UCLA
UCLA Electronic Theses and Dissertations

Title

Palladium-Catalyzed Reactions of Cyclic Allenes and Strain-Promoted Reactions of Cyclic 1,2,3-Trienes

Permalink

https://escholarship.org/uc/item/0594f2qp

Author

Witkowski, Dominick Christopher

Publication Date

2025

Peer reviewed|Thesis/dissertation

eScholarship.org Powered by the California Digital Library
University of California

UNIVERSITY OF CALIFORNIA

Los Angeles

Palladium-Catalyzed Reactions of Cyclic Allenes and Strain-Promoted Reactions of Cyclic 1,2,3-Trienes

A dissertation submitted in partial satisfaction of the

requirements for the degree Doctor of Philosophy

in Chemistry

by

Dominick Christopher Witkowski

2025

© Copyright by

Dominick Christopher Witkowski

2025

ABSTRACT OF THE DISSERTATION

Palladium-Catalyzed Reactions of Cyclic Allenes and

Strain-Promoted Reactions of Cyclic 1,2,3-Trienes

by

Dominick Christopher Witkowski

Doctor of Philosophy in Chemistry

University of California, Los Angeles, 2025

Professor Neil Kamal Garg, Chair

This dissertation describes the development of methodologies that engage strained cyclic intermediates in complexity-generating reactions. One major effort involves the transition metal-catalyzed interception of strained cyclic allenes, which has been accomplished using palladium catalysis. Additionally, the study of alternative minimally explored strained intermediates including cyclic 1,2,3-trienes and heterocyclic 1,2,3-trienes are reported. These studies contribute to fundamental understanding of structure and reactivity of transient strained compounds and give

rise to polycyclic products. Computational studies relating to the mechanism of strained intermediate generation from Kobayashi precursors are also reported.

Chapters one and two are related to the development of palladium-catalyzed reactions of strained cyclic allenes. Chapter one describes the development of a modular annulation reaction of strained allenes and arylpalladium species. This methodology employs aryl halides and cyclic allene precursors to generate fused heterocyclic products via the formation of two new bonds and a new center. Chapter two described the development of a catalyst-controlled annulation reaction of strained allenes and π-allylpalladium species. This methodology employs vinyl benzoxazinones and cyclic allenes precursors to generate two isomeric products with high selectivity based on the ligand employed. The development of these palladium-catalyzed reactions demonstrates that despite their high reactivity and short lifetimes, strained cyclic allenes efficiently engaged in catalytic processes, to access complex products, including examples with absolute stereocontrol.

Chapter three describes the development of strained 1,2,3-cyclohexatrienes, which have remained underexplored historically, as synthetic building blocks. Studies of the reactivity of the unsubstituted 1,2,3-cyclohexatriene, as well as its mono- and disubstituted derivatives are reported, drastically expanding the scope of reactions known for such intermediates. Combined computational and experimental studies elucidate the factors controlling regioselectivity in reactions of an unsymmetrical strained triene. Furthermore, the potential utility of strained trienes in rapidly generating complex scaffolds is demonstrated through the integration of triene trapping reactions into multistep synthetic sequences to access polycyclic products. These studies highlight the potential of these traditionally avoided species for broader use in synthetic chemistry.

Chapter four details the study of six-membered heterocyclic 1,2,3-trienes, particularly 4,5-didehydropyridones. Computational studies of the structure of such species, as well as the

development of a synthetic route to access precursors to the same, are reported. Scope studies demonstrate the utility of six-membered azacyclic 1,2,3-trienes for accessing complex nitrogen-containing heterocycles, and trends in the regioselectivity observed therein are explored through computational studies. Collectively, this study demonstrates the value of six-membered azacyclic 1,2,3-trienes, a previously unexplored class of strained cyclic intermediates, in heterocycle synthesis, while pushing the limits of strained intermediate chemistry.

Chapter five describes the reaction mechanisms of the fluoride-mediated generation of selected strained intermediates from Kobayashi precursors. We interrogate several mechanistic aspects using Density Functional Theory (DFT) calculations and find that the eliminations to form alkynes and alkenes can take place through primarily two different mechanisms. This study is one of the few theoretical studies on Kobayashi eliminations for the generation of strained intermediates. It is anticipated that this report will enable the rational design of new strained intermediate precursors for future uses in synthesis.

The dissertation of Dominick Christopher Witkowski is approved.

Abigail Gutmann Doyle

Kendall N. Houk

Yi Tang

Neil Kamal Garg, Committee Chair

University of California, Los Angeles

2025

"The chymists are a strange class of mortals impelled by an almost insane impulse to seek their pleasure among smoke and vapor, soot and flame, poisons and poverty; yet among all these evils I seem to live so sweetly, that I may die if I would change places with the Persian King."

– Johann Joachim Becher

For my family

TABLE OF CONTENTS

ABSTRACT OF THE DISSERTATION ii

COMMITTEE PAGE v

DEDICATION PAGE vi

TABLE OF CONTENTS vii

LIST OF FIGURES xv

LIST OF SCHEMES xxxvi

LIST OF TABLES xxxvii

LIST OF EQUATIONS xli

LIST OF ABBREVIATIONS xlii

ACKNOWLEDGEMENTS xlviii

BIOGRAPHICAL SKETCH liv

CHAPTER ONE: Palladium-Catalyzed Annulations of Strained Cyclic Allenes 1

1.1 Abstract 1

1.2 Introduction 1

1.3 Reaction Design 3

1.4 Reaction Optimization 4

1.5 Scope of the Annulation Reaction 5

1.6 Development of Stereoselective Variants 8

1.7 Conclusion 11

1.8 Experimental Section 11

1.8.1 Materials and Methods 11

1.8.2 Experimental Procedures 14

1.8.2.1 Syntheses of Annulation Partners 14

1.8.2.1.1 Syntheses of *N*-Tosyl-Arylamines 14

1.8.2.1.2 Synthesis of Alcohol **1.43** 21

1.8.2.2 Synthesis of Silyl Triflate **1.46** 22

1.8.2.3 Optimization of the Racemic Annulation 25

1.8.2.4 Scope of the Racemic Annulation 28

1.8.2.5 Diastereoselective Annulation 43

1.8.2.6 Optimization of the Asymmetric Annulation 45

1.8.2.7 Synthesis of **(–)-1.47** via Asymmetric Annulation 51

1.8.2.8 Elaboration of Annulation Product of **(–)-1.47** 53

1.9 Spectra Relevant to Chapter One 59

1.10 Notes and References 103

CHAPTER TWO: Catalyst-Controlled Annulations of Strained Cyclic Allenes with π-Allylpalladium Complexes 111

2.1 Abstract 111

2.2 Introduction 111

2.3 Reaction Optimization 114

2.4 Scope of the Annulation Reactions 115

2.5 Reaction Mechanisms 119

2.6 Development of Enantioselective Variant 120

2.7 Conclusion 123

2.8 Experimental Section 123

2.8.1 Materials and Methods 123

2.8.2 Experimental Procedures 126

2.8.2.1 Synthesis of *N*-Tosyl-vinyl Benzoxazinones 126

2.8.2.2 Optimization of the Racemic Annulation 135

2.8.2.3 Scope of the Racemic Annulation 140

2.8.2.4 Representative Asymmetric Annulations 168

2.8.2.5 Extended Evaluation of Chiral Ferrocenyl Phosphine Ligands 172

2.8.2.6 Assignment of Absolute Stereochemical Configuration 176

2.9 Spectra Relevant to Chapter Two 187

2.10 Notes and References 231

CHAPTER THREE: Strain-Promoted Reactions of 1,2,3-Cyclohexatriene and Its Derivatives 240

3.1 Abstract 240

3.2 Introduction 241

3.3 Computational Structural Analysis 245

3.4 Reactivity of 1,2,3-Cyclohexatriene (**3.5**) 246

3.5 Reactivity of a Substituted 1,2,3-Cyclohexatriene Derivative 248

3.6 Regioselective Reactions of a Silyl-Substituted Triene 252

3.7 Leveraging Cyclic Trienes to Access Complex Scaffolds 255

3.8 Conclusion 257

3.9 Experimental Section 257

3.9.1 Method for Literature Searches for Strained Intermediate Studies 257

3.9.2 Materials and Methods 257

3.9.3 Experimental Procedures 260

3.9.3.1 Optimization of Trapping Reactions of 1,2,3-Cyclohexatriene (**3.5**) 260

3.9.3.2 Scope of Trapping Reactions of 1,2,3-Cyclohexatriene (**3.5**) 262

3.9.3.3 Synthesis of Silyl Triflate **3.42** 267

3.9.3.4 Scope of Trapping Reactions of Triene **3.43** 270

3.9.3.5 Synthesis of Silyl Triflate **3.76** 282

3.9.3.6 Trapping Reactions of Silyl Triene **3.75** 285

3.9.3.7 Synthetic Elaboration of Triene Trapping Products 287

3.9.3.8 Competition Experiment with 1,2,3-Cyclohexatriene (**3.5**) and Benzyne (**3.20**) 304

3.9.4 Computational Section 304

3.9.4.1 Computational Methods 304

3.9.4.2 Calculated Energies of Selected C_6H_6 Isomers 305

3.9.4.3 Structure of 1,2,3-Cyclohexatriene (**3.5**) 305

3.9.4.4 Transition State Analysis for Reaction of Triene **3.80** with Phenoxide **3.34** 306

3.9.4.5 Relative Stereochemical Assignment of Thietanes **3.69** and **3.93** 308

3.9.4.6 Cartesian Coordinates of Optimized Geometries 310

3.10 Spectra Relevant to Chapter Three 311

3.11 Notes and References 365

CHAPTER FOUR: Synthesis and Reactivity of Nitrogen-Containing Cyclic 1,2,3-Trienes 377

4.1 Abstract 377

4.2 Introduction 378

4.3 Geometric and Electronic Structure of Cyclic 1,2,3-Trienes 379

4.4 Synthesis of Azacyclic 1,2,3-Triene Precursor 381

4.5 Generation and Trapping of Azacyclic 1,2,3-Trienes in (4+2) Cycloadditions 383

4.6 Regioselective Trapping Experiments 388

4.7 Computational Analysis of Regioselective Trapping Reactions 390

4.8 Conclusion 394

4.9 Experimental Section 394
4.9.1 Materials and Methods 394
4.9.2 Experimental Procedures 398
4.9.2.1 Synthesis of Unsubstituted Silyl Nonaflate and Silyl Triflate Precursors 398
4.9.2.2 Synthesis of Substituted Silyl Nonaflate Precursors 408
4.9.2.3 Optimization of Trapping Reactions of Azacyclic 1,2,3-Triene **4.12** 415
4.9.2.4 Scope of (4+2) Trapping Reactions 418
4.9.2.5 Scope of Regioselective Trapping Reactions 431
4.9.2.6 Synthesis and Trapping of **4.12** via Isomeric Silyl Nonaflate **4.75** 441
4.9.2.7 1 mmol Scale Trapping Reaction 447
4.9.3 Computational Section 448
4.9.3.1 Computational Methods 448
4.9.3.2 Choice of Computational Method 448
4.9.3.3 Structure of 1,2,3-Cyclohexatriene (**4.8**) 449
4.9.3.4 Structure of Azacyclic 1,2,3-Triene **4.12** 450
4.9.3.5 Energy of Dehydrogenation Calculation for Azacyclic 1,2,3-Triene **4.12** 451
4.9.3.6 Structure of Pyridone **4.76** 451
4.9.3.7 Structures of Cyclic 1,2,3-Trienes **4.78** and **4.79** 451
4.9.3.8 Geometric Distortions of 1,2,3-Triene **4.80a**–**4.80c** 453

4.9.3.9 Structure of Azacyclic 1,2,3-Triene Isomer **4.81**.....454

4.9.3.10 Structures of Azacyclic 1,2,3-Trienes **4.29** and **4.31**.....455

4.9.3.11 Structures of Azacyclic 1,2,3-Trienes **4.35** and **4.37**.....455

4.9.3.12 Transition State Analysis for Reaction of **4.12** with **4.42**.....456

4.9.3.13 Transition State Analysis for Reaction of **4.37** with **4.42**.....458

4.9.3.14 Reaction Energy Profile and Mechanism for Reaction of **4.12** with **4.42**.....460

4.9.3.15 Cartesian Coordinates of Optimized Geometries 461

4.10 Spectra Relevant to Chapter Four.....462

4.11 Notes and References.....516

CHAPTER FIVE: Mechanisms of Kobayashi Eliminations for the Formation of Highly-Strained Arynes, Cyclic Cumulenes, adn Anti-Bredt Olefins.....528

5.1 Abstract.....528

5.2 Introduction.....529

5.3 Thermodynamics of Kobayashi Eliminations to Form Strained Intermediates.....532

5.4 Kobayashi Elimination to Form Benzyne (**5.3**).....534

5.5 Mechanisms of Kobayashi Eliminations to Form Cyclohexyne (**5.5**) and 1,2,3-Cyclohexatriene (**5.9**).....537

5.6 Kobayashi Eliminations to Form Anti-Bredt Olefins.....540

5.7 Study of Impact of Dihedral Angle on Kobayashi Eliminations of Aliphatic Systems 542

5.8 Conclusion 544

5.9 Computational Section.....545

5.9.1 Methods for Literature Searches for Kobayashi Precursors and Reactions 545
5.9.2 Computational Methods.....546
5.9.3 Calculated Energies of Selected Kobayashi Precursors and Strained Intermediates.....546
5.9.4 Transition State Analysis for Reaction of Precursor **5.1** to Form Benzyne (**5.3**) 547
5.9.5 Control Experiments to Support Proposed Mechanism.....548
5.9.6 Reaction Energy Profile and Mechanism for Formation of Cyclohexyne (**5.5**) 550
5.9.7 Reaction Energy Profile and Mechanism for Formation of 1,2,3-Cyclohexatriene (**5.9**).....552
5.9.8 Reaction Energy Profile and Mechanism for Formation of 1,2,3-Triene **5.45** 554
5.9.9 Reaction Energy Profile and Mechanism for Formation of 1,2,3-Triene **5.50** 556
5.9.10 Reaction Energy Profile and Mechanism for Formation of Anti-Bredt Olefin **5.11**.....561
5.9.11 Reaction Energy Profile and Mechanism for Formation of Anti-Bredt Olefin ***epi*-5.11** 562
5.9.12 Effect of Dihedral Angle on Kobayashi Eliminations 565
5.9.13 Cartesian Coordinates of Optimized Geometries 567
5.10 Notes and References.....568

LIST OF FIGURES

CHAPTER ONE

Figure 1.1 Selected in situ-generated strained cyclic intermediates and overview of strained cyclic allene reactivity 3

Figure 1.2 Scope of the annulation reaction with iodoaniline derivatives **1.20** 7

Figure 1.3 Variation of the pronucleophile to furnish structurally diverse products ... 8

Figure 1.4 Stereocontrolled annulations and synthetic elaboration of an annulation product 10

Figure 1.5 Ligand families evaluated during asymmetric reaction development 46

Figure 1.6 ORTEP representation of X-ray crystallographic structure **(+)-1.50**. 55

Figure 1.7 SFC trace for **(±)-1.47**. 58

Figure 1.8 SFC trace for **(–)-1.47** 58

Figure 1.9 ^{1}H NMR (400 MHz, $CDCl_3$) of compound **1.56** 60

Figure 1.10 ^{13}C NMR (100 MHz, $CDCl_3$) of compound **1.56** 60

Figure 1.11 ^{1}H NMR (500 MHz, $CDCl_3$) of compound **1.58** 61

Figure 1.12 ^{13}C NMR (125 MHz, $CDCl_3$) of compound **1.58** 61

Figure 1.13 ^{1}H NMR (400 MHz, $CDCl_3$) of compound **1.60** 62

Figure 1.14 ^{13}C NMR (125 MHz, $CDCl_3$) of compound **1.60** 62

Figure 1.15 ^{19}F NMR (376 MHz, $CDCl_3$) of compound **1.60** 63

Figure 1.16 ^{1}H NMR (500 MHz, CD_3OD) of compound **1.62** 64

Figure 1.17 ^{13}C NMR (125 MHz, CD_3OD) of compound **1.62** 64

Figure 1.18 ^{1}H NMR (500 MHz, $CDCl_3$) of compound **1.64** 65

Figure 1.19 ^{13}C NMR (125 MHz, $CDCl_3$) of compound **1.64** 65

Figure 1.20 ^{1}H NMR (500 MHz, CD_3OD) of compound **1.66** 66

Figure 1.21 ^{13}C NMR (125 MHz, CD_3OD) of compound **1.66** 66

Figure 1.22 ^{1}H NMR (500 MHz, $CDCl_3$) of compound **1.45** 67

Figure 1.23 ^{13}C NMR (125 MHz, $CDCl_3$) of compound **1.45** 67

Figure 1.24 ^{1}H NMR (500 MHz, $CDCl_3$) of compound **1.69** 68

Figure 1.25 ^{13}C NMR (125 MHz, $CDCl_3$) of compound **1.69** 68

Figure 1.26 ^{1}H NMR (500 MHz, $CDCl_3$) of compound **1.71** 69

Figure 1.27 ^{13}C NMR (125 MHz, $CDCl_3$) of compound **1.71** 69

Figure 1.28 ^{1}H NMR (500 MHz, $CDCl_3$) of compound **1.73** 70

Figure 1.29 ^{13}C NMR (125 MHz, $CDCl_3$) of compound **1.73** 70

Figure 1.30 ^{1}H NMR (500 MHz, $CDCl_3$) of compound **1.43** 71

Figure 1.31 ^{13}C NMR (125 MHz, $CDCl_3$) of compound **1.43** 71

Figure 1.32 ^{1}H NMR (400 MHz, $CDCl_3$) of compound **1.75** 72

Figure 1.33 ^{13}C NMR (100 MHz, $CDCl_3$) of compound **1.75** 72

Figure 1.34 ^{1}H NMR (400 MHz, $CDCl_3$) of compound **1.76** 73

Figure 1.35 ^{13}C NMR (100 MHz, $CDCl_3$) of compound **1.76** 73

Figure 1.36 ^{1}H NMR (500 MHz, $CDCl_3$) of compound **1.46** 74

Figure 1.37 ^{13}C NMR (125 MHz, $CDCl_3$) of compound **1.46** 74

Figure 1.38 ^{1}H NMR (500 MHz, $CDCl_3$) of compound **1.19a** 75

Figure 1.39 ^{1}H NMR (500 MHz, DMSO-d_6) of compound **1.19b**.....76

Figure 1.40 ^{13}C NMR (100 MHz, DMSO-d_6) of compound **1.19b**.....76

Figure 1.41 ^{1}H NMR (500 MHz, DMSO-d_6) of compound **1.19c** 77

Figure 1.42 ^{13}C NMR (125 MHz, DMSO-d_6) of compound **1.19c** 77

Figure 1.43 ^{1}H NMR (400 MHz, C_6D_6) of compound **1.22** 78

Figure 1.44 ^{13}C NMR (100 MHz, C_6D_6) of compound **1.22** 78

Figure 1.45 ^{1}H NMR (500 MHz, $CDCl_3$) of compound **1.23** 79

Figure 1.46 ^{13}C NMR (125 MHz, $CDCl_3$) of compound **1.23** 79

Figure 1.47 ^{1}H NMR (600 MHz, $CDCl_3$) of compound **1.24** 80

Figure 1.48 ^{13}C NMR (125 MHz, $CDCl_3$) of compound **1.24** 80

Figure 1.49 ^{19}F NMR (376 MHz, $CDCl_3$) of compound **1.24** 81

Figure 1.50 ^{1}H NMR (500 MHz, $CDCl_3$) of compound **1.25** 82

Figure 1.51 ^{13}C NMR (125 MHz, $CDCl_3$) of compound **1.25** 82

Figure 1.52 ^{1}H NMR (400 MHz, $CDCl_3$) of compound **1.26** 83

Figure 1.53 ^{13}C NMR (100 MHz, $CDCl_3$) of compound **1.26** 83

Figure 1.54 ^{1}H NMR (500 MHz, $CDCl_3$) of compound **1.27** 84

Figure 1.55 ^{13}C NMR (125 MHz, $CDCl_3$) of compound **1.27** 84

Figure 1.56 ^{1}H NMR (500 MHz, $CDCl_3$) of compound **1.28** 85

Figure 1.57 ^{13}C NMR (125 MHz, $CDCl_3$) of compound **1.28** 85

Figure 1.58 ^{1}H NMR (500 MHz, C_6D_6) of compound **1.29** 86

Figure 1.59 ^{13}C NMR (125 MHz, $CDCl_3$) of compound **1.29** 86

Figure 1.60 ^{1}H NMR (500 MHz, $CDCl_3$) of compound **1.30** 87

Figure 1.61 ^{13}C NMR (125 MHz, $CDCl_3$) of compound **1.30** 87

Figure 1.62 ^{19}F NMR (376 MHz, $CDCl_3$) of compound **1.30** 88

Figure 1.63 ^{1}H NMR (500 MHz, $CDCl_3$) of compound **1.31** 89

Figure 1.64 ^{13}C NMR (125 MHz, $CDCl_3$) of compound **1.31** 89

Figure 1.65 ^{1}H NMR (500 MHz, $CDCl_3$) of compound **1.32** 90

Figure 1.66 ^{13}C NMR (125 MHz, $CDCl_3$) of compound **1.26** 90

Figure 1.67 ^{1}H NMR (600 MHz, $CDCl_3$) of compound **1.33** 91

Figure 1.68 ^{13}C NMR (125 MHz, $CDCl_3$) of compound **1.33** 91

Figure 1.69 ^{1}H NMR (500 MHz, $CDCl_3$) of compound **1.34** 92

Figure 1.70 ^{13}C NMR (125 MHz, $CDCl_3$) of compound **1.34** 92

Figure 1.71 ^{1}H NMR (500 MHz, $CDCl_3$) of compound **1.36** 93

Figure 1.72 ^{13}C NMR (100 MHz, $CDCl_3$) of compound **1.36** 93

Figure 1.73 ^{1}H NMR (500 MHz, $CDCl_3$) of compound **1.38** 94

Figure 1.74 ^{13}C NMR (100 MHz, $CDCl_3$) of compound **1.38** 94

Figure 1.75 ^{1}H NMR (500 MHz, $CDCl_3$) of compound **1.40** 95

Figure 1.76 ^{1}H NMR (600 MHz, $CDCl_3$) of compound **1.42** 96

Figure 1.77 ^{13}C NMR (100 MHz, $CDCl_3$) of compound **1.42** 96

Figure 1.78 ^{1}H NMR (500 MHz, $CDCl_3$) of compound **1.44** 97

Figure 1.79 ^{13}C NMR (125 MHz, $CDCl_3$) of compound **1.44** 97

Figure 1.80 ^{1}H NMR (500 MHz, $CDCl_3$) of compound **1.86** 98

Figure 1.81 ^{13}C NMR (125 MHz, $CDCl_3$) of compound **1.86** 98

Figure 1.82 NOESY (500 MHz, $CDCl_3$) of compound **1.86** 99

Figure 1.83 ^{1}H NMR (500 MHz, $CDCl_3$) of compound (–)-**1.47** 100

Figure 1.84 ^{13}C NMR (125 MHz, $CDCl_3$) of compound (–)-**1.47** 100

Figure 1.85 ^{1}H NMR (500 MHz, $CDCl_3$) of compound (+)-**1.49** 101

Figure 1.86 ^{13}C NMR (125 MHz, $CDCl_3$) of compound (+)-**1.49** 101

Figure 1.87 ^{1}H NMR (500 MHz, $CDCl_3$) of compound (+)-**1.50** 102

Figure 1.88 ^{13}C NMR (125 MHz, $CDCl_3$) of compound (+)-**1.50** 102

CHAPTER TWO

Figure 2.1A Strained cyclic intermediates **2.1**–**2.4** 113

Figure 2.1B Approaches for metal-catalyzed reactions of strained cyclic allenes 113

Figure 2.1C Overview of current study 113

Figure 2.2 Scope of the annulation reaction using PPh_3 as the ligand 117

Figure 2.3 Scope of the annulation reaction using dppf as the ligand..... 118

Figure 2.4 Proposed catalytic cycle..... 120

Figure 2.5 Unsuccessful and low yielding substrates evaluated during scope studies 167

Figure 2.6 Ligand families evaluated during asymmetric reaction development 174

Figure 2.7 ORTEP representation of X-ray crystallographic structure **(–)-2.43**.....178

Figure 2.8 SFC trace of (±)-**2.43** 182

Figure 2.9 SFC trace of **(–)-2.43** (from reaction mixture).....182

Figure 2.10 SFC trace of **(–)-2.43** (Crystals used for X-ray analysis) 183

Figure 2.11 SFC trace of **(±)-2.52** 184

Figure 2.12 SFC trace of **(–)-2.52** 184

Figure 2.13 SFC trace of **(±)-2.51** 185

Figure 2.14 SFC trace of **2.51** 185

Figure 2.15 SFC trace of **(±)-2.91** 186

Figure 2.16 SFC trace of **2.91** 186

Figure 2.17 ^{1}H NMR (500 MHz, $CDCl_3$) of compound **2.54** 188

Figure 2.18 ^{13}C NMR (125 MHz, $CDCl_3$) of compound **2.54** 188

Figure 2.19 ^{1}H NMR (500 MHz, $CDCl_3$) of compound **2.56** 189

Figure 2.20 ^{13}C NMR (125 MHz, $CDCl_3$) of compound **2.56** 189

Figure 2.21 ^{1}H NMR (500 MHz, $CDCl_3$) of compound **2.49** 190

Figure 2.22 ^{13}C NMR (125 MHz, $CDCl_3$) of compound **2.49** 190

Figure 2.23 ^{1}H NMR (600 MHz, $CDCl_3$) of compound **2.58** 191

Figure 2.24 ^{13}C NMR (125 MHz, $CDCl_3$) of compound **2.58** 191

Figure 2.25 ^{1}H NMR (500 MHz, $CDCl_3$) of compound **2.60**. 192

Figure 2.26 ^{13}C NMR (125 MHz, $CDCl_3$) of compound **2.60** 192

Figure 2.27 ^{1}H NMR (500 MHz, $CDCl_3$) of compound **2.61** 193

Figure 2.28 ^{13}C NMR (125 MHz, $CDCl_3$) of compound **2.61** 193

Figure 2.29 ^{1}H NMR (500 MHz, $CDCl_3$) of compound **2.63** 194

Figure 2.30 ^{13}C NMR (125 MHz, $CDCl_3$) of compound **2.63** 194

Figure 2.31 ^{1}H NMR (600 MHz, $CDCl_3$) of compound **2.65** 195

Figure 2.32 ^{13}C NMR (125 MHz, $CDCl_3$) of compound **2.65** 195

Figure 2.33 ^{1}H NMR (500 MHz, $CDCl_3$) of compound **2.66** 196

Figure 2.34 ^{13}C NMR (125 MHz, $CDCl_3$) of compound **2.66** 196

Figure 2.35 ^{1}H NMR (600 MHz, $CDCl_3$) of compound **2.67** 197

Figure 2.36 ^{13}C NMR (150 MHz, $CDCl_3$) of compound **2.67** 197

Figure 2.37 ^{1}H NMR (500 MHz, $CDCl_3$) of compounds **2.17** and **2.68** 198

Figure 2.38 ^{13}C NMR (125 MHz, $CDCl_3$) of compounds **2.17** and **2.68** 198

Figure 2.39 NOESY (500 MHz, $CDCl_3$) of compound **2.17** 199

Figure 2.40 ^{1}H NMR (500 MHz, $CDCl_3$) of compound **2.22** 200

Figure 2.41 ^{13}C NMR (125 MHz, $CDCl_3$) of compound **2.22** 200

Figure 2.42 ^{1}H NMR (500 MHz, $CDCl_3$) of compound **2.23** 201

Figure 2.43 ^{13}C NMR (125 MHz, $CDCl_3$) of compound **2.23** 201

Figure 2.44 ^{1}H NMR (600 MHz, $CDCl_3$) of compounds **2.24** and **2.72** 202

Figure 2.45 ^{13}C NMR (150 MHz, $CDCl_3$) of compounds **2.24** and **2.72** 202

Figure 2.46 ^{1}H NMR (500 MHz, $CDCl_3$) of compound **2.25** 203

Figure 2.47 ^{13}C NMR (125 MHz, $CDCl_3$) of compound **2.25** 203

Figure 2.48 ^{19}F NMR (282 MHz, $CDCl_3$) of compound **2.25**.....204

Figure 2.49 ^{1}H NMR (500 MHz, $CDCl_3$) of compounds **2.26**, **2.75**, and **2.39** 205

Figure 2.50 ^{13}C NMR (125 MHz, $CDCl_3$) of compounds **2.26**, **2.75**, and **2.39** 205

Figure 2.51 ^{19}F NMR (282 MHz, $CDCl_3$) of compounds **2.26**, **2.75**, and **2.39** 206

Figure 2.52 ^{1}H NMR (500 MHz, $CDCl_3$) of compounds **2.27** and **2.77** 207

Figure 2.53 ^{13}C NMR (125 MHz, $CDCl_3$) of compounds **2.27** and **2.77** 207

Figure 2.54 ^{1}H NMR (500 MHz, $CDCl_3$) of compounds **2.28** and **2.78** 208

Figure 2.55 ^{13}C NMR (125 MHz, $CDCl_3$) of compounds **2.28** and **2.78** 208

Figure 2.56 ^{1}H NMR (500 MHz, $CDCl_3$) of compounds **2.29** and **2.79** 209

Figure 2.57 ^{13}C NMR (125 MHz, $CDCl_3$) of compounds **2.29** and **2.79** 209

Figure 2.58 ^{1}H NMR (500 MHz, $CDCl_3$) of compounds **2.30** and **2.80** 210

Figure 2.59 ^{13}C NMR (125 MHz, $CDCl_3$) of compounds **2.30** and **2.80** 210

Figure 2.60 ^{1}H NMR (500 MHz, $CDCl_3$) of compounds **2.31** and **2.82** 211

Figure 2.61 ^{13}C NMR (125 MHz, $CDCl_3$) of compounds **2.31** and **2.82** 211

Figure 2.62 NOESY (600 MHz, $CDCl_3$) of compound **2.31** 212

Figure 2.63 ^{1}H NMR (500 MHz, $CDCl_3$) of compounds **2.32** and **2.83** 213

Figure 2.64 ^{13}C NMR (125 MHz, $CDCl_3$) of compounds **2.32** and **2.83** 213

Figure 2.65 ^{1}H NMR (500 MHz, $CDCl_3$) of compounds **2.33** and **2.85** 214

Figure 2.66 ^{13}C NMR (125 MHz, $CDCl_3$) of compounds **2.33** and **2.85** 214

Figure 2.67 NOESY (500 MHz, $CDCl_3$) of compound **2.85** 215

Figure 2.68 ^{1}H NMR (500 MHz, $CDCl_3$) of compounds **2.18** and **2.17** 216

Figure 2.69 ^{13}C NMR (125 MHz, $CDCl_3$) of compounds **2.18** and **2.17** 216

Figure 2.70 ^{1}H NMR (500 MHz, $CDCl_3$) of compound **2.35** 217

Figure 2.71 ^{13}C NMR (125 MHz, $CDCl_3$) of compound **2.35** 217

Figure 2.72 ^{1}H NMR (500 MHz, $CDCl_3$) of compounds **2.36** and **2.23** 218

Figure 2.73 ^{13}C NMR (125 MHz, $CDCl_3$) of compound **2.36** and **2.23**.....218

Figure 2.74 ^{1}H NMR (500 MHz, $CDCl_3$) of compounds **2.37** and **2.24** 219

Figure 2.75 ^{13}C NMR (125 MHz, $CDCl_3$) of compound **2.37** and **2.24**.....219

Figure 2.76 ^{1}H NMR (500 MHz, $CDCl_3$) of compounds **2.38** and **2.25** 220

Figure 2.77 ^{13}C NMR (125 MHz, $CDCl_3$) of compound **2.38** and **2.25**.....220

Figure 2.78 ^{19}F NMR (282 MHz, $CDCl_3$) of compound **2.38** and **2.25** 221

Figure 2.79 ^{1}H NMR (500 MHz, $CDCl_3$) of compounds **2.39** and **2.26** 222

Figure 2.80 ^{13}C NMR (125 MHz, $CDCl_3$) of compound **2.39** and **2.26**.....222

Figure 2.81 ^{19}F NMR (282 MHz, $CDCl_3$) of compound **2.39** and **2.26** 223

Figure 2.82 ^{1}H NMR (600 MHz, $CDCl_3$) of compounds **2.40** and **2.27** 224

Figure 2.83 ^{13}C NMR (150 MHz, $CDCl_3$) of compound **2.40** and **2.27**.....224

Figure 2.84 ^{1}H NMR (500 MHz, $CDCl_3$) of compounds **2.41**, **2.28**, and **2.78** 225

Figure 2.85 ^{13}C NMR (125 MHz, $CDCl_3$) of compounds **2.41**, **2.28**, and **2.78** 225

Figure 2.86 ^{1}H NMR (500 MHz, $CDCl_3$) of compound **2.42** 226

Figure 2.87 ^{13}C NMR (125 MHz, $CDCl_3$) of compound **2.42** 226

Figure 2.88 ^{1}H NMR (500 MHz, $CDCl_3$) of compound **2.43** 227

Figure 2.89 ^{13}C NMR (125 MHz, $CDCl_3$) of compound **2.43** 227

Figure 2.90 ^{1}H NMR (600 MHz, $CDCl_3$) of compound **2.44** 228

Figure 2.91 ^{13}C NMR (125 MHz, $CDCl_3$) of compound **2.44** 228

Figure 2.92 ^{1}H NMR (500 MHz, $CDCl_3$) of compound (–)-**2.52** 229

Figure 2.93 ^{13}C NMR (125 MHz, $CDCl_3$) of compound (–)-**2.52** 229

Figure 2.94 ^{1}H NMR (500 MHz, $CDCl_3$) of compounds **2.51** and **2.91** 230

Figure 2.95 ^{13}C NMR (125 MHz, $CDCl_3$) of compounds **2.51** and **2.91** 230

CHAPTER THREE

Figure 3.1 Selected strained isomers of benzene (**3.1**) and comparison of reaction coordinate diagrams 242

Figure 3.2 Strained cyclic intermediates and overview of current study 244

Figure 3.3A Geometry-optimized structures and frontier molecular orbitals of benzene (**3.1**), 1,2,3-cyclohexatriene (**3.5**), and benzyne (**3.20**) 246

Figure 3.3B Scope of reactions of triene **3.5** 247

Figure 3.4A Synthesis of silyl triflate **3.42** 249

Figure 3.4B Scope of reactions of triene **3.43** 251

Figure 3.5 Structure and regioselective reactions of a monosubstituted cyclic triene 254

Figure 3.6 Strained 1,2,3-cyclohexatrienes in multistep synthesis 256

Figure 3.7 ORTEP representation of X-ray crystallographic structure **3.81** 290

Figure 3.8 ORTEP representation of X-ray crystallographic structure **3.84** 295

Figure 3.9 SFC trace for **(±)-3.78** 302

Figure 3.10 SFC trace for **(+)-3.78** 302

Figure 3.11 SFC trace for **(±)-3.19** 303

Figure 3.12 SFC trace for **(+)-3.19** 303

Figure 3.13 Geometry of 1,2,3-cyclohexatriene (**3.5**) 305

Figure 3.14 DIAS strain analysis along a relaxed scan of the forming C–O bond for attack of phenoxide **3.34** (Na^+ omitted) on triene **3.80** at C2 or C3 307

Figure 3.15 Transition state structures for the attack of **3.34** (Na^+ omitted) onto **3.80** 308

Figure 3.16 Atom numbers used in Table 3.8 and Table 3.9 310

Figure 3.17 ^{1}H NMR (600 MHz, C_6D_6) of compound **3.27** 312

Figure 3.18 ^{1}H NMR (600 MHz, C_6D_6) of compound **3.28** 313

Figure 3.19 ^{13}C NMR (150 MHz, C_6D_6) of compound **3.28** 313

Figure 3.20 ^{1}H NMR (600 MHz, C_6D_6) of compound **3.29** 314

Figure 3.21 ^{13}C NMR (150 MHz, C_6D_6) of compound **3.29** 314

Figure 3.22 ^{1}H NMR (500 MHz, CD_2Cl_2) of compound **3.30** 315

Figure 3.23 ^{13}C NMR (125 MHz, CD_2Cl_2) of compound **3.30** 315

Figure 3.24 ^{1}H NMR (500 MHz, C_6D_6) of compound **3.35** 316

Figure 3.25 ^{13}C NMR (100 MHz, C_6D_6) of compound **3.35** 316

Figure 3.26 ^{1}H NMR (500 MHz, C_6D_6) of compound **3.36** 317

Figure 3.27 ^{13}C NMR (125 MHz, C_6D_6) of compound **3.36** 317

Figure 3.28 ^{1}H NMR (600 MHz, C_6D_6) of compound **3.37** 318

Figure 3.29 ^{13}C NMR (150 MHz, C_6D_6) of compound **3.37** 318

Figure 3.30 ^{1}H NMR (500 MHz, C_6D_6) of compound **3.38** 319

Figure 3.31 ^{13}C NMR (125 MHz, C_6D_6) of compound **3.38** 319

Figure 3.32 ^{1}H NMR (500 MHz, $CDCl_3$) of compound **3.40** 320

Figure 3.33 ^{13}C NMR (150 MHz, $CDCl_3$) of compound **3.40** 320

Figure 3.34 ^{1}H NMR (400 MHz, $CDCl_3$) of compound **3.41** 321

Figure 3.35 ^{13}C NMR (100 MHz, $CDCl_3$) of compound **3.41** 321

Figure 3.36 ^{1}H NMR (600 MHz, $CDCl_3$) of compound **3.42** 322

Figure 3.37 ^{13}C NMR (150 MHz, $CDCl_3$) of compound **3.42** 322

Figure 3.38 ^{19}F NMR (376 MHz, $CDCl_3$) of compound **3.42**.....323

Figure 3.39 ^{1}H NMR (600 MHz, C_6D_6) of compound **3.50**.....324

Figure 3.40 ^{13}C NMR (150 MHz, C_6D_6) of compound **3.50**.....324

Figure 3.41 ^{1}H NMR (500 MHz, $CDCl_3$) of compound **3.51** 325

Figure 3.42 ^{13}C NMR (125 MHz, $CDCl_3$) of compound **3.51** 325

Figure 3.43 ^{1}H NMR (600 MHz, $CDCl_3$) of compound **3.52** 326

Figure 3.44 ^{13}C NMR (150 MHz, $CDCl_3$) of compound **3.52** 326

Figure 3.45 ^{1}H NMR (500 MHz, $CDCl_3$) of compound **3.53** 327

Figure 3.46 ^{13}C NMR (125 MHz, $CDCl_3$) of compound **3.53** 327

Figure 3.47 ^{1}H NMR (500 MHz, C_6D_6) of compound **3.54**.....328

Figure 3.48 ^{13}C NMR (125 MHz, C_6D_6) of compound **3.54**.....328

Figure 3.49 ^{1}H NMR (500 MHz, CD_3CN) of compound **3.55**.....329

Figure 3.50 ^{13}C NMR (150 MHz, C_6D_6) of compound **3.55**.....329

Figure 3.51 ^{1}H NMR (500 MHz, C_6D_6) of compound **3.56**.....330

Figure 3.52 ^{13}C NMR (125 MHz, C_6D_6) of compound **3.56**.....330

Figure 3.53 ^{1}H NMR (500 MHz, C_6D_6) of compound **3.57**.....331

Figure 3.54 ^{13}C NMR (150 MHz, CD_2Cl_2) of compound **3.57**.....331

Figure 3.55 ^{1}H NMR (600 MHz, $CDCl_3$) of compound **3.58** 332

Figure 3.56 ^{13}C NMR (150 MHz, $CDCl_3$) of compound **3.58** 332

Figure 3.57 ^{1}H NMR (600 MHz, $CDCl_3$) of compound **3.66** 333

Figure 3.58 ^{13}C NMR (150 MHz, CD_3CN) of compound **3.66**.....333

Figure 3.59 ^{1}H NMR (500 MHz, C_6D_6) of compound **3.67**.....334

Figure 3.60 ^{13}C NMR (125 MHz, $CDCl_3$) of compound **3.67** 334

Figure 3.61 ^{1}H NMR (500 MHz, C_6D_6) of compound **3.68**.....335

Figure 3.62 ^{13}C NMR (125 MHz, C_6D_6) of compound **3.68**.....335

Figure 3.63 ^{1}H NMR (600 MHz, C_6D_6) of compound **3.69**.....336

Figure 3.64 ^{13}C NMR (150 MHz, C_6D_6) of compound **3.69**.....336

Figure 3.65 ^{13}C NMR (125 MHz, C_6D_6) of compound **3.69** and **3.93**.....337

Figure 3.66 ^{1}H NMR (500 MHz, C_6D_6) of compound **3.70**.....338

Figure 3.67 ^{13}C NMR (125 MHz, C_6D_6) of compound **3.70**.....338

Figure 3.68 ^{1}H NMR (500 MHz, C_6D_6) of compound **3.71**.....339

Figure 3.69 ^{13}C NMR (150 MHz, $CDCl_3$) of compound **3.71** 339

Figure 3.70 ^{1}H NMR (600 MHz, CD_2Cl_2) of compound **3.72** 340

Figure 3.71 ^{13}C NMR (150 MHz, CD_2Cl_2) of compound **3.72**.....340

Figure 3.72 ^{1}H NMR (500 MHz, $CDCl_3$) of compound **3.73** 341

Figure 3.73 ^{13}C NMR (150 MHz, $CDCl_3$) of compound **3.73** 341

Figure 3.74 ^{1}H NMR (500 MHz, C_6D_6) of compound **3.74**.....342

Figure 3.75 ^{13}C NMR (125 MHz, C_6D_6) of compound **3.74**.....342

Figure 3.76 ^{1}H NMR (600 MHz, $CDCl_3$) of compound **3.94** 343

Figure 3.77 ^{13}C NMR (150 MHz, $CDCl_3$) of compound **3.94** 343

Figure 3.78 ^{1}H NMR (600 MHz, $CDCl_3$) of compound **3.96** 344

Figure 3.79 ^{13}C NMR (150 MHz, $CDCl_3$) of compound **3.96** 344

Figure 3.80 ^{1}H NMR (600 MHz, C_6D_6) of compound **3.76** 345

Figure 3.81 ^{13}C NMR (150 MHz, C_6D_6) of compound **3.76** 345

Figure 3.82 ^{19}F NMR (376 MHz, C_6D_6) of compound **3.76** 346

Figure 3.83 ^{1}H NMR (600 MHz, $CDCl_3$) of compound **3.78** 347

Figure 3.84 ^{13}C NMR (150 MHz, $CDCl_3$) of compound **3.78** 347

Figure 3.85 ^{1}H NMR (600 MHz, C_6D_6) of compound **3.79** 348

Figure 3.86 ^{13}C NMR (150 MHz, C_6D_6) of compound **3.79** 348

Figure 3.87 ^{1}H NMR (500 MHz, C_6D_6) of compound **3.81** 349

Figure 3.88 ^{13}C NMR (125 MHz, C_6D_6) of compound **3.81** 349

Figure 3.89 NOESY (600 MHz, acetone-d_6) of compound **3.81** 350

Figure 3.90 ^{1}H NMR (600 MHz, acetone-d_6) of compound **3.97** 351

Figure 3.91 ^{13}C NMR (125 MHz, acetone-d_6) of compound **3.97** 351

Figure 3.92 NOESY (600 MHz, acetone-d_6) of compound **3.97** 352

Figure 3.93 ^{1}H NMR (600 MHz, C_6D_6) of compound **3.82** 353

Figure 3.94 ^{13}C NMR (150 MHz, C_6D_6) of compound **3.82** 353

Figure 3.95 NOESY (600 MHz, C_6D_6) of compound **3.82** 354

Figure 3.96 ^{1}H NMR (600 MHz, C_6D_6) of compound **3.98** 355

Figure 3.97 ^{13}C NMR (125 MHz, C_6D_6) of compound **3.98** 355

Figure 3.98 NOESY (600 MHz, C_6D_6) of compound **3.98** 356

Figure 3.99 ^{1}H NMR (600 MHz, C_6D_6) of compounds **3.83** and **3.99** 357

Figure 3.100 ^{13}C NMR (125 MHz, C_6D_6) of compounds **3.83** and **3.99** 357

Figure 3.101 NOESY (600 MHz, C_6D_6) of compounds **3.83** and **3.99**.....358

Figure 3.102 ^{1}H NMR (500 MHz, C_6D_6) of compound **3.84**.....359

Figure 3.103 ^{13}C NMR (150 MHz, CD_3OD) of compound **3.84**.....359

Figure 3.104 ^{1}H NMR (600 MHz, $CDCl_3$) of compound (–)-**3.87**.....360

Figure 3.105 ^{13}C NMR (150 MHz, $CDCl_3$) of compound (–)-**3.87**.....360

Figure 3.106 ^{1}H NMR (400 MHz, $CDCl_3$) of compound (–)-**3.100**.....361

Figure 3.107 ^{13}C NMR (100 MHz, $CDCl_3$) of compound (–)-**3.100**.....361

Figure 3.108 NOESY (400 MHz, $CDCl_3$) of compound (–)-**3.100**.....362

Figure 3.109 ^{1}H NMR (600 MHz, $CDCl_3$) of compound (+)-**3.19**.....363

Figure 3.110 ^{13}C NMR (150 MHz, $CDCl_3$) of compound (+)-**3.19**.....363

Figure 3.111 NOESY (800 MHz, $CDCl_3$) of compound (+)-**3.19**.....364

CHAPTER FOUR

Figure 4.1 Background and overview.....379

Figure 4.2A Geometry-optimized structures of 1,2,3-cyclohexatriene (**4.8**) and azacyclic 1,2,3-triene **4.12**.....381

Figure 4.2B Electrostatic potential map with C4 and C5 natural bond orbital charges and frontier molecular orbitals of azacyclic 1,2,3-triene **4.12**.....381

Figure 4.3A Synthesis of triene precursor **4.17**.....383

Figure 4.3B Survey of fluoride sources for 1,2,3-triene generation and trapping.....385

Figure 4.4 Trapping reactions of azacyclic 1,2,3-trienes **4.9** with dienes **4.21** to give (4+2) cycloadducts **4.22**.....387

Figure 4.5 Regioselective reactions of azacyclic 1,2,3-trienes.....389

Figure 4.6 Transition state analysis at 353.15 K of additions of 1,3-dimethyl-2-imidazolidinone (**4.42**) to azacyclic 1,2,3-trienes **4.12** and **4.37** 393

Figure 4.7 Synthesis of silyl nonaflate **4.44**. 409

Figure 4.8 Unsuccessful substrates evaluated during scope studies 441

Figure 4.9 Geometry of 1,2,3-cyclohexatriene (**4.8**).....450

Figure 4.10 Geometry of azacyclic 1,2,3-triene **4.12**.....450

Figure 4.11 Equation used to calculate energy of dehydrogenation 451

Figure 4.12 Geometry of pyridone **4.76**.....452

Figure 4.13 Geometry of cyclic 1,2,3-trienes **4.78** and **4.79**.....453

Figure 4.14 Geometry of 1,2,3-trienes **4.80a**–**4.80c** 454

Figure 4.15 Geometry of 4,5-pyridyne **4.81**.....455

Figure 4.16 Geometry of azacyclic 1,2,3-trienes **4.29** and **4.31**.....455

Figure 4.17 Geometry of azacyclic 1,2,3-trienes **4.35** and **4.37**.....456

Figure 4.18 Distortion/interaction activation strain analysis along the reaction coordinate of the forming C–N bond for attack of 1,3-dimethyl-2-imidazolidinone (**4.42**) on azacyclic 1,2,3-triene **4.12** at C4 and C5.....458

Figure 4.19 Distortion/interaction activation strain analysis along the reaction coordinate of the forming C–N bond for attack of 1,3-dimethyl-2-imidazolidinone (**4.42**) on azacyclic 1,2,3-triene **4.37** at C4 and C5.....460

Figure 4.20 Calculated free energy profile for formal C–N bond insertion.....461

Figure 4.21 ^{1}H NMR (500 MHz, $CDCl_3$) of compound **4.14** 463

Figure 4.22 ^{1}H NMR (600 MHz, C_6D_6) of compound **4.15**.....464

Figure 4.23 ^{13}C NMR (150 MHz, C_6D_6) of compound **4.15**.....464

Figure 4.24 ^{1}H NMR (600 MHz, $CDCl_3$) of compound **4.16** 465

Figure 4.25 ^{13}C NMR (125 MHz, $CDCl_3$) of compound **4.16** 465

Figure 4.26 ^{19}F NMR (565 MHz, $CDCl_3$) of compound **4.16**.....466

Figure 4.27 ^{1}H NMR (600 MHz, $CDCl_3$) of compound **4.17** 467

Figure 4.28 ^{13}C NMR (150 MHz, $CDCl_3$) of compound **4.17** 467

Figure 4.29 ^{19}F NMR (565 MHz, $CDCl_3$) of compound **4.17**.....468

Figure 4.30 ^{1}H NMR (500 MHz, $CDCl_3$) of compound **4.47** 469

Figure 4.31 ^{1}H NMR (600 MHz, $CDCl_3$) of compound **4.48** 470

Figure 4.32 ^{13}C NMR (150 MHz, $CDCl_3$) of compound **4.48** 470

Figure 4.33 ^{19}F NMR (282 MHz, $CDCl_3$) of compound **4.48**.....471

Figure 4.34 ^{1}H NMR (600 MHz, acetone-d_6) of compound **4.49** 472

Figure 4.35 ^{13}C NMR (150 MHz, acetone-d_6) of compound **4.49** 472

Figure 4.36 ^{19}F NMR (376 MHz, acetone-d_6) of compound **4.49**.....473

Figure 4.37 ^{1}H NMR (600 MHz, acetone-d_6) of compound **4.50** 474

Figure 4.38 ^{13}C NMR (150 MHz, acetone-d_6) of compound **4.50** 474

Figure 4.39 ^{19}F NMR (376 MHz, acetone-d_6) of compound **4.50**.....475

Figure 4.40 ^{1}H NMR (600 MHz, acetone-d_6) of compound **4.51** 476

Figure 4.41 ^{13}C NMR (150 MHz, acetone-d_6) of compound **4.51** 476

Figure 4.42 ^{19}F NMR (282 MHz, acetone-d_6) of compound **4.51**.....477

Figure 4.43 ^{1}H NMR (600 MHz, $CDCl_3$) of compound **4.52** 478

Figure 4.44 ^{13}C NMR (150 MHz, $CDCl_3$) of compound **4.52** 478

Figure 4.45 ^{19}F NMR (376 MHz, $CDCl_3$) of compound **4.52**.....479

Figure 4.46 ^{1}H NMR (600 MHz, $CDCl_3$) of compound **4.53** 480

Figure 4.47 ^{13}C NMR (150 MHz, $CDCl_3$) of compound **4.53** 480

Figure 4.48 ^{1}H NMR (600 MHz, $CDCl_3$) of compound **4.54** 481

Figure 4.49 ^{13}C NMR (150 MHz, $CDCl_3$) of compound **4.54** 481

Figure 4.50 ^{1}H NMR (600 MHz, $CDCl_3$) of compound **4.55** 482

Figure 4.51 ^{13}C NMR (150 MHz, $CDCl_3$) of compound **4.55** 482

Figure 4.52 ^{1}H NMR (600 MHz, $CDCl_3$) of compound **4.56** 483

Figure 4.53 ^{13}C NMR (150 MHz, $CDCl_3$) of compound **4.56** 483

Figure 4.54 ^{1}H NMR (600 MHz, acetone-d_6) of compound **4.44** 484

Figure 4.55 ^{13}C NMR (125 MHz, acetone-d_6) of compound **4.44** 484

Figure 4.56 ^{19}F NMR (376 MHz, acetone-d_6) of compound **4.44**.....485

Figure 4.57 ^{1}H NMR (500 MHz, $CDCl_3$) of compound **4.19** 486

Figure 4.58 ^{13}C NMR (125 MHz, $CDCl_3$) of compound **4.19** 486

Figure 4.59 ^{1}H NMR (500 MHz, $CDCl_3$) of compound **4.24** 487

Figure 4.60 ^{13}C NMR (125 MHz, $CDCl_3$) of compound **4.24** 487

Figure 4.61 ^{1}H NMR (600 MHz, acetone-d_6) of compound **4.26** 488

Figure 4.62 ^{13}C NMR (150 MHz, acetone-d_6) of compound **4.26** 488

Figure 4.63 ^{1}H NMR (600 MHz, acetone-d_6) of compound **4.28** 489

Figure 4.64 ^{13}C NMR (150 MHz, acetone-d_6) of compound **4.28** 489

Figure 4.65 ^{1}H NMR (400 MHz, acetone-d_6) of compound **4.30** 490

Figure 4.66 ^{13}C NMR (125 MHz, acetone-d_6) of compound **4.30** 490

Figure 4.67 ^{1}H NMR (400 MHz, acetone-d_6) of compound **4.32** 491

Figure 4.68 ^{13}C NMR (125 MHz, acetone-d_6) of compound **4.32** 491

Figure 4.69 ^{1}H NMR (600 MHz, acetone-d_6) of compound **4.34** 492

Figure 4.70 ^{13}C NMR (150 MHz, acetone-d_6) of compound **4.34** 492

Figure 4.71 ^{1}H NMR (600 MHz, acetone-d_6) of compound **4.36** 493

Figure 4.72 ^{13}C NMR (125 MHz, acetone-d_6) of compound **4.36** 493

Figure 4.73 ^{1}H NMR (600 MHz, acetone-d_6) of compound **4.39** 494

Figure 4.74 ^{13}C NMR (150 MHz, acetone-d_6) of compound **4.39** 494

Figure 4.75 ^{1}H NMR (600 MHz, acetone-d_6) of compound **4.60** 495

Figure 4.76 ^{13}C NMR (150 MHz, acetone-d_6) of compound **4.60** 495

Figure 4.77 ^{1}H NMR (400 MHz, CD_2Cl_2) of compound **4.62** 496

Figure 4.78 ^{13}C NMR (125 MHz, CD_2Cl_2) of compound **4.62** 496

Figure 4.79 ^{1}H NMR (500 MHz, acetone-d_6) of compound **4.41** 497

Figure 4.80 ^{13}C NMR (125 MHz, acetone-d_6) of compound **4.41** 497

Figure 4.81 NOESY (400 MHz, acetone-d_6) of compound **4.41** 498

Figure 4.82 ^{1}H NMR (500 MHz, acetone-d_6) of compound **4.43** 499

Figure 4.83 ^{13}C NMR (125 MHz, acetone-d_6) of compound **4.43** 499

Figure 4.84 NOESY (400 MHz, acetone-d_6) of compound **4.43** 500

Figure 4.85 ^{1}H NMR (600 MHz, acetone-d_6) of compound **4.45** 501

Figure 4.86 ^{13}C NMR (150 MHz, acetone-d_6) of compound **4.45** 501

Figure 4.87 NOESY (600 MHz, acetone-d_6) of compound **4.45** 502

Figure 4.88 ^{1}H NMR (600 MHz, acetone-d_6) of compound **4.46** 503

Figure 4.89 ^{13}C NMR (125 MHz, acetone-d_6) of compound **4.46** 503

Figure 4.90 NOESY (600 MHz, acetone-d_6) of compound **4.46** 504

Figure 4.91 ^{1}H NMR (600 MHz, acetone-d_6) of compound **4.65** and **4.66** 505

Figure 4.92 ^{13}C NMR (150 MHz, acetone-d_6) of compound **4.65** and **4.66** 505

Figure 4.93 NOESY (600 MHz, acetone-d_6) of compound **4.65** 506

Figure 4.94 ^{1}H NMR (600 MHz, acetone-d_6) of compound **4.68** 507

Figure 4.95 ^{13}C NMR (150 MHz, acetone-d_6) of compound **4.68** 507

Figure 4.96 NOESY (600 MHz, acetone-d_6) of compound **4.68** 508

Figure 4.97 ^{1}H NMR (600 MHz, acetone-d_6) of compound **4.70** 509

Figure 4.98 ^{13}C NMR (150 MHz, acetone-d_6) of compound **4.70** 509

Figure 4.99 NOESY (600 MHz, acetone-d_6) of compound **4.70** 510

Figure 4.100 ^{1}H NMR (500 MHz, acetone-d_6) of compound **4.72** 511

Figure 4.101 ^{13}C NMR (125 MHz, acetone-d_6) of compound **4.72** 511

Figure 4.102 NOESY (400 MHz, acetone-d_6) of compound **4.72** 512

Figure 4.103 ^{1}H NMR (600 MHz, acetone-d_6) of compound **4.74** 513

Figure 4.104 ^{13}C NMR (150 MHz, acetone-d_6) of compound **4.74** 513

Figure 4.105 ^{1}H NMR (600 MHz, acetone-d_6) of compound **4.75** 514

Figure 4.106 ^{13}C NMR (150 MHz, acetone-d_6) of compound **4.75** 514

Figure 4.107 ^{19}F NMR (282 MHz, acetone-d_6) of compound **4.75**.....515

CHAPTER FIVE

Figure 5.1 Background and overview 531

Figure 5.2 ΔG values for the fluoride-mediated generation of strained intermediates from their trimethylsilyltriflate precursors.....534

Figure 5.3 Calculated energy profile for the fluoride-mediated elimination of silyltriflate **5.1** to generate benzyne (**5.3**) 537

Figure 5.4A Abbreviated energy profiles for the generation of cyclohexyne (**5.5**).....539

Figure 5.4B Abbreviated energy profiles for the generation of 1,2,3-cyclohexatriene (**5.9**) 539

Figure 5.5 Mechanism and energy profile for the fluoride-mediated generation of anti-Bredt olefin **5.11** from silyltriflate **5.22** 541

Figure 5.6 Study of unreactive substrate (***epi*-22**) under fluoride-mediated conditions 542

Figure 5.7A Computational study of fluoride-mediated generation of ethylene (**5.34**) from silyltriflate **5.32** with varying Si–C–C–O dihedral angle θ 544

Figure 5.7B Key transition states **TS-5.10a-c** and geometric parameters 544

Figure 5.8 Geometries of **TS-5.1**–**TS-5.4** 548

Figure 5.9 Calculated free energy profile for formation of cyclohexyne (**5.5**) from precursor **5.6** 551

Figure 5.10 Geometries of **TS-5.11**, **TS-5.12**, and **TS-5.6** 552

Figure 5.11 Calculated free energy profile for formation of 1,2,3-cyclohexatriene (**5.9**) from precursor **5.10** 553

Figure 5.12 Geometries of **TS-5.14**, **TS-5.15**, and **TS-5.7** 554

Figure 5.13 Calculated free energy profile for formation of 1,2,3-triene **5.45** from precursor **5.42** 555

Figure 5.14 Geometries of **TS-5.17**–**TS-5.19** 556

Figure 5.15 Calculated free energy profile for formation of azacyclic 1,2,3-triene **5.50** from precursor **5.46** 558

Figure 5.16 Geometries of **TS-5.20**–**TS-5.22** 559

Figure 5.17 Calculated free energy profile for formation of azacyclic 1,2,3-triene **5.50** from precursor **5.51**.....560

Figure 5.18 Geometries of **TS-5.24**–**TS-5.26**.....561

Figure 5.19 Geometries of **TS-5.8** and **TS-5.9**.....562

Figure 5.20 Calculated free energy profile for formation of silicate ***epi*-5.30** from precursor ***epi*-5.22**.....563

Figure 5.21 Geometry of ***epi*-TS-5.8**.....563

Figure 5.22 Unlocated transition states ***epi*-TS-5.9** and **TS-5.28**, anion ***epi*-5.31**, and ABO ***epi*-5.11**.....564

Figure 5.23 Calculated generalized pathway for formation of ethylene **5.34** from precursor **5.32**.....566

Figure 5.24 Geometry of **TS-5.10** at various dihedral angles.....566

LIST OF SCHEMES

CHAPTER ONE

Scheme 1.1 Envisioned reaction design 4

LIST OF TABLES

CHAPTER ONE

Table 1.1 Reaction optimization 5

Table 1.2 Temperature screening results 26

Table 1.3 Base screening results 26

Table 1.4 CsF loading screening results 27

Table 1.5 Ligand screening results 27

Table 1.6 Chiral ligand screen results 47

Table 1.7 Solvent screening results 48

Table 1.8 Fluoride source screening results 49

Table 1.9 Palladium source screening results 49

Table 1.10 Base screening results 50

Table 1.11 Crystal data and structure refinement for epoxide **(+)-1.50** 55

Table 1.12 SFC conditions and data 57

CHAPTER TWO

Table 2.1 Select Results from Optimization Studies 115

Table 2.2 Evaluation of Select Chiral Ligands in the Annulation Reaction 122

Table 2.3 Evaluation of Vinyl Benzoxazinone Equivalents 138

Table 2.4 Evaluation of Temperature 138

Table 2.5 Evaluation of H_2O Loading 139

Table 2.6 Evaluation of Catalyst Loading 139

Table 2.7 Evaluation of Concentration 139

Table 2.8 Evaluation of Ligands 140

Table 2.9 Ligand evaluation results. 175

Table 2.10 Crystal data and structure refinement for compound **(–)-2.43**.....178

Table 2.11 SFC conditions and data. 180

CHAPTER THREE

Table 3.1 Selected Optimization Screening Results 261

Table 3.2 Crystal data and structure refinement for compound **3.81**.....290

Table 3.3 Crystal data and structure refinement for compound **3.84**.....296

Table 3.4 SFC conditions and data 301

Table 3.5 Computed energies of selected C_6H_6 isomers.....305

Table 3.6 Computed energies for the reaction of triene **3.80** with phenoxide **3.34** (Na^+ omitted).....306

Table 3.7 Distortion/Interaction-Activation Strain Analysis (DIAS) of the phenolate additions (**TS3.1** & **TS3.2**) 306

Table 3.8 Comparison of Experimental and Computed NMR Chemical Shifts for Structure **3.69**.....309

Table 3.9 Comparison of Experimental and Computed NMR Chemical Shifts for Structure **3.93**.....310

CHAPTER FOUR

Table 4.1 Selected results from the optimization of trapping reaction of 1,2,3-triene **4.12**.....416

Table 4.2 Selected results from the optimization of trapping reaction of 1,2,3-triene **4.12**.....418

Table 4.3 Computed structural properties of azacyclic 1,2,3-triene **4.12** at differing levels of theory.....449

Table 4.4 Computed energies for the reaction of azacyclic 1,2,3-triene **4.12** with 1,3-dimethyl-2-imidazolidinones (**4.42**) 457

Table 4.5 Computed energies for the reaction of azacyclic 1,2,3-triene **4.12** with 1,3-dimethyl-2-imidazolidinones (**4.42**) 457

Table 4.6 Distortion/Interaction Activation Strain (DIAS) Analysis of the urea addition (**TS-4.1a** & **TS-4.1b**).....457

Table 4.7 Computed energies for the reaction of azacyclic 1,2,3-triene **4.37** with 1,3-dimethyl-2-imidazolidinones (**4.42**) 459

Table 4.8 Computed energies for the reaction of azacyclic 1,2,3-triene **4.37** with 1,3-dimethyl-2-imidazolidinones (**4.42**) 459

Table 4.9 Distortion/Interaction Activation Strain (DIAS) Analysis of the urea addition (**TS-4.2a** & **TS-4.2b**).....459

Table 4.10 Computed energies for the reaction of azacyclic 1,2,3-triene **4.12** with 1,3-dimethyl-2-imidazolidinones (**4.42**) 461

CHAPTER FIVE

Table 5.1 Computed energies for formation of benzyne (**5.3**), cyclohexyne (**5.5**), and 1,2-cyclohexadiene (**5.7**).....546

Table 5.2 Computed energies for formation of 1,2,3-cyclohexatriene (**5.9**) 547

Table 5.3 Computed energies for formation of anti-Bredt olefin (**5.11**).....547

Table 5.4 Computed energies for the reaction of **5.1** to form benzyne (**5.3**).....548

Table 5.5 Computed energies for the reaction of **5.6** to form cyclohexyne (**5.5**) 552

Table 5.6 Computed energies for the reaction of **5.10** to form 1,2,3-cyclohexatriene (**5.9**).....554

Table 5.7 Computed energies for the reaction of **5.42** to form 1,2,3-triene **5.45** 556

Table 5.8 Computed energies for the reaction of **5.46** to form 1,2,3-triene **5.50** 559

Table 5.9 Computed energies for the reaction of **5.51** to form 1,2,3-triene **5.50** 561

Table 5.10 Computed energies for the reaction of **5.22** to form ABO **5.11** 562

Table 5.11 Computed energies for the investigation of the unobserved reaction of ***epi*-5.22** to for ABO ***epi*-5.11**.....564

Table 5.12 Computed energies for the elimination from **5.32** to form **5.34** 567

LIST OF EQUATIONS

CHAPTER THREE

Equation 3.1 Modified Karplus equation 294

Equation 3.2 Empirical scaling of computed shifts.....309

LIST OF ABBREVIATIONS

α	alpha
β	beta
γ	gamma
Δ	delta; heat or difference
δ	delta; chemical shift
ε	epsilon; dielectric constant
η	eta
θ	theta; bond angle
λ	lambda; wavelength
μ	mu; micro
π	pi
Σ	sigma
σ	sigma; computed isotropic shielding constant
ϕ	phi; dihedral angle
χ	chi; bond length
ω	omega
$[\alpha]_D$	specific rotation at wavelength of sodium D line
(Het)	hetero, heterocycle
ABO	anti-Bredt olefin
Ac	acetyl
acac	acetylacetonate
anth	anthracene
app.	apparent
APCI	atmospheric-pressure chemical ionization
aq.	aqueous
Ar	aryl
b	intercept from empirical scaling data
B3LYP	Becke, 3-parameter, Lee–Yang–Parr (functional)
BDE	bond dissociation energy
BINAP	(2,2′-bis(diphenylphosphino)-1,1′-binaphthyl)
BIPHEP	(2,2’-bis(diphenylphosphino)-1,1′-biphenyl)
Bn	benzyl
Boc	*tert*-butyloxy carbonyl

BOX	bis(oxazoline)
br	broad
BRSM	based on recovered starting material
Bu	butyl
n-Bu	butyl (linear)
t-Bu	*tert*-butyl
Bz	benzoyl
c	concentration for specific rotation measurements
°C	degrees Celsius
ca.	calculated
calcd	calculated
Cbz	carboxybenzyl
CCDC	Cambridge Crystallographic Data Centre
cm	centimeter
CMAD	corrected mean absolute deviation
cod	1,5-cyclooctadiene
conc.	concentration
Cp	cyclopentadienyl
CREST	conformer-rotamer ensemble sampling tool
Cy	cyclohexyl
DABCO	1,4-diazabicyclo[2.2.2]octane
DART-MS	Direct Analysis in Real Time – Mass Spectroscopy
dba	dibenzylideneacetone
d	doublet
dd	doublet of doublets
ddd	doublet of doublet of doublets
dddd	doublet of doublet of doublet of doublets
ddt	doublet of doublet of triplets
DMI	1,3-dimethy-2-imidazolidinone
dq	doublet of quartets
dr	diastereomeric ratio
dt	doublet of triplets
DBU	1,8-diazabicyclo(5.4.0)undec-7-ene
DCE	1,2-dichloroethane

DFT	density functional theory
DIAS	distortion/interaction activation strain
DIBAL	diisobutylaluminum hydride
DIOP	(2,3-*O*-isopropylidene-2,3-dihydroxy-1,4-bis(diphenylphosphino)butane)
dist	distortion
DME	1,2-dimethoxyethane
DMF	*N*,*N*-dimethylformamide
DMSO	dimethyl sulfoxide
DNA	deoxyribonucleic acid
dppe	1,2-bis(diphenylphosphino)ethane
dppf	1,1'-bis(diphenylphosphino)ferrocene
dtbpf	1,1′-bis(di-tert-butylphosphino)ferrocene
E	electronic energy; energy
ee	enantiomeric excess
equiv	equivalent
er	enantiomeric ratio
ESI	electrospray ionization
ESP	electrostatic potential map
Et	ethyl
EtOAc	ethyl acetate
eV	electron volts
Et_3N	triethylamine
FMO	frontier molecular orbital
FT	Fourier transform
g	gram(s)
G	Gibb's free energy
G(T)	Gibb's free energy
G3	generation 3
GIAO	gauge-including atomic orbitals
H	enthalpy
h	hour(s)
HF	Hartree Fock
HOMO	highest occupied molecular orbital
HRMS	high resolution mass spectroscopy

Hz	hertz
int	interaction
IR	infrared (spectroscopy)
i-Pr	iso-propyl
J	coupling constant
kcal/mol	kilocalories to mole ratio
KHMDS	potassium hexamethyldisilazide
L	liter or ligand
LDA	lithium diisopropylamide
LUMO	lowest unoccupied molecular orbital
m	multiplet or milli; slope from empirical scaling data
m	meta
M	molar
m/z	mass to charge ratio
*m*CPBA	*meta*-chloroperoxybenzoic acid
Me	methyl
MeCN	acetonitrile
MeOH	methanol
Mes	mesityl
MHz	megahertz
min	minute(s)
mm	millimeter
mol	mole(s)
mp	melting point
Ms	mesyl
n-BuLi	*n*-butyllithium
NaHMDS	sodium bis(trimethylsilyl)amide
NBS	*N*-bromosuccinimide
NBO	natural bond orbital
Nf	nonafluorobutylsulfonyl
NMR	nuclear magnetic resonance
NOESY	Nuclear Overhauser Enhancement Spectroscopy
o	ortho
ORTEP	Oak Ridge Thermal-Ellipsoid Plot Program

p	para
Ph	phenyl
PhCN	benzonitrile
PHOX	phosphinooxazoline
PPFA	(*S*)-*N*,*N*-Dimethyl-1-[(*R*)-2-(diphenylphosphino)ferrocenyl]ethylamine
ppm	parts per million
pyr	pyridine
Piv	pivaloyl
PivCl	pivaloyl chloride
q	quartet
qh-G(T)	quasi-harmonic corrected Gibbs free energy
qh-S	quasi-harmonic corrected entropy
quant	quantitative
QUINAP	1-(2-diphenylphosphino-1-naphthyl)isoquinoline
quint	quintet
rac	racemic
rr	regioisomeric ratio; ratio of regioisomers
R_f	retention factor
S	entropy
s	singlet
sat.	saturated
SFC	supercritical fluid chromatography
SMD	solvation model based on density
SPC	single point energy correction; single point energy calculation
T	temperature
t	triplet
td	triplet of doublets
temp	temperature
TASF	tris(dimethylamino)sulfonium difluorotrimethylsilicate
TBAF	tetrabutylammonium fluoride; tetra-*n*-butylammonium fluoride
TBAT	tetrabutylammonium difluorotriphenylsilicate
Tf	trifluoromethanesulfonyl
THF	tetrahydrofuran
TIPSCl	triisopropylsilyl chloride

TLC	thin layer chromatography
TMAF	tetramethylammonium fluoride
Ts	*p*-toluenesulfonyl (tosyl)
TsCl	4-toluenesulfonyl chloride
TS	transition state
U	unrestricted
UHP	ultra high purity
UV	ultraviolet
w/w	weight by weight
wt%	percentage by mass
ZPE	zero-point energy

ACKNOWLEDGEMENTS

I would first like to thank Professor Neil K. Garg for his support, guidance, mentorship, and friendship. I felt very fortunate to have been accepted into UCLA for graduate school and to have the opportunity to begin working in his laboratory my first summer here. From the start, his enthusiasm and dedication for research has been very inspiring and his support, assistance, and advice as a mentor and teacher has been extraordinary. I am very grateful for everything he has done for me over the past five years.

I would like to thank the members of my committee, Professors Abigail Doyle, Kendall Houk, and Yi Tang. I am grateful for the support, advice, guidance, and mentorship they have given me during my time at UCLA. I am particularly grateful to Prof. Houk for providing invaluable insight and assistance regarding my computational chemistry projects. It has been an honor to collaborate together on many different projects.

I would also like to acknowledge and thank several professors and mentors from my time as an undergraduate at Boston University, beginning with Professor John A. Porco, Jr. I am extremely grateful to him for giving me the chance to get involved in research in his lab during my time at Boston University. His continuing support over the years has been greatly appreciated. While there, I had the privilege of learning from a number of great scientists, particularly Xiaowei Wu. His mentorship and friendship were formative for me as a chemist. I am also grateful to all of the members of the Porco Lab that I had the privilege of overlapping with. My positive experience in the Porco Lab was the reason I chose to pursue graduate school. I am also grateful to the other professors that supported me in the chemistry department at Boston University, particularly Professors John Snyder and John Caradonna.

Finally, I would like to acknowledge my high school chemistry teachers Catherine Burchat and Ken Wieder for sparking my interest in chemistry.

I am also grateful to Ta-Chung Ong, Saeed Khan, Robert Taylor, Robert Peterson, Tyler Kerr, and Greg Khitrov for their work to provide the department with invaluable instrumentation resources.

During my time in the Garg lab, I have had the privilege of working alongside many talented scientists and good friends. This includes a number of postdocs who each contributed uniquely to the lab. When I first started, I had the pleasure of overlapping with Logan Bachman and Veronica Tona. Logan and I worked in 5235 together and I loved chatting with him about coffee, music, and chemistry. Veronica and I became good friends and I really enjoyed spending time with her both in and out of lab. Nathan Adamson and Dan Nasrallah joined the lab during my first year. Nathan is a phenomenal chemist and I really enjoyed learning new things from him. Dan was an amazing coworker and I am very grateful for his mentorship and friendship during a majority of my graduate school career. During my third year, Jacob Sorrentino and Lukas Wein joined the lab. I really loved chatting with Jacob about chemistry and we had fun working on various MOM exercises together. Lukas's knowledge of chemistry and strong sense of humor have made him a great lab mate. During my fourth year, Jiaming Ding and Sarah French joined the lab. It has been fun getting to work with Jiaming on the cubene/quadricyclene project. And finally, it has been an absolute blast working on "the cube" with Sarah.

While in the Garg Lab, I also overlapped briefly with a visiting student from Germany, Lisa Kamecke, and an undergraduate student, Lauren Van Auken. It was fun to get to know them and work with them on various group activities.

During my first year as a graduate student Sarah Anthony, Tim Boit, and Melissa Ramirez were fifth years. I am grateful for Sarah for her mentorship and friendship during my first year and I have a lot of great memories of working Friday nights in lab on the π-allyl project and going to Manhattan Beach on the weekends. Tim is a great leader and I appreciated his intensity in group meetings and subgroup. Finally, I am appreciative of Melissa for always being there to answer my computational chemistry questions.

The next class was Jason Chari, Rachel Knapp, and Francesca Ippoliti. Jason is a very positive person and I always appreciated his creativity when it came to putting together a slide or a figure. One of my favorite memories is when we brought 3D glasses to our synthetic exercise presentation so the group could look at our helicene in 3D. I had the greatest time working in 5235 and 5234 with Francesca. I always appreciated that we could always have fun and laugh together even when working on really hard chemistry. The pothos clipping she gave me is still going strong. Finally, Rachel and I got to know each other well both in and out of lab. I always admired her leadership, work ethic, and personality.

Andrew Kelleghan, Milauni Mehta, and Katie Spence were the next class and they had the largest influence on my time in graduate school. First and foremost, I want to thank Andrew for being the greatest friend and mentor. I learned so much from him and always appreciated him being there for me. I am grateful for our many chats about music and Dark Souls and our hot tub hangouts. Milauni is an amazing person and I really enjoyed hanging out with her in and out of lab. I really appreciated our coffee walks, beach days, pool parties, and brunches and had a lot of fun planning parties and maintaining the glovebox together. Finally, Katie was a very positive influence on me. I really appreciated her attitude and outlook and had a blast working next to her in 5234.

The next class is Ana Bulger, Matt McVeigh, and Laura Wonilowicz. Ana is an awesome person and she has been a really great project partner over the years. I appreciated the opportunity to check your *Org. Synth.* and it's been really fun to work on the cyclic triene projects together. Matt was a really great lab mate and project partner. I always had fun working on our catalysis projects together and sharing weird music with each other. Finally, Laura was a great lab mate and safety officer. I enjoyed the opportunity to work together in 5234 and on our various education projects.

The next class is my very own cohort consisting of Luca McDermott and Arismel Tena Meza. Luca has been a great friend and lab mate over the past five years. His enthusiasm and approach to problem solving is admirable. It was so fun to work on our two *Org. Synth.* projects together. I am also very grateful to him for always being there to watch my cat when I was out of town. Ari has also been a great friend and lab mate over the past five years. It has been fun to work on various educational projects together as well as the cubene/quadricyclene project and it is cool that we both ended up in process chemistry careers! The last five years together has been so important to me and I am so grateful to have spent it together.

The current fourth years are Jordan Gonzalez and Georgia Scherer. Jordan is a great labmate and friend and it was really fun to work in 5234 together. Georgia was my mentee when she first joined the lab. She has been a great friend, project partner, and an amazing group celebration co-coordinator.

The current third years are Allison Hands, Dani Turner, and Zach Walters. Allison has become a very good friend and I have really appreciated our coffee breaks and chemistry chats over the past few years. Dani has been a really great project partner and it was really fun to work on the azacyclic 1,2,3-triene project together. Finally, Zach has been a really awesome lab mate

and project partner and I have really enjoyed working together on the Kobayashi computational study together and chatting about video games.

The current second years are Allison Clark, Ben Janda, Giulianna Miseo, and Christina Rivera. The four of them have brought so much energy to the lab and it has been fun engage with them in group meeting and subgroup. Importantly, I have had a great time working with Christina on the cubene project.

Finally, the current first years, Noah Gilbertson, Aimee Long, and Marianna Tonoyan, are a strong group and I look forward to seeing their future successes.

Outside of the Garg lab there are a few people (and animals) that I would like to thank. Firstly, I am indebted to my partner Max for his unconditional love and support. Second, I want to acknowledge my cat, Mystique, for being a great companion. Finally, I am endlessly grateful to my family, Stephen, Laura, Brittany, and Victoria.

Chapter 1 is a version of Kelleghan, A. V.; Witkowski, D. C.; McVeigh, M. S.; Garg, N. K. Palladium-Catalyzed Annulations of Strained Cyclic Allenes. *J. Am. Chem Soc.* **2021**, *143*, 9338–9342. Kelleghan, Witkowski, and McVeigh were responsible for experiments.

Chapter 2 is a version Witkowski, D. C.; McVeigh, M. S.; Scherer, G. M.; Anthony, S. M.; Garg, N. K. Catalyst-Controlled Annulations of Strained Cyclic Allenes with π-Allylpalladium Complexes. *J. Am. Chem. Soc.* **2023**, *145*, 10491–10496. Witkowski, McVeigh, Scherer, and Anthony were responsible for experiments.

Chapter 3 is a version of Kelleghan, A. V. †; Bulger, A. S. †; Witkowski, D. C.; Garg, N. K. Strain-Promoted Reactions of 1,2,3-Cyclohexatriene and its Derivatives. *Nature* **2023**, *618*, 748–754. Kelleghan, Bulger, and Witkowski were responsible for experiments. Kelleghan and Witkowski were responsible for computations.

Chapter 4 is a version of Witkowski, D. C.; Bulger, A. S.; Turner, D. W.; Houk, K. N.; Garg, N. K. Synthesis and Reactivity of Nitrogen-Containing Cyclic 1,2,3-Trienes. *Nat. Synth.* **2025**, DOI: 10.1038/s44160-025-00793-9. Witkowski, Bulger, and Turner were responsible for experiments. Witkowski was responsible for computations.

Chapter 5 is a version of Walters, Z. G. †; Witkowski, D. C. †; Houk, K. N.; Garg, N. K. Mechanisms of Kobayashi Eliminations for the Generation of Highly-Strained Arynes, Cyclic Cumulenes, and Anti-Bredt Olefins. *Manuscript submitted*. Walters and Witkowski were responsible for experiments. Walters and Witkowski were responsible for computations.

BIOGRAPHICAL SKETCH

Education:

University of California, Los Angeles, CA

- Ph.D. in Organic Chemistry, anticipated Spring 2025
- Current GPA: 3.99/4.00

Boston University, Boston, MA

- B.A. in Chemistry, minor in Computer Science, May 2020
- Cumulative GPA: 3.47/4.00
- Graduated with honors in Chemistry
- Senior Honors Thesis: *Synthetic Studies Towards Phomoxanthone A*

Professional and Academic Experience:

Graduate Research Assistant: University of California, Los Angeles, CA

- Advisor: Prof. Neil K. Garg; Aug. 2020 – present
  - Developed a general method for the synthesis of diverse polycyclic products leveraging cyclic allenes and arylpalladium species.
  - Demonstrated new catalyst-controlled reactivity of cyclic allenes and π-allylpalladium species and demonstrated the feasibility of an asymmetric variant.
  - Demonstrated new reactivity of unsubstituted and substituted strained cyclic 1,2,3-cyclohexatrienes, explored the derivatization of the trapping products, and assisted in computational studies.
  - Designed syntheses of silyl nonaflate and silyl triflate precursors to six-membered azacyclic 1,2,3-trienes, developed scope of trapping reactions, and conducted computational studies.
  - Investigated the mechanism of the fluoride-mediated generation of strained intermediates from Kobayashi precursors computationally
  - Optimized a large-scale procedure for the synthesis of phenanthridinones using strained intermediate chemistry.
  - Demonstrated new reactivity of cubene, explored the derivatization of trapping products, and investigated new routes to cubene precursors.
  - Demonstrated laboratory techniques and presentations skills while mentoring graduate students in the laboratory.

Graduate Teaching Assistant: University of California, Los Angeles, CA

- Undergraduate organic chemistry discussion sections; Sept. 2020 – Jun. 2021
  - Developed lesson plans and led discussion sections to teach students concepts relating to physical organic chemistry, organic reactions, mechanisms, and organic chemistry of pharmaceuticals.

Undergraduate Research Assistant: Boston University, Boston, MA

- Advisor: Prof. John A. Porco, Jr.; Jan. 2018 – May 2020
  - Synthesized intermediates toward the total synthesis of phomoxanthone A.
  - Synthesized mono- and dimeric chromone derivatives for biological testing as potential STING agonists.

Honors and Awards:

- Herbert Newby McCoy Commencement Award, UCLA, 2025
- Dissertation Year Fellowship, UCLA, 2024 – 2025
- Horizon Prize in Organic Chemistry, Royal Society of Chemistry, 2024
- Ralph and Charlene Bauer Award, UCLA, 2024
- Department of Chemistry and Biochemistry Research Fellowship UCLA, 2024
- John Stauffer Excellence in 2nd Year Academics and Research Award, UCLA, 2023
- Michael E. Jung Excellence in Teaching Award, UCLA 2022
- NSF Graduate Research Fellowship Program Honorable Mention, UCLA, 2022
- College of Letters and Science Stone Fellowship, UCLA, 2021
- Graduate Dean's Scholar Award, UCLA, 2020 – 2021
- Graduated with Honors in Chemistry, Boston University, 2020
- Undergraduate Research Opportunities Program, Boston University, 2019
- Laursen Research Scholarship Award, Boston University, 2018
- Dean's List, Boston University, 2018 – 2020

Publications:

1. **Strained "Alkenes" with Bond Orders Approaching 1.5: Cubene and 1,7-Quadricyclene**. Ding, J. M.[†]; French, S. A.[†]; Riviera, C. A.[‡]; Tena Meza, A.[‡]; Witkowski, D. C.[‡]; Houk, K. N.; Garg, N. K. *Manuscript submitted*.
2. **Mechanisms of Kobayashi Eliminations for the Generation of Highly-Strained Arynes, Cyclic Cumulenes, and Anti-Bredt Olefins**. Walters, Z. G.[†]; Witkowski, D. C.[†]; Houk, K. N.; Garg, N. K. *Manuscript submitted*.
3. **Synthesis and Reactivity of Nitrogen-Containing Cyclic 1,2,3-Trienes**. Witkowski, D. C.; Bulger, A. S.; Turner, D. W.; Houk, K. N.; Garg, N. K. *Nat. Synth.* **2025**, DOI: 10.1038/s44160-025-00793-9.
4. **Catalyst-Controlled Annulations of Strained Cyclic Allenes with π-Allylpalladium Complexes**. Witkowski, D. C.; McVeigh, M. S.; Scherer, G. M.; Anthony, S. M.; Garg, N. K. *J. Am. Chem. Soc.* **2023**, *145*, 10491–10496.
5. **Strain-Promoted Reactions of 1,2,3-Cyclohexatriene and Its Derivatives**. Kelleghan, A. V.[†]; Bulger, A. S.[†]; Witkowski, D. C.; Garg, N. K. *Nature* **2023**, *618*, 748–754.
6. **Synthesis of Phenanthridinones via the Palladium-Catalyzed Annulation of Benzyne**. Witkowski, D. C.; McDermott, L.; Garg, N. K. Org. Synth. **2022**, *99*, 159–173.
7. **Synthesis of Carboxylic Acids from Benzamide Precursors Using Nickel Catalysis**. Bulger, A. S.; Witkowski, D. C.; Garg, N. K. *Org. Synth.* **2022**, *99*, 305–325.
8. **A Convenient Method for the Removal of Tetrabutylammonium Salts from Desilylation Reactions**. McDermott, L.; Witkowski, D. C.; Garg, N. K. *Org. Synth.* **2022**, *99*, 53–67.
9. **Palladium-Catalyzed Annulations of Strained Cyclic Allenes**. Kelleghan, A. V.; Witkowski, D. C.; McVeigh, M. S.; Garg, N. K. *J. Am. Chem Soc*. **2021**, *143*, 9338–9342.

[†,‡]These authors contributed equally

CHAPTER ONE

Palladium-Catalyzed Annulations of Strained Cyclic Allenes

Andrew V. Kelleghan, Dominick C. Witkowski, Matthew S. McVeigh, and Neil K. Garg

J. Am. Chem. Soc. **2021**, *143*, 9338–9342.

1.1 Abstract

We report Pd-catalyzed annulations of in situ-generated strained cyclic allenes. This methodology employs aryl halides and cyclic allene precursors as the reaction partners in order to generate fused heterocyclic products. The annulation proceeds via the formation of two new bonds and a sp^3 center. Moreover, both diastereo- and enantioselective variants of this methodology are validated, with the latter ultimately enabling the rapid enantioselective synthesis of a complex hexacyclic product. Studies leveraging transition metal catalysis to intercept cyclic allenes represent a departure from the more common, historical modes of cyclic allene trapping which rely on nucleophiles or cycloaddition partners. As such, this study is expected to fuel the development of reactions that strategically merge transition metal catalysis and transient strained intermediate chemistry for the synthesis of complex scaffolds.

1.2 Introduction

Since the early 1900s, transient strained cyclic intermediates, exemplified by benzyne (**1.1**, Figure 1.1A), have stimulated interest in the chemical community.[1] Although the proposal of benzyne (**1.1**) as a reactive intermediate led to significant controversy in the early 20th century, pioneering experiments by Roberts[2] and Wittig[3,4] in the 1950s validated its existence, despite the

high degree of ring strain. Indeed, this ring strain gives rise to unique and synthetically useful reactivity, which in turn has motivated the development of heterocyclic arynes, such as **1.2**[5] and **1.3**,[6] and more highly saturated analogs of benzyne (**1.1**), such as cyclohexyne (**1.4**).[7,8] These in situ-generated intermediates have become increasingly prominent in the modern synthetic toolbox, finding applications in the construction of heterocycles,[9] ligands for catalysis,[10] natural products,[11,12,13] agrochemicals,[14] and organic materials.[15]

Whereas strained cyclic alkynes have received significant attention from the synthetic community, reactions of a related class of fleeting intermediates, strained cyclic allenes (e.g., 1,2-cyclohexadiene (**1.5**)), are relatively less developed.[16,17] This is notable as cyclic allenes and alkynes were both discovered around the same time and share similar strain-promoted reactivity.[18] Moreover, cyclic allenes are advantageous for the synthesis of sp^3-rich and stereochemically complex targets, which are becoming increasingly more valuable.[19] However, to date, only three major intermolecular reaction classes have been reported for these intermediates (Figure 1.1B), the most frequently studied being nucleophilic trappings (e.g., **1.7** + KO*t*-Bu → **1.6**) and cycloadditions (e.g., **1.7** + **1.8** → **1.9**).[16] More than fifty studies detailing such reactions have been reported, including more recent studies by Guitián,[20,21] West,[22,23,24,25] Okano and Mori,[26,27] Schreiber,[28] and our laboratory.[29,30,31,32] A complementary, albeit rarely studied, approach utilizes transition metal catalysis to intercept the cyclic allene (e.g., **1.7** + **1.10** → **1.11**).[20,33] However, this strategy poses an inherent kinetic challenge due to the requirement for reaction between a catalytically generated intermediate and an in situ-generated fleeting cyclic allene, both of which are present in low concentration.

Previous efforts to intercept strained cyclic allenes with transition metal catalysis have been limited, with only two examples known in the literature. The first was a single example wherein

an in situ-generated cyclic allene was intercepted in a Pd-catalyzed [2 + 2 + 2] reaction to generate a mixture of tetralin products, as demonstrated by Guitián and co-workers in 2009.[20] Subsequently, our laboratory developed a Ni-catalyzed annulation of cyclic allenes with benzotriazinones, including an asymmetric variant.[33] These studies demonstrate that the combination of transition metal catalysis and cyclic allenes provides an exciting new avenue in strained intermediate chemistry.

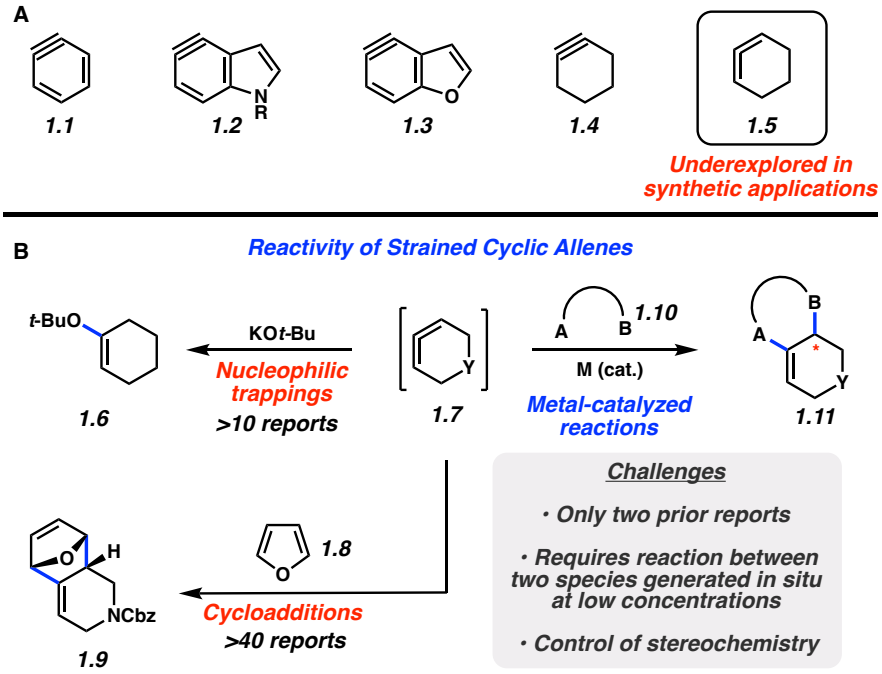

Figure 1.1. (A) Selected in situ-generated strained cyclic intermediates and (B) overview of strained cyclic allene reactivity.

1.3 Reaction Design

With the aim of developing a modular new method for the metal-catalyzed interception of strained cyclic allenes, we designed the transformation depicted in Scheme 1.1.[34] We envisioned that bifunctional annulation partners **1.12** containing an aryl iodide and a pendant pronucleophile (XH) would first react with a transition metal catalyst, generating oxidative addition intermediate **1.15**. Concurrently, silyl triflate **1.13** would be converted to strained cyclic allene **1.7** via fluoride-

mediated desilylation. Cyclic allene **1.7** would then undergo migratory insertion into the Ar–M bond of **1.15**, ultimately giving rise to η^3-coordinated complex **1.16**. Cyclization of the pendant pronucleophile would deliver tricycle **1.14** with regeneration of the catalyst. Herein, we demonstrate the successful implementation of this approach to annulate in situ-generated cyclic allenes using Pd catalysis. An array of fused polycyclic products is obtained in synthetically useful yields by varying the cyclic allene precursor and the aryl halide substrate. Stereoselective examples are also demonstrated. These results highlight the value of merging transition metal catalysis with strained cyclic allene chemistry and should enable future reaction development in this emerging area.

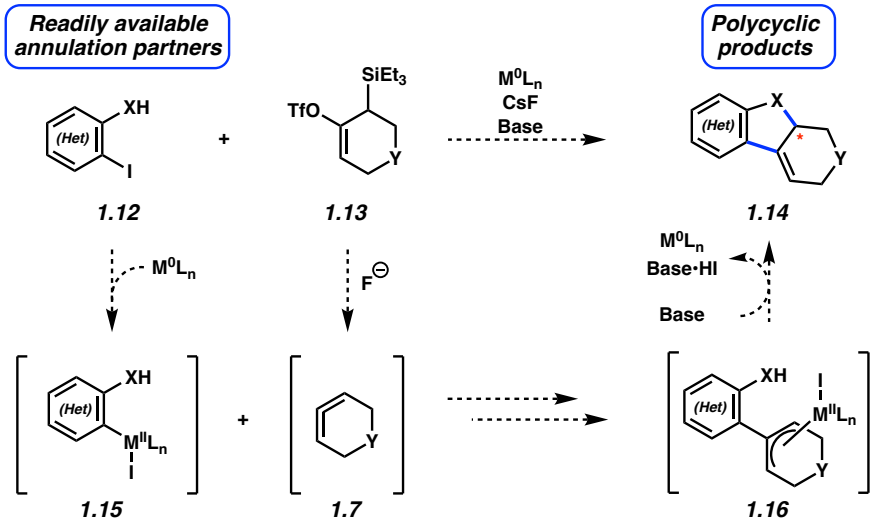

Scheme 1.1. Envisioned reaction design.

1.4 Reaction Optimization

To validate our proposed reaction design, we studied the reaction of *o*-iodoaniline derivative **1.17** with silyl triflate **1.18** using fluoride-based conditions (Table 1.1). The conditions we had identified previously for the aforementioned Ni-catalyzed reaction of benzotriazinones with cyclic allenes[33] were deemed a suitable starting point for reaction discovery. Unfortunately, no desired product was observed with a $Ni(cod)_2$/dppf catalyst system, even at increased

temperature (entries 1 and 2). Given the widespread use of palladium in academic and industrial settings, along with its well-established competency in heteroannulation reactions,[34] we turned to Pd catalysis. We were gratified to observe that the use of a Pd catalyst enabled the desired reactivity, leading to tetrahydrocarbazole **1.19a**, albeit only in 8% yield (entry 3). Because unreacted silyl triflate **1.18** was observed under these conditions, we increased the loading of CsF. This led to a significant improvement in the yield, as shown in entry 4.[35] After evaluating other ligands (see Section 1.8.2.3 for details), we found that employing the bulky monophosphine DavePhos was most effective,[36] generating **1.19a** in 71% yield (entry 5). Further optimization led to the use of DMF as solvent, Bu_4NOTf[37] as an additive, and a slight excess of silyl triflate **1.18**. Employing these conditions delivered **1.19a** in nearly quantitative yield after 1 h at 80 °C (entry 6).

Table 1.1. Reaction optimization.

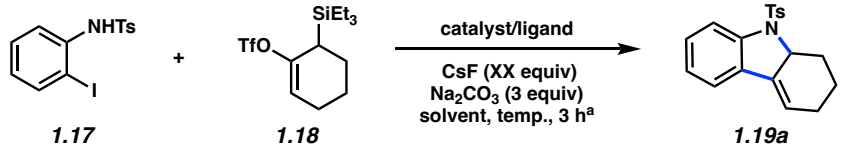

Entry	*Catalyst/Ligand*	*Solvent*	*Equiv. CsF*	*Temperature*	*Yield[b]*
1[c]	$Ni(cod)_2$/dppf	MeCN	2.5	35 °C	0%
2	$Ni(cod)_2$/dppf	MeCN	2.5	80 °C	0%
3	$Pd(OAc)_2$/dppf	MeCN	2.5	80 °C	8%
4	$Pd(OAc)_2$/dppf	MeCN	10	80 °C	51%
5	$Pd(OAc)_2$/DavePhos	MeCN	10	80 °C	71%
6[d]	$Pd(OAc)_2$/DavePhos	DMF	10	80 °C	97%

[a] Reaction conditions: **1.17** (1.0 equiv), **1.18** (1.0 equiv), catalyst (10 mol%), ligand (20 mol%), CsF (as shown), Na_2CO_3 (3 equiv), solvent (0.1 M), 3 h. [b] Yield determined by ^1H NMR analysis using 1,3,5-trimethoxybenzene as an external standard. [c] 24 h. [d] **1.18** (1.5 equiv), Bu_4NOTf (5.0 equiv), 1 h.

1.5 Scope of the Annulation Reaction

To assess the generality of this reaction, we tested a range of *o*-iodoaniline derivatives **1.20** and silyl triflates **1.13** (Figure 1.2). Although our conditions shown in Table 1.1, entry 6 were

generally useful, some modifications were made to obtain optimal yields based on empirical observations. Three different *N*-substituents were examined, namely tosyl (Ts), *tert*-butyloxycarbonyl (Boc), and acetyl (Ac), with Ts providing the highest yield (90% of **1.19a**). Electronic and steric perturbations of the annulation partner were also tolerated, as evidenced by the formation of tetrahydrocarbazoles **1.22**–**1.30**. Of note, the annulation exhibits good functional group compatibility, leading to products bearing nitriles or esters (**1.26** and **1.27**), as well as aryl bromides, chlorides, or fluorides (**1.28**–**1.30**).[38] Given the importance of heterocycles in medicinal chemistry, we also assessed the compatibility of the reaction with heterocyclic annulation partners and heterocyclic allenes. Gratifyingly, an iodopyridyl annulation partner underwent the desired reaction to afford product **1.31** in excellent yield. The corresponding bromopyridine substrate could also be employed to give **1.31**, albeit in slightly diminished yield (78%).[39] Lastly, we varied silyl triflate **1.13** to enable further modulation of the product structure. Oxa- and aza-derivatives of **1.13**, readily available through known routes,[30,31] were employed to furnish heterocycles **1.32** and **1.33**, respectively. This highlights the value of heterocyclic allenes in our methodology for the modular assembly of more complex heterocyclic products. Likewise, substituting a 7-membered cyclic allene precursor in place of a 6-membered cyclic allene precursor gave straightforward access to the 6–5–7 ring system seen in **1.34**.

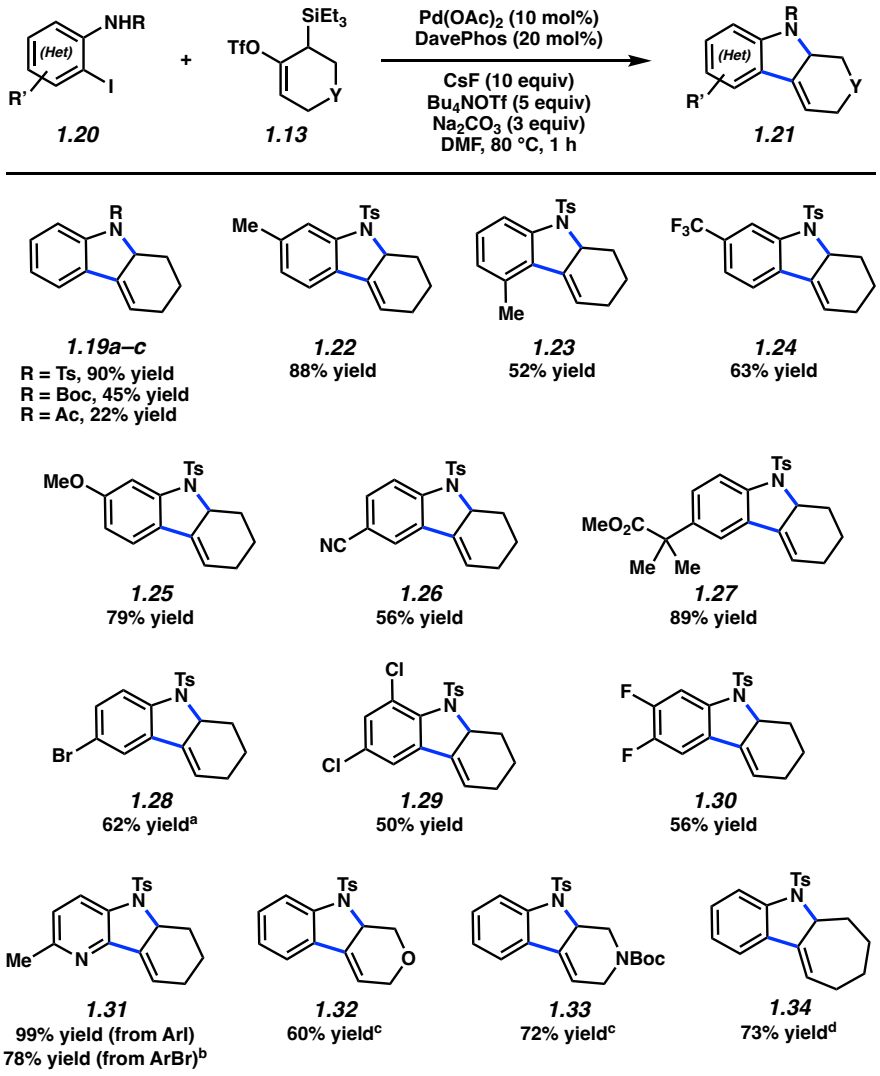

Figure 1.2. Scope of the annulation reaction with iodoaniline derivatives **1.20**. Reactions performed with **1.20** (1.0 equiv) and **1.13** (1.5 equiv). [a] Reaction was performed using 2-(*N*,*N*-dimethylaminomethyl)-1-diphenylphosphanylferrocene as ligand in MeCN at 60 °C for 3 h. [b] ArX = 2-halo-6-methyl-3-*N*-tosylaminopyridine. [c] Reaction was performed using 2-(*N*,*N*-dimethylaminomethyl)-1-diphenylphosphanylferrocene as ligand with CsF (2.5 equiv) in MeCN at 60 °C for 24 h; performed in the absence of Bu_4NOTf. [d] A silyl tosylate was used as the allene precursor (see ref. 40).

We also questioned whether other pronucleophiles, beyond iodoaniline derivatives, could be employed in Pd-catalyzed reactions of strained cyclic allenes (Figure 1.3). With regard to oxygen nucleophiles, we found that benzyl alcohol **1.35** and benzoic acid **1.37** were successful in

delivering **1.36** and **1.38**, respectively, under our standard reaction conditions. Using modified conditions with Xantphos as the ligand, we found that amide **1.39** was a suitable *N*-pronucleophile, delivering **1.40** in 71% yield. Lastly, we tested the viability of a C-based pronucleophile by employing diester **1.41**. Using our standard reaction conditions, we obtained tetrahydrofluorene **1.42**, which bears a newly formed quaternary carbon. These examples underscore that the union of strained cyclic allenes and Pd catalysis provides a rapid entryway to the synthesis of structurally diverse polycyclic products, including 6–6–6 and 6–5–6 ring systems bearing ethers, lactones, amides, or all-carbon frameworks.

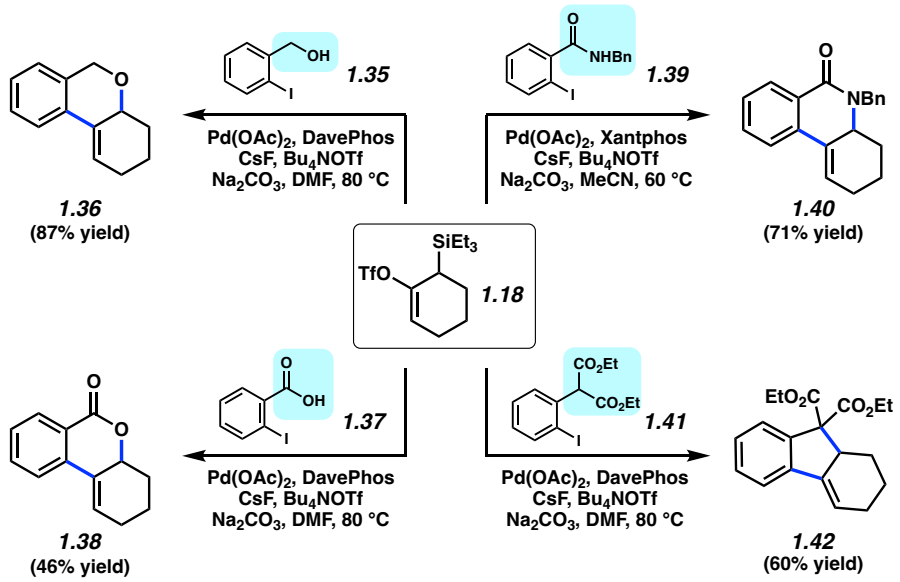

Figure 1.3. Variation of the pronucleophile to furnish structurally diverse products.

1.6 Development of Stereoselective Variants

The feasibility of diastereo- and enantioselective variants of the methodology was established as shown in Figure 1.4. In both cases, heterocyclic substrates were utilized to evaluate the strengths and limitations of the methodology, while providing access to polycyclic scaffolds. Regarding the diastereoselective annulation, it should be noted that diastereoselective reactions of strained cyclic allenes have been reported in the context of cycloadditions,[16] but there are no prior

examples involving transition metal catalysis. Given our success in employing a benzylic alcohol (i.e., **1.35**, Figure 1.3), we prepared tertiary benzylic alcohol **1.43**. This substrate, rapidly accessed from a commercially available isatin precursor, was treated with 1,2-cyclohexadiene precursor **1.18** under standard annulation conditions. Tetracycle **1.44** was obtained as the major product, with dr = 5.6:1, thus providing the first example of substrate-guided stereocontrol in a metal-catalyzed reaction of cyclic allenes.[41]

To probe the feasibility of an enantioselective variant, we tested the reaction of iodopyridine **1.45** with silyl triflate **1.46** (Figure 1.4). Evaluation of chiral ligands led to the identification of $Pd_2(dba)_3$/Mandyphos as the optimal catalyst system. Moreover, with CH_2Cl_2 as solvent at decreased temperature (3 °C) (see Section 1.8.2.6 for extended optimization details), tricycle (–)-**1.47** was generated in 90% ee.[42] As catalytic asymmetric reactions of in-situ-generated strained cyclic intermediates (i.e., arynes, cyclohexynes, cyclic allenes, etc.) are rare, we hope this result will promote further efforts in this area.

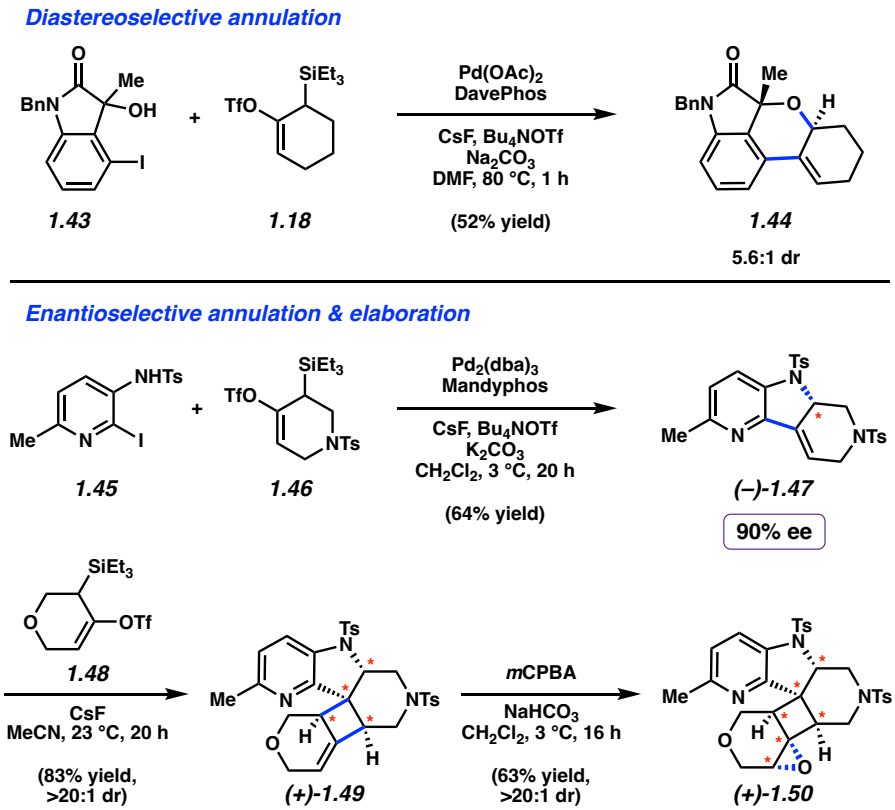

Figure 1.4. Stereocontrolled annulations and synthetic elaboration of an annulation product.

Finally, with unique polyheterocyclic product (–)-**1.47** in hand, we questioned if the styrenyl olefin present in the annulation products could be leveraged as a handle for further elaboration. (–)-**1.47** was subjected to oxacyclic allene precursor **1.48** in the presence of CsF to furnish (+)-**1.49** via a highly diastereoselective [2+2] cycloaddition. The olefin in (+)-**1.49**, newly introduced in the cyclic allene [2+2] reaction, then underwent diastereoselective epoxidation to furnish (+)-**1.50**. This short sequence leverages the asymmetric Pd-catalyzed annulation of an azacyclic allene to ultimately generate an enantioenriched hexacyclic compound (i.e., (+)-**1.50**) bearing five different fused heterocycles, a highly substituted cyclobutane, and six contiguous stereocenters, one of which is quaternary.

1.7 Conclusion

In summary, we have developed Pd-catalyzed annulations of in situ-generated strained cyclic allenes. The methodology employs aryl halides and cyclic allene precursors as the reaction partners, ultimately forming two new bonds and generating an array of fused heterocyclic products. Moreover, through the syntheses of **1.44** and (–)-**1.47** (see Figure 1.4), we demonstrate stereoselective variants of this methodology. The catalytic asymmetric annulation and resulting swift access to hexacycle (+)-**1.50** highlight some of the opportunities afforded by the combination of strained intermediates and Pd catalysis. As this strategy represents a departure from the more common, historical modes of cyclic allene trapping using nucleophiles or cycloaddition partners, we hope this study will stimulate the future development of reactions that strategically merge transition metal catalysis and transient strained intermediate chemistry for the synthesis of complex scaffolds.[43]

1.8 Experimental Section

1.8.1 Materials and Methods

Unless stated otherwise, reactions were conducted in flame-dried glassware under an atmosphere of nitrogen, and commercially obtained reagents were used as received unless otherwise specified. Anhydrous solvents were either freshly distilled or passed through activated alumina columns, unless otherwise stated. Non-commercially available substrates were synthesized according to known preparations or following protocols specified in the Experimental Procedures. Prior to use, acetonitrile, dimethylformamide (DMF), 1,2-dichloroethane (DCE), 1,2-dimethoxyethane (DME), and dichloromethane were passed through activated alumina columns and degassed by five freeze-pump-thaw cycles. *n*-Butyllithium (*n*-BuLi), *N*-(5-chloro-2-

pyridyl)bis(trifluoromethanesulfonamide) (Comins' Reagent), potassium *tert*-butoxide, potassium fluoride, tetrabutylammonium difluorotriphenylsilicate (TBAT), tetrabutylammonium fluoride monohydrate (TBAF•H_2O), sodium hydride (60 wt% in oil), 4-iodoindoline-2,3-dione (**1.72**), 2'-(dicyclohexylphosphino)-*N*,*N*-dimethyl-[1,1'-biphenyl]-2-amine (DavePhos), sodium bicarbonate, *meta*-chloroperoxybenzoic acid (*m*CPBA), sodium *tert*-butoxide, allylpalladium chloride dimer ($[Pd(allyl)Cl]_2$), sodium acetate trihydrate, sodium bis(trimethylsilyl)amide (NaHMDS), methylmagnesium bromide (3.0 M in diethyl ether), benzyl bromide, and tris(dimethylamino)sulfonium difluorotrimethylsilicate (TASF) were obtained from Sigma-Aldrich. 1,4-diazabicyclo[2.2.2]octane (DABCO) and pyridine were obtained from Acros Organics. Triethylsilyl chloride, 4-toluenesulfonyl chloride (TsCl), 2-iodobenzyl alcohol (**1.35**), and 2-iodobenzoic acid (**1.37**) were obtained from Oakwood Chemical. 1,4,7,10,13,16-Hexaoxacyclooctadecane (18-crown-6) was obtained from Chem-Impex. Diisopropylamine was obtained from Alfa Aesar. Bis(1,5-cyclooctadiene)nickel(0) ($Ni(cod)_2$), 1,1'-bis(diphenylphosphino)ferrocene (dppf), cesium fluoride, palladium(II) acetate, bis(dibenzylideneacetone)palladium(0) ($Pd(dba)_2$), tris(dibenzylideneacetone)dipalladium(0) ($Pd_2(dba)_3$), palladium(II) chloride, and palladium(II) acetylacetonate ($Pd(acac)_2$) were obtained from Strem Chemicals. Tetrabutylammonium trifluoromethanesulfonate was obtained from TCI America. Potassium phosphate dibasic and potassium carbonate were obtained from Fisher Scientific. All ligands used for reaction optimization (Sections 1.8.2.3 and 1.8.2.6) were obtained from Strem Chemicals, TCI America, Sigma-Aldrich, or Solvias. All commercially available *o*-iodoanilines were obtained from Sigma-Aldrich, Enamine, or Combi-Blocks. Triethylsilyl chloride, pyridine, and diisopropylamine were distilled over CaH_2 prior to use. Na_2CO_3 and K_2CO_3 were dried in an oven heated to 120 °C for 48 h prior to use. Reaction temperatures at or above 23

°C were controlled using an IKAmag temperature modulator, and unless stated otherwise, performed at room temperature (approximately 23 °C). Reactions conducted at 3 °C were performed in a refrigerator set to 3 °C and equipped with a stir plate. Thin-layer chromatography (TLC) was conducted with EMD gel 60 F_{254} pre-coated plates (0.25 mm for analytical chromatography and 0.50 mm for preparative chromatography) and visualized using a combination of UV and potassium permanganate staining techniques. Silicycle Siliaflash P60 (particle size 40–63 μm) was used for flash column chromatography. ^{1}H-NMR and 2D-NOESY spectra were recorded on Bruker spectrometers (at 400, 500, and 600 MHz) and are reported relative to the residual solvent signal. Data for ^{1}H-NMR spectra are reported as follows: chemical shift (δ ppm), multiplicity, coupling constant (Hz) and integration. ^{13}C-NMR spectra were recorded on Bruker spectrometers (at 100 and 125 MHz) and are reported relative to the residual solvent signal. Data for ^{13}C-NMR spectra are reported in terms of chemical shift (δ ppm) and, when necessary, multiplicity, and coupling constant (Hz). ^{19}F NMR spectra were recorded on Bruker spectrometers (at 376 MHz) and are reported in terms of chemical shift (δ ppm), multiplicity, coupling constant (Hz) and integration. IR spectra were recorded on a Perkin-Elmer UATR Two FT-IR spectrometer and are reported in terms of frequency absorption (cm^{-1}). DART-MS spectra were collected on a Thermo Exactive Plus MSD (Thermo Scientific) equipped with an ID-CUBE ion source and a Vapur Interface (IonSense Inc.). Both the source and MSD were controlled by Excalibur software version 3.0. The analyte was spotted onto OpenSpot sampling cards (IonSense Inc.) using $CDCl_3$ or CH_2Cl_2 as the solvent. Ionization was accomplished using UHP He plasma with no additional ionization agents. The mass calibration was carried out using Pierce LTQ Velos ESI (+) and (–) Ion calibration solutions (Thermo Fisher Scientific). Optical rotations were measured with a Rudolf Autopol III Automatic Polarimeter. Determination of

enantiopurity was carried out on a Mettler Toledo SFC (supercritical fluid chromatography) using a Daicel ChiralPak AD-H column. Data for SFC chromatograms are reported in enantiomeric excess (ee).

Aniline derivatives **1.17**[44], **1.57**[45], **1.79**[46], **1.80**[47], **1.81**[48], **1.82**[49], and **1.83**[50], benzamide **1.39**[51], diester **1.41**[52], bromoketone **1.74**[53], ferrocenyl ligands **1.78**[54] and **1.87**[55], and allene precursors **1.18**[29], **1.48**[31], **1.84**[33], and **1.85**[32] are all known compounds. The ^{1}H NMR spectral data matched those reported in literature.

1.8.2 Experimental Procedures

1.8.2.1 Syntheses of Annulation Partners

1.8.2.1.1 Syntheses of *N*-Tosyl-Arylamines

Annulation partners **1.45**, **1.56**, **1.58**, **1.60**, **1.62**, **1.64**, **1.66**, **1.69**, and **1.71** were synthesized from the corresponding amines using the general procedures shown below.

General Procedure 1.1 for the synthesis of *N*-tosyl-iodoanilines:

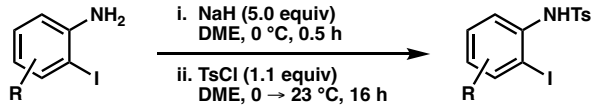

1.51 *1.52*

***N*-tosyl-iodoanilines 1.52.** To a solution of NaH (60 wt%, 5.0 equiv) in DME (5.8 M) at 0 °C was added iodoaniline **1.51** (1.0 equiv) in DME (1.2 M) dropwise over 2 min. The mixture was stirred at this temperature for 30 min prior to the rapid dropwise addition of TsCl (1.1 equiv) in DME (1.3 M) over 2 min. The resulting mixture was gradually warmed to 23 °C over 16 h then quenched by the addition of 1 M HCl (10 mL). The resulting mixture was extracted with EtOAc (3 x 15 mL).

The combined organic layers were dried with Na_2SO_4, filtered, and concentrated under reduced pressure. The crude material was purified by flash column chromatography to provide *N*-tosyl-iodoaniline **1.52**.

General Procedure 1.2 for the synthesis of *N*-tosyl-iodoanilines:

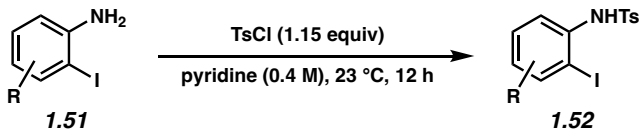

1.51 *1.52*

***N*-tosyl-iodoanilines 1.52.** Iodoaniline **1.51** (1.0 equiv) and TsCl (1.15 equiv) were dissolved in pyridine (0.4 M) at 23 °C, and the resulting mixture was stirred at this temperature for 12 h. The reaction was quenched by the addition of 1 M HCl (20 mL). The resulting mixture was extracted with EtOAc (3 x 20 mL), and the combined organic layers were then washed with water (2 x 20 mL) and saturated aqueous $NaHCO_3$ (20 mL). The combined organic layers were dried with Na_2SO_4, filtered, and concentrated under reduced pressure. The crude material was purified by flash column chromatography to provide *N*-tosyl-iodoaniline **1.52**.

General Procedure 1.3 for the synthesis of *N*-tosyl-arylamines:

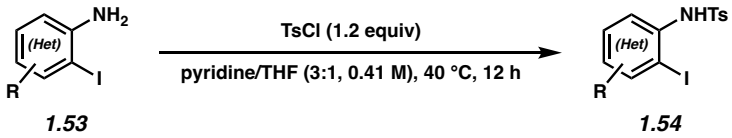

1.53 *1.54*

***N*-tosyl-arylamines 1.54.** Iodoamine **1.53** (1.0 equiv) and TsCl (1.2 equiv) were dissolved in a mixture of pyridine and THF (3:1, 0.41 M), and the resulting mixture was stirred at 40 °C in a sealed vial for 12 h, leading to the formation of a white precipitate. After 12 h, the solvent was removed under reduced pressure, and the crude residue was redissolved in EtOAc (10 mL) then washed with water (2 x 10 mL). The organic layer was dried with Na_2SO_4, filtered, and

concentrated under reduced pressure. The crude material was purified by flash column chromatography to provide *N*-tosyl-arylamine **1.54**.

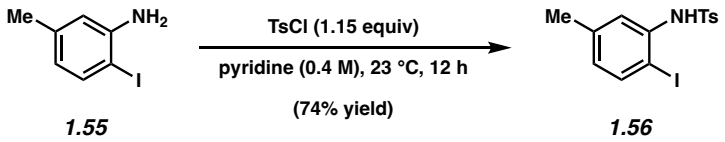

1.55 ***1.56***

***N*-tosyl-iodoaniline 1.56**. Followed General Procedure 1.2 using **1.55** (250 mg, 1.07 mmol). Purification by flash column chromatography (9:1 hexanes:EtOAc) provided *N*-tosyl-iodoaniline **1.56** (317 mg, 74% yield) as a white solid. ***N*-tosyl-iodoaniline 1.56**: Mp: 120 °C; R_f 0.27 (9:1 hexanes:EtOAc); ^{1}H NMR (400 MHz, $CDCl_3$): δ 7.62 (d, *J* = 8.3, 2H), 7.49 (d, *J* = 1.8, 1H), 7.48 (d, *J* = 8.2, 1H), 7.21 (d, *J* = 8.0, 2H), 6.71 (br s, 1H), 6.65 (ddd, *J* = 8.1, 2.0, 0.6, 1H), 2.38 (s, 3H), 2.30 (s, 3H); ^{13}C NMR (100 MHz, $CDCl_3$): δ 144.2, 140.0, 138.6, 137.2, 136.0, 129.6, 128.0, 127.5, 123.4, 88.4, 21.6, 21.2; IR (film): 3244, 2917, 1475, 1336, 1161 cm^{-1}; HRMS-APCI (*m/z*) $[M + H]^+$ calcd for $C_{14}H_{15}INO_2S^+$, 387.9863; found 387.9839.

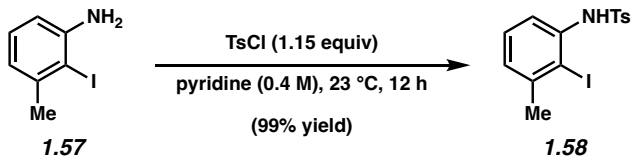

1.57 ***1.58***

***N*-tosyl-iodoaniline 1.58**. Followed General Procedure 1.2 using **1.57** (532 mg, 2.28 mmol). Purification by flash column chromatography (2:1 benzene:hexanes) provided *N*-tosyl-iodoaniline **1.58** (883 mg, 99% yield) as a white solid. ***N*-tosyl-iodoaniline 1.58**: Mp: 95–96 °C; R_f 0.61 (9:1 benzene:Et_2O); ^{1}H NMR (500 MHz, $CDCl_3$): δ 7.65 (d, *J* = 8.3, 2H), 7.45 (d, *J* = 8.4, 1H), 7.19 (d, *J* = 8.4, 2H), 7.15 (t, *J* = 8.0, 1H), 7.04 (br s, 1H), 6.96 (d, *J* = 8.0, 1H), 2.36 (s, 3H), 2.35 (s,

3H); ^{13}C NMR (100 MHz, $CDCl_3$): δ 144.1, 142.9, 137.7, 136.0, 129.6, 128.7, 127.5, 126.5, 119.1, 99.5, 29.7, 21.6; IR (film): 3302, 2949, 1459, 1374, 1159 cm^{-1}; HRMS-APCI (*m/z*) $[M - H]^-$ calcd for $C_{14}H_{13}INO_2S^-$, 385.9706; found 385.9725.

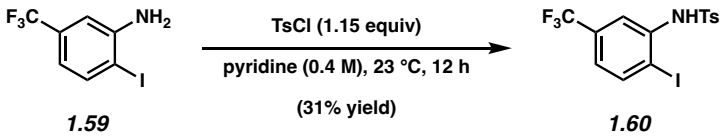

1.59 ***1.60***

***N*-tosyl-iodoaniline 1.60**. Followed General Procedure 1.2 using **1.59** (300 mg, 1.05 mmol). Purification by flash column chromatography (9:1 hexanes:EtOAc) provided *N*-tosyl-iodoaniline **1.60** (48 mg, 31% yield) as an off-white solid. ***N*-tosyl-iodoaniline 1.60**: Mp: 171 °C; R_f 0.11 (9:1 hexanes:EtOAc); ^{1}H NMR (400 MHz, $CDCl_3$): δ 7.88 (d, *J* = 1.8, 1H), 7.78 (d, *J* = 8.2, 1H), 7.66 (d, *J* = 8.3, 2H), 7.24 (d, *J* = 8.1, 2H), 7.05 (ddd, *J* = 8.3, 2.1, 0.6, 1H), 6.94 (br s, 1H), 2.39 (s, 3H); ^{13}C NMR (125 MHz, $CDCl_3$): δ 144.8, 139.7, 138.4, 135.5, 132.1 (q, *J* = 33.3), 129.9, 127.5, 123.3 (q, *J* = 272.6), 122.8 (q, *J* = 3.8), 118.2 (q, *J* = 3.8), 95.7 (q, *J* = 1.4), 21.6; ^{19}F NMR (376 MHz, $CDCl_3$) δ –63.11 (s, 3F); IR (film): 3247, 1388, 1325, 1169, 1118 cm^{-1}; HRMS-APCI (*m/z*) $[M + H]^+$ calcd for $C_{14}H_{12}F_3INO_2S^+$, 441.9580; found 441.9587.

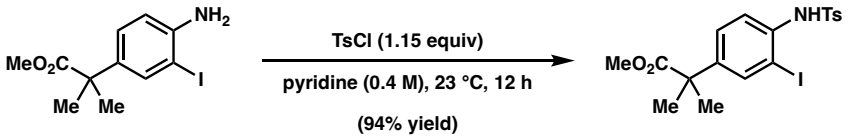

1.61 ***1.62***

***N*-tosyl-iodoaniline 1.62.** Followed General Procedure 1.2 using **1.61** (100 mg, 0.313 mmol). Purification by flash column chromatography (5:1 hexanes:EtOAc) afforded *N*-tosyl-iodoaniline **1.62** (140 mg, 94% yield) as an off-white solid. ***N*-tosyl-iodoaniline 1.62**: Mp: 85–86 °C; R_f 0.42 (9:1 benzene:Et_2O); ^{1}H NMR (500 MHz, MeOD): δ 6.11 (d, *J* = 2.0, 1H), 6.04 (d, *J* = 8.3, 2H),

5.76–5.72 (m, 4H), 2.07 (s, 3H), 1.74 (br s, 1H), 0.83 (s, 3H), 0.07 (s, 6H); ^{13}C NMR (125 MHz, MeOD): δ 176.6, 144.6, 143.9, 137.4, 137.0, 136.7, 129.3, 127.2, 126.3, 126.0, 95.2, 51.5, 45.7, 25.4, 20.1; IR (film): 3267, 2950, 1728, 1336, 1161 cm^{-1}; HRMS-APCI (*m/z*) [M – H]$^-$ calcd for $C_{18}H_{19}INO_4S^-$, 472.0074; found 472.0095.

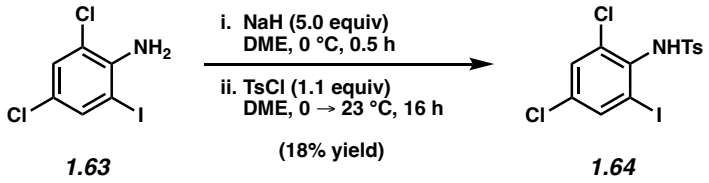

1.63 ***1.64***

***N*-tosyl-iodoaniline 1.64**. Followed General Procedure 1.1 using **1.63** (100 mg, 0.347 mmol). Purification by flash column chromatography (benzene) provided *N*-tosyl-iodoaniline **1.64** (28 mg, 18% yield) as an off-white solid. ***N*-tosyl-iodoaniline 1.64**: Mp: 181 °C; R_f 0.24 (5:1 hexanes:EtOAc); ^{1}H NMR (500 MHz, $CDCl_3$): δ 7.78 (d, *J* = 2.4, 1H), 7.68 (d, *J* = 8.3, 2H), 7.39 (d, *J* = 2.4, 1H), 7.29 (d, *J* = 8.3, 2H), 6.28 (s, 1H), 2.44 (s, 3H); ^{13}C NMR (125 MHz, $CDCl_3$): δ 144.4, 138.3, 137.6, 134.7, 134.5, 133.9, 130.4, 129.7, 127.8, 101.2, 21.7; IR (film): 3252, 2923, 1436, 1336, 1162 cm^{-1}; HRMS-APCI (*m/z*) [M – H]$^-$ calcd for $C_{13}H_9Cl_2INO_2S^-$, 439.8770; found 439.8787.

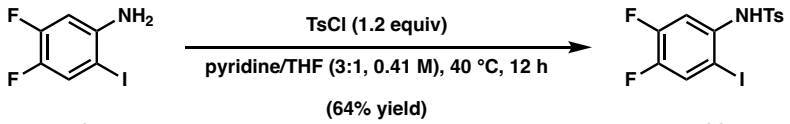

1.65 ***1.66***

***N*-tosyl-iodoaniline 1.66**. Followed General Procedure 1.3 using **1.65** (100 mg, 0.392 mmol). Purification by flash column chromatography (9:1 hexanes:EtOAc → 5:1 hexanes:EtOAc) provided *N*-tosyl-iodoaniline **1.66** (102 mg, 64% yield) as a white solid. ***N*-tosyl-iodoaniline 1.66**:

Mp: 131–133 °C; R_f 0.56 (9:1 benzene:Et_2O); ^{1}H NMR (500 MHz, MeOD): δ 6.11 (dd, *J* = 9.5, 8.7, 1H), 6.03 (d, *J* = 8.5, 2H), 5.78–5.73 (m, 3H), 0.84 (s, 3H); ^{13}C NMR (125 MHz, MeOD): δ 149.8 (dd, *J* = 248.5, 13.2), 147.1 (dd, *J* = 251.7, 13.1), 144.1, 137.0, 135.6 (dd, *J* = 8.5, 3.8), 129.4, 127.2, 127.1 (d, *J* = 19.6), 115.4 (d, *J* = 20.2), 88.0 (dd, *J* = 6.2,4.1), 20.1; IR (film): 3268, 3063, 1598, 1493, 1340 cm^{-1}; HRMS-APCI (*m/z*) $[M - H]^-$ calcd for $C_{13}H_9F_2INO_2S^-$, 407.9361; found 407.9373.

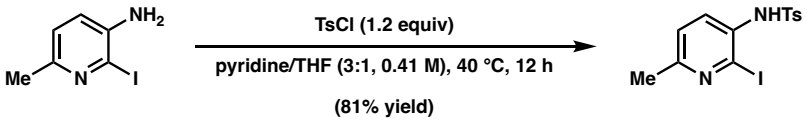

1.67 ***1.45***

***N*-tosyl-aminopyridine 1.45.** Followed General Procedure 1.3 using **1.67** (175 mg, 0.748 mmol). Purification by flash column chromatography (98:2 benzene:Et_3N → 80:20:2 benzene:acetone:Et_3N) provided *N*-tosyl-aminopyridine **1.45** (235 mg, 81% yield) as a white solid. ***N*-tosyl-aminopyridine 1.45**: Mp: 121–123 °C; R_f 0.68 (1:1 $CHCl_3$:Et_2O); ^{1}H NMR (500 MHz, $CDCl_3$): δ 7.77 (d, *J* = 8.2, 1H), 7.60 (d, *J* = 8.3, 2H), 7.23 (d, *J* = 8.4, 2H), 7.06 (d, *J* = 8.2, 1H), 6.71 (br s, 1H), 2.46 (s, 3H), 2.39 (s, 3H); ^{13}C NMR (125 MHz, $CDCl_3$): δ 157.2, 144.7, 135.5, 133.3, 130.1, 129.9, 127.4, 123.3, 116.4, 23.5, 21.6; IR (film): 3269, 2970, 1739, 1454, 1315 cm^{-1}; HRMS-APCI (*m/z*) $[M + H]^+$ calcd for $C_{13}H_{14}IN_2O_2S^+$, 388.9815; found 388.9814.

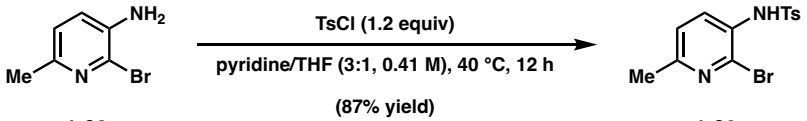

1.68 ***1.69***

***N*-tosyl-aminopyridine 1.69.** Followed General Procedure 1.3 using **1.68** (200 mg, 1.07 mmol). Purification by flash column chromatography (98:2 benzene:Et_3N → 80:20:2

benzene:acetone:Et_3N) provided *N*-tosyl-aminopyridine **1.69** (316 mg, 87% yield) as a white solid.

***N*-tosyl-aminopyridine 1.69**: Mp: 127 °C; R_f 0.68 (1:1 $CHCl_3$:Et_2O); ^{1}H NMR (500 MHz, $CDCl_3$): δ 7.85 (d, *J* = 8.9, 1H), 7.63–7.59 (m, 2H), 7.22 (d, *J* = 8.5, 2H), 7.08 (d, *J* = 8.4, 1H), 6.88 (br s, 1H), 2.45 (s, 3H), 2.37 (s, 3H); ^{13}C NMR (125 MHz, $CDCl_3$): δ 156.1, 144.7, 135.5, 135.0, 131.1, 129.91, 129.88, 127.3, 123.3, 23.5, 21.6; IR (film): 3259, 2924, 1458, 1317, 1161 cm^{-1}; HRMS-APCI (*m/z*) $[M + H]^+$ calcd for $C_{13}H_{14}BrN_2O_2S^+$, 340.9954; found 340.9955.

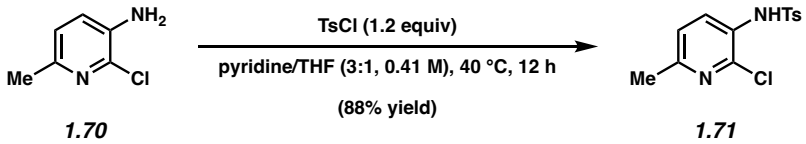

1.70 *1.71*

***N*-tosyl-aminopyridine 1.71.** Followed General Procedure 1.3 using **1.70** (200 mg, 1.40 mmol). Purification by flash column chromatography (98:2 benzene:Et_3N → 80:20:2 benzene:acetone:Et_3N) provided *N*-tosyl-aminopyridine **1.71** (368 mg, 88% yield) as a beige solid.

***N*-tosyl-aminopyridine 1.71**: Mp: 125–128 °C; R_f 0.62 (1:1 $CHCl_3$:Et_2O); ^{1}H NMR (500 MHz, $CDCl_3$): δ 7.88 (d, *J* = 8.1, 1H), 7.62 (d, *J* = 8.3, 2H), 7.22 (d, *J* = 8.3, 2H), 7.06 (d, *J* = 8.2, 1H), 6.93 (br s, 1H), 2.43 (s, 3H), 2.36 (s, 3H); ^{13}C NMR (125 MHz, $CDCl_3$): δ 155.5, 144.6, 141.7, 135.6, 131.5, 129.9, 128.0, 127.2, 123.0, 23.5, 21.6; IR (film): 3257, 1739, 1597, 1463, 1320 cm^{-1}; HRMS-APCI (*m/z*) $[M + H]^+$ calcd for $C_{13}H_{14}ClN_2O_2S^+$, 297.0459; found 297.0460.

1.8.2.1.2 Synthesis of Alcohol 1.43

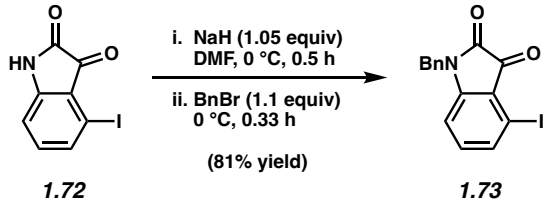

1.72 *1.73*

Isatin 1.73. To a solution of NaH (washed with hexanes, 46.1 mg, 1.92 mmol, 1.05 equiv) in DMF (2.5 mL) at 0 °C was added isatin **1.72** (500 mg, 1.83 mmol, 1.00 equiv) in DMF (2.5 mL) dropwise over 2 min, giving a deep purple solution. The reaction was stirred at 0 °C for 30 min followed by the dropwise addition of BnBr (240 μL, 2.01 mmol, 1.10 equiv) over 2 min. The reaction was stirred for an additional 20 min at this temperature, then water (10 mL) was added in a single portion to precipitate the product. The resulting suspension was filtered, and the solid was washed with water (3 x 10 mL) then collected. The slightly wet solid was then dissolved in benzene (10 mL) and concentrated under reduced pressure. This process of dissolution and concentration was repeated twice more to provide isatin **1.73** (536 mg, 81% yield) as an orange solid. **Isatin 1.73**: Mp: 161 °C; R_f 0.43 (2:1 Hexanes:EtOAc); ^{1}H NMR (500 MHz, $CDCl_3$): δ 7.52 (dd, J = 8.0, 0.5, 1H), 7.36–7.28 (m, 5H), 7.10 (t, J = 8.0, 1H), 6.75 (dd, J = 8.0, 0.5, 1H), 4.93 (s, 2H); ^{13}C NMR (125 MHz, $CDCl_3$): δ 181.5, 157.4, 152.6, 138.0, 135.1, 134.2, 129.1, 128.3, 127.4, 119.3, 110.5, 92.9, 43.8; IR (film): 3063, 1735, 1594, 1445, 1328 cm^{-1}; HRMS-APCI (*m/z*) $[M + H]^+$ calcd for $C_{15}H_{11}INO_2^+$, 363.9829; found 363.9816.

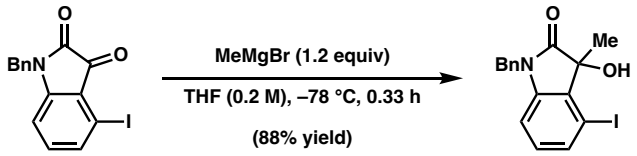

1.73 *1.43*

Alcohol 1.43. A solution of isatin **1.73** (250 mg, 0.688 mmol, 1.0 equiv) in THF (3.44 mL, 0.20 M) was cooled to –78 °C. MeMgBr (299 μL, 2.76 M in THF, 0.826 mmol, 1.2 equiv) was added dropwise over 2 min, and the solution was stirred at –78 °C for 20 min. The reaction mixture was then quenched with a saturated aqueous solution of NH_4Cl (10 mL) and extracted with EtOAc (3 x 10 mL). The organic layers were combined, dried over Na_2SO_4, filtered, and concentrated to afford the crude residue. Purification by flash column chromatography (9:1 benzene:Et_2O) afforded alcohol **1.43** (231 mg, 88% yield) as a light yellow solid. **Alcohol 1.43**: Mp: 148 °C; R_f 0.10 (9:1 benzene:Et_2O); ^{1}H NMR (500 MHz, $CDCl_3$): δ 7.44 (d, J = 8.0, 1H), 7.34–7.23 (m, 5H), 6.89 (t, J = 8.0, 1H), 6.68 (d, J = 8.0, 1H), 4.96 (d, J = 15.6, 1H), 4.80 (d, J = 15.6, 1H), 2.85 (s, 1H), 1.81 (s, 3H); ^{13}C NMR (125 MHz, $CDCl_3$): δ 177.7, 143.7, 135.0, 133.6, 132.3, 130.8, 129.0, 127.9, 127.1, 109.4, 90.3, 75.6, 43.6, 22.7; IR (film): 3394, 2925, 1710, 1600, 1577 cm^{-1}; HRMS-APCI (*m/z*) $[M - HI + OH]^-$ calcd for $C_{16}H_{14}NO_3^-$, 268.0968; found 268.0978.

1.8.2.2 Synthesis of Silyl Triflate 1.46

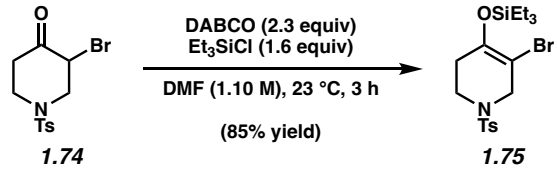

1.74 *1.75*

Silyl enol ether 1.75. To a solution of bromoketone **1.74** (1.40 g, 4.21 mmol, 1.0 equiv) in DMF (3.80 mL, 1.10 M) was added Et_3SiCl (1.14 mL, 6.74 mmol. 1.6 equiv) and DABCO (1.09 g, 9.69 mmol, 2.3 equiv) sequentially, and the resulting heterogeneous mixture was allowed to stir at 23 °C

for 3 h. The reaction was then quenched with saturated aqueous $NaHCO_3$ (20 mL) and diluted with water (20 mL). The resulting mixture was extracted with EtOAc (3 x 10 mL). The combined organic layers were washed sequentially with water (2 x 15 mL) and brine (1 x 15 mL), dried with Na_2SO_4, filtered, and concentrated under reduced pressure to provide the crude silyl enol ether as a colorless oil. The crude product was purified by flash column chromatography (19:1 hexanes:EtOAc) to provide silyl enol ether **1.75** (1.60 g, 85% yield) as a colorless oil. **Silyl enol ether 1.75**: R_f 0.23 (9:1 hexanes:EtOAc); ^{1}H NMR (400 MHz, $CDCl_3$): δ 7.67 (d, *J* = 8.4, 2H), 7.33 (d, *J* = 8.0, 2H), 3.81 (t, *J* = 2.1, 2H), 3.30 (t, *J* = 5.8, 2H), 2.43 (s, 3H), 2.30–2.26 (m, 2H), 0.96 (t, *J* = 8.5, 9H), 0.65 (q, *J* = 7.5, 6H); ^{13}C NMR (100 MHz, $CDCl_3$): δ 145.4, 143.9, 133.7, 129.9, 127.6, 95.1, 50.1, 43.3, 31.3, 21.6, 6.6, 5.5; IR (film): 2955, 2876, 1972, 1340, 1163 cm^{-1}; HRMS-APCI (*m/z*) $[M + H]^+$ calcd for $C_{18}H_{29}BrNO_3SSi^+$, 446.0815; found 446.0802.

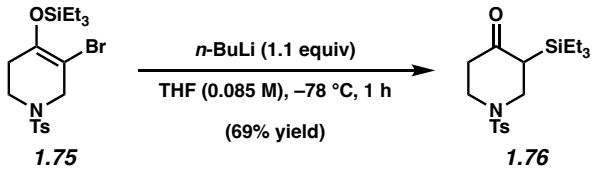

Silyl ketone 1.76. To a solution of silyl enol ether **1.75** (1.60 g, 3.57 mmol, 1.0 equiv) in THF (42 mL, 0.085 M) at –78 °C was added *n*-BuLi (2.63 M in hexanes, 1.50 mL, 3.93 mmol, 1.1 equiv) dropwise over 5 min. After stirring for 1 h at –78 °C, the reaction was quenched with saturated aqueous $NaHCO_3$ (25 mL) and allowed to warm to 23 °C. The mixture was extracted with EtOAc (3 x 25 mL). The combined organic layers were then dried over Na_2SO_4, filtered, and concentrated under reduced pressure. The resulting crude oil was purified by flash column chromatography (9:1 hexanes:EtOAc) to afford silyl ketone **1.76** (0.91 g, 69% yield) as a colorless oil. **Silyl Ketone 1.76**: R_f 0.28 (4:1 hexanes:EtOAc); ^{1}H NMR (400 MHz, $CDCl_3$): δ 7.63 (d, *J* = 8.2, 2H), 7.32 (d,

J = 8.2, 2H), 3.87–3.82 (m, 1H), 3.79 (dt, J = 11.6, 2.7, 1H), 2.90 (dd, J = 11.8, 5.1, 1H), 2.68 (td, 11.5, 4.1, 1H), 2.59–2.50 (m, 1H), 2.41 (s, 3H), 2.40–2.35 (m, 2H), 0.97 (t, J = 8.1, 9H), 0.72 (qd, J = 7.4, 2.1, 6H); ^{13}C NMR (100 MHz, $CDCl_3$): δ 206.6, 144.0, 132.7, 129.8, 127.7, 46.4, 45.4, 42.4, 40.1, 21.5, 7.3, 2.9; IR (film): 2954, 2876, 1688, 1361, 1163 cm^{-1}; HRMS-APCI (*m/z*) [M + H]$^+$ calcd for $C_{18}H_{30}NO_3SSi^+$, 368.1710; found 368.1694.

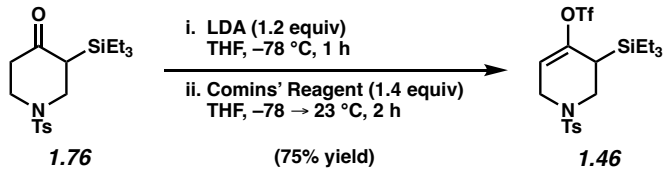

Silyl triflate 1.46. To a solution of diisopropylamine (0.40 mL, 2.80 mmol, 1.25 equiv) in THF (4.0 mL) at –78 °C was added *n*-BuLi (2.63 M in hexanes, 1.02 mL, 2.69 mmol, 1.20 equiv) dropwise over 2 min. The reaction was stirred at –78 °C for 30 min, warmed to 23 °C over 15 min, then re-cooled to –78 °C over 15 min. A solution of silyl ketone **1.76** (824 mg, 2.24 mmol, 1.00 equiv) in THF (4.0 mL) was then added dropwise over 3 min. The mixture was stirred at –78 °C for 1 h followed by the dropwise addition of Comins' Reagent (1.23 g, 3.14 mmol, 1.40 equiv) in THF (4.0 mL) over 3 min. The resulting mixture was stirred for 10 min at –78 °C before being warmed to 23 °C. After stirring for an additional 2 h at this temperature, the reaction mixture was quenched by the addition of saturated aqueous $NaHCO_3$ (20 mL), and the layers were separated. The aqueous layer was extracted with Et_2O (3 x 20 mL), and the combined organic layers were dried over Na_2SO_4, filtered, and concentrated under reduced pressure. The resulting crude oil was purified by flash column chromatography (3:1 hexanes:benzene → 1:1 hexanes:benzene) to give silyl triflate **1.46** (531 mg, 75% yield) as a colorless oil which solidified on standing at –20 °C. **Silyl triflate 1.46**: Mp: 36 °C; R_f 0.82 (9:1 benzene:Et_2O); ^{1}H NMR (500 MHz, $CDCl_3$): δ 7.68–

7.63 (m, 2H), 7.36–7.32 (m, 2H), 5.56–5.52 (m, 1H), 3.94 (ddd, J = 16.4, 3.6, 2.3, 1H), 3.67 (dd, J = 11.8, 3.6, 1H), 3.41 (dt, J = 16.4, 3.1, 1H), 2.99 (dd, J = 11.8, 4.5, 1H), 2.44 (s, 3H), 2.08–2.03 (m, 1H), 0.99 (t, J = 8.1, 9H), 0.78–0.72 (m, 6H); ^{13}C NMR (125 MHz, $CDCl_3$): δ 150.4, 144.2, 132.4, 129.9, 127.7, 118.4 (q, J = 320.7), 110.0, 45.2, 43.7, 28.0, 21.6, 7.2, 2.7; IR (film): 2957, 2914, 1419, 1210, 1168 cm^{-1}; HRMS-APCI (*m/z*) $[M + H]^+$ calcd for $C_{19}H_{29}F_3NO_5S_2Si^+$, 533.0957; found 533.0974.

1.8.2.3 Optimization of the Racemic Annulation

Results from the optimization of the reaction between **1.17** and **1.18** appear below. Temperature, base, CsF loading, and ligand were varied using General Procedure 1.4, and results appear below in Tables 1.2, 1.3, 1.4, and 1.5 respectively.

General Procedure 1.4 for the optimization of the racemic annulation:

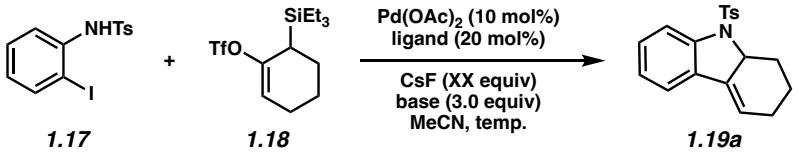

1.17 *1.18* *1.19a*

Annulation Product 1.19a. A 1-dram vial containing a magnetic stir bar was charged with iodoaniline **1.17** (11.3 mg, 0.03 mmol, 1.0 equiv). A separate 1-dram vial was charged with silyl triflate **1.18** (10.3 mg, 0.03 mmol, 1.0 equiv). A third 1-dram vial was charged with $Pd(OAc)_2$ (0.674 mg, 0.003 mmol, 10 mol%). All three vials were taken into a glovebox where the ligand (0.006 mmol, 20 mol%), the base (0.09 mmol, 3.0 equiv), and CsF were added to the vial containing iodoaniline **1.17**. The vial containing the $Pd(OAc)_2$ and the vial containing silyl triflate **1.18** were then each treated with an aliquot of solvent (0.20 mL each) and agitated vigorously to ensure full dissolution. The solution of $Pd(OAc)_2$ and the solution of silyl triflate were then

transferred sequentially to the reaction vial containing iodoaniline **1.17**, and the vial was sealed with a Teflon-lined cap, removed from the glovebox, and stirred for 3 h at the desired reaction temperature. The mixture was then filtered through a pad of silica gel, eluting with EtOAc (10 mL). The eluate was concentrated to provide a crude residue, which was analyzed by ^{1}H NMR using 1,3,5-trimethoxybenzene an external standard.

Table 1.2. Temperature screening results.

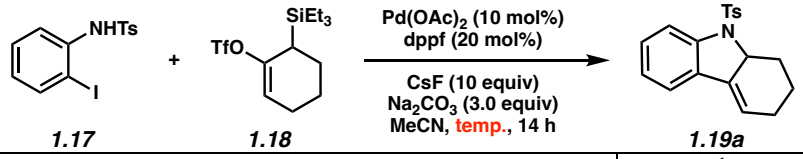

1.17 ***1.18*** ***1.19a***

Entry	Temperature (°C)	^{1}H NMR Yield[a]
1	35	35%
2	50	49%
3	65	49%
4	80	53%

[a] ^{1}H NMR yield determined using 1,3,5-trimethoxybenzene as an external standard.

Table 1.3. Base screening results.

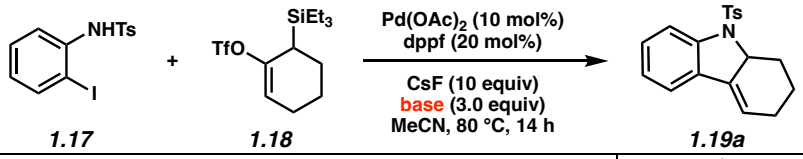

1.17 ***1.18*** ***1.19a***

Entry	Base	^{1}H NMR Yield[a]
1	Na_2CO_3	53%
2	Et_3N	46%
3	NaO*t*Bu	0%

[a] ^{1}H NMR yield determined using 1,3,5-trimethoxybenzene as an external standard.

Table 1.4. CsF loading screening results.

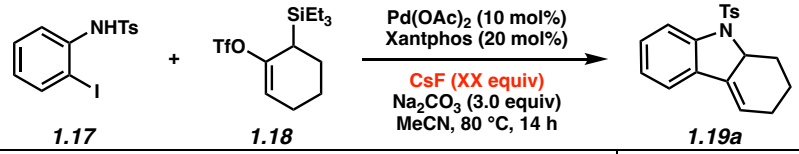

1.17 *1.18* *1.19a*

Entry	Equiv. CsF	^{1}H NMR Yield[a]
1	2.5	11%
2	5	39%
3	7.5	45%
4	10	56%

[a] ^{1}H NMR yield determined using 1,3,5-trimethoxybenzene as an external standard.

Table 1.5. Ligand screening results.

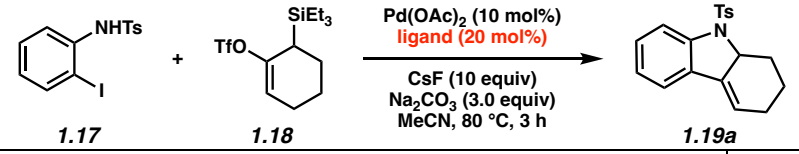

1.17 *1.18* *1.19a*

Entry	Ligand	^{1}H NMR Yield[a]
1	PCy_3	20%
2	dppe	22%
3	rac. BINAP	19%
4	dtbpf	29%
5	Xantphos	56%
6	dppf	53%
7	dppf Gen. 3 (10 mol%)[b]	42%
8	RuPhos Gen. 3 (10 mol%)[b]	44%
9	SPhos Gen. 4 (10 mol%)[b]	55%
10	Johnphos	37%
11	Xphos	54%
12	DPEphos	55%
13	2-(*N*,*N*-dimethylaminomethyl)-1-diphenylphosphinoferrocene (**1.78**)[c]	74%
14	DavePhos	72%

[a] ^{1}H NMR yield determined using 1,3,5-trimethoxybenzene as an external standard.
[b] $Pd(OAc)_2$ omitted from the reaction.
[c] Reaction carried out at 60 °C.

1.8.2.4 Scope of the Racemic Annulation

General Procedure 1.5 for the scope of the racemic annulation:

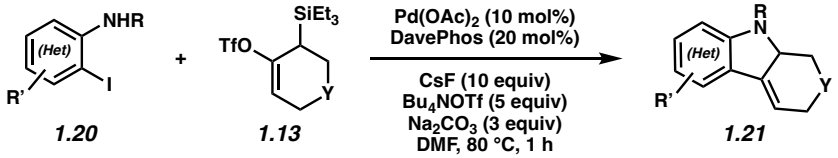

Annulation Products 1.21. A 1-dram vial containing a magnetic stir bar was charged with iodoaniline **1.20** (0.05 mmol, 1.0 equiv) and Bu_4NOTf (98.7 mg, 0.25 mmol, 5.0 equiv). A separate 1-dram vial was charged with silyl triflate **1.13** (0.075 mmol, 1.5 equiv). A third 1-dram vial was charged with $Pd(OAc)_2$ (1.12 mg, 0.005 mmol, 10 mol%). All three vials were taken into a glovebox where Na_2CO_3 (15.9 mg, 0.15 mmol, 3.0 equiv) and CsF (76.0 mg, 0.50 mmol, 10 equiv) were added to the vial containing iodoaniline **1.20**. DavePhos (3.94 mg, 0.010 mmol, 20 mol%) was then added to the vial containing $Pd(OAc)_2$. The vial containing the $Pd(OAc)_2$/DavePhos and the vial containing silyl triflate **1.13** were then each treated with an aliquot of DMF (0.25 mL each) and agitated vigorously to ensure full dissolution. The solution of $Pd(OAc)_2$/DavePhos and the solution of silyl triflate were then transferred sequentially to the reaction vial containing iodoaniline **1.20**, and the vial was sealed with a Teflon-lined cap, removed from the glovebox, and stirred for 1 h at 80 °C. The mixture was then filtered through a pad of silica gel, eluting with EtOAc (10 mL). The eluate was concentrated by iteratively azeotroping with *n*-heptane (4 x 5 mL). The crude residue was redissolved in CH_2Cl_2 (1 mL) and filtered through a pad of silica gel eluting with CH_2Cl_2 (20 mL) to remove excess Bu_4NOTf. The eluate was concentrated and purified by preparative thin layer chromatography to provide annulation products **1.21**.

General Procedure 1.6 for the scope of the racemic annulation:

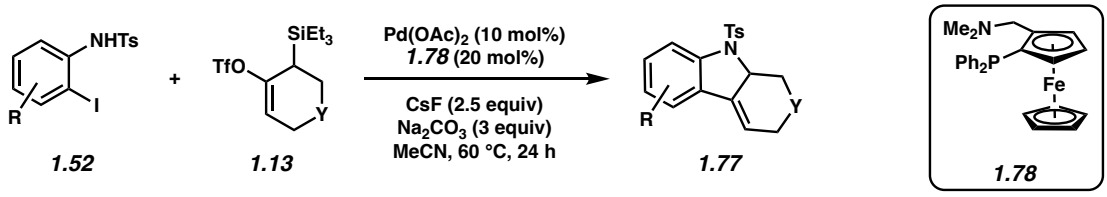

Annulation Products 1.77. A 1-dram vial containing a magnetic stir bar was charged with iodoaniline **1.52** (0.05 mmol, 1.0 equiv). A separate 1-dram vial was charged with silyl triflate **1.13** (0.075 mmol, 1.5 equiv). A third 1-dram vial was charged with $Pd(OAc)_2$ (1.12 mg, 0.005 mmol, 10 mol%). All three vials were taken into a glovebox where Na_2CO_3 (15.9 mg, 0.15 mmol, 3.0 equiv) and CsF (19.0 mg, 0.125 mmol, 2.5 equiv) were added to the vial containing iodoaniline **1.52**. Ligand **1.78** (4.27 mg, 0.010 mmol, 20 mol%) was then added to the vial containing $Pd(OAc)_2$. The vial containing the $Pd(OAc)_2$/ligand and the vial containing silyl triflate **1.13** were then each treated with an aliquot of MeCN (0.25 mL each) and agitated vigorously to ensure full dissolution. The solution of $Pd(OAc)_2$/ligand and the solution of silyl triflate were then transferred sequentially to the reaction vial containing iodoaniline **1.52**, and the vial was sealed with a Teflon-lined cap, removed from the glovebox, and stirred for 24 h at 60 °C. The mixture was then filtered through a pad of silica gel, eluting with EtOAc (10 mL). The eluate was concentrated and purified by preparative thin layer chromatography to provide annulation products **1.77**.

Any modification of the conditions shown in the general procedure above are specified in the following schemes.

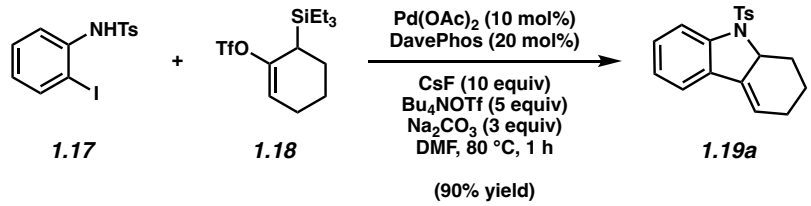

1.19a. Followed General Procedure 1.5. Purification by preparative thin layer chromatography (4:1 hexanes:acetone) generated annulation product **1.19a** (90% yield, average of two experiments: 92% yield and 88% yield) as a white solid. **Annulation product 1.19a**: Spectral data matched those reported in the literature.[56]

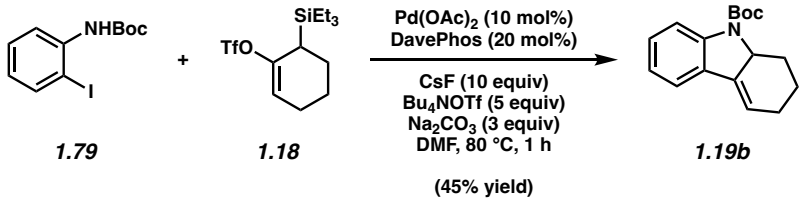

1.19b. Followed General Procedure 1.5. Purification by preparative thin layer chromatography (2:1 hexanes:CH_2Cl_2, eluted three times) generated annulation product **1.19b** (45% yield, average of two experiments: 42% yield and 48% yield) as a colorless oil. **Annulation product 1.19b**: R_f 0.32 (3:1 benzene:hexanes); ^{1}H NMR (500 MHz, DMSO-d_6): δ 7.75–7.59 (m, 1H), 7.39 (d, J = 7.6, 1H), 7.14 (t, J = 7.8, 1H), 6.93 (t, J = 7.7, 1H), 5.95 (q, J = 3.4, 1H), 4.46–4.36 (m, 1H), 2.70–2.61 (m, 1H), 2.29–2.16 (m, 2H), 1.87–1.78 (m, 1H), 1.69–1.59 (m, 1H), 1.48 (s, 9H), 1.29–1.16 (m, 1H); ^{13}C NMR (100 MHz, DMSO-d_6): δ 152.6, 144.0, 136.8, 129.1, 128.9, 123.1, 120.3, 117.7, 115.2, 81.2, 61.8, 28.4, 28.1, 24.4, 19.9; IR (film): 2975, 2932, 1704, 1384, 1158 cm^{-1}; HRMS-APCI (*m/z*) $[M + H]^+$ calcd for $C_{17}H_{22}NO_2^+$, 272.1645; found 272.1651.

*Note: **1.19b** was obtained as a mixture of rotamers. These data represent empirically observed chemical shifts from the ^{1}H and ^{13}C NMR spectra.*

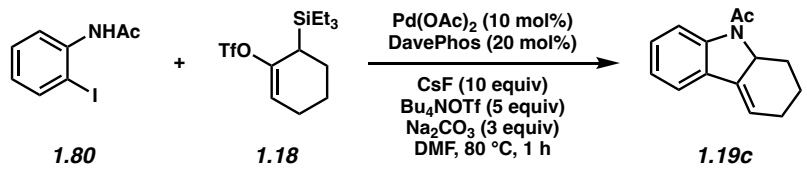

1.80 *1.18* *1.19c*

1.19c. Followed General Procedure 1.5. Purification by preparative thin layer chromatography (4:1 hexanes:acetone) generated annulation product **1.19c** (22% yield, average of two experiments: 22% yield and 22% yield) as an off-white solid. **Annulation product 1.19c**: Mp: 105–107 °C; R_f 0.29 (4:1 hexanes:acetone); ^{1}H NMR (500 MHz, DMSO-d_6): δ 8.04 (br s, 1H), 7.44 (d, J = 7.6, 1H), 7.14 (t, J = 7.6, 1H), 6.99 (t, J = 7.6, 1H), 6.00 (q, J = 3.6, 1H), 4.64 (br s, 1H), 2.67–2.49 (m, 1H), 2.31–2.18 (m, 5H), 1.84–1.76 (m, 1H), 1.75–1.62 (m, 1H), 1.32–1.21 (m, 1H); ^{13}C NMR (125 MHz, DMSO-d_6): δ 170.2, 144.3, 137.4, 129.2, 129.0, 123.9, 120.2, 117.5, 116.8, 61.8, 28.8, 24.9, 24.1, 19.5; IR (film): 2933, 1662, 1461, 1383, 1319 cm^{-1}; HRMS-APCI (*m/z*) $[M + H]^+$ calcd for $C_{14}H_{16}NO^+$, 214.1226; found 214.1226.

*Note: **1.19c** was obtained as a mixture of rotamers. These data represent empirically observed chemical shifts from the ^{1}H and ^{13}C NMR spectra.*

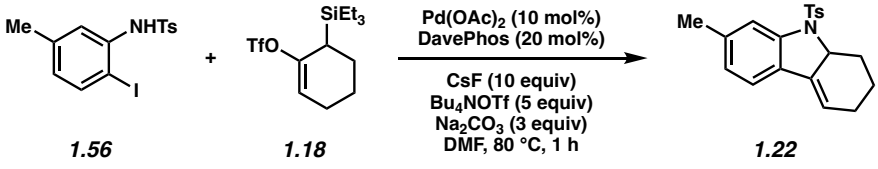

1.56 *1.18* *1.22*

1.22. Followed General Procedure 1.5. Purification by preparative thin layer chromatography (9:1 hexanes:EtOAc) generated annulation product **1.22** (89% yield, average of two experiments: 86% yield and 91% yield) as an off-white solid. **Annulation product 1.22**: Mp: 148–150 °C; R_f 0.32

(9:1 hexanes:EtOAc); ^{1}H NMR (400 MHz, C_6D_6): δ 8.03–8.00 (m, 1H), 7.72 (d, *J* = 8.3, 2H), 6.90 (d, *J* = 7.9, 1H), 6.58–6.55 (m, 1H), 6.55–6.52 (m, 2H), 5.36 (q, *J* = 3.6, 1H), 4.27–4.16 (m, 1H), 2.95 (dq, *J* = 12.1, 3.8, 1H), 2.07 (s, 3H), 1.84–1.71 (m, 2H), 1.66 (s, 3H), 1.63–1.57 (m, 1H), 1.55–1.45 (m, 1H), 1.36–1.23 (m, 1H); ^{13}C NMR (100 MHz, C_6D_6): δ 144.4, 143.4, 139.1, 135.7, 134.2, 129.3, 128.2, 127.1, 124.7, 119.8, 116.39, 116.35, 64.4, 29.2, 24.2, 21.5, 20.7, 20.1; IR (film): 2934, 1599, 1356, 1169, 665 cm^{-1}; HRMS-APCI (*m/z*) $[M + H]^+$ calcd for $C_{20}H_{22}NO_2S^+$, 340.1366; found 340.1375.

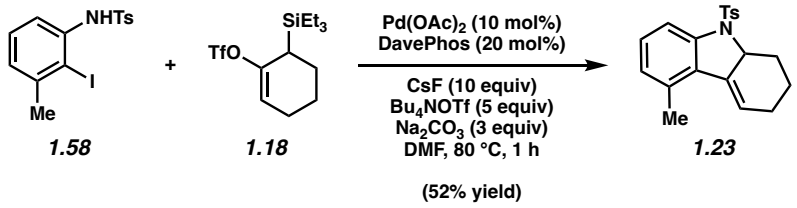

1.23. Followed General Procedure 1.5. Purification by preparative thin layer chromatography (9:1 hexanes:acetone, eluted twice) generated annulation product **1.23** (52% yield, average of two experiments: 52% yield and 51% yield) as a white solid. **Annulation product 1.23**: Mp: 99–101 °C; R_f 0.68 (9:1 benzene:Et_2O); ^{1}H NMR (500 MHz, $CDCl_3$): δ 7.68 (d, *J* = 8.5, 2H), 7.65 (d, *J* = 8.3, 1H), 7.21 (d, *J* = 8.5, 2H), 7.07 (t, *J* = 7.7, 1H), 6.78 (d, *J* = 7.7, 1H), 5.90 (q, *J* = 3.6, 1H), 4.20–4.11 (m, 1H), 2.88–2.81 (m, 1H), 2.35 (s, 3H), 2.32 (s, 3H), 2.32–2.27 (m, 2H), 1.96–1.89 (m, 1H), 1.76–1.64 (m, 2H); ^{13}C NMR (100 MHz, $CDCl_3$): δ 144.1, 143.7, 136.3, 133.7, 133.4, 129.6, 128.0, 127.8, 127.3, 126.1, 120.7, 112.8, 63.9, 29.3, 25.1, 21.5, 20.6, 19.8; IR (film): 2942, 1585, 1458, 1356, 1168 cm^{-1}; HRMS-APCI (*m/z*) $[M + H]^+$ calcd for $C_{20}H_{22}NO_2S^+$, 340.1366; found 340.1373.

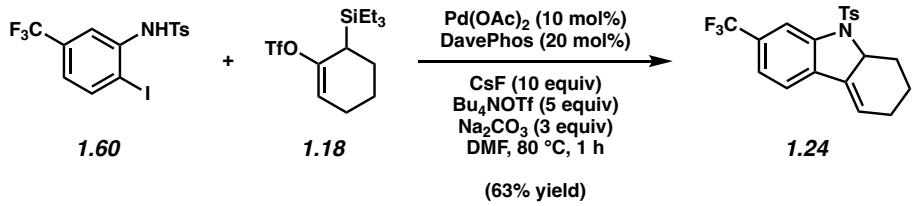

1.24. Followed General Procedure 1.5. Purification by preparative thin layer chromatography (9:1 hexanes:EtOAc) generated annulation product **1.24** (63% yield, average of two experiments: 63% yield and 63% yield) as an off-white solid. **Annulation product 1.24**: Mp: 128–130 °C; R_f 0.22 (9:1 hexanes:EtOAc); ^{1}H NMR (400 MHz, $CDCl_3$): δ 7.99 (s, 1H), 7.69 (d, J = 8.3, 2H), 7.29 (d, J = 7.9, 1H), 7.26 (d, J = 8.2, 2H), 7.22 (d, J = 8.0, 1H), 5.98 (q, J = 3.6, 1H), 4.26–4.23 (m, 1H), 2.83–2.80 (m, 1H), 2.37 (s, 3H), 2.30–2.29 (m, 2H), 2.00–1.97 (m, 1H), 1.71–1.67 (m, 2H); ^{13}C NMR (125 MHz, $CDCl_3$): δ 144.7, 143.7, 134.7, 133.1, 132.7, 130.8 (q, J = 32.4), 129.8, 127.7, 124.0 (q, J = 272.4), 121.1, 120.9 (q, J = 4.0), 120.1, 112.3 (q, J = 4.0), 64.5, 29.0, 24.6, 21.6, 20.0; ^{19}F NMR (376 MHz, $CDCl_3$) δ –62.25 (s, 3F); IR (film): 2935, 1430, 1324, 1167, 1124 cm^{-1}; HRMS-APCI (*m/z*) $[M + H]^+$ calcd for $C_{20}H_{19}F_3NO_2S^+$, 394.1087; found 394.1083.

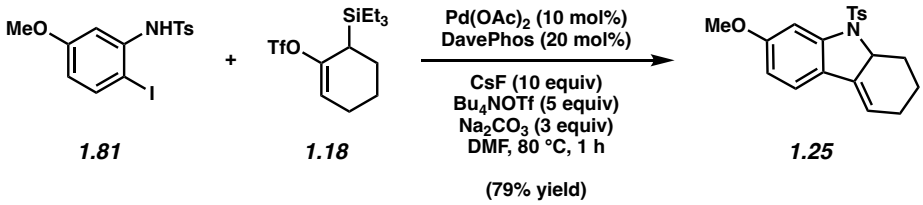

1.25. Followed General Procedure 1.5. Purification by preparative thin layer chromatography (4:1 hexanes:acetone, eluted twice) generated annulation product **1.25** (79% yield, average of two experiments: 78% yield and 79% yield) as a white solid. **Annulation product 1.25**: Mp: 104–107 °C; R_f 0.58 (9:1 benzene:Et_2O); ^{1}H NMR (500 MHz, $CDCl_3$): δ 7.70 (d, J = 8.2, 2H), 7.38 (d, J = 2.4, 1H), 7.24 (d, J = 8.2, 2H), 7.13 (d, J = 8.2, 1H), 6.54 (dd, J = 8.2, 2,4, 1H), 5.67 (q, J = 3.6,

1H), 4.20–4.10 (m, 1H), 3.84 (s, 3H), 2.81–2.74 (m, 1H), 2.37 (s, 3H), 2.29–2.17 (m, 2H), 1.98–1.90 (m, 1H), 1.75–1.59 (m, 2H); ^{13}C NMR (100 MHz, $CDCl_3$): δ 160.8, 144.8, 144.2, 135.1, 133.4, 129.7, 127.7, 122.4, 120.6, 115.4, 110.4, 101.2, 64.8, 55.7, 29.2, 24.4, 21.6, 20.2; IR (film): 2938, 1738, 1607, 1489, 1355 cm^{-1}; HRMS-APCI (*m/z*) [M + H]$^+$ calcd for $C_{20}H_{22}NO_3S^+$, 356.1315; found 356.1312.

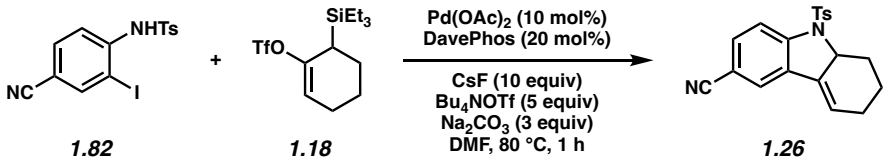

1.26. Followed General Procedure 1.5. Purification by preparative thin layer chromatography (4:1 hexanes:EtOAc) generated annulation product **1.26** (56% yield, average of two experiments: 56% yield and 56% yield) as a yellow solid. **Annulation product 1.26**: Mp: 187 °C; R_f 0.11 (9:1 hexanes:EtOAc); ^{1}H NMR (400 MHz, $CDCl_3$): δ 7.79 (d, *J* = 8.9, 1H), 7.72–7.67 (m, 2H), 7.49–7.43 (m, 2H), 7.30–7.26 (m, 2H), 5.96 (q, *J* = 3.6, 1H), 4.31–4.21 (m, 1H), 2.86–2.74 (m, 1H), 2.39 (s, 3H), 2.34–2.22 (m, 2H), 2.05–1.93 (m, 1H), 1.75–1.59 (m, 2H); ^{13}C NMR (100 MHz, $CDCl_3$): δ 146.9, 145.0, 133.7, 133.4, 133.1, 130.4, 130.0, 127.5, 123.7, 121.3, 118.9, 115.4, 107.0, 64.7, 28.9, 24.6, 21.6, 19.9; IR (film): 2937, 2225, 1608, 1469, 1365 cm^{-1}; HRMS-APCI (*m/z*) [M + H]$^+$ calcd for $C_{20}H_{19}N_2O_2S^+$, 351.1162; found 351.1169.

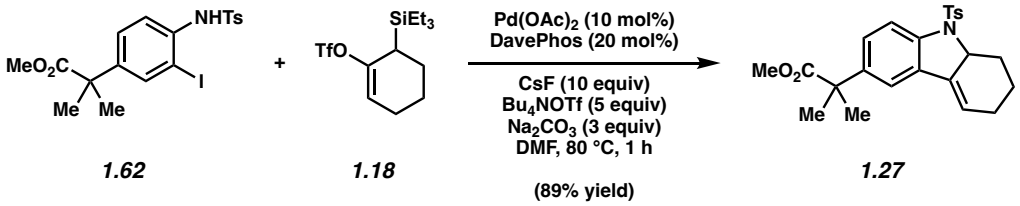

1.27. Followed General Procedure 1.5. Purification by preparative thin layer chromatography (4:1 hexanes:acetone, eluted three times) afforded annulation product **1.27** (89% yield, average of two experiments: 87% yield and 91% yield) as a white solid. **Annulation product 1.27**: Mp: 123–125; R_f 0.30 (4:1 hexanes:acetone); ^{1}H NMR (500 MHz, $CDCl_3$): δ 7.60 (d, J = 8.2, 2H), 7.57 (d, J = 8.6, 1H), 7.16–7.10 (m, 3H), 7.05 (dd, J = 9.0, 1.9, 1H), 5.76 (q, J = 3.5, 1H), 4.12–4.04 (m, 1H), 3.53 (s, 3H), 2.73–2.64 (m, 1H), 2.27 (s, 3H), 2.21–2.10 (m, 2H), 1.90–1.81 (m, 1H), 1.61–1.53 (m, 2H), 1.43 (s, 6H); ^{13}C NMR (125 MHz, $CDCl_3$): δ 177.1, 144.2, 142.2, 140.3, 135.6, 133.6, 129.7, 129.4, 127.7, 126.5, 118.2, 117.2, 115.0, 64.4, 52.3, 46.1, 29.0, 26.7 26.5, 24.5, 21.6, 20.2; IR (film): 2947, 1730, 1478, 1361, 1167 cm^{-1}; HRMS-APCI (*m/z*) [M + H]$^+$ calcd for $C_{24}H_{28}NO_4S^+$, 426.1734; found 426.1730.

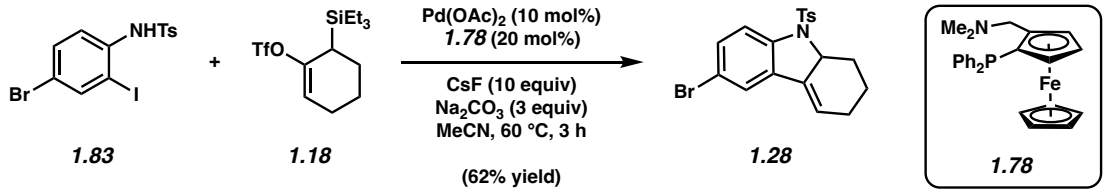

1.28. Followed a modified version of General Procedure 1.6 by altering the amount of silyl triflate **1.18** (17.2 mg, 0.05 mmol, 1.0 equiv), CsF (76.0 mg, 0.500 mmol, 10.0 equiv), and MeCN (0.66 mL in total, 0.075 M) used and by decreasing the reaction time to 3 h. Purification by preparative thin layer chromatography (9:1 hexanes:EtOAc) afforded annulation product **1.28** (62% yield, average of two experiments: 63% yield and 61% yield) as a white solid. **Annulation product 1.28**: Mp: 165–166 °C; R_f 0.4 (9:1 hexanes:EtOAc); ^{1}H NMR (500 MHz, C_6D_6): δ 7.82 (d, J = 8.7, 1H),

7.63 (d, J = 8.3, 2H), 7.11–7.07 (m, 2H), 6.57 (d, J = 8.2, 2H), 5.12 (q, J = 3.7, 1H), 4.15–4.07 (m, 1H), 2.91–2.85 (dq, J = 12.0, 4.19, 1H), 1.71 (s, 3H), 1.69–1.63 (m, 2H), 1.52–1.42 (m, 2H), 1.27–1.18 (m, 1H); ^{13}C NMR (125 MHz, $CDCl_3$): δ 144.5, 142.5, 134.5, 133.0, 131.6, 131.5, 129.8, 127.7, 123.1, 119.8, 116.9, 116.8, 64.4, 29.0, 24.6, 21.6, 20.1; IR (film): 2935, 1458, 1361, 1166, 665 cm^{-1}; HRMS-APCI (m/z) $[M + H]^+$ calcd for $C_{19}H_{19}BrNO_2S^+$, 404.0314; found 404.0310.

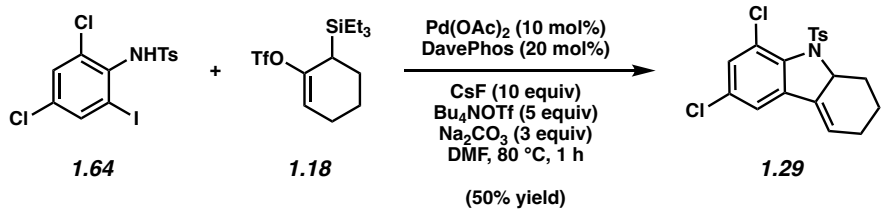

1.29. Followed General Procedure 1.5. Purification by preparative thin layer chromatography (4:1 hexanes:acetone, eluted twice) generated annulation product **1.29** (50% yield, average of two experiments: 49% yield and 50% yield) as a white solid. **Annulation product 1.29**: Mp: 119–121 °C; R_f 0.41 (4:1 hexanes:acetone); ^{1}H NMR (500 MHz, C_6D_6): δ 7.76 (d, J = 8.3, 2H), 6.93 (d, J = 1.8, 1H), 6.84 (d, J = 1.8, 1H), 6.71 (d, J = 8.3, 2H), 5.15 (q, J = 3.5, 1H), 5.01–4.93 (m, 1H), 2.64–2.54 (m, 1H), 1.81 (s, 3H), 1.76–1.67 (m, 2H), 1.44–1.36 (m, 1H), 1.35–1.17 (m, 2H); ^{13}C NMR (125 MHz, $CDCl_3$): δ 143.6, 139.9, 138.1, 134.9, 134.4, 130.2, 130.1, 129.3, 127.0, 122.7, 120.5, 118.4, 65.1, 28.9, 24.6, 21.6, 19.8; IR (film): 2933, 1563, 1443, 1341, 1162 cm^{-1}; HRMS-APCI (m/z) $[M + H]^+$ calcd for $C_{19}H_{18}Cl_2NO_2S^+$, 394.0430; found 394.0434.

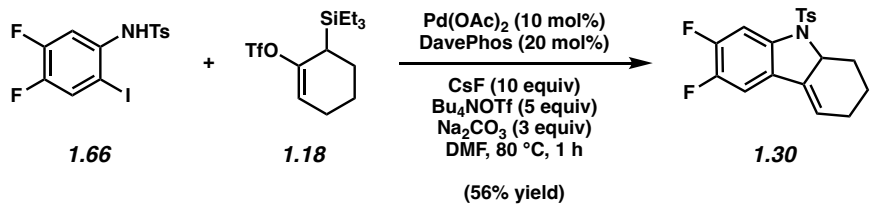

1.30. Followed General Procedure 1.5. Purification by preparative thin layer chromatography (4:1 hexanes:acetone, eluted twice) generated annulation product **1.30** (56% yield, average of two experiments: 53% yield and 59% yield) as a colorless crystalline solid. **Annulation product 1.30**: Mp: 169–171 °C; R_f 0.39 (4:1 hexanes:acetone); ^{1}H NMR (500 MHz, C_6D_6): δ 7.97 (dd, J = 11.4, 7.0, 1H), 7.59 (d, J = 8.3, 2H), 6.59 (d, J = 8.3, 2H), 6.51 (dd, J = 9.1, 8.3, 1H), 5.08 (q, J = 3.7, 1H), 4.17–4.04 (m, 1H), 2.89 (dq, J = 11.1, 3.3, 1H), 1.77–1.67 (m, 2H), 1.73 (s, 3H), 1.58–1.45 (m, 2H), 1.30–1.17 (m, 1H); ^{13}C NMR (100 MHz, $CDCl_3$): δ 150.4 (dd, J = 247.7, 14.3), 147.6 (dd, J = 245.0, 14.3), 144.7, 139.3 (dd, J = 9.1, 1.6), 134.2 (app. t, J = 2.1), 132.8, 129.9, 127.7, 125.5 (dd, J = 6.3, 3.4), 118.9 (d, J = 1.8), 108.3 (d, J = 19.8), 105.2 (d, J = 24.4), 64.5, 28.9, 24.4, 21.6, 19.9; ^{19}F NMR (376 MHz, C_6D_6): δ –134.7 (ddd, J = 20.8, 11.3, 7.8, 1F), –143.2 (ddd; J = 20.8, 9.6, 6.9, 1F); IR (film): 2936, 1610, 1599, 1487, 1359 cm^{-1}; HRMS-APCI (*m/z*) $[M + H]^+$ calcd for $C_{19}H_{18}F_2NO_2S^+$, 362.1021; found 362.1020.

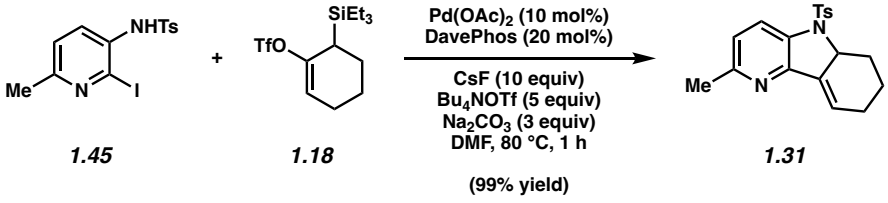

1.31. Followed General Procedure 1.5. Purification by preparative thin layer chromatography (9:1 benzene:MeCN) afforded annulation product **1.31** (99% yield, average of two experiments: 99% yield and 99% yield) as a white solid. **Annulation product 1.31**: Mp: 168–170 °C; R_f 0.27 (4:1

hexanes:acetone); ^{1}H NMR (500 MHz, C_6D_6): δ 8.04 (d, *J* = 8.3, 1H), 7.65 (d, *J* = 8.2, 2H), 6.59 (d, *J* = 8.1, 2H), 6.49 (d, *J* = 8.4, 1H), 6.32 (q, *J* = 3.5, 1H), 4.24–4.17 (m, 1H), 2.89 (m, *J* = 4.1, 1H), 2.27 (s, 3H), 1.79–1.73 (m, 2H), 1.72 (s, 3H), 1.61–1.52 (m, 1H), 1.48–1.41 (m, 1H), 1.30–1.18 (m, 1H); ^{13}C NMR (125 MHz, $CDCl_3$): δ 154.1, 148.1, 144.6, 136.2, 135.1, 132.9, 129.8, 127.7, 122.7, 122.4, 121.6, 63.1, 29.0, 24.6, 23.8, 21.6, 20.2; IR (film): 3034, 2933, 1425, 1360, 1166 cm^{-1}; HRMS-APCI (*m/z*) $[M + H]^+$ calcd for $C_{19}H_{21}N_2O_2S^+$, 341.1318; found 341.1313.

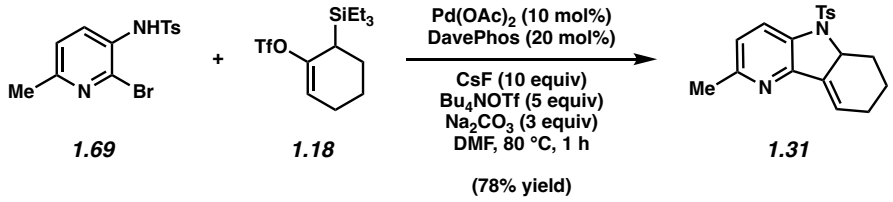

1.31. Followed General Procedure 1.5. Purification by preparative thin layer chromatography (9:1 benzene:MeCN) generated annulation product **1.31** (78% yield, average of two experiments: 75% yield and 80% yield) as a white solid. **Annulation product 1.31**: Spectral data matched those observed for the product obtained from the annulation of **1.45**.

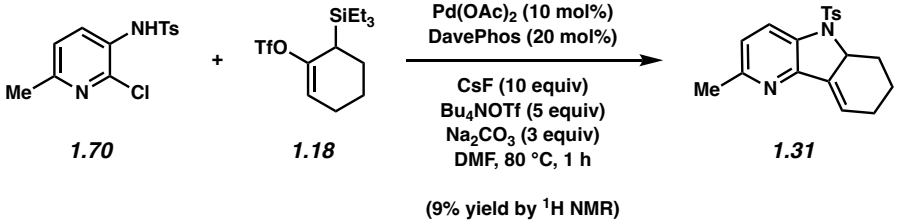

1.31. Followed modified version of General Procedure 1.5 by adding 1,3,5-trimethoxybenzene (0.33 equiv) as an external standard following the workup. Analysis of the crude reaction material by ^{1}H NMR showed annulation product **1.31** (9% yield, average of two experiments: 7% yield and

11% yield). **Annulation product 1.31**: Spectral data matched those observed for the product obtained from the annulation of **1.45**.

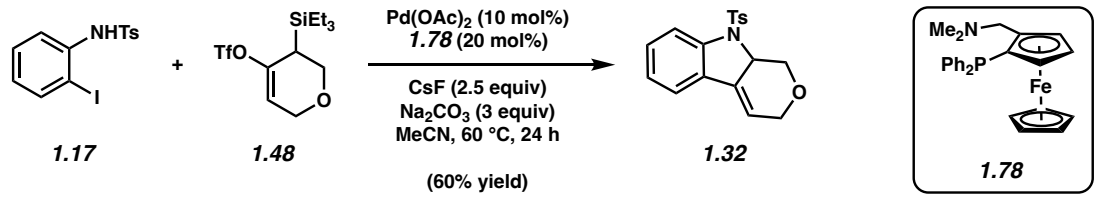

1.32. Followed General Procedure 1.6. Purification by preparative thin layer chromatography (9:1 benzene:Et_2O) afforded annulation product **1.32** (60% yield, average of two experiments: 58% yield and 62% yield) as a white solid. **Annulation product 1.32**: Mp: 161–163 °C; R_f 0.47 (9:1 benzene:Et_2O); ^{1}H NMR (500 MHz, $CDCl_3$): δ 7.79 (d, *J* = 8.1, 1H), 7.73 (d, *J* = 8.3, 2H), 7.28–7.22 (m, 4H), 7.02 (t, *J* = 7.5, 1H), 5.81 (q, *J* = 2.8, 1H), 4.77 (dd, *J* = 10.1, 5.1, 1H), 4.46–4.23 (m, 3H), 3.57 (t, *J* = 9.8, 1H), 2.36 (s, 3H); ^{13}C NMR (125 MHz, $CDCl_3$): δ 144.7, 143.5, 133.8, 132.4, 129.8, 129.7, 128.4, 127.9, 124.2, 120.7, 115.6, 115.3, 67.4, 65.5, 59.9, 21.6; IR (film): 2925, 2874, 1599, 1459, 1354 cm^{-1}; HRMS-APCI (*m/z*) $[M + H]^+$ calcd for $C_{18}H_{18}NO_3S^+$, 328.1002; found 328.0999.

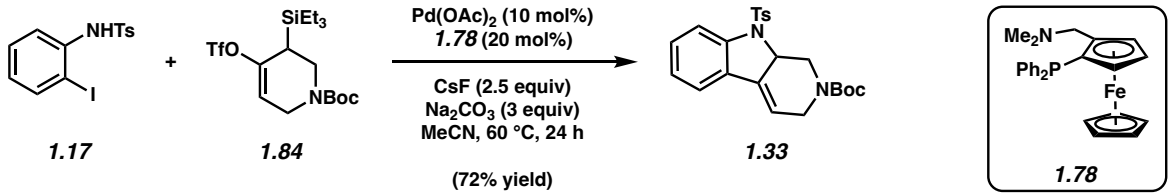

1.33. Followed General Procedure 1.6. Purification by preparative thin layer chromatography (9:1 benzene:Et_2O) afforded annulation product **1.33** (72% yield, average of two experiments: 74% yield and 69% yield) as a beige solid. **Annulation product 1.33**: Mp: 185–188 °C; R_f 0.41 (9:1 benzene:Et_2O); ^{1}H NMR (600 MHz, $CDCl_3$): δ 7.81 (d, *J* = 8.3, 1H), 7.79–7.63 (m, 2H), 7.29–

7.26 (m, 1H), 7.26–7.21 (m, 3H), 7.02 (t, J = 7.6, 1H), 5.90–5.75 (m, 1H), 5.25–4.96 (m, 1H), 4.58–4.25 (m, 1H), 4.25–4.02 (m, 1H), 3.91–3.67 (m, 1H), 2.99–2.78 (m, 1H), 2.37 (s, 3H), 1.61–1.40 (m, 9H); ^{13}C NMR (125 MHz, $CDCl_3$): δ 154.8, 144.7, 143.7, 135.0, 132.8, 132.5, 129.8, 129.7, 128.1, 127.8, 124.3, 120.6, 115.4, 114.5, 113.9, 80.4, 60.9, 46.4, 45.1, 43.9, 43.3, 29.7, 28.5, 21.6; IR (film): 2976, 2930, 1698, 1459, 1365 cm^{-1}; HRMS-APCI (*m/z*) [M + H]$^+$ calcd for $C_{23}H_{27}N_2O_4S^+$, 427.1686; found 427.1679.

*Note: **1.33** was obtained as a mixture of rotamers. These data represent empirically observed chemical shifts from the ^{1}H and ^{13}C NMR spectra.*

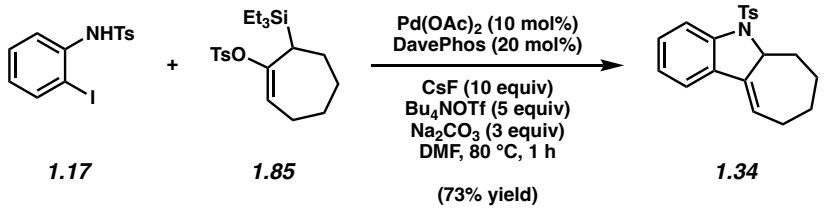

1.34. Followed General Procedure 1.5. Purification by preparative thin layer chromatography (97:3 benzene:Et_2O) afforded annulation product **1.34** (73% yield, average of two experiments: 74% yield and 73% yield) as a white solid. **Annulation product 1.34**: Mp: 186–188 °C; R_f 0.36 (9:1 hexanes:EtOAc); ^{1}H NMR (500 MHz, $CDCl_3$): δ 7.69 (d, J = 8.3, 1H), 7.60 (d, J = 8.3, 2H), 7.23–7.15 (m, 4H), 6.99 (t, J = 7.6, 1H), 6.20 (ddd, J = 9.0, 5.2, 2.9, 1H), 4.63 (dq, J = 11.1, 1.8, 1H), 2.50–2.43 (m, 1H), 2.32 (s, 3H), 2.31–2.28 (m, 1H), 2.18–2.04 (m, 2H), 1.85–1.74 (m, 2H), 1.68–1.60 (m, 1H), 1.37–1.23 (m, 1H); ^{13}C NMR (125 MHz, $CDCl_3$): δ 143.9, 143.1, 141.7, 134.3, 129.7, 129.6, 128.8, 127.3, 124.2, 119.9, 119.8, 116.2, 68.1, 34.7, 30.0, 28.6, 27.5, 21.6; IR (film): 2923, 1462, 1353, 1168, 578 cm^{-1}; HRMS-APCI (*m/z*) [M + H]$^+$ calcd for $C_{20}H_{22}NO_2S^+$, 340.1366; found 340.1365.

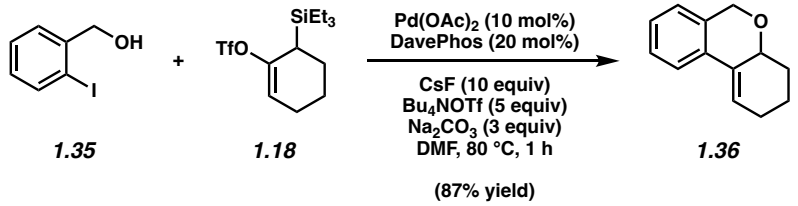

1.35 *1.18* *1.36*

1.36. Followed General Procedure 1.5. Purification by preparative thin layer chromatography (9:1 hexanes:EtOAc, eluted twice) generated annulation product **1.36** (87% yield, average of two experiments: 84% yield and 89% yield) as a colorless oil. **Annulation product 1.36**: R_f 0.58 (4:1 hexanes:acetone); ^{1}H NMR (500 MHz, $CDCl_3$): δ 7.58 (d, J = 7.9, 1H), 7.23–7.13 (m, 2H), 7.00 (d, J = 7.4, 1H), 6.40–6.34 (m, 1H), 4.89 (d, J = 15.0, 1H), 4.81 (d, J = 14.8, 1H), 4.26–4.17 (m, 1H), 2.39–2.17 (m, 3H), 1.96–1.83 (m, 1H), 1.68–1.59 (m, 2H); ^{13}C NMR (100 MHz, $CDCl_3$): δ 133.8, 132.1, 131.4, 126.9, 126.8, 124.6, 122.6, 121.3, 73.9, 68.3, 29.7, 26.0, 20.3; IR (film): 3032, 2938, 2863, 1721, 1447 cm^{-1}; HRMS-APCI (*m/z*) $[M + H]^+$ calcd for $C_{13}H_{15}O^+$, 187.1174; found 187.1172.

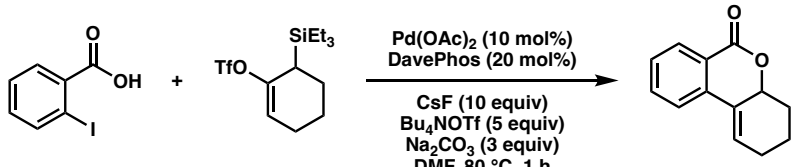

1.37 *1.18* *1.38*

1.38. Followed General Procedure 1.5. Purification by preparative thin layer chromatography (19:1 benzene:Et_2O) generated annulation product **1.38** (46% yield, average of two experiments: 45% yield and 47% yield) as a colorless oil. **Annulation product 1.38**: R_f 0.44 (CH_2Cl_2); ^{1}H NMR (500 MHz, $CDCl_3$): δ 8.11 (d, J = 7.8, 1H), 7.57 (t, J = 7.6, 1H), 7.50 (d, J = 7.8, 1H), 7.40 (t, J = 7.6, 1H), 6.52–6.43 (m, 1H), 5.11 (app. s, 1H), 2.44–2.21 (m, 3H), 2.03–1.86 (m, 2H), 1.75–1.62 (m, 1H); ^{13}C NMR (100 MHz, $CDCl_3$): δ 165.3, 137.9, 133.9, 130.3, 129.3, 128.9, 128.2, 123.4, 122.7,

75.3, 29.0, 25.8, 19.8; IR (film): 3063, 1719, 1657, 1599, 1276 cm^{-1}; HRMS-APCI (*m/z*) $[M + H]^+$ calcd for $C_{13}H_{13}O_2^+$, 201.0910; found 201.0888.

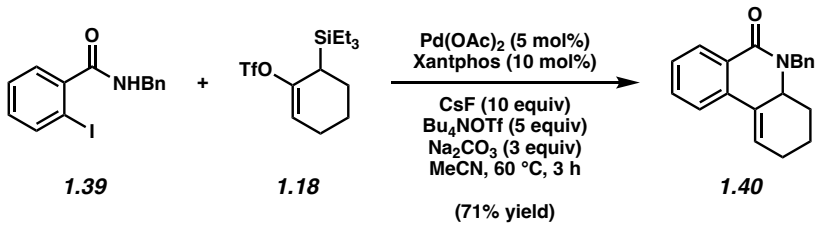

1.40. A 1-dram vial containing a magnetic stir bar was charged with benzamide **1.39** (16.9 mg, 0.05 mmol, 1.0 equiv), Bu_4NOTf (98.7 mg, 0.25 mmol, 5.0 equiv), and Xantphos (2.9 mg, 0.005 mmol, 10 mol%). A separate 1-dram vial was charged with silyl triflate **1.18** (17.2 mg, 0.075 mmol, 1.5 equiv). Both vials were taken into a glovebox where Na_2CO_3 (15.9 mg, 0.150 mmol, 3.0 equiv) and CsF (76.0 mg, 0.500 mmol, 10.0 equiv) were added to the vial containing benzamide **1.39**. The vial containing silyl triflate **1.18** was then treated with an aliquot of MeCN (0.33 mL) and agitated to ensure full dissolution. $Pd(OAc)_2$ (0.6 mg, 0.0025 mmol, 5 mol%) in MeCN (0.33 mL) was then added to the vial containing benzamide **1.39** from a freshly prepared stock solution. Subsequently, silyl triflate **1.18** in MeCN was also transferred to the reaction vial containing benzamide **1.39**. The vial was sealed with a Teflon-lined cap, removed from the glovebox, and stirred for 3 h at 60 °C. The mixture was then filtered through a pad of silica gel, eluting with EtOAc (10 mL). The eluate was concentrated and purified by preparative thin layer chromatography (9:1 benzene:MeCN) to provide annulation product **1.40** as a white solid (71% yield, average of two experiments: 71% yield and 72% yield). **Annulation product 1.40**: Spectral data matched those reported in the literature.[33]

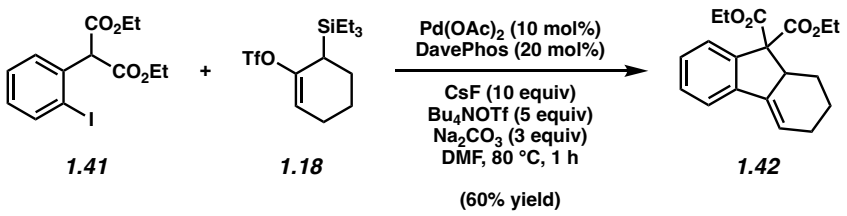

1.42. Followed General Procedure 1.5. Purification by preparative thin layer chromatography (99:1 benzene:MeCN, eluted twice) generated annulation product **1.42** (60% yield, average of two experiments: 59% yield and 60% yield) as a colorless oil. **Annulation product 1.42**: R_f 0.77 (CH_2Cl_2); ^{1}H NMR (500 MHz, $CDCl_3$): δ 7.64 (d, J = 7.7, 1H), 7.45 (d, J = 7.7, 1H), 7.30 (dt, J = 7.5, 1.0, 1H), 7.24 (dt, J = 7.5, 1.0, 1H), 6.10 (q, J = 3.5, 1H), 4.38–4.29 (m, 2H), 4.18 (dq, J = 10.9, 7.1, 1H), 4.10 (dq, J = 10.9, 7.1, 1H), 3.64–3.54 (m, 1H), 2.32–2.15 (m, 3H), 2.03–1.95 (m, 1H), 1.76–1.65 (m, 1H), 1.37 (t, J = 7.0, 3H), 1.35–1.27 (m, 1H), 1.20 (t, J = 7.1, 3H); ^{13}C NMR (100 MHz, $CDCl_3$): δ 170.0, 169.6, 141.5, 140.1, 139.7, 128.7, 127.8, 125.9, 120.1, 118.6, 67.1, 61.7, 61.3, 47.6, 25.1, 24.9, 22.6, 14.2; IR (film): 2981, 2833, 1728, 1467, 1248 cm^{-1}; HRMS-APCI (*m/z*) $[M + H]^+$ calcd for $C_{19}H_{23}O_4^+$, 315.1591; found 315.1554.

1.8.2.5 Diastereoselective Annulation

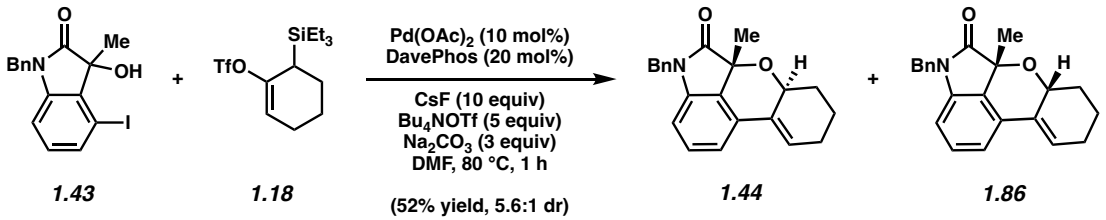

1.44 and **1.86**. Followed General Procedure 1.5. Purification by preparative TLC (4:1 hexanes:acetone, eluted 3 times) afforded major diastereomer **1.44** and minor diastereomer **1.86**, each as a waxy amorphous solid (52% combined yield, 5.6:1 dr (determined by ^{1}H NMR analysis of the crude mixture), average of two experiments: 53% combined yield, 5.6:1 dr and 51%

combined yield, 5.6:1 dr). **Annulation Product 1.44** (major diastereomer): R_f 0.35 (4:1 hexanes:acetone); ^{1}H NMR (500 MHz, $CDCl_3$): δ 7.33–7.23 (m, 5H), 7.14 (t, *J* = 7.8, 1H), 6.91 (d, *J* = 7.7, 1H), 6.53 (d, *J* = 7.7, 1H), 6.25–6.21 (m, 1H), 5.07 (d, *J* = 15.6, 1H), 4.58 (d, *J* = 15.6, 1H), 4.34–4.28 (m, 1H), 2.40–2.18 (m, 3H), 1.93–1.80 (m, 2H), 1.75–1.63 (m, 1H), 1.57 (s, 3H); ^{13}C NMR (125 MHz, $CDCl_3$): δ 178.8, 139.9, 136.0, 132.4, 131.9, 129.4, 129.2, 128.8, 127.7, 127.4, 126.5, 117.1, 107.4, 74.6, 74.4, 43.8, 32.2, 25.9, 25.7, 21.1; IR (film): 2924, 2854, 1730, 1608, 1473 cm^{-1}; HRMS-APCI (*m/z*) $[M + H]^+$ calcd for $C_{22}H_{22}NO_2^+$, 332.1645; found 332.1634. **Annulation product 1.86** (minor diastereomer): R_f 0.32 (4:1 hexanes:acetone); ^{1}H NMR (500 MHz, $CDCl_3$): δ 7.34–7.28 (m, 5H), 7.13–7.03 (m, 2H), 6.44 (d, *J* = 7.2, 1H), 6.35–6.31 (m, 1H), 5.13 (d, *J* = 15.7, 1H), 4.88–4.83 (m, 1H), 4.46, (d, *J* = 15.7, 1H), 2.32–2.23 (m, 3H), 2.01–1.93 (m, 1H), 1.83–1.71 (m, 1H), 1.77 (s, 3H), 1.68–1.61 (m, 1H); ^{13}C NMR (125 MHz, $CDCl_3$): δ 179.2, 140.9, 136.0, 131.1, 129.2, 129.1, 128.8, 128.4, 127.7, 127.4, 124.2, 114.9, 106.7, 75.4, 71.1, 43.7, 29.3, 25.8, 22.5, 20.7; IR (film): 2930, 2865, 1729, 1604, 1469 cm^{-1}; HRMS-APCI (*m/z*) $[M + H]^+$ calcd for $C_{22}H_{22}NO_2^+$, 332.1645; found 332.1638.

The structure of **1.86** was verified by 2D-NOESY, as the following interaction was observed:

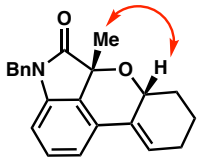

1.86

1.8.2.6 Optimization of the Asymmetric Annulation

Results from the optimization of the asymmetric annulation reaction between **1.17** and **1.18** appear below. Ligand, solvent, fluoride source, palladium source, and base were varied using General Procedure 1.7, and results appear below in Tables 1.6, 1.7, 1.8, 1.9, and 1.10 respectively.

General Procedure 1.7 for the optimization of the asymmetric annulation:

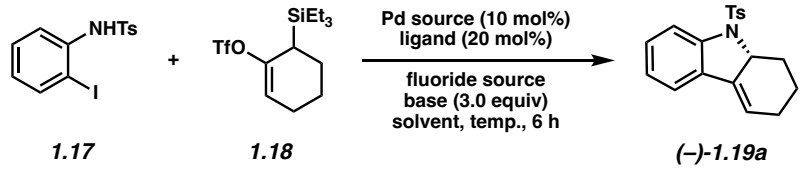

1.17 *1.18* *(–)-1.19a*

(–)-1.19a. Inside a glovebox, a 1-dram vial was charged with the base (0.09 mmol, 3.0 equiv), the ligand (0.006 mmol, 20 mol%), and the fluoride source as solids. The vial was then treated sequentially with separate freshly prepared stock solutions of iodoaniline **1.17** (11.3 mg, 0.03 mmol, 1.0 equiv), the palladium source (10 mol% Pd), and silyl triflate **1.18** (10.3 mg, 0.03 mmol, 1.0 equiv) to give a final reaction concentration of 0.075 M. The vial was sealed with a Teflon-lined cap, removed from the glovebox, and stirred for 6 h at the desired reaction temperature. After 6 h, 6-acetylbenzothiophene (2.0 mg, 0.011 mmol, 0.38 equiv) was added to the reaction as an external standard for subsequent quantitative analysis by SFC. The mixture was then filtered through a pad of silica gel, eluting with MeCN (10 mL). The eluate was analyzed directly by SFC to determine the yield of **(–)-1.19a** and degree of enantioenrichment.

*The stereochemistry depicted for **(–)-1.19a** is not necessarily representative of the major enantiomer observed for all ligands screened. Any modification of the conditions shown in the general procedure above are specified in the following tables.*

A range of ligands (see Figure 1.5 below for ligand structures) were screened using General Procedure 1.7, and results of these screening reactions appear below in Table 1.6.

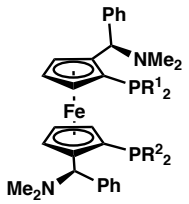

Mandyphos

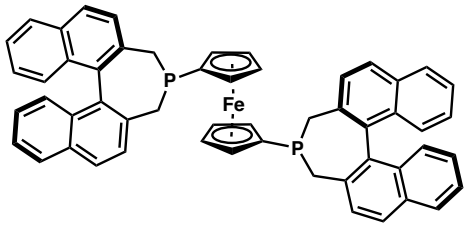

BINAPHANE

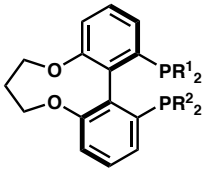

Tunephos

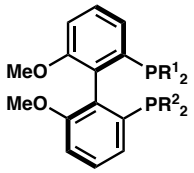

MeO-BIPHEP

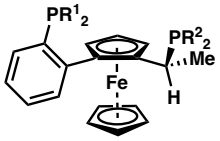

Walphos

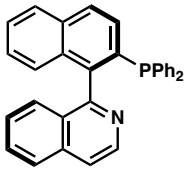

QUINAP

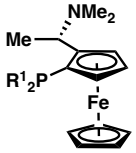

PPFA

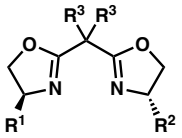

BOX

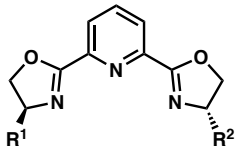

PyBOX

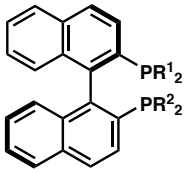

BINAP

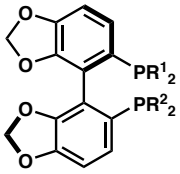

SEGPHOS

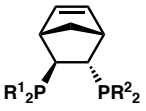

Norphos

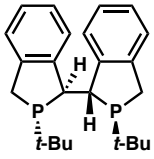

DuanPhos

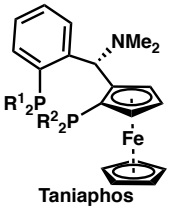

Taniaphos

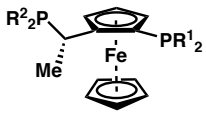

Josiphos

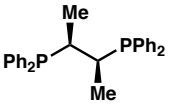

Chiraphos

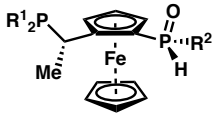

JosPOphos

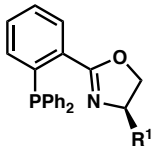

PHOX

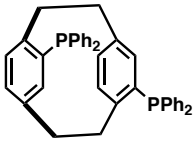

Phanephos

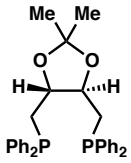

DIOP

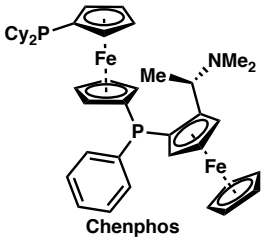

Chenphos

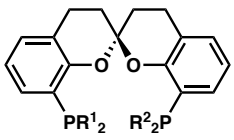

SKP

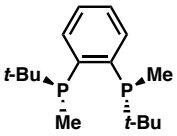

BenzP*

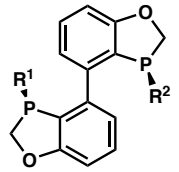

BABIBOP

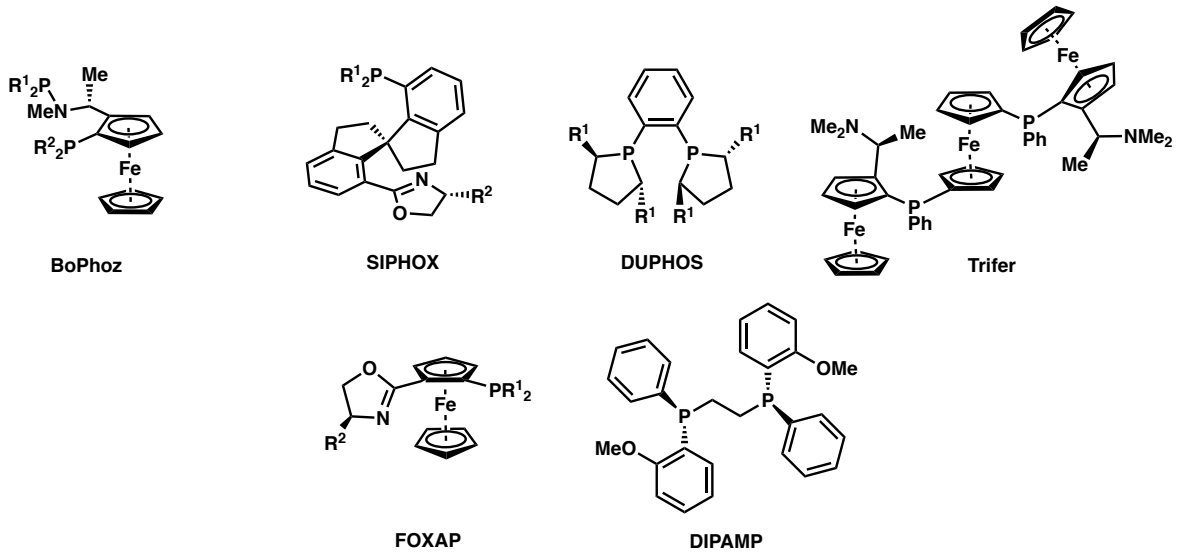

Figure 1.5. Ligand families evaluated during asymmetric reaction development.

Table 1.6. Chiral ligand screen results. See Figure 1.5 above for ligand classes (absolute stereochemistry of product may differ between table entries).

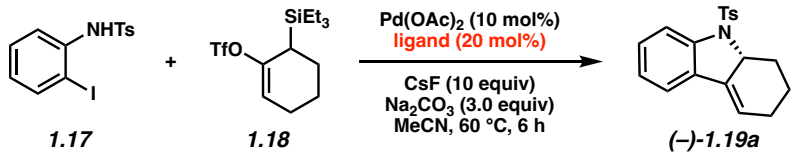

Entry	Ligand Class	R^1	R^2	Yield[a]	%ee
1	Mandyphos	3,5-bis(trifluoromethyl) phenyl	3,5-bis(trifluoromethyl) phenyl	69%	69%
2	Mandyphos	3,5-xylyl	3,5-xylyl	74%	41%
3	Mandyphos	4-methoxy-3,5-xylyl	4-methoxy-3,5-xylyl	63%	47%
4	Mandyphos	Cy	Cy	68%	47%
5	Mandyphos	Ph	Ph	52%	35%
6	Binaphane	N/A	N/A	28%	4%
7	Tunephos	Ph	Ph	37%	5%
8	MeO-BIPHEP	Ph	Ph	40%	1%
9	Walphos	Ph	3,5-bis(trifluoromethyl) phenyl	14%	13%
10	QUINAP	N/A	N/A	29%	8%
11	PPFA	Cy	N/A	95%	40%
12	BOX (R^3 = Me)	*t*-Bu	*t*-Bu	18%	1%

13	PyBOX	*i*-Pr	*i*-Pr	6%	6%
14	BINAP	3,5-xylyl	3,5-xylyl	4%	21%
15	SEGPHOS	Ph	Ph	6%	38%
16	Norphos	Ph	Ph	1%	33%
17	Duanphos	N/A	N/A	7%	28%
18	Taniaphos	Ph	Ph	43%	9%
19	Josiphos	Ph	Cy	0%	N/A
20	Chiraphos	N/A	N/A	0%	N/A
21	JosPOphos	*t*-Bu	Ph	12%	15%
22	PHOX	*i*-Pr	N/A	7%	23%
23	Phanephos	N/A	N/A	61%	18%
24	DIOP	N/A	N/A	13%	3%
25	Chenphos	N/A	N/A	77%	26%
26	SKP	Ph	Ph	71%	10%
27	BenzP*	N/A	N/A	0%	N/A
28	BABIBOP	*t*-Bu	*t*-Bu	4%	73%
29	BoPhoz	Ph	Ph	74%	0%
30	SiPHOX	Ph	Bn	3%	6%
31	DUPHOS	Me	N/A	18%	6%
32	Trifer	N/A	N/A	80%	60%
33	FOXAP	Ph	*i*-Pr	9%	12%
34	DIPAMP	N/A	N/A	10%	15%

[a] Yield determined by quantitative SFC analysis using 6-acetylbenzothiophene as an external standard.

Table 1.7. Solvent screening results.

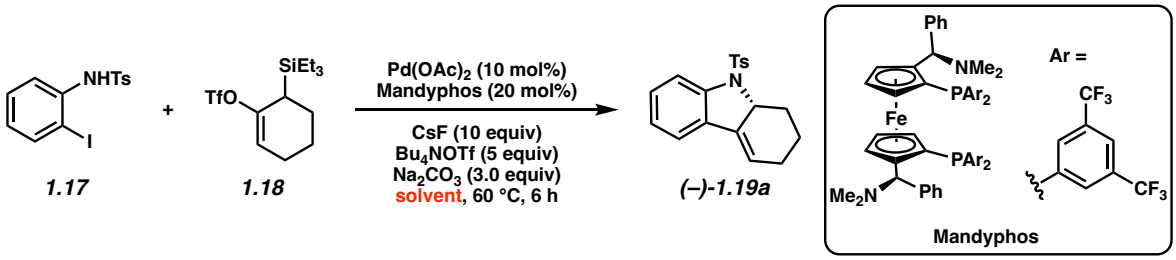

Entry	Solvent	Yield[a]	%ee
1[b]	CH_2Cl_2	24%	80%
2	1,2-dichloroethane	16%	72%
3	acetonitrile	90%	65%
4	THF	63%	65%
5	1,2-dimethoxyethane	40%	61%
6	1,4-dioxane	79%	61%

7	DMF	28%	45%
8	PhMe	68%	43%
9	pyridine	42%	34%

[a] Yield determined by quantitative SFC analysis using 6-acetylbenzothiophene as an external standard. [b] Reaction carried out at 35 °C due to solvent volatility.

Table 1.8. Fluoride source screening results.

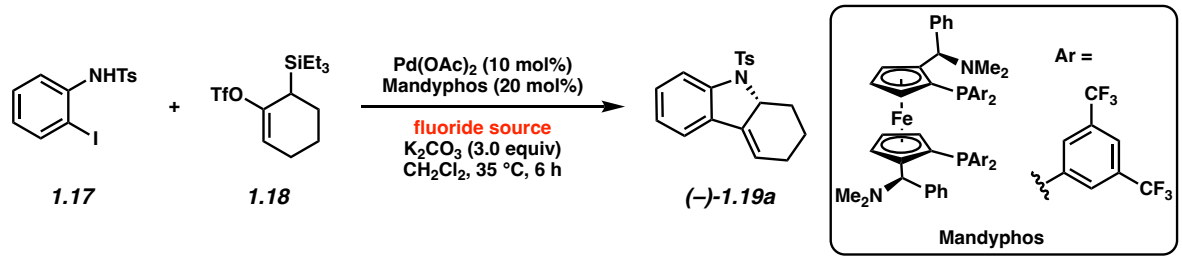

Entry	Fluoride source	NMR Yield[a]	%ee
1	CsF (10 equiv) Bu_4NOTf (5 equiv)	14%	85%
2	TBAF•H_2O (1.5 equiv)	22%	85%
3	TASF (1.5 equiv)	38%	83%
4	TBAT (1.5 equiv)	29%	78%
5	KF (5 equiv) 18-crown-6 (5 equiv)	14%	79%

[a] Yield determined by quantitative SFC analysis using 6-acetylbenzothiophene as an external standard.

Table 1.9. Palladium source screening results.

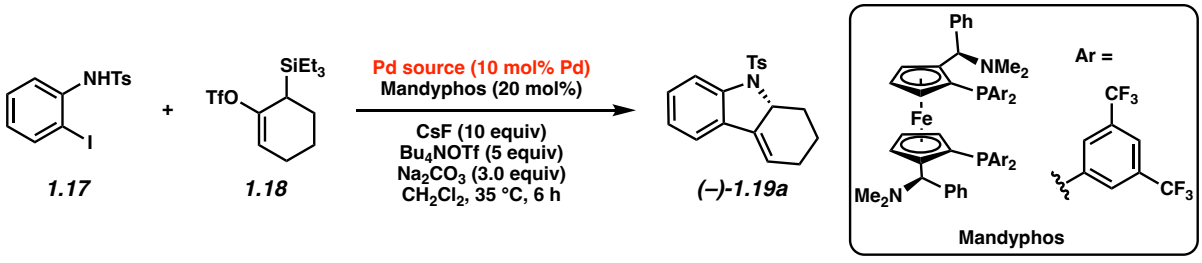

Entry	Pd source	Yield[a]	%ee
1	$Pd_2(dba)_3$	20%	83%
2	$Pd(dba)_2$	43%	82%

3	$[Pd(allyl)Cl]_2$	49%	80%
4	$Pd(OAc)_2$	37%	76%
5	$PdCl_2$	44%	67%
6	$Pd(acac)_2$	16%	63%

[a] Yield determined by quantitative SFC analysis using 6-acetylbenzothiophene as an external standard.

Table 1.10. Base screening results.

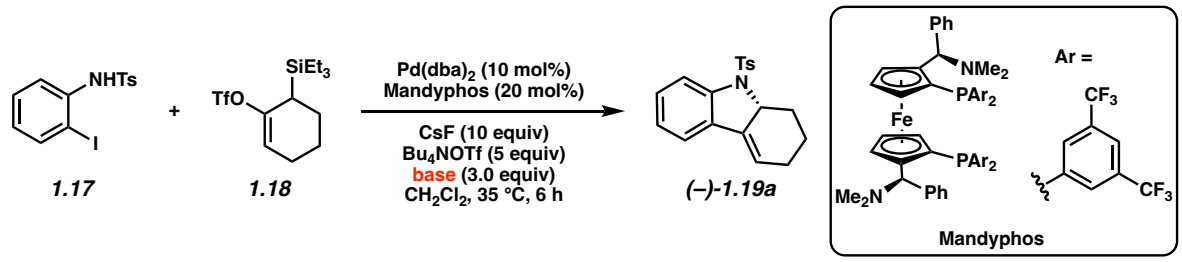

Entry	Base	Yield[a]	%ee
1	K_2CO_3	14%	85%
2	K_2HPO_4	15%	85%
3	KO*t*Bu	12%	84%
4	Et_3N	27%	82%
5	$NaOAc•3H_2O$	15%	79%
6	NaHMDS	4%	51%

[a] Yield determined by quantitative SFC analysis using 6-acetylbenzothiophene as an external standard.

1.8.2.7 Synthesis of (–)-1.47 via Asymmetric Annulation

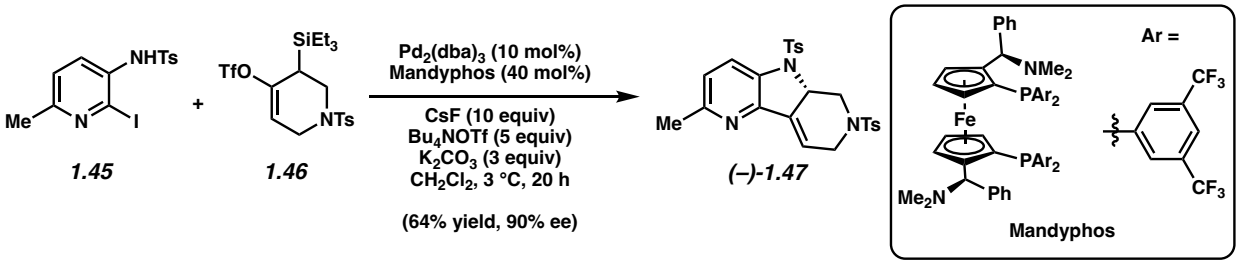

(–)-1.47. A 1-dram vial containing a magnetic stir bar was charged with iodopyridine **1.45** (23.3 mg, 0.06 mmol, 1.2 equiv) and Bu_4NOTf (98.7 mg, 0.25 mmol, 5.0 equiv). A separate 1-dram vial was charged with silyl triflate **1.46** (25.0 mg, 0.05 mmol, 1.0 equiv). Both vials were taken into a glovebox where K_2CO_3 (20.7 mg, 0.15 mmol, 3.0 equiv) and CsF (76.0 mg, 0.50 mmol, 10 equiv) were added to the vial containing iodopyridine **1.45**. An empty vial equipped with a stir bar was then charged with Mandyphos (27.3 mg, 0.020 mmol, 40 mol%) and $Pd_2(dba)_3$ (4.6 mg, 0.005 mmol, 10 mol%) then treated with CH_2Cl_2 (0.33 mL) to give a deep purple solution. This vial was sealed with a Teflon-lined cap and stirred at 45 °C for 45 min then cooled back to 23 °C, yielding a yellow/brown solution. The vial containing silyl triflate **1.46** was then treated with an aliquot of CH_2Cl_2 (0.33 mL) and agitated to ensure full dissolution. The solution of $Pd_2(dba)_3$/Mandyphos and the solution of silyl triflate were then transferred sequentially to the reaction vial containing iodopyridine **1.45**, and the vial was sealed with a Teflon-lined cap, removed from the glovebox, and stirred for 20 h at 3 °C. The mixture was then filtered through a pad of silica gel, eluting with 9:1 benzene:MeCN (30 mL). The eluate was concentrated and purified by preparative thin layer chromatography (9:1 benzene:MeCN) to provide annulation product **(–)-1.47** (64% yield, average of two experiments: 63% yield, 90% ee and 65% yield, 90% ee) as a white solid. **Annulation product (–)-1.47**: Mp: 161–163 °C; R_f 0.29 (9:1 benzene:MeCN); ^{1}H NMR (500 MHz, $CDCl_3$): δ 7.89 (d, J = 8.5, 1H), 7.76 (d, J = 8.3, 2H), 7.66 (d, J = 8.3, 2H), 7.35 (d, J = 8.0, 2H), 7.27 (d, J

= 8.0, 2H), 6.98 (d, *J* = 8.5, 1H), 6.22 (q, *J* = 3.2, 1H), 4.84 (dd, *J* = 11.3, 5.1, 1H), 4.41 (dt, *J* = 18.5, 3.6, 1H), 4.29–4.22 (m, 1H), 3.54 (dt, *J* = 18.5, 3.6, 1H), 2.70 (dd, *J* = 11.3, 9.9, 1H), 2.452 (s, 3H), 2.448 (s, 3H), 2.40 (s, 3H); ^{13}C NMR (125 MHz, $CDCl_3$): δ 154.8, 146.4, 145.3, 143.9, 136.6, 134.5, 134.2, 131.7, 130.1, 129.9, 127.9, 127.4, 123.3, 122.7, 116.2, 60.0, 47.0, 44.9, 23.8, 21.63, 21.59; IR (film): 2924, 1441, 1360, 1166, 1093 cm^{-1}; HRMS-APCI (*m/z*) $[M + H]^+$ calcd for $C_{25}H_{26}N_3O_4S_2^+$, 496.1359; found 496.1351; $[\alpha]^{20.9}_D$ –168° (*c* = 0.500, CH_2Cl_2).

Note: 3 °C was selected for the practical convenience of being able to perform long reactions in a refrigerator.

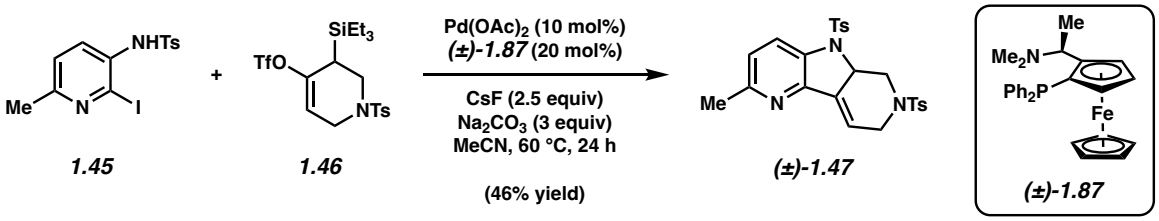

(±)-1.47. Followed a modified version of General Procedure 1.6 by using ligand **(±)-1.87**. Purification by preparative thin layer chromatography (9:1 benzene:MeCN) afforded annulation product **(±)-1.47** (46% yield) as a white solid. **Annulation product (±)-1.47**: Spectral data matched those obtained for **(–)-1.47**.

1.8.2.8 Elaboration of Annulation Product (–)-1.47

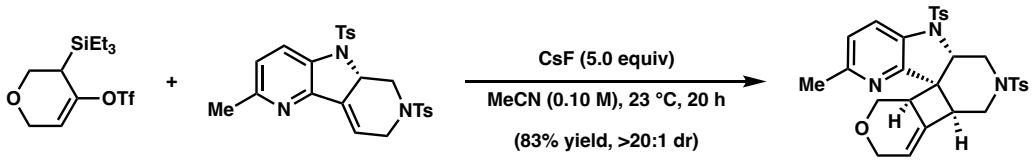

1.48 *(–)-1.47* *(+)-1.49*

Pentacycle (+)-1.49. A 1-dram vial was charged with annulation product **(–)-1.47** (17.3 mg, 0.035 mmol, 1.0 equiv) and silyl triflate **1.48** (18.2 mg, 0.053 mmol, 1.5 equiv) then purged with nitrogen for 5 min. The reactants were then dissolved in MeCN (0.35 mL, 0.10 M) before the rapid addition of CsF (26.6 mg, 0.175 mmol, 5.0 equiv) in a single portion. The vial was sealed with a Teflon-lined cap and stirred at 23 °C for 20 h. The mixture was then filtered through pad of silica gel, eluting with EtOAc (10 mL). The eluate was concentrated to provide a crude residue, which was purified by flash column chromatography (19:1 benzene:Et_2O → 7:3 benzene:Et_2O) to provide a single diastereomer of pentacycle **(+)-1.49** (16.8 mg, 83% yield) as a white crystalline solid. Relative and absolute stereochemistry were assigned by single crystal X-ray diffraction studies of epoxide **(+)-1.50**. **Pentacycle (+)-1.49**: Mp: 110 ºC; R_f 0.21 (9:1 benzene:MeCN); ^{1}H NMR (500 MHz, $CDCl_3$): δ 7.77 (d, *J* = 8.3, 1H), 7.65 (d, *J* = 8.1, 2H), 7.61 (d, *J* = 8.1, 2H), 7.29 (app t, *J* = 8.9, 4H), 6.99 (d, *J* = 8.3, 1H), 5.63–5.58 (m, 1H), 4.38 (dd, *J* = 10.0, 6.7, 1H), 4.23 (dd, *J* = 11.8, 7.1, 1H), 4.17–4.05 (m, 2H), 4.04–3.92 (m, 2H), 3.01–2.91 (m, 1H), 2.59 (app. d, *J* = 2.59, 2H), 2.48 (s, 3H), 2.40 (s, 6H), 2.28 (dd, *J* = 12.4, 4.8, 1H), 1.93 (t, *J* = 11.4, 1H); ^{13}C NMR (125 MHz, $CDCl_3$): δ 155.3, 152.8, 145.0, 143.8, 135.1, 133.4, 132.44, 132.37, 130.1, 129.8, 127.6, 126.9, 123.0, 122.6, 113.3, 65.1, 61.6, 58.3, 50.5, 49.9, 48.1, 45.8, 44.3, 23.8, 21.6, 21.5; IR (film): 2922, 2850, 1447, 1357, 1164 cm^{-1}; HRMS-APCI (*m/z*) $[M + H]^+$ calcd for $C_{30}H_{32}N_3O_5S_2^+$, 578.1778; found 578.1752; $[\alpha]^{23.8}_D$ +38.7° (*c* = 0.500, CH_2Cl_2).

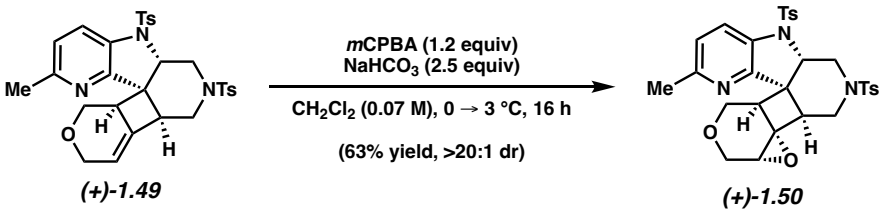

(+)-1.49 *(+)-1.50*

Epoxide (+)-1.50. A 1-dram vial was charged with pentacycle **(+)-1.49** (11.2 mg, 0.019 mmol, 1.0 equiv) and CH_2Cl_2 (0.28 mL, 0.07 M) then cooled to 0 °C. $NaHCO_3$ (4.1 mg, 0.049 mmol, 2.5 equiv) and *m*CPBA (77 wt% purity, 5.0 mg, 0.022 mmol, 1.2 equiv) were added sequentially as solids, and the reaction was moved to a cold room set to 3 °C where it was stirred for 16 h. The reaction was quenched by addition of EtOAc (5 mL), and the organic layer was washed with saturated aqueous $NaHCO_3$ (3 x 5 mL), dried with Na_2SO_4, filtered, and concentrated under reduced pressure. The resulting crude solid was purified by preparative thin layer chromatography (9:1 benzene:MeCN) to provide a single diastereomer of epoxide **(+)-1.50** (7.4 mg, 63% yield) as a white crystalline solid. Crystals suitable for X-ray diffraction studies were obtained by recrystallization from a mixture of EtOAc and cyclohexane. **Epoxide (+)-1.50**: Mp: decomposes at 220 ºC; R_f 0.69 (4:1 benzene:MeCN); ^{1}H NMR (500 MHz, $CDCl_3$): δ 7.78 (d, *J* = 8.3, 1H), 7.68 (d, *J* = 8.2, 2H), 7.62 (d, *J* = 8.2, 2H), 7.29 (app. t, *J* = 7.6, 4H), 6.98 (d, *J* = 8.3, 1H), 4.89 (dd, *J* = 10.4, 6.5, 1H), 4.36 (ddd, *J* = 11.7, 6.5, 1.3, 1H), 4.30 (dd, *J* = 13.2, 4.3, 1H), 3.79 (t, *J* = 3.2, 1H), 3.68 (d, *J* = 4.2, 1H), 3.58 (d, *J* = 12.6, 1H), 3.29 (dd, *J* = 13.4, 2.4, 1H), 2.66–2.56 (m, 2H), 2.46 (s, 3H), 2.393 (s, 3H), 2.390 (s, 3H), 2.19 (dd, *J* = 12.7, 4.6, 1H), 2.14 (dd, *J* = 12.4, 2.2, 1H), 1.97 (t, *J* = 11.6, 1H); ^{13}C NMR (125 MHz, $CDCl_3$): δ 155.2, 152.2, 144.9, 144.0, 134.8, 132.7, 132.6, 130.1, 129.9, 127.7, 127.0, 122.9, 122.1, 68.0, 60.5, 58.2, 53.7, 50.6, 48.9, 46.4, 44.5, 43.3, 42.0, 23.7, 21.6, 21.5; IR (film): 2924, 2848, 1597, 1449, 1358 cm^{-1}; HRMS-APCI (*m/z*) $[M + H]^+$ calcd for $C_{30}H_{32}N_3O_6S_2^+$, 594.1727; found 594.1695; $[\alpha]^{24.8}_D$ +50.0° (*c* = 1.00, CH_2Cl_2).

Crystal Structure Analysis

Diffraction intensities were collected at 100 K on a Bruker Smart ApexII CCD diffractometer with CuKα radiation, 1.54178 Å. Absorption corrections were applied by SADABS[57]. All calculations were performed by the SHELXL-2014 packages[58]. Deposition Number 2065022 contains the supplementary crystallographic data for this paper. These data are provided free of charge by the joint Cambridge Crystallographic Data Centre and Fachinformationszentrum Karlsruhe Access Structures service www.ccdc.cam.ac.uk/structures.

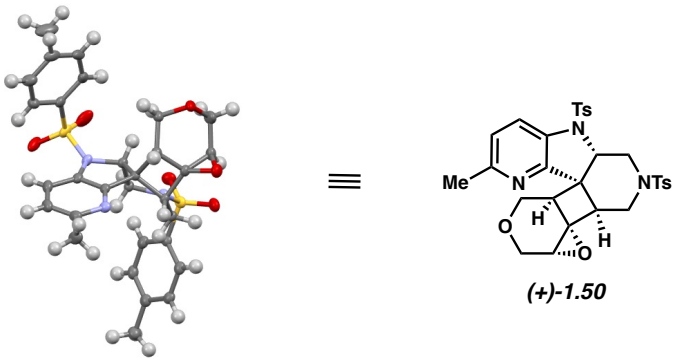

Figure 1.6. ORTEP representation of X-ray crystallographic structure **(+)-1.50**. EtOAc omitted for clarity. (CCDC Registry # 2065022).

Table 1.11. Crystal data and structure refinement for epoxide **(+)-1.50**.

Identification code	cu_garg2006s	
Empirical formula	C34 H39 N3 O8 S2	
Formula weight	681.80	
Temperature	100(2) K	
Wavelength	1.54178 Å	
Crystal system	Monoclinic	
Space group	$P2_1$	
Unit cell dimensions	a = 10.0508(2) Å	a= 90°.
	b = 14.2935(3) Å	b= 105.5148(7)°.
	c = 12.0393(3) Å	g = 90°.
Volume	1666.56(6) $Å^3$	
Z	2	
Density (calculated)	1.359 Mg/m^3	
Absorption coefficient	1.917 mm^{-1}	
F(000)	720	
Crystal size	0.300 x 0.200 x 0.200 mm^3	
Theta range for data collection	3.810 to 69.338°.	

Index ranges	-12<=h<=12, -16<=k<=17, -14<=l<=12
Reflections collected	27146
Independent reflections	5940 [R(int) = 0.0190]
Completeness to theta = 67.679°	97.4 %
Absorption correction	Semi-empirical from equivalents
Max. and min. transmission	0.75 and 0.60
Refinement method	Full-matrix least-squares on F^2
Data / restraints / parameters	5940 / 1 / 463
Goodness-of-fit on F^2	1.054
Final R indices [I>2sigma(I)]	R1 = 0.0308, wR2 = 0.0828
R indices (all data)	R1 = 0.0311, wR2 = 0.0831
Absolute structure parameter	0.031(2)
Extinction coefficient	n/a
Largest diff. peak and hole	0.428 and -0.291 $eÅ^{-3}$

Table 1.12. SFC conditions and data.

Compound	Column	Solvent	Flow Rate	Retention Times (min)	Enantiomeric Ratio (er)
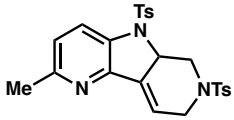 ***(±)-1.47***	ChiralPak AD-H/40 °C	20% isopropanol in CO_2	3.5 mL/min	3.61/5.00	49.8 : 50.2
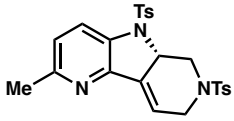 ***(–)-1.47***	ChiralPak AD-H/40 °C	20% isopropanol in CO_2	3.5 mL/min	3.64/5.03	4.9 : 95.1

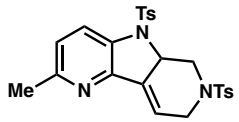

(±)-1.47

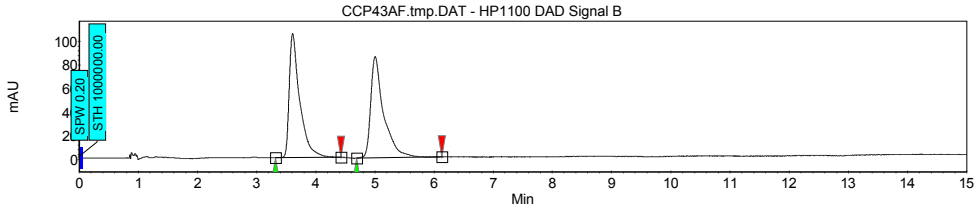

Index	Name	Start	Time	End	RT Offset	Quantity	Height	Area	Area
		[Min]	[Min]	[Min]	[Min]	[% Area]	[µV]	[µV.Min]	[%]
1	UNKNOWN	3.32	3.61	4.42	0.00	49.79	105.0	21.5	49.791
2	UNKNOWN	4.69	5.00	6.13	0.00	50.21	85.8	21.7	50.209
Total						100.00	190.8	43.3	100.000

Figure 1.7. SFC trace for **(±)-1.47**.

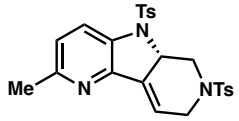

(–)-1.47

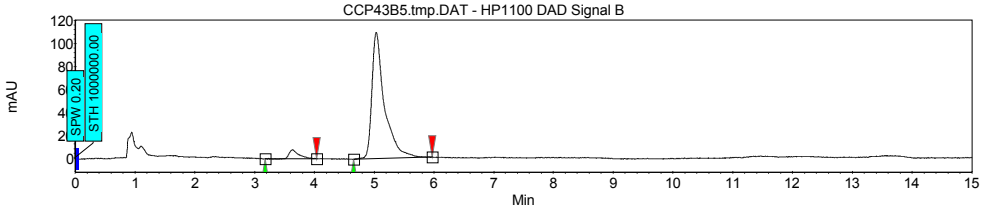

Index	Name	Start	Time	End	RT Offset	Quantity	Height	Area	Area
		[Min]	[Min]	[Min]	[Min]	[% Area]	[µV]	[µV.Min]	[%]
2	UNKNOWN	3.18	3.64	4.04	0.00	4.93	7.7	1.4	4.931
1	UNKNOWN	4.65	5.03	5.97	0.00	95.07	110.1	26.9	95.069
Total						100.00	117.9	28.3	100.000

Figure 1.8. SFC trace for **(–)-1.47**.

1.9 Spectra Relevant to Chapter One:

Palladium-Catalyzed Annulations of Strained Cyclic Allenes

Andrew V. Kelleghan, Dominick C. Witkowski, Matthew S. McVeigh, and Neil K. Garg

J. Am. Chem. Soc. **2021**, *143*, 9338–9342.

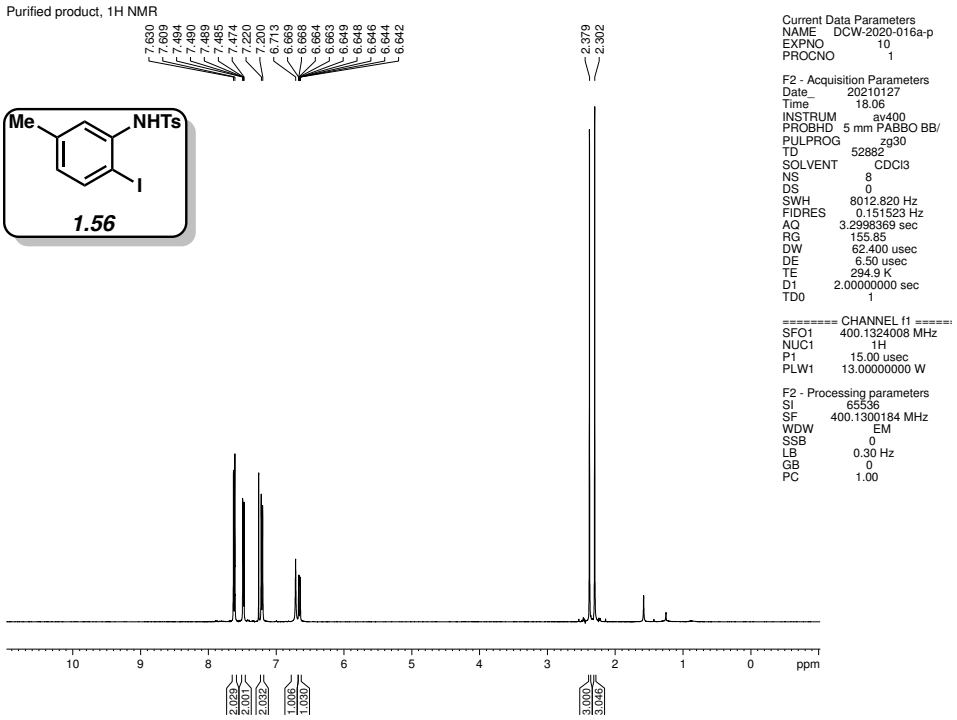

Figure 1.9. ^{1}H NMR (400 MHz, $CDCl_3$) of compound **1.56**.

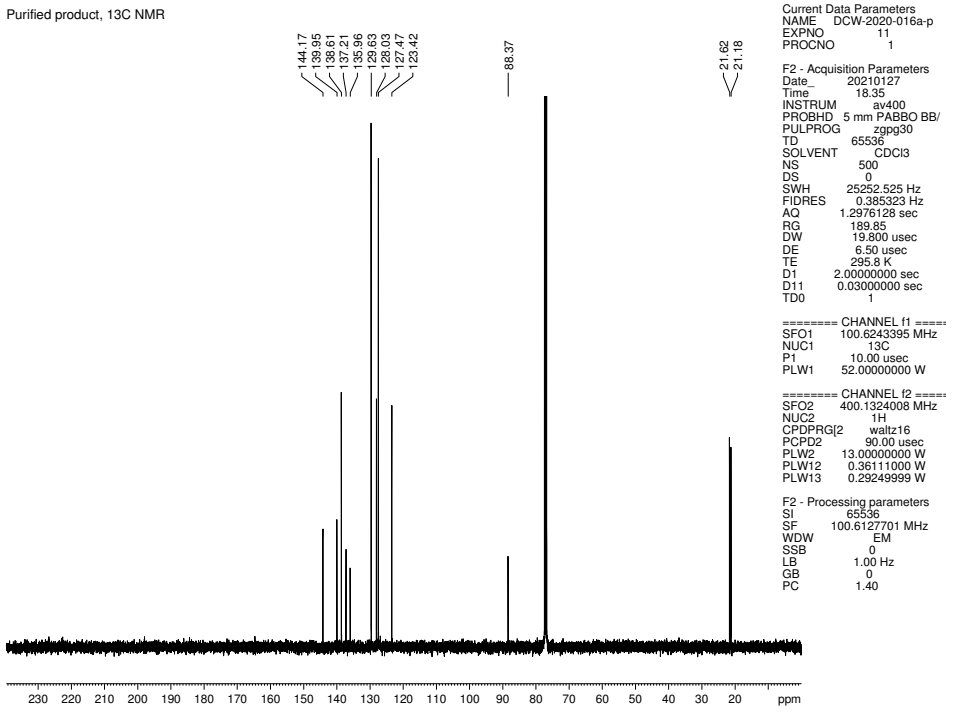

Figure 1.10. ^{13}C NMR (100 MHz, $CDCl_3$) of compound **1.56**.

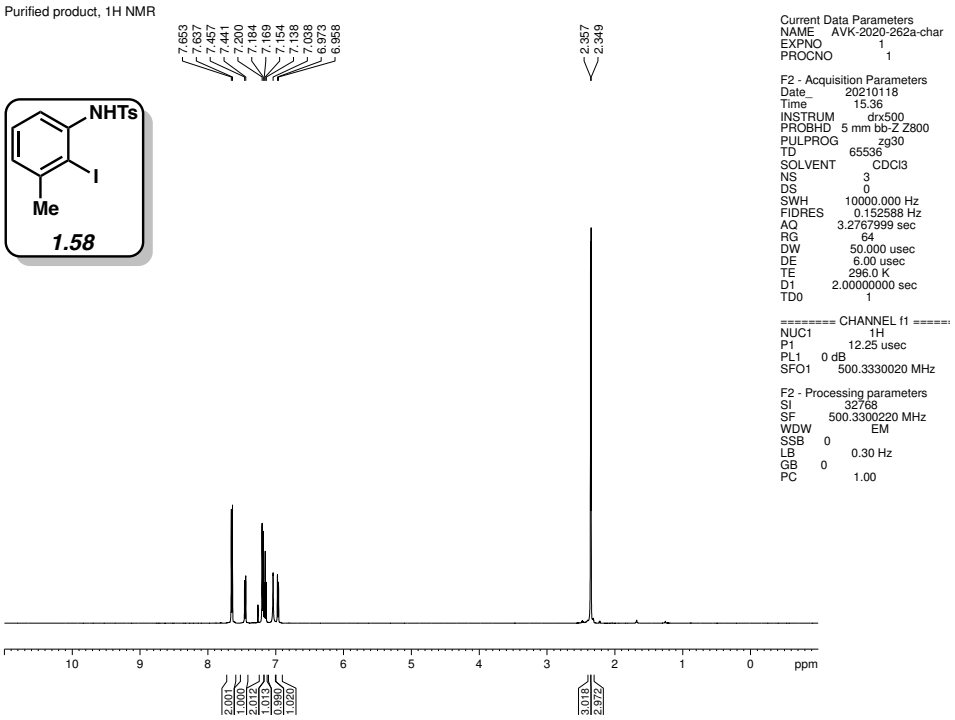

Figure 1.11. ^{1}H NMR (500 MHz, $CDCl_3$) of compound **1.58**.

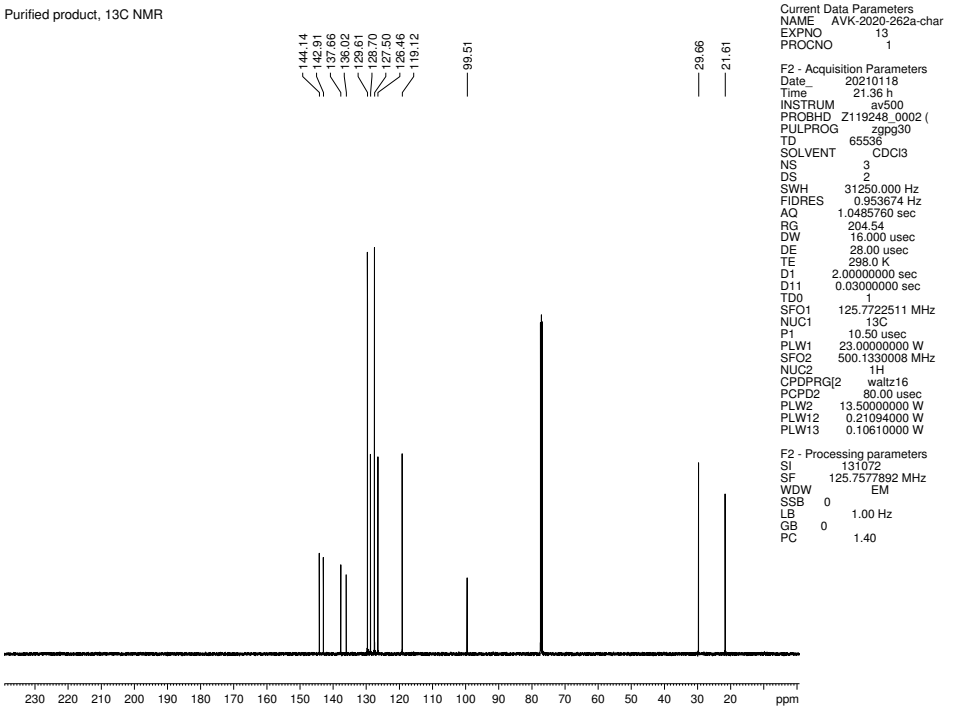

Figure 1.12. ^{13}C NMR (125 MHz, $CDCl_3$) of compound **1.58**.

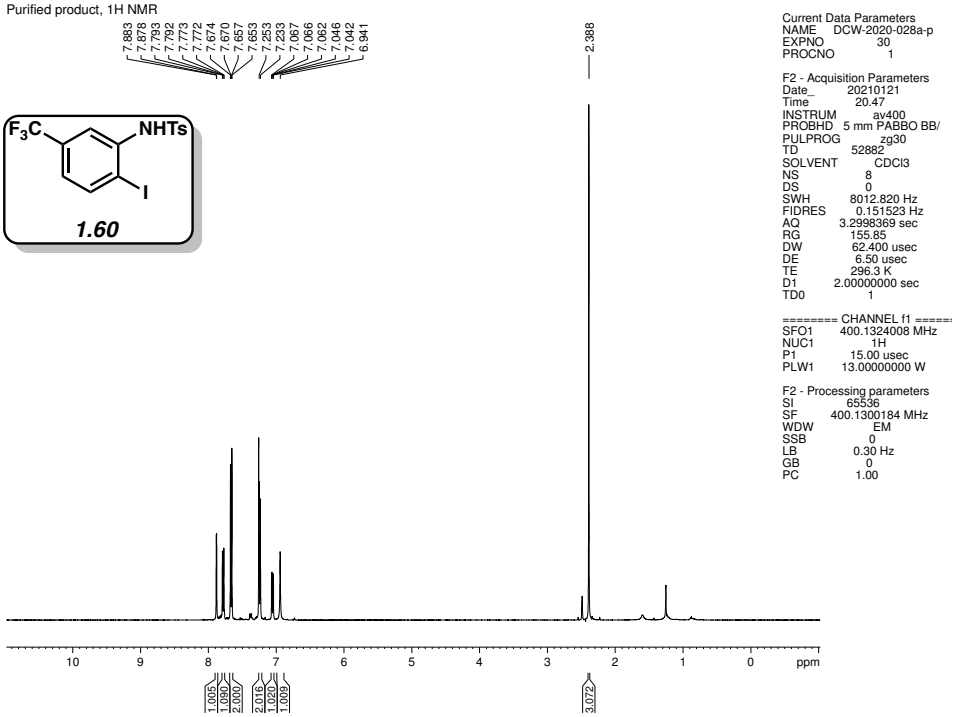

Figure 1.13. ^{1}H NMR (400 MHz, $CDCl_3$) of compound **1.60**.

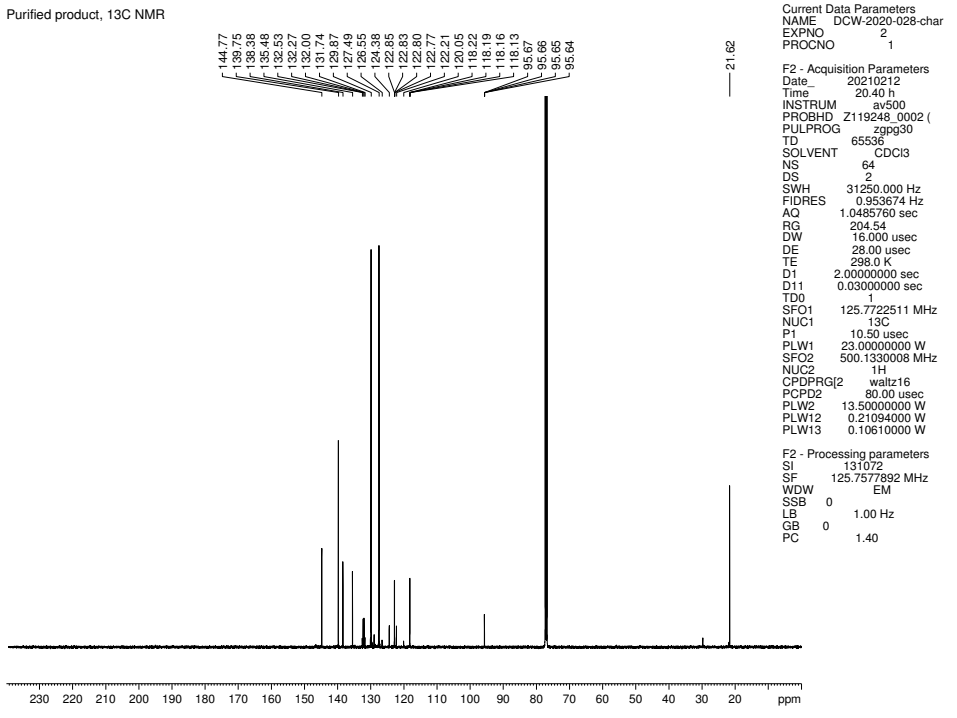

Figure 1.14. ^{13}C NMR (125 MHz, $CDCl_3$) of compound **1.60**.

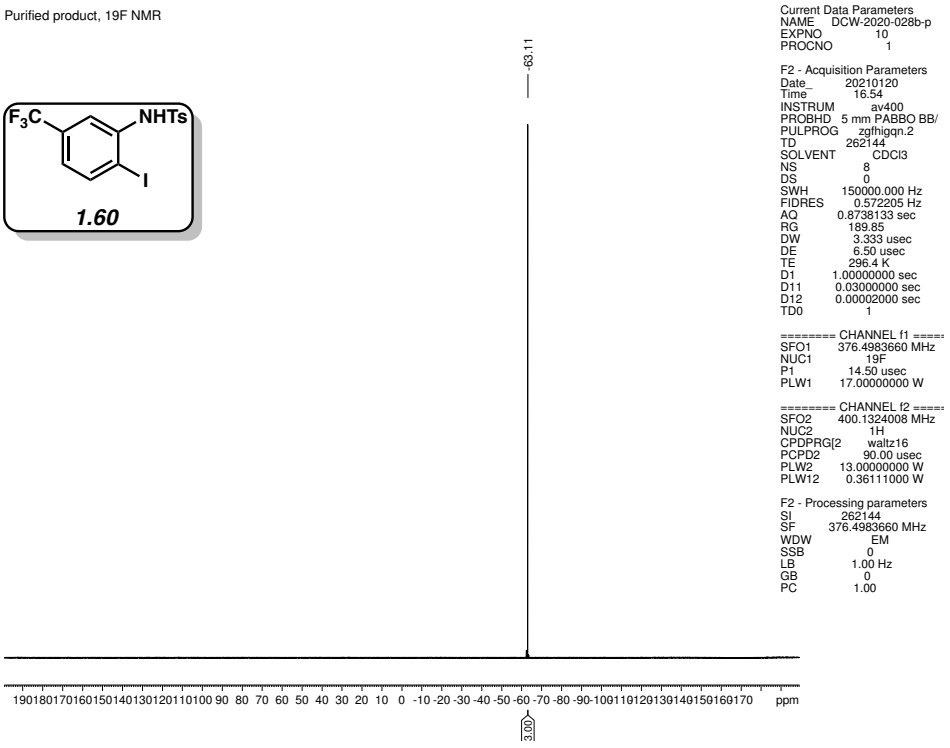

Figure 1.15. ^{19}F NMR (376 MHz, $CDCl_3$) of compound **1.60**.

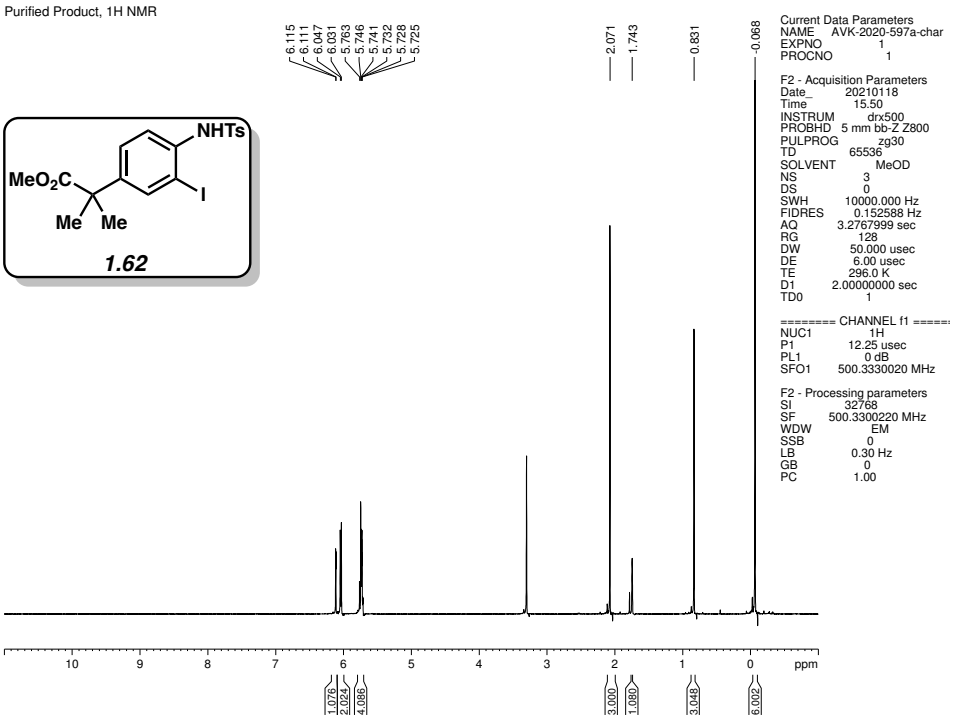

Figure 1.16. ^{1}H NMR (500 MHz, CD_3OD) of compound **1.62**.

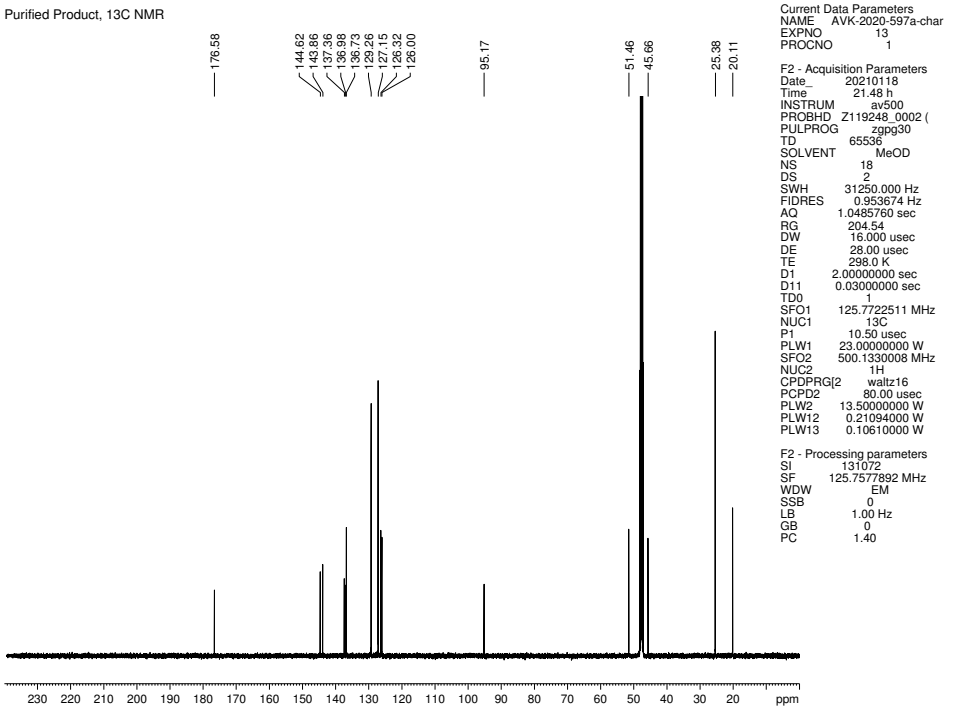

Figure 1.17. ^{13}C NMR (125 MHz, CD_3OD) of compound **1.62**.

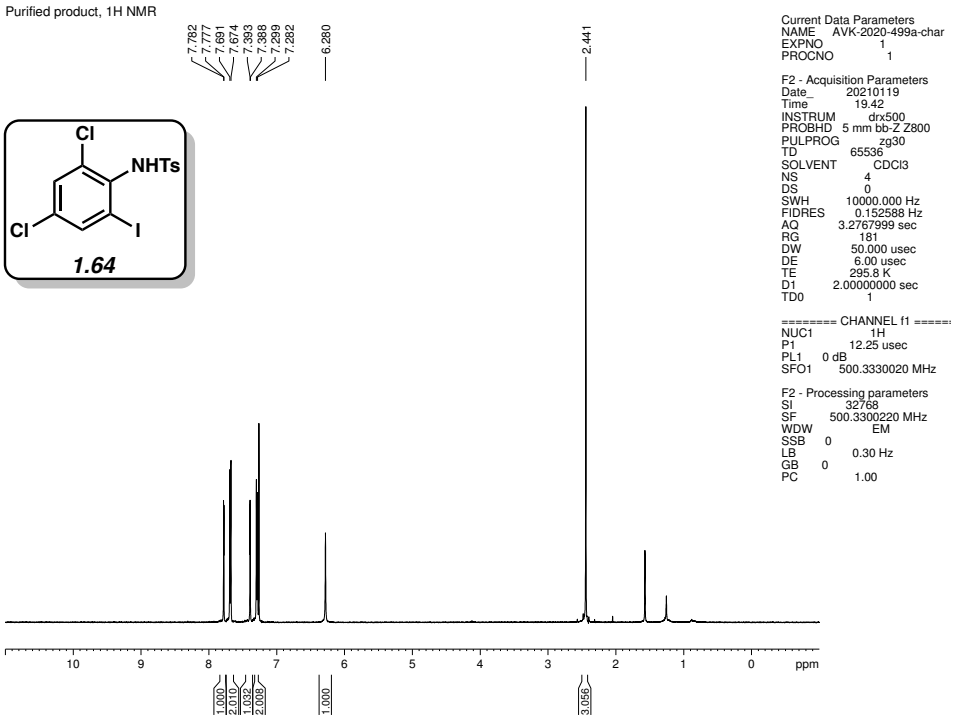

Figure 1.18. ^{1}H NMR (500 MHz, $CDCl_3$) of compound **1.64**.

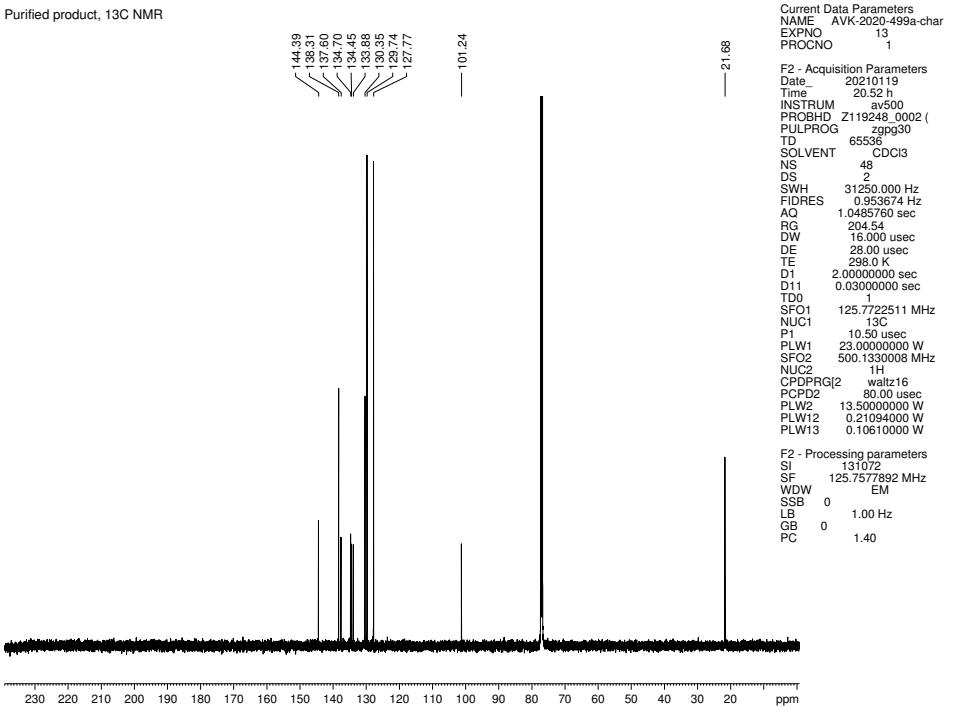

Figure 1.19. ^{13}C NMR (125 MHz, $CDCl_3$) of compound **1.64**.

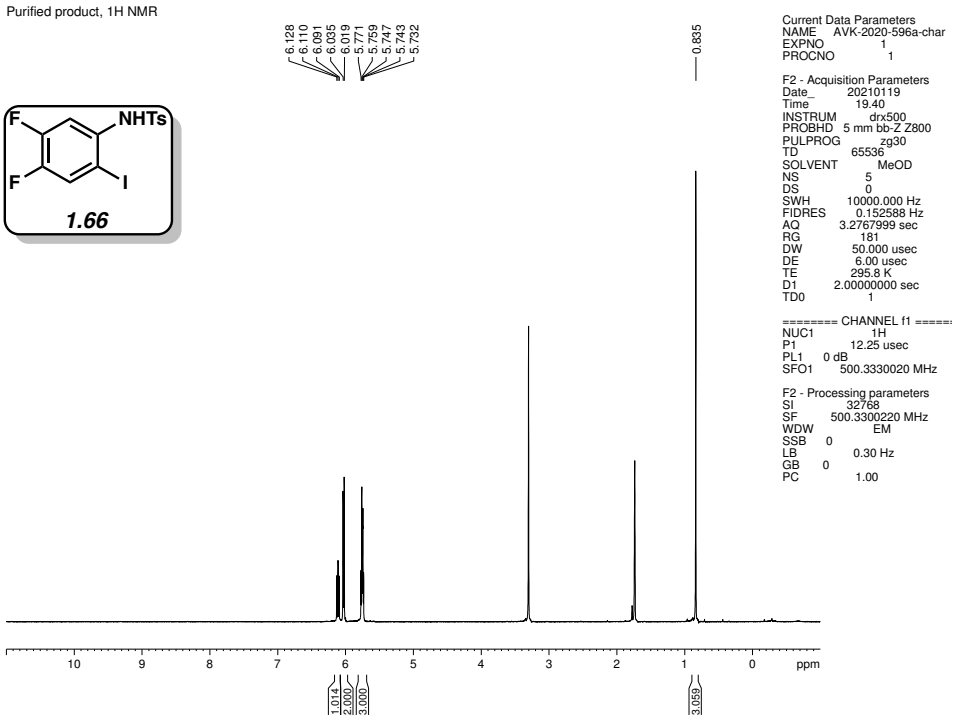

Figure 1.20. ^{1}H NMR (500 MHz, CD_3OD) of compound **1.66**.

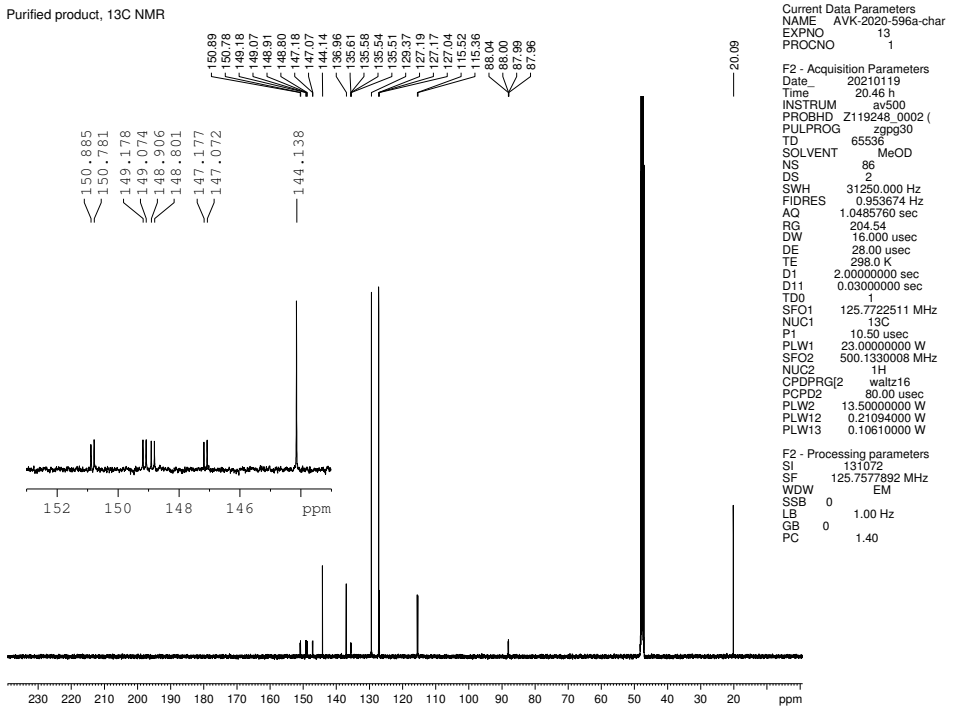

Figure 1.21. ^{13}C NMR (125 MHz, CD_3OD) of compound **1.66**.

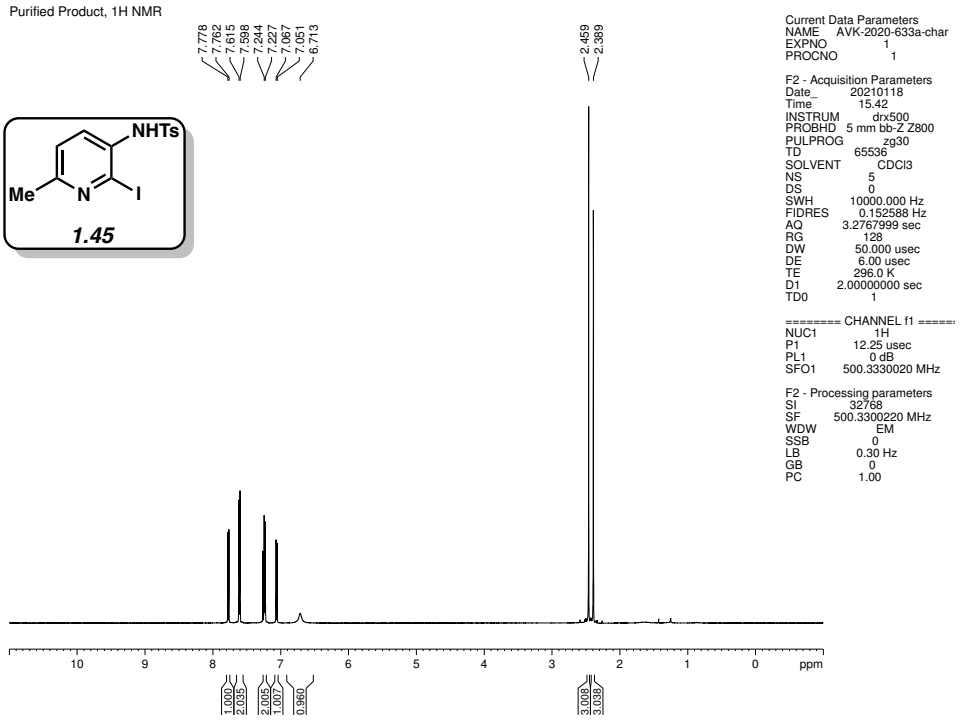

Figure 1.22. ^{1}H NMR (500 MHz, $CDCl_3$) of compound **1.45**.

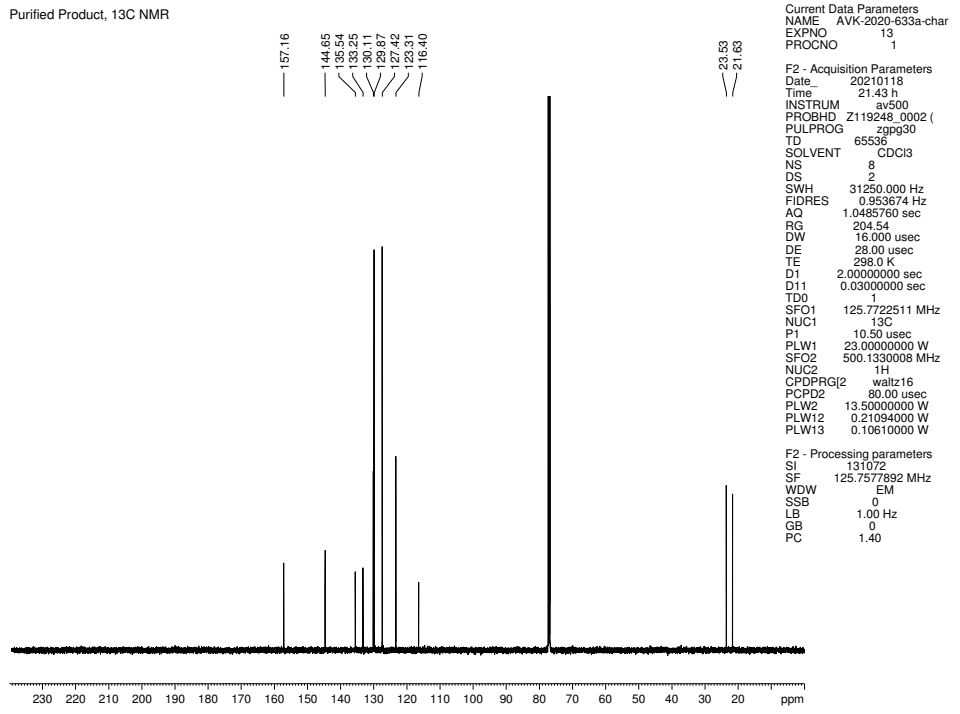

Figure 1.23. ^{13}C NMR (125 MHz, $CDCl_3$) of compound **1.45**.

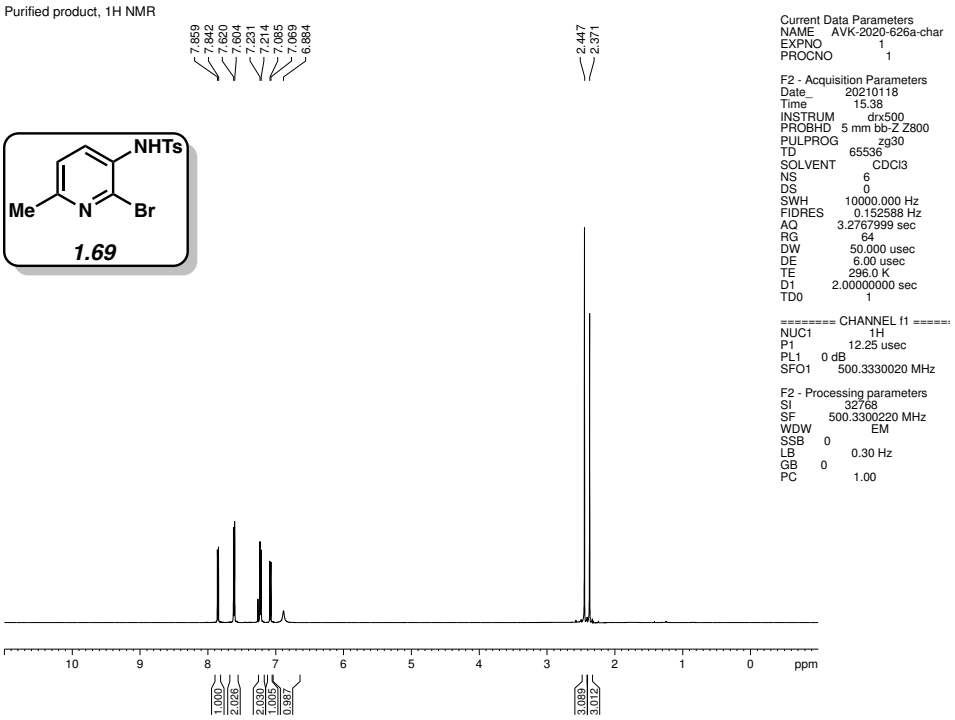

Figure 1.24. ^{1}H NMR (500 MHz, $CDCl_3$) of compound **1.69**.

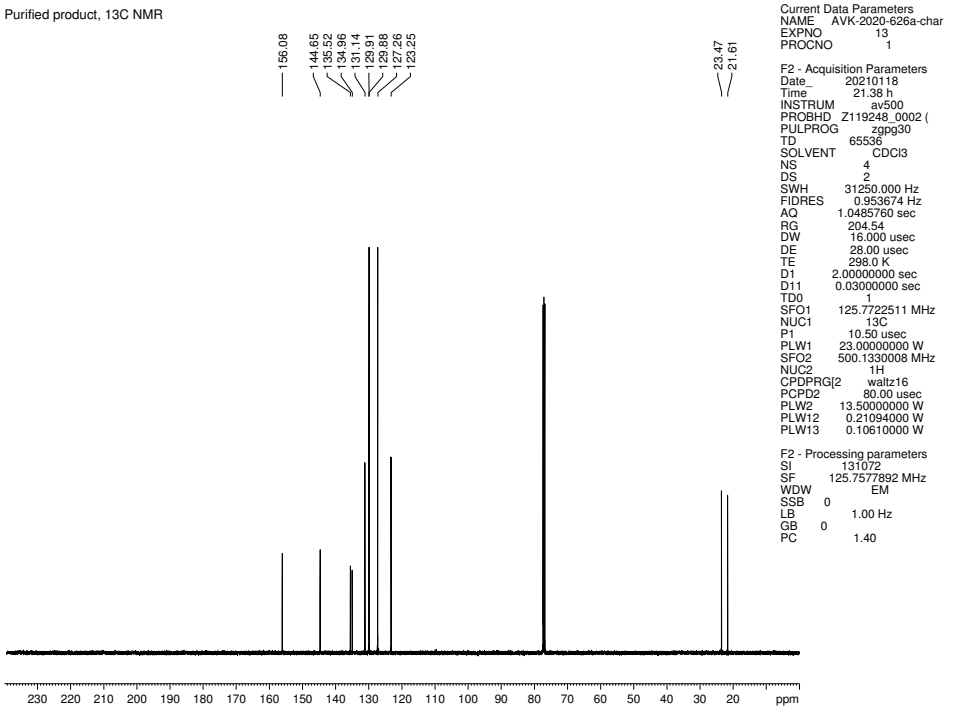

Figure 1.25. ^{13}C NMR (125 MHz, $CDCl_3$) of compound **1.69**.

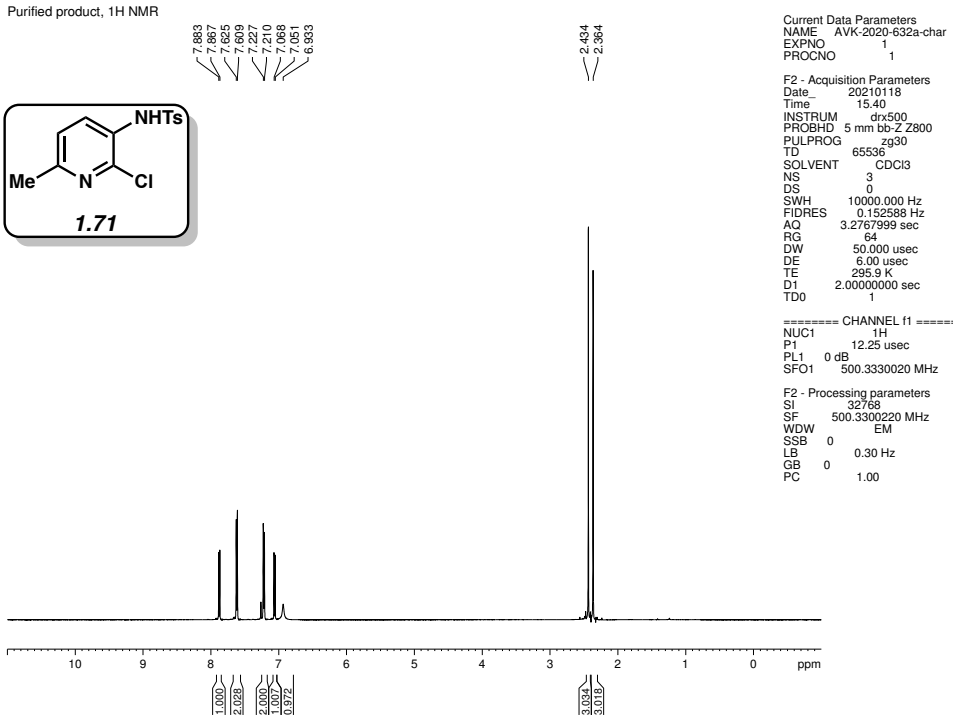

Figure 1.26. ^{1}H NMR (500 MHz, $CDCl_3$) of compound **1.71**.

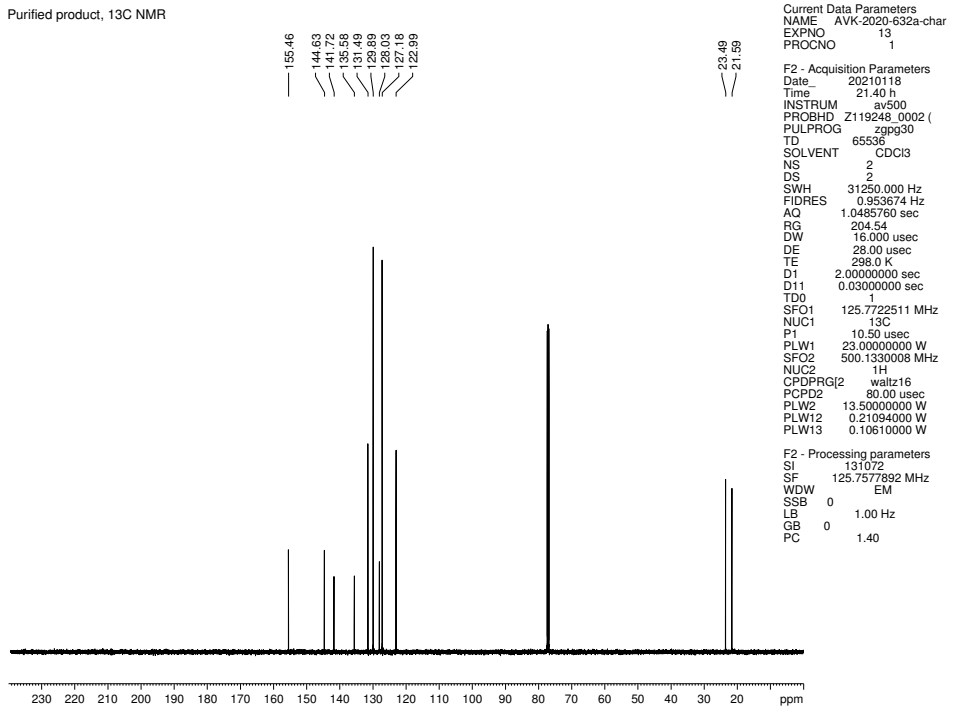

Figure 1.27. ^{13}C NMR (125 MHz, $CDCl_3$) of compound **1.71**.

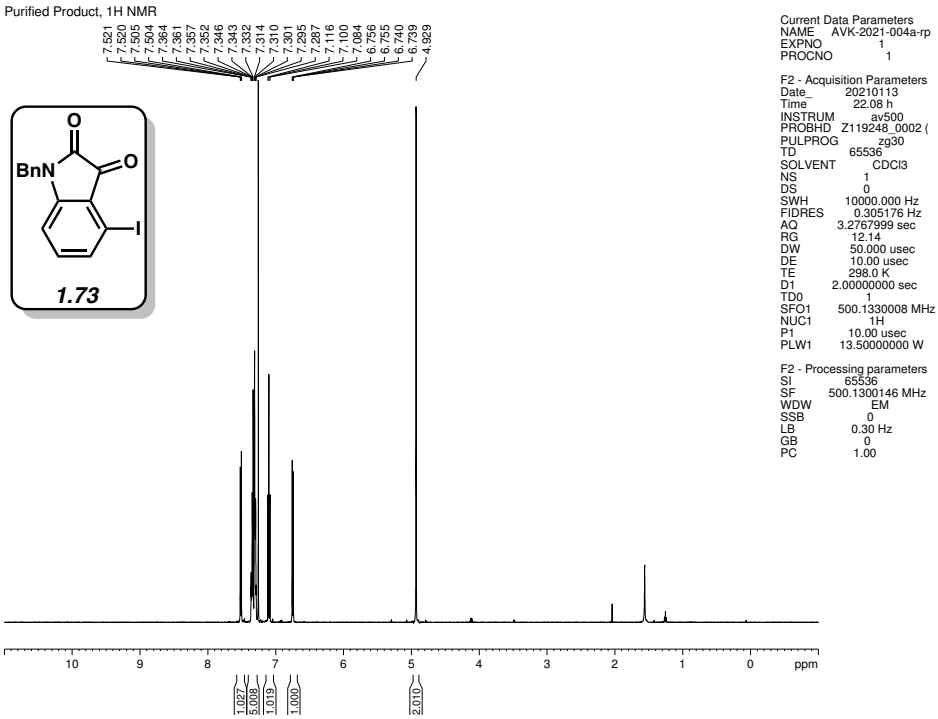

Figure 1.28. ^{1}H NMR (500 MHz, $CDCl_3$) of compound **1.73**.

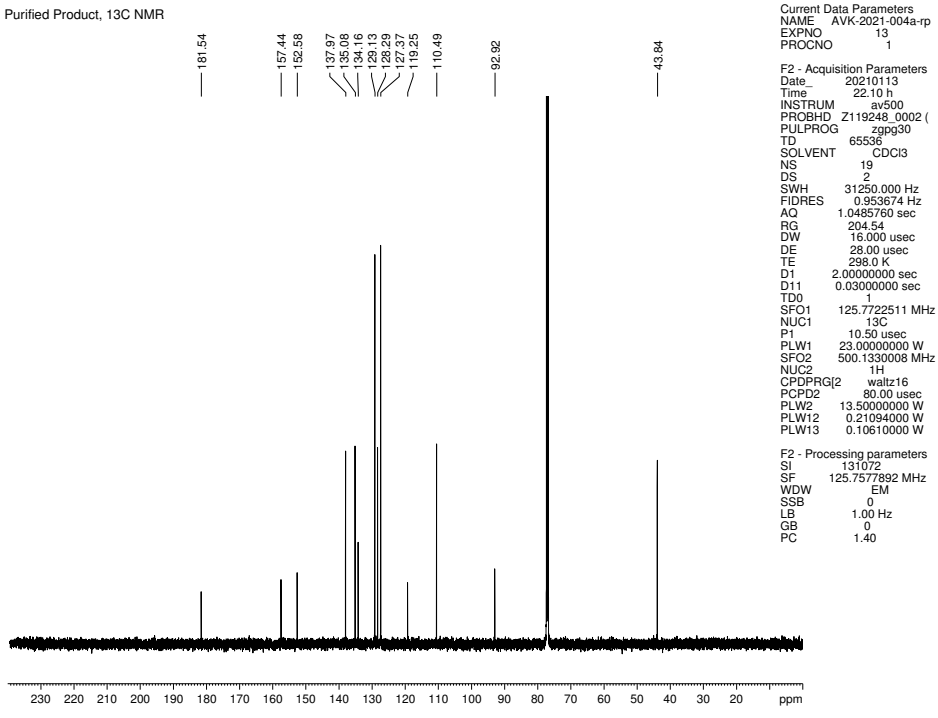

Figure 1.29. ^{13}C NMR (125 MHz, $CDCl_3$) of compound **1.73**.

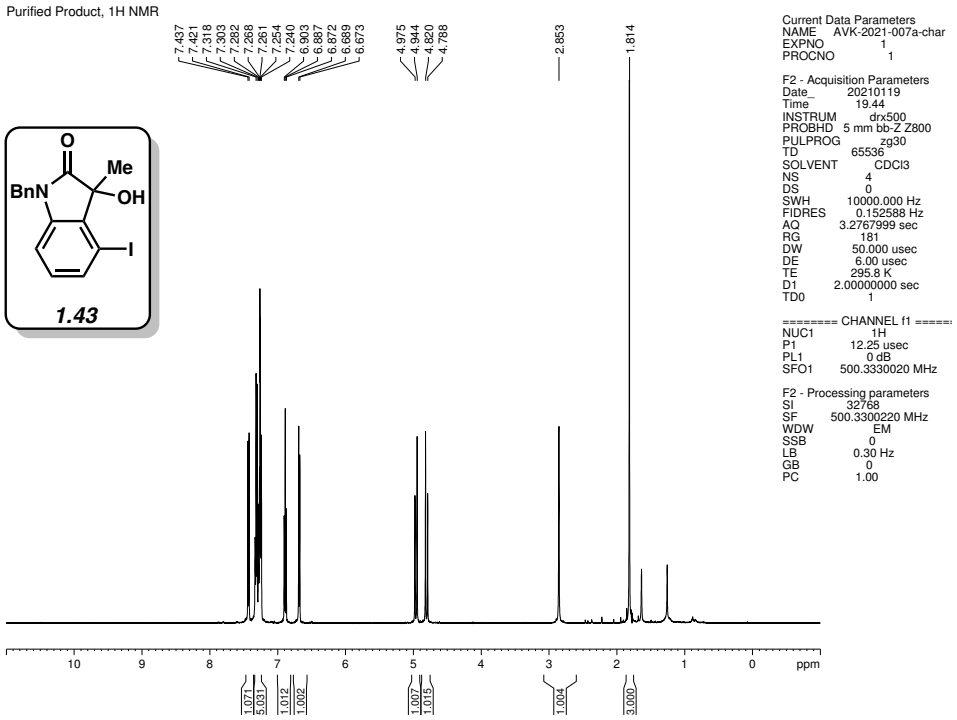

Figure 1.30. ^{1}H NMR (500 MHz, $CDCl_3$) of compound **1.43**.

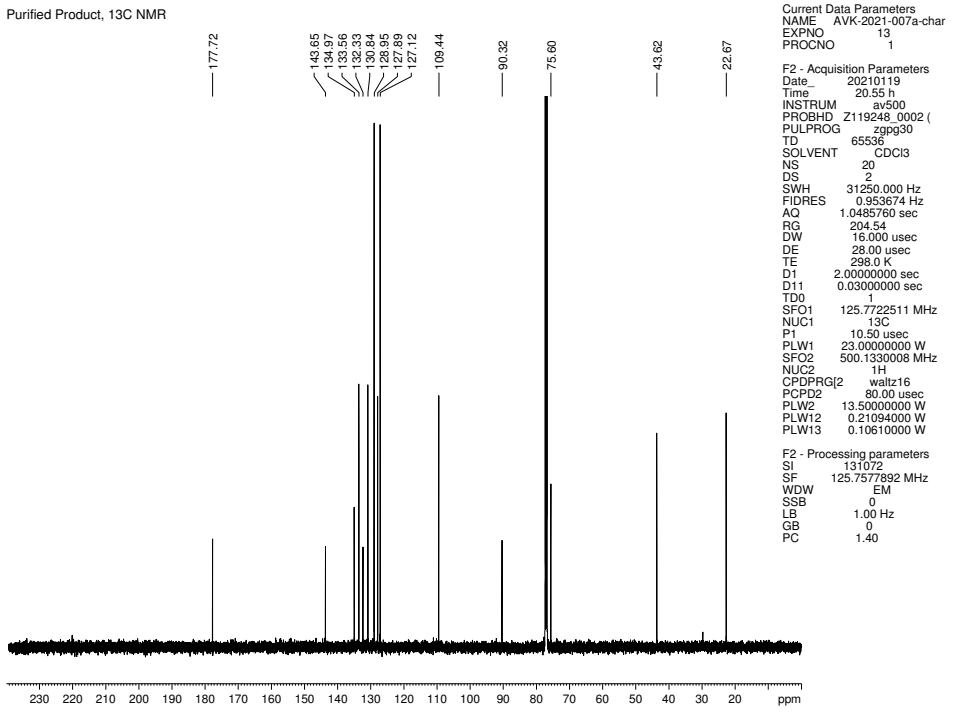

Figure 1.31. ^{13}C NMR (125 MHz, $CDCl_3$) of compound **1.43**.

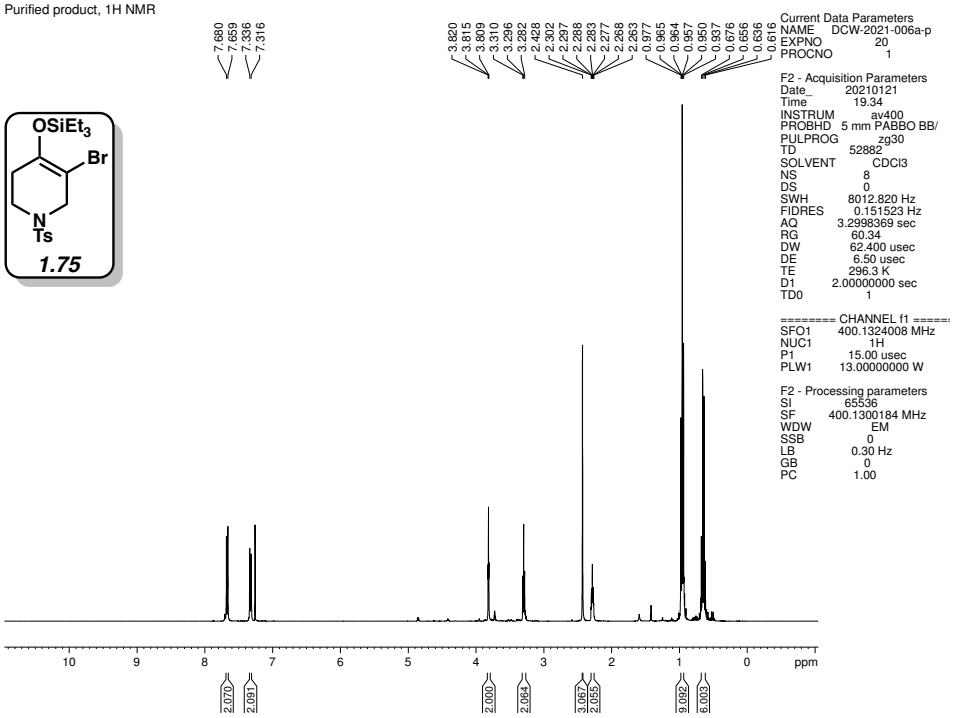

Figure 1.32. ^{1}H NMR (400 MHz, $CDCl_3$) of compound **1.75**.

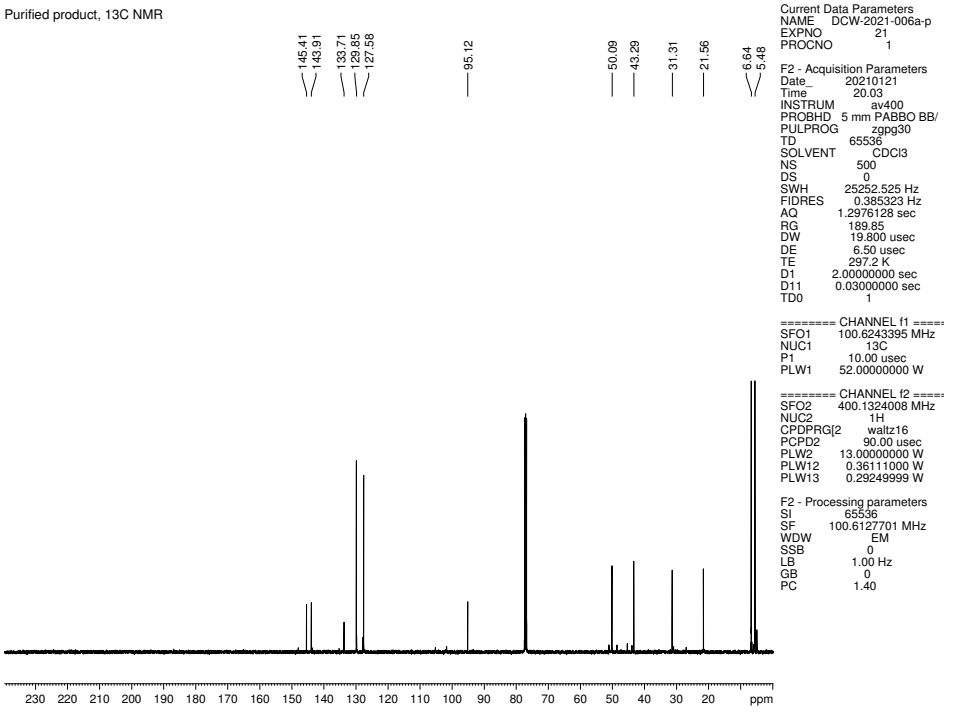

Figure 1.33. ^{13}C NMR (100 MHz, $CDCl_3$) of compound **1.75**.

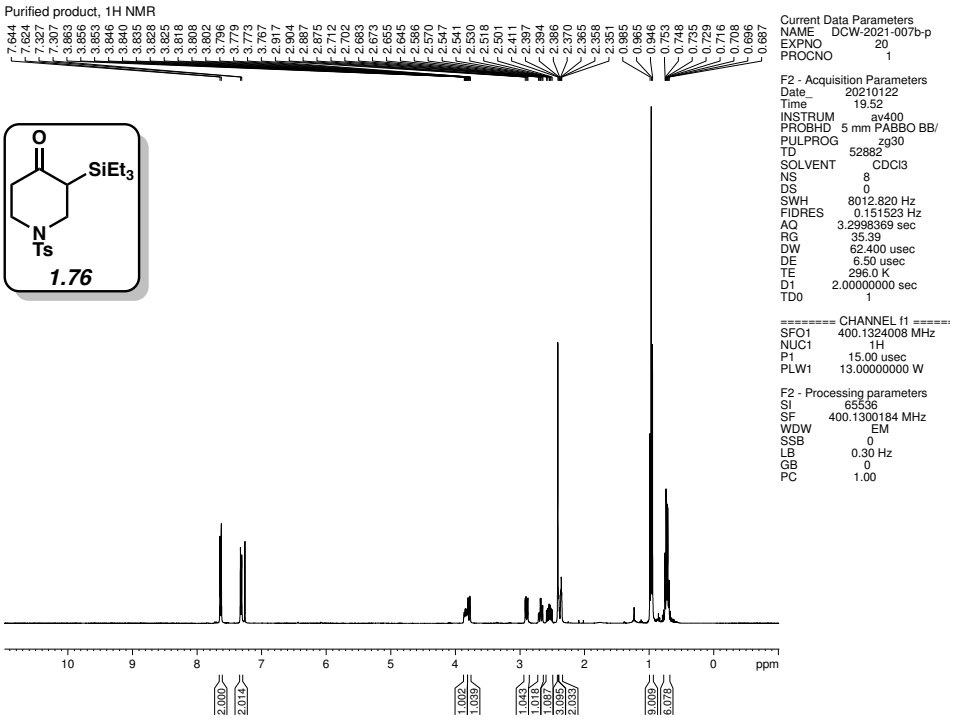

Figure 1.34. ^{1}H NMR (400 MHz, $CDCl_3$) of compound **1.76**.

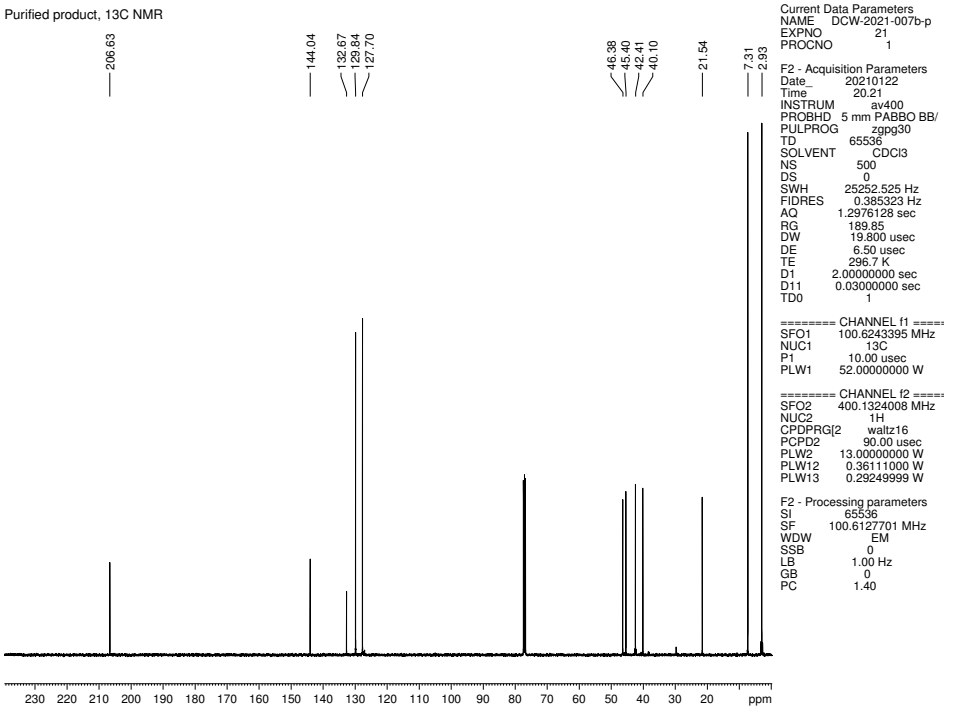

Figure 1.35. ^{13}C NMR (100 MHz, $CDCl_3$) of compound **1.76**.

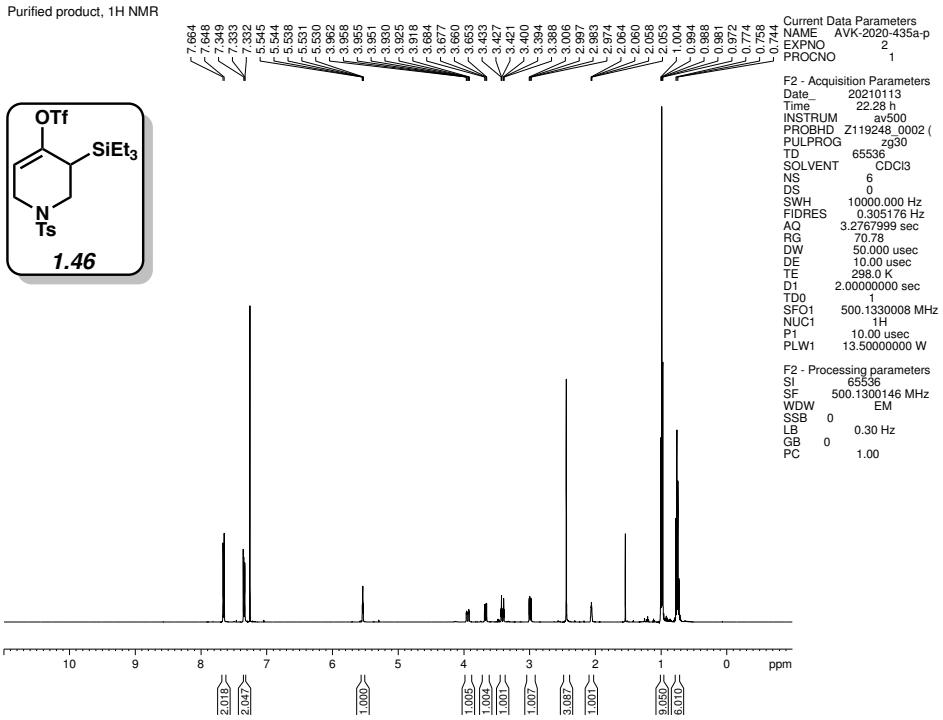

Figure 1.36. ^{1}H NMR (500 MHz, $CDCl_3$) of compound **1.46**.

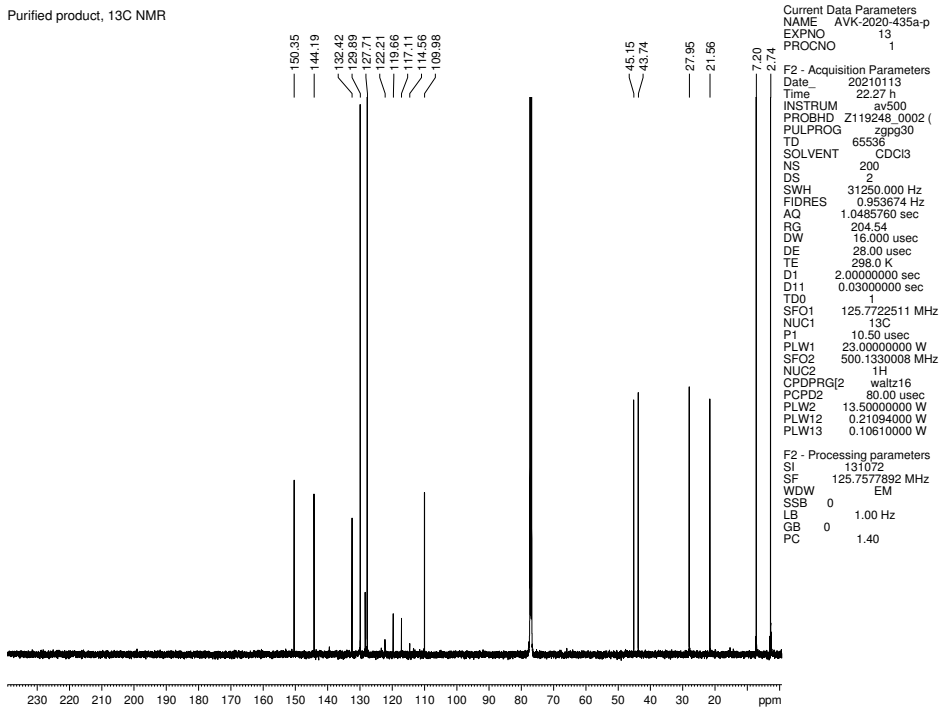

Figure 1.37. ^{13}C NMR (125 MHz, $CDCl_3$) of compound **1.46**.

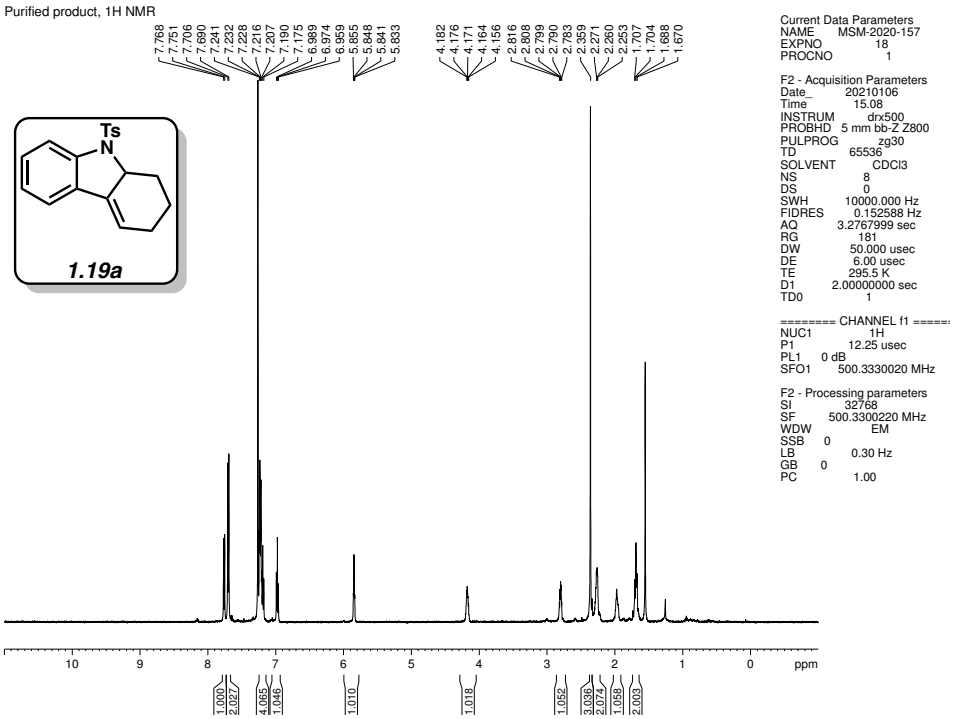

Figure 1.38. ^{1}H NMR (500 MHz, $CDCl_3$) of compound **1.19a**.

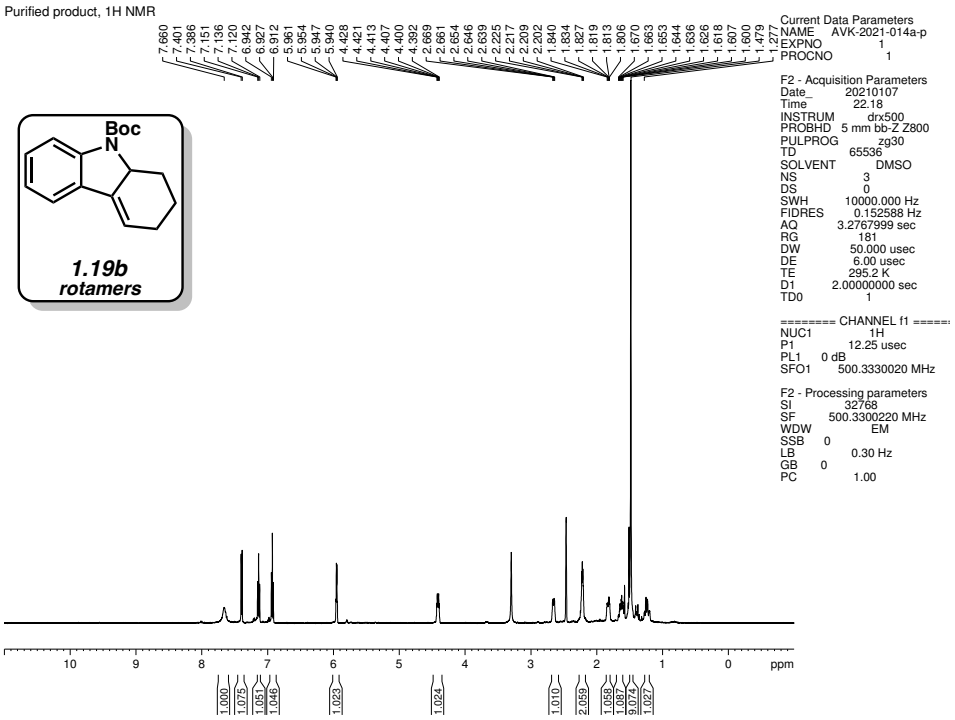

Figure 1.39. ^{1}H NMR (500 MHz, DMSO-d_6) of compound **1.19b**.

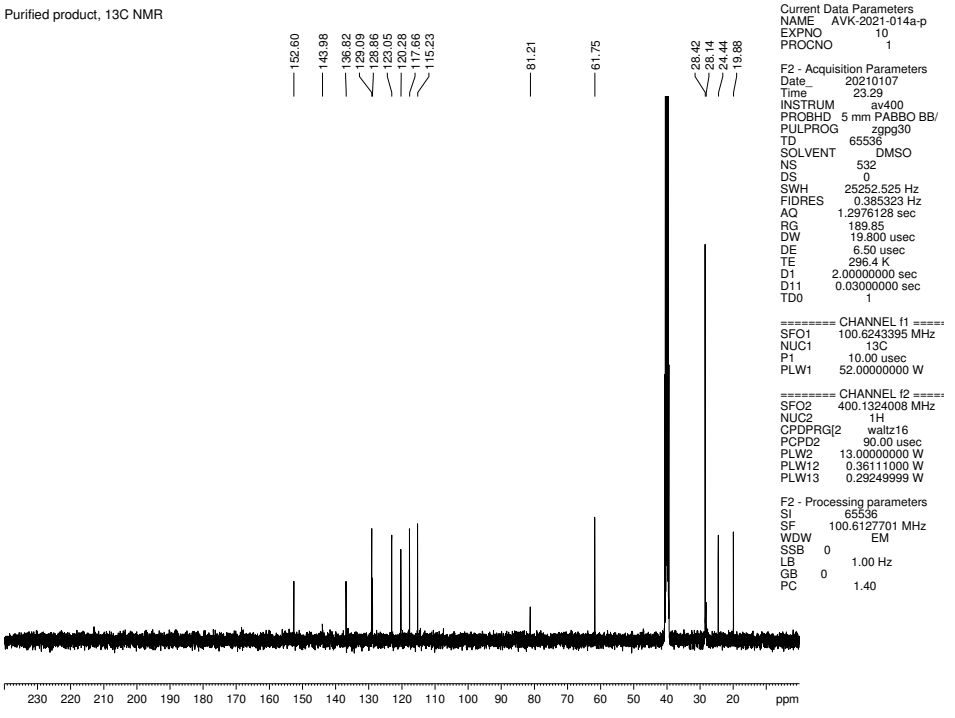

Figure 1.40. ^{13}C NMR (100 MHz, DMSO-d_6) of compound **1.19b**.

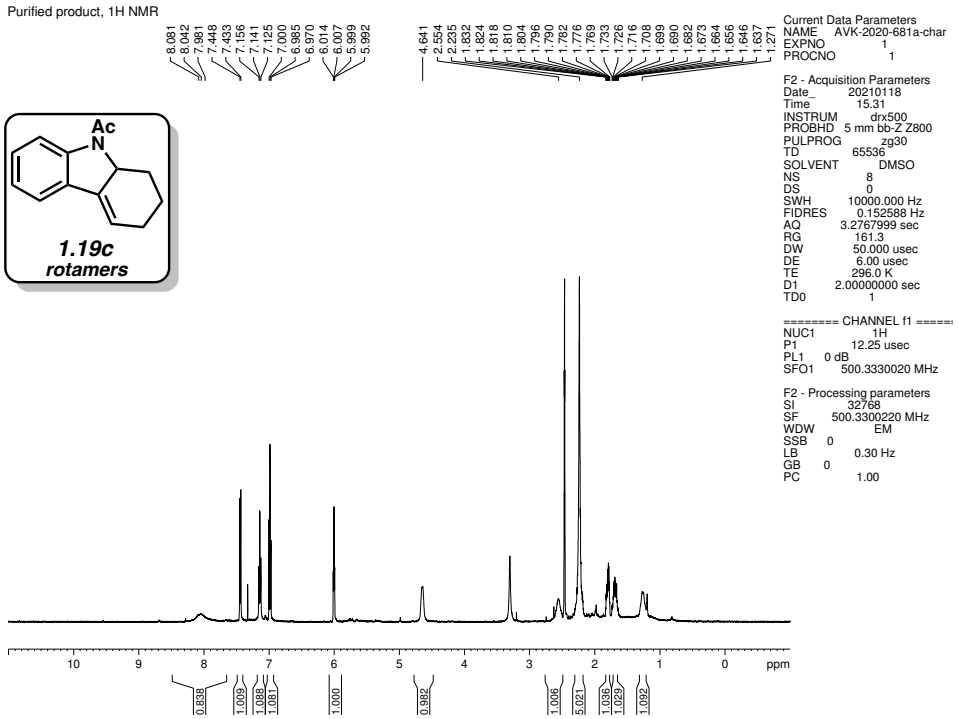

Figure 1.41. ^{1}H NMR (500 MHz, DMSO-d_6) of compound **1.19c**.

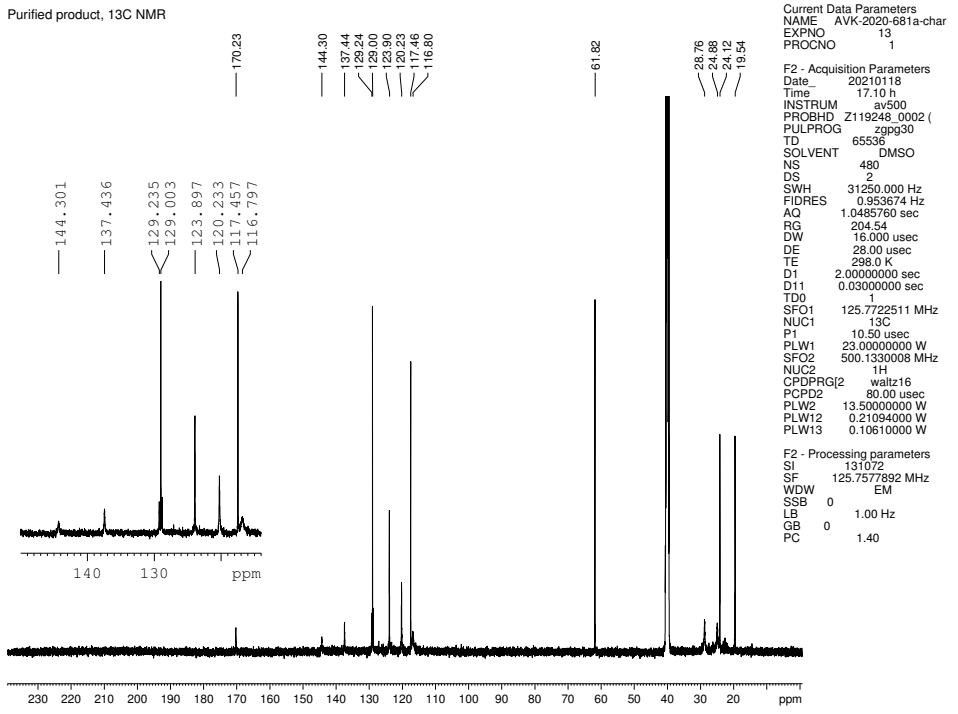

Figure 1.42. ^{13}C NMR (125 MHz, DMSO-d_6) of compound **1.19c**.

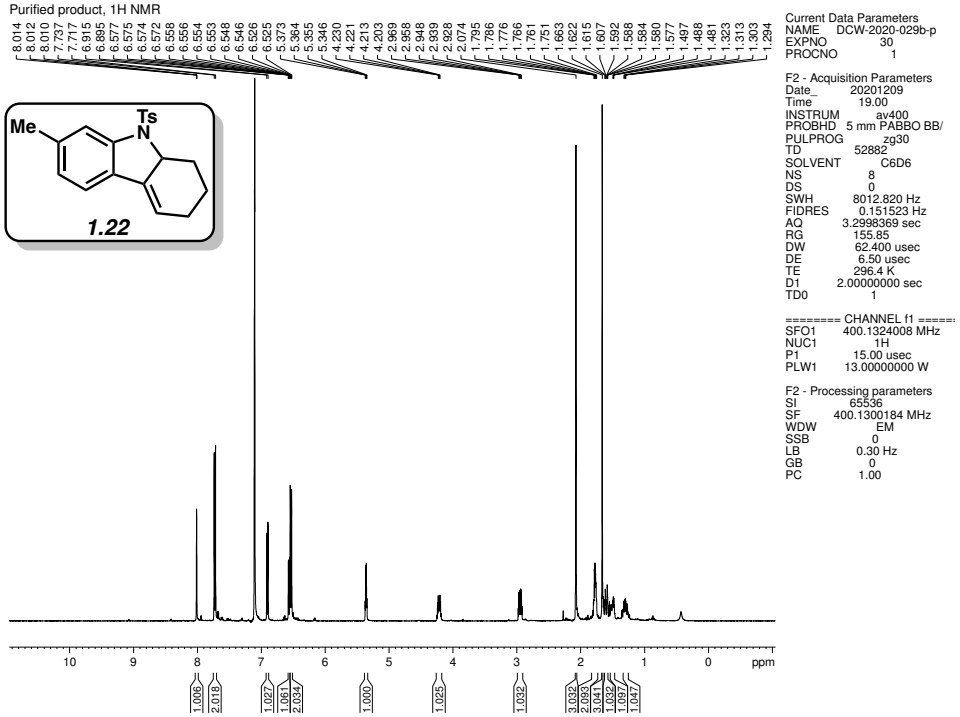

Figure 1.43. ^{1}H NMR (400 MHz, C_6D_6) of compound **1.22**.

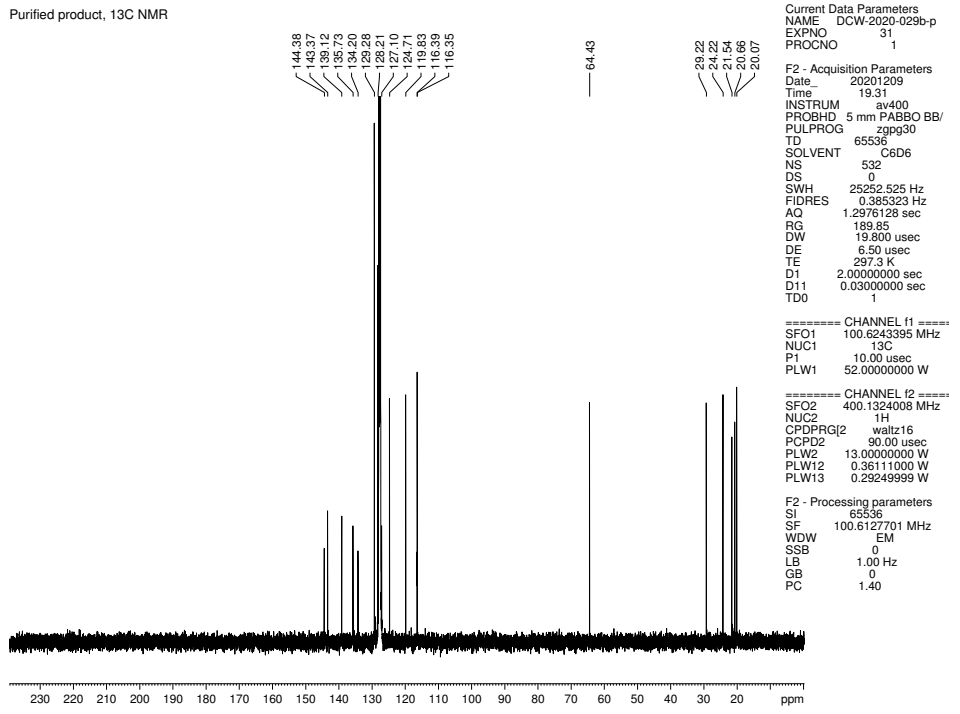

Figure 1.44. ^{13}C NMR (100 MHz, C_6D_6) of compound **1.22**.

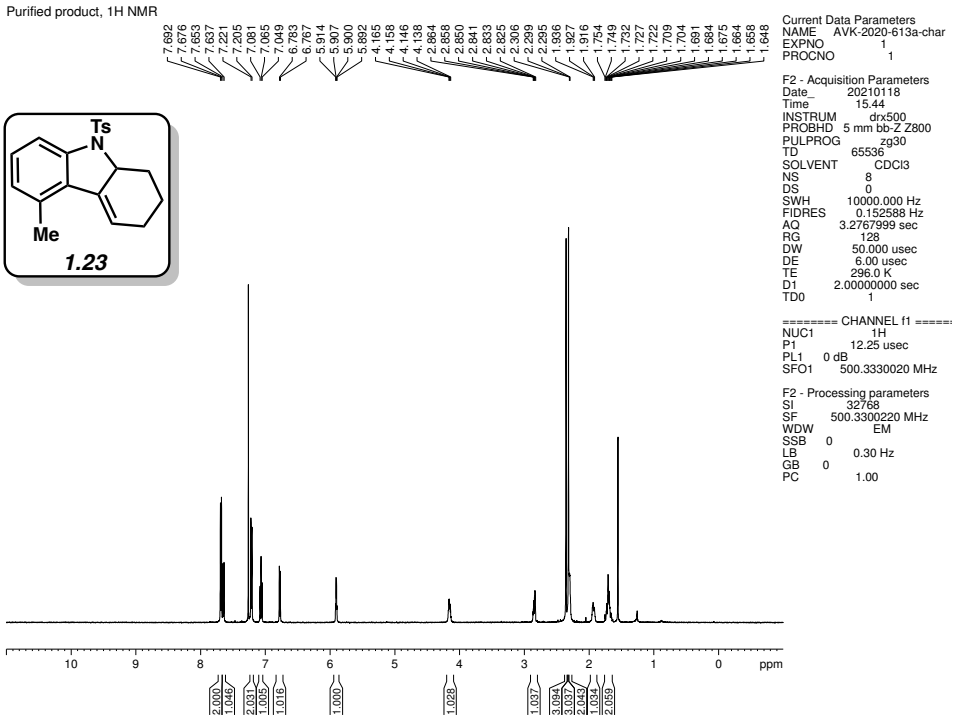

Figure 1.45. ^{1}H NMR (500 MHz, $CDCl_3$) of compound **1.23**.

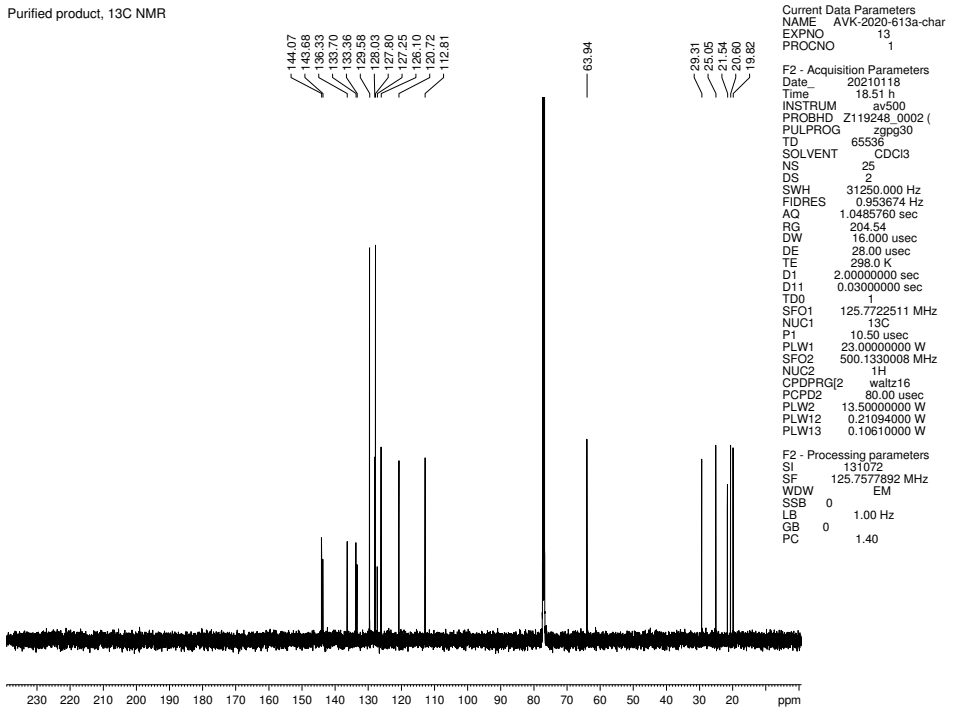

Figure 1.46. ^{13}C NMR (125 MHz, $CDCl_3$) of compound **1.23**.

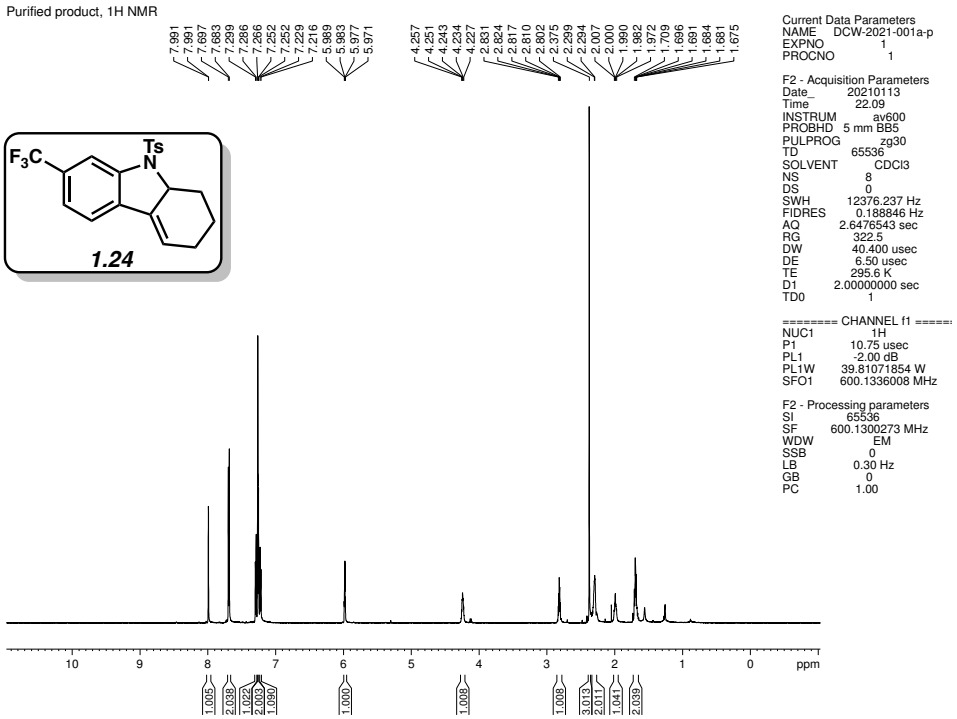

Figure 1.47. ^{1}H NMR (600 MHz, $CDCl_3$) of compound **1.24**.

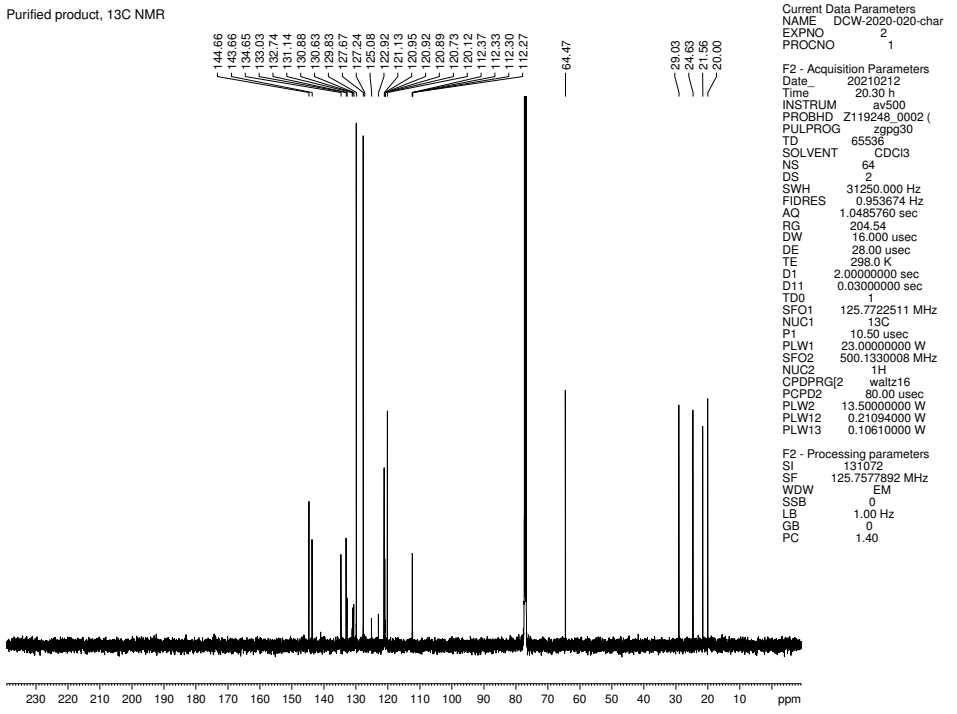

Figure 1.48. ^{13}C NMR (125 MHz, $CDCl_3$) of compound **1.24**.

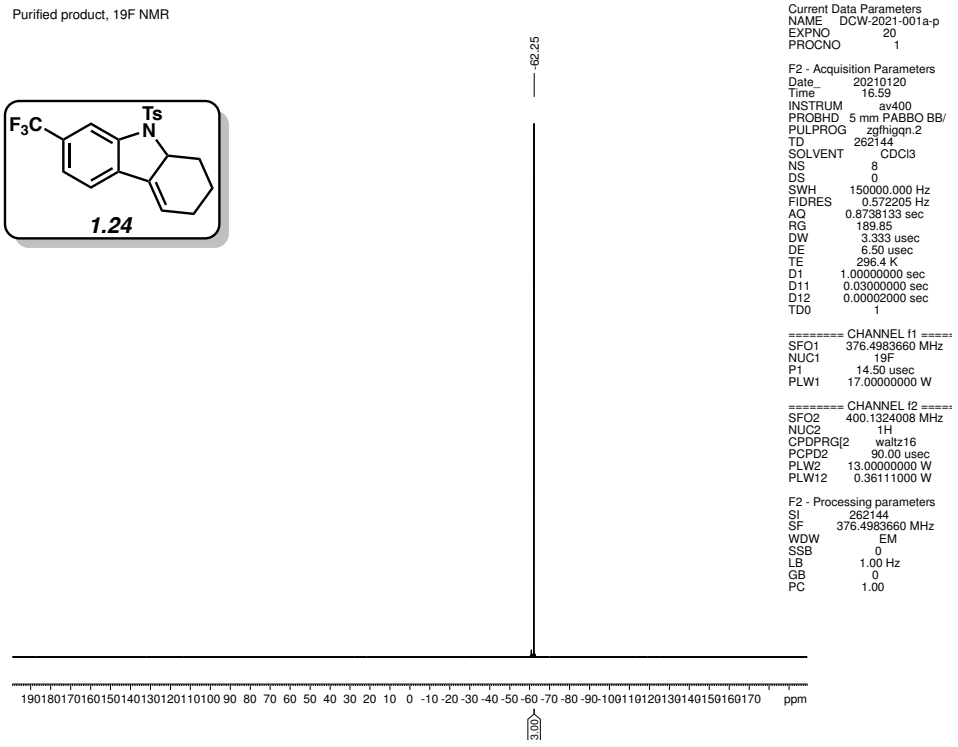

Figure 1.49. ^{19}F NMR (376 MHz, $CDCl_3$) of compound **1.24**.

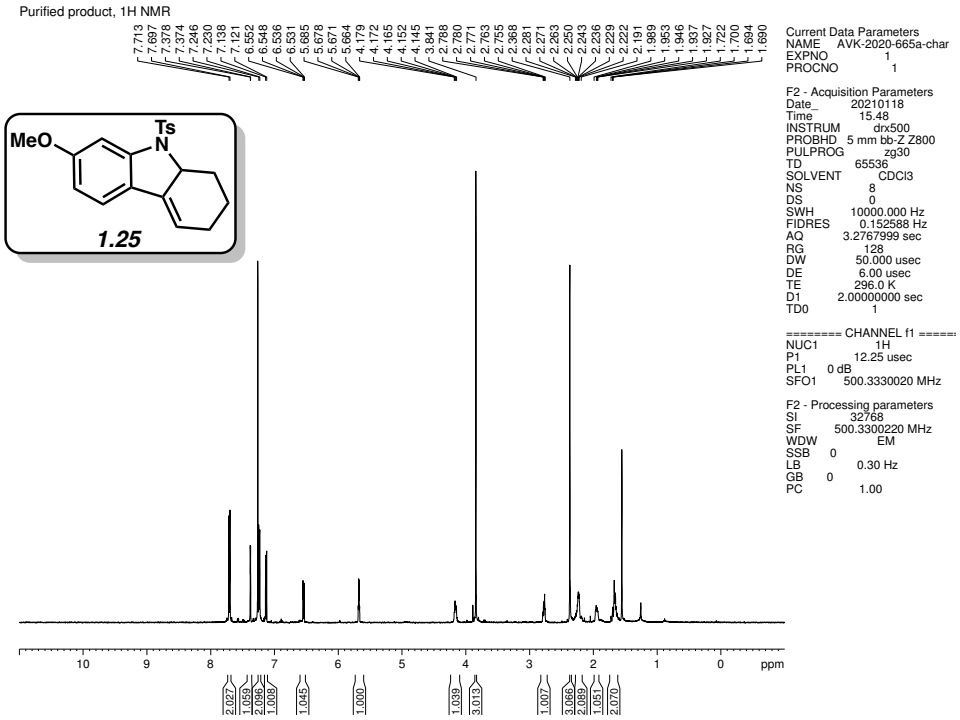

Figure 1.50. ^{1}H NMR (500 MHz, $CDCl_3$) of compound **1.25**.

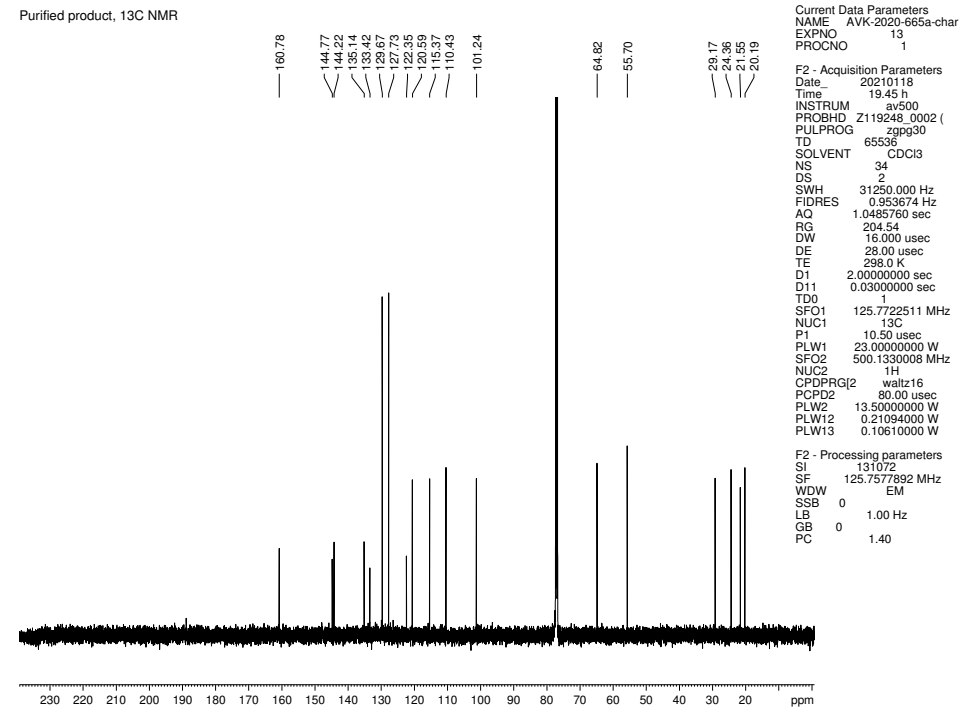

Figure 1.51. ^{13}C NMR (125 MHz, $CDCl_3$) of compound **1.25**.

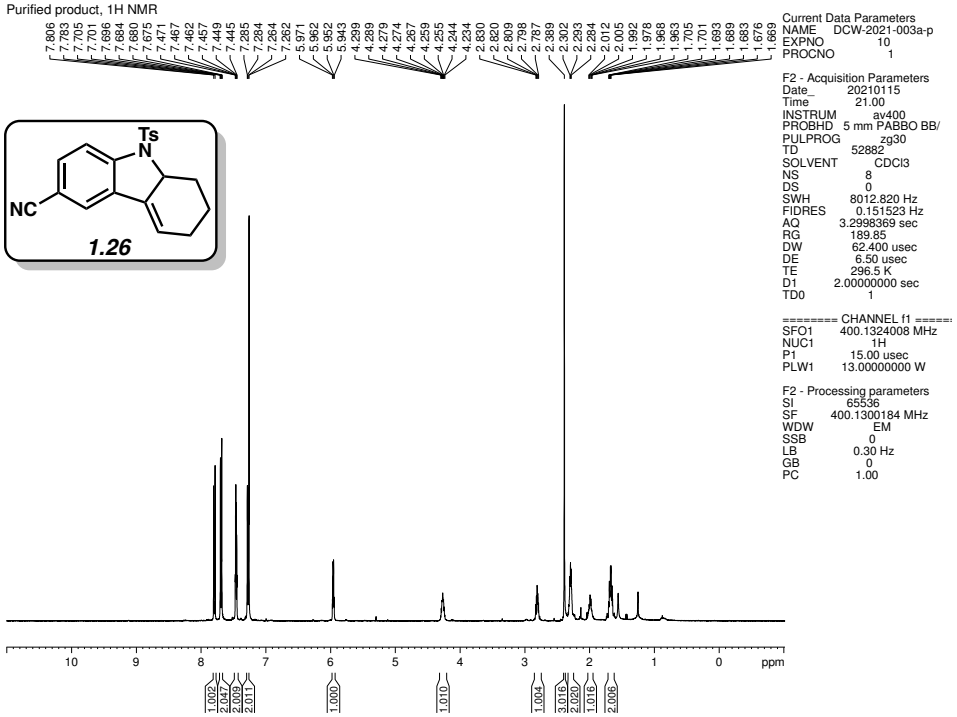

Figure 1.52. ^{1}H NMR (400 MHz, $CDCl_3$) of compound **1.26**.

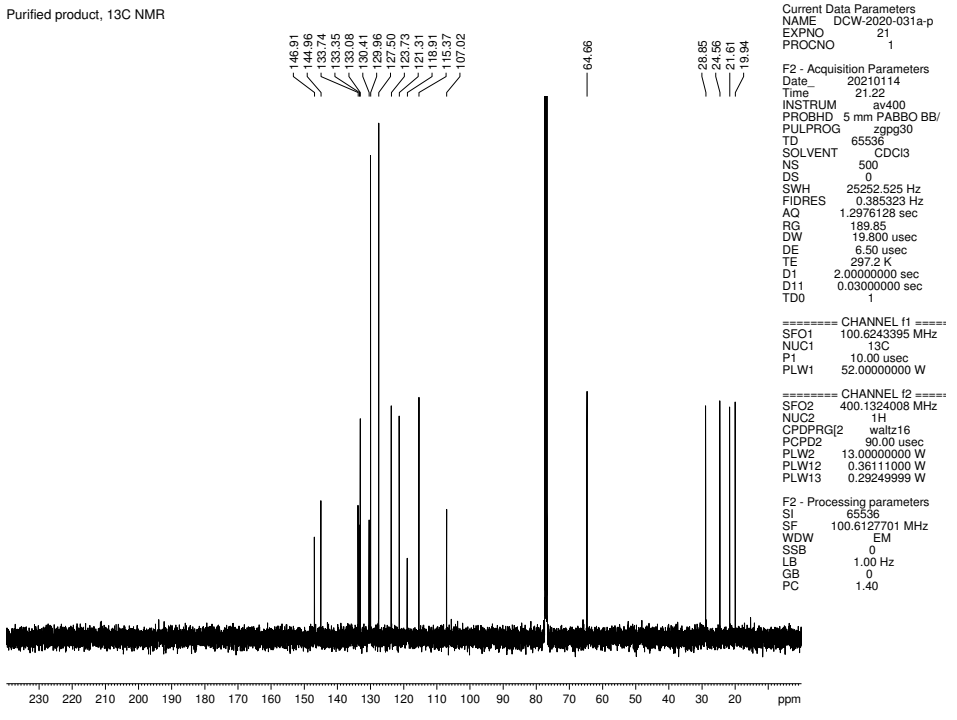

Figure 1.53. ^{13}C NMR (100 MHz, $CDCl_3$) of compound **1.26**.

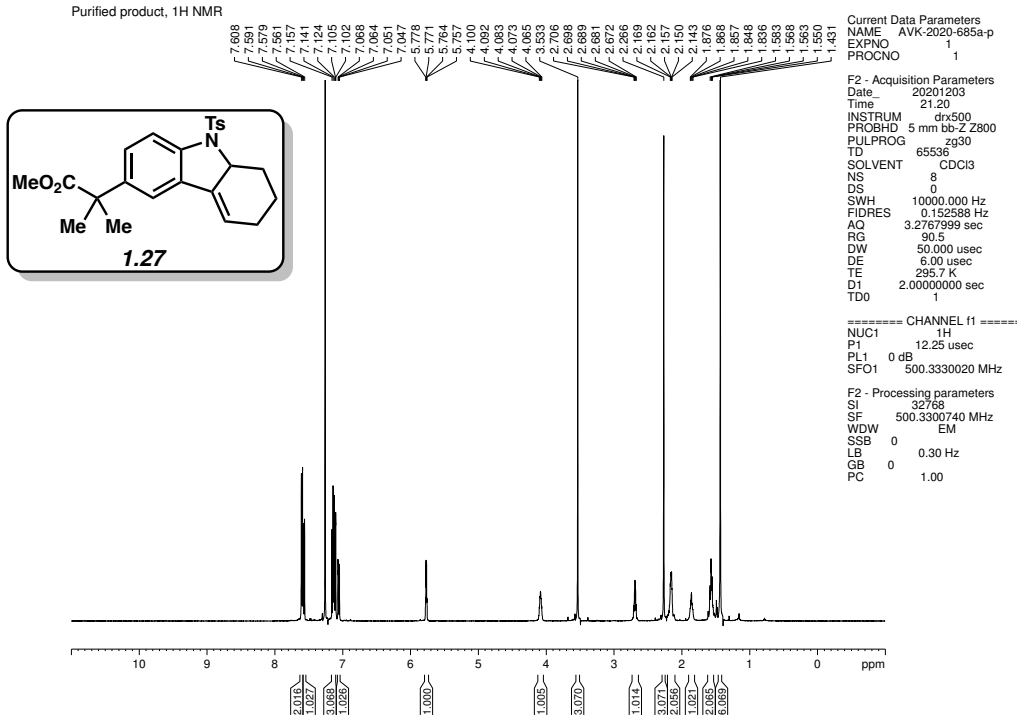

Figure 1.54. ^{1}H NMR (500 MHz, $CDCl_3$) of compound **1.27**.

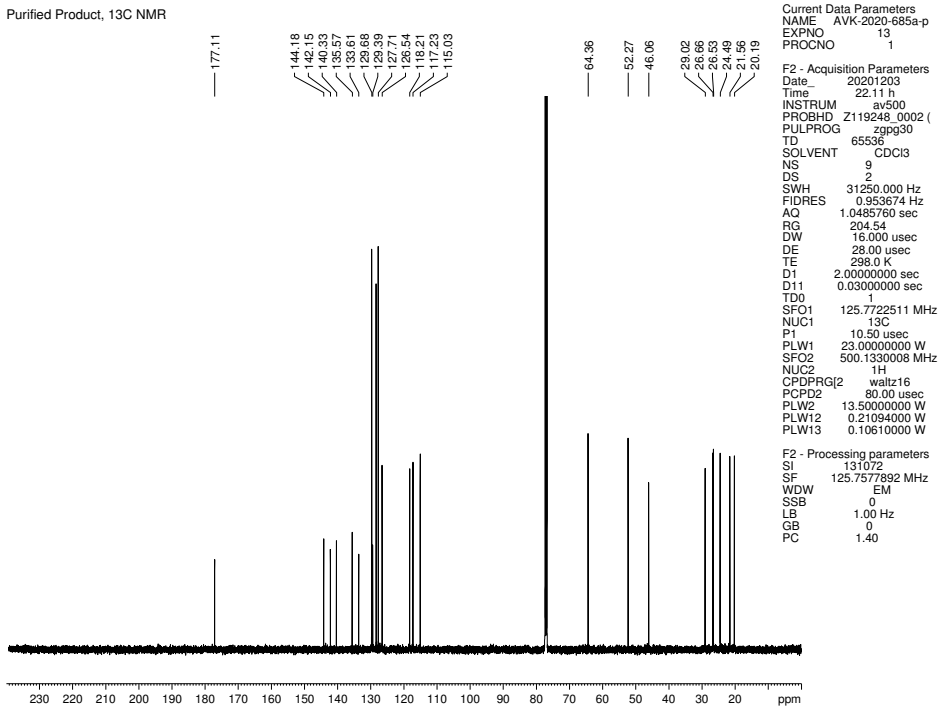

Figure 1.55. ^{13}C NMR (125 MHz, $CDCl_3$) of compound **1.27**.

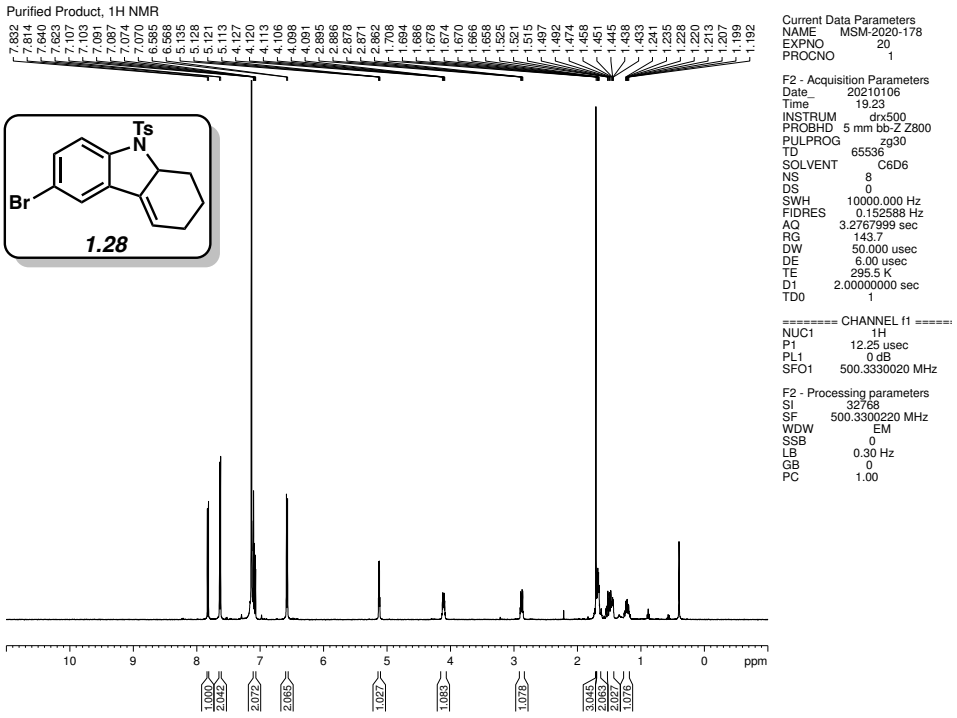

Figure 1.56. ^{1}H NMR (500 MHz, C_6D_6) of compound **1.28**.

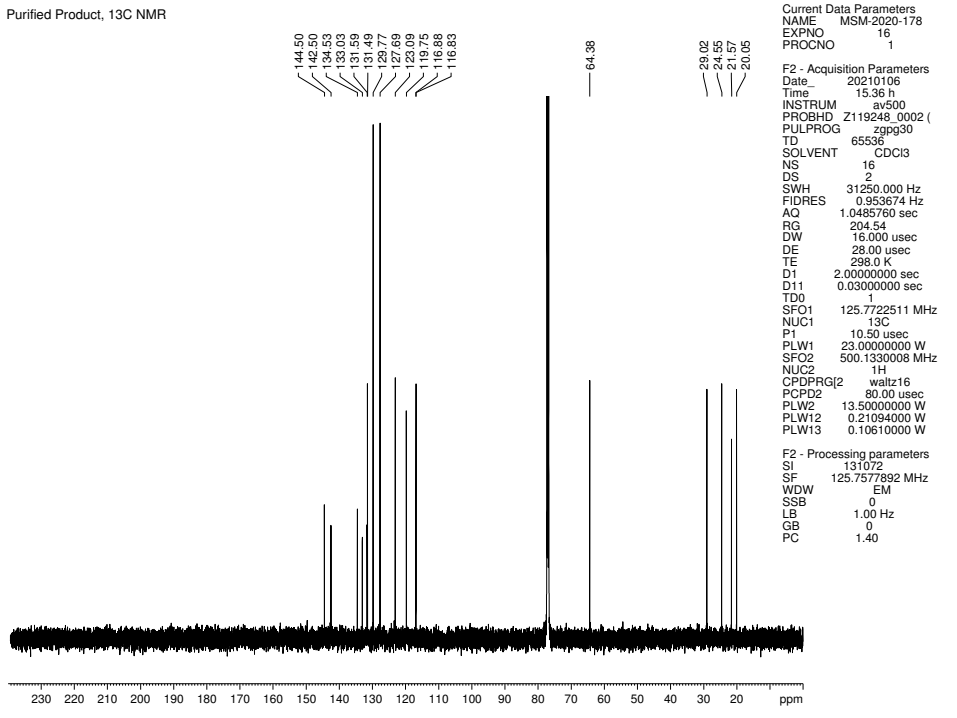

Figure 1.57. ^{13}C NMR (125 MHz, $CDCl_3$) of compound **1.28**.

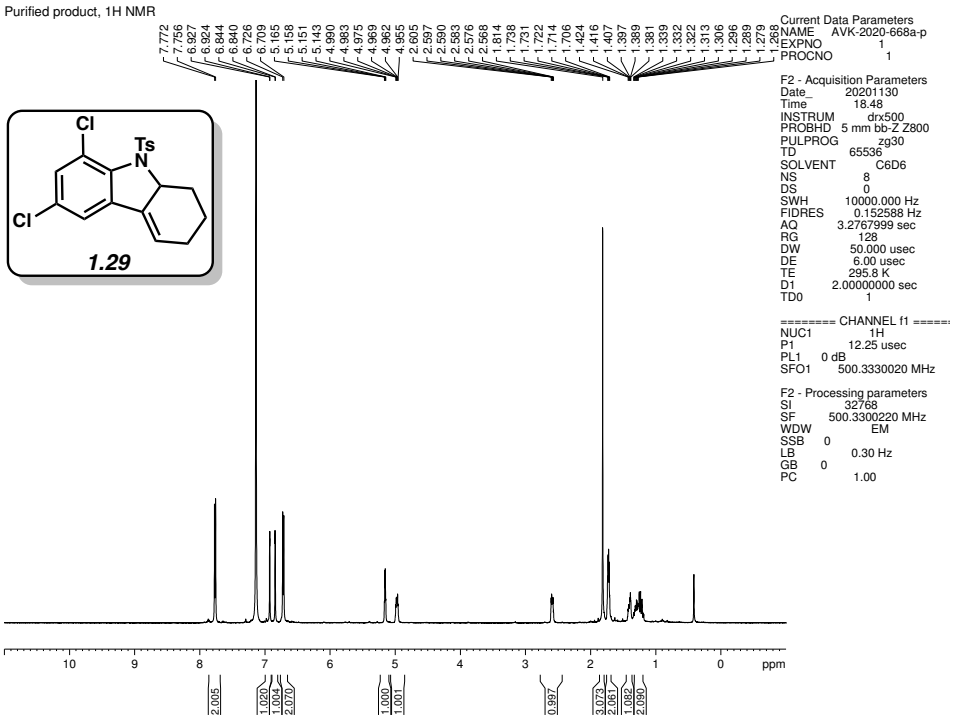

Figure 1.58. ^{1}H NMR (500 MHz, C_6D_6) of compound **1.29**.

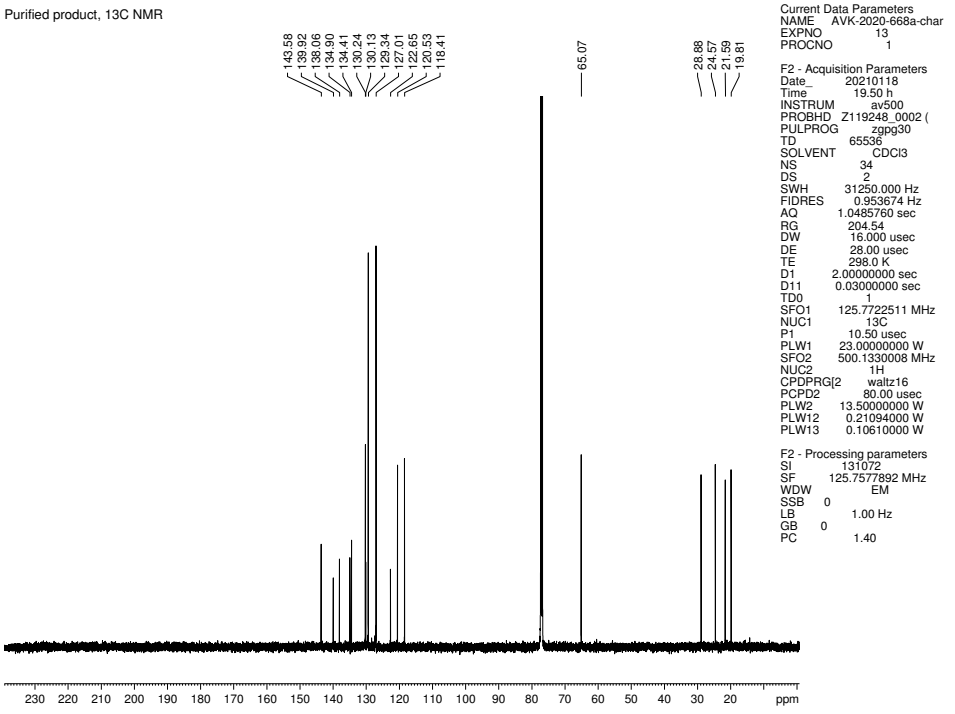

Figure 1.59. ^{13}C NMR (125 MHz, $CDCl_3$) of compound **1.29**.

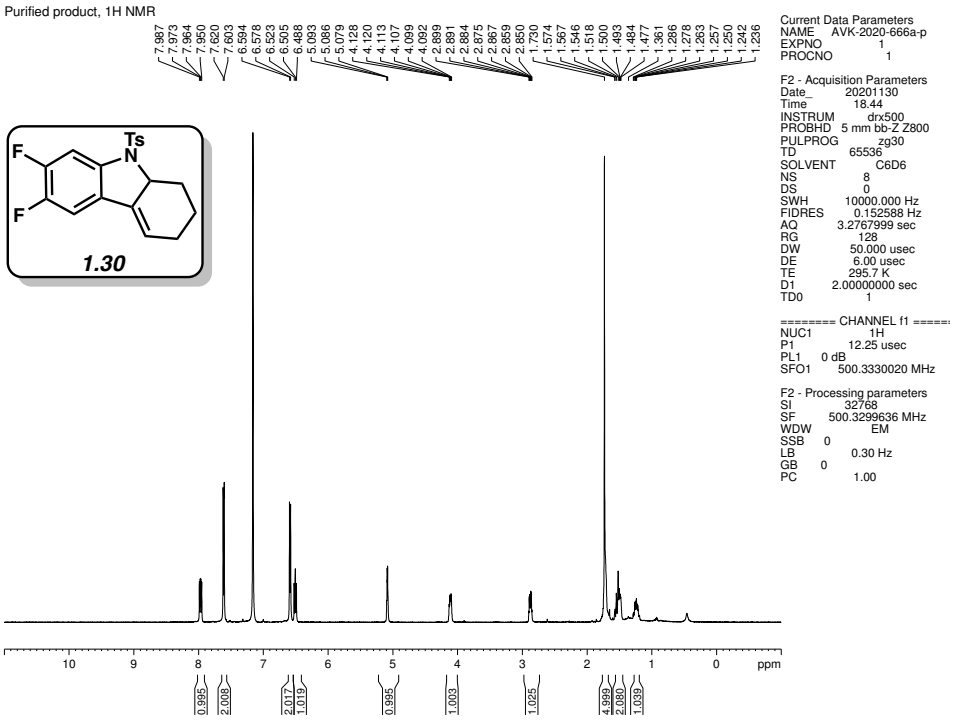

Figure 1.60. ^{1}H NMR (500 MHz, C_6D_6) of compound **1.30**.

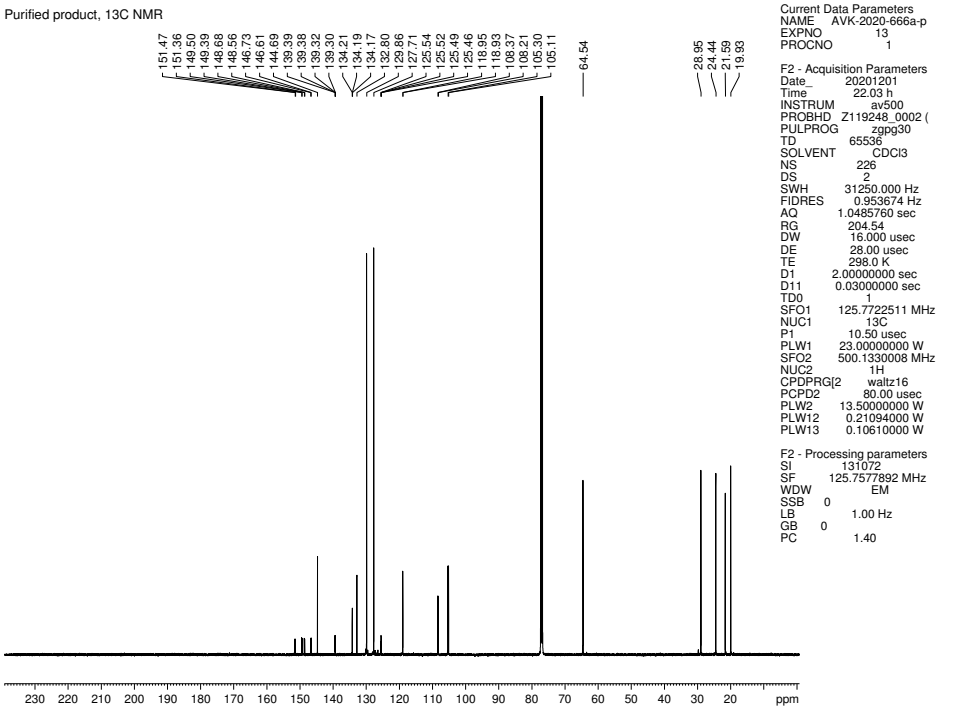

Figure 1.61. ^{13}C NMR (125 MHz, $CDCl_3$) of compound **1.30**.

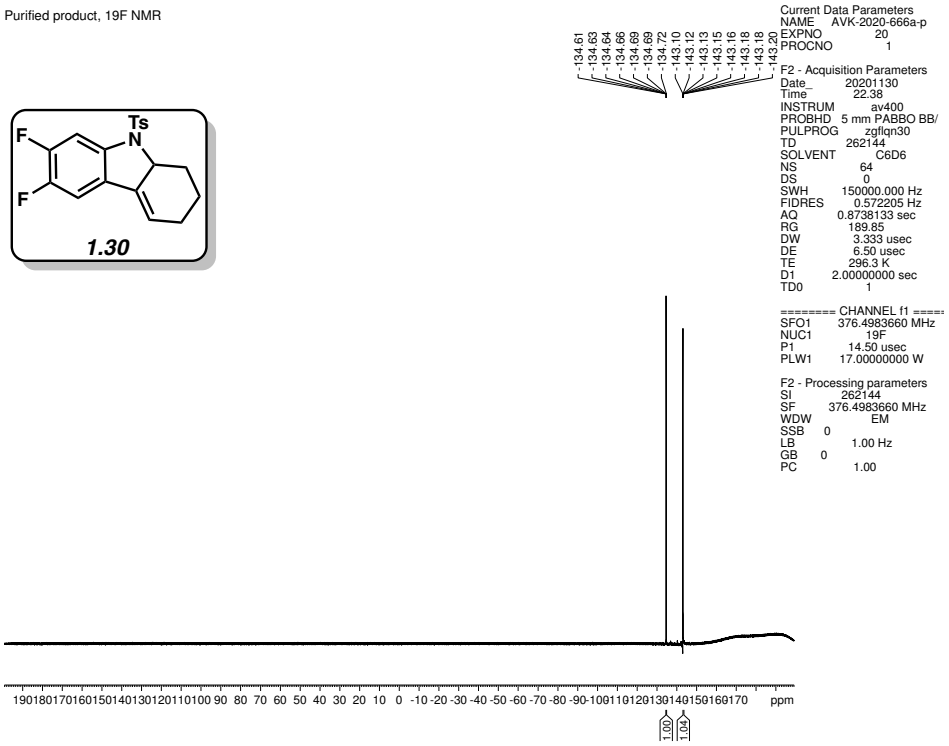

Figure 1.62. ^{19}F NMR (376 MHz, C_6D_6) of compound **1.30**.

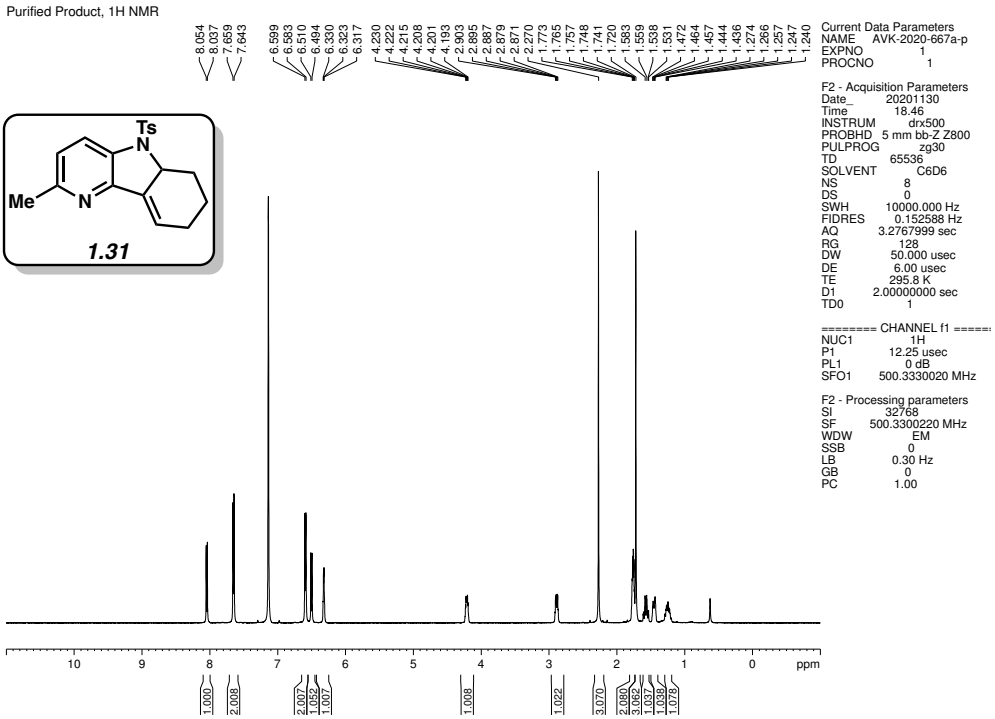

Figure 1.63. ^{1}H NMR (500 MHz, C_6D_6) of compound **1.31**.

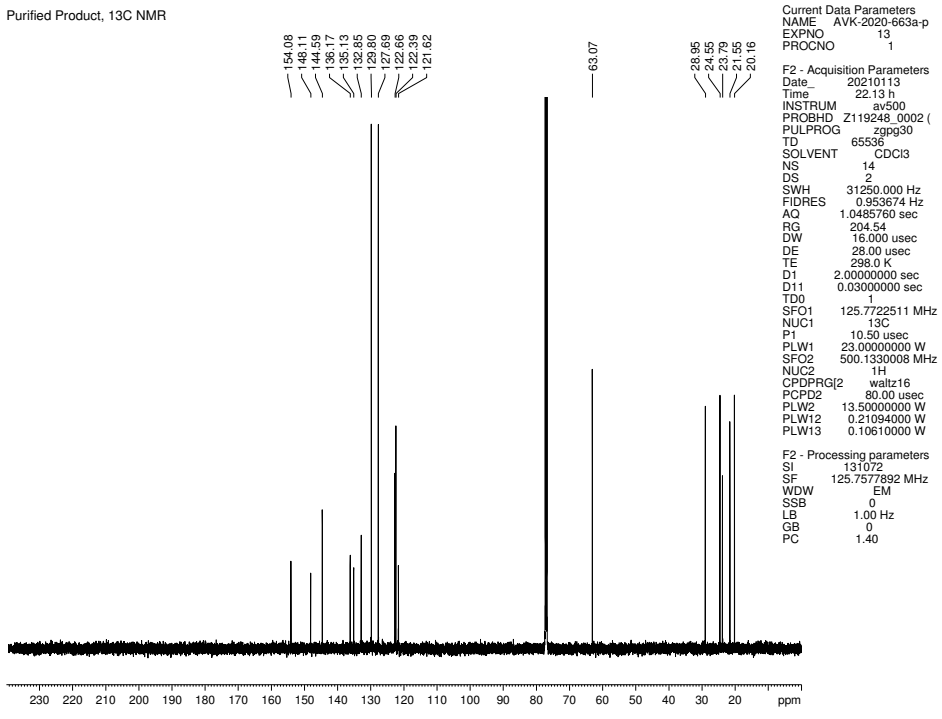

Figure 1.64. ^{13}C NMR (125 MHz, $CDCl_3$) of compound **1.31**.

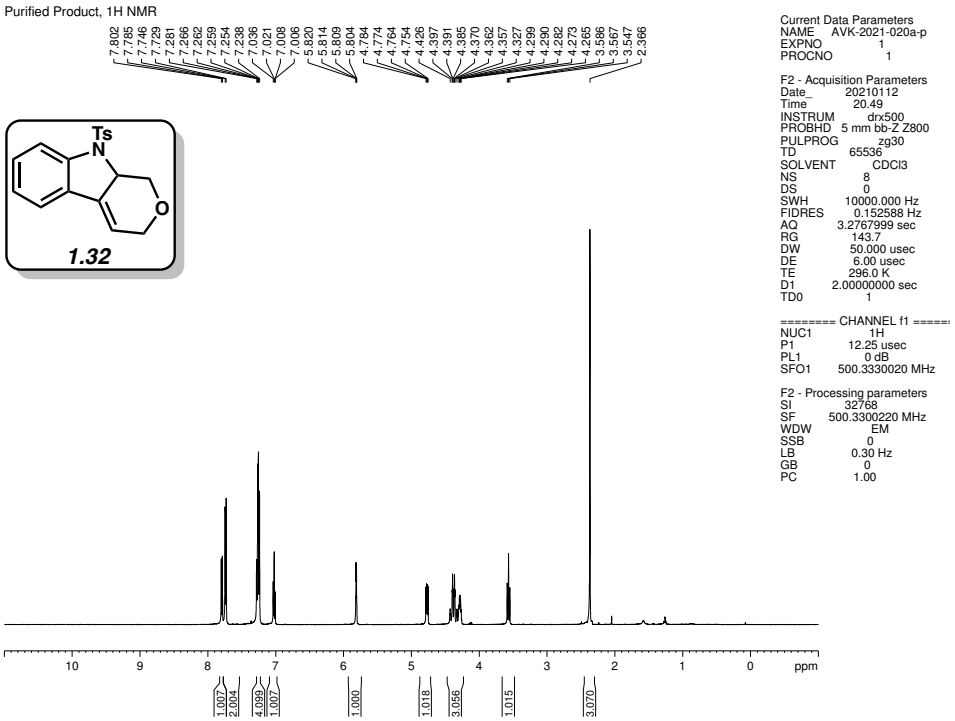

Figure 1.65. ^{1}H NMR (500 MHz, $CDCl_3$) of compound **1.32**.

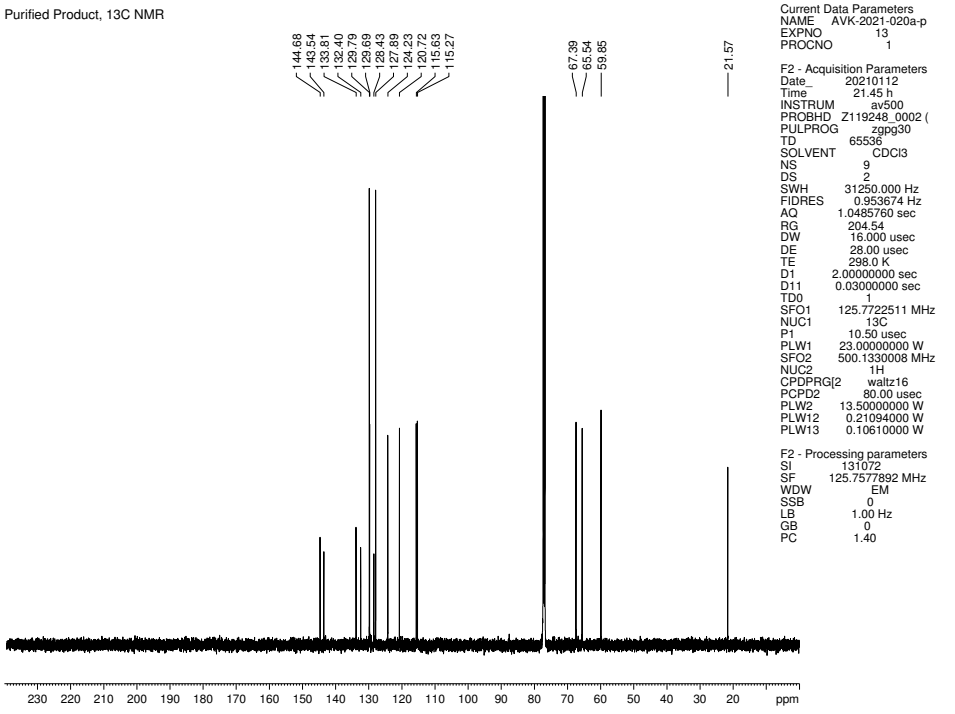

Figure 1.66. ^{13}C NMR (125 MHz, $CDCl_3$) of compound **1.32**.

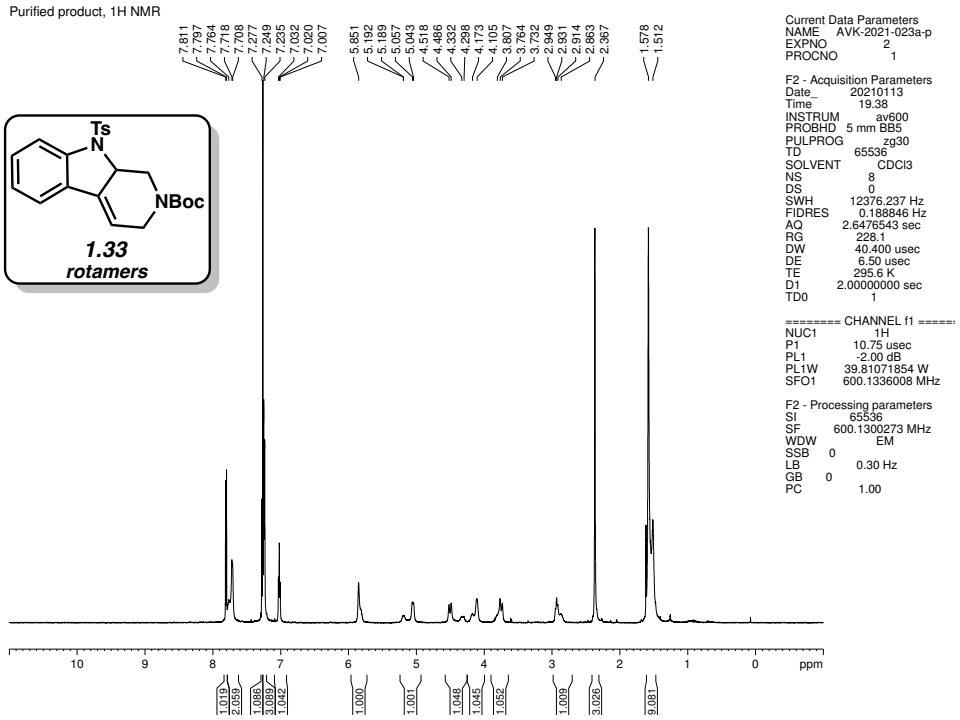

Figure 1.67. ^{1}H NMR (600 MHz, $CDCl_3$) of compound **1.33**.

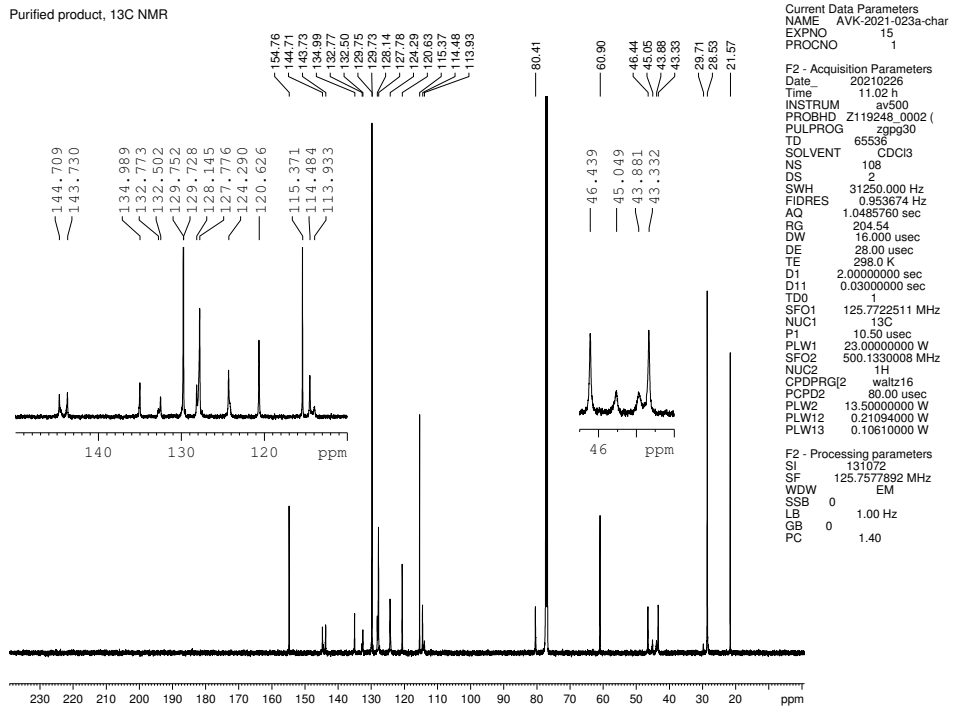

Figure 1.68. ^{13}C NMR (125 MHz, $CDCl_3$) of compound **1.33**.

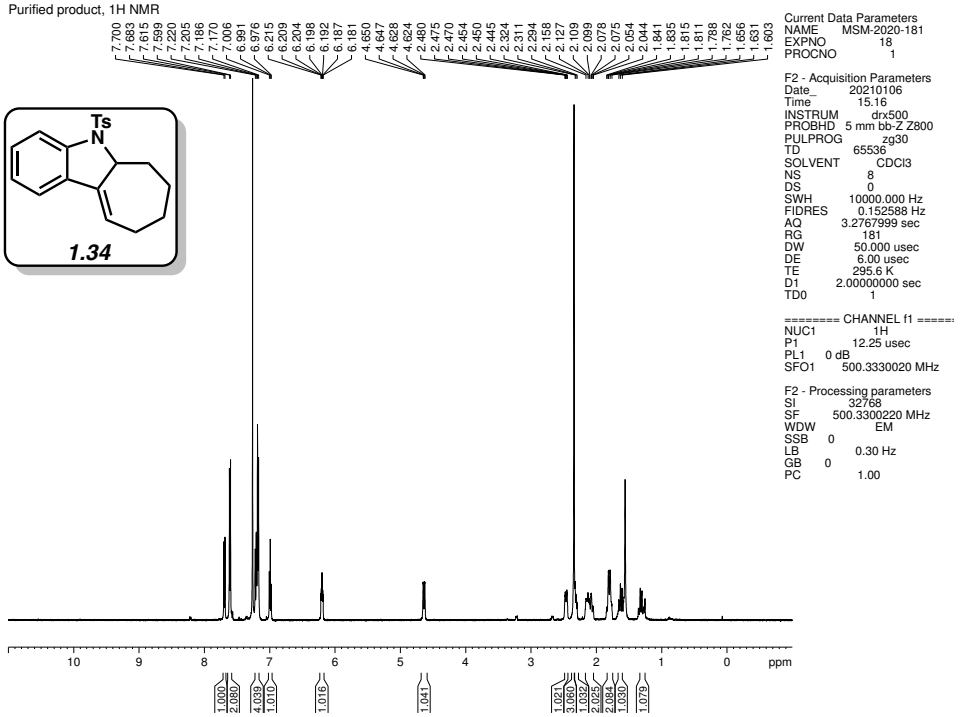

Figure 1.69. ^{1}H NMR (500 MHz, $CDCl_3$) of compound **1.34**.

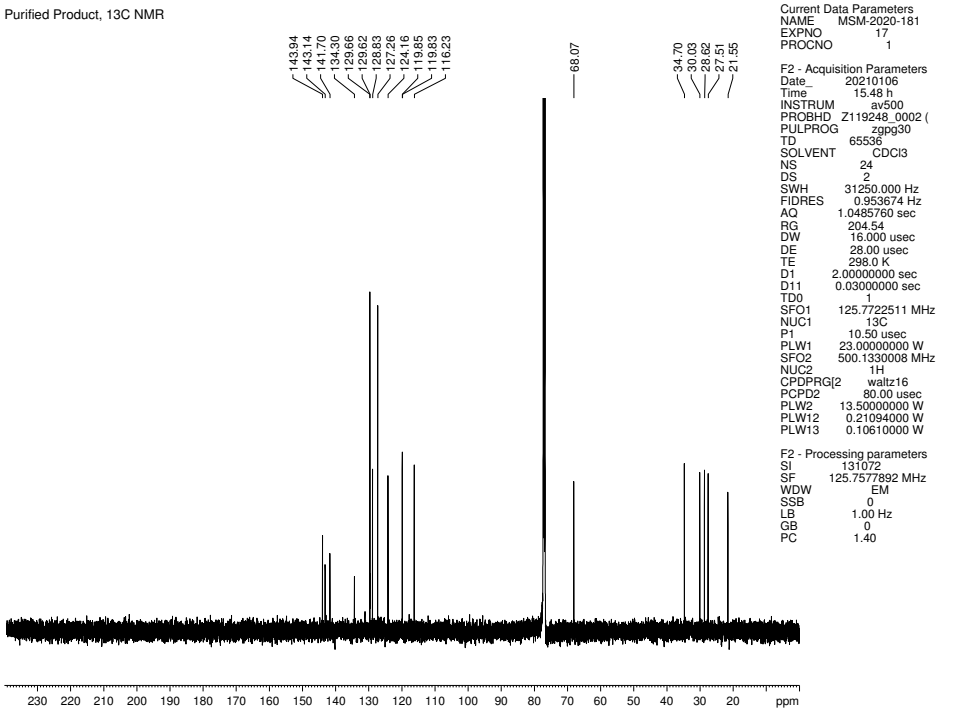

Figure 1.70. ^{13}C NMR (125 MHz, $CDCl_3$) of compound **1.34**.

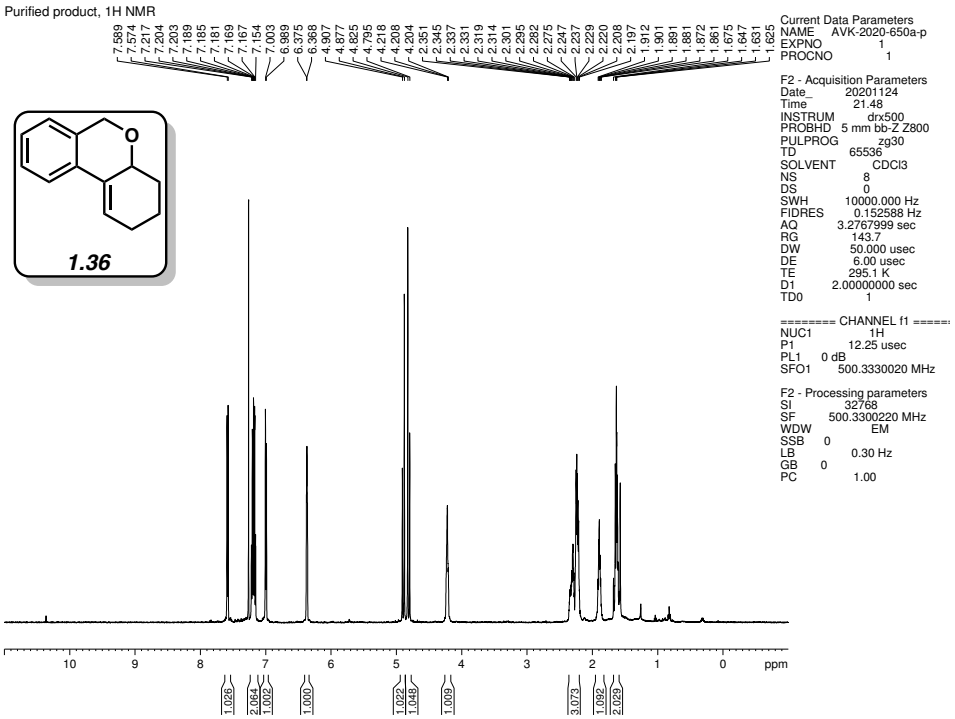

Figure 1.71. ^{1}H NMR (500 MHz, $CDCl_3$) of compound **1.36**.

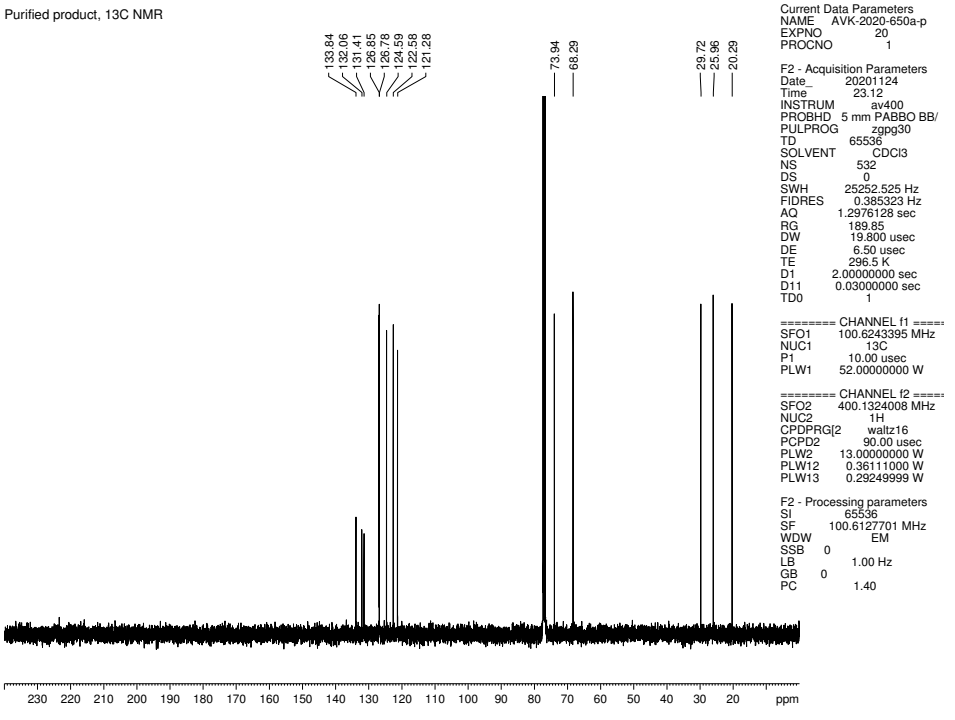

Figure 1.72. ^{13}C NMR (100 MHz, $CDCl_3$) of compound **1.36**.

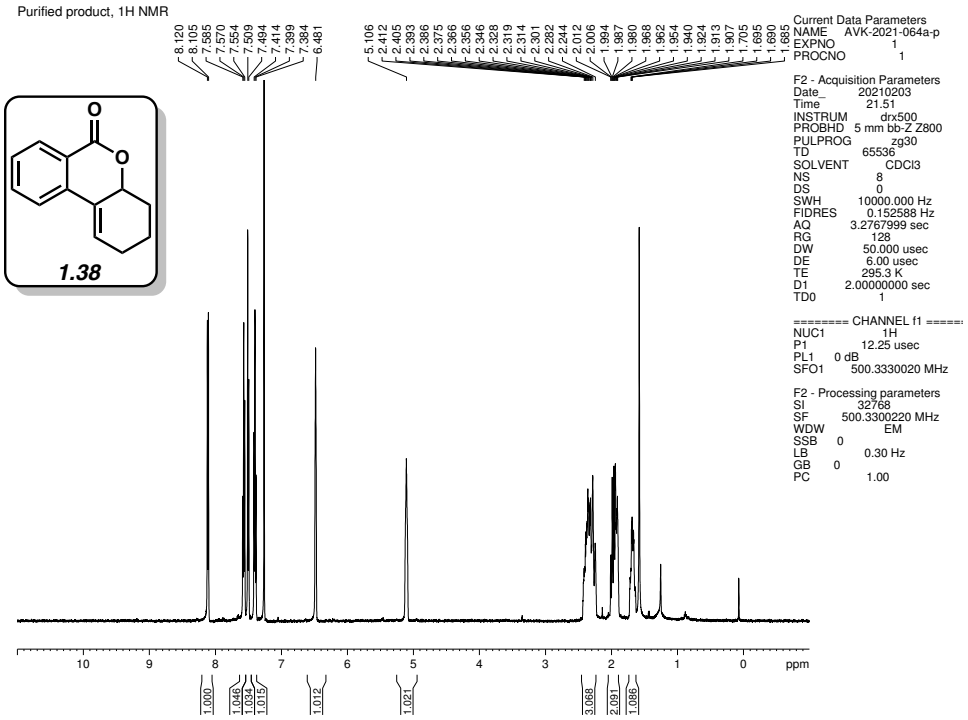

Figure 1.73. ^{1}H NMR (500 MHz, $CDCl_3$) of compound **1.38**.

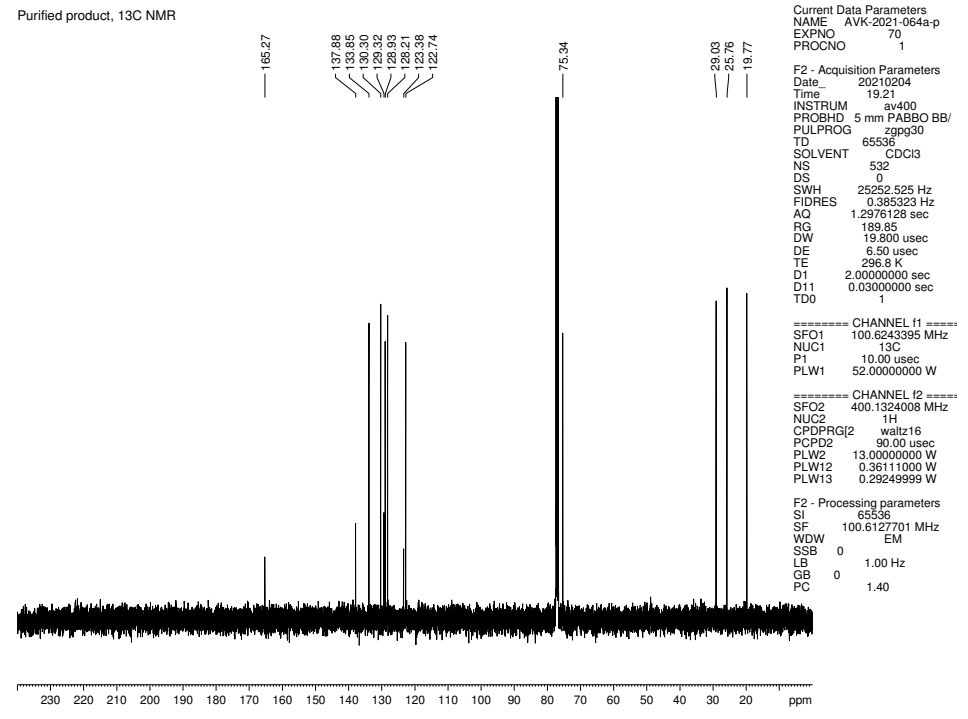

Figure 1.74. ^{13}C NMR (100 MHz, $CDCl_3$) of compound **1.38**.

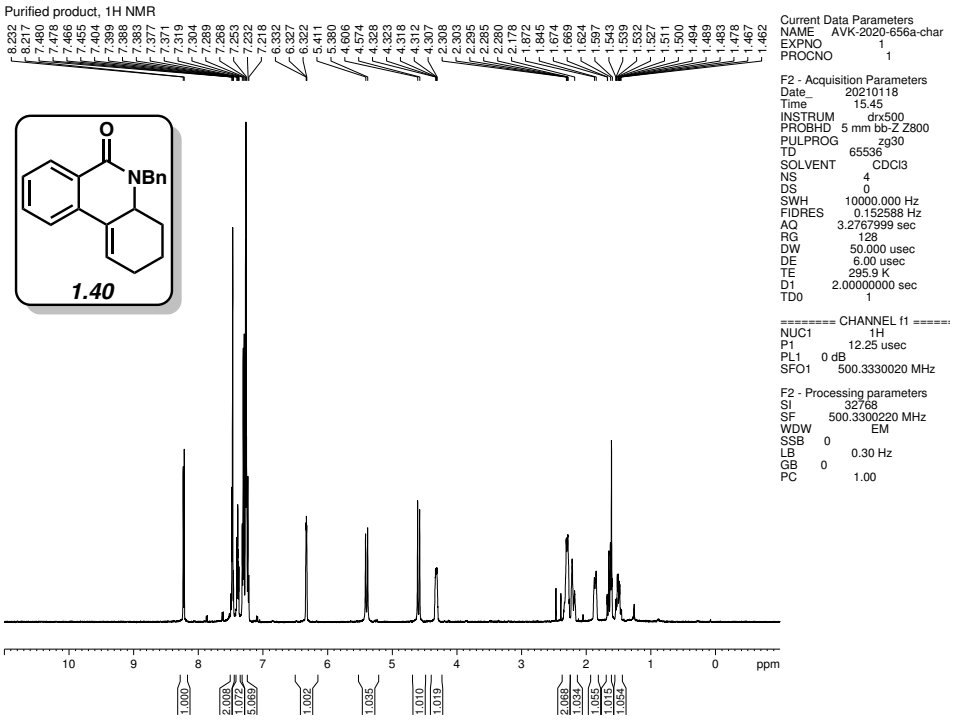

Figure 1.75. ^{1}H NMR (500 MHz, $CDCl_3$) of compound **1.40**.

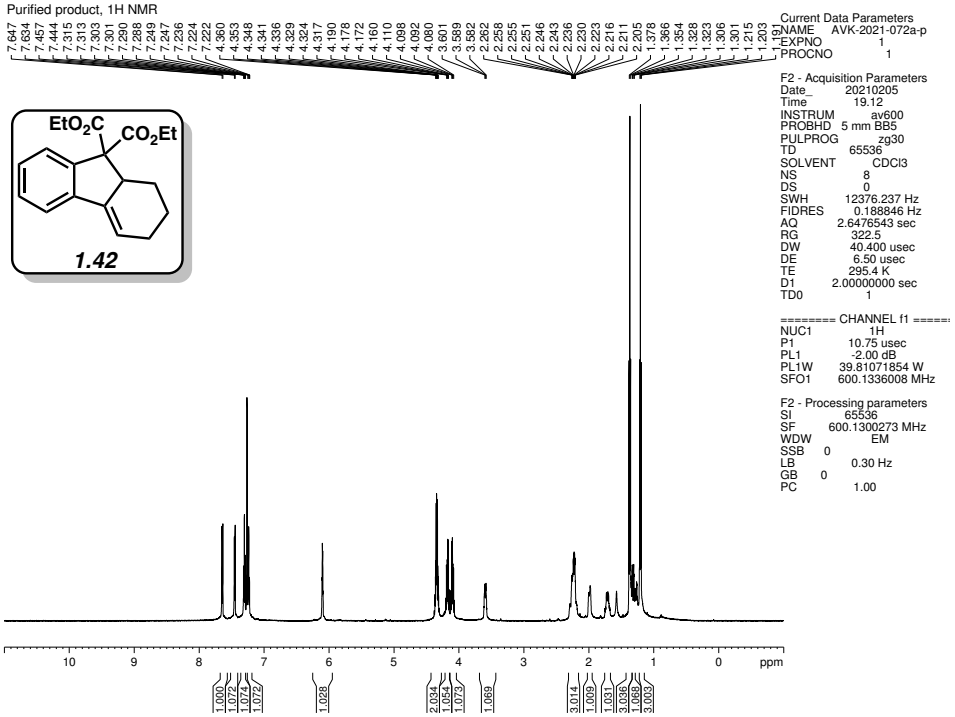

Figure 1.76. ^{1}H NMR (600 MHz, $CDCl_3$) of compound **1.42**.

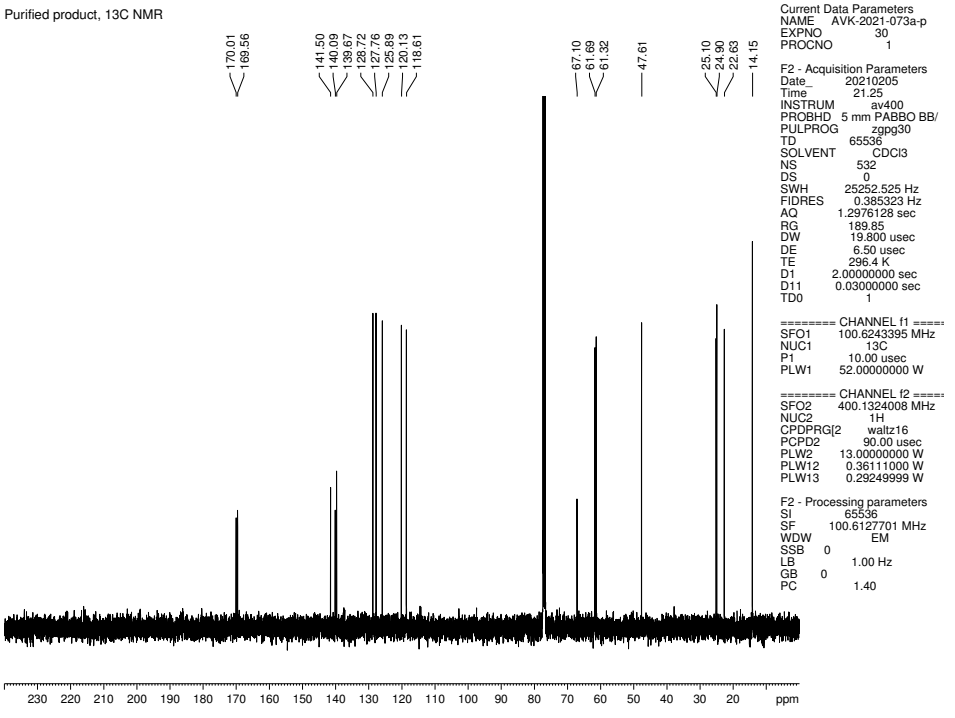

Figure 1.77. ^{13}C NMR (100 MHz, $CDCl_3$) of compound **1.42**.

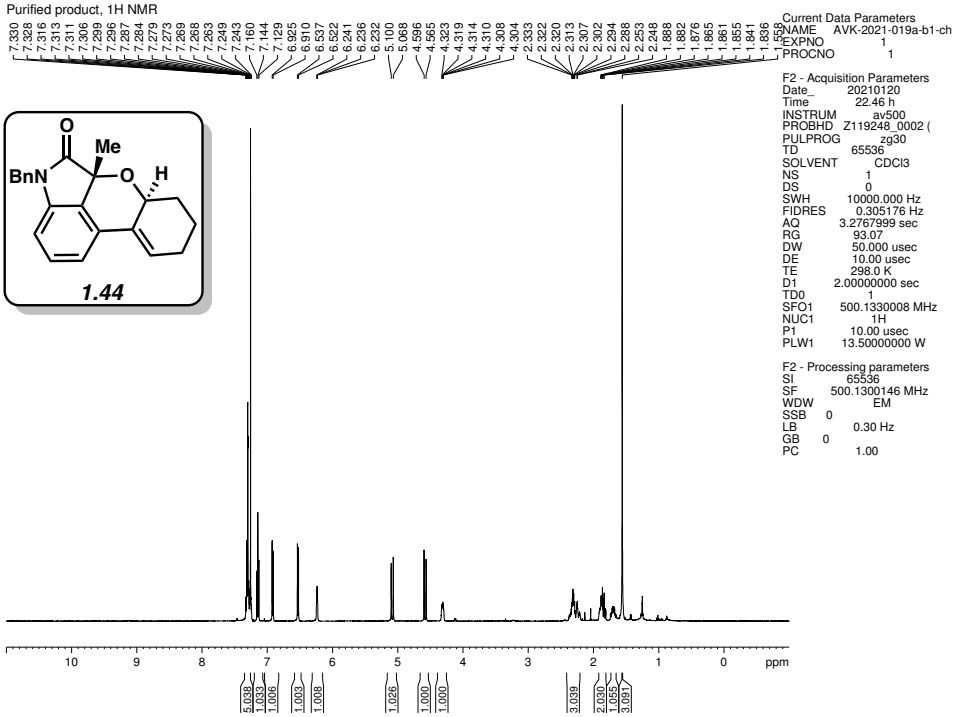

Figure 1.78. ^{1}H NMR (500 MHz, $CDCl_3$) of compound **1.44**.

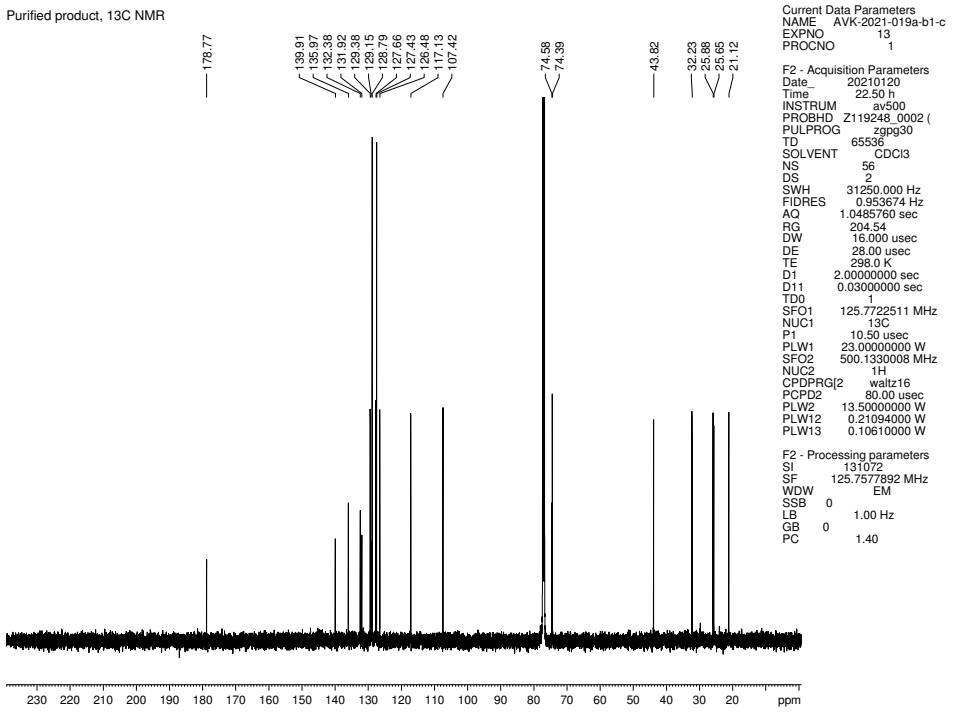

Figure 1.79. ^{13}C NMR (125 MHz, $CDCl_3$) of compound **1.44**.

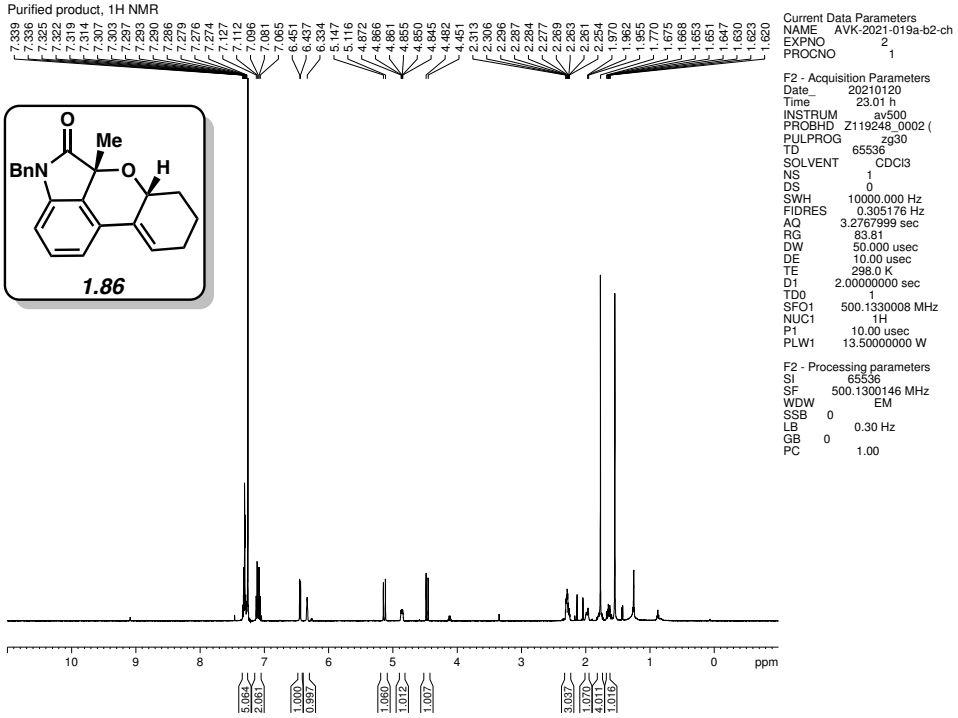

Figure 1.80. ^{1}H NMR (500 MHz, $CDCl_3$) of compound **1.86**.

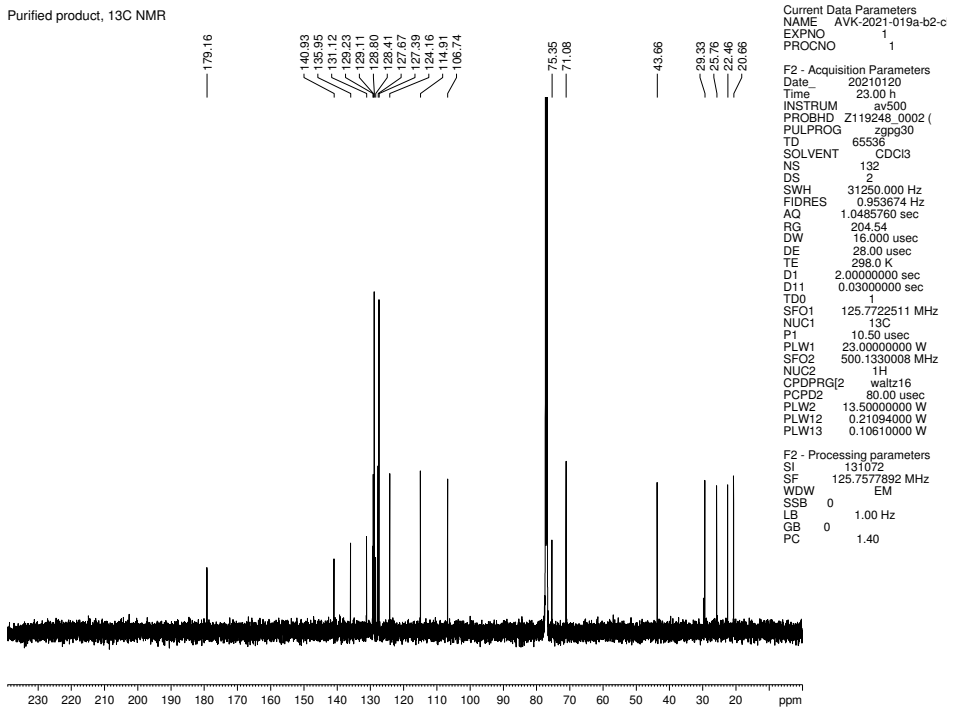

Figure 1.81. ^{13}C NMR (125 MHz, $CDCl_3$) of compound **1.86**.

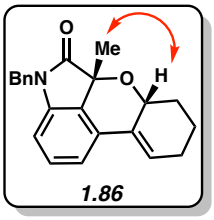

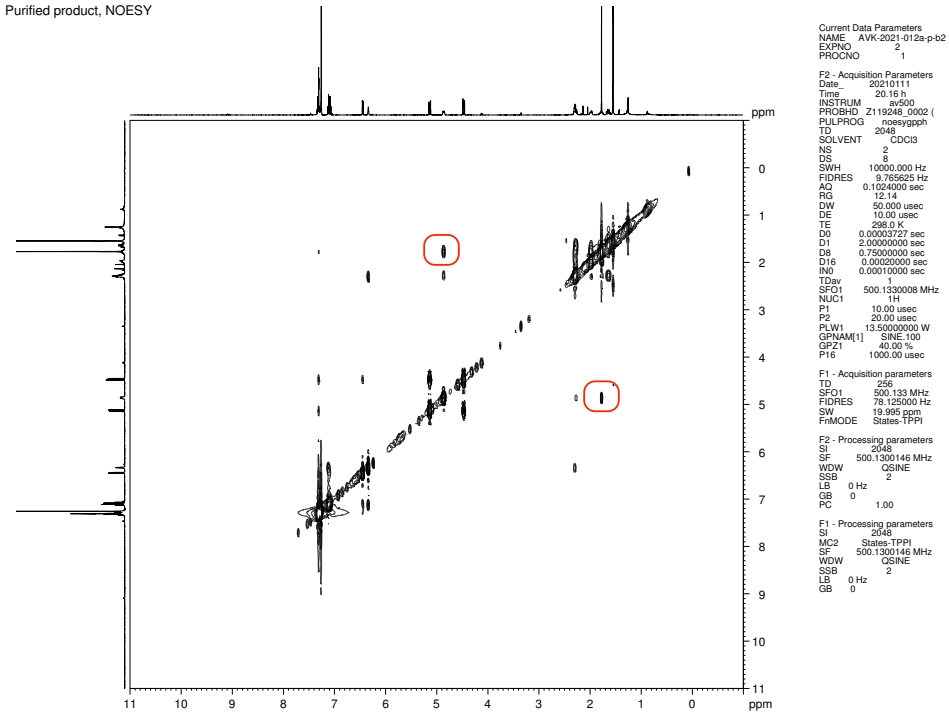

Figure 1.82. NOESY (500 MHz, $CDCl_3$) of compound **1.86**.

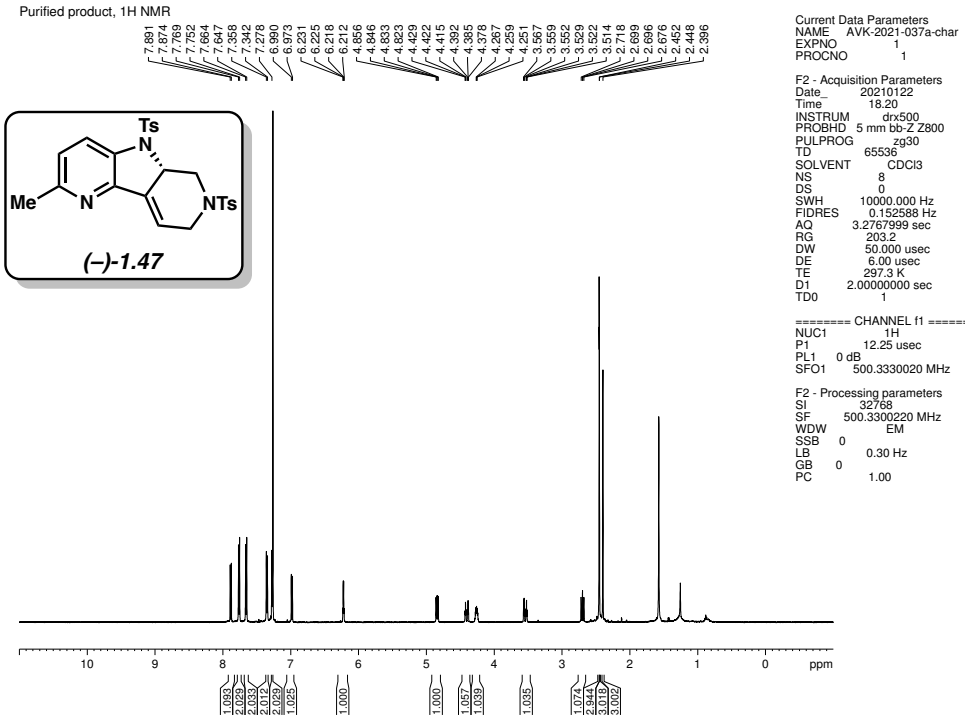

Figure 1.83. ^{1}H NMR (500 MHz, $CDCl_3$) of compound (–)-**1.47**.

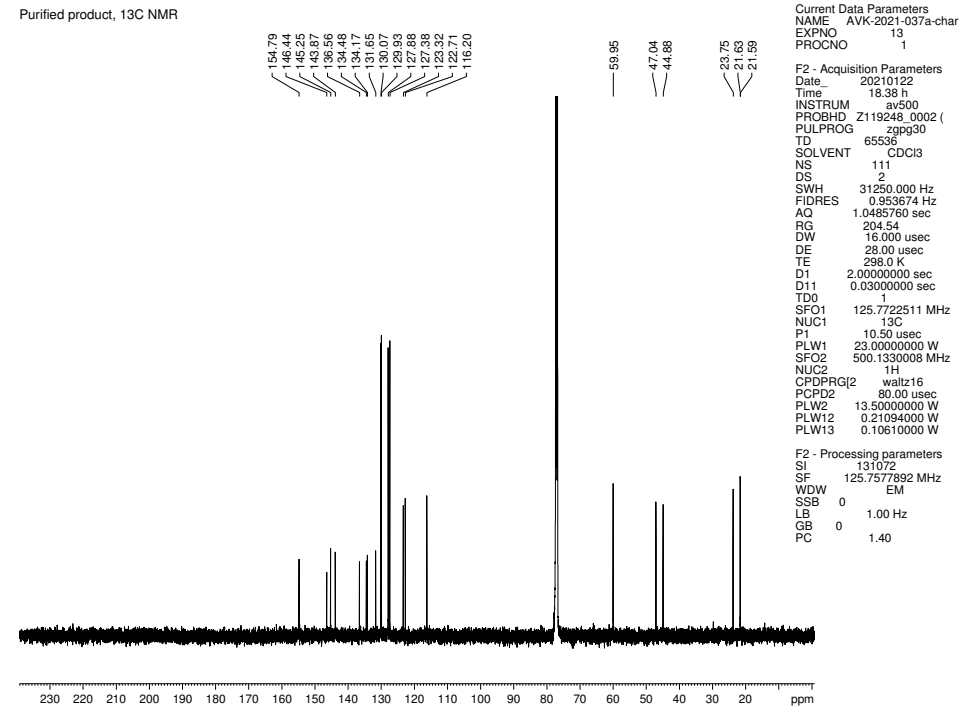

Figure 1.84. ^{13}C NMR (125 MHz, $CDCl_3$) of compound (–)-**1.47**.

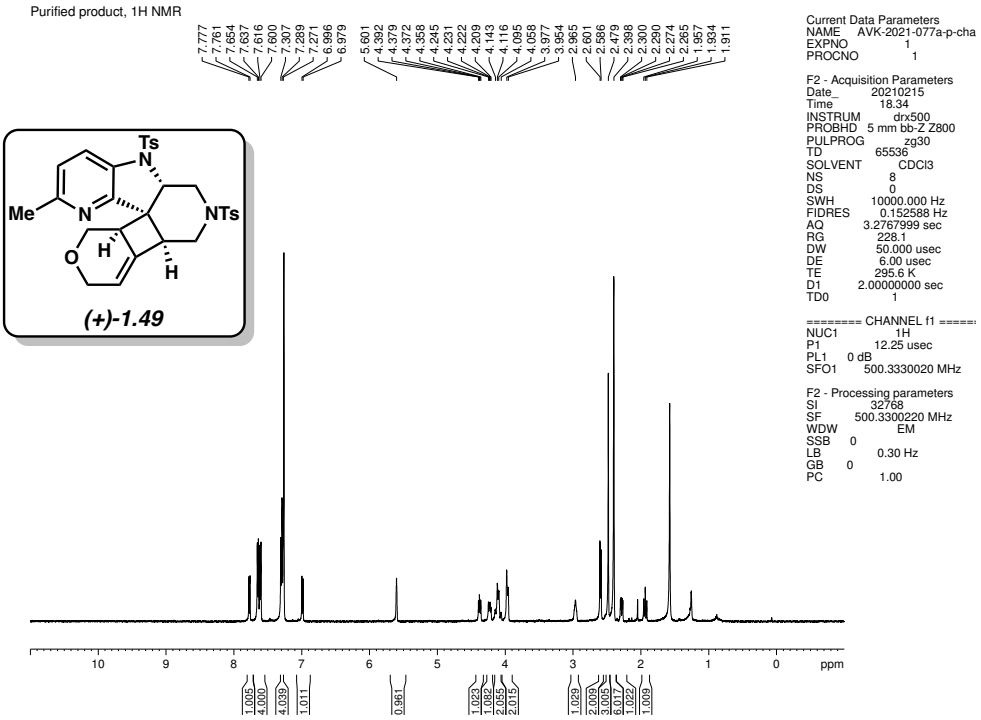

Figure 1.85. ^{1}H NMR (500 MHz, $CDCl_3$) of compound (+)-**1.49**.

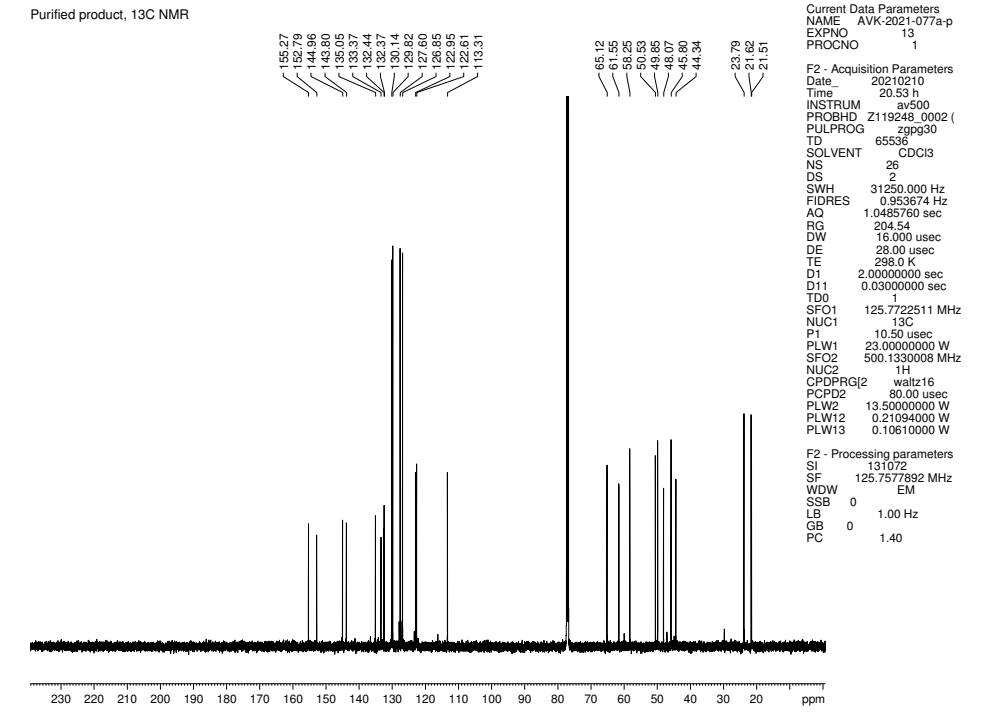

Figure 1.86. ^{13}C NMR (125 MHz, $CDCl_3$) of compound (+)-**1.49**.

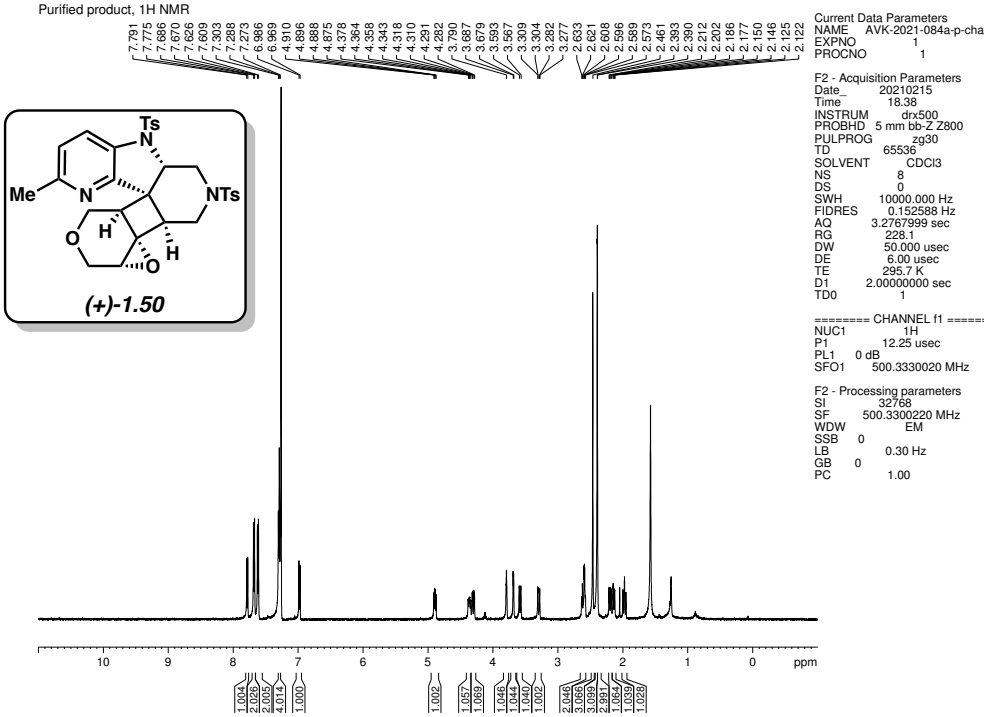

Figure 1.87. ^{1}H NMR (500 MHz, $CDCl_3$) of compound (+)-**1.50**.

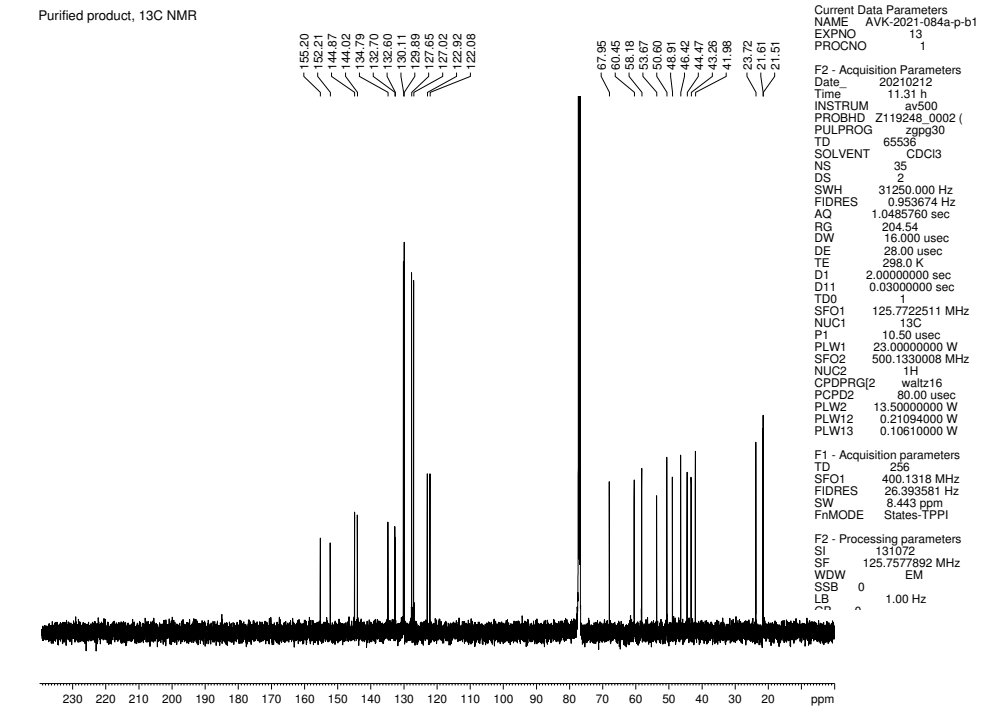

Figure 1.88. ^{13}C NMR (125 MHz, $CDCl_3$) of compound (+)-**1.50**.

1.10 Notes and References

(1) Wenk, H. H.; Winkler, M.; Sander, W. One century of aryne chemistry. *Angew. Chem., Int. Ed.* **2003**, *42*, 502–528.

(2) Roberts, J. D.; Simmons, H. E.; Carlsmith, L. A.; Vaughan, C. W. Rearrangement in the reaction of chlorobenzene-1-C^{14} with potassium amide. *J. Am. Chem. Soc.* **1953**, *75*, 3290–3291.

(3) Wittig, G. Phenyl-lithium, der Schlüssel zu einer neuen Chemie metallorganischer Verbindungen. *Naturwissenschaften* **1942**, *30*, 696–703.

(4) Wittig, G.; Pohmer, L. Intermediäre Bildung von Dehydrobenzol (Cyclohexa-dienin). *Angew. Chem.* **1955**, *67*, 348.

(5) Julia, M.; Huang, Y.; Igolen, J. Synthesis of 4- or 5-aminoindoles by arsenic substitution. *C. R. Acad. Sci., Ser. C* **1967**, *265*, 110–112.

(6) Shah, T. K.; Medina, J. M.; Garg, N. K. Expanding the strained alkyne toolbox: Generation and utility of oxygen-containing strained alkynes. *J. Am. Chem. Soc.* **2016**, *138*, 4948–4954.

(7) Scardiglia, F.; Roberts, J. D. Evidence for cyclohexyne as an intermediate in the coupling of phenyllithium with 1-chlorocyclohexene. *Tetrahedron* **1957**, *1*, 343−344.

(8) For a review describing a wide range of in situ-generated strained intermediates, see: Shi, J.; Li, L.; Li, Y. *o*-Silylaryl triflates: A journey of Kobayashi aryne precursors. *Chem. Rev.* **2021**, *121*, 3892–4044.

(9) Dubrovskiy, A. V.; Markina, N. A.; Larock, R. C. Use of benzynes for the synthesis of heterocycles. *Org. Biomol. Chem.* **2013**, *11*, 191–218.

(10) Mauger, C. C.; Mignani, G. A. An efficient and safe procedure for the large-scale Pd-catalyzed hydrazonation of aromatic chlorides using Buchwald technology. *Org. Process Res. Dev.* **2004**, *8*, 1065–1071.

(11) Takikawa, H.; Nishii, A.; Sakai, T.; Suzuki, K. Aryne-based strategy in the total synthesis of naturally occurring polycyclic compounds. *Chem. Soc. Rev.* **2018**, *47*, 8030–8056.

(12) Tadross, P. M.; Stoltz, B. M. A comprehensive history of arynes in natural product total synthesis. *Chem. Rev.* **2012**, *112*, 3550–3577.

(13) Gampe, C. M.; Carreira, E. M. Arynes and cyclohexyne in natural product synthesis. *Angew. Chem., Int. Ed.* **2012**, *51*, 3766–3778.

(14) Schleth, F.; Vettiger, T.; Rommel, M.; Tobler, H. Process for the preparation of pyrazole carboxylic acid amides. International patent WO2011131544 A1, Oct 27, 2011.

(15) Lin, J. B.; Shah, T. J.; Goetz, A. E.; Garg, N. K.; Houk, K. N. Conjugated trimeric scaffolds accessible from indolyne cyclotrimerizations: Synthesis, structures, and electronic properties. *J. Am. Chem. Soc.* **2017**, *139*, 10447–10455.

(16) Whereas cyclic allenes have not seen synthetic development to the extent that their alkyne counterparts have, invaluable studies on methods for allene generation and trapping have been put forward by Christl, Balci & Jones, Elliot, Guitián, West, and many others. For a comprehensive view of strained cyclic allene chemistry through 2003, see: Christl, M. *Cyclic allenes up to seven-membered rings. Modern Allene Chemistry*; Krause, N.; Kashmi, S. A. K., Eds.; Wiley-VCH: Weinheim, 2004; pp 243–357.

(17) The disparity between the development of these related intermediates is clearly seen by comparison of the wealth of reactions discovered for cyclic alkynes (nucleophilic

trappings, cycloadditions, ene reactions, C–H insertions, transition-metal-catalyzed processes, multicomponent couplings, and many others – see ref. 8) to the few known modes of cyclic allene reactivity.

(18) Wittig, G.; Fritze, P. On the intermediate occurrence of 1,2-cyclohexadiene. *Angew. Chem., Int. Ed. Engl.* **1966**, *5*, 846.

(19) Lovering, F.; Bikker, J.; Humblet, C. Escape from flatland: Increasing saturation as an approach to improving clinical success. *J. Med. Chem.* **2009**, *52*, 6752–6756.

(20) Quintana, I.; Peña, D.; Pérez, D.; Guitián, E. Generation and reactivity of 1,2-cyclohexadiene under mild reaction conditions. *Eur. J. Org. Chem.* **2009**, *2009*, 5519−5524.

(21) Peña, D.; Iglesias, B.; Quintana, I.; Pérez, D.; Guitián, E.; Castedo, L. Synthesis and reactivity of new strained cyclic allene and alkyne precursors. *Pure Appl. Chem.* **2009**, *78*, 451–455.

(22) Lofstrand, V. A.; West, F. G. Efficient trapping of 1,2-cyclohexadienes with 1,3-dipoles. *Chem. Eur. J.* **2016***, 22*, 10763–10767.

(23) Lofstrand, V. A.; McIntosh, K. C.; Almehmadi, Y. A.; West, F. G. Strain-activated Diels–Alder trapping of 1,2-cyclohexadienes: Intramolecular capture by pendent furans. *Org. Lett.* **2019**, *21*, 6231–6234.

(24) Almehmadi, Y. A.; West, F. G. A mild method for the generation and interception of 1,2-cycloheptadienes with 1,3-dipoles. *Org. Lett.* **2020**, *22*, 6091–6095.

(25) Wang, B.; Constantin, M.-G.; Singh, S.; Zhou, Y.; Davis, R. L.; F. G. West. Generation and trapping of electron-deficient 1,2-cyclohexadienes. Unexpected hetero-Diels–Alder reactivity. *Org. Biomol. Chem.* **2021**, *19*, 399–405.

(26) Hioki, Y.; Mori, A.; Okano, K. Steric effects on deprotonative generation of cyclohexynes and 1,2-cyclohexadienes from cyclohexenyl triflates by magnesium amides. *Tetrahedron* **2020**, *76*, 131103.

(27) Inoue, K.; Nakura, R.; Okano, K.; Mori, A. One-pot synthesis of silylated enol triflates from silyl enol ethers for cyclohexynes and 1,2-cyclohexadienes. *Eur. J. Org. Chem.* **2018**, *2018*, 3343–3347.

(28) Westphal, M. V.; Hudson, L.; Mason, J. W.; Pradeilles, J. A.; Zecri, F. J.; Briner, K.; Schreiber, S. L. Water-compatible cycloadditions of oligonucleotide-conjugated strained allenes for DNA-encoded library synthesis. *J. Am. Chem. Soc.* **2020**, *142*, 7776–7782.

(29) Barber, J. S.; Styduhar, E. D.; Pham, H. V.; McMahon, T. C.; Houk, K. N.; Garg, N. K. Nitrone cycloadditions of 1,2-cyclohexadiene. *J. Am. Chem. Soc*. **2016**, *138*, 2512–2515.

(30) Barber, J. S.; Yamano, M. M.; Ramirez, M.; Darzi, E. R.; Knapp, R. R.; Liu, F.; Houk, K. N.; Garg, N. K. Diels–Alder cycloadditions of strained azacyclic allenes. *Nat. Chem.* **2018**, *10*, 953–960.

(31) Yamano, M. M.; Knapp, R. R.; Ngamnithiporn, A.; Ramirez, M.; Houk, K. N.; Stoltz, B. M.; Garg, N. K. Cycloadditions of oxacyclic allenes and a catalytic asymmetric entryway to enantioenriched cyclic allenes. *Angew. Chem., Int. Ed.* **2019**, *58*, 5653–5657.

(32) McVeigh, M. S.; Kelleghan, A. V.; Yamano, M. M.; Knapp, R. R.; Garg, N. K. Silyl tosylate precursors to cyclohexyne, 1,2-cyclohexadiene, and 1,2-cycloheptadiene. *Org. Lett.* **2020**, *22*, 4500–4504.

(33) Yamano, M. M.; Kelleghan, A. V.; Shao, Q.; Giroud, M.; Simmons, B. J.; Li, B.; Chen, S.; Houk, K. N.; Garg, N. K. Intercepting fleeting cyclic allenes with asymmetric nickel catalysis. *Nature* **2020**, *586*, 242–247.

(34) Analogous transformations of linear allenes have been reported. For a representative study, see: Larock, R. C.; Berrios-Peña, N. G.; Fried, C. A. Regioselective, palladium-catalyzed hetero- and carboannulation of 1,2-dienes using functionally substituted aryl halides. *J. Org. Chem.* **1991**, *56*, 2615–2617.

(35) When the experiment shown in entry 4 was performed in the absence of exogenous ligand, product **1.19a** was obtained in 17% yield.

(36) 2-(*N*,*N*-dimethylaminomethyl)-1-diphenylphosphinoferrocene was found to provide similar results to DavePhos, but the latter was chosen for further study given its widespread commercial availability.

(37) Tetrabutylammonium salts have been shown to increase the rate of strained intermediate generation, presumably by improving CsF solubility; for a relevant study, see: Feng, M.; Tang, B.; Wang, N.; Xiu, H.-X.; Jiang, X. Ligand controlled regiodivergent C_1 insertion on arynes for construction of phenanthridinone and acridone alkaloids. *Angew. Chem., Int. Ed.* **2015**, *54*, 14960–14964.

(38) Despite the general ability of Pd to activate Ar–Br and Ar–Cl bonds, brominated and chlorinated products **1.28** and **1.29** were obtained in synthetically useful yields, thus

highlighting the chemoselectivity of this transformation. Moreover, the halides provide versatile synthetic handles for further functionalization.

(39) The bromo derivative of **1.17** performs modestly in the annulation reaction to give 41% yield of **1.19a**. We attribute the nearly twofold increase in yield when using the 2-bromopyridine to the well-documented 2-halopyridine effect. Of note, even a chloride electrophile could generate product **1.31** in this pyridyl system, albeit in 9% yield, see Section 1.8.2.4 for details. For a reference documenting the origins of such effects, see: Legault, C. Y.; Garcia, Y.; Merlic, C. A.; Houk, K. N. Origin of regioselectivity in palladium-catalyzed cross-coupling reactions of polyhalogenated heterocycles. *J. Am. Chem. Soc.* **2007**, *129*, 12664–12665.

(40) The corresponding silyl triflate has been found to be unstable, leading to the development of a silyl tosylate as an alternative allene precursor, see ref. 32.

(41) We hypothesize that the *trans* diastereomer is obtained as the major product due to a destabilizing steric interaction in the presumed transition state leading to the *cis* diastereomer. Specifically, a steric interaction between the methyl group adjacent to the alcohol and the π-allyl fragment may disfavor formation of the *cis* product.

(42) The origin of asymmetric induction is presumed to be similar to that recently reported in the Ni-catalyzed annulation of benzotriazinones involving desymmetrization of an intermediate π-allyl metal complex (e.g., **1.16**); see ref 33.

(43) This topic, along with other recent advances in the chemistry of strained intermediates for the introduction of structure complexity, has recently been reviewed, see: Anthony, S. M.;

Wonilowicz, L. G.; McVeigh, M. S.; Garg, N. K. Leveraging fleeting strained intermediates to access complex scaffolds. *JACS Au* **2021**, *1*, 897–912.

(44) Zenner, Z. M.; Larock, R. C. Palladium-catalyzed, asymmetric hetero- and carboannulation of allenes using functionally-substituted aryl and vinylic iodides. *J. Org. Chem.* **1999**, *64*, 7312–7322.

(45) Fra, L.; Millán, A.; Souto, J. A.; Muñiz, K. Indole synthesis based on a modified Koser Reagent. *Angew. Chem., Int. Ed.* **2014**, *53*, 7349–7353.

(46) Zhang, L.; Si, X.; Rominger, F.; Hashmi, A. S. K. Visible-light-induced radical carbo-cyclization/*gem*-diborylation through triplet energy transfer between a gold catalyst and aryl iodides. *J. Am. Chem. Soc.* **2020**, *142*, 10485–10493.

(47) Shen, H.; Fu, J.; Yuan, H.; Gong, J.; Yang, Z. Synthesis of 2,3-disubstituted indoles and benzofurans by the tandem reaction of rhodium(II)-catalyzed intramolecular C–H insertion and oxygen-mediated oxidation. *J. Org. Chem.* **2016**, *81*, 10180–10192.

(48) Ji, Q.; Peng, X.; Wong, H. N. C. Brønsted acid-catalyzed synthesis of carbazoles from 2-substituted indoles. *Org. Chem. Front.* **2014**, *1*, 1197–1200.

(49) Seath, C. P.; Wilson, K. L.; Campbell, A.; Mowat, J. M.; Watson, A. J. B. Synthesis of 2-BMIDA 6,5-bicyclic heterocycles by Cu(I)/Pd(0)/Cu(II) cascade catalysis of 2-iodoaniline/phenols. *Chem. Commun.* **2016**, *52*, 8703–8706.

(50) Chen, C.; Chandru Senadi, G.; Liu, M-C.; Wang, J-J. Halogenation of arenes via an in situ generated hypohalous acid from *m*-CPBA and HX: Mechanistic insights from cyclic voltammetry. *ChemistrySelect* **2016**, *1*, 2207–2211.

(51) Medina, J. M.; Moreno, J.; Racine, S.; Du, S.; Garg, N. K. Mizoroki-Heck cyclizations of amide derivatives for the introduction of quaternary centers. *Angew. Chem., Int. Ed.* **2017**, *56*, 6567–6571.

(52) Zhang, D.; Yum, E. K.; Liu, Z.; Larock, R. C. Synthesis of indenes by the palladium-catalyzed carboannulation of internal alkynes. *Org. Lett.* **2005**, *7*, 4963–4966.

(53) Alekseyev, R. S.; Kurkin, A. V.; Yuroskaya, M. A. The Piloty-Robinson reaction of *N*-substituted piperidin-4-one azines. A novel route for the synthesis of 3,6-diazacarbazole. *Chem. Heterocycl. Comp.* **2011**, *47*, 584–596.

(54) Marr, G.; Hunt, T. Unsymmetrically disubstituted ferrocenes. Part VIII. Synthesis and reactivity of some 2-substituted ferrocenylphosphines. *J. Chem. Soc. C* **1969**, 1070–1072.

(55) Tamio, H.; Takaya, M.; Motoo, F.; Masahiro, K.; Nobuo, N.; Yuji, H.; Akira, M.; Sota, K.; Mitsuo, K.; Keiji, Y.; Makoto, K. Asymmetric synthesis catalyzed by chiral ferrocenylphosphine-transition metal complexes. I. Preparation of chiral ferrocenylphosphines. *Bull. Chem. Soc. Jpn.* **1980**, *53*, 1138–1151.

(56) Arisawa, M.; Terada, Y.; Takahasi, K.; Nakagawa, M.; Nishida, A. Development of isomerization and cycloisomerization with use of ruthenium hydride with *N*-heterocyclic carbene and its application to the synthesis of heterocycles. *J. Org. Chem.* **2006**, *71*, 4255–4261.

CHAPTER TWO

Catalyst-Controlled Annulations of Strained Cyclic Allenes with π-Allylpalladium Complexes

Dominick C. Witkowski, Matthew S. McVeigh, Georgia M. Scherer, Sarah M. Anthony, and Neil K. Garg

J. Am. Chem. Soc. **2023**, *145*, 10491–10496.

2.1 Abstract

Strained cyclic allenes are a class of in situ-generated fleeting intermediates that, despite being discovered more than 50 years ago, has received significantly less attention from the synthetic community compared to related strained intermediates. Examples of trapping strained cyclic allenes that involve transition metal catalysis are especially rare. We report the first annulations of highly reactive cyclic allenes with in situ-generated π-allylpalladium species. By varying the ligand employed, either of two isomeric polycyclic scaffolds can be obtained with high selectivity. The products are heterocyclic, sp^3-rich, and bear two or three new stereocenters. This study should encourage the further development of fragment couplings that rely on transition metal catalysis and strained cyclic allenes for the rapid assembly of complex scaffolds.

2.2 Introduction

In situ-generated strained intermediates that bear a functional group with a preferred linear geometry within a small ring have emerged as valuable synthetic building blocks. Arynes[1,2,3,4,5,6] and cyclic alkynes[7,8] (e.g., **2.1**–**2.3**, Figure 2.1A) have been most well-studied with applications

spanning the synthesis of heterocycles,[9,10] ligands (such as XPhos),[11] natural products,[12,13,14] agrochemicals,[15] and organic materials.[16,17] A related class of strained intermediates discovered around the same time as arynes and cyclic alkynes is strained cyclic allenes, such as 1,2-cyclohexadiene (**2.4**).[18,19] The cumulated diene confined to a small ring leads to ~30 kcal/mol of strain energy, making cyclic allenes well-suited for strain-promoted reactions.[20,21,22] However, these intermediates have received significantly less attention compared to arynes and cyclic alkynes despite possessing many attractive attributes[23] that substantiate their value as building blocks for the synthesis of complex sp^3-rich scaffolds. Recent studies of strained cyclic allenes have led to advances in cyclic allene generation protocols,[24,25,26] cycloaddition reactions,[27,28,29,30,31,32,33,34,35,36] metal-catalyzed processes,[37,38] trapping in a single-electron process,[39] DNA-encoded library synthesis,[40] and total synthesis.[41]

An attractive yet underdeveloped approach to leveraging strained cyclic allenes in synthesis utilizes transition metal catalysis.[42,43] Only three reports of such transformations have been demonstrated in the literature.[44] In these reactions, an organometallic intermediate **2.5** is generated catalytically and intercepts a transient cyclic allene (e.g., **2.6**) (Figure 2.1B). This gives rise to annulated product **2.7**. In the known literature reports, only σ-bound metal species have been used, namely, palladacycle **2.8**,[24,45] nickelacycle **2.9**,[37] and arylpalladium species **2.10**.[38] With the aim of expanding the types of organometallic intermediates that can be used in reactions of strained cyclic allenes, we became interested in the use of π-allylpalladium species **2.11**. The ability of **2.11** to undergo C–C bond formation at either of its termini[46,47,48] is distinct from the reactivity of organometallic intermediates used previously in cyclic allene annulations. As will be described herein, the use of π-allylpalladium complexes[49,50] to trap cyclic allenes provides

opportunities to control regiochemistry and stereoselectivity, while building diverse and sp^3-rich scaffolds.

In this chapter, we demonstrate the first use of π-allylmetal complexes to trap strained cyclic allenes (**2.12** and **2.6**, respectively, Figure 2.1C). By varying the ligand employed, either of two different polycyclic scaffolds, **2.13** or **2.14**, can be formed preferentially, via the formation of multiple bonds and stereocenters. Studies toward an enantioselective variant are also reported. These studies demonstrate the merger of transition metal catalysis and strained cyclic allenes for the rapid assembly of complex, sp^3-rich scaffolds.

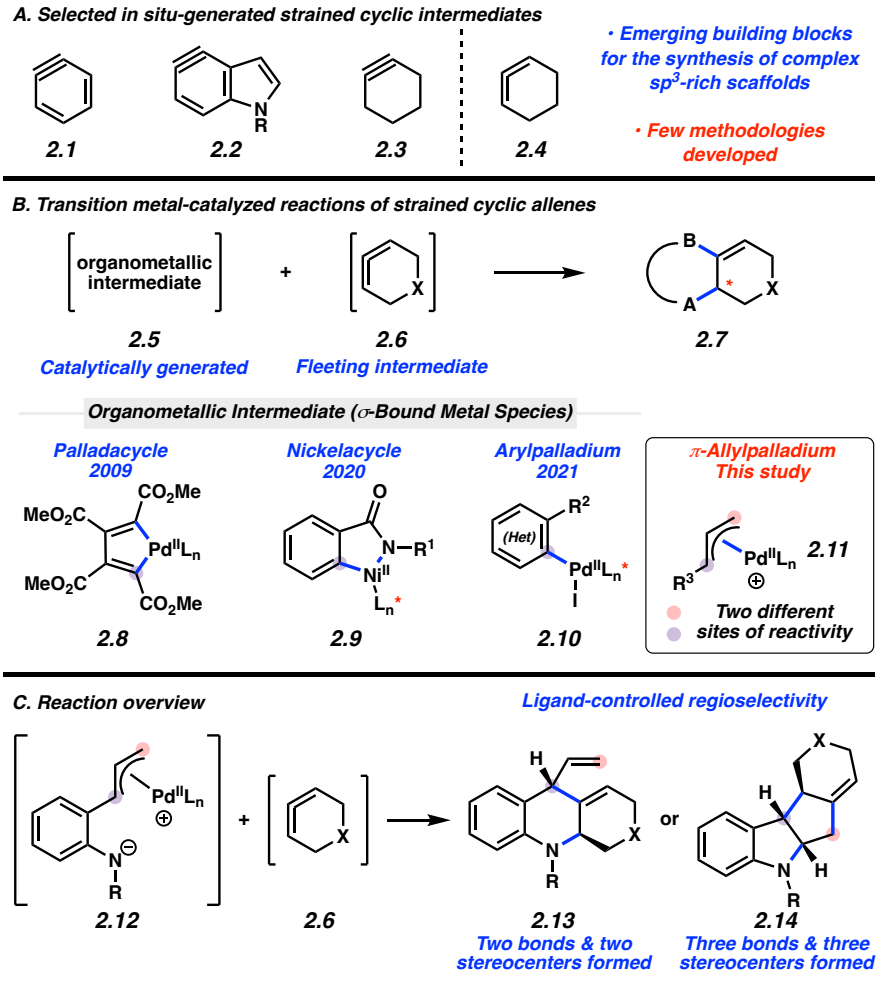

Figure 2.1. (A) Strained cyclic intermediates **2.1**–**2.4**, (B) approaches for metal-catalyzed reactions of strained cyclic allenes, and (C) overview of current study.

2.3 Reaction Optimization

To initiate our studies, we investigated the reaction of vinyl benzoxazinone **2.15** with silyl triflate **2.16** using palladium catalysis (Table 2.1). Of note, benzoxazinone **2.15**, a known π-allylmetal precursor,[51,52,53,54,55] was selected for these studies as it had been demonstrated to be compatible with fluoride-mediated generation of benzyne.[56] Based on known reactivity of **2.15**, two products could plausibly arise, tricycle **2.17** or tetracycle **2.18**. To generate soluble fluoride ions, CsF and Bu_4NOTf[57] were used in combination. Furthermore, elevated temperatures were employed to facilitate efficient generation of reactive intermediates. Select key results from reaction optimization are depicted, and additional data are available in Section 2.8.2.2.

The use of the dialkylbiaryl ligand DavePhos, which had previously been identified as a competent ligand in a cyclic allene annulation,[38] did not lead to a productive reaction (Table 2.1, entry 1). However, switching to the PPh_3 ligand gave tricyclic annulation product **2.17**, albeit in a low yield of 20% (entry 2). Alternatively, the use of the bidentate ferrocene ligand dppf delivered constitutional isomer **2.18** as the major product (entry 3). With initial results for the selective formation of annulation products **2.17** or **2.18**, we performed optimization to selectively access each of the constitutional isomers. For practical reasons, we elected to pursue the use of $Pd(PPh_3)_4$, which gave **2.17** in slightly improved yield and excellent selectivity (entry 4; compared with entry 2). Because a significant amount of decomposition of benzoxazinone **2.15** was observed under these conditions,[58] we explored additives to mitigate deleterious side reactions. Empirically, the addition of water led to significant improvement, generating tricycle **2.17** in 65% yield after 2 h (entry 5). Extensive efforts were made to selectively generate tetracycle **2.18**. We ultimately identified that the use of Buchwald precatalyst dppf Pd G3 and water as an additive delivered **2.18** in 73% yield after 2 h (entry 6; compared with entry 3). Thus, either tricycle **2.17** or tetracycle

2.18 could be accessed by the judicious choice of ligand. It should be noted that the annulation of benzyne with benzoxazinone **2.15** only delivers the tetracyclic counterpart to **2.18**, without formation of the tricyclic counterpart to **2.17**.[56]

Table 2.1. Select Results from Optimization Studies.

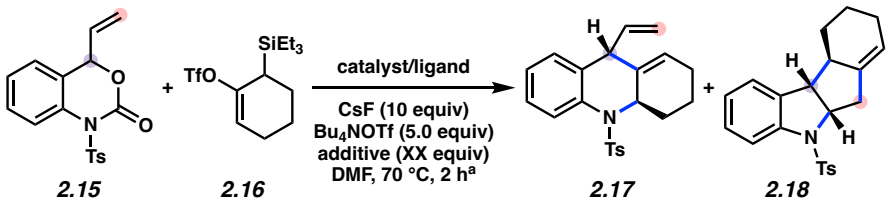

Entry	*Catalyst*	*Ligand*	*Additive*	*Yield*[b]	*2.17:2.18*[c]
1	$Pd(OAc)_2$	DavePhos (10 mol%)	–	0%	–
2	$Pd(OAc)_2$	PPh_3 (10 mol%)	–	20%	>20:1
3	$Pd(OAc)_2$	dppf (10 mol%)	–	10%	1:14
4	$Pd(PPh_3)_4$	–	–	24%	18:1
5	$Pd(PPh_3)_4$	–	H_2O (9.0 equiv)	65%	19:1
6[d]	dppf Pd G3	–	H_2O (9.0 equiv)	73%	1:13

[a] Reactions conditions: **2.15** (3.0 equiv), **2.16** (1.0 equiv), catalyst (5 mol%), ligand (as shown), CsF (10 equiv), Bu_4NOTf (5.0 equiv), additive (as shown), DMF (0.050 M), 70 °C, 2 h. [b] Yield determined by an isolation experiment. [c] Ratio of **2.17**:**2.18** and dr were determined by ^1H NMR analysis. In entries where **2.17** is the major product, dr = 11:1; in entries where **2.18** is the major product dr = >20:1. [d] [Pd] (10 mol%), 0.025 M.

2.4 Scope of the Annulation Reactions

Having identified suitable reaction conditions for the selective formation of either constitutional isomer **2.17** or **2.18**, we examined the scope of the methodology beginning with the formation of tricyclic products **2.21** (Figure 2.2). The parent substrate, along with its *N*-mesyl derivative, each gave 60% yield of tricyclic product (**2.17** and **2.22**, respectively). A variety of substituents on the arene (R^2 = Me, F, OMe, Ph, 2-thiophene) were also tolerated, as evidenced by the formation of tricycles **2.23**–**2.29**.[59] The use of a naphthalene-derived substrate proceeded smoothly to furnish **2.30** in 64% yield. Additionally, we evaluated a benzoxazinone bearing an isopropenyl group, which afforded tricycle **2.31**. Lastly, heterocyclic allene precursors (i.e., **2.20**)

could be employed under modified reaction conditions to enable further modulation of the product structure. More specifically, interception of oxa-[29] and aza-derivatives[28] of **2.20** delivered heterocycles **2.32** and **2.33**, respectively. It should be noted that formation of the corresponding tetracyclic products was either negligible or not observed for the results shown in Figure 2.2. Additionally, in most cases, the observed diastereoselectivities are synthetically useful.

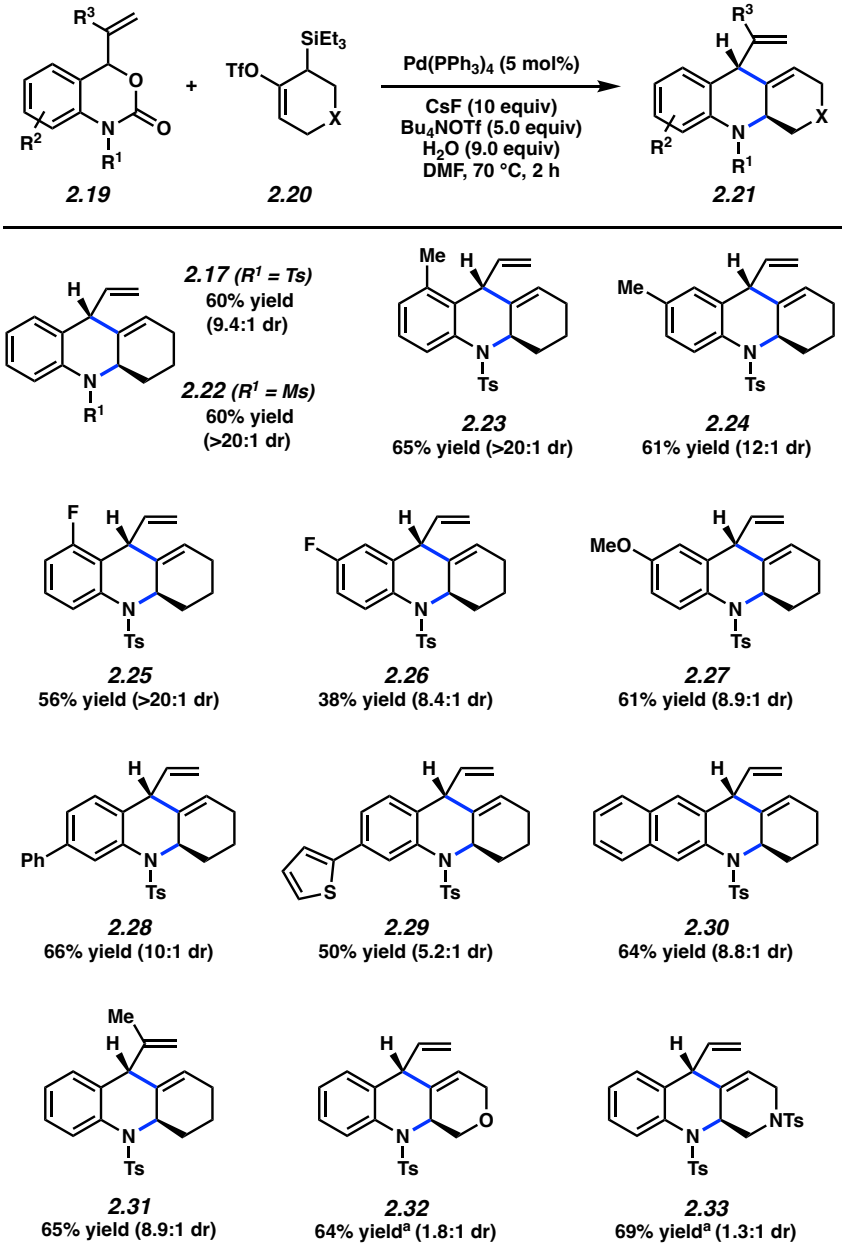

Figure 2.2. Scope of the annulation reaction using PPh_3 as the ligand. Reactions performed on 0.05 mmol scale with **2.19** (3.0 equiv) and **2.20** (1.0 equiv) at 0.050 M. Yields reflect an average of two isolation experiments. [a] Reactions were performed with CsF (5.0 equiv) in MeCN (0.050 M) at 60 °C for 6 h, without Bu_4NOTf additive.

Subsequently, the scope of the methodology for preparing tetracycles utilizing the dppf Pd G3 catalyst was assessed (Figure 2.3). Although our conditions shown in Table 2.1, entry 6 were generally useful, some modifications were made to obtain optimal yields based on empirical

observations. Beginning with the parent substrate combination, **2.18** was isolated in 70% yield and >20:1 dr. Variation of the *N*-substituent, as well as steric and electronic perturbations of the aryl ring, were tolerated as seen by the formation of **2.35**–**2.43** in good yields. Finally, trapping of an oxacyclic allene gave tetracycle **2.44**. Notably, the annulations to afford tetracycles **2.34** proceed via the formation of three new bonds and three stereocenters with excellent diastereoselectivity (>20:1 dr in all cases).

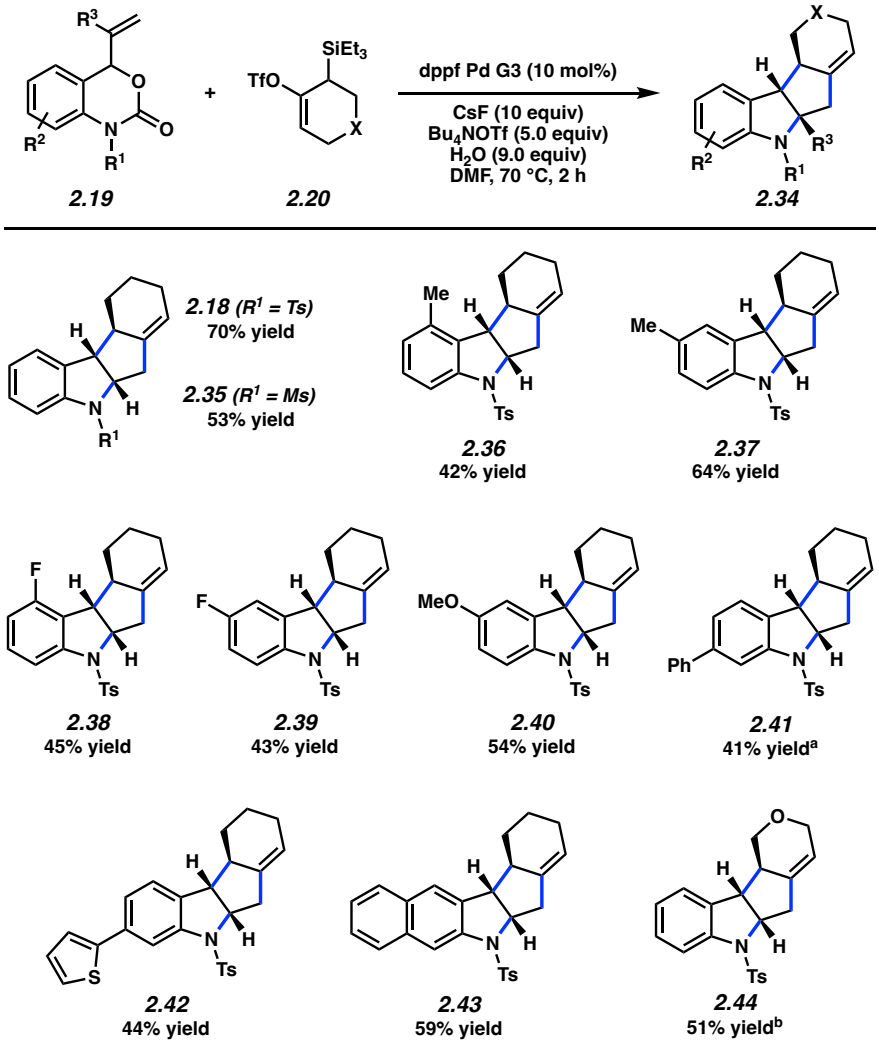

Figure 2.3. Scope of the annulation reaction using dppf as the ligand. Reactions performed on 0.05 mmol scale with **2.19** (3.0 equiv) and **2.20** (1.0 equiv) at 0.025 M. Yields reflect an average of two isolation experiments. For all isolations, dr = >20:1 and ratios of **2.34**:**2.21** range from 6.3:1 to

>20:1; see Section 2.8.2.3 for details. [a] Reaction was performed at 100 °C. [b] Reaction was performed in MeCN (0.0125 M) at 30 °C for 14 h, without Bu_4NOTf additive.

2.5 Reaction Mechanisms

Plausible mechanisms for the transformations we have developed are depicted in Figure 2.4. The Pd(0) catalyst coordinates to **2.45**. Oxidative addition of the Pd(0) catalyst into the allylic C–O bond of **2.46** followed by decarboxylation affords zwitterionic π-allylpalladium intermediate **2.12**.[51] Ligand-controlled migratory insertion of cyclic allene **2.6** (formed from fluoride-mediated 1,2-elimination of silyl triflate **2.20**) gives π-allylpalladium intermediates **2.47** and **2.48**.[60] These intermediates arise from C–C bond formation at either of the two sites of reactivity of π-allylpalladium species **2.12**. The branched or linear selectivity of the migratory insertion is proposed to be a result of the ligands employed.[61] Cyclizations of **2.47** and **2.48** afford tricycle **2.13**[62] and tetracycle **2.14**, respectively, through the formation of one or two new bonds.

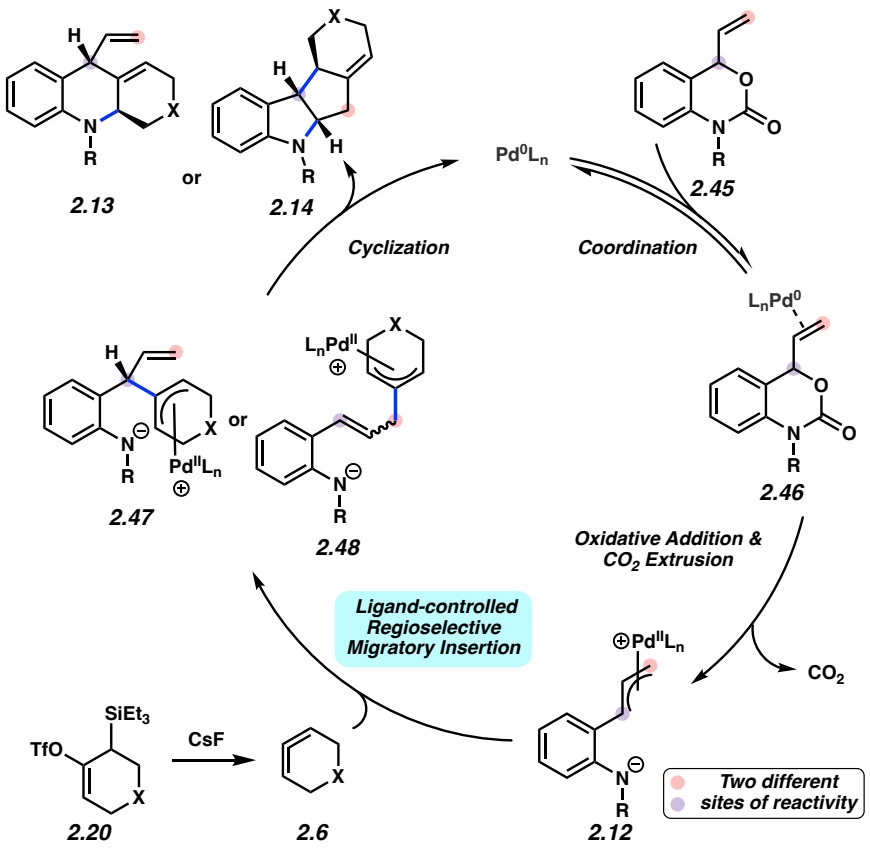

Figure 2.4. Proposed catalytic cycle.

2.6 Development of Enantioselective Variant

Given the notable impact of ligands on selectivity in these transformations, the feasibility of an enantioselective variant was investigated using vinyl benzoxazinone **2.49** and oxacyclic allene precursor **2.50**. Notably, the use of two chiral racemic starting materials would represent a departure from previous studies that use an achiral trapping partner.[37,38] Select key results are shown in Table 2.2, with additional information being available in the Section 2.8.2.5.[63] The use of PHOX ligand **L2.1** and Trost's ligand **L2.2**, which are commonly employed in π-allylpalladium chemistry,[50] provided no desired reactivity (entries 1 and 2, respectively). However, using phosphoramidite ligand **L2.3** (entry 3), annulation product **2.51** was formed as the major isomer, thus demonstrating the feasibility of rendering the annulation to form both products

enantioselective. Given the greater structural complexity of isomer (–)-**2.52**, we elected to assess other chiral diphosphine ligands in pursuit of (–)-**2.52**. The use of Phanephos **L2.4**, Segphos ligand **L2.5**, and Josiphos ligand **L2.6** each gave the desired product (–)-**2.52** in varying yields and enantioselectivities. The employment of Walphos ligand **L2.7** and Mandyphos ligand **L2.8** each resulted in increased yields and enantioselectivities. Of these, use of **L2.8** provided superior results and delivered (–)-**2.52** in 54% yield and 70% ee.[64] We surmise that the absolute configuration of (–)-**2.52** is as depicted, on the basis of an X-ray crystal structure obtained for carbocyclic derivative (–)-**2.43**. Although improving the enantioselectivity was challenging in our initial efforts,[65] the results shown provide the most structurally complex products accessible from the merger of strained cyclic allenes and asymmetric catalysis to date. As enantioselective transformations of fleeting strained cyclic intermediates remain exceedingly rare, we hope these results will promote further efforts in this area.

Table 2.2. Evaluation of Select Chiral Ligands in the Annulation Reaction.

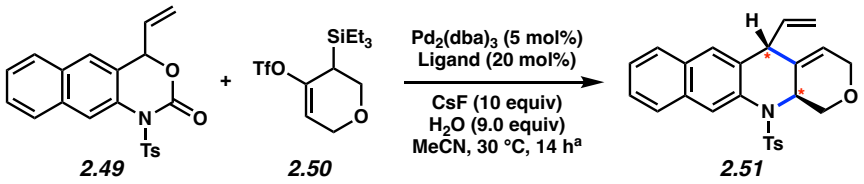

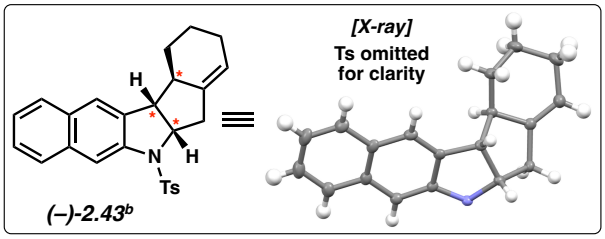

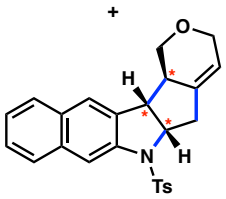

Entry	*Ligand*	*Yield (51/52)[c]*	*dr (2.51/2.52)*	*ee (2.51/2.52)*
1	L2.1	– / –	– / –	– / –
2	L2.2	– / –	– / –	– / –
3	L2.3	26% / 11%	2.8:1 / >20:1	~38% / 12%
4	L2.4	– / 32%	– / >20:1	– / 14%
5	L2.5	– / 24%	– / >20:1	– / 82%
6	L2.6	– / 10%	– / >20:1	– / 14%
7	L2.7	– / 34%	– / >20:1	– / 60%
8	L2.8	– / 54%	– / >20:1	– / 70%

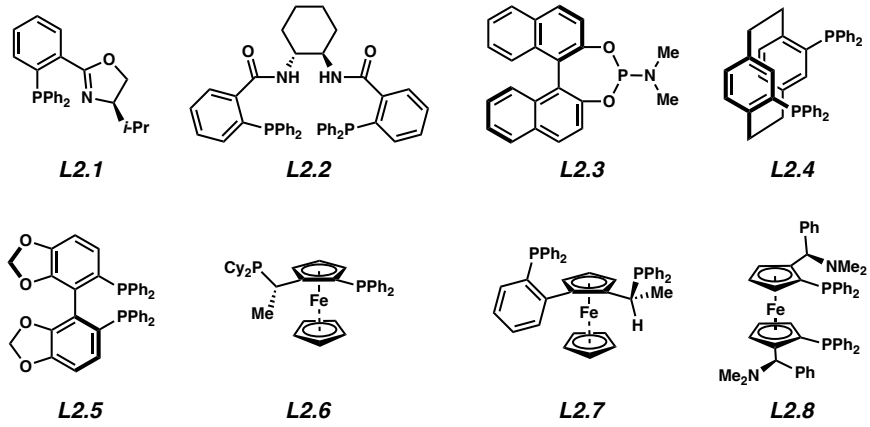

[a] Reaction conditions: **2.49** (3.0 equiv), **2.50** (1.0 equiv), $Pd_2(dba)_3$ (5 mol%), ligand (20 mol%), CsF (10 equiv), H_2O (9.0 equiv), MeCN (0.0125 M), 30 °C, 14 h. [b] See Section 2.8.2.6 for details and crystallographic data. [c] Yield determined by an isolation experiment.

2.7 Conclusion

We have developed the first strategy for engaging strained cyclic allenes with π-allyl metal species. These are rare examples of cyclic allene reactions in transition metal-catalyzed processes. By the judicious choice of ligands, selectivity can be controlled, leading to the preferential formation of tri- or tetracyclic heterocycles with significant structural complexity. Of note, the transformations proceed by formation of either two or three new bonds and two or three new stereocenters. We also demonstrate the feasibility of an enantioselective variant, thus providing a crucial proof-of-principle study for further asymmetric reaction development. Overall, the union of strained cyclic allenes and π-allylpalladium chemistry expands the types of organometallic intermediates that can be used in cyclic allene reactions to access complex sp^3-rich scaffolds. We hope this study promotes the further development and understanding of transition metal-catalyzed reactions of strained cyclic allenes.

2.8 Experimental Section

2.8.1 Materials and Methods

Unless stated otherwise, reactions were conducted in flame-dried glassware under an atmosphere of nitrogen, and commercially obtained reagents were used as received unless otherwise specified. Anhydrous solvents were either freshly distilled or passed through activated alumina columns, unless otherwise stated. Non-commercially available substrates were synthesized according to known preparations or following protocols specified in the Experimental Procedures. Prior to use, acetonitrile (MeCN), dimethylformamide (DMF), 1,4-dioxane, methanol (MeOH), methylene chloride, and tetrahydrofuran (THF) were passed through activated alumina columns and degassed by five freeze-pump-thaw cycles. Water and 1,4-dioxane were degassed by

sparging with N_2 gas before use. Hydrochloric acid, sodium bicarbonate, sodium hydride, ethyl chloroformate, phenylboronic acid pinacol ester (**2.59**), and thiophene-2-boronic acid (**2.64**) pinacol ester were obtained from Sigma-Aldrich. Sodium carbonate was obtained from EMD Millipore. 4-Toluenesulfonyl chloride (TsCl) was obtained from Oakwood Chemical. Vinylmagnesium bromide (**2.55**) was obtained from Acros Organics. Palladium(II) acetate, tris(dibenzylideneacetone)dipalladium(0) ($Pd_2(dba)_3$), methanesulfonato[1,1'-bis(diphenylphosphino)ferrocene)](2'-amino-1,1'-biphenyl-2-yl)palladium(II) (DPPF Palladacycle Gen. 3), cesium fluoride, manganese dioxide, and tetrakis(triphenylphosphine)palladium(0) were obtained from Strem Chemicals. Tetrabutylammonium trifluoromethanesulfonate (Bu_4NOTf) was obtained from TCI America. Potassium carbonate was obtained from Fisher Scientific. 2-Amino-4-bromobenzaldehyde (**2.58**) was obtained from AmBeed. All ligands used for reaction optimization (Sections 2.8.2.2, 2.8.2.4, and 2.8.2.5) were obtained from Strem Chemicals, TCI America, Sigma-Aldrich, or Solvias. Ethyl chloroformate was distilled over CaH_2 prior to use. MnO_2, Na_2CO_3, and K_2CO_3 were dried in an oven heated to 120 °C for 48 h prior to use. Reaction temperatures at or above 23 °C were controlled using an IKAmag temperature modulator, and unless stated otherwise, performed at room temperature (approximately 23 °C). Thin-layer chromatography (TLC) was conducted with EMD gel 60 F_{254} pre-coated plates (0.25 mm for analytical chromatography and 0.50 mm for preparative chromatography) and visualized using a combination of UV light and potassium permanganate staining techniques. Silicycle Siliaflash P60 (particle size 40–63 μm) was used for flash column chromatography. ^{1}H-NMR and 2D-NOESY spectra were recorded on Bruker spectrometers (at 400, 500, and 600 MHz) and are reported relative to the residual solvent signal. Data for ^{1}H-NMR spectra are reported as follows: chemical shift (δ ppm), multiplicity, coupling

constant (Hz) and integration. ^{13}C-NMR spectra were recorded on Bruker spectrometers (at 100, 125, and 150 MHz) and are reported relative to the residual solvent signal. Data for ^{13}C-NMR spectra are reported in terms of chemical shift (δ ppm) and, when necessary, multiplicity, and coupling constant (Hz). ^{19}F-NMR spectra were recorded on Bruker spectrometers (at 282 MHz) and are reported in terms of chemical shift (δ ppm), multiplicity, coupling constant (Hz) and integration. IR spectra were recorded on a Perkin-Elmer UATR Two FT-IR spectrometer and a JASCO FT/IR-4100 spectrometer and are reported in terms of frequency absorption (cm^{-1}). Uncorrected melting points were measured using a Digimelt MPA160 melting point apparatus. DART-MS spectra were collected on a Thermo Exactive Plus MSD (Thermo Scientific) equipped with an ID-CUBE ion source and a Vapur Interface (IonSense Inc.). Both the source and MSD were controlled by Excalibur software version 3.0. The analyte was spotted onto OpenSpot sampling cards (IonSense Inc.) using deuterated chloroform ($CDCl_3$) or CH_2Cl_2 as the solvent. Ionization was accomplished using UHP He plasma with no additional ionization agents. The mass calibration was carried out using Pierce LTQ Velos ESI (+) and (–) Ion calibration solutions (Thermo Fisher Scientific). Optical rotations were measured with a Rudolf Autopol III Automatic Polarimeter. Determination of enantiopurity was carried out on a JASCO SFC (supercritical fluid chromatography) using a Daicel ChiralPak ID column and a Daicel ChiralPak IE column. Data for SFC chromatograms are reported in enantiomeric excess (ee).

Alcohol **2.53**,[66] vinyl benzoxazinone derivatives **2.15**[67], **2.69**[56], **2.70**[56], **2.71**[68], **2.73**[67], **2.74**[68], **2.76**[68], **2.81**[69], **2.86**[70], **2.87**[69], **2.89**[67], and **2.90**[69], and allene precursors **2.16**[27], **2.50**[29], **2.84**[38], and **2.88**[25] are all known compounds. The ^{1}H NMR spectral data matched those reported in literature.

2.8.2 Experimental Procedures

2.8.2.1 Synthesis of *N*-Tosyl-vinyl Benzoxazinones

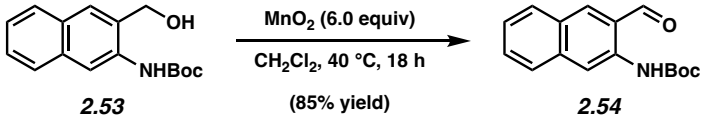

Aldehyde 2.54. To a solution of alcohol **2.53** (2.37 g, 8.67 mmol, 1.0 equiv) in CH_2Cl_2 (28.9 mL, 0.30 M) was added MnO_2 (4.52 g, 52.0 mmol, 6.0 equiv) in a single portion. The reaction vessel was fitted with an air condenser and the resulting mixture was stirred at 40 °C for 18 h. After 18 h, the reaction mixture was cooled to 23 °C and filtered over a celite plug eluting with ethyl acetate (500 mL). The filtrate was then concentrated under reduced pressure to afford aldehyde **2.54** (1.99 g, 85% yield) as a yellow solid, which was used in the subsequent step without purification. **Aldehyde 2.54**: Mp: 132–133 °C; R_f 0.57 (5:1 hexanes:EtOAc); ^{1}H NMR (500 MHz, $CDCl_3$): δ 10.19 (br s, 1H), 10.07 (s, 1H), 8.78 (s, 1H), 8.18 (s, 1H), 7.87 (d, J = 8.2, 1H), 7.82 (d, J = 8.3, 1H), 7.59 (t, J = 7.3, 1H), 7.42 (t, J = 7.5, 1H), 1.57 (s, 9H); ^{13}C NMR (125 MHz, $CDCl_3$): δ 195.2, 153.4, 140.4, 137.5, 136.5, 130.4, 129.1, 128.2, 127.8, 125.4, 122.8, 115.2, 80.9, 28.5; IR (film): 3314, 2980, 1728, 1673, 1541 cm^{-1}; HRMS-APCI (*m/z*) $[M - H]^-$ calcd for $C_{16}H_{16}NO_3^-$, 270.1125; found 270.1112.

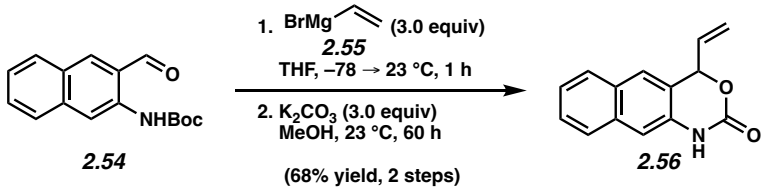

Vinyl benzoxazinone 2.56. To a solution of aldehyde **2.54** (750 mg, 2.77 mmol, 1.0 equiv) in THF (6.0 mL, 0.46 M) at –78 °C was added vinylmagnesium bromide **2.55** (0.32 M in THF, 25.9 mL, 8.29 mmol, 3.0 equiv) dropwise over 25 min. The solution was warmed to 23 °C and stirred

at this temperature for 1 h. The reaction was then cooled to 0 °C and quenched with dropwise addition of saturated aqueous $NaHCO_3$ (40 mL). The resulting mixture was extracted with diethyl ether (3 x 50 mL). The combined organic layers were dried with Na_2SO_4, filtered, and concentrated under reduced pressure to afford a dark orange oil (828 mg). To a solution of the dark orange oil in MeOH (9.1 mL, 0.30 M) was added K_2CO_3 (1.15 g, 8.30 mmol, 3.0 equiv) and the resulting heterogeneous mixture was allowed to stir at 23 °C for 60 h. The reaction was then neutralized with 2 M HCl (4 mL) and the resulting mixture was extracted with EtOAc (3 x 50 mL). The combined organic layers were washed with brine (1 x 50 mL), dried with Na_2SO_4, filtered, and concentrated under reduced pressure. The crude material was purified by flash column chromatography (5:1 → 4:1 hexanes:EtOAc) to provide vinyl benzoxazinone **2.56** (425 mg, 68% yield over 2 steps) as an off-white solid. **Vinyl benzoxazinone 2.56**: Mp: 165 °C; R_f 0.33 (2:1 hexanes:EtOAc); ^{1}H NMR (500 MHz, $CDCl_3$): δ 9.33 (s, 1H), 7.77 (d, *J* = 8.1, 1H), 7.74 (d, *J* = 8.2, 1H), 7.58 (s, 1H), 7.47 (ddd, *J* = 8.1, 6.9, 1.2, 1H), 7.40 (ddd, *J* = 8.1, 6.9, 1.2, 1H), 7.29 (s, 1H), 6.17 (ddd, *J* = 17.0, 10.4, 6.4, 1H), 5.97 (dd, *J* = 6.4, 1.0, 1H), 5.49 (dt, *J* = 10.4, 0.9, 1H), 5.44 (dt, *J* = 17.1, 1.0, 1H); ^{13}C NMR (125 MHz, $CDCl_3$): δ 153.4, 133.9, 133.8, 132.9, 130.2, 128.1, 127.4, 127.1, 125.2, 124.8, 121.1, 120.3, 110.4, 80.3; IR (film): 3099, 2927, 1706, 1379, 1032 cm^{-1}; HRMS-APCI (*m/z*) $[M + H]^+$ calcd for $C_{14}H_{12}NO_2^+$, 226.0863; found 226.0866.

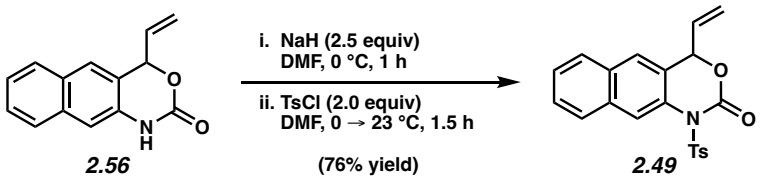

***N*-tosyl-vinyl benzoxazinone 2.49**. To a solution of vinyl benzoxazinone **2.56** (350 mg, 1.55 mmol, 1.0 equiv) in DMF (10.4 mL, 0.15 M) at 0 °C was added NaH (60 wt% dispersion in mineral

oil, 160 mg, 3.88 mmol, 2.5 equiv) in one portion. The mixture was stirred at this temperature for 1 h prior to the addition of TsCl (592 mg, 3.11 mmol, 2.0 equiv) in one portion. The resulting mixture was gradually warmed to 23 °C over 1.5 h then quenched by pouring into an Erlenmeyer flask filled with ice. The resulting mixture was extracted with EtOAc (3 x 50 mL). The combined organic layers were washed with water (3 x 40 mL), dried with Na_2SO_4, filtered, and concentrated under reduced pressure. The crude material was purified by flash column chromatography (9:1 hexanes:EtOAc) to provide *N*-tosyl-vinyl benzoxazinone **2.49** (449 mg, 76% yield) as a white solid. ***N*-tosyl-vinyl benzoxazinone 2.49**: Mp: 148–149 °C; R_f 0.57 (2:1 hexanes:EtOAc); ^{1}H NMR (500 MHz, $CDCl_3$): δ 8.14 (dt, *J* = 8.7, 1.9, 2H), 8.04 (s, 1H), 7.88 (d, *J* = 8.0, 1H), 7.81 (d, *J* = 8.0, 1H), 7.65 (s, 1H), 7.55 (ddd, *J* = 8.2, 6.9, 1.4, 1H), 7.51 (ddd, *J* = 8.1, 7.0, 1.5, 1H), 7.43–7.38 (m, 2H), 6.11 (ddd, *J* = 17.2, 10.5, 6.0, 1H), 5.78 (dd, *J* = 6.1, 1.1, 1H), 5.52 (dt, *J* = 10.6, 1.1, 1H), 5.42 (ddd, *J* = 17.2, 1.3, 0.7, 1H), 2.47 (s, 3H); ^{13}C NMR (125 MHz, $CDCl_3$): δ 149.4, 145.8, 135.7, 133.2, 132.2, 131.1, 130.8, 129.8 129.3, 128.3, 127.8 127.5, 126.9, 126.0, 124.7, 121.7, 118.9, 79.8, 21.9; IR (film): 3065, 2927, 1744, 1368, 1168 cm^{-1}; HRMS-APCI (*m/z*) $[M + H]^+$ calcd for $C_{21}H_{18}NO_4S^+$, 380.0951; found 380.0957.

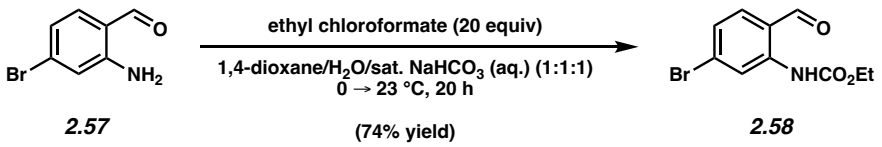

2.57 *2.58*

Carbamate 2.58. To a solution of amino benzaldehyde **2.57** (1.50 g, 7.50 mmol, 1.0 equiv) in 1:1:1 1,4-dioxane/water/sat. $NaHCO_3$ (30 mL, 0.25 M) at 0 °C was added ethyl chloroformate (8.00 mL, 80.0 mmol, 20.0 equiv) dropwise over 5 min. The reaction was then warmed to 23 °C over 20 h before being diluted with brine (40 mL). The resulting mixture was extracted with EtOAc (3 x 30 mL). The combined organic layers were dried with Na_2SO_4, filtered, and concentrated

under reduced pressure. The crude material was purified by flash column chromatography (49:1 hexanes:EtOAc) to provide carbamate **2.58** (1.51 g, 74% yield) as a pale yellow solid. **Carbamate 2.58**: Mp: 66–67 °C; R_f 0.58 (5:1 hexanes:EtOAc); ^{1}H NMR (600 MHz, $CDCl_3$): δ 10.60 (br s, 1H), 9.86 (s, 1H), 8.73 (d, *J* = 1.2, 1H), 7.48 (d, *J* = 8.2, 1H), 7.31 (dd, *J* = 8.2, 1.7, 1H), 4.26 (q, *J* = 7.2, 2H), 1.34 (t, *J* = 7.2, 3H); ^{13}C NMR (125 MHz, $CDCl_3$): δ 194.3, 153.6, 142.2, 137.0, 131.9, 125.4, 121.6, 120.1, 61.9, 14.6; IR (film): 3231, 2995, 1728, 1515, 1216 cm^{-1}; HRMS-APCI (*m/z*) $[M + H]^+$ calcd for $C_{10}H_{11}BrNO_3^+$, 271.9917; found 271.9919.

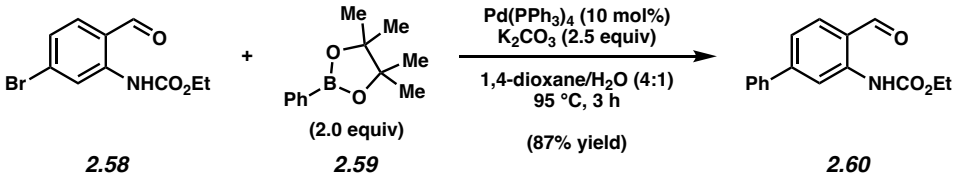

2.58 *2.59* *2.60*

Carbamate 2.60. An 8-dram vial containing a magnetic stir bar was charged with carbamate **2.58** (600 mg, 2.21 mmol, 1.0 equiv), potassium carbonate (762 mg, 5.51 mmol, 2.5 equiv), and phenylboronic acid pinacol ester **2.59** (900 mg, 4.41 mmol, 2.0 equiv). The vial was taken into a glovebox where $Pd(PPh_3)_4$ (255 mg, 0.221 mmol, 0.1 equiv) was added. The reaction was sealed with a septum cap, removed from the glovebox, and placed under a flow of N_2. Then, 4:1 1,4-dioxane:water (16 mL, 0.138 M) was added. The septum cap was then carefully replaced with a Teflon-lined cap and stirred for 3 h at 95 °C. The reaction mixture was then cooled to 23 °C, concentrated under reduced pressure, diluted with water (10 mL) and extracted with CH_2Cl_2 (3 x 20 mL). The combined organic layers were dried with Na_2SO_4, filtered, and concentrated under reduced pressure. The crude material was purified by flash column chromatography (49:1 hexanes:EtOAc) to provide carbamate **2.60** (515 mg, 87% yield) as a white solid. **Carbamate 2.60**: Mp: 109–110 °C; R_f 0.66 (5:1 hexanes:EtOAc); ^{1}H NMR (500 MHz, $CDCl_3$): δ 10.65 (br s,

1H), 9.94 (d, J = 0.6, 1H), 8.78 (d, J = 1.5, 1H), 7.73–7.66 (m, 3H), 7.49–7.44 (m, 2H), 7.44–7.38 (m, 2H), 4.27 (q, J = 7.1, 2H), 1.36 (t, J = 7.1, 3H); ^{13}C NMR (125 MHz, $CDCl_3$): δ 194.7, 154.0, 148.8, 141.9, 139.7, 136.6, 129.1, 128.9, 127.7, 120.7, 120.3, 117.0, 61.6, 14.6; IR (film): 3272, 2928, 1724, 1564, 1211 cm^{-1}; HRMS-APCI (*m/z*) $[M + H]^+$ calcd for $C_{16}H_{16}NO_3^+$, 270.1125; found 270.1127.

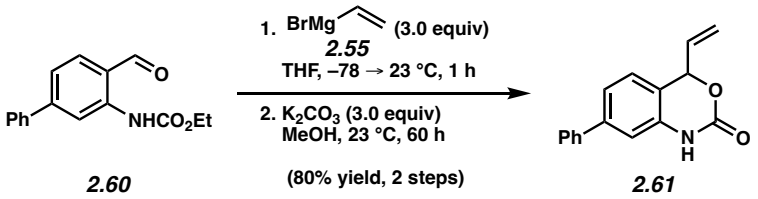

Vinyl benzoxazinone 2.61. To a solution of aldehyde **2.60** (495 mg, 1.84 mmol, 1.0 equiv) in THF (1.0 mL, 2 M) at –78 °C was added vinylmagnesium bromide **2.55** (0.46 M in THF, 12.0 mL, 5.51 mmol, 3.0 equiv) dropwise over 7 min. The solution was warmed to 23 °C and stirred at this temperature for 30 min. The reaction was then cooled to 0 °C and quenched with dropwise addition of saturated aqueous $NaHCO_3$ (6 mL). The resulting mixture was extracted with diethyl ether (3 x 7 mL). The combined organic layers were dried with Na_2SO_4, filtered, and concentrated under reduced pressure to afford an oil (550 mg). To a solution of the oil in MeOH (6.17 mL, 0.30 M) was added K_2CO_3 (767 mg, 5.55 mmol, 3.0 equiv) and the resulting heterogeneous mixture was allowed to stir at 23 °C for 60 h. The reaction was neutralized with 1 M HCl (6 mL), and the resulting mixture was extracted with EtOAc (3 x 20 mL). The combined organic layers were washed with brine (10 mL), dried with Na_2SO_4, filtered, and concentrated under reduced pressure. The crude product was purified by flash column chromatography (5:1 hexanes:EtOAc) to provide vinyl benzoxazinone **2.61** (373 mg, 80% yield over 2 steps) as an pale yellow solid. **Vinyl benzoxazinone 2.61**: Mp: 159–161 °C; R_f 0.15 (5:1 hexanes:EtOAc); ^{1}H NMR (500 MHz,

$CDCl_3$): δ 7.62 (br s, 1H), 7.57–7.53 (m, 2H), 7.48–7.42 (m, 2H), 7.38 (tt, *J* = 7.4, 1.3, 1H), 7.30 (dd, *J* = 7.9, 1.7, 1H), 7.17 (d, *J* = 7.8, 1H), 7.00 (d, *J* = 1.7, 1H), 6.10 (ddd, *J* = 16.9, 10.3, 6.4, 1H), 5.87–5.84 (m, 1H), 5.56–5.38 (m, 2H); ^{13}C NMR (125 MHz, $CDCl_3$, 13 of 14 signals observed): δ 143.0, 139.9, 135.5, 133.9, 129.0, 128.1, 127.3, 125.6, 122.4, 119.9, 118.9, 113.0, 80.3; IR (film): 3235, 2971, 1704, 1366, 760 cm^{-1}; HRMS-APCI (*m/z*) $[M + H]^+$ calcd for $C_{16}H_{14}NO_2^+$, 252.1019; found 252.1018.

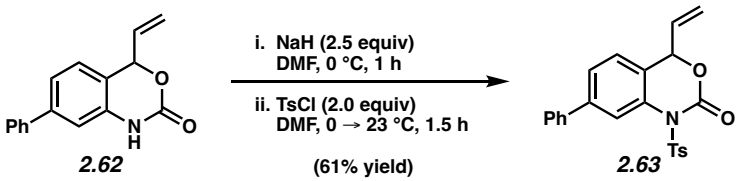

***N*-tosyl-vinyl benzoxazinone 2.63**. To a solution of vinyl benzoxazinone **2.62** (370 mg, 1.47 mmol, 1.0 equiv) in DMF (9.82 mL, 0.15 M) at 0 °C was added NaH (60 wt% dispersion in mineral oil, 150 mg, 3.68 mmol, 2.5 equiv) in one portion. The mixture was stirred at this temperature for 1 h prior to the addition of TsCl (561 mg, 2.94 mmol, 2.0 equiv) in one portion. The resulting mixture was gradually warmed to 23 °C over 3 h then quenched by pouring into an Erlenmeyer flask filled with ice. The resulting mixture was extracted with EtOAc (3 x 20 mL). The combined organic layers were washed with water (3 x 30 mL), dried with Na_2SO_4, filtered, and concentrated under reduced pressure. The crude material was purified by flash column chromatography (7:1 hexanes:EtOAc) to provide *N*-tosyl-vinyl benzoxazinone **2.63** (365 mg, 61% yield) as a yellow solid. ***N*-tosyl-vinyl benzoxazinone 2.63**: Mp: 120–121 °C; R_f 0.23 (5:1 hexanes:EtOAc); ^{1}H NMR (500 MHz, $CDCl_3$): δ 8.12 (d, *J* = 8.3, 2H), 7.85 (s, 1H), 7.59 (d, *J* = 7.4, 2H), 7.51–7.45 (m, 3H), 7.44–7.37 (m, 3H), 7.25 (overlapped with residual solvent peak, 1H), 6.07 (ddd, *J* = 16.9, 10.4, 6.2, 1H), 5.69 (d, *J* = 6.0, 1H), 5.49 (d, *J* = 10.4, 1H), 5.41 (d, *J* = 17.1, 1H), 2.47 (s, 3H);

^{13}C NMR (125 MHz, $CDCl_3$): δ 149.3, 145.8, 142.8, 140.0, 135.8, 134.6, 132.2, 129.9, 129.3, 129.2, 128.3, 127.4, 125.5, 125.3, 124.9, 121.4, 119.9, 79.5, 21.9; IR (film): 3025, 2970, 1747, 1364, 1166 cm^{-1}; HRMS-APCI (*m/z*) $[M + H]^+$ calcd for $C_{23}H_{20}NO_4S^+$, 406.1108; found 406.1109.

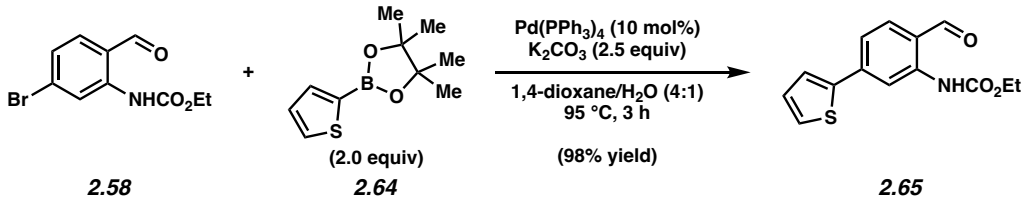

2.58 ***2.64*** ***2.65***

Carbamate 2.65. A 50-mL round-bottomed flask containing a magnetic stir bar was charged with carbamate **2.58** (750 mg, 2.76 mmol, 1.0 equiv), potassium carbonate (952 mg, 6.89 mmol, 2.5 equiv), and thiophene-2-boronic acid pinacol ester **2.64** (1.16 g, 5.51 mmol, 2.0 equiv). The flask was taken into a glovebox where $Pd(PPh_3)_4$ (319 mg, 0.276 mmol, 0.10 equiv) was added. The reaction was sealed with a septum cap, removed from the glovebox, and placed under a flow of N_2. Then, 4:1 1,4-dioxane:water (18.8 mL, 0.147 M) was added. The reaction mixture was stirred for 3 h at 95 °C. The reaction mixture was then cooled to 23 °C, concentrated under reduced pressure, diluted with water (10 mL), and extracted with CH_2Cl_2 (3 x 20 mL). The combined organic layers were dried with Na_2SO_4, filtered, and concentrated under reduced pressure. The crude material was purified by flash column chromatography (19:1 hexanes:EtOAc) to provide carbamate **2.65** (745 mg, 98% yield) as a yellow solid. **Carbamate 2.65**: Mp: 105–106 °C; R_f 0.68 (1:1 hexanes:CH_2Cl_2); ^{1}H NMR (600 MHz, $CDCl_3$): δ 10.66 (br s, 1H), 9.87 (s, 1H), 8.82 (d, *J* = 1.4, 1H), 7.62 (d, *J* = 8.0, 1H), 7.54 (dd, *J* = 3.7, 1.1, 1H), 7.43–7.38 (m, 2H), 7.13 (dd, *J* = 5.0, 3.7, 1H), 4.27 (q, *J* = 7.2, 2H), 1.36 (t, *J* = 7.2, 3H); ^{13}C NMR (125 MHz, $CDCl_3$): δ 194.2, 153.9, 142.9, 142.1, 141.7, 136.9, 128.6, 127.5, 125.9, 120.2, 119.1, 115.0, 61.7, 14.6; IR (film): 3263,

1734, 1610, 1212, 703 cm^{-1}; HRMS-APCI (*m/z*) $[M + H]^+$ calcd for $C_{14}H_{14}NO_3S^+$, 276.0694; found 276.0690.

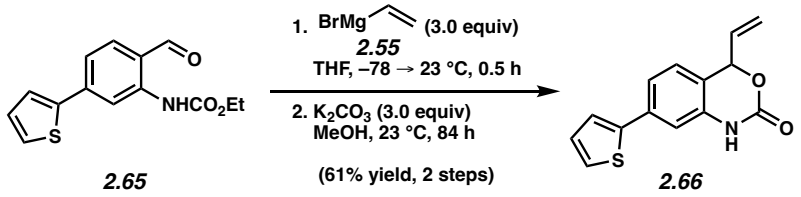

Vinyl benzoxazinone 2.66. To a solution of aldehyde **2.65** (500 mg, 1.82 mmol, 1.0 equiv) in THF (22.7 mL, 0.080 M) at –78 °C was added vinylmagnesium bromide **2.55** (0.46 M in THF, 11.8 mL, 5.45 mmol, 3.0 equiv) dropwise over 7 min. The solution was warmed to 23 °C and stirred at this temperature for 30 min. The reaction was then cooled to 0 °C and quenched with dropwise addition of saturated aqueous $NaHCO_3$ (8 mL). The resulting mixture was extracted with diethyl ether (3 x 10 mL). The combined organic layers were dried with Na_2SO_4, filtered, and concentrated under reduced pressure to afford an oil (551 mg). To a solution of the oil in MeOH (20.0 mL, 0.091 M) was added K_2CO_3 (753 mg, 5.45 mmol, 3.0 equiv) and the resulting heterogeneous mixture was allowed to stir at 23 °C for 84 h. The reaction was neutralized with 1 M HCl (6 mL), and the resulting mixture was extracted with EtOAc (3 x 20 mL). The combined organic layers were washed with brine (10 mL), dried with Na_2SO_4, filtered, and concentrated under reduced pressure. The crude product was purified by flash column chromatography (5:1 hexanes:EtOAc) to provide vinyl benzoxazinone **2.66** (284 mg, 61% yield over 2 steps) as an off-white solid. **Vinyl benzoxazinone 2.66**: Mp: 163 °C; R_f 0.11 (5:1 hexanes:EtOAc); ^{1}H NMR (500 MHz, $CDCl_3$): δ 7.57 (br s, 1H), 7.33–7.30 (m, 3H), 7.12–7.07 (m, 2H), 7.02 (d, *J* = 1.4, 1H), 6.08 (ddd, *J* = 16.9, 10.3, 6.4, 1H), 5.82 (d, *J* = 6.4, 1H), 5.44 (d, *J* = 10.3, 1H), 5.39 (d, *J* = 17.1, 1H); ^{13}C NMR (125 MHz, $CDCl_3$): δ 151.8, 142.9, 136.0, 135.6, 133.8, 128.3, 125.9, 125.8, 124.1,

121.2, 120.0, 119.0, 111.4, 80.2; IR (film): 3108, 2925, 1706, 1376, 1268 cm^{-1}; HRMS-APCI (*m/z*) $[M + H]^+$ calcd for $C_{14}H_{12}NO_2S^+$, 258.0589; found 258.0590.

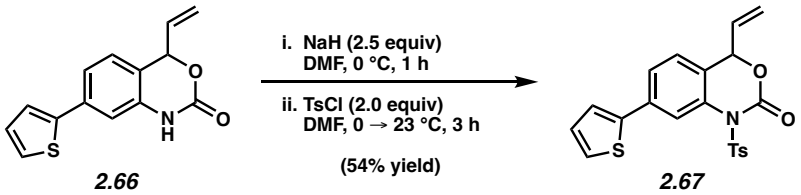

***N*-tosyl-vinyl benzoxazinone 2.67**. To a solution of vinyl benzoxazinone **2.66** (284 mg, 1.10 mmol, 1.0 equiv) in DMF (7.35 mL, 0.15 M) at 0 °C was added NaH (60 wt% dispersion in mineral oil, 110 mg, 2.75 mmol, 2.5 equiv) in one portion. The mixture was stirred at this temperature for 1 h prior to the addition of TsCl (420 mg, 2.20 mmol, 2.0 equiv) in one portion. The resulting mixture was gradually warmed to 23 °C over 3 h then quenched by pouring into an Erlenmeyer flask filled with ice. The resulting mixture was extracted with EtOAc (3 x 20 mL). The combined organic layers were washed with water (30 mL), dried with Na_2SO_4, filtered, and concentrated under reduced pressure. The crude material was purified by flash column chromatography (7:1 hexanes:EtOAc) to provide *N*-tosyl-vinyl benzoxazinone **2.67** (246 mg, 54% yield) as a white solid. ***N*-tosyl-vinyl benzoxazinone 2.67**: Mp: 119 °C; R_f 0.18 (5:1 hexanes:EtOAc); ^1H NMR (600 MHz, $CDCl_3$): δ 8.15 (dt, *J* = 8.7, 2.0, 2H), 7.84 (d, *J* = 1.6, 1H), 7.48 (dd, *J* = 8.0, 1.6, 1H), 7.44–7.39 (m, 2H), 7.37–7.33 (m, 2H), 7.18 (d, *J* = 8.0, 1H), 7.12 (dd, *J* = 5.0, 3.7, 1H), 6.05 (ddd, *J* = 17.0, 10.4, 6.1, 1H), 5.58–5.63 (m, 1H), 5.52–5.46 (m, 1H), 5.40 (ddd, *J* = 17.2, 1.3, 0.6, 1H), 2.48 (s, 3H); ^{13}C NMR (150 MHz, $CDCl_3$): δ 149.2, 145.9, 142.9, 135.87, 135.86, 134.9, 132.1, 129.9, 129.3, 128.5, 126.1, 125.7, 125.4, 124.5, 123.5, 121.5, 118.3, 79.5, 21.9; IR (film): 2977, 2367, 1758, 1173, 823 cm^{-1}; HRMS-APCI (*m/z*) $[M + H]^+$ calcd for $C_{21}H_{18}NO_4S_2^+$, 412.0677; found 412.0668.

2.8.2.2 Optimization of the Racemic Annulation

Results from the optimization of the reactions between **2.15** and **2.16** and between **2.15** and **2.50** appear below. Reactant stoichiometry and temperature were varied using General Procedure 2.1, and results appear below in Table 2.3 and 2.4, respectively. Water loading, catalyst loading, and concentration were varied using General Procedure 2.2, and results appear below in Table 2.5, 2.6, and 2.7, respectively. Ligands were varied using General Procedure 2.3, and results appear below in Table 2.8. Initial efforts to use other metals (e.g., Ir and Ni) were unsuccessful. As such, we focused on Pd.

Any modification of the conditions shown in the general procedures above are specified in the following schemes. Although reactions were performed in a glovebox for consistency, reactions setup on the bench-top did not suffer from a significant loss in yield.

General Procedure 2.1 for the optimization of the racemic annulation:

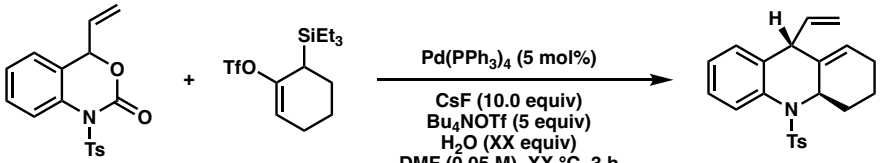

(XX equiv) *2.15* (1.0 equiv) *2.16* *2.17*

Annulation Product 2.17. A 1-dram vial containing a magnetic stir bar was charged with vinyl benzoxazinone **2.15** and Bu_4NOTf (49 mg, 0.13 mmol, 5.0 equiv). A separate 1-dram vial was charged with silyl triflate **2.16**. The two vials were taken into a glovebox where $Pd(PPh_3)_4$ (1.4 mg, 0.0013 mmol, 0.05 equiv) and CsF (38 mg, 0.25 mmol, 10.0 equiv) were added to the vial containing vinyl benzoxazinone **2.15**. To the vial containing silyl triflate **2.16** was added the appropriate amount of DMF to afford a 0.05 M solution. The vial was capped and shaken to ensure

full dissolution. The necessary amount of the solution of silyl triflate **2.16** (0.05 M in DMF, 500 µL, 8.6 mg, 0.025 mmol, 1.0 equiv) was then transferred via micropipette to the reaction vial containing vinyl benzoxazinone **2.15**. The reaction was sealed with a septum cap, removed from the glovebox, and placed under a flow of N_2. Then, deionized water was added to the reaction vessel via microsyringe. The septum cap was then carefully replaced with a Teflon-lined cap under a stream of N_2 and stirred for 3 h at the desired reaction temperature. The mixture was then filtered through a pad of silica gel, eluting with EtOAc (8 mL). The eluate was concentrated by iteratively azeotroping with *n*-heptane (4 x 5 mL). The crude residue was then redissolved in CH_2Cl_2 (1 mL) and filtered through a pad of silica gel eluting with CH_2Cl_2 (20 mL) to remove excess Bu_4NOTf. The eluate was concentrated to afford a crude residue, which was analyzed by ^1H NMR using mesitylene as an external standard.

General Procedure 2.2 for the optimization of the racemic annulation:

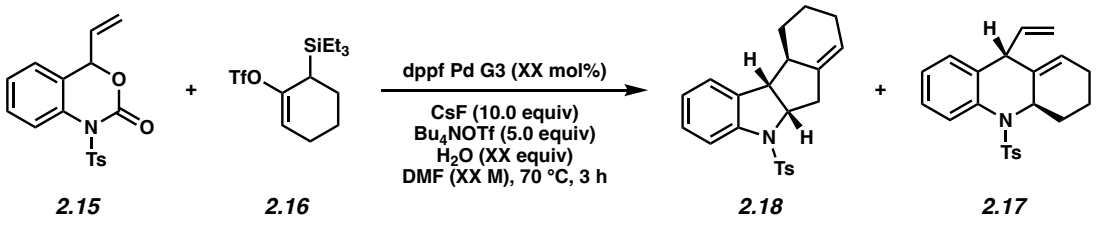

Annulation Products 2.17 and **2.18**. A 1-dram vial containing a magnetic stir bar was charged with vinyl benzoxazinone **2.15** (25 mg, 0.075 mmol, 3.0 equiv) and Bu_4NOTf (49 mg, 0.13 mmol, 5.0 equiv). A separate 1-dram vial was charged with silyl triflate **2.16**. The two vials were taken into a glovebox where dppf Pd G3 and CsF (38 mg, 0.25 mmol, 10.0 equiv) were added to the vial containing vinyl benzoxazinone **2.15**. To the vial containing silyl triflate **2.16** was added the appropriate amount of DMF to afford a solution of desired concentration. The vial was capped and shaken to ensure full dissolution. The necessary amount of the solution of silyl triflate **2.16** (8.6

mg, 0.025 mmol, 1.0 equiv) was then transferred via micropipette to the reaction vial containing vinyl benzoxazinone **2.15**. The reaction was sealed with a septum cap, removed from the glovebox, and placed under a flow of N_2. Then, deionized water was added to the reaction vessel via microsyringe. The septum cap was then carefully replaced with a Teflon-lined cap under a stream of N_2 and stirred for 3 h at 70 °C. The mixture was then filtered through a pad of silica gel, eluting with EtOAc (8 mL). The eluate was washed with water (2 x 5 mL), dried with Na_2SO_4, filtered, and concentrated under reduced pressure. The crude residue was redissolved in CH_2Cl_2 (1 mL) and filtered through a pad of silica gel eluting with CH_2Cl_2 (20 mL) to remove excess Bu_4NOTf. The eluate was concentrated and purified by preparative thin layer chromatography (4:1:1 hexanes:CH_2Cl_2:Et_2O) to provide annulation products **2.17** and **2.18**.

General Procedure 2.3 for the optimization of the racemic annulation:

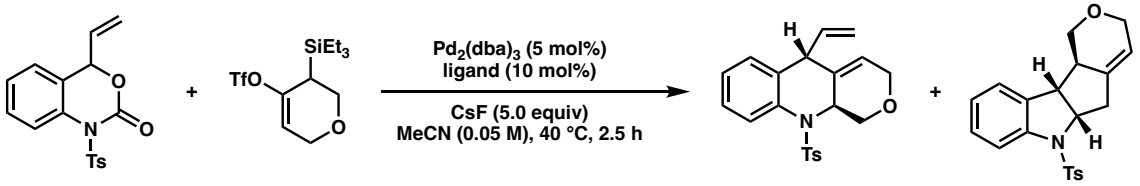

2.15 *2.50* *2.32* *2.44*

Annulation Products 2.32 and **2.44**. A 1-dram vial containing a magnetic stir bar was charged with vinyl benzoxazinone **2.15** (25 mg, 0.075 mmol, 3.0 equiv). A separate 1-dram vial was charged with silyl triflate **2.50**. The two vials were taken into a glovebox where $Pd_2(dba)_3$ (1.1 mg, 0.0013 mmol, 5 mol%), ligand (0.0025 mmol, 10 mol%) and CsF (38 mg, 0.25 mmol, 10.0 equiv) were added to the vial containing vinyl benzoxazinone **2.15**. To the vial containing silyl triflate **2.50** was added the appropriate amount of MeCN to afford a 0.05 M solution. The vial was capped and shaken to ensure full dissolution. The necessary amount of the solution of silyl triflate **2.50** (0.05 M in MeCN, 500 µL, 8.6 mg, 0.025 mmol, 1.0 equiv) was then transferred via micropipette

to the reaction vial containing vinyl benzoxazinone **2.15**. The reaction was sealed with a Teflon-lined cap, removed from the glovebox, and stirred for 2.5 h at 40 °C. The mixture was then filtered through a pad of silica gel, eluting with EtOAc (8 mL). The eluate was concentrated to provide a crude residue, which was analyzed by ^{1}H NMR using mesitylene as an external standard.

Table 2.3. Evaluation of Vinyl Benzoxazinone Equivalents.

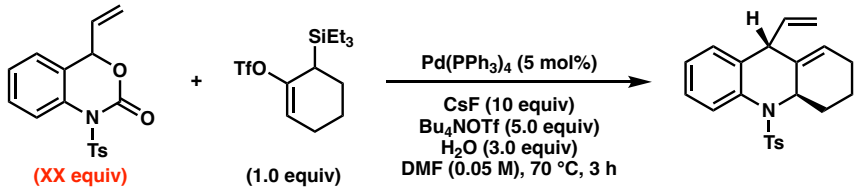

2.15 ***2.16*** ***2.17***

Entry	Equiv. 2.15	^{1}H NMR Yield[a]	dr
1	1.0	31%	7.4:1[b]
2	3.0	54%	11:1[b]
3	5.0	47%	9.3:1[c]

[a] ^{1}H NMR yield determined using mesitylene as an external standard.
[b] dr was determined by ^{1}H NMR analysis of crude reaction mixture.
[c] dr was determined by ^{1}H NMR analysis of isolated mixture of diastereomers.

Table 2.4. Evaluation of Temperature.

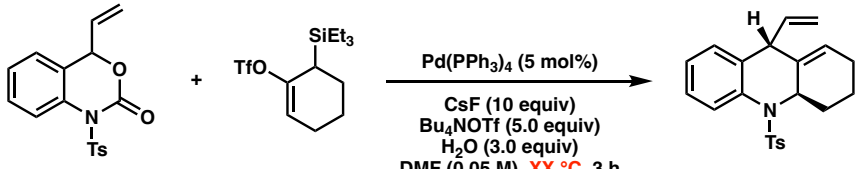

2.15 ***2.16*** ***2.17***

Entry	Temperature (°C)	^{1}H NMR Yield[a]	dr[b]
1	50	46%	8.4:1
2	70	54%	11:1
3	90	47%	7.8:1

[a] ^{1}H NMR yield determined using mesitylene as an external standard. [b] dr was determined by ^{1}H NMR analysis of crude reaction mixture.

Table 2.5. Evaluation of H_2O Loading.

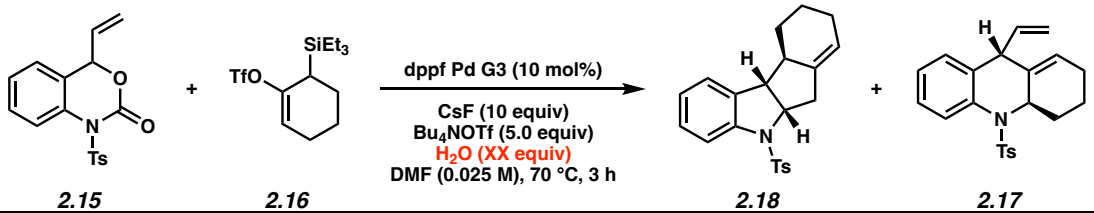

2.15 *2.16* *2.18* *2.17*

Entry	Equiv. H_2O	Isolated Yield[a]	2.18:2.17[b]
1	0.0	28%	>20:1
2	3.0	59%	10:1
3	6.0	65%	11:1
4	9.0	74%	10:1
5	12.0	73%	3.8:1

[a] Products isolated as a mixture. [b] For **2.18** dr = >20:1. For **2.17** dr could not be determined. Ratio of **2.18**:**2.17** and dr were determined by ^{1}H NMR analysis of the isolated mixture.

Table 2.6. Evaluation of Catalyst Loading.

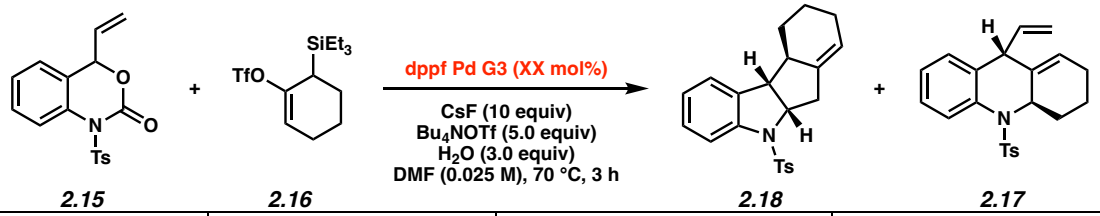

2.15 *2.16* *2.18* *2.17*

Entry	Mol% [Pd]	Isolated Yield[a]	2.18:2.17[b]
1	5 mol%	44%	11:1
2	10 mol%	59%	10:1
3	15 mol%	61%	11:1

[a] Products isolated as a mixture. [b] For **2.18** dr = >20:1. For **2.17** dr could not be determined. Ratio of **2.18**:**2.17** and dr were determined by ^{1}H NMR analysis of the isolated mixture.

Table 2.7. Evaluation of Concentration.

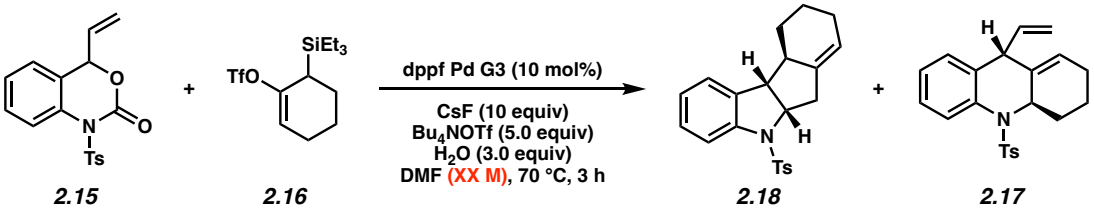

2.15 *2.16* *2.18* *2.17*

Entry	Concentration	Isolated Yield[a]	2.18:2.17[b]
1	0.05	64%	7.6:1
2	0.025	59%	10:1
3	0.0125	51%	15:1

[a] Products isolated as a mixture. [b] For **2.18** dr = >20:1. For **2.17** dr could not be determined. Ratio of **2.18**:**2.17** and dr were determined by ^{1}H NMR analysis of the isolated mixture.

Table 2.8. Evaluation of Ligands.

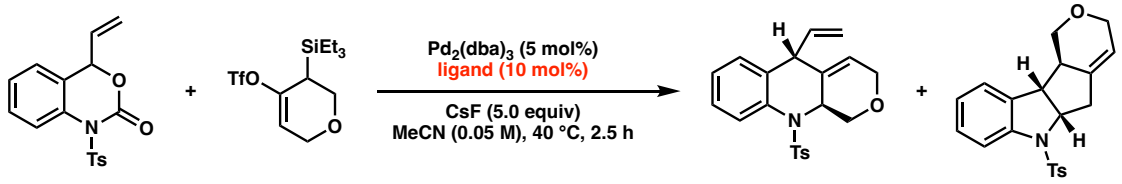

2.15 *2.50* *2.32* *2.44*

Entry	Ligand	^{1}H NMR Yield (2.32)[a,b]	^{1}H NMR Yield (2.44)[a,c]
1	$Pd(PPh_3)_4$ (5 mol%)[d]	54%	0%
2	PCy_3	18%	4%
3	DavePhos	13%	0%
4	Ruphos	10%	0%
5	Xantphos	8%	0%
6	SPhos	8%	0%
7	XPhos	6%	0%
8	dppe	0%	0%
9	dtbpf	0%	0%
10	rac-BINAP	0%	0%
11	DPEphos	0%	8%
12	dppf	0%	36%
13	dppf Pd G3 (5 mol%)[d]	0%	44%

[a] ^{1}H NMR yield determined using mesitylene as an external standard. [b] ~1:1 dr as determined by ^{1}H NMR analysis of crude reaction mixture. [c] >20:1 dr as determined by ^{1}H NMR analysis of crude reaction mixture. [d] $Pd_2(dba)_3$ omitted from the reaction.

2.8.2.3. Scope of the Racemic Annulation

General Procedure 2.4 for the scope of the racemic annulation:

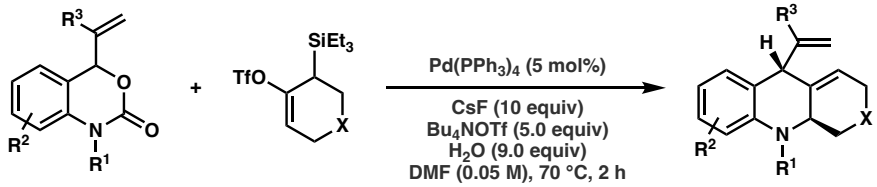

2.19 *2.20* *2.21*

Annulation Products 2.21. A 1-dram vial containing a magnetic stir bar was charged with vinyl benzoxazinone **2.19** (0.15 mmol, 3.0 equiv) and Bu_4NOTf (98 mg, 0.25 mmol, 5.0 equiv). A separate 1-dram vial was charged with silyl triflate **2.20**. The two vials were taken into a glovebox where $Pd(PPh_3)_4$ (2.9 mg, 0.0025 mmol, 5 mol%) and CsF (76 mg, 0.50 mmol, 10.0 equiv) were

added to the vial containing vinyl benzoxazinone **2.19**. To the vial containing silyl triflate **2.20** was added the appropriate amount of DMF to afford a 0.05 M solution. The vial was capped and shaken to ensure full dissolution. The necessary amount of the solution of silyl triflate **2.20** (0.05 M in DMF, 1.0 mL, 0.05 mmol, 1.0 equiv) was then transferred via micropipette to the reaction vial containing vinyl benzoxazinone **2.19**. The reaction was sealed with a septum cap, removed from the glovebox, and placed under a flow of N_2. Then, deionized water (8.1 μL, 0.45 mmol, 9.0 equiv) was added to the reaction vessel via microsyringe. The septum cap was then carefully replaced with a Teflon-lined cap under a stream of N_2 and stirred for 2 h at 70 °C. The mixture was then filtered through a pad of silica gel, eluting with EtOAc (8 mL). The eluate was washed with water (4 x 5 mL), dried with Na_2SO_4, filtered, and concentrated under reduced pressure. The crude residue was redissolved in CH_2Cl_2 (1 mL) and filtered through a pad of silica gel eluting with CH_2Cl_2 (20 mL) to remove excess Bu_4NOTf. The eluate was concentrated and purified by preparative thin layer chromatography to provide annulation products **2.21**.

General Procedure 2.5 for the scope of the racemic annulation:

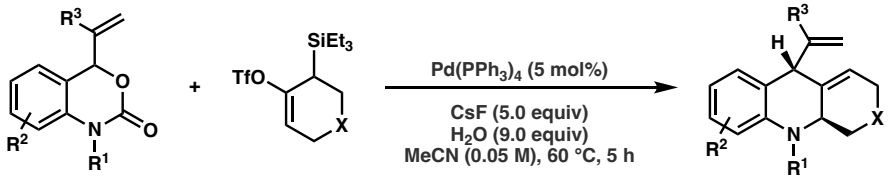

2.19 *2.20* *2.21*

Annulation Products 2.21. A 1-dram vial containing a magnetic stir bar was charged with vinyl benzoxazinone **2.19** (0.15 mmol, 3.0 equiv). A separate 1-dram vial was charged with silyl triflate **2.20**. The two vials were taken into a glovebox where $Pd(PPh_3)_4$ (2.9 mg, 0.0025 mmol, 5 mol%) and CsF (38 mg, 0.25 mmol, 5.0 equiv) were added to the vial containing vinyl benzoxazinone **2.19**. To the vial containing silyl triflate **2.20** was added the appropriate amount of MeCN to afford

a 0.05 M solution. The vial was capped and shaken to ensure full dissolution. The necessary amount of the solution of silyl triflate **2.20** (0.05 M in MeCN, 1.0 mL, 0.05 mmol, 1.0 equiv) was then transferred via micropipette to the reaction vial containing vinyl benzoxazinone **2.19**. The reaction was sealed with a septum cap, removed from the glovebox, and placed under a flow of N_2. Then, deionized water (8.1 μL, 0.45 mmol, 9.0 equiv) was added to the reaction vessel via microsyringe. The septum cap was then carefully replaced with a Teflon-lined cap under a stream of N_2 and stirred for 5 h at 60 °C. The mixture was then filtered through a pad of silica gel, eluting with EtOAc (8 mL). The eluate was concentrated and purified by preparative thin layer chromatography to provide annulation products **2.21**.

General Procedure 2.6 for the scope of the racemic annulation:

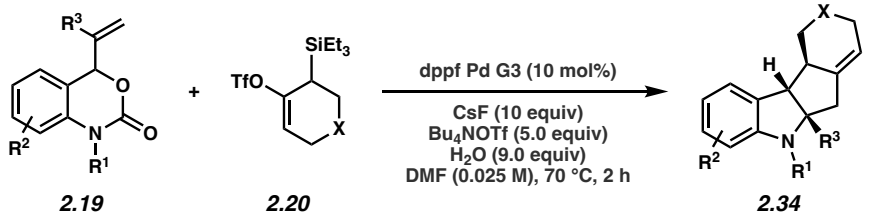

2.19 *2.20* *2.34*

Annulation Products 2.34. A 1-dram vial containing a magnetic stir bar was charged with vinyl benzoxazinone **2.19** (0.15 mmol, 3.0 equiv) and Bu_4NOTf (98 mg, 0.25 mmol, 5.0 equiv). A separate 1-dram vial was charged with silyl triflate **2.20**. The two vials were taken into a glovebox where dppf Pd G3 (4.7 mg, 0.0050 mmol, 10 mol%) and CsF (76 mg, 0.50 mmol, 10.0 equiv) were added to the vial containing vinyl benzoxazinone **2.19**. To the vial containing silyl triflate **2.20** was added the appropriate amount of DMF to afford a 0.025 M solution. The vial was capped and shaken to ensure full dissolution. The necessary amount of the solution of silyl triflate **2.20** (0.025 M in DMF, 2.0 mL, 0.05 mmol, 1.0 equiv) was then transferred via micropipette to the reaction vial containing vinyl benzoxazinone **2.19**. The reaction was sealed with a septum cap, removed

from the glovebox, and placed under a flow of N_2. Then, deionized water (8.1 μL, 0.45 mmol, 9.0 equiv) was added to the reaction vessel via microsyringe. The septum cap was then carefully replaced with a Teflon-lined cap under a stream of N_2 and stirred for 2 h at 70 °C. The mixture was then filtered through a pad of silica gel, eluting with EtOAc (8 mL). The eluate was washed with water (4 x 5 mL), dried with Na_2SO_4, filtered, and concentrated under reduced pressure. The crude residue was redissolved in CH_2Cl_2 (1 mL) and filtered through a pad of silica gel eluting with CH_2Cl_2 (20 mL) to remove excess Bu_4NOTf. The eluate was concentrated and purified by preparative thin layer chromatography to provide annulation products **2.34**.

General Procedure 2.7 for the scope of the racemic annulation:

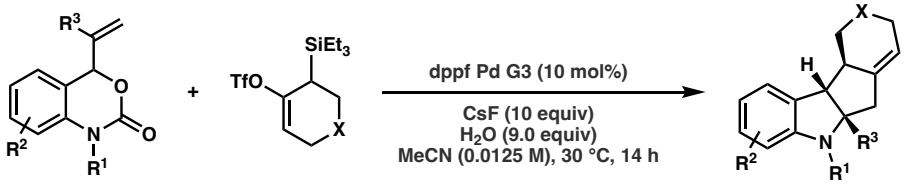

Annulation Products 2.34. A 2-dram vial containing a magnetic stir bar was charged with vinyl benzoxazinone **2.19** (0.15 mmol, 3.0 equiv). A separate 1-dram vial was charged with silyl triflate **2.20**. The two vials were taken into a glovebox where dppf Pd G3 (4.7 mg, 0.0050 mmol, 10 mol%) and CsF (75 mg, 0.50 mmol, 10.0 equiv) were added to the vial containing vinyl benzoxazinone **2.19**. To the vial containing silyl triflate **2.20** was added the appropriate amount of MeCN to afford a 0.0125 M solution. The vial was capped and shaken to ensure full dissolution. The necessary amount of the solution of silyl triflate **2.20** (0.0125 M in MeCN, 4.0 mL, 0.05 mmol, 1.0 equiv) was then transferred via micropipette to the reaction vial containing vinyl benzoxazinone **2.19**. The reaction was sealed with a septum cap, removed from the glovebox, and placed under a flow of N_2. Then, deionized water (8.1 μL, 0.45 mmol, 9.0 equiv) was added to the reaction vessel via

microsyringe. The septum cap was then carefully replaced with a Teflon-lined cap under a stream of N_2 and stirred for 14 h at 30 °C. The mixture was then filtered through a pad of silica gel, eluting with EtOAc (8 mL). The eluate was concentrated and purified by preparative thin layer chromatography to provide annulation products **2.34**.

Any modification of the conditions shown in the general procedures above are specified in the following schemes. Although reactions were performed in a glovebox for consistency, reactions setup on the bench-top did not suffer from a significant loss in yield.

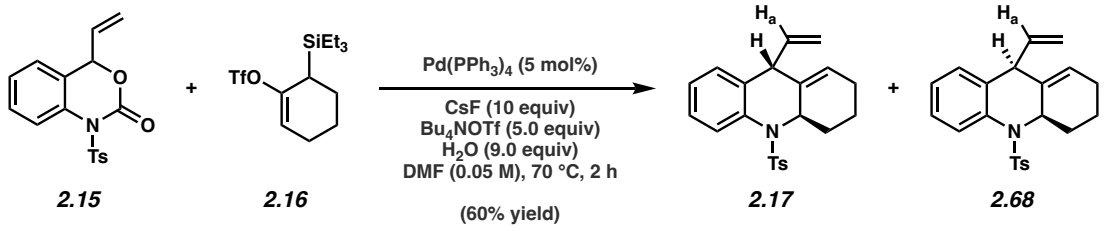

2.17 and **2.68**. Followed General Procedure 2.4. Purification by preparative thin layer chromatography (4:1:1 hexanes:CH_2Cl_2:Et_2O) afforded a mixture of major diastereomer **2.17** and minor diastereomer **2.68** (60% combined yield, 9.4:1 dr, average of two experiments) as a white solid. Diastereomeric ratio was determined by integrating the following peaks in the ^{1}H NMR spectrum of the isolated mixture (H_a **2.17**: 4.81 ppm; **2.68**: 5.88 ppm). **Annulation Products 2.17** and **2.68**: R_f 0.70 (4:1:1 hexanes:CH_2Cl_2:Et_2O); ^{1}H NMR (500 MHz, $CDCl_3$, **2.17**): 7.85 (dd, J = 8.2, 0.9, 1H), 7.43 (dt, J = 8.3, 1.7, 2H), 7.26–7.21 (overlapped with residual solvent peak, 1H), 7.16–7.12 (m, 2H), 7.10 (td, J = 7.4, 1.2, 1H), 6.96 (dd, J = 7.5, 1.5, 1H), 5.57–5.53 (m, 1H), 4.81 (ddd, J = 17.1, 10.0, 5.4, 1H), 4.70–4.58 (m, 2H), 4.42 (dt, J = 9.9, 1.8, 1H), 3.68–3.65 (m, 1H), 2.60 (dq, J = 11.7, 4.3, 1H), 2.35 (s, 3H), 2.08–1.90 (m, 2H), 1.85–1.79 (m, 1H), 1.77–1.65 (m, 1H), 1.62–1.52 (overlapped with residual H_2O peak, 1H); ^{13}C NMR (125 MHz, $CDCl_3$, **2.17**): δ

143.5, 137.5, 136.3, 136.2, 135.9, 134.9, 129.4, 127.8, 127.7, 127.5, 126.0, 125.7, 124.8, 115.2, 56.4, 51.8, 32.7, 24.5, 21.6, 21.2; IR (film): 2972, 2864, 1484, 1359, 1164 cm^{-1}; HRMS-APCI (*m/z*) $[M + H]^+$ calcd for $C_{22}H_{24}NO_2S^+$, 366.1522; found 366.1522.

The structure of **2.17** was verified by 2D-NOESY, as the following interaction was observed:

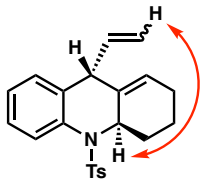

2.17

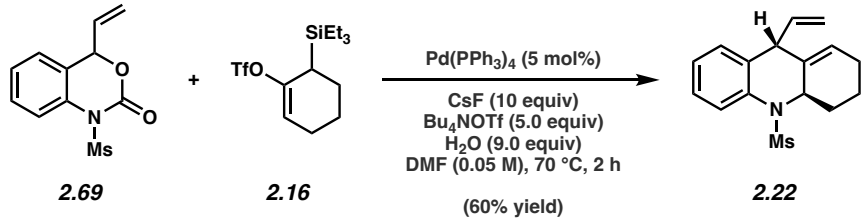

2.69 *2.16* *2.22*

2.22. Followed General Procedure 2.4. Purification by preparative thin layer chromatography (4:1:1 hexanes:CH_2Cl_2:Et_2O) afforded **2.22** (60% yield, >20:1 dr (determined by ^1H NMR analysis of the crude mixture), average of two experiments) as a white solid. **Annulation Product 2.22**: Mp: 107–108 °C; R_f 0.52 (4:1:1 hexanes:CH_2Cl_2:Et_2O); ^1H NMR (500 MHz, $CDCl_3$): δ 7.70 (d, *J* = 8.2, 1H), 7.26–7.22 (overlapped with residual solvent peak, 1H), 7.17–7.10 (m, 2H), 5.94 (ddd, *J* = 17.3, 10.3, 3.6, 1H), 5.69–5.64 (m, 1H), 5.20–5.15 (m, 1H), 5.08–5.02 (m, 1H), 4.75–4.69 (m, 1H), 3.93–3.89 (m, 1H), 2.80 (s, 3H), 2.44 (dq, *J* = 11.7, 3.9, 1H), 2.11–2.05 (m, 1H), 2.04–1.94 (m, 1H), 1.84–1.79 (m, 1H), 1.77–1.65 (m, 1H), 1.56–1.46 (overlapped with residual H_2O peak, 1H); ^{13}C NMR (125 MHz, $CDCl_3$): δ 139.0, 135.7, 135.2, 135.0, 128.1, 128.0, 125.7, 125.4, 124.6, 116.8, 56.5, 51.3, 39.5, 32.5, 24.5, 21.1; IR (film): 2931, 2862, 1485, 1341, 1155 cm^{-1}; HRMS-

APCI (*m/z*) $[M + H]^+$ calcd for $C_{16}H_{20}NO_2S^+$, 290.1209; found 290.1209. Relative stereochemistry was assigned by analogy to the ^1H NMR data of **2.17** and **2.68**.

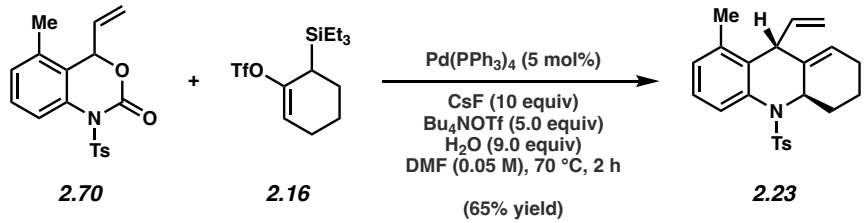

2.70 *2.16* *2.23*

2.23. Followed General Procedure 2.4. Purification by preparative thin layer chromatography (4:1:1 hexanes:CH_2Cl_2:Et_2O) afforded **2.23** (65% yield, >20:1 dr (determined by ^1H NMR analysis of the crude mixture), average of two experiments) as a white solid. **Annulation Product 2.23**: Mp: 109–111 °C; R_f 0.62 (4:1:1 hexanes:CH_2Cl_2:Et_2O); ^1H NMR (500 MHz, $CDCl_3$): δ 7.69 (d, *J* = 8.2, 1H), 7.43 (dt, *J* = 8.3, 1.9, 2H), 7.16–7.09 (m, 3H), 6.96 (d, *J* = 7.4, 1H), 5.57–5.53 (m, 1H), 4.83 (ddd, *J* = 17.1, 10.1, 5.5, 1H), 4.68–4.60 (m, 2H), 4.48 (dt, *J* = 10.0, 1.8, 1H), 3.89–3.84 (m, 1H), 2.58 (dq, *J* = 12.0, 4.3, 1H), 2.35 (s, 3H), 2.19 (s, 3H), 2.07–1.90 (m, 2H), 1.84–1.79 (m, 1H), 1.76–1.65 (m, 1H), 1.60–1.52 (overlapped with residual H_2O peak, 1H); ^{13}C NMR (125 MHz, $CDCl_3$): δ 143.4, 136.6, 136.5, 136.3, 134.92, 134.89, 134.1, 129.3, 127.9, 127.3, 126.7, 124.6, 123.9, 115.6, 56.2, 48.0, 32.6, 24.5, 21.6, 21.2, 19.0; IR (film): 2926, 1739, 1351, 1163, 665 cm^{-1}; HRMS-APCI (*m/z*) $[M + H]^+$ calcd for $C_{23}H_{26}NO_2S^+$, 380.1684; found 380.1685. Relative stereochemistry was assigned by analogy to the ^1H NMR data of **2.17** and **2.68**.

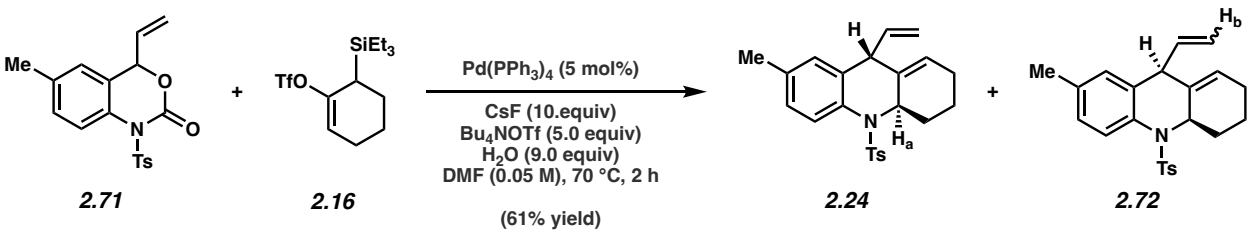

2.24 and **2.72**. Followed General Procedure 2.4. Purification by preparative thin layer chromatography (4:1:1 hexanes:CH_2Cl_2:Et_2O) afforded a mixture of major diastereomer **2.24** and minor diastereomer **2.72** (61% combined yield, 12:1 dr, average of two experiments) as a white solid. Diastereomeric ratio was determined by integrating the following peaks in the ^{1}H NMR spectrum of the crude reaction mixture (H_a **2.24**: 4.62–4.55 ppm; H_b **2.72**: 5.16 ppm). **Annulation Products 2.24** and **2.72**: R_f 0.69 (4:1:1 hexanes:CH_2Cl_2:Et_2O); ^{1}H NMR (600 MHz, $CDCl_3$, **2.24**): δ 7.72 (d, J = 8.2, 1H), 7.43 (dt, J = 8.3, 1.6, 2H), 7.17–7.13 (m, 2H), 7.04 (dd, J = 8.3, 1.8, 1H), 6.77 (d, J = 1.8, 1H), 5.54–5.52 (m, 1H), 4.76 (ddd, J = 17.0, 9.9, 5.5, 1H), 4.68 (dt, J = 17.1, 1.8, 1H), 4.62–4.55 (m, 1H), 4.40 (dt, J = 9.8, 1.8, 1H), 3.62–3.59 (m, 1H), 2.58 (dq, J = 11.9, 4.3, 1H), 2.36 (s, 3H), 2.29 (s, 3H), 2.04–1.90 (m, 2H), 1.83–1.78 (m, 1H), 1.75–1.65 (m, 1H), 1.60–1.52 (overlapped with residual H_2O peak, 1H); ^{13}C NMR (150 MHz, $CDCl_3$, **2.24**): δ 143.4, 137.6, 136.42, 136.36, 135.7, 135.6, 132.2, 129.4, 128.20, 128.19, 127.8, 126.0, 124.6, 115.0, 56.3, 52.0, 32.6, 24.5, 21.6, 21.2, 21.0; IR (film): 2925, 1494, 1351, 1166, 567 cm^{-1}; HRMS-APCI (*m/z*) [M + H]$^+$ calcd for $C_{23}H_{26}NO_2S^+$, 380.1684; found 380.1685. Relative stereochemistry was assigned by analogy to the ^{1}H NMR data of **2.17** and **2.68**.

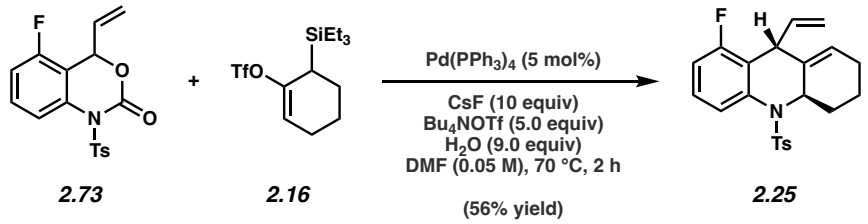

2.25. Followed General Procedure 2.4. Purification by preparative thin layer chromatography (4:1:1 hexanes:CH_2Cl_2:Et_2O) afforded **2.25** (56% yield, >20:1 dr (determined by ^{1}H NMR analysis of the crude mixture), average of two experiments) as a white solid. **Annulation Product 2.25**: Mp: 150–154 °C; R_f 0.67 (4:1:1 hexanes:CH_2Cl_2:Et_2O); ^{1}H NMR (500 MHz, $CDCl_3$): δ 7.67 (d, *J* = 8.4, 1H), 7.47–7.39 (m, 2H), 7.21–7.13 (m, 3H), 6.85 (td, *J* = 8.5, 0.7, 1H), 5.64–5.60 (m, 1H), 4.79 (ddd, *J* = 17.1, 9.8, 5.1, 1H), 4.68 (dt, *J* = 17.1, 1.5 1H), 4.65–4.58 (m, 1H), 4.46 (dt, *J* = 9.9, 1.8, 1H), 4.10–4.06 (m, 1H), 2.62 (dq, *J* = 11.8, 4.3, 1H), 2.36 (s, 3H), 2.08–1.92 (m, 2H), 1.86–1.80 (m, 1H), 1.77–1.65 (m, 1H), 1.62–1.52 (overlapped with residual H_2O peak, 1H); ^{13}C NMR (125 MHz, $CDCl_3$): δ 158.8 (d, *J* = 244.1), 143.8, 136.5 (d, *J* = 6.4), 136.1, 136.0, 135.0, 129.5, 127.8, 127.6 (d, *J* = 9.3), 125.8, 123.2 (d, *J* = 19.9), 121.6 (d, *J* = 3.2), 115.8, 112.1 (d, *J* = 22.0), 56.3, 43.4 (d, *J* = 3.7), 32.8, 24.5, 21.6, 21.1; ^{19}F NMR (282 MHz, $CDCl_3$): δ –121.39 (m, 1F); IR (film): 2928, 2864, 1584, 1465, 1352 cm^{-1}; HRMS-APCI (*m/z*) $[M + H]^+$ calcd for $C_{22}H_{23}FNO_2S^+$, 384.1428; found 384.1428. Relative stereochemistry was assigned by analogy to the ^{1}H NMR data of **2.17** and **2.68**.

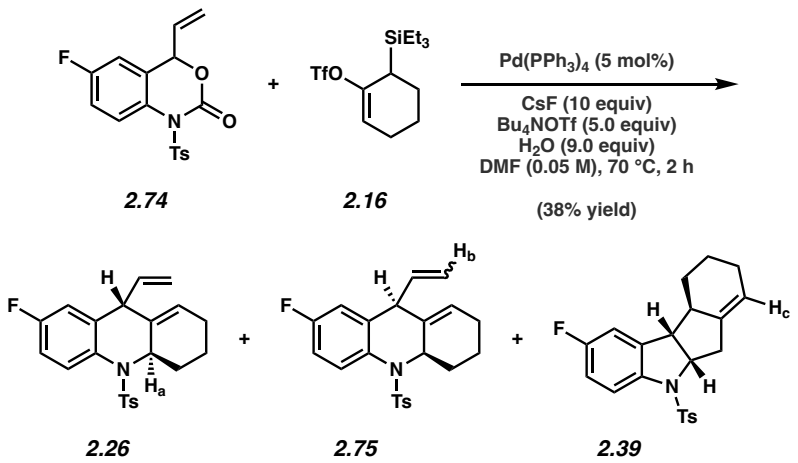

2.26, **2.75**, and **2.39**. Followed General Procedure 2.4. Purification by preparative thin layer chromatography (4:1:1 hexanes:CH_2Cl_2:Et_2O) afforded a mixture of major diastereomer **2.26**, minor diastereomer **2.75**, and constitutional isomer **2.39** (38% combined yield, 8.4:1 dr, 14:2.3:1.0 **2.26**:**2.75**:**2.39**, average of two experiments) as a waxy white solid. Diastereomeric ratio was determined by integrating the following peaks in the ^{1}H-NMR spectrum of the crude reaction mixture (H_a **2.26**: 4.59–4.54 ppm; H_b **2.75**: 5.25 ppm). Ratio of constitutional isomers was determined by integrating the following peaks in the ^{1}H-NMR spectrum of the isolated mixture (H_a **2.26**: 4.59–4.54 ppm; H_b **2.75**: 5.25 ppm; H_c **2.39**: 5.51–5.49 ppm). **Annulation Products 2.26**, **2.75**, and **2.39**: R_f 0.63 (4:1:1 hexanes:CH_2Cl_2:Et_2O); ^{1}H NMR (500 MHz, $CDCl_3$, **2.26**): δ 7.82 (dd, J = 9.0, 5.1, 1H), 7.43–7.39 (m, 2H), 7.18–7.14 (m, 2H), 6.93 (td, J = 8.5, 3.0, 1H), 6.68 (dd, J = 8.3, 3.0, 1H), 5.57–5.54 (m, 1H), 4.77–4.64 (m, 2H), 4.59–4.54 (m, 1H), 4.41 (dt, J = 9.3, 2.1, 1H), 3.63–3.60 (m, 1H), 2.59 (dq, J = 11.7, 4.1, 1H), 2.37 (s, 3H), 2.07–1.91 (m, 2H), 1.85–1.80 (m, 1H), 1.76–1.64 (m, 1H), 1.60–1.50 (overlapped with residual H_2O peak, 1H); ^{13}C NMR (125 MHz, $CDCl_3$, **2.26**): δ 160.4 (d, J = 246.6), 143.7, 138.1 (d, J = 7.4), 136.7, 136.1, 135.7, 129.5, 127.9, 127.8, 127.1, 125.4, 115.6, 114.3 (d, J = 16.7), 114.1 (d, J = 16.2), 56.2, 51.8, 32.6, 24.5, 21.6, 21.2; ^{19}F NMR (282 MHz, $CDCl_3$): δ –116.79 (m, 1F); IR (film): 2929, 1741, 1488,

1351, 1164 cm^{-1}; HRMS-APCI (*m/z*) $[M + H]^+$ calcd for $C_{22}H_{23}FNO_2S^+$, 384.1428; found 384.1430. Relative stereochemistry was assigned by analogy to the ^1H NMR data of **2.17** and **2.68**.

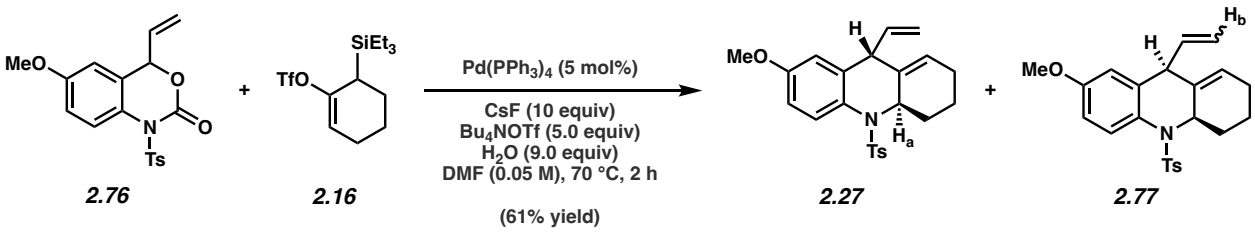

2.27 and **2.77**. Followed General Procedure 2.4. Purification by preparative thin layer chromatography (4:1:1 hexanes:CH_2Cl_2:Et_2O) afforded a mixture of major diastereomer **2.27** and minor diastereomer **2.77** (61% combined yield, 8.9:1 dr, average of two experiments) as a colorless clear oil. Diastereomeric ratio was determined by integrating the following peaks in the ^1H NMR spectrum of the crude reaction mixture (H_a **2.27**: 4.59–4.51 ppm; H_b **2.77**: 5.23 ppm). **Annulation Products 2.27** and **2.77**: R_f 0.54 (4:1:1 hexanes:CH_2Cl_2:Et_2O); ^1H NMR (500 MHz, $CDCl_3$, **2.27**): δ 7.76 (d, *J* = 9.0, 1H), 7.40 (dt, *J* = 8.3, 2.0, 2H), 7.17–7.13 (m, 2H), 6.78 (dd, *J* = 9.0, 3.0, 1H), 6.51 (d, *J* = 3.0, 1H), 5.55–5.51 (m, 1H), 4.72–4.67 (m, 2H), 4.59–4.51 (m, 1H), 4.39–4.35 (m, 1H), 3.78 (s, 3H), 3.61–3.58 (m, 1H), 2.57 (dq, *J* = 11.8, 4.3, 1H), 2.36 (s, 3H), 2.06–1.90 (m, 2H), 1.84–1.78 (m, 1H), 1.75–1.64 (m, 1H), 1.61–1.50 (overlapped with residual H_2O peak, 1H); ^{13}C NMR (125 MHz, $CDCl_3$, **2.27**): δ 157.5, 143.4, 137.5, 137.2, 136.24, 136.18, 129.4, 127.8, 127.7, 127.5, 124.9, 115.2, 112.9, 112.5, 56.2, 55.5, 52.1, 32.6, 24.5, 21.6, 21.2; IR (film): 2935, 1600, 1494, 1163, 567 cm^{-1}; HRMS-APCI (*m/z*) $[M + H]^+$ calcd for $C_{23}H_{26}NO_3S^+$, 396.1633; found 396.1631. Relative stereochemistry was assigned by analogy to the ^1H NMR data of **2.17** and **2.68**.

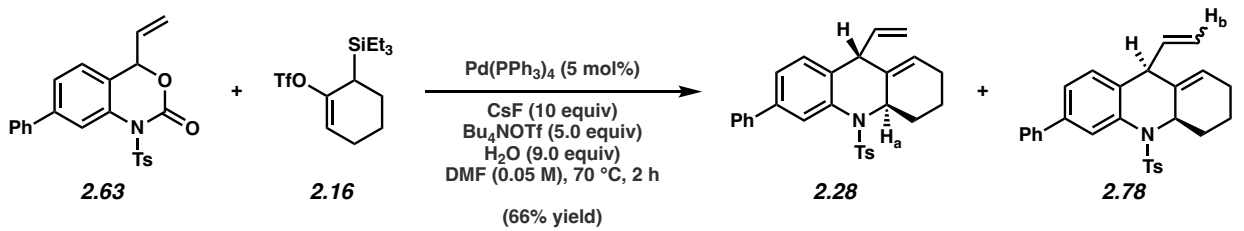

2.28 and **2.78**. Followed General Procedure 2.4. Purification by preparative thin layer chromatography (4:1:1 hexanes:CH_2Cl_2:Et_2O) afforded a mixture of major diastereomer **2.28** and minor diastereomer **2.78** (66% combined yield, 10:1 dr, average of two experiments) as a colorless clear oil. Diastereomeric ratio was determined by integrating the following peaks in the ^{1}H NMR spectrum of the crude reaction mixture (H_a **2.28**: 4.67–4.63 ppm; H_b **2.78**: 5.27 ppm). **Annulation Products 2.28** and **2.78**: R_f 0.76 (4:1:1 hexanes:CH_2Cl_2:Et_2O); ^{1}H NMR (500 MHz, $CDCl_3$, **2.28**): δ 8.12 (d, *J* = 1.8, 1H), 7.66–7.62 (m, 2H), 7.49–7.42 (m, 4H), 7.37–7.33 (m, 2H), 7.17–7.13 (m, 2H), 7.03 (d, *J* = 7.8, 1H), 5.60–5.56 (m, 1H), 4.85 (ddd, *J* = 17.1, 10.0, 5.4, 1H), 4.70 (dt, *J* = 17.1, 1.6, 1H), 4.67–4.63 (m, 1H), 4.45 (dt, *J* = 10.0, 1.8, 1H), 3.73–3.70 (m, 1H), 2.63 (dq, *J* = 11.8, 4.3, 1H), 2.35 (s, 3H), 2.05–1.95 (m, 2H), 1.86–1.81 (m, 1H), 1.78–1.67 (m, 1H), 1.66–1.59 (overlapped with residual H_2O peak, 1H); ^{13}C NMR (125 MHz, $CDCl_3$, **2.28**): δ 143.6, 140.54, 140.52, 137.5, 136.3, 136.1, 135.3, 134.8, 129.4, 128.9, 128.0, 127.9, 127.6, 127.2, 125.0, 124.7, 124.3, 115.3, 56.4, 51.6, 32.7, 24.6, 21.6, 21.2; IR (film): 2927, 1599, 1482, 1165, 665 cm^{-1}; HRMS-APCI (*m/z*) $[M + H]^+$ calcd for $C_{28}H_{28}NO_2S^+$, 442.1841; found 442.1841. Relative stereochemistry was assigned by analogy to the ^{1}H NMR data of **2.17** and **2.68**.

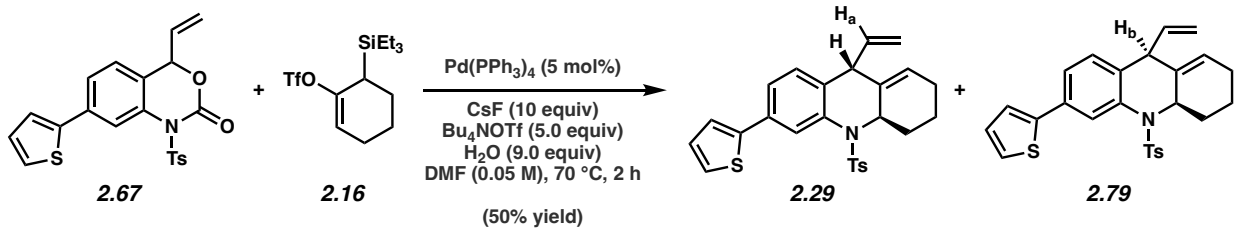

2.29 and **2.79**. Followed General Procedure 2.4. Purification by preparative thin layer chromatography (4:1:1 hexanes:CH_2Cl_2:Et_2O) afforded a mixture of major diastereomer **2.29** and minor diastereomer **2.79** (50% combined yield, 5.2:1 dr, average of two experiments) as an off-white solid. Diastereomeric ratio was determined by integrating the following peaks in the ^{1}H NMR spectrum of the crude reaction mixture (H_a **2.29**: 4.88 ppm; H_b **2.79**: 4.59–4.55 ppm). **Annulation Products 2.29** and **2.79**: R_f 0.57 (4:1:1 hexanes:CH_2Cl_2:Et_2O); ^{1}H NMR (500 MHz, $CDCl_3$, **2.29**): δ 8.12 (d, *J* = 1.8, 1H), 7.50 (dt, *J* = 8.3, 1.9, 2H), 7.36–7.31 (m, 2H), 7.28 (dd, *J* = 5.1, 1.1, 1H), 7.17–7.14 (m, 2H), 7.11–7.07 (m, 1H), 6.96 (d, *J* = 7.8, 1H), 5.59–5.56 (m, 1H), 4.88 (ddd, *J* = 17.0, 10.1, 5.3, 1H), 4.71–4.64 (m, 2H), 4.47 (dt, *J* = 10.0, 1.9, 1H), 3.70–3.67 (m, 1H), 2.64 (dq, *J* = 11.6, 4.2, 1H), 2.35 (s, 3H), 2.05–1.95 (m, 2H), 1.86–1.81 (m, 1H), 1.78–1.67 (m, 1H), 1.65–1.56 (overlapped with residual H_2O peak, 1H); ^{13}C NMR (125 MHz, $CDCl_3$, **2.29**, 23 of 24 signals observed): δ 144.0, 143.7, 137.4, 136.2, 136.0, 135.5, 134.8, 133.8, 129.4, 128.2, 128.1, 128.0, 125.01, 125.00, 123.5, 123.1, 115.4, 56.4, 51.5, 32.7, 24.5, 21.6, 21.2; IR (film): 2973, 2363, 1742, 1165, 667 cm^{-1}; HRMS-APCI (*m/z*) $[M + H]^+$ calcd for $C_{26}H_{26}NO_2S_2^+$, 448.1405; found 448.1408. Relative stereochemistry was assigned by analogy to the ^{1}H NMR data of **2.17** and **2.68**.

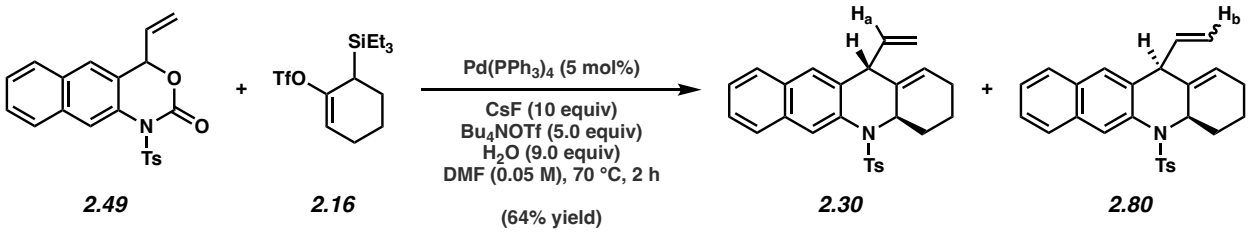

2.30 and **2.80**. Followed General Procedure 2.4. Purification by preparative thin layer chromatography (4:1:1 hexanes:CH_2Cl_2:Et_2O) afforded a mixture of major diastereomer **2.30** and minor diastereomer **2.80** (64% combined yield, 8.8:1 dr, average of two experiments) as a white solid. Diastereomeric ratio was determined by integrating the following peaks in the ^{1}H NMR spectrum of the crude reaction mixture (H_a **2.30**: 5.03 ppm; H_b **2.80**: 5.30 ppm). **Annulation Products 2.30** and **2.80**: R_f 0.61 (4:1:1 hexanes:CH_2Cl_2:Et_2O); ^{1}H NMR (500 MHz, $CDCl_3$, **2.30**): δ 8.32 (s, 1H), 7.86–7.82 (m, 1H), 7.72–7.68 (m, 1H), 7.48 (dt, *J* = 8.3, 2.0, 2H), 7.47–7.38 (m, 3H), 7.11–7.07 (m, 2H), 5.64–5.60 (m, 1H), 5.03 (ddd, *J* = 17.1 10.1, 5.0, 1H), 4.82–4.75 (m, 1H), 4.71 (ddd, *J* = 17.2, 1.9, 1.7, 1H), 4.52 (ddd, *J* = 10.1, 2.1, 1.6, 1H), 3.90–3.87 (m, 1H), 2.64 (dq, *J* = 11.8, 4.3, 1H), 2.31 (s, 3H), 2.09–2.02 (m, 1H), 2.01–1.90 (m, 1H), 1.87–1.81 (m, 1H), 1.81–1.69 (m, 1H), 1.65–1.55 (m, 1H); ^{13}C NMR (125 MHz, $CDCl_3$, **2.30**): δ 143.6, 137.6, 136.5, 136.0, 135.0, 133.1, 132.9, 131.4, 129.3, 128.2, 127.9, 127.1, 126.0, 125.8, 125.5, 123.4, 115.7, 56.6, 52.0, 32.5, 24.7, 21.6, 21.2; IR (film): 2927, 2862, 1460, 1353, 1165 cm^{-1}; HRMS-APCI (*m/z*) [M + H]$^+$ calcd for $C_{26}H_{26}NO_2S^+$, 416.1679; found 416.1676. Relative stereochemistry was assigned by analogy to the ^{1}H NMR data of **2.17** and **2.68**.

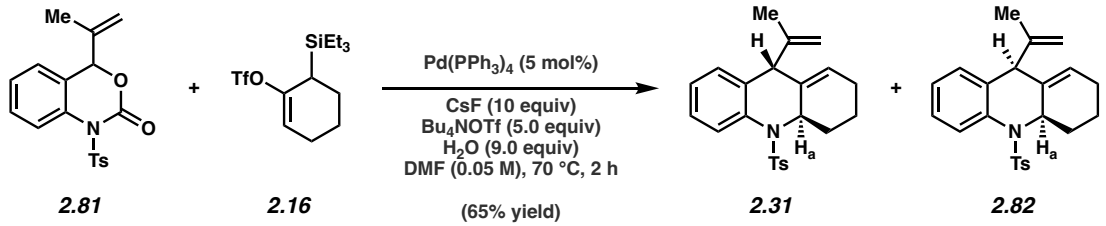

2.81 *2.16* *2.31* *2.82*

2.31 and **2.82**. Followed General Procedure 2.4. Purification by preparative thin layer chromatography (4:1:1 hexanes:CH_2Cl_2:Et_2O) afforded a mixture of major diastereomer **2.31** and minor diastereomer **2.82** (65% combined yield, 8.9:1 dr, average of two experiments) as a white solid. Diastereomeric ratio was determined by integrating the following peaks in the ^{1}H NMR spectrum of the isolated mixture (H_a **2.31**: 4.78–4.71 ppm; **2.82**: 4.56–4.51 ppm). **Annulation Products 2.31** and **2.82**: R_f 0.63 (4:1:1 hexanes:CH_2Cl_2:Et_2O); ^{1}H NMR (500 MHz, $CDCl_3$, **2.31**): δ 7.86–7.83 (m, 1H), 7.50 (dt, *J* = 8.3, 2.0, 2H), 7.24–7.19 (m, 1H), 7.12–7.08 (m, 2H), 7.05 (td, *J* = 7.5, 1.2, 1H), 6.95 (dd, *J* = 7.5, 1.6, 1H), 5.60–5.57 (m, 1H), 4.78–4.71 (m, 1H), 4.35–4.30 (m, 1H), 4.15–4.13 (m, 1H), 3.60 (s, 1H), 2.59 (dq, *J* = 11.8, 4.3, 1H), 2.34 (s, 3H), 2.11–2.04 (m, 1H), 2.04–1.93 (m, 1H), 1.86–1.81 (m, 1H), 1.80–1.68 (m, 1H), 1.59–1.54 (m, 1H), 1.26–1.24 (m, 3H); ^{13}C NMR (125 MHz, $CDCl_3$, **2.31**): δ 143.3, 143.0, 136.9, 135.8, 135.01, 134.95, 129.5, 129.1, 129.0, 128.1, 127.4, 127.0, 126.0, 125.05, 125.01, 112.5, 56.7, 54.5, 32.6, 24.6, 21.7, 21.6, 21.3; IR (film): 2928, 2863, 1484, 1344, 1160 cm^{-1}; HRMS-APCI (*m/z*) [M + H]$^+$ calcd for $C_{23}H_{26}NO_2S^+$, 380.1679; found 380.1678.

The structure of **2.31** was verified by 2D-NOESY, as the following interaction was observed:

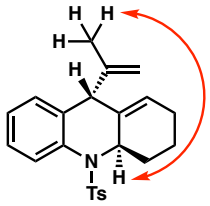

2.31

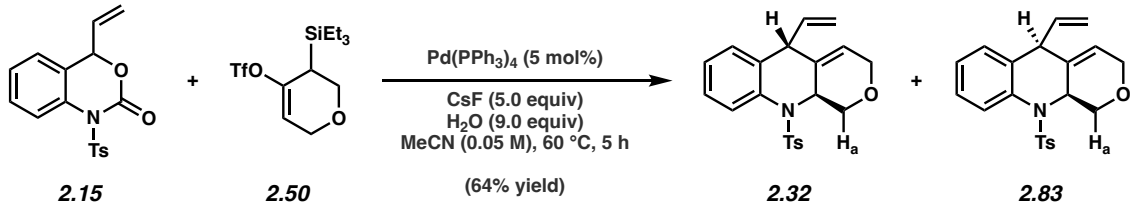

2.32 and **2.83**. Followed General Procedure 2.5. Purification by preparative thin layer chromatography (4:1:1 hexanes:CH_2Cl_2:Et_2O) afforded a mixture of major diastereomer **2.32** and minor diastereomer **2.83** (64% combined yield, 1.8:1 dr, average of two experiments) as a white solid. Diastereomeric ratio was determined by integrating the following peaks in the ^{1}H NMR spectrum of the crude reaction mixture (H_a **2.32**: 3.36 ppm; **2.83**: 3.30 ppm). **Annulation Products 2.32** and **2.83**: R_f 0.37 (4:1:1 hexanes:CH_2Cl_2:Et_2O); ^{1}H NMR (500 MHz, $CDCl_3$, **2.32**): δ 7.91–7.88 (m, 1H), 7.40 (dt, *J* = 8.3, 2.0, 2H), 7.31–7.27 (m, 1H), 7.17–7.11 (m, 3H), 6.98 (dd, *J* = 7.5, 1.6, 1H), 5.58 (q, *J* = 2.7, 1H), 4.71 (ddd, *J* = 17.1, 9.9, 5.0, 1H), 4.67–4.55 (m, 3H), 4.35 (dt, 9.8, 2.0, 1H), 4.20–4.10 (m, 1H), 4.05 (ddd, *J* = 16.7, 3.9, 2.0, 1H), 3.76–3.73 (m, 1H), 3.36 (dd, *J* = 10.0, 9.3, 1H), 2.36 (s, 3H); ^{1}H NMR (500 MHz, $CDCl_3$, **2.83**): δ 7.66 (dd, *J* = 8.0, 1.2, 1H), 7.34–7.30 (m, 3H), 7.22–7.17 (m, 3H), 6.94 (dt, *J* = 7.7, 1.3, 1H), 5.85 (dt, *J* = 16.8, 10.0, 1H), 5.32–5.27 (m, 2H), 4.76 (ddd, *J* = 17.0, 1.8, 0.3, 1H), 4.67–4.55 (m, 1H), 4.39 (dd, *J* = 10.4, 5.6, 1H), 4.20–4.10 (m, 1H), 3.98 (ddt, *J* = 18.6, 4.1, 2.3, 1H), 3.30 (t, J = 10.0, 1H), 2.40 (s, 3H), 2.28 (d, *J* = 9.3, 1H); ^{13}C NMR (125 MHz, $CDCl_3$, **2.32** and **2.83**): δ 144.0, 143.9, 137.4, 136.7, 136.6, 135.3, 135.2, 134.8, 134.6, 134.4, 134.2, 133.3, 129.7, 129.6, 128.6, 128.0, 127.9, 127.8, 127.6, 127.2, 126.9, 126.4, 126.1, 124.3, 122.3, 120.2, 118.5, 115.6, 69.1, 68.6, 64.9, 64.9, 54.0, 52.2, 50.5, 45.3, 21.63, 21.61; IR (film): 2925, 2852, 1349, 1165, 1088 cm^{-1}; HRMS-APCI (*m/z*) [M + H]$^+$ calcd for $C_{21}H_{22}NO_3S^+$, 368.1315; found 368.1332. Relative stereochemistry was assigned by analogy to the ^{1}H NMR data of **2.33** and **2.85**.

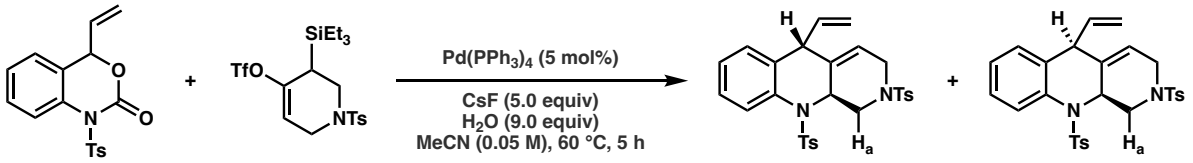

2.15 *2.84* *2.33* *2.85*

2.33 and **2.85**. Followed General Procedure 2.5. Purification by preparative thin layer chromatography (4:1:1 hexanes:CH_2Cl_2:Et_2O) afforded a mixture of major diastereomer **2.33** and minor diastereomer **2.85** (69% combined yield, 1.3:1 dr, average of two experiments) as a waxy white-yellow solid. Diastereomeric ratio was determined by integrating the following peaks in the ^{1}H NMR spectrum of the crude reaction mixture (H_a **2.33**: 3.14 ppm; **2.85**: 3.05 ppm). To obtain an analytical sample, the mixture of diastereomers was then purified by preparative thin layer chromatography (2:1 Et_2O:hexanes) to afford **2.85** as a waxy pale yellow solid. **Annulation Products 2.33** and **2.85**: R_f 0.33 (4:1:1 hexanes:CH_2Cl_2:Et_2O); ^{1}H NMR (500 MHz, $CDCl_3$, **2.33**): δ 7.85 (dd, *J* = 8.2, 1.0, 1H), 7.74 (dt, *J* = 8.3, 1.9, 2H), 7.37 (dt, *J* = 8.3, 1.9, 2H), 7.35–7.27 (m, 2H), 7.26–7.21 (overlapped with residual solvent peak, 1H), 7.21–7.13 (m, 2H), 7.10 (td, *J* = 7.5, 1.2, 1H), 6.92 (dd, *J* = 7.5, 1.6, 1H), 5.50 (dt, *J* = 4.0, 2.3, 1H), 4.68–4.58 (m, 3H), 4.53–4.47 (m, 1H), 4.29 (ddd, *J* = 9.9, 2.1, 1.4, 1H), 4.14–4.07 (m, 1H), 3.71–3.66 (m, 1H), 3.14 (ddd, *J* = 17.2, 3.5, 2.3, 1H), 2.43–2.35 (m, 7H); ^{1}H NMR (500 MHz, $CDCl_3$, **2.85**): δ 7.70 (dt, *J* = 8.3, 1.9, 2H), 7.62 (dd, *J* = 8.0, 1.2, 1H), 7.35–7.27 (m, 5H), 7.21–7.13 (m, 3H), 6.88 (dt, *J* = 7.6, 1.2, 1H), 5.76 (dt, *J* = 16.9, 9.9, 1H), 5.27 (dd, *J* = 10.1, 1.8, 1H), 5.20 (sext, *J* = 2.3, 1H), 4.71 (dd, *J* = 17.0, 1.3, 1H), 4.68–4.58 (m, 1H), 4.43–4.39 (m, 1H), 4.03 (dq, *J* = 16.9, 3.1, 1H), 3.05 (ddt, *J* = 17.1, 3.5, 2.5, 1H), 2.43–2.35 (m, 6H), 2.31 (dd, *J* = 11.1, 10.1, 1H), 2.21 (d, *J* = 9.2, 1H); ^{13}C NMR (125 MHz, $CDCl_3$, **2.33** and **2.85**): δ 144.0, 143.9, 143.72, 143.70, 137.3, 137.1, 136.1, 135.2, 135.1, 135.0, 134.6, 134.2, 133.84, 133.77, 133.4, 132.7, 129.8, 129.6, 129.4, 128.5, 127.81, 127.75, 127.70, 127.66, 127.5, 127.1, 127.0, 126.3, 126.1, 124.1, 120.4, 119.5, 115.7, 115.5, 54.9, 52.9,

50.2, 48.7, 48.3, 45.1, 44.1, 44.0, 21.53, 21.50; IR (film): 3065, 2923, 1483, 1348, 1162 cm^{-1}; HRMS-APCI (*m/z*) $[M + H]^+$ calcd for $C_{28}H_{29}N_2O_4S_2^+$, 521.1563; found 521.1567.

The structure of **2.85** was verified by 2D-NOESY, as the following interaction was observed:

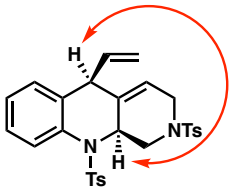

2.85

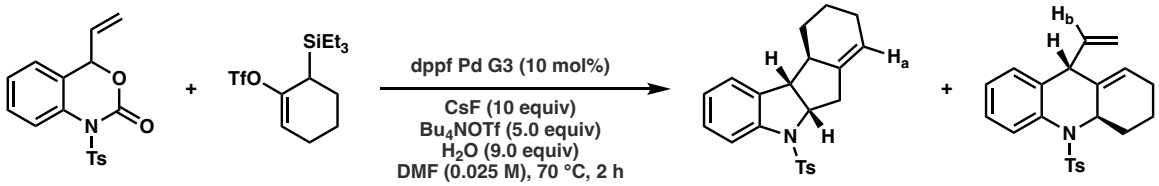

2.15 ***2.16*** ***2.18*** ***2.17***

2.18. Followed General Procedure 2.6. Purification by preparative thin layer chromatography (4:1:1 hexanes:CH_2Cl_2:Et_2O) afforded a mixture of **2.18** and constitutional isomer **2.17** (70% combined yield, >20:1 dr (determined by ^1H NMR analysis of the crude mixture), 12:1 **2.18**:**2.17**, average of two experiments) as a white solid. Ratio of constitutional isomers was determined by integrating the following peaks in the ^1H NMR spectrum of the isolated mixture (H_a **2.18**: 5.51–5.49 ppm; H_b **2.17**: 4.81 ppm). **Annulation Products 2.18** and **2.17**: R_f 0.57 (4:1:1 hexanes:CH_2Cl_2:Et_2O); ^1H NMR (500 MHz, $CDCl_3$, **2.18**): 7.67–7.63 (m, 3H), 7.23–7.17 (m, 3H), 7.09 (d, J = 7.3, 1H), 7.00 (t, J = 7.4, 1H), 5.51–5.49 (br m, 1H), 4.42 (dt, J = 10.2, 7.6, 1H), 3.09–3.03 (m, 1H), 2.98 (dd, J = 15.6, 7.9, 1H), 2.75–2.69 (m, 1H), 2.35 (s, 3H), 2.24–2.17 (m, 2H), 2.01–1.99 (m, 2H), 1.82–1.78 (m, 1H), 1.50–1.39 (m, 1H), 1.23–1.14 (m, 1H); ^{13}C NMR (125 MHz, $CDCl_3$, **2.18**): δ 143.9, 141.2, 140.3, 135.4, 134.7, 129.6, 128.0, 127.3, 124.2, 124.0, 118.9, 115.4, 65.7, 52.1, 46.0, 41.3, 29.2, 24.7, 22.3, 21.5; IR (film): 2924, 2854, 1478, 1355, 1167 cm^{-}

[1]; HRMS-APCI (*m/z*) $[M + H]^+$ calcd for $C_{22}H_{24}NO_2S^+$, 366.1522; found 366.1523. Relative stereochemistry was assigned by analogy to the ^1H NMR data of **2.43**.

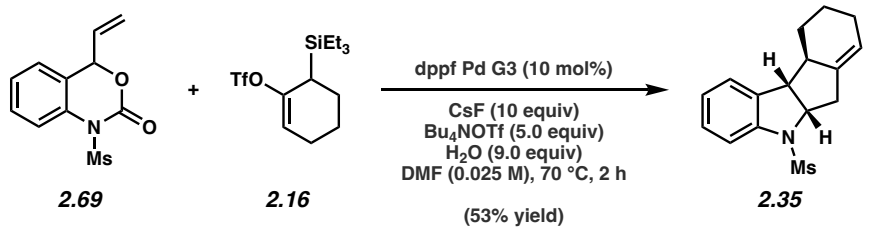

2.35. Followed General Procedure 2.6. Purification by preparative thin layer chromatography (4:1:1 hexanes:CH_2Cl_2:Et_2O) afforded **2.35** (53% yield, >20:1 dr (determined by ^1H NMR analysis of the crude mixture), average of two experiments) as a white solid. **Annulation Product 2.35**: Mp: 126–128 °C; R_f 0.42 (4:1:1 hexanes:CH_2Cl_2:Et_2O); ^1H NMR (500 MHz, $CDCl_3$): δ 7.41 (d, *J* = 8.2, 1H), 7.25–7.20 (m, 2H), 7.05 (t, *J* = 7.4, 1H), 5.52–5.50 (br m, 1H), 4.55 (dt, *J* = 10.1, 7.3, 1H), 3.34 (t, *J* = 9.3, 1H), 2.94 (dd, *J* = 15.9, 8.0, 1H), 2.86 (s, 3H), 2.73–2.68 (m, 1H), 2.30–2.27 (m, 2H), 2.05–2.01 (m, 2H), 1.87–1.82 (m, 1H), 1.53–1.42 (m ,1H), 1.34–1.24 (m, 1H); ^{13}C NMR (125 MHz, $CDCl_3$): δ 141.3, 140.3, 135.0, 128.5, 124.7, 124.1, 119.3, 114.2, 66.7, 52.7, 46.2, 41.3, 35.5, 29.2, 24.9, 22.4; IR (film): 2926, 2854, 1479, 1348, 1159 cm^{-1}; HRMS-APCI (*m/z*) $[M + H]^+$ calcd for $C_{16}H_{20}NO_2S^+$, 290.1209; found 290.1211. Relative stereochemistry was assigned by analogy to the ^1H NMR data of **2.43**.

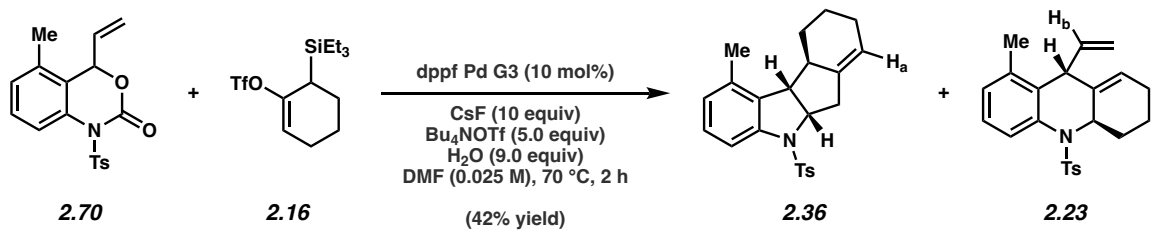

2.36. Followed General Procedure 2.6. Purification by preparative thin layer chromatography (4:1:1 hexanes:CH_2Cl_2:Et_2O) afforded a mixture of **2.36** and constitutional isomer **2.23** (42% combined yield, >20:1 dr (determined by ^{1}H NMR analysis of the crude mixture), 7.6:1 **2.36**:**2.23**, average of two experiments) as a white solid. Ratio of constitutional isomers was determined by integrating the following peaks in the ^{1}H NMR spectrum of the isolated mixture (H_a **2.36**: 5.52–5.50 ppm; H_b **2.23**: 4.83 ppm). **Annulation Products 2.36** and **2.23**: R_f 0.61 (4:1:1 hexanes:CH_2Cl_2:Et_2O); ^{1}H NMR (500 MHz, $CDCl_3$, **2.36**): δ 7.62 (d, J = 8.2, 2H), 7.49 (d, J = 8.0, 1H), 7.18 (d, J = 8.0, 2H), 7.10 (t, J = 7.9, 1H), 6.80 (d, J = 7.6, 1H), 5.52–5.50 (br m, 1H), 4.41 (dt, J = 9.8, 7.5, 1H), 3.12–3.07 (m, 1H), 2.96 (dd, J = 15.6, 7.7, 1H), 2.79–2.73 (m, 1H), 2.35 (s, 3H), 2.31–2.26 (m, 2H), 2.23 (s, 3H), 2.02–1.99 (m, 2H), 1.83–1.78 (m, 1H), 1.51–1.40 (m, 1H), 1.26–1.17 (m, 1H); ^{13}C NMR (125 MHz, $CDCl_3$, **2.36**): δ 143.9, 141.4, 140.6, 134.9, 134.8, 133.8, 129.7, 128.0, 127.5, 125.6, 119.2, 113.0, 66.1, 51.9, 45.1, 41.2, 30.1, 24.9, 22.7, 21.7, 20.2; IR (film): 2923, 1739, 1355, 1166, 663 cm^{-1}; HRMS-APCI (*m/z*) $[M + H]^+$ calcd for $C_{23}H_{26}NO_2S^+$, 380.1684; found 380.1683. Relative stereochemistry was assigned by analogy to the ^{1}H NMR data of **2.43**.

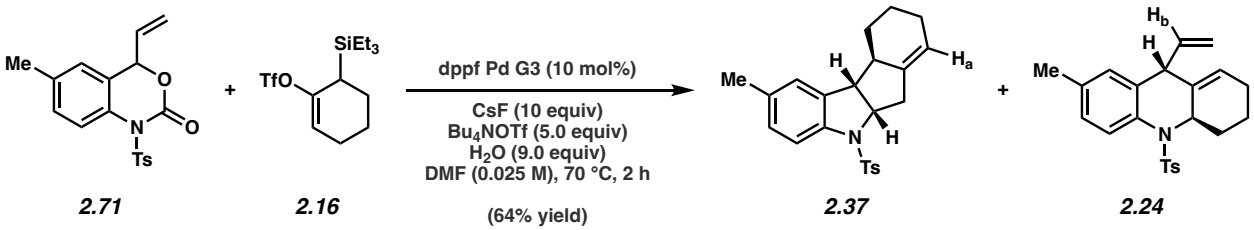

2.37. Followed General Procedure 2.6. Purification by preparative thin layer chromatography (4:1:1 hexanes:CH_2Cl_2:Et_2O) afforded a mixture of **2.37** and constitutional isomer **2.24** (64% combined yield, >20:1 dr (determined by ^{1}H NMR analysis of the crude mixture), 6.3:1 **2.37**:**2.24**, average of two experiments) as a colorless clear oil. Ratio of constitutional isomers was determined by integrating the following peaks in the ^{1}H NMR spectrum of the isolated mixture (H_a **2.37**: 5.50–5.48 ppm; H_b **2.24**: 4.76 ppm). **Annulation Products 2.37** and **2.24**: R_f 0.74 (4:1:1 hexanes:CH_2Cl_2:Et_2O); ^{1}H NMR (500 MHz, $CDCl_3$, **2.37**): δ 7.63 (dt, J = 8.3, 1.9, 2H), 7.53 (d, J = 8.3, 1H), 7.20–7.16 (m, 2H), 7.03–6.99 (m, 1H), 6.91–6.88 (m, 1H), 5.50–5.48 (br m, 1H), 4.39 (dt, J = 10.0, 7.7, 1H), 3.02–2.93 (m, 2H), 2.73–2.66 (m, 1H), 2.35 (s, 3H), 2.28 (s, 3H), 2.24–2.17 (m, 2H), 2.02–1.98 (m, 2H), 1.83–1.77 (m, 1H), 1.51–1.40 (m, 1H), 1.23–1.13 (m, 1H); ^{13}C NMR (125 MHz, $CDCl_3$, **2.37**): δ 143.9, 140.5, 139.0, 135.8, 134.7, 133.9, 129.7, 128.7, 127.4, 124.9, 119.0, 115.4, 65.9, 52.2, 46.1, 41.3, 29.4, 24.9, 22.4, 21.7, 21.1; IR (film): 2922, 1739, 1485, 1354, 1165 cm^{-1}; HRMS-APCI (*m/z*) $[M + H]^+$ calcd for $C_{23}H_{26}NO_2S^+$, 380.1684; found 380.1684. Relative stereochemistry was assigned by analogy to the ^{1}H NMR data of **2.43**.

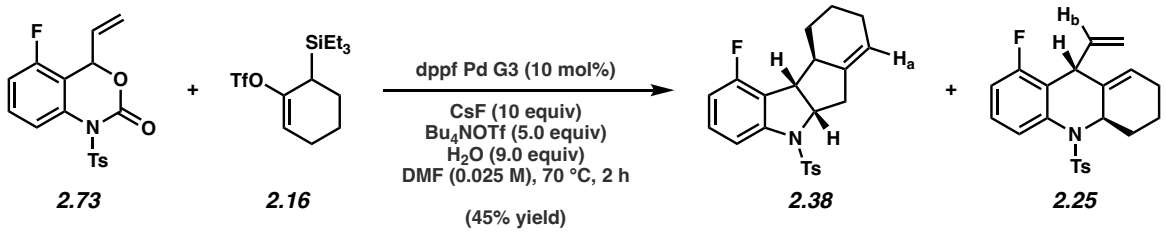

2.38. Followed General Procedure 2.6. Purification by preparative thin layer chromatography (4:1:1 hexanes:CH_2Cl_2:Et_2O) afforded a mixture of **2.38** and constitutional isomer **2.25** (45% combined yield, >20:1 dr (determined by ^{1}H NMR analysis of the crude mixture), 11:1 **2.38**:**2.25**, average of two experiments) as a waxy light yellow solid. Ratio of constitutional isomers was determined by integrating the following peaks in the ^{1}H NMR spectrum of the isolated mixture (H_a **2.38**: 5.54–5.50 ppm; H_b **2.25**: 4.79 ppm). **Annulation Products 2.38** and **2.25**: R_f 0.65 (4:1:1 hexanes:CH_2Cl_2:Et_2O); ^{1}H NMR (500 MHz, $CDCl_3$, **2.38**): δ 7.65 (dt, *J* = 8.3, 2.2, 2H), 7.44 (d, *J* = 8.1, 1H), 7.23–7.14 (m, 3H), 6.73–6.67 (m, 1H), 5.54–5.50 (br m, 1H), 4.46 (dt, *J* = 10.5, 7.6, 1H), 3.20 (dd, *J* = 10.3, 7.7, 1H), 3.00 (dd, *J* = 15.6, 8.0, 1H), 2.75–2.67 (m, 1H), 2.37 (s, 3H), 2.35–2.31 (m, 2H), 2.02–1.96 (m, 2H), 1.83–1.76 (m, 1H), 1.51–1.39 (m, 1H), 1.23–1.13 (m, 1H); ^{13}C NMR (125 MHz, $CDCl_3$, **2.38**): δ 159.6 (d, *J* = 246.1), 144.3, 144.0 (d, *J* = 8.7), 139.9, 134.6, 129.8, 129.7, 127.4, 121.7 (d, *J* = 22.4), 119.6, 111.1 (d, *J* = 3.4), 110.9 (d, *J* = 20.3), 66.5, 49.7 (d, *J* = 1.4), 45.5, 41.5, 29.1 (d, *J* = 2.4), 24.9, 22.4, 21.7; ^{19}F NMR (282 MHz, $CDCl_3$): δ –116.72 (m, 1F); IR (film): 2926, 2856, 1620, 1457, 1355 cm^{-1}; HRMS-APCI (*m/z*) $[M + H]^+$ calcd for $C_{22}H_{23}FNO_2S^+$, 384.1428; found 384.1431. Relative stereochemistry was assigned by analogy to the ^{1}H NMR data of **2.43**.

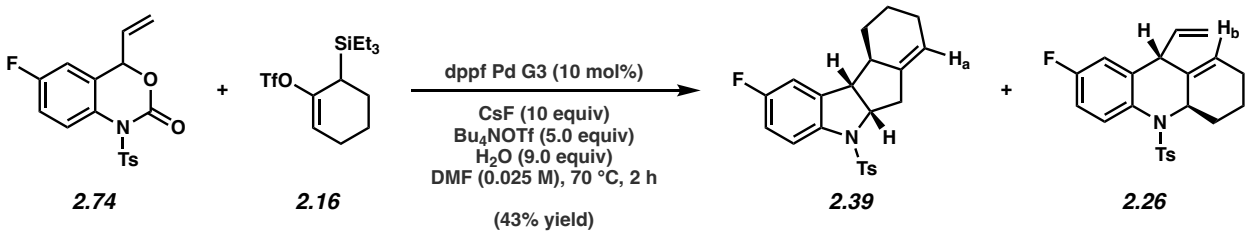

2.39. Followed General Procedure 2.6. Purification by preparative thin layer chromatography (4:1:1 hexanes:CH_2Cl_2:Et_2O) afforded a mixture of **2.39** and constitutional isomer **2.26** (43% combined yield, >20:1 dr (determined by ^{1}H NMR analysis of the crude mixture), 13:1 **2.39**:**2.26**, average of two experiments) as a light yellow solid. Ratio of constitutional isomers was determined by integrating the following peaks in the ^{1}H NMR spectrum of the isolated mixture (H_a **2.39**: 5.51–5.49 ppm; H_b **2.26**: 5.57–5.54 ppm). **Annulation Products 2.39** and **2.26**: R_f 0.72 (4:1:1 hexanes:CH_2Cl_2:Et_2O); ^{1}H NMR (500 MHz, $CDCl_3$, **2.39**): δ 7.62–7.58 (m, 3H), 7.22–7.18 (m, 2H), 6.90 (tdd, *J* = 8.8, 2.7, 0.6, 1H), 6.78 (ddd, *J* = 8.0, 2.6, 0.8, 1H), 5.51–5.49 (br m, 1H), 4.42 (dt, *J* = 10.3, 7.5, 1H), 3.02–2.93 (m, 2H), 2.73–2.65 (m, 1H), 2.36 (s, 3H), 2.24–2.14 (m, 2H), 2.03–1.96 (m, 2H), 1.83–1.78 (m, 1H), 1.51–1.39 (m, 1H), 1.21–1.12 (m, 1H); ^{13}C NMR (125 MHz, $CDCl_3$, **2.39**): δ 160.1 (d, *J* = 242.5), 144.2, 139.9, 137.7 (d, *J* = 8.1), 137.4, 134.4, 129.8, 127.4, 119.4, 116.8 (d, *J* = 8.6), 114.7 (d, *J* = 23.4), 111.5 (d, *J* = 23.7), 66.3, 52.1 (d, *J* = 1.7), 46.0, 41.2, 29.3, 24.8, 22.3, 21.7; ^{19}F NMR (282 MHz, $CDCl_3$): δ –119.18 (m, 1F); IR (film): 2926, 2853, 1479, 1355, 1166 cm^{-1}; HRMS-APCI (*m/z*) $[M + H]^+$ calcd for $C_{22}H_{23}FNO_2S^+$, 384.1428; found 384.1430. Relative stereochemistry was assigned by analogy to the ^{1}H NMR data of **2.43**.

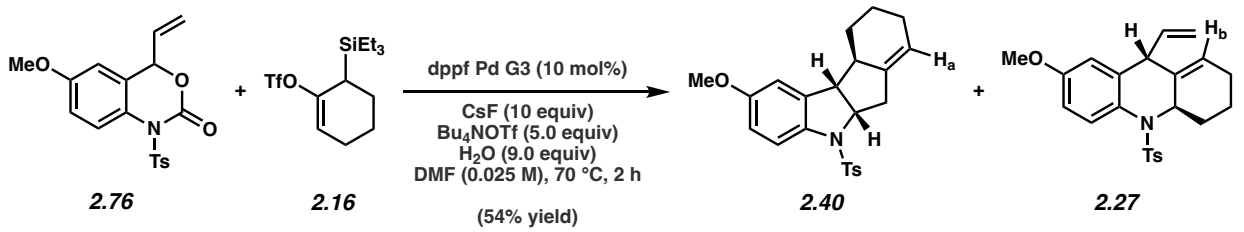

2.40. Followed General Procedure 2.6. Purification by preparative thin layer chromatography (4:1:1 hexanes:CH_2Cl_2:Et_2O) afforded a mixture of **2.40** and constitutional isomer **2.27** (54% combined yield, >20:1 dr (determined by ^{1}H NMR analysis of the crude mixture), 8.5:1 **2.40**:**2.27**, average of two experiments) as a colorless clear oil. Ratio of constitutional isomers was determined by integrating the following peaks in the ^{1}H NMR spectrum of the isolated mixture (H_a **2.40**: 5.49–5.47 ppm; H_b **2.27**: 5.55–5.51 ppm). **Annulation Products 2.40** and **2.27**: R_f 0.57 (4:1:1 hexanes:CH_2Cl_2:Et_2O); ^{1}H NMR (600 MHz, $CDCl_3$, **2.40**): δ 7.60–7.56 (m, 3H), 7.19–7.16 (m, 2H), 6.75 (dd, J = 8.8, 2.4, 1H), 6.63–6.61 (m, 1H), 5.49–5.47 (br m, 1H), 4.37 (dt, J = 10.2, 7.6, 1H), 3.77 (s, 3H), 2.98–2.91 (m, 2H), 2.71–2.65 (m, 1H), 2.35 (s, 3H), 2.24–2.14 (m, 2H), 2.02–1.98 (m, 2H), 1.82–1.77 (m, 1H), 1.49–1.40 (m, 1H), 1.20–1.12 (m, 1H); ^{13}C NMR (150 MHz, $CDCl_3$, **2.40**): δ 157.1, 143.9, 140.3, 137.6, 134.7, 134.4, 129.7, 127.5, 119.1, 116.9, 113.0, 110.2, 66.1, 55.8, 52.2, 45.9, 41.1, 29.4, 24.8, 22.4, 21.7; IR (film): 2928, 1597, 1485, 1164, 665 cm^{-1}; HRMS-APCI (*m/z*) $[M + H]^+$ calcd for $C_{23}H_{26}NO_3S^+$, 396.1633; found 396.1632. Relative stereochemistry was assigned by analogy to the ^{1}H NMR data of **2.43**.

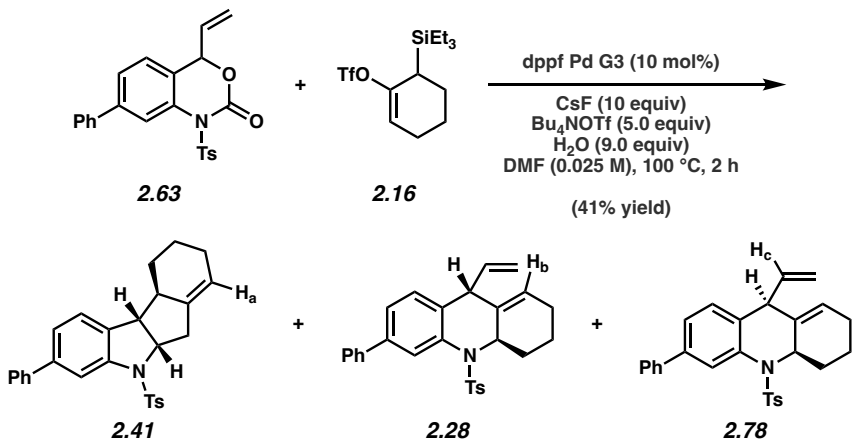

2.41. Followed a modified version of General Procedure 2.6 by altering the temperature (100 °C). Purification by preparative thin layer chromatography (4:1:1 hexanes:CH_2Cl_2:Et_2O) afforded a mixture of **2.41** and constitutional isomers **2.28** and **2.78** (41% combined yield, >20:1 dr (determined by ^{1}H NMR analysis of the crude mixture), 20:1.1:1.0 **2.41**:**2.28:2.78**, average of two experiments) as an off-white solid. Ratio of constitutional isomers was determined by integrating the following peaks in the ^{1}H NMR spectrum of the isolated mixture (H_a **2.41**: 5.53–5.49ppm; H_b **2.28**: 5.60–5.56 ppm; H_b **2.78**: 5.92 ppm). **Annulation Products 2.41**, **2.28**, and **2.78**: R_f 0.82 (4:1:1 hexanes:CH_2Cl_2:Et_2O); ^{1}H NMR (500 MHz, $CDCl_3$, **2.41**): δ 7.90 (d, *J* = 1.6, 1H), 7.68 (dt, *J* = 8.4, 1.6, 2H), 7.63–7.59 (m, 2H), 7.48–7.43 (m, 2H), 7.39–7.34 (m, 1H), 7.24 (dd, *J* = 7.8, 1.7, 1H), 7.22–7.18 (m, 2H), 7.15 (d, *J* = 7.8, 1H), 5.53–5.49 (br m, 1H), 4.48 (dt, *J* = 10.2, 7.6, 1H), 3.09 (dd, *J* = 10.1, 8.0, 1H), 3.01 (dd, *J* = 15.6, 7.9, 1H), 2.79–2.72 (m, 1H), 2.35 (s, 3H), 2.30–2.21 (m, 2H), 2.05–1.99 (m, 2H), 1.85–1.78 (m, 1H), 1.53–1.43 (m, 1H), 1.27–1.17 (m, 1H); ^{13}C NMR (125 MHz, $CDCl_3$, **2.41**): δ 144.0, 142.0, 141.4, 140.9, 140.3, 134.7, 134.6, 129.7, 128.8, 127.4, 127.3, 127.2, 124.4, 123.1, 119.0, 113.9, 66.1, 51.9, 46.0, 41.3, 29.2, 24.8, 22.3, 21.5; IR (film): 3220, 2928, 2367, 1483, 1356 cm^{-1}; HRMS-APCI (*m/z*) $[M + H]^+$ calcd for $C_{28}H_{28}NO_2S^+$, 442.1841; found 442.1842. Relative stereochemistry was assigned by analogy to the ^{1}H NMR data of **2.43**.

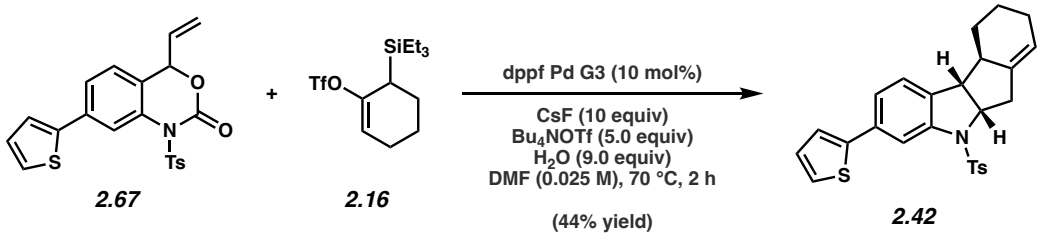

2.67 *2.16* *2.42*

2.42. Followed General Procedure 2.6. Purification by preparative thin layer chromatography (4:1:1 hexanes:CH_2Cl_2:Et_2O) afforded **2.42** (44% yield, >20:1 dr (determined by ^1H NMR analysis of the crude mixture), average of two experiments) as a white solid. **Annulation Product 2.42**: Mp: 188–190 °C; R_f 0.74 (4:1:1 hexanes:CH_2Cl_2:Et_2O); ^1H NMR (500 MHz, $CDCl_3$): δ 7.92 (s, 1H), 7.68 (d, J = 8.1, 2H), 7.35 (d, J = 3.5, 1H), 7.29 (d, J = 5.0, 1H), 7.25–7.23 (overlapped with residual solvent peak, 1H), 7.20 (d, J = 8.0, 2H), 7.11–7.06 (m, 2H), 5.52–5.50 (br m, 1H), 4.47 (dt, J = 10.0, 7.6, 1H), 3.09–2.97 (m, 2H), 2.78–2.71 (m, 1H), 2.35 (s, 3H), 2.27–2.19 (m, 2H), 2.03–1.99 (m, 2H), 1.84–1.79 (m, 1H), 1.51–1.41 (m, 1H), 1.26–1.15 (m, 1H); ^{13}C NMR (125 MHz, $CDCl_3$): δ 144.4, 144.2, 142.2, 140.3, 134.9, 134.73, 134.66, 129.8, 128.2, 127.5, 125.0, 124.7, 123.5, 122.1, 119.2, 112.7, 66.3, 52.1, 46.2, 41.4, 29.3, 24.9, 22.4, 21.7; IR (film): 2965, 2367, 1423, 1356, 1212 cm^{-1}; HRMS-APCI (*m/z*) $[M + H]^+$ calcd for $C_{26}H_{26}NO_2S_2^+$, 448.1405; found 448.1409. Relative stereochemistry was assigned by analogy to the ^1H NMR data of **2.42**.

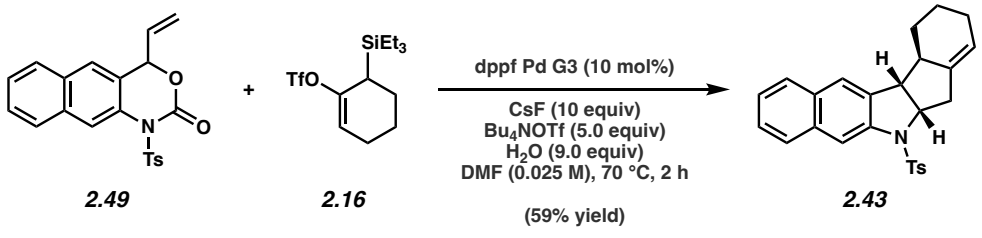

2.49 *2.16* *2.43*

2.43. Followed General Procedure 2.6. Purification by preparative thin layer chromatography (4:1:1 hexanes:CH_2Cl_2:Et_2O) afforded **2.43** (59% yield, >20:1 dr (determined by ^1H NMR analysis of the crude mixture), average of two experiments) as a white solid. **Annulation Product 2.43**:

Mp: 181–183 °C; R_f 0.64 (4:1:1 hexanes:CH_2Cl_2:Et_2O); ^{1}H NMR (500 MHz, $CDCl_3$): δ 8.01 (s, 1H), 7.84–7.80 (m, 1H), 7.72 (dt, *J* = 8.3, 2.0, 2H), 7.71–7.67 (m, 1H), 7.53–7.5 (m, 1H), 7.43 (ddd, *J* = 8.2, 6.9, 1.3, 1H), 7.36 (ddd, *J* = 8.1, 6.8, 1.2, 1H), 7.19–7.15 (m, 2H), 5.54–5.50 (br m, 1H), 4.53 (ddd, *J* = 10.3, 7.5, 6.8, 1H), 3.24–3.19 (m, 1H), 3.03 (dd, *J* = 15.8, 7.9, 1H), 2.83–2.76 (m, 1H), 2.35–2.28 (m, 5H), 2.07–2.00 (m, 2H), 1.88–1.81 (m, 1H), 1.52–1.42 (m, 1H), 1.33–1.22 (m, 1H); ^{13}C NMR (125 MHz, $CDCl_3$): δ 144.2, 140.7, 140.2, 136.4, 134.8, 133.9, 131.1, 129.8, 127.9, 127.41, 127.39, 126.0, 124.8, 122.9, 119.2, 111.3, 66.2, 51.9, 46.5, 41.4, 29.3, 24.9, 22.4, 21.6; IR (film): 2923, 2852, 1454, 1356, 1163 cm^{-1}; HRMS-APCI (*m/z*) $[M + H]^+$ calcd for $C_{26}H_{26}NO_2S^+$, 416.1678; found 416.1682. Relative stereochemistry was assigned by X-ray crystallography; see Section 2.8.2.6 for details. See Table 2.11, Entry 1 and Figure 2.8 for SFC data.

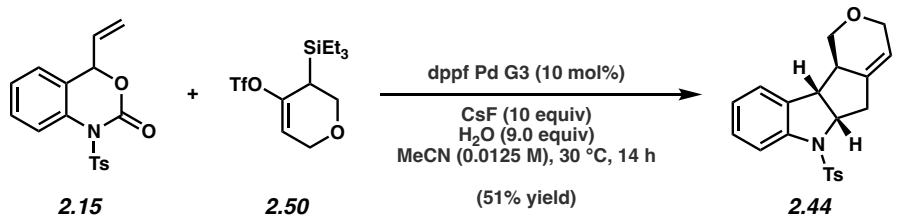

2.44. Followed General Procedure 2.7. Purification by preparative thin layer chromatography (4:1:1 hexanes:CH_2Cl_2:Et_2O) afforded **2.44** (51% yield, >20:1 dr (determined by ^{1}H NMR analysis of the crude mixture), average of two experiments) as a white solid. **Annulation Product 2.44**: Mp: 128–130 °C; R_f 0.22 (4:1:1 hexanes:CH_2Cl_2:Et_2O); ^{1}H NMR (600 MHz, $CDCl_3$): δ 7.68–7.62 (m, 3H), 7.25–7.22 (m, 1H), 7.21–7.18 (m, 2H), 7.05–7.00 (m, 2H), 5.54–5.51 (m, 1H), 4.45 (dt, *J* = 10.4, 7.5, 1H), 4.33 (dd, *J* = 10.5, 6.1, 1H), 4.16 (dq, *J* = 16.2, 3.0, 1H), 4.10–4.03 (m, 1H), 3.19 (t, *J* = 10.3, 1H), 3.10–3.04 (m, 2H), 2.77–2.70 (m, 1H), 2.60–2.56 (m, 1H), 2.35 (s, 3H); ^{13}C

NMR (125 MHz, $CDCl_3$): δ 144.2, 141.3, 138.3, 134.8, 134.5, 129.8, 128.5, 127.4, 124.53, 124.52, 117.4, 115.8, 69.0, 65.6, 65.0, 47.9, 44.6, 40.9, 21.7; IR (film): 2955, 2819, 1460, 1349, 1158 cm^{-1}; HRMS-APCI (*m/z*) $[M + H]^+$ calcd for $C_{21}H_{22}NO_3S^+$, 368.1315; found 368.1331. Relative stereochemistry was assigned by analogy to the ^1H NMR data of **2.43**.

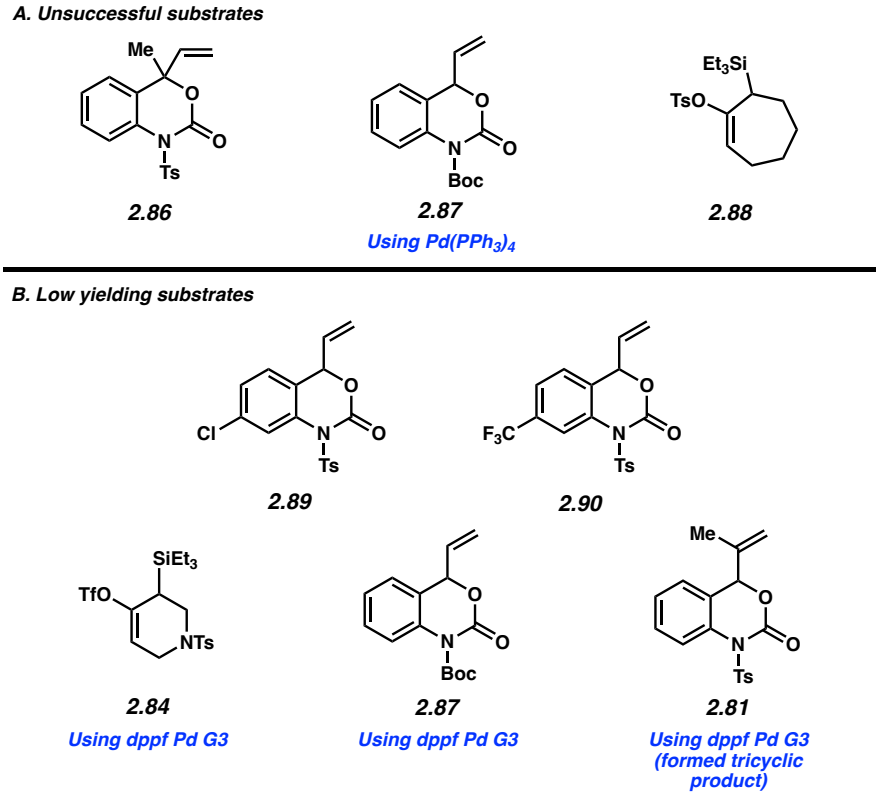

Figure 2.5. Unsuccessful and low yielding substrates evaluated during scope studies.

2.8.2.4 Representative Asymmetric Annulations

General Procedure 2.8 for the asymmetric annulation:

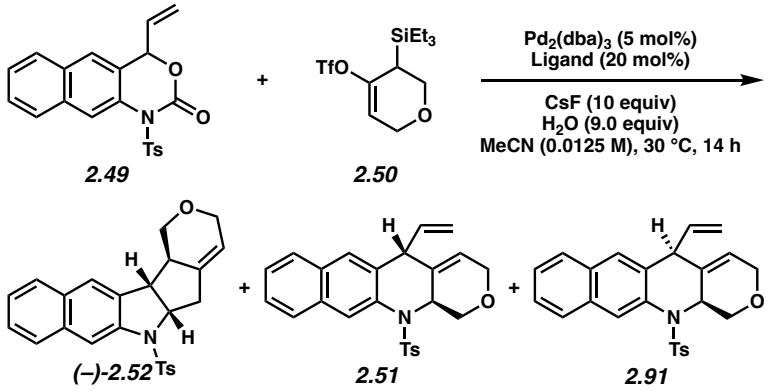

A 1-dram vial containing a magnetic stir bar was charged with vinyl benzoxazinone **2.49** (28 mg, 0.075 mmol, 3.0 equiv). A separate 1-dram vial was charged with silyl triflate **2.50**. The two vials were taken into a glovebox where $Pd_2(dba)_3$ (1.1 mg, 0.0013 mmol, 5 mol%), ligand (0.005 mmol, 20 mol%), and CsF (38 mg, 0.25 mmol, 10 equiv) were added to the vial containing vinyl benzoxazinone **2.49**. To the vial containing silyl triflate **2.50** was added the appropriate amount of MeCN to afford a 0.0125 M solution. The vial was capped and shaken to ensure full dissolution. The necessary amount of the solution of silyl triflate **2.50** (0.0125 M in MeCN, 2.0 mL, 8.7 mg, 0.025 mmol, 1.0 equiv) was then transferred via micropipette to the reaction vial containing vinyl benzoxazinone **2.49**. The reaction was sealed with a septum cap, removed from the glovebox, and placed under a flow of N_2. Then, deionized water (4.1 μL, 0.23 mmol, 9.0 equiv) was added to the reaction vessel via microsyringe. The septum cap was then carefully replaced with a Teflon-lined cap under a stream of N_2 and stirred for 14 h at 30 °C. The mixture was then filtered through a pad of silica gel, eluting with EtOAc (8 mL). The eluate was concentrated and purified by preparative thin layer chromatography to provide annulation products (–)-**2.52**, **2.51**, and **2.91** which were analyzed by SFC using a chiral stationary phase.

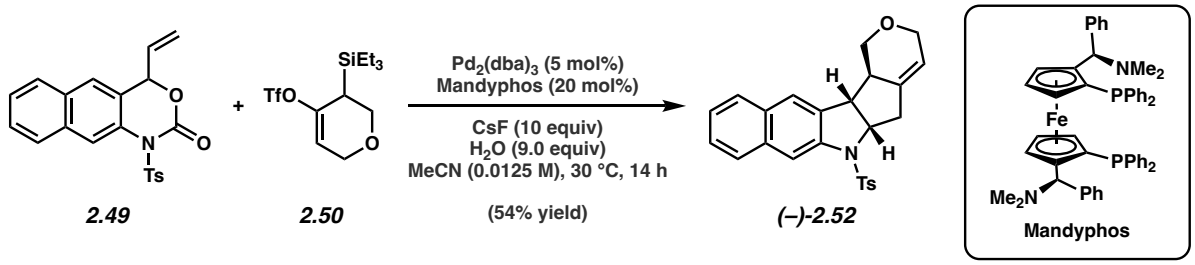

2.49 *2.50* *(–)-2.52*

(–)-2.52. Followed General Procedure 2.8. Purification by preparative thin layer chromatography (8:3:3 hexanes:CH_2Cl_2:Et_2O) afforded annulation product **(–)-2.52** (54% yield, >20:1 dr (determined by ^{1}H NMR analysis of the crude mixture), 70% ee) as a white solid. **(–)-2.52**: Mp: 157–159 °C; R_f 0.37 (8:3:3 hexanes:CH_2Cl_2:Et_2O); ^{1}H NMR (500 MHz, $CDCl_3$): δ 8.02, (s, 1H), 7.83 (d, J = 8.1, 1H), 7.73–7.68 (m, 3H), 7.47–7.42 (m, 2H), 7.40–7.35 (m, 1H), 7.17 (d, J = 8.0, 2H), 5.56–5.54 (br m, 1H), 4.56 (dt, J = 10.0, 7.5, 1H), 4.44 (dd, J = 10.4, 6.1, 1H), 4.21–4.15 (m, 1H), 4.12–4.06 (m, 1H), 3.31–3.20 (m, 2H), 3.11 (dd, J = 15.6, 7.7, 1H), 2.84–2.76 (m, 1H), 2.69–2.65 (m, 1H), 2.33 (s, 3H); ^{13}C NMR (125 MHz, $CDCl_3$): δ 144.4, 140.0, 138.6, 135.4, 134.8, 134.0, 131.2, 129.9, 127.9, 127.5, 127.3, 126.3, 125.0, 123.3, 117.6, 111.7, 69.0, 66.0, 65.0, 47.5, 44.9, 40.9 21.7; IR (film): 2926, 1457, 1356, 1164, 590 cm^{-1}; HRMS-APCI (*m/z*) $[M + H]^+$ calcd for $C_{25}H_{24}NO_3S^+$, 418.1471; found 418.1505. $[\alpha]^{19.9}_D$–8.0° (*c* = 1.00, CH_2Cl_2). Relative stereochemistry was assigned by analogy to the ^{1}H NMR data of **2.43**. See Table 2.11, Entry 5 and Figure 2.12 for SFC data.

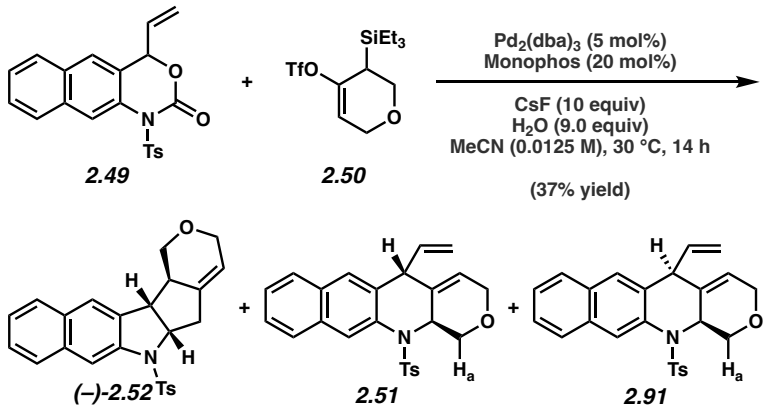

(–)-2.52, 2.51, and **2.91**. Followed General Procedure 2.8. Purified by preparative thin layer chromatography (8:3:3 hexanes:CH_2Cl_2:Et_2O) afforded **(–)-2.52** (11% yield, >20:1 dr (determined by ^{1}H NMR analysis of the crude mixture), 12% ee) as a white solid and an mixture of major diastereomer **2.51** and minor diastereomer **2.91** (26% yield, 2.8:1 dr, ~38% ee and ~38% ee, respectively) as an off-white solid. Diastereomeric ratio was determined by integrating the following peaks in the ^{1}H-NMR spectrum of the crude reaction mixture (H_a **2.51**: 3.41–3.31 ppm; **2.91**: 3.41–3.31 ppm). Spectral data matched those obtained for **(–)-2.52**. **2.51** and **2.91**: R_f 0.54 (8:3:3 hexanes:CH_2Cl_2:Et_2O); ^{1}H NMR (500 MHz, $CDCl_3$, **2.51**): δ 8.37 (s, 1H), 7.91–7.86 (m, 1H), 7.76–7.70 (m, 1H), 7.50–7.41 (m, 3H), 7.35–7.31 (m, 2H), 7.13–7.09 (m, 2H), 5.65 (q, *J* = 2.7, 1H), 4.89 (ddd, *J* = 17.1, 10.1, 4.9, 1H), 4.81–4.72 (m, 1H), 4.67 (ddd, *J* = 17.2, 2.0, 1.4, 1H), 4.62 (dd, *J* = 10.4, 5.5, 1H), 4.45–4.39 (m, 1H), 4.22–4.11 (m, 1H), 4.04 (ddd, 16.9, 3.9, 1.9, 1H), 4.01–3.94 (m, 1H), 3.41–3.31 (m, 1H), 2.33 (s, 3H); ^{1}H NMR (500 MHz, $CDCl_3$, **2.91**): δ 8.15 (s, 1H), 7.91–7.86 (m, 1H), 7.76–7.70 (m, 1H), 7.50–7.41 (m, 5H), 7.19–7.15 (m, 2H), 5.99 (dt, *J* = 19.4, 9.9, 1H), 5.40–5.34 (m, 2H), 4.83 (dd, *J* = 17.1, 1.5, 1H), 4.81–4.72 (m, 1H), 4.45–4.39 (m, 1H),), 4.22–4.11 (m, 1H), 4.01–3.94 (m, 1H), 3.41–3.31 (m, 1H), 2.48–2.44 (m, 1H), 2.39 (s, 3H); ^{13}C NMR (125 MHz, $CDCl_3$, **2.51** and **2.91**, 45 of 46 signals observed): δ 144.0, 143.9, 136.7, 136.1, 136.0, 135.7, 135.6, 134.3, 133.9, 133.2, 133.1, 132.7, 132.4, 132.0, 131.5, 129.7, 129.5,

128.3, 128.2, 127.9, 127.5, 127.2, 127.11, 127.05, 126.6, 126.3, 126.22, 126.21, 126.17, 124.1, 123.0, 122.9, 120.3, 119.1, 116.1, 69.0, 68.5, 65.1, 65.1, 54.3, 52.4, 50.7, 45.7, 21.63, 21.60; IR (film): 2926, 2853, 1356, 1167, 1091 cm^{-1}; HRMS-APCI (*m/z*) $[M + H]^+$ calcd for $C_{25}H_{24}NO_3S^+$, 418.1471; found 418.1465. Optical rotation could not be determined for **2.51** and **2.91** due to difficulty of separation. Relative stereochemistry was assigned by analogy to the ^1H NMR data of **2.33** and **2.85**. See Table 2.11, Entry 7 and Figure 2.14 for SFC data for **2.51** and see Table 2.11, Entry 9 and Figure 2.16 for SFC data for **2.91**.

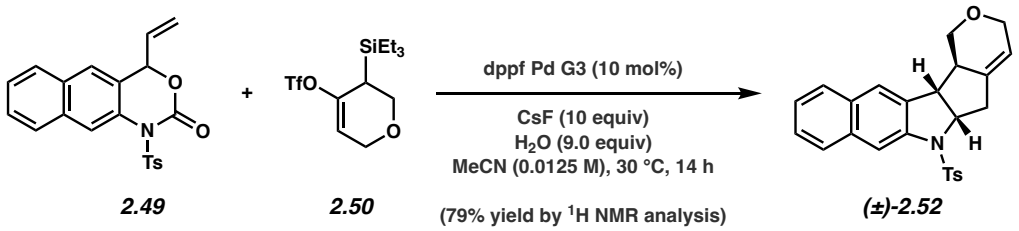

(±)-2.52. Followed a modified version of General Procedure 2.7 by performing on 0.025 mmol scale. Purification by preparative thin layer chromatography (4:1:1 hexanes:CH_2Cl_2:Et_2O) afforded an analytical sample of annulation product **(±)-2.52** (79% yield by ^1H NMR using mesitylene as an internal standard, >20:1 dr (determined by ^1H NMR analysis of the crude mixture)) as a white solid. **Annulation Product (±)-2.52**: Spectral data matched those obtained for **(–)-2.52**. See Table 2.11, Entry 4 and Figure 2.11 for SFC data**.**

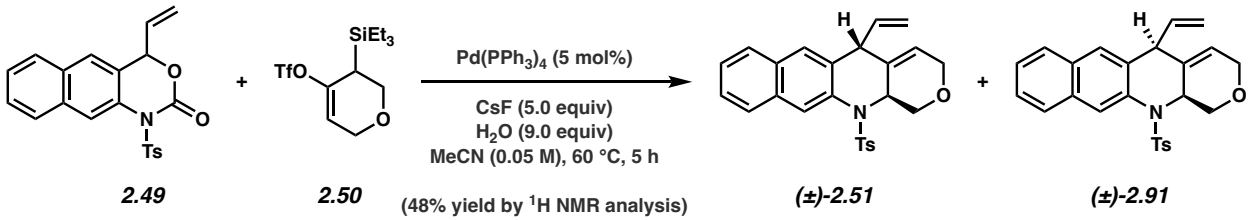

2.49 *2.50* *(±)-2.51* *(±)-2.91*

(±)-2.51 and **(±)-2.91**. Followed a modified version of General Procedure 2.5 by performing on 0.025 mmol scale. Purification by preparative thin layer chromatography (8:3:3 hexanes:CH_2Cl_2:Et_2O) afforded an analytical sample of a mixture of major diastereomer **(±)-2.51** and minor diastereomer **(±)-2.91** (48% yield by ^{1}H NMR using mesitylene as an internal standard, 1.3:1 dr) as a white solid. Diastereomeric ratio was determined by integrating the following peaks in the ^{1}H-NMR spectrum of the crude reaction mixture (H_a **(±)-2.51**: 3.41–3.31 ppm; **(±)-2.91**: 3.41–3.31 ppm). Spectral data matched those obtained for **2.51** and **2.91**. See Table 2.11, Entry 6 and Figure 2.13 for SFC data for **(±)-2.51** and see Table 2.11, Entry 8 and Figure 2.15 for SFC data for **(±)-2.91**.

2.8.2.5. Extended Evaluation of Chiral Ferrocenyl Phosphine Ligands

General Procedure 2.9 for the evaluation of the asymmetric annulation:

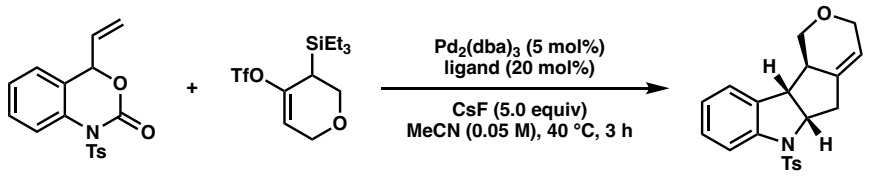

2.15 *2.50* *(–)-2.44*

A 1-dram vial containing a magnetic stir bar was charged with vinyl benzoxazinone **2.15** (28 mg, 0.075 mmol, 3.0 equiv). A separate 1-dram vial was charged with silyl triflate **2.50**. The two vials were taken into a glovebox where $Pd_2(dba)_3$ (1.1 mg, 0.0013 mmol, 5 mol%), ligand (0.005 mmol, 20 mol%), and CsF (17 mg, 0.13 mmol, 5.0 equiv) were added to the vial containing vinyl

benzoxazinone **2.15**. To the vial containing silyl triflate **2.50** was added the appropriate amount of MeCN to afford a 0.05 M solution. The vial was capped and shaken to ensure full dissolution. The necessary amount of the solution of silyl triflate **2.50** (0.05 M in MeCN, 500 μL, 8.7 mg, 0.025 mmol, 1.0 equiv) was then transferred via micropipette to the reaction vial containing vinyl benzoxazinone **2.15**. The reaction was sealed with a Teflon-lined cap, removed from the glovebox, and stirred for 3 h at 40 °C. The mixture was then filtered through a pad of silica gel, eluting with EtOAc (8 mL). The eluate was concentrated and purified by preparative thin layer chromatography to provide annulation products **(–)-2.44** which were analyzed by SFC using a chiral stationary phase.

*The stereochemistry depicted for **(–)-2.44** is not necessarily representative of the major enantiomer observed for all ligands evaluated. Any modification of the conditions shown in the general procedure above are specified in the following scheme.*

A range of ligands (see Figure 2.6 below for ligand structures) were tested using General Procedure 2.9, and results of these studies appear below in Table 2.9.

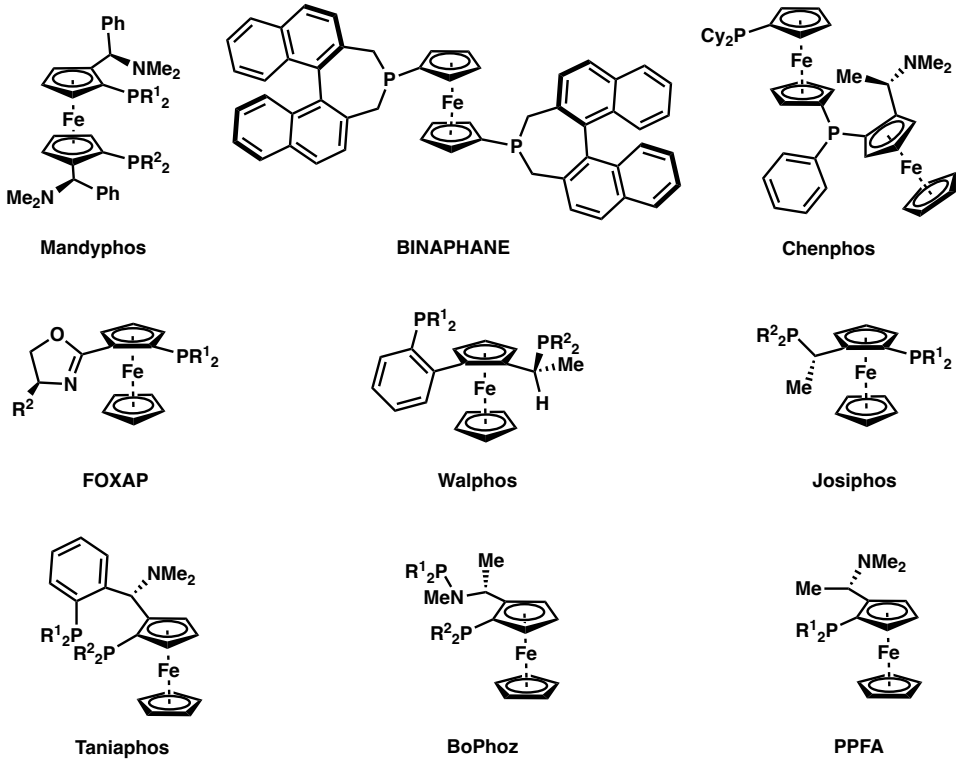

Figure 2.6. Ligand families evaluated during asymmetric reaction development.

Table 2.9. Ligand evaluation results. See Figure 2.6 above for ligand classes (absolute stereochemistry of product may differ between table entries).

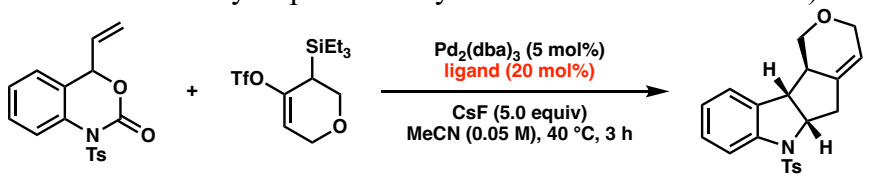

2.15 *2.50* *(–)-2.44*

Entry	Ligand Class	R^1	R^2	Yield[a]	%ee
1	Mandyphos[b]	Ph	Ph	19%	77%
2	Mandyphos[b]	4-methoxy-3,5-xylyl	4-methoxy-3,5-xylyl	18%	73%
3	Mandyphos[b]	3,5-bis(trifluoromethyl) phenyl	3,5-bis(trifluoromethyl) phenyl	0%	N/A
4	Mandyphos[b]	3,5-xylyl	3,5-xylyl	5%	19%
5	Mandyphos[b]	Cy	Cy	0%	N/A
6	BINAPHANE	N/A	N/A	0%	N/A
7	Chenphos	N/A	N/A	0%	N/A
8	FOXAP	Ph	*i*-Pr	0%	N/A
9	Walphos	Ph	Ph	13%	46%
10	Walphos	Ph	3,5-xylyl	5%	N/A
11	Walphos	3,5-xylyl	3,5-xylyl	5%	N/A
12	Walphos	Ph	Cy	10%	N/A
13	Josiphos[b]	Ph	Cy	0%	N/A
14	Josiphos	2-furyl	3,5-xylyl	16%	N/A
15	Josiphos	1-naphthyl	3,5-xylyl	4%	N/A
16	Josiphos	Ph	*t*-Bu	8%	N/A
17	Taniaphos	Ph	Ph	0%	N/A
18	BoPhoz	Ph	Ph	18%	0%
19	PPFA[b]	Ph	N/A	0%	N/A
20[c]	No ligand	N/A	N/A	0%	N/A

[a] ^{1}H NMR yield determined using mesitylene as an external standard. [b] 10 mol% ligand. [c] Conditions: $Pd_2(dba)_3$ (2.5 mol%), CsF (10 equiv), H_2O (3.0 equiv), MeCN (0.0125 M), 30 °C, 16 h.

2.8.2.6. Assignment of Absolute Stereochemical Configuration

To determine the major enantiomer formed in the annulation reaction, annulation product **(–)-2.43** was synthesized.

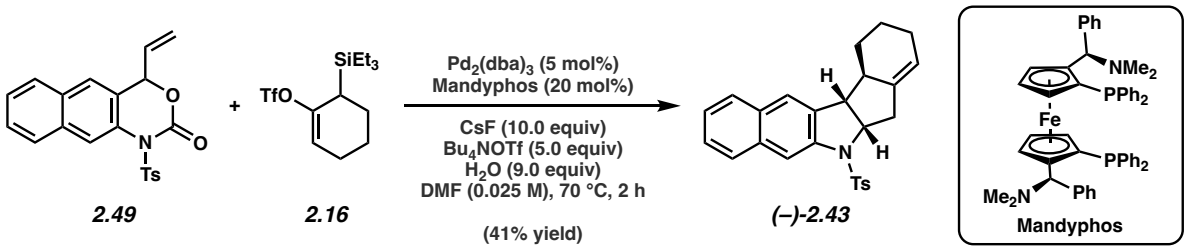

(–)-2.43. A 1-dram vial containing a magnetic stir bar was charged with vinyl benzoxazinone **2.49** (28 mg, 0.075 mmol, 3.0 equiv) and Bu_4NOTf (49 mg, 0.13 mmol, 5.0 equiv). A separate 1-dram vial was charged with silyl triflate **2.16**. The two vials were taken into a glovebox where $Pd_2(dba)_3$ (1.1 mg, 0.0013 mmol, 5 mol%), Mandyphos (4.1 mg, 0.005 mmol, 20 mol%), and CsF (38 mg, 0.25 mmol, 10.0 equiv) were added to the vial containing vinyl benzoxazinone **2.49**. To the vial containing silyl triflate **2.16** was added the appropriate amount of DMF to afford a 0.025 M solution. The vial was capped and shaken to ensure full dissolution. The necessary amount of the solution of silyl triflate **2.16** (0.025 M in DMF, 1.0 mL, 8.6 mg, 0.025 mmol, 1.0 equiv) was then transferred via micropipette to the reaction vial containing vinyl benzoxazinone **2.49**. The reaction was sealed with a septum cap, removed from the glovebox, and placed under a flow of N_2. Then, deionized water (4.1 µL, 0.23 mmol, 9.0 equiv) was added to the reaction vessel via microsyringe. The septum cap was then carefully replaced with a Teflon-lined cap under a stream of N_2 and stirred for 2 h at 70 °C. The mixture was then filtered through a pad of silica gel, eluting with EtOAc (8 mL). The eluate was washed with water (2 x 5 mL), dried with Na_2SO_4, filtered, and

concentrated under reduced pressure. The crude residue was redissolved in CH_2Cl_2 (1 mL) and filtered through a pad of silica gel eluting with CH_2Cl_2 (20 mL) to remove excess Bu_4NOTf. The eluate was concentrated and purified by preparative thin layer chromatography (4:1:1 hexanes:CH_2Cl_2:Et_2O) to provide annulation product **(–)-2.43** (41% yield, >20:1 dr, 58% ee) as an off-white solid. Crystals suitable for X-ray diffraction studies were obtained by liquid diffusion crystallization: **(–)-2.43** in a 1-dram vial was dissolved in minimal amounts of CH_2Cl_2 then EtOH was layered on top resulting in ~1:5 CH_2Cl_2:EtOH (solvents were filtered through a 0.22 μm filter prior to use). The ee for the crystals of **(–)-2.43** evaluated by X-ray analysis was ~80%, with the major enantiomer seen by SFC analysis corresponding to the major enantiomer observed after chromatography. **(–)-2.43**: Spectral data matched those previous reported in Section 2.8.2.3 for **2.43**. $[\alpha]^{18.1}_{D}$–203° (*c* = 1.00, CH_2Cl_2). See Table 2.11, Entries 2 and 3 and Figures 2.9 and 2.10 for SFC data.

Crystal Structure Analysis

Diffraction intensities were collected at 100 K on a Bruker Smart ApexII CCD diffractometer with CuKα radiation, 1.54178 Å. Absorption corrections were applied by SADABS.[71] All calculations were performed by the SHELXL-2014 packages.[72] Deposition Number 2238913 contains the supplementary crystallographic data for this paper. These data are provided free of charge by the joint Cambridge Crystallographic Data Centre and Fachinformationszentrum Karlsruhe Access Structures service www.ccdc.cam.ac.uk/structures.

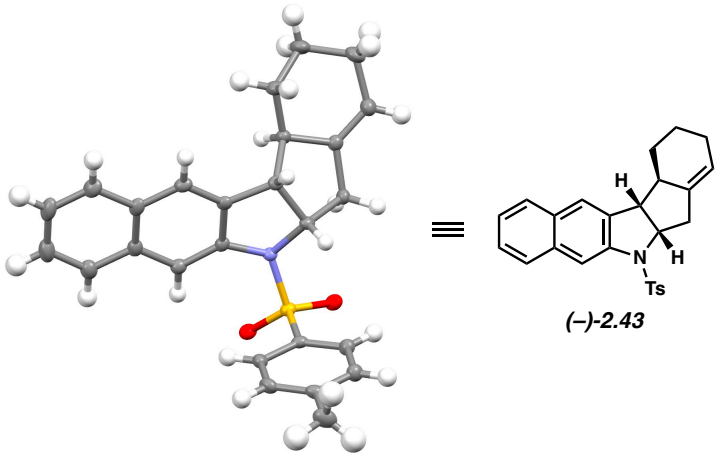

Figure 2.7. ORTEP representation of X-ray crystallographic structure **(–)-2.43**. (CCDC Registry # 2238913).

Table 2.10. Crystal data and structure refinement for compound **(–)-2.43**.

Identification code	cu_garg2209_a	
Empirical formula	C26 H25 N O2 S	
Formula weight	415.53	
Temperature	100(2) K	
Wavelength	1.54178 Å	
Crystal system	Monoclinic	
Space group	$P2_1$	
Unit cell dimensions	a = 14.1629(10) Å	α = 90°
	b = 5.4284(4) Å	β = 107.696(3)°
	c = 14.3334(10) Å	γ = 90°
Volume	1049.84(13) $Å^3$	
Z	2	
Density (calculated)	1.314 Mg/m^3	
Absorption coefficient	1.544 mm^{-1}	
F(000)	440	
Crystal size	0.400 x 0.030 x 0.030 mm^3	
Theta range for data collection	3.236 to 69.429 °	

Index ranges	–17<=h<=15, –5<=k<=6, –14<=I<=17
Reflections collected	13355
Independent reflections	3750 [R(int) = 0.0405]
Completeness to theta = 67.679°	97.9
Absorption correction	Semi-empirical from equivalents
Max. and min. transmission	0.75 and 0.58
Refinement method	Full-matrix least-squares on F^2
Data / restraints / parameters	3750 / 1 / 272
Goodness-of-fit on F^2	1.061
Final R indices [I>2sigma(I)]	R1 = 0.0295, wR2 = 0.0742
R indices (all data)	R1 = 0.0311, wR2 = 0.0748
Absolute structure parameter	0.037(7)
Extinction coefficient	n/a
Largest diff. peak and hole	0.180 and –0.333 e.$Å^{-3}$

Table 2.11. SFC conditions and data.

Compound	Column	Solvent	Flow Rate	Retention Times (min)	Enantiomeric Ratio (er)
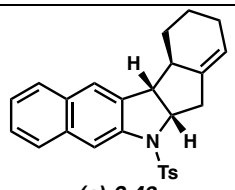 ***(±)-2.43***	Daicel ChiralPak IE / 30 °C	5–40% isopropanol in CO_2	4.0 mL/min	12.463/13.523	47.7 : 52.3
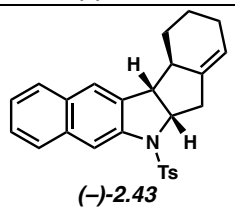 ***(–)-2.43*** *From reaction mixture*	Daicel ChiralPak IE / 30 °C	5–40% isopropanol in CO_2	4.0 mL/min	12.485/13.522	20.9 : 79.1
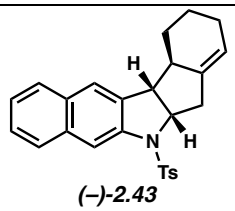 ***(–)-2.43*** *Crystals used for X-ray analysis*	Daicel ChiralPak IE / 30 °C	5–40% isopropanol in CO_2	4.0 mL/min	12.507/13.567	10 : 90[a]
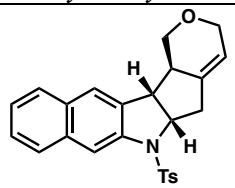 ***(±)-2.52***	Daicel ChiralPak ID / 30 °C	5–40% isopropanol in CO_2	4.0 mL/min	11.740/12.933	49.2 : 50.8
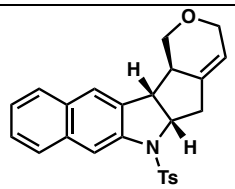 ***(–)-2.52***	Daicel ChiralPak ID / 30 °C	5–40% isopropanol in CO_2	4.0 mL/min	11.730/12.940	84.9 : 15.1
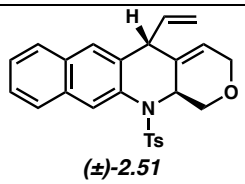 ***(±)-2.51***	Daicel ChiralPak ID / 30 °C	5–40% isopropanol in CO_2	4.0 mL/min	9.830/10.103	48.6 : 51.4[b]

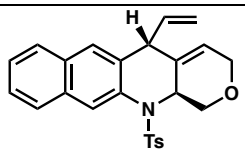 **2.51**	Daicel ChiralPak ID / 30 °C	5–40% isopropanol in CO_2	4.0 mL/min	9.890/10.170	69 : 31[b]
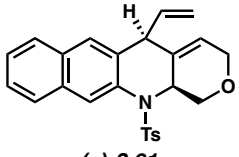 **(±)-2.91**	Daicel ChiralPak ID / 30 °C	5–40% isopropanol in CO_2	4.0 mL/min	9.017/9.453	52.3 : 47.7[b]
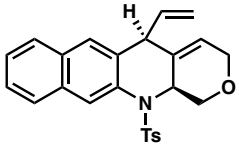 **2.91**	Daicel ChiralPak ID / 30 °C	5–40% isopropanol in CO_2	4.0 mL/min	9.070/9.500	69 : 31[b]

[a] The ee for (–)-**2.43** (Crystals) is approximated due to low concentration and a non-zero baseline.
[b] Due to difficulty resolving peaks, the ee reported for **2.51** and **2.94** (see Section 2.8.2.4) is approximated.

DCW-2022-092_112 DCW-2022-092-IE5-40iPrOH 1/20/2023 11:26:46 AM

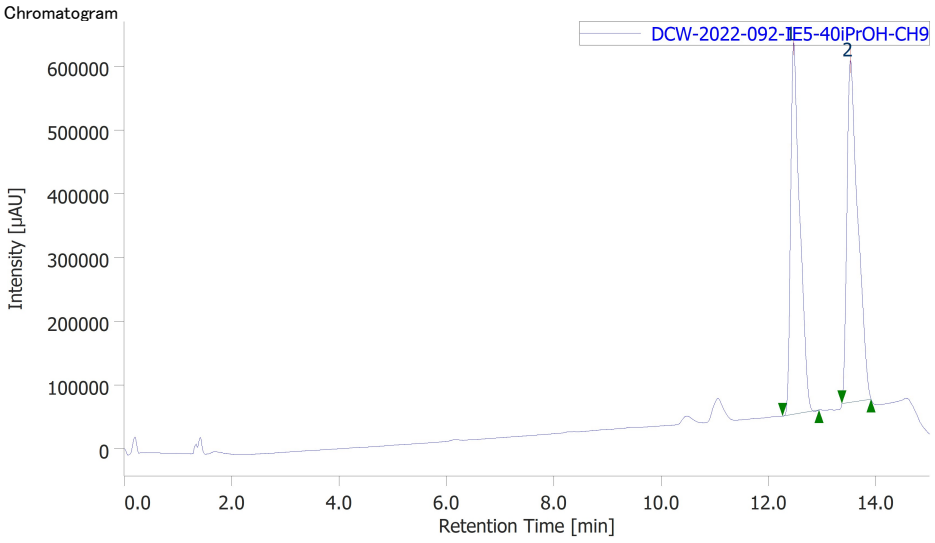

Peak Information

#	Peak Name	CH	tR [min]	Area [µV·sec]	Height [µV]	Area%	Height%	Quantity	NTP	Resolution	Symmetry Factor	Warning
1	Unknown	9	12.463	6871405	583880	47.675	52.105	N/A	25133	3.072	1.669	
2	Unknown	9	13.523	7541748	536710	52.325	47.895	N/A	20546	N/A	1.713	

Figure 2.8. SFC trace of **(±)-2.43**.

DCW-2022-092_112 DCW-2022-112-IE5-40iPrOH 1/20/2023 11:30:46 AM

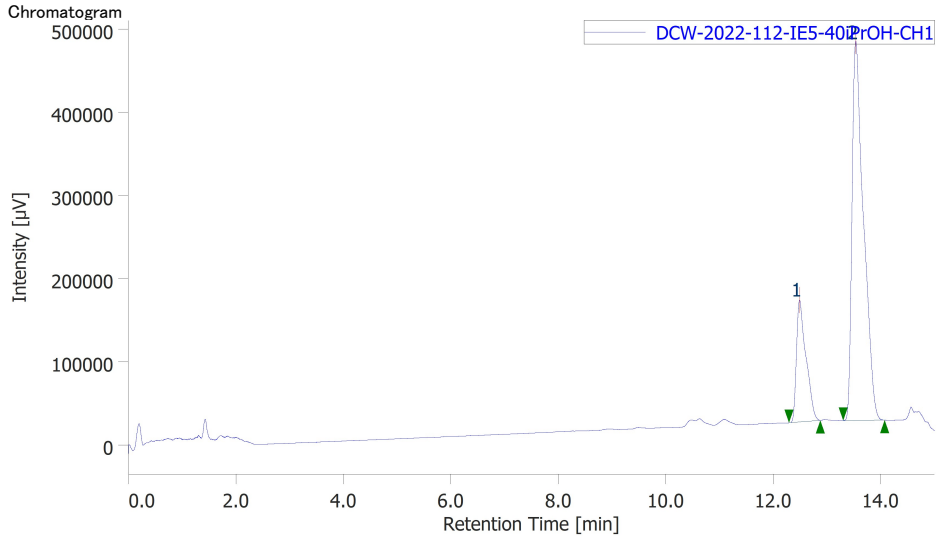

Peak Information

#	Peak Name	CH	tR [min]	Area [µV·sec]	Height [µV]	Area%	Height%	Quantity	NTP	Resolution	Symmetry Factor	Warning
1	Unknown	1	12.485	1792991	146467	20.943	24.323	N/A	23046	2.900	1.692	
2	Unknown	1	13.528	6768170	455706	79.057	75.677	N/A	19000	N/A	1.770	

Figure 2.9. SFC trace of **(–)-2.43** (from reaction mixture).

DCW-2022-112-redux DCW-2022-112-redux-IE5-40iPrOH 3/22/2023 2:01:54 PM

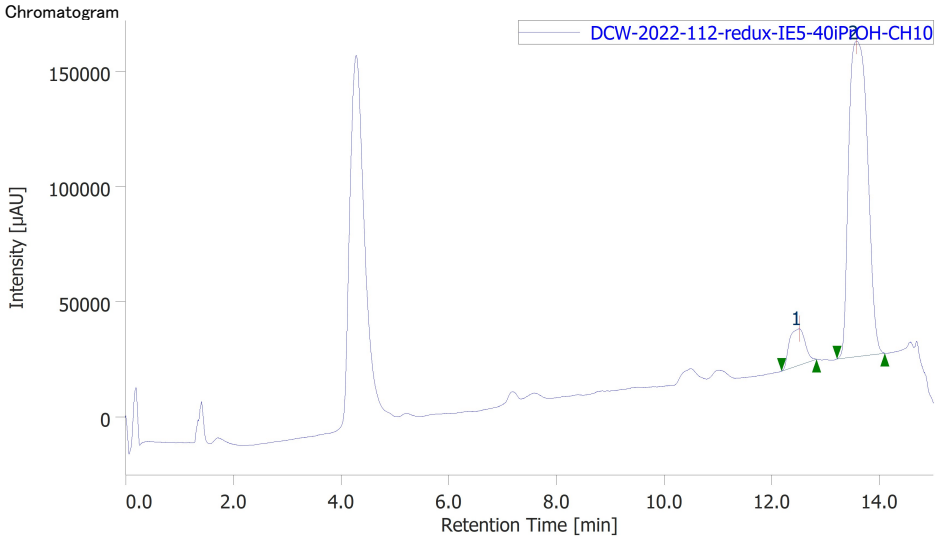

Peak Information

#	Peak Name	CH	tR [min]	Area [µV·sec]	Height [µV]	Area%	Height%	Quantity	NTP	Resolution	Symmetry Factor	Warning
1	Unknown	10	12.507	322576	15742	8.856	10.315	N/A	7675	1.696	0.951	
2	Unknown	10	13.567	3319743	136876	91.144	89.685	N/A	6319	N/A	1.274	

Figure 2.10. SFC trace of **(–)-2.43** (Crystals used for X-ray analysis).

DCW-2022-183-rp DCW-2022-183-rp-ID5-40iPrOH 1/20/2023 11:32:36 AM

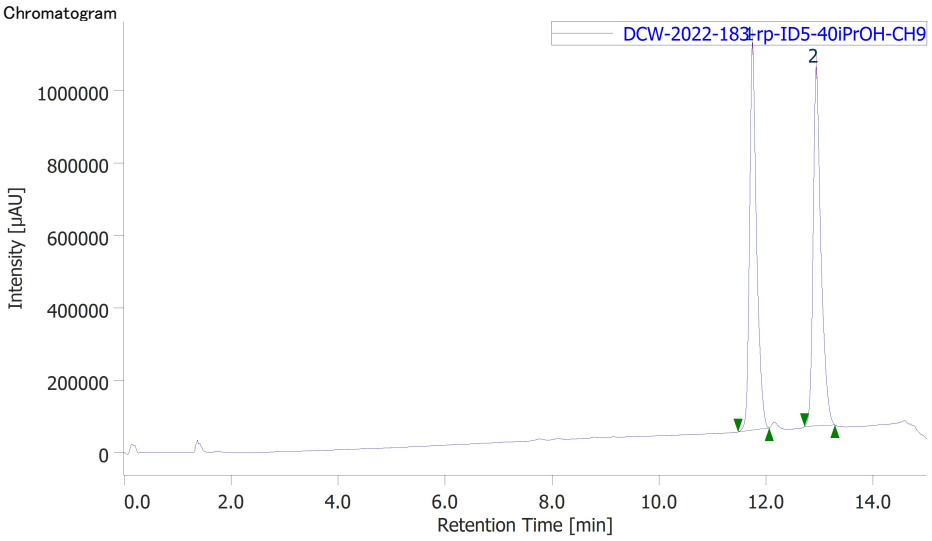

Peak Information

#	Peak Name	CH	tR [min]	Area [μV·sec]	Height [μV]	Area%	Height%	Quantity	NTP	Resolution	Symmetry Factor	Warning
1	Unknown	9	11.740	9762221	1072140	49.248	51.904	N/A	43994	5.060	1.362	
2	Unknown	9	12.933	10060552	993464	50.752	48.096	N/A	43154	N/A	1.404	

Figure 2.11. SFC trace of **(±)-2.52**.

DCW-2023-004_005_006 DCW-2023-004-ID5-40iPrOH 1/20/2023 11:33:43 AM

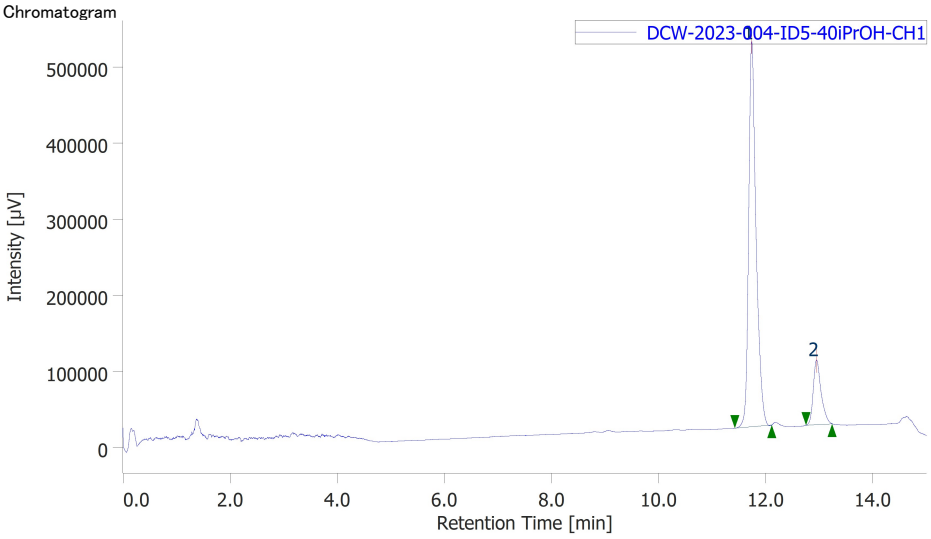

Peak Information

#	Peak Name	CH	tR [min]	Area [μV·sec]	Height [μV]	Area%	Height%	Quantity	NTP	Resolution	Symmetry Factor	Warning
1	Unknown	1	11.730	4861803	506817	84.904	85.612	N/A	38918	4.927	1.359	
2	Unknown	1	12.940	864424	85178	15.096	14.388	N/A	41315	N/A	1.339	

Figure 2.12. SFC trace of **(–)-2.52**.

DCW-2023-011 DCW-2023-011-ID5-40iPrOH 1/20/2023 11:34:21 AM

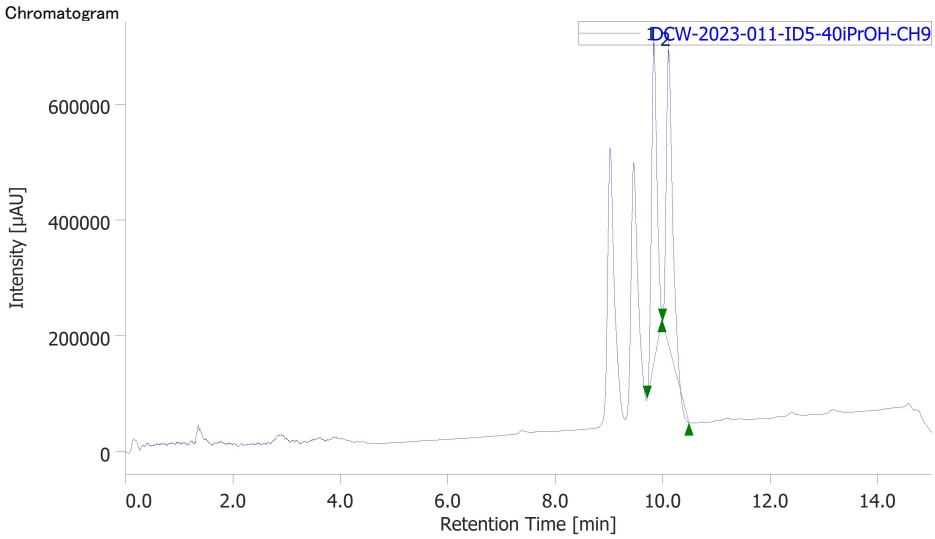

Peak Information

#	Peak Name	CH	tR [min]	Area [μV·sec]	Height [μV]	Area%	Height%	Quantity	NTP	Resolution	Symmetry Factor	Warning
1	Unknown	9	9.830	3912441	554563	48.564	52.160	N/A	44701	1.399	1.217	
2	Unknown	9	10.103	4143789	508642	51.436	47.840	N/A	38548	N/A	1.579	

Figure 2.13. SFC trace of **(±)-2.51**.

DCW-2022-305 DCW-2022-305-2-ID5-40iPrOH 1/20/2023 11:41:20 AM

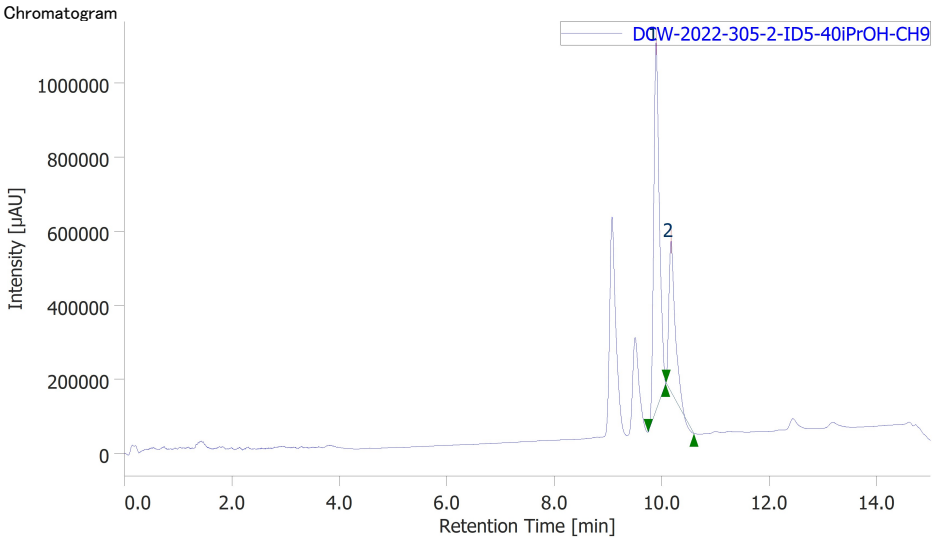

Peak Information

#	Peak Name	CH	tR [min]	Area [μV·sec]	Height [μV]	Area%	Height%	Quantity	NTP	Resolution	Symmetry Factor	Warning
1	Unknown	9	9.890	7222036	993611	68.556	70.879	N/A	44561	1.465	1.280	
2	Unknown	9	10.170	3312508	408236	31.444	29.121	N/A	43101	N/A	1.785	

Figure 2.14. SFC trace of **2.51**.

DCW-2023-011 DCW-2023-011-ID5-40iPrOH 1/20/2023 11:38:42 AM

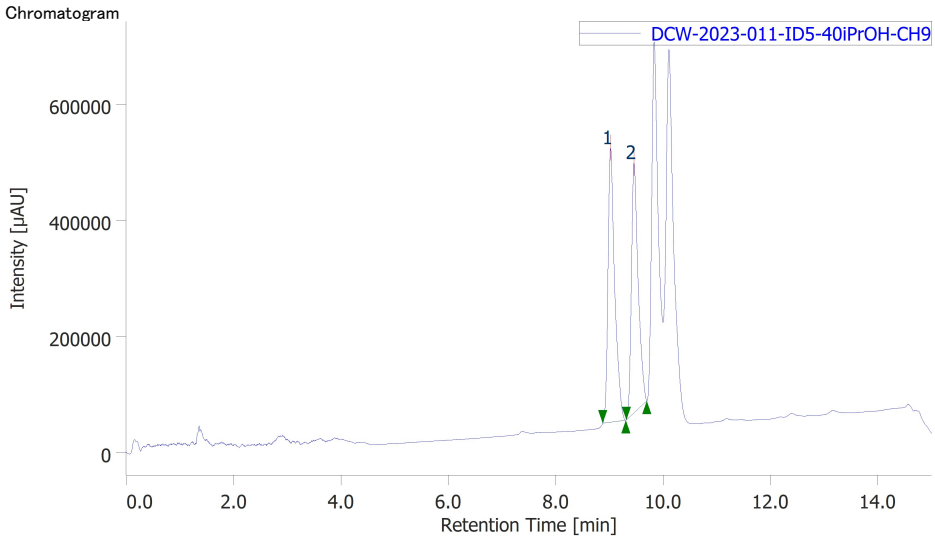

Peak Information

#	Peak Name	CH	tR [min]	Area [μV·sec]	Height [μV]	Area%	Height%	Quantity	NTP	Resolution	Symmetry Factor	Warning
1	Unknown	9	9.017	4091997	472755	52.309	52.338	N/A	28612	2.019	1.522	
2	Unknown	9	9.453	3730678	430511	47.691	47.662	N/A	29389	N/A	1.484	

Figure 2.15. SFC trace of **(±)-2.91**.

DCW-2022-305 DCW-2022-305-2-ID5-40iPrOH 1/20/2023 11:40:05 AM

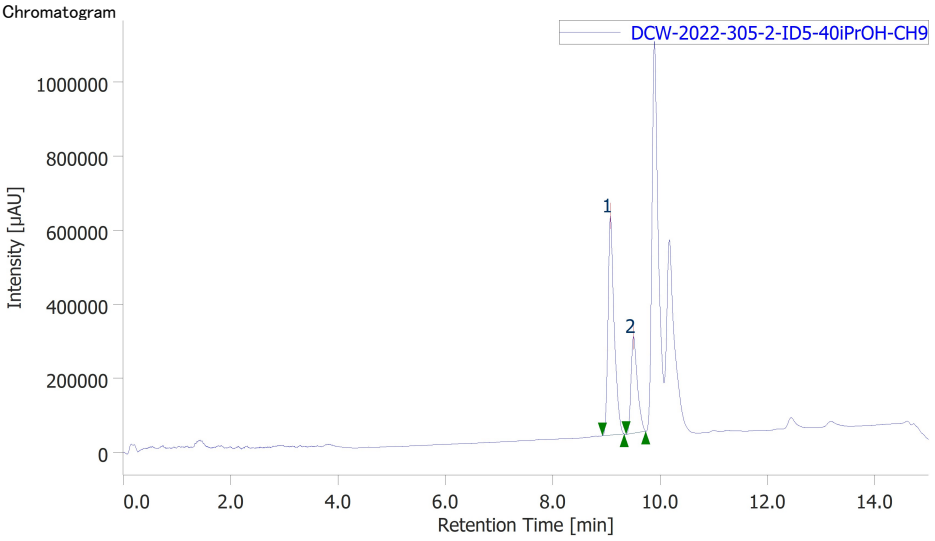

Peak Information

#	Peak Name	CH	tR [min]	Area [μV·sec]	Height [μV]	Area%	Height%	Quantity	NTP	Resolution	Symmetry Factor	Warning
1	Unknown	9	9.070	4706828	591021	68.734	69.396	N/A	33228	2.102	1.464	
2	Unknown	9	9.500	2141035	260642	31.266	30.604	N/A	32369	N/A	1.450	

Figure 2.16. SFC trace of **2.91**.

2.9 Spectra Relevant to Chapter Two:

Catalyst-Controlled Annulations of Strained Cyclic Allenes with π-Allylpalladium Complexes

Dominick C. Witkowski, Matthew S. McVeigh, Georgia M. Scherer, Sarah M. Anthony, and Neil K. Garg

J. Am. Chem. Soc. **2023**, *145*, 10491–10496.

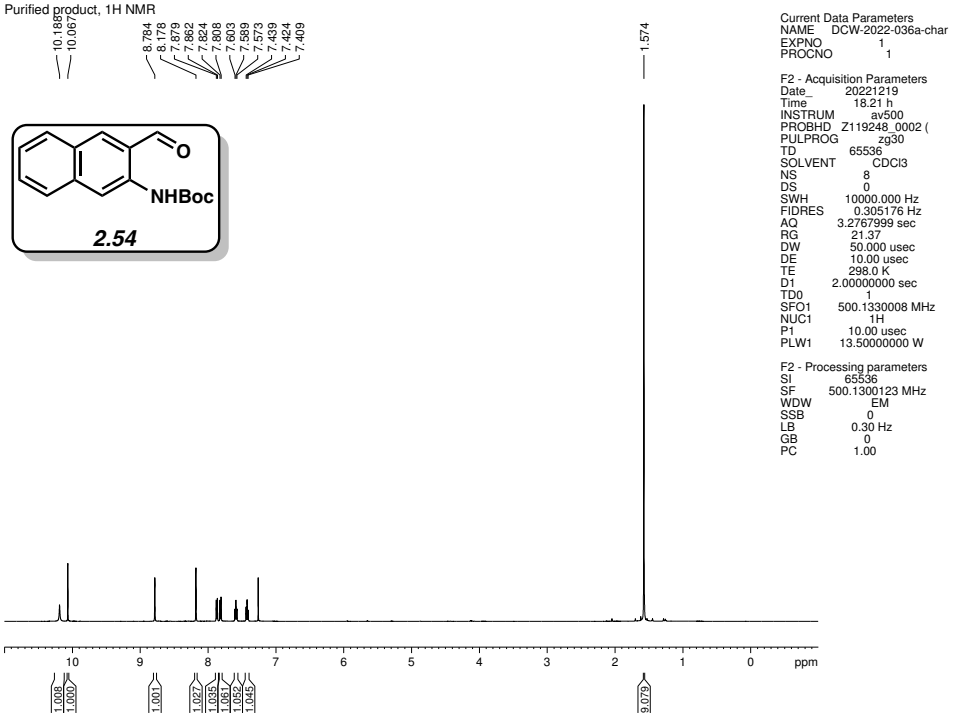

Figure 2.17. ^{1}H NMR (500 MHz, $CDCl_3$) of compound **2.54**.

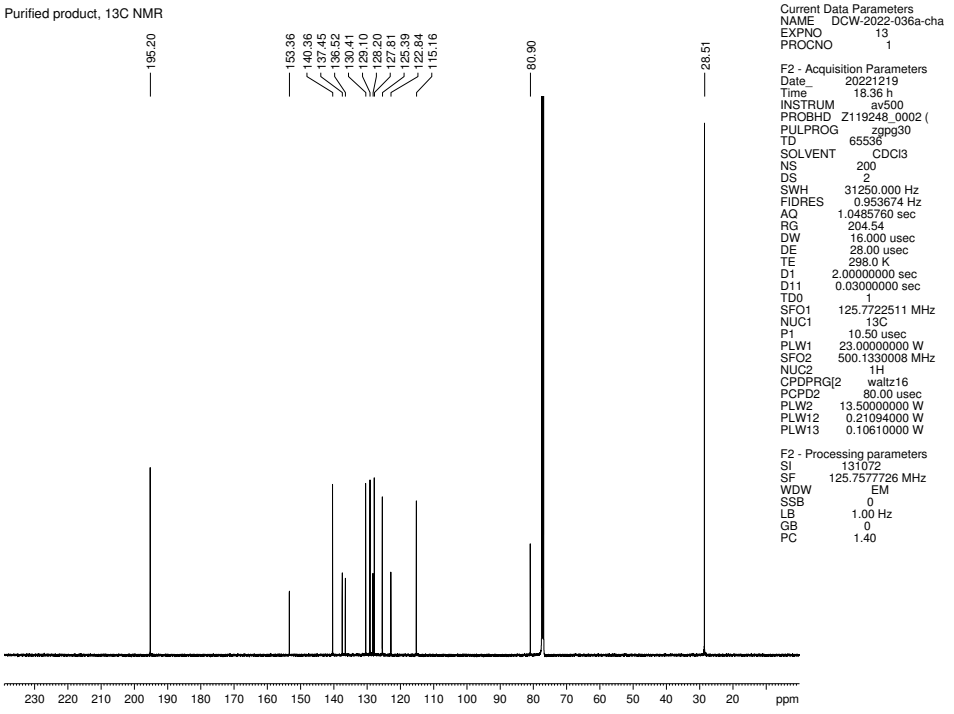

Figure 2.18. ^{13}C NMR (125 MHz, $CDCl_3$) of compound **2.54**.

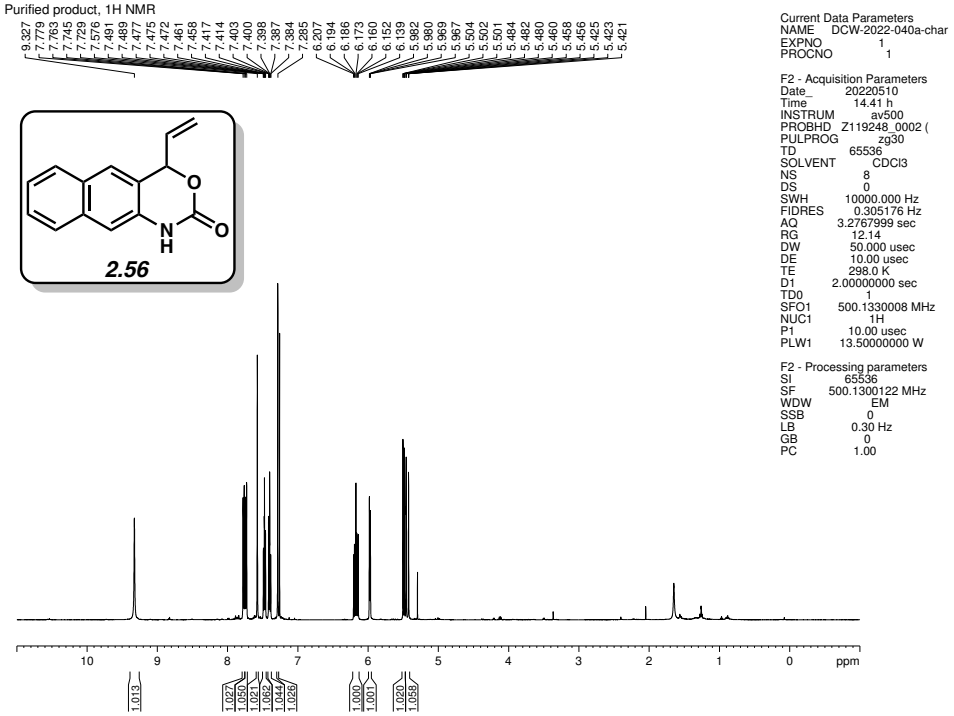

Figure 2.19. ^{1}H NMR (500 MHz, $CDCl_3$) of compound **2.56**.

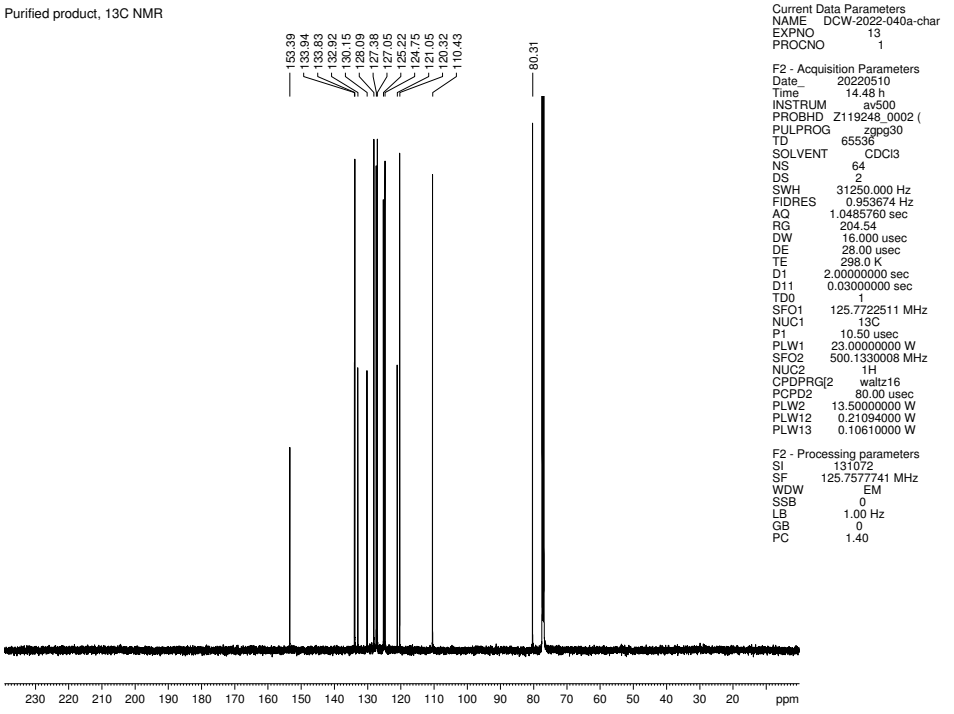

Figure 2.20. ^{13}C NMR (125 MHz, $CDCl_3$) of compound **2.56**.

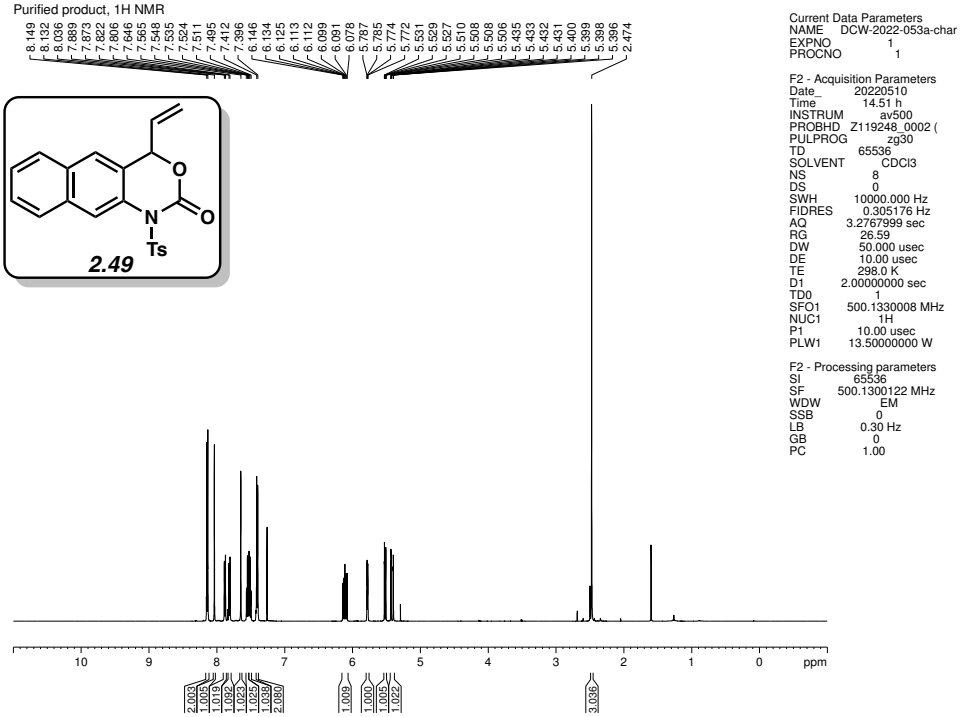

Figure 2.21. ^{1}H NMR (500 MHz, $CDCl_3$) of compound **2.49**.

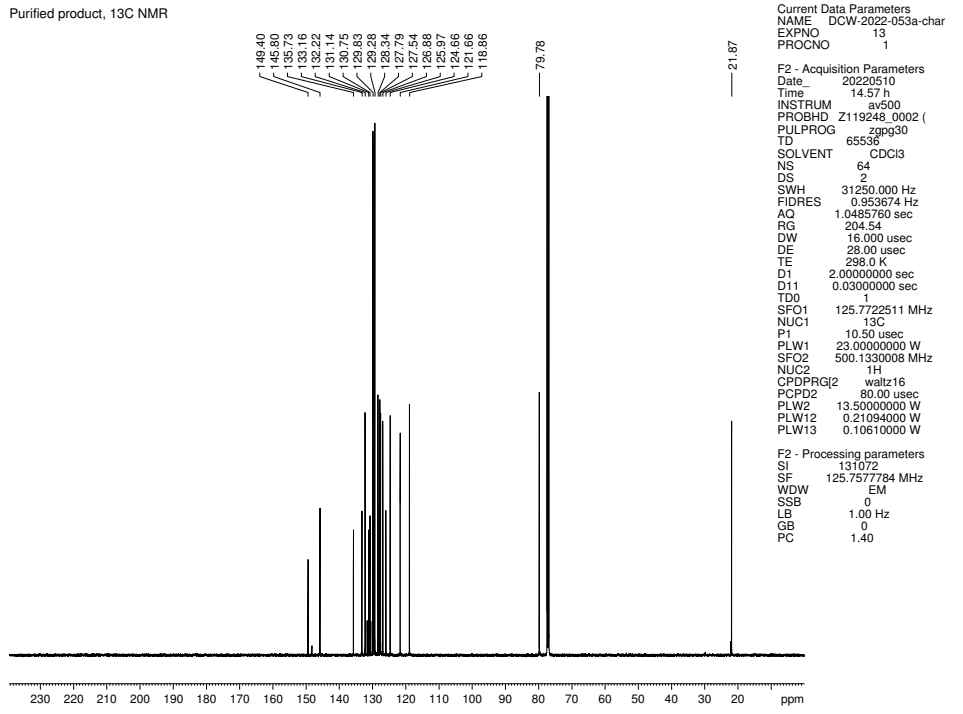

Figure 2.22. ^{13}C NMR (125 MHz, $CDCl_3$) of compound **2.49**.

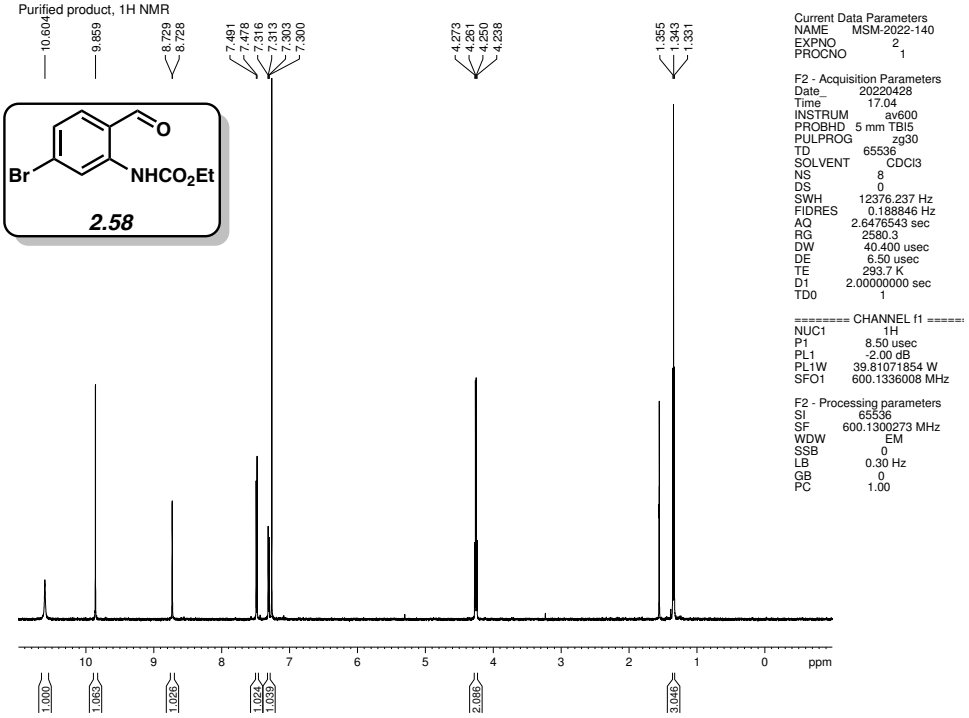

Figure 2.23. ^{1}H NMR (600 MHz, $CDCl_3$) of compound **2.58**.

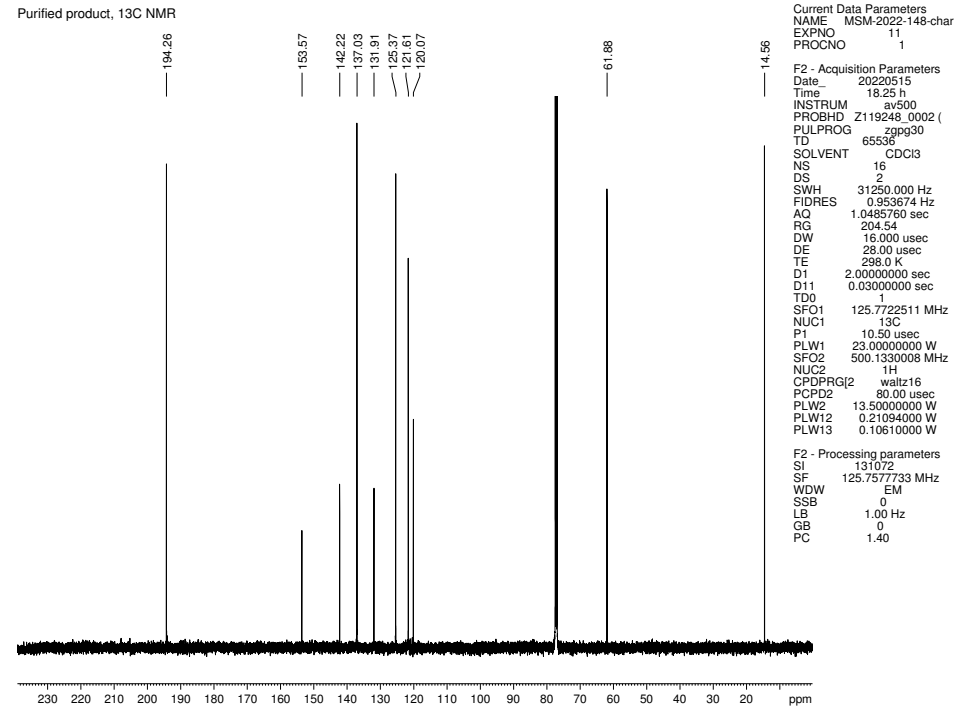

Figure 2.24. ^{13}C NMR (125 MHz, $CDCl_3$) of compound **2.58**.

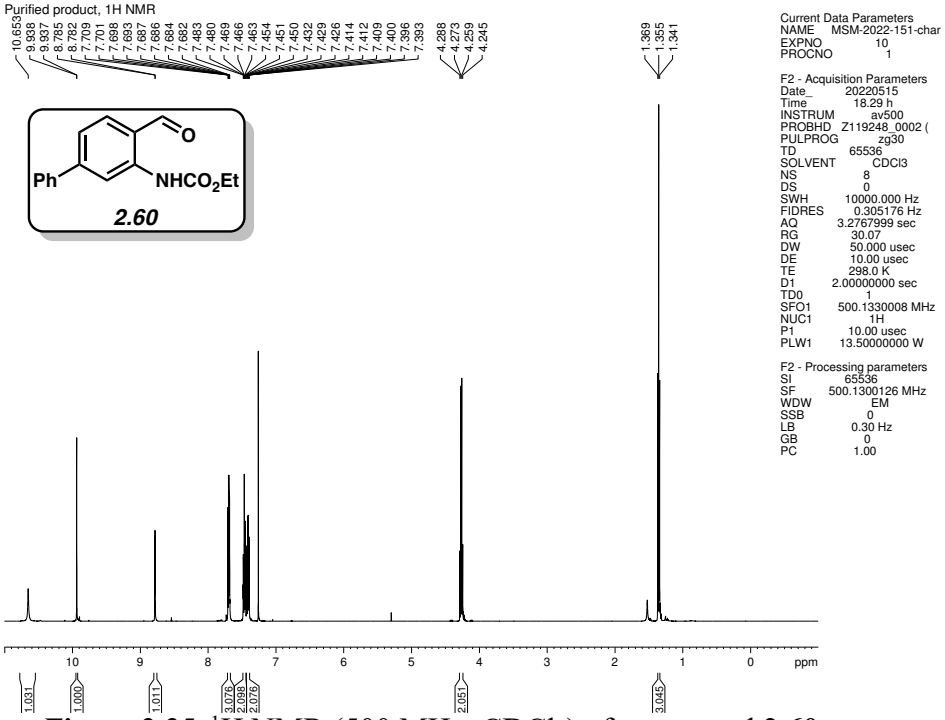

Figure 2.25. ^{1}H NMR (500 MHz, $CDCl_3$) of compound **2.60**.

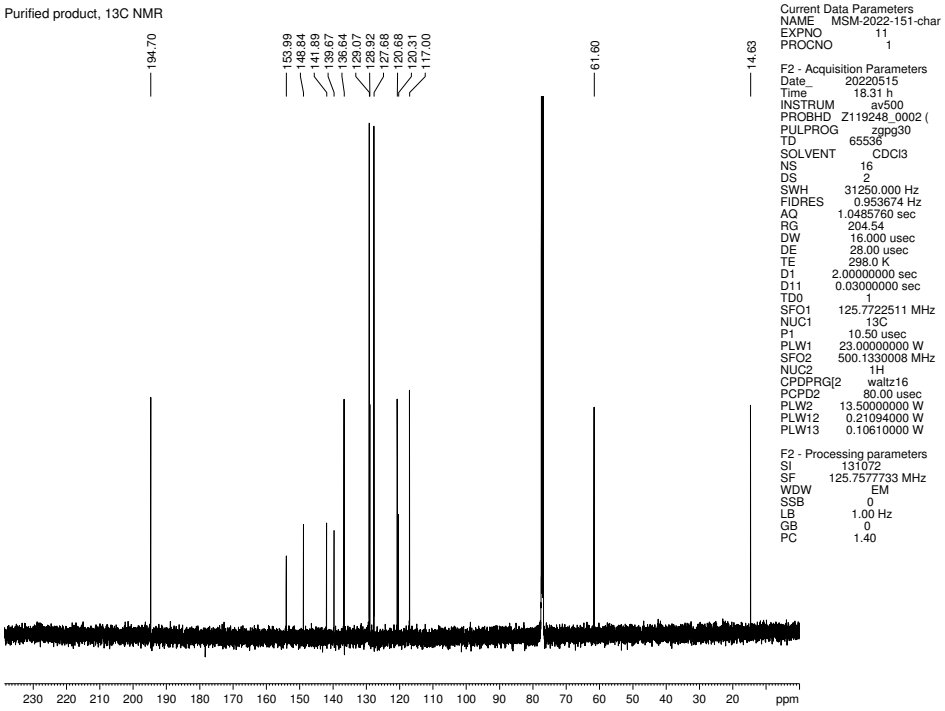

Figure 2.26. ^{13}C NMR (125 MHz, $CDCl_3$) of compound **2.60**.

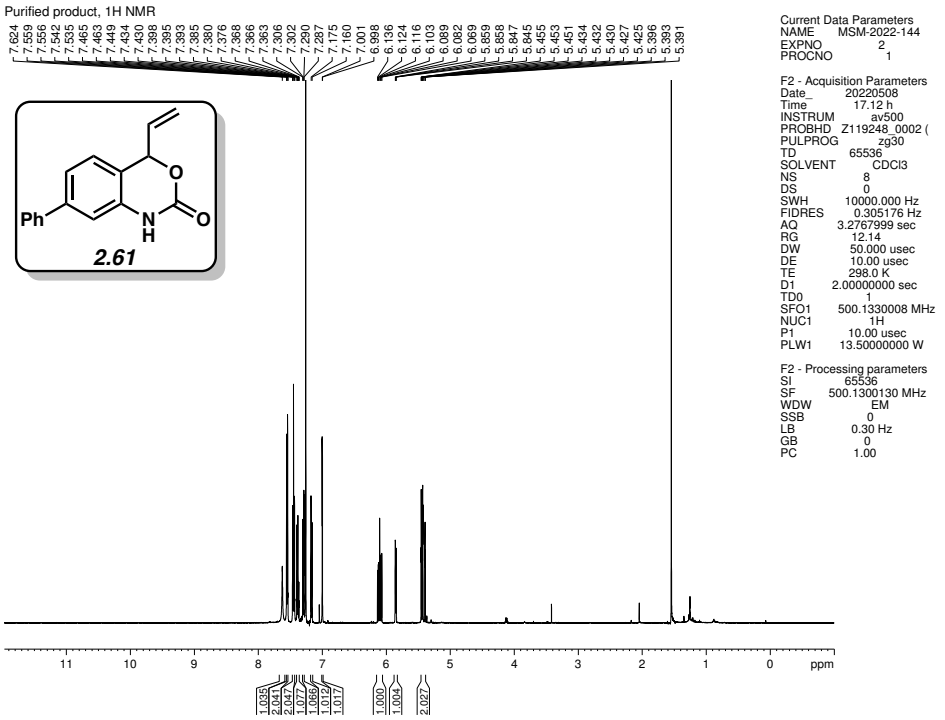

Figure 2.27. ^{1}H NMR (500 MHz, $CDCl_3$) of compound **2.61**.

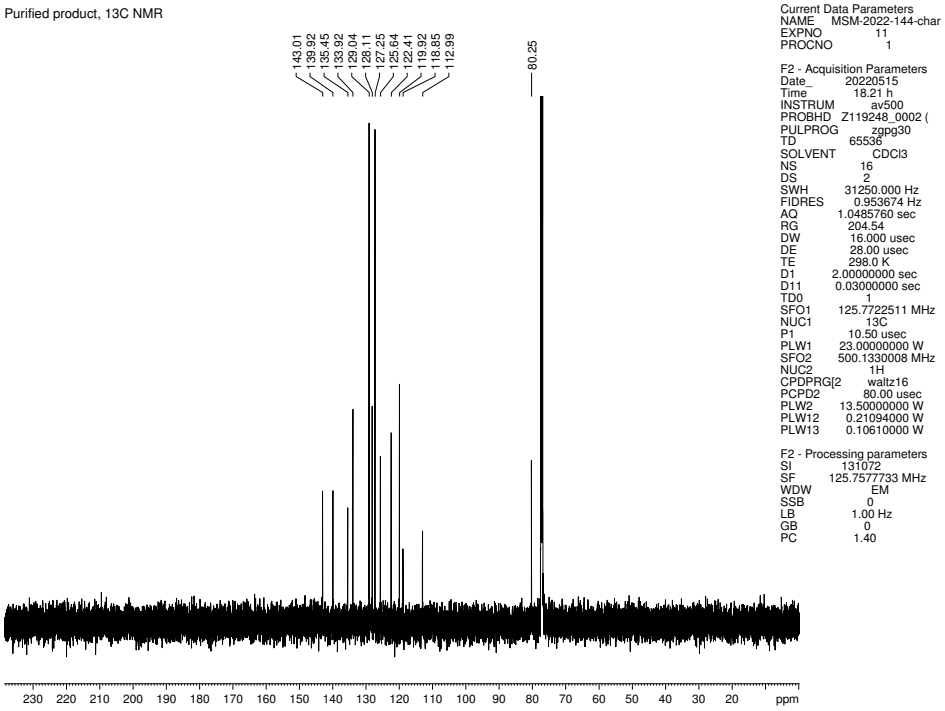

Figure 2.28. ^{13}C NMR (125 MHz, $CDCl_3$) of compound **2.61**.

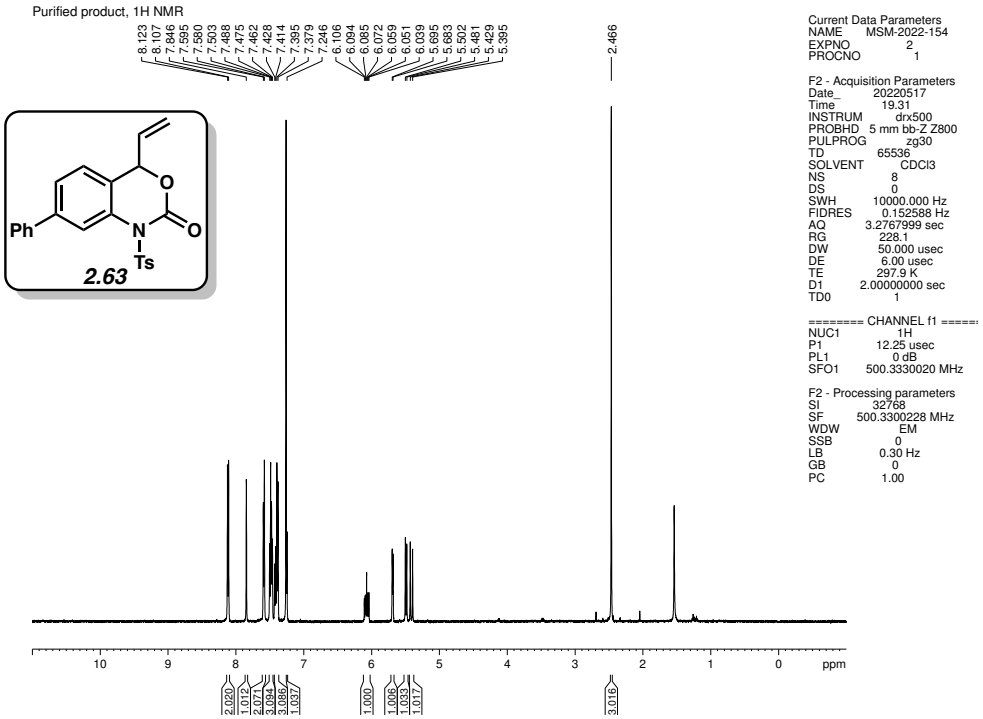

Figure 2.29. ^{1}H NMR (500 MHz, $CDCl_3$) of compound **2.63**.

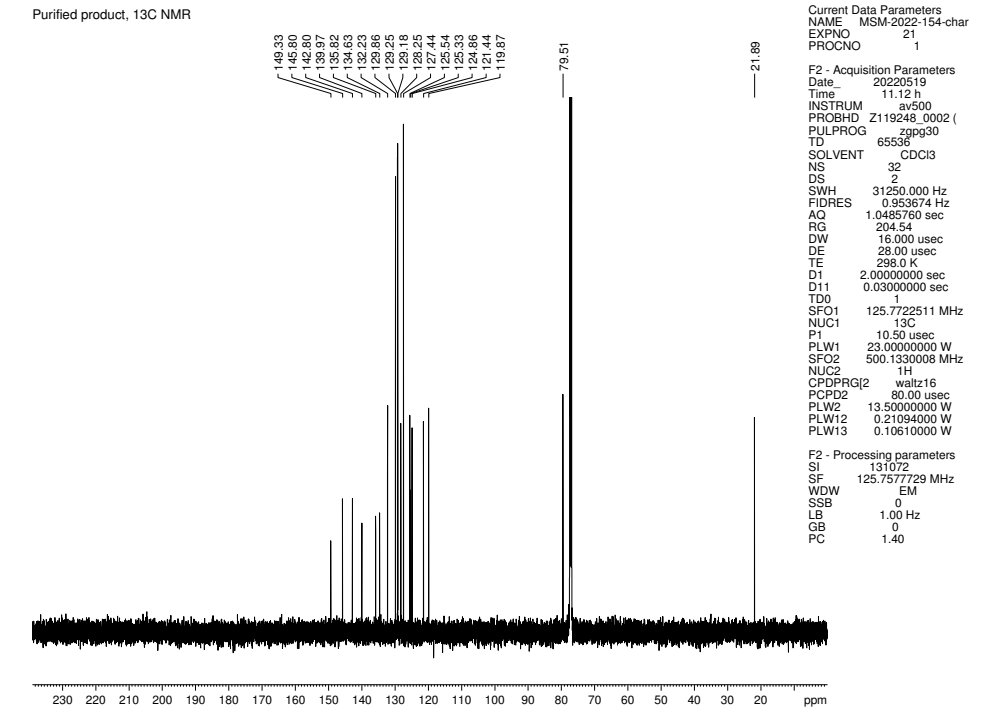

Figure 2.30. ^{13}C NMR (125 MHz, $CDCl_3$) of compound **2.63**.

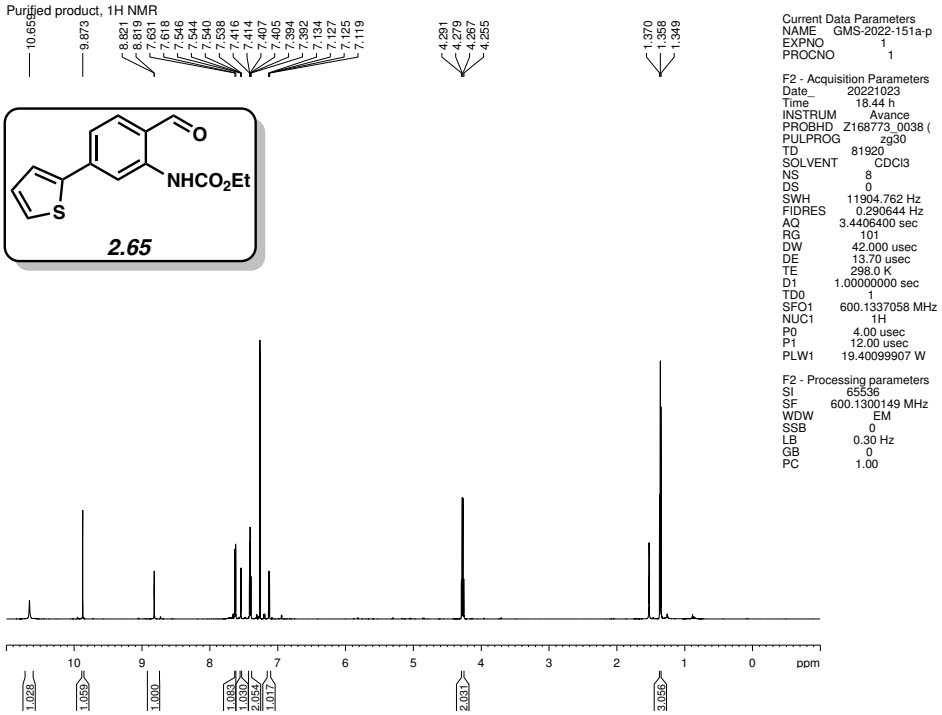

Figure 2.31. ^{1}H NMR (600 MHz, $CDCl_3$) of compound **2.65**.

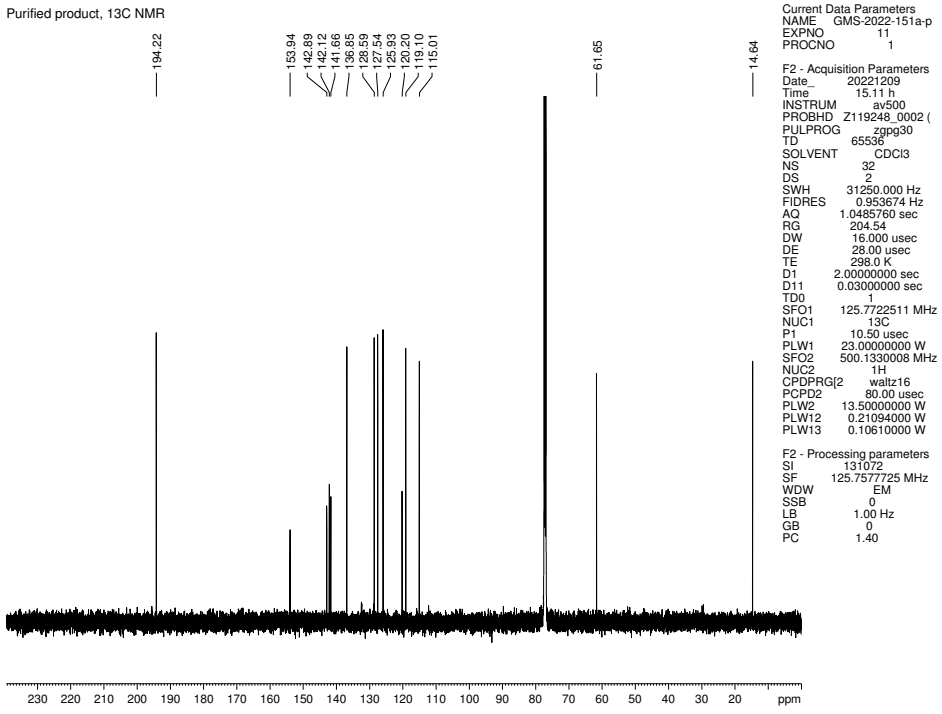

Figure 2.32. ^{13}C NMR (125 MHz, $CDCl_3$) of compound **2.65**.

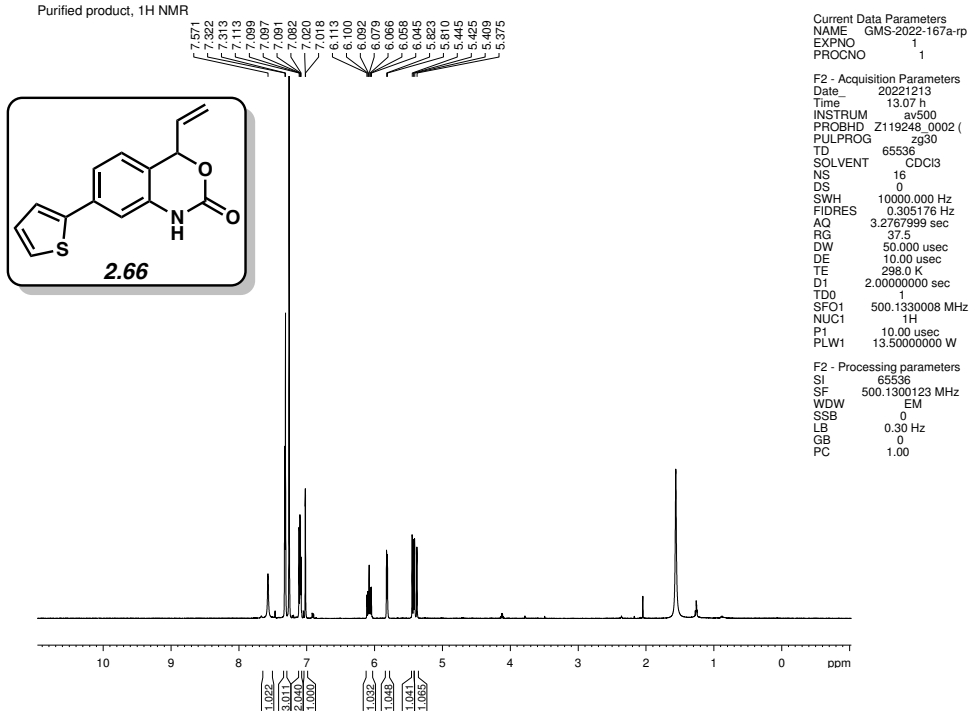

Figure 2.33. ^{1}H NMR (500 MHz, $CDCl_3$) of compound **2.66**.

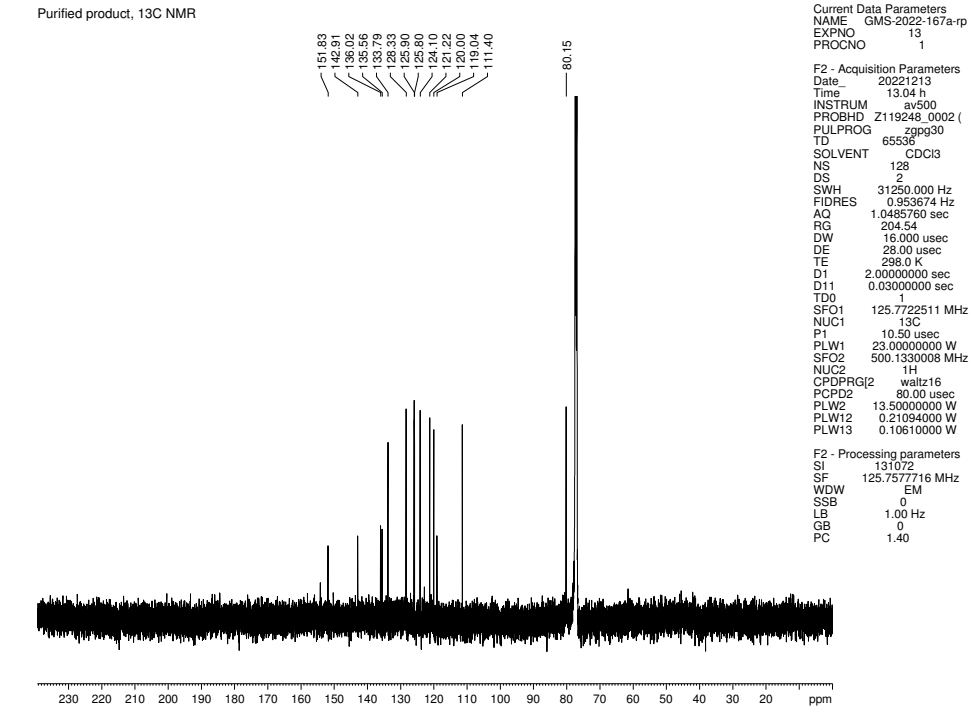

Figure 2.34. ^{13}C NMR (125 MHz, $CDCl_3$) of compound **2.66**.

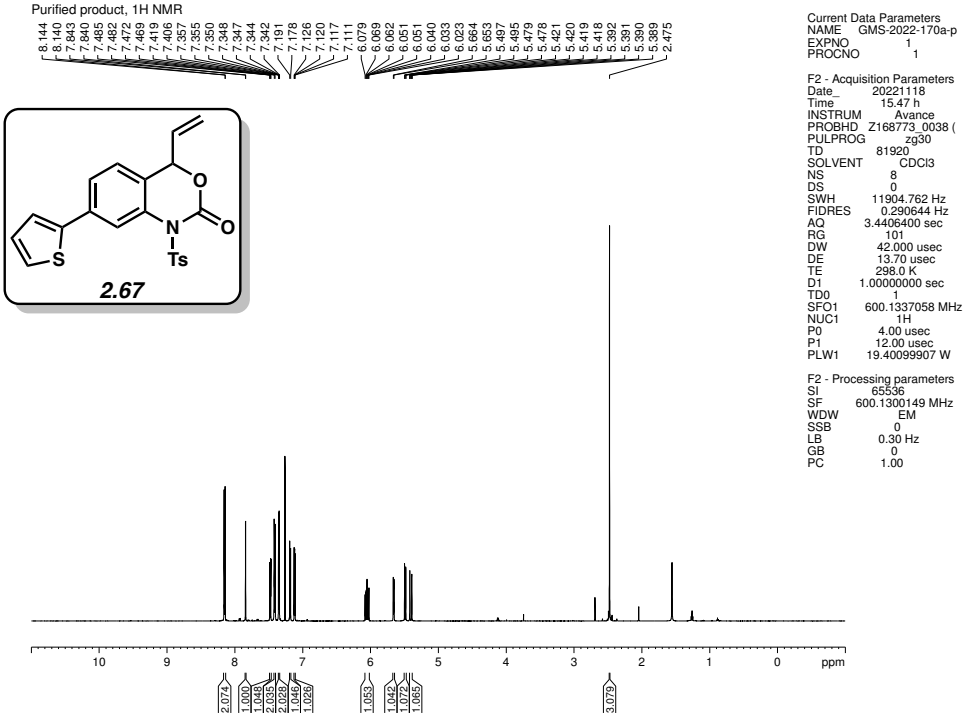

Figure 2.35. ^{1}H NMR (600 MHz, $CDCl_3$) of compound **2.67**.

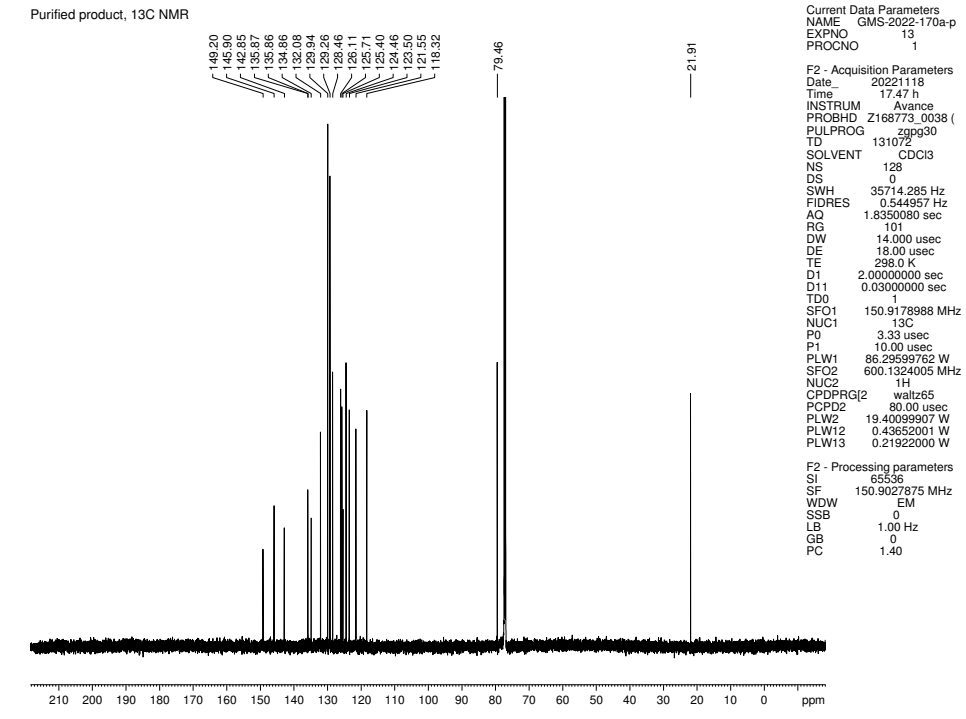

Figure 2.36. ^{13}C NMR (150 MHz, $CDCl_3$) of compound **2.67**.

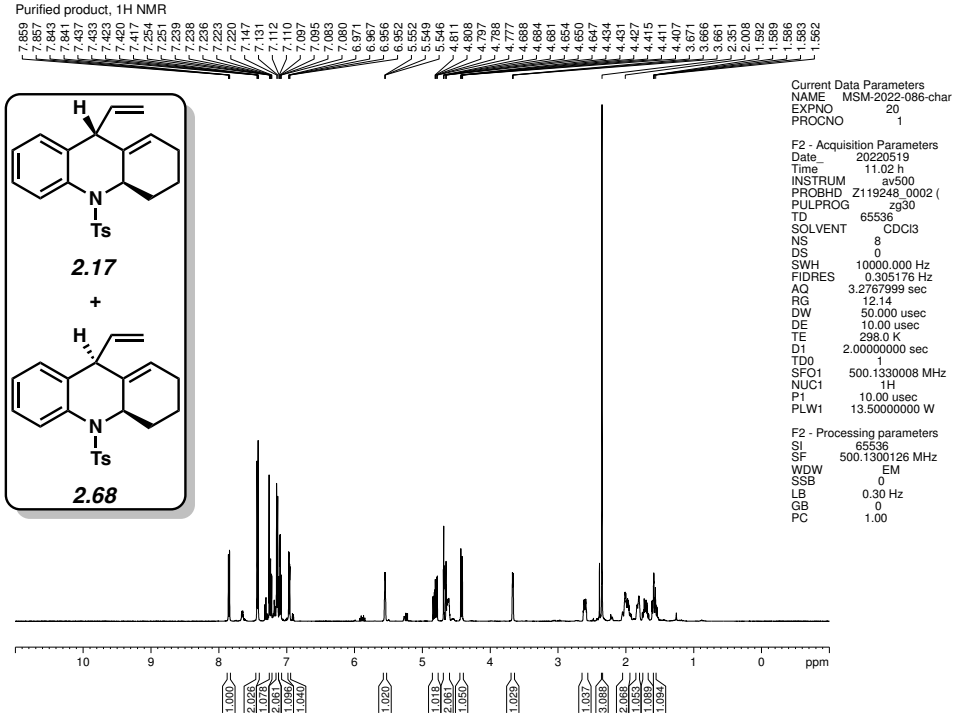

Figure 2.37. ^{1}H NMR (500 MHz, $CDCl_3$) of compounds **2.17** and **2.68**.

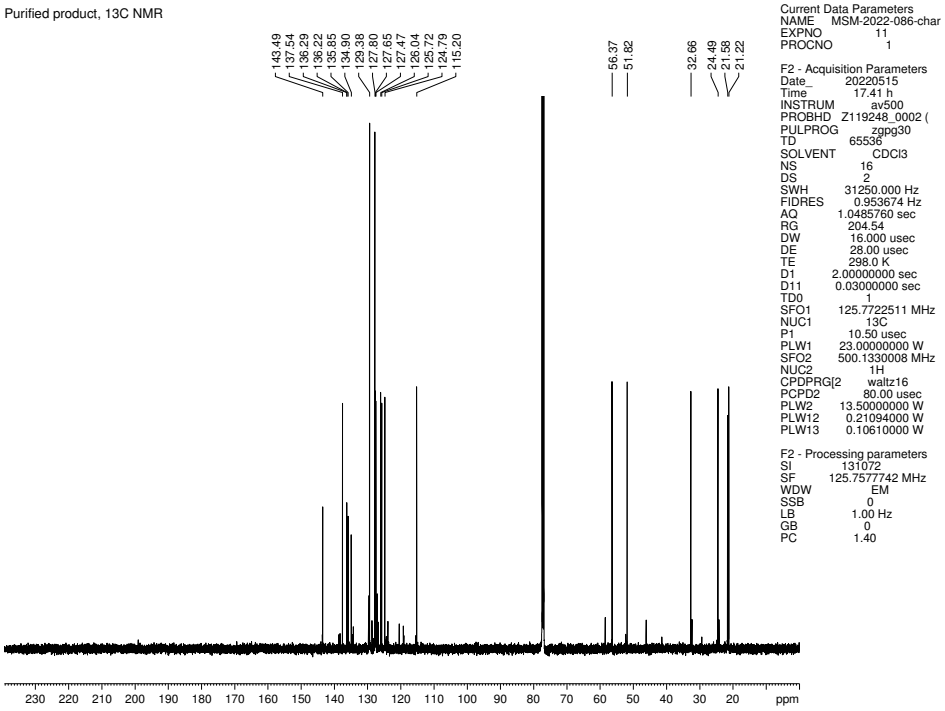

Figure 2.38. ^{13}C NMR (125 MHz, $CDCl_3$) of compounds **2.17** and **2.68**.

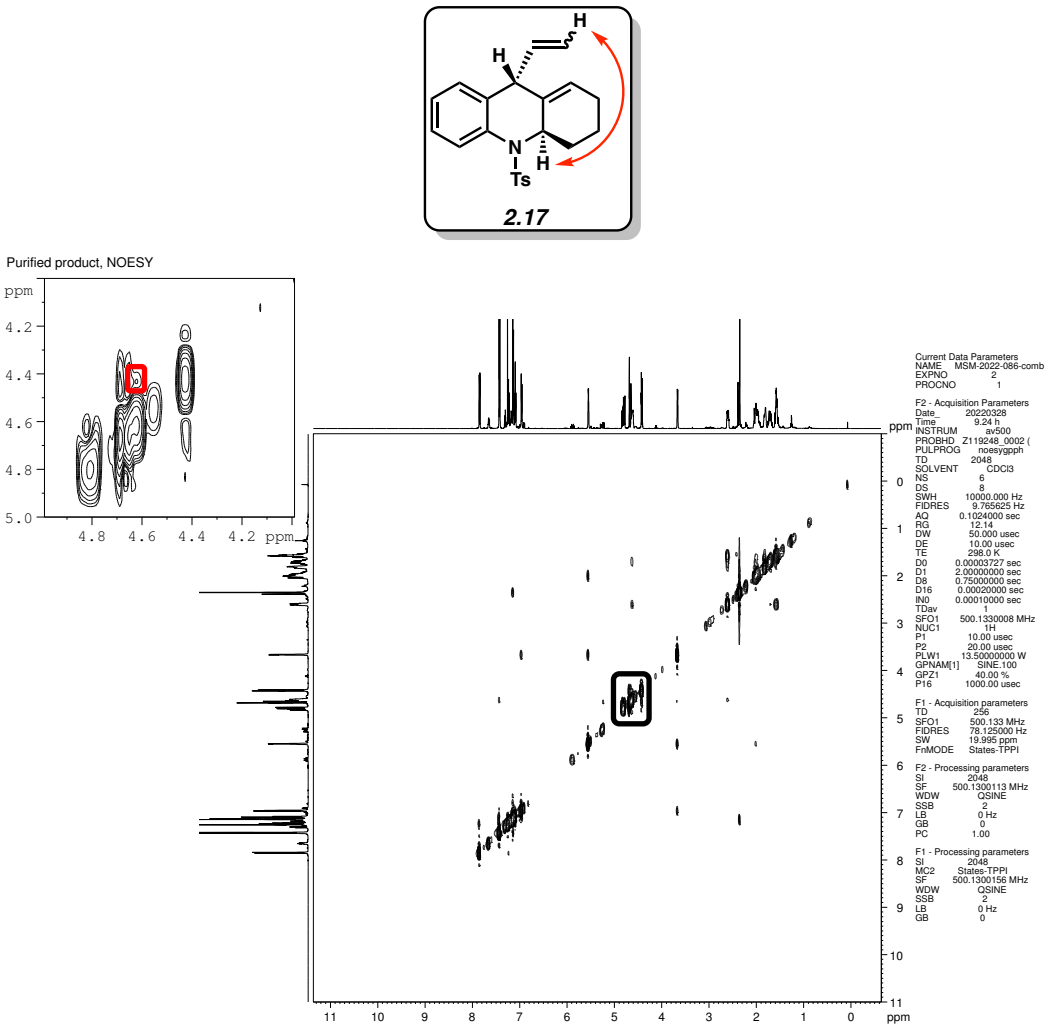

Figure 2.39. NOESY (500 MHz, $CDCl_3$) of compound **2.17**.

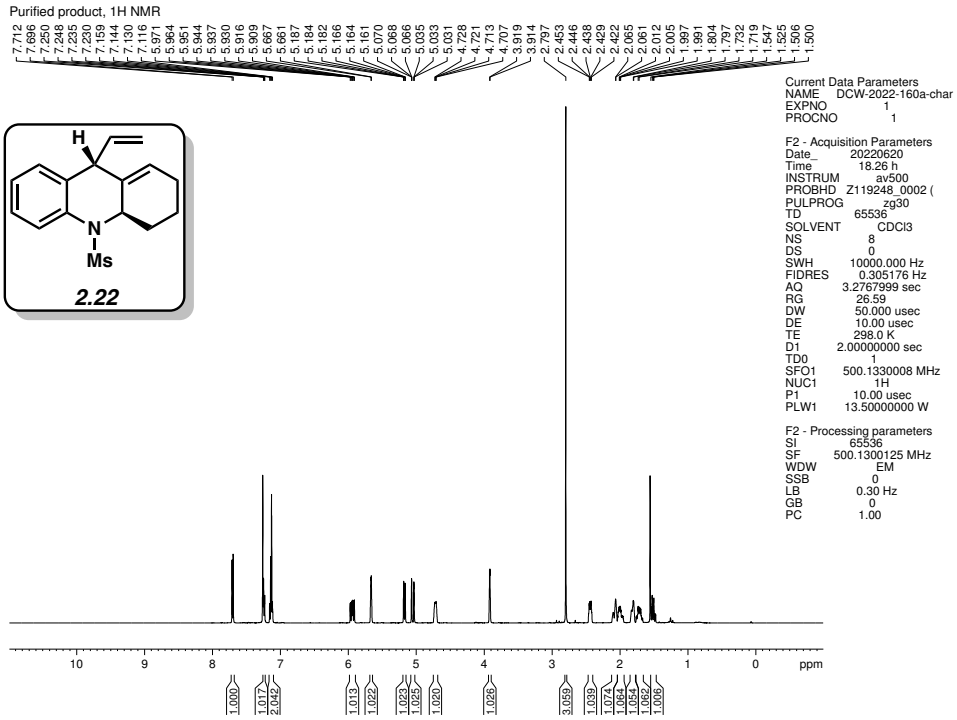

Figure 2.40. ^{1}H NMR (500 MHz, $CDCl_3$) of compound **2.22**.

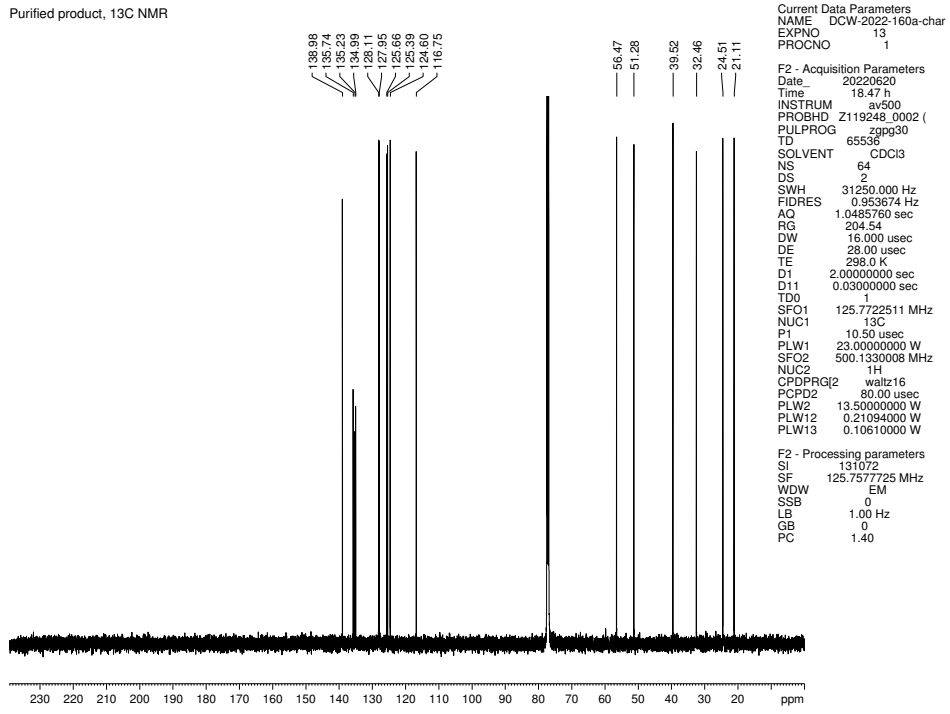

Figure 2.41. ^{13}C NMR (125 MHz, $CDCl_3$) of compound **2.22**.

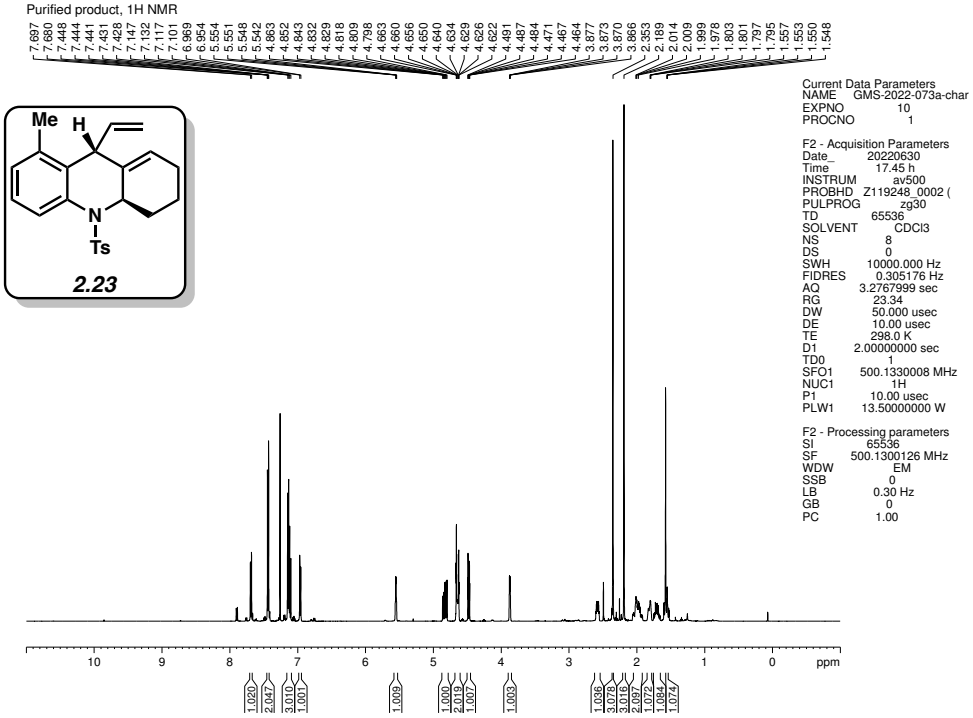

Figure 2.42. ^{1}H NMR (500 MHz, $CDCl_3$) of compound **2.23**.

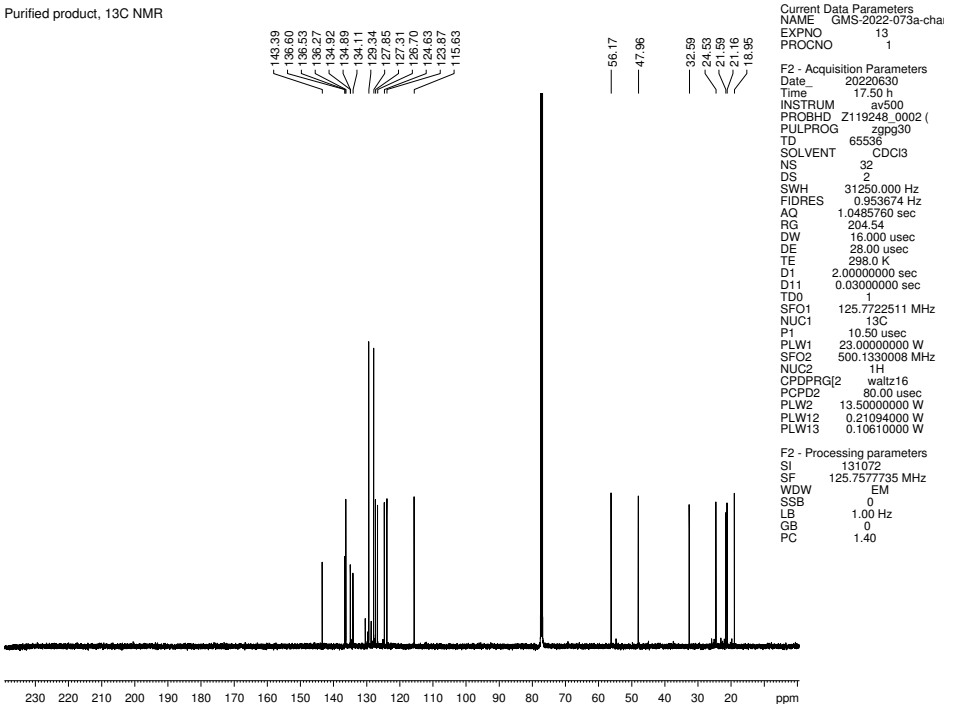

Figure 2.43. ^{13}C NMR (125 MHz, $CDCl_3$) of compound **2.23**.

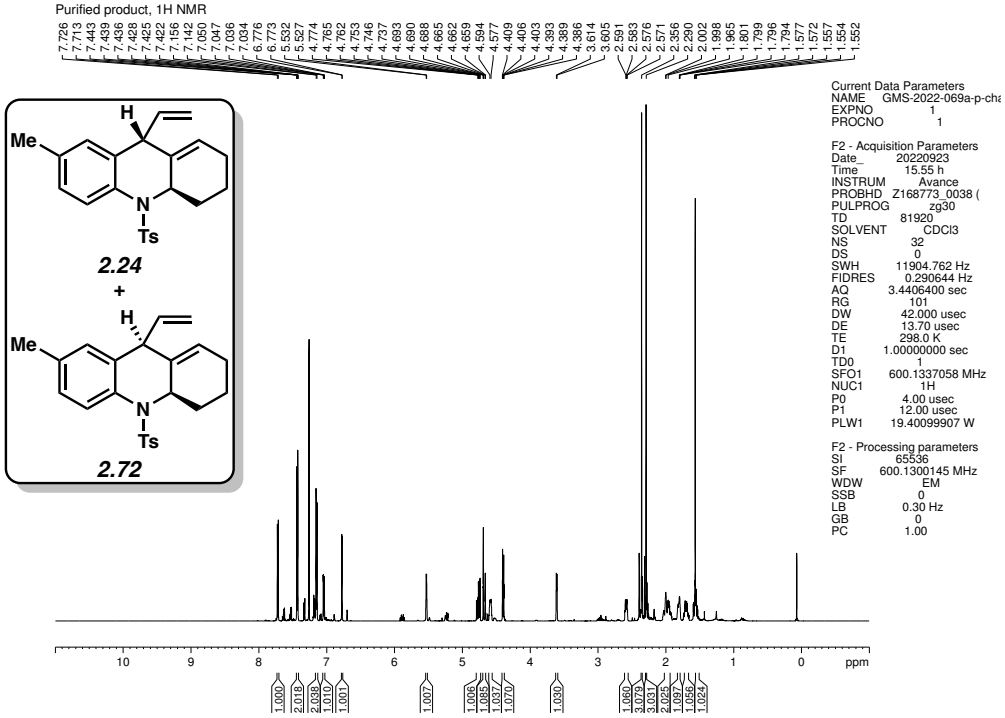

Figure 2.44. ^{1}H NMR (600 MHz, $CDCl_3$) of compounds **2.24** and **2.72**.

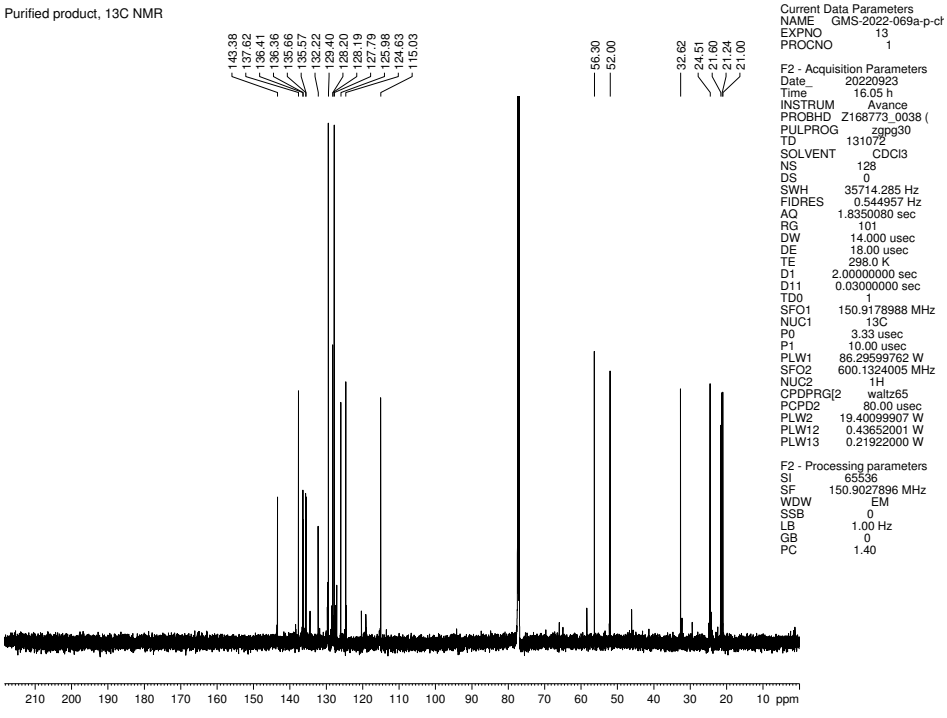

Figure 2.45. ^{13}C NMR (150 MHz, $CDCl_3$) of compounds **2.24** and **2.72**.

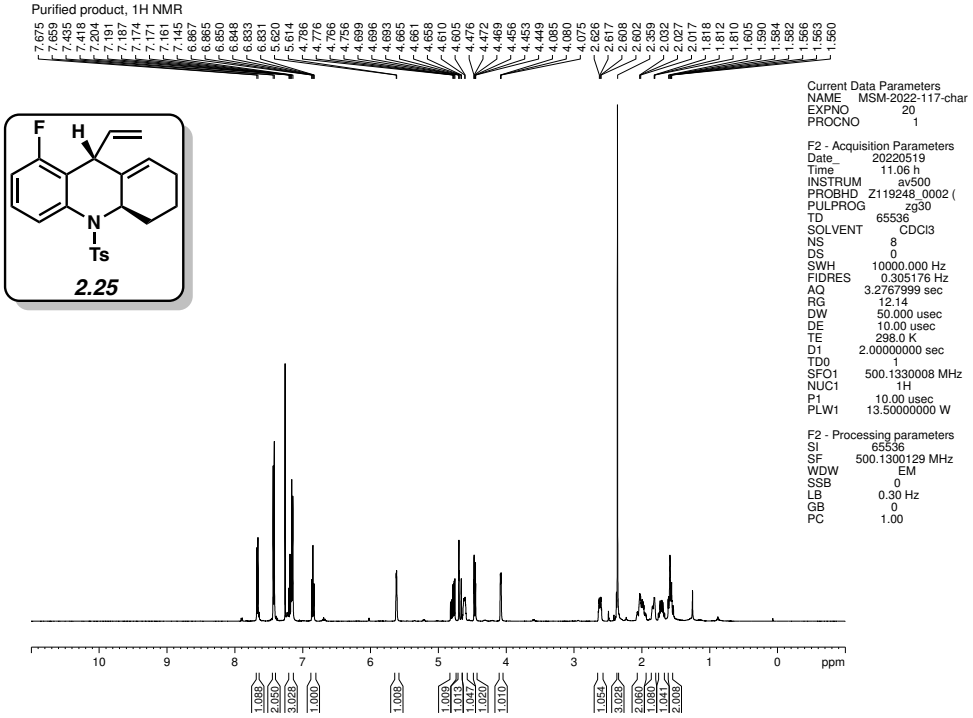

Figure 2.46. ^{1}H NMR (500 MHz, $CDCl_3$) of compound **2.25**.

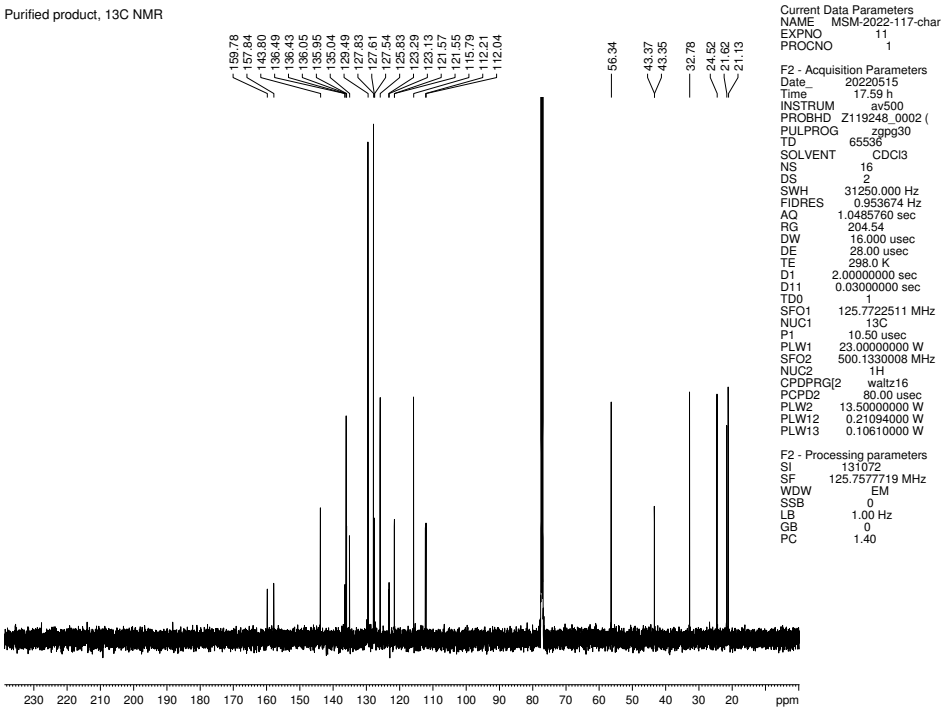

Figure 2.47. ^{13}C NMR (125 MHz, $CDCl_3$) of compound **2.25**.

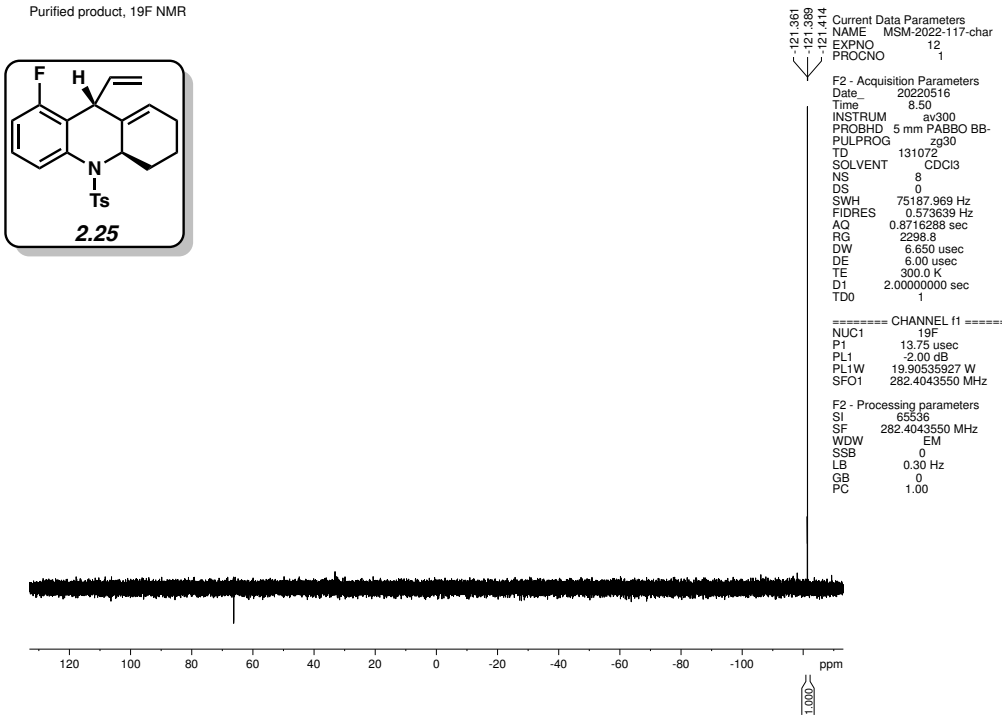

Figure 2.48. ^{19}F NMR (282 MHz, $CDCl_3$) of compound **2.25**.

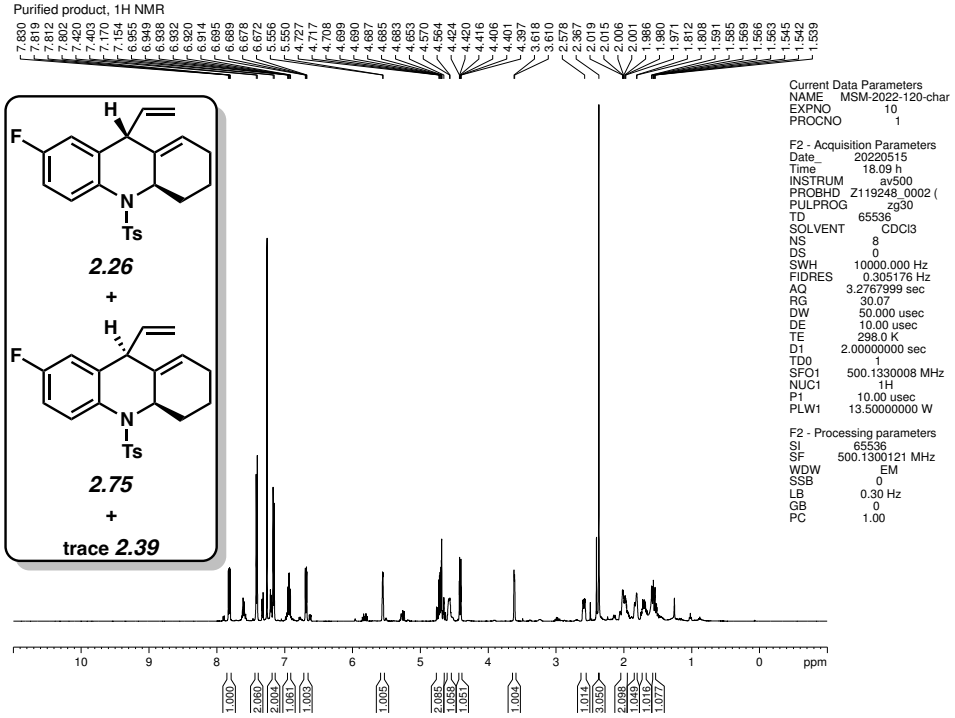

Figure 2.49. ^{1}H NMR (500 MHz, $CDCl_3$) of compounds **2.26**, **2.75**, and **2.39** (trace).

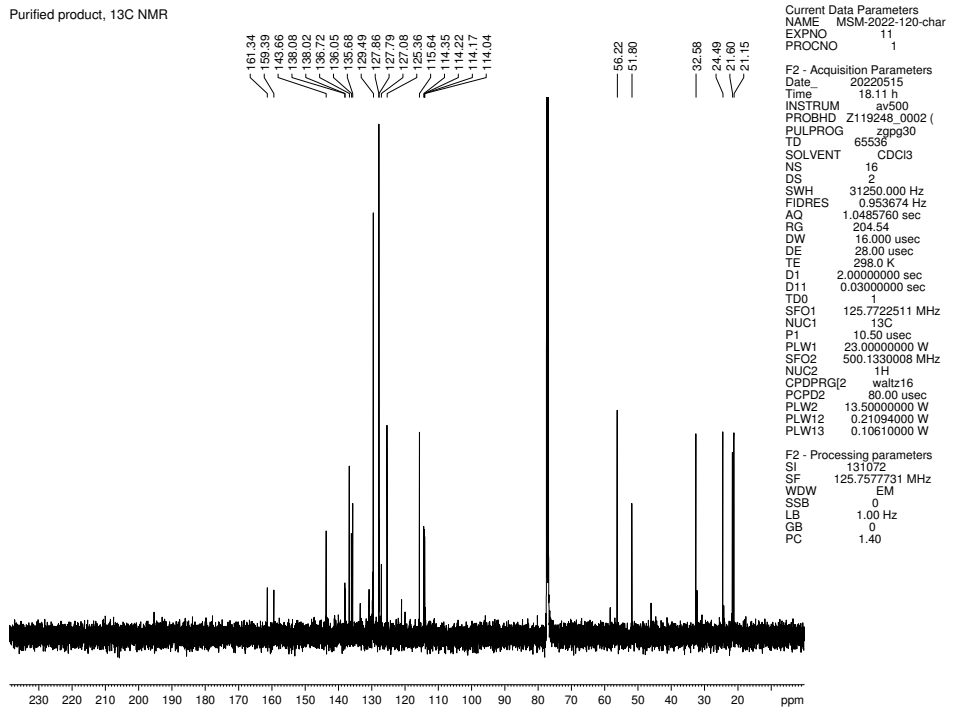

Figure 2.50. ^{13}C NMR (125 MHz, $CDCl_3$) of compounds **2.26**, **2.75**, and **2.39** (trace).

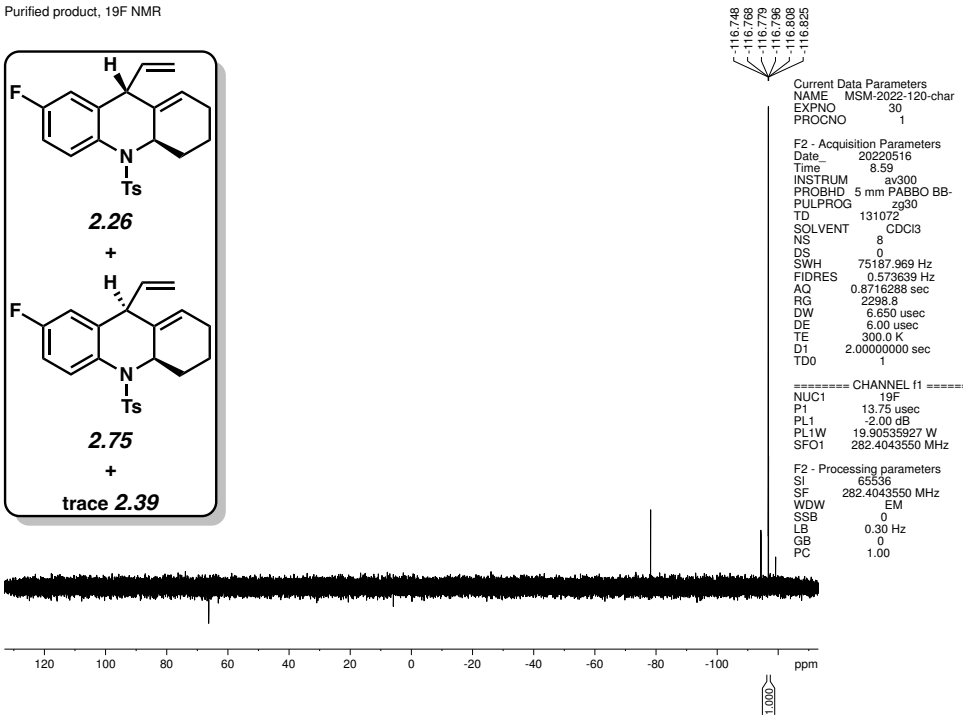

Figure 2.51. ^{19}F NMR (282 MHz, $CDCl_3$) of compounds **2.26**, **2.75**, and **2.39** (trace).

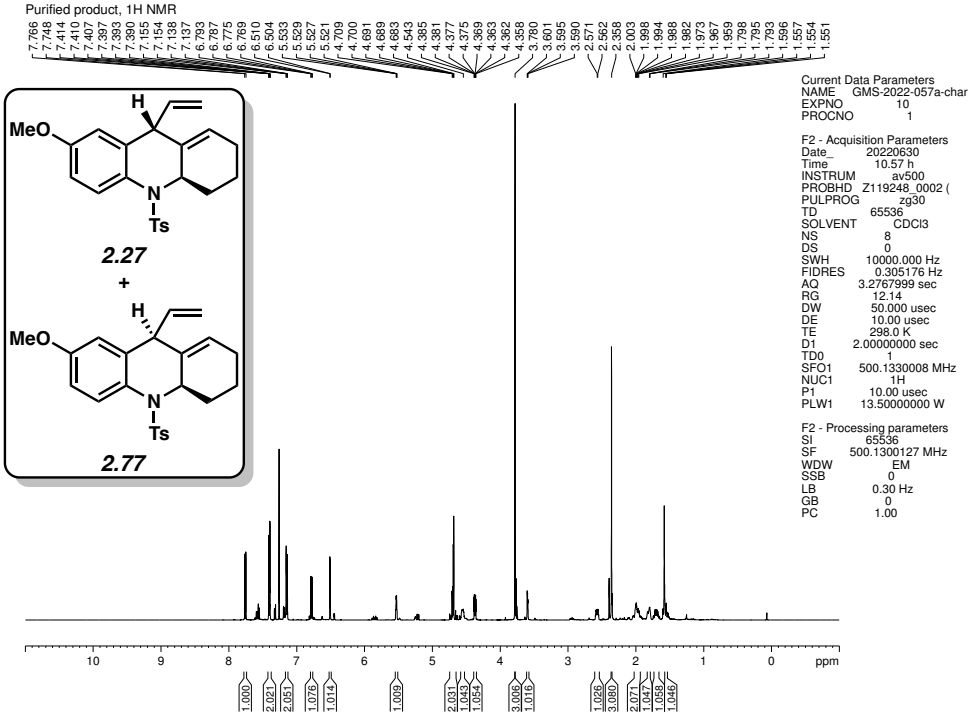

Figure 2.52. ^{1}H NMR (500 MHz, $CDCl_3$) of compounds **2.27** and **2.77**.

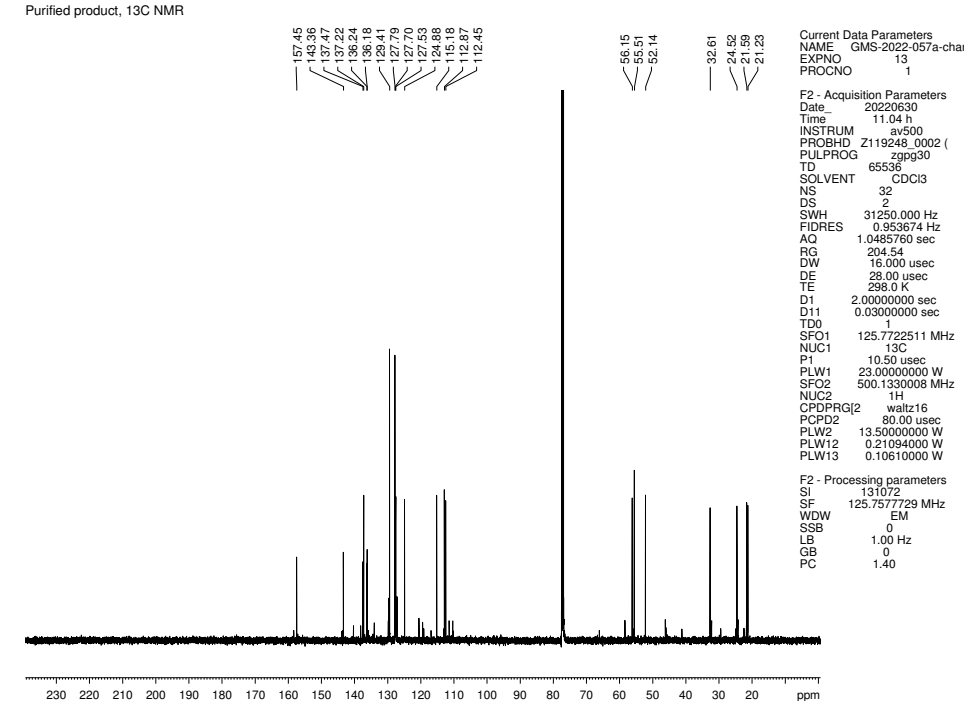

Figure 2.53. ^{13}C NMR (125 MHz, $CDCl_3$) of compounds **2.27** and **2.77**.

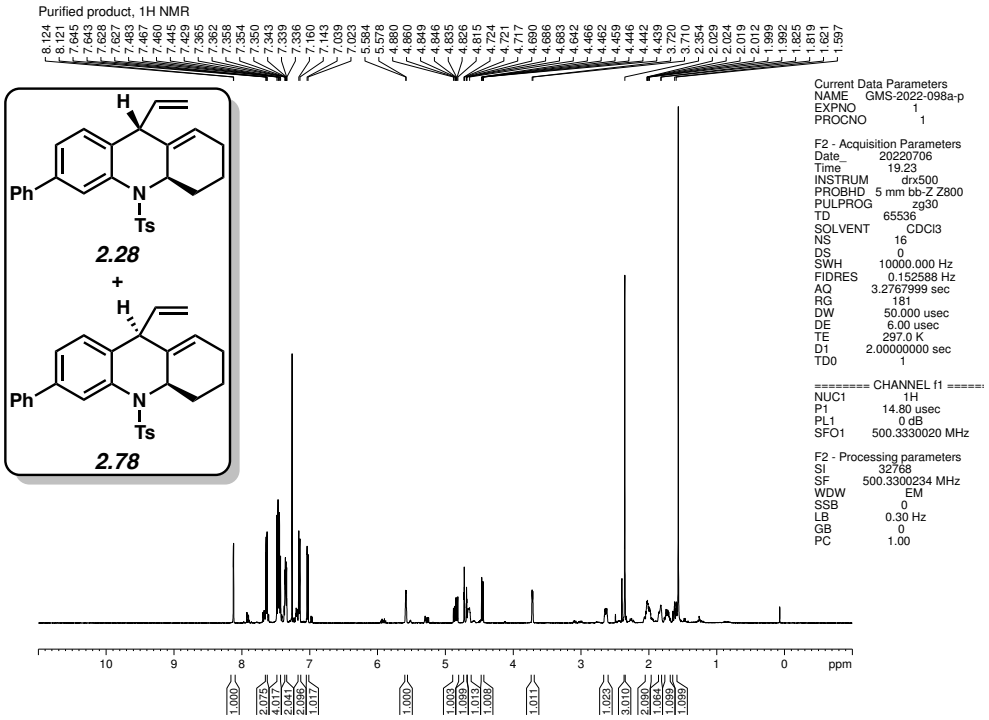

Figure 2.54. ^{1}H NMR (500 MHz, $CDCl_3$) of compounds **2.28** and **2.78**.

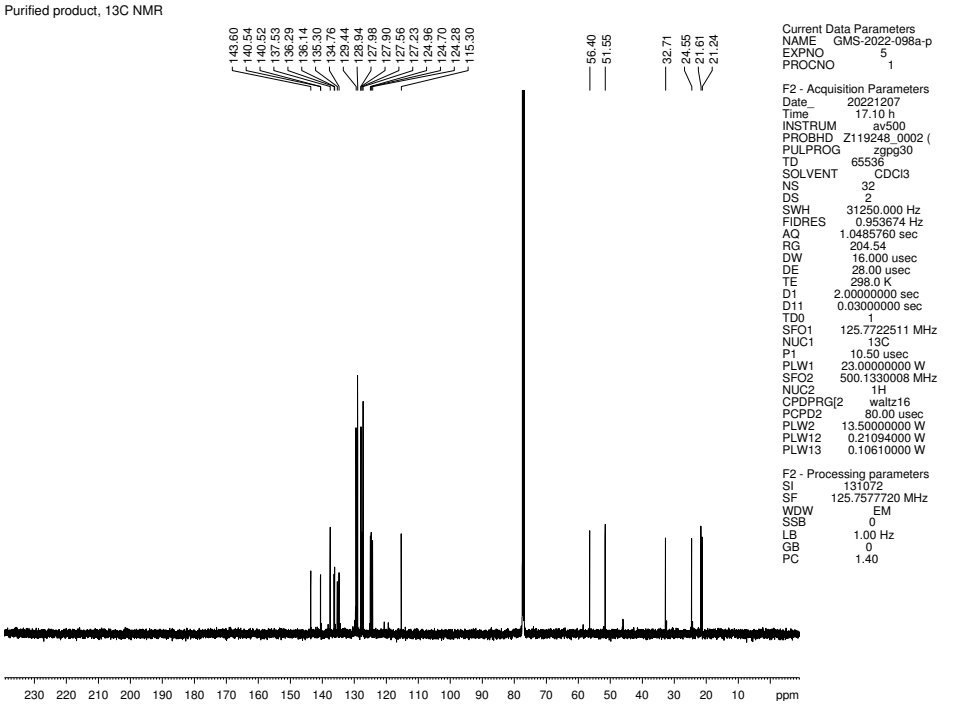

Figure 2.55. ^{13}C NMR (125 MHz, $CDCl_3$) of compounds **2.28** and **2.78**.

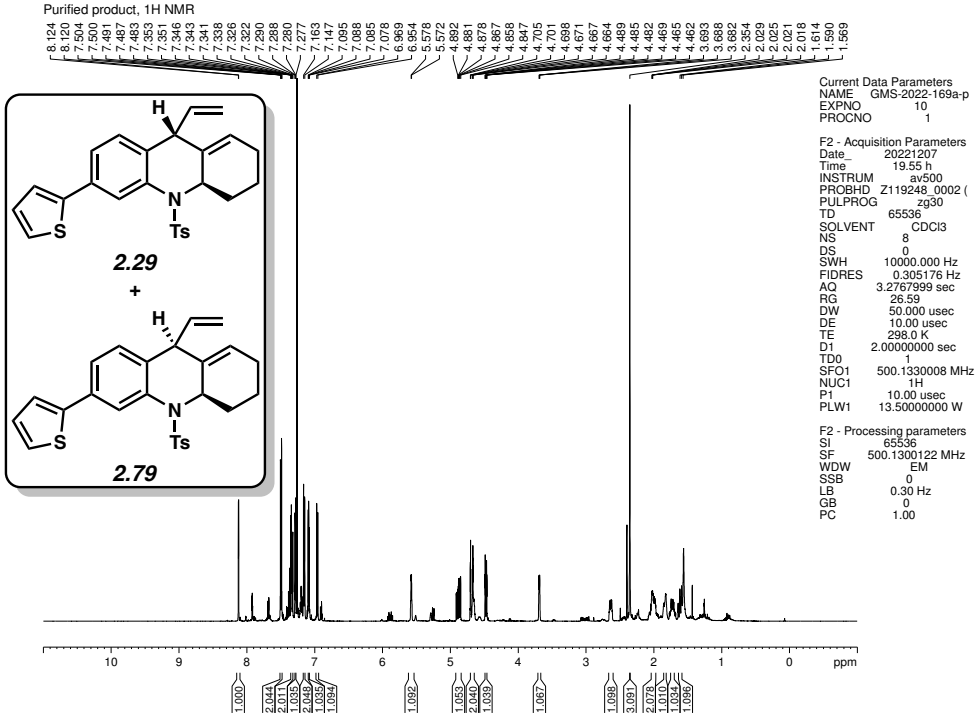

Figure 2.56. ^{1}H NMR (500 MHz, $CDCl_3$) of compounds **2.29** and **2.79**.

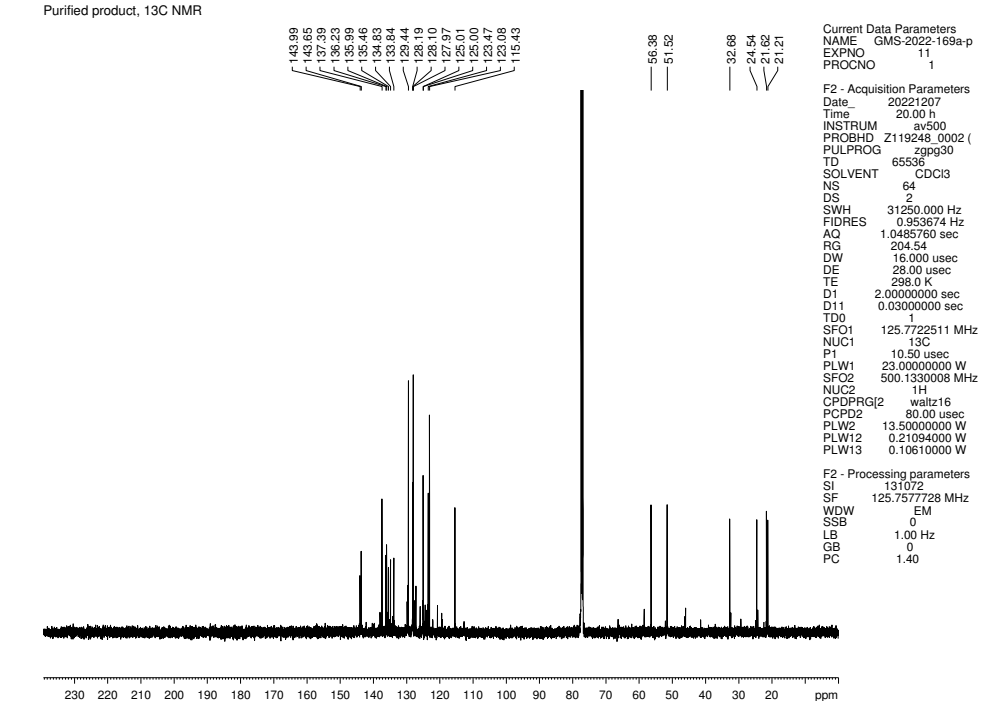

Figure 2.57. ^{13}C NMR (125 MHz, $CDCl_3$) of compounds **2.29** and **2.79**.

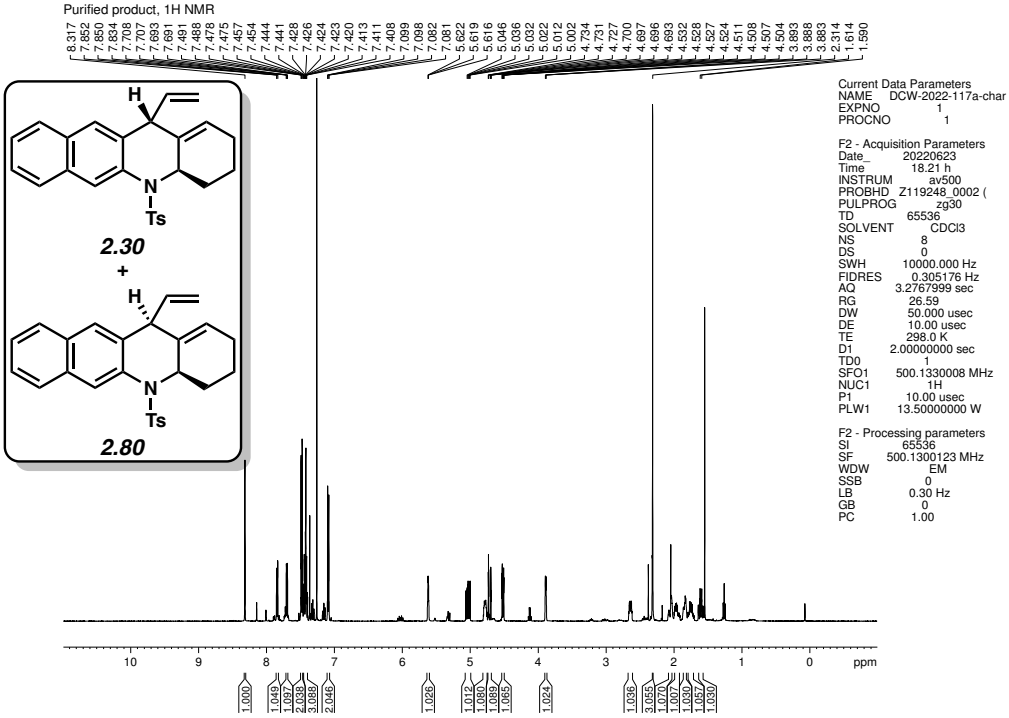

Figure 2.58. ^{1}H NMR (500 MHz, $CDCl_3$) of compounds **2.30** and **2.80**.

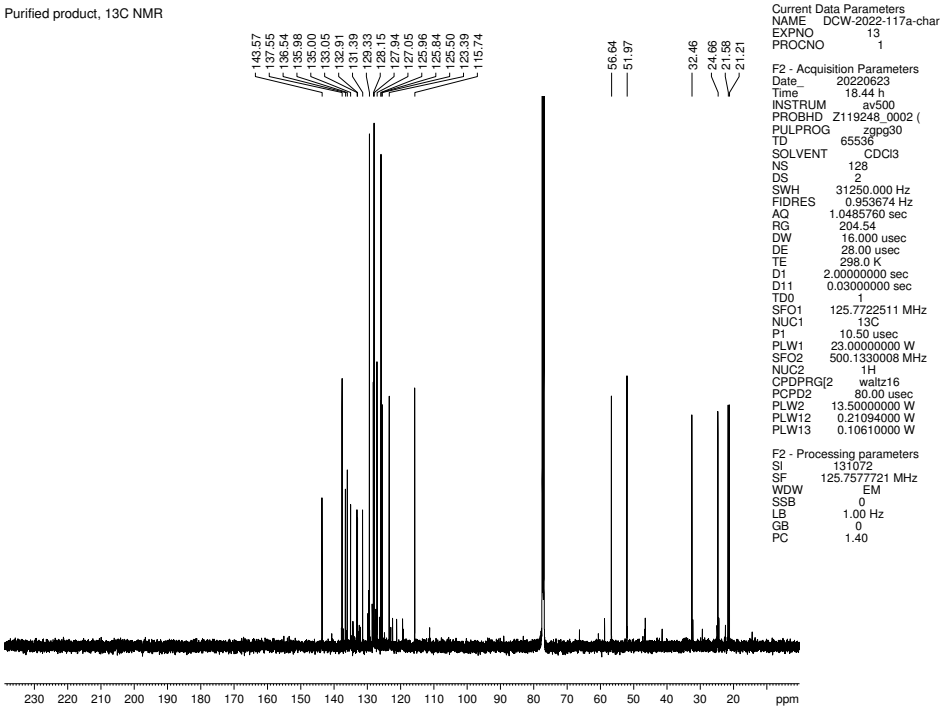

Figure 2.59. ^{13}C NMR (125 MHz, $CDCl_3$) of compounds **2.30** and **2.80**.

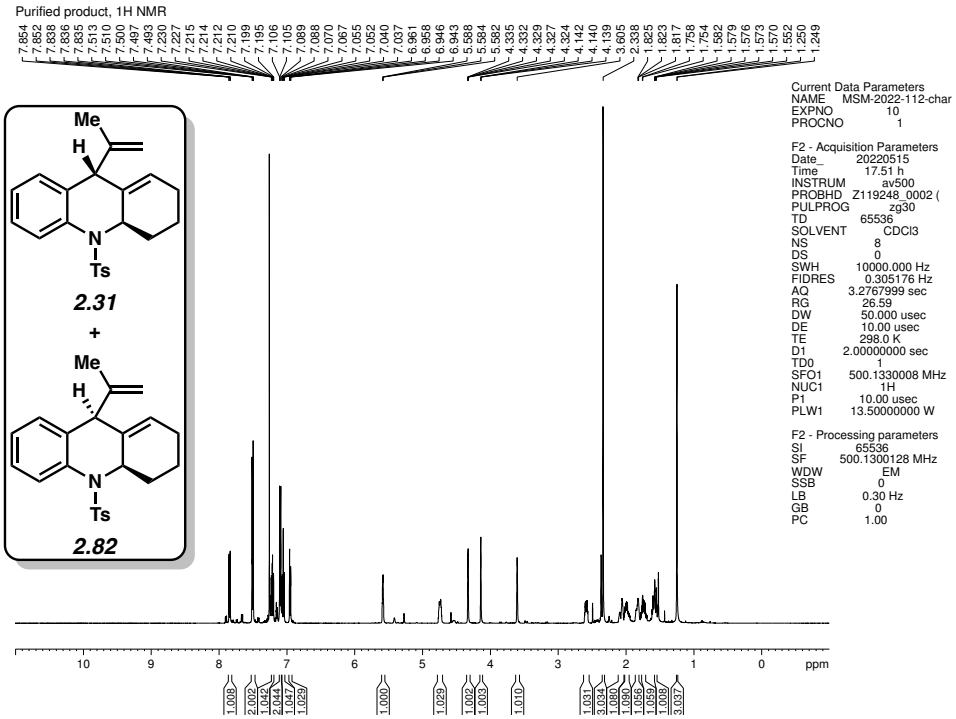

Figure 2.60. ^{1}H NMR (500 MHz, $CDCl_3$) of compounds **2.31** and **2.82**.

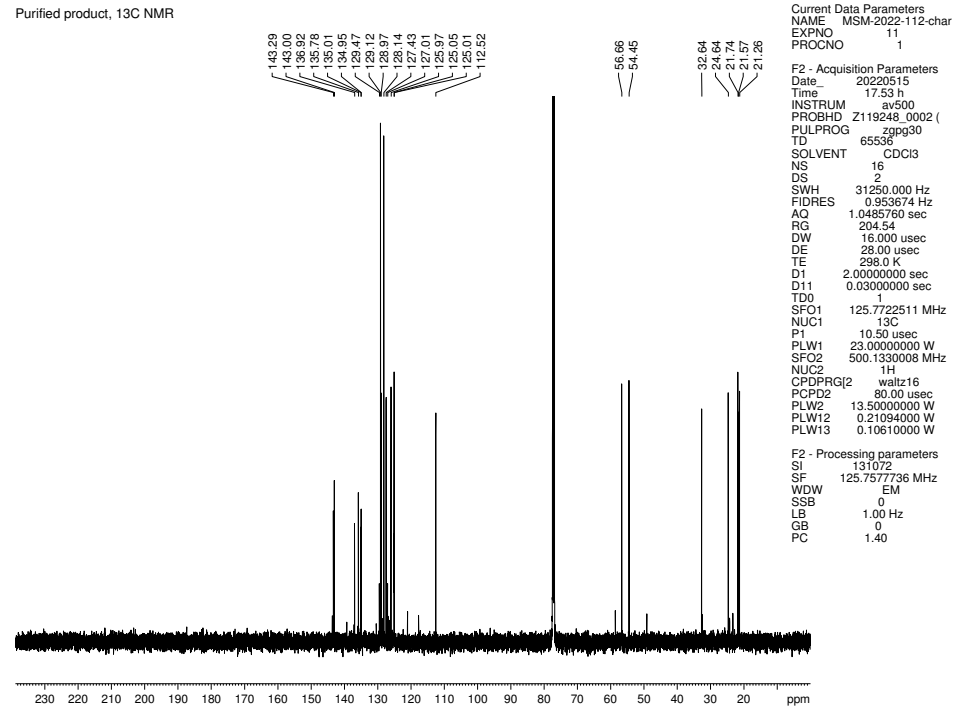

Figure 2.61. ^{13}C NMR (125 MHz, $CDCl_3$) of compounds **2.31** and **2.82**.

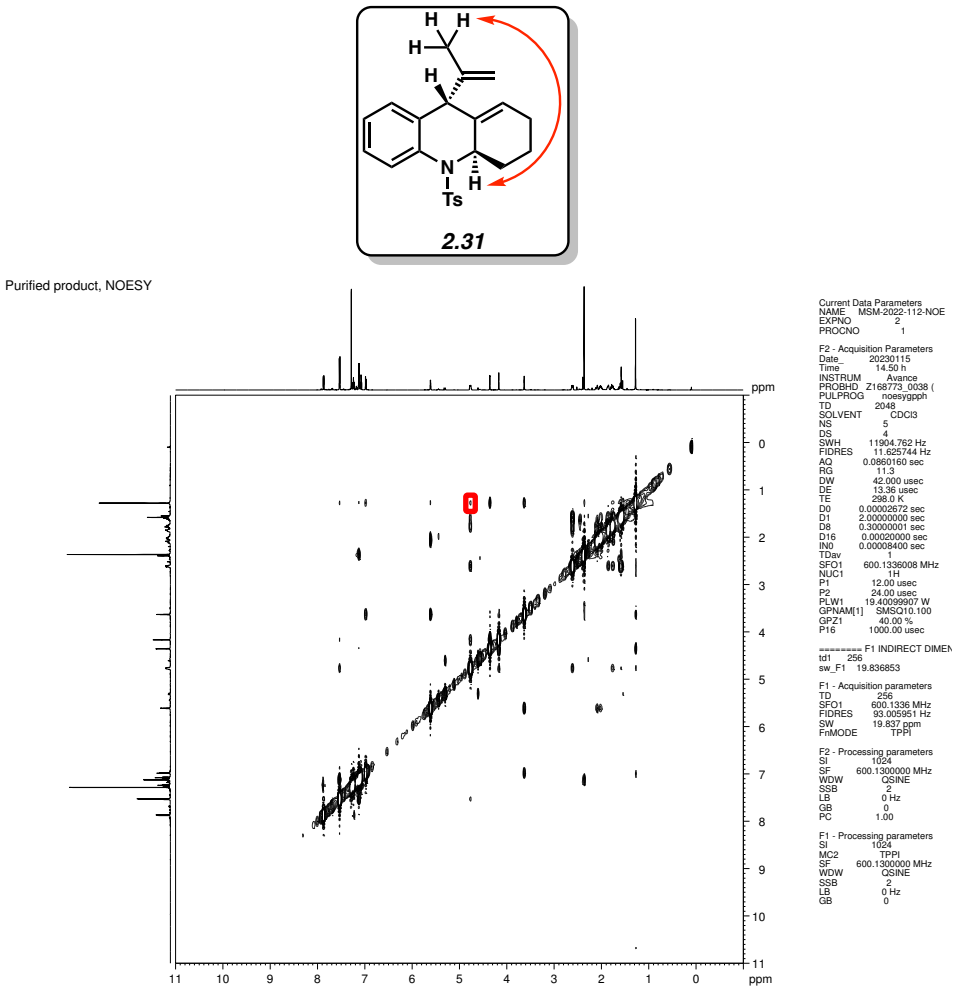

Figure 2.62. NOESY (600 MHz, $CDCl_3$) of compound **2.31**.

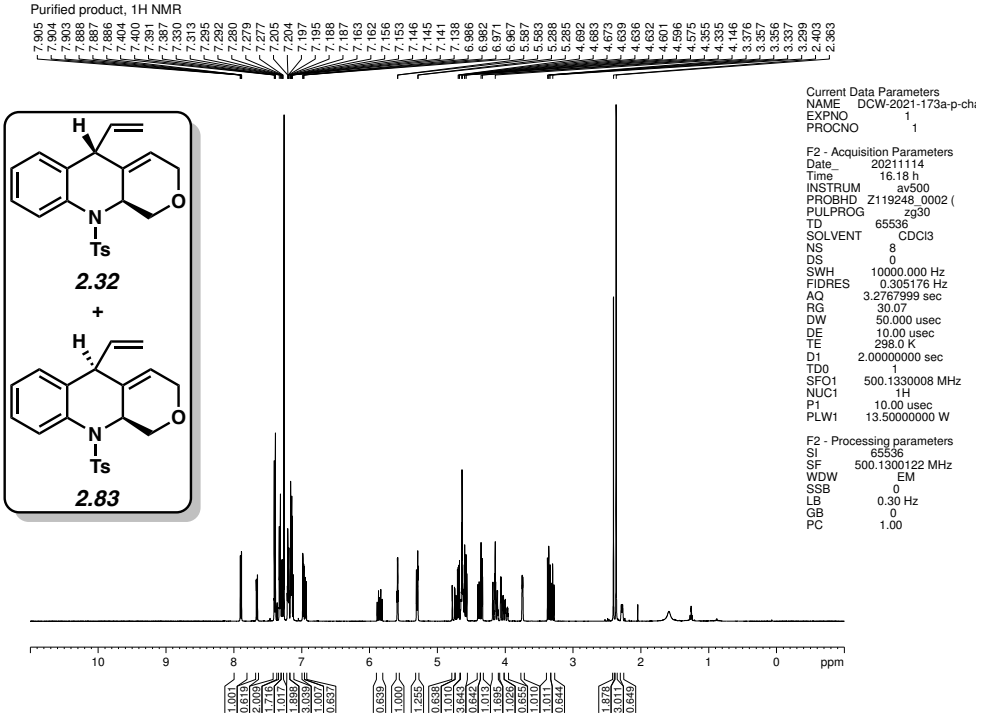

Figure 2.63. ^{1}H NMR (500 MHz, $CDCl_3$) of compounds **2.32** and **2.83**.

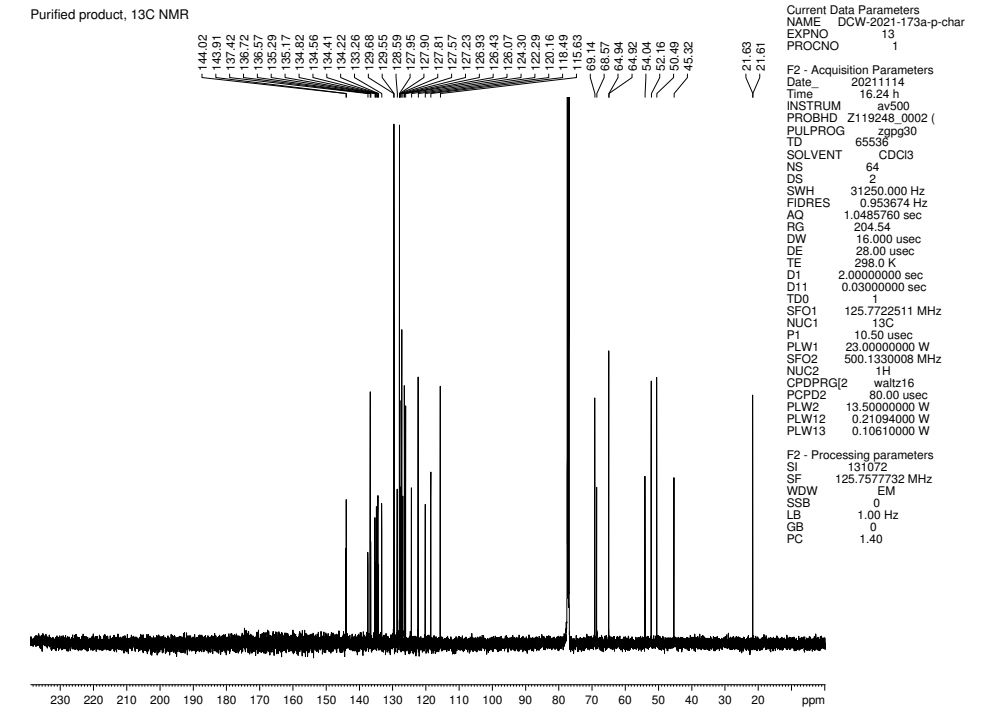

Figure 2.64. ^{13}C NMR (125 MHz, $CDCl_3$) of compounds **2.32** and **2.83**.

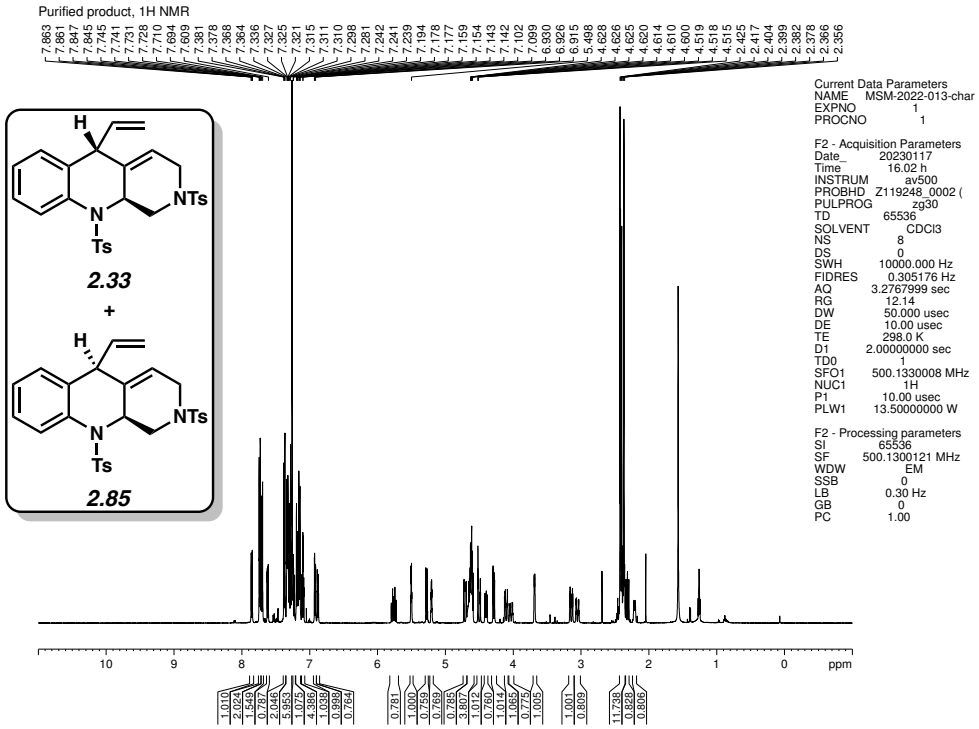

Figure 2.65. ^{1}H NMR (500 MHz, $CDCl_3$) of compounds **2.33** and **2.85**.

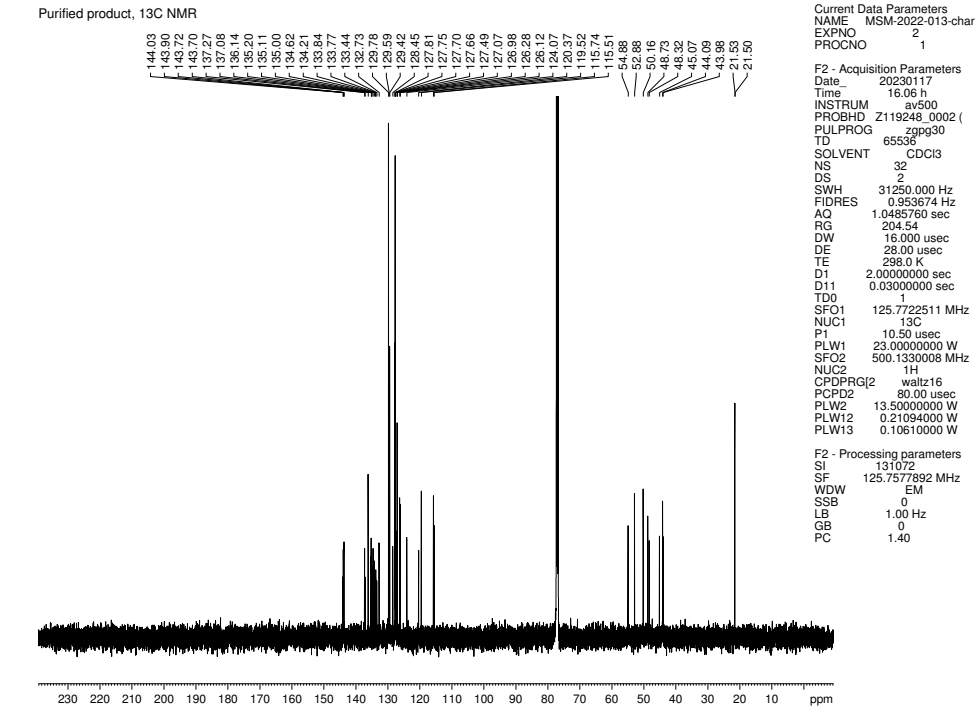

Figure 2.66. ^{13}C NMR (125 MHz, $CDCl_3$) of compounds **2.33** and **2.85**.

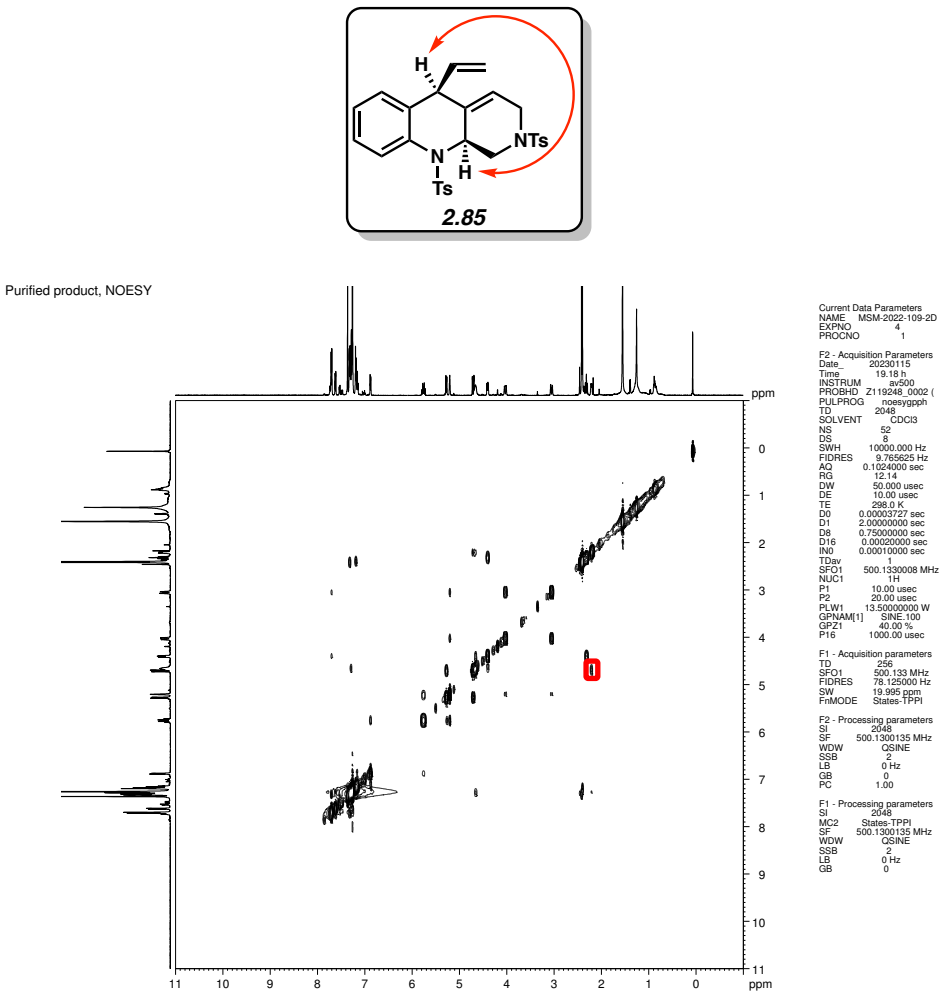

Figure 2.67. NOESY (500 MHz, $CDCl_3$) of compound **2.85**.

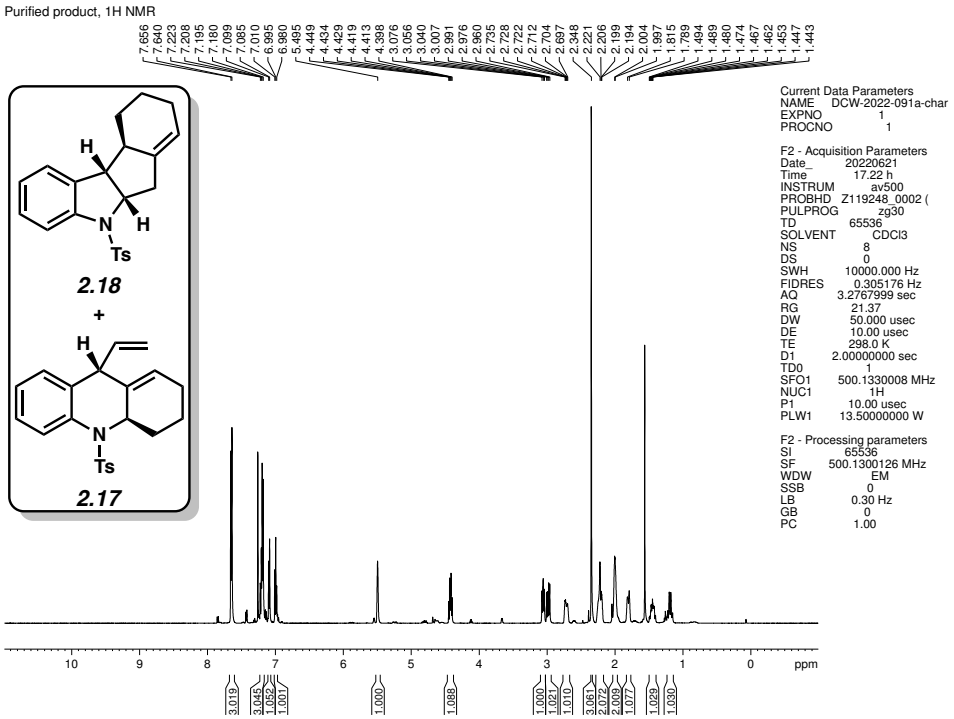

Figure 2.68. ^{1}H NMR (500 MHz, $CDCl_3$) of compounds **2.18** and **2.17**.

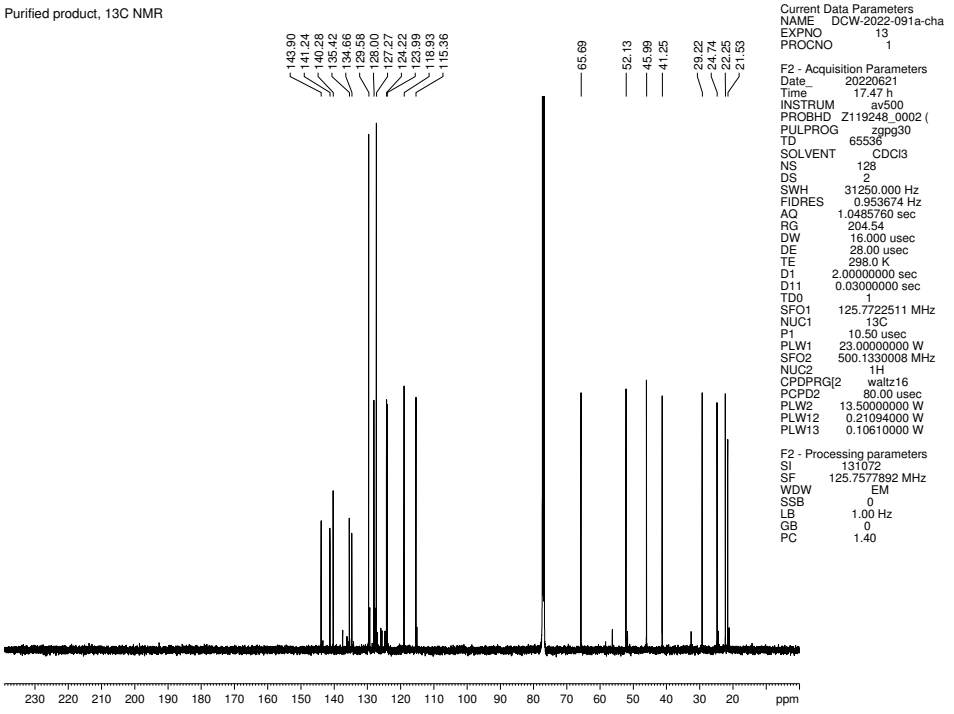

Figure 2.69. ^{13}C NMR (125 MHz, $CDCl_3$) of compounds **2.18** and **2.17**.

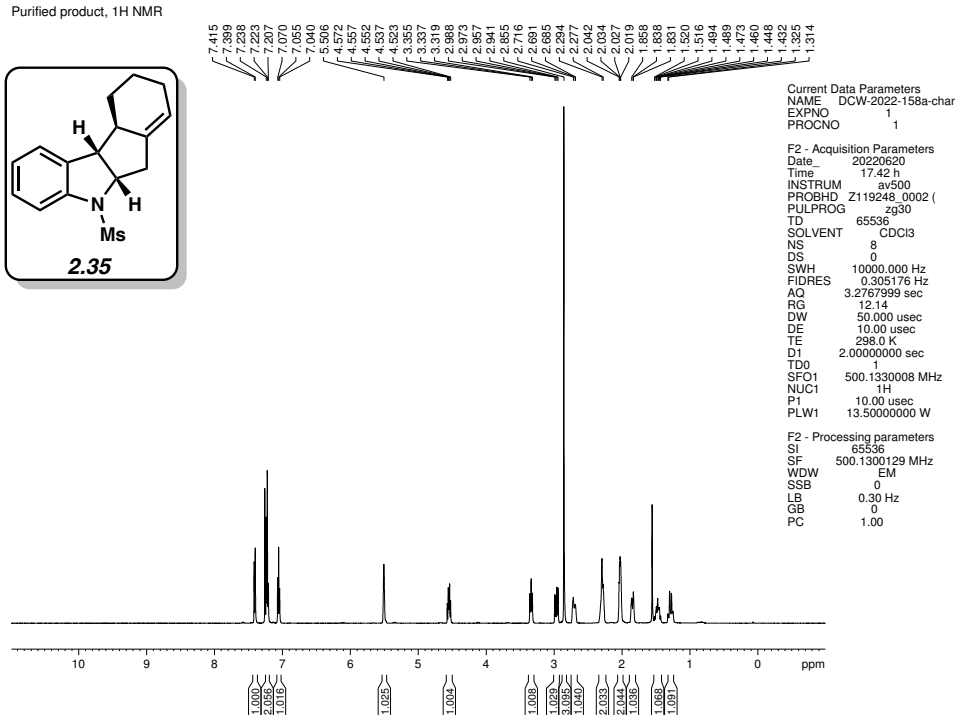

Figure 2.70. ^{1}H NMR (500 MHz, $CDCl_3$) of compound **2.35**.

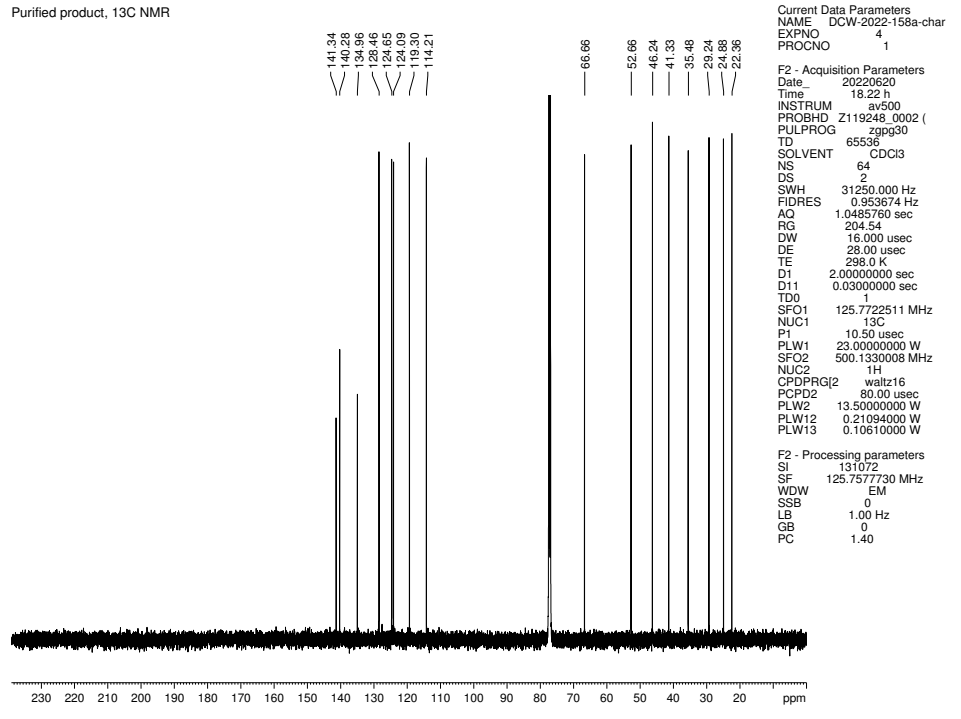

Figure 2.71. ^{13}C NMR (125 MHz, $CDCl_3$) of compound **2.35**.

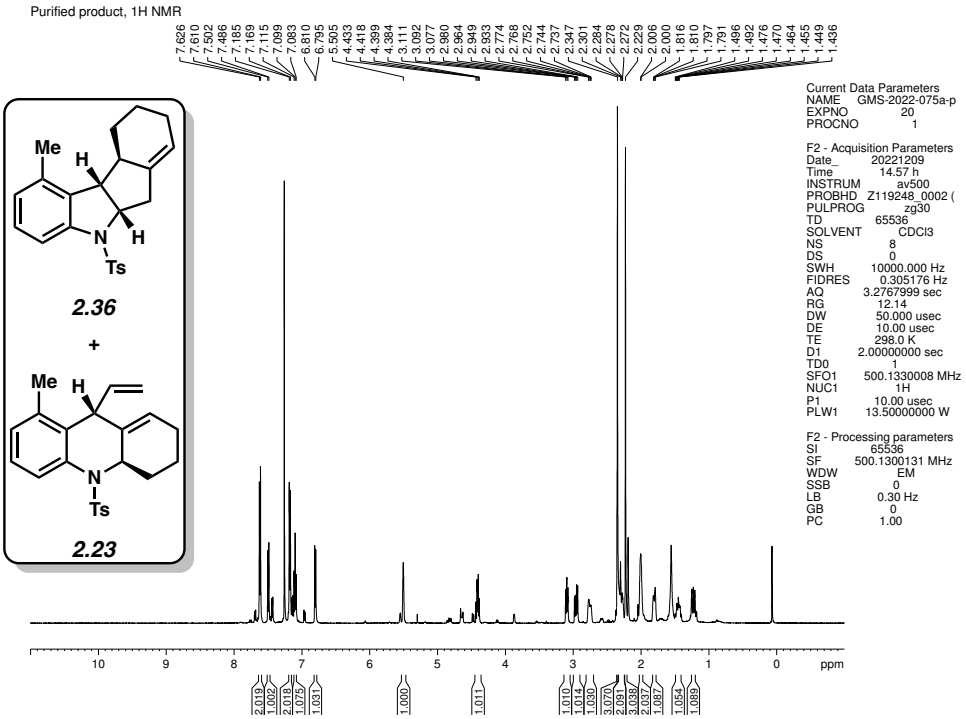

Figure 2.72. ^{1}H NMR (500 MHz, $CDCl_3$) of compounds **2.36** and **2.23**.

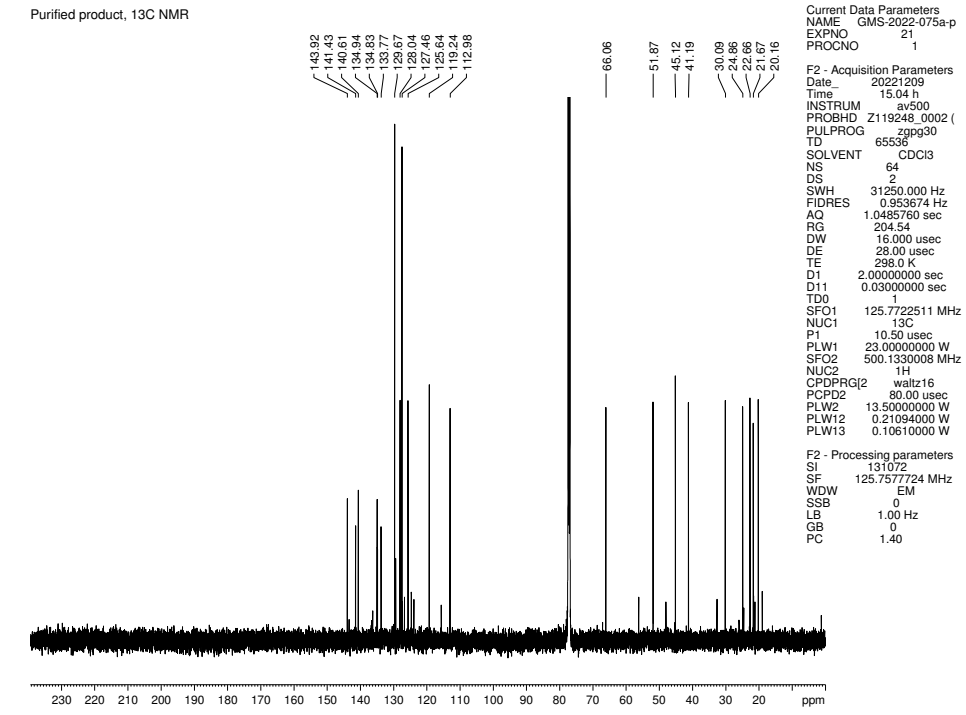

Figure 2.73. ^{13}C NMR (125 MHz, $CDCl_3$) of compound **2.36** and **2.23**.

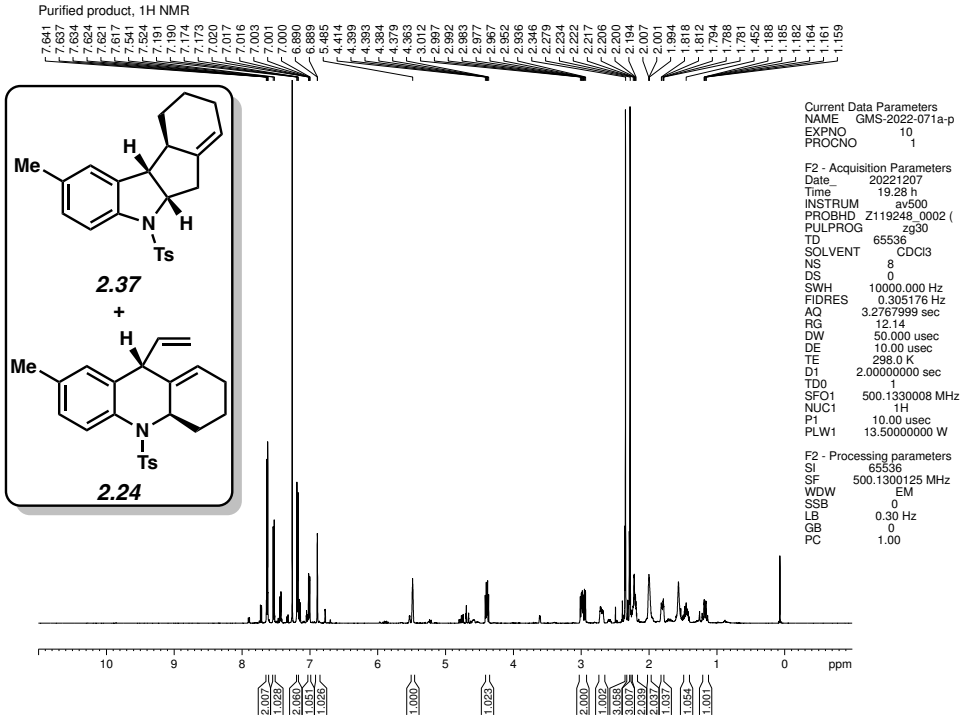

Figure 2.74. ^{1}H NMR (500 MHz, $CDCl_3$) of compounds **2.37** and **2.24**.

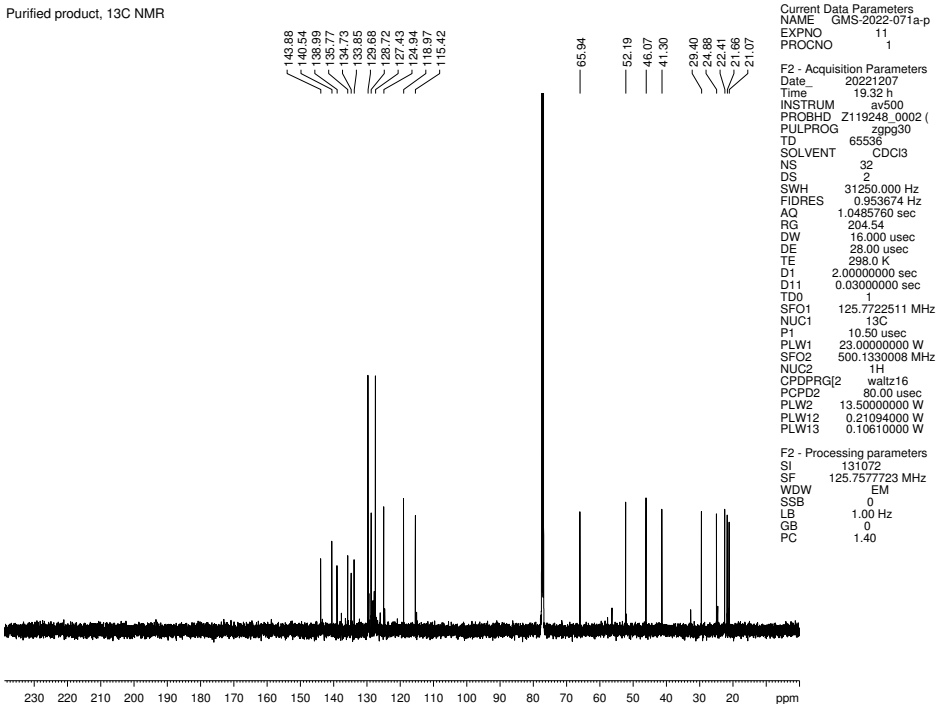

Figure 2.75. ^{13}C NMR (125 MHz, $CDCl_3$) of compound **2.37** and **2.24**.

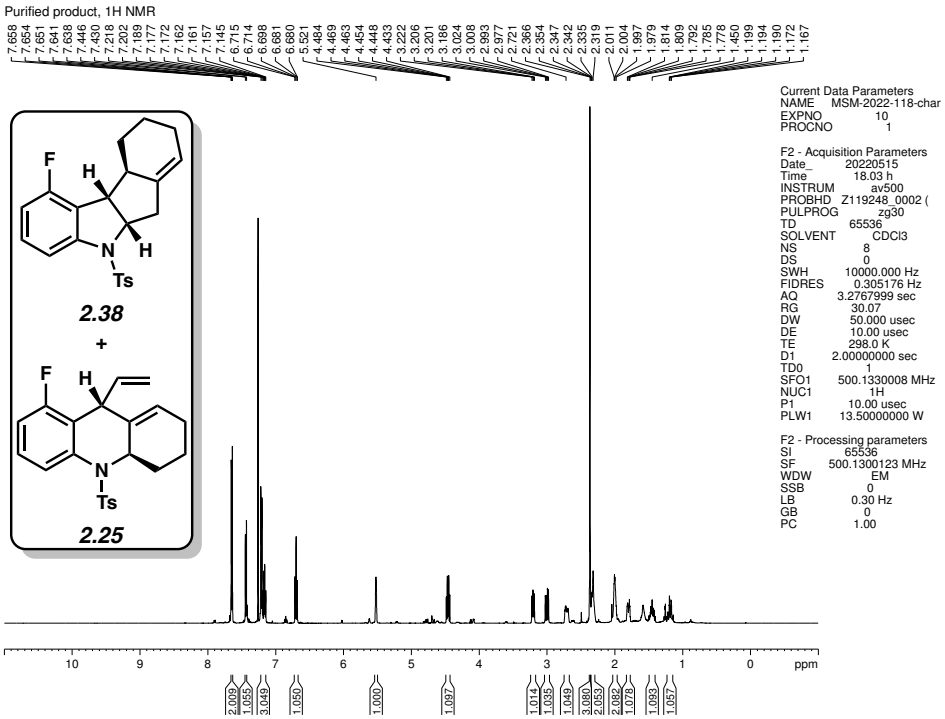

Figure 2.76. ^{1}H NMR (500 MHz, $CDCl_3$) of compounds **2.38** and **2.25**.

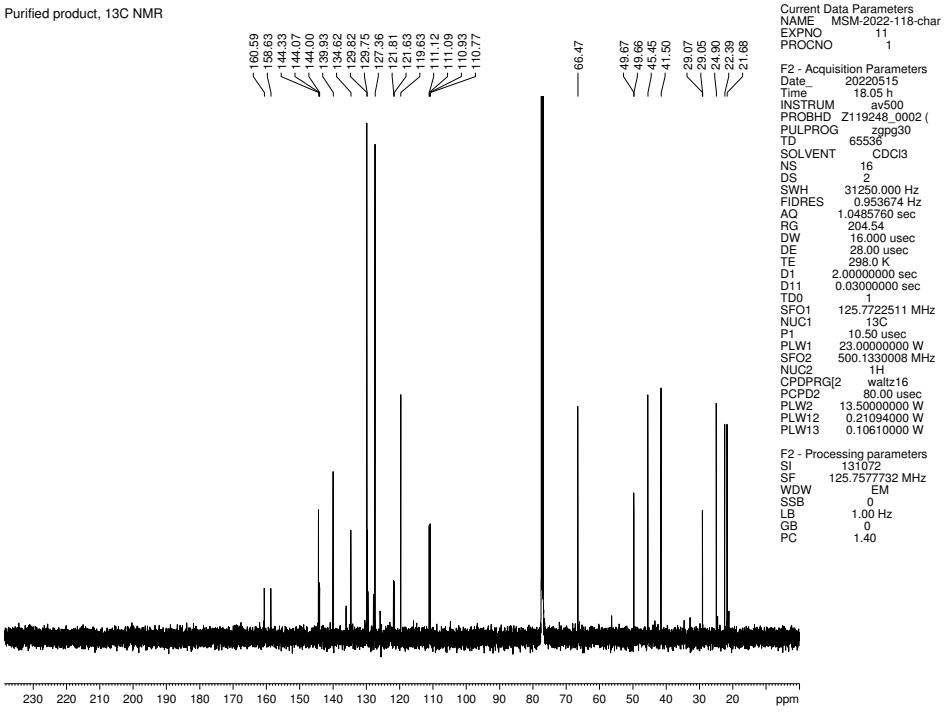

Figure 2.77. ^{13}C NMR (125 MHz, $CDCl_3$) of compound **2.38** and **2.25**.

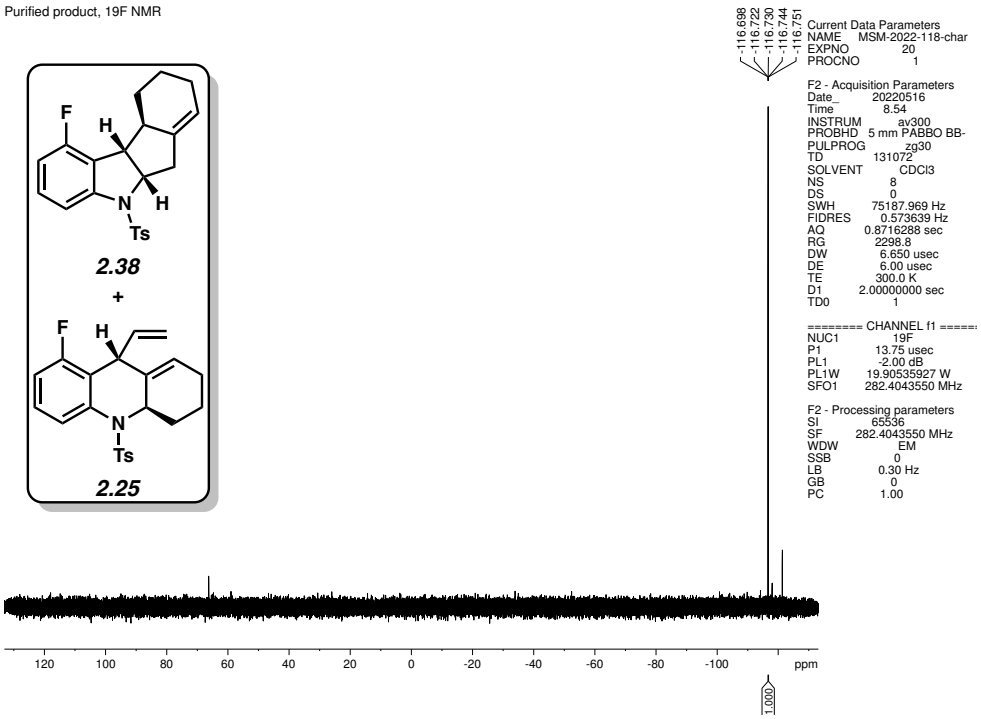

Figure 2.78. ^{19}F NMR (282 MHz, $CDCl_3$) of compound **2.38** and **2.25**.

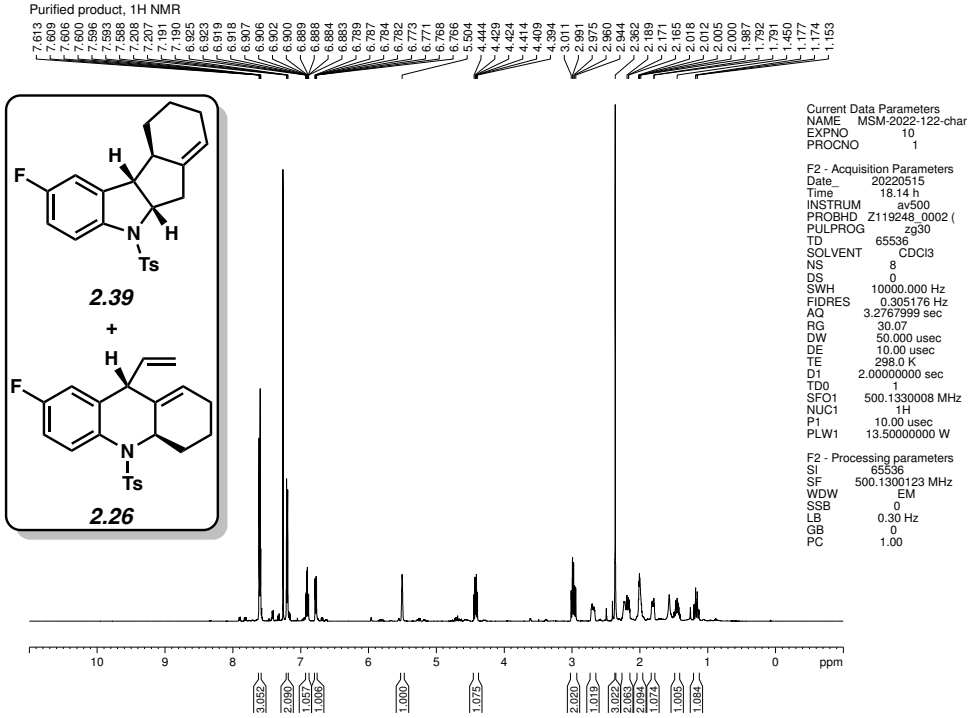

Figure 2.79. ^{1}H NMR (500 MHz, $CDCl_3$) of compounds **2.39** and **2.26**.

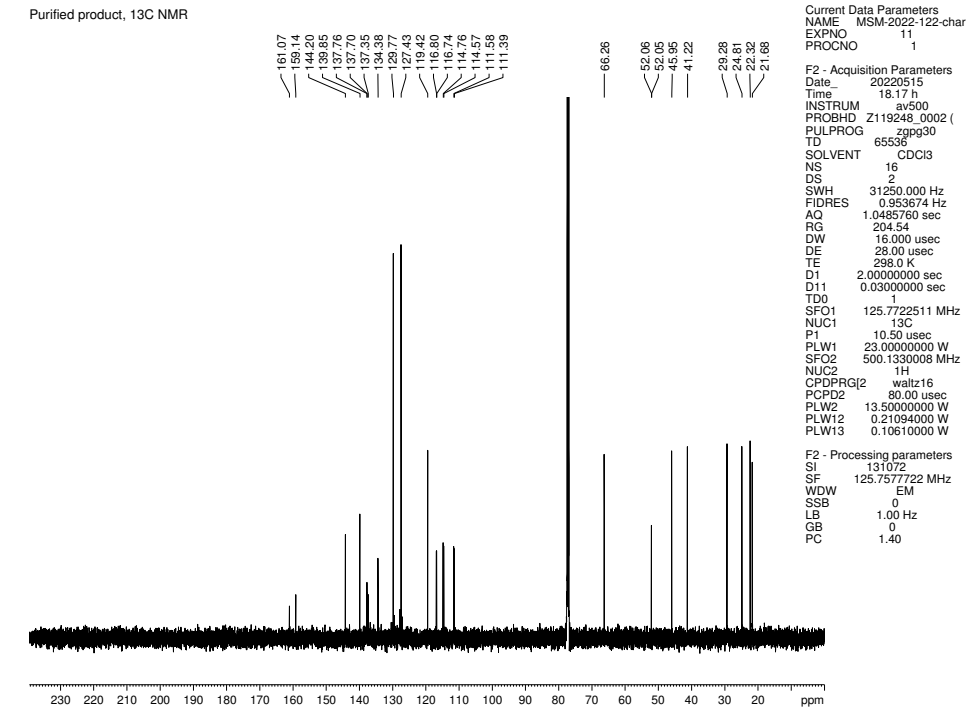

Figure 2.80. ^{13}C NMR (125 MHz, $CDCl_3$) of compound **2.39** and **2.26**.

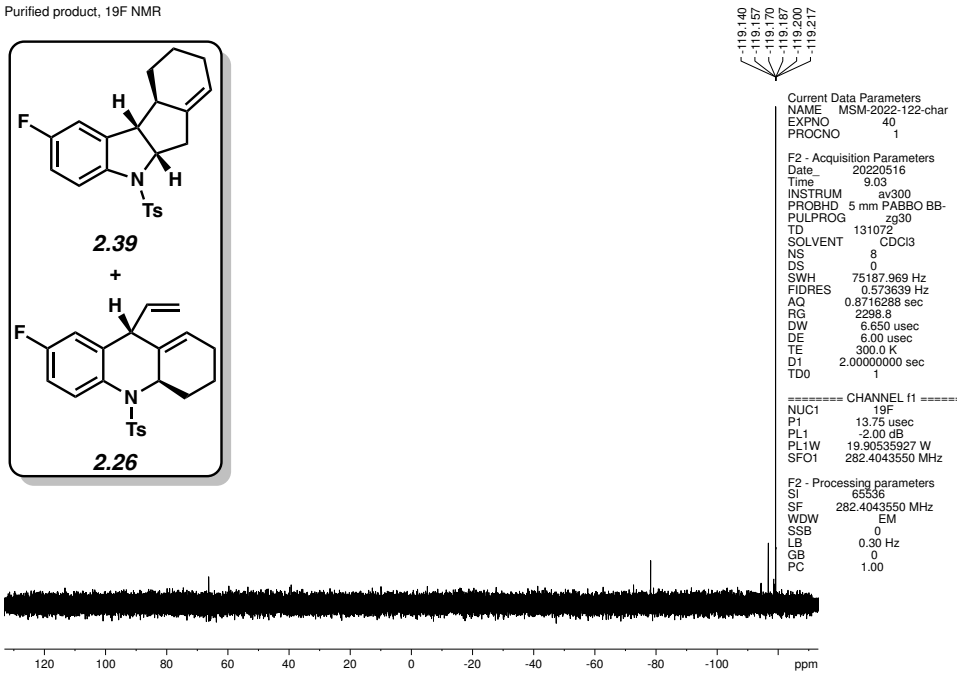

Figure 2.81. ^{19}F NMR (282 MHz, $CDCl_3$) of compound **2.39** and **2.26**.

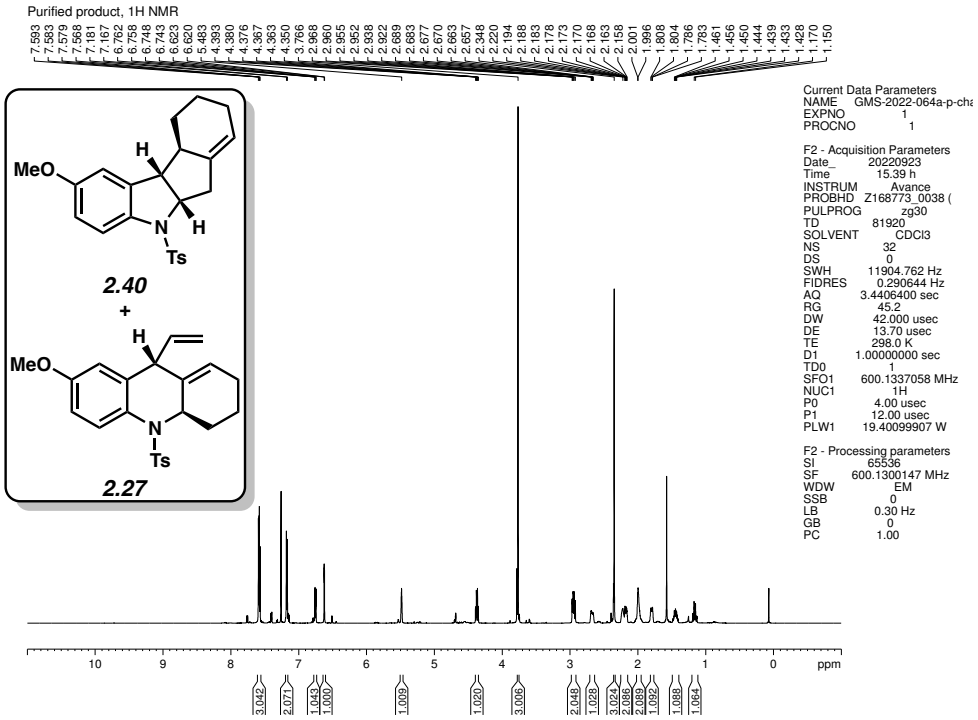

Figure 2.82. ^{1}H NMR (600 MHz, $CDCl_3$) of compounds **2.40** and **2.27**.

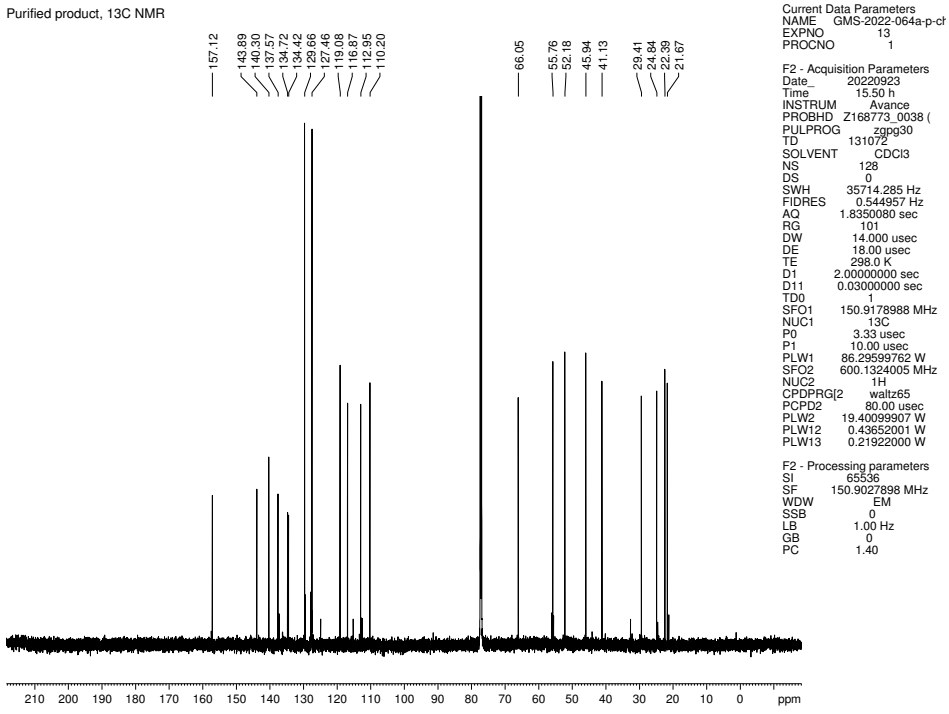

Figure 2.83. ^{13}C NMR (150 MHz, $CDCl_3$) of compound **2.40** and **2.27**.

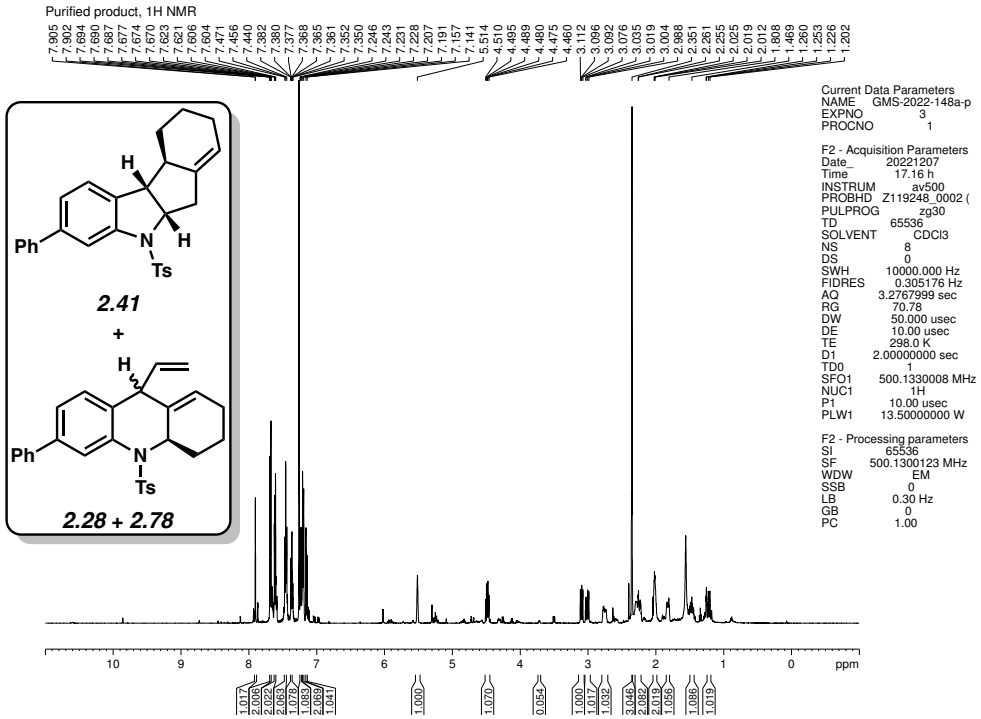

Figure 2.84. ^{1}H NMR (500 MHz, $CDCl_3$) of compounds **2.41**, **2.28**, and **2.78**.

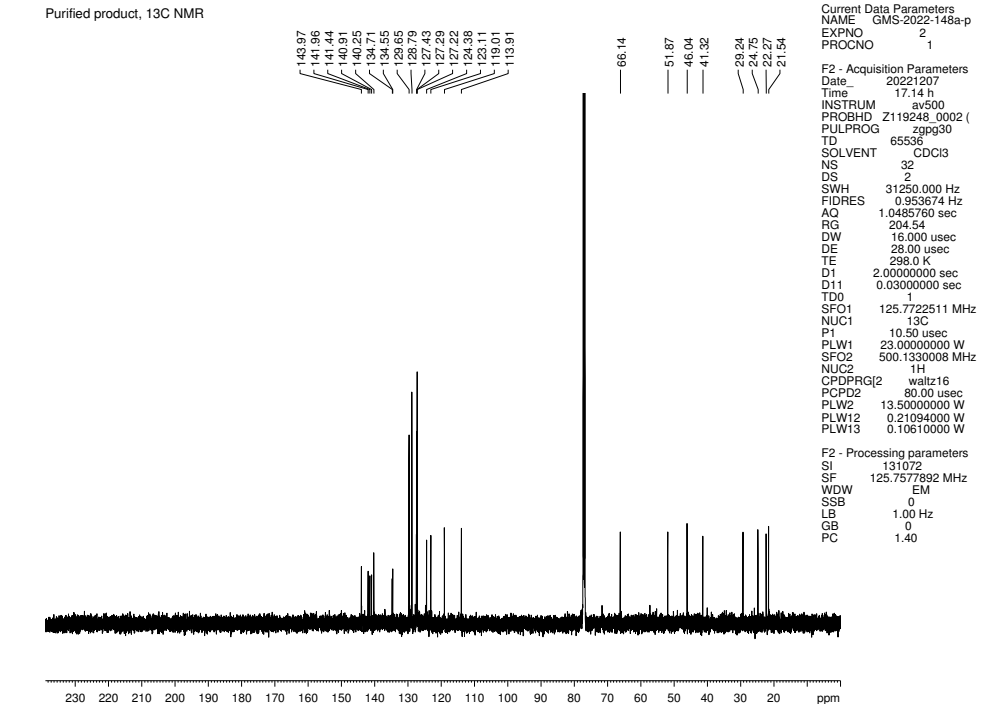

Figure 2.85. ^{13}C NMR (125 MHz, $CDCl_3$) of compounds **2.41**, **2.28**, and **2.78**.

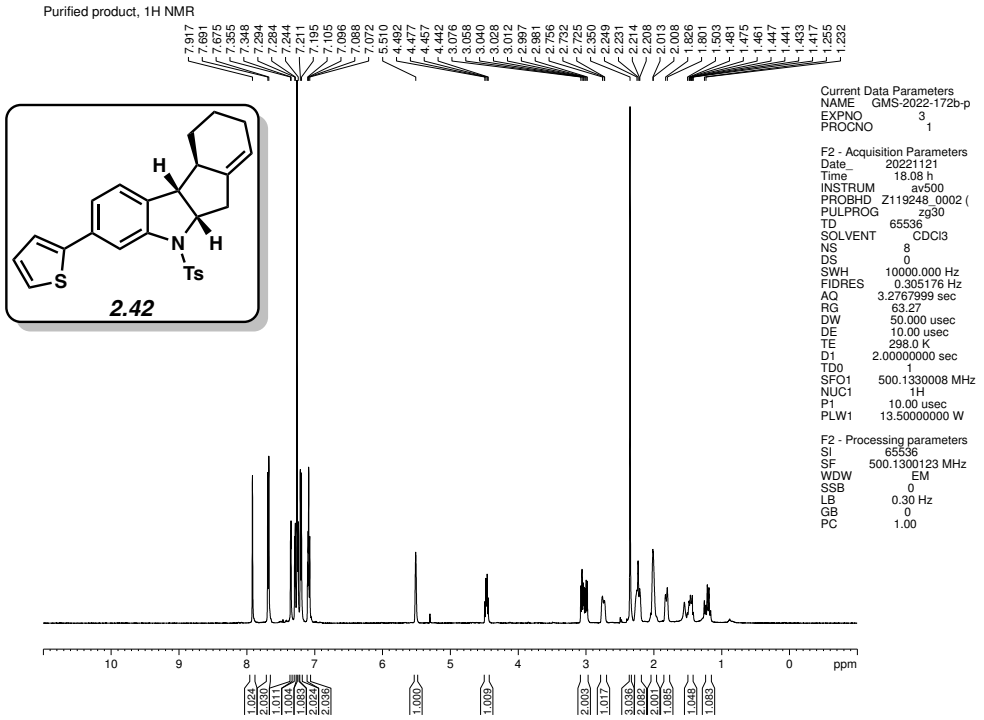

Figure 2.86. ^{1}H NMR (500 MHz, $CDCl_3$) of compound **2.42**.

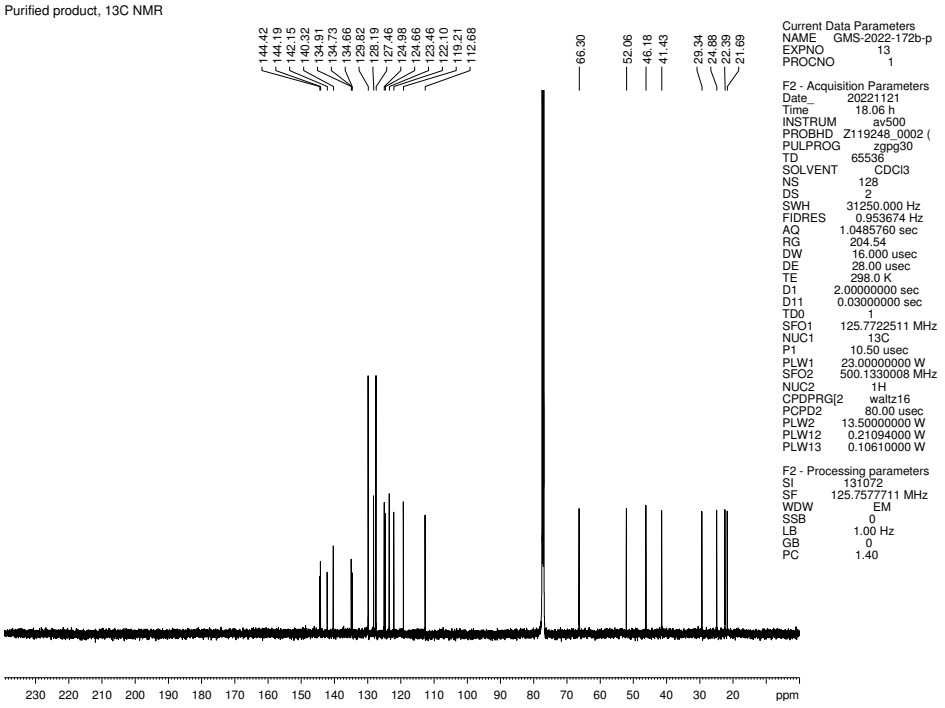

Figure 2.87. ^{13}C NMR (125 MHz, $CDCl_3$) of compound **2.42**.

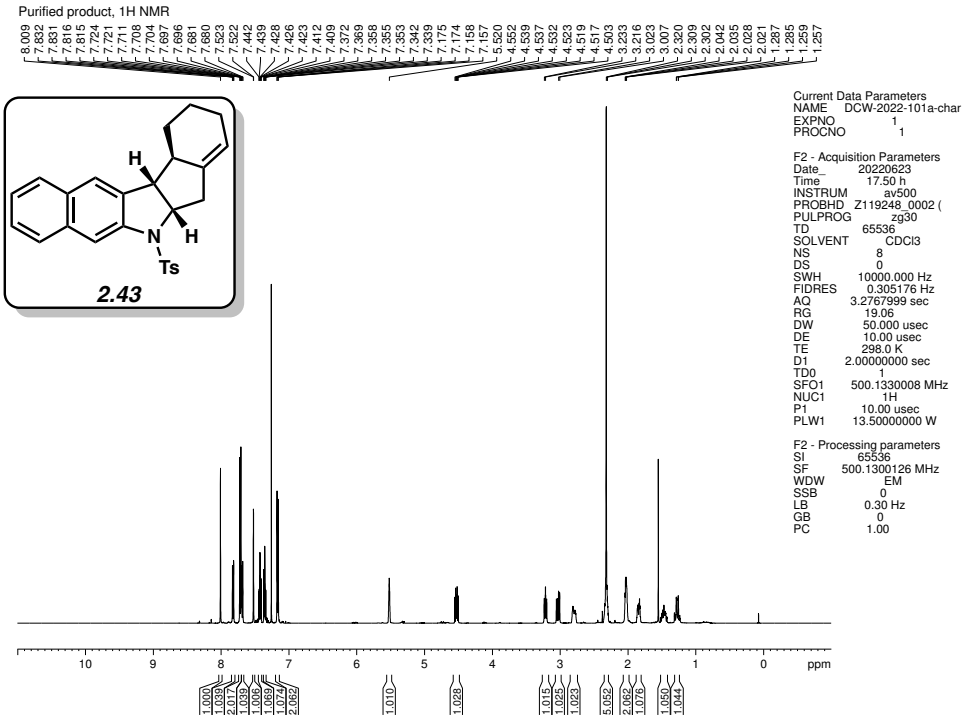

Figure 2.88. ^{1}H NMR (500 MHz, $CDCl_3$) of compound **2.43**.

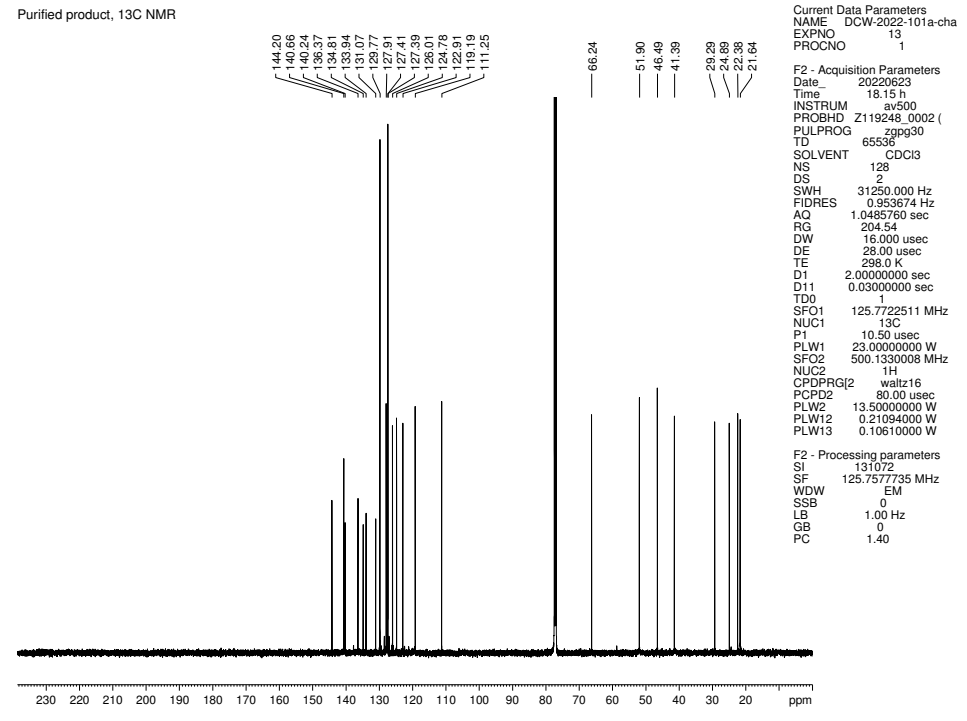

Figure 2.89. ^{13}C NMR (125 MHz, $CDCl_3$) of compound **2.43**.

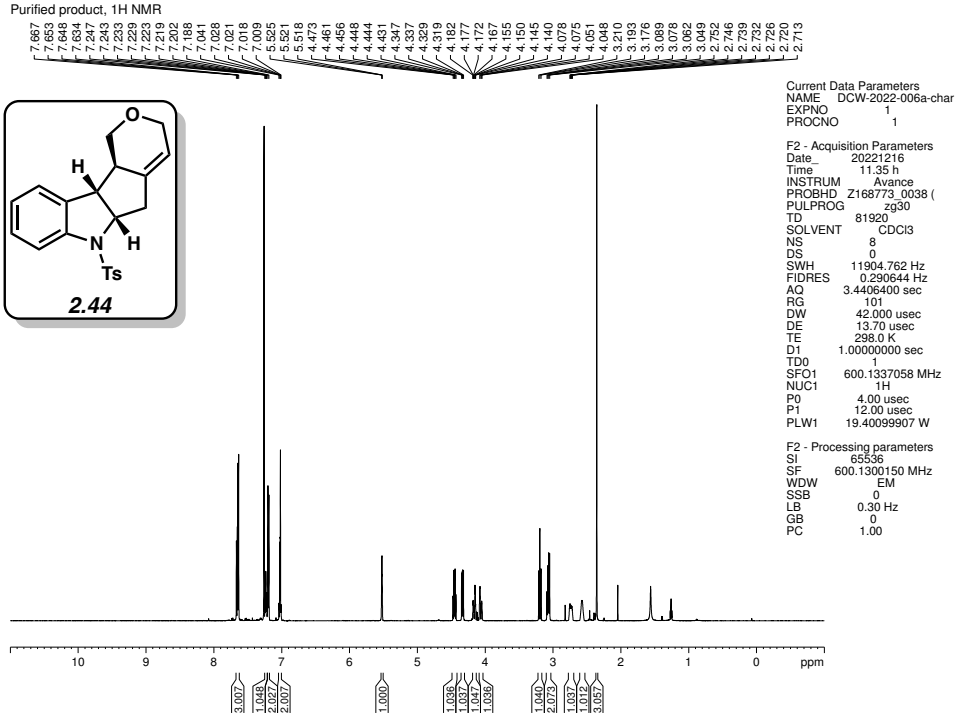

Figure 2.90. ^{1}H NMR (600 MHz, $CDCl_3$) of compound **2.44**.

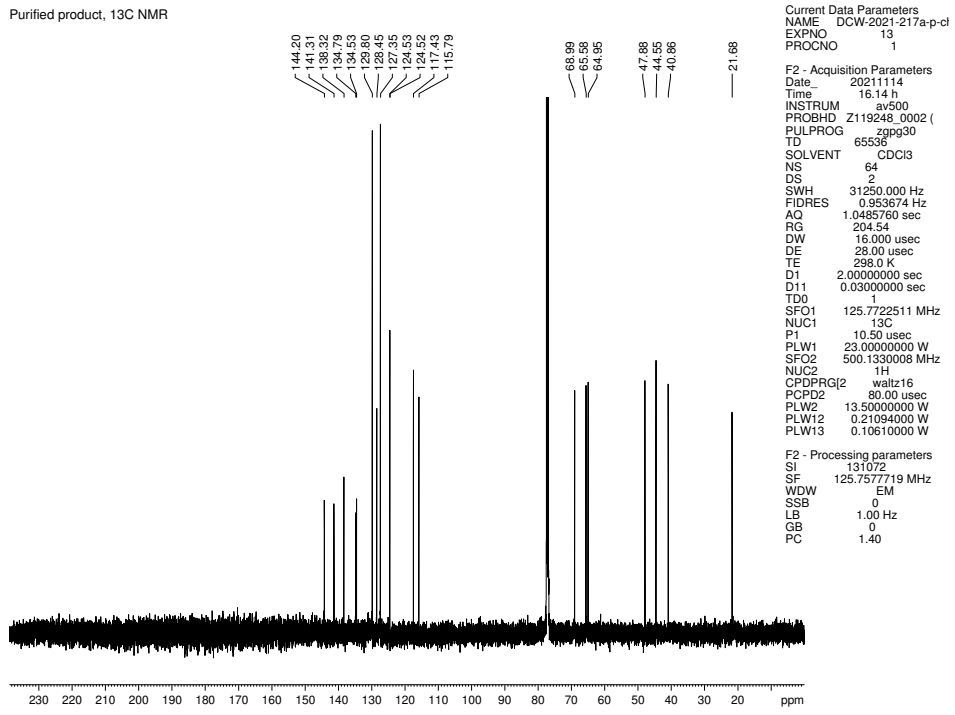

Figure 2.91. ^{13}C NMR (125 MHz, $CDCl_3$) of compound **2.44**.

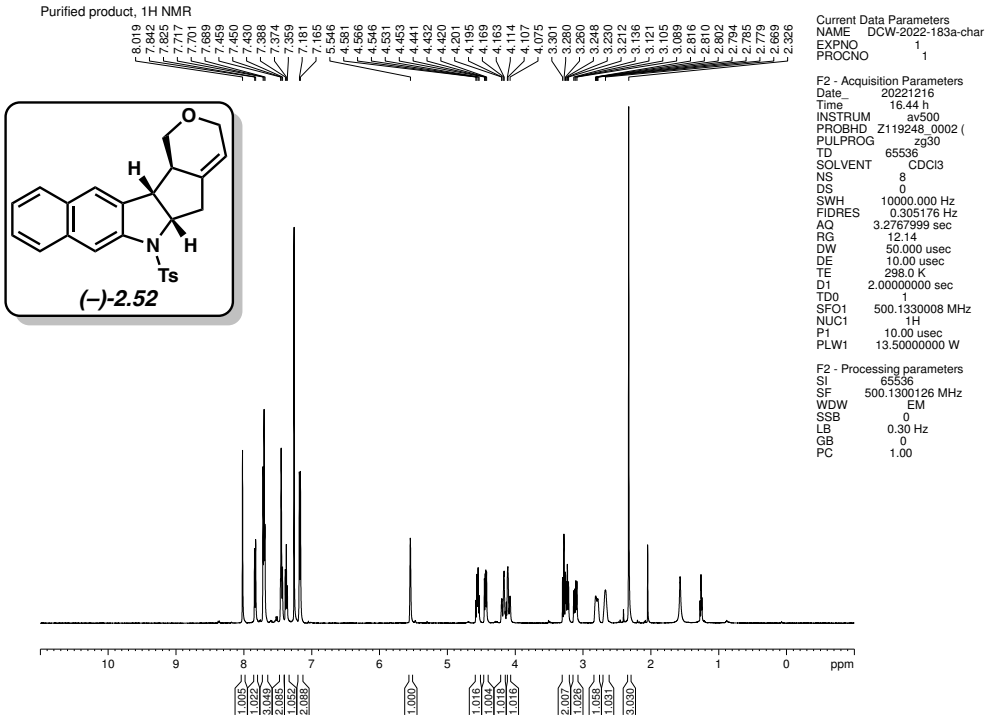

Figure 2.92. ^{1}H NMR (500 MHz, $CDCl_3$) of compound (–)-**2.52**.

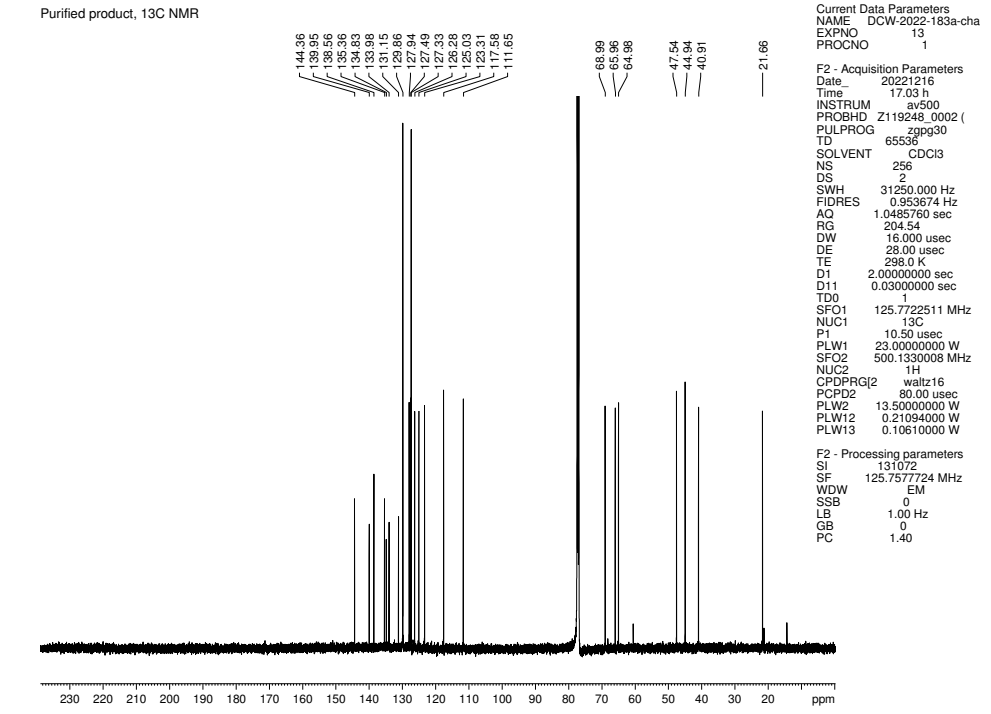

Figure 2.93. ^{13}C NMR (125 MHz, $CDCl_3$) of compound (–)-**2.52**.

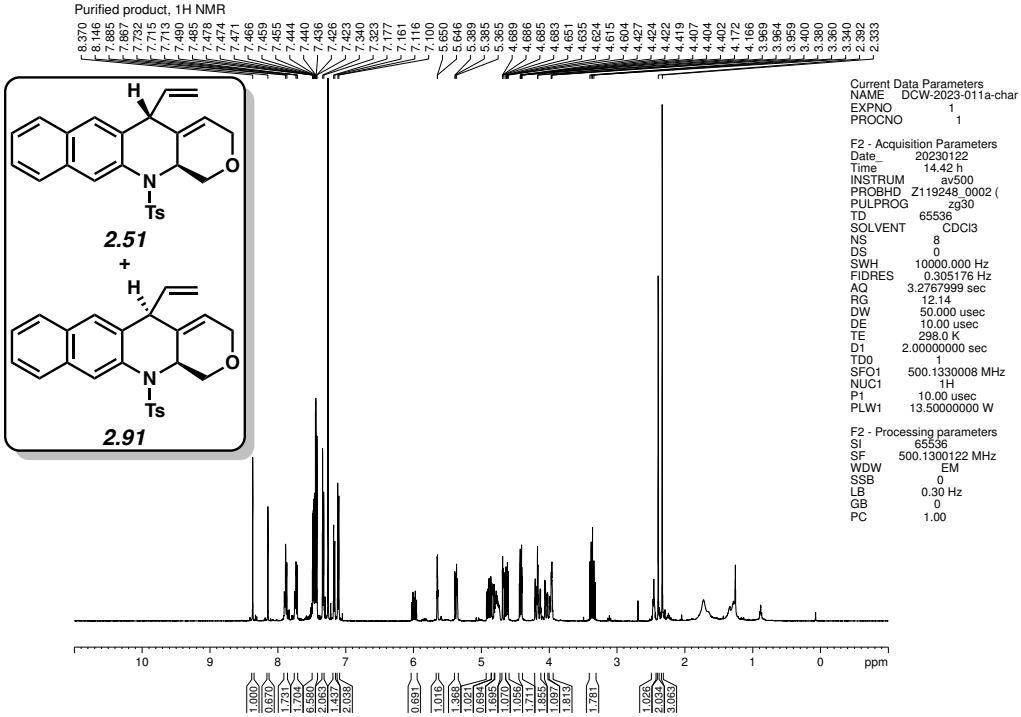

Figure 2.94. ^{1}H NMR (500 MHz, $CDCl_3$) of compounds **2.51** and **2.91**.

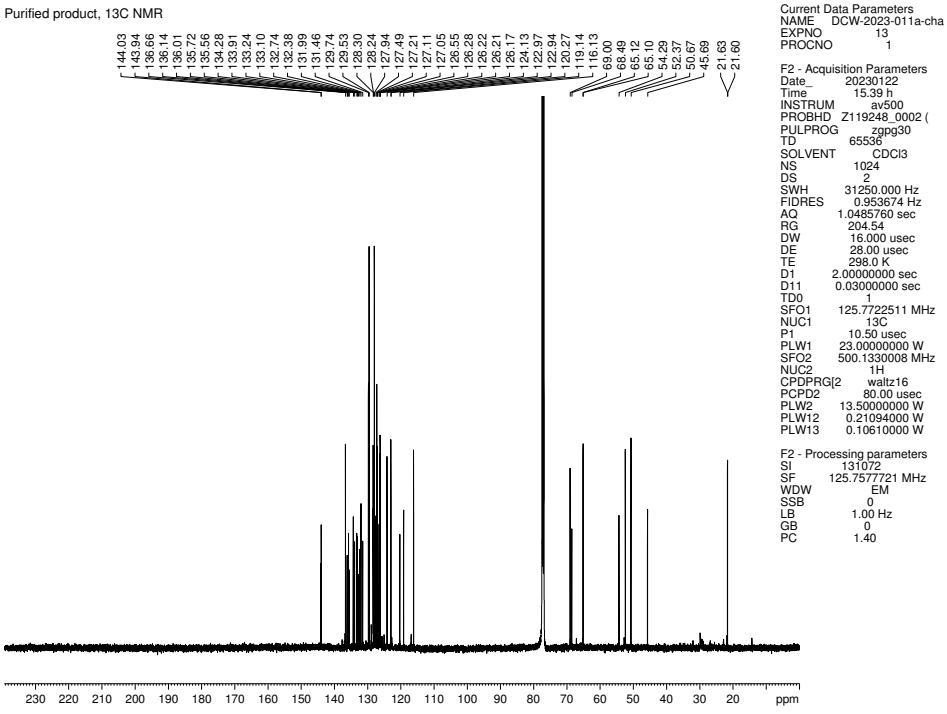

Figure 2.95. ^{13}C NMR (125 MHz, $CDCl_3$) of compounds **2.51** and **2.91**.

2.10 Notes and References

(1) Roberts, J. D.; Simmons, H. E.; Carlsmith, L. A.; Vaughn, C. W. Rearrangement in the reaction of chlorobenzene-1-C^{14} with potassium amide. *J. Am. Chem. Soc.* **1953**, *75*, 3290–3291.

(2) Wenk, H. H.; Winkler, M.; Sander, W. One century of aryne chemistry. *Angew. Chem., Int. Ed.* **2003**, *42*, 502–528.

(3) Dhokale, R. A.; Mhaske, S. B. Transition-metal-catalyzed reactions involving arynes. *Synthesis* **2018**, *50*, 1–16.

(4) Bhunia, A.; Yetra, S. R.; Biju, A. T. Recent advances in transition-metal-free carbon–carbon and carbon–heteroatom bond-forming reaction using arynes. *Chem. Soc. Rev.* **2012**, *41*, 3140–3152.

(5) Goetz, A. E.; Garg, N. K.; Enabling the use of heterocyclic arynes in chemical synthesis. *J. Org. Chem.* **2014**, *79*, 846–851.

(6) Nakamura, Y.; Yoshida, S.; Hosya, T. Recent advances in synthetic hetaryne chemistry. *Hetereocycles* **2019**, *98*, 1623–1677.

(7) Scardiglia, F.; Roberts, J. D. Evidence for cyclohexyne as an intermediate in the coupling of phenyllithium with 1-chlorocyclohexene. *Tetrahedron* **1957**, *1*, 343–344.

(8) For a review describing a wide range of in situ-generated strained intermediates, see: Shi, J.; Li, L.; Li, Y. *o*-Silylaryl triflates: A journey of Kobayashi aryne precursors. *Chem. Rev.* **2021**, *121*, 3892–4044.

(9) Dubrovskiy, A. V.; Markina, N. A.; Larock, R. C. Use of benzynes for the synthesis of heterocycles. *Org. Biomol. Chem.* **2013**, *11*, 191–218.

(10) Goetz, A. E.; Shah, T. K.; Garg, N. K. Pyridynes and indolynes as building blocks for functionalized heterocycles and natural products. *Chem. Commun.* **2015**, *51*, 34–45.

(11) Mauger, C. C.; Mignani, G. A. An efficient and safe procedure for the large-scale Pd-catalyzed hydrazonation of aromatic chlorides using Buchwald technology. *Org. Proc. Res. Dec.* **2004**, *8*, 1065–1071.

(12) Tadross, P. M.; Stoltz, B. M. A comprehensive history of arynes in natural product total synthesis. *Chem. Rev.* **2012**, *112*, 3550–3577.

(13) Gampe, C. M.; Carreira, E. M. Arynes and cyclohexyne in natural product total synthesis. *Angew. Chem., Int. Ed.* **2012**, *51*, 3766–3778.

(14) Takikawa, H.; Nishii, A.; Sakai, T.; Suzuki, K. Aryne-based strategy in the total synthesis of naturally occurring polycyclic compounds. *Chem. Soc. Rev.* **2018**, *47*, 8030–8056.

(15) Schleth, F.; Vettiger, T.; Rommel, M.; Tobler, H. Process for the preparation of pyrazole carboxylic acid amides. International patent WO 2011131544 A1, Oct 27, 2011.

(16) Lin, J. B.; Shah, T. J.; Goetz, A. E.; Garg, N. K.; Houk, K. N. Conjugated trimeric scaffolds accessible from indolyne cyclotrimerizations: Synthesis, structures, and electronic properties. *J. Am. Chem. Soc.* **2017**, *139*, 10447–10455.

(17) Darzi, E. R.; Barber, J. S.; Garg, N. K. Cyclic alkyne approach to heteroatom-containing polycyclic aromatic hydrocarbon scaffolds. *Angew. Chem., Int. Ed.* **2019**, *58*, 9419–9424.

(18) Wittig, G.; Fritze, P. On the intermediate occurrence of 1,2-cyclohexadiene. *Angew. Chem., Int. Ed.* **1966**, *5*, 846.

(19) Moser, W. R. *The reactions of gem-dihalocyclopropanes with organometallic reagents*. Ph.D. Dissertation, Massachusetts Institute of Technology Cambridge, MA, 1964.

(20) Christl, M. *Cyclic allenes up to seven-membered rings*. *Modern Allene Chemistry*; Krause, N., Kashmi, S. A. K., Eds.; Wiley-VCH: Weinheim, 2004; pp 243–357.

(21) Angus, R. O., Jr.; Schmidt, M. W.; Johnson, R. P. Small-ring cyclic cumulenes: Theoretical studies of the structure and barrier to inversion of cyclic allenes. *J. Am. Chem. Soc.* **1985**, *107*, 532–537.

(22) Daoust, K. J.; Hernandez, S. M.; Konrad, K. M.; Mackie, I. D.; Winstanley, J.; Johnson, R. P. Strain estimates for small-ring cyclic allenes and butatrienes. *J. Org. Chem.* **2006**, *71*, 5708–5714.

(23) Strained cyclic allenes have several attractive attributes that include their (a) generation under mild reaction conditions; (b) ability to undergo two or one electron processes leading to a wide scope of reactions; (c) inherent chirality, which can allow for stereoselective transformations; (d) participation in regioselective reactions based on substituent effects; and (e) relatively understudied nature, which allows numerous opportunities for discovery.

(24) Quintana, I.; Peña, D.; Pérez, D.; Guitián, E. Generation and reactivity of 1,2-cyclohexadiene under mild reaction conditions. *Eur. J. Org. Chem.* **2009**, 5519–5524.

(25) McVeigh, M. S.; Kelleghan, A. V.; Yamano, M. M.; Knapp, R. R.; Garg, N. K. Silyl tosylate precursors to cyclohexynes, 1,2-cyclohexadienes, and 1,2-cycloheptadiene. *Org. Lett.* **2020**, *22*, 4500–4504.

(26) Hioki, Y.; Mori, A.; Okano, K. Steric effects on deprotonative generation of cyclohexynes and 1,2-cyclohexadienes from cyclohexenyl triflates by magnesium amides. *Tetrahedron* **2020**, *76*, 131103.

(27) Barber, J. S.; Styduhar, E. D.; Pham, H. V.; McMahon, T. C.; Houk, K. N.; Garg, N. K. Nitrone cycloadditions of 1,2-cyclohexadiene. *J. Am. Chem. Soc.* **2016**, *138*, 2512–2515.

(28) Barber, J. S.; Yamano, M. M.; Ramirez, M.; Darzi, E. R.; Knapp, R. R.; Liu, F.; Houk, K. N.; Garg, N. K. Diels–Alder cycloadditions of strained azacyclic allenes. *Nat. Chem.* **2018**, *10*, 953–960.

(29) Yamano, M. M.; Knapp, R. R.; Ngamnithiporn, A.; Ramirez, M.; Houk, K. N.; Stoltz, B. M.; Garg, N. K. Cycloadditions of oxacyclic allenes and a catalytic asymmetric entryway to enantioenriched cyclic allenes. *Angew. Chem., Int. Ed.* **2019**, *58*, 5633–5657.

(30) Ramirez, M.; Svatunek, D.; Liu, F.; Garg, N. K.; Houk, K. N. Origins of endo selectivity in Diels–Alder reactions of cyclic allene dienophiles. *Angew. Chem., Int. Ed.* **2021**, *60*, 14989–14997.

(31) Lofstrand, V. A.; West, F. G. Efficient trapping of 1,2-cyclohexadienes with 1,3-dipoles. *Chem. Eur. J.* **2016**, *22*, 10763–10767.

(32) Lofstrand, V. A.; McIntosh, K. C.; Almehmadi, Y. A.; West, F. G. Strain-activated Diels–Alder trapping of 1,2-cyclohexadienes: Intramolecular capture by pendant furans. *Org. Lett.* **2019**, *21*, 6231–6234.

(33) Almehmadi, Y. A.; West, F. G. A mild method for the generation and interception of 1,2-cycloheptadienes with 1,3-dipoles. *Org. Lett.* **2020**, *22*, 6091–6095.

(34) Wang, B.; Constantin, M.-G.; Singh, S.; Zhou, Y.; Davis, R. L.; West, F. G. Generation and trapping of electron-deficient 1,2-cyclohexadienes. Unexpected hetero-Diels–Alder reactivity. *Org. Biomol. Chem.* **2021**, *19*, 399–405.

(35) Jankovic, C. L.; West, F. G. 2 + 2 Trapping of acyloxy-1,2-cyclohexadienes with styrenes and electron-deficient olefins. *Org. Lett.* **2022**, *24*, 9497–9501.

(36) Nendel, M.; Tolbert, L. M.; Herring, L. E.; Islam, M. N.; Houk, K. N. Strained allenes as dienophiles in the Diels–Alder reaction: An experimental and computational study. *J. Org. Chem.* **1999**, *64*, 976–983.

(37) Yamano, M. M.; Kelleghan, A. V.; Shao, Q.; Giroud, M.; Simmons, B. J.; Li, B.; Chen, S.; Houk. K. N.; Garg, N. K. Interception fleeting cyclic allenes with asymmetric nickel catalysis. *Nature* **2020**, *586*, 242–247.

(38) Kelleghan, A. V.; Witkowski, D. C.; McVeigh, M. S.; Garg, N. K. Palladium-catalyzed annulations of strained cyclic allenes. *J. Am. Chem. Soc.* **2021**, *143*, 9338–9342.

(39) McVeigh, M. S.; Garg, N. K. Interception of 1,2-cyclohexadiene with TEMPO radical. *Tetrahedron Lett.* **2021**, *87*, 153539–153543.

(40) Westphal, M. V.; Hudson, L.; Mason, J. W.; Pradeilles, J. A.; Zécri, F. J.; Briner, K.; Schreiber, S. L. Water-compatible cycloadditions of oligonucleotide-conjugated strained allenes for DNA-encoded library synthesis. *J. Am. Chem. Soc.* **2020**, *142*, 7776–7782.

(41) Ippoliti, F. M.; Adamson, N. J.; Wonilowicz, L. G.; Nasrallah, D. J.; Darzi, E. R.; Donaldson, J. S.; Garg, N. K. Total synthesis of lissodendoric acid A via stereospecific trapping of a strained cyclic allene. *Science* **2023**, *379*, 261–265.

(42) Anthony, S. M.; Wonilowicz, L. G.; McVeigh, M. S.; Garg, N. K. Leveraging fleeting strained intermediates to access complex scaffolds. *JACS Au* **2021**, *1*, 897–912.

(43) Spence, K. A.; Tena Meza, A.; Garg, N. K. Merging metals and strained intermediates. *Chem Catalysis* **2022**, *2*, 1870–1879.

(44) In contrast, over 50 studies of cycloadditions or nucleophilic additions of 6-membered strained cyclic allenes are available in the literature. Similarly, arynes have been widely used in metal-catalyzed processes (for reviews, see: ref 3, 8, 42, 43).

(45) For a report of palladacycle **2.8** being invoked in strained intermediate cocyclotrimerizations, see: Peña, D.; Pérez, D.; Guitián, E.; Castedo L. Selective palladium-catalyzed cocyclotrimerization of arynes with dimethyl acetylenedicarboxylate: A versatile method for the synthesis of polycyclic aromatic hydrocarbons. *J. Org. Chem.* **2000**, *65*, 6944–6950.

(46) Baker, R. π-Allylmetal derivatives in organic synthesis. *Chem. Rev.* **1973**, *73*, 487–530.

(47) Trost, B. Metal catalyzed allylic alkylations: Its development in the Trost laboratories. *Tetrahedron* **2015**, *71*, 5708–5733.

(48) Dutta, S.; Bhattacharya, T.; Werz, D. B.; Maiti, D. Transition-metal-catalyzed C–H allylation reactions. *Chem* **2021**, *7*, 555–605.

(49) Trost, B. M.; Crawley, M. L. Asymmetric transition-metal-catalyzed allylic alkylations: Applications in total synthesis. *Chem. Rev.* **2003**, *103*, 2921–2944.

(50) Pàmies, O.; Margalef, J.; Cañellas, S.; James, J.; Judge, E.; Guiry, P. J.; Moberg, C.; Bäckvall, J.-E.; Pfaltz, A.; Pericàs, M. A.; Diégeuz, M. Recent advances in enantioselective Pd-catalyzed allylic substitution: From design to applications. *Chem. Rev.* **2021**, *121*, 4373–4505.

(51) Wang, C.; Pahadi, N.; Tunge, J. A. Decarboxylative cyclizations and cycloadditions of palladium-polarized aza-*ortho*-xylylenes. *Tetrahedron* **2009**, *65*, 5102–5109.

(52) Li, T.-R.; Wang, Y.-N.; Xiao, W.-J.; Lu, L.-Q. Transition-metal-catalyzed cyclization reactions using vinyl and ethynyl benzoxazinones as dipole precursors. *Tetrahedron Lett.* **2018**, *59*, 1521–1530.

(53) Zuo, L.; Liu, T.; Chang, X.; Guo, W. An update of transition metal-catalyzed decarboxylative transformations of cyclic carbonates and carbamates. *Molecules* **2019**, *24*, 3930–3945.

(54) Tian, Y.; Duan, M.; Liu, J.; Fu, S.; Dong, K.; Yue, H.; Hou, Y.; Zhao, Y. Recent advances in metal-catalyzed decarboxylative reactions of vinyl benzoxazinones. *Adv. Synth. Catal.* **2021**, *363*, 4461–4474.

(55) You, Y.; Li, Q.; Zhang, Y.-P.; Zhao, J.-Q.; Wang, Z.-H.; Yuan, W.-C. Advances in palladium-catalyzed decarboxylative cycloadditions of cyclic carbonates, carbamates, and lactones. *ChemCatChem* **2022**, *14*, e202101887.

(56) Duan, S.; Cheng, B.; Duan, X.; Bao, B.; Li, Y.; Zhai, H. Synthesis of *cis*-5,5a,6,10b-tetrahydroindeno[2,1-*b*]indoles through palladium-catalyzed decarboxylative coupling of vinyl benzoxazinanones with arynes. *Org. Lett.* **2018**, *20*, 1417–1420.

(57) Feng, M.; Tang, B.; Wang, N.; Xu, H.-X.; Jiang, X. Ligand controlled regiodivergent C_1 insertion on arynes for construction of phenanthridinone and acridone alkaloids. *Angew. Chem., Int. Ed.* **2015**, *54*, 14960–14964.

(58) We hypothesize that fluoride-mediated detosylation of the vinyl benzoxazinone could be responsible for decomposition, see: Carato, P.; Yous, S.; Sellier, D.; Poupaert, J. H.; Lebegue, N.; Berthelot, P. Efficient and selective deprotection method for *N*-protected 2(*3H*)-benzoxazolones and 2(*3H*)-benzothiazolones. *Tetrahedron* **2004**, *60*, 10321–10324.

(59) Yield of **2.26** represents a combined yield of tri- and tetracyclic isomers (16:1), see Section 2.8.2.3 for details.

(60) Zimmer, R.; Dinesh, C. U.; Nandanan, E.; Khan, F. A. Palladium-catalyzed reactions of allenes. *Chem. Rev.* **2000**, *100*, 3067–3125.

(61) How specific ligands influence regioselectivity in the migratory insertion step of the proposed mechanism is not presently understood. However, ligand-guided regioselectivity in trapping π-allylpalladium species with conventional nucleophiles is not uncommon; see refs 46, 47.

(62) We hypothesize that the *trans* diastereomer is obtained as the major product due to a destabilizing steric interaction in the presumed transition state leading to the *cis* diastereomer. Specifically, a steric interaction between the vinyl group and the π-allyl fragment may disfavor formation of the cis product.

(63) Empirically, **2.49** and **2.50** gave optimal yields and ee in comparison to other substrate combinations and, therefore, were used in subsequent optimization.

(64) **2.49** was recovered (<30%) in 10% ee. This finding will be subject to further investigation.

(65) Efforts to improve ee by varying easily-modifiable parameters such as solvent, concentration, and stoichiometry, led to no improvement. Future efforts beyond the present proof-of-principle study will be aimed toward improving enantioselectivity.

(66) Havlík, M.; Dolenský, B.; Jakubek, M.; Král, V. Synthesis of unsymmetrical Tröger's bases bearing groups sensitive to reduction. *Eur. J. Org. Chem.* **2014**, *2014*, 2798–2805.

(67) Li, T.-R.; Tan, F.; Lu, L.-Q.; Wei, Y.; Wang, Y.-N.; Liu, Y.-Y.; Yang, Q.-Q.; Chen, J.-R.; Shi, D.-Q.; Xiao, W.-J. Asymmetric trapping of zwitterionic intermediates by sulphur

ylides in a palladium-catalysed decarboxylation-cycloaddition sequence. *Nat. Commun.* **2014**, *5*, 5500–5509.

(68) Guo, C.; Fleige, M.; Janssen-Müller, D.; Daniliuc, C. G.; Glorius, F. Cooperative N-heterocyclic carbene/palladium-catalyzed enantioselective umpolung annulations. *J. Am. Chem. Soc.* **2016**, *138*, 7840–7843.

(69) Tucker, Z. D.; Hill, H. M.; Smith, A. L.; Ashfeld, B. L. Diverting β-hydride elimination of a π-allyl Pd^{II} carbene complex for the assembly of disubstituted indolines via a highly diastereoselective (4+1)-cycloaddition. *Org. Lett.* **2020**, *22*, 6605–6609.

(70) Lu, C.-H.; Darvishi, S.; Khakyzadeh, V.; Li, C. Pd-catalyzed enantioselective synthesis of 2-methy-3-methyleneindoline. *Chin. Chem. Lett.* **2021**, *32*, 405–407.

(71) Sheldrick, G. M. (1996). *SADABS*. University of Göttingen, Germary.

(72) Sheldrick, G. M. Crystal structure refinement with SHELXL. *Acta Cryst. C* **2015**, *71*, 3–8.

CHAPTER THREE

Strain-Promoted Reactions of 1,2,3-Cyclohexatriene and Its Derivatives

Andrew V. Kelleghan,† Ana S. Bulger,† Dominick C. Witkowski, and Neil K. Garg

Nature **2023**, *618*, 748–754.

3.1 Abstract

Since 1825,[1] studies of compounds with the molecular formula C_6H_6–most notably benzene–have been the subject of rigorous scientific investigation.[2,3,4,5,6,7] Of these compounds, 1,2,3-cyclohexatriene has been largely overlooked. This strained isomer is substantially (approximately 100 kcal/mol) higher in energy compared to benzene and, like its relatives benzyne and 1,2-cyclohexadiene, should undergo strain-promoted reactions. However, few experimental studies of 1,2,3-cyclohexatriene are known.[8,9,10,11,12] We demonstrate that 1,2,3-cyclohexatriene and its derivatives participate in a host of reaction modes including diverse cycloadditions, nucleophilic additions, and σ-bond insertions. Experimental and computational studies of an unsymmetrical derivative of 1,2,3-cyclohexatriene demonstrate the potential for highly selective reactions of strained trienes despite their high reactivity and short lifetimes. Finally, integration of 1,2,3-cyclohexatrienes into multistep synthetic sequences demonstrates their utility in rapidly assembling topologically and stereochemically complex molecules. Collectively, these efforts should fuel the further investigation of the strained C_6H_6 isomer 1,2,3-cyclohexatriene and its derivatives, as well as their strategic application in the synthesis of important compounds.

3.2 Introduction

Since Faraday's isolation of an unidentified compound of the formula C_6H_6 in 1825,[1] studies of benzene (**3.1**, Figure 3.1A) and its isomers have fueled significant advances in diverse areas including the development of resonance theory,[13,14,15] the discovery of aromaticity,[16] and the development of countless synthetic methodologies.[2] Of the hundreds of known and postulated benzene isomers, strained isomers (e.g., **3.2**–**3.4**) have a particularly rich history in organic chemistry. For example, Dewar benzene (**3.2**) and prismane (**3.4**), which often appear even in introductory textbooks, evolved from being hypothetical structures in the 19th century to intriguing synthetic targets in the 20th century.[3,4] Despite the nearly two hundred years since the original isolation of benzene, investigation of strained isomers of benzene and their derivatives continues to provide new opportunities for discovery in modern organic chemistry.[5,6,7]

A strained benzene isomer that has remained largely underexplored is 1,2,3-cyclohexatriene (**3.5**), which was not validated experimentally until 1990.[8] The three olefins in **3.5**, unlike those in benzene itself, are cumulated to give a highly strained structure. This strain, coupled with the lack of aromatic stabilization present in benzene, translates to a substantially higher free energy. The free energy of **3.5** calculated using density functional theory (DFT) compared with benzene (**3.1**) is +101 kcal/mol (ΔG_{rel}). As such, the strong ground state destabilization of **3.5** should yield kinetically and thermodynamically favorable reactions that are difficult or not possible for benzene (Figure 3.1B). More specifically, in the case of benzene, a transformation of the type **3.1** $\rightarrow$ **3.6** would be disfavored because of the loss of aromatic stabilization, which is expected to result in an energetic penalty in the relevant transition state and comparatively destabilize the corresponding product **3.6**. By contrast, analogous reactions of 1,2,3-

cyclohexatriene (**3.5** → **3.7**) should be kinetically and thermodynamically favored because of the considerable strain release along the reaction coordinate.

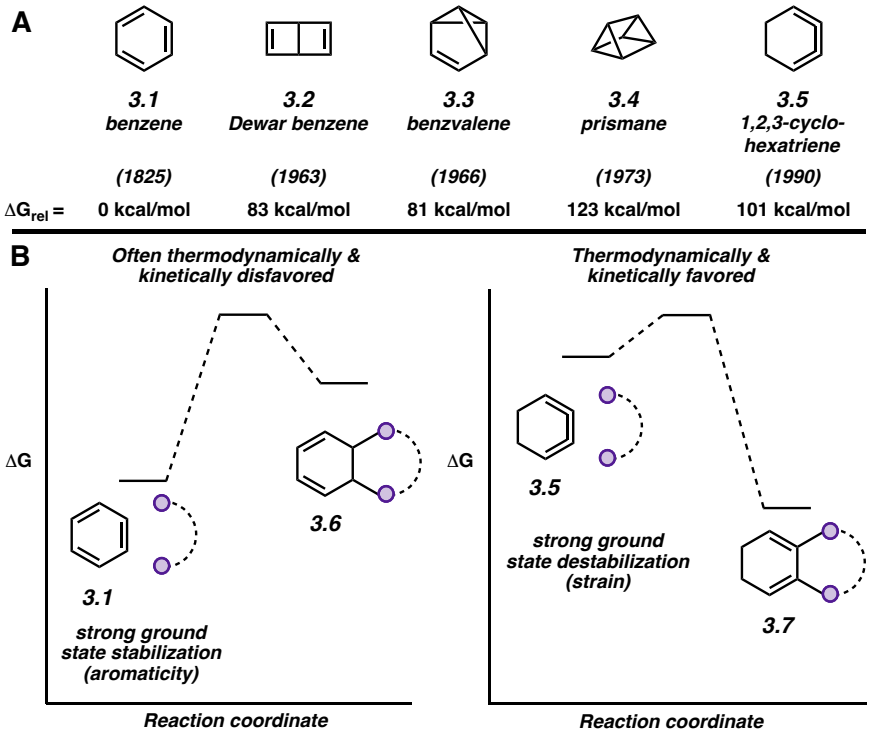

Figure 3.1. Selected strained isomers of benzene (**3.1**) and comparison of reaction coordinate diagrams. (A) Benzene (**3.1**) and several of its strained isomers with the year each was first isolated–or generated in situ in the case of 1,2,3-cyclohexatriene (**3.5**). Free energies at 298.15 K are reported relative to benzene (B3LYP-D3/6-311+G(d,p)). (B) Hypothetical reaction coordinate diagrams for transformations of benzene and 1,2,3-cyclohexatriene (**3.5**).

Conceptually, strained benzene isomer **3.5** is closely related to arynes and strained cyclic alkynes (**3.8**) and strained cyclic allenes (e.g., **3.9**, Figure 3.2A). Each of these intermediates incorporates a functional group with a preferred linear geometry into a small ring. Although the cyclic alkynes and allenes were initially mere scientific curiosities when first validated in the 1950s and 1960s,[17,18,19,20] they have since emerged as powerful tools for the construction of diverse target molecules.[21] Strained intermediates **3.11**–**3.14** are used in agrochemistry,[22] materials chemistry,[23] heterocycle synthesis,[24] and natural product total synthesis, respectively.[25] Numerous studies

pertaining to strained cyclic alkynes and strained cyclic allenes are available in the literature (about 4,600 reports and 160 reports, respectively, see Section 3.9.1 for details).

By contrast, 1,2,3-cyclohexatrienes (e.g., **3.5**) have remained underexplored despite the fact that 1,2,3-trienes constrained to cyclic systems have been studied by chemists since the 1960s.[26,27] Only four experimental studies pertaining to **3.5** are available in the literature. Two Diels–Alder trapping experiments involving 1,2,3-cyclohexatriene (**3.5**) have been reported previously[8,9,10] using 1,3-diphenylisobenzofuran and cyclopentadiene, respectively. The intermediacy of a fused bicyclic 1,2,3-cyclohexatriene during flash vacuum pyrolysis of a linear precursor has also been reported.[11] Furthermore, a [4+2] cycloaddition reaction presumed to proceed between 1,2,3-cyclohexatriene (**3.5**) and nitrones, ultimately leading to products arising from rearrangement pathways rather than the expected primary cycloadducts, has also been reported.[12] Substituted derivatives of 1,2,3-cyclohexatriene (**3.5**) are largely unexplored.[28] These limitations are notable given the diverse transformations known for strained alkynes, which include (8+2), (7+2), (5+2), (4+2), (3+2), and (2+2) cycloadditions, nucleophilic trappings, ene reactions, transition metal-catalyzed reactions, formal σ-bond insertions, and many others. Furthermore, the lack of study of substituted trienes is surprising given that substituted strained cyclic alkynes and allenes have been studied extensively and proven crucial for enabling synthetic applications of strained intermediates.[21]

We now report an investigation of 1,2,3-cyclohexatriene (**3.5**) and its derivatives, which we expect will fuel further research in this long-understudied area (Figure 3.2B). We describe: (a) a computational comparison of 1,2,3-cyclohexatriene (**3.5**) to its isomer benzene (**3.1**) and its close relative benzyne (**3.20**), (b) (4+2), (3+2), (2+2) and nucleophilic trapping reactions (e.g., **3.15** + **3.17** → **3.18**), (c) syntheses and trappings of new substituted cyclic 1,2,3-hexatrienes, including a

geometrically-distorted silyl substituted cyclic triene that undergoes regioselective reactions, and (d) the elaboration of cyclic triene cycloadducts by leveraging the embedded 1,3-diene to rapidly access diverse product scaffolds (e.g., **3.18** → **3.19**).

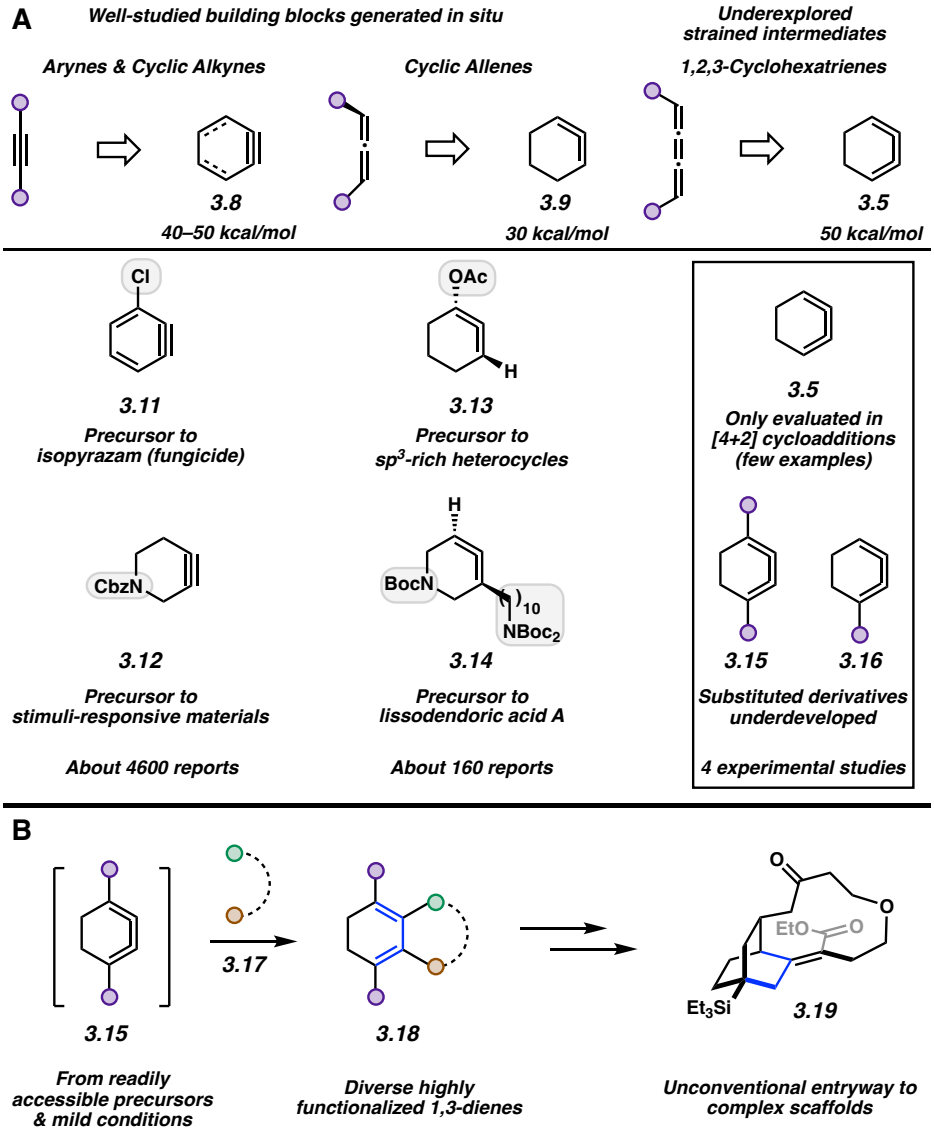

Figure 3.2. Strained cyclic intermediates and overview of current study. (A) Representative classes of strained cyclic intermediates with synthetically useful derivatives **3.11**–**3.14**. (B) Overview of our current study.

3.3 Computational Structural Analysis

We performed DFT studies to directly compare the geometric and electronic structures of 1,2,3-cyclohexatriene (**3.5**) with those of its isomer benzene (**3.1**) and its relative benzyne (**3.20**) (Figure 3.3A). Whereas the geometry of benzene is characterized by equivalent interior angles of 120°, the isomeric 1,2,3-triene **3.5** and benzyne (**3.20**) each show a wider internal angle at the positions shown (131° and 127°, respectively) as a consequence of constraining two formally sp-hybridized carbons to a six-membered ring. This structural deformation leads to a calculated strain energy of approximately 50 kcal/mol for both 1,2,3-cyclohexatriene (**3.5**)[29] and benzyne (**3.20**).[30] This calculated geometry for triene **3.5** is in good agreement with earlier reports.[29] However, to our knowledge, the electronic structure of **3.5** has not been reported previously. We find that the highest occupied molecular orbitals (HOMOs) of benzene (**3.1**), its isomer 1,2,3-cyclohexatriene (**3.5**), and benzyne (**3.20**)[31] are all localized to the conjugated π-systems, but the lowest unoccupied molecular orbital (LUMO) structures differ substantially. Unlike the LUMO of benzene, the LUMO of **3.5** is largely localized to the central, in plane π-bond of the triene and is 1.5 eV lower in energy. Although the LUMO structure and energy is very different between cyclic triene **3.5** and benzene (**3.1**), there is a strong similarity in comparison with benzyne (**3.20**). This similarity suggests that triene **3.5**, unlike its well-studied isomer benzene (**3.1**), should share the strong electrophilicity of benzyne and its propensity to undergo cycloaddition reactions.

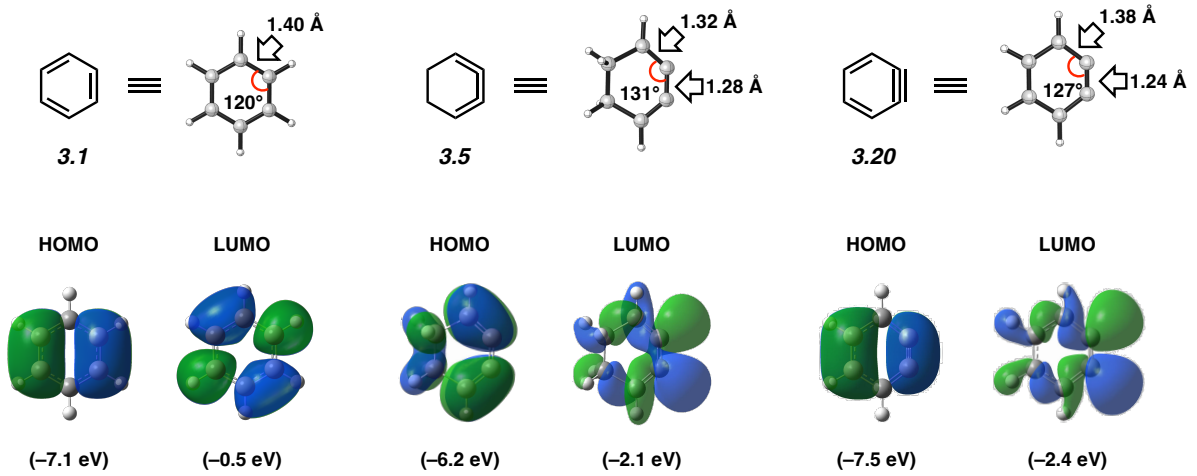

Figure 3.3A. Geometry-optimized structures and frontier molecular orbitals of benzene (**3.1**), 1,2,3-cyclohexatriene (**3.5**), and benzyne (**3.20**) (B3LYP-D3/6-311+G(d,p)).

3.4 Reactivity of 1,2,3-Cyclohexatriene (3.5)

To initiate the experimental study of 1,2,3-cyclohexatriene (**3.5**), we prepared silyl triflate **3.21**, a readily available compound known from a 1990 study,[8] and performed trapping experiments (Figure 3.3B). The use of a Kobayashi silyl triflate precursor was considered ideal, as Kobayashi precursors typically require mild fluoride sources to trigger in situ formation of the desired strained intermediate.[21] After optimization (see Section 3.9.3.1 for details), we found that generation and trapping of **3.5** proceeded best using CsF as the fluoride source, tetrabutylammonium triflate as a fluoride-solubilizing agent,[32] and THF as the solvent at 60 °C. Triene **3.5** reacts smoothly with various dienes including an isobenzofuran, furans, and a pyrrole to furnish (4+2) cycloadducts **3.27**–**3.30** in good yields (entries 1–4). We found that triene **3.5** undergoes dipolar (3+2) cycloadditions with azomethine imines **3.31** and **3.32** to give cycloadducts **3.35** and **3.36**, respectively (entries 5 and 6). A formal (2+2) cycloaddition could also be achieved by using ketene acetal **3.33** as a trap, giving cyclobutane **3.37** (entry 7). Moreover, the use of phenoxide **3.34** as a nucleophile gives direct addition product **3.38**. These results indicate that

triene **3.5** is indeed a versatile intermediate capable of undergoing a range of trapping reactions despite having been minimally exploited in earlier experimental studies.

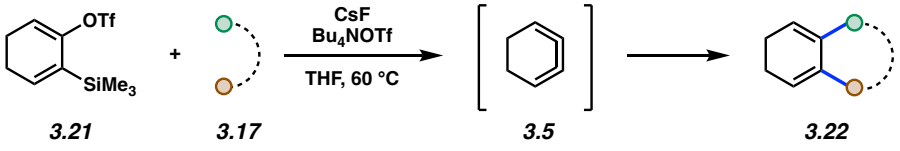

3.21 *3.17* *3.5* *3.22*

Entry	*Trapping Agent*		*Product*		*Yield*
1	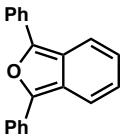	*3.23*	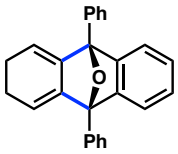	*3.27*	65%
2	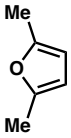	*3.24*	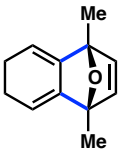	*3.28*	62%
3		*3.25*	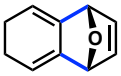	*3.29*	72%
4	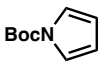	*3.26*	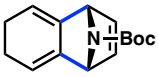	*3.30*	61%
5	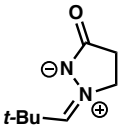	*3.31*	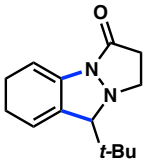	*3.35*	59%
6	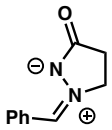	*3.32*	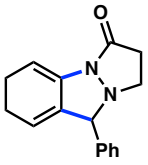	*3.36*	51%
7	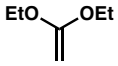	*3.33*	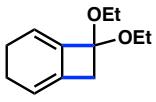	*3.37*	44%
8[a]	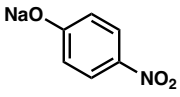	*3.34*	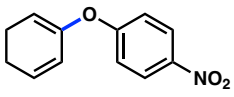	*3.38*	51%

Figure 3.3B. Trapping reactions of triene **3.5**. Reaction conditions are as follows: **3.21** (1 equiv), trapping partner **3.17** (5–20 equiv), CsF (10 equiv), Bu_4NOTf (2 equiv), THF (0.1 M), 60 °C, 24

h. Yields were determined by an average of two isolation experiments. [a] Modified reaction conditions: CsF (20 equiv), Bu_4NOTf (4 equiv), MeCN (0.1 M), 60 °C, 22 h (see Section 3.9.3.2 for details).

3.5 Reactivity of a Substituted 1,2,3-Cyclohexatriene Derivative

Substituted 1,2,3-cyclohexatrienes are largely unknown. To our knowledge, a single literature example suggestive of a substituted derivative of 1,2,3-cyclohexatriene (**3.5**) is available,[11] which required pyrolytic temperatures (600 °C) and led to unimolecular rearrangement processes of the presumed triene intermediate yielding a mixture of products. By contrast, substituted arynes, cyclic alkynes, and cyclic allenes have been investigated extensively in both fundamental and applied studies to control regioselectivity in trappings and to synthesize complex structures.[21,33,34,35] As such, we undertook the study of two new substituted 1,2,3-cyclohexatrienes (di- and mono-substituted) to validate their intermediacy and assess their synthetic potential.

To evaluate a disubstituted 1,2,3-cyclohexatriene, we prepared dimethylated silyl triflate **3.42**, the presumed precursor to **3.43**, using the sequence shown in Figure 3.4A. Known brominated vinylogous ester **3.39**[36] was first converted to the corresponding silylated vinylogous ester **3.40** via a retro-Brook rearrangement of the corresponding silyl enol ether.[37] Subsequent 1,2-addition and Stork–Danheiser transposition afforded enone **3.41**. α-Methylation followed by triflation then delivered desired silyl triflate **3.42**. This synthetic route has proven flexible and scalable, thus providing a roadmap for future studies of substituted cyclic trienes.

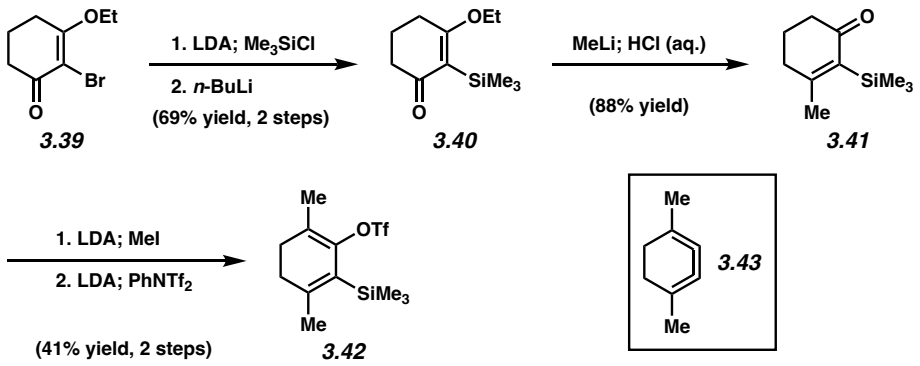

Figure 3.4A. Synthesis of silyl triflate **3.42**. See Section 3.9.3.3 for reaction details.

With silyl triflate **3.42**, we studied the generation and trapping of disubstituted triene **3.43** (Figure 3.4B). Our previously optimized reaction conditions led to low conversion, but we found that switching the solvent to acetonitrile and increasing the loading of Bu_4NOTf facilitated full conversion and good yields in trappings of **3.43**. More generally, we observed that trappings of disubstituted triene **3.43** proceeded in higher yields and with broader scope compared to trappings of the parent compound, 1,2,3-cyclohexatriene (**3.5**), despite **3.43** bearing an increased steric profile. The results shown highlight the engagement of disubstituted triene **3.43** in: (a) (4+2) cycloadditions with either electron-rich or electron-deficient dienes affording **3.50**–**3.52** (entries 1–3), (b) (3+2) cycloadditions using azomethine imines (**3.31** and **3.32**), nitrones (**3.46** and **3.47**), a quinolinium imide (**3.48**), or an isoquinolinium imide (**3.49**) to generate products **3.53**–**3.58** (entries 4–9), (c) a (5+2) cycloaddition of oxidopyridinium **3.59** to give [3.2.1] bicycle **3.66** (entry 10), (d) formal (2+2) reactions using nucleophilic 2π-systems, such as ketene acetal **3.33**, enamine **3.60**, and thioketone **3.61**, to afford the corresponding cyclobutane or thietane products **3.67–3.69** (entries 11–13), and (e) nucleophilic additions using oxygen, sulfur, nitrogen, or carbon nucleophiles **3.34** and **3.62**–**3.65** to give dienes **3.70**–**3.74**, respectively (entries 14–18). Notably, in the case of carbon nucleophiles **3.64** and **3.65**, formal C–C σ-bond insertion products were isolated, analogous to known aryne insertion reactions.[38] Collectively, these data showcase that

1,2,3-cyclic trienes may engage in a host of trappings akin to what has long been established for arynes, but largely overlooked for cyclic trienes. Moreover, a variety of structurally distinct scaffolds are accessible, including fused polycyclic compounds, bridged structures, and complex heterocycles. All of the products bear functional handles for further manipulation, particularly the 1,3-diene motif.

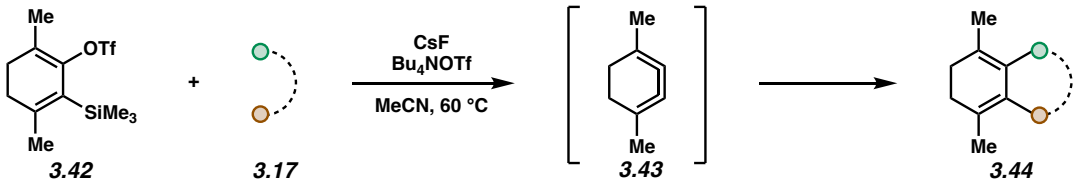

Entry	Trapping Agent	Product & Yield
1 2	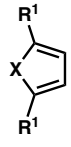	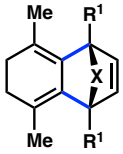
	X = O, R^1 = Me, ***3.24***	***3.50***, 80%
	X = NBoc, R^1 = H, ***3.26***	***3.51***, 82%
3	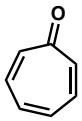	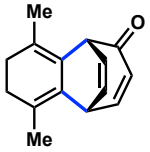
	3.45	***3.52***, 40%
4 5	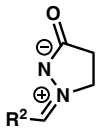	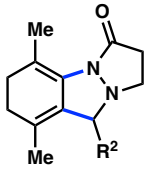
	R^2 = *t*-Bu, ***3.31***	***3.53***, 86%
	R^2 = Ph, ***3.32***	***3.54***, 87%
6 7	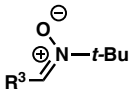	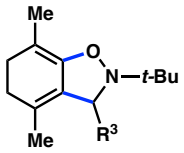
	R^3 = Ph, ***3.46***	***3.55***, 74%
	R^3 = *t*-Bu, ***3.47***	***3.56***, 75%
8	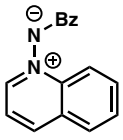	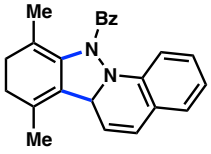
	3.48	***3.57***, 79%
9		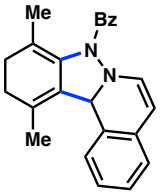
	3.49	***3.58***, 51%

Entry	Trapping Agent	Product & Yield
10	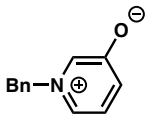	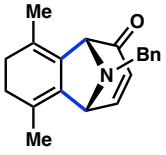
	3.59	***3.66***, 68%
11[a] 12[a]		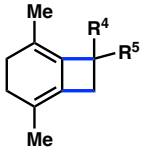
	R^4 = R^5 = OEt, ***3.33***	***3.67***, 47%
	R^4 = $N(Boc)_2$, R^5 = CO_2Me, ***3.60***	***3.68***, 48%
13	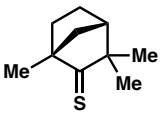	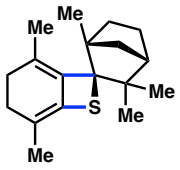
	3.61	***3.69***, 77% (2.7:1 dr)
14 15[a]	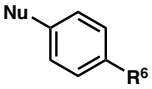	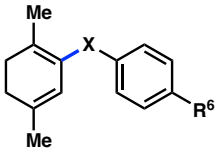
	Nu = NaO, R^6 = NO_2, ***3.34***	***3.70***, 83%
	Nu = SH, R^6 = H, ***3.62***	***3.71***, 81%
16		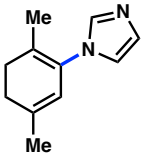
	3.63	***3.72***, 58%
17 18	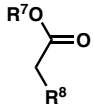	
	R^7 = Et, R^8 = CN, ***3.64***	***3.73***, 47%
	R^7 = Me, R^8 = CO_2Me, ***3.65***	***3.74***, 82%

Figure 3.4B. Scope of reactions of triene **3.43**. Reaction conditions are as follows: **3.42** (1 equiv), trapping partner **3.17** (5–20 equiv), CsF (20 equiv), Bu_4NOTf (4 equiv), MeCN (0.1 M), 60 °C, 24 h. Yields were determined by an average of two isolation experiments unless otherwise noted (see Section 3.9.3.4 for details). [a] Yield determined by ^1H NMR with mesitylene as external standard.

3.6 Regioselective Reactions of a Silyl-Substituted Triene

Figure 3.5 highlights studies related to **3.75**, an unsymmetrical monosubstituted 1,2,3-cyclic triene bearing a triethylsilyl substituent. Silyl substituents have previously been used to study the origins of regioselectivity in aryne trappings,[39,40,41,42] but similar studies relating to reactions of substituted 1,2,3-cyclic trienes have not been reported. The structure of **3.75** was optimized using DFT calculations (Figure 3.5A). Polarization of the C1–Si bond toward C1 leads to rehybridization of the internal, formally sp-hybridized carbons of triene **3.75** in accordance with Bent's Rule,[43,44] which states that 'atomic s-character concentrates in orbitals directed toward electropositive substituents' and has been applied in previous studies of silyl-substituted arynes.[39] This rehybridization strongly distorts the ground state geometry, leading to a significantly flattened C1=C2=C3 bond angle (θ_{C2} = 146°) and a contracted C2=C3=C4 bond angle (θ_{C3} = 118°) relative to those of unsubstituted triene **3.5** ($\theta_{C2} = \theta_{C3}$ = 131°). This geometric distortion also yields a shift in the electron distribution in the substituted triene, with C2 now bearing a slight positive charge, and C3 bearing a slight negative charge, consistent with the observed rehybridization. We inferred that **3.75** could undergo regioselective trapping given that analogous ground state distortion has previously led to regioselectivity in trapping reactions of silyl-substituted arynes.[39]

To test this hypothesis, we prepared triethylsilyl-substituted silyl triflate **3.76** (see Section 3.9.3.5 for details) and performed the key trapping experiments shown in Figure 3.5B. With the large enamine **3.77** as the trap, adduct **3.78** was obtained, arising from a sterically-controlled addition onto C3 of the triene, distal to the bulky triethylsilyl substituent. Conversely, with smaller phenoxide nucleophile **3.34** as the trap, a complete switch in regioselectivity was observed; adduct

3.79 was the sole product, arising from proximal attack at C2. We proposed that this contrasteric outcome could arise from reactant pre-distortion, wherein the geometric distortion in the ground state discussed above probably mirrors the geometry of the transition state, leading to the observed product. Such effects have been observed extensively in aryne chemistry and have been codified previously in the 'aryne distortion model,' an application of distortion/interaction activation strain (DIAS) analysis,[45] which enables the prediction of regiochemical outcomes in reactions of substituted arynes.[46,47,48,49,50] DFT studies of the phenoxide trapping were performed (using a trimethylsilyl group instead of a triethylsilyl group and omitting the Na^+ counterion) to validate the pre-distortion hypothesis (Figure 3.5C). Consistent with our experiments, addition at C2 (see **TS-3.1**) was found to be favored over addition at C3 (see **TS-3.2)** by 3.1 kcal/mol ($\Delta\Delta G^{\ddagger}$; $\Delta\Delta E^{\ddagger}$ = 4.6 kcal/mol). To explain the origin of this difference, we performed DIAS analysis to decompose $\Delta\Delta E^{\ddagger}$ into two separate contributions from reactant distortion energies and interaction energies.[45] Regarding distortion, $\Delta\Delta E^{\ddagger}_{distortion}$ for nucleophile **3.34** was negligible. However, $\Delta\Delta E^{\ddagger}_{distortion}$ for triene **3.80** is 1.4 kcal/mol, indicating greater distortion of triene **3.80** in **TS-3.2** compared to **TS-3.1**. The geometry of the triene in **TS-3.1** is indeed very similar to that of ground state triene **3.80**, thus requiring minimal geometric distortion to reach **TS-3.1** geometry ($\Delta\theta_{C3}$ = –4°; $\Delta\theta_{C2}$ = 0°). Conversely, arriving at **TS-3.2** requires substantial geometric reorganization ($\Delta\theta_{C3}$ = 18°; $\Delta\theta_{C2}$ = –21°). This supports the notion that triene pre-distortion contributes to **TS-3.1** being favored as proposed. DIAS analysis also indicates strong differences in interaction energies ($\Delta\Delta E^{\ddagger}_{interaction}$ = 3.2 kcal/mol.), which contribute significantly to the observed selectivity (see Section 3.9.4.4 for details). Overall, the results shown in Figure 3.5 suggest that sterics, distortion, and interaction all contribute to controlling selectivity and that substituted 1,2,3-cyclohexatrienes can be employed in regioselective reactions with potentially predictable outcomes.

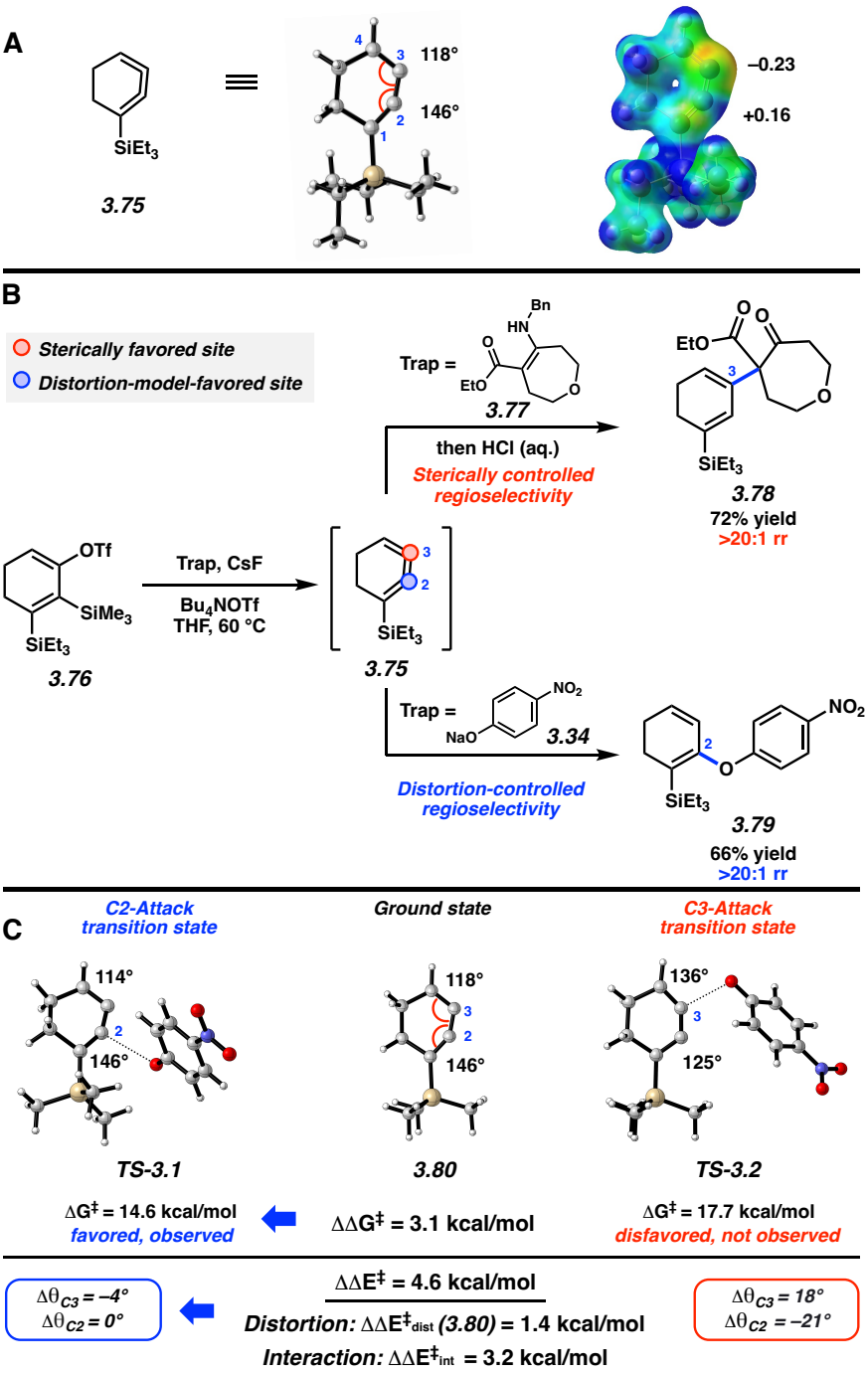

Figure 3.5. Structure and regioselective reactions of a monosubstituted cyclic triene. (A) Geometry-optimized structure of triene **3.75** and electrostatic potential map (B3LYP-D3/6-311+G(d,p)) (natural bond orbital (NBO) charges shown). (B) Yields determined by isolation experiments (see Section 3.9.3.6 for reaction details). rr, regioisomeric ratio. (C) Transition state analysis at 333.15 K using a trimethyl silyl group to model the triethyl silyl group in **3.75** and omitting the Na^+ cation of **3.34** (B3LYP-D3/6-311+G(d,p)/SMD(THF)) (see Section 3.9.4.4 for details).

3.7 Leveraging Cyclic Trienes to Access Complex Scaffolds

Figure 3.6 shows the previously untapped value of strained cyclic trienes for the construction of complex scaffolds. Tricyclic diene **3.35**, prepared by azomethine imine cycloaddition of triene **3.5** (see Figure 3.3B), was elaborated to four compounds with different skeletons (**3.81**–**3.84**, Figure 3.6A). Diene **3.35** underwent a Diels–Alder reaction with *N*-Ph-maleimide with high facial control guided by the *t*-Bu substituent to generate [2.2.2]-bicycle **3.81**. The diene of **3.35** can instead serve as a 2π–component in cycloaddition reactions with either a strained cyclic allene or a nitrile oxide to generate fused polycycles **3.82** and **3.83**, respectively. These transformations occur with high regioselectivity with respect to both the diene and trap and give rise to unusual heterocyclic scaffolds. Alternatively, the diene motif of **3.35** can be preserved through chemoselective reduction of the *N*–*N* bond[51] to reveal the 6/8 fused ring system of **3.84**.

The synthetic sequence shown in Figure 3.6B establishes that 1,2,3-cyclic trienes can be used to quickly assemble complex scaffolds in a highly selective manner. Silyl-substituted triene **3.75** was trapped using enantioenriched enamine **3.85**. After hydrolytic workup, diene (+)-**3.78** was obtained regioselectively in 92% ee. Subsequent allylation of (+)-**3.78** yielded diene (–)-**3.87** bearing a pendant alkene. Thermolysis of (–)-**3.87** effected a Diels–Alder (see **TS-3.3**) and retro-carbonyl-ene cascade to yield (+)-**3.19** in 91% ee; (+)-**3.19** bears considerable structural complexity as exemplified by the 11-membered ring, a highly substituted [2.2.2]-bicycle, and three stereocenters. This concise, three-step elaboration of triene **3.75** to (+)-**3.19** demonstrates that, despite their high reactivity and minimal use in prior experimental studies, strained cyclic trienes can be engaged in regio- and stereoselective reactions to ultimately access complex products.

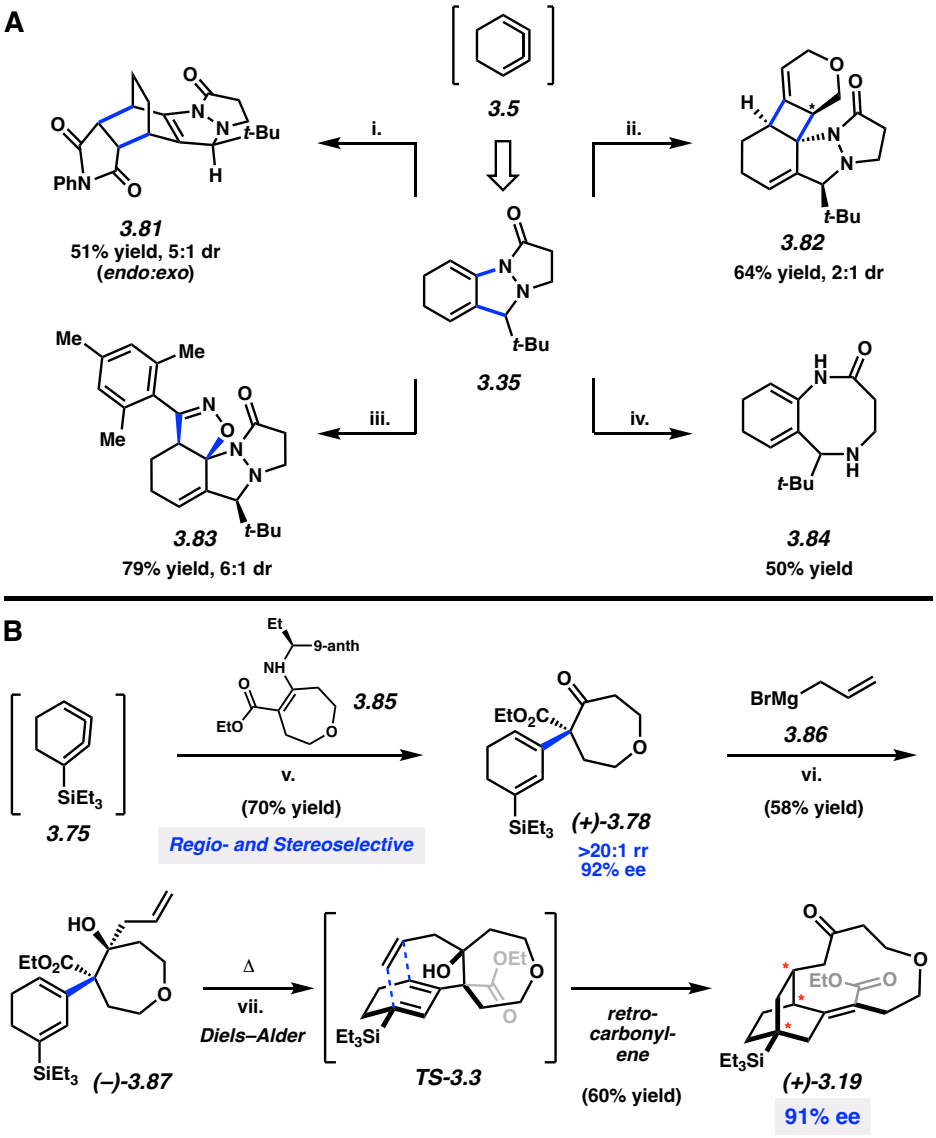

Figure 3.6. Strained 1,2,3-cyclohexatrienes in multistep synthesis. (A) Reaction conditions are as follows: (i) *N*-Ph maleimide (2.5 equiv), benzene, 80 °C, 51% yield, 5:1 dr. (ii) oxacyclic allene precursor (1.5 equiv), CsF (5 equiv), MeCN, 23 °C, 64% yield, 2:1 dr at the stereocenter indicated by an *. (iii) mesitylene nitrile oxide (1.5 equiv), CH_2Cl_2, 0 to 40 °C, 79% yield, 6:1 dr. (iv) sodium naphthalenide (3 equiv), THF, 0 °C, 50% yield. See Section 3.9.3.7 for full reaction details. dr, diastereomeric ratio (B) Reaction conditions are as follows: (v) enamine **3.85** (5 equiv), CsF, (10 equiv), Bu_4NOTf (2 equiv), THF, 60 °C, then HCl (1 M), 23 °C, 70% yield, >20:1 rr, 92% ee. (vi) allylMgBr (2 equiv), THF, –78 °C, 58% yield, >20:1 dr. (vii) hexadecane, 220 °C, 60% yield (see Section 3.9.3.7 for full reaction details). rr, regioisomeric ratio.

3.8 Conclusion

These studies establish that the unusual benzene isomer 1,2,3-cyclohexatriene, along with its derivatives, can be harnessed in chemical synthesis. As such, these efforts should prompt the further investigation of the fundamental properties of strained cyclic 1,2,3-hexatrienes and their strategic application in the synthesis of important compounds.

3.9 Experimental Section

3.9.1 Method for Literature Searches for Strained Intermediate Studies.

The values included for the number of literature reports for various strained intermediates were obtained using keyword searching in SciFinder^n with the following keywords. For strained cyclic alkynes: "benzyne", "aryne" or "strained alkyne". For strained cyclic allenes: "1,2-cyclohexadiene", "1,2-cycloheptadiene", "1,2-cyclooctadiene" or "strained allene".

3.9.2 Materials and Methods

Unless stated otherwise, reactions were conducted in flame-dried glassware under an atmosphere of nitrogen, and commercially obtained reagents were used as received unless otherwise specified. Anhydrous solvents were either freshly distilled or passed through activated alumina columns, unless otherwise stated. Non-commercially available substrates were synthesized according to known preparations or following protocols specified in the Experimental Procedures. Prior to use in trapping experiments, acetonitrile (MeCN) and tetrahydrofuran (THF) were passed through an activated alumina column and degassed by five freeze-pump-thaw cycles. Dimethylformamide (DMF), benzonitrile (PhCN), 1,4-dioxane, 1,2-dichloroethane (DCE), 1,2-dimethoxyethane (DME), dichloromethane, benzene, and triethylamine (Et_3N) were passed

through an activated alumina column prior to use. Diisopropylamine, pyridine, trimethylsilyl chloride, and triethylsilyl chloride were distilled over CaH_2 prior to use. Tetrabutylammonium iodide (Bu_4NI), tetrabutylammonium fluoride (TBAF) solution (1.0 M in THF), tris(dimethylamino)sulfonium difluorotrimethylsilicate (TASF), tetrabutylammonium trifluoromethanesulfonate (Bu_4NOTf), *n*-butyllithium (*n*-BuLi), hexadecane, methyllithium, magnesium bromide diethyl etherate, *N*-phenyl maleimide, *N*-Boc-pyrrole (**3.26**), tropone (**3.45**), thiophenol (**3.62**), imidazole (**3.63**), ethyl cyanoacetate (**3.64**), dimethyl malonate (**3.65**), pyridinium perbromide, benzoic anhydride, Florisil® (<200 mesh, fine powder), and Brockman Grade activated basic alumina (60 mesh powder) were all purchased from Sigma-Aldrich and used as received. Cesium fluoride was obtained from Strem Chemicals, stored in a glovebox, and used as received. Methyl iodide was obtained from Thermofisher Scientific. *N*-(5-chloro-2-pyridyl)bis(trifluoromethanesulfonimide) (Comins' Reagent), 2,5-dimethylfuran (**3.24**), diphenylisobenzofuran (**3.23**), and *N*-*tert*-butyl α-phenylnitrone (**3.46**), were purchased from Combi Blocks. *N*-phenyl-bis(trifluoromethanesulfonimide) ($PhNTf_2$) was obtained from Oakwood Chemicals. Furan (**3.25**) was obtained from Acros Organics. 1,1-Diethoxyethene (**3.33**) was obtained from Fluka Chemicals. Reaction temperatures at or above 23 °C were controlled using an IKAmag temperature modulator, and unless stated otherwise, performed at room temperature (approximately 23 °C). Thin-layer chromatography (TLC) was conducted with EMD gel 60 F_{254} pre-coated plates (0.25 mm for analytical chromatography and 0.50 mm for preparative chromatography) and visualized using a combination of UV, anisaldehyde, and potassium permanganate staining techniques. Silicycle Siliaflash P60 (particle size 40–63 μm) was used for flash column chromatography unless otherwise specified. ^{1}H-NMR and 2D-NOESY spectra were recorded on Bruker spectrometers (at 400, 500, 600, and 800 MHz) and are reported relative to the

residual solvent signal. Data for ^{1}H-NMR spectra are reported as follows: chemical shift (δ ppm), multiplicity, coupling constant (Hz), and integration. ^{13}C-NMR spectra were recorded on Bruker spectrometers (at 100, 125, and 150 MHz) and are reported relative to the residual solvent signal. Data for ^{13}C-NMR spectra are reported in terms of chemical shift (δ ppm) and, when necessary, multiplicity, and coupling constant (Hz). ^{19}F-NMR spectra were recorded on Bruker spectrometers (at 376 MHz) and are reported in terms of chemical shift (δ ppm), multiplicity, and integration. ^{1}H NMR yields were determined by addition of an aliquot of a stock solution of external standard, 2,5-dimethylfuran or mesitylene, in C_6D_6 to the concentrated crude reaction mixture followed by further dilution with C_6D_6 and subsequent ^{1}H NMR analysis. Control experiments demonstrated agreement within 2% between 2,5-dimethylfuran and mesitylene as external standards. IR spectra were recorded on a Perkin-Elmer UATR Two FT-IR spectrometer and are reported in terms of frequency absorption (cm^{-1}). DART-MS spectra were collected on a Thermo Exactive Plus MSD (Thermo Scientific) equipped with an ID-CUBE ion source and a Vapur Interface (IonSense Inc.). Both the source and MSD were controlled by Excalibur software version 3.0. The analyte was spotted onto OpenSpot sampling cards (IonSense Inc.) using $CDCl_3$ or CH_2Cl_2 as the solvent. Ionization was accomplished using UHP He plasma with no additional ionization agents. The mass calibration was carried out using Pierce LTQ Velos ESI (+) and (–) Ion calibration solutions (Thermo Fisher Scientific). Optical rotations were measured with a Rudolf Autopol III Automatic Polarimeter. Determination of enantiopurity was carried out on a JASCO SFC (supercritical fluid chromatography) using a Daicel ChiralPak AD-H column. Data for SFC chromatograms are reported in enantiomeric excess (ee). Diastereomeric ratios (dr) and regioisomeric ratios (rr) were determined by ^{1}H analysis of crude reaction mixtures.

Silyl triflate **3.21**[8], cycloadduct **3.27**[8], azomethine imines **3.31**[52] and **3.32**[53], phenoxide **3.34**[54], vinylogous ester **3.39**[55], nitrone **3.47**[56], quinolinium imide **3.48**[57], isoquinolinium imide **3.49**[57], oxidopyridinium **3.59**[58], enamine **3.60**[59], thioketone **3.61**[60], ketal **3.88**[61], enamines **3.77** and **3.85**[62], silyl triflate **3.89**[63], and nitrile oxide **3.90**[64] are all known compounds. The ^{1}H NMR spectral data matched those reported in literature.

3.9.3 Experimental Procedures

3.9.3.1 Optimization of Trapping Reactions of 1,2,3-Cyclohexatriene (3.5)

Selected results from the optimization of the reaction between silyl triflate **3.21** and azomethine imine **3.31** commencing from the closest literature precedent[8] appear below. Solvent, fluoride source, and additives were varied using General Procedure 3.1, and results appear below in Table 3.1. For the use of tetrabutylammonium salts as phase transfer reagents in combination with alkali metal fluorides, see references 32 and 65.

General Procedure 3.1 for the optimization of trapping reactions of triene 3.5:

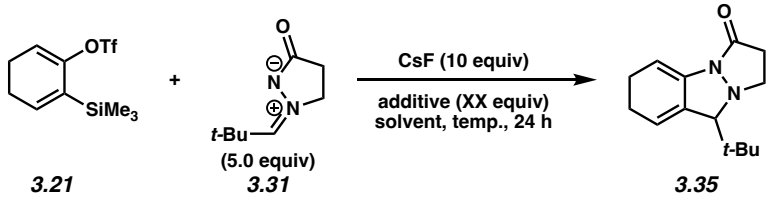

3.21 *3.31* *3.35*

A flame-dried 1-dram vial containing a magnetic stir bar was charged sequentially with silyl triflate **3.21** (10.0 mg, 0.03 mmol, 1.0 equiv), additive (0–2.0 equiv), azomethine imine **3.31** (25.7 mg, 0.16 mmol, 5.0 equiv), solvent (0.320 mL, 0.1 M), and CsF (48.5 mg, 0.32 mmol, 10 equiv) in a glovebox. The vial was then sealed with a Teflon-lined cap, removed from the glovebox, and stirred for 24 h at the desired reaction temperature. The mixture was then filtered over a pad of

Celite, eluting with EtOAc (10 mL). The eluate was concentrated then analyzed by ^{1}H NMR using 2,5-dimethylfuran as an external standard.

Table 3.1. Selected Optimization Screening Results.

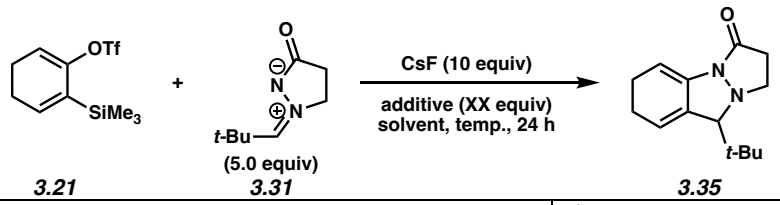

3.21 *3.31* *3.35*

Entry	Conditions	^{1}H NMR Yield[a]	Yield BRSM
1	DMSO, 23 °C	26%	26%
2	MeCN, 23 °C	2%	100%
3	Bu_4NI (1.0 equiv), MeCN, 60 °C	24%	32%
Solvent Screen			
4	Bu_4NI (1.0 equiv), DMSO, 60 °C	24%	24%
5	Bu_4NI (1.0 equiv), DMF, 60 °C	28%	28%
6	Bu_4NI (1.0 equiv), PhCN, 60 °C	19%	23%
7	Bu_4NI (1.0 equiv), Dioxane, 60 °C	14%	61%
8	Bu_4NI (1.0 equiv), DME, 60 °C	13%	25%
9	Bu_4NI (1.0 equiv), PhH, 60 °C	12%	40%
10	Bu_4NI (1.0 equiv), DCE, 60 °C	0%	N/A
11	Bu_4NI (1.0 equiv), THF, 60 °C	38%	42%
Fluoride Source Screen			
12	–CsF, +TBAF (5.0 equiv), THF, 23 °C	9%	17%
13	–CsF, +TASF (5.0 equiv), THF, 23 °C	16%	16%
14	CsF (5 equiv), Bu_4NOTf (2.0 equiv), THF, 23 °C	44%	46%
Additive Loading Screen			
15	Bu_4NOTf (1.0 equiv), THF, 60 °C	42%	76%
16	Bu_4NOTf (2.0 equiv), THF, 60 °C	54%	54%
17[b]	Bu_4NOTf (2.0 equiv), THF, 60 °C	36%[c]	40%

[a] ^{1}H NMR yield determined using 2,5-dimethylfuran as an external standard. [b] Reaction was set up according to General Procedure 3.1, but the procedure was performed entirely outside of the glovebox. [c] Yields for reactions performed outside of a glovebox under these conditions were found to vary between 36–67%. The value reported represents the low end of reaction efficiency observed in these experiments.

3.9.3.2 Scope of Trapping Reactions of 1,2,3-Cyclohexatriene (3.5)

General Procedure 3.2 for the scope of trapping reactions of 1,2,3-cyclohexatriene (3.5):

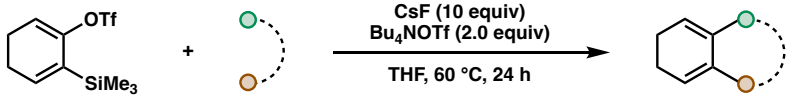

3.21 *3.17* *3.22*

A flame-dried 1-dram vial containing a magnetic stir bar was charged sequentially with silyl triflate **3.21** (31.3 mg, 0.10 mmol, 1.0 equiv), Bu_4NOTf (78.3 mg, 0.20 mmol, 2.0 equiv), trapping partner **3.17** (5.0–20 equiv), THF (1.00 mL, 0.1 M), and CsF (152 mg, 1.0 mmol, 10 equiv) in a glovebox. The vial was then sealed with a Teflon-lined cap, removed from the glovebox, and stirred for 24 h at 60 °C. The mixture was then filtered over a pad of Celite, eluting with EtOAc (10 mL). The eluate was concentrated under reduced pressure then purified by chromatography to provide adducts **3.22**.

Any modification of the conditions shown in the general procedure above are specified in the following schemes. Deviations in trapping partner stoichiometry result from cursory empirical optimization. In most cases, higher loadings of trapping reagents led to higher yields, though exceptions were observed.

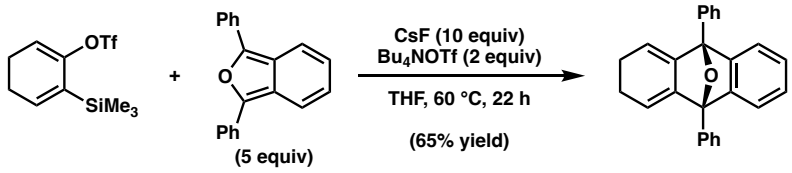

3.21 *3.23* *3.27*

Cycloadduct 3.27. Followed General Procedure 3.2. Analysis of the crude reaction mixture by ^1H NMR using 2,5-dimethylfuran as an external standard showed 71% yield. Purification by flash

chromatography on Florisil (hexanes → 40:3 hexanes:EtOAc) afforded cycloadduct **3.27** (65% yield, average of two experiments) as a pale yellow solid. **Cycloadduct 3.27**: Spectral data matched those reported in the literature.[8]

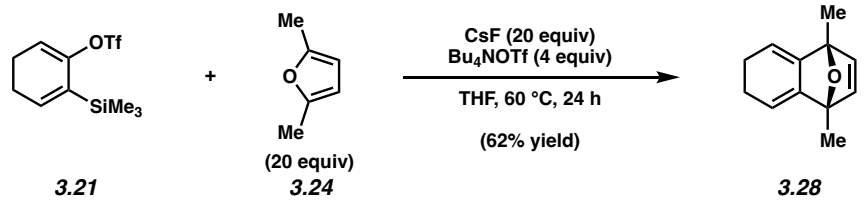

3.21 *3.24* *3.28*

Cycloadduct 3.28. Followed a modified version of General Procedure 3.2 by altering the amount of Bu_4NOTf (157 mg, 0.4 mmol, 4.0 equiv) and CsF (304 mg, 2.0 mmol, 20 equiv). Purification by flash chromatography on Florisil (pentane → 10:1 pentane:Et_2O) afforded cycloadduct **3.28** (62% yield, average of two experiments) as a colorless oil. **Cycloadduct 3.28**: R_f 0.50 (9:1 hexanes:EtOAc); ^1H NMR (600 MHz, C_6D_6): δ 5.97 (s, 2H), 5.33–5.26 (m, 2H), 2.13–1.99 (m, 4H), 1.57 (s, 6H); ^{13}C NMR (150 MHz, C_6D_6): δ 141.1, 139.1, 110.6, 86.0, 22.8, 15.2; IR (film): 3058, 2930, 2877, 1381, 1145 cm^{-1}; HRMS-APCI (*m/z*) $[M + H]^+$ calcd for $C_{12}H_{15}O^+$, 175.1117; found 175.1112.

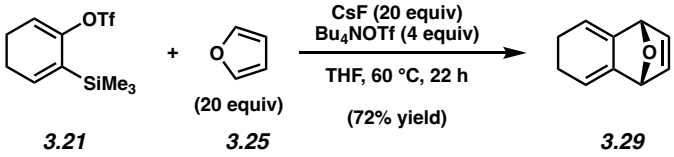

3.21 *3.25* *3.29*

Cycloadduct 3.29. Followed a modified version of General Procedure 3.2 by altering the amount of Bu_4NOTf (157 mg, 0.4 mmol, 4.0 equiv) and CsF (304 mg, 2.0 mmol, 20 equiv). Purification by flash chromatography on Florisil (pentane → 10:1 pentane:Et_2O) afforded cycloadduct **3.29** (72% yield, average of two experiments) as a colorless oil. **Cycloadduct 3.29**: R_f 0.62 (9:1

hexanes:EtOAc); ^{1}H NMR (600 MHz, C_6D_6): δ 6.04 (s, 2H), 5.39–5.35 (m, 2H), 4.97 (s, 2H), 2.13–2.03 (m, 2H), 2.02–1.92 (m, 2H); ^{13}C NMR (150 MHz, C_6D_6): δ 135.6, 135.1, 112.8, 80.4, 23.0; IR (film): 3010, 2925, 2829, 998, 823 cm^{-1}; HRMS-APCI (m/z) $[M + H]^+$ calcd for $C_{10}H_{11}O^+$, 147.0804; found 147.0799.

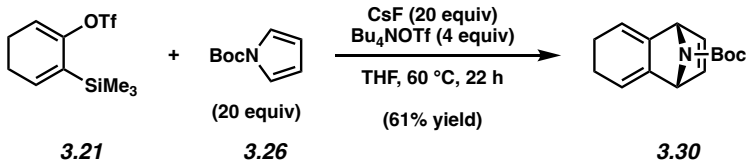

Cycloadduct 3.30. Followed a modified version of General Procedure 3.2 by altering the amount of Bu_4NOTf (157 mg, 0.4 mmol, 4.0 equiv) and CsF (304 mg, 2.0 mmol, 20 equiv). Purification by flash chromatography on Florisil (pentane → 10:1 pentane:Et_2O) afforded cycloadduct **3.30** (61% yield, average of two experiments) as a light yellow oil. **Cycloadduct 3.30**: R_f 0.38 (9:1 hexanes:EtOAc); ^{1}H NMR (500 MHz, CD_2Cl_2): δ 6.31 (s, 2H), 5.64 (s, 2H), 4.87 (s, 2H), 2.30–2.08 (m, 4H), 1.38 (s, 9H); ^{13}C NMR (125 MHz, CD_2Cl_2): δ 155.1, 135.1, 134.5, 114.1, 80.0, 64.3, 63.6, 27.9, 22.7; IR (film): 3037, 2929, 1704, 1337, 1251 cm^{-1}; HRMS-APCI (*m/z*) $[M + H]^+$ calcd for $C_{15}H_{20}NO_2^+$, 246.1489; found 246.1504.

*Note: **3.30** was obtained as a mixture of rotamers. These data represent empirically observed chemical shifts from the ^{1}H and ^{13}C NMR spectra.*

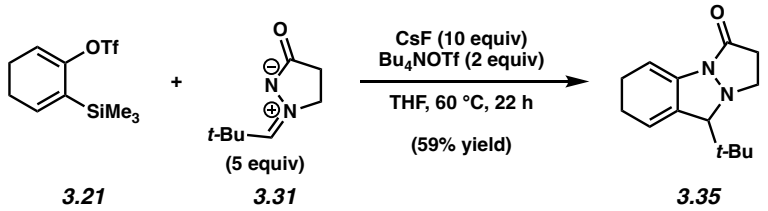

3.21 *3.31* *3.35*

Cycloadduct 3.35. Followed General Procedure 3.2. Purification by flash chromatography on Florisil (3:1 hexanes:EtOAc) afforded **3.35** (59% yield, average of two experiments) as an off-white solid. **Cycloadduct 3.35**: Mp: 106 °C; R_f 0.21 (5:1 hexanes:EtOAc); ^{1}H NMR (500 MHz, C_6D_6): δ 6.08–6.04 (m, 1H), 5.41–5.37 (m, 1H), 2.88 (t, *J* = 8.0, 1H), 2.58 (q, *J* = 2.7, 1H), 2.46 (ddd, *J* = 15.3, 13.8, 7.9, 1H), 2.16–1.91 (m, 6H), 0.86 (s, 9H); ^{13}C NMR (100 MHz, C_6D_6): δ 165.0, 136.1, 131.4, 121.4, 99.6, 76.1, 57.0, 35.7, 35.0, 26.4, 24.1, 21.2; IR (film): 2928, 2867, 1699, 1661, 1400 cm^{-1}; HRMS-APCI (*m/z*) $[M + H]^+$ calcd for $C_{14}H_{21}N_2O^+$, 233.1648; found 233.1649.

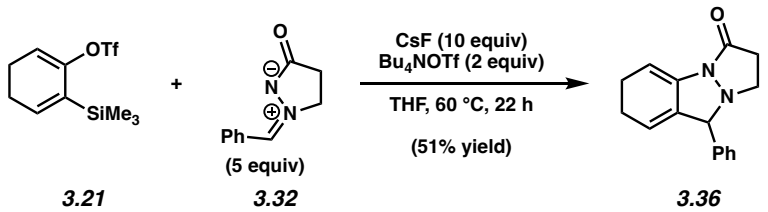

3.21 *3.32* *3.36*

Cycloadduct 3.36. Followed General Procedure 3.2. Purification by flash chromatography on Florisil (4:1 hexanes:EtOAc → 2:1 hexanes:EtOAc) afforded **3.36** (51% yield, average of two experiments) as a white solid. **Cycloadduct 3.36**: Mp: 107–108 °C; R_f 0.20 (3:1 hexanes:EtOAc); ^{1}H NMR (500 MHz, C_6D_6): δ 7.26 (d, *J* = 7.7, 2H), 7.18 (overlapped with residual solvent peak, 2H), 7.14–7.09 (m, 1H), 6.14 (dd, *J* = 5.4, 3.1, 1H), 4.98–4.92 (m, 1H), 3.70–3.62 (m, 1H), 2.80 (t, *J* = 8.5, 1H), 2.44 (ddd, *J* = 15.8, 13.1, 8.7, 1H), 2.16–2.01 (m, 3H), 2.00–1.92 (m, 1H), 1.90–1.79 (m, 1H), 1.78–1.69 (m, 1H); ^{13}C NMR (125 MHz, C_6D_6): δ 162.8, 140.1, 137.7, 129.8, 128.8,

128.7, 128.5, 120.0, 99.9, 73.6, 52.1, 36.0, 22.1, 21.7; IR (film): 3033, 2926, 2827, 1699, 1673 cm^{-1}; HRMS-APCI (*m/z*) $[M + H]^+$ calcd for $C_{16}H_{17}N_2O^+$, 253.1335; found 253.1351.

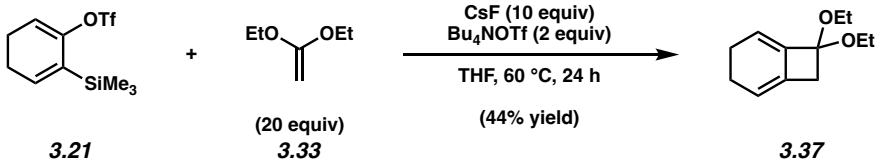

Cycloadduct 3.37. Followed General Procedure 3.2. Analysis of the crude reaction mixture by ^1H NMR using 2,5-dimethylfuran as an external standard showed 48% yield. Purification by preparative thin layer chromatography (10:1 hexanes:EtOAc) afforded cycloadduct **3.37** (44% yield, average of two experiments) as a yellow oil. **Cycloadduct 3.37**: R_f 0.31 (19:1 hexanes:EtOAc); ^1H NMR (600 MHz, C_6D_6): δ 5.52.–5.50 (m, 1H), 5.33–5.28 (m, 1H), 3.59 (qd, *J* = 9.3, 7.1, 2H), 3.51 (qd, *J* = 9.3, 7.1, 2H), 2.99–2.95 (m, 2H), 2.08–2.04 (m, 4H), 1.15 (t, *J* = 7.1, 6H); ^{13}C NMR (150 MHz, C_6D_6): δ 143.6, 133.9, 114.3, 114.2, 105.1, 58.5, 42.8, 23.5, 23.3, 15.5; IR (film): 3046, 2975, 2824, 1251, 1055 cm^{-1}; HRMS-APCI (*m/z*) $[M – OEt]^+$ calcd for $C_{10}H_{13}O^+$, 149.0961; found 149.0957.

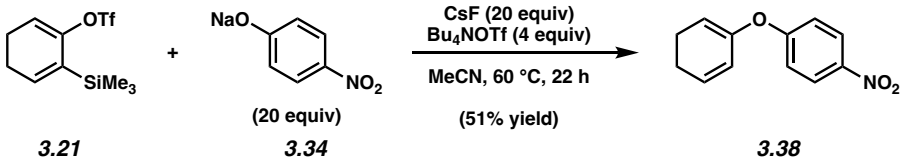

Adduct 3.38. Followed a modified version of General Procedure 3.2 by altering the amount of Bu_4NOTf (157 mg, 0.4 mmol, 4.0 equiv) and CsF (304 mg, 2.0 mmol, 20 equiv) and by switching the solvent to MeCN. Analysis of the crude reaction mixture by ^1H NMR using mesitylene as an external standard showed 50% yield. Purification by flash chromatography on Florisil (pentane → 4:1 pentane:Et_2O) afforded **3.38** (51% yield, average of two experiments) as a light yellow oil.

Adduct 3.38: R_f 0.57 (5:1 hexanes:EtOAc); ^{1}H NMR (500 MHz, C_6D_6): δ 7.84–7.79 (m, 2H), 6.59–6.54 (m, 2H), 5.65–5.58 (m, 1H), 5.55–5.49 (m, 1H), 5.07–5.02 (m, 1H), 1.95–1.87 (m, 2H), 1.86–1.78 (m, 2H); ^{13}C NMR (125 MHz, C_6D_6): δ 161.8, 149.2, 143.0, 130.8, 125.8, 122.8, 117.0, 109.0, 22.4, 21.4; IR (film): 3080, 2933, 1589, 1512, 1241 cm^{-1}; HRMS-APCI (*m/z*) $[M + H]^+$ calcd for $C_{12}H_{12}NO_3^+$, 218.0812; found 218.0819.

3.9.3.3 Synthesis of Silyl Triflate 3.42

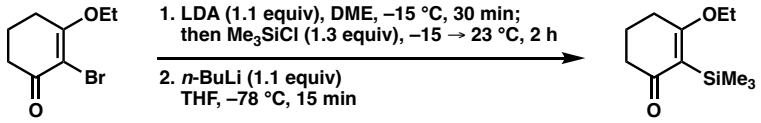

3.39 (69% yield, two steps) *3.40*

α-Silyl Vinylogous Ester 3.40. To a solution of diisopropylamine (9.15 g, 12.8 mL, 90.4 mmol, 1.2 equiv) in DME (150 mL) at –15 °C was added *n*-BuLi (2.5 M in hexanes, 33.1 mL, 1.1 equiv) dropwise over 5 min. The resulting solution was stirred at this temperature for 25 min, then vinylogous ester **3.39** (16.5 g, 75.3 mmol, 1.0 equiv) in DME (150 mL) was added dropwise via cannula over 20 min to give a bright yellow solution. Stirring was continued at this temperature for 30 min then trimethylsilyl chloride (11.9 mL, 97.9 mmol, 1.3 equiv) was added dropwise over 5 min. The cooling bath was removed, and stirring was continued for 2 h. After this time, the solvent was removed in vacuo, and the flask was evacuated and backfilled with nitrogen (3x). The heterogeneous yellow residue was suspended in pentane and filtered through Celite under a nitrogen atmosphere into a flame-dried round bottom flask (4 x 25 mL aliquots of pentane). The resulting eluate was concentrated under reduced pressure to give a yellow oil (20.8 g) which was dissolved in THF (476 mL, 0.15 M) and cooled to –78 °C. To this solution was added *n*-BuLi (2.5 M in hexanes, 31.4 mL, 1.1 equiv) dropwise over 15 min giving an orange solution. Stirring was

continued for 15 min then the reaction was quenched with a mixture of saturated ammonium chloride:water (1:20; 200 mL). The mixture was diluted with Et_2O (150 mL), and the layers were separated. The aqueous layer was extracted with Et_2O (2 x 150 mL), and the organic layers were combined, dried over magnesium sulfate, filtered, and concentrated under reduced pressure. The crude residue was purified by flash chromatography (4:1 → 7:3 hexanes:EtOAc) to provide α-silyl vinylogous ester **3.40** (10.4 g, 49.0 mmol, 69% yield, two steps) as a yellow solid. **α-Silyl Vinylogous Ester 3.40**: Mp: 46 °C; R_f 0.67 (9:1 benzene:MeCN); ^{1}H NMR (500 MHz, $CDCl_3$): δ 4.05 (q, *J* = 7.0, 2H), 2.51 (t, *J* = 6.3, 2H), 2.26 (t, *J* = 6.3, 2H), 1.95 (p, *J* = 6.3, 2H), 1.33 (t, *J* = 7.0, 3H), 0.16 (s, 9H); ^{13}C NMR (150 MHz, $CDCl_3$): δ 202.7, 182.3, 115.4, 63.4, 37.3, 26.2, 21.1, 15.0, 0.9; IR (film): 2950, 2894, 1633, 155.8, 1187 cm^{-1}; HRMS-APCI (*m/z*) $[M + H]^+$ calcd for $C_{11}H_{21}O_2Si^+$, 213.1305; found 213.1299.

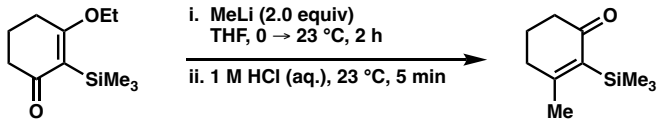

3.40 (88% yield) *3.41*

α-Silyl Enone 3.41. To a solution of vinylogous ester **3.40** (3.20 g, 15.0 mmol, 1.0 equiv) in THF (15 mL, 1 M) at 0 °C was added methyllithium (2.5 M in dimethoxymethane, 12.0 mL, 30.0 mmol, 2.0 equiv) dropwise over 2 min. The cooling bath was removed, and stirring was continued for 2 h. At this time, 1 M aqueous HCl (40 mL) was added carefully causing gas evolution. The biphasic mixture was stirred for 5 min then diluted with water (50 mL) and Et_2O (50 mL). The layers were separated, and the aqueous layer was extracted with Et_2O (2 x 50 mL). The organic layers were combined, dried over sodium sulfate, filtered, and concentrated. The crude residue was purified by flash chromatography (19:1 hexanes:Et_2O → 9:1 hexanes:Et_2O) to give α-silyl enone **3.41** (2.43

g, 13.3 mmol, 88% yield) as a clear colorless oil. **α-Silyl Enone 3.41**: R_f 0.78 (7:3 hexanes:EtOAc); ^{1}H NMR (400 MHz, $CDCl_3$): δ 2.34–2.23 (m, 4H), 2.02 (s, 3H), 1.95–1.85 (m, 2H), 0.21 (s, 9H); ^{13}C NMR (100 MHz, $CDCl_3$): δ 203.2, 169.5, 136.6, 37.9, 34.7, 24.8, 22.2, 1.7; IR (film): 2948, 1739, 1654, 1583, 1245 cm^{-1}; HRMS-APCI (*m/z*) $[M + H]^+$ calcd for $C_{10}H_{19}OSi^+$, 183.1200; found 183.1199.

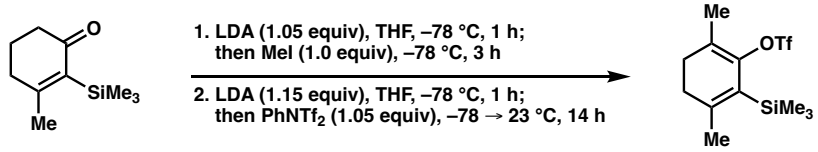

3.41 (41% yield, two steps) *3.42*

Silyl Triflate 3.42. To a solution of diisopropylamine (2.50 mL, 17.7 mmol, 1.1 equiv) in THF (25 mL) at –78 °C was added *n*-BuLi (2.4 M in hexanes, 7.05 mL, 16.9 mmol, 1.05 equiv) dropwise over 5 min. The resulting mixture was stirred for 15 min at this temperature, then the cooling bath was removed, and stirring was continued for an additional 15 min. The mixture was again cooled to –78 °C and then a solution of enone **3.41** (2.94 g, 16.1 mmol, 1.0 equiv) in THF (25 mL) was added dropwise via cannula over 8 min. The mixture was allowed to stir at –78 °C for 1 h and then iodomethane (1.00 mL, 16.1 mmol, 1.0 equiv) was added dropwise over 5 min at –78 °C. The reaction was stirred for an additional 3 h at –78 °C. At this time, the mixture was quenched with saturated ammonium chloride:water (1:20; 100 mL), diluted with Et_2O (50 mL), and the layers were separated. The aqueous layer was extracted with Et_2O (2 x 50 mL). The organic layers were combined, dried over magnesium sulfate, filtered, and concentrated to give a light yellow oil (2.98 g). The residue was dissolved in THF (14 mL) and added dropwise to a solution of LDA at –78 °C (prepared as described previously; 1.06 M in THF, 14 mL, 1.15 equiv). The resulting yellow solution was stirred at this temperature for 1 h then treated dropwise with a solution of $PhNTf_2$

(4.87 g, 13.6 mmol, 1.05 equiv) in THF (14 mL) via cannula over 4 min. The cooling bath was left in place, and the reaction was allowed to warm gradually from –78 °C to 23 °C over 14 h. After this time, the reaction was quenched with water (50 mL) and hexanes (50 mL). The layers were separated, and the aqueous layer was extracted with hexanes (2 x 50 mL). The organic layers were combined, dried over sodium sulfate, filtered, and concentrated. The residue was purified by flash chromatography on basic alumina (pentane) to give silyl triflate **3.42** (2.24 g, 6.57 mmol, 41% yield, two steps) as a light yellow oil. Note: Discoloration of silyl triflate **3.42** was observed within 5 minutes if left exposed to air. ^{1}H NMR analysis showed no change following discoloration, but samples of **3.42** were typically stored in a glovebox to avoid air exposure. **Silyl Triflate 3.42**: R_f 0.66 (19:1 hexanes:EtOAc); ^{1}H NMR (600 MHz, $CDCl_3$): δ 2.14–2.04 (m, 4H), 2.00 (s, 3H), 1.85 (s, 3H), 0.27 (s, 9H); ^{13}C NMR (150 MHz, $CDCl_3$): δ 150.5, 145.3, 127.3, 123.3, 118.6 (q, J = 318), 30.9, 29.5, 24.0, 16.7, 1.2; ^{19}F NMR (376 MHz, $CDCl_3$): δ –73.9 (s, 3F); IR (film): 2936, 1414, 1398, 1200, 1139 cm^{-1}; HRMS-APCI (*m/z*) $[M + H]^+$ calcd for $C_{12}H_{20}F_3O_3SSi^+$, 328.0771; found 328.0762.

3.9.3.4 Scope of Trapping Reactions of Triene 3.43

Empirically, we observed that reactions of substituted trienes occurred in higher yield compared to those of the unsubstituted 1,2,3-cyclohexatriene (**3.5**). The substituents on **3.43** likely help to suppress deleterious side reactions involving the reactive 1,2,3-triene or its precursor. The nature of this beneficial effect is currently unknown and will be subject to further investigation.

General Procedure 3.3 for the scope of trapping reactions of triene 3.43:

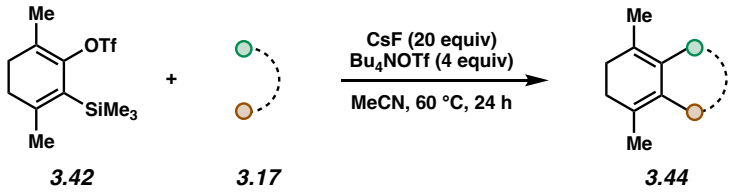

3.42 *3.17* *3.44*

A flame-dried 1-dram vial containing a magnetic stir bar was charged sequentially with silyl triflate **3.42** (34.2 mg, 0.10 mmol, 1.0 equiv), Bu_4NOTf (157 mg, 0.40 mmol, 4.0 equiv), trapping partner **3.17** (2.0–20 equiv), MeCN (1.00 mL, 0.1 M), and CsF (304 mg, 2.0 mmol, 20 equiv) in a glovebox. The vial was then sealed with a Teflon-lined cap, removed from the glovebox, and stirred for 24 h at 60 °C. The mixture was then filtered over a pad of Celite, eluting with EtOAc (10 mL). The eluate was concentrated under reduced pressure then purified by chromatography to provide adducts **3.44**.

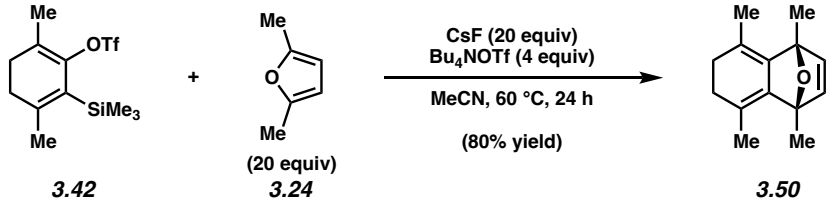

3.42 *3.24* *3.50*

Cycloadduct 3.50. Followed General Procedure 3.3. Purification by flash chromatography on Florisil (pentane → 10:1 pentane:Et_2O) afforded cycloadduct **3.50** (80% yield, average of two experiments) as a colorless oil. **Cycloadduct 3.50**: R_f 0.23 (19:1 hexanes:EtOAc); ^1H NMR (600 MHz, C_6D_6): δ 6.02 (s, 2H), 2.10–2.00 (m, 2H), 1.93–1.84 (m, 2H), 1.77 (s, 6H), 1.65 (s, 6H); ^{13}C NMR (150 MHz, C_6D_6): δ 138.9, 134.1, 118.9, 86.9, 31.6, 18.9, 18.1; IR (film): 3068, 2913, 2824, 1381, 1141 cm^{-1}; HRMS-APCI (*m/z*) $[M + H]^+$ calcd for $C_{14}H_{19}O^+$, 203.1430; found 203.1422.

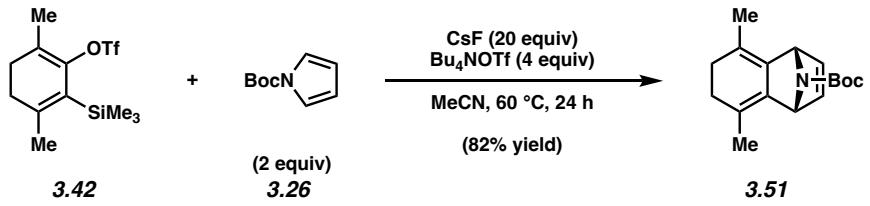

Cycloadduct 3.51. Followed General Procedure 3.3. Purification by flash chromatography on basic alumina (10:1 pentane:Et_2O → 1:1 pentane:Et_2O) afforded cycloadduct **3.51** (82% yield, average of two experiments) as a yellow oil. **Cycloadduct 3.51**: R_f 0.32 (5:1 hexanes:EtOAc); ^{1}H NMR (500 MHz, $CDCl_3$): δ 6.51–6.11 (m, 2H), 5.32–4.92 (m, 2H), 2.23–2.03 (m, 4H), 1.77 (s, 6H), 1.39 (s, 9H); ^{13}C NMR (125 MHz, $CDCl_3$): δ 155.8, 135.1, 133.7, 128.3, 127.7, 121.3, 120.8, 80.3, 62.7, 62.0, 29.5, 28.3, 19.1; IR (film): 3032, 2972, 1710, 1366, 1092 cm^{-1}; HRMS-APCI (*m/z*) $[M + H]^+$ calcd for $C_{17}H_{24}NO_2^+$, 274.1802; found 274.1794.

*Note: **3.51** was obtained as a mixture of rotamers. These data represent empirically observed chemical shifts from the ^{1}H and ^{13}C NMR spectra.*

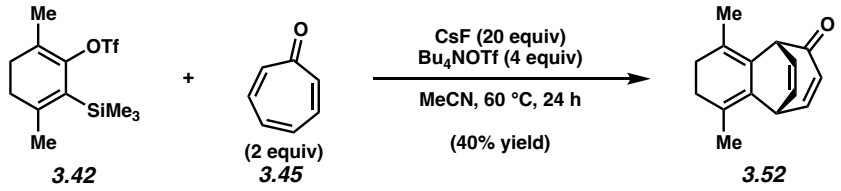

Cycloadduct 3.52. Followed General Procedure 3.3. Purification by preparative thin layer chromatography (5:1 benzene:Et_2O) afforded cycloadduct **3.52** (40% yield, average of two experiments) as a yellow oil. **Cycloadduct 3.52**: R_f 0.19 (9:1 hexanes:EtOAc); ^{1}H NMR (600 MHz, $CDCl_3$): δ 6.98 (dd, *J* = 10.9, 8.8, 1H), 6.54 (ddd, *J* = 8.3, 7.3, 1.0, 1H), 6.15 (ddd, *J* = 8.3, 7.3, 1.0, 1H), 5.65 (dd, *J* = 10.9, 1.9, 1H), 4.47–4.42 (m, 1H), 4.18 (t, *J* = 8.0, 1H), 2.27–2.17 (m, 2H), 2.16–2.01 (m, 2H), 1.85 (s, 3H), 1.82 (s, 3H); ^{13}C NMR (150 MHz, $CDCl_3$): δ 192.4, 150.5, 137.4, 131.3, 129.0, 127.4, 127.2, 124.2, 122.1, 56.9, 39.6, 31.0, 30.5, 19.3; 19.0; IR (film): 3053,

2984, 2852, 1662, 1379 cm^{-1}; H1RMS-APCI (*m/z*) $[M + H]^+$ calcd for $C_{15}H_{17}O^+$, 213.1274; found 213.1267.

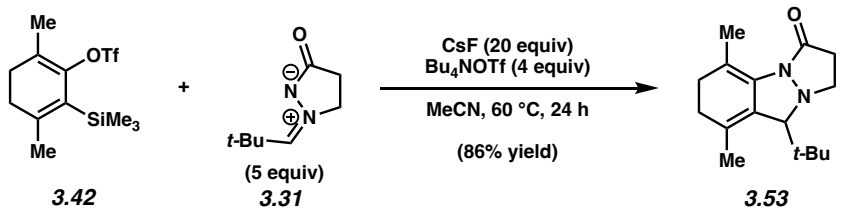

Cycloadduct 3.53. Followed General Procedure 3.3. Purification by flash chromatography on Florisil (4:1 pentane:Et_2O → 2:1 pentane:Et_2O) afforded cycloadduct **3.53** (86% yield, average of two experiments) as a white solid. **Cycloadduct 3.53**: Mp: 131–133 °C; R_f 0.28 (5:1 hexanes:EtOAc); ^1H NMR (500 MHz, $CDCl_3$): δ 3.58–3.52 (m, 1H), 3.05 (s, 1H), 3.02–2.87 (m, 2H), 2.45–2.38 (m, 1H), 2.28–2.14 (m, 2H), 2.06–1.98 (m, 2H), 1.97 (s, 3H), 1.74 (s, 3H), 1.54 (s, 9H); ^{13}C NMR (125 MHz, $CDCl_3$): δ 168.1, 129.1, 129.0, 128.8, 110.6, 73.8, 57.0, 38.4, 35.3, 32.0, 29.7, 26.6, 21.5, 20.2; IR (film): 2922, 2867, 1684, 1360, 1096 cm^{-1}; HRMS-APCI (*m/z*) $[M + H]^+$ calcd for $C_{16}H_{25}N_2O^+$, 261.1961; found 261.1949.

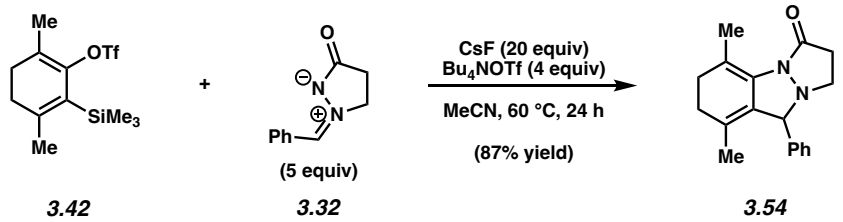

Cycloadduct 3.54. Followed General Procedure 3.3. Purification by flash chromatography on Florisil (1:1 hexanes:Et_2O → Et_2O) afforded cycloadduct **3.54** (87% yield, average of two experiments) as a white solid. **Cycloadduct 3.54**: Mp: 111 °C; R_f 0.08 (4:1 hexanes:EtOAc); ^1H NMR (500 MHz, C_6D_6): δ 7.25–7.19 (m, 2H), 7.14–7.09 (m, 2H), 7.09–7.04 (m, 1H), 3.81 (br s,

1H), 2.89 (dt, J = 10.3, 7.5, 1 H), 2.43 (q, J = 9.3, 1H), 2.29 (s, 3H), 2.24–1.94 (m, 5H), 1.91–1.80 (m, 1H), 1.11 (s, 3H); ^{13}C NMR (125 MHz, C_6D_6, 14 of 16 signals observed): δ 169.0, 140.2, 132.8, 129.9, 129.1, 125.9, 113.4, 72.2, 47.9, 33.6, 30.9, 29.7, 20.7, 18.8; IR (film): 3028, 2924, 2855, 1728, 1664 cm^{-1}; HRMS-APCI (*m/z*) $[M + H]^+$ calcd for $C_{18}H_{21}N_2O^+$, 281.1648; found 281.1635.

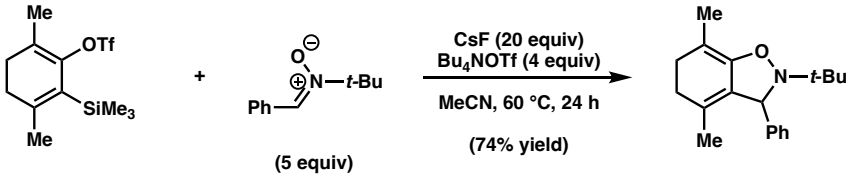

3.42 ***3.46*** ***3.55***

Cycloadduct 3.55. Followed General Procedure 3.3. Purification by flash chromatography on basic alumina (hexanes → 1:1 hexanes:CH_2Cl_2) afforded cycloadduct **3.55** (74% yield, average of two experiments) as a clear colorless oil. **Cycloadduct 3.55**: R_f 0.51 (19:1 hexanes:EtOAc); ^{1}H NMR (500 MHz, CD_3CN): δ 7.34–7.28 (m, 4H), 7.27–7.21 (m, 1H), 4.99 (s, 1H), 2.35–2.02 (m, 4H), 1.68 (s, 3H), 1.64 (s, 3H), 1.11 (s, 9H); ^{13}C NMR (150 MHz, C_6D_6): δ 148.7, 143.9, 133.2, 128.7, 128.1, 127.2, 125.0, 92.4, 64.1, 61.0, 30.9, 29.0, 26.2, 19.3, 15.5; IR (film): 3036, 2971, 2920, 1479, 1390 cm^{-1}; HRMS-APCI (*m/z*) $[M + H]^+$ calcd for $C_{19}H_{26}NO^+$, 284.2009; found 284.1996.

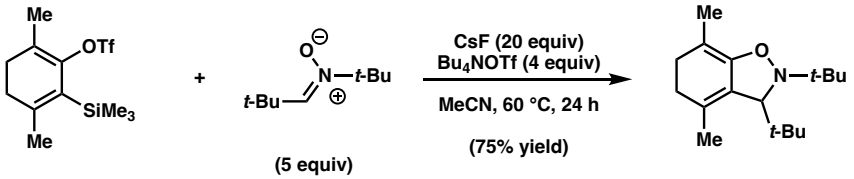

3.42 ***3.47*** ***3.56***

Cycloadduct 3.56. Followed General Procedure 3.3. Purification by flash chromatography on basic alumina (hexanes → 5:1 hexanes:CH_2Cl_2) afforded cycloadduct **3.56** (75% yield, average of

two experiments) as a clear colorless oil. **Cycloadduct 3.56**: R_f 0.33 (1:1 hexanes:CH_2Cl_2); ^{1}H NMR (500 MHz, C_6D_6): δ 3.39 (s, 1H), 2.30 (td, *J* = 16.6, 8.3, 1H), 2.02 (td, *J* = 17.2, 8.3, 1H), 1.92–1.78 (m, 2H), 1.82 (s, 3H), 1.54 (s, 3H), 1.08 (s, 9H), 1.05 (s, 9H); ^{13}C NMR (125 MHz, C_6D_6): δ 150.3, 131.4, 126.5, 90.6, 68.1, 60.6, 37.0, 31.7, 29.2, 27.3, 26.5, 21.1, 15.3; IR (film): 2973, 2916, 2868, 1700, 1363 cm^{-1}; HRMS-APCI (*m/z*) $[M + H]^+$ calcd for $C_{17}H_{30}NO^+$, 264.2322; found 264.2315.

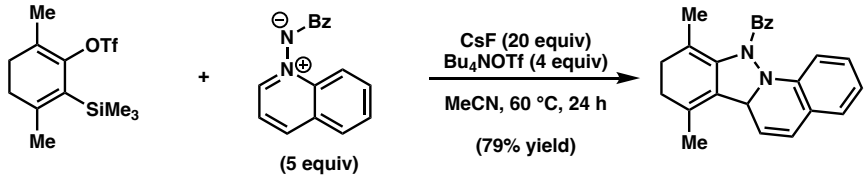

Cycloadduct 3.57. Followed General Procedure 3.3. Purification by flash chromatography on Florisil (hexanes → 9:1 hexanes:EtOAc) afforded cycloadduct **3.57** (79% yield, average of two experiments) as an off-white solid. **Cycloadduct 3.57**: Mp: 158–159 °C; R_f 0.39 (17:3 hexanes:EtOAc); ^{1}H NMR (500 MHz, C_6D_6): δ 8.11 (d, *J* = 7.3, 2H), 7.35 (d, *J* = 7.9, 1H), 7.04–6.91 (m, 4H), 6.68–6.60 (m, 2H), 5.93 (d, *J* = 9.9, 1H), 5.50 (dd, *J* = 9.9, 5.6, 1H), 4.18 (br s, 1H), 2.10–1.86 (m, 2H), 2.00 (s, 3H), 1.89–1.74 (m, 1H), 1.72–1.60 (m, 1H), 1.37 (s, 3H); ^{13}C NMR (150 MHz, CD_2Cl_2): δ 171.4, 144.2, 134.6, 131.1, 130.9, 129.5, 128.6, 128.1, 127.7, 127.0, 125.09, 125.06, 123.2, 122.5, 122.2, 118.9, 115.1, 61.8, 30.6, 28.6, 19.1, 19.0; IR (film): 3070, 3034, 2910, 1663, 1482 cm^{-1}; HRMS-APCI (*m/z*) $[M + H]^+$ calcd for $C_{24}H_{23}N_2O^+$, 355.1805; found 355.1787.

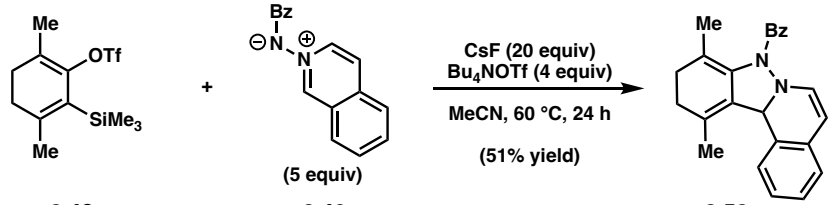

3.42 *3.49* *3.58*

Cycloadduct 3.58. Followed General Procedure 3.3. Purification by flash chromatography on Florisil (hexanes → 18:1 hexanes:EtOAc) afforded cycloadduct **3.58** (51% yield, average of two experiments) as an off-white solid. **Cycloadduct 3.58**: Mp: 146 °C; R_f 0.29 (9:1 hexanes:EtOAc); ^{1}H NMR (600 MHz, $CDCl_3$): δ 7.74–7.67 (m, 2H), 7.43 (tt, *J* = 7.4, 1.2, 1H), 7.40–7.34 (m, 2H), 7.19–7.13 (m, 2H), 7.04 (t, *J* = 7.5, 1H), 6.92 (d, *J* = 7.3, 1H), 6.25 (d, *J* = 7.9, 1H), 5.66 (d, *J* = 7.9, 1H), 4.68 (s, 1H), 2.51–2.40 (m, 1H), 2.36–2.14 (m, 3H), 1.83 (s, 3H), 1.34 (s, 3H); ^{13}C NMR (150 MHz, $CDCl_3$): δ 171.4, 139.4, 134.8, 131.8, 131.1, 130.7, 130.3, 129.6, 129.1, 128.8, 128.5, 127.9, 127.7, 127.3, 125.9, 124.8, 117.7, 108.4, 65.0, 31.7, 29.0, 20.0, 17.4; IR (film): 3060, 3022, 2917, 1712, 1667 cm^{-1}; HRMS-APCI (*m/z*) $[M + H]^+$ calcd for $C_{24}H_{23}N_2O^+$, 355.1805; found 355.1785.

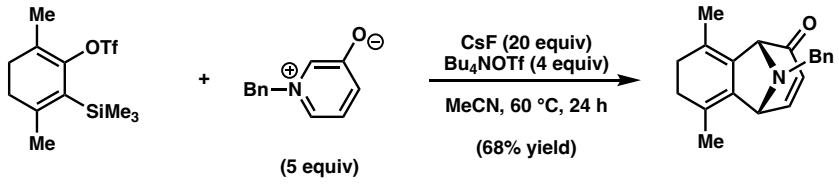

3.42 *3.59* *3.66*

Cycloadduct 3.66. Followed General Procedure 3.3. Purification by flash chromatography (benzene → 9:1 benzene:Et_2O) afforded cycloadduct **3.66** (68% yield, average of two experiments) as a light yellow oil. **Cycloadduct 3.66**: R_f 0.42 (7:3 hexanes:EtOAc); ^{1}H NMR (600 MHz, CD_3CN): δ 7.36–7.31 (m, 2H), 7.30–7.24 (m, 3H), 7.15 (dd, *J* = 9.6, 5.8, 1H), 5.79 (dd, *J* = 9.6, 1.3, 1H), 4.16 (d, *J* = 5.8, 1H), 3.99 (s, 1H), 3.47 (d, *J* = 13.1, 1H), 3.44 (d, *J* = 13.1, 1H),

2.39–2.08 (m, 4H), 1.77 (s, 3H), 1.73 (s, 3H); ^{13}C NMR (150 MHz, CD_3CN): δ 194.5, 150.8, 139.2, 131.8, 130.1, 129.6, 129.4, 128.3, 126.6, 125.9, 125.2, 73.4, 61.6, 56.4, 30.8, 30.1, 19.9, 19.6; IR (film): 3028, 2970, 2911, 1683, 1373 cm^{-1}; HRMS-APCI (*m/z*) $[M + H]^+$ calcd for $C_{20}H_{22}NO^+$, 292.1696; found 292.1696.

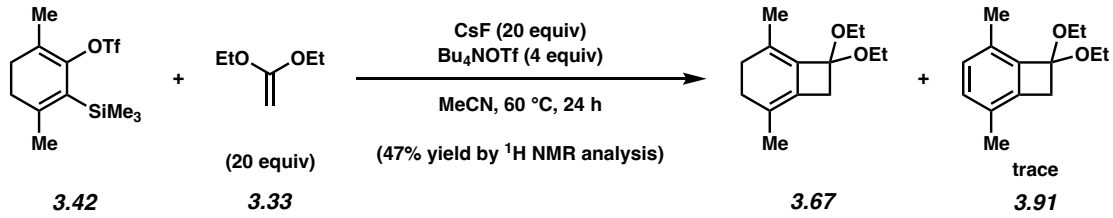

Cycloadduct 3.67. Followed General Procedure 3.3. ^{1}H NMR analysis of the reaction mixture after workup indicated 47% yield (average of two experiments) of cycloadduct **3.67** relative to a mesitylene standard. To obtain an analytical sample, the reaction mixture was then purified by preparative thin-layer chromatography (10:1 hexanes:EtOAc) to afford an inseparable mixture of **3.67** and **3.91** as a yellow oil. **Cycloadduct 3.67**: R_f 0.49 (9:1 hexanes:EtOAc); ^{1}H NMR (500 MHz, C_6D_6): δ 3.69–3.56 (m, 4H), 2.92 (s, 2H), 2.11–2.01 (m, 4H), 1.77 (s, 3H), 1.55 (s, 3H), 1.18 (t, J = 7.0, 6H); ^{13}C NMR (125 MHz, $CDCl_3$): δ 136.2, 126.5, 122.2, 120.3, 105.2, 58.8, 41.2, 30.9, 29.7, 19.1, 17.5, 15.5; IR (film): 2975, 2911, 1441, 1242, 1148, 1057 cm^{-1}; HRMS-APCI (*m/z*) $[M - OEt]^+$ calcd for $C_{12}H_{17}O^+$, 177.1274; found 177.1269. **Cycloadduct 3.91** was assigned by analogy of its ^{1}H NMR spectrum to known cycloadduct **3.92** (see below).

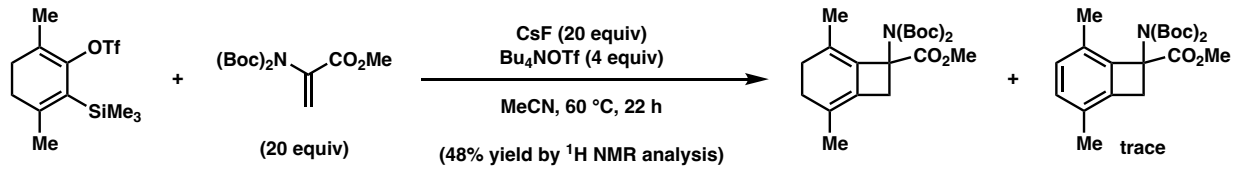

Cycloadduct 3.68 and **3.92.** Followed General Procedure 3.3. ^{1}H NMR analysis of the reaction mixture purification by flash chromatography (5:1 hexanes:EtOAc) indicated 48% yield (average of two experiments) of cycloadduct **3.68** relative to a mesitylene standard. To obtain an analytical sample, the reaction mixture was then purified by preparative thin-layer chromatography (4:1 hexanes:EtOAc) to afford an inseparable mixture of **3.68** and **3.92**[66] as a colorless oil. **Cycloadduct 3.68**: R_f 0.64 (4:1 hexanes:EtOAc); ^{1}H NMR (500 MHz, C_6D_6): δ 4.14 (d, J = 15.2, 1H), 3.46 (s, 3H), 3.17 (d, J = 15.2, 1H), 2.10–1.87 (m, 4H), 1.82 (s, 3H), 1.45 (s, 3H), 1.38 (s, 18H); ^{13}C NMR (125 MHz, C_6D_6): δ 170.4, 152.4, 132.7, 129.1, 125.6, 119.6, 82.0, 67.5, 52.1, 40.6, 31.3, 29.7, 27.8, 17.5, 16.9; IR (film): 2979, 1744, 1711, 1251, 1116 cm^{-1}; HRMS-APCI (*m/z*) $[M + H]^+$ calcd for $C_{22}H_{34}NO_6^+$, 408.2381; found 408.2395. **Cycloadduct 3.92**: Spectral data matched those reported in the literature.[8]

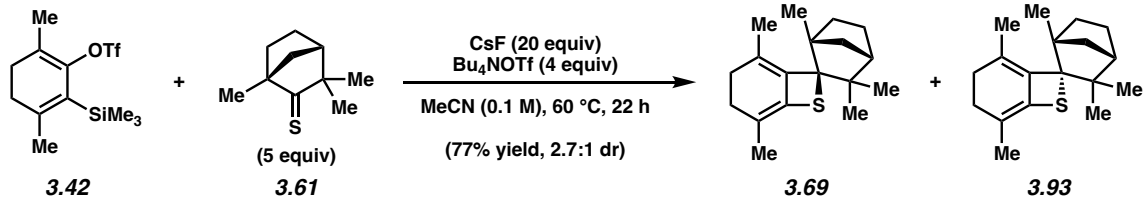

Cycloadduct 3.69 and **3.93.** Followed General Procedure 3.3. Filtration through a pad of Florisil, eluting with benzene (10 mL) followed by filtration through a second pad of Florisil, eluting with 4:1 hexanes:EtOAc (10 mL) afforded major diastereomer **3.69** and minor diastereomer **3.93** (77% combined yield, 2.7:1 dr (determined by ^{1}H NMR analysis of the crude mixture) (average of two

experiments)) as a colorless oil. To obtain an analytical sample, the mixture of **3.69** and **3.93** was purified by flash chromatography (pentane) to afford major diastereomer **3.69** as a colorless oil. **Cycloadduct 3.69** and **3.93**: R_f 0.46 (100% hexanes); ^{1}H NMR (600 MHz, C_6D_6, major diastereomer **3.69**): δ 2.25–2.06 (m, 2H), 2.02–1.87 (m, 2H), 1.80–1.72 (m, 1H), 1.69–1.66 (m, 1H), 1.65–1.59 (m, 5H), 1.57 (s, 3H), 1.55 (s, 3H), 1.42–1.32 (m, 2H), 1.31 (s, 3H), 1.15 (s, 3H), 1.07 (d, J = 10.6, 1H); ^{13}C NMR (150 MHz, C_6D_6, major diastereomer **3.69**): δ 135.3, 127.0, 122.2, 112.8, 86.8, 55.2, 50.0, 45.6, 42.6, 34.4, 33.0, 32.5, 29.4, 25.5, 24.0, 21.9, 20.1, 16.6; ^{13}C NMR (125 MHz, C_6D_6, minor diastereomer **3.93**): δ 136.3, 125.8, 121.3, 112.5, 87.0, 52.6, 49.2, 45.8, 42.2, 35.0, 32.6, 29.9, 29.3, 28.3, 25.3, 20.2, 17.9, 16.7; IR (film): 2930, 2872, 1450, 1206, 1145 cm^{-1}; HRMS-APCI (*m/z*) $[M + H]^+$ calcd for $C_{18}H_{27}S^+$, 275.1828; found 275.1844. The relative stereochemistry of **3.69** and **3.93** were assigned by comparison of experimental and computed NMR chemical shift data, see Section 3.9.4.5 for details.

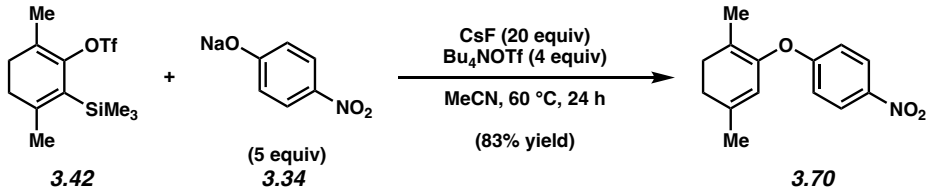

Adduct 3.70. Followed General Procedure 3.3. Purification by flash chromatography on Florisil (hexanes → 3:1 hexanes:Et_2O) afforded adduct **3.70** (83% yield, average of two experiments) as a yellow oil. **Adduct 3.70**: R_f 0.69 (5:1 hexanes:EtOAc); ^{1}H NMR (500 MHz, C_6D_6): δ 7.91–7.83 (m, 2H), 6.65–6.57 (m, 2H), 5.28 (s, 1H), 1.97 (t, J = 9.5, 2H), 1.85 (t, J = 9.4, 2H), 1.51 (s, 3H), 1.49 (s, 3H); ^{13}C NMR (125 MHz, C_6D_6): δ 162.5, 142.9, 142.6, 137.6, 126.0, 118.0, 116.8, 115.6, 28.8, 28.6, 22.6, 15.3; IR (film): 3039, 2926, 2824, 1513, 1340 cm^{-1}; HRMS-APCI (*m/z*) $[M + H]^+$ calcd for $C_{14}H_{16}NO_3^+$, 246.1125; found 246.1121

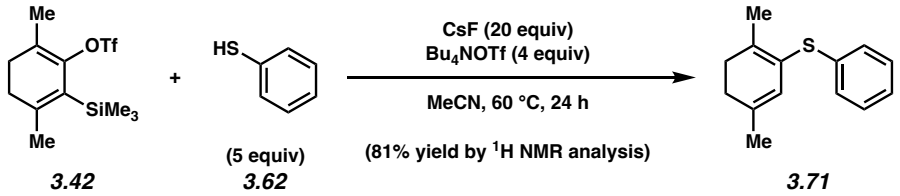

Adduct 3.71. Followed General Procedure 3.3. ^{1}H NMR analysis of the reaction mixture after workup indicated 81% yield (average of two experiments) of adduct **3.71** relative to a mesitylene standard. To obtain an analytical sample, the reaction mixture was then purified by sequential preparative thin layer chromatography (10:1 hexanes:EtOAc) and flash silica column chromatography (10:1 pentane:Et_2O) to afford adduct **3.71** as a colorless oil. **Adduct 3.71**: R_f 0.90 (10:1 hexanes:EtOAc); ^{1}H NMR (500 MHz, C_6D_6): δ 7.35–7.30 (m, 2H), 7.06–7.01 (m, 2H), 6.89 (tt, J = 7.4, 1.4, 1H), 5.80 (q, J = 1.5, 1H), 2.05 (t, J = 9.4, 2H), 1.97 (s, 3H), 1.86 (t, J = 9.4, 2H), 1.48 (s, 3H); ^{13}C NMR (150 MHz, $CDCl_3$): δ 138.7, 137.4, 134.9, 128.9, 127.6, 125.1, 123.8, 121.1, 31.4, 28.4, 22.8, 21.3; IR (film): 3058, 2922, 2822, 1477, 1025 cm^{-1}; HRMS-APCI (*m/z*) $[M + H]^+$ calcd for $C_{14}H_{17}S^+$, 217.1046; found 217.1042.

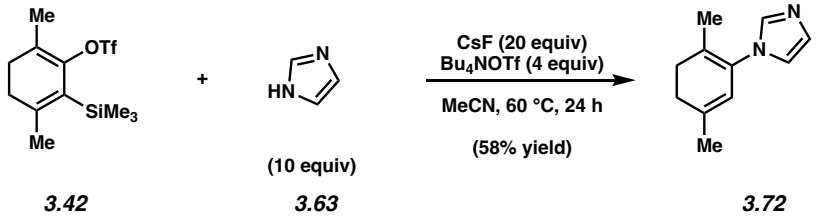

Adduct 3.72. Followed General Procedure 3.3. Purification by flash chromatography (7:3 hexanes:EtOAc → 3:7 hexanes:EtOAc) afforded adduct **3.72** (58% yield, average of two experiments) as a light yellow oil. **Adduct 3.72**: R_f 0.25 (1:1 hexanes:EtOAc); ^{1}H NMR (600 MHz, CD_2Cl_2): δ 7.44 (s, 1H), 7.05 (s, 1H), 6.91 (s, 1H), 5.55 (q, J = 1.5, 1H), 2.35 (t, J = 9.6, 2H), 2.21 (t, J = 9.6, 2H), 1.81 (s, 3H), 1.65 (s, 3H); ^{13}C NMR (150 MHz, CD_2Cl_2): δ 136.7, 136.5, 128.1,

127.9, 125.9, 119.6, 119.3, 29.5, 27.9, 22.3, 17.5; IR (film): 3443, 3108, 2925, 2826, 1738 cm^{-1}; HRMS-APCI (*m/z*) $[M + H]^+$ calcd for $C_{11}H_{15}N_2^+$, 175.1230; found 175.1223.

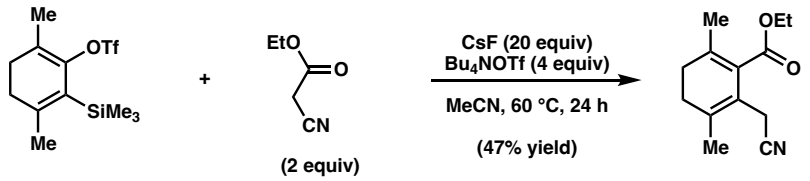

3.42 *3.64* *3.73*

Diene 3.73. Followed General Procedure 3.3. Purification by preparative thin layer chromatography (4:1 hexanes:acetone) afforded diene **3.73** (47% yield, average of two experiments) as a clear colorless oil. **Diene 3.73**: R_f 0.21 (9:2:1 hexanes:CH_2Cl_2:Et_2O); ^1H NMR (500 MHz, $CDCl_3$): δ 4.31 (q, *J* = 7.3, 2H), 3.22 (s, 2H), 2.16 (app. s, 4H), 1.99 (s, 3H), 1.89 (s, 3H), 1.37 (t, *J* = 7.3, 3H); ^{13}C NMR (150 MHz, $CDCl_3$): δ 168.2, 140.8, 134.2, 126.4, 118.0, 117.4, 61.0, 30.1, 29.6, 21.3, 19.6, 18.0, 14.2; IR (film): 2982, 2930, 2248, 1716, 1252 cm^{-1}; HRMS-APCI (*m/z*) $[M + H]^+$ calcd for $C_{13}H_{18}NO_2^+$, 220.1332; found 220.1346.

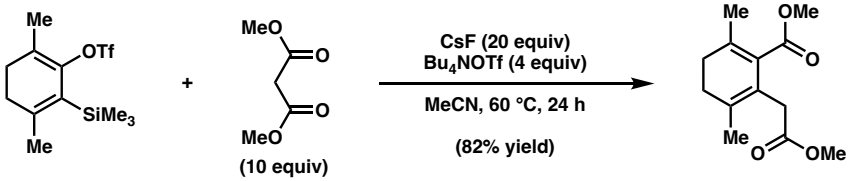

3.42 *3.65* *3.74*

Diene 3.74. Followed a modified version of General Procedure 3.3 by filtering the crude reaction mixture over a basic alumina plug (5 cm) instead of Celite, eluting with EtOAc (10 mL). Purification by preparative thin layer chromatography (5:1 hexanes:EtOAc) afforded diene **3.74** (82% yield, average of two experiments) as a colorless oil. **Diene 3.74**: R_f 0.31 (5:1 hexanes:EtOAc); ^1H NMR (500 MHz, C_6D_6): δ 3.49 (s, 3H), 3.34 (s, 3H), 3.30 (s, 2H), 1.81 &

1.79 (app. overlapping s, 7H), 1.62 (s, 3H); ^{13}C NMR (125 MHz, C_6D_6): δ 171.4, 169.1, 137.2, 131.9, 128.8, 121.3, 51.3, 50.9, 34.9, 30.0, 29.8, 21.2, 19.7; IR (film): 2951, 2879, 1725, 1434, 1251 cm^{-1}; HRMS-APCI (*m/z*) $[M + H]^+$ calcd for $C_{13}H_{19}O_4^+$, 239.1278; found 239.1272.

3.9.3.5. Synthesis of Silyl Triflate 3.76

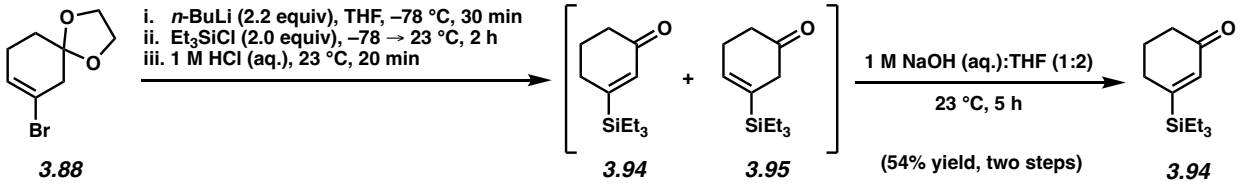

Enone 3.94. To a solution of bromide **3.88** (6.00 g, 27.4 mmol, 1.0 equiv) in THF (304 mL, 0.09 M) at –78 °C was added dropwise *n*-BuLi (2.4 M in hexanes, 25.1 mL, 60.3 mmol, 2.2 equiv) over 10 min to give a clear pink solution. The mixture was stirred at this temperature for 30 min, at which point it had become heterogeneous. To this solution was added triethylsilyl chloride (9.19 mL, 54.8 mmol, 2.0 equiv) dropwise over 5 min, and the resulting solution was stirred at –78 °C for 1 h. The cooling bath was then removed, and stirring was continued for an additional 1 h at 23 °C. After this time, the reaction was poured into a vigorously stirring 1 M HCl (aq.) solution (150 mL) and stirred at 23 °C for 20 min. The resulting solution was then diluted with Et_2O (100 mL), and the layers were separated. The aqueous layer was extracted with Et_2O (2 x 100 mL), and the organic layers were combined, dried over sodium sulfate, filtered, and concentrated under reduced pressure. The crude residue was purified by flash chromatography (23:2 → 9:1 EtOAc:hexanes) giving partial separation of isomers **3.94** and **3.95**. The mixed fractions were combined, concentrated, resuspended in THF (100 mL), and treated with 1 M NaOH (aq.) (50 mL). The resulting brown solution was stirred for 5 h then diluted with Et_2O (200 mL), and the layers were separated. The aqueous layer was extracted with Et_2O (2 x 200 mL), dried over sodium sulfate,

filtered, and concentrated. The resulting crude oil was filtered through a silica plug eluting with 9:1 EtOAc:hexanes (300 mL), and the eluate was concentrated then combined with the pure **3.94** obtained from the initial column to give enone **3.94** (3.08 g, 27.4 mmol, 54% yield) as a clear colorless oil. **Enone 3.94**: R_f = 0.39 (9:2:1 hexanes:CH_2Cl_2:Et_2O); ^{1}H NMR (600 MHz, $CDCl_3$): δ 6.23 (t, *J* = 1.8, 1H), 2.43–2.38 (m, 2H), 2.33 (td, *J* = 5.6, 1.8, 2H), 1.99 (p, *J* = 6.1, 2H), 0.94 (t, *J* = 8.0, 9H), 0.67 (q, *J* = 8.0, 6H); ^{13}C NMR (150 MHz, $CDCl_3$): δ 198.5, 166.0, 137.1, 38.2, 28.6, 23.6, 7.3, 2.1; IR (film): 3072, 3036, 2954, 2876, 1671 cm^{-1}; HRMS-APCI (*m/z*) $[M + H]^+$ calcd for $C_{12}H_{23}OSi^+$, 211.1513; found 211.1507

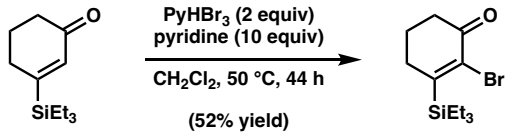

3.94 *3.96*

Bromo enone 3.96. A round bottom flask equipped with a reflux condenser was charged with enone **3.94** (2.70 g, 12.8 mmol, 1.0 equiv), CH_2Cl_2 (128 mL, 0.10 M), and pyridine (10.4 mL, 128.3 mmol, 10.0 equiv) sequentially at 23 °C. Pyridinium perbromide (8.21 g, 25.7 mmol, 2.0 equiv) was then added rapidly in a single portion, and the reaction was heated at 50 °C with vigorous stirring for 44 h. After this time, the reaction was quenched with saturated sodium bicarbonate (50 mL), and the layers were separated. The aqueous layer was extracted with CH_2Cl_2 (2 x 50 mL), and the organic layers were combined then washed sequentially with saturated sodium thiosulfate (50 mL) and 0.5 M HCl (aq.) (50 mL). The organic layer was dried over sodium sulfate, filtered, and concentrated then purified by flash chromatography (19:1 → 9:1 petroleum ether:Et_2O) to give bromo enone **3.96** (1.91 g, 6.6 mmol, 52% yield) as a white solid. **Bromo enone 3.96**: Mp: 53 °C; R_f 0.43 (9:2:1 hexanes:CH_2Cl_2:Et_2O); ^{1}H NMR (600 MHz, $CDCl_3$): δ

2.64–2.58 (m, 2H), 2.47 (t, J = 5.7, 2H), 2.04–1.98 (m, 2H), 0.97 (t, J = 7.5, 9H), 0.89–0.84 (m, 6H); ^{13}C NMR (150 MHz, $CDCl_3$): δ 189.9, 164.0, 132.9, 38.3, 34.0, 23.3, 7.5, 3.0; IR (film): 2954, 2875, 1739, 1691, 1549 cm^{-1}; HRMS-APCI (*m/z*) [M + H]$^+$ calcd for $C_{12}H_{22}OBrSi^+$, 289.0618; found 289.0620.

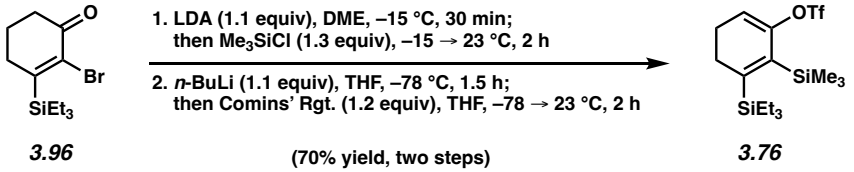

3.96 ***3.76***

Silyl triflate 3.76. To a solution of diisopropylamine (1.12 mL, 7.92 mmol, 1.2 equiv) in DME (13 mL) at –15 °C was added *n*-BuLi (2.1 M in hexanes, 3.4 mL, 7.3 mmol, 1.1 equiv) dropwise over 5 min. The resulting solution was stirred at this temperature for 25 min then treated dropwise with a solution of bromo enone **3.96** (1.91 g, 6.60 mmol, 1.0 equiv) in DME (13 mL) over 3 min. The resulting solution was stirred for 30 min then treated with trimethylsilyl chloride (1.04 mL, 8.58 mmol, 1.3 equiv) rapidly dropwise. The cooling bath was then removed, stirring of the reaction continued, and the reaction warmed to 23 °C over 2 h. After this time, the solvent was removed in vacuo, and the flask was evacuated and backfilled with nitrogen (3x). The heterogeneous yellow residue was suspended in pentane and filtered through Celite under a nitrogen atmosphere into a flame-dried round bottom flask (4 x 15 mL aliquots of pentane). The resulting eluate was concentrated under reduced pressure to give a yellow oil (2.39 g) which was dissolved in THF (44 mL, 0.15 M) and cooled to –78 °C. To this solution was added *n*-BuLi (2.4 M in hexanes, 3.03 mL, 1.1 equiv) dropwise over 12 min giving a solution which progressed from red to green to yellow over the course of addition. Stirring was continued for 1.5 h at this temperature before Comins' Reagent (3.11 g, 7.92 mmol, 1.2 equiv) in THF (13 mL) was added

rapidly dropwise. The resulting pink solution was stirred at –78 °C for 15 min, then the cooling bath was removed and the reaction was stirred and gradually warmed to 23 °C over 2 h. The reaction was then quenched with water (50 mL) and diluted with hexanes (50 mL). The layers were separated, and the aqueous layer was extracted with hexanes (2 x 50 mL). The organic layers were combined, dried over magnesium sulfate, filtered, and concentrated under reduced pressure. The crude residue was purified by flash chromatography on basic alumina (petroleum ether) to provide silyl triflate **3.76** (1.94 g, 4.68 mmol, 70% yield, two steps) as a yellow oil which was stored in a glovebox. **Silyl triflate 3.76**: R_f 0.65 (19:1 hexanes:EtOAc); ^{1}H NMR (600 MHz, C_6D_6): δ 5.64 (t, J = 5.4, 1H), 1.84–1.76 (m, 2H), 1.57–1.48 (m, 2H), 0.89 (t, J = 7.9, 9H), 0.64 (q, J = 7.9, 6H), 0.33 (s, 9H); ^{13}C NMR (150 MHz, C_6D_6): δ 158.5, 151.9, 144.9, 118.9 (q, J = 319), 114.4, 29.7, 21.6, 7.5, 4.0, 1.6; ^{19}F NMR (376 MHz, C_6D_6) –73.15 (s, 3F); IR (film): 2956, 2878, 1418, 1203, 1141 cm^{-1}; HRMS-APCI (*m/z*) [M – OTf]$^+$ calcd for $C_{15}H_{29}Si_2^+$, 265.1802; found 265.1785.

3.9.3.6 Trapping Reactions of Silyl Triene 3.75

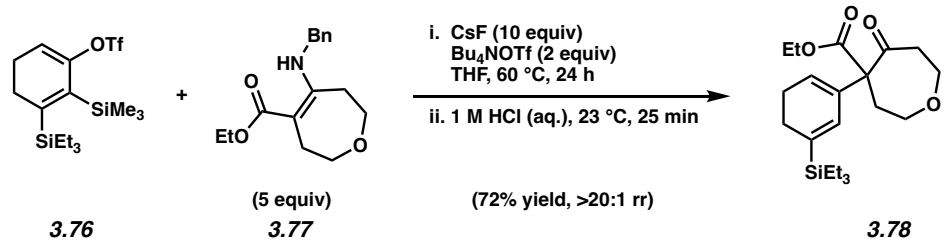

Ketoester 3.78. Inside a glove box, a dram vial containing silyl triflate **3.76** (100.0 mg, 0.241 mmol, 1.0 equiv) was charged sequentially with enamine **3.77** (332.0 mg, 1.21 mmol, 5 equiv), Bu_4NOTf (188.9 mg, 0.482 mmol, 2.0 equiv) and THF (2.4 mL, 0.1 M). CsF (366.4 mg, 2.41 mmol, 10 equiv) was then added in a single portion, and the vial was sealed, brought out of the

glovebox, and stirred at 60 °C for 24 h. After this time, the reaction was diluted with Et_2O (5 mL) and filtered through a Celite plug eluting with Et_2O (5 mL). The eluate was concentrated, and the resulting residue was resuspended in THF (3 mL) then treated with 1 M HCl (aq.) (3 mL). The mixture was stirred vigorously for 25 min, then diluted with water (5 mL) and Et_2O (5 mL). The layers were separated, and the aqueous layer was extracted with Et_2O (2 x 5 mL). The organic layers were combined, dried over sodium sulfate, filtered, and concentrated under reduced pressure. The crude residue was purified by flash chromatography (benzene → 97:3 benzene:Et_2O) to give ketoester **3.78** (65.5 mg, 0.173 mmol, 72% yield) as a clear colorless oil. **Ketoester 3.78**: R_f 0.55 (9:1 benzene:Et_2O); ^{1}H NMR (600 MHz, $CDCl_3$): δ 5.98 (q, *J* = 1.6, 1H), 5.66 (td, *J* = 4.5, 2.0, 1H), 4.21 (q, *J* = 7.2, 2H), 3.99 (ddd, *J* = 13.5, 7.2, 1.7, 1H), 3.89 (ddd, *J* = 12.3, 6.5, 3.6, 1H), 3.75 (ddd, *J* = 13.5, 8.3, 1.7, 1H), 3.63 (ddd, *J* = 12.3, 9.1, 2.8, 1H), 2.90 (ddd, *J* = 14.3, 9.1, 3.7, 1H), 2.71 (ddd, *J* = 14.3, 6.5, 2.8, 1H), 2.45 (ddd, *J* = 15.5, 7.2, 1.6, 1H), 2.19–1.99 (m, 5H), 1.25 (t, *J* = 7.2, 3H), 0.92 (t, *J* = 8.0, 9H), 0.59 (q, *J* = 8.0, 6H); ^{13}C NMR (150 MHz, $CDCl_3$): δ 206.5, 171.5, 138.1, 134.2, 133.3, 125.0, 68.7, 67.1, 66.8, 61.5, 46.2, 33.6, 24.5, 22.6, 14.0, 7.4, 2.5; IR (film): 2953, 2874, 1736, 1464, 1231 cm^{-1}; HRMS-APCI (*m/z*) $[M + H]^+$ calcd for $C_{21}H_{35}O_4Si^+$, 379.2299; found 379.2287.

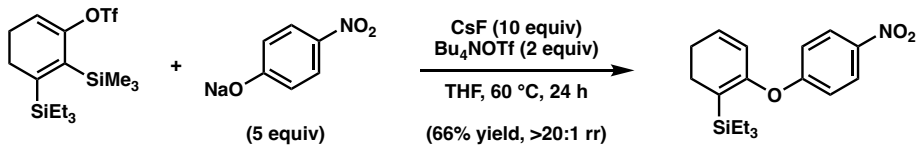

Adduct 3.79. Inside a glovebox, a dram vial containing phenoxide **3.34** (60.6 mg, 0.376 mmol, 5.0 equiv) was sequentially charged with CsF (114.0 mg, 0.752 mmol, 10 equiv) and Bu_4NOTf (58.9 mg, 0.150 mmol, 2.0 equiv). To this vial was then added a solution of silyl triflate **3.76** (31.2

mg, 75.2 μmol, 1.0 equiv) in THF (752 μL, 0.1 M). The vial was sealed, brought out of the glovebox, and stirred at 60 °C for 24 h. After this time, the reaction was diluted with Et_2O (5 mL) and filtered through a Celite plug eluting with Et_2O (5 mL). The eluate was concentrated, and the resulting residue was purified by flash chromatography (9:1 hexanes:CH_2Cl_2 → 4:1 hexanes:CH_2Cl_2) to afford adduct **3.79** (16.5 mg, 49.8 μmol, 66% yield) as a clear colorless oil. **Adduct 3.79**: R_f 0.44 (19:1 hexanes:EtOAc); ^{1}H NMR (600 MHz, C_6D_6): δ 7.84–7.79 (m, 2H), 6.56–6.51 (m, 2H), 5.76 (dt, *J* = 9.8, 4.4, 1H), 5.42 (dt, *J* = 9.8, 2.0, 1H), 2.11–2.05 (m, 2H), 1.85 (app. tdd, *J* = 9.4, 4.3, 1.9, 2H), 0.96 (t, *J* = 8.0, 9H), 0.62 (q, *J* = 8.0, 6H); ^{13}C NMR (150 MHz, C_6D_6): δ 161.8, 154.7, 142.8, 132.6, 126.0, 123.3, 118.4, 116.2, 25.4, 22.6, 7.8, 3.7; IR (film): 2951, 2874, 1582, 1516, 1340 cm^{-1}; HRMS-APCI (*m/z*) [M + H]$^+$ calcd for $C_{18}H_{26}SiNO_3^+$, 332.1677; found 332.1678.

3.9.3.7 Synthetic Elaboration of Triene Trapping Products

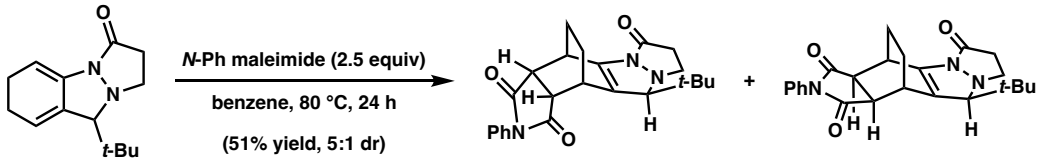

3.35 *3.81* *3.97*

Cycloadducts 3.81 and **3.97.** A 1-dram vial was charged with diene **3.35** (15.0 mg, 0.065 mmol, 1.0 equiv), *N*-phenyl maleimide (28.0 mg, 0.16 mmol, 2.5 equiv), and benzene (0.646 mL, 0.1 M). The vial was sealed with a Teflon-lined cap and stirred at 80 °C for 24 h. After this time, the reaction was cooled to 23 °C and concentrated under reduced pressure. The crude product was purified by preparative thin layer chromatography (2:1 hexanes:EtOAc) to afford a mixture of major diastereomer **3.81** and minor diastereomer **3.97** (13.3 mg, 0.033 mmol, 51% combined yield,

5:1 dr (determined by ^{1}H NMR analysis of the crude reaction mixture)) as a waxy-white solid. Analytical samples were obtained by preparative thin layer chromatography (1:1:1 hexanes:CH_2Cl_2:Et_2O) to provide major diastereomer **3.81** as a white crystalline solid and minor diastereomer **3.97** as a white powder. Crystals of **3.81** suitable for X-ray diffraction studies were obtained by recrystallization from Et_2O. **Cycloadduct 3.81** (major diastereomer, *endo* product): Mp: 188–190 °C; R_f 0.16 (1:1:1 hexanes:CH_2Cl_2:Et_2O); ^{1}H NMR (500 MHz, C_6D_6): δ 7.62–7.56 (m, 2H), 7.15–7.11 (overlapped with residual solvent peak, 2H), 6.99 (t, *J* = 7.4, 1H), 4.24–4.20 (m, 1H), 3.28 (s, 1H), 3.19–3.15 (m, 1H), 2.69 (t, *J* = 8.2, 1H), 2.38 (ddd, *J* = 15.5, 13.9, 7.8, 1H), 2.32–2.26 (m, 2H), 2.17 (ddd, *J* = 14.7, 8.2, 6.5, 1H), 2.01 (dd, *J* = 15.7, 6.4, 1H), 1.09–1.00 (m, 2H), 0.99–0.88 (m, 2H), 0.79 (s, 9H); ^{13}C NMR (125 MHz, C_6D_6, 19 of 20 signals observed): δ 176.1, 175.2, 166.2, 137.2, 132.9, 128.9, 125.7, 119.4, 82.8, 56.7, 46.6, 44.2, 35.8, 34.9, 32.8, 31.3, 26.5, 25.5, 23.0; IR (film): 2955, 2871, 1716, 1376, 1180 cm^{-1}; HRMS-APCI (*m/z*) $[M + H]^+$ calcd for $C_{24}H_{28}N_3O_3^+$, 406.2125; found 406.2126. **Cycloadduct 3.97** (minor diastereomer, *exo* product): Mp: 144–146 °C; R_f 0.08 (1:1:1 hexanes:CH_2Cl_2:Et_2O); ^{1}H NMR (600 MHz, $(CD_3)_2CO$): δ 7.53–7.47 (m, 2H), 7.43 (tt, *J* = 7.5, 1.2, 1H), 7.33–7.30 (m, 2H), 3.95 (q, *J* = 2.8, 1H), 3.85 (s, 1H), 3.63 (t, *J* = 8.2, 1H), 3.31–3.28 (m, 1H), 3.20–3.13 (m, 2H), 3.01 (ddd, *J* = 14.0, 8.6, 6.7, 1H), 2.91–2.84 (overlapped with H_2O peak, 1H), 2.40 (dd, *J* = 15.7, 6.7, 1H), 1.91–1.79 (m, 2H), 1.60–1.53 (m, 1H), 1.52–1.45 (m, 1H), 0.97 (s, 9H); ^{13}C NMR (125 MHz, $(CD_3)_2CO$): δ 177.6, 177.3, 168.3, 141.3, 133.8, 129.8, 129.3, 127.84, 127.76, 123.0, 83.3, 57.5, 47.8, 46.7, 36.5, 35.2, 34.2, 27.0, 22.5, 22.0; IR (film): 2925, 2856, 1708, 1379, 1180 cm^{-1}; HRMS-APCI (*m/z*) $[M + H]^+$ calcd for $C_{24}H_{28}N_3O_3^+$, 406.2125; found 406.2125.

The structure of **3.81** was verified by single crystal X-ray diffraction and 2D-NOESY, as the following interactions were observed:

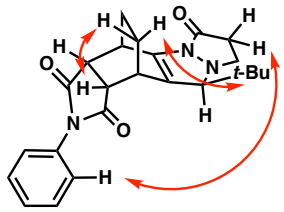

3.81

The structure of **3.97** was verified by 2D-NOESY, as the following interactions were observed:

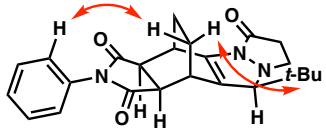

3.97

Crystal Structure Analysis for 3.81

Diffraction intensities were collected at 100 K on a Bruker Smart ApexII CCD diffractometer with CuKα radiation, 1.54178 Å. Absorption corrections were applied by SADABS.[67] All calculations were performed by the SHELXL-2014 packages.[68] Deposition Number 2239633 contains the supplementary crystallographic data for compound **3.81**. These data are provided free of charge by the joint Cambridge Crystallographic Data Centre and Fachinformationszentrum Karlsruhe Access Structures service www.ccdc.cam.ac.uk/structures.

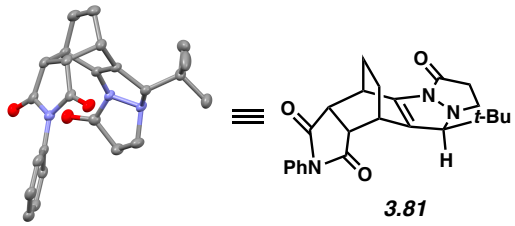

Figure 3.7. ORTEP representation of X-ray crystallographic structure **3.81**. (CCDC Registry # 2239633).

Table 3.2. Crystal data and structure refinement for compound **3.81**.

Identification code	cu_garg2301sa_a	
Empirical formula	C24 H27 N3 O3	
Formula weight	405.48	
Temperature	100(2) K	
Wavelength	1.54178 Å	
Crystal system	Monoclinic	
Space group	$P2_1/C$	
Unit cell dimensions	a = 11.7285(6) Å	a = 90°
	b = 18.1222(10) Å	b = 90.648(3)°
	c = 9.9897(6) Å	g = 90°
Volume	2123.1(2) $Å^3$	
Z	4	
Density (calculated)	1.269 Mg/m^3	
Absorption coefficient	0.679 mm^{-1}	
F(000)	864	
Crystal size	0.250 x 0.200 x 0.040 mm^3	
Theta range for data collection	3.769 to 70.042 °	
Index ranges	–12<=h<=14, –17<=k<=21, –10<=I<=11	
Reflections collected	16613	
Independent reflections	3912 [R(int) = 0.0719]	
Completeness to theta = 67.679°	99.3%	
Absorption correction	Semi-empirical from equivalents	
Max. and min. transmission	0.75 and 0.64	
Refinement method	Full-matrix least-squares on F^2	
Data / restraints / parameters	3912 / 0 / 274	
Goodness-of-fit on F^2	0.888	
Final R indices [I>2sigma(I)]	R1 = 0.0413, wR2 = 0.0864	
R indices (all data)	R1 = 0.0654, wR2 = 0.0902	
Extinction coefficient	n/a	
Largest diff. peak and hole	0.189 and –0.225 e.$Å^{-3}$	

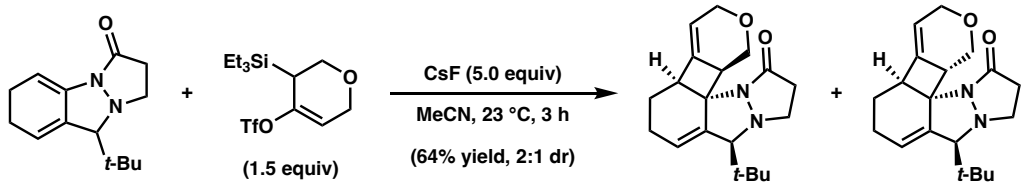

Cycloadducts 3.82 and **3.98.** A 1-dram vial was charged with diene **3.35** (15.0 mg, 0.065 mmol, 1.0 equiv) and silyl triflate **3.89** (34.0 mg, 0.097 mmol, 1.5 equiv) and taken into a glovebox where MeCN (0.646 mL, 0.1 M) was added followed by CsF (49.3 mg, 0.097 mmol, 5.0 equiv). The vial was sealed with a Teflon-lined cap, removed from the glovebox, and stirred at 23 °C for 3 h. After this time, the reaction was filtered through a silica gel plug eluting with EtOAc (8 mL), and the eluate was concentrated under reduced pressure. The crude product was purified by preparative thin layer chromatography (2:1 hexanes:EtOAc) to afford a mixture of major diastereomer **3.82** and minor diastereomer **3.98** (12.9 mg, 0.041 mmol, 64% combined yield, 2:1 dr (determined by ^{1}H NMR analysis of the crude mixture)) as a white solid. Analytical samples of **3.82** and **3.98** were obtained by preparative thin layer chromatography (3:1 benzene:acetonitrile) to provide major diastereomer **3.82** as a colorless oil and minor diastereomer **3.98** as a white solid. **Cycloadduct 3.82** (major diastereomer): R_f 0.29 (3:1 benzene:MeCN); ^{1}H NMR (600 MHz, C_6D_6): δ 5.78 (br s, 1H), 5.61–5.56 (m, 1H), 4.96–4.92 (m, 1H), 4.25–4.19 (m, 1H), 4.05 (dd, *J* = 9.6, 6.3, 1H), 3.92 (dq, 16.2, 3.1, 1H), 3.85–3.79 (m, 1H), 2.97 (t, *J* = 9.7, 1H), 2.93 (t, *J* = 8.7, 1H), 2.51–2.48 (m, 1H), 2.37 (ddd, *J* = 15.8, 12.7, 8.6, 1H), 2.17 (dd, *J* = 15.8, 8.0, 1H), 2.08 (dt, *J* = 12.6, 8.5, 1H), 1.97–1.89 (m, 1H), 1.69–1.62 (m, 1H), 1.55–1.50 (m, 1H), 1.00 (tt, *J* = 13.1, 4.7, 1H), 0.76 (s, 9H); ^{13}C NMR (150 MHz, C_6D_6): δ 163.7, 141.4, 136.3, 126.9, 114.7, 79.1, 65.5, 64.3, 61.2, 54.6, 52.2, 45.5, 35.9, 34.8, 27.5, 21.7, 21.5; IR (film): 2926, 2856, 1679, 1417, 1100 cm^{-1}; HRMS-APCI (*m/z*) $[M + H]^+$ calcd for $C_{19}H_{27}N_2O_2^+$, 315.2067; found 315.2070. **Cycloadduct 3.98** (minor diastereomer): Mp: 161–163 °C; R_f 0.37 (3:1 benzene:MeCN); ^{1}H NMR (600 MHz, C_6D_6): δ 5.56–

5.52 (m, 1H), 5.51 (app. br s, 1H), 5.05–4.98 (m, 1H), 4.34–4.27 (m, 1H), 4.26–4.17 (m, 2H), 3.60 (t, J = 9.6, 1H), 3.03–2.97 (m, 1H), 2.92 (t, J = 8.3, 1H), 2.55–2.51 (m, 1H), 2.37 (ddd, J = 17.8, 15.2, 8.7, 1H), 2.15–2.08 (m, 2H), 1.93–1.79 (m, 2H), 1.70 (dq, J = 13.0, 3.6, 1H), 1.25–1.17 (m, 1H), 0.76 (s, 9H); ^{13}C NMR (125 MHz, C_6D_6): δ 164.3, 145.2, 138.1, 122.9, 117.0, 78.3, 66.0, 63.9, 61.9, 55.2, 53.4, 45.0, 35.5, 34.9, 26.6, 23.8, 22.8; IR (film): 2956, 2860, 1684, 1417, 1095 cm^{-1}; HRMS-APCI (*m/z*) $[M + H]^+$ calcd for $C_{19}H_{27}N_2O_2^+$, 315.2067; found 315.2068.

The structure of **3.82** was verified by 2D-NOESY, as the following interactions were observed:

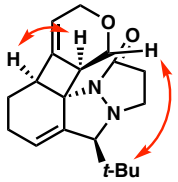

3.82

The structure of **3.98** was verified by 2D-NOESY, as the following interactions were observed:

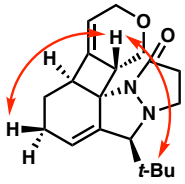

3.98

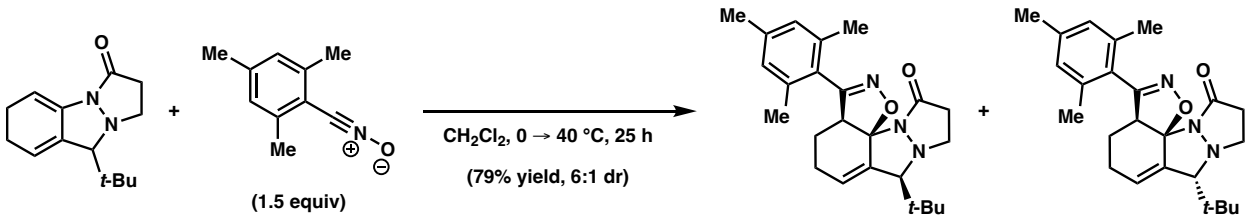

3.35 ***3.90*** ***3.83*** ***3.99***

Cycloadducts 3.83 and **3.99.** A 1-dram vial was charged with nitrile oxide **3.90** (16.2 mg, 0.097 mmol, 1.5 equiv) and CH_2Cl_2 (0.646 mL, 0.1 M) and cooled to 0 °C. Diene **3.35** (15.0 mg, 0.065 mmol, 1.0 equiv) was then added in one portion, and the reaction was stirred at 0 °C for 1 h. After

1 h, the reaction was warmed to 40 °C and stirred for an additional 24 h at this temperature. After this time, the reaction was cooled to 23 °C and concentrated under reduced pressure. The crude product was purified by preparative thin layer chromatography (2:1 hexanes:EtOAc) to afford an inseparable mixture of major diastereomer **3.83** and minor diastereomer **3.99** (20.0 mg, 0.051 mmol, 79% combined yield, 6:1 dr (determined by ^{1}H NMR analysis of the crude mixture)) as a waxy-amorphous solid. **Cycloadducts 3.83** and **3.99**: Mp: 187–189 °C; R_f 0.50 (2:1 hexanes:EtOAc); ^{1}H NMR (600 MHz, C_6D_6, major diastereomer **3.83**): δ 6.74 (s, 2H), 5.70 (ddd, J = 7.5, 2.9, 2.2, 1H), 5.38 (dd, J = 8.3, 2.3, 1H), 3.01 (td, J = 8.5, 1.8, 1H), 2.67–2.64 (m, 1H), 2.58 (s, 6H), 2.29 (ddd, J = 15.6, 12.4, 8.4, 1H), 2.21–2.14 (m, 1H), 2.08 (s, 3H), 2.08–2.02 (m, 1H), 1.96–1.87 (m, 1H), 1.62–1.55 (m, 1H), 1.50–1.43 (m, 1H), 1.20–1.11 (m, 1H), 1.03 (s, 9H); ^{13}C NMR (125 MHz, C_6D_6, mixture of **3.83** and **3.99**, 35 of 38 signals observed): δ 170.4, 165.1, 159.2, 157.5, 140.2, 139.8, 138.74, 138.65, 138.45, 138.42, 129.54, 129.46, 126.3, 126.1, 93.8, 91.9, 77.4, 75.4, 59.4, 54.8, 51.5, 47.1, 36.5, 35.7, 35.4, 33.6, 27.5, 27.2, 23.3, 22.6, 22.0, 21.4, 21.3, 21.2, 21.0; IR (film): 2956, 2865, 1694, 1392, 1095 cm^{-1}; HRMS-APCI (*m/z*) $[M + H]^+$ calcd for $C_{24}H_{32}N_3O_2^+$, 394.2489; found 394.2489.

The structure of **3.83** was verified by comparison of computed and observed $^4J_{HH}$ coupling constants as well as 2D-NOESY experiments. $^4J_{HH}$ coupling constants were calculated from the computationally derived H1-C2-C3-C4 dihedral angles (geometry optimized at the ωB97XD/6-31G(d) level of theory) using the modified Karplus equation in Equation 3.1. These calculated $^4J_{HH}$ coupling constants were then compared to the observed $^4J_{HH}$ coupling constants for each diastereomer (**3.83** and **3.99**), supporting **3.83** as bearing a syn relationship between the isooxazoline and *tert*-butyl substituent, and **3.99** bearing a trans relationship.

$$^4J = 1.3\cos^2(\phi) - 2.6\sin^2(\phi)$$

Equation 3.1. Modified Karplus equation.[69]

These assignments were further supported by comparison of H5–H1 NOESY signal strength to the calculated H5–H1 distances in the optimized geometries. **3.83** shows a strong H5–H1 NOE with a calculated H5–H1 distance of 2.45 Å whereas **3.99** shows a weak H5–H1 and a substantially larger H5–H1 distance of 3.34 Å.

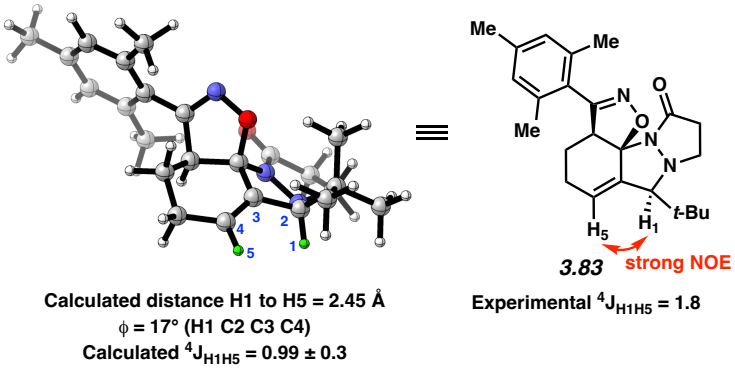

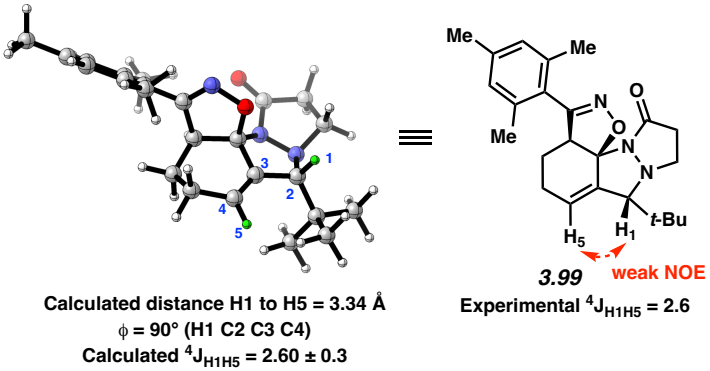

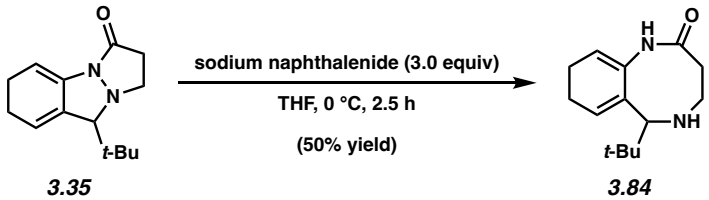

Diene 3.84. To a solution of diene **3.35** (15.0 mg, 0.065 mmol, 1.0 equiv) in THF (0.646 mL, 0.1 M) at 0 °C was added sodium naphthalenide[70] (2.0 M in THF, 97 µL, 0.194 mmol, 3.0 equiv)

slowly down the side of the vial. The reaction was allowed to stir at this temperature for 2.5 h. After 2.5 h the reaction was quenched with MeOH (3.0 mL) and concentrated under reduced pressure. The crude product was purified by flash chromatography (benzene → 1:1 benzene:EtOAc → EtOAc) to afford diene **3.84** (7.6 mg, 0.032 mmol, 50% yield) as a white solid. Crystals suitable for X-ray diffraction studies were obtained by recrystallization from a mixture of CH_2Cl_2 and cyclohexane. **Diene 3.84**: Mp: 186–187 °C; R_f 0.22 (EtOAc); ^{1}H NMR (500 MHz, C_6D_6): δ 8.38 (s, 1H), 5.51–5.41 (m, 1H), 5.24–5.14 (m, 1H), 3.22–3.11 (m, 1H), 2.85 (s, 1H), 2.75–2.58 (m, 2H), 2.12 (dd, J = 10.4, 8.5, 1H), 1.75–1.56 (m, 5H), 0.90 (s, 9H); ^{13}C NMR (150 MHz, CD_3OD): δ 176.7, 137.5, 136.6, 131.7, 118.8, 76.2, 42.9, 36.2, 35.6, 28.3, 23.9, 22.9; IR (film): 3353, 3045, 2930, 2817, 1669 cm^{-1}; HRMS-APCI (*m/z*) $[M + H]^+$ calcd for $C_{14}H_{23}N_2O^+$, 235.1805; found 235.1800.

Crystal Structure Analysis for 3.84

Data collection and analysis were performed as detailed above for compound **3.81**. Deposition Number 2238912 contains the supplementary crystallographic data for compound **3.84**. These data are provided free of charge by the joint Cambridge Crystallographic Data Centre and Fachinformationszentrum Karlsruhe Access Structures service www.ccdc.cam.ac.uk/structures.

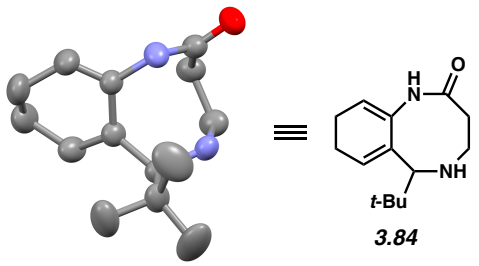

Figure 3.8. ORTEP representation of X-ray crystallographic structure **3.84**. (CCDC Registry # 2238912).

Table 3.3. Crystal data and structure refinement for compound **3.84**.

Identification code	cu_garg2207s	
Empirical formula	C14 H22 N2 O	
Formula weight	234.33	
Temperature	293(2) K	
Wavelength	1.54178 Å	
Crystal system	Triclinic	
Space group	P–1	
Unit cell dimensions	a = 7.4706(10) Å	a = 75.818(10)°
	b = 7.7662(11) Å	b = 82.253(10)°
	c = 12.6574(18) Å	g = 78.737(10)°
Volume	695.34(17) $Å^3$	
Z	2	
Density (calculated)	1.119 Mg/m^3	
Absorption coefficient	0.553 mm^{-1}	
F(000)	256	
Crystal size	0.30 x 0.20 x 0.06 mm^3	
Theta range for data collection	3.617 to 69.270 °	
Index ranges	–9<=h<=9, –9<=k<=7, –15<=I<=14	
Reflections collected	11182	
Independent reflections	2460 [R(int) = 0.0723]	
Completeness to theta = 67.679°	96.1%	
Absorption correction	Semi-empirical from equivalents	
Max. and min. transmission	0.75 and 0.55	
Refinement method	Full-matrix least-squares on F^2	
Data / restraints / parameters	2460 / 0 / 163	
Goodness-of-fit on F^2	1.065	
Final R indices [I>2sigma(I)]	R1 = 0.0684, wR2 = 0.1587	
R indices (all data)	R1 = 0.1003, wR2 = 0.1895	
Extinction coefficient	n/a	
Largest diff. peak and hole	0.228 and –0.190 e.$Å^{-3}$	

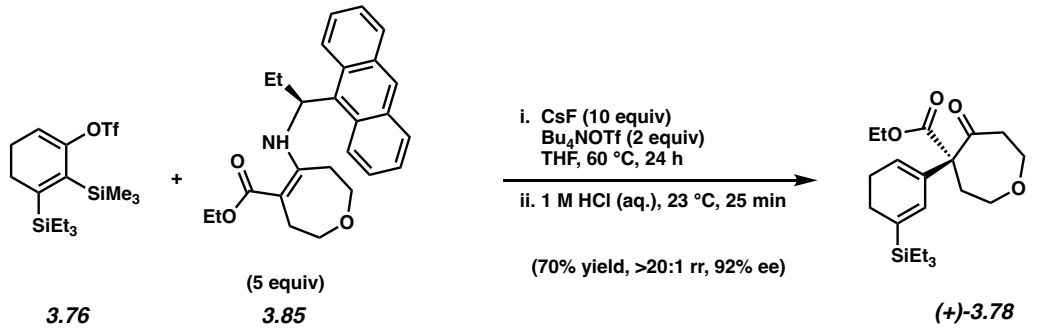

3.76 *3.85* *(+)-3.78*

Ketoester (+)-3.78. Prepared according to the procedure above for **(±)-3.78** using silyl triflate **3.76** (50.0 mg, 0.121 mmol, 1.0 equiv) and enantioenriched enamine **3.85** (243 mg, 0.603 mmol, 5.0 equiv) to generate ketoester **(+)-3.78** (31.8 mg, 84.0 μmol, 70% yield). Absolute stereochemistry was assigned by analogy to the literature.[62] Spectral data matched those reported above for **(±)-3.78**. **Ketoester (+)-3.78**: $[\alpha]^{23.1}_{D}$ +91° (*c* = 1.00, CH_2Cl_2).

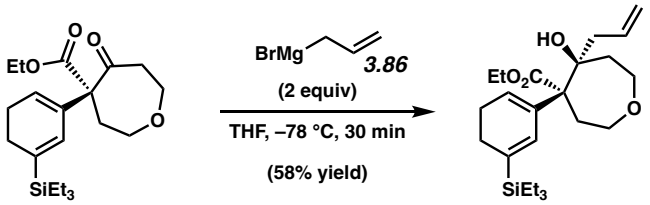

(+)-3.78 *(–)-3.87*

Alcohol (–)-3.87. To a solution of ketoester **(+)-3.78** (17.0 mg, 44.9 μmol, 1.0 equiv) in THF (449 μL, 0.10 M) at –78 °C was added dropwise a freshly prepared solution of allyl Grignard **3.86**[71] (1.0 M in Et_2O, 89.8 μL, 2.0 equiv) over 1 min. The resulting solution was stirred at this temperature for 30 min then quenched with saturated ammonium chloride (5 mL) and diluted with Et_2O (5 mL). The layers were separated, and the aqueous layer was extracted with Et_2O (2 x 5 mL). The organic layers were combined, dried over sodium sulfate, filtered, and concentrated under reduced pressure. The resulting residue was purified by preparative thin layer chromatography (plate pre-treated by developing in 9:1 hexanes:Et_2O with 2% Et_3N, then the

compound was loaded and eluted with the same solvent) to afford alcohol **(–)-3.87** (10.9 mg, 25.9 μmol, 58% yield) as a clear colorless oil. The relative stereochemistry was assigned by conversion to benzoate **3.100** (see below). **Alcohol (–)-3.87**: R_f 0.45 (19:1 benzene:MeCN); ^{1}H NMR (600 MHz, $CDCl_3$): 6.20 (s, 1H), 5.94–5.86 (m, 1H), 5.72–5.66 (m, 1H), 5.10–5.05 (m, 1H), 5.02 (tdd, *J* = 17.0, 2.1, 1.2, 1H), 4.25 (dq, *J* = 10.8, 7.1, 1H), 4.15 (dq, *J* = 10.8, 7.1, 1H), 3.79 (td, *J* = 11.4, 5.6, 1H), 3.73 (ddd, *J* = 11.5, 7.3, 1.6, 1H), 3.70–3.62 (m, 2H), 2.99 (ddd, *J* = 14.7, 11.1, 7.3, 1H), 2.91 (dd, *J* = 14.2, 8.1, 1H), 2.30 (ddd, *J* = 14.8, 8.7, 6.5, 1H), 2.20–2.14 (m, 1H), 2.13–2.17 (m, 2H), 2.07–1.94 (m, 3H), 1.88 (ddd, *J* = 14.5, 5.5, 1.7, 1H), 1.71 (dt, *J* = 15.0, 3.0, 1H), 1.28 (t, *J* = 7.1, 3H), 0.92 (t, *J* = 8.0, 9H), 0.59 (q, *J* = 8.0, 6H); ^{13}C NMR (150 MHz, $CDCl_3$, 19 of 20 signals observed): δ 173.5, 137.6, 136.8, 135.1, 124.4, 118.1, 75.4, 66.6, 64.6, 60.4, 60.1, 44.6, 38.5, 31.8, 24.5, 22.5, 14.1, 7.4, 2.5; IR (film): 3464, 3073, 2951, 2874, 1736 cm^{-1}; HRMS-APCI (*m/z*) [M + H]$^+$ calcd for $C_{24}H_{41}O_4Si^+$, 421.2769; found 421.2766.

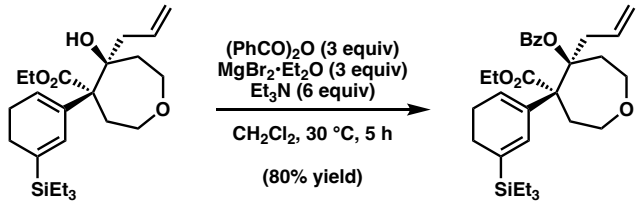

(–)-3.87 *(–)-3.100*

Benzoate (–)-3.100. In a glovebox, a 1-dram vial containing alcohol **(–)-3.87** (2.2 mg, 5.2 μmol, 1.0 equiv) was treated sequentially with CH_2Cl_2 (150 μL, 0.03 M), Et_3N (4.4 μL, 31 μmol, 6.0 equiv), $(PhCO)_2O$ (3.5 mg, 5.2 μmol, 3.0 equiv), and $MgBr_2$•Et_2O (4.1 mg, 16 μmol, 3.0 equiv). The vial was sealed, brought out of the glovebox, and stirred at 30 °C for 5 h. After this time, the reaction was diluted with saturated sodium bicarbonate (5 mL) and Et_2O (5 mL). The layers were separated, and the aqueous layer was extracted with Et_2O (2 x 5 mL). The organic layers were

combined, dried over sodium sulfate, filtered, and concentrated under reduced pressure. The residue was purified by preparative thin layer chromatography (9:2:1 hexanes:CH_2Cl_2:Et_2O) to give benzoate **(–)-3.100** (2.2 mg, 4.2 μmol, 80% yield) as a clear colorless oil. **Benzoate (–)-3.100**: R_f 0.24 (97:3 benzene:Et_2O); ^{1}H NMR (400 MHz, $CDCl_3$): δ 8.03–7.94 (m, 2H), 7.57 (tt, *J* = 7.5, 1.3, 1H), 7.50–7.42 (m, 2H), 6.33–6.24 (m, 1H), 5.88–5.74 (m, 1H), 5.74–5.66 (m, 1H), 5.03–4.93 (m, 1H), 4.87 (tdd, *J* = 10.3, 2.4, 1.2, 1H), 4.29 (dq, *J* = 10.8, 7.1, 1H), 4.90–4.84 (m, 1H), 3.95 (ddd, *J* = 11.4, 9.9, 7.3, 1H), 3.79 (dt, *J* = 13.0, 3.7, 1H), 3.72 (ddd, *J* = 11.4, 8.1, 1.8, 1H), 3.49–3.39 (m, 1H), 3.22–3.17 (m, 2H), 3.12 (ddd, *J* = 14.8, 9.6, 8.2, 1H), 2.96 (ddd, *J* = 16.0, 3.0, 1.4, 1H), 2.59 (ddd, *J* = 16.0, 12.0, 3.9, 1H), 2.21–1.92 (m, 5H), 1.30 (t, *J* = 7.2, 3H), 0.82 (t, *J* = 8.0, 9H), 0.56–0.39 (m, 6H); ^{13}C NMR (100 MHz, C_6D_6): 172.9, 165.0, 136.9, 136.6, 135.2, 134.9, 132.8, 132.2, 129.4, 128.6, 126.0, 117.2, 89.8, 66.8, 65.5, 60.7, 60.3, 42.6, 36.9, 32.1, 24.1, 22.9, 14.2, 7.5, 2.6; IR (film): 3076, 2929, 2873, 1729, 1696 cm^{-1}; HRMS-APCI (*m/z*) $[M + H]^+$ calcd for $C_{31}H_{45}O_5Si^+$, 525.3031; found 525.3014. $[\alpha]^{21.6}_D$ –62° (*c* = 1.00, CH_2Cl_2).

The structure of **(–)-3.100** was verified by 2D-NOESY, as the following interactions were observed:

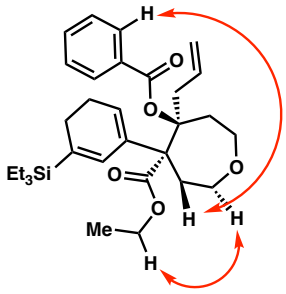

(–)-3.100

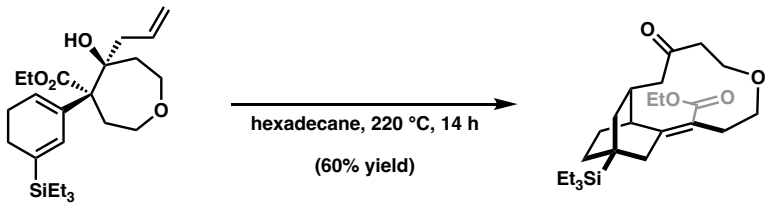

(–)-3.87 *(+)-3.19*

Product (+)-3.19. A flask equipped with a Teflon stopcock was charged with a solution of alcohol **(–)-3.87** (7.0 mg, 17 μmol, 1.0 equiv) in hexadecane (1.7 mL, 0.01 M). The solution was sparged vigorously with nitrogen for 15 min, then the stopcock was sealed, and the reaction was immersed in a sand bath and stirred at 220 °C for 14 h. After this time, the reaction was cooled to 23 °C then loaded onto a silica plug (5 cm) eluting first with hexanes (10 mL) to remove hexadecane then Et_2O (10 mL) to elute the remaining material. The eluate was concentrated, and the product was isolated by preparative thin layer chromatography (7:2:1 hexanes:CH_2Cl_2:Et_2O, eluted 2x) to afford product **(+)-3.19** (4.2 mg, 10 μmol, 60% yield) as a clear colorless oil. **Product (+)-3.19**: R_f 0.33 (4:1 hexanes:acetone); ^{1}H NMR (600 MHz, $CDCl_3$): 4.23 (qd, *J* = 7.1, 2.6, 2H), 4.13 (ddd, *J* = 11.8, 9.6, 2.4, 1H), 3.97 (ddd, *J* = 10.7, 4.8, 3.2, 1H), 3.56–3.48 (m, 2H), 3.33 (ddd, *J* = 11.5, 6.1, 2.6, 1H), 2.89 (ddd, *J* = 16.5, 9.4, 2.2, 1H), 2.60–2.45 (m, 3H), 2.33–2.20 (m, 4H), 2.13–2.06 (m, 1H), 1.92 (dt, *J* = 13.7, 2.6, 1H), 1.84–1.76 (m, 1H), 1.70 (ddd, *J* = 13.4, 10.9, 2.3, 1H), 1.68–1.61 (m, 1H), 1.58–1.51 (m, 1H), 1.39–1.34 (m, 1H), 1.34 (t, *J* = 7.1, 3H), 1.02 (t, *J* = 8.0, 9H), 0.61 (q, *J* = 8.0, 6H); ^{13}C NMR (150 MHz, $CDCl_3$): δ 210.7, 169.0, 157.6, 123.8, 69.9, 67.3, 60.0, 47.9, 44.3, 36.1, 35.5, 35.1, 30.6, 29.6, 27.0, 26.7, 20.8, 14.3, 8.1, 1.4; IR (film): 2927, 2875, 1739, 1366, 1217 cm^{-1}; HRMS-APCI (*m/z*) $[M + H]^+$ calcd for $C_{24}H_{41}O_4Si^+$, 421.2769; found 421.2760. $[\alpha]^{24.4}_D$ +37° (*c* = 1.00, CH_2Cl_2).

The structure of **(+)-3.19** was verified by 2D-NOESY, as the following interactions were observed:

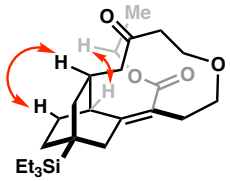

(+)-3.19

Table 3.4. SFC conditions and data.

Compound	Column	Solvent	Flow Rate	Retention Times (min)	Enantiomeric Ratio (er)
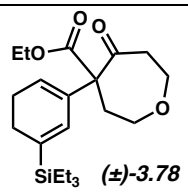 *(±)-3.78*	Daicel ChiralPak IC / 30 °C	15% isopropanol in CO_2	10.0 mL/min	3.07/3.71	49.6 : 50.4
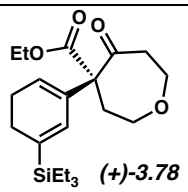 *(+)-3.78*	Daicel ChiralPak IC / 30 °C	15% isopropanol in CO_2	10.0 mL/min	3.01/3.64	4.0 : 96.0
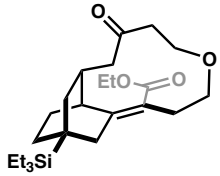 *(±)-3.19*	Daicel ChiralPak IB / 30 °C	5% isopropanol in CO_2	4.0 mL/min	5.18/6.29	49.8 : 50.2
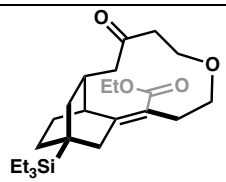 *(+)-3.19*	Daicel ChiralPak IB / 30 °C	5% isopropanol in CO_2	4.0 mL/min	5.14/6.31	95.3 : 4.7

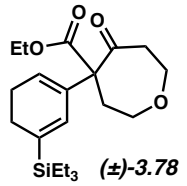

(±)-3.78

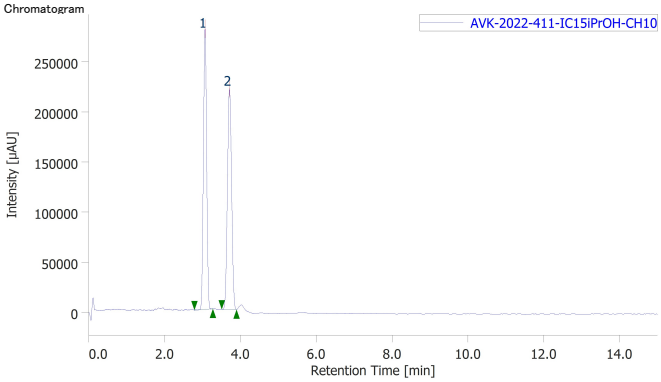

Peak Information

#	Peak Name	CH	tR [min]	Area [µV·sec]	Height [µV]	Area%	Height%	Quantity	NTP	Resolution	Symmetry Factor	Warning
1	Unknown	10	3.067	1655092	279970	49.613	55.920	N/A	6006	3.568	1.026	
2	Unknown	10	3.713	1680926	220689	50.387	44.080	N/A	5241	N/A	1.018	

Figure 3.9. SFC trace for **(±)-3.78**.

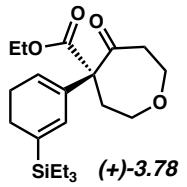

(+)-3.78

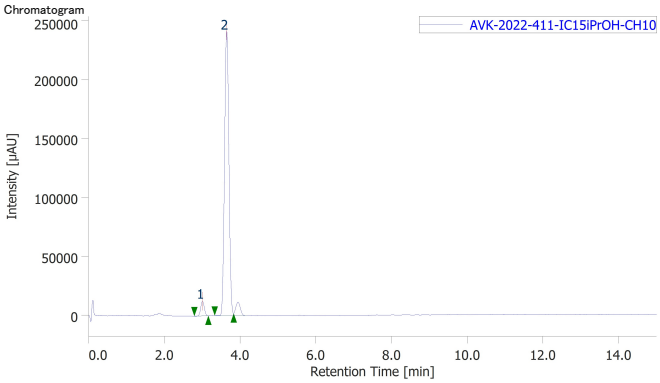

Peak Information

#	Peak Name	CH	tR [min]	Area [µV·sec]	Height [µV]	Area%	Height%	Quantity	NTP	Resolution	Symmetry Factor	Warning
1	Unknown	10	3.010	80547	12303	4.001	4.847	N/A	4634	3.256	1.018	
2	Unknown	10	3.647	1932514	241499	95.999	95.153	N/A	4593	N/A	1.047	

Figure 3.10. SFC trace for **(+)-3.78**.

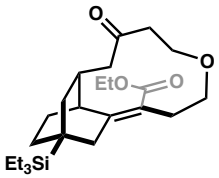

(±)-3.19

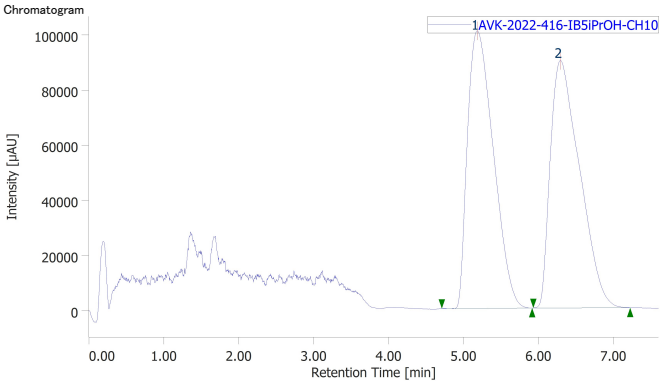

Peak Information

#	Peak Name	CH	tR [min]	Area [µV·sec]	Height [µV]	Area%	Height%	Quantity	NTP	Resolution	Symmetry Factor	Warning
1	Unknown	10	5.180	2418253	100574	49.777	52.866	N/A	967	1.563	1.545	
2	Unknown	10	6.290	2439916	89671	50.223	47.134	N/A	1103	N/A	1.687	

Figure 3.11. SFC trace for **(±)-3.19**.

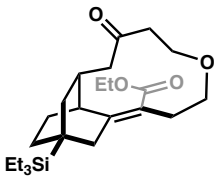

(+)-3.19

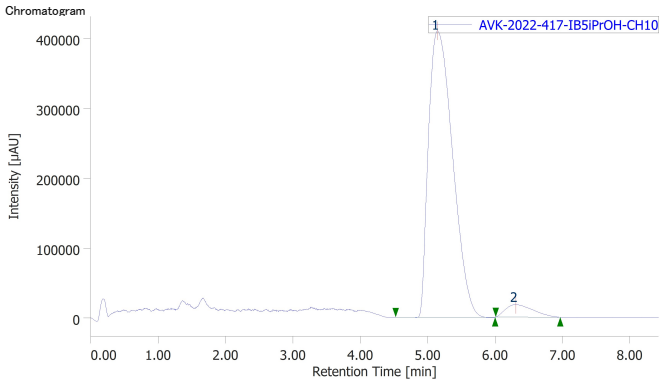

Peak Information

#	Peak Name	CH	tR [min]	Area [µV·sec]	Height [µV]	Area%	Height%	Quantity	NTP	Resolution	Symmetry Factor	Warning
1	Unknown	10	5.143	10189703	409937	95.268	95.814	N/A	900	1.576	1.560	
2	Unknown	10	6.307	506147	17911	4.732	4.186	N/A	1007	N/A	1.513	

Figure 3.12. SFC trace for **(+)-3.19**.

3.9.3.8 Competition Experiment with 1,2,3-Cyclohexatriene (3.5) and Benzyne (3.20)

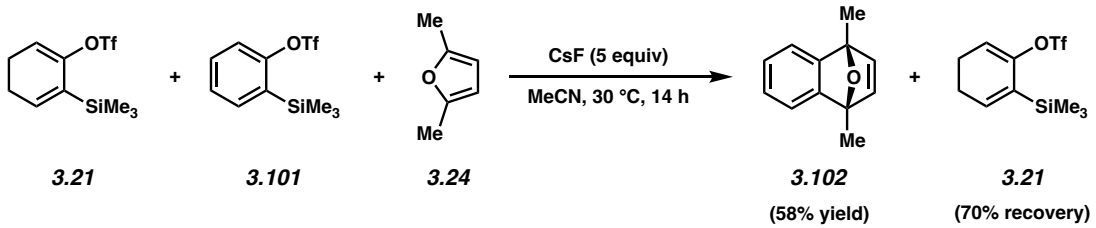

3.21 *3.101* *3.24* *3.102* (58% yield) *3.21* (70% recovery)

A flame-dried 1-dram vial containing a magnetic stir bar was charged sequentially with silyl triflate **3.21** (25.0 mg, 0.08 mmol, 1.0 equiv), silyl triflate **3.101** (25.0 mg, 0.08 mmol, 1.0 equiv), and trapping partner **3.24** (8.0 mg, 0.08 mmol, 1.0 equiv), MeCN (0.810 mL, 0.1 M), and CsF (63.0 mg, 0.42 mmol, 5.0 equiv). The vial was then sealed with a Teflon-lined cap and stirred for 14 h at 30 °C. The mixture was then filtered over a pad of Celite, eluting with EtOAc (10 mL). The eluate was concentrated. Analysis of the crude reaction mixture by ^{1}H NMR using mesitylene as an external standard showed 58% yield of **3.102**, 70% recovery of **3.21**, and no formation of the cycloadduct derived from **3.21** (i.e., **3.28**). **Cycloadduct 3.102**: Spectral data matched those reported in the literature.[72]

3.9.4 Computational Section

3.9.4.1 Computational Methods

Conformational searches were performed in Spartan '20 V1.1.4[73] using Molecular Mechanics. Conformers were then optimized in Gaussian 16 A.03[74] at the B3LYP[75,76] -D3[77]/6-311+G(d,p), SMD[78](THF) level of theory. Structures for NMR calculations were optimized at the B3LYP/6-31+G(d,p) level of theory. NMR single point calculations (GIAO)[79,80,81,82,83] were performed on these geometries at the mPW1PW91[84]/6-311+G(d,p), SMD(benzene) level of theory. All geometries were verified as stationary points on the potential energy surface and characterized as transition states or minima by frequency calculations. Intrinsic reaction coordinate (IRC)

calculations were performed at the same level of theory to confirm the intermediates linked by each transition state. GoodVibes[85] (v. 3.2) with quasi-harmonic entropy[86] and enthalpy[87] treatment (frequency cut-off value: 100 cm^{-1}) was used to obtain corrected Gibbs free energies and enthalpies at either 298.15 K or 333.15 K and 1 atm. Optimized structures are presented using CYLview.[88]

3.9.4.2 Calculated Energies of Selected C_6H_6 Isomers

Table 3.5. Computed energies of selected C_6H_6 isomers at 25 °C at the B3LYP-D3/6-311+G(d,p) level of theory. All units are in Hartrees.

Structure	E	ZPE	H	T.qh-S	G(T)	qh-G(T)
Benzene (**3.1**)	-232.31633	0.10013	-232.21086	0.03281	-232.24367	-232.24368
Dewar benzene (**3.2**)	-232.18184	0.09680	-232.07952	0.03233	-232.11184	-232.11184
Benzvalene (**3.3**)	-232.18557	0.09690	-232.08340	0.03175	-232.11514	-232.11514
Prismane (**3.4**)	-232.11823	0.09635	-232.01682	0.03026	-232.04708	-232.04708
Triene **3.5**	-232.14988	0.09616	-232.04731	0.03490	-232.08221	-232.08221

3.9.4.3 Structure of 1,2,3-Cyclohexatriene (3.5)

The annotated structure of 1,2,3-cyclohexatriene (**3.5**) appears below in Figure 3.13 and was used to obtain the frontier molecular orbitals shown in Figure 3.3A. Comparison of LUMO energy with benzyne (**3.20**) suggests strong similarities in electronic structure which correlate with the similarity in reactivity reported herein. Notably, whereas the absolute magnitude of DFT-derived LUMO eigenvalues is known to deviate from experimental benchmarks,[89] the relative energies support similarity between triene **3.5** and benzyne (**3.20**).

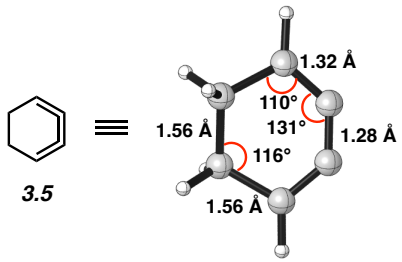

Figure 3.13. Geometry of 1,2,3-cyclohexatriene (**3.5**) at the B3LYP-D3/6-311+G(d,p) level of theory.

3.9.4.4 Transition State Analysis for Reaction of Triene 3.80 with Phenoxide 3.34

The reaction between Et_3Si-substituted triene **3.75** and phenoxide **3.34** was studied computationally using Me_3Si-substituted triene **3.80** and omitting the Na^+ cation in **3.34**. The latter approximation was motivated in part by the possibility for cation exchange with other cations in the reaction (Na^+, Bu_4N^+, and Cs^+), which convolutes the determination of the exact identity of the relevant species. Additionally, this omission circumvents potentially complex solvent-cation interactions. Analogous simplifications involving substitution of Me_3Si for Et_3Si[90] and omission of the cation[47] in computational modeling of nucleophilic additions to strained intermediates have been reported in the literature, and the resulting models demonstrate good correlation with experimentally observed outcomes.

Table 3.6. Computed energies for the reaction of triene **3.80** with phenoxide **3.34** (Na^+ omitted) at 60 °C at the B3LYP-D3/6-311+G(d,p), SMD(THF) level of theory. All units are in Hartrees.

Structure	E	ZPE	H	T.qh-S	G(T)	qh-G(T)
Triene **3.80**	-640.91356	0.19670	-640.69956	0.06186	-640.76342	-640.76142
Phenoxide **3.34**	-511.67626	0.09324	-511.57249	0.04813	-511.62142	-511.62062
TS-3.1	-1152.59402	0.29171	-1152.27476	0.08405	-1152.36413	-1152.35881
TS-3.2	-1152.58660	0.29074	-1152.26784	0.08610	-1152.36088	-1152.35393

Table 3.7. Distortion/Interaction-Activation Strain Analysis (DIAS) of the phenolate addition (**TS3.1** & **TS3.2**). All units are in kcal/mol.

	TS-3.1	**TS-3.2**
$E_{dist,triene\ \mathbf{3.80}}$	1.54	2.98
$E_{dist,triene\ \mathbf{3.34}}$	0.09	0.08
E_{int}	-4.27	-1.05

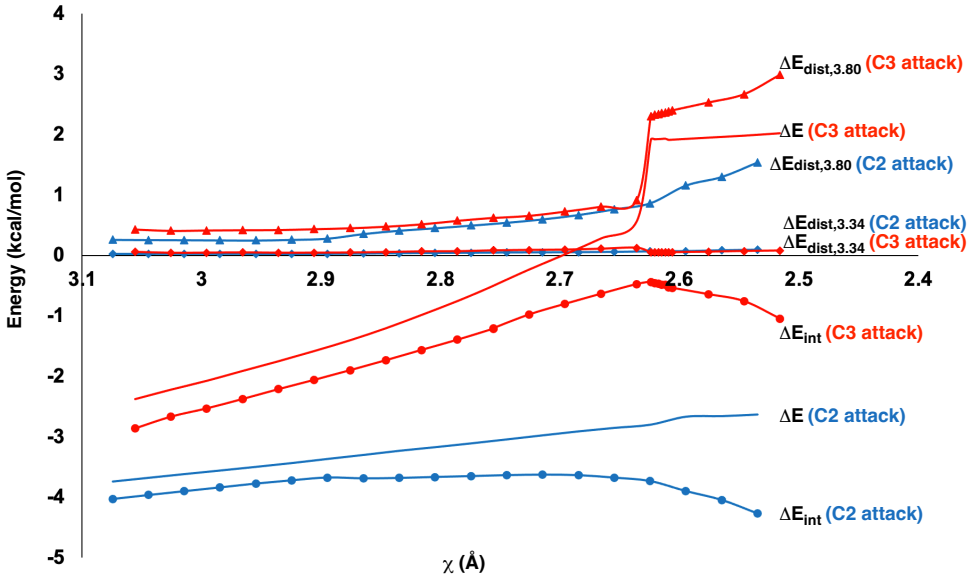

Figure 3.14. DIAS strain analysis along a relaxed scan of the forming C–O bond for attack of phenoxide **3.34** (Na^+ omitted) on triene **3.80** at C2 or C3 (B3LYP-D3/6-311+G(d,p), SMD(THF)). The x-axis corresponds to reaction progress, (i.e., the C–O bond distance for the forming bond).

DIAS analysis performed along the two competing approaches for nucleophilic attack of **3.34** onto **3.80** demonstrates that C2 attack is favored due to both distortion and interaction effects (Figure 3.14). Whereas distortion of phenoxide **3.34** is negligible for both approaches, attack at C3 requires significant geometric distortion of triene **3.80** as bond formation advances while attack at C2 does not (as a result of the previously discussed ground state distortion). This difference is reflected in a substantially higher (1.4–1.9 kcal/mol) distortion energy for **3.80** at C–O bond lengths under 2.65 Å. C2 attack also benefits from more favorable interaction energies. Significant additional stabilization arises from attractive CH–π and C–H···O interactions between the incoming nucleophile **3.34** and the C–H groups of the $SiMe_3$ substituent, whereas the approach and transition state geometry of **TS-3.2** place the nucleophile increasingly out of reach of the $SiMe_3$ substituent as the forming C3–O bond length decreases (see Figure 3.15 below).

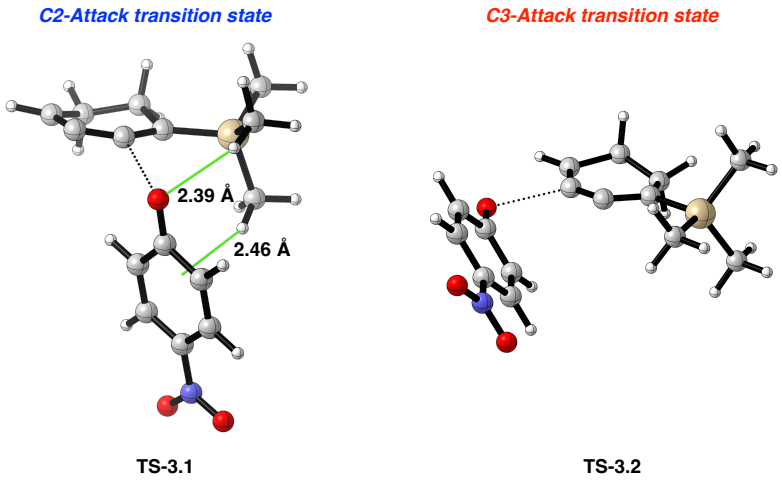

Figure 3.15. Transition state structures for the attack of **3.34** (Na^+ omitted) onto **3.80** at the B3LYP-D3/6-311+G(d,p), SMD(THF) level of theory. Stabilizing CH–π and C–H···O interactions present in **TS-3.1** are designated with green highlighting and the corresponding distances.

3.9.4.5 Relative Stereochemical Assignment of Thietanes 3.69 and 3.93

Extensive overlapping signals prevented assignment of the relative stereochemistry of thietane **3.69** using 2D-NOESY experiments, so the structural assignment was instead accomplished by comparison to computed NMR shift data (see below).

Computed NMR Shift Data

Structures used for NMR calculations were optimized at the B3LYP/6-31+G(d,p) level of theory. NMR single point calculations (GIAO) were performed on these geometries at the mPW1PW91/6-311+G(d,p), SMD(benzene) level of theory to obtain computed isotropic shielding constants (σ). Corrected chemical shifts were obtained by empirically scaling these shielding constants according to Equation 3.2 using scaling factors (m and b) from http://cheshirenmr.info which are given below.[91,92,93,94]

$$\delta = \frac{b-\sigma}{-m}$$

Equation 3.2. Empirical scaling of computed shifts.

δ = computed chemical shift relative to Me_4Si
σ = computed isotropic shielding constant
m = slope from empirical scaling data (here, –1.0286)
b = intercept from empirical scaling data (here, 185.5899)

Table 3.8. Comparison of Experimental and Computed NMR Chemical Shifts for Structure **3.69**.

	^{13}C NMR Chemical Shifts (ppm)		
Nucleus #[a]	Expt.	Computed (**3.69**)[b]	Computed (**3.93**)[b]
1	112.82	116.31	115.23
2	135.30	138.16	138.56
3	34.43	33.34	32.69
4	122.22	127.24	126.79
5	29.38	29.63	29.45
6	126.96	133.21	132.30
11	16.62	15.14	15.16
15	21.89	21.27	19.24
20	86.80	93.89	94.17
21	45.63	50.54	49.87
22	55.23	58.42	56.19
23	32.48	32.66	35.39
26	25.49	25.21	25.14
29	50.02	51.19	50.26
31	32.97	31.94	25.86
35	23.96	21.49	27.30
39	42.57	42.02	42.29
42	20.05	18.33	16.00
	CMAD[c]	2.42	2.91

[a] Nucleus labels correspond to those shown in the Figure 3.16 below Table 3.9. [b] Largest outliers are indicated in red. Note that higher than average errors are expected for the carbon atoms bearing a sulfur atom (e.g., C6 and C20) – due to heavy-atom effects. [c] CMAD = corrected mean absolute deviation and is computed as $\frac{1}{n}\sum_i^n \left|\delta_{comp} - \delta_{exp}\right|$ where δ_{comp} refers to the scaled computed chemical shifts and δ_{exp} refers to experimentally observed chemical shifts.

Table 3.9. Comparison of Experimental and Computed NMR Chemical Shifts for Structure **3.93**.

	^{13}C NMR Chemical Shifts (ppm)		
Nucleus #[a]	Expt.	Computed (**3.69**)[b]	Computed (**3.93**)[b]
1	112.48	116.31	115.23
2	136.27	138.16	138.56
3	32.57	33.34	32.69
4	121.27	127.24	126.79
5	29.31	29.63	29.45
6	125.83	133.21	132.30
11	16.71	15.14	15.16
15	20.20	21.27	19.24
20	87.00	93.89	94.17
21	45.75	50.54	49.87
22	52.60	58.42	56.19
23	35.04	32.66	35.39
26	25.25	25.21	25.14
29	49.21	51.19	50.26
31	29.85	31.94	25.86
35	28.28	21.49	27.30
39	42.17	42.02	42.29
42	17.86	18.33	16.00
	CMAD[c]	3.07	2.68

[a] Nucleus labels correspond to those shown in Figure 3.16 below. [b] Largest outliers are indicated in red. Note that higher than average errors are expected for the carbon atoms bearing a sulfur atom (CSS) – due to heavy-atom effects. [c] CMAD = corrected mean absolute deviation and is computed as $\frac{1}{n}\sum_i^n \left|\delta_{comp} - \delta_{exp}\right|$ where δ_{comp} refers to the scaled computed chemical shifts.

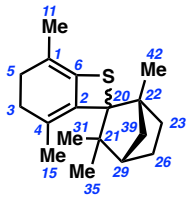

Figure 3.16. Atom numbers used in Table 3.8 and Table 3.9.

3.9.4.6 Cartesian Coordinates of Optimized Geometries

Cartesian coordinates for the optimized structures were reported in the literature.[95]

3.10 Spectra Relevant to Chapter Three:

Strain-Promoted Reactions of 1,2,3-Cyclohexatriene and Its Derivatives

Andrew V. Kelleghan,[†] Ana S. Bulger,[†] Dominick C. Witkowski, and Neil K. Garg

Nature **2023**, *618*, 748–754.

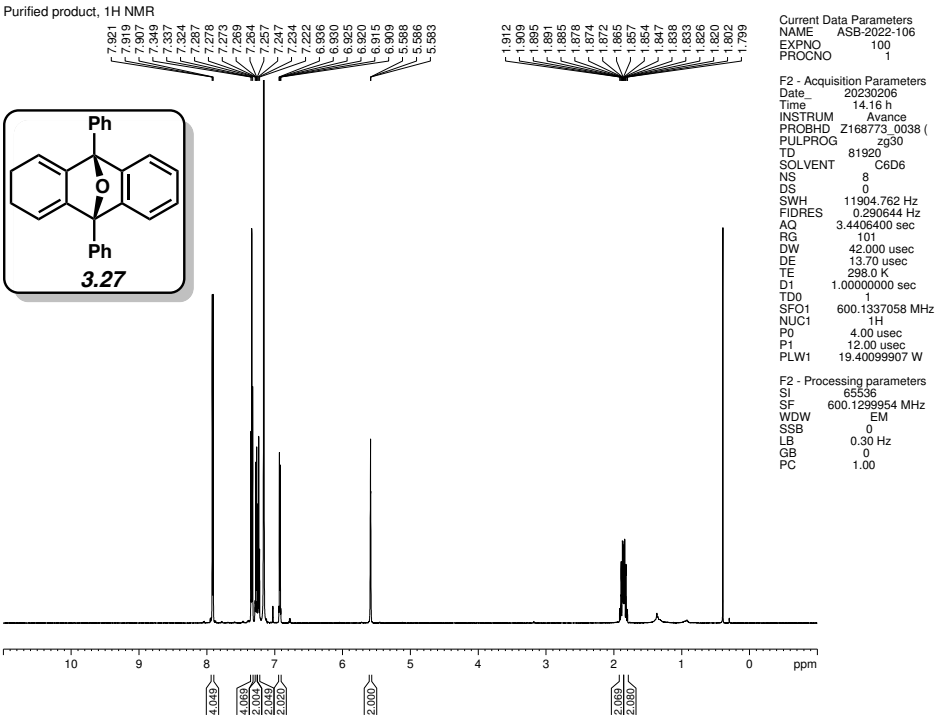

Figure 3.17. ^{1}H NMR (600 MHz, C_6D_6) of compound **3.27**.

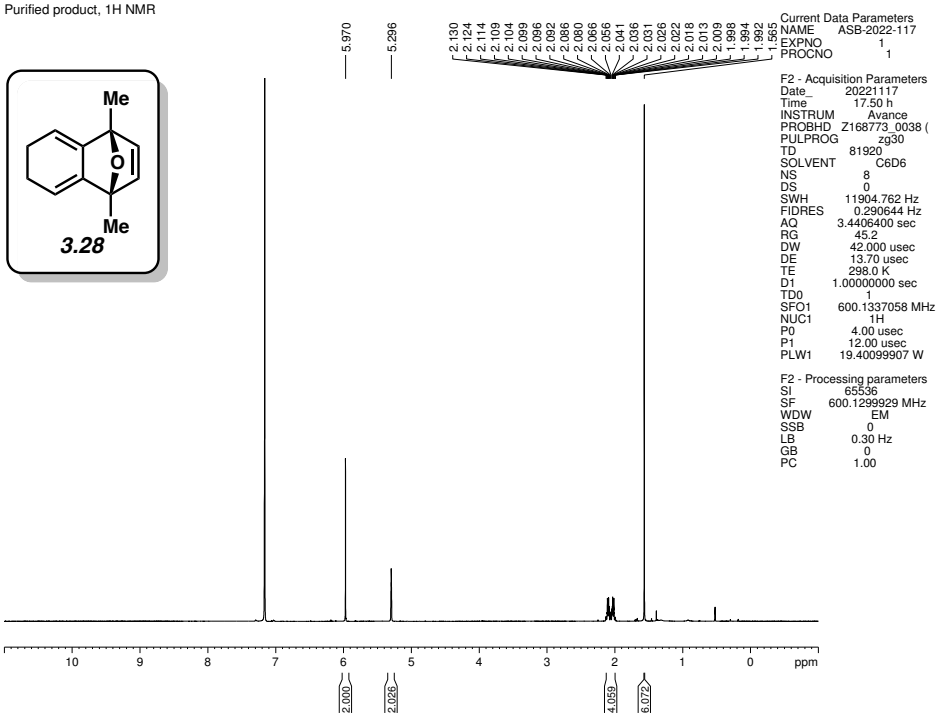

Figure 3.18. ^{1}H NMR (600 MHz, C_6D_6) of compound **3.28**.

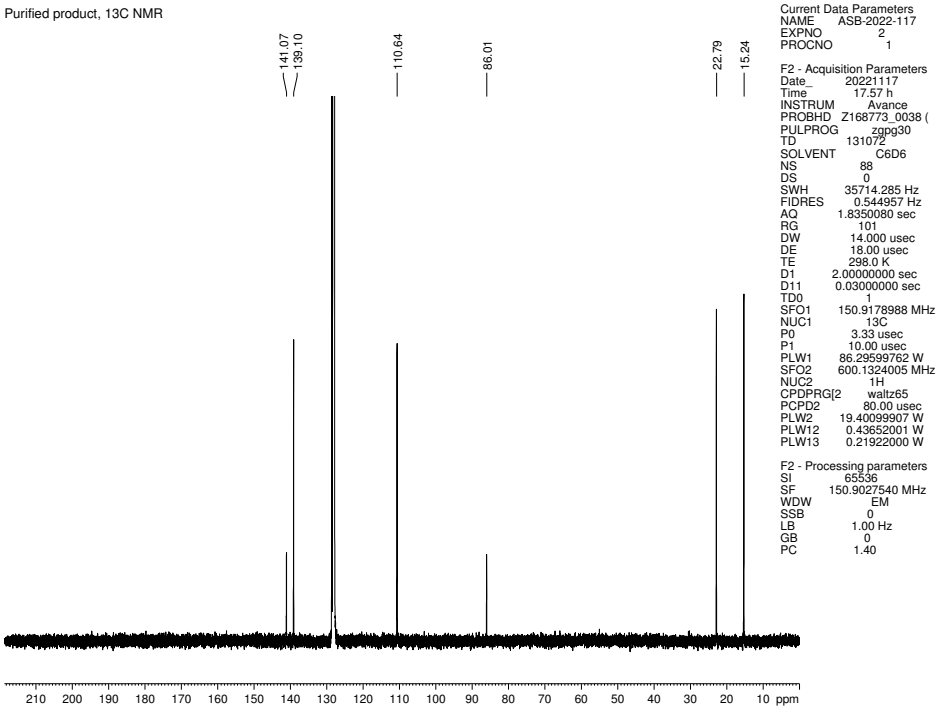

Figure 3.19. ^{13}C NMR (150 MHz, C_6D_6) of compound **3.28**.

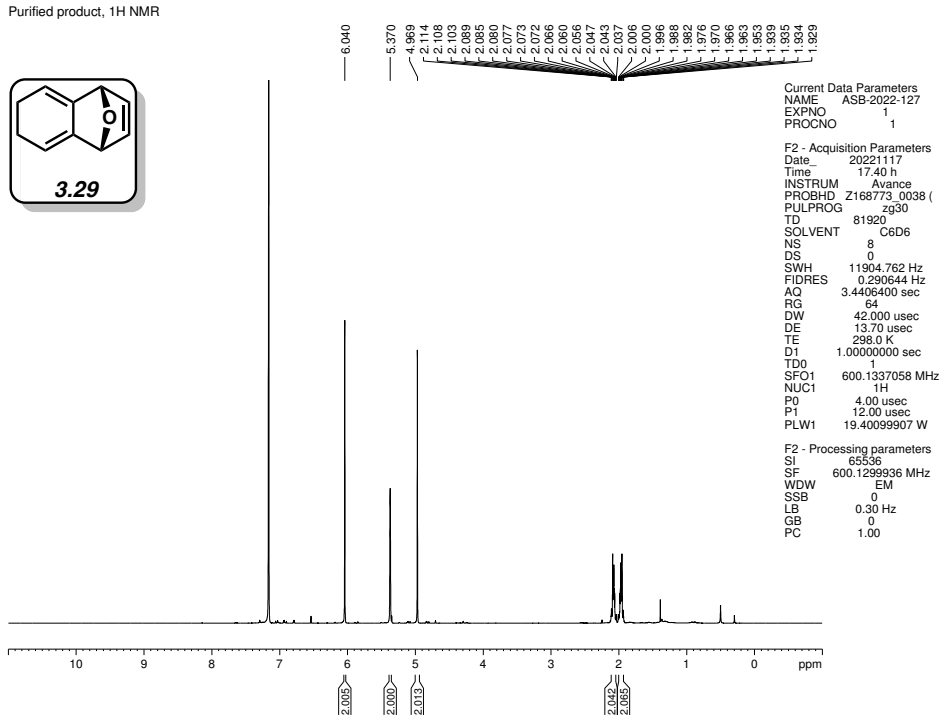

Figure 3.20. ^{1}H NMR (600 MHz, C_6D_6) of compound **3.29**.

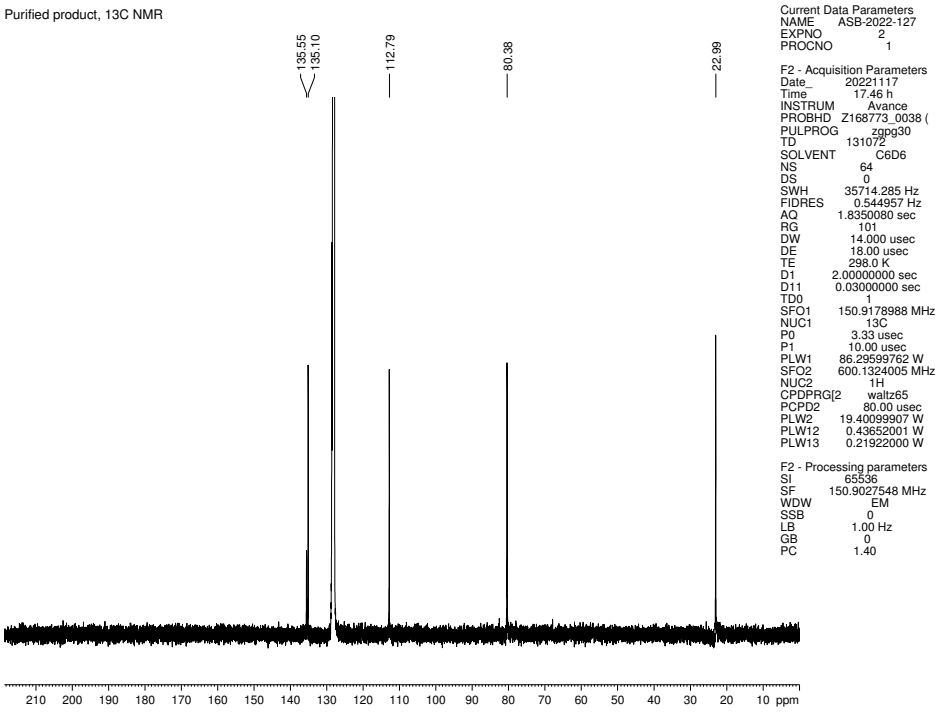

Figure 3.21. ^{13}C NMR (150 MHz, C_6D_6) of compound **3.29**.

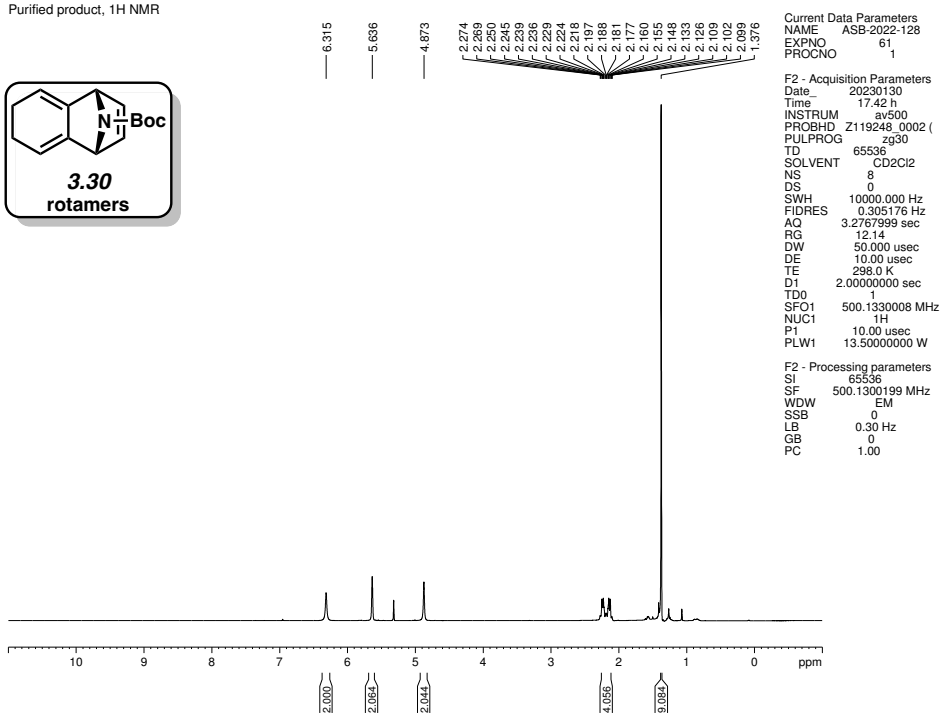

Figure 3.22. ^{1}H NMR (500 MHz, CD_2Cl_2) of compound **3.30**.

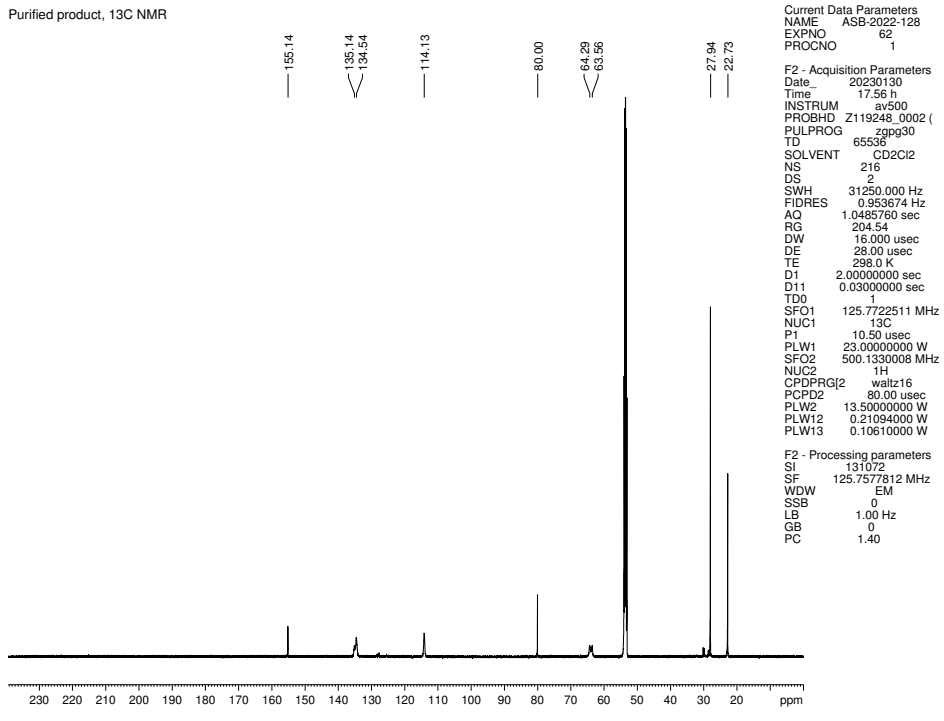

Figure 3.23. ^{13}C NMR (125 MHz, CD_2Cl_2) of compound **3.30**.

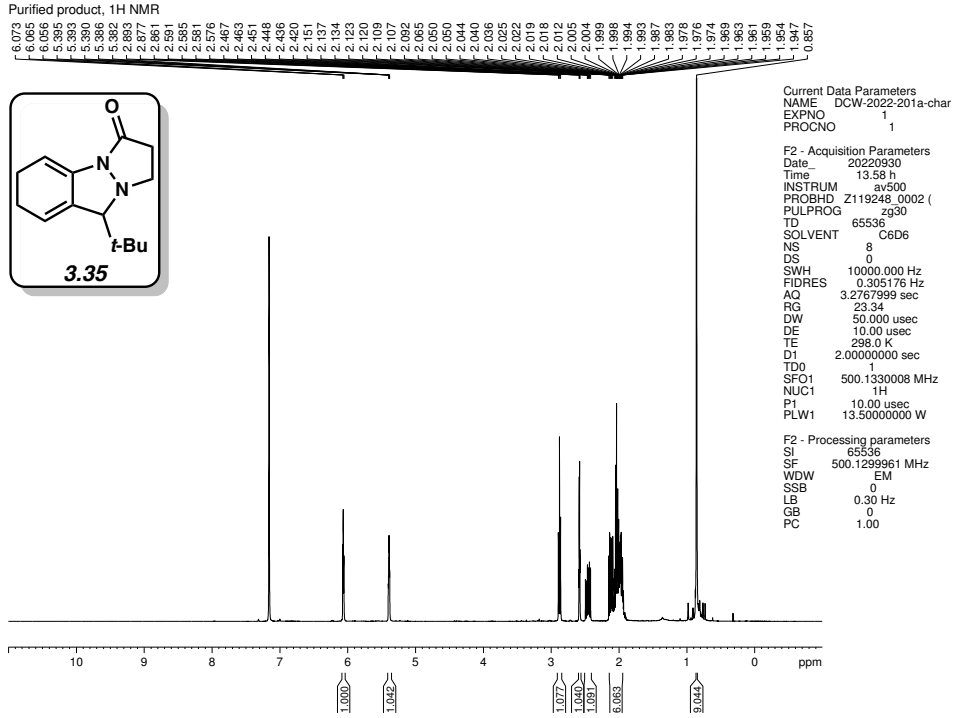

Figure 3.24. ^{1}H NMR (500 MHz, C_6D_6) of compound **3.35**.

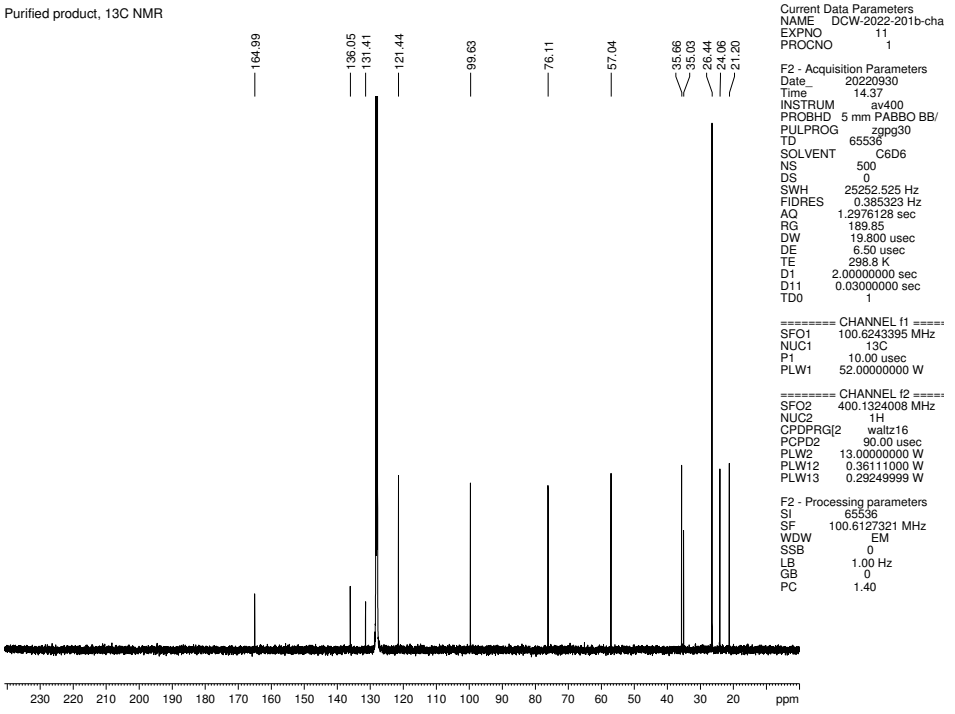

Figure 3.25. ^{13}C NMR (100 MHz, C_6D_6) of compound **3.35**.

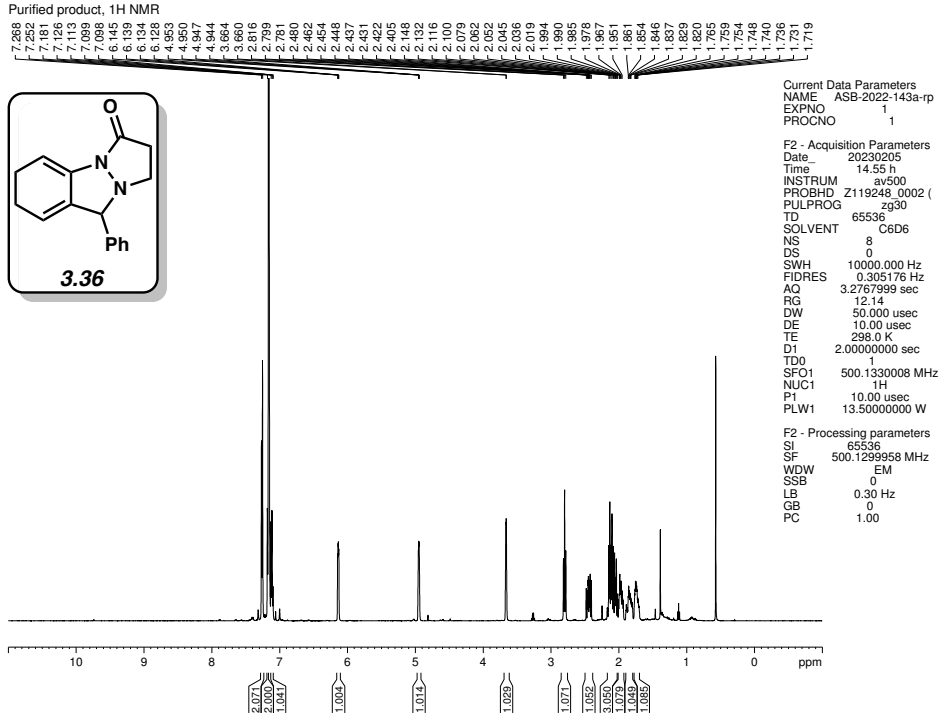

Figure 3.26. ^{1}H NMR (500 MHz, C_6D_6) of compound **3.36**.

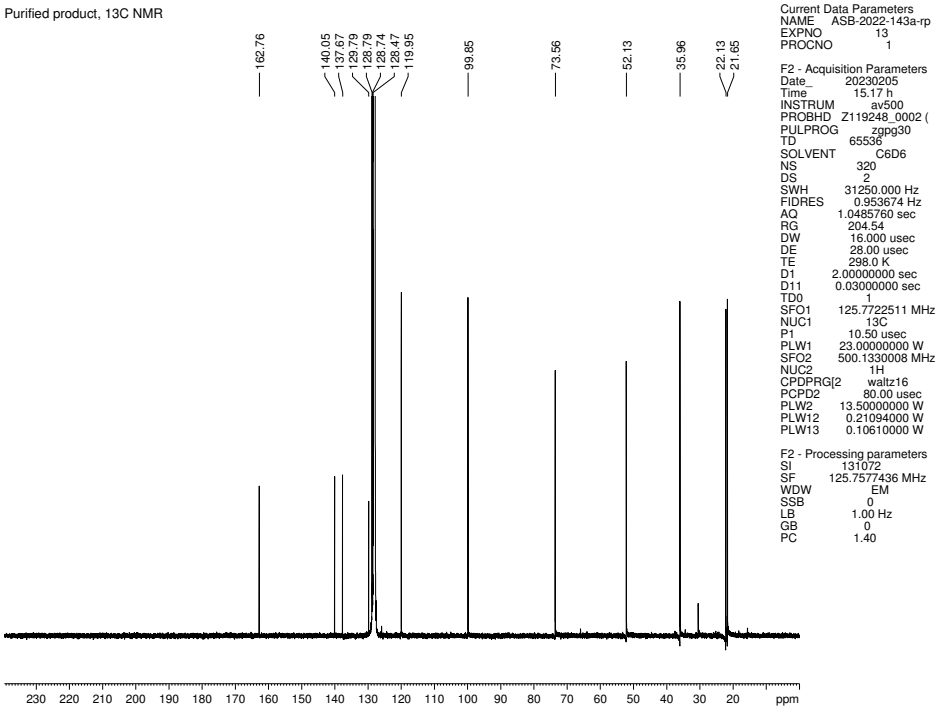

Figure 3.27. ^{13}C NMR (125 MHz, C_6D_6) of compound **3.36**.

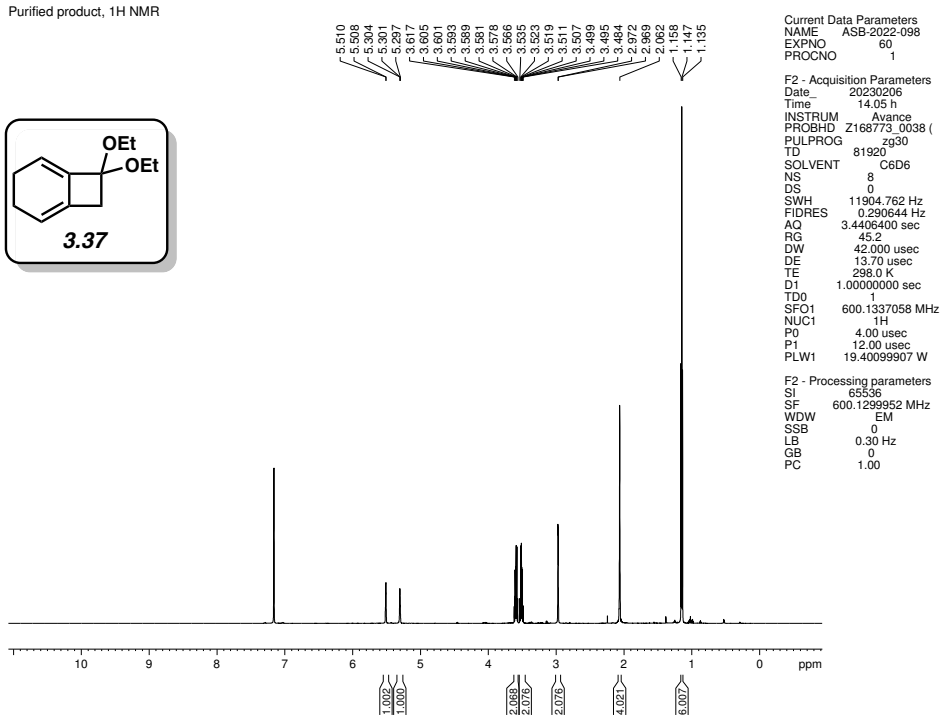

Figure 3.28. ^{1}H NMR (600 MHz, C_6D_6) of compound **3.37**.

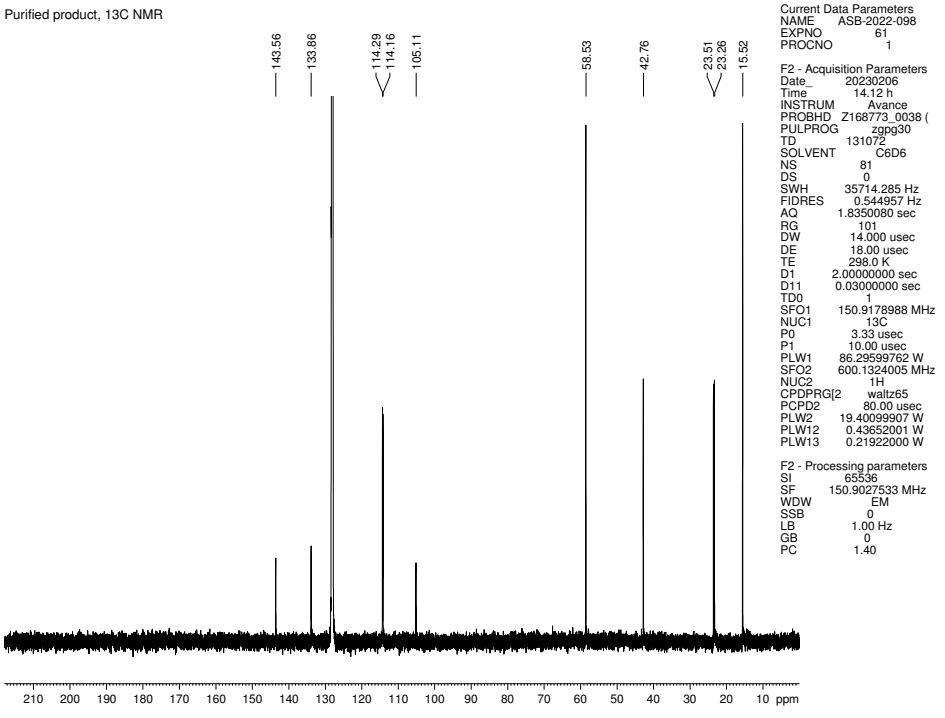

Figure 3.29. ^{13}C NMR (150 MHz, C_6D_6) of compound **3.37**.

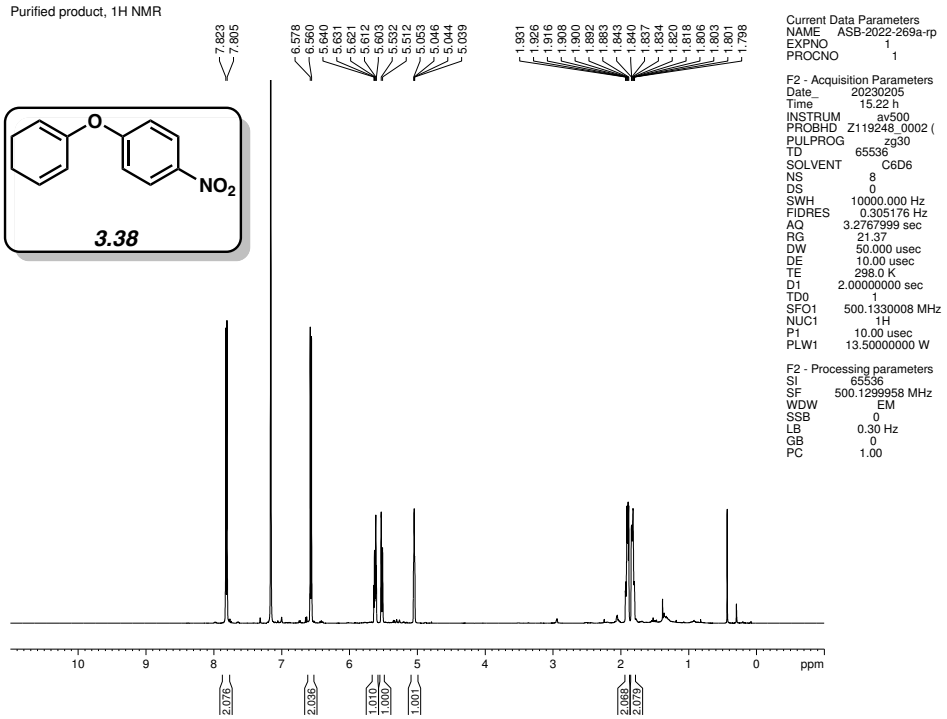

Figure 3.30. ^{1}H NMR (500 MHz, C_6D_6) of compound **3.38**.

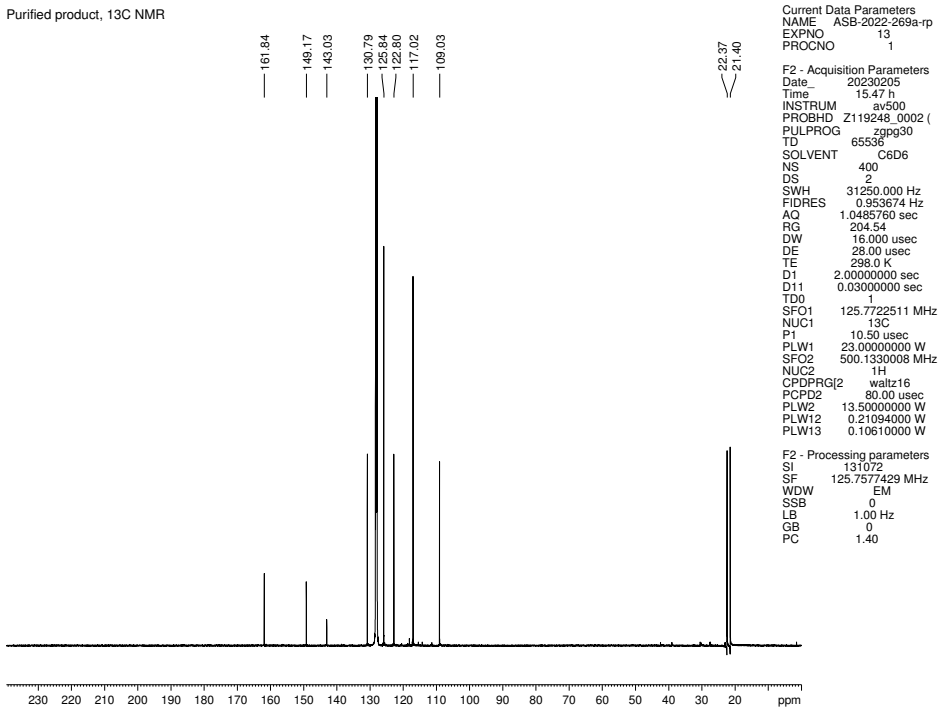

Figure 3.31. ^{13}C NMR (125 MHz, C_6D_6) of compound **3.38**.

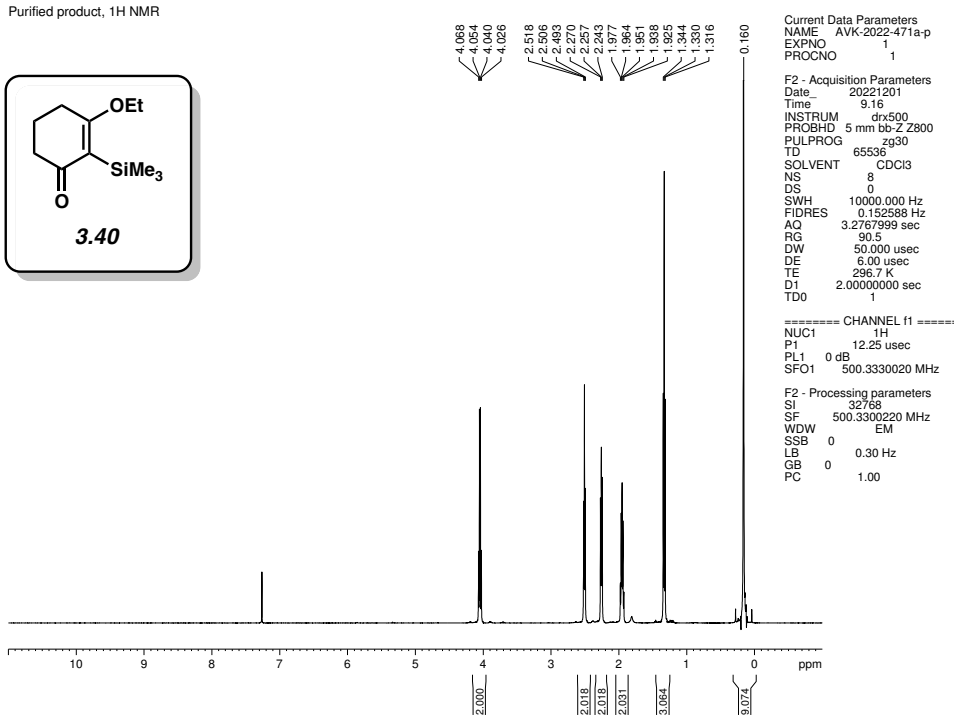

Figure 3.32. ^{1}H NMR (500 MHz, $CDCl_3$) of compound **3.40**.

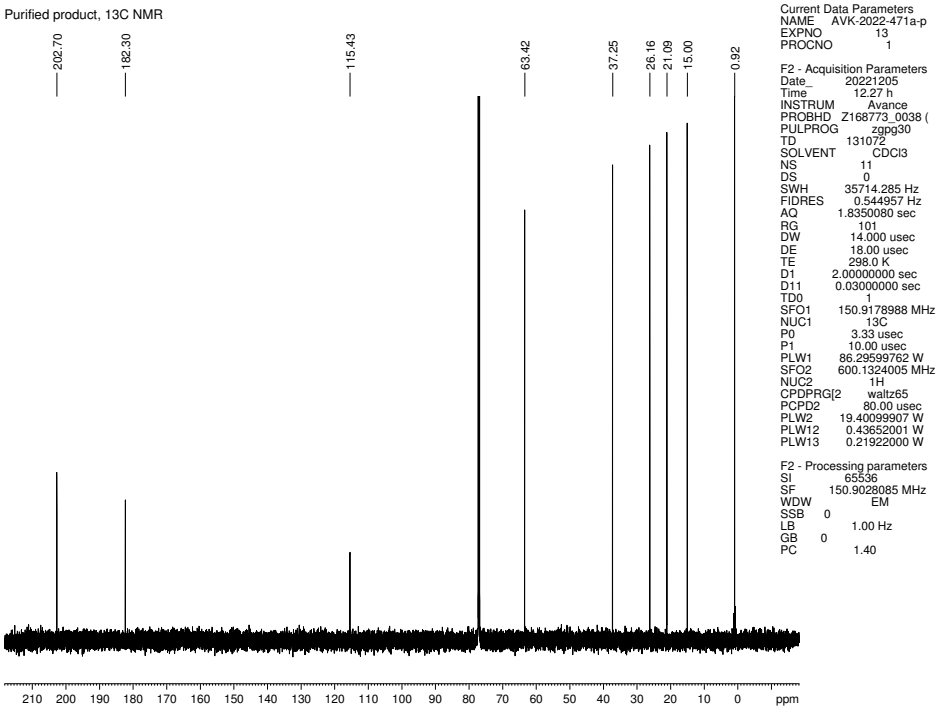

Figure 3.33. ^{13}C NMR (150 MHz, $CDCl_3$) of compound **3.40**.

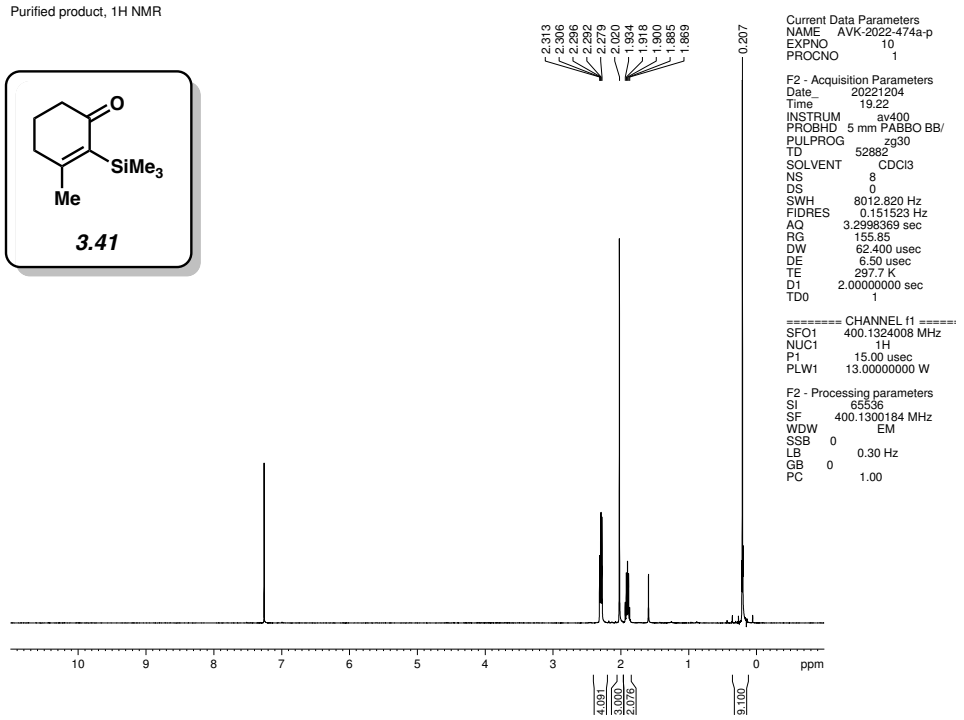

Figure 3.34. ^{1}H NMR (400 MHz, $CDCl_3$) of compound **3.41**.

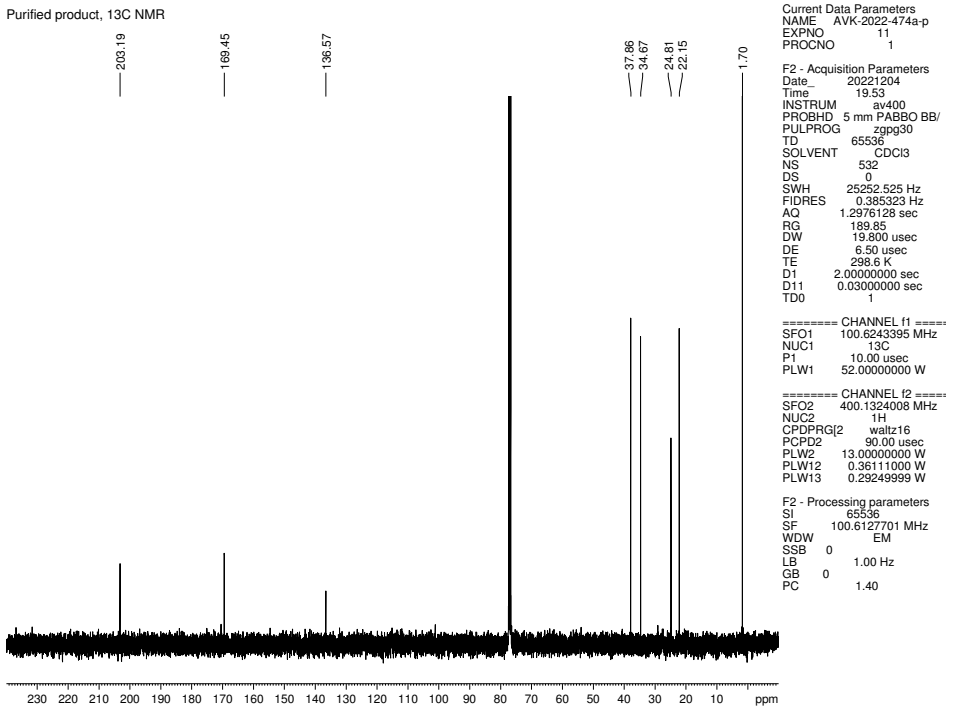

Figure 3.35. ^{13}C NMR (100 MHz, $CDCl_3$) of compound **3.41**.

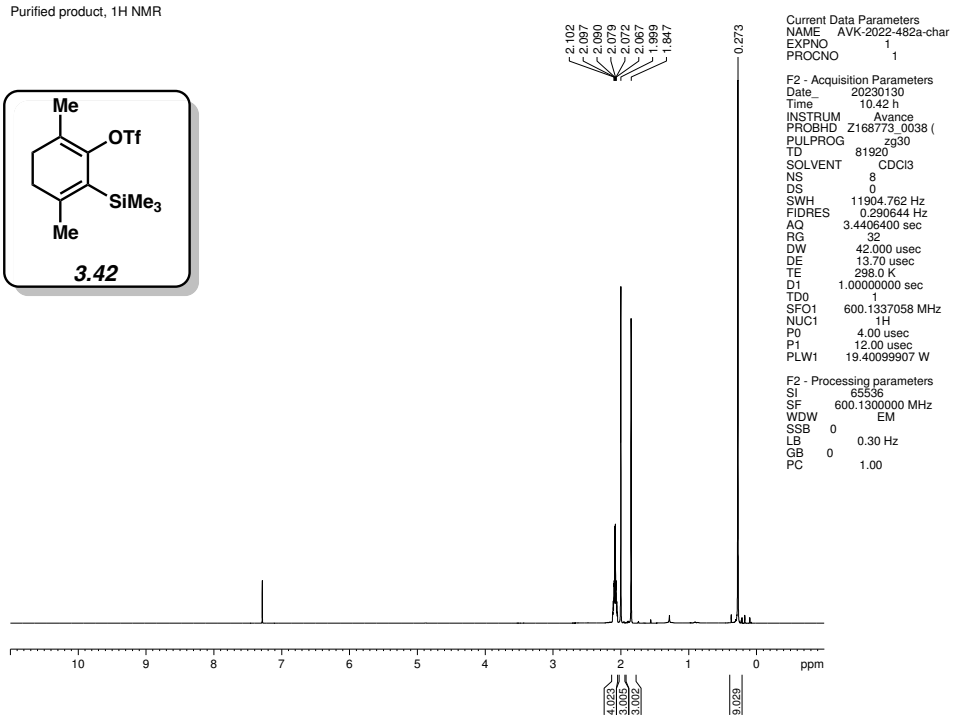

Figure 3.36. ^{1}H NMR (600 MHz, $CDCl_3$) of compound **3.42**.

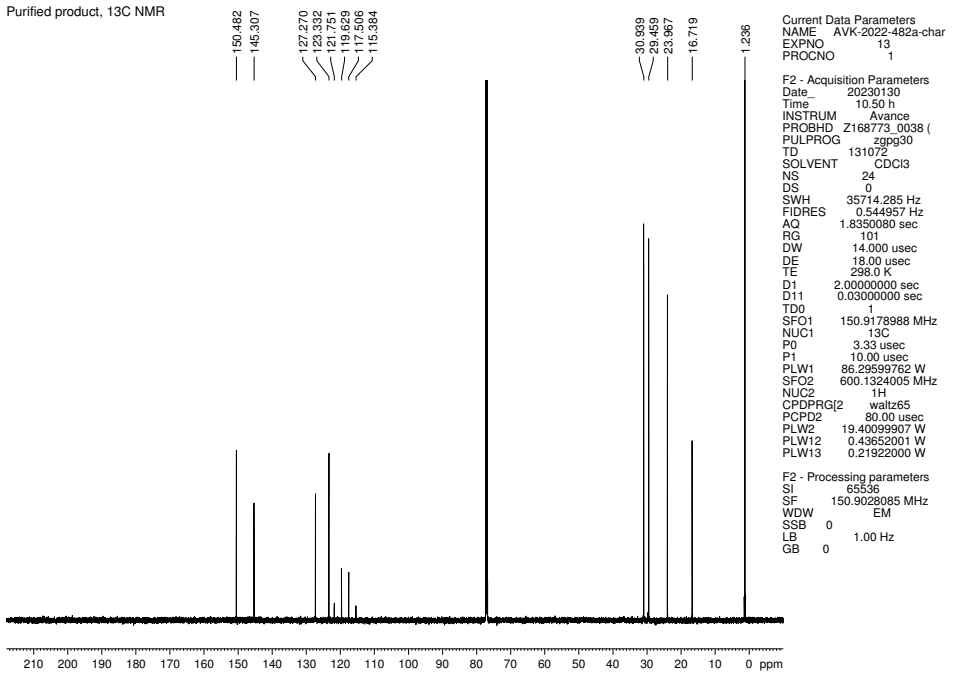

Figure 3.37. ^{13}C NMR (150 MHz, $CDCl_3$) of compound **3.42**.

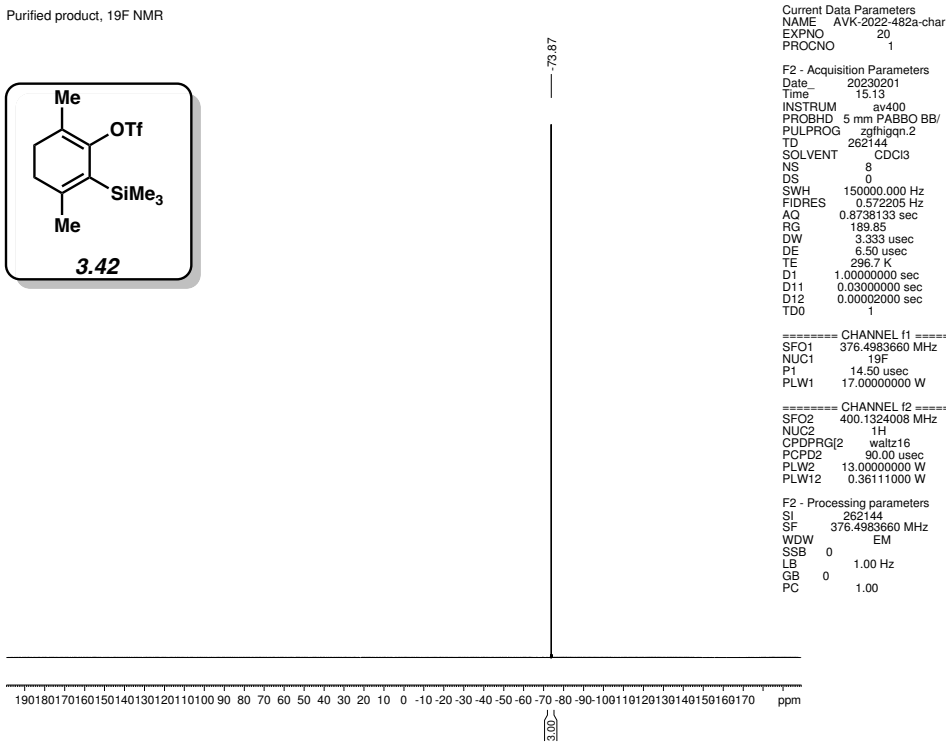

Figure 3.38. ^{19}F NMR (376 MHz, $CDCl_3$) of compound **3.42**.

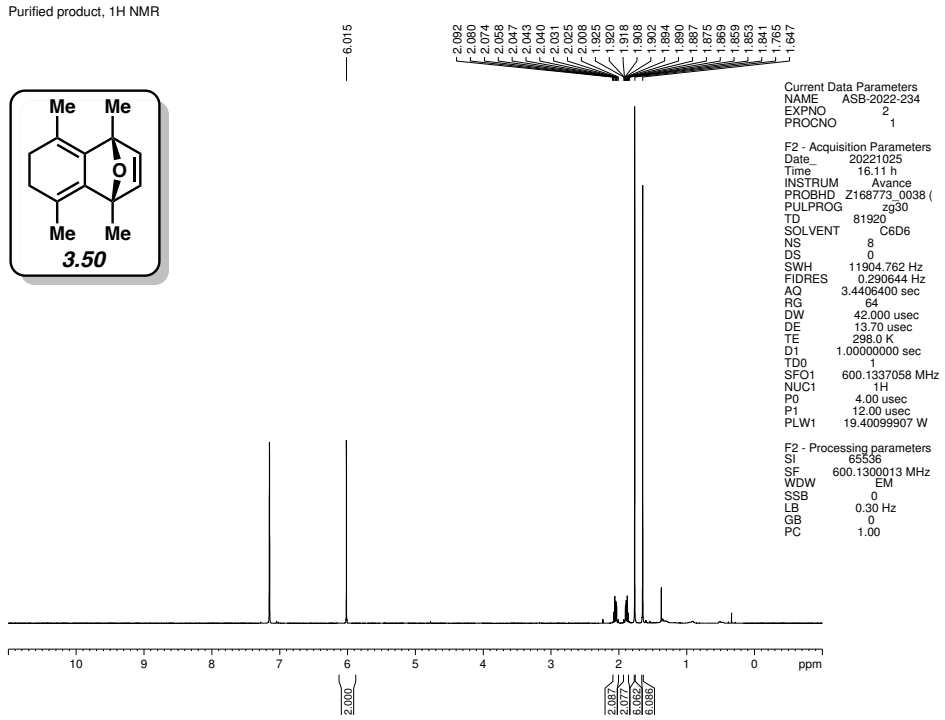

Figure 3.39. ^{1}H NMR (600 MHz, C_6D_6) of compound **3.50**.

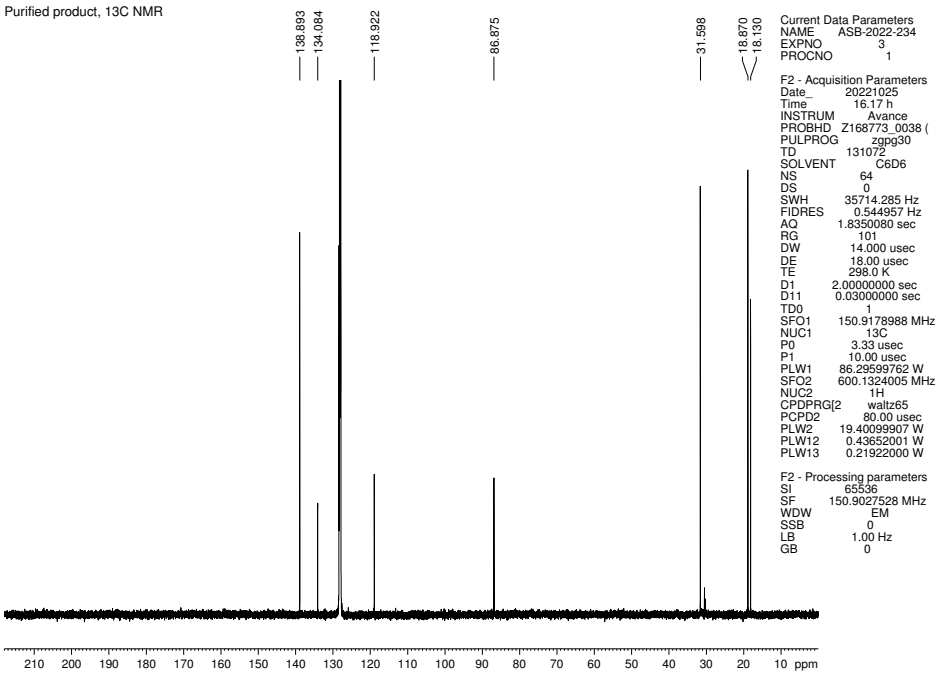

Figure 3.40. ^{13}C NMR (150 MHz, C_6D_6) of compound **3.50**.

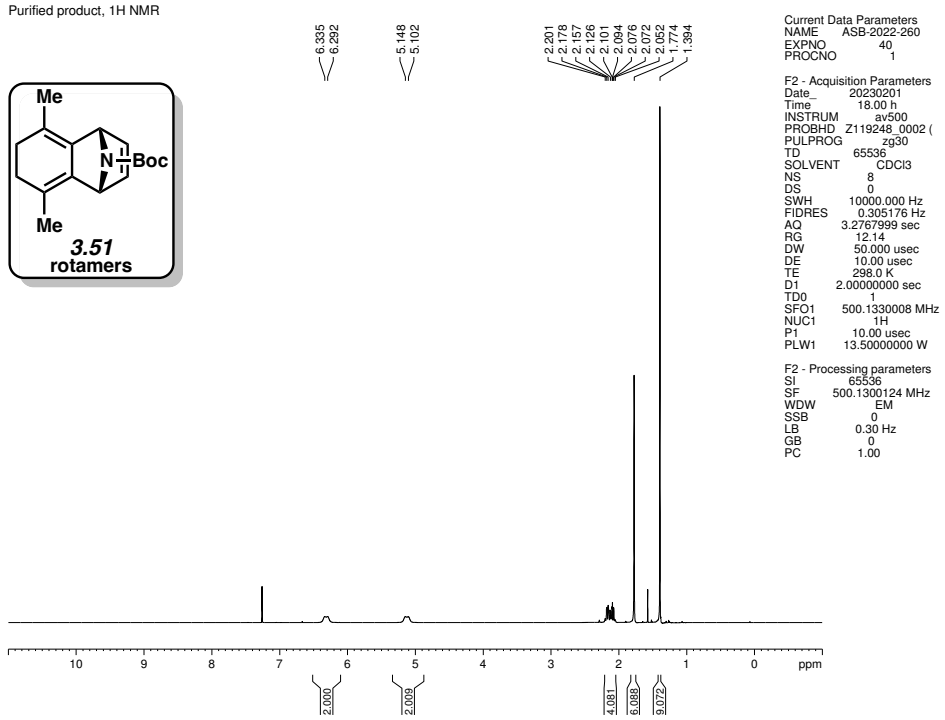

Figure 3.41. ^{1}H NMR (500 MHz, $CDCl_3$) of compound **3.51**.

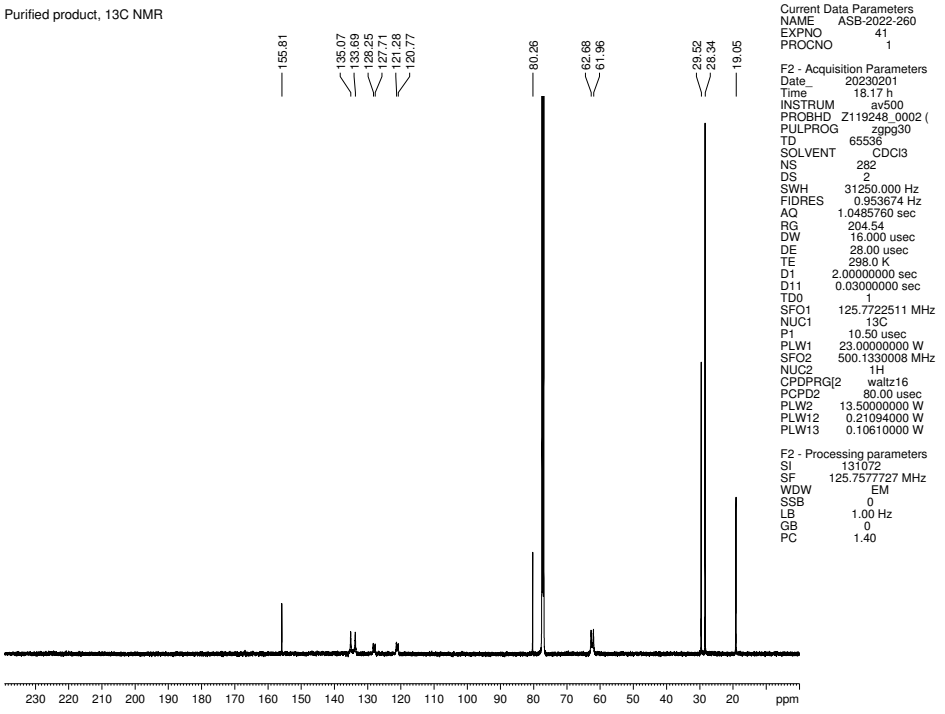

Figure 3.42. ^{13}C NMR (125 MHz, $CDCl_3$) of compound **3.51**.

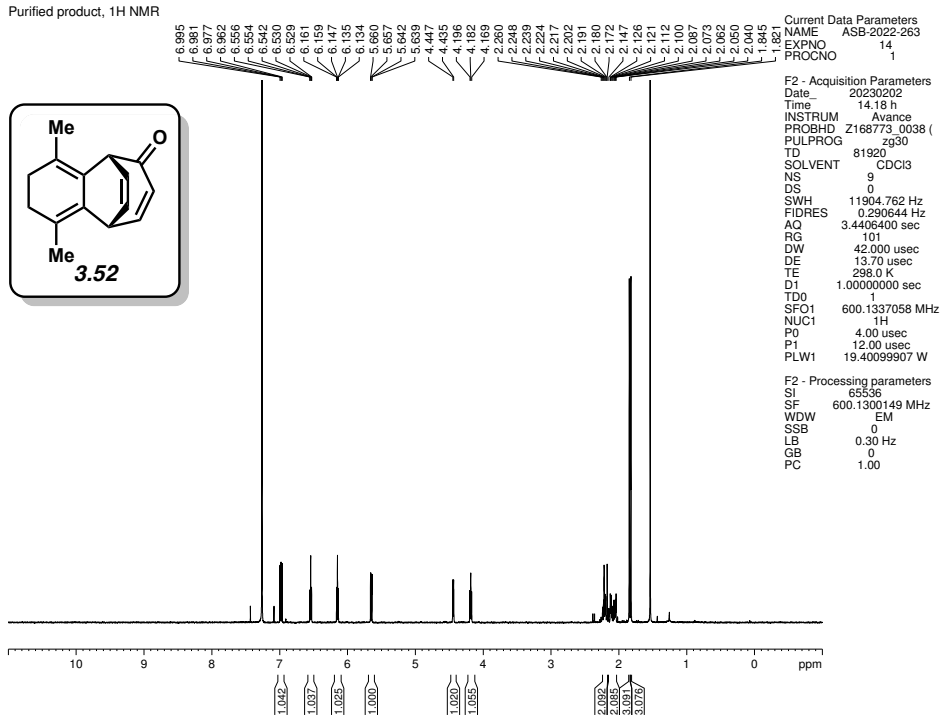

Figure 3.43. ^{1}H NMR (600 MHz, $CDCl_3$) of compound **3.52**.

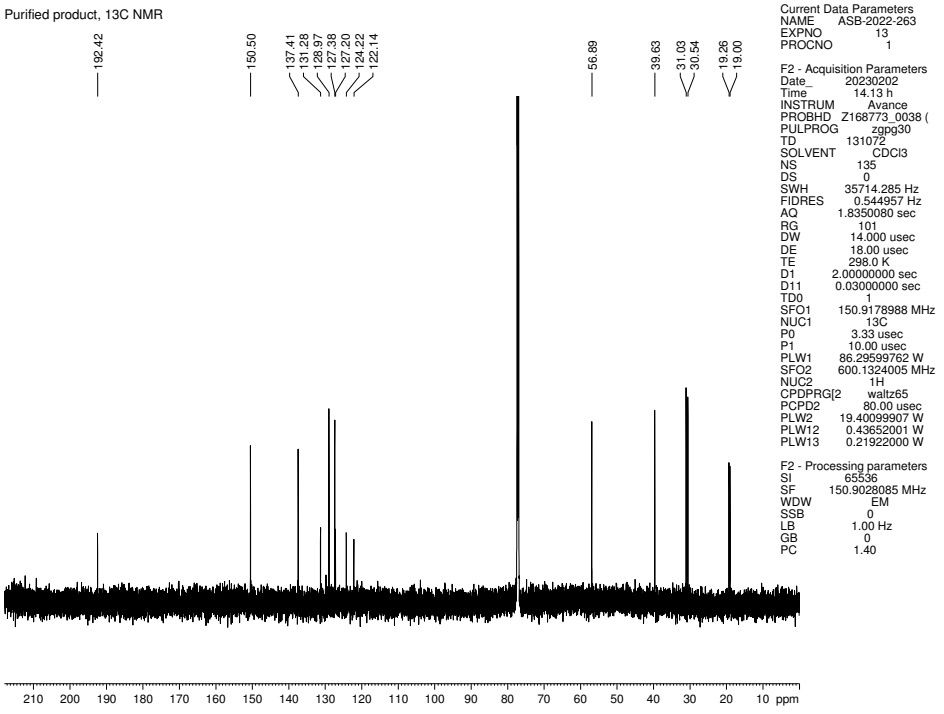

Figure 3.44. ^{13}C NMR (150 MHz, $CDCl_3$) of compound **3.52**.

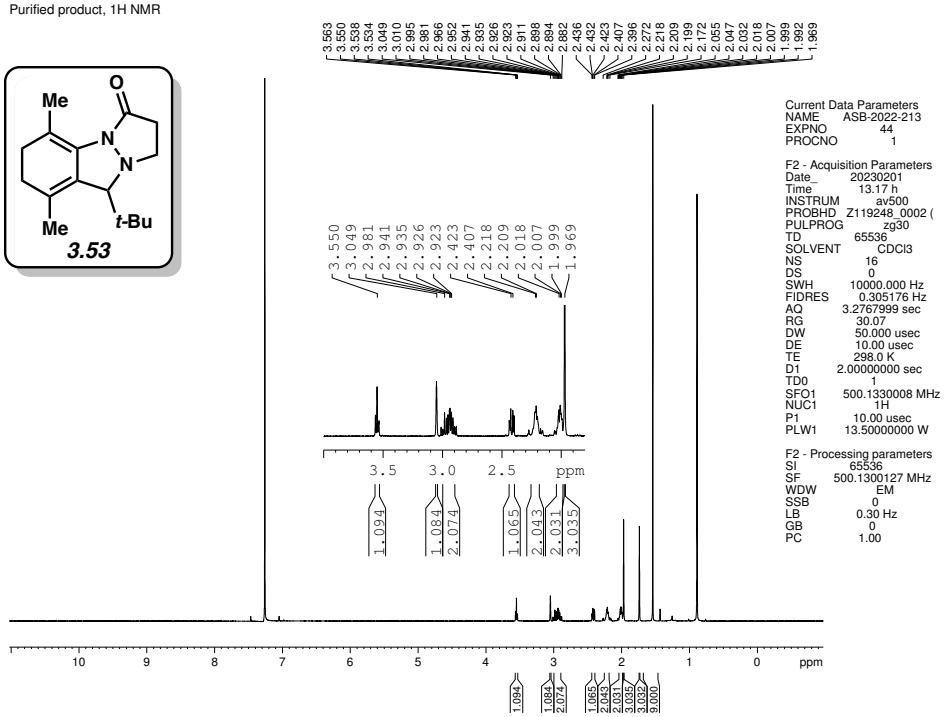

Figure 3.45. ^{1}H NMR (500 MHz, $CDCl_3$) of compound **3.53**.

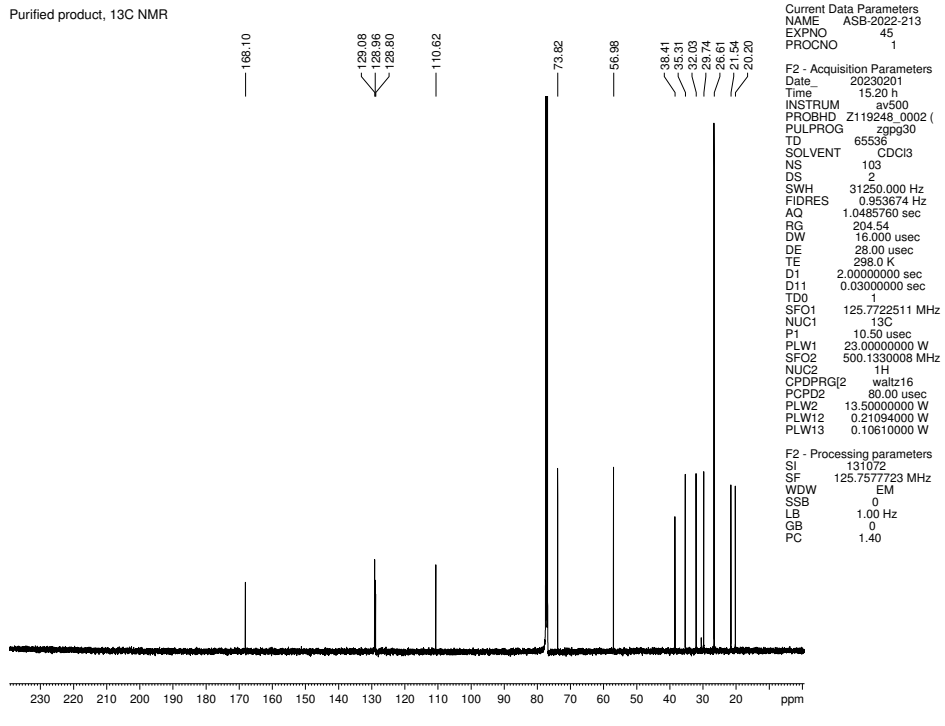

Figure 3.46. ^{13}C NMR (125 MHz, $CDCl_3$) of compound **3.53**.

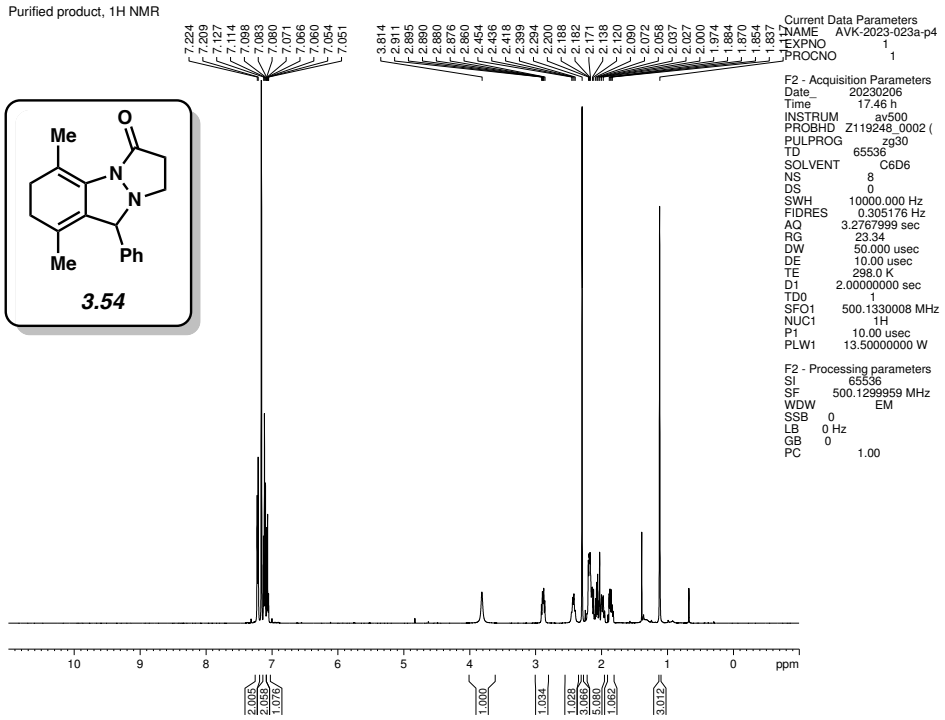

Figure 3.47. ^{1}H NMR (500 MHz, C_6D_6) of compound **3.54**.

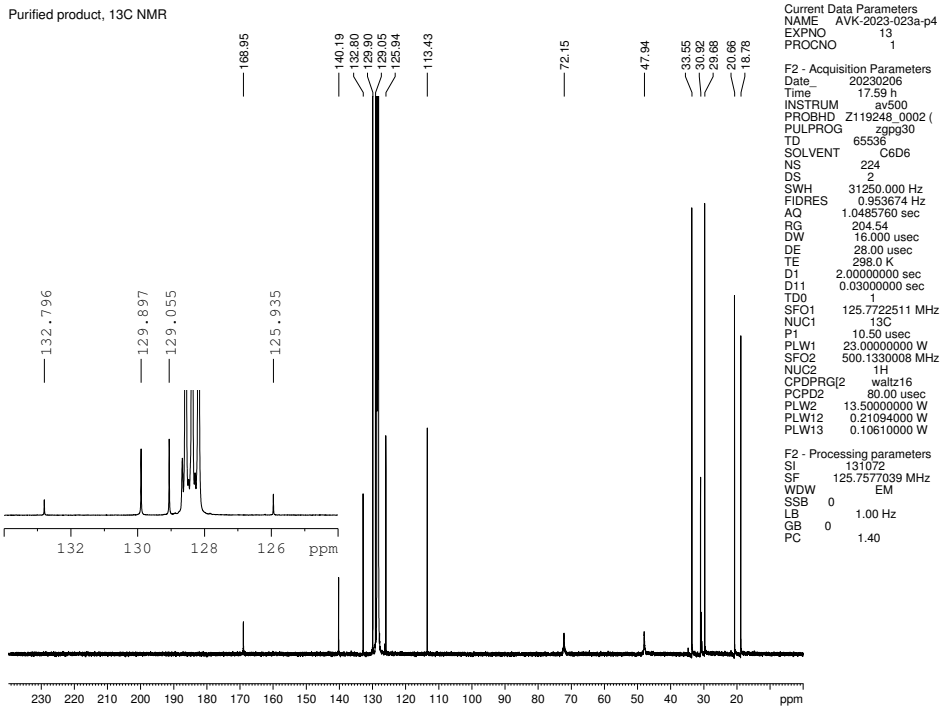

Figure 3.48. ^{13}C NMR (125 MHz, C_6D_6) of compound **3.54**.

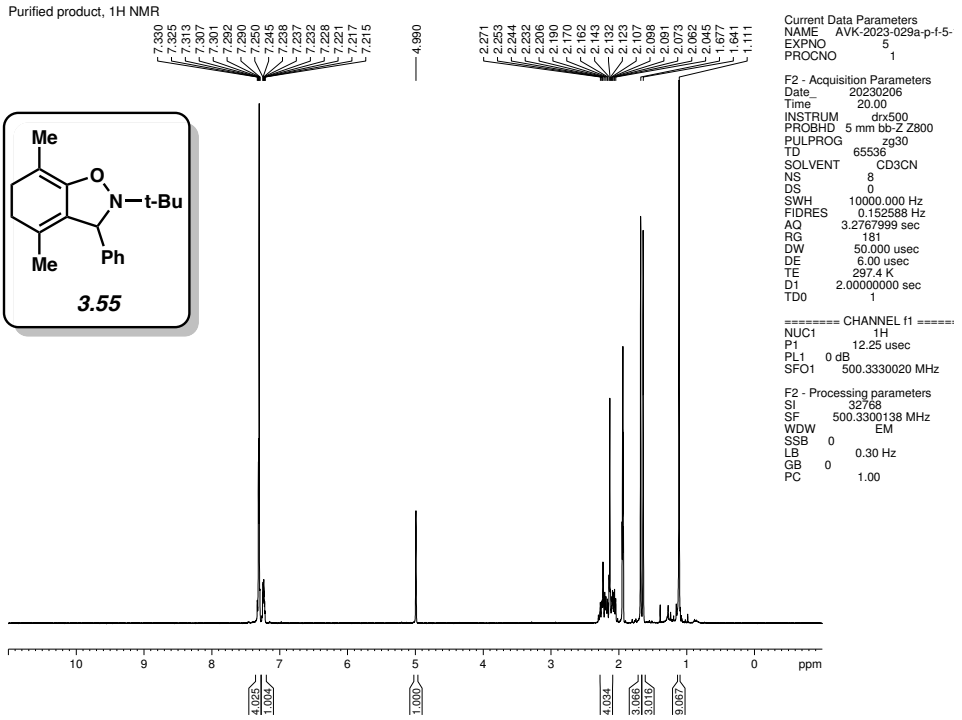

Figure 3.49. ^{1}H NMR (500 MHz, CD_3CN) of compound **3.55**.

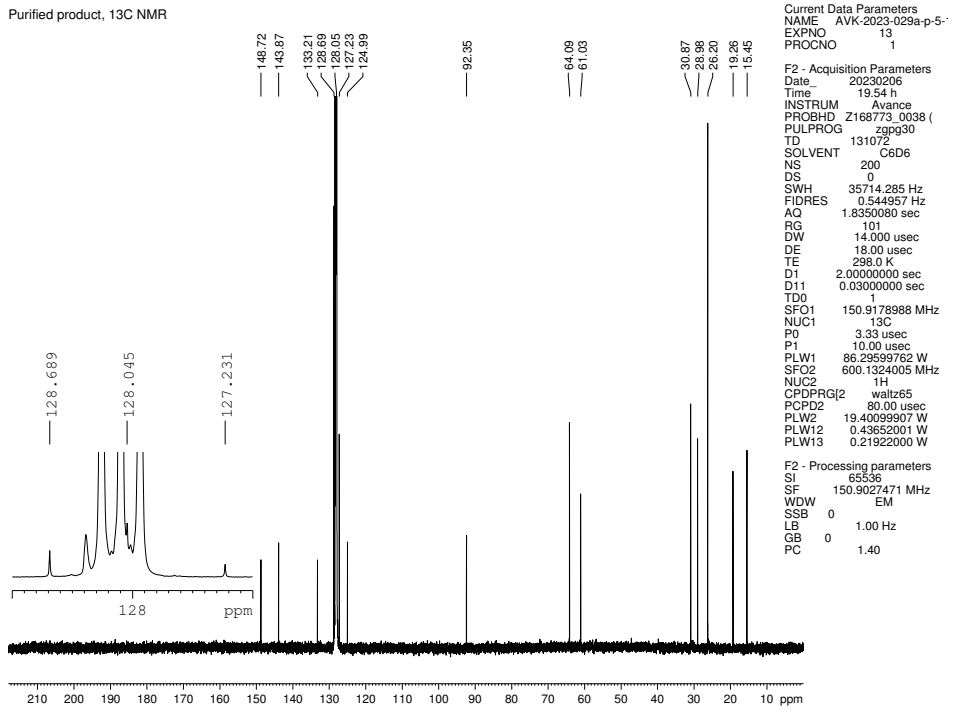

Figure 3.50. ^{13}C NMR (150 MHz, C_6D_6) of compound **3.55**.

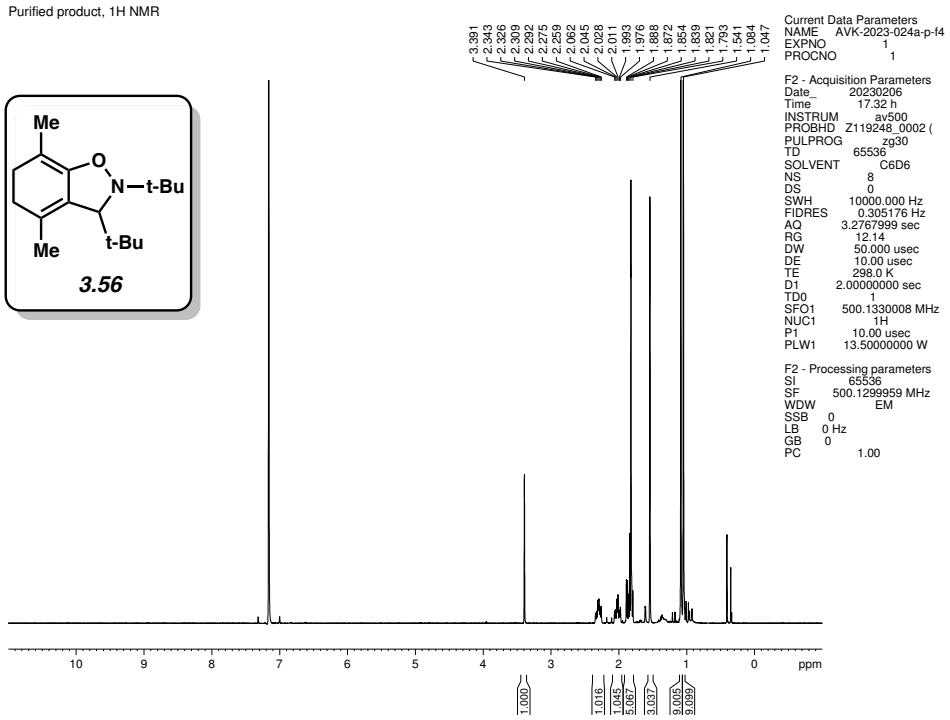

Figure 3.51. ^{13}C NMR (500 MHz, C_6D_6) of compound **3.56**.

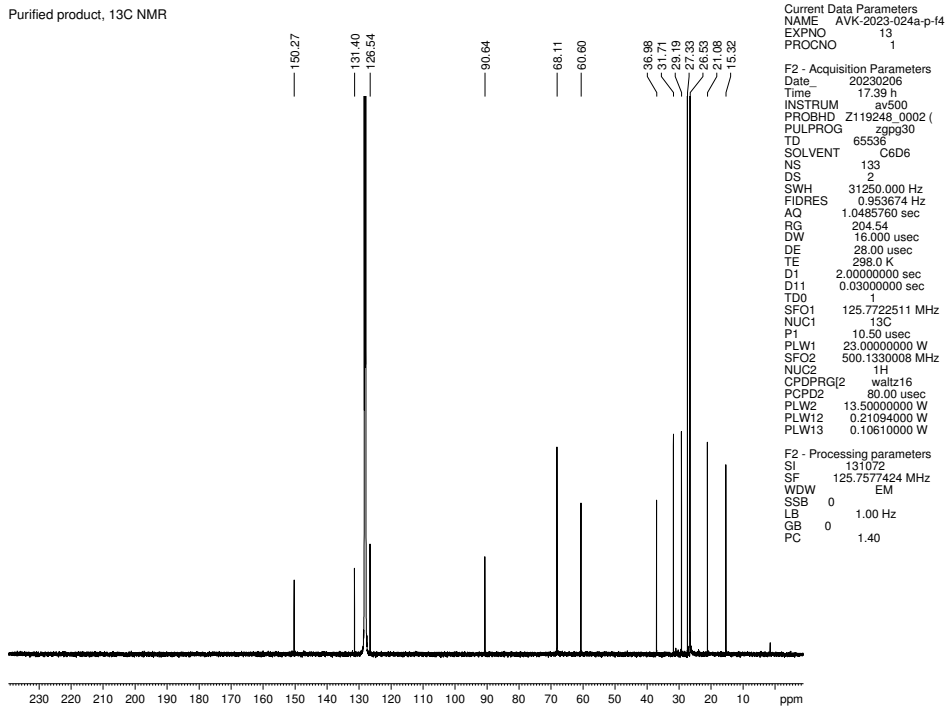

Figure 3.52. ^{13}C NMR (125 MHz, C_6D_6) of compound **3.56**.

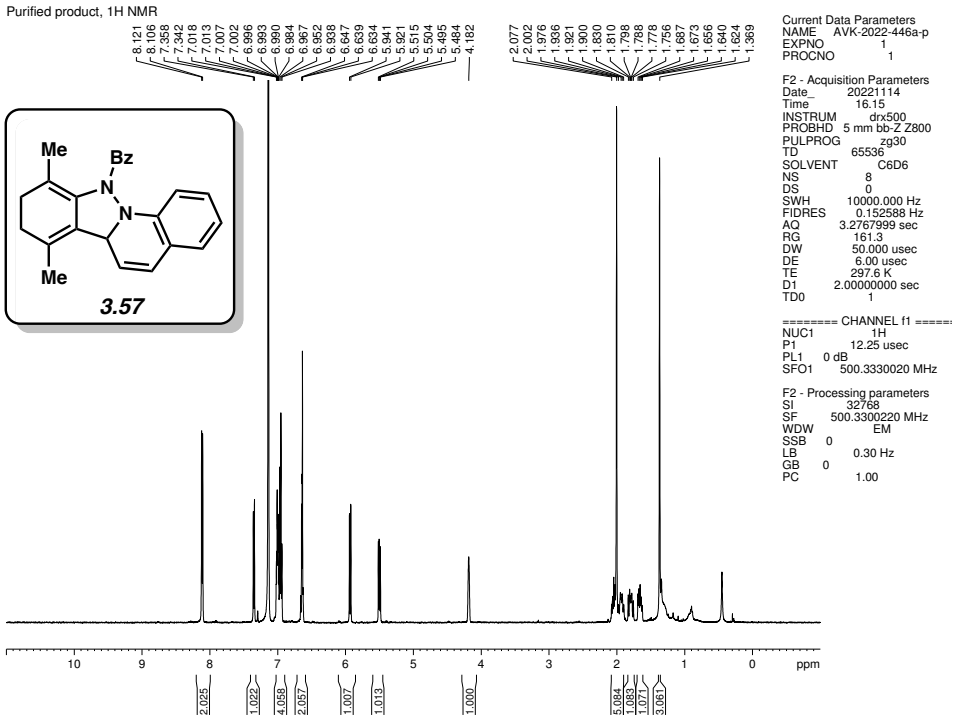

Figure 3.53. ^{1}H NMR (500 MHz, C_6D_6) of compound **3.57**.

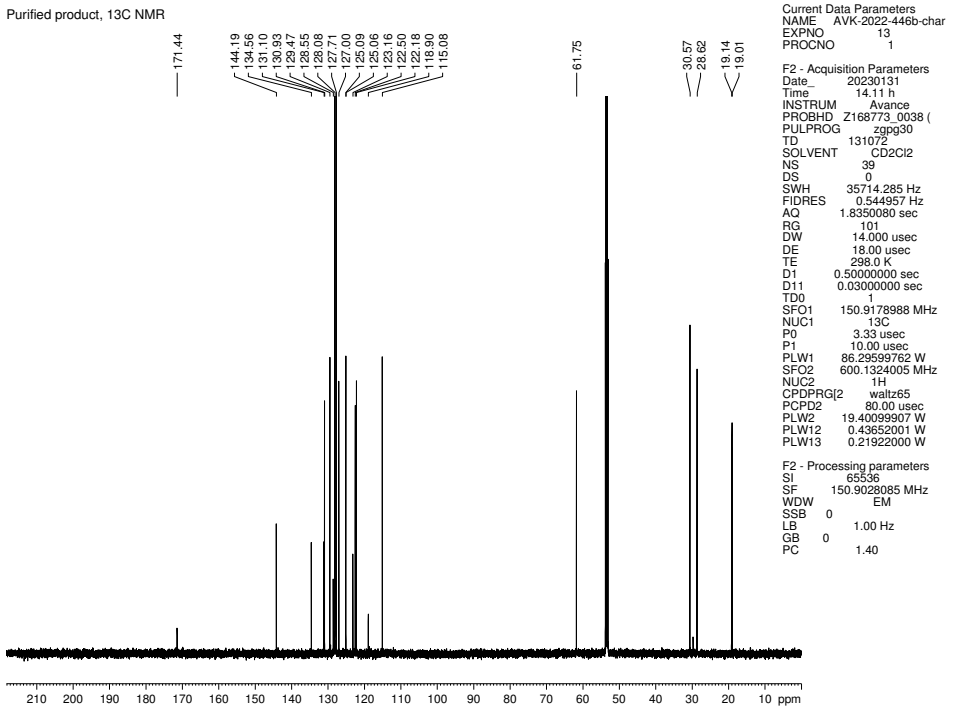

Figure 3.54. ^{13}C NMR (150 MHz, CD_2Cl_2) of compound **3.57**.

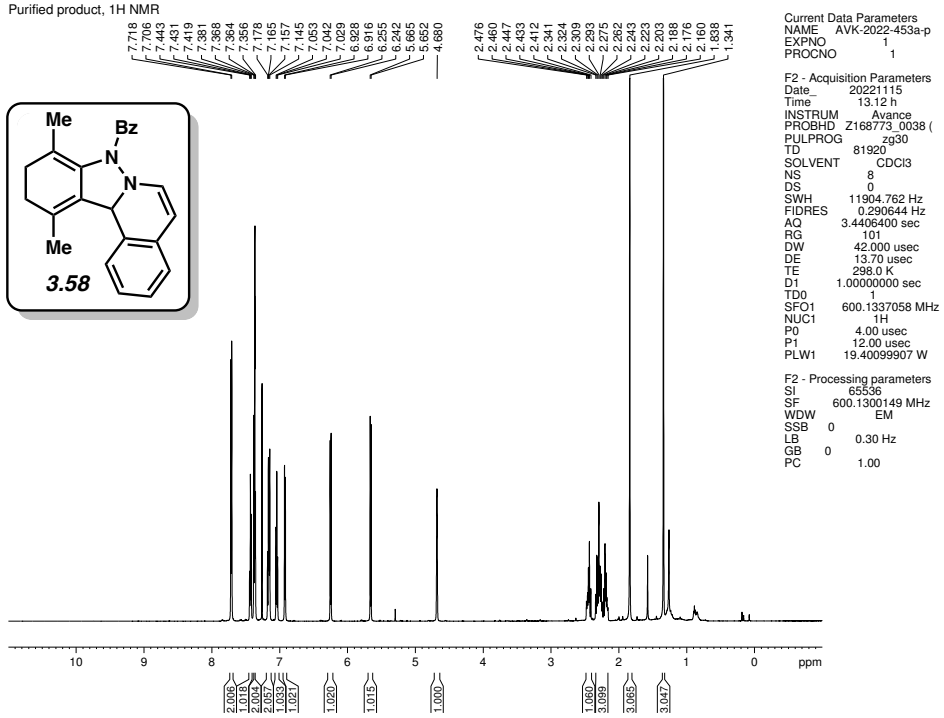

Figure 3.55. ^{1}H NMR (600 MHz, $CDCl_3$) of compound **3.58**.

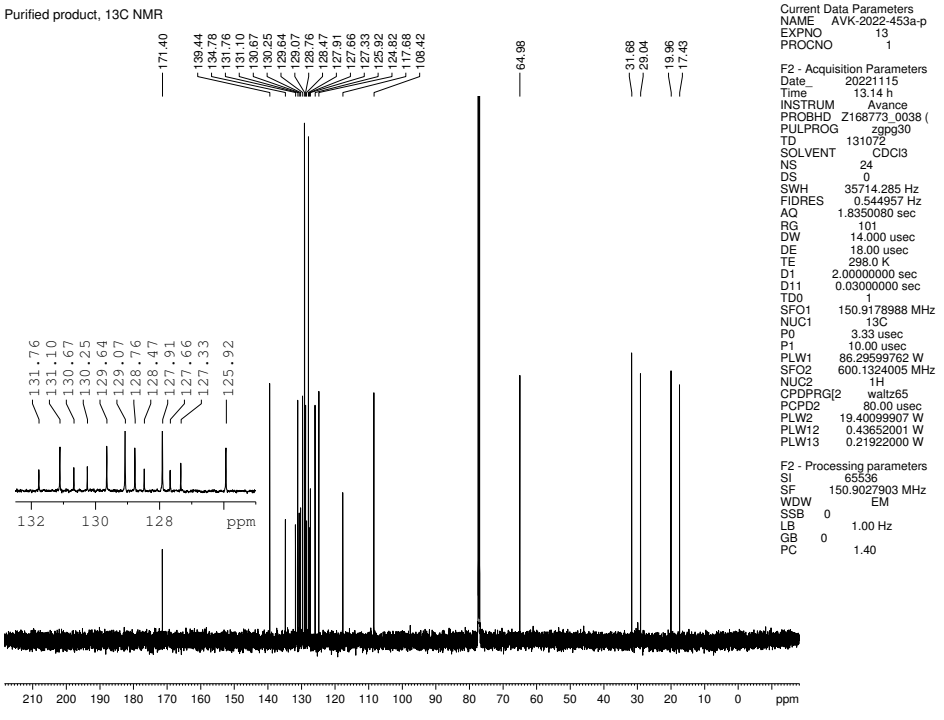

Figure 3.56. ^{13}C NMR (150 MHz, $CDCl_3$) of compound **3.58**.

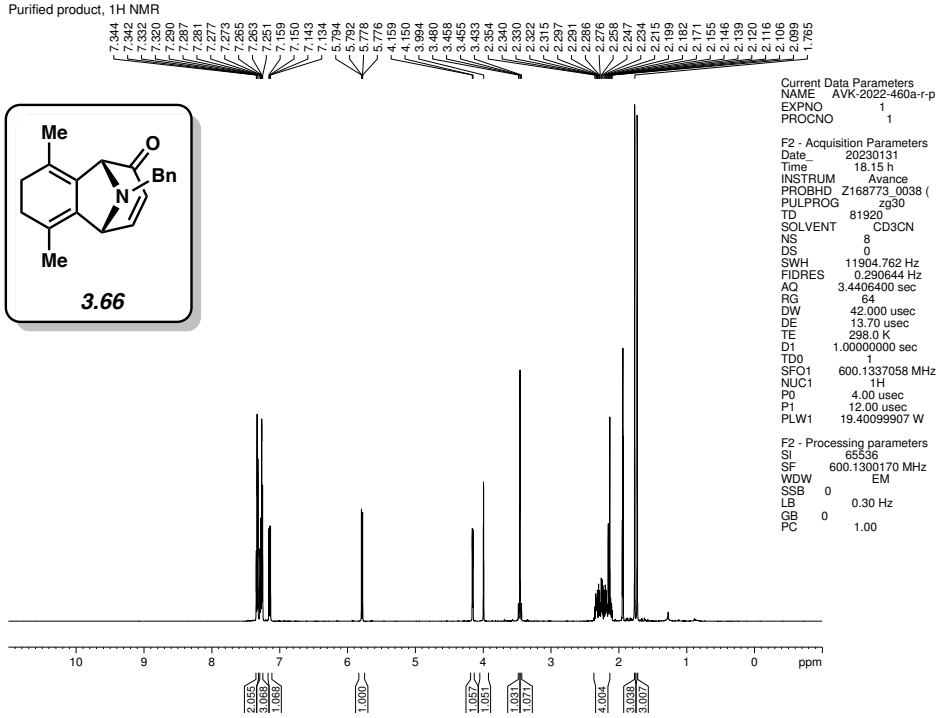

Figure 3.57. ^{1}H NMR (600 MHz, CD_3CN) of compound **3.66**.

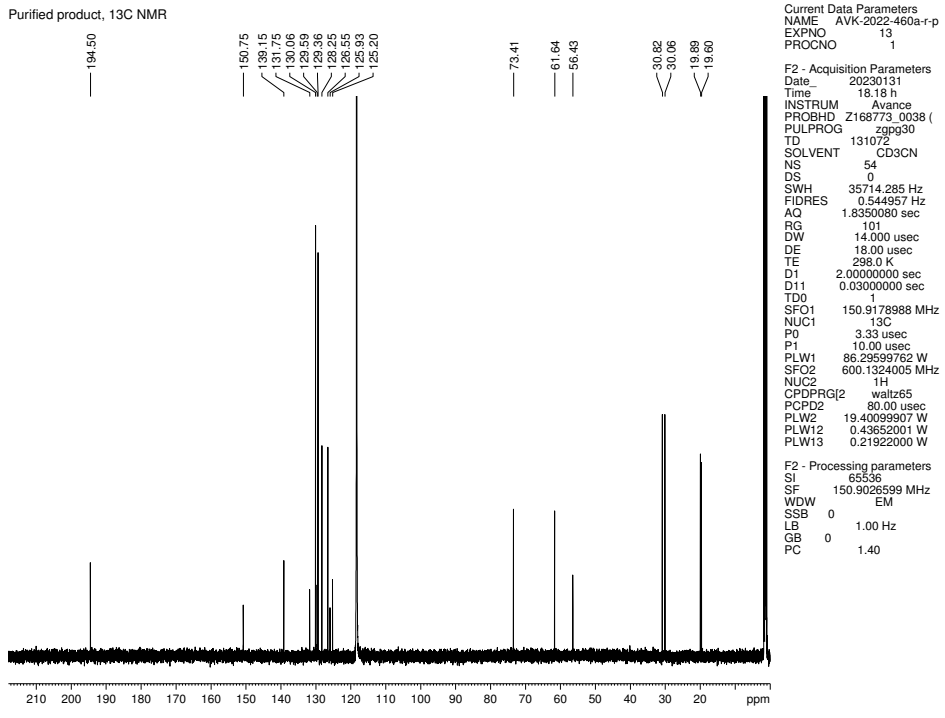

Figure 3.58. ^{13}C NMR (150 MHz, CD_3CN) of compound **3.66**.

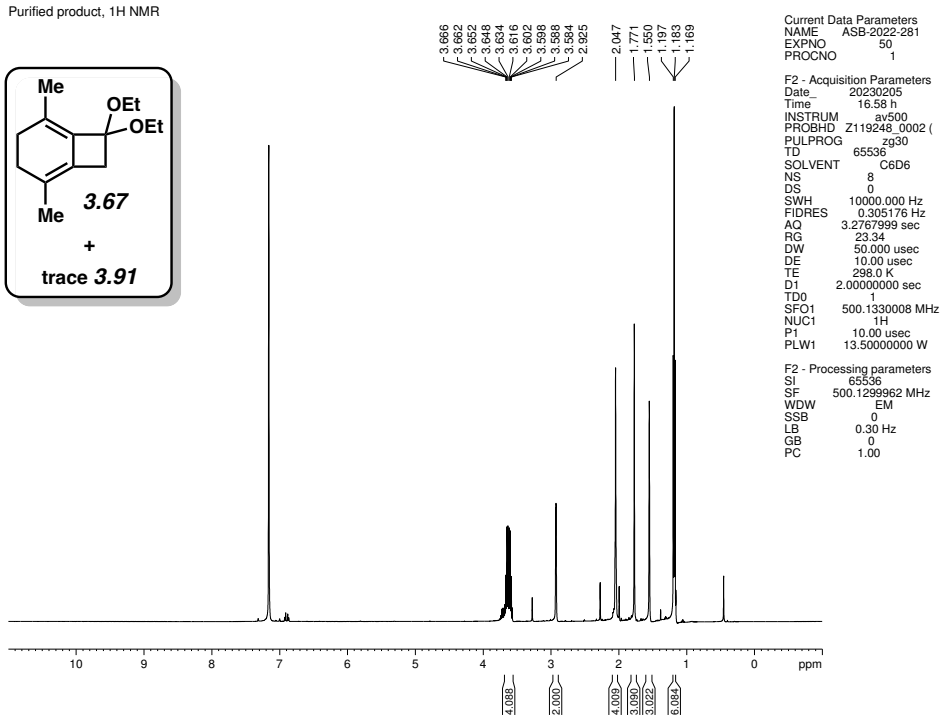

Figure 3.59. ^{1}H NMR (500 MHz, C_6D_6) of compound **3.67**.

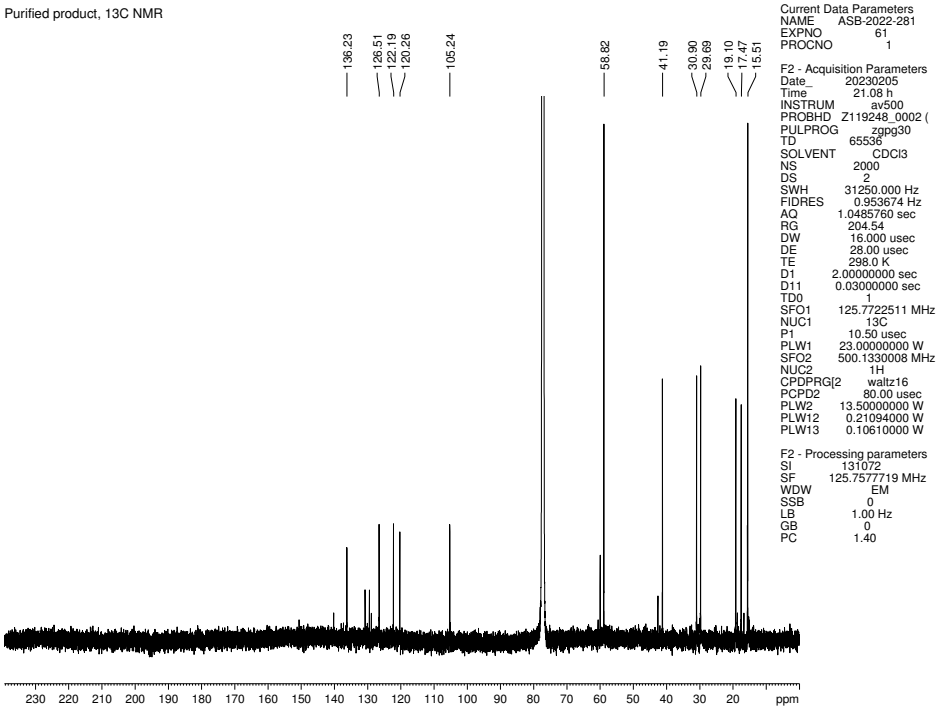

Figure 3.60. ^{13}C NMR (125 MHz, $CDCl_3$) of compound **3.67**.

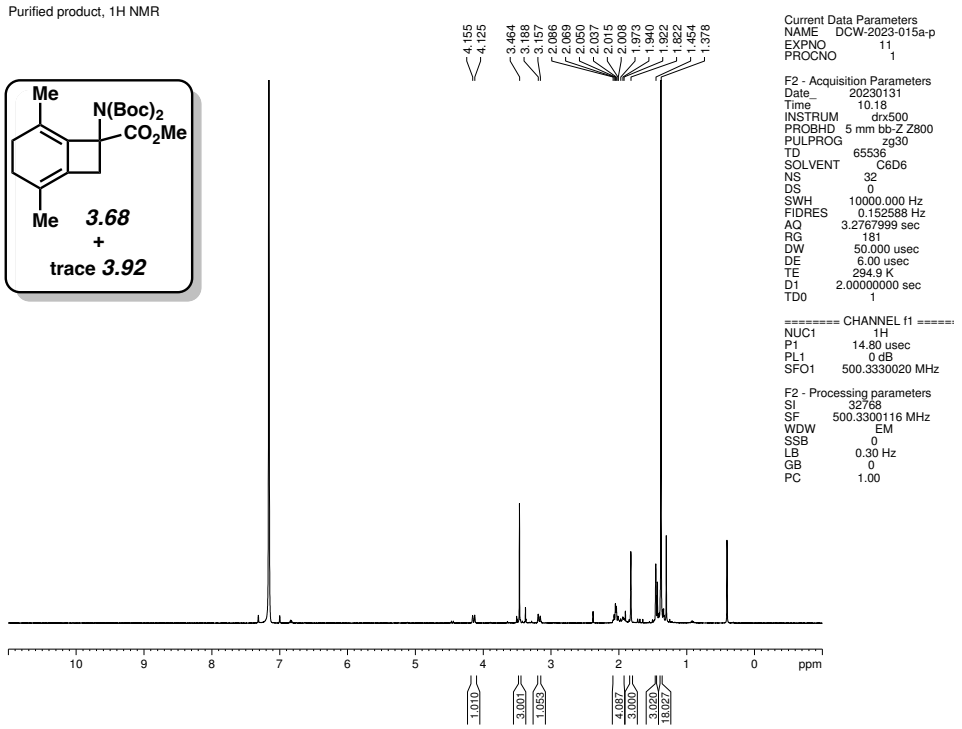

Figure 3.61. ^{1}H NMR (500 MHz, C_6D_6) of compound **3.68**.

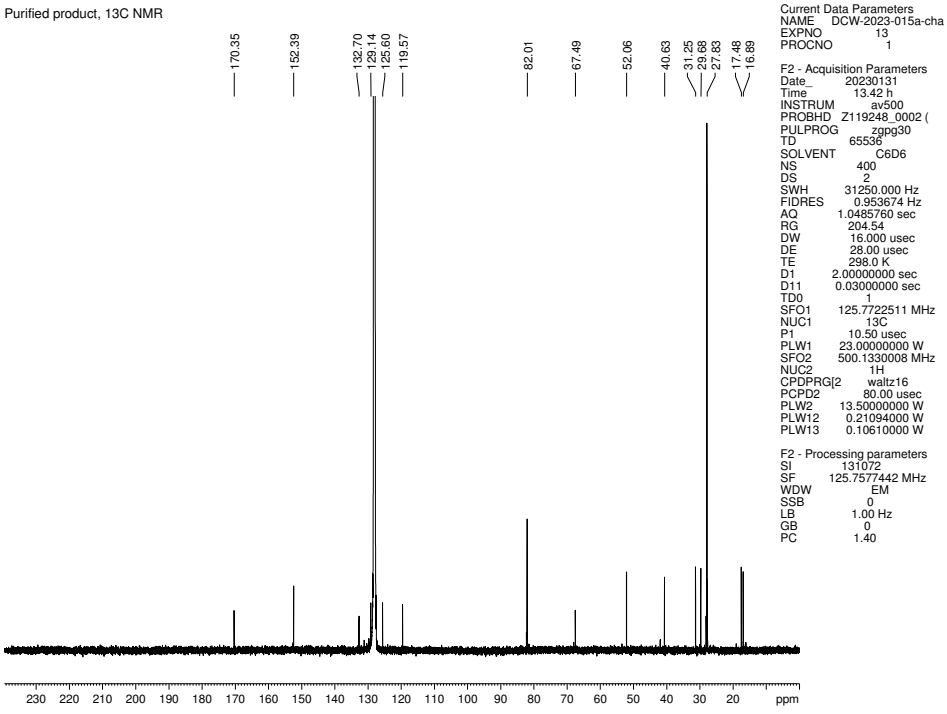

Figure 3.62. ^{13}C NMR (125 MHz, C_6D_6) of compound **3.68**.

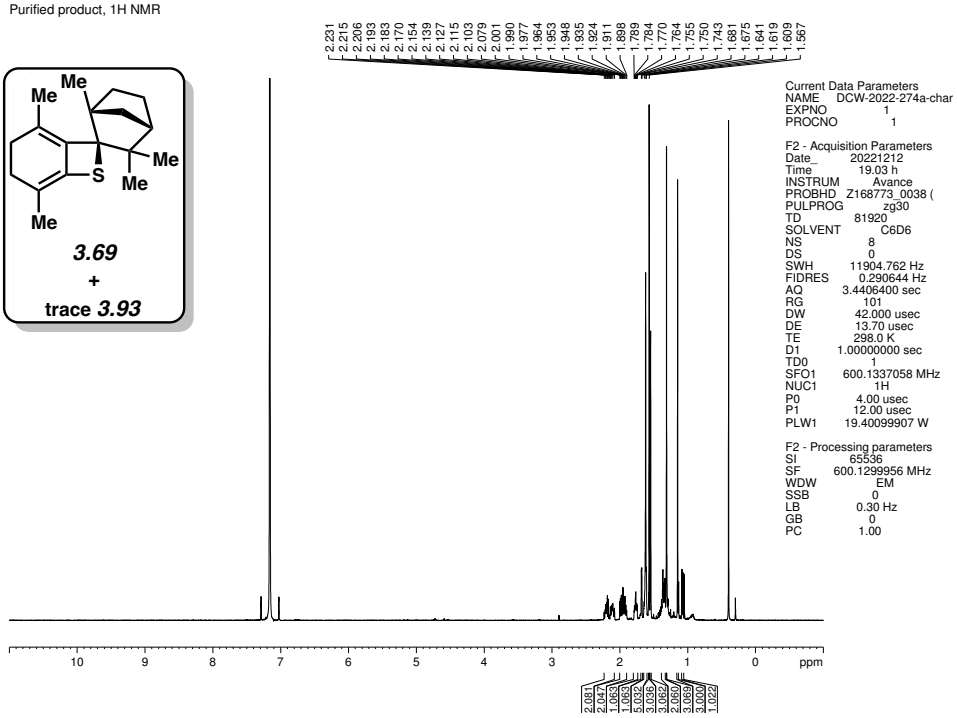

Figure 3.63. ^{1}H NMR (600 MHz, C_6D_6) of compound **3.69**.

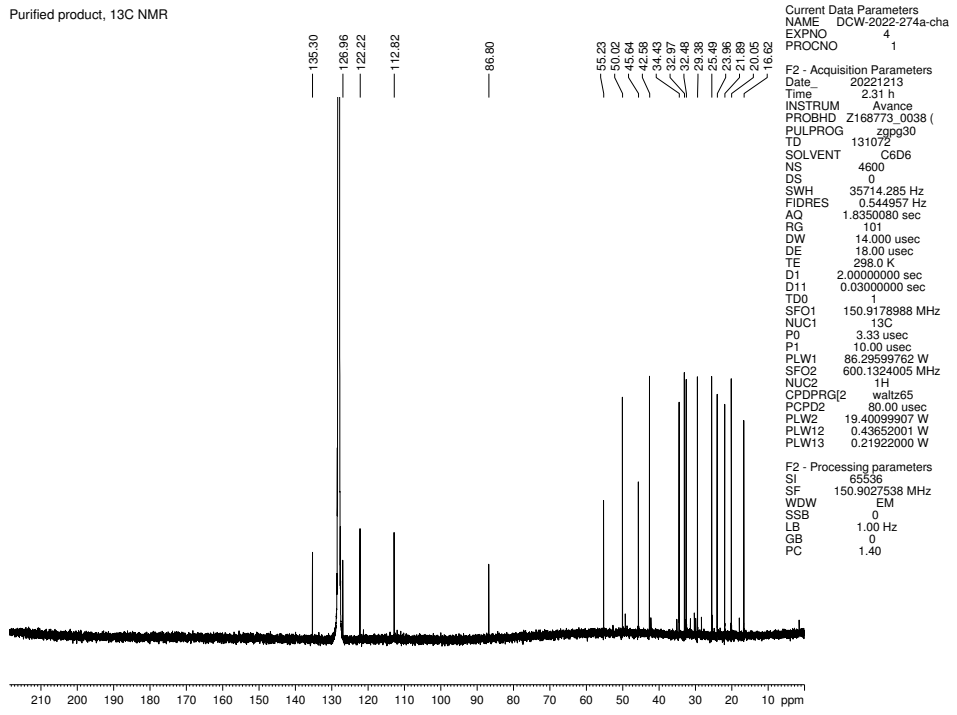

Figure 3.64. ^{13}C NMR (150 MHz, C_6D_6) of compound **3.69**.

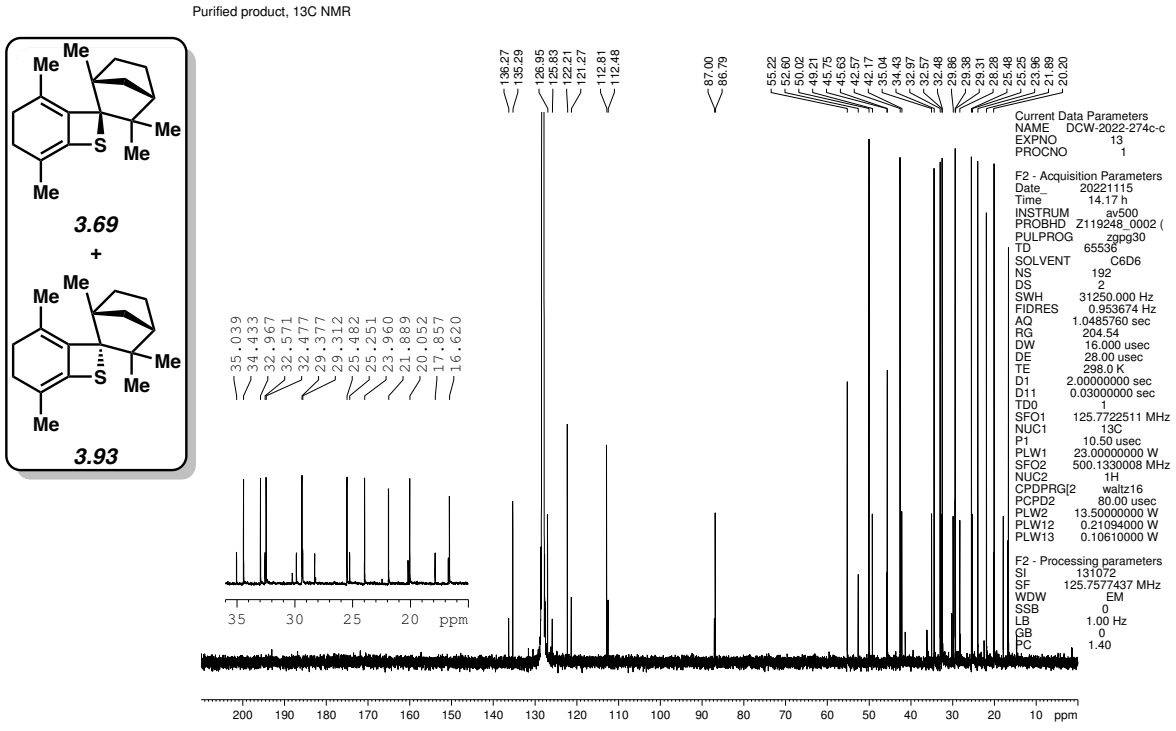

Figure 3.65. ^{13}C NMR (125 MHz, C_6D_6) of compound **3.69** and **3.93**.

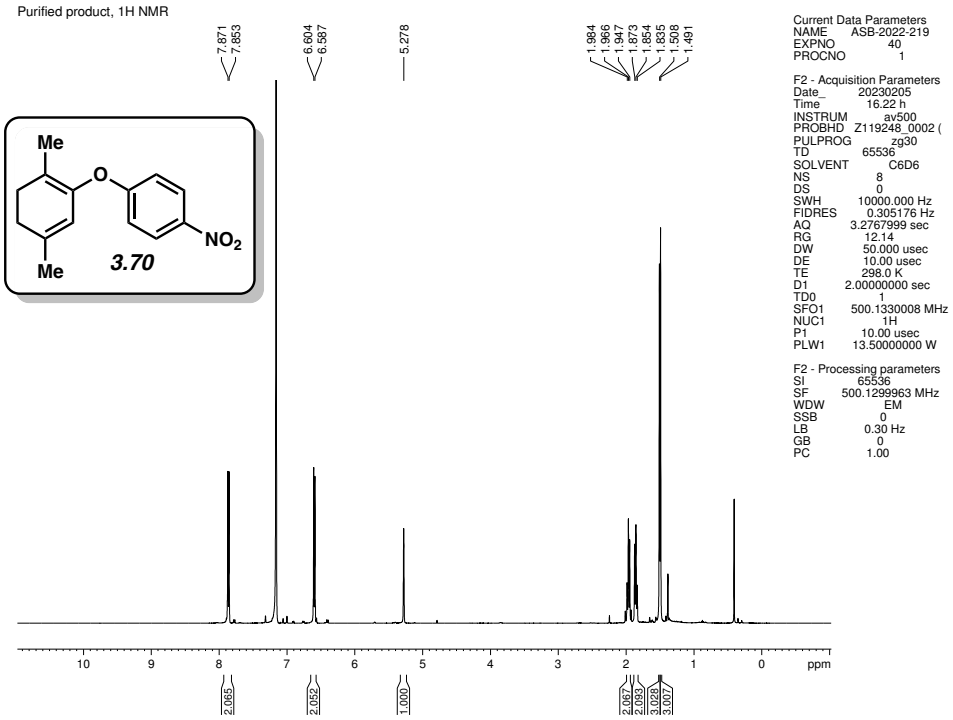

Figure 3.66. ^{1}H NMR (500 MHz, C_6D_6) of compound **3.70**.

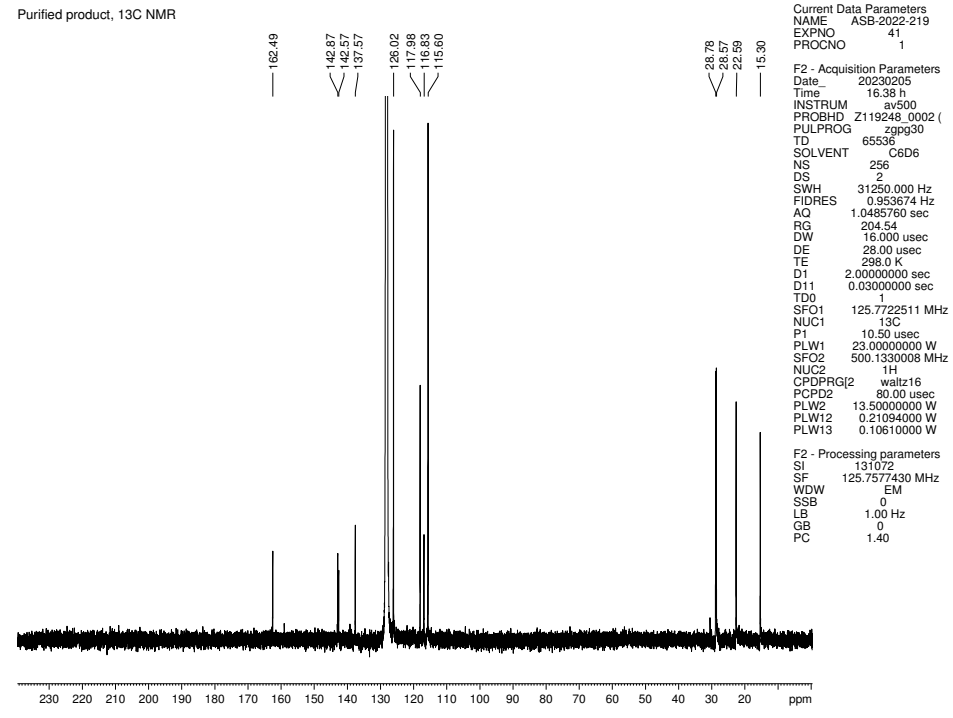

Figure 3.67. ^{13}C NMR (125 MHz, C_6D_6) of compound **3.70**.

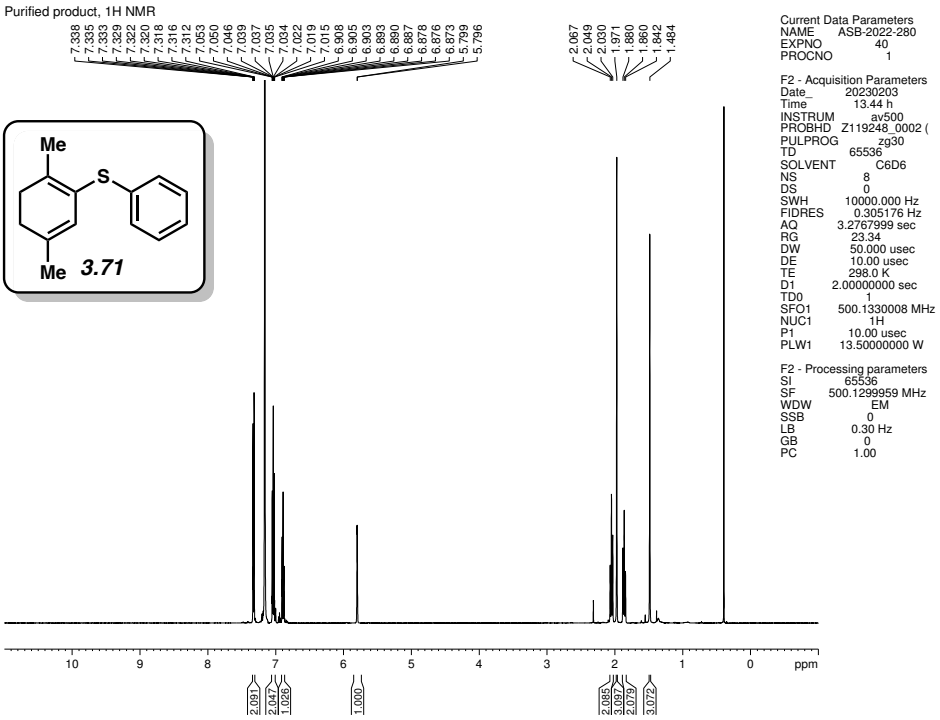

Figure 3.68. ^{1}H NMR (500 MHz, C_6D_6) of compound **3.71**.

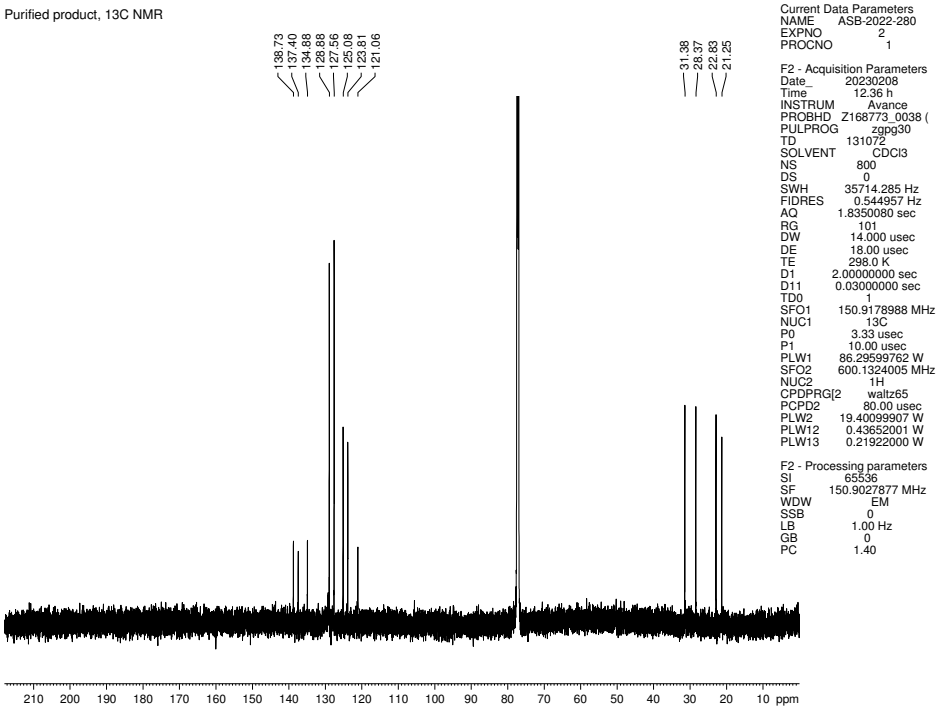

Figure 3.69. ^{13}C NMR (150 MHz, $CDCl_3$) of compound **3.71**.

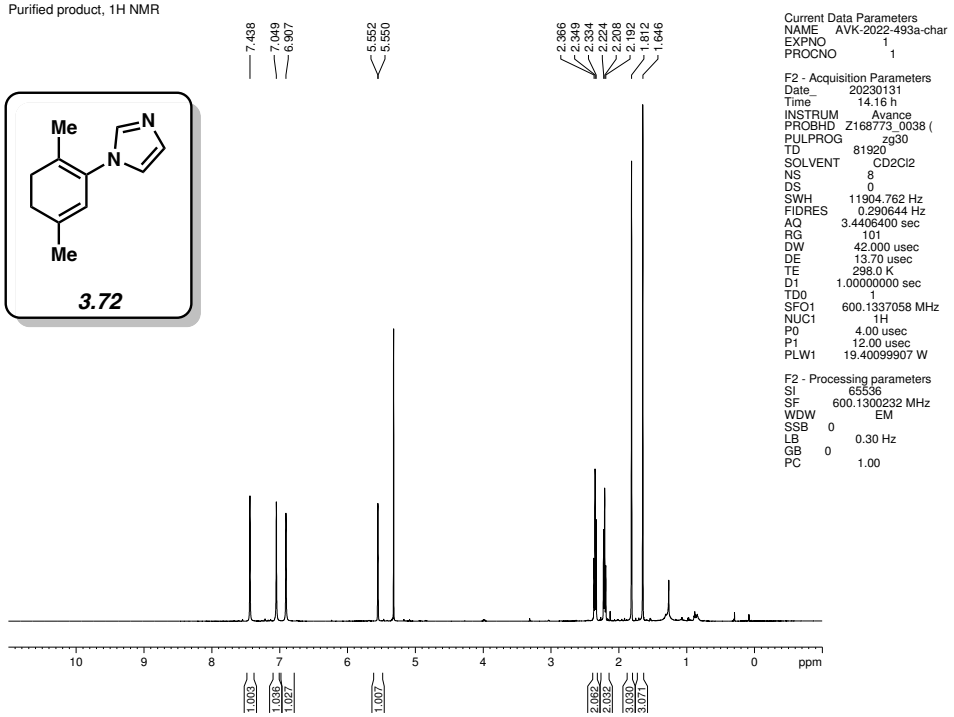

Figure 3.70. ^{1}H NMR (600 MHz, CD_2Cl_2) of compound **3.72**.

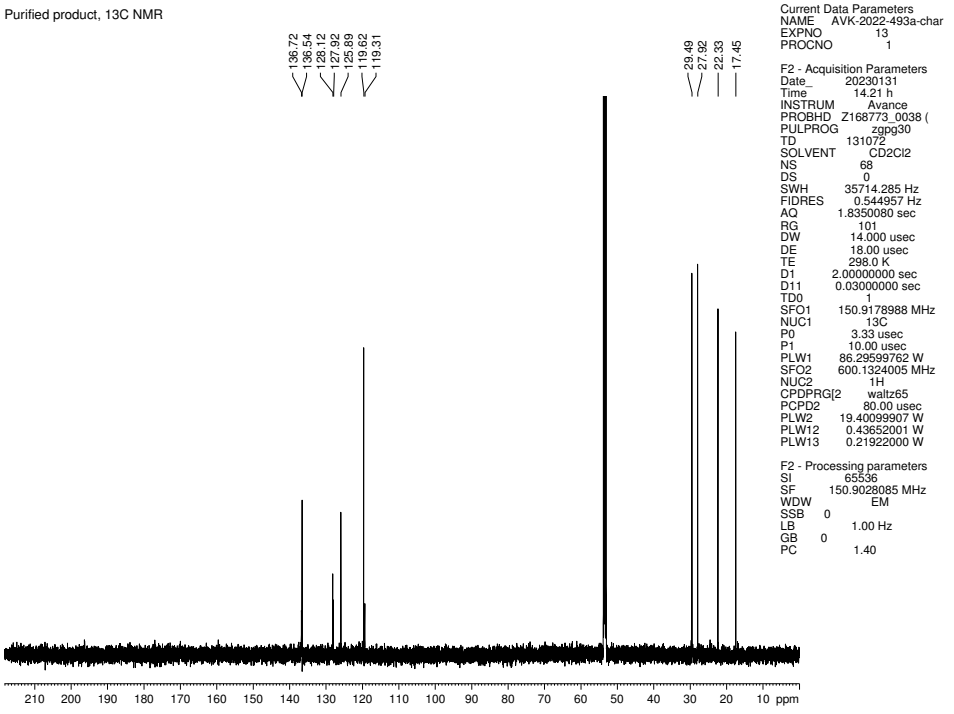

Figure 3.71. ^{13}C NMR (150 MHz, CD_2Cl_2) of compound **3.72**.

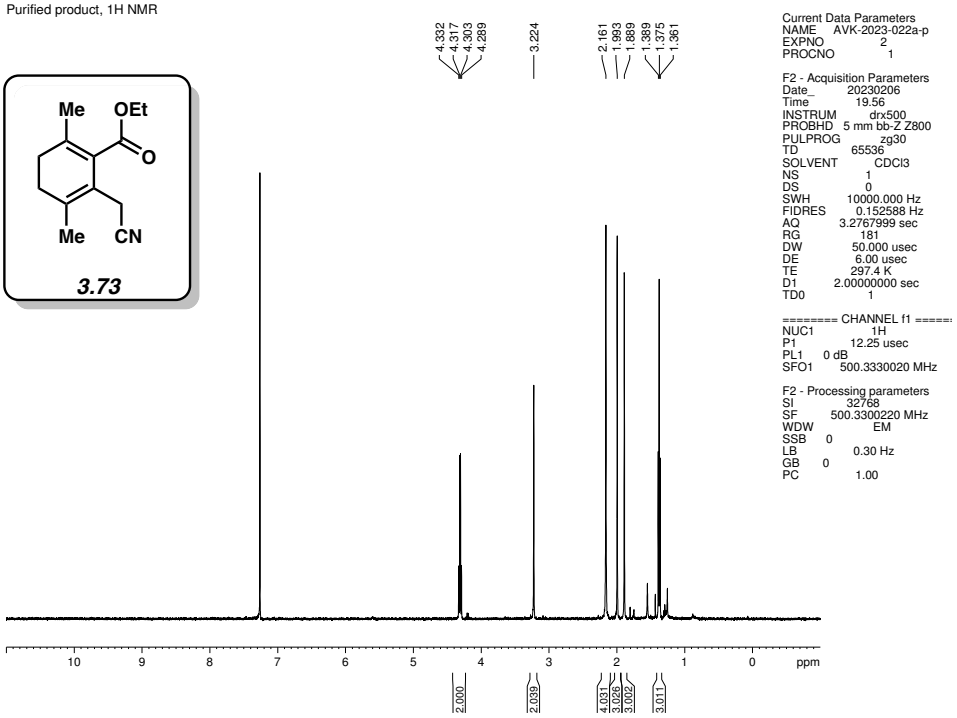

Figure 3.72. ^{1}H NMR (500 MHz, $CDCl_3$) of compound **3.73**.

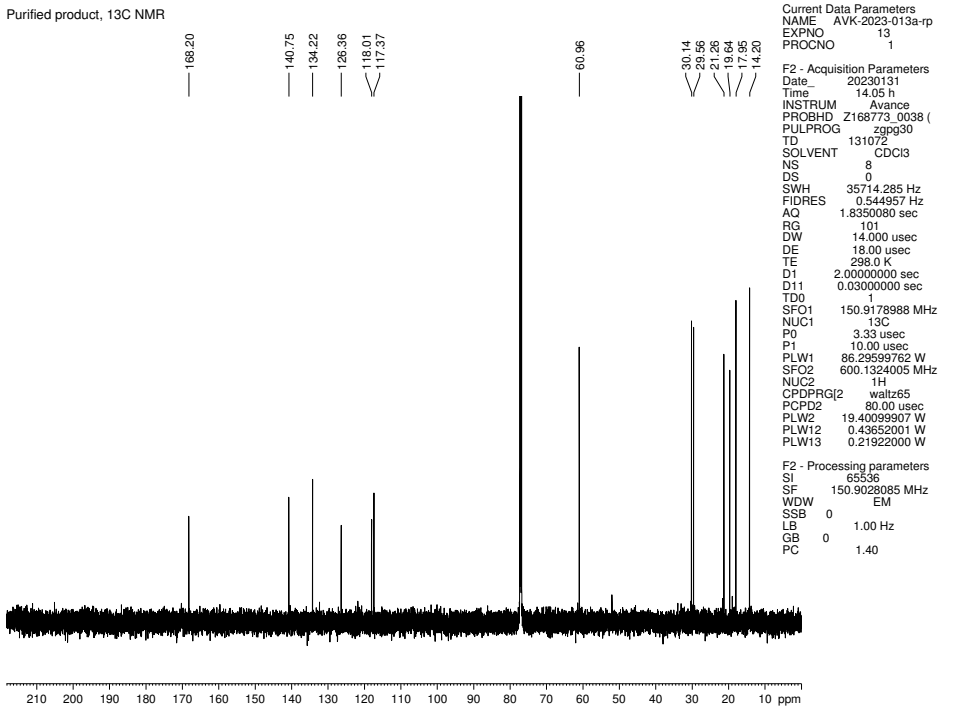

Figure 3.73. ^{13}C NMR (150 MHz, $CDCl_3$) of compound **3.73**.

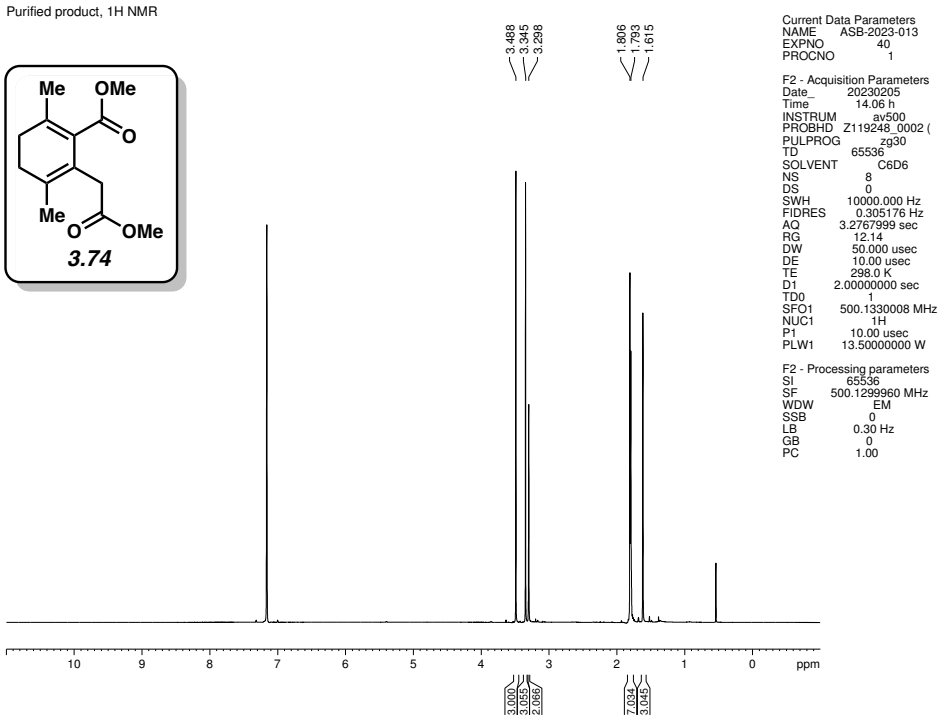

Figure 3.74. ^{1}H NMR (500 MHz, C_6D_6) of compound **3.74**.

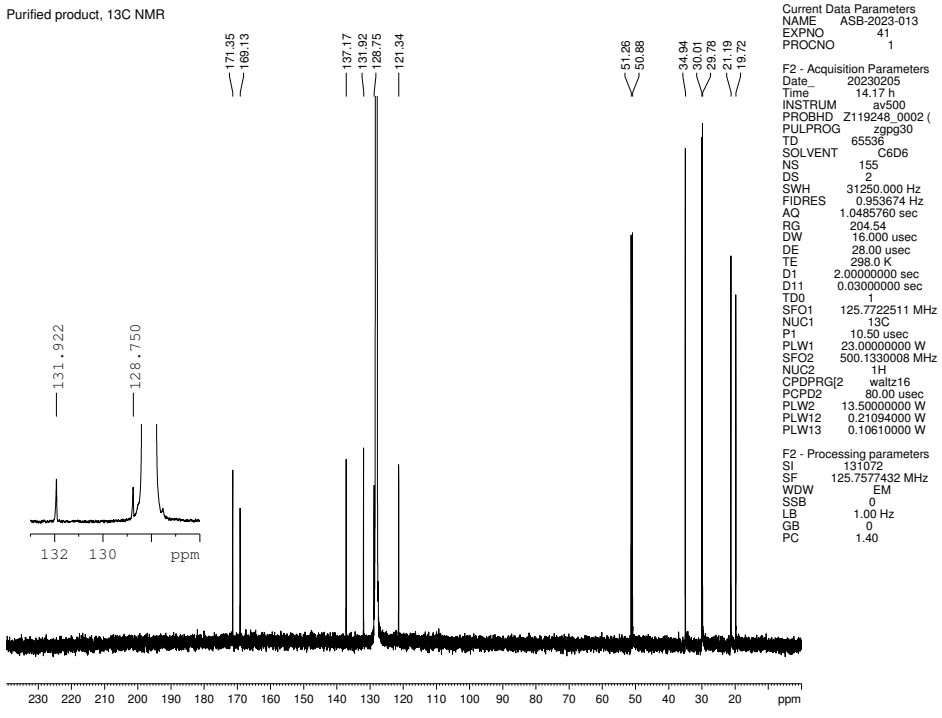

Figure 3.75. ^{13}C NMR (125 MHz, C_6D_6) of compound **3.74**.

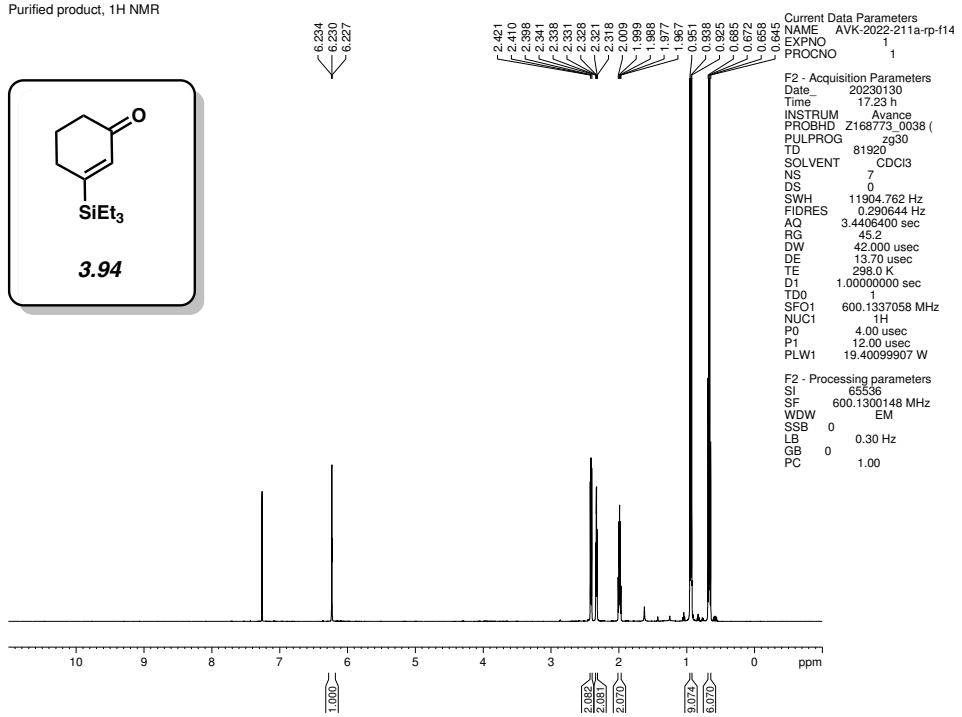

Figure 3.76. ^{1}H NMR (600 MHz, $CDCl_3$) of compound **3.94**.

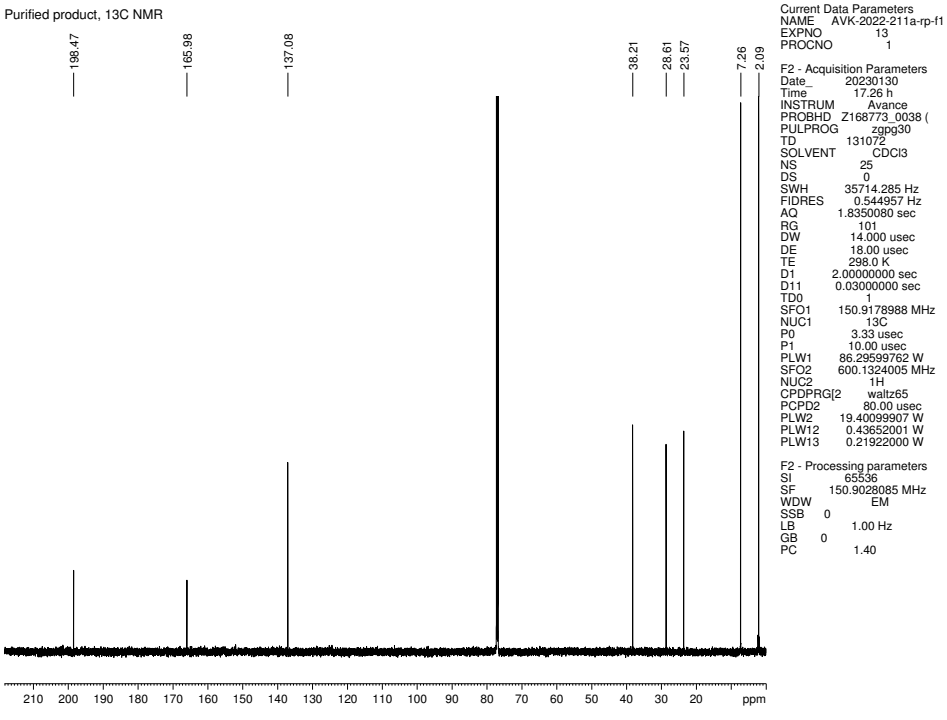

Figure 3.77. ^{13}C NMR (150 MHz, $CDCl_3$) of compound **3.94**.

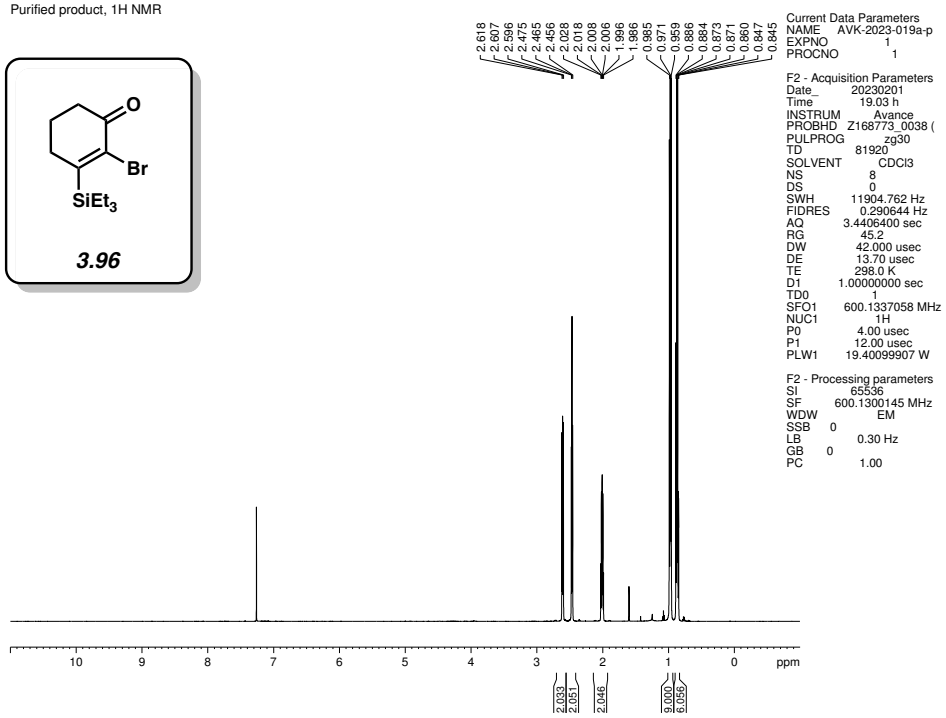

Figure 3.78. ^{1}H NMR (600 MHz, $CDCl_3$) of compound **3.96**.

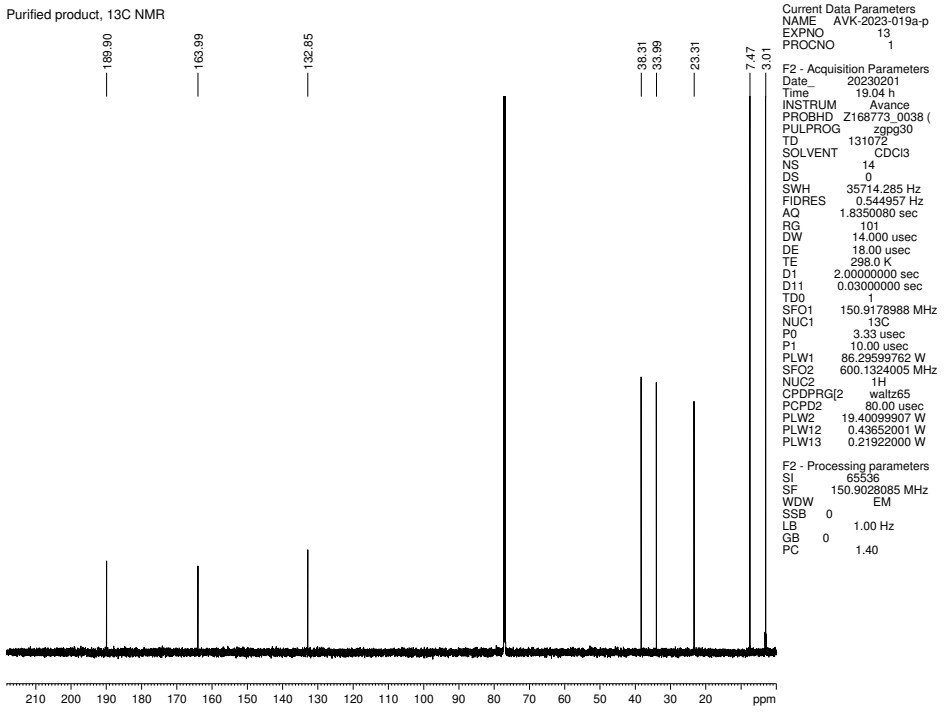

Figure 3.79. ^{13}C NMR (150 MHz, $CDCl_3$) of compound **3.96**.

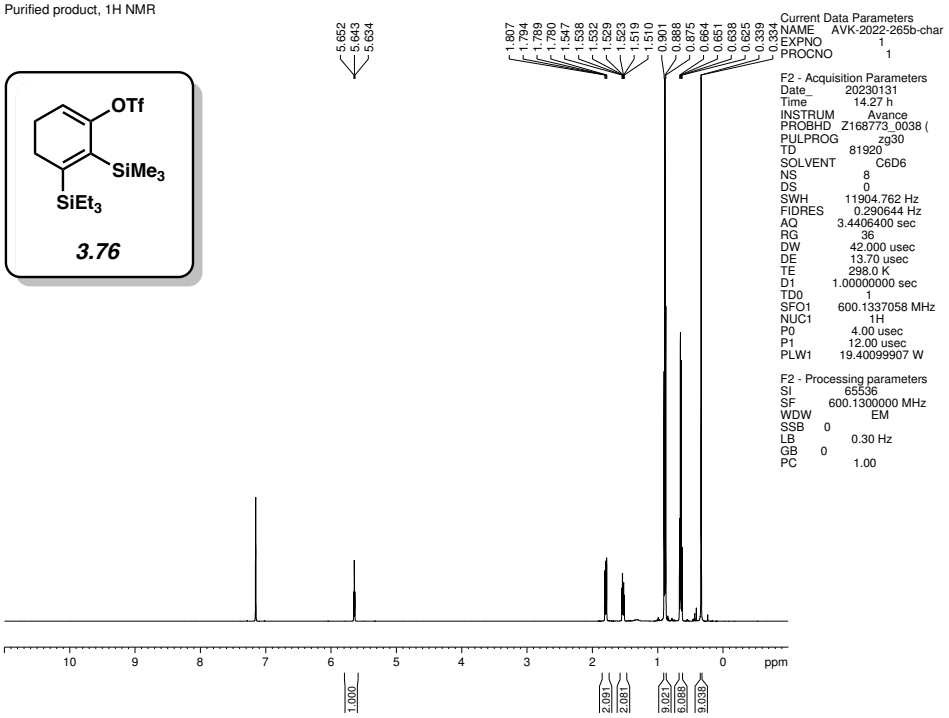

Figure 3.80. ^{1}H NMR (600 MHz, C_6D_6) of compound **3.76**.

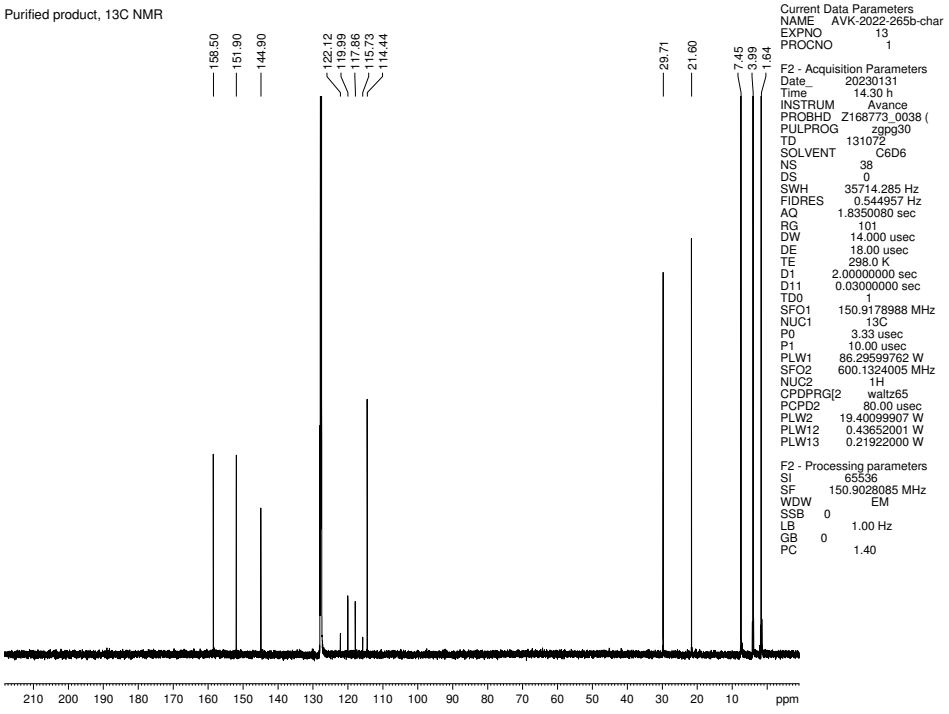

Figure 3.81. ^{13}C NMR (150 MHz, C_6D_6) of compound **3.76**.

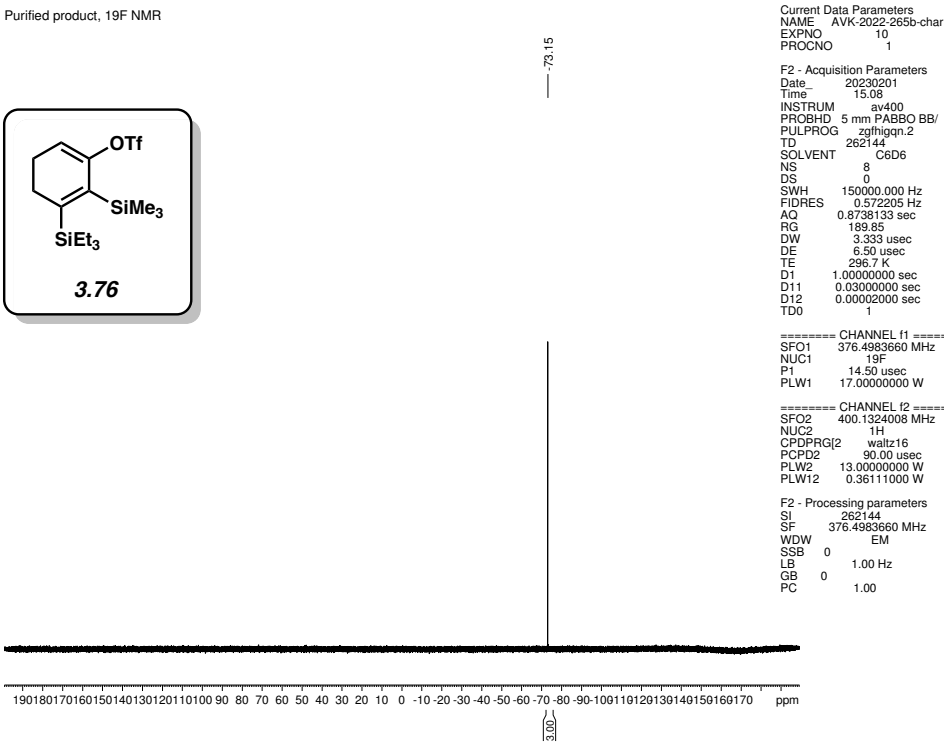

Figure 3.82. ^{19}F NMR (376 MHz, C_6D_6) of compound **3.76**.

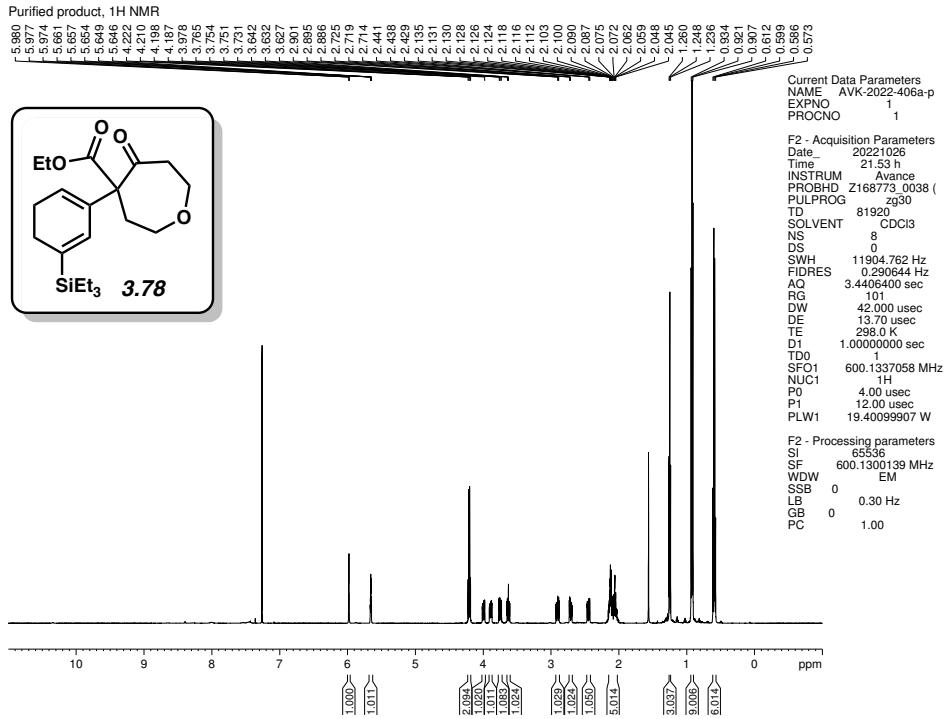

Figure 3.83. ^{1}H NMR (600 MHz, $CDCl_3$) of compound **3.78**.

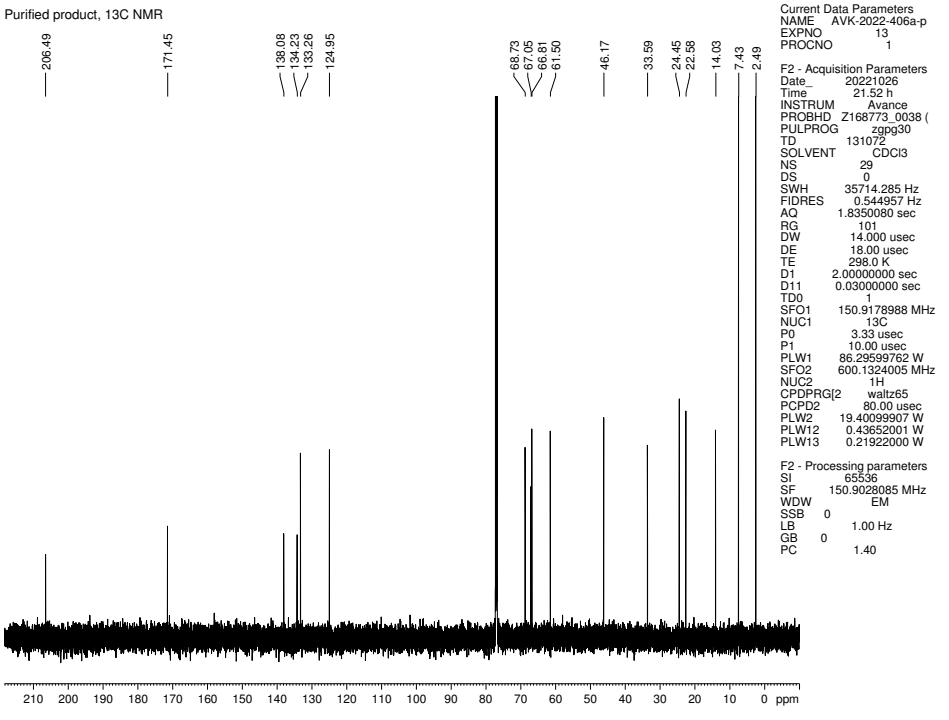

Figure 3.84. ^{13}C NMR (150 MHz, $CDCl_3$) of compound **3.78**.

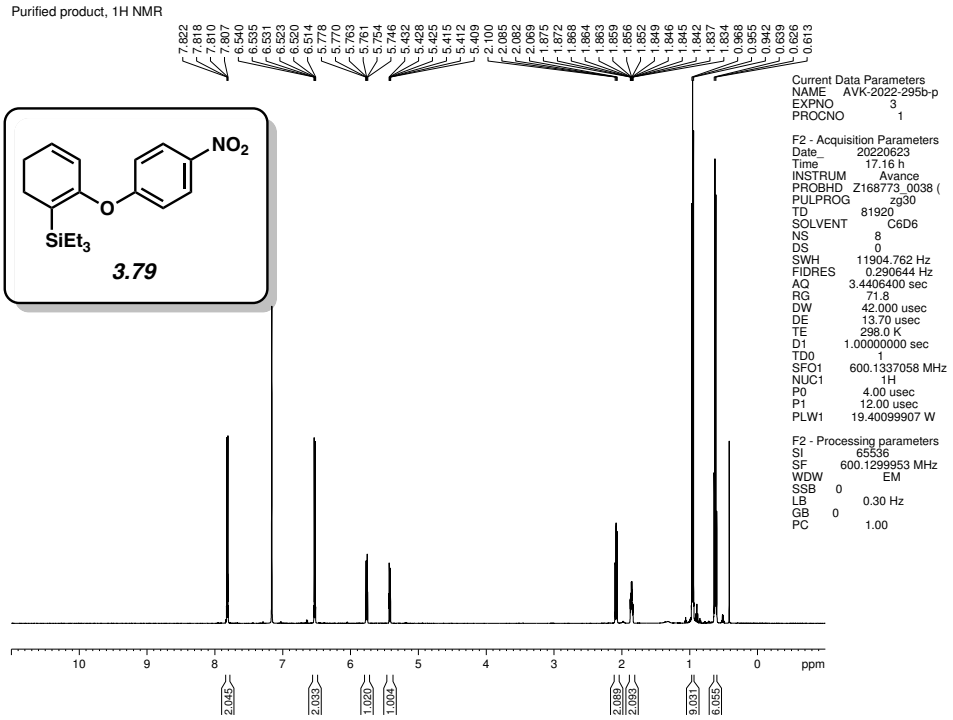

Figure 3.85. ^{1}H NMR (600 MHz, C_6D_6) of compound **3.79**.

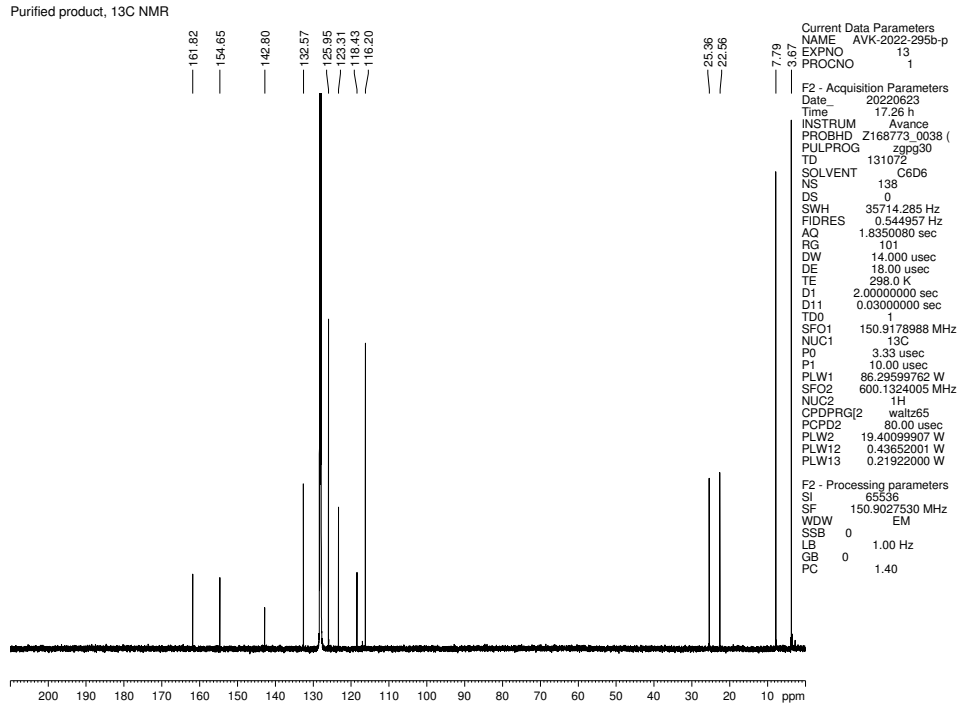

Figure 3.86. ^{13}C NMR (150 MHz, C_6D_6) of compound **3.79**.

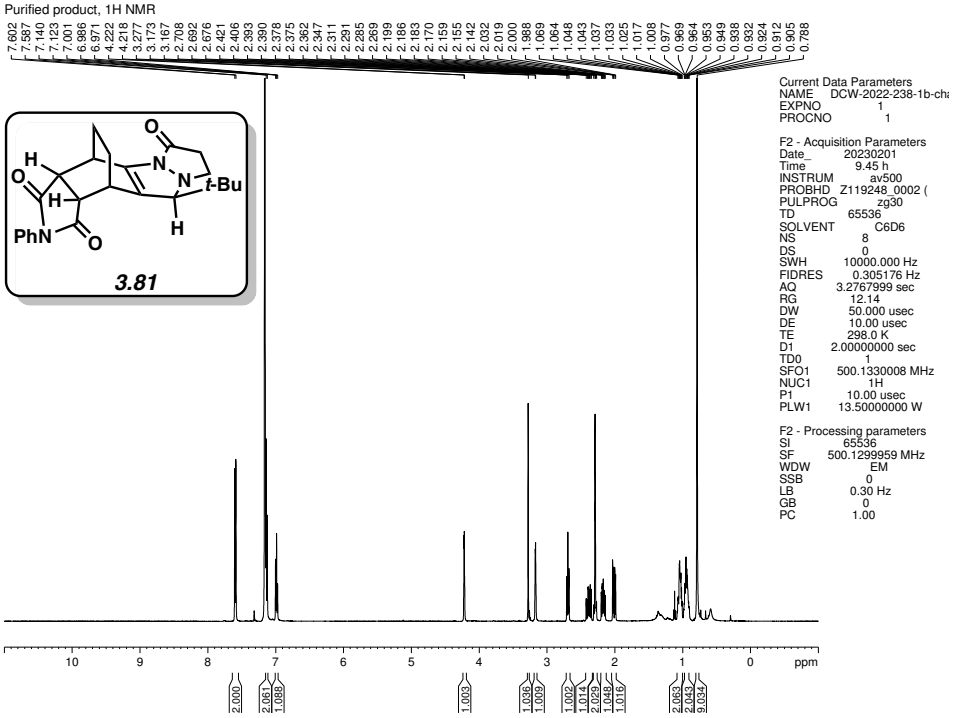

Figure 3.87. ^{1}H NMR (500 MHz, C_6D_6) of compound **3.81**.

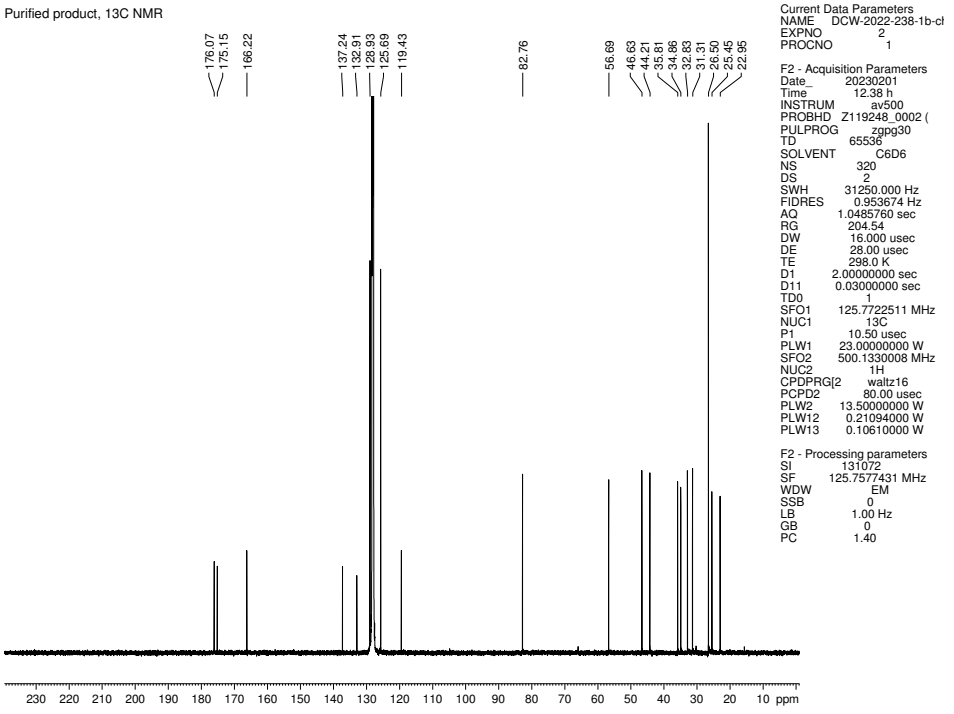

Figure 3.88. ^{13}C NMR (125 MHz, C_6D_6) of compound **3.81**

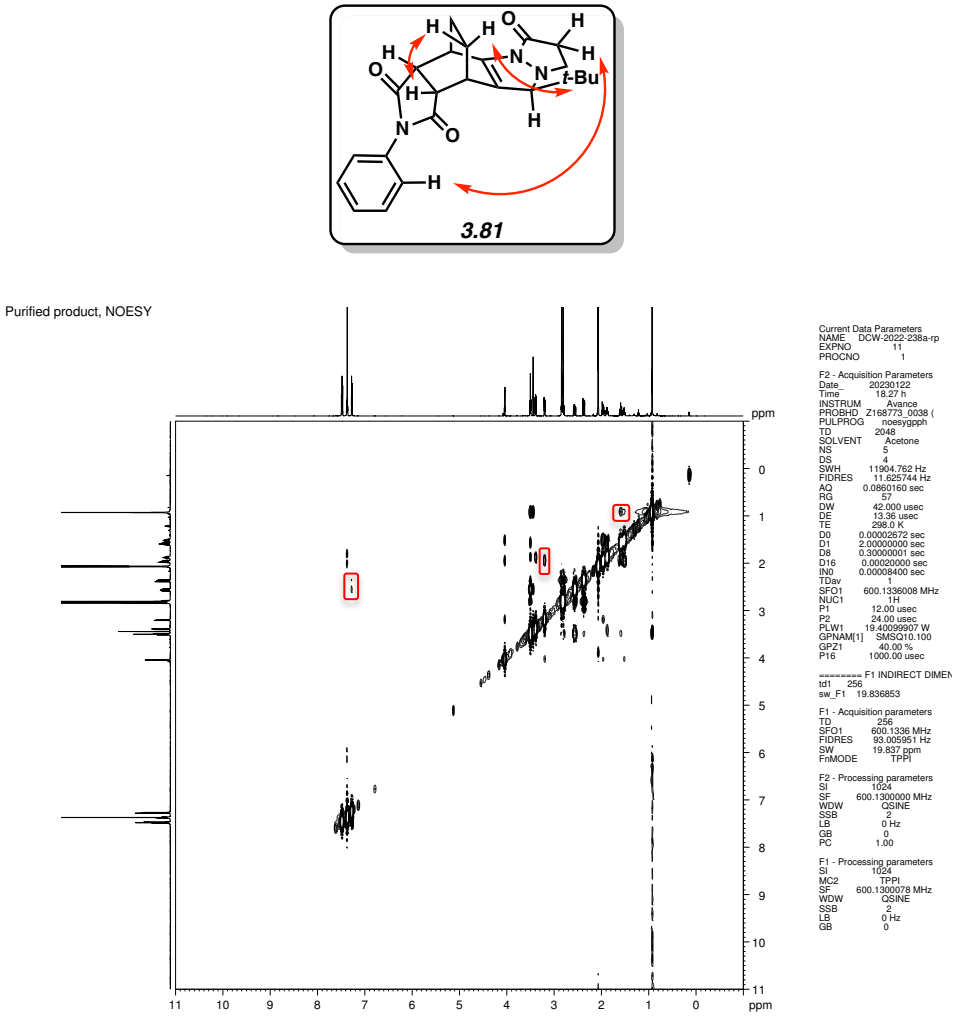

Figure 3.89. NOESY (600 MHz, acetone-d_6) of compound **3.81**.

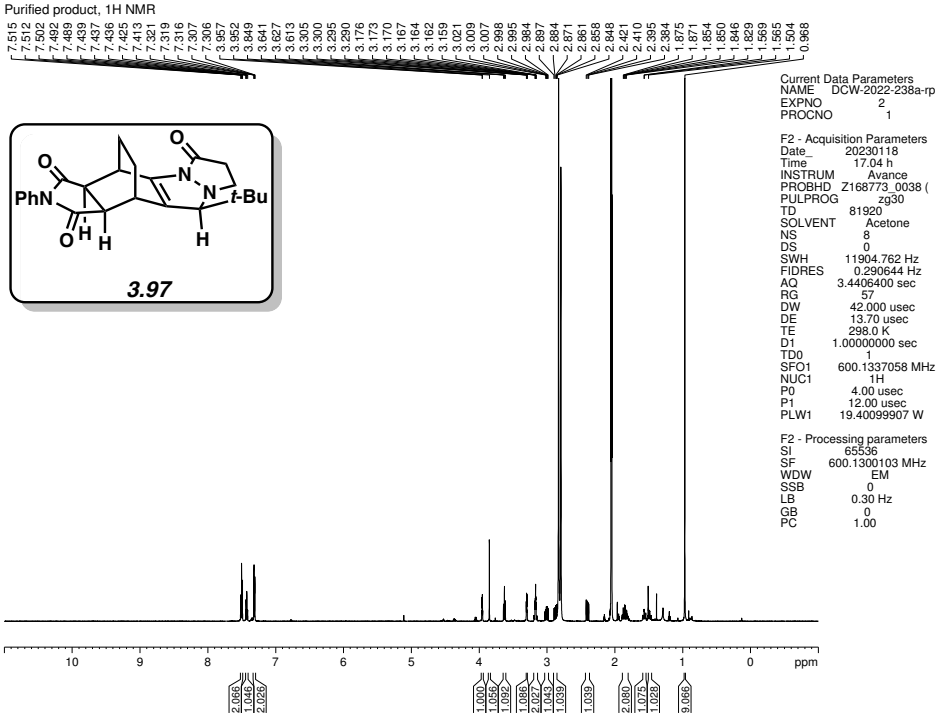

Figure 3.90. ^{1}H NMR (600 MHz, acetone-d_6) of compound **3.97**.

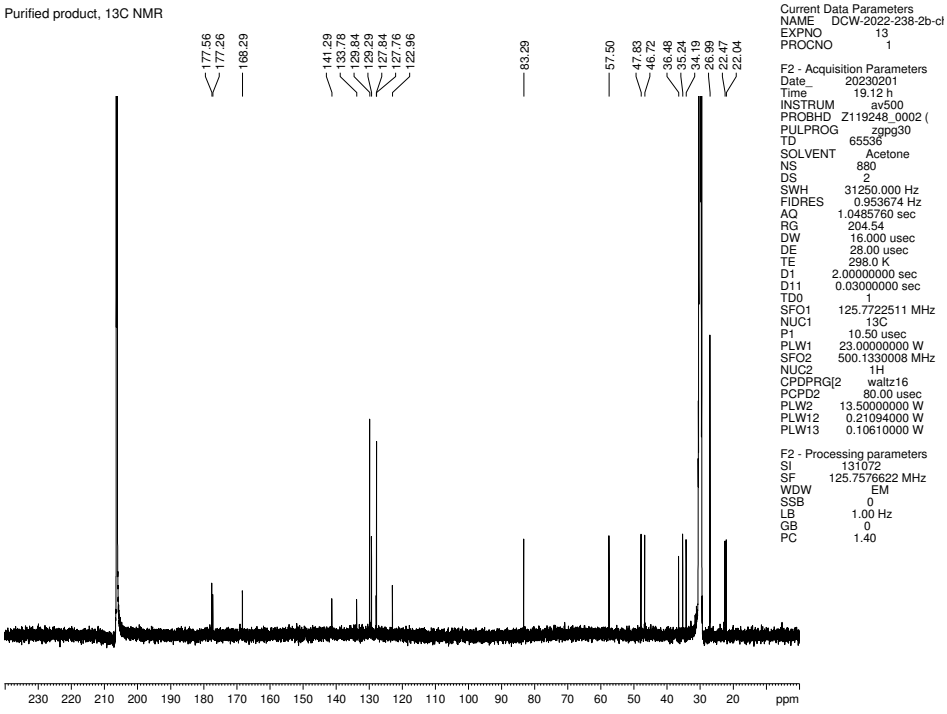

Figure 3.91. ^{13}C NMR (125 MHz, acetone-d_6) of compound **3.97**.

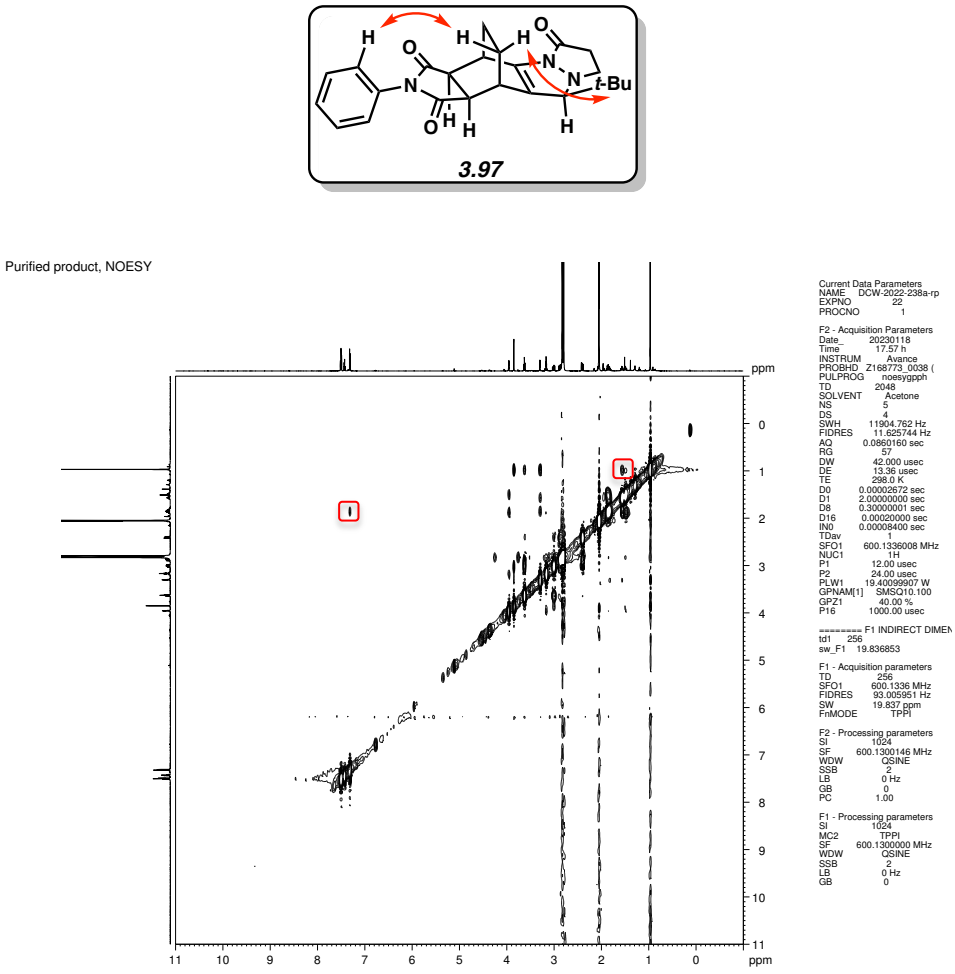

Figure 3.92. NOESY (600 MHz, acetone-d_6) of compound **3.97**.

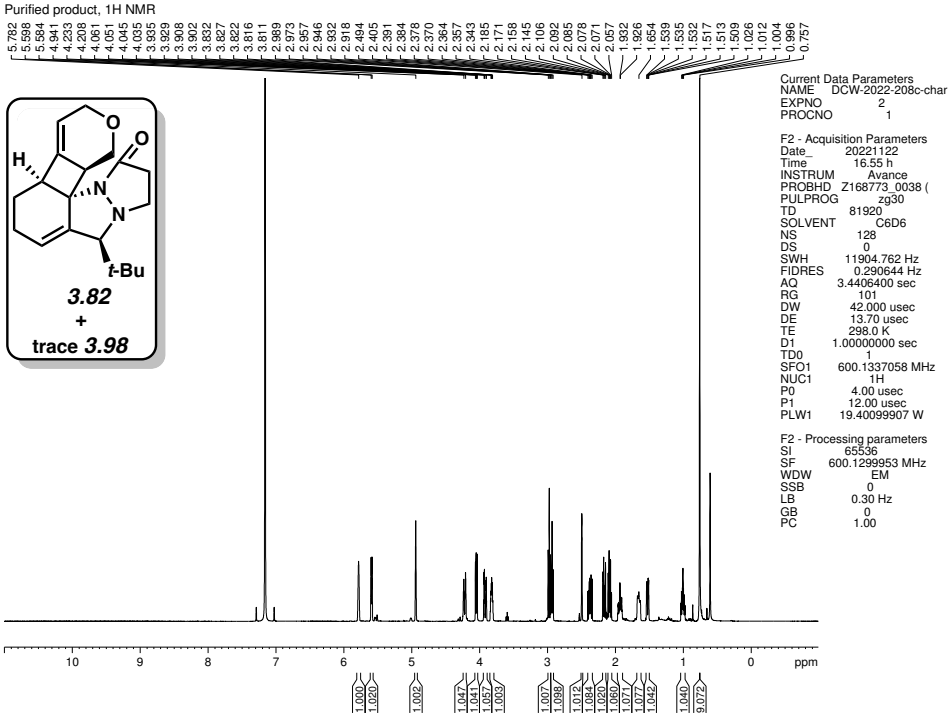

Figure 3.93. ^{1}H NMR (600 MHz, C_6D_6) of compound **3.82**.

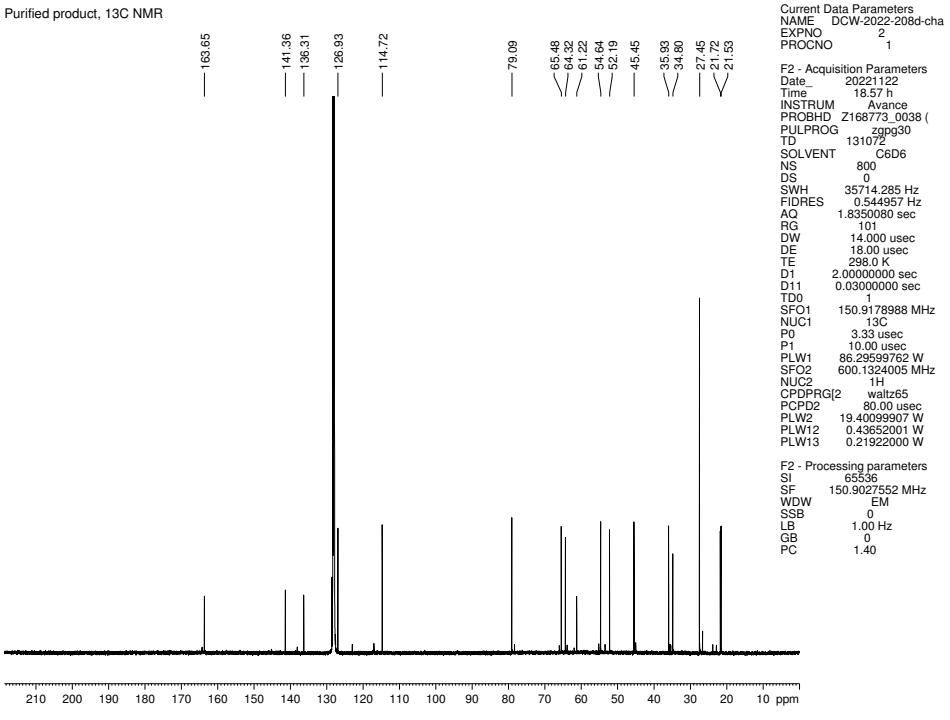

Figure 3.94. ^{13}C NMR (150 MHz, C_6D_6) of compound **3.82**.

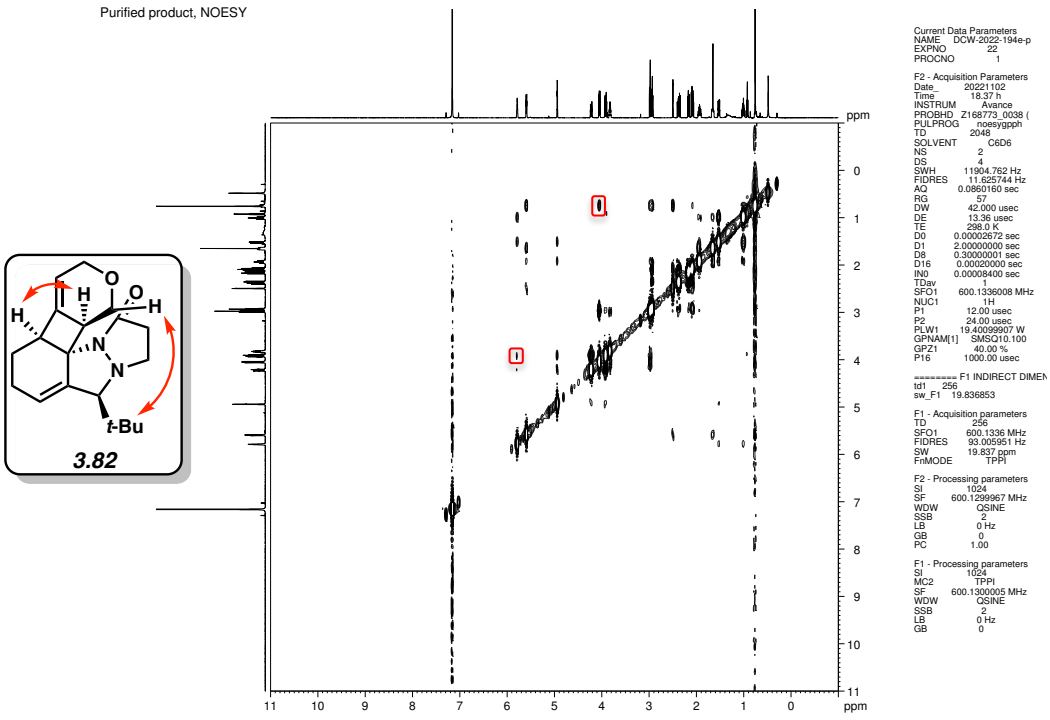

Figure 3.95. NOESY (600 MHz, C_6D_6) of compound **3.82**.

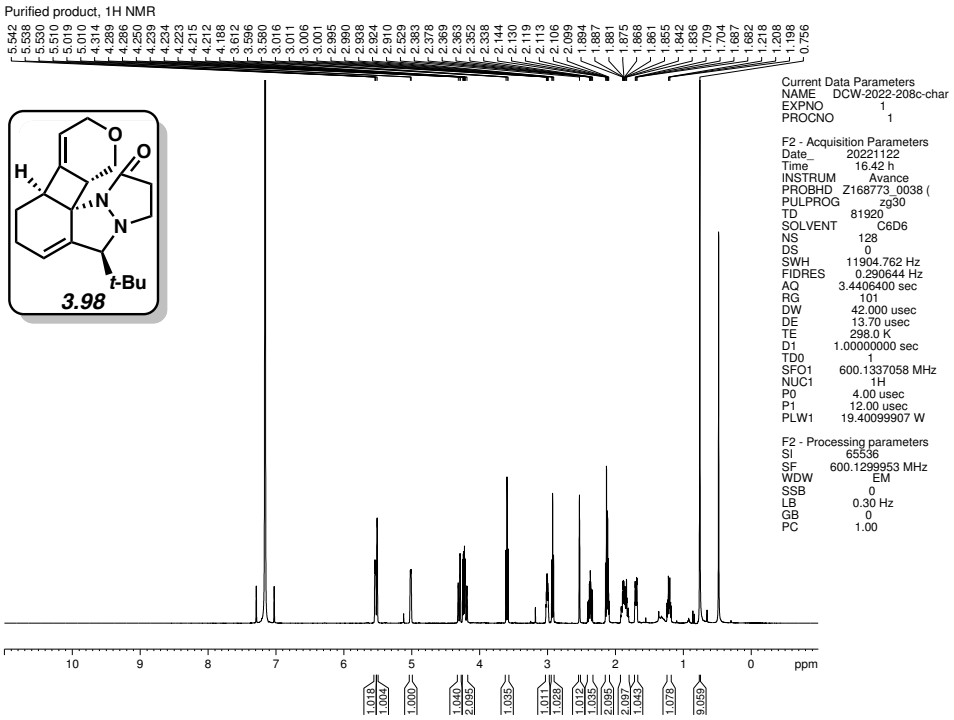

Figure 3.96. ^{1}H NMR (600 MHz, C_6D_6) of compound **3.98**.

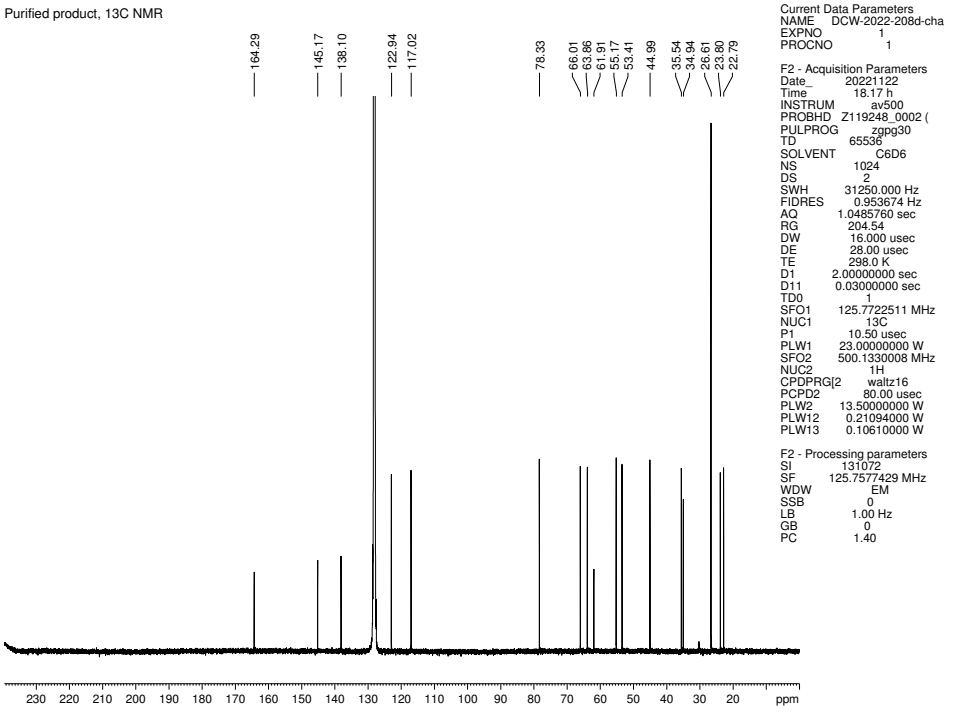

Figure 3.97. ^{13}C NMR (125 MHz, C_6D_6) of compound **3.98**.

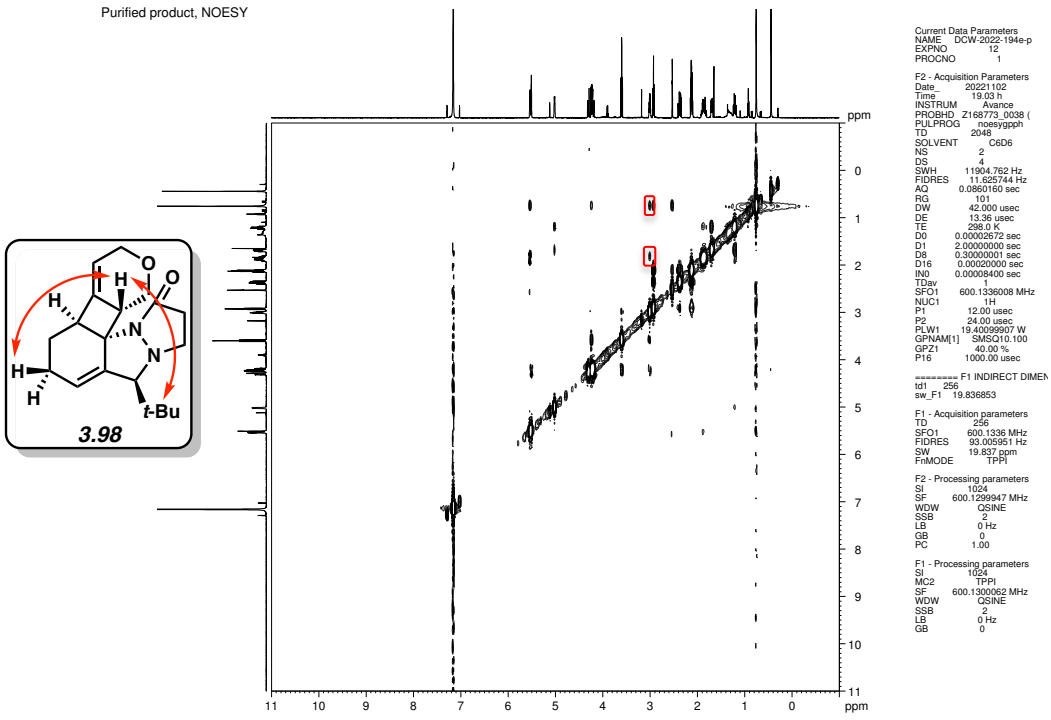

Figure 3.98. NOESY (600 MHz, C_6D_6) of compound **3.98**.

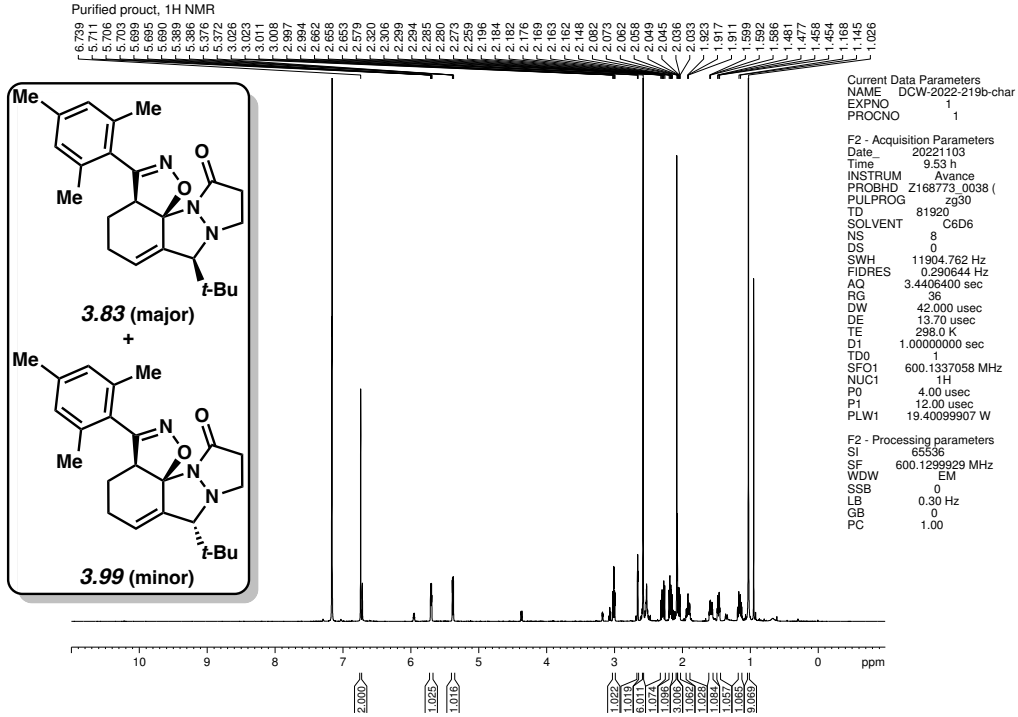

Figure 3.99. ^{1}H NMR (600 MHz, C_6D_6) of compounds **3.83** and **3.99**.

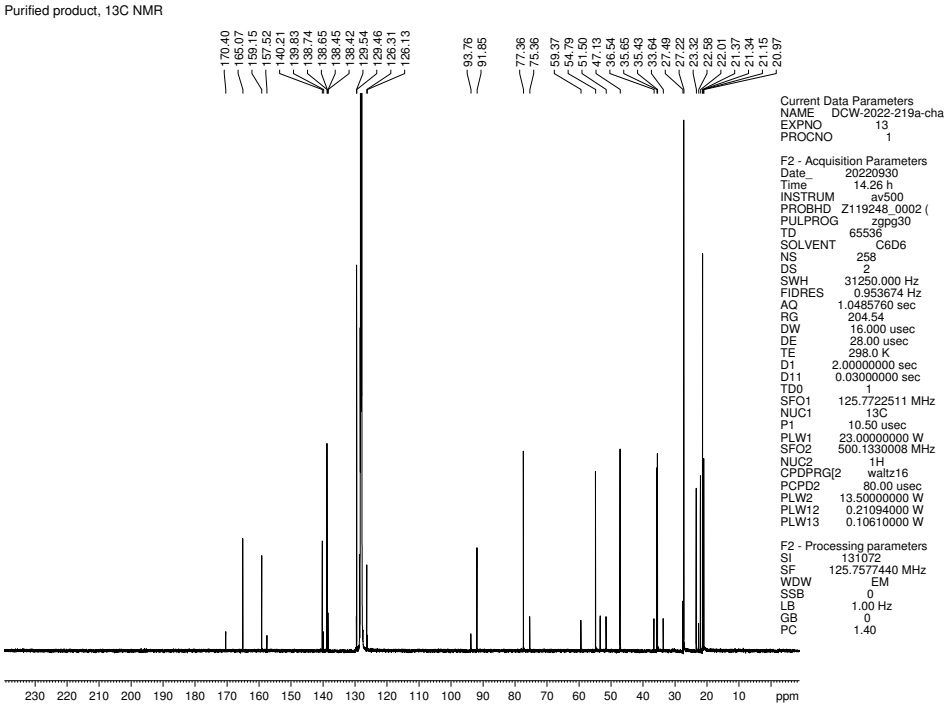

Figure 3.100. ^{13}C NMR (125 MHz, C_6D_6) of compounds **3.83** and **3.99**.

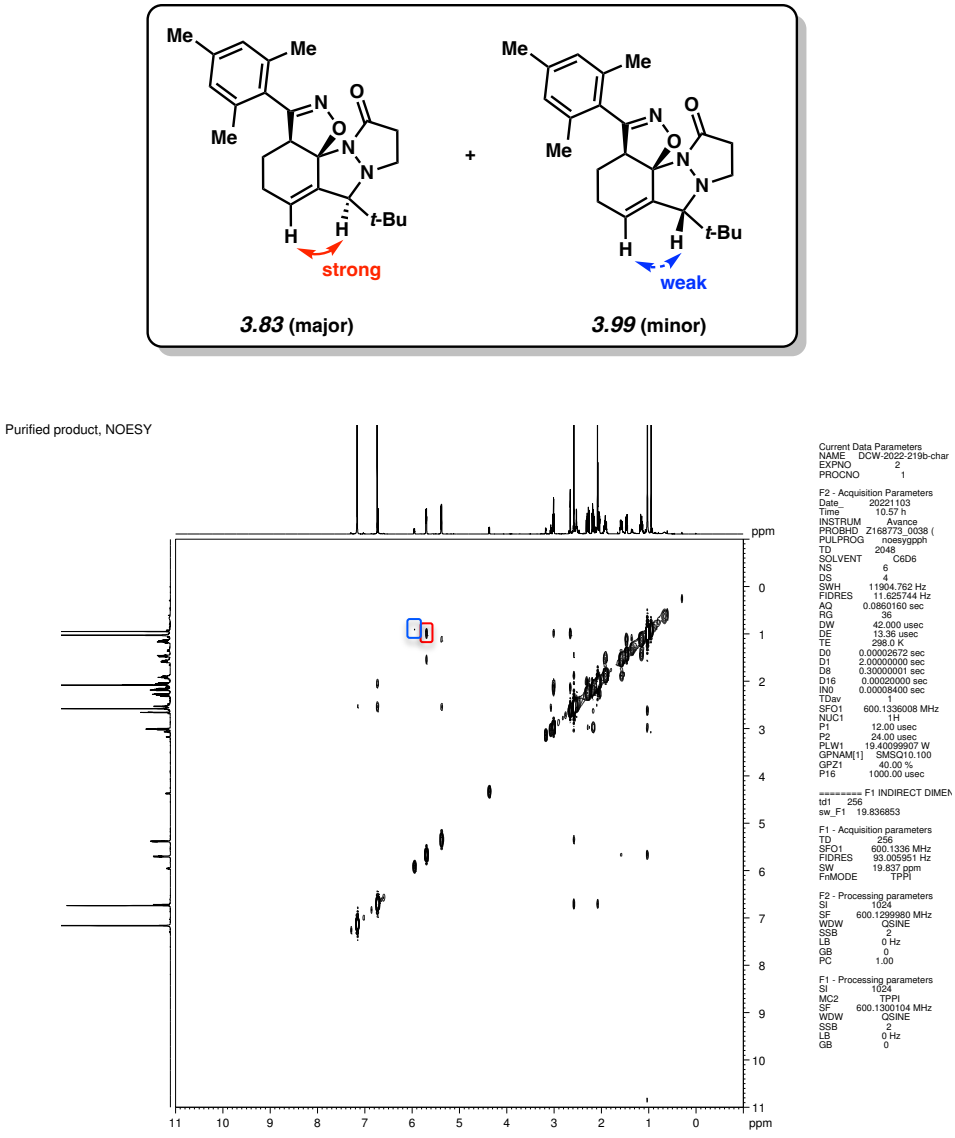

Figure 3.101. NOESY (600 MHz, C_6D_6) of compounds **3.83** and **3.99**.

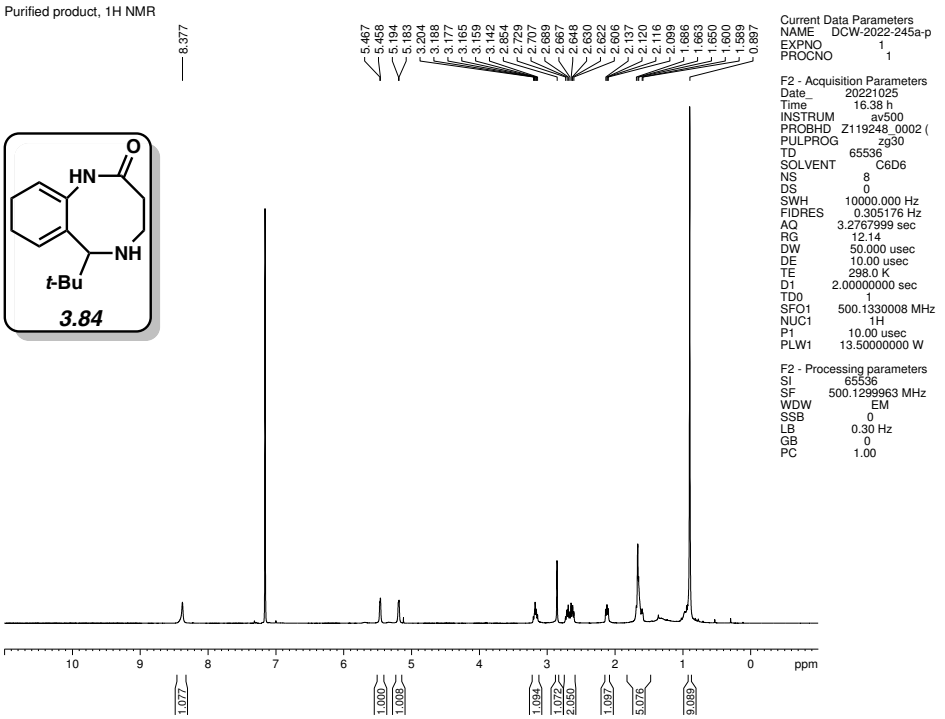

Figure 3.102. ^{1}H NMR (500 MHz, C_6D_6) of compound **3.84**.

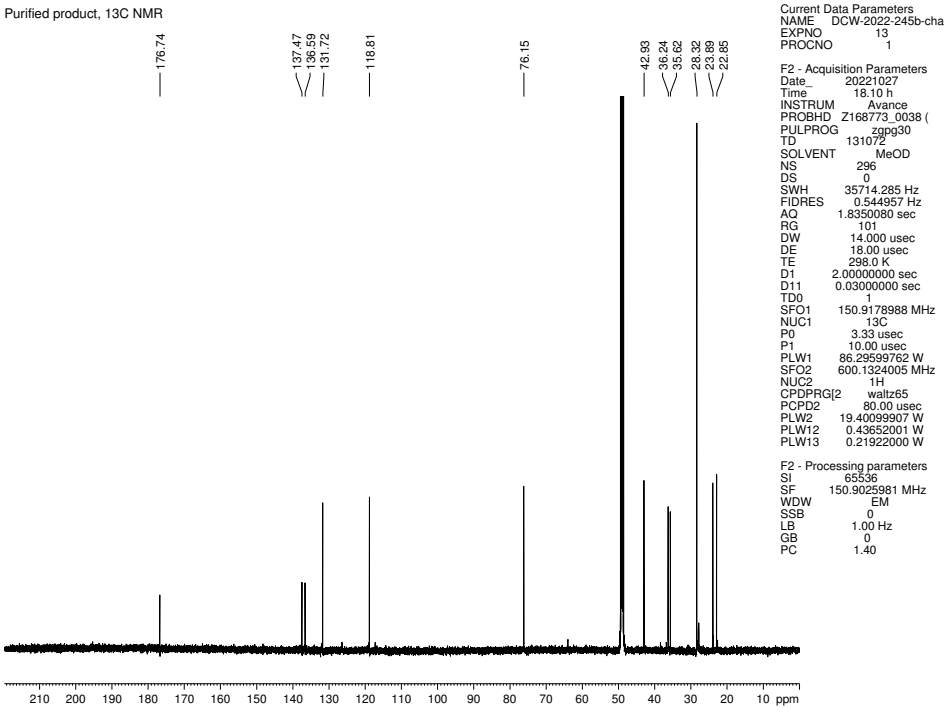

Figure 3.103. ^{13}C NMR (150 MHz, CD_3OD) of compound **3.84**.

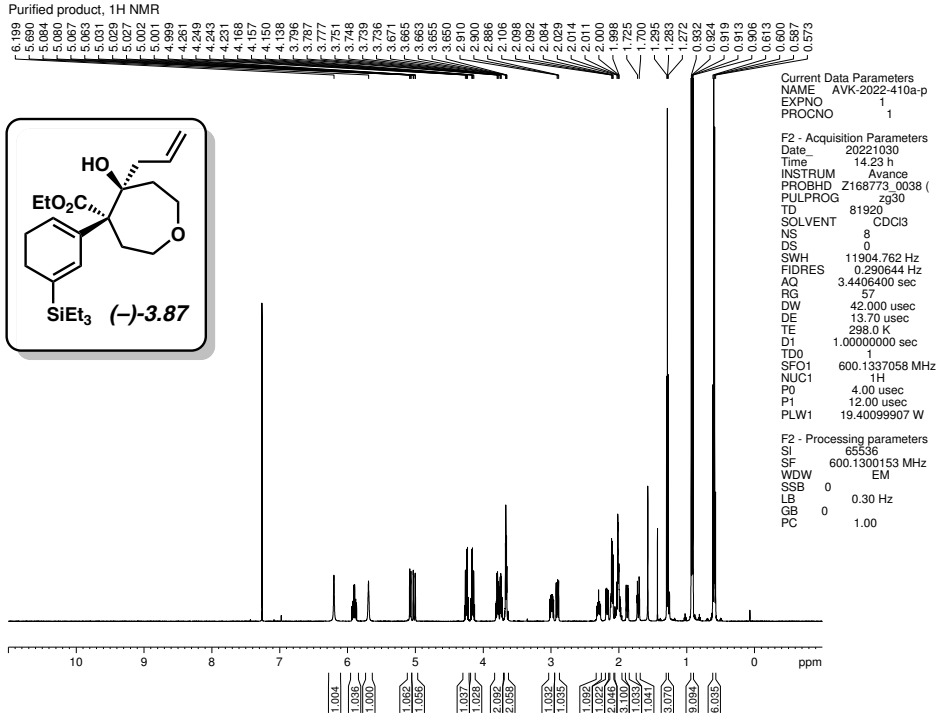

Figure 3.104. ^{1}H NMR (600 MHz, $CDCl_3$) of compound (–)-**3.87**.

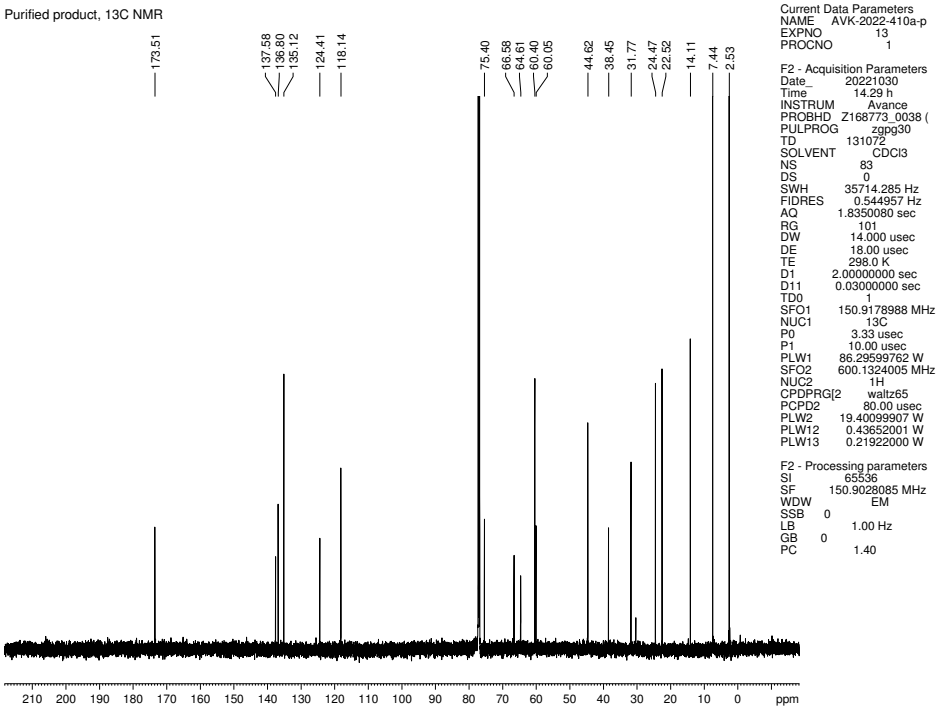

Figure 3.105. ^{13}C NMR (150 MHz, $CDCl_3$) of compound (–)-**3.87**.

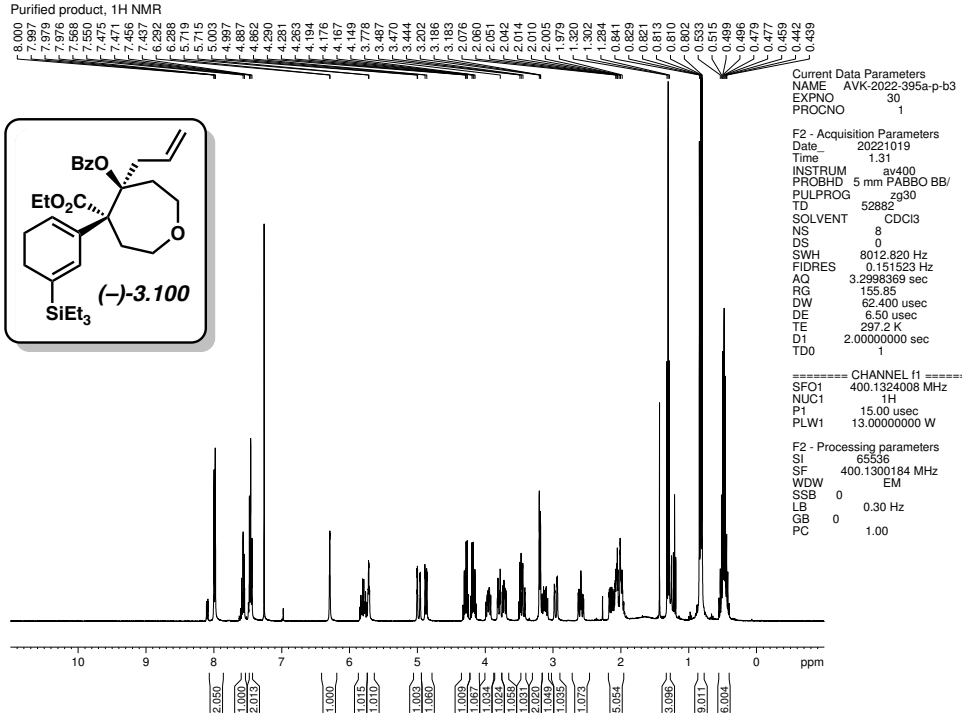

Figure 3.106. ^{1}H NMR (400 MHz, $CDCl_3$) of compound (–)-**3.100**.

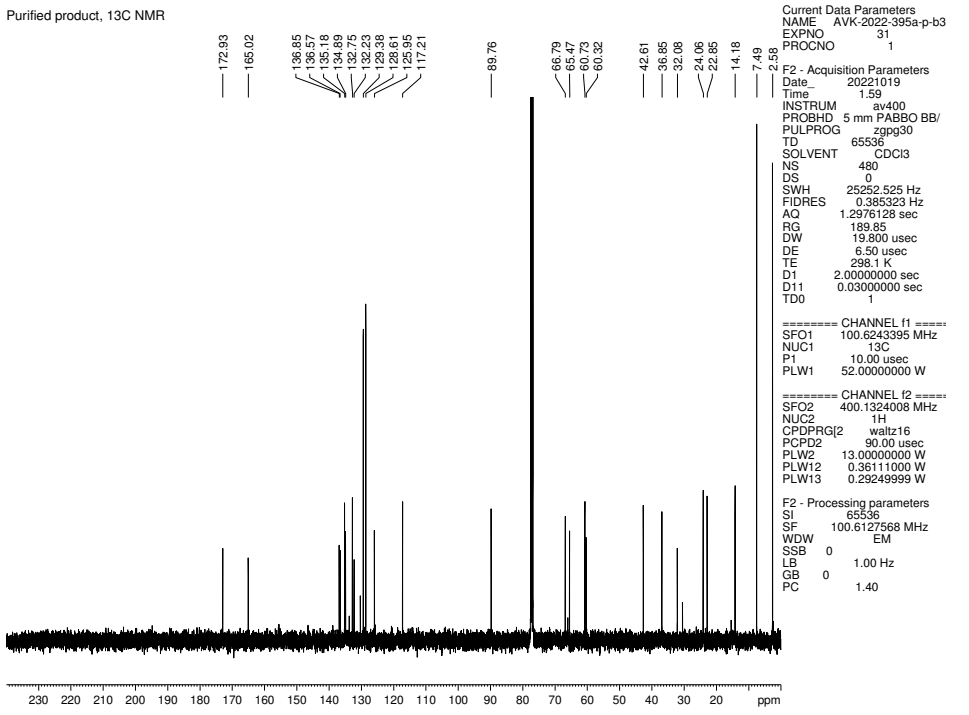

Figure 3.107. ^{13}C NMR (100 MHz, $CDCl_3$) of compound (–)-**3.100**.

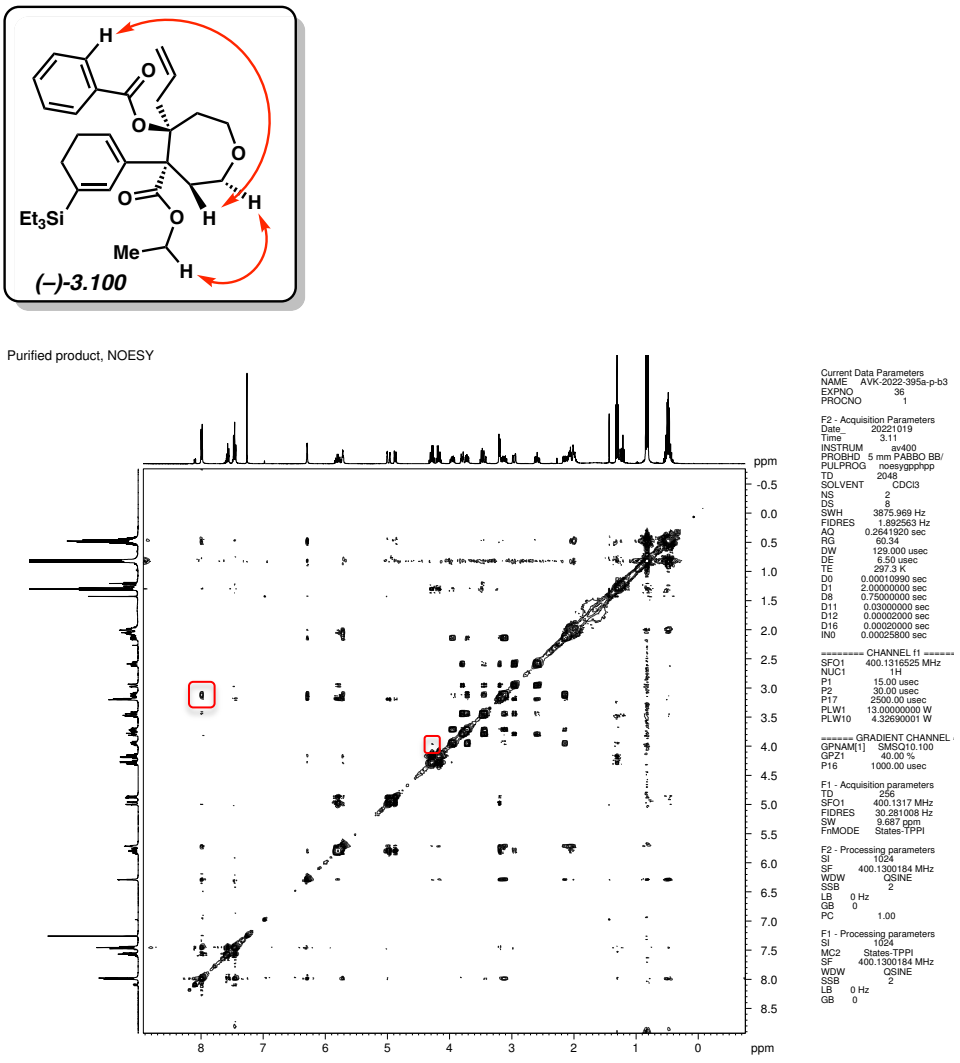

Figure 3.108. NOESY (400 MHz, $CDCl_3$) of compound (–)-**3.100**.

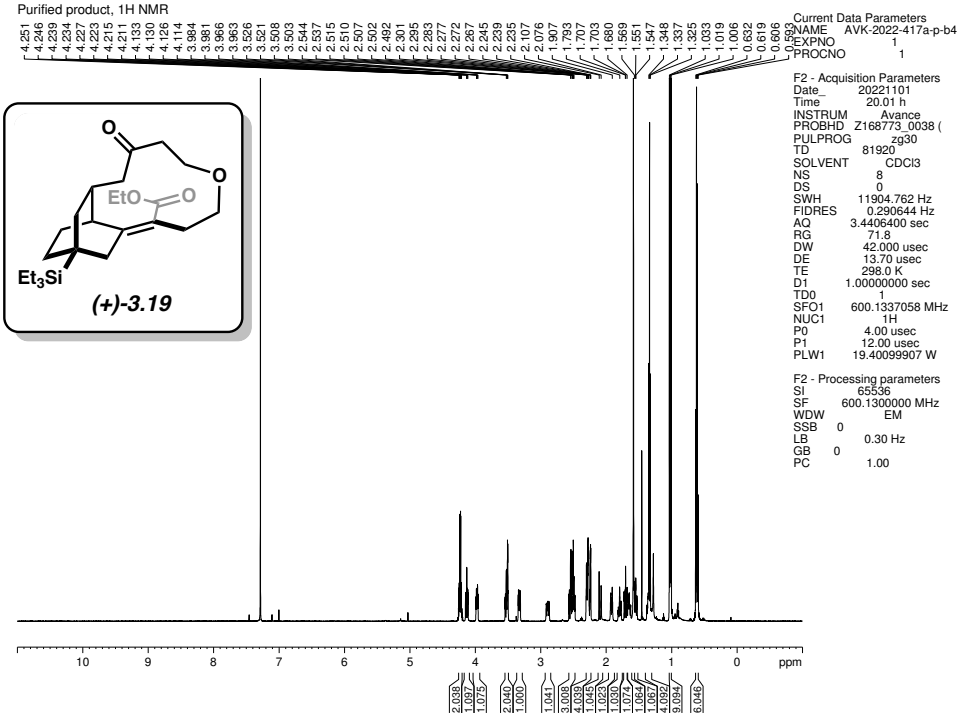

Figure 3.109. ^{1}H NMR (600 MHz, $CDCl_3$) of compound (+)-**3.19**.

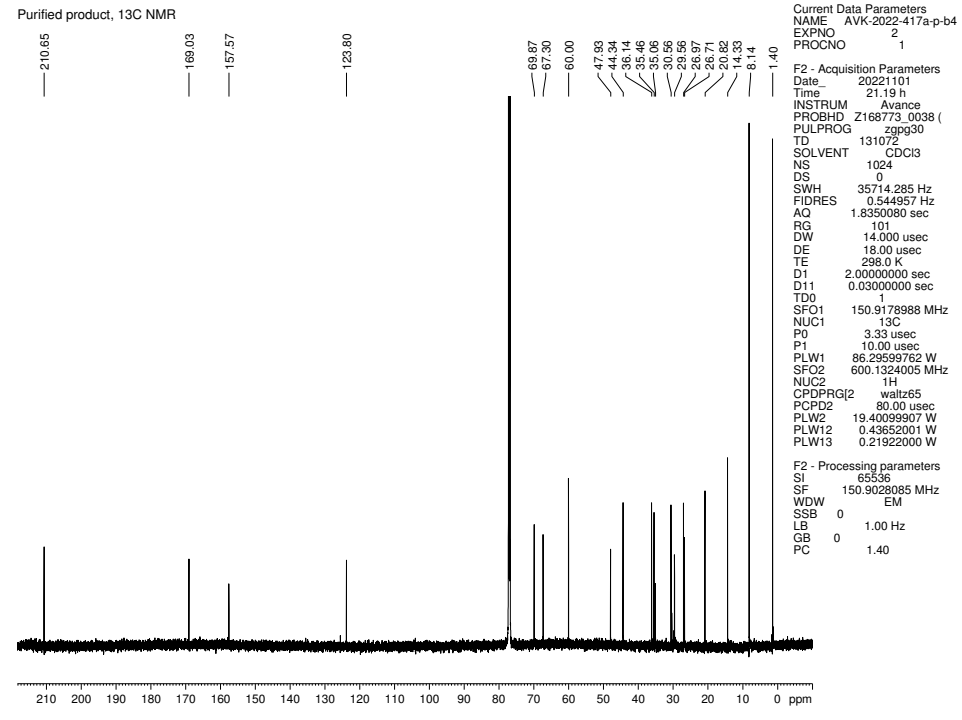

Figure 3.110. ^{13}C NMR (150 MHz, $CDCl_3$) of compound (+)-**3.19**.

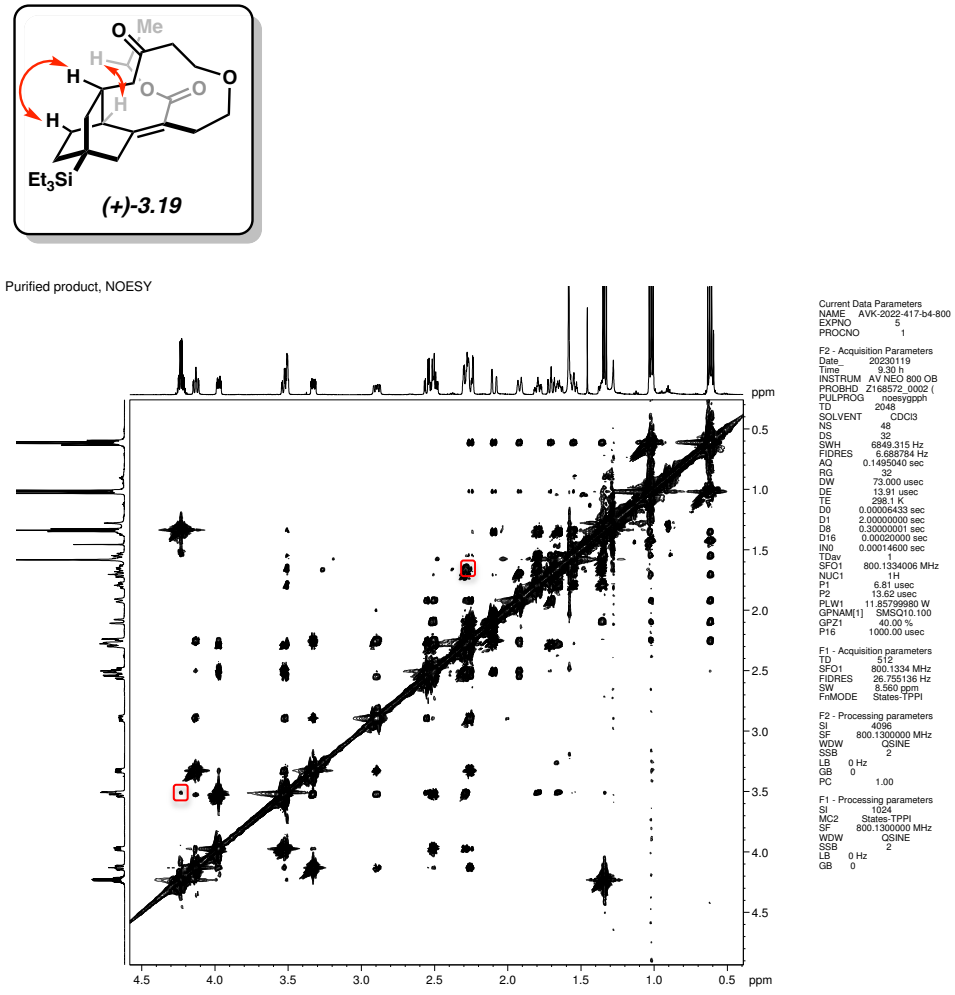

Figure 3.111. NOESY (800 MHz, $CDCl_3$) of compound (+)-**3.19**.

3.11 Notes and References

(1) Faraday, M. XX. On new compounds of carbon and hydrogen, and on certain other products obtained during the decomposition of oil by heat. *Philos. Trans. R. Soc.* **1825**, *115*, 440–466.

(2) Mortier, J. *Arene Chemistry: Reaction Mechanisms and Methods for Aromatic Compounds*. John Wiley & Sons, Inc. 2016.

(3) van Tamelen, E. E.; Pappas, S. P. Bicyclo [2.2.0]hexa-2,5-diene. *J. Am. Chem. Soc.* **1963**, *85*, 3297–3298.

(4) Katz, T. J.; Acton, N. Synthesis of prismane. *J. Am. Chem. Soc.* **1973**, *95*, 2738–2739.

(5) Huang, X.; Chen, B.-Z.; Li, P.; Ji, D.-W.; Liu, J.; Zheng, H.; Yang, S.-N.; Hu, Y.-C.; Wan, B.; Hu, X.-P.; Fu, C.; Huang, Y.; Zheng, J.; Chen, Q.-A.; Ma, S. Palladium-catalysed construction of butafulvenes. *Nat. Chem.* **2022**, *14*, 1185–1192.

(6) Preethalayam, P.; Krishnan, K. S.; Thulasi, S.; Chand, S. S.; Joseph, J.; Nair, V.; Jaroschik, F.; Radhakrishnan, K. V. Recent advances in the chemistry of pentafulvenes. *Chem. Rev.* **2017**, *117*, 3930–3989.

(7) Seo, J.; Lee, S. Y.; Bielawski, C. W. Unveiling a masked polymer of Dewar benzene reveals trans-poly(acetylene). *Macromolecules* **2019**, *52*, 2923–2931.

(8) Shakespeare, W. C.; Johnson, R. P. 1,2,3-Cyclohexatriene and cyclohexen-3-yne: Two new highly strained C_6H_6 isomers. *J. Am. Chem. Soc.* **1990**, *112*, 8578–8579.

(9) Hickey, E. R.; Paquette, L. A. Torsional angle decompression is not the source of facial selectivity in Diels–Alder cycloadditions involving cyclic dienes fused to bicyclic

frameworks. The case study of 1,2,3,4,6,7-hexahydro-1,4-methanonaphthalene. *Tetrahedron Lett.* **1994**, *35* 2309–2312.

(10) Hickey, E. R.; Paquette, L. A. Experimental and theoretical analysis of the effects of strain diminution on the stereoselectivity of dienophilic capture by π-facially nonequivalent homologues of isodicyclopentadiene. *J. Am. Chem. Soc.* **1995**, *117*, 163–176.

(11) Burrell, R. C.; Daoust, K. J.; Bradley, A. Z.; DiRico, K. J.; Johnson, R. P. Strained cyclic cumulene intermediates in Diels–Alder cycloadditions of enynes and diynes. *J. Am. Chem. Soc.* **1996**, *118*, 4218–4219.

(12) Sakura, M.; Ando, S.; Hattori, A.; Saito, K. Reaction of cyclohexa-1,2,3-triene with *N*,α-diphenylnitrone: Formation of seven-membered cyclic amines via piradone derivatives. *Heterocycles* **1999**, *51*, 547–556.

(13) Slater, J. C. Directed valence in polyatomic molecules. *Phys. Rev.* **1931**, *37*, 481–489.

(14) Pauling, L.; Wheland, G. W. The nature of the chemical bond. V. The quantum-mechanical calculation of the resonance energy of benzene and naphthalene and the hydrocarbon free radicals. *J. Chem. Phys.* **1933**, *1*, 362–374.

(15) L. Pauling. The theory of resonance in chemistry. *Proc. R. Soc. Lond. A* **1977**, *356*, 433–441.

(16) Garratt, P. J. *Aromaticity*. Wiley-Interscience, 1986.

(17) Roberts, J. D.; Simmons, H. E.; Carlsmith, L. A.; Vaughan, C. W. Rearrangement in the reaction of chlorobenzene-1-C^{14} with potassium amide. *J. Am. Chem. Soc.* **1953**, *75*, 3290–3291.

(18) Scardiglia, F.; Roberts, J. D. Evidence for cyclohexyne as an intermediate in the coupling of phenyllithium with 1-chlorocyclohexene. *Tetrahedron* **1957**, *1*, 343–344.

(19) Wittig, G.; Fritze, P. On the intermediate occurrence of 1,2-cyclohexadiene. *Angew. Chem., Int. Ed.* **1966**, *5*, 846.

(20) Moser, W. R. The reactions of *gem*-dihalocyclopropanes with organometallic reagents. Ph.D. Dissertation, Massachusetts Institute of Technology, Cambridge, MA, 1964.

(21) Shi, J.; Li, L.; Li, Y. *o*-Silylaryl triflates: A journey of Kobayashi aryne precursors. *Chem. Rev.* **2021**, *121*, 3892– 4044.

(22) Schleth, F., Vettiger, T., Rommel, M. & Tobler, H. Process for the preparation of pyrazole carboxylic acid amides. International patent WO2011131544A1, 2011.

(23) Darzi, E. R.; Barber, J. S.; Garg, N. K. Cyclic alkyne approach to heteroatom-containing polycyclic aromatic hydrocarbon scaffolds. *Angew. Chem., Int. Ed.* **2019**, *58*, 9419– 9424.

(24) Yamano, M. M.; Knapp, R. R.; Ngamnithiporn, A.; Ramirez, M.; Houk, K. N.; Stoltz, B. M.; Garg, N. K. Cycloadditions of oxacyclic allenes and a catalytic asymmetric entryway to enantioenriched cyclic allenes. *Angew. Chem., Int. Ed.* **2019**, *58*, 5653– 5657.

(25) Ippoliti, F.; Adamsonn, N. J.; Wonilowicz, L. G.; Darzi, E. R.; Donaldson, J. S.; Garg, N. K. Total synthesis of lissodendoric acid A via stereospecific trapping of a strained cyclic allene. *Science* **2023**, *379*, 261–265.

(26) Moore, W. M.; Ozretich, T. M. Cyclic cumulenes. The synthesis and some reactions of 1,2,3-cyclodecatriene. *Tetrahedron Lett.* **1967**, *33* 3205–3207.

(27) Johnson, R. P. Strained cyclic cumulenes. *Chem. Rev.* **1989**, *89*, 1111–1124.

(28) Yin, J.; Abboud, K. A.; Jones, W. M. Synthesis of zirconocene complexes of a 1,2,3-cyclohexatriene and a cyclohexen-3-yne. *J. Am. Chem. Soc.* **1993**, *115*, 8859–8860.

(29) Daoust, K. J.; Hernandez, S. M.; Konrad, K. M.; Mackie, I. D.; Winstanley, J.; Johnson, R. P. Strain estimates for small-ring cyclic allenes and butatrienes. *J. Org. Chem.* **2006**, *71*, 5708– 5714.

(30) Liebman, J. F.; Greenberg, A. A survey of strained organic molecules. *Chem. Rev.* **1976**, *76*, 311–365.

(31) Newton, M. D.; Fraenkel, H. A. The equilibrium geometry, electronic structure, and heat of formation of ortho-benzyne. *Chem. Phys. Lett.* **1973**, *18*, 244–246.

(32) Carpino, L. A.; Sau, A. C. Convenient source of 'naked' fluoride: Tetra-n-butylammonium chloride and potassium fluoride dihydrate. *J. Chem. Soc., Chem. Commun.* **1979**, 514–515.

(33) Anthony, S. M.; Wonilowicz, L. G.; McVeigh, M. S.; Garg, N. K. Leveraging fleeting strained intermediates to access complex scaffolds. *JACS Au* **2021**, *1*, 897–912.

(34) Spence, K. A.; Tena Meza, A.; Garg, N. K. Merging metals and strained intermediates. *Chem Catalysis* **2022**, *2*, 1870–1879.

(35) Wenk, H. H.; Winkler, M.; Sander, W. One century of aryne chemistry. *Angew. Chem., Int. Ed.* **2003**, *42*, 502–528.

(36) Schepens, W.; Van Haver, D.; Vandewalle, M.; Bouillon, R.; Verstuyf, A.; De Clercq, P. J. Synthesis of spiro[4.5]decane CF-ring analogues of 1α,25-dihydroxyvitamin D3. *Org. Lett.* **2006**, *8*, 4247–4250.

(37) Chari, J. V.; Ippoliti, F. M.; Garg, N. K. Concise approach to cyclohexyne and 1,2-cyclohexadiene precursors. *J. Org. Chem.* **2019**, *84*, 3652–3655.

(38) Asmadi, M.; Chikhalia, K. H. Aryne insertion into σ bonds. *Asian J. Org. Chem.* **2017**, *6*, 1331–1348.

(39) Bronner, S. M.; Mackey, J. L.; Garg, N. K. Steric effects compete with aryne distortion to control regioselectivities of nucleophilic additions to 3-silylarynes. *J. Am. Chem. Soc.* **2012**, *134*, 13966–13969

(40) Shi, J.; Li, L.; Shan, C.; Wang, J.; Chen, Z.; Gu, R.; He, J.; Tan, M.; Lan, Y.; Li, Y. Aryne 1,2,3,5-tetrasubstitution enabled by 3-silylaryne and allyl sulfoxide via an aromatic 1,3-silyl migration. *J. Am. Chem. Soc.* **2021**, *143*, 2178–2184.

(41) Ikawa, T.; Nishiyama, T.; Shigeta, T.; Mohri, S.; Morita, S.; Takayanagi, S.-i.; Terauchi, Y.; Morikawa, Y.; Takagi, A.; Ishikawa, Y.; Fujii, S.; Kita, Y.; Akai, S. *ortho*-Selective nucleophilic addition of primary amines to silylbenzynes: synthesis of 2-silylanilines. *Angew. Chem., Int. Ed.* **2011**, *50*, 5674–5677.

(42) Matsumoto, T.; Sohma, T.; Hatazaki, S.; Suzuki, K. On the regiochemistry of cycloaddition of unsymmetrical aryne with nitrone remarkable effect of trialkylsilyl substituent. *Synlett* **1993**, *1993*, 843−846.

(43) Bent, H. A. An appraisal of valence-bond structures and hybridization in compounds of the first-row elements. *Chem. Rev.* **1961**, *61*, 275–311.

(44) Medina, J. M.; McMahon, T. C.; Jiménez-Osés, G.; Houk, K. N.; Garg, N. K. Cycloadditions of cyclohexynes and cyclopentyne. *J. Am. Chem. Soc.* **2014**, *136*, 14706–14709.

(45) Bickelhaupt, F. M.; Houk, K. N. Analyzing reaction rates with the distortion/interaction-activation strain model. *Angew. Chem., Int. Ed.* **2017**, *56*, 10070–10086.

(46) Medina, J. M.; Mackey, J. L.; Garg, N. K.; Houk, K. N. The role of aryne distortions, steric effects, and charges in regioselectivities of aryne reactions. *J. Am. Chem. Soc.* **2014**, *136*, 15798–15805.

(47) Cheong, P. H.-Y.; Paton, R. S.; Bronner, S. M.; Im, G.-Y. J.; Garg, N. K.; Houk, K. N. Indolyne and aryne distortions and nucleophilic regioselectivities. *J. Am. Chem. Soc.* **2010**, *132*, 1267–1269.

(48) Goetz, A. E.; Garg, N. K. Regioselective reactions of 3,4-pyridynes enabled by the aryne distortion model. *Nature Chem.* **2013**, *5*, 54–60.

(49) Bronner, S. M.; Goetz, A. E.; Garg, N. K. Overturning indolyne regioselectivities and synthesis of indolactam V. *J. Am. Chem. Soc.* **2011**, *133*, 3832–3835.

(50) Goetz, A. E.; Shah, T. K.; Garg, N. K. Pyridynes and indolynes as building blocks for functionalized heterocycles and natural products. *Chem. Commun.* **2015**, *51*, 34–45.

(51) Kemp, D. S.; Sidell, M. D.; Shortridge, T. J. Synthetic routes to 1,5-diazacyclooctanes via 2,6-diketo-1,5-diazabicyclo[3.3.1]octanes. *J. Org. Chem.* **1979**, *44*, 4473–4476.

(52) Shintani, R.; Hayashi, T. Palladium-catalyzed [3 + 3] cycloaddition of trimethylenemethane with azomethine imines. *J. Am. Chem. Soc.* **2006**, *128*, 6330–6331.

(53) Shintani, R.; Fu, G. C. A new copper-catalyzed [3 + 2] cycloaddition: Enantioselective coupling of terminal alkynes with azomethine imines to generate five-membered nitrogen heterocycles. *J. Am. Chem. Soc.* **2003**, *125*, 10778–10779.

(54) Arellano, L. M.; Yue, S.; Atienzar, P.; Gómez-Escalonilla, M. J.; Ortega-Higueruelo, F. J.; Fierro, J. L. G.; García, H.; Langa, F. Modulating charge carrier density and mobility in doped graphene by covalent functionalization. *Chem. Commun.* **2019**, *67*, 9999–10002.

(55) Schepens, W.; Van Haver, D.; Vandewalle, M.; Bouillon, R.; Verstuyf, A.; De Clercq, P. J. Synthesis of spiro[4.5]decane CF-ring analogues of 1α,25-dihydroxyvitamin D3. *Org. Lett.* **2006**, *8*, 4247–4250.

(56) Reeves, J. T.; Lorenc, C.; Camara, K.; Li, Z.; Lee, H.; Busacca, C. A.; Senanayake, C. H. Carbamoyl anion addition to nitrones. *J. Org. Chem*. **2014**, *79*, 5895–5902.

(57) Kumar, R.; Chaudhary, S.; Kumar, R.; Upadhyay, P.; Sahal, D.; Sharma, U. Catalyst and additive-free diastereoselective 1,3-dipolar cycloaddition of quinolinium imides with olefins, maleimides, and benzynes: Direct access to fused *N*,*N*′-heterocycles with promising activity against a drug-resistant malaria parasite. *J. Org. Chem.* **2018**, *83,* 11552–11570.

(58) Shapiro, S. L.; Weinberg, K.; Freedman, L. N-Substituted-3-oxypyridyl betaines. *J. Am. Chem. Soc.* **1959**, *81*, 5140–5145.

(59) Adams, L. A.; Aggarwal, V. K.; Bonnert, R. V.; Bressel, B.; Cox, R. J.; Shepherd, J.; de Vicente, J.; Walter, M.; Whittingham, W. G.; Winn, C. L. Diastereoselective synthesis of cyclopropane amino acids using diazo compounds generated in situ. *J. Org. Chem.* **2003**, *68*, 9433–9440.

(60) Sánchez-Arroyo, A. J.; Pardo, Z. D.; Moreno-Jiménez, F.; Herrera, A.; Martín, N.; García-Fresnadillo, D. Photochemical oxidation of thioketones by singlet molecular oxygen revisited: Insights into photoproducts, kinetics, and reaction mechanism. *J. Org. Chem.* **2015**, *80*, 10575–10584.

(61) Shih, C.; Swenton, J. S. An efficient and simple β-acylvinyl anion equivalent for cyclohexenones. *Tetrahedron Lett.* **1981**, *22*, 4217–4220.

(62) Picazo, E.; Anthony, S. M.; Giroud, M.; Simon, A.; Miller, M. A.; Houk, K. N.; Garg, N. K. Arynes and cyclic alkynes as synthetic building blocks for stereodefined quaternary centers. *J. Am. Chem. Soc.* **2018**, *140*, 7605–7610.

(63) Yamano, M. M.; Knapp, R. R.; Ngamnithiporn, A.; Ramirez, M.; Houk, K. N.; Stoltz, B. M.; Garg, N. K. Cycloadditions of oxacyclic allenes and a catalytic asymmetric entryway to enantioenriched cyclic allenes. *Angew. Chem., Int. Ed.* **2019**, *58*, 5653–5657.

(64) Altintas, O.; Glassner, M.; Rodriguez-Emmenegger, C.; Welle, A.; Trouillet, V.; Barner-Kowollik, C. Macromolecular surface design: Photopatterning of functional stable nitrile oxides. *Angew. Chem., Int. Ed.* **2015**, *54*, 5777–5783.

(65) Feng, M.; Tang, B.; Wang, N.; Xiu, H.-X.; Jiang, X. Ligand controlled regiodivergent C1 insertion on arynes for construction of phenanthridinone and acridone alkaloids. *Angew. Chem., Int. Ed.* **2015**, *54*, 14960–14964.

(66) Picard, A.; Ciblat, S.; Ramtohul, Y. K. Synthesis of α,α,-disubstituted benzocyclobutane amino acids through [2+2] annulation of benzyne and dehydroalanine. *Synlett* **2020**, *31*, 507–511.

(67) Sheldrick, G. M. (1996). *SADABS*. University of Göttingen, Germany.

(68) Sheldrick, G. M. Crystal structure refinement with SHELXL. *Acta Cryst. C*, **2015**, *71*, 3–8.

(69) Garbisch Jr., E. W. Conformations. VI. Vinyl-allylic proton spin couplings. *J. Am. Chem. Soc*. **1964**, *86,* 5561–5564.

(70) Hancock, E. N.; Kuker, E. L.; Tantillo, D. J.; Brown, M. K. Lessons in strain and stability: Enantioselective synthesis of (+)-[5]-ladderanoic acid. *Angew. Chem., Int. Ed.* **2019**, *59*, 436–441.

(71) Hauser, F. M.; Baghdanov, V. M. Regiospecific total synthesis of (±)-daunomycinone from an 11-deoxydaunomycinone precursor. *Tetrahedron* **1984**, *40*, 4719–4724.

(72) Sumida, Y.; Kato, T.; Hosoya, T. Generation of arynes via ate complexes of arylboronic esters with an *ortho*-leaving group. *Org. Lett.* **2013**, *15*, 2806–2809.

(73) Spartan'20 Wavefunction, Inc., Irvine, CA.

(74) Frisch, M. J.; Trucks, G. W.; Schlegel, H. B.; Scuseria, G. E.; Robb, M. A.; Cheeseman, J. R.; Scalmani, G.; Barone, V.; Petersson, G. A.; Nakatsuji, H.; Li, X.; Caricato, M.; Marenich, A. V.; Bloino, J.; Janesko, B. G.; Gomperts, R.; Mennucci, B.; Hratchian, H. P.; Ortiz, J. V.; Izmaylov, A. F.; Sonnenberg, J. L.; Williams-Young, D.; Ding, F.; Lipparini, F.; Egidi, F.; Goings, J.; Peng, B.; Petrone, A.; Henderson, T.; Ranasinghe, D.; Zakrzewski, V. G.; Gao, J.; Rega, N.; Zheng, G.; Liang, W.; Hada, M.; Ehara, M.; Toyota, K.; Fukuda, R.; Hasegawa, J.; Ishida, M.; Nakajima, T.; Honda, Y.; Kitao, O.; Nakai, H.; Vreven, T.; Throssell, K.; Montgomery, Jr., J. A.; Peralta, J. E.; Ogliaro, F.; Bearpark, M. J.; Heyd, J. J.; Brothers, E. N.; Kudin, K. N.; Staroverov, V. N.; Keith, T. A.; Kobayashi, R.; Normand, J.; Raghavachari, K.; Rendell, A. P.; Burant, J. C.; Iyengar, S. S.; Tomasi, J.; Cossi, M.; Millam, J. M.; Klene, M.; Adamo, C.; Cammi, R.; Ochterski, J. W.; Martin, R. L.; Morokuma, K.; Farkas, O.; Foresman, J. B.; Fox, D. J. *Gaussian 16 Revision C.01*, Gaussian, Inc., Wallingford, CT, 2016

(75) Becke, A. D. Density-functional thermochemistry. III. The role of exact exchange. *J. Chem. Phys.* **1993**, *98*, 5648.

(76) Lee, C.; Yang, W.; Parr, R. G. Development of the Colle–Salvetti correlation-energy formula into a functional of the electron density. *Phys. Rev. B* **1988**, *37*, 785–789.

(77) Grimme, S.; Antony, J.; Ehrlich, S.; Krieg, H. A consistent and accurate ab initio parametrization of density functional dispersion correction (DFT-D) for the 94 Elements H-Pu. *J. Chem. Phys.* **2010**, *132*, 154104.

(78) Marenich, A. V.; Cramer, C. J.; Truhlar, D. G. Universal solvation model based on solute electron density and on a continuum model of the solvent defined by the bulk dielectric constant and atomic surface tensions. *J. Phys. Chem. B* **2009**, *113*, 6378–6396.

(79) London, F. J. Théorie quantique des courants interatomiques dans les combinaisons aromatiques. *J. Phys. Radium* **1937**, *8*, 397–409.

(80) McWeeny, R. Perturbation theory for the Fock-Dirac density matrix. *Phys. Rev.* **1974**, *124*, 1028–1034.

(81) Ditchfield, R. Self-consistent perturbation theory of diamagnetism. *Mol. Phys.* **1974**, *27*, 789–807.

(82) Wolinski, K.; Hinton, J. F.; Pulay, P. Efficient implementation of the gauge-independent atomic orbital method for NMR chemical shift calculations. *J. Am. Chem. Soc.* **1990**, *112*, 8251–8260.

(83) Cheeseman, J. R.; Trucks, G. W.; Keith, T. A.; Frisch, M. J. A comparison of models for calculating nuclear magnetic resonance shielding tensors. *J. Chem. Phys.* **1996**, *104*, 5497–5509.

(84) Adamo, C.; Barone, V. J. Exchange functionals with improved long-range behavior and adiabatic connection methods without adjustable parameters: The mPW and mPW1PW models. *J. Chem. Phys.* **2009**, *113*, 6378–6396.

(85) Luchini, G.; Alegre-Requena, J. V.; Funes-Ardoiz, I.; Paton, R. S. GoodVibes: Automated thermochemistry for heterogeneous computational chemistry data. *F1000Research* **9**, 291 (2020).

(86) Grimme, S. Supramolecular binding thermodynamics by dispersion-corrected density functional theory. *Chem. Eur. J.* **2012**, *18*, 9955–9964.

(87) Li, Y.; Gomes, J.; Sharada, S. M.; Bell, A. T.; Head-Gordon, M. Improved force-field parameters for QM/MM simulations of the energies of adsorption for molecules in zeolites and a free rotor correction to the rigid rotor harmonic oscillator model for adsorption enthalpies. *J. Phys. Chem. C* **2015**, *119*, 1840–1850.

(88) Legault, C. Y. CYLView, 1.0b; Université de Sherbrooke: Quebec, Montreal, Canada, http://www.cylview.org (2009).

(89) Zhang, G.; Musgrave, C. B. Comparison of DFT methods for molecular orbital eigenvalue calculations. *J. Phys. Chem. A* **2007**, *111*, 1554–1561.

(90) Bronner, S. M.; Mackey, J. L.; Garg, N. K. Steric effects compete with aryne distortion to control regioselectivities of nucleophilic additions to 3-silylarynes. *J. Am. Chem. Soc.* **2012**, *134*, 13966–13969.

(91) Lodewyk, M. W.; Siebert, M. R.; Tantillo, D. J. Computational prediction of 1H and 13C chemical shifts: A useful tool for natural product, mechanistic, and synthetic organic chemistry. *Chem. Rev.* **2012**, *112*, 1839–1862.

(92) Rablen, P. R.; Pearlman, S. A.; Finkbiner, J. A comparison of density functional methods for the estimation of proton chemical shifts with chemical accuracy. *J. Phys. Chem. A* **1999**, *103*, 7357–7362.

(93) Jain, R.; Bally, T.; Rablen, P. R. Calculating accurate proton chemical shifts of organic molecules with density functional methods and modest basis sets. *J. Org. Chem.* **2009**, *74*, 4017–4023.

(94) Jain, R.; Bally, T.; Rablen, P. R. Quantum-chemical simulation of 1H NMR spectra. 2.† Comparison of DFT-based procedures for computing proton–proton coupling constants in organic molecules. *J. Org. Chem.* **2011**, *76*, 4818–4830.

(95) Kelleghan, A. V.; Bulger, A. S.; Witkowski, D. C.; Garg, N. K. Strain-promoted reactions of 1,2,3-cyclohexatriene and its derivatives. *Nature* **2023**, *618*, 748–754.

CHAPTER FOUR

Synthesis and Reactivity of Nitrogen-Containing Strained Cyclic 1,2,3-Trienes

Dominick C. Witkowski, Daniel W. Turner, Ana S. Bulger, K. N. Houk, and Neil K. Garg

Nat. Synth. **2025**, *In press*. doi.org/10.1038/s44160-025-00793-9

4.1 Abstract

Cyclic 1,2,3-trienes are a class of intermediates that confine a functional group with a preferred linear geometry into a ring. When the ring is sufficiently small, the 1,2,3-triene geometry becomes bent, leading to substantial strain and high reactivity. Whereas advances in cyclic 1,2,3-triene chemistry have focused on carbocyclic derivatives, the corresponding chemistry of their heteroatom-containing counterparts remains unexplored. Here we report the fluoride-mediated generation and trapping of six-membered azacyclic 1,2,3-trienes in a host of reactions, including (4+2) and (3+2) cycloadditions and σ-bond insertions, allowing for the synthesis of annulated pyridones. Moreover, computational studies provide insight into their structure and reactivity. This study pushes the limits of strained intermediate chemistry, while also laying the foundation for the further strategic use of strained cyclic 1,2,3-trienes as unconventional, but useful synthetic building blocks.

4.2 Introduction

Strained cyclic intermediates with functionality that is geometrically distorted from a preferred geometry are of great interest to the synthetic community.[1,2] Breakthroughs in this field include the synthetic chemistry of *o*-benzyne (**4.1**),[3,4,5] cyclohexyne (**4.2**),[6] and 1,2-cyclohexadiene (**4.3**)[7,8,9] (Figure 4.1A). Moreover, heterocyclic variants (e.g., **4.4**–**4.7**) provide an entryway to access functionalized nitrogen-containing heterocycles.[10,11] These compounds (e.g., **4.4**–**4.7**) have been used for the synthesis of bioactive molecules and natural products,[12,13,14,15] materials,[16] DNA-encoded libraries,[17] and more.[11]

Another intriguing class of strained intermediates is cyclic 1,2,3-trienes (e.g., **4.8**, Figure 4.1B). In contrast to arynes, strained nonaromatic cyclic alkynes, and strained cyclic allenes, for which thousands of reports on their study and usage exist, cyclic 1,2,3-trienes are much less explored. These species have largely been the subject of theoretical investigations[18,19,20,21,22,23,24] historically, although 1,2,3-cyclohexatriene (**4.8**) was validated experimentally in 1990 by the Johnson group.[25] Following this seminal report, evidence for the formation of 1,2,3-cyclohexatrienes has been reported in the literature using a range of different methods.[26,27,28,29,30,31,32] Recently, further studies from our laboratory showed that 1,2,3-cyclohexatriene (**4.8**) and substituted derivatives can engage in several types of cycloaddition and nucleophilic addition reactions, providing an unconventional means to access structurally complex molecules.[33,34]

Strained heterocyclic 1,2,3-trienes (e.g., **4.9**, Figure 4.1B) remain an underexplored frontier in strained intermediate chemistry. The development of chemistry to generate and trap such intermediates could provide an entryway into accessing a variety of functionalized nitrogen-containing heterocycles, which are important motifs in pharmaceuticals[35,36,37] and natural

products.[38] Additionally, in comparison to 1,2,3-triene **4.8**, the direct attachment of a heteroatom to the cumulated triene could plausibly lead to regioselective trapping reactions based on analogy to results seen for other azacyclic strained intermediates.[39,40,41]

With these considerations in mind, we pursued the generation and trapping of 1,2,3-triene **4.9** and its derivatives. We show that trapping of this previously unknown species with cycloaddition partners **4.10** provides a means to access functionalized pyridones **4.11**. Functionalized pyridones are present in medicines and natural products, and are well poised for further elaboration.[42,43] Moreover, we report computational studies that shed light on the structure and reactivity of this unusual strained intermediate, including an analysis of regioselectivities using the distortion/interaction activation strain (DIAS) model.[44]

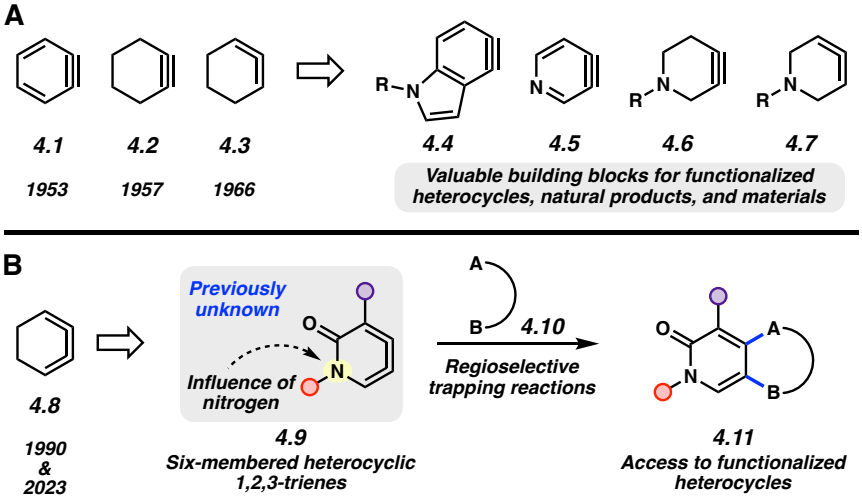

Figure 4.1. Background and overview. (A) Survey of strained alkynes and allenes. (B) Focus of present study involving azacyclic 1,2,3-trienes **4.9**.

4.3 Geometric and Electronic Structure of Cyclic 1,2,3-Trienes

We initiated our studies by assessing the impact of the amide on the geometry and electronic structure of the cyclic 1,2,3-triene structure. Figure 4.2A displays the geometry-optimized structure of 1,2,3-cyclohexatriene (**4.8**), and the targeted azacyclic 1,2,3-triene **4.12**

obtained from DFT calculations using B3LYP/6-31G(d). This level of theory was selected because of its previous application to the study of related strained intermediate structure and reactivity (see Section 4.9.3.2 for details).[45,46] 1,2,3-Cyclohexatriene (**4.8**) has C_2 symmetry and shows deformed internal angles of 131° at C2 and C3, in agreement with previous studies (see Section 4.9.3.3 for details).[18,33] Analysis of the structure of azacyclic 1,2,3-triene **4.12** shows that it is unsymmetrically distorted in comparison to 1,2,3-triene **4.8**, with internal angles of 139° and 115° at C4 and C5, respectively. We attribute this to the inductive effects imparted by the electronegative nitrogen atom, analogous to prior studies of heterocyclic alkynes.[45,47] More specifically, in accordance with Bent's rule and prior studies of related strained intermediates,[48,49,50] polarization of the C6–N bond toward *N* leads to rehybridization of the orbitals of the internal carbons on triene **4.12**. The hybrid bonding orbitals at C5 (closer to the *N*-atom) possess more p character than on C4, which translates to the compressed internal angle at C5.

Figure 4.2B provides the calculated electrostatic potential (ESP) map, natural bond orbital (NBO) charges, and frontier molecular orbitals (FMOs) of azacyclic 1,2,3-triene **4.12**. Consistent with the aforementioned rehybridization due to inductive effects, C5 bears a partial negative charge of –0.16, whereas C4 has a partial positive charge of +0.17. With regard to the FMOs of azacyclic 1,2,3-triene **4.12**, the calculated highest occupied molecular orbital (HOMO) and lowest unoccupied molecular orbital (LUMO) are depicted, showcasing that the HOMO is largely localized to the conjugated diene π-system (C3=C4–C5=C6). The LUMO is largely localized to the central, in-plane C4=C5 π-bond that lies orthogonal to the diene. Energetically, **4.12** has a HOMO energy of –8.4 eV and a LUMO energy of 1.5 eV. We also find that the HOMO–1 is largely localized to the in-plane C4=C5 π-bond and has an energy of –10.5 eV (see Section 4.9.3.4

for details). Overall, the electronic structure of **4.12** shares many similarities with related carbocyclic trienes (e.g., **4.8**),[33] albeit with the significant unsymmetrical distortion imparted by the *N*-atom. The carbonyl also has a small effect on the unsymmetric distortion (see Section 4.9.3.7 for details). Given previous studies of unsymmetrically distorted transient strained intermediates,[50] we posited that **4.12** could undergo regioselective trapping reactions and probed this notion in studies described below.

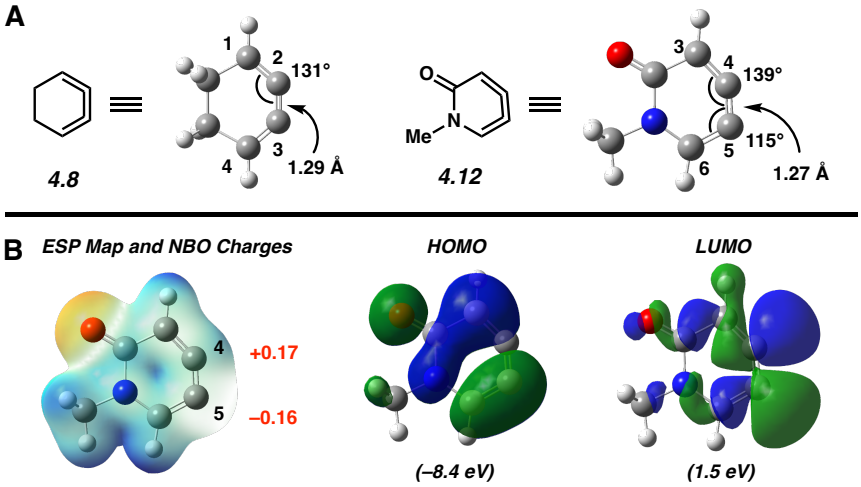

Figure 4.2. (A) Geometry-optimized structures of 1,2,3-cyclohexatriene (**4.8**) and azacyclic 1,2,3-triene **4.12** (B3LYP/6-31G(d)). (B) Electrostatic potential (ESP) map with C4 and C5 natural bond orbital (NBO) charges (B3LYP/6-31G(d)) and frontier molecular orbitals (FMOs) of azacyclic 1,2,3-triene **4.12** (HF/6-31G(d)//B3LYP/6-31G(d)).

4.4 Synthesis of Azacyclic 1,2,3-Triene Precursor

Encouraged by our initial computational findings, we pursued a means to access azacyclic 1,2,3-triene **4.12**. We ultimately synthesized silyl nonaflate **4.17** (Figure 4.3A) following extensive consideration and evaluation of possible azacyclic triene precursors. Silyl sulfonates have proven to be valuable precursors to various strained intermediates based on Kobayashi's versatile approach that relies on mild fluoride-mediated elimination.[11] Although triflates are most commonly used in analogous Kobayashi-type eliminations, nonaflates were attractive due to the

potential stability of cyclic triene precursors[51,52] and their comparable leaving group ability.[53,54] Moreover, empirically we found that the use of silyl nonaflate **4.17** led to slightly improved outcomes in trapping experiments compared to when the corresponding triflate was employed (see Section 4.9.2.3 for details). The use of a bromide in place of a sulfonate was deemed ineffective. The identity of the silyl substituent was also evaluated during our exploratory studies. Although different silyl substituents could be employed, we focused on triethylsilyl, which provides an adequate balance of substrate stability and reactivity in strained intermediate generation.

With regard to synthetic routes to **4.17**, unsuccessful strategies that were pursued to access silyl sulfonates involved directed metalations and cross-couplings of pyridones in attempts to access silylated pyridones. Furthermore, attempts were made to directly access the desired 1,2,3-triene precursor by oxidation of Kobayashi precursors to 3,4-pyridynes. We ultimately found that 1,2,3-triene precursor **4.17** could be derived from 5-bromo-2-methoxypyridine (**4.13**), which is commercially available. *ortho*-Silylation of **4.13** proceeded smoothly to deliver known silyl bromide **4.14**.[55] Next, a one-pot procedure involving lithium-halogen exchange, borylation, and oxidation[56] provided pyridinol **4.15**. Following nonaflation,[57] *O*-demethylation with in situ-generated Me_3SiI[58] followed by *N*-methylation[59] gave silyl nonaflate **4.17**.

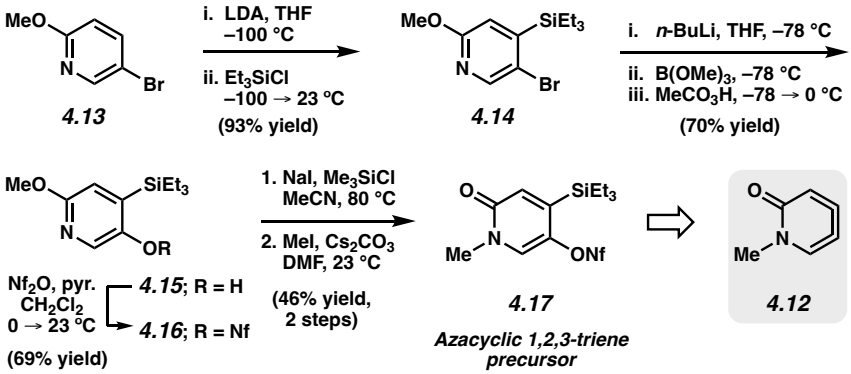

Figure 4.3A. Synthesis of triene precursor **4.17**.

4.5 Generation and Trapping of Azacyclic 1,2,3-Trienes in (4+2) Cycloadditions

With a suitable precursor in hand, we studied azacyclic 1,2,3-triene generation and trapping. Selected results are shown in Figure 4.3B, wherein precursor **4.17** was treated with a fluoride source in the presence of 2,5-dimethylfuran (**4.18**) using THF as solvent. We were delighted to observe the formation of cycloadduct **4.19** under several conditions, albeit with variable yields. For example, the use of tetra-*n*-butylammonium fluoride hydrate (TBAF•H_2O) at 60 °C (entry 1) furnished 19 in 23% yield. Changing the fluoride source to tetramethylammonium fluoride (TMAF) or tris(dimethylamino)sulfonium difluorotrimethylsilicate (TASF) led to slight increases in yields (entries 2 and 3, respectively). We also evaluated alkali fluoride salts and additives. Whereas the use of CsF was ultimately found to give comparable results to TBAF•H_2O (entry 4; compared with entry 1), the use of CsF with fluoride solubilizing agent *n*-Bu_4NOTf led to an improved yield of 50% (entry 7). Finally, it was found that the use of KF and 18-crown-6 led to further improvement, generating cycloadduct **4.19** in 56% yield after 2.5 h (entry 8).

These empirical findings highlight the important role of fluoride solubility and the challenges associated with strained intermediate generation and trapping. We posit that the use of an inorganic fluoride source (i.e., KF) with a crown ether leads to sparing fluoride solubility, which, in turn, leads to slow formation and low effective concentration of the highly reactive

azacyclic 1,2,3-triene intermediate. As ^{1}H NMR spectra of the crude reaction mixtures typically show the desired product with few impurities, we speculate that the remainder of mass is lost to nonspecific decomposition pathways involving the transient 1,2,3-triene **4.12**. This is consistent with prior studies of 1,2,3-triene **4.8**[33] and 2,3-pyridynes[40] and can be rationalized by the high strain and severe geometric distortion present in the azacyclic triene intermediate.

The proposed azacyclic 1,2,3-triene **4.12** has not been directly observed, but evidence exists for its intermediacy. First and foremost, analogous to the well-established chemistry of arynes, cyclic nonaromatic alkynes, cyclic allenes, and other highly strained intermediates, the intermediacy of **4.12** is supported by the formation of various cycloadducts, as is shown further below. Moreover, we highlight that: (1) reactions do not proceed unless fluoride is present (see Section 4.9.2.3 for details), (2) an isomeric silyl nonaflate, wherein the positioning of the silyl and nonaflate substituents were swapped, was tested and performs comparably in this methodology, which supports the likelihood of a common transient intermediate (see Section 4.9.2.6 for details), and (3) preliminary calculations are in-line with earlier computational studies of arynes,[60,61] and demonstrate that azacyclic 1,2,3-triene formation and trapping is kinetically and thermodynamically feasible using Kobayashi-type conditions. A more thorough discussion of these energetics will be reported elsewhere.

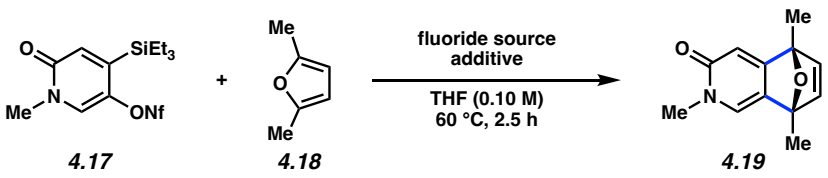

Entry	Fluoride Source	Additive	Yield[a]
1	TBAF·H_2O (1.5 equiv)	–	23%
2	TMAF (1.5 equiv)	–	30%
3	TASF (1.5 equiv)	–	33%
4	CsF (10 equiv)	–	24%
5	CsF (10 equiv)	*n*-Bu_4NBr (2.0 equiv)	24%
6	CsF (10 equiv)	*n*-Bu_4NI (2.0 equiv)	24%
7	CsF (10 equiv)	*n*-Bu_4NOTf (2.0 equiv)	50%
8	KF (2.0 equiv)	18-crown-6 (2.0 equiv)	56%

Figure 4.3B. Survey of fluoride sources for 1,2,3-triene generation and trapping. [a] Yields determined by ^{1}H NMR spectroscopic analysis using mesitylene as an external standard.

As shown in Figure 4.4, by varying the two fragments, azacyclic 1,2,3-triene precursors **4.20** and dienes **4.21**, a variety of (4+2) cycloadducts **4.22** could be obtained. Azacyclic 1,2,3-triene **4.12** underwent trapping with various dienes, including a furan **4.18**, isobenzofuran **4.23**, cyclopentadiene (**4.25**), and pyrrole **4.27**, to provide fused pyridone-containing cycloadducts **4.19**, **4.24**, **4.26**, and **4.28** (entries 1–4, respectively). Other Diels–Alder trapping agents, such as *N*-Boc pyrrole and tetraphenylcyclopentadienone, were also successful, although led to lower yields of annulation products (see Section 4.9.2.4 for details). Azacyclic 1,2,3-trienes with different substituents were also accessible, with routes to suitable precursors and calculated ground state structures being shown in Sections 4.9.2 and 4.9.3, respectively. As seen in entries 5 and 6, *N*-phenyl (Ph) and *N*-benzyl (Bn) substituents on the triene fragment were tolerated, giving rise to cycloadducts **4.30** and **4.32**, respectively. In addition, two trienes bearing bromide substituents were trapped, *N*-benzyl derivative **4.33** and bromo-triene **4.35**, allowing access to cycloadducts **4.34** and **4.36** (entries 7 and 8, respectively) and providing a potential means for further manipulation. Lastly, cycloaddition of phenyl-substituted triene **4.37** gave **4.39** (entry 9). In all

cases, a large excess of diene **4.21** was used to maximize productive trapping, prior to decomposition of the highly reactive azacyclic 1,2,3-triene **4.9**. Furthermore, the general instability of **4.9** limits the scope of the trapping partners in comparison to what is seen in the chemistry of other strained intermediates (for unsuccessful trapping partners, see Section 4.9.2.4). Nonetheless, these results not only validate that azacyclic 1,2,3-trienes **4.9** can be generated, but also demonstrate how these intermediates allow for the rapid generation of pyridone-fused bridged bicycles that are well poised for further elaboration.

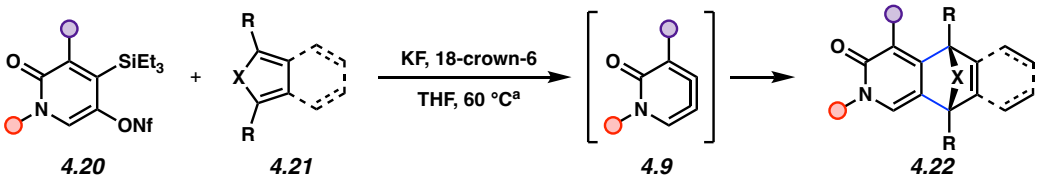

4.20 *4.21* *4.9* *4.22*

Entry	1,2,3-Triene		Diene		Product (yield)	
1	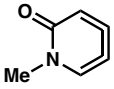	*4.12*	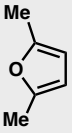	*4.18*	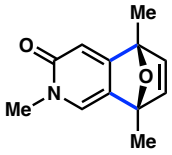	***4.19*** (56% yield)
2		*4.12*	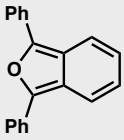	*4.23*	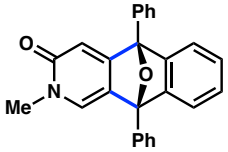	***4.24*** (51% yield)
3		*4.12*		*4.25*		***4.26*** (52% yield)[b]
4		*4.12*	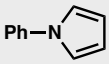	*4.27*	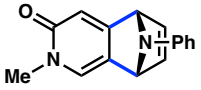	***4.28*** (48% yield)
5 6	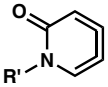	*4.29*; R' = Ph *4.31*; R' = Bn		*4.27*	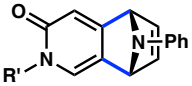	***4.30***; R' = Ph (44% yield) ***4.32***; R' = Bn (41% yield)
7	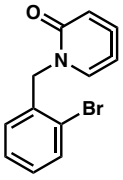	*4.33*		*4.23*	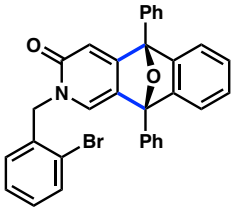	***4.34*** (46% yield)
8		*4.35*		*4.18*	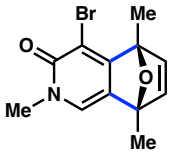	***4.36*** (47% yield)
9	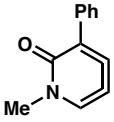	4.37		4.38	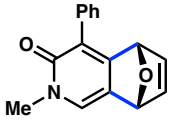	***4.39*** (64% yield)

Figure 4.4. Trapping reactions of azacyclic 1,2,3-trienes **4.9** with dienes **4.21** to give (4+2) cycloadducts **4.22**. Reactions were performed on 0.1 mmol scale. Yields reflect an average of two experiments. [a] Reactions conditions: **4.20** (1.0 equiv), **4.21** (5.0–20 equiv), KF (2.0 equiv), 18-crown-6 (2.0 equiv), THF (0.10 M), 60 °C, 2.5–6 h. [b] Yield determined by ^{1}H NMR spectroscopic analysis using mesitylene as an external standard.

4.6 Regioselective Trapping Experiments

As alluded to earlier, azacyclic 1,2,3-trienes have the potential to undergo regioselective trappings (see Figure 4.2 discussion). Heteroatom influence on such systems, where the heteroatom is directly attached to the 1,2,3-triene in a small ring, has not been tested previously. Thus, reactions were performed using azacyclic 1,2,3-triene precursor **4.17** in combination with either unsymmetrical cycloaddition partner **4.40** or nucleophilic annulation partner **4.42**[62] (Figure 4.5). Employing these trapping agents delivered adducts **4.41** and **4.43**, via (3+2) cycloaddition or formal C–N bond insertion, respectively. In both cases, regioselectivities were high, reflective of the pronounced distortion in **4.12**. We note that the use of other unsymmetrical trapping agents, such as 9-methoxyanthracene, an azomethine imine, a bicyclobutane, and a ketene acetal, led to lower yields of products, but provide further examples of regioselective trappings and access to additional functionalized pyridone products (see Section 4.9.2.5). In the case of trapping with nitrile oxide **4.40**, regioselectivity is attributed to the high nucleophilicity of C5 in the intermediate triene **4.12**, arising from the C5 angle constraint of 115° (see Figure 4.2). This results in low distortion energy for the transition state that involves C5 attack at the electrophilic terminus of the nitrile oxide, leading to **4.41**.[63] With nucleophile **4.42**, initial C4–N bond formation occurs leading to **4.43**, as the geometry at C4 in triene **4.12** (see Figure 4.2) is more distorted toward linearity (vide infra).[64] Interestingly, the analogous reaction of 2-methoxy-4,5-pyridyne, a constitutional isomer of azacyclic 1,2,3-triene **4.12** that possesses far less unsymmetrical geometric distortion (see Section 4.9.3.9), has been studied previously.[65] Trapping of 2-methoxy-4,5-pyridyne with

nucleophile **4.42** has been shown to proceed with poor regioselectivity (1.5:1), consistent with the 'aryne distortion model'.[46,50,64] This comparison underscores the substantial differences in geometric distortion between 2-methoxy-4,5-pyridyne and the isomeric azacyclic 1,2,3-triene **4.12**, despite these two species having very similar structures at a cursory level.

We also performed trapping with phenyl-substituted triene precursor **4.44** (Figure 4.5). In the case of (3+2) cycloaddition using **4.40**, cycloadduct **4.45** was obtained as the major product, analogous to the formation of **4.41**. However, when using trapping agent **4.42**, annulated product **4.46** was the major product, reflective of a switch in regioselectivity in comparison to the formation of **4.43** (vide infra). The results shown in Figure 4.5 not only highlight the influence of substituent effects, but also demonstrate that other annulations of azacyclic 1,2,3-trienes are possible and allow access to unique pyridone-containing products.

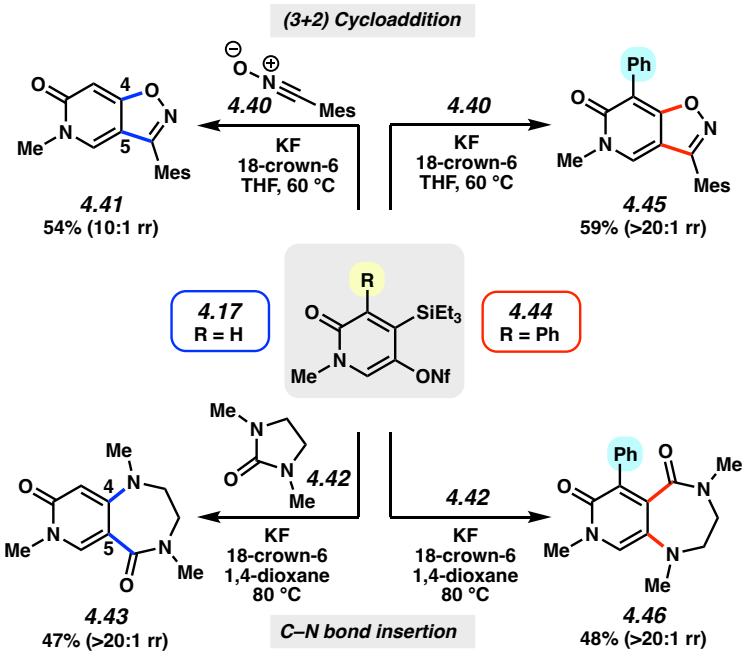

Figure 4.5. Regioselective reactions of azacyclic 1,2,3-trienes. See Section 4.9.2.5 for reaction details. Regioselectivities reported as a ratio of isomers formed (rr) as determined by ^{1}H NMR spectroscopic analysis of the crude reaction mixtures.

4.7 Computational Analysis of Regioselective Trapping Reactions

Given the varying sense of regioselectivities observed in the aforementioned trapping experiments involving 1,3-dimethyl-2-imidazolidinone (**4.42**), we performed DFT calculations to analyze competing transition states for the trapping reactions of trienes **4.12** and **4.37**. Key aspects are provided here; further details are available in the Sections 4.9.3.12–4.9.3.14. Regarding the trapping of 1,2,3-triene **4.12**, the competing transition states are **TS-4.1a** and **TS-4.1b**, with favorable activation barriers of 14.6 kcal mol^{-1} and 17.5 kcal mol^{-1}, respectively (Figure 4.6). The addition of **4.42** to C4 of azacyclic 1,2,3-triene **4.12** (**TS-4.1a**) was found to be favored over attack at C5 (**TS-4.1b**) by 2.9 kcal mol^{-1}. Consistent with prior studies of related strained intermediates, flattening at the carbon undergoing attack is seen in both **TS-4.1a** and **TS-4.1b**. For **TS-4.1a**, this requires minimal change in the geometry of the triene fragment. More specifically, the internal angle at C4 is 139° in **4.12** and 142° in **TS-4.1a**. On the other hand, significant geometric reorganization of the triene geometry is required to reach **TS-4.1b** from **4.12**, as judged by the change in the C5 internal angle (115° in **4.12** versus 129° in **TS-4.1b**), and the C4 internal angle (139° in **4.12** versus 121° **in TS-4.1b**).

To further probe this notion, a distortion/interaction strain (DIAS) analysis[44] of **TS-4.1a** and **TS-4.1b** was performed (Figure 4.6A). Thus, the $\Delta E^{\ddagger}$ for each transition state was broken down into the $\Delta E^{\ddagger}$ for distortion ($\Delta E_{dist,total}^{\ddagger}$) and the $\Delta E^{\ddagger}$ for interaction ($\Delta E_{int}^{\ddagger}$). The $\Delta E_{dist,total}^{\ddagger}$ was further broken down into $\Delta E^{\ddagger}$ for distortion of each fragment, **4.12** and **4.14** ($\Delta E_{dist,(\mathbf{4.12})}\ddagger$ and $\Delta E_{dist,(\mathbf{4.42})}^{\ddagger}$, respectively). For the disfavored transition state, **TS-4.1b**, the notable $\Delta E_{dist,total}^{\ddagger}$ of 6.6 kcal mol^{-1} is mostly attributed to the change in geometry of the triene fragment based on the $\Delta E_{dist,(\mathbf{4.12})}^{\ddagger}$ of 5.4 kcal mol^{-1}. Thus, the DIAS analysis corroborates the notion that C4 attack is highly favored due to triene **4.12** being pre-distorted toward the favorable transition state geometry

seen in **TS-4.1a**. The large magnitude of both $\Delta E_{int}^{\ddagger}$ and $\Delta E_{dist,total}^{\ddagger}$ for attack at C5 also arises from the shift to a much later transition state (2.20 Å in **TS-4.1b** versus 2.99 Å in **TS-4.1a**) to overcome the distortion.

Figure 4.6B shows the corresponding competing transition states for the reaction of triene **4.37** with trapping agent **4.42**. Consistent with experiments, computations show that attack at C5 (**TS-4.2b**) is favored over attack at C4 (**TS-4.2a**) by 5.8 kcal mol^{-1} primarily due to the ~10 kcal mol^{-1} destabilization of **TS-4.2a** versus **TS-4.1a**. Thus, both experiments and computations reflect a flip in regioselectivity for the reaction of triene **4.37** compared to triene **4.12**. The changes in internal angles at C4 and C5 in considering **4.37** versus **TS-4.2a** and **TS-4.2b** are comparable to what is seen in the analysis of **4.12** shown in Figure 4.6A. However, a significant steric clash between the nucleophile with the phenyl substituent is present in **TS-4.2a**, which presumably leads to this transition state (i.e., attack at C4) being disfavored.

We performed a DIAS analysis of **TS-4.2a** and **TS-4.2b** to further interrogate the regioselectivity (Figure 4.6B). The $\Delta\Delta E_{dist,total}^{\ddagger}$ was calculated to be –12.0 kcal mol^{-1}, versus the $\Delta\Delta E_{int}^{\ddagger}$ of 7.6 kcal mol^{-1}, showing the important role that geometric distortion plays in the favorability of **TS-4.2b**. For **TS-4.2b** (C5 attack), the $\Delta E_{dist,(\mathbf{4.37})}^{\ddagger}$ is calculated to be 6.4 kcal mol^{-1}, which reflects a small energetic penalty needed for **4.37** to undergo geometric reorganization to achieve the geometry in **TS-4.2b** (e.g., the internal angle at C5 is 115° in 37 and 129° in **TS-4.2b**). However, the corresponding $\Delta E_{dist,(\mathbf{4.37})}^{\ddagger}$ is more severe in **TS-4.2a** (C4 attack), with a calculated value of 13.7 kcal mol^{-1}. The $\Delta E_{dist,(\mathbf{4.42})}^{\ddagger}$ is also higher in **TS-4.2a** compared to **TS-4.2b** (6.5 versus 1.8 kcal mol^{-1}, respectively). Collectively, these distortion values for each fragment lead to a high $\Delta E_{dist,total}^{\ddagger}$ in **TS-4.2a** of 20.2 kcal mol^{-1}, which is attributed to the steric clash between the Ph substituent and fragment **4.42**.

We summarize by highlighting that: (1) geometric pre-distortion of the triene fragment toward a transition state geometry is generally favorable (i.e., **TS-4.1a** favored over **TS-4.1b**); (2) however, if large substituents are present, additional steric factors may override this preference, leading to a relative flip in regioselectivity (i.e., **TS-4.2b** favored over **TS-4.2a**). Nonetheless, findings from DFT calculations correlate with experimental results; regioselective outcomes of reactions of heterocyclic 1,2,3-trienes can plausibly be predicted in future studies.

A

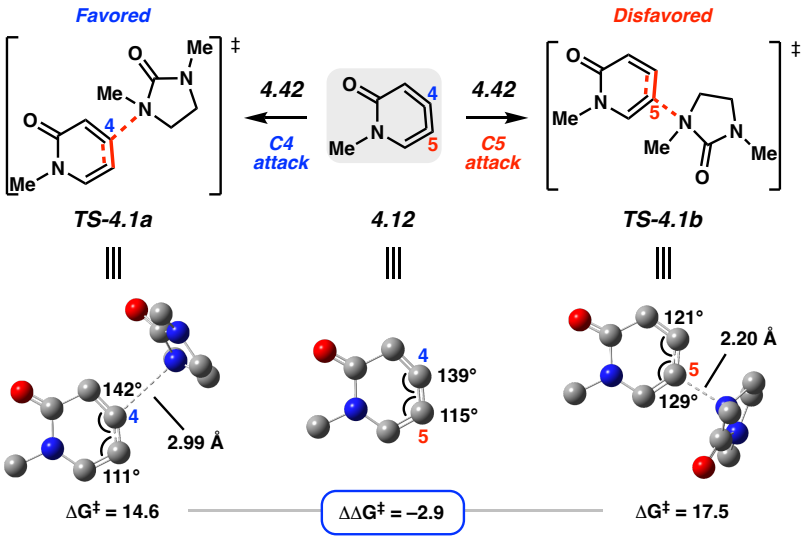

DIAS Analysis

	TS-4.1a / C4 attack	*TS-4.1b* / C5 attack	Difference (ΔΔE‡)
Energy (ΔE‡)	–0.9	0.6	–1.5
• Interaction Energy ($\Delta E_{int}^{\ddagger}$)	–1.3	–6.0	4.7
• Distortion Energy ($\Delta E_{dist,total}^{\ddagger}$)	0.4	6.6	–6.2
○ $\Delta E_{dist,(4.12)}^{\ddagger}$	0.4	5.4	–5.0
○ $\Delta E_{dist,(4.42)}^{\ddagger}$	0.0	1.2	–1.2

B

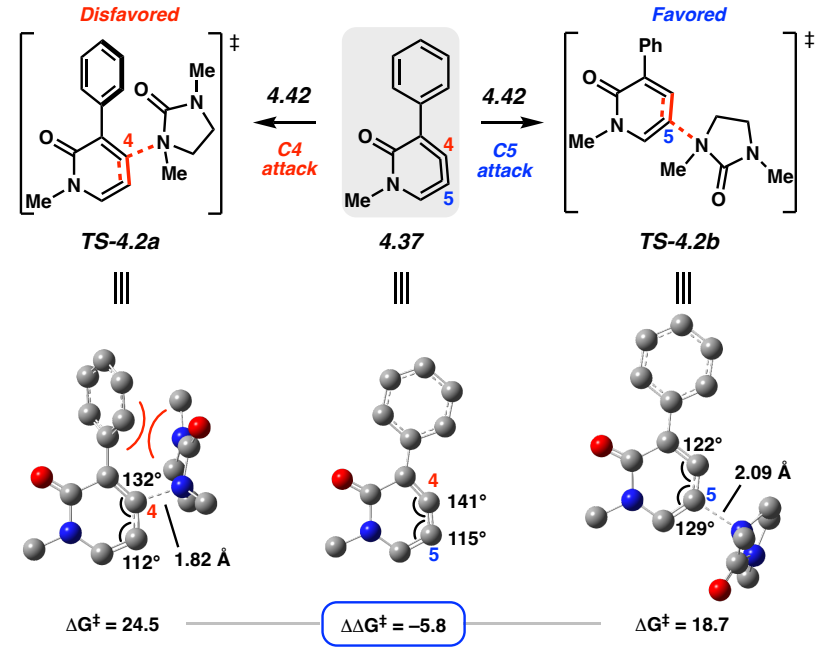

DIAS Analysis

	TS-4.2a / C4 attack	*TS-4.2b* / C5 attack	Difference (ΔΔE‡)
Energy (ΔE‡)	5.5	1.1	–4.4
• Interaction Energy ($\Delta E_{int}^{\ddagger}$)	–14.7	–7.1	7.6
• Distortion Energy ($\Delta E_{dist,total}^{\ddagger}$)	20.2	8.2	–12.0
○ $\Delta E_{dist,(4.37)}^{\ddagger}$	13.7	6.4	–7.3
○ $\Delta E_{dist,(4.42)}^{\ddagger}$	6.5	1.8	–4.7

Figure 4.6. Transition state analysis at 353.15 K of additions of 1,3-dimethyl-2-imidazolidinone (**4.42**) to azacyclic 1,2,3-trienes **4.12** and **4.37** (B3LYP/6-311+G(d,p)/SMD(1,4-dioxane)//B3LYP/6-31G(d)). (A) Transition state analysis of addition of **4.42** to **4.12** and distortion/interaction activation strain (DIAS) analysis. (B) Transition state analysis of addition of **4.42** to **4.37** and distortion/interaction activation strain (DIAS) analysis. The $\Delta G^{\ddagger}$ (Gibbs free energy) and the $\Delta E^{\ddagger}$ (electronic energy) values were consistent with experimental regiochemical observations. A distortion/interaction activation strain (DIAS) analysis was performed, where the $\Delta E^{\ddagger}$ was broken down into $\Delta E^{\ddagger}$ of interaction and $\Delta E^{\ddagger}$ of distortion. $\Delta E^{\ddagger}$ of distortion was further broken down into the $\Delta E^{\ddagger}$ of distortion for each reactant. Energies are provided in kcal mol^{-1}.

4.8 Conclusion

We have detailed the generation and trapping of six-membered azacyclic 1,2,3-trienes. These reactive intermediates are geometrically distorted from a typical linear geometry of 1,2,3-trienes. Moreover, inductive effects as a result of the directly attached *N*-atom leads to unsymmetric distortion with respect to the 1,2,3-triene unit. Trapping of the azacyclic trienes allows for the synthesis of annulated pyridones. When an unsymmetrical cycloaddition partner or nucleophilic annulation partner is used, reactions occur regioselectively. Selectivities are rationalized by transition state modeling and a distortion/interaction activation strain analysis. Overall, this study pushes the limits of strained intermediate chemistry, while also laying the foundation for the further strategic use of strained cyclic 1,2,3-trienes as unconventional, but useful synthetic building blocks.

4.9 Experimental Section

4.9.1 Materials and Methods

Unless stated otherwise, reactions were conducted in flame-dried glassware under an atmosphere of nitrogen, and commercially obtained reagents were used as received unless otherwise specified. Anhydrous solvents were either freshly distilled or passed through activated alumina columns, unless otherwise stated. Non-commercially available substrates were

synthesized according to known preparations or following protocols specified in the Experimental Procedures. Prior to use in trapping experiments, tetrahydrofuran (THF) and 1,4-dioxane were passed through an activated alumina column and degassed by five freeze-pump-thaw cycles. Dimethylformamide (DMF), 1,2-dimethoxyethane (DME), acetonitrile (MeCN), dichloromethane, toluene, and triethylamine (Et_3N) were passed through an activated alumina column prior to use. Diisopropylamine, pyridine, trimethylsilyl chloride, and triethylsilyl chloride were distilled over CaH_2 prior to use. Triflic anhydride (Tf_2O) was distilled over P_2O_5 prior to use. Dicyclopentadiene was cracked and cyclopentadiene (**4.25**) was stored at –24 °C prior to use. Potassium fluoride (KF), *n*-butyllithium (*n*-BuLi), nonafluorobutanesulfonic anhydride (Nf_2O), peracetic acid (39 wt. % in acetic acid), tetrabutylammonium trifluoromethanesulfonate (Bu_4NOTf), tetrabutylammonium bromide (Bu_4NBr), tetrabutylammonium iodide (Bu_4NI), tris(dimethylamino)sulfonium difluorotrimethylsilicate (TASF), tetramethylammonium fluoride (TMAF), tetrabutylammonium fluoride (TBAF) solution (1.0 M in THF), diisobutylaluminum hydride (DIBAL) solution (1.0 M in hexanes), 2,5-dimethylfuran (**4.18**), *N*-Ph pyrrole (**4.27**), dicyclopentadiene, tetraphenylcyclopentadienone (**4.61**), imidazole, 10% palladium on activated carbon powder (Pd/C), Kryptofix® 222, copper (I) chloride, benzyl bromide (BnBr), mesitylene, triglyme, allyl bromide, *N*-bromosuccinimide (NBS), and Florisil® (<200 mesh, fine powder) were all purchased from Sigma-Aldrich. Cesium carbonate, tetrakis(triphenylphosphine)palladium(0), tetrabutylammonium fluoride hydrate ($TBAF•H_2O$), and cesium fluoride (CsF) were obtained from Strem Chemicals and used as received. Methyl iodide (MeI), hydrochloric acid, and trimethyl borate (99%, metals basis) were obtained from Thermofisher Scientific. Tripotassium phosphate, ethyl alcohol (EtOH), 2-methyltetrahydrofuran (2-MeTHF) were obtained from Acros Organics. 1,3-Dimethyl-2-imidazolidinone (DMI) (**4.42**)

was obtained from Alfa Aesar. 5-bromo-2-methoxy-pyridine (**4.13**) and 1,3-diphenylisobenzofuran (**4.23**) were purchased from Combi Blocks. *N*-Boc pyrrole (**4.59**) and 5-bromo-2-methoxypyridin-4-ol (**4.73**) were purchased from AmBeed. Methyl 3-(4-bromophenyl)bicyclo[1.1.0]butane-1-carboxylate (**4.69**) was purchased from Enamine and purified on silica prior to use (hexanes:EtOAc). 18-Crown-6 was purchased from Chem Impex International, azeotroped with benzene, and stored in a glovebox prior to use. Sodium iodide, triflic anhydride (Tf_2O), trimethylsilyl chloride, trielthylsilyl chloride, triisopropylsilyl chloride (TIPSCl), pivaloyl chloride (PivCl), phenylboronic acid, and 2-bromobenzyl bromide were purchased from Oakwood chemicals.

Reaction temperatures at or above 23 °C were controlled using an IKAmag temperature modulator, and unless stated otherwise, performed at room temperature (approximately 23 °C). Thin-layer chromatography (TLC) was conducted with EMD gel 60 F_{254} pre-coated plates (0.25 mm for analytical chromatography and 0.50 mm for preparative chromatography) and visualized using a combination of UV, anisaldehyde, potassium permanganate, and Dragendorff's reagent staining techniques. Silicycle Siliaflash P60 (particle size 40–63 μm) was used for flash column chromatography and RediSep Gold Silica (20–40 μm) and RediSep Gold C18 (20–40 μm) were used for automated column chromatography on a CombiFlash NextGen 300+ instrument unless otherwise specified. Monster pipette refers to "Kimble 5-3/4 Soda Lime Disposable Glass Monster Pipette" and was purchased from VWR (catalog #50880-040). ^{1}H-NMR and 2D-NOESY spectra were recorded on Bruker spectrometers (at 300, 400, 500, and 600 MHz) and are reported relative to the residual solvent signal. Data for ^{1}H-NMR spectra are reported as follows: chemical shift (δ ppm), multiplicity, coupling constant (Hz) and integration. ^{13}C-NMR spectra were recorded on

Bruker spectrometers (at 100, 125, and 150 MHz) and are reported relative to the residual solvent signal. Data for ^{13}C-NMR spectra are reported in terms of chemical shift (δ ppm) and, when necessary, multiplicity, and coupling constant (Hz). ^{19}F NMR spectra were recorded on Bruker spectrometers (at 282, 376, and 565 MHz) and are reported in terms of chemical shift (δ ppm), multiplicity, and integration. ^{1}H NMR yields were determined by addition of an aliquot of a stock solution of mesitylene in acetone-d_6 to the concentrated crude reaction mixture followed by further dilution with acetone-d_6 and subsequent ^{1}H NMR analysis. IR spectra were recorded on a Perkin-Elmer UATR Two FT-IR spectrometer and are reported in terms of frequency absorption (cm^{-1}). DART-MS spectra were collected on a Thermo Exactive Plus MSD (Thermo Scientific) equipped with an ID-CUBE ion source and a Vapur Interface (IonSense Inc.). Both the source and MSD were controlled by Excalibur software version 3.0. The analyte was spotted onto OpenSpot sampling cards (IonSense Inc.) using $CDCl_3$, CH_2Cl_2 or acetone as the solvent. Ionization was accomplished using UHP He plasma with no additional ionization agents. The mass calibration was carried out using Pierce LTQ Velos ESI (+) and (–) Ion calibration solutions (Thermo Fisher Scientific). ESI-TOF measurements were carried out in positive ionization mode on an Agilent 6545 Q-TOF LC/MS system with 1260 Infinity LC and electrospray ionization (ESI) controlled by Agilent Mass Hunter Workstation Data Acquisition version 10.1 software, or a Waters LCT-Premier TOF LC/MS with Acquity UPLC and electrospray ionization (ESI) controlled by MassLynx 4.1 software (Waters Corporation, Milford MA). Analytes were dissolved in MeCN or MeOH. Data collection and analysis were performed using Mass Hunter Acquisition and Qualitative Analysis software (Agilent). Melting points were measure using a DigiMelt MPA160 melting point apparatus.

Silyl bromide **4.14**[55], silyl triflate **4.47**[66], nitrile oxide **4.40**[67], bis(phenyl)iodonium triflate ($Ph_2(I)OTf$)[68], 9-methoxyanthracene (**4.64**)[69], azomethine imine **4.67**[70], and 1,2-diethyoxyethene (**4.71**) [71] are all known compounds. The ^1H NMR spectral data matches those reported in literature.

4.9.2 Experimental Procedures

4.9.2.1 Synthesis of Unsubstituted Silyl Nonaflate and Silyl Triflate Precursors

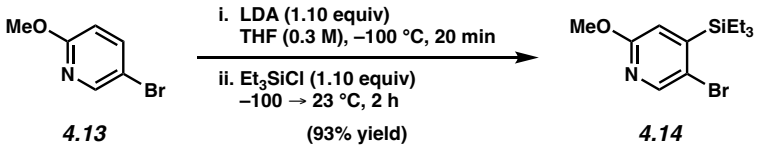

4.13 (93% yield) *4.14*

Silyl Bromide 4.14. To a solution of diisopropylamine (6.31 g, 8.80 mL, 62.4 mmol, 1.15 equiv) in THF (130 mL) at –100 °C under nitrogen atmosphere was added *n*-BuLi (2.3 M in hexanes, 25.9 mL, 59.7 mmol, 1.10 equiv) dropwise over 5 min. The cooling bath was removed and the resulting solution was stirred for 30 min. The mixture was again cooled to –100 °C and stirring was continued for 10 min. A solution of pyridine **4.13** (10.2 g, 54.2 mmol, 1.00 equiv) in THF (51 mL) was added slowly dropwise via cannula over 30 min. The mixture was allowed to stir at –100 °C for 20 minutes and then triethylsilyl chloride (8.99 g, 10.0 mL, 59.7 mmol, 1.10 equiv) was added dropwise over 5 min at –100 °C. The cooling bath was removed and stirring was continued for 2 h while the reaction warmed to 23 °C. After this time, the mixture was quenched with deionized water (80 mL), diluted Et_2O (50 mL), and the layers were separated. The aqueous layer was extracted Et_2O (2 x 50 mL). The combined organic layers were combined, washed with brine (50 mL), dried over sodium sulfate, filtered, and concentrated under reduced pressure to give a dark orange oil. The crude residue was purified by flash chromatography (hexanes → 9:11 hexanes:Et_2O) to provide silyl bromide **4.14** (15.2 g, 50.3 mmol, 93% yield) as a light yellow oil.

Silyl Bromide 4.14: R_f 0.65 (1:1 hexanes:benzene); ^{1}H NMR (500 MHz, $CDCl_3$): δ 8.18 (s, 1H), 6.77 (s, 1H), 3.90 (s, 3H), 0.97–0.91 (m, 15H). Spectral data match those previously reported.[55]

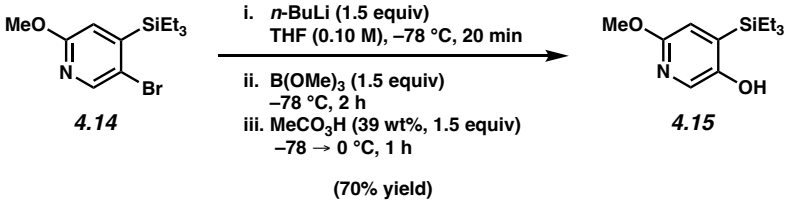

Silyl alcohol 4.15. To a solution of silyl bromide **4.14** (2.9 g, 9.6 mmol, 1.0 equiv) in THF (96 mL, 0.10 M) at –78 °C was added *n*-BuLi (2.3 M in hexanes, 6.3 mL, 14 mmol, 1.5 equiv) dropwise over 5 min. The resulting solution was stirred at this temperature for 20 min, then trimethyl borate (1.5 g, 1.6 mL, 14 mmol, 1.5 equiv) was added dropwise over 5 min. Stirring was continued at this temperature for 2 h then peracetic acid (2.8 g of a 39 wt% solution in glacial acetic acid, 2.5 mL, 14 mmol, 1.5 equiv) was added dropwise over 5 min. The reaction was then allowed to warm to 0 °C and stirring was continued for 1 h. After this time, the mixture was quenched at 0 °C with saturated aqueous sodium hydrogenosulfite (30 mL), which was added dropwise over 1 minute, and the resulting mixture was allowed to warm to 23 °C and stirred for 10 min. The mixture was then diluted further with deionized water (50 mL) and CH_2Cl_2 (50 mL) and the layers were separated. The aqueous layer was extracted CH_2Cl_2 (2 x 50 mL). The organic layers were combined, dried over sodium sulfate, filtered, and concentrated under reduced pressure. The crude residue was purified by flash chromatography (hexanes → Et_2O) to provide silyl alcohol **4.15** (1.6 g, 6.7 mmol, 70% yield) as a white solid. **Silyl alcohol 4.15**: Mp: 76–77 °C; R_f 0.37 (3:1 hexanes:EtOAc); ^{1}H NMR (600 MHz, C_6D_6): δ 7.29 (s, 1H), 6.94 (s, 1H), 4.29 (s, 1H), 3.86 (s, 3H), 0.98–0.93 (m, 9H), 0.87–0.80 (m, 6H); ^{13}C NMR (150 MHz, C_6D_6): δ 159.1, 152.1, 137.6,

131.4, 117.7, 53.3, 7.6, 3.3; IR (film): 3111, 2954, 1377, 1210, 724 cm^{-1}; HRMS-APCI (m/z) $[M + H]^+$ calcd for $C_{12}H_{22}NO_2Si^+$, 240.1414; found 240.1414.

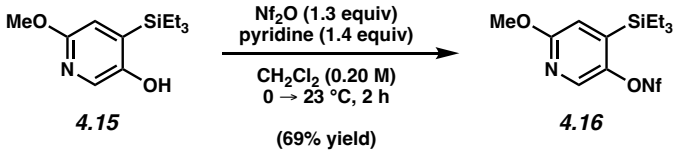

Silyl nonaflate 4.16. To a solution of silyl alcohol **4.15** (1.00 g, 4.18 mmol, 1.0 equiv) in CH_2Cl_2 (20.9 mL, 0.20 M) were added sequentially pyridine (463 mg, 473 μL, 5.85 mmol, 1.4 equiv) dropwise over 1 min and Nf_2O (3.16 g, 1.67 mL, 5.43 mmol, 1.3 equiv) dropwise over 1 min at 0 °C. After stirring at this temperature for 1 h, the reaction was warmed to 23 °C and stirred for an additional 1 h. After this time, the reaction was quenched with deionized water (15 mL) and diluted with CH_2Cl_2 (20 mL). The layers were then poured into a separatory funnel containing a mixture of saturated aqueous sodium bicarbonate (40 mL) and deionized water (20 mL). The organic and aqueous layers were separated and the aqueous layer was extracted CH_2Cl_2 (2 x 20 mL). The combined organic layers were dried over sodium sulfate, filtered, and concentrated under reduced pressure. The crude residue was purified by flash chromatography (hexanes → 3:1 hexanes:CH_2Cl_2) to provide silyl nonaflate **4.16** (1.49 g, 2.86 mmol, 69% yield) as a yellow oil. **Silyl nonaflate 4.16**: R_f 0.78 (3:1 hexanes:EtOAc); ^1H NMR (600 MHz, $CDCl_3$): δ 8.13 (s, 1H), 6.82 (s, 1H), 3.94 (s, 3H), 0.98–0.93 (m, 9H), 0.93–0.86 (m, 6H); ^{13}C NMR (125 MHz, $CDCl_3$): δ 162.3, 147.3, 144.0, 138.1 (t, J = 3.6), 120.9–106.0 (m), 118.6, 54.1, 7.2, 3.0; ^{19}F NMR (565 MHz, $CDCl_3$): δ –80.6–(–80.7) (m, 3F), –109.3–(–109.4) (m, 2F), –120.8–(–121.1) (m, 2F), –125.7–(–125.9) (m, 2F); IR (film): 2960, 1348, 1238, 1143, 1032 cm^{-1}; HRMS-ESI (m/z) $[M + H]^+$ calcd for $C_{16}H_{21}F_9NO_4SSi^+$, 522.0817; found 522.0833.

*Perfluorobutanesulfonyl fluoride (NfF), a less expensive alternative to Nf_2O, can also employed in these nonaflations. However, lower yields were obtained when using NfF in initial experiments. Furthermore, the corresponding triflates (e.g., **4.48**) are also viable precursors, as shown below. As reaction times for this chemistry are typically governed by the sparing solubility of inorganic fluoride sources (i.e., CsF and KF) in organic solvents, the reaction times when using nonaflates or triflates are generally comparable.*

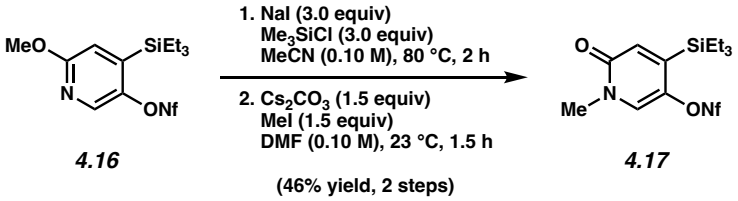

Silyl nonaflate 4.17. To a solution of silyl nonaflate **4.16** (1.89 g, 3.63 mmol, 1.0 equiv) in MeCN (36.3 mL, 0.10 M) were added sequentially NaI (1.63 g, 10.9 mmol, 3.0 equiv) in a single portion and trimethylsilyl chloride (1.18 g, 1.4 mL, 10.9 mmol, 3.0 equiv) dropwise over 1 min at 23 °C. The reaction flask was then fitted with an air condenser and heated to 80 °C in an oil bath. After stirring at this temperature for 2 h, the reaction was cooled to 23 °C and poured into a separatory funnel containing a 5 wt% solution of aqueous disodium thiosulfate (50 mL). The mixture was then diluted with EtOAc (50 mL), and the layers were separated. The aqueous layer was extracted with EtOAc (3 x 50 mL). The organic layers were combined, dried over sodium sulfate, filtered, and concentrated under reduced pressure to provide a light yellow solid (1.84 g) which was dissolved in DMF (36 mL, 0.10 M). To this solution were added sequentially Cs_2CO_3 (1.77 g, 5.44 mmol, 1.5 equiv) in a single portion and MeI (772 mg, 340 μL, 5.44 mmol, 1.5 equiv) dropwise over 1 min at 23 °C. The mixture was stirred at this temperature for 1.5 h. The reaction was then quenched with deionized water (20 mL). The biphasic mixture was then poured into a separatory

funnel containing deionized water (500 mL) and EtOAc (200 mL) and the layers were separated. The aqueous layer was extracted with EtOAc (3 x 100 mL). The organic layers were combined, washed with deionized water (3 x 100 mL), dried over sodium sulfate, filtered, and concentrated under reduced pressure. The crude residue was purified by flash chromatography (hexanes → 1:3 hexanes:EtOAc) to provide silyl nonaflate **4.17** (863 mg, 1.66 mmol, 46% yield, two steps) as an amber oil. **Silyl nonaflate 4.17**: R_f 0.58 (1:1 hexanes:EtOAc); ^{1}H NMR (600 MHz, $CDCl_3$): δ 7.34 (s, 1H), 6.67 (s, 1H), 3.54 (s, 3H), 0.97–0.92 (m, 9H), 0.88–0.82 (m, 6H); ^{13}C NMR (150 MHz, $CDCl_3$): δ 160.5, 147.0, 137.1, 129.7–129.6 (m), 129.1, 120.2–106.4 (m), 38.2, 7.2, 2.9; ^{19}F NMR (565 MHz, $CDCl_3$): δ –80.5–(–80.7) (m, 3F), –109.5–(–109.7) (m, 2F), –120.7–(–121.0) (m, 2F), –125.6–(–125.8) (m, 2F); IR (film): 2958, 1666, 1600, 1421, 1199 cm^{-1}; HRMS-ESI (m/z) [M + H]$^+$ calcd for $C_{16}H_{21}F_9NO_4SSi^+$, 522.0817; found 522.0840.

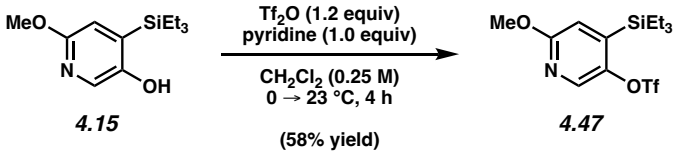

Silyl triflate 4.47. To a solution of silyl alcohol **4.15** (1.50 g, 6.27 mmol, 1.0 equiv) in CH_2Cl_2 (25 mL, 0.25 M) were added sequentially pyridine (496 mg, 507 μL, 6.27 mmol, 1.0 equiv) and Tf_2O (2.12 g, 1.26 mL, 7.52 mmol, 1.2 equiv) dropwise over 3 min at 0 °C. After stirring at this temperature for 3 h, the reaction was warmed to 23 °C and stirred for an additional 1 h. After this time, the reaction was quenched with saturated aqueous sodium bicarbonate (40 mL) and diluted with deionized water (70 mL). The organic and aqueous layers were separated and the aqueous layer was extracted CH_2Cl_2 (3 x 100 mL). The combined organic layers were dried over sodium sulfate, filtered, and concentrated under reduced pressure. The crude residue was purified by flash

chromatography (hexanes → 9:1 hexanes:EtOAc) to provide silyl triflate **4.47** (1.36 g, 3.66 mmol, 58% yield) as a light yellow oil. **Silyl triflate 4.47**: R_f 0.43 (9:1 hexanes:EtOAc); ^{1}H NMR (500 MHz, $CDCl_3$): δ 8.13 (s, 1H), 6.82 (s, 1H), 3.94 (s, 3H), 0.97–0.87 (m, 15H). Spectral data match those previously reported.[66]

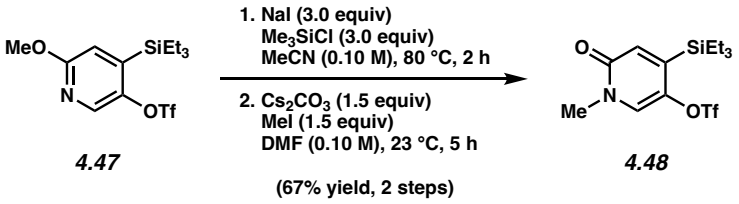

Silyl triflate 4.48. To a solution of silyl triflate **4.47** (1.38 g, 3.72 mmol, 1.0 equiv) in MeCN (37 mL, 0.10 M) were added sequentially NaI (1.67 g, 11.1 mmol, 3.0 equiv) in a single portion and trimethylsilyl chloride (1.21 g, 1.41 mL, 11.1 mmol, 3.0 equiv) dropwise over 1 min at 23 °C. The reaction flask was then fitted with an air condenser and heated to 80 °C in an oil bath. After stirring at this temperature for 2 h, the reaction was cooled to 23 °C and poured into a separatory funnel containing a 5 wt% solution of aqueous disodium thiosulfate (75 mL) and brine (75 mL). The mixture was then diluted with Et_2O (100 mL) and the layers were separated. The aqueous layer was extracted with Et_2O (2 x 100 mL). The organic layers were combined, dried over sodium sulfate, filtered, and concentrated under reduced pressure to provide a light yellow solid (1.33 g) which was dissolved in DMF (37 mL, 0.10 M). To this solution were added sequentially Cs_2CO_3 (1.82 g, 5.58 mmol, 1.5 equiv) in a single portion and MeI (792 mg, 349 μL, 5.58 mmol, 1.5 equiv) dropwise over 1 min at 23 °C. The mixture was stirred at this temperature for 5 h. The reaction was then quenched with deionized water (200 mL). The biphasic mixture was then poured into a separatory funnel containing brine (400 mL) and EtOAc (100 mL) and the layers were separated. The aqueous layer was extracted with EtOAc (2 x 100 mL). The organic layers were combined,

washed with deionized water (3 x 100 mL), dried over sodium sulfate, filtered, and concentrated under reduced pressure. The crude residue was purified by flash chromatography (hexanes → 3:2 hexanes:EtOAc) to provide silyl triflate **4.48** (921 mg, 2.48 mmol, 67% yield, two steps) as a pale yellow solid. **Silyl triflate 4.48**: Mp: 35–37 °C; R_f 0.63 (1:1 hexanes:EtOAc); ^{1}H NMR (600 MHz, $CDCl_3$): δ 7.37 (s, 1H), 6.68 (s, 1H), 3.54 (s, 3H), 0.97–0.92 (m, 9H), 0.87–0.81 (m, 6H); ^{13}C NMR (150 MHz, $CDCl_3$): δ 160.5, 146.9, 136.9, 129.4, 129.2, 118.5 (q, J = 319.9), 38.2, 7.2, 2.9; ^{19}F NMR (282 MHz, $CDCl_3$): δ –73.7 (m, 3F); IR (film): 2959, 2880, 1666, 1601, 1421 cm^{-1}; HRMS-APCI (m/z) $[M + H]^+$ calcd for $C_{13}H_{21}F_3NO_4SSi^+$, 372.0907; found 372.0906.

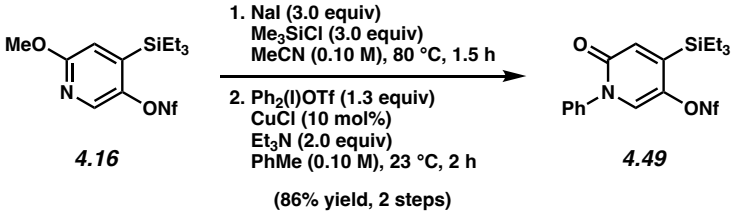

Silyl nonaflate 4.49. To a solution of silyl nonaflate **4.16** (500 mg, 959 μmol, 1.0 equiv) in MeCN (9.59 mL, 0.10 M) were added sequentially NaI (431 mg, 2.88 mmol, 3.0 equiv) in a single portion and trimethylsilyl chloride (313 mg, 364 μL, 2.88 mmol, 3.0 equiv) dropwise over 1 min at 23 °C. The reaction flask was then fitted with an air condenser and heated to 80 °C in an oil bath. After stirring at this temperature for 1.5 h, the reaction was cooled to 23 °C and poured into a separatory funnel containing a 5 wt% solution of aqueous disodium thiosulfate (50 mL) and brine (50 mL). The mixture was then diluted with EtOAc (50 mL), and the layers were separated. The aqueous layer was extracted with EtOAc (2 x 50 mL). The organic layers were combined, dried over sodium sulfate, filtered, and concentrated under reduced pressure to provide a light yellow solid (487 mg) which was transferred to a vial. To this vial were added sequentially bis(phenyl)iodonium triflate

(536 mg, 1.25 mmol, 1.3 equiv), CuCl (9.5 mg, 96 μmol, 0.10 equiv), triethylamine (194 mg, 267 μL, 1.92 mmol, 2.0 equiv), and toluene (9.59 mL, 0.10 M) at 23 °C. The mixture was stirred at this temperature for 2 h. The reaction was filtered over a Celite plug eluting with EtOAc (100 mL). The eluate was concentrated under reduced pressure. The crude material was purified by flash chromatography (19:1 hexanes:EtOAc → 9:1 hexanes:EtOAc) to provide silyl nonaflate **4.49** (480 mg, 822 μmol, 86% yield, two steps) as a white solid. **Silyl nonaflate 4.49**: Mp: 53–54 °C; R_f 0.13 (9:1 hexanes:EtOAc); ^{1}H NMR (600 MHz, acetone-d_6): δ 7.75 (s, 1H), 7.57–7.52 (m, 2H), 7.51–7.46 (m, 3H), 6.62 (s, 1H), 1.06–1.01 (m, 9H), 1.00–0.94 (m, 6H); ^{13}C NMR (150 MHz, acetone-d_6): δ 159.5, 147.2, 141.2, 137.5, 131.4, 130.6, 130.1, 129.6, 127.4, 7.4, 3.4 (Note: ^{13}C signals of nonaflate carbons are not visible[72]); ^{19}F NMR (376 MHz, acetone-d_6): δ –81.5–(–81.6) (m, 3F), –110.0–(–110.3) (m, 2F), –121.3–(–121.6) (m, 2F), –126.3–(–126.5) (m, 2F); IR (film): 2959, 2883, 1667, 1585, 1196 cm^{-1}; HRMS-ESI (m/z) [M + H]$^+$ calcd for $C_{21}H_{23}F_9NO_4SSi^+$, 584.0973; found 584.1015.

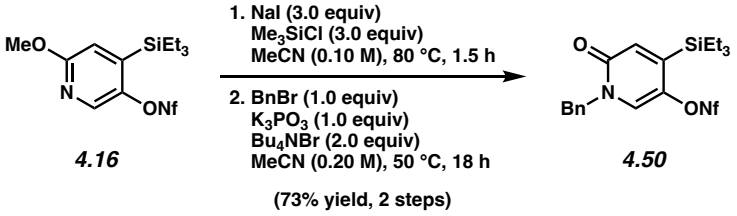

Silyl nonaflate 4.50. To a solution of silyl nonaflate **4.16** (505 mg, 967 μmol, 1.0 equiv) in MeCN (9.69 mL, 0.10 M) were added sequentially NaI (436 mg, 2.91 mmol, 3.0 equiv) in a single portion and trimethylsilyl chloride (316 mg, 368 μL, 2.91 mmol, 3.0 equiv) dropwise over 1 min at 23 °C. The reaction flask was then fitted with an air condenser and heated to 80 °C in an oil bath. After stirring at this temperature for 1.5 h, the reaction was cooled to 23 °C and poured into a separatory

funnel containing a 5 wt% solution of aqueous disodium thiosulfate (50 mL) and brine (50 mL). The mixture was then diluted with EtOAc (50 mL), and the layers were separated. The aqueous layer was extracted with EtOAc (2 x 50 mL). The organic layers were combined, dried over sodium sulfate, filtered, and concentrated under reduced pressure to provide a light yellow solid (492 mg) which was transferred to a vial and dissolved in MeCN (4.85 mL, 0.20 M). To this solution were added sequentially K_3PO_4 (206 mg, 967 μmol, 1.0 equiv), Bu_4NBr (625 mg, 1.94 mmol, 2.0 equiv), and benzyl bromide (166 mg, 115 μL, 967 μmol, 1.0 equiv) dropwise over 1 min at 23 °C. The reaction vial was fitted with a Teflon-lined cap and heated to 50 °C in an oil bath. After stirring at this temperature for 18 h, the reaction was cooled to 23 °C and filtered over a Celite plug eluting with EtOAc (100 mL). The eluate was concentrated under reduced pressure. The crude material was purified by flash chromatography (19:1 hexanes:EtOAc → 9:1 hexanes:EtOAc) to provide silyl nonaflate **4.50** (423 mg, 709 μmol, 73% yield, two steps) as a yellow oil. **Silyl nonaflate 4.50**: R_f 0.19 (9:1 hexanes:EtOAc); ^{1}H NMR (600 MHz, acetone-d_6): δ 7.83 (s, 1H), 7.42–7.35 (m, 4H), 7.35–7.30 (m, 1H), 6.57 (s, 1H), 5.20 (s, 2H), 1.01–0.96 (m, 9H), 0.95–0.88 (m, 6H); ^{13}C NMR (150 MHz, acetone-d_6): δ 159.9, 146.6, 137.3 (d, J = 3.9), 131.2 (t, J = 2.6), 129.7, 129.6, 129.2, 128.9, 52.7, 7.4, 3.4 (Note: ^{13}C signals of nonaflate carbons are not visible[72]); ^{19}F NMR (376 MHz, acetone-d_6): δ –81.4–(–81.6) (m, 3F), –109.9–(–110.1) (m, 2F), –121.4–(–121.6) (m, 2F), –126.3–(–126.5) (m, 2F); IR (film): 2960, 2881, 1666, 1596, 1199 cm^{-1}; HRMS-ESI (m/z) $[M + H]^+$ calcd for $C_{22}H_{25}F_9NO_4SSi^+$, 598.1130; found 598.1155.

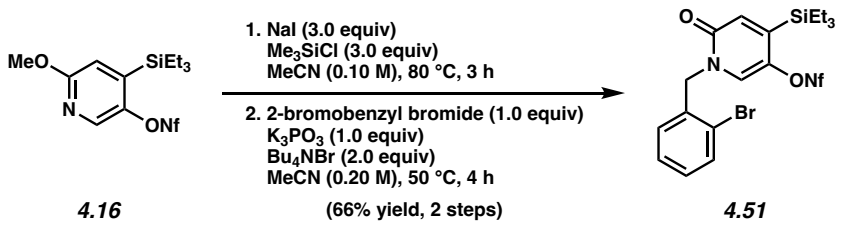

4.16 *4.51*

Silyl nonaflate 4.51. To a solution of silyl nonaflate **4.16** (2.47 g, 4.73 mmol, 1.0 equiv) in MeCN (47.3 mL, 0.10 M) were added sequentially NaI (2.13 g, 14.2 mmol, 3.0 equiv) in a single portion and trimethylsilyl chloride (1.54 g, 1.80 mL, 14.2 mmol, 3.0 equiv) dropwise over 1 min at 23 °C. The reaction flask was then fitted with an air condenser and heated to 80 °C in an oil bath. After stirring at this temperature for 3 h, the reaction was cooled to 23 °C and poured into a separatory funnel containing a 5 wt% solution of aqueous disodium thiosulfate (40 mL). The mixture was then diluted with EtOAc (40 mL), and the layers were separated. The aqueous layer was extracted with EtOAc (2 x 40 mL). The organic layers were combined, dried over sodium sulfate, filtered, and concentrated under reduced pressure to provide a light yellow solid (2.40 g) which was transferred to a round bottom flask and dissolved in MeCN (24 mL, 0.20 M). To this solution were added sequentially K_3PO_4 (1.00 g, 4.73 mmol, 1.0 equiv), Bu_4NBr (3.05 g, 9.46 mmol, 2.0 equiv), and 2-bromobenzyl bromide (1.18 g, 4.73 mmol, 1.0 equiv) at 23 °C. The reaction flask was then fitted with an air condenser and heated to 50 °C in an oil bath. After stirring at this temperature for 4 h, the reaction was cooled to 23 °C and filtered over a Celite plug eluting with EtOAc (100 mL). The eluate was concentrated under reduced pressure. The crude material was purified by flash chromatography (hexanes → 5:2 hexanes:EtOAc) to provide silyl nonaflate **4.51** (2.10 g, 3.10 mmol, 66% yield, two steps) as an orange wax. **Silyl nonaflate 4.51**: R_f 0.48 (5:1 hexanes:EtOAc); ^{1}H NMR (600 MHz, acetone-d_6): δ 7.77 (s, 1H), 7.68 (dd, J = 8.0, 1.0, 1H), 7.40 (td, J = 7.5, 1.1, 1H), 7.30 (td, J = 7.8, 1.6, 1H), 7.24 (dd, J = 7.7, 1.4, 1H), 6.60 (s, 1H), 5.25 (s, 2H), 1.03–0.98 (m, 9H), 0.97–0.91 (m, 6H); ^{13}C NMR (150 MHz, acetone-d_6): δ 159.9, 146.9, 137.5, 136.0, 134.0,

131.2, 130.83, 130.78, 129.5, 129.0, 123.9, 53.1, 7.4, 3.4 (Note: ^{13}C signals of nonaflate carbons are not visible[72]); ^{19}F NMR (282 MHz, acetone-d_6): δ –81.4–(–81.6) (m, 3F), –109.9–(–110.1) (m, 2F), –121.4–(–121.7) (m, 2F), –126.3–(–126.6) (m, 2F); IR (film): 2960, 2880, 1668, 1598, 1199 cm^{-1}; HRMS-APCI (m/z) $[M + H]^+$ calcd for $C_{22}H_{24}BrF_9NO_4SSi^+$, 676.0230; found 676.0248.

4.9.2.2 Synthesis of Substituted Silyl Nonaflate Precursors

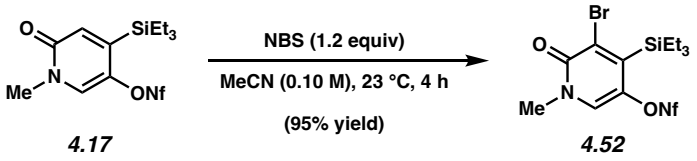

Silyl nonaflate 4.52. To a solution of silyl nonaflate **4.17** (422 mg, 809 μmol, 1.0 equiv) in MeCN (8.09 mL, 0.10 M) in a dark hood was added NBS (173 mg, 971 μmol, 1.2 equiv) in one portion at 23 °C. The reaction vessel was wrapped in aluminum foil to exclude light. After stirring at this temperature for 4 h, the reaction was quenched with saturated aqueous sodium thiosulfate (20 mL) and diluted with ethyl acetate (50 mL) and brine (50 mL). The layers were then poured into a separatory funnel and the organic and aqueous layers were separated. The aqueous layer was extracted with EtOAc (2 x 50 mL). The combined organic layers were dried over sodium sulfate, filtered, and concentrated under reduced pressure. The crude residue was purified by flash chromatography (hexanes → 13:7 hexanes:EtOAc) to provide silyl nonaflate **4.52** (460 mg, 766 μmol, 95% yield) as an light yellow solid. **Silyl nonaflate 4.52**: Mp: 43–44 °C; R_f 0.26 (5:1 hexanes:EtOAc); ^1H NMR (600 MHz, $CDCl_3$): δ 7.37 (s, 1H), 3.62 (s, 3H), 1.10–1.04 (m, 6H), 1.01–0.96 (m, 9H); ^{13}C NMR (150 MHz, $CDCl_3$): δ 157.2, 147.0, 135.6, 129.0, 127.4, 39.7, 7.7, 4.5 (Note: ^{13}C signals of nonaflate carbons are not visible[72]); ^{19}F NMR (376 MHz, $CDCl_3$): δ –80.4–(–80.6) (m, 3F), –108.6–(–108.8) (m, 2F), –120.6–(–120.8) (m, 2F), –125.6–(–125.8) (m,

2F); IR (film): 2968, 2883, 1646, 1601, 1433 cm^{-1}; HRMS-APCI (m/z) $[M + H]^+$ calcd for $C_{16}H_{20}BrF_9NO_4SSi^+$, 599.9917; found 599.9948.

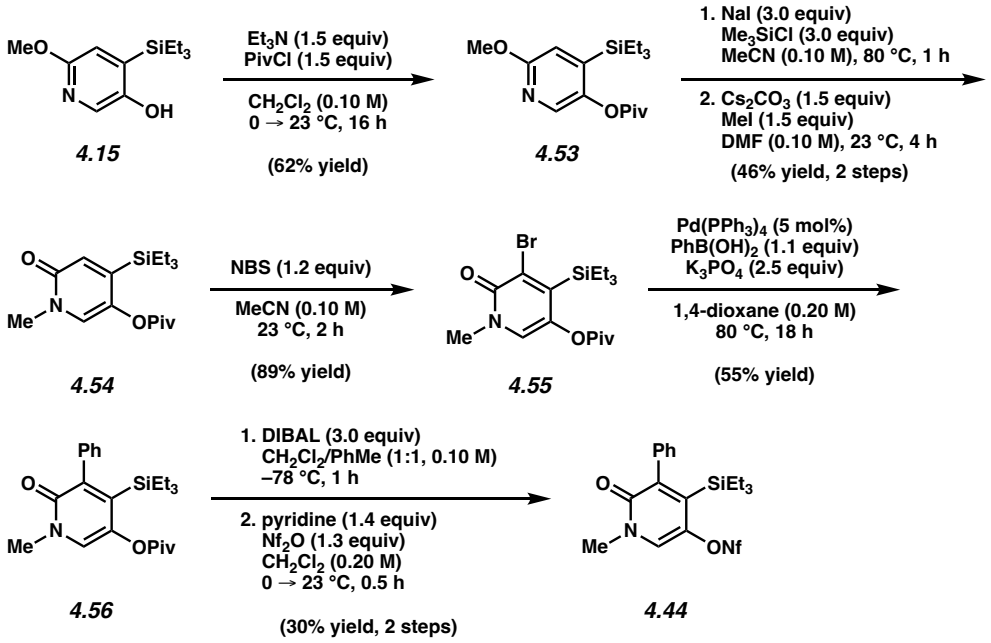

Figure 4.7. Synthesis of silyl nonaflate **4.44**.

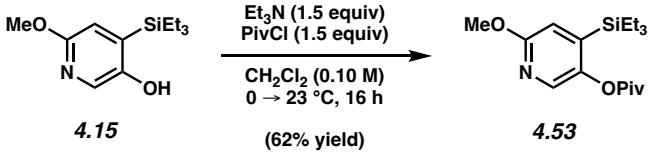

Silyl pivalate 4.53. To a solution of silyl alcohol **4.15** (5.20 g, 21.7 mmol, 1.0 equiv) in CH_2Cl_2 (217 mL, 0.10 M) were added sequentially triethylamine (3.30 g, 4.54 mL, 32.6 mmol, 1.5 equiv) dropwise over 3 min and pivaloyl chloride (3.93 g, 4.00 mL, 32.6 mmol, 1.5 equiv) dropwise over 3 min at 0 °C. The reaction was warmed to 23 °C and stirred for 16 h. After this time, the reaction was quenched with saturated aqueous ammonium chloride (100 mL). The organic and aqueous layers were separated and the aqueous layer was extracted CH_2Cl_2 (3 x 200 mL). The combined

organic layers were washed with brine (200 mL), dried over sodium sulfate, filtered, and concentrated under reduced pressure. The crude residue was purified by flash chromatography (hexanes → 9:1 hexanes:EtOAc) to provide silyl pivalate **4.53** (4.34 g, 13.4 mmol, 62% yield) as a colorless oil. **Silyl pivalate 4.53:** R_f 0.65 (5:1 hexanes:EtOAc); ^{1}H NMR (600 MHz, $CDCl_3$): δ 7.74 (s, 1H), 6.79 (s, 1H), 3.90 (s, 3H), 1.36 (s, 9H), 0.94–0.89 (m, 9H), 0.82–0.75 (m, 6H); ^{13}C NMR (150 MHz, $CDCl_3$): δ 177.7, 161.0, 147.3, 142.5, 139.5, 117.1, 53.7, 39.3, 27.5, 7.3, 3.0; IR (film): 2958, 2877, 1751, 1467, 1348 cm^{-1}; HRMS-APCI (m/z) $[M + H]^+$ calcd for $C_{17}H_{30}NO_3Si^+$, 324.1990; found 324.2012.

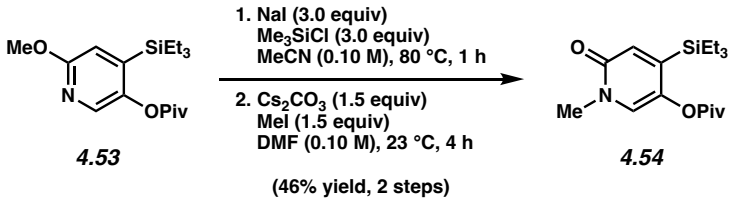

Silyl pivalate 4.54. To a solution of silyl pivalate **4.53** (4.33 g, 13.4 mmol, 1.0 equiv) in MeCN (134 mL, 0.10 M) were added sequentially NaI (6.02 g, 40.2 mmol, 3.0 equiv) in a single portion and trimethylsilyl chloride (4.36 g, 5.08 mL, 40.2 mmol, 3.0 equiv) dropwise over 1 min at 23 °C. The reaction flask was then fitted with an air condenser and heated to 80 °C in an oil bath. After stirring at this temperature for 1 h, the reaction was cooled to 23 °C and poured into a separatory funnel containing a 5 wt% solution of aqueous disodium thiosulfate (25 mL) and brine (100 mL). The mixture was then diluted with CH_2Cl_2 (100 mL), and the layers were separated. The aqueous layer was extracted with CH_2Cl_2 (2 x 100 mL). The organic layers were combined, dried over sodium sulfate, filtered, and concentrated under reduced pressure. The crude residue was purified by flash chromatography (2:1 hexanes:EtOAc → 1:2 hexanes:EtOAc) to provide the surmised silyl

pivalate intermediate (2.63 g, 8.50 mmol, 64% yield) as a light yellow solid, which was used in the subsequent step without rigorous characterization.

To a solution of silyl pivalate (1.80 g, 5.82 mmol, 1.0 equiv) in DMF (58.2 mL, 0.10 M) were added sequentially Cs_2CO_3 (2.84 g, 8.72 mmol, 1.5 equiv) in a single portion and MeI (1.24 g, 546 μL, 8.72 mmol, 1.5 equiv) dropwise over 1 min at 23 °C. The mixture was stirred at this temperature for 4 h. The reaction was then quenched with deionized water (200 mL). The biphasic mixture was then poured into a separatory funnel containing brine (400 mL) and EtOAc (150 mL) and the layers were separated. The aqueous layer was extracted with EtOAc (2 x 150 mL). The organic layers were combined, washed with deionized water (300 mL), dried over sodium sulfate, filtered, and concentrated under reduced pressure. The crude residue was purified by flash column chromatography (4:1 hexanes:EtOac → EtOAc) to provide silyl pivalate **4.54** (1.35 g, 4.17 mmol, 72% yield) as a white solid. **Silyl pivalate 4.54**: Mp: 92–93 °C; R_f 0.26 (1:1 hexanes:EtOAc); ^{1}H NMR (600 MHz, $CDCl_3$): δ 7.05 (s, 1H), 6.66 (s, 1H), 3.50 (s, 3H), 1.32 (s, 9H), 0.94–0.89 (m, 9H), 0.78–0.72 (m, 6H); ^{13}C NMR (150 MHz, $CDCl_3$): δ 177.6, 160.8, 147.1, 137.2, 129.7, 128.1, 39.3, 37.8, 27.5, 7.2, 2.9; IR (film): 2960, 2874, 1755, 1655, 1587 cm^{-1}; HRMS-APCI (m/z) [M + H]$^+$ calcd for $C_{17}H_{30}NO_3Si^+$, 324.1990; found 324.2013.

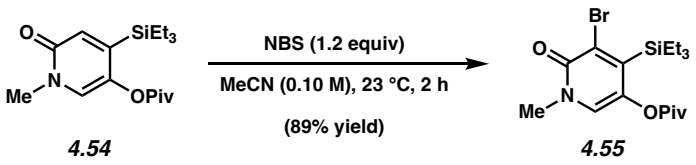

Silyl pivalate 4.55. To a solution of silyl pivalate **4.54** (2.47 g, 7.64 mmol, 1.0 equiv) in MeCN (76.4 mL, 0.10 M) in a dark hood was added NBS (1.63 g, 9.16 mmol, 1.2 equiv) in three portions over 5 minutes at 23 °C. The reaction vessel was wrapped in aluminum foil to exclude light. After

stirring at this temperature for 2 h, the reaction was quenched with saturated aqueous sodium thiosulfate (40 mL) and diluted with EtOAc (200 mL) and brine (200 mL). The layers were then poured into a separatory funnel and the organic and aqueous layers were separated. The organic layer was dried over sodium sulfate, filtered, and concentrated under reduced pressure. The crude residue was purified by flash chromatography (hexanes → 1:1 hexanes:EtOAc) to provide silyl pivalate **4.55** (2.73 g, 6.78 mmol, 89% yield) as a light orange solid. **Silyl pivalate 4.55**: Mp: 116–118 °C; R_f 0.61 (1:1 hexanes:EtOAc); ^{1}H NMR (600 MHz, $CDCl_3$): δ 6.87 (s, 1H), 3.57 (s, 3H), 1.33 (s, 9H), 0.95 (app s, 15H); ^{13}C NMR (150 MHz, $CDCl_3$): δ 178.6, 157.3, 147.7, 137.3, 128.7, 126.2, 39.5, 39.2, 27.5, 7.6, 4.6; IR (film): 2960, 2875, 1752, 1645, 1595 cm^{-1}; HRMS-APCI (m/z) $[M + H]^+$ calcd for $C_{17}H_{29}BrNO_3Si^+$, 402.1095; found 402.1123.

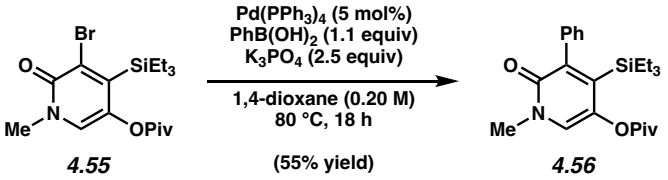

Silyl pivalate 4.56. To a flame dried round bottom flask containing a stir bar were added silyl pivalate **4.55** (550 mg, 1.37 mmol, 1.0 equiv), phenylboronic acid (183 mg, 1.50 mmol, 1.1 equiv), and K_3PO_4 (725 mg, 3.42 mmol, 2.5 equiv). The flask was taken into a glovebox and $Pd(PPh_3)_4$ (79.0 mg, 68.3 μmol, 5 mol%) and 1,4-dioxane (6.83 mL, 0.20 M) were added. The reaction was fitted with an air condenser, removed from the glovebox, and heated to 80 °C in an oil bath. After 18 h, the reaction was cooled to 23 °C and quenched with deionized water (55 mL). The aqueous layer was extracted with CH_2Cl_2 (3 x 50 mL). The organic layers were combined, dried over sodium sulfate, filtered, and concentrated under reduced pressure. The crude residue was purified by flash chromatography (2:1 hexanes:EtOAc → EtOAc) to provide silyl pivalate **4.56** (301 mg,

753 μmol, 55% yield) as a light yellow solid. **Silyl pivalate 4.56**: Mp: 138–139 °C; R_f 0.41 (1:1 hexanes:EtOAc); ^{1}H NMR (600 MHz, $CDCl_3$): δ 7.37–7.31 (m, 3H), 7.22–7.18 (m, 2H), 6.97 (s, 1H), 3.52 (s, 3H), 1.36 (s, 9H), 0.79–0.74 (m, 9H), 0.40–0.34 (m, 6H); ^{13}C NMR (150 MHz, $CDCl_3$): δ 178.1, 160.6, 143.8, 141.4, 138.7, 137.3, 130.5, 128.6, 127.92, 127.89, 39.4, 38.1, 27.5, 7.6, 3.6; IR (film): 2959, 2877, 1747, 1644, 1591 cm^{-1}; HRMS-APCI (m/z) $[M + H]^+$ calcd for $C_{23}H_{34}NO_3Si^+$, 400.2303; found 400.2333.

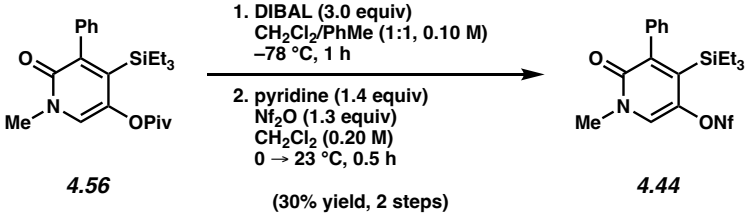

Silyl nonaflate 4.44. To a solution of silyl pivalate **4.56** (450 mg, 1.13 mmol, 1.0 equiv) in CH_2Cl_2 (5.63 mL) and toluene (5.63 mL) was added DIBAL (1.0 M in hexanes, 2.26 mL, 2.26 mmol, 2.0 equiv) dropwise over 5 minutes at –78 °C. After stirring for 1 h, a second portion of DIBAL (1.0 M in hexanes, 1.13 mL, 1.13 mmol, 1.0 equiv) was added dropwise over 5 minutes at –78 °C and stirring at this temperature was continued for 1 h. After this time, the reaction was warmed to 0 °C and quenched with saturated aqueous potassium sodium tartrate (1 mL). The reaction was diluted with EtOAc (100 mL) and saturated aqueous potassium sodium tartrate (200 mL) and stirred vigorously for 1 h at 23 °C. After this time, the organic and aqueous layers were separated and the aqueous layer was extracted EtOAc (3 x 50 mL). The combined organic layers were dried over sodium sulfate, filtered, and concentrated under reduced pressure to provide a yellow solid (355 mg) which was transferred to a round bottom flask and dissolved in CH_2Cl_2 (5.63 mL, 0.20 M). To this solution were added sequentially pyridine (125 mg, 127 μL, 1.58 mmol, 1.4 equiv) and

Nf_2O (852 mg, 449 μL, 1.46 mmol, 1.3 equiv) dropwise over 5 min at 0 °C. The reaction was warmed to 23 °C and stirred for 0.5 h. After this time, the reaction was quenched with deionized water (1 mL) and diluted with CH_2Cl_2 (5 mL). The layers were then poured into a separatory funnel containing a mixture of saturated aqueous sodium bicarbonate (5 mL) and deionized water (5 mL). The organic and aqueous layers were separated and the aqueous layer was extracted with CH_2Cl_2 (2 x 5 mL). The combined organic layers were dried over sodium sulfate, filtered, and concentrated under reduced pressure. The crude residue was purified by flash chromatography (hexanes → 3:2 hexanes:EtOAc) to provide silyl nonaflate **4.44** (203 mg, 340 μmol, 30% yield, two steps) as a tan solid. **Silyl nonaflate 4.44:** Mp: 96–98 °C; R_f 0.61 (2:1 hexanes:EtOAc); ^{1}H NMR (600 MHz, acetone-d_6): δ 7.85 (s, 1H), 7.42–7.38 (m, 3H), 7.29–7.26 (m, 2H), 3.58 (s, 3H), 0.85–0.81 (m, 9H), 0.55–0.49 (m, 6H); ^{13}C NMR (125 MHz, acetone-d_6): δ 160.6, 143.0, 142.5, 139.2, 137.4, 131.7, 130.9, 129.1, 128.4, 38.2, 7.9, 5.0 (Note: ^{13}C signals of nonaflate carbons are not visible[72]); ^{19}F NMR (376 MHz, acetone-d_6): δ –81.5–(–81.6) (m, 3F), –109.9–(–110.1) (m, 2F), –121.4–(–121.6) (m, 2F), –126.2–(–126.5) (m, 2F); IR (film): 2959, 2880, 1645, 1598, 1428 cm^{-1}; HRMS-APCI (m/z) $[M + H]^+$ calcd for $C_{22}H_{25}F_9NO_4SSi^+$, 598.1124; found 598.1129.

4.9.2.3 Optimization of Trapping Reactions of Azacyclic 1,2,3-Triene 4.12

General Procedure 4.1 for the optimization of trapping reactions of azacyclic 1,2,3-triene 4.12:

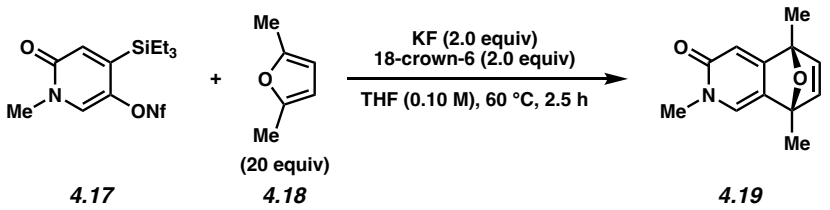

4.17 *4.18* *4.19*

A flame-dried 1-dram vial containing a magnetic stir bar was charged sequentially with silyl nonaflate **4.17** (20.0 mg, 38.4 μmol, 1.0 equiv), furan **4.18** (73.7 mg, 0.767 mmol, 20 equiv), THF (0.384 mL, 0.10 M), 18-crown-6 (20.3 mg, 76.7 μmol, 2.0 equiv), and KF (4.5 mg, 76.7 μmol, 2.0 equiv) in a glovebox. The vial was then sealed with a Teflon-lined cap, removed from the glovebox, and stirred for 2.5 h at 60 °C. The mixture was then filtered over a 2 cm pad of Celite in a monster pipette with cotton, eluting with acetone (10 mL). The eluate was concentrated under reduced pressure and analyzed with mesitylene as an external standard to determine the yield.

The results of deviation from standard conditions are tabulated in Table 4.1 below.

Table 4.1. Selected results from the optimization of trapping reaction of 1,2,3-triene **4.12**. [a] ^{1}H NMR yields determined using mesitylene as an external standard. [b] Without 18-crown-6 additive. [c] Quantitative recovery of silyl nonaflate **4.17** by ^{1}H NMR analysis determined using mesitylene as an external standard [d] Yields for reactions performed outside of a glovebox under these conditions were found to vary between 39–53%. The value reported represents the low end of reaction efficiency observed in these experiments.

Entry	Deviation from General Procedure 4.1	^{1}H NMR Yield[a]
1	None	56%
2	40 °C	50%
3	25 °C	39%
4	KF (5.0 equiv), 18-crown-6 (5.0 equiv), 6 h	53%
5	KF (5.0 equiv), 18-crown-6 (5.0 equiv), 1,4-dioxane, 6 h	44%
6	KF (1.3 equiv), 18-crown-6 (1.3 equiv), 16 h	42%
7	KF (1.3 equiv), 18-crown-6 (1.3 equiv), 25 °C, 16 h	44%
8[b]	CsF (10 equiv), Bu_4NOTf (2.0 equiv)	50%
9[b]	CsF (10 equiv), Bu_4NI (2.0 equiv)	24%
10[b]	CsF (10 equiv), Bu_4NBr (2.0 equiv)	24%
11[b]	CsF (10 equiv)	24%
12[b]	TMAF (1.5 equiv)	30%
13[b]	TASF (1.5 equiv)	33%
14[b]	TBAF•H_2O (1.5 equiv)	23%
15[c]	without KF and without 18-crown-6	0%
16[d]	reaction setup on the benchtop	39%

General Procedure 4.2 for the optimization of trapping reactions of azacyclic 1,2,3-triene 4.12:

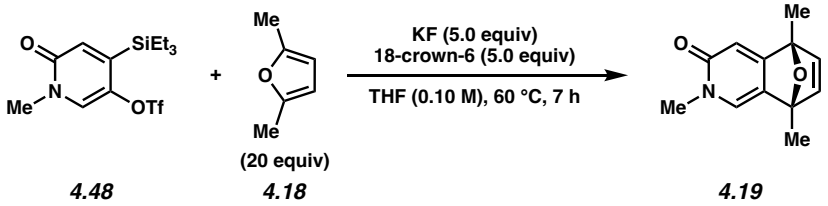

4.48 *4.18* *4.19*

A flame-dried 1-dram vial containing a magnetic stir bar was charged sequentially with silyl triflate **4.48** (14.4 mg, 38.8 μmol, 1.0 equiv), furan **4.18** (74.5 mg, 0.775 mmol, 20 equiv), THF (0.388 mL, 0.10 M), 18-crown-6 (51.2 mg, 0.194 mmol, 5.0 equiv), and KF (11.3 mg, 0.194 mmol, 5.0 equiv) in a glovebox. The vial was then sealed with a Teflon-lined cap, removed from the glovebox, and stirred for 7 h at 60 °C. The mixture was then filtered over a 2 cm pad of Celite in a monster pipette with cotton, eluting with acetone (10 mL). The eluate was concentrated under reduced pressure and analyzed with mesitylene as an external standard to determine the yield.

The results of deviation from standard conditions are tabulated in Table 4.2 below.

Table 4.2. Selected results from the optimization of trapping reaction of 1,2,3-triene **4.12**. [a] ^{1}H NMR yields determined using mesitylene as an external standard. [b] Without 18-crown-6 additive.

Entry	Deviation from General Procedure 4.2	^{1}H NMR Yield[a]
1	None	44%
2	KF (2.5 equiv), 18-crown-6 (2.5 equiv), 4 h	38%
3	KF (10 equiv), 18-crown-6 (10 equiv), 4 h	45%
4	1,4-dioxane, 80 °C, 4 h	50%
5	THF/PhMe (1:1), 80 °C, 4 h	44%
6	2-MeTHF, 80 °C, 4 h	40%
7	DME, 6 h	43%
8	MeCN, 6 h	38%
9	23 °C, 17 h	27%
10[b]	CsF (5.0 equiv), Bu_4NOTf (1.0 equiv), 6 h	43%
11[b]	KF (5.0 equiv), Kryptofix 222 (5.0 equiv), 3 h	50%
12[b]	TMAF (5.0 equiv), 23 °C, 17 h	14%
13[b]	TASF (5.0 equiv), 23 °C, 16 h	16%
14[b]	TBAF (5.0 equiv), 23 °C, 16 h	13%

4.9.2.4 Scope of (4+2) Trapping Reactions

General procedure 4.3 for the scope of (4+2) trapping experiments

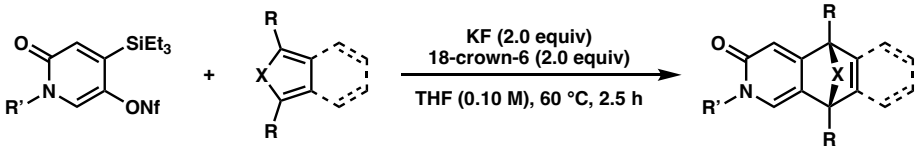

4.57 *4.21* *4.58*

A flame-dried 1-dram vial containing a magnetic stir bar was charged sequentially with silyl nonaflate **4.57** (0.10 mmol, 1.0 equiv), trapping partner **4.21** (2.5–20 equiv), THF (1.0 mL, 0.10 M), 18-crown-6 (53.1 mg, 0.20 mmol, 2.0 equiv), and KF (11.7 mg, 0.20 mmol, 2.0 equiv) in a glovebox. The vial was then sealed with a Teflon-lined cap, removed from the glovebox, and

stirred for 2.5 h at 60 °C. The mixture was then filtered over a 2 cm pad of Celite in a monster pipette with cotton, eluting with acetone (15 mL). The eluate was concentrated under reduced pressure then purified by chromatography to provide adducts **4.58**.

Any deviation from the above procedure is designated in the schemes below. Deviations in trapping partner stoichiometry result from cursory empirical optimization. In most cases, higher loadings of trapping reagents led to higher yields, though exceptions were observed. Unless stated otherwise, all average yields reported for scope studies reflect the results of two isolation experiments with isolated yields within 5%. For all compounds in which regioisomeric ratios were >20:1, the minor isomers were not observed in the ^{1}H-NMR spectrum of the crude reaction mixture.

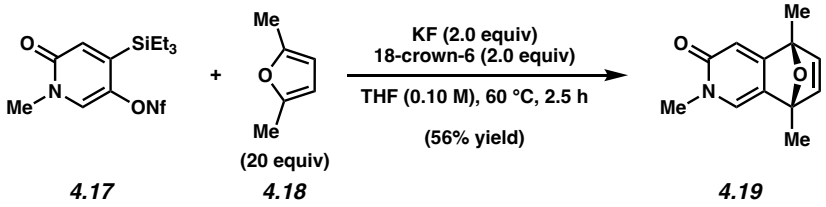

Cycloadduct 4.19. Followed General Procedure 4.3. A flame-dried 1-dram vial containing a magnetic stir bar was charged sequentially with silyl nonaflate **4.17** (55.2 mg, 0.11 mmol, 1.0 equiv), trapping partner **4.18** (203 mg, 2.1 mmol, 20 equiv), THF (1.1 mL, 0.10 M), 18-crown-6 (56.0 mg, 0.21 mmol, 2.0 equiv), and KF (12.3 mg, 0.21 mmol, 2.0 equiv) in a glovebox. The vial was then sealed with a Teflon-lined cap, removed from the glovebox, and stirred for 2.5 h at 60 °C. The mixture was then filtered over a 2 cm pad of Celite in a monster pipette with cotton, eluting with acetone (15 mL). The eluate was concentrated under reduced pressure. Purification by flash chromatography on silica (9:1 hexanes:acetone → 1:4 hexanes:acetone) afforded cycloadduct **4.19**

(12.2 mg, 60 μmol). This experiment was performed 2X with an average yield of 56% yield for the two runs. An analytical sample was obtained by flash chromatography on silica (hexanes → EtOAc) to afford **4.19** as a colorless oil. **Cycloadduct 4.19**: R_f 0.22 (EtOAc); ^{1}H NMR (500 MHz, $CDCl_3$): δ 6.91 (s, 1H), 6.60 (d, J = 5.4, 1H), 6.51 (d, J = 5.4, 1H), 6.36 (s, 1H), 3.41 (s, 3H), 1.80 (s, 3H), 1.77 (s, 3H); ^{13}C NMR (125 MHz, $CDCl_3$): δ 163.1, 162.6, 145.2, 142.2, 128.0, 126.3, 110.7, 87.7, 86.7, 37.5, 15.3, 14.8; IR (film): 2933, 1680, 1607, 1424, 1140 cm^{-1}; HRMS-APCI (m/z) $[M + H]^+$ calcd for $C_{12}H_{14}NO_2^+$, 204.1019; found 204.1019.

*Note: In the absence of KF and 18-crown-6, under otherwise the same reaction conditions specified above, no decomposition of **4.17** occurs and **4.19** is not observed.*

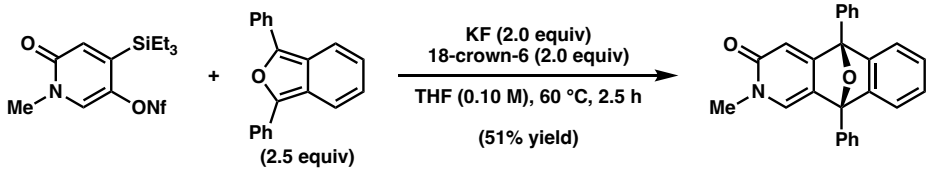

Cycloadduct 4.24. Followed General Procedure 4.3. A flame-dried 1-dram vial containing a magnetic stir bar was charged sequentially with silyl nonaflate **4.17** (62.1 mg, 0.12 mmol, 1.0 equiv), trapping partner **4.23** (80.5 mg, 0.30 mmol, 2.5 equiv), THF (1.2 mL, 0.10 M), 18-crown-6 (62.9 mg, 0.24 mmol, 2.0 equiv), and KF (13.8 mg, 0.24 mmol, 2.0 equiv) in a glovebox. The vial was then sealed with a Teflon-lined cap, removed from the glovebox, and stirred for 2.5 h at 60 °C. The mixture was then filtered over a 2 cm pad of Celite in a monster pipette with cotton, eluting with acetone (15 mL). The eluate was concentrated under reduced pressure. Purification by flash chromatography on Florisil (benzene to elute excess trapping partner, then 3:1 hexanes:EtOAc → 1:1 hexanes:EtOAc) afforded cycloadduct **4.24** (23.5 mg, 62 μmol) as a beige

solid. This experiment was performed 2X with an average yield of 51% yield for the two runs. **Cycloadduct 4.24**: Mp: **4.24** turned brown and appeared to decompose at 118 °C; R_f 0.17 (1:1 hexanes:EtOAc); ^{1}H NMR (500 MHz, $CDCl_3$): δ 7.86–7.81 (m, 4H), 7.63–7.54 (m, 4H), 7.54–7.47 (m, 2H), 7.43–7.38 (m, 1H), 7.37–7.32 (m, 1H), 7.21–7.14 (m, 2H), 7.13 (app s, 1H), 6.59 (app s, 1H), 3.39 (s, 3H); ^{13}C NMR (125 MHz, $CDCl_3$): δ 162.4, 160.7, 148.8, 146.8, 134.2, 133.4, 129.2, 129.03, 128.96, 128.89, 127.4, 127.01, 126.96, 126.7, 126.3, 121.3, 119.9, 112.2, 89.8, 88.7, 37.8 (21 of 22 signals observed); IR (film): 3065, 2918, 1679, 1618, 990 cm^{-1}; HRMS-ESI (m/z) $[M + H]^+$ calcd for $C_{26}H_{20}NO_2^+$, 378.1494; found 378.1511.

*Note: Yields for reactions performed with different loadings of trapping partner **4.23** (1.5, 2.5, and 5.0 equiv) were found to vary (44%, 50%, and 54%, respectively).*

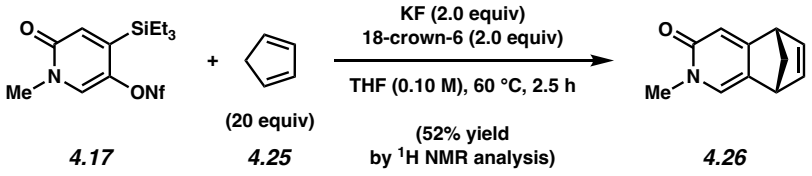

Cycloadduct 4.26. Followed General Procedure 4.3. A flame-dried 1-dram vial containing a magnetic stir bar was charged sequentially with silyl nonaflate **4.17** (52.2 mg, 0.10 mmol, 1.0 equiv), trapping partner **4.25** (132 mg, 2.0 mmol, 20 equiv), THF (1.0 mL, 0.10 M), 18-crown-6 (52.9 mg, 0.20 mmol, 2.0 equiv), and KF (11.6 mg, 0.20 mmol, 2.0 equiv) in a glovebox. The vial was then sealed with a Teflon-lined cap, removed from the glovebox, and stirred for 2.5 h at 60 °C. The mixture was then filtered over a 2 cm pad of Celite in a monster pipette with cotton, eluting with acetone (15 mL). The eluate was concentrated under reduced pressure. ^{1}H NMR analysis of the reaction mixture after workup indicated 52% yield (average of two experiments) of

cycloadduct **4.26** relative to a mesitylene standard. Purification by flash chromatography on silica (hexanes → 1:1 hexanes:acetone), then filtration through a 2 cm pad of Florisil in a pipette with cotton, eluting with EtOAc, then filtration through a 2 cm pad of silica in a pipette with cotton, eluting with EtOAc, afforded cycloadduct **4.26** as a colorless oil. Diminished isolated yields (i.e., <50%) for **4.26** were observed and can be attributed to the volatility of the neat compound. **Cycloadduct 4.26**: R_f 0.29 (1:1 hexanes:acetone); ^{1}H NMR (600 MHz, acetone-d_6): δ 7.22 (s, 1H), 6.63 (dd, *J* = 5.3, 3.0, 1H), 6.50 (dd, *J* = 5.1, 3.1, 1H), 6.29 (s, 1H), 3.74 (br s, 2H), 3.31 (s, 3H), 2.13–2.07 (m, 1H), 1.97–1.92 (m, 1H); ^{13}C NMR (150 MHz, acetone-d_6): δ 164.1, 162.6, 142.8, 139.5, 129.5, 126.6, 113.1, 63.2, 50.4, 46.8, 36.8; IR (film): 2989, 2935, 1675, 1596, 1306 cm^{-1}; HRMS-APCI (m/z) $[M + H]^+$ calcd for $C_{11}H_{12}NO^+$, 174.0913; found 174.0914.

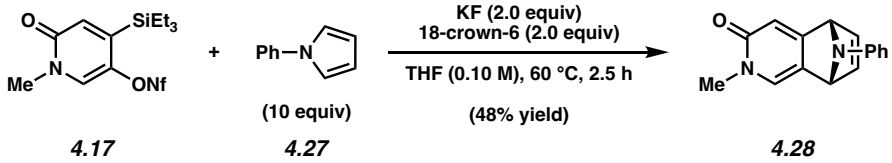

Cycloadduct 4.28. Followed General Procedure 4.3. A flame-dried 1-dram vial containing a magnetic stir bar was charged sequentially with silyl nonaflate **4.17** (54.0 mg, 0.10 mmol, 1.0 equiv), trapping partner **4.27** (144 mg, 1.0 mmol, 10 equiv), THF (1.0 mL, 0.10 M), 18-crown-6 (53.1 mg, 0.20 mmol, 2.0 equiv), and KF (11.7 mg, 0.20 mmol, 2.0 equiv) in a glovebox. The vial was then sealed with a Teflon-lined cap, removed from the glovebox, and stirred for 2.5 h at 60 °C. The mixture was then filtered over a 2 cm pad of Celite in a monster pipette with cotton, eluting with acetone (15 mL). The eluate was concentrated under reduced pressure. Purification by flash chromatography on silica (hexanes → 1:1 hexanes:acetone) then filtration through a 2 cm pad of Florisil in a pipette with cotton, eluting with acetone, afforded cycloadduct **4.28** (12.6 mg, 50

μmol) as a white solid. This experiment was performed 2X with an average yield of 48% yield for the two runs. **Cycloadduct 4.28**: Mp: **4.28** turned brown and appeared to decompose at 172 °C; R_f 0.32 (1:1 hexanes:acetone); ^{1}H NMR (600 MHz, acetone-d_6): δ 7.31 (s, 1H), 7.16–7.11 (m, 2H), 6.89–6.84 (m, 3H), 6.79–6.74 (m, 2H), 6.36 (s, 1H), 5.46–5.44 (m, 2H), 3.25 (s, 3H); ^{13}C NMR (150 MHz, acetone-d_6): δ 162.4, 160.2, 147.6, 142.0, 138.4, 130.5, 129.7, 123.5, 121.2, 118.2, 114.1, 68.0, 65.9, 36.8; IR (film): 2925, 1679, 1600, 1495, 1256 cm^{-1}; HRMS-ESI (m/z) $[M + H]^+$ calcd for $C_{16}H_{15}N_2O^+$, 251.1184; found 251.1184.

*Note: Yields for reactions performed with different loadings of trapping partner **4.27** (2.5, 5.0, and 10 equiv) were found to vary (46%, 50%, and 55%, respectively).*

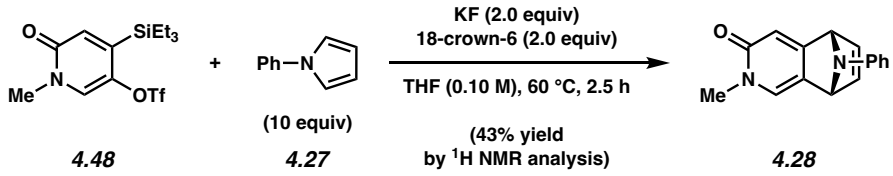

Cycloadduct 4.28. A flame-dried 1-dram vial containing a magnetic stir bar was charged sequentially with silyl triflate **4.48** (37.7 mg, 0.10 mmol, 1.0 equiv), trapping partner **4.27** (145 mg, 1.0 mmol, 10 equiv), THF (1.0 mL, 0.10 M), 18-crown-6 (53.7 mg, 0.20 mmol, 2.0 equiv), and KF (11.8 mg, 0.20 mmol, 2.0 equiv) in a glovebox. The vial was then sealed with a Teflon-lined cap, removed from the glovebox, and stirred for 2.5 h at 60 °C. The mixture was then filtered over a 2 cm pad of Celite in a monster pipette with cotton, eluting with acetone (15 mL). The eluate was concentrated under reduced pressure. ^{1}H NMR analysis of the reaction mixture after workup indicated 43% yield (average of two experiments) of cycloadduct **4.28** relative to a mesitylene

standard. **Cycloadduct 4.28**: Spectral data matched those observed for the product obtained from the cycloaddition of **4.17** (see page 422).

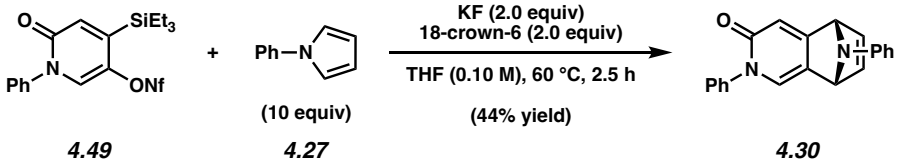

4.49 *4.27* *4.30*

Cycloadduct 4.30. Followed General Procedure 4.3. A flame-dried 1-dram vial containing a magnetic stir bar was charged sequentially with silyl nonaflate **4.49** (58.5 mg, 0.10 mmol, 1.0 equiv), trapping partner **4.27** (144 mg, 1.0 mmol, 10 equiv), THF (1.0 mL, 0.10 M), 18-crown-6 (53.0 mg, 0.20 mmol, 2.0 equiv), and KF (11.6 mg, 0.20 mmol, 2.0 equiv) in a glovebox. The vial was then sealed with a Teflon-lined cap, removed from the glovebox, and stirred for 2.5 h at 60 °C. The mixture was then filtered over a 2 cm pad of Celite in a monster pipette with cotton, eluting with acetone (15 mL). The eluate was concentrated under reduced pressure. Purification by flash chromatography on silica (hexanes → 2:1 hexanes:acetone) then filtration through a 2 cm pad of Florisil in a pipette with cotton, eluting with EtOAc, afforded cycloadduct **4.30** (14.2 mg, 46 μmol) as a light brown solid. This experiment was performed 2X with an average yield of 44% yield for the two runs. **Cycloadduct 4.30**: Mp: 183–184 °C; R_f 0.45 (1:1 hexanes:acetone); ^{1}H NMR (400 MHz, acetone-d_6): δ 7.46–7.40 (m, 2H), 7.38–7.32 (m, 2H), 7.31–7.26 (m, 2H), 7.21–7.14 (m, 2H), 6.94–6.87 (m, 3H), 6.83–6.76 (m, 2H), 6.44 (s, 1H), 5.56–5.49 (m, 2H); ^{13}C NMR (125 MHz, acetone-d_6): δ 161.8, 160.3, 147.4, 142.9, 141.9, 138.0, 129.9, 129.73, 129.67, 128.3, 127.7, 123.8, 121.4, 118.3, 114.8, 68.2, 65.8; IR (film): 3077, 2928, 1681, 1616, 1586 cm^{-1}; HRMS-ESI (m/z) $[M + H]^+$ calcd for $C_{21}H_{17}N_2O^+$, 313.1341; found 313.1353.

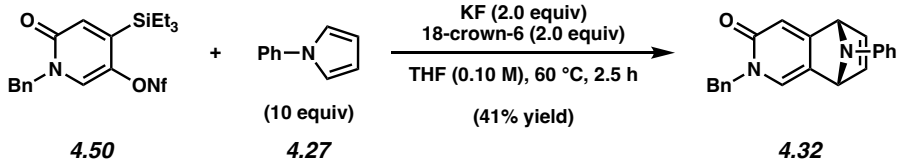

4.50 *4.27* *4.32*

Cycloadduct 4.32. Followed General Procedure 3. A flame-dried 1-dram vial containing a magnetic stir bar was charged sequentially with silyl nonaflate **4.50** (60.1 mg, 0.10 mmol, 1.0 equiv), trapping partner **4.27** (144 mg, 1.0 mmol, 10 equiv), THF (1.0 mL, 0.10 M), 18-crown-6 (53.2 mg, 0.20 mmol, 2.0 equiv), and KF (11.7 mg, 0.20 mmol, 2.0 equiv) in a glovebox. The vial was then sealed with a Teflon-lined cap, removed from the glovebox, and stirred for 2.5 h at 60 °C. The mixture was then filtered over a 2 cm pad of Celite in a monster pipette with cotton, eluting with acetone (15 mL). The eluate was concentrated under reduced pressure. Purification by flash chromatography on silica (hexanes → 2:1 hexanes:acetone) then filtration through a 2 cm pad of Florisil in a pipette with cotton, eluting with EtOAc, afforded cycloadduct **4.32** (14.1 mg, 43 μmol) as a light yellow solid. This experiment was performed 2X with an average yield of 41% yield for the two runs. **Cycloadduct 4.32**: Mp: 184–186 °C; R_f 0.45 (1:1 hexanes:acetone); ^{1}H NMR (400 MHz, acetone-d_6): δ 7.37 (s, 1H), 7.30–7.18 (m, 5H), 7.17–7.11 (m, 2H), 6.89–6.84 (m, 2H), 6.84–6.76 (m, 2H), 6.74 (ddd, J = 5.7, 2.7, 0.6, 1H), 6.42 (s, 1H), 5.48–5.42 (m, 2H), 5.03 (d, J = 14.7, 1H), 4.87 (d, J = 14.7, 1H); ^{13}C NMR (125 MHz, acetone-d_6): δ 162.0, 160.1, 147.5, 141.8, 139.1, 138.1, 129.63, 129.56, 129.3, 128.5, 128.2, 124.0, 121.3, 118.3, 114.5, 68.2, 65.9, 51.6; IR (film): 2925, 2854, 1679, 1602, 1591 cm^{-1}; HRMS-ESI (m/z) $[M + H]^+$ calcd for $C_{22}H_{19}N_2O^+$, 327.1497; found 327.1496.

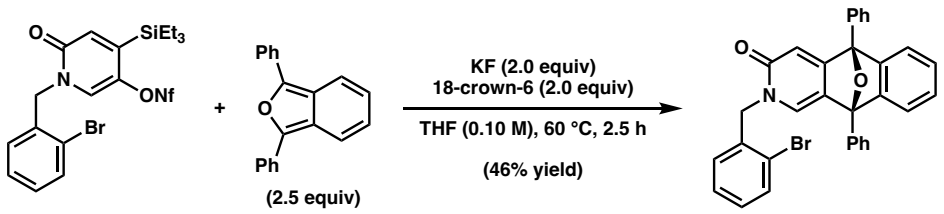

4.51 *4.23* *4.34*

Cycloadduct 4.34. A flame-dried 1-dram vial containing a magnetic stir bar was charged sequentially with silyl nonaflate **4.51** (67.7 mg, 0.10 mmol, 1.0 equiv), trapping partner **4.23** (67.6 mg, 0.25 mmol, 2.5 equiv), THF (1.0 mL, 0.10 M), 18-crown-6 (52.9 mg, 0.20 mmol, 2.0 equiv), and KF (11.6 mg, 0.20 mmol, 2.0 equiv) in a glovebox. The vial was then sealed with a Teflon-lined cap, removed from the glovebox, and stirred for 2.5 h at 60 °C. The mixture was then filtered over a 2 cm pad of Celite in a monster pipette with cotton, eluting with acetone (15 mL). The eluate was concentrated under reduced pressure. Purification by flash chromatography on silica (hexanes → 5:1 hexanes:EtOAc) afforded cycloadduct **4.34** (25.2 mg, 47 μmol) as a white amorphous solid. This experiment was performed 2X with an average yield of 46% yield for the two runs. **Cycloadduct 4.34**: R_f 0.19 (5:1 hexanes:acetone); ^{1}H NMR (600 MHz, acetone-d_6): δ 7.97–7.94 (m, 2H), 7.93–7.89 (m, 2H), 7.70–7.65 (m, 3H), 7.61–7.54 (m, 4H), 7.52–7.47 (m, 2H), 7.36–7.32 (m, 1H), 7.25–7.20 (m, 3H), 7.16 (td, *J* = 7.8, 1.6, 1H), 6.89 (dd, *J* = 7.7, 1.2, 1H), 6.47 (s, 1H), 5.19 (d, *J* = 15.8, 1H), 4.99 (d, *J* = 15.7, 1H); ^{13}C NMR (150 MHz, acetone-d_6): δ 160.8, 160.7, 149.1, 146.6, 136.3, 134.4, 134.0, 132.7, 129.4, 129.11, 128.96, 128.92, 128.6, 128.5, 128.3, 127.8, 127.4, 126.8, 126.2, 126.1, 125.8, 122.3, 120.8, 119.7, 111.2, 89.3, 88.6, 52.0; IR (film): 3062, 2931, 1677, 1620, 1246 cm^{-1}; HRMS-APCI (m/z) $[M + H]^+$ calcd for $C_{32}H_{23}BrNO_2^+$, 532.0907; found 532.0914.

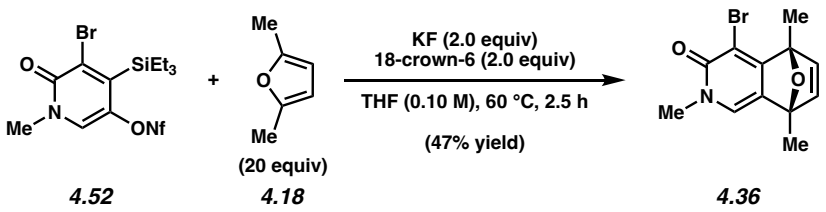

4.52 *4.18* *4.36*

Cycloadduct 4.36. A flame-dried 1-dram vial containing a magnetic stir bar was charged sequentially with silyl nonaflate **4.52** (63.8 mg, 0.10 mmol, 1.0 equiv), trapping partner **4.18** (198 mg, 2.0 mmol, 20 equiv), THF (1.0 mL, 0.10 M), 18-crown-6 (54.5 mg, 0.20 mmol, 2.0 equiv), and KF (12.0 mg, 0.20 mmol, 2.0 equiv) in a glovebox. The vial was then sealed with a Teflon-lined cap, removed from the glovebox, and stirred for 2.5 h at 60 °C. The mixture was then filtered over a 2 cm pad of Celite in a monster pipette with cotton, eluting with acetone (15 mL). The eluate was concentrated under reduced pressure. Purification by flash chromatography on silica (hexanes → 3:1 hexanes:acetone) afforded cycloadduct **4.36** (13.8 mg, 49 μmol) as a tan solid. This experiment was performed 2X with an average yield of 47% yield for the two runs. **Cycloadduct 4.36**: Mp: **4.36** turned brown and appeared to decompose at 143–146 °C; R_f 0.19 (3:1 hexanes:acetone); ^{1}H NMR (600 MHz, acetone-d_6): δ 7.30 (s, 1H), 6.76 (d, J = 5.3, 1H), 6.69 (d, J = 5.3, 1H), 3.41 (s, 3H), 1.90 (s, 3H), 1.75 (s, 3H); ^{13}C NMR (125 MHz, acetone-d_6): δ 161.2, 158.7, 147.2, 142.4, 129.1, 126.7, 107.4, 90.9, 87.4, 38.2, 17.1, 15.2; IR (film): 2927, 2856, 1669, 1614, 1304 cm^{-1}; HRMS-APCI (m/z) $[M + H]^+$ calcd for $C_{12}H_{13}BrN_2O_2^+$, 282.0124; found 282.0138.

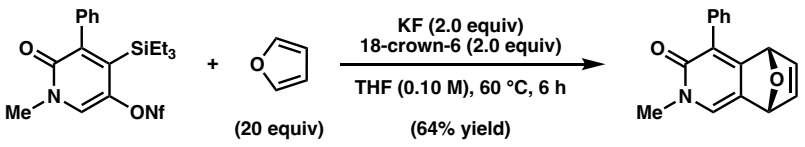

4.44 *4.38* *4.39*

Cycloadduct 4.39. A flame-dried 1-dram vial containing a magnetic stir bar was charged sequentially with silyl nonaflate **4.44** (60.1 mg, 0.10 mmol, 1.0 equiv), trapping partner **4.38** (137 mg, 2.0 mmol, 20 equiv), THF (1.0 mL, 0.10 M), 18-crown-6 (53.2 mg, 0.20 mmol, 2.0 equiv), and KF (11.7 mg, 0.20 mmol, 2.0 equiv) in a glovebox. The vial was then sealed with a Teflon-lined cap, removed from the glovebox, and stirred for 6 h at 60 °C. The mixture was then filtered over a 2 cm pad of Celite in a pipette with cotton, eluting with acetone (15 mL). The eluate was concentrated under reduced pressure. Purification by flash chromatography on silica (5:1 hexanes:acetone → 1:1 hexanes:acetone) then filtration through a 2 cm pad of Florisil in a pipette with cotton, eluting with acetone, afforded cycloadduct **4.39** (16.2 mg, 65 μmol) as a yellow solid. This experiment was performed 2X with an average yield of 64% yield for the two runs. **Cycloadduct 4.39**: Mp: >200 °C; R_f 0.14 (3:1 hexanes:acetone); ^{1}H NMR (600 MHz, acetone-d_6): δ 7.49–7.36 (m, 2H), 7.44–7.39 (m, 3H), 7.37–7.32 (m, 1H), 7.06 (dd, *J* = 5.6, 1.8, 1H), 7.00 (dd, *J* = 5.6, 1.8, 1H), 5.70–5.68 (m, 1H), 5.49–5.47 (m, 1H), 3.42 (s, 3H); ^{13}C NMR (150 MHz, MeOD): δ 163.1, 158.5, 143.3, 139.4, 135.6, 130.6, 129.3, 129.12, 129.09, 125.9, 125.6, 82.5, 81.3, 38.4; IR (film): 3077, 1675, 1601, 1444, 1287 cm^{-1}; HRMS-APCI (m/z) $[M + H]^+$ calcd for $C_{16}H_{14}NO_2^+$, 252.1019; found 252.1031.

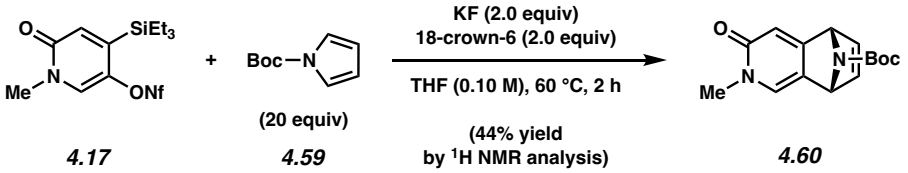

Cycloadduct 4.60. A flame-dried 1-dram vial containing a magnetic stir bar was charged sequentially with silyl nonaflate **4.17** (17.1 mg, 32.9 μmol, 1.0 equiv), trapping partner **4.59** (110 mg, 657 μmol, 20 equiv), THF (329 μL, 0.10 M), 18-crown-6 (17.4 mg, 65.7 μmol, 2.0 equiv), and KF (3.8 mg, 65.7 μmol, 2.0 equiv) in a glovebox. The vial was then sealed with a Teflon-lined cap, removed from the glovebox, and stirred for 2 h at 60 °C. The mixture was then filtered over a 2 cm pad of Celite in a monster pipette with cotton, eluting with acetone (10 mL). The eluate was concentrated under reduced pressure. ^{1}H NMR analysis of the reaction mixture after workup indicated 44% yield of cycloadduct **4.60** relative to a trimethoxybenzene standard. Purification by flash chromatography on silica (9:1 hexanes:acetone → 1:1 hexanes:acetone) then filtration through a 2 cm pad of Florisil in a pipette with cotton, eluting with acetone, afforded an analytical sample of cycloadduct **4.60** as a colorless oil. **Cycloadduct 4.60**: R_f 0.29 (1:1 hexanes:acetone); ^{1}H NMR (600 MHz, acetone-d_6): δ 7.37 (s, 1H), 6.86 (br s, 1H), 6.75 (br s, 1H), 6.38 (s, 1H), 5.33 (br s, 2H), 3.33 (s, 3H), 1.36 (s, 9H); ^{13}C NMR (150 MHz, acetone-d_6): δ 162.2, 159.2, 155.2, 142.9, 142.2, 139.2, 138.5, 130.0, 122.9, 113.3, 112.8, 80.9, 66.4, 65.7, 64.4, 63.6, 36.9, 28.3; IR (film): 2926, 1688, 1608, 1337, 1164 cm^{-1}; HRMS-APCI (m/z) $[M + H]^+$ calcd for $C_{15}H_{19}N_2O_3^+$, 275.1390; found 275.1388.

*Note: **4.60** was obtained as a mixture of rotamers. These data represent empirically observed chemical shifts from the ^{1}H and ^{13}C NMR spectra.*

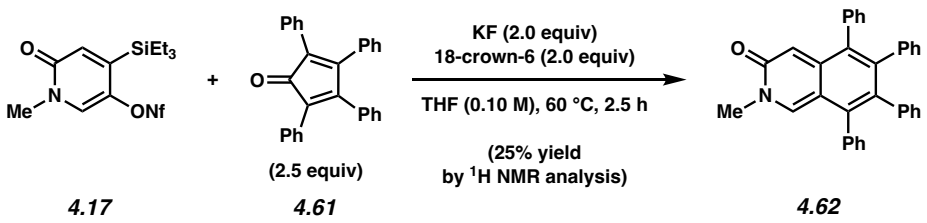

4.17 *4.61* *4.62*

Cycloadduct 4.62. A flame-dried 1-dram vial containing a magnetic stir bar was charged sequentially with silyl nonaflate **4.17** (16.3 mg, 31.3 μmol, 1.0 equiv), trapping partner **4.61** (30.0 mg, 78.1 μmol, 2.5 equiv), THF (313 μL, 0.10 M), 18-crown-6 (16.5 mg, 62.5 μmol, 2.0 equiv), and KF (3.6 mg, 62.5 μmol, 2.0 equiv) in a glovebox. The vial was then sealed with a Teflon-lined cap, removed from the glovebox, and stirred for 2.5 h at 60 °C. The mixture was then filtered over a 2 cm pad of Celite in a monster pipette with cotton, eluting with acetone (10 mL). The eluate was concentrated under reduced pressure. ^{1}H NMR analysis of the reaction mixture after workup indicated 25% yield of cycloadduct **4.62** relative to a mesitylene standard. Purification by flash chromatography on silica (hexanes → EtOAc), then flash chromatography on silica (9:1 benzene:MeCN → 1:1 benzene:MeCN), then preparative thin layer chromatography (9:1 CH_2Cl_2:MeOH) afforded an analytical sample of cycloadduct **4.62** as a yellow amorphous solid. **Cycloadduct 4.62**: R_f 0.56 (9:1 CH_2Cl_2:MeOH); ^{1}H NMR (400 MHz, CD_2Cl_2): δ 7.98 (s, 1H), 7.32–7.14 (m, 10H), 6.92–6.80 (m, 11H), 3.78 (s, 3H); ^{13}C NMR (125 MHz, CD_2Cl_2): δ 142.3, 139.4, 138.9, 138.4, 137.0, 136.5, 135.8, 131.1, 130.93, 130.87, 130.5, 128.2,128.1, 127.7, 127.3, 126.90, 126. 86, 126.1, 126.0, 108.5, 40.7 (21 of 26 signals observed); IR (film): 3060, 3029, 2928, 1648, 699 cm^{-1}; HRMS-APCI (m/z) $[M + H]^+$ calcd for $C_{34}H_{26}NO^+$, 464.2009; found 464.2010.

*Note: **4.62** slowly decomposes upon removal of solvent. We surmise that its instability may be a consequence of its π-expansive nature.*

4.9.2.5 Scope of Regioselective Trapping Reactions

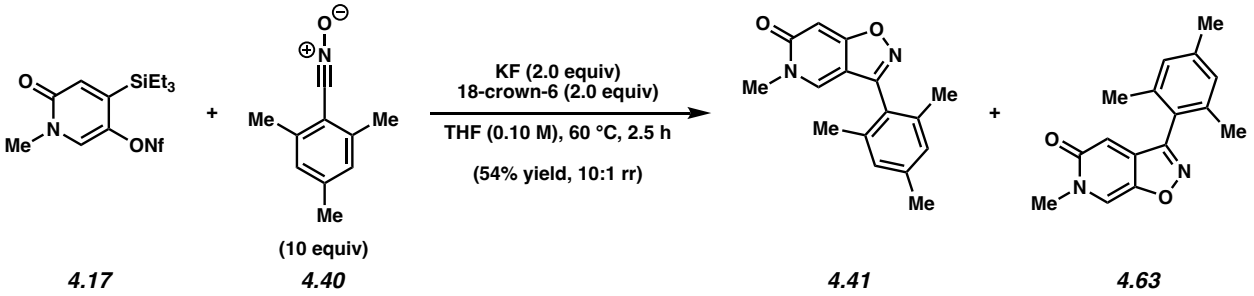

Cycloadduct 4.41. A flame-dried 1-dram vial containing a magnetic stir bar was charged sequentially with silyl nonaflate **4.17** (54.0 mg, 0.10 mmol, 1.0 equiv), nitrile oxide **4.40** (162 mg, 1.0 mmol, 10 equiv), THF (1.0 mL, 0.10 M), 18-crown-6 (53.1 mg, 0.20 mmol, 2.0 equiv), and KF (11.7 mg, 0.20 mmol, 2.0 equiv) in a glovebox. The vial was then sealed with a Teflon-lined cap, removed from the glovebox, and stirred for 2.5 h at 60 °C. The mixture was then filtered over a 2 cm pad of Celite in a monster pipette with cotton, eluting with acetone (15 mL). The eluate was concentrated under reduced pressure to obtain the crude residue (10:1 rr; average of two experiments). Purification by flash chromatography on silica (hexanes → 1:2 hexanes:acetone) afforded cycloadducts **4.41** and **4.63** (13.6 mg, 51 μmol) as a tan solid. This experiment was performed 2X with an average yield of 54% combined yield for the two runs. An analytical sample was obtained by preparative thin layer chromatography (1:1 hexanes:acetone) to provide major regioisomer **4.41** as a white solid. **Cycloadduct 4.41**: Mp: >200 °C; R_f 0.67 (1:1 hexanes:acetone); ^{1}H NMR (500 MHz, acetone-d_6): δ 8.26 (s, 1H), 7.04 (s, 2H), 6.22 (s, 1H), 3.61 (s, 3H), 2.34 (s, 3H), 2.13 (s, 6H); ^{13}C NMR (125 MHz, acetone-d_6): δ 169.7, 162.9, 158.1, 140.6, 138.3, 138.2, 129.4, 123.6, 109.6, 90.8, 38.7, 21.2, 20.0; IR (film): 3027, 2923, 1668, 1583, 1336 cm^{-1}; HRMS-ESI (m/z) $[M + H]^+$ calcd for $C_{16}H_{17}N_2O_2^+$, 269.1290; found 269.1290.

The structure of **4.41** was verified by 2D-NOESY, as the following interactions were observed:

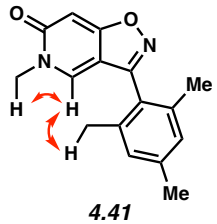

4.41

*Note: Yields for reactions performed with different loadings of trapping partner **4.40** (2.5, 5.0, and 10 equiv) were found to vary (28%, 34%, and 56%, respectively).*

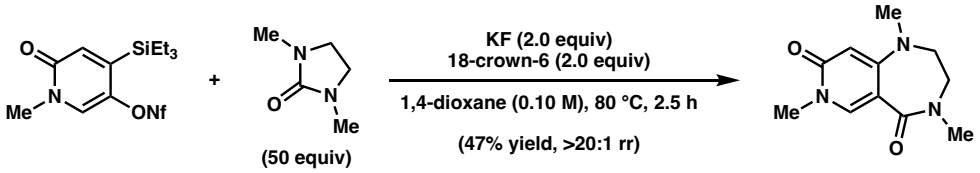

4.17 ***4.42*** ***4.43***

Adduct 4.43. A flame-dried 1-dram vial containing a magnetic stir bar was charged sequentially with silyl nonaflate **4.17** (52.1 mg, 0.10 mmol, 1.0 equiv), cyclic urea **4.42** (570 mg, 5.0 mmol, 50 equiv), 1,4-dioxane (1.0 mL, 0.10 M), 18-crown-6 (52.8 mg, 0.20 mmol, 2.0 equiv), and KF (11.6 mg, 0.20 mmol, 2.0 equiv) in a glovebox. The vial was then sealed with a Teflon-lined cap, removed from the glovebox, and stirred for 2.5 h at 80 °C. The mixture was then filtered over a 2 cm pad of Celite in a monster pipette with cotton, eluting with acetone (15 mL). The eluate was concentrated under reduced pressure to obtain the crude residue (>20:1 rr; average of two experiments). Purification by flash chromatography on silica (3:1 hexanes:acetone → 19:1 acetone:MeOH) then filtration through a pad of Florisil, eluting with acetone, afforded adduct **4.43** (10.6 mg, 47.9 μmol) as a light brown oil. This experiment was performed 2X with an average yield of 47% yield for the two runs. An analytical sample was obtained by preparative thin layer chromatography (9:1 CH_2Cl_2:MeOH) to provide **4.43** as a colorless oil. **Adduct 4.43**: R_f 0.31 (9:1

CH_2Cl_2:MeOH); ^1H NMR (500 MHz, $CDCl_3$): δ 7.88 (s, 1H), 5.67 (s, 1H), 3.54–3.50 (m, 2H), 3.49 (s, 3H), 3.45–3.41 (m, 2H), 3.12 (s, 3H), 2.84 (s, 3H); ^{13}C NMR (125 MHz, $CDCl_3$): δ 167.2, 163.6, 154.7, 143.7, 110.0, 98.9, 55.8, 48.0, 40.5, 37.0, 35.5; IR (film): 2925, 2855, 1652, 1612, 1487 cm^{-1}; HRMS-APCI (m/z) $[M + H]^+$ calcd for $C_{11}H_{16}N_3O_2^+$, 222.1237; found 222.1235.

The structure of **4.43** was verified by 2D-NOESY, as the following interactions were observed:

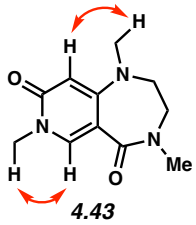

4.43

*Note: In the absence of KF and 18-crown-6, under otherwise the same reaction conditions specified above, slight decomposition of **4.17** occurs and **4.43** is not observed.*

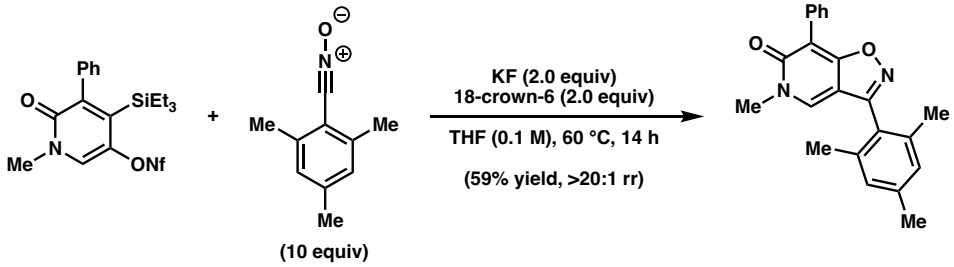

4.44 ***4.40*** ***4.45***

Cycloadduct 4.45. A flame-dried 1-dram vial containing a magnetic stir bar was charged sequentially with silyl nonaflate **4.44** (61.0 mg, 0.10 mmol, 1.0 equiv), nitrile oxide **4.40** (165 mg, 1.0 mmol, 10 equiv), THF (1.0 mL, 0.1 M), 18-crown-6 (54.0 mg, 0.20 mmol, 2.0 equiv), and KF (11.9 mg, 0.20 mmol, 2.0 equiv) in a glovebox. The vial was then sealed with a Teflon-lined cap, removed from the glovebox, and stirred for 14 h at 60 °C. The mixture was then filtered over a 2 cm pad of Celite in a monster pipette with cotton, eluting with acetone (15 mL). The eluate was

concentrated under reduced pressure to obtain the crude residue (>20:1 rr; average of two experiments). Purification by flash chromatography on silica (5:1 hexanes:EtOAc → 1:1 hexanes:EtOAc) afforded cycloadduct **4.45** (19.9 mg, 58 μmol) as a beige solid This experiment was performed 2X with an average yield of 59% combined yield for the two runs. **Cycloadduct 4.45**: Mp: >200 °C; R_f 0.32 (1:1 hexanes:EtOAc); ^{1}H NMR (600 MHz, acetone-d_6): δ 8.27 (s, 1H), 8.08–8.04 (m, 2H), 7.46 (t, *J* = 7.7, 2H), 7.36–7.31 (m, 1H), 7.06 (s, 2H), 3.70 (s, 3H), 2.35 (s, 3H), 2.17 (s, 6H); ^{13}C NMR (150 MHz, acetone-d_6): δ 166.2, 161.8, 158.4, 140.6, 138.3, 136.6, 133.3, 130.4, 129.4, 128.6, 128.1, 123.6, 109.8, 104.7, 39.5, 21.2, 20.0; IR (film): 2923, 2351, 1733, 1652, 1351 cm^{-1}; HRMS-APCI (m/z) $[M + H]^+$ calcd for $C_{22}H_{21}N_2O_2^+$, 345.1598; found 345.1588.

The structure of **4.45** was verified by 2D-NOESY, as the following interactions were observed:

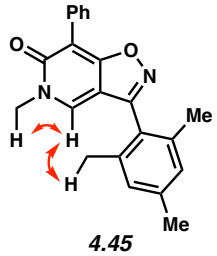

4.45

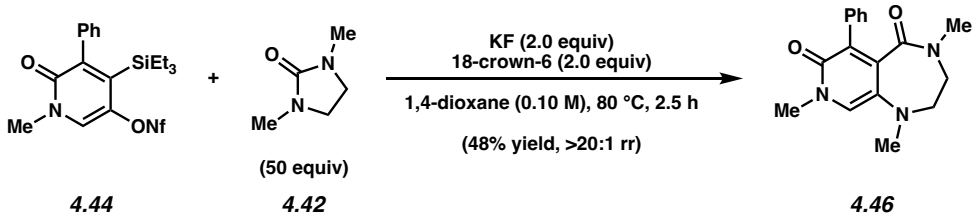

4.44 ***4.42*** ***4.46***

Adduct 4.46. A flame-dried 1-dram vial containing a magnetic stir bar was charged sequentially with silyl nonaflate **4.44** (20.2 mg, 33.8 μmol, 1.0 equiv), cyclic urea **4.42** (193 mg, 1.69 mmol,

50 equiv), 1,4-dioxane (338 µL, 0.10 M), 18-crown-6 (17.9 mg, 67.6 µmol, 2.0 equiv), and KF (3.9 mg, 67.6 µmol, 2.0 equiv) in a glovebox. The vial was then sealed with a Teflon-lined cap, removed from the glovebox, and stirred for 2.5 h at 80 °C. The mixture was then filtered over a pad of Celite, eluting with acetone (10 mL). The eluate was concentrated under reduced pressure to obtain the crude residue (>20:1 rr; average of two experiments). Purification by flash chromatography on C18 reversed-phase (9:1 H_2O:MeCN → 4:1 H_2O:MeCN) then filtration through a 2 cm pad of Florisil in a pipette with cotton, eluting with acetone, afforded adduct **4.46** (4.7 mg, 16 µmol) as a yellow oil. This experiment was performed 2X with an average yield of 48% yield for the two runs. An analytical sample was obtained by preparative thin layer chromatography (acetone) to provide **4.46** as a yellow oil. **Adduct 4.46**: R_f 0.24 (3:1 acetone:hexanes); ^{1}H NMR (600 MHz, acetone-d_6): δ 7.36–7.33 (m, 2H), 7.28–7.20 (m, 3H), 7.16 (s, 1H), 3.96–3.85 (m, 1H), 3.55–3.43 (m, 5H), 2.96 (s, 3H), 2.71 (s, 3H), 2.54–2.47 (m, 1H); ^{13}C NMR (125 MHz, acetone-d_6): δ 167.3, 161.0, 145.2, 137.3, 130.8, 130.1, 128.01, 127.99, 127.9, 126.4, 56.8, 48.2, 40.5, 37.9, 32.7; IR (film): 2924, 2847, 2356, 1647, 1196 cm^{-1}; HRMS-APCI (m/z) $[M + H]^+$ calcd for $C_{17}H_{20}N_3O_2^+$, 298.1550; found 298.1557.

The structure of **4.46** was verified by 2D-NOESY, as the following interactions were observed:

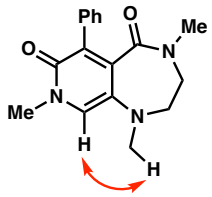

4.46

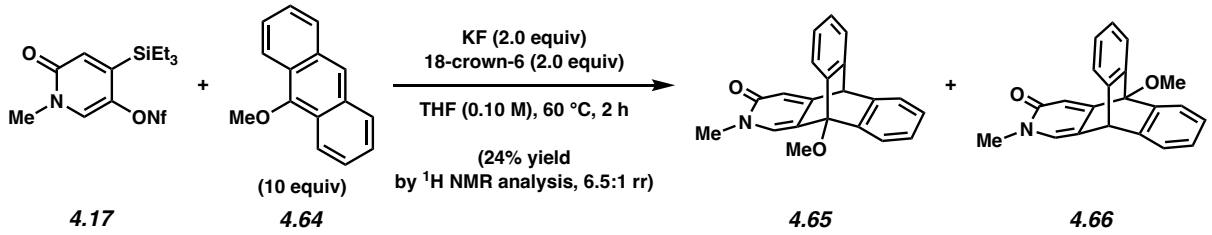

4.17 *4.64* *4.65* *4.66*

Cycloadducts 4.65 and **4.66**. A flame-dried 1-dram vial containing a magnetic stir bar was charged sequentially with silyl nonaflate **4.17** (16.3 mg, 31.3 μmol, 1.0 equiv), trapping partner **4.64** (65.1 mg, 313 μmol, 10 equiv), THF (313 μL, 0.10 M), 18-crown-6 (16.5 mg, 62.5 μmol, 2.0 equiv), and KF (3.6 mg, 62.5 μmol, 2.0 equiv) in a glovebox. The vial was then sealed with a Teflon-lined cap, removed from the glovebox, and stirred for 2 h at 60 °C. The mixture was then filtered over a 2 cm pad of Celite in a monster pipette with cotton, eluting with acetone (10 mL). The eluate was concentrated under reduced pressure. ^{1}H NMR analysis of the reaction mixture after workup indicated 24% yield of cycloadducts **4.65** and **4.66** relative to a mesitylene standard (6.5:1 rr). Purification by preparative thin-layer chromatography (2:1 hexanes:acetone) afforded an analytical sample of an inseparable mixture of cycloadducts **4.65** and **4.66** as a white solid. **Cycloadducts 4.65** and **4.66**: R_f 0.62 (acetone); ^{1}H NMR (600 MHz, acetone-d_6, major regioisomer **4.65**): δ 7.63–7.60 (m, 2H), 7.59 (s, 1H), 7.47 (dd, J = 7.3, 0.7, 2H), 7.16 (td, J = 7.6, 1,4, 2H), 7.11 (td, J = 7.6, 1.4, 2H), 6.43 (s, 1H), 5.40 (s, 1H), 4.30 (s, 3H), 3.38 (s, 3H); ^{13}C NMR (150 MHz, acetone-d_6, mixture of **4.65** and **4.66**, 27 of 30 signals observed): δ 161.9, 155.9, 145.0, 144.4, 143.5, 142.9, 132.5, 132.0, 127.1, 126.8, 126.6, 126.3, 124.8, 124.1, 122.9, 122.5, 121.8, 113.3, 112.0, 85.8, 64.3, 57.7, 57.5, 52.5, 48.6, 37.0, 36.7; IR (film): 2964, 2925, 1672, 1605, 1261 cm^{-1}; HRMS-APCI (m/z) $[M + H]^+$ calcd for $C_{21}H_{18}NO_2^+$, 316.1332; found 316.1319.

The structure of **4.65** was verified by 2D-NOESY, as the following interactions were observed:

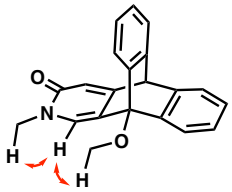

4.65

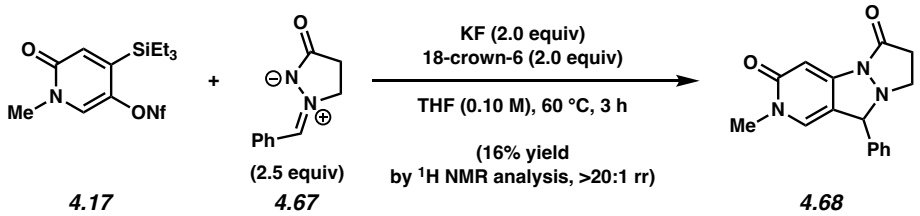

4.17 ***4.67*** ***4.68***

Cycloadduct 4.68. A flame-dried 1-dram vial containing a magnetic stir bar was charged sequentially with silyl nonaflate **4.17** (16.6 mg, 31.8 μmol, 1.0 equiv), trapping partner **4.67** (13.9 mg, 79.6 μmol, 2.5 equiv), THF (318 μL, 0.10 M), 18-crown-6 (16.8 mg, 63.7 μmol, 2.0 equiv), and KF (3.7 mg, 63.7 μmol, 2.0 equiv) in a glovebox. The vial was then sealed with a Teflon-lined cap, removed from the glovebox, and stirred for 3 h at 60 °C. The mixture was then filtered over a 2 cm pad of Celite in a monster pipette with cotton, eluting with acetone (10 mL). The eluate was concentrated under reduced pressure. ^{1}H NMR analysis of the reaction mixture after workup indicated 16% yield of cycloadduct **4.68** relative to a mesitylene standard (>20:1 rr). Purification by preparative thin-layer chromatography (acetone) afforded an analytical sample of cycloadduct **4.68** as a yellow oil. **Cycloadduct 4.68**: R_f 0.63 (acetone); ^{1}H NMR (600 MHz, acetone-d_6): δ 7.53–7.50 (m, 2H), 7.45–7.42 (m, 2H), 7.41–7.37 (m, 1H), 7.14 (d, J = 1.6, 1H), 6.26 (s, 1H), 5.03 (d, J = 1.6, 1H), 3.59–3.55 (m, 1H), 3.35 (s, 3H), 3.30–3.24 (m, 1H), 3.05–2.97 (m, 1H), 2.78–2.72 (overlapped with residual water peak, 1H); ^{13}C NMR (150 MHz, acetone-d_6): δ 165.5, 163.3, 143.6, 139.0, 135.1, 129.7, 129.4, 129.1, 118.0, 97.4, 71.7, 53.0, 37.2, 36.8; IR (film): 3066, 2927,

1722, 1670, 1382cm^{-1}; HRMS-APCI (m/z) [M + H]$^+$ calcd for $C_{16}H_{16}N_3O_2^+$, 282.1237; found 282.1231.

The structure of **4.68** was verified by 2D-NOESY, as the following interactions were observed:

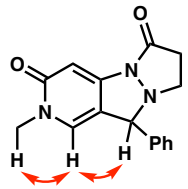

4.68

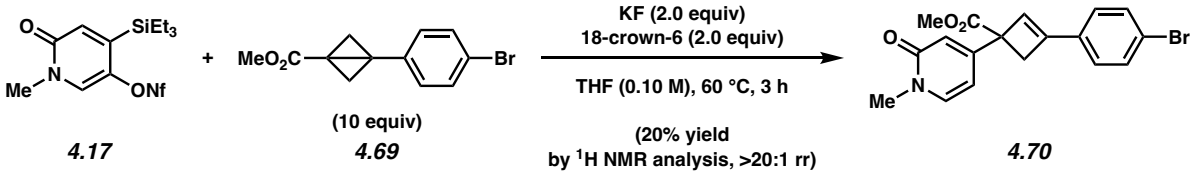

4.17 ***4.69*** ***4.70***

Adduct 4.70. A flame-dried 1-dram vial containing a magnetic stir bar was charged sequentially with silyl nonaflate **4.17** (15.3 mg, 29.3 μmol, 1.0 equiv), trapping partner **4.69** (78.4 mg, 293 μmol, 10 equiv), THF (293 μL, 0.10 M), 18-crown-6 (15.5 mg, 58.7 μmol, 2.0 equiv), and KF (3.4 mg, 58.7 μmol, 2.0 equiv) in a glovebox. The vial was then sealed with a Teflon-lined cap, removed from the glovebox, and stirred for 3 h at 60 °C. The mixture was then filtered over a 2 cm pad of Celite in a monster pipette with cotton, eluting with acetone (10 mL). The eluate was concentrated under reduced pressure. ^{1}H NMR analysis of the reaction mixture after workup indicated 20% yield of cycloadduct **4.70** relative to a mesitylene standard (>20:1 rr). Purification by preparative thin-layer chromatography (9:1 CH_2Cl_2:MeOH) afforded an analytical sample of adduct **4.70** as a white solid. **Adduct 4.70**: R_f 0.38 (1:1 hexanes:acetone); ^{1}H NMR (600 MHz, acetone-d_6): δ 7.60–7.57 (m, 2H), 7.55 (d, J = 7.3, 1H), 7.46–7.43 (m, 2H), 6.79 (s, 1H), 6.34 (d,

J = 1.8, 1H), 6.20 (dd, J = 7.1, 1.8, 1H), 3.70 (s, 3H), 3.61 (d, J = 12.9, 1H), 3.44 (s, 3H), 2.98 (d, J = 12.9, 1H); ^{13}C NMR (150 MHz, acetone-d_6): δ 172.8, 162.8, 153.6, 148.0, 139.9, 133.4, 132.6, 128.7, 127.9, 123.2, 117.7, 104.5, 54.9, 52.8, 41.1, 36.8; IR (film): 2960, 1730, 1661, 1587, 813 cm^{-1}; HRMS-APCI (m/z) $[M + H]^+$ calcd for $C_{18}H_{17}BrNO_3^+$, 374.0386; found 374.0372.

The structure of **4.70** was verified by 2D-NOESY, as the following interactions were observed:

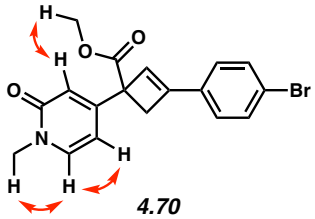

4.70

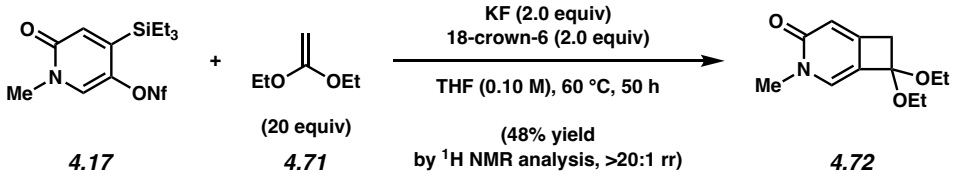

4.17 ***4.71*** ***4.72***

Cycloadduct 4.72. A flame-dried 1-dram vial containing a magnetic stir bar was charged sequentially with silyl nonaflate **4.17** (39.7 mg, 76.1 μmol, 1.0 equiv), trapping partner **4.71** (177 mg, 1.52 mmol, 20 equiv), THF (761 μL, 0.10 M), 18-crown-6 (40.2 mg, 152 μmol, 2.0 equiv), and KF (8.9 mg, 152 μmol, 2.0 equiv) in a glovebox. The vial was then sealed with a Teflon-lined cap, removed from the glovebox, and stirred for 50 h at 60 °C. The mixture was then filtered over a 2 cm pad of Celite in a monster pipette with cotton, eluting with acetone (10 mL). The eluate was concentrated under reduced pressure. ^{1}H NMR analysis of the reaction mixture after workup indicated 48% yield of cycloadduct **4.72** relative to a mesitylene standard (>20:1 rr). Purification by preparative thin-layer chromatography (1:1 hexanes:acetone) then preparative thin-layer chromatography (acetone) afforded an analytical sample of adduct **4.72** as a yellow oil.

Cycloadduct 4.72: R_f 0.37 (1:1 hexanes:acetone); ^{1}H NMR (500 MHz, acetone-d_6): δ 7.61 (s, 1H), 6.18 (s, 1H), 3.67–3.53 (m, 4H), 3.42 (s, 3H), 3.25 (s, 2H), 1.17 (t, J = 7.1, 6H); ^{13}C NMR (125 MHz, acetone-d_6): δ 164.1, 154.3, 132.5, 125.3, 113.7, 104.3, 59.7, 44.7, 37.7, 15.5; IR (film): 3042, 2959, 1662, 1230, 850 cm^{-1}; HRMS-APCI (m/z) $[M + H]^+$ calcd for $C_{12}H_{18}NO_3^+$, 224.1282; found 224.1276.

The structure of **4.72** was verified by 2D-NOESY, as the following interactions were observed:

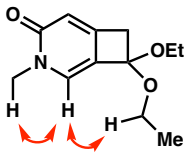

4.72

Unsuccessful Trapping Partners in Attempted (3+2) and (2+2) cycloadditions, nucleophilic additions, and transition metal-mediated reactions.

As shown in Figure 4.8, several other types of trapping reactions were unsuccessful. We attribute this to the azacyclic 1,2,3-triene intermediate undergoing deleterious decomposition pathways faster than trapping with the partners shown below. The propensity for the azacyclic 1,2,3-triene to decompose is likely due to its high strain and severe unsymmetrical geometric distortion.

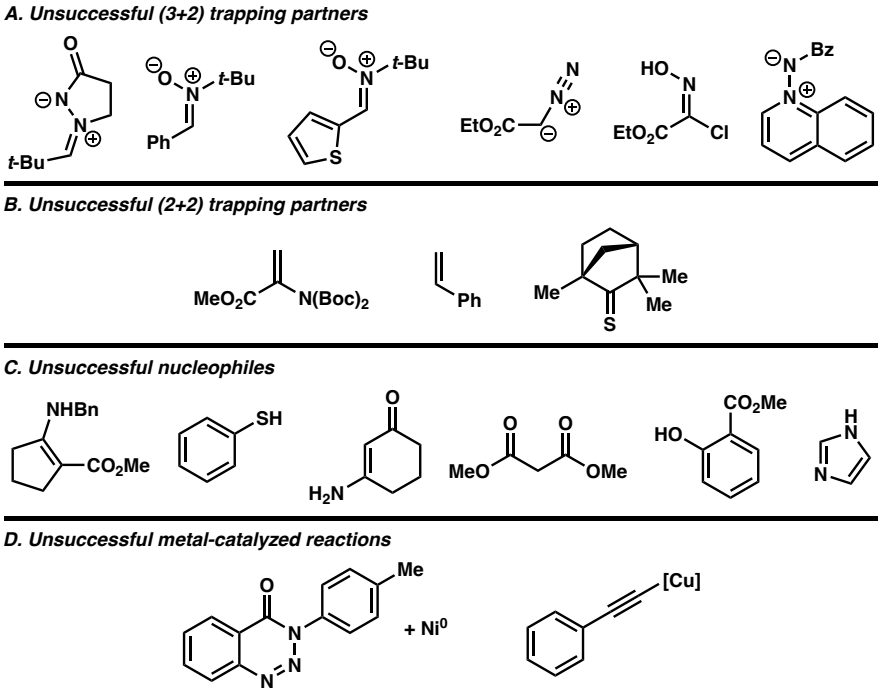

Figure 4.8. Unsuccessful substrates evaluated during scope studies.

4.9.2.6 Synthesis and Trapping of 4.12 via Isomeric Silyl Nonaflate 4.75

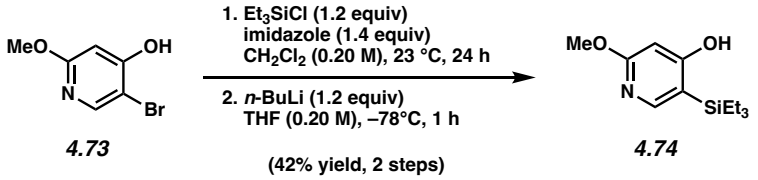

Silyl alcohol 4.74. To a solution of pyridinol **4.73** (300 mg, 1.47 mmol, 1.0 equiv) and imidazole (140 mg, 2.06 mmol, 1.4 equiv) in CH_2Cl_2 (7.25 mL, 0.20 M) was added triethylsilyl chloride (266 mg, 297 μL, 1.76 mmol, 1.2 equiv) dropwise over 1 min at 23 °C. After stirring at this temperature for 24 h, the reaction was quenched with deionized water (25 mL). The mixture was then diluted with CH_2Cl_2 (25 mL), and the layers were separated. The aqueous layer was extracted with CH_2Cl_2 (2 x 25 mL). The organic layers were combined, washed with brine (25 mL), dried over sodium sulfate, filtered, and concentrated under reduced pressure to provide a colorless oil (468 mg) which

was dissolved in THF (7.35 mL, 0.20 M). To this solution at –78 °C was added *n*-BuLi (2.4 M in hexanes, 735 μL, 1.76 mmol, 1.2 equiv) dropwise over 5 min. The resulting mixture was stirred at this temperature for 1 h. Then, deionized water (10 mL) was added dropwise over 5 min. The solution was allowed to warm to 23 °C over 10 min and the mixture was further diluted with deionized water (15 mL) and CH_2Cl_2 (25 mL). The layers were separated and the aqueous layer was extracted with CH_2Cl_2 (2 x 25 mL). The organic layers were combined, dried over sodium sulfate, filtered, and concentrated under reduced pressure. The crude material was purified by flash chromatography (5:1 hexanes:EtOAc) to provide silyl alcohol **4.74** (146 mg, 611 μmol, 42% yield, two steps) as a white solid. **Silyl alcohol 4.74**: Mp: 127–129 °C; R_f 0.22 (5:1 hexanes:EtOAc); ^{1}H NMR (600 MHz, acetone-d_6): δ 7.84 (s, 1H), 6.13 (s, 1H), 3.84 (s, 3H), 0.99–0.94 (m, 9H), 0.89–0.83 (m, 6H); ^{13}C NMR (150 MHz, acetone-d_6): δ 174.4, 166.9, 152.4, 113.4, 95.2, 53.9, 7.8, 3.8; IR (film): 2952, 2874, 2453, 1204, 715 cm^{-1}; HRMS-ESI (m/z) $[M + H]^+$ calcd for $C_{12}H_{22}NO_2Si^+$, 240.1414; found 240.1454.

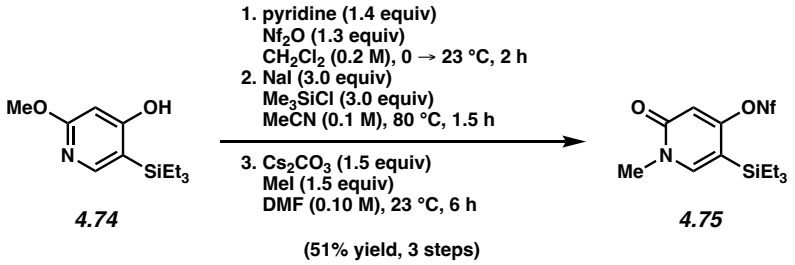

Silyl nonaflate 4.75. To a solution of silyl alcohol **4.74** (146 mg, 610 μmol, 1.0 equiv) in CH_2Cl_2 (3.05 mL, 0.20 M) were added sequentially pyridine (67.5 mg, 69.1 μL, 854 μmol, 1.4 equiv) dropwise over 1 min and Nf_2O (462 mg, 243 μL, 793 μmol, 1.3 equiv) dropwise over 1 min at 0 °C. After stirring at this temperature for 1 h, the reaction was warmed to 23 °C and stirred for an additional 1 h. After this time, the reaction was quenched with deionized water (10 mL) and diluted

with CH_2Cl_2 (25 mL). The layers were then poured into a separatory funnel containing a mixture of saturated aqueous sodium bicarbonate (7.5 mL) and deionized water (7.5 mL). The organic and aqueous layers were separated and the aqueous layer was extracted CH_2Cl_2 (2 x 25 mL). The combined organic layers were dried over sodium sulfate, filtered, and concentrated under reduced pressure to provide an orange oil (318 mg) which was dissolved in MeCN (6.10 mL, 0.10 M). To this solution were added sequentially NaI (274 mg, 610 μmol, 3.0 equiv) in a single portion and trimethylsilyl chloride (199 mg, 232 μL, 610 μmol, 3.0 equiv) dropwise over 1 min at 23 °C. The reaction vial was sealed with a Teflon-lined cap and heated to 80 °C in an oil bath. After stirring at this temperature for 1.5 h, the reaction was cooled to 23 °C and poured into a separatory funnel containing a 5 wt% solution of aqueous disodium thiosulfate (25 mL) and brine (25 mL). The mixture was then diluted with EtOAc (30 mL), and the layers were separated. The aqueous layer was extracted with EtOAc (2 x 30 mL). The organic layers were combined, dried over sodium sulfate, filtered, and concentrated under reduced pressure. The crude residue was purified by flash chromatography (5:1 hexanes:EtOAc → 2:1 hexanes:EtOAc) to provide the surmised silyl nonaflate intermediate (192 mg, 378 μmol, 62% yield, two steps) as a light yellow oil, which was used in the subsequent step without rigorous characterization.

To a solution of silyl nonaflate (192 mg, 378 μmol, 1.0 equiv) in DMF (3.78 mL, 0.10 M) were added sequentially Cs_2CO_3 (185 mg, 568 μmol, 1.5 equiv) in a single portion and MeI (80.6 mg, 35.5 μL, 568 μmol, 1.5 equiv) dropwise over 1 min at 23 °C. The mixture was stirred at this temperature for 6 h. The reaction was then quenched with deionized water (25 mL). The biphasic mixture was then poured into a separatory funnel containing deionized water (75 mL), brine (10 mL), and EtOAc (50 mL) and the layers were separated. The aqueous layer was extracted with EtOAc (3 x 50 mL). The organic layers were combined, washed with deionized water (3 x 50 mL),

dried over sodium sulfate, filtered, and concentrated under reduced pressure. The crude residue was purified by flash chromatography (5:1 hexanes:EtOAc → 3:1 hexanes:EtOAc) to provide silyl nonaflate **4.75** (162 mg, 314 μmol, 82% yield) as a yellow wax. **Silyl nonaflate 4.75**: R_f 0.38 (3:1 hexanes:EtOAc); ^{1}H NMR (600 MHz, acetone-d_6): δ 7.74 (s, 1H), 6.40 (s, 1H), 3.56 (s, 3H), 0.99–0.94 (m, 9H), 0.89–0.83 (m, 6H); ^{13}C NMR (150 MHz, acetone-d_6): δ 163.9, 162.9, 148.8, 108.0 (t, J = 2.5), 104.1, 37.3, 7.4, 3.6 (Note: ^{13}C signals of nonaflate carbons are not visible[72]); ^{19}F NMR (282 MHz, acetone-d_6): δ –81.4–(–81.6) (m, 3F), –109.8–(–110.0) (m, 2F), –121.5–(–121.7) (m, 2F), –126.3–(–126.5) (m, 2F); IR (film): 2959, 2881, 1659, 1427, 1201 cm^{-1}; HRMS-ESI (m/z) [M + H]$^+$ calcd for $C_{16}H_{21}F_9NO_4SSi^+$, 522.0811; found 522.0801.

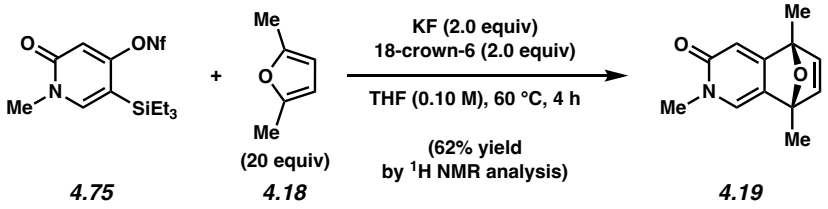

Cycloadduct 4.19. A flame-dried 1-dram vial containing a magnetic stir bar was charged sequentially with silyl nonaflate **4.75** (37.5 mg, 76.1 μmol, 1.0 equiv), trapping partner **4.18** (146 mg, 1.52 mmol, 20 equiv), THF (0.761 mL, 0.10 M), 18-crown-6 (40.2 mg, 152 μmol, 2.0 equiv), and KF (8.9 mg, 152 μmol, 2.0 equiv) in a glovebox. The vial was then sealed with a Teflon-lined cap, removed from the glovebox, and stirred for 4 h at 60 °C. The mixture was then filtered over a 2 cm pad of Celite in a monster pipette with cotton, eluting with acetone (10 mL). The eluate was concentrated under reduced pressure. ^{1}H NMR analysis of the reaction mixture after workup indicated 62% yield of cycloadduct **4.19** relative to a mesitylene standard. **Cycloadduct 4.19**:

Spectral data matched those observed for the product obtained from the cycloaddition of **4.17** (see page 419).

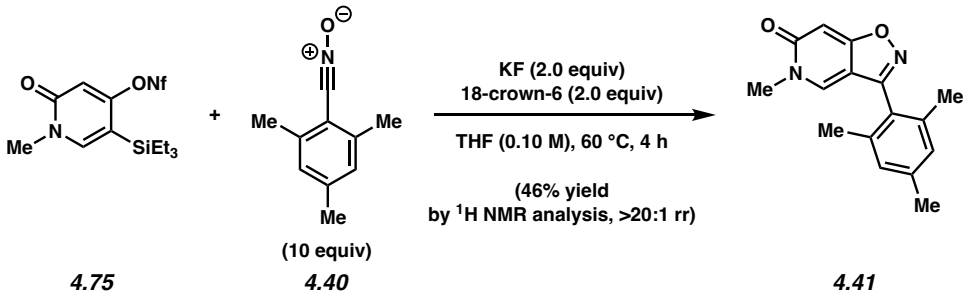

Cycloadduct 4.41. A flame-dried 1-dram vial containing a magnetic stir bar was charged sequentially with silyl nonaflate **4.75** (23.5 mg, 45.1 μmol, 1.0 equiv), nitrile oxide **4.40** (72.6 mg, 451 μmol, 10 equiv), THF (0.451 mL, 0.10 M), 18-crown-6 (23.8 mg, 90.1 μmol, 2.0 equiv), and KF (5.2 mg, 90.1 μmol, 2.0 equiv) in a glovebox. The vial was then sealed with a Teflon-lined cap, removed from the glovebox, and stirred for 4 h at 60 °C. The mixture was then filtered over a 2 cm pad of Celite in a monster pipette with cotton, eluting with acetone (10 mL). The eluate was concentrated under reduced pressure. ^{1}H NMR analysis of the reaction mixture after workup indicated 46% yield of cycloadduct **4.41** relative to a mesitylene standard (>20:1 rr). **Cycloadduct 4.41**: Spectral data matched those observed for the major product obtained from the cycloaddition of **4.17** (see page 431).

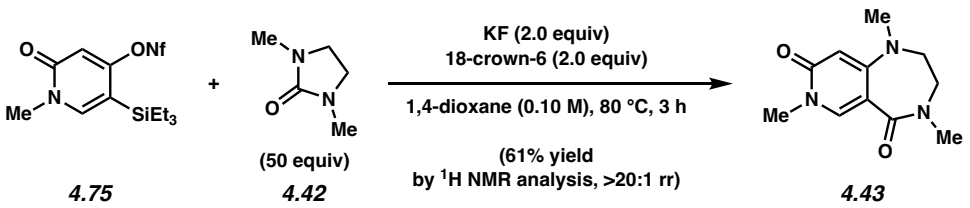

Adduct 4.43. A flame-dried 1-dram vial containing a magnetic stir bar was charged sequentially with silyl nonaflate **4.75** (15.8 mg, 30.3 μmol, 1.0 equiv), cyclic urea **4.42** (173 mg, 1.51 mmol, 50 equiv), 1,4-dioxane (0.303 mL, 0.10 M), 18-crown-6 (16.0 mg, 60.6 μmol, 2.0 equiv), and KF (3.5 mg, 60.6 μmol, 2.0 equiv) in a glovebox. The vial was then sealed with a Teflon-lined cap, removed from the glovebox, and stirred for 3 h at 80 °C. The mixture was then filtered over a 2 cm pad of Celite in a monster pipette with cotton, eluting with acetone (10 mL). The eluate was concentrated under reduced pressure. ^{1}H NMR analysis of the reaction mixture after workup indicated 61% yield of adduct **4.43** relative to a mesitylene standard (>20:1 rr). **Adduct 4.43**: Spectral data matched those observed for the product obtained from the cycloaddition of **4.17** (see page 432).

4.9.2.7 1 mmol Scale Trapping Reaction

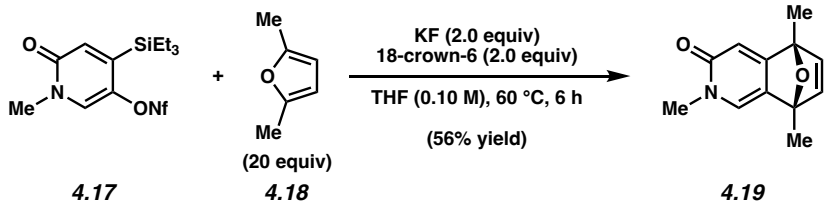

Cycloadduct 4.19 (1 mmol scale). A flame-dried 25 mL round bottom flask containing a magnetic stir bar was charged sequentially with silyl nonaflate **4.17** (530 mg, 1.02 mmol, 1.0 equiv), trapping partner **4.18** (1.95 g, 20.3 mmol, 20 equiv), THF (10.2 mL, 0.10 M), 18-crown-6 (537 mg, 2.03 mmol, 2.0 equiv), and KF (118 mg, 2.03 mmol, 2.0 equiv) in a glovebox. The flask was then fitted with an air condenser, removed from the glovebox, and stirred for 6 h at 60 °C. The mixture was then filtered over a 2 cm pad of Celite in a fritted funnel, eluting with acetone (100 mL). The eluate was concentrated under reduced pressure. Purification by flash chromatography (7:1 hexanes:acetone → 1:1 hexanes:acetone) then filtration through a 2 cm pad of Florisil in a 12 mL syringe with cotton, eluting with acetone, afforded cycloadduct **4.19** (117 mg, 0.57 mmol, 56% yield) as a colorless oil. **Cycloadduct 4.19**: Spectral data matched those observed for the product obtained from the cycloaddition of **4.17** on 0.10 mmol scale (see page 419).

4.9.3 Computational Section

4.9.3.1 Computational Methods

Conformational searches were performed in Spartan '20 V1.1.4[73] using Molecular Mechanics and CREST conformer-rotamer ensemble sampling tool[74,75] version 2.7.1 with xtb version 6.2 RC2 (SAW190805)[76,77,78]. Conformers were then optimized in Gaussian 16 A.03[79] at the B3LYP[80,81]/6-31G(d) level of theory. The frontier molecular orbital structures and energies were obtained by single point energy calculations at the HF/6-31G(d) level of theory. All geometries were verified as stationary points on the potential energy surface and characterized as transition states or minima by frequency calculations. A stability check of the restricted wavefunction was performed to ensure that open-shell wavefunctions are not more stable ("stable" keyword added to all single-point calculations). Intrinsic reaction coordinate (IRC) calculations were performed at the same level of theory to confirm the intermediates linked by each transition state. Single point energies were computed at the B3LYP/6-311+G(d,p), SMD[82](1,4-dioxane). GoodVibes[83] (v. 3.2) with quasi-harmonic entropy[84] and enthalpy[85] treatment (frequency cut-off value: 100 cm^{-1}) was used to obtain corrected Gibbs free energies and enthalpies at either 298.15 K or 353.15 K and 1 atm. Optimized structures are presented using GaussView 6.0.16.[86]

4.9.3.2 Choice of Computational Method

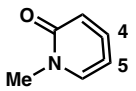

4.12

A variety of methods were compared to study the ground state structures of azacyclic 1,2,3-triene **4.12**. All DFT methods showed similar results for the geometry of **4.12**, especially with regards to the internal angles at C4 and C5 and the C4=C5 bond length. B3LYP/6-31G(d) was utilized for

further geometry optimization, frequency calculations, and transition state analysis as it has been previously shown to be effective for studying other strained intermediates.[45,46]

Table 4.3. Computed structural properties of azacyclic 1,2,3-triene **4.12** at differing levels of theory.

Level of Theory	Internal Angle (C4)	Internal Angle (C5)	Length (C4=C5)
B3LYP/6-31G(d)	139°	115°	1.27 Å
B3LYP/6-311+G(d,p) /SMD(THF)	139°	115°	1.26 Å
B3LYP-D3/6-311+G(d,p) /SMD(THF)	140°	115°	1.26 Å
B3LYP-D3(BJ)/6-311+G(d,p) /SMD(THF)	139°	115°	1.26 Å
ωB97X-D/6-31G(d)	140°	114°	1.27 Å
ωB97X-D/def2-TZVP	140°	114°	1.26 Å
M06-2X/6-31G(d)	140°	114°	1.27 Å
M06-2X/def2-TZVP	140°	114°	1.26 Å
HF/6-31G(d)	143°	110°	1.26 Å

4.9.3.3 Structure of 1,2,3-Cyclohexatriene (4.8)

The annotated structure of 1,2,3-cyclohexatriene (**4.8**) appears below in Figure 4.9 and was used in Figure 4.2. Energetically, **4.8** has a HOMO–1 energy of –9.2 eV, a HOMO energy of –8.2 eV, and a LUMO energy of 2.3 eV. The charges found on the central carbons of the triene are +0.001, which are negligible.[50]

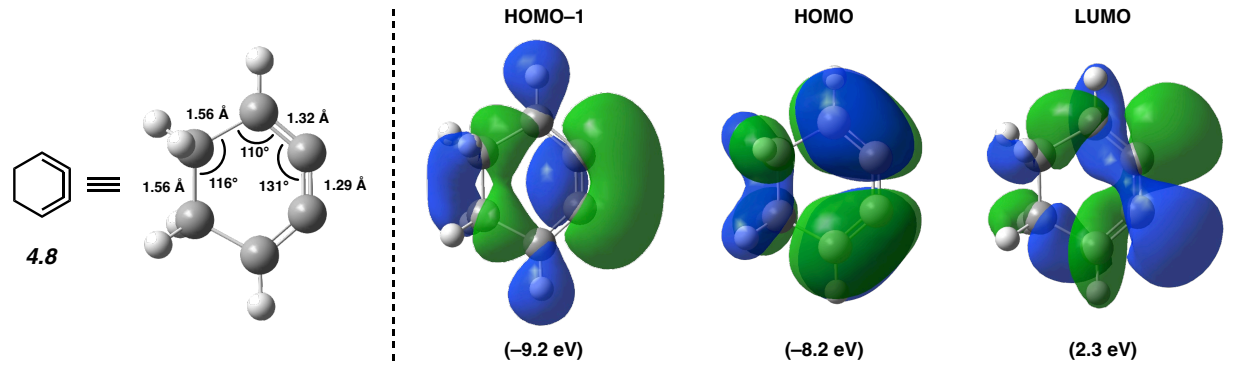

Figure 4.9. Geometry of 1,2,3-cyclohexatriene (**4.8**) calculated at B3LYP/6-31G(d) level of theory and frontier molecular orbitals (FMOs) of 1,2,3-cyclohexatriene (**4.8**) (HF/6-31G(d)//B3LYP/6-31G(d)).

4.9.3.4 Structure of Azacyclic 1,2,3-Triene 4.12

The annotated structure of azacyclic 1,2,3-triene **4.12** appears below in Figure 4.10 and was used to obtain the frontier molecular orbitals and electrostatic potential map shown in Figure 4.2. Energetically, **4.8** has a HOMO–1 energy of –10.5 eV, a HOMO energy of –8.4 eV, and a LUMO energy of 1.5 eV. Given that azacyclic 1,2,3-triene **4.12** is a dehydropyridone, we were interested in the structural and energy differences between **4.12** and its pyridone counterpart. See Section 4.9.3.5 for the energy of dehydrogenation and Section 4.9.3.6 for the annotated structure of pyridone **4.76**, the parent pyridone of 1,2,3-triene **4.12**.

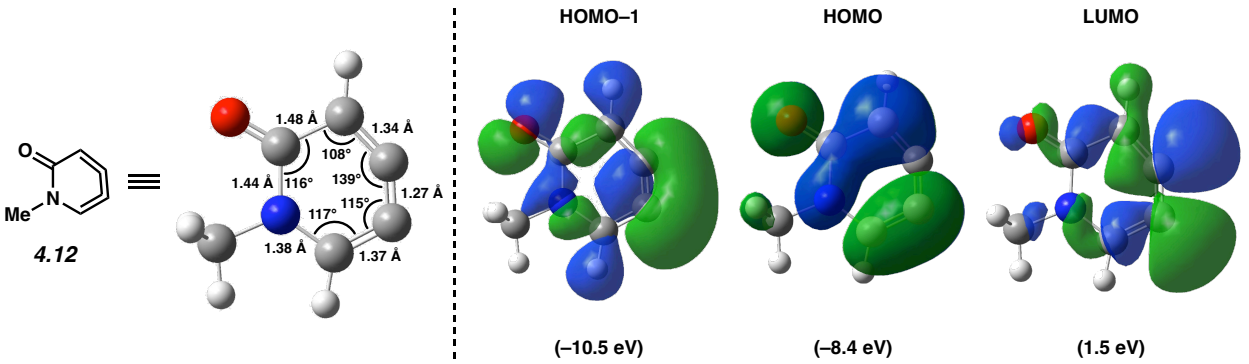

Figure 4.10. Geometry of azacyclic 1,2,3-triene **4.12** calculated at B3LYP/6-31G(d) level of theory.

4.9.3.5 Energy of Dehydrogenation Calculation for Azacyclic 1,2,3-Triene 4.12

The chemical equation in Figure 4.11 below was used to estimate the energy of dehydrogenation of pyridone **4.76**, which was found to be 105 kcal mol^{-1}. For arynes, an energy difference of approximately 115 kcal mol^{-1} or less suggests that the strained intermediate can be readily generated.[87]

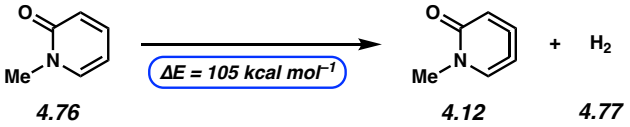

Figure 4.11. Equation used to calculate energy of dehydrogenation. Geometry optimization of **4.76**, **4.12**, and **4.77** were conducted using DFT (B3LYP/6-31G(d)).

4.9.3.6 Structure of Pyridone 4.76

The annotated structure of pyridone **4.76** appears below in Figure 4.12. Azacyclic 1,2,3-triene **4.12**, a dehydropyridone, has distinct geometric differences when compared to the parent pyridone **4.76**. Though overall the bond lengths are relatively the same, the internal angles differ greatly between structures. Specifically, the internal angle for C3 is 122° compared to 108° in **4.12**. Furthermore, the internal angles at C4 and C5 are very similar (121° and 118°, respectively) and only differ by 3°. This is in contrast to the internal angles at C4 and C5 for triene **4.12** being 139° and 115°, respectively. For a DFT and ab-initio computational study of 2-pyridones see study from Maes and coworkers.[88]

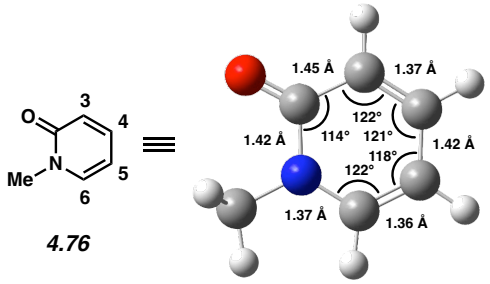

Figure 4.12. Geometry of pyridone **4.76** calculated at the B3LYP/6-31G(d) level of theory.

4.9.3.7 Structures of Cyclic 1,2,3-Trienes 4.78 and 4.79

In order to assess the relative impact of the *N*-substituent and the carbonyl on the geometry of cyclic 1,2,3-triene **4.12**, we analyzed the geometry-optimized structure of cyclic 1,2,3-trienes **4.78** and **4.79** (Figure 4.13). **4.78** lacks the amide carbonyl, whereas **4.79** lacks the *N*-atom. The annotated structures for **4.78** and **4.79** appear below in Figure 4.13. Given the similar distortion present in **4.78** (internal angles at C3 and C4 are 113° and 137°, respectively) compared to **4.12**, we conclude that the *N*-atom is a significant contributor to the geometric distortion of **4.12**. The resonance electron donation by the *N*-lone pair is reflected in the shortened C2–N bond length of 1.37 Å and the lengthened C2=C3 bond length of 1.37 Å (normally 1.34 Å). This electron donation further increases the nucleophilicity of C3 and C5. In contrast, minimal geometric distortion is seen in **4.79** as judged by the internal angles of 133° (C3) and 129° (C4). The strength of inductive effects are dependent on distance, therefore, the *O*-atom being one atom removed from the 1,2,3-triene in comparison to the *N*-atom likely weakens its contribution to the geometric distortion.

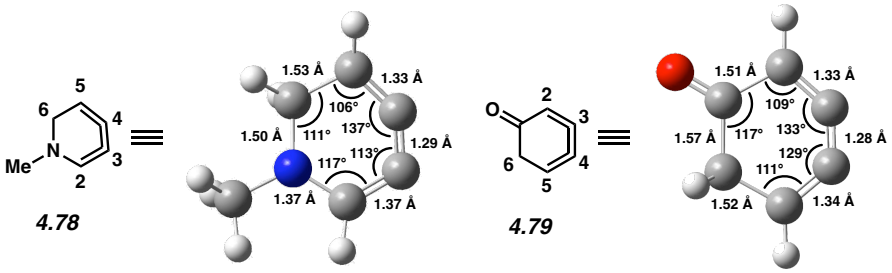

Figure 4.13. Geometry of cyclic 1,2,3-trienes **4.78** and **4.79** at B3LYP/6-31G(d) level of theory.

4.9.3.8 Geometric Distortions of 1,2,3-Trienes 4.80a–4.80c

To better understand the electronic structure of the cyclic 1,2,3-triene, we systematically constrained linear 1,2,3-triene **4.80a** to the 1,2,3-cyclohexatriene (**4.8**) geometry (see Section 4.9.3.3) and the azacyclic 1,2,3-triene **4.12** geometry (see Section 4.9.3.4). The annotated structures of 1,2,3-trienes **4.80a–4.80c** appear below in Figure 4.14. Energetically, unstrained linear 1,2,3-triene **4.80a** has a HOMO energy of –8.9 eV and a LUMO energy of 2.5 eV. The charges found on the central carbons of the triene are –0.03, which is negligible.[50] The bending of the triene (e.g., **4.80b**) to adopt the internal angles and C=C bond lengths calculated for 1,2,3-cyclohexatriene (**4.8**) (see Section 4.9.3.3), lowers the triene LUMO with respect to that of the unstrained triene **4.80a**, but has little effect on the HOMO. For benzyne, the low LUMO energy results from the acetylene bending enforced by the benzyne geometry.[89] Finally, the unsymmetric bending of the 1,2,3-triene **4.80c** to adopt the internal angles and C=C bond lengths calculated for azacyclic 1,2,3-triene **4.12** (see Section 4.9.3.4) has little effect on the HOMO and LUMO with respect to strained triene **4.80b**. However, the carbon with the internal angle of 139° now bears a slight positive charge of +0.13 and the carbon with the internal angle of 115° bears a slight negative charge of –0.09. As these charges are comparable to the charges observed for azacyclic 1,2,3-

triene **4.12** (Figure 4.2), we conclude that the differentiated charges are a result of the rehybridization of the central carbons of the triene.

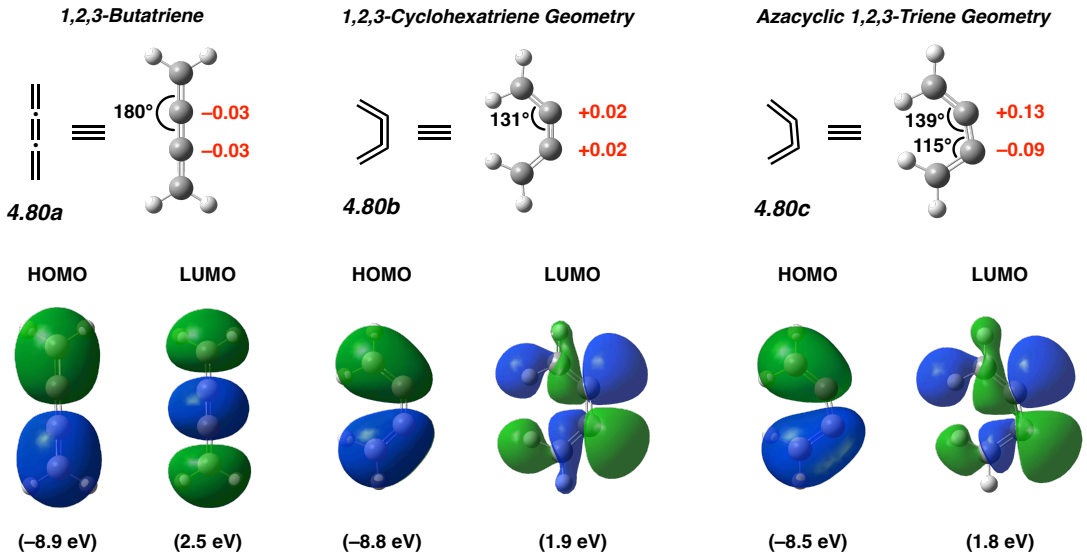

Figure 4.14. Geometry of 1,2,3-trienes **4.80a**–**4.80c** and natural bond orbital (NBO) charges at B3LYP/6-31G(d) level of theory and frontier molecular orbitals (FMOs) of 1,2,3-trienes **4.80a**–**4.80c** at HF/6-31G(d)//B3LYP/6-31G(d) level of theory.

4.9.3.9 Structure of Azacyclic 1,2,3-Triene Isomer 4.81

The structure of **4.81** was computed and analyzed, as this is an aromatic isomer of 1,2,3-triene **4.12**, and would provide an interesting point of comparison. The annotated structure of 4,5-pyridyne **4.81** appears below in Figure 4.15. The distortion caused by the electronegativity of the *N*-heteroatom is offset by the in-plane overlap of the nitrogen lone pair with the π and π* orbitals of the alkyne localized at C5.[45] Therefore, despite being an isomer of azacyclic 1,2,3-triene **4.12**, it displays a less distorted ground state geometry. It is the sum of these two opposing effects that leads to a 4° difference between the two internal angles at C4 and C5 (127° and 123°, respectively). Consequently, due to the minimal difference between the two internal angles, trapping reactions of **4.81** proceed without significant regioselectivity.[65]

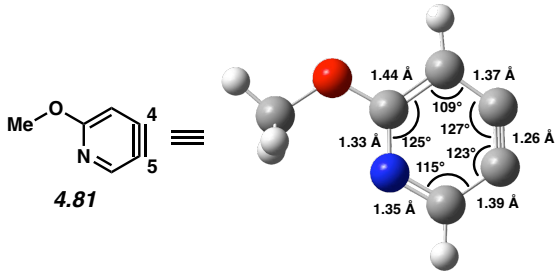

Figure 4.15. Geometry of 4,5-pyridyne **4.81** at B3LYP/6-31G(d) level of theory.

4.9.3.10 Structure of Azacyclic 1,2,3-Trienes 4.29 and 4.31

The structures of **4.29** and **4.31** were computed and analyzed to assess the impact of the *N*-substituent on the geometry. The annotated structures of azacyclic 1,2,3-trienes **4.29** and **4.31** appear below in Figure 4.16. Given that **4.29** and **4.31** have the same internal angles of 139° and 115° at C4 and C5, respectively, we can conclude that the exact *N*-substituent has little impact on the unsymmetrical geometric distortion seen in azacyclic triene **4.12** (see Section 4.9.3.4).

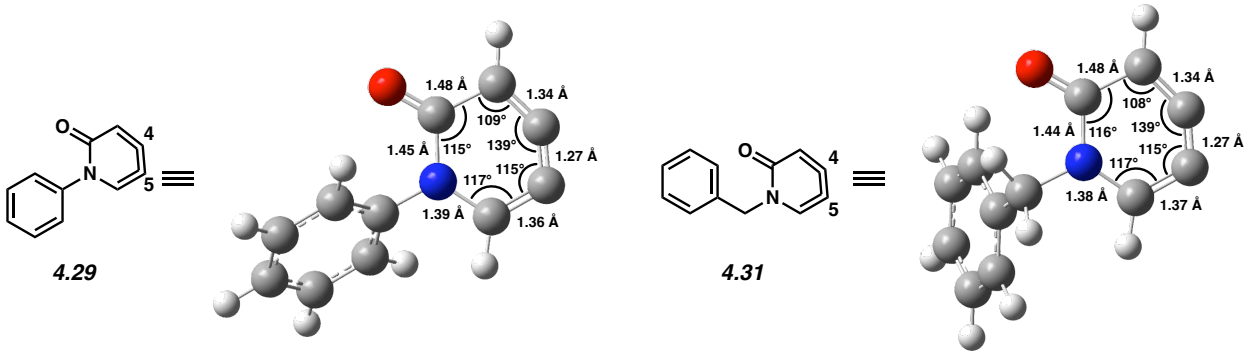

Figure 4.16. Geometry of azacyclic 1,2,3-trienes **4.29** and **4.31** at B3LYP/6-31G(d) level of theory.

4.9.3.11 Structure of Azacyclic 1,2,3-Trienes 4.35 and 4.37

The structures of **4.35** and **4.37** were computed and analyzed to assess the impact of the substituents at C3 on the geometry. The annotated structures of azacyclic 1,2,3-trienes **4.35** and

4.37 appear below in Figure 4.17. For **4.35**, we note that the inductively withdrawing Br partially counters the influence of the N resulting in internal angles of 135° and 119° at C4 and C5, respectively, but does not lead to a significant change. For **4.37**, we note that the phenyl substituent leads to internal angles of 141° and 115° at C4 and C5, respectively, which reflects a minimal change.

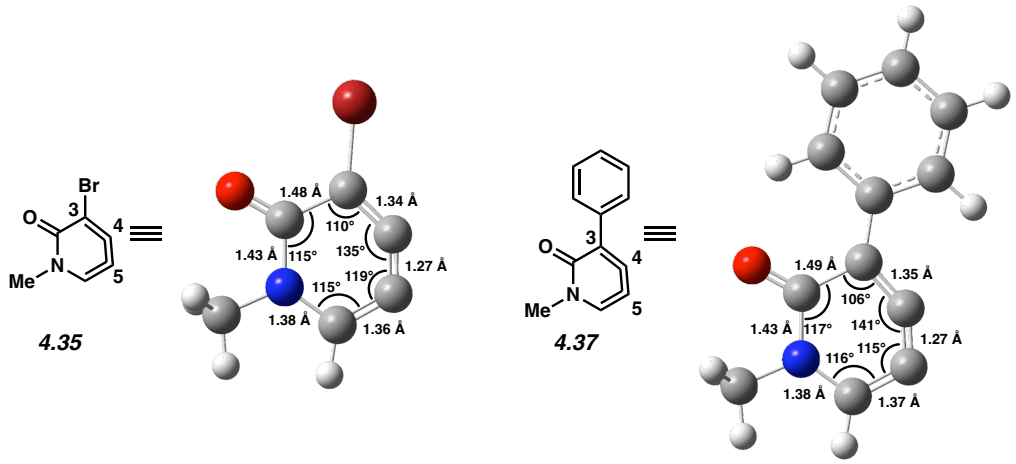

Figure 4.17. Geometry of azacyclic 1,2,3-trienes **4.35** and **4.37** at B3LYP/6-31G(d) level of theory.

4.9.3.12 Transition State Analysis for Reaction of 4.12 with 4.42

The reactions between azacyclic 1,2,3-triene **4.12** and 1,3-dimethyl-2-imidazolidinone (**4.42**) was studied computationally. The transition state geometries of nucleophilic attack of **4.42** at C4 and C5 of **4.12** were found (**TS-4.1a** and **TS-4.1b**, respectively). These transition states represent the initial C–N bond formation (see Section 4.9.3.14 for full mechanism) and attack at C4 was found to be favored over attack at C5 by 2.9 kcal mol^{-1} (**Table 4.4**). Additional single-point energy calculations were performed with B3LYP-D3, ωB97X-D and M06-2X and were able to predict the observed regioselectivity (**Table 4.5**). Distortion/interaction strain analysis (DIAS) was performed in order to understand the role distortion and interaction play in the activation barrier

for the nucleophilic additions (**Table 4.6**). The analysis was also performed along the two competing approaches (**Figure 4.18**). Given that **TS-4.1a** is a very early transition state, only two points on the reaction coordinate are available. Overall, this analysis showed that **4.12** is highly predistorted towards the **TS-4.1a** geometry.

Table 4.4. Computed energies for the reaction of azacyclic 1,2,3-triene **4.12** with 1,3-dimethyl-2-imidazolidinone (**4.42**) at 80 °C (353.15 K) at the B3LYP/6-311+G(d,p)/SMD(1,4-dioxane)//B3LYP/6-31G(d) level of theory. All units are in Hartrees. E = electronic energy; ZPE = zero-point energy; H = enthalpy; T = temperature; S = entropy; G(T) = Gibbs free energy; qh-S = quasi-harmonic corrected entropy; qh-G(T) = quasi-harmonic corrected Gibbs free energy.

Structure	E_SPC	E	ZPE	H_SPC	T.S	T.qh-S	G(T)_SPC	qh-G(T)_SPC
4.12	-361.59685	-361.48683	0.09432	-361.49196	0.04899	0.04883	-361.54095	-361.5408
4.42	-381.42033	-381.30065	0.15295	-381.25502	0.05226	0.05207	-381.30728	-381.3071
TS-4.1a	-743.01855	-742.79321	0.24825	-742.74697	0.08233	0.77676	-742.82930	-742.82464
TS-4.1b	-743.01619	-742.79009	0.24909	-742.74435	0.07862	0.07568	-742.82297	-742.82003

Table 4.5. Computed energies for the reaction of azacyclic 1,2,3-triene **4.12** with 1,3-dimethyl-2-imidazolidinone (**4.42**) at 80 °C (353.15 K) at the Level of Theory//B3LYP/6-31G(d) level of theory. All units are in kcal mol^{-1}.

Level of Theory	**TS-4.1a ($\Delta G^{\ddagger}$)**	**TS-4.1b ($\Delta G^{\ddagger}$)**
B3LYP/6-311+G(d,p)/SMD(1,4-dioxane)	14.6	17.5
B3LYP-D3/6-311+G(d,p)/SMD(1,4-dioxane)	9.7	11.1
ωB97X-D/6-311+G(d,p)/SMD(1,4-dioxane)	9.6	11.5
M06-2X/6-311+G(d,p)/SMD(1,4-dioxane)	10.1	11.7
M06-2X/def2-TZVPP/SMD(1,4-dioxane)	11.0	13.4

Table 4.6. Distortion/Interaction Activation Strain (DIAS) Analysis of the urea addition (**TS-4.1a** & **TS-4.1b**). All units are in kcal mol^{-1}.

	TS-4.1a	**TS-4.1b**
$E_{dist,(\mathbf{4.12})}$	0.40	5.35
$E_{dist,(\mathbf{4.42})}$	0.02	1.23
E_{int}	–1.28	–5.96

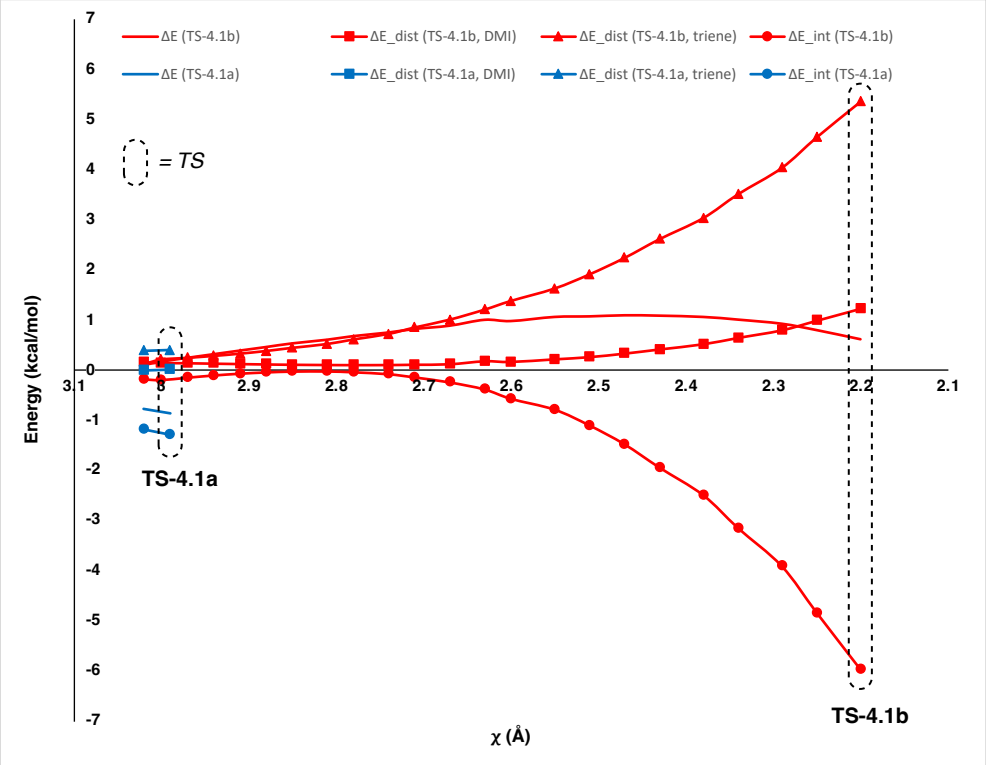

Figure 4.18. Distortion/interaction activation strain analysis along the reaction coordinate of the forming C–N bond for attack of 1,3-dimethyl-2-imidazolidinone (**4.42**) on azacyclic 1,2,3-triene **4.12** at C4 or C5. The x-axis corresponds to reaction progress (i.e., the C–N bond distance for the forming bond). The last points to the right side of the graph are the respective transition states.

4.9.3.13 Transition State Analysis for Reaction of 4.37 with 4.42

The reactions between azacyclic 1,2,3-triene **4.37** and 1,3-dimethyl-2-imidazolidinone (**4.42**) was studied computationally. The transition state geometries of nucleophilic attack of **4.42** at C4 and C5 of **4.37** were found (**TS-4.2a** and **TS-4.2b**, respectively). These transition states represent the initial C–N bond formation and attack at C5 was found to be favored over attack at C4 by 5.8 kcal mol^{-1} (**Table 4.7**). Additional single-point energy calculations with performed using B3LYP-D3, ωB97X-D and M06-2X. B3LYP-D3 was able to predict the observed regioselectivity but ωB97X-D and M06-2X were not able to predict the observed regioselectivity (**Table 4.8**). Distortion/interaction strain analysis (DIAS) was performed in order to understand the role

distortion and interaction play in the activation barrier for the nucleophilic additions (**Table 4.9**). The analysis was also performed along the two competing approaches (**Figure 4.19**). Overall, this analysis showed that significant steric clash in **TS-4.2a** likely leads to this transition state being disfavored.

Table 4.7. Computed energies for the reaction of azacyclic 1,2,3-triene **4.37** with 1,3-dimethyl-2-imidazolidinone (**4.42**) at 80 °C (353.15 K) at the B3LYP/6-311+G(d,p)/SMD(1,4-dioxane)//B3LYP/6-31G(d) level of theory. All units are in Hartrees. E = electronic energy; ZPE = zero-point energy; H = enthalpy; T = temperature; S = entropy; G(T) = Gibbs free energy; qh-S = quasi-harmonic corrected entropy; qh-G(T) = quasi-harmonic corrected Gibbs free energy.

Structure	E_SPC	E	ZPE	H_SPC	T.S	T.qh-S	G(T)_SPC	qh-G(T)_SPC
4.37	-592.71489	-592.54993	0.17389	-592.52393	0.06505	0.06342	-592.58898	-592.58734
4.42	-381.42033	-381.30065	0.15295	-381.25502	0.05226	0.05207	-381.30728	-381.3071
TS-4.2a	-974.12632	-973.84505	0.32929	-973.76850	0.09096	0.08682	-973.85946	-973.85532
TS-4.2b	-974.13337	-973.85242	0.32860	-973.7756	0.09402	0.08897	-973.86961	-973.86456

Table 4.8. Computed energies for the reaction of azacyclic 1,2,3-triene **4.37** with 1,3-dimethyl-2-imidazolidinone (**4.42**) at 80 °C (353.15 K) at the Level of Theory//B3LYP/6-31G(d) level of theory. All units are in kcal mol^{-1}.

Level of Theory	**TS-4.1a ($\Delta G^{\ddagger}$)**	**TS-4.1b ($\Delta G^{\ddagger}$)**
B3LYP/6-311+G(d,p)/SMD(1,4-dioxane)	24.5	18.7
B3LYP-D3/6-311+G(d,p)/SMD(1,4-dioxane)	12.6	11.8
ωB97X-D/6-311+G(d,p)/SMD(1,4-dioxane)	8.6	11.4
M06-2X/6-311+G(d,p)/SMD(1,4-dioxane)	8.6	11.4
M06-2X/def2-TZVPP/SMD(1,4-dioxane)	11.7	13.2

Table 4.9. Distortion/Interaction Activation Strain (DIAS) Analysis of the urea addition (**TS-4.2a** & **TS-4.2b**). All units are in kcal mol^{-1}.

	TS-4.2a	**TS-4.2b**
$E_{dist,\ (\mathbf{4.37})}$	13.73	6.43
$E_{dist,\ (\mathbf{4.42})}$	6.52	1.82
E_{int}	–14.67	–7.10

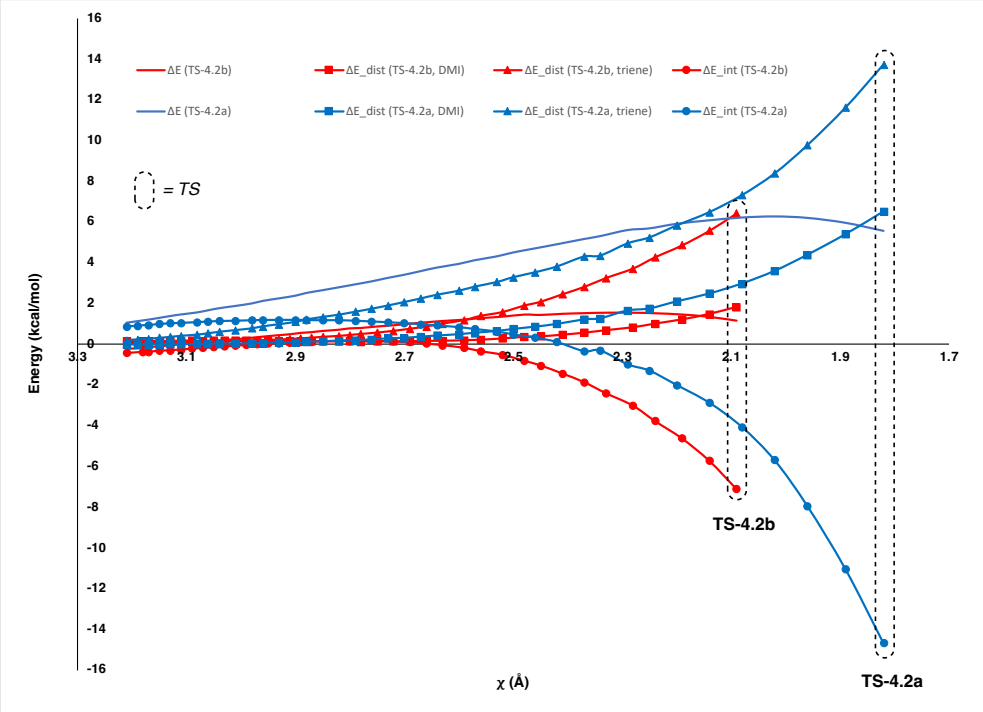

Figure 4.19. Distortion/interaction activation strain analysis along the reaction coordinate of the forming C–N bond for attack of 1,3-dimethyl-2-imidazolidinone (**4.42**) on azacyclic 1,2,3-triene **4.37** at C4 or C5. The x-axis corresponds to reaction progress (i.e., the C–N bond distance for the forming bond). The last points to the right side of the graph are the respective transition states.

4.9.3.14 Reaction Energy Profile and Mechanism for Reaction of 4.12 with 4.42

We propose a plausible stepwise mechanism for the reaction between azacyclic 1,2,3-triene **4.12** and 1,3-dimethyl-2-imidazolidinone (**4.42**), as outlined in Figure 4.20. This stepwise pathway begins with initial regioselective C–N bond formation ($\Delta G^{\ddagger}$ = 14.6 kcal mol^{-1}) to afford zwitterionic intermediate **4.82**. Then, we located the transition state **TS-4.3** for the final C–C bond forming step to afford **4.43**. The free energy barrier for this cyclization was found to be 2.9 kcal mol^{-1}. This mechanism is supported by DFT results on related reactions from Akai and coworkers.[90]

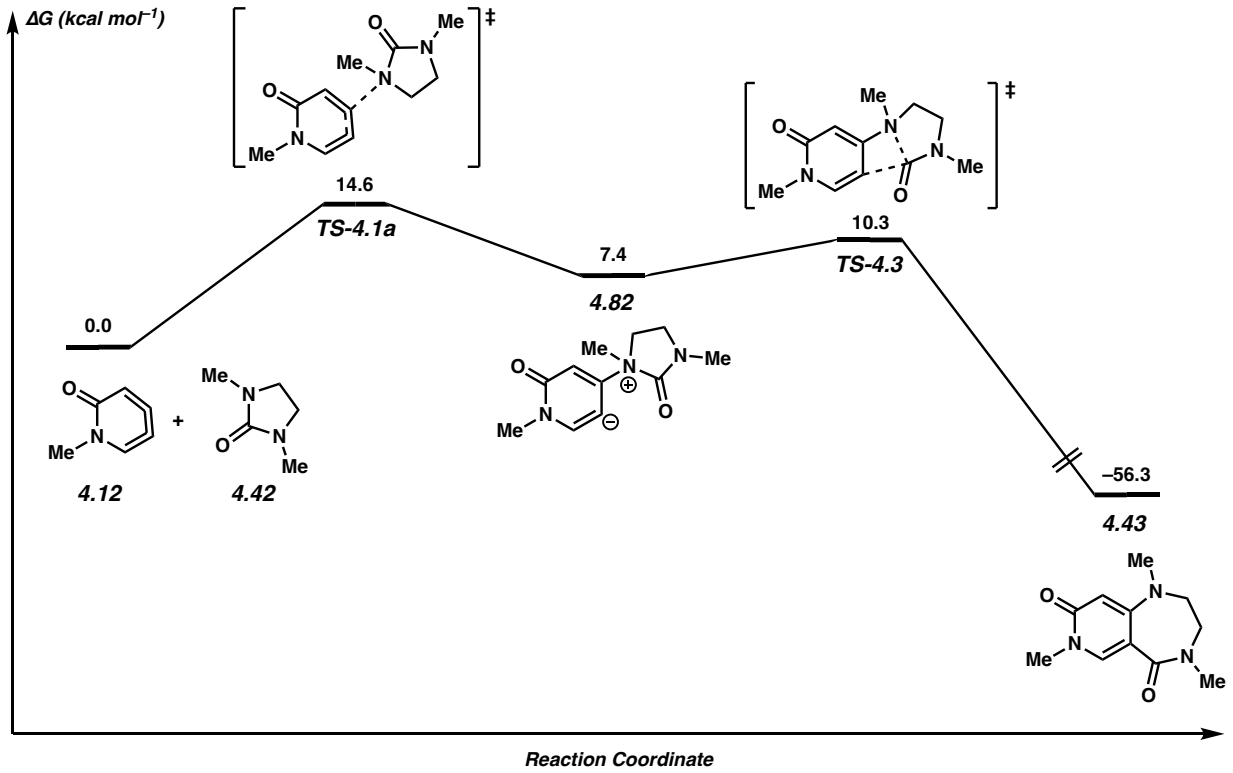

Figure 4.20. Calculated free energy profile for formal C–N bond insertion at 80 °C (353.15 K) at the B3LYP/6-311+G(d,p)/SMD(1,4-dioxane)//B3LYP/6-31G(d) level of theory. Energies are in kcal mol^{-1}.

Table 4.10. Computed energies for the reaction of azacyclic 1,2,3-triene **4.12** with 1,3-dimethyl-2-imidazolidinone (**4.42**) at 80 °C (353.15 K) at the B3LYP/6-311+G(d,p)/SMD(1,4-dioxane)//B3LYP/6-31G(d) level of theory. All units are in Hartrees. E = electronic energy; ZPE = zero-point energy; H = enthalpy; T = temperature; S = entropy; G(T) = Gibbs free energy; qh-S = quasi-harmonic corrected entropy; qh-G(T) = quasi-harmonic corrected Gibbs free energy.

Structure	E_SPC	E	ZPE	H_SPC	T.S	T.qh-S	G(T)_SPC	qh-G(T)_SPC
4.12	-361.59685	-361.48683	0.09432	-361.49196	0.04899	0.04883	-361.54095	-361.5408
4.42	-381.42033	-381.30065	0.15295	-381.25502	0.05226	0.05207	-381.30728	-381.3071
TS-4.1a	-743.01855	-742.79321	0.24825	-742.74697	0.08233	0.77676	-742.82930	-742.82464
4.82	-743.03496	-742.80394	0.25115	-742.76142	0.07741	0.07468	-742.83883	-742.83609
TS-4.3	-743.03314	-742.80033	0.25186	-742.76017	0.07267	0.07134	-742.83284	-742.83151
4.43	-743.13954	-742.91960	0.25353	-742.86409	0.07527	0.07333	-742.93936	-742.93742

4.9.3.15 Cartesian Coordinates of Optimized Geometries

Cartesian coordinates for the optimized structures were reported in the literature.[91]

4.10 Spectra Relevant to Chapter Four:

Synthesis and Reactivity of Nitrogen-Containing Strained Cyclic 1,2,3-Trienes

Dominick C. Witkowski, Daniel W. Turner, Ana S. Bulger, K. N. Houk and Neil K. Garg

Nat. Synth. **2025**, *In press*. doi.org/10.1038/s44160-025-00793-9

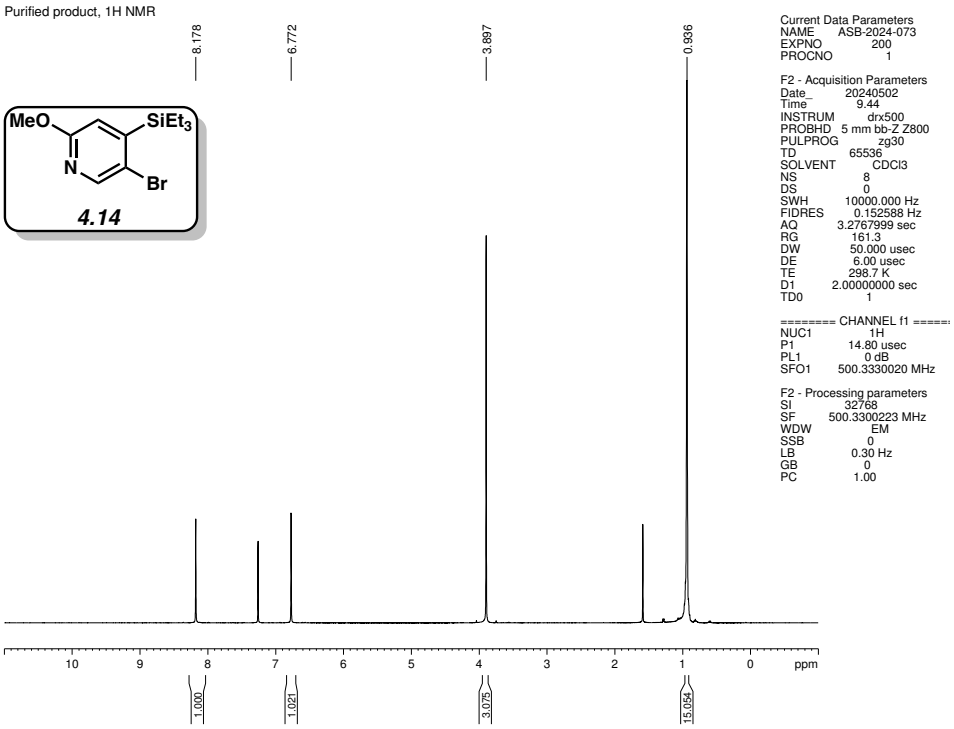

Figure 4.21. ^{1}H NMR (500 MHz, $CDCl_3$) of compound **4.14**.

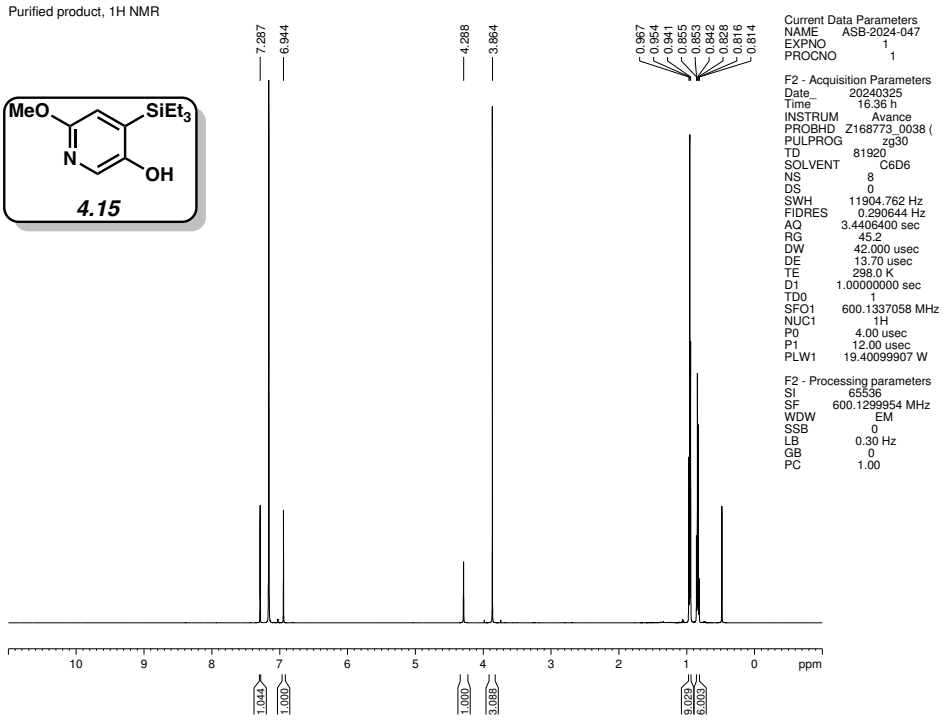

Figure 4.22. ^{1}H NMR (600 MHz, C_6D_6) of compound **4.15**.

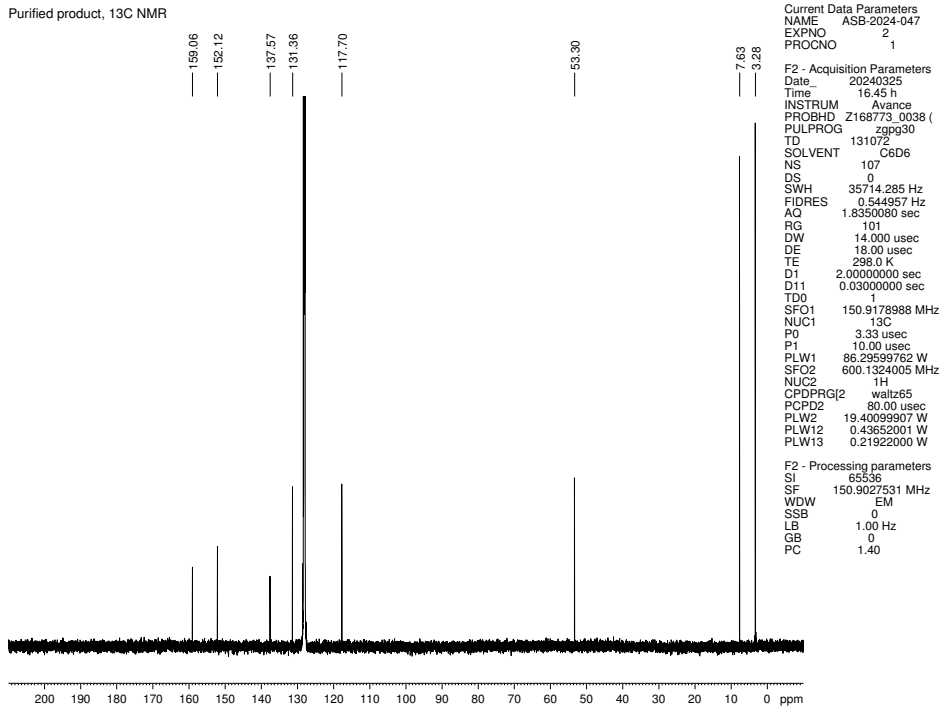

Figure 4.23. ^{13}C NMR (150 MHz, C_6D_6) of compound **4.15**.

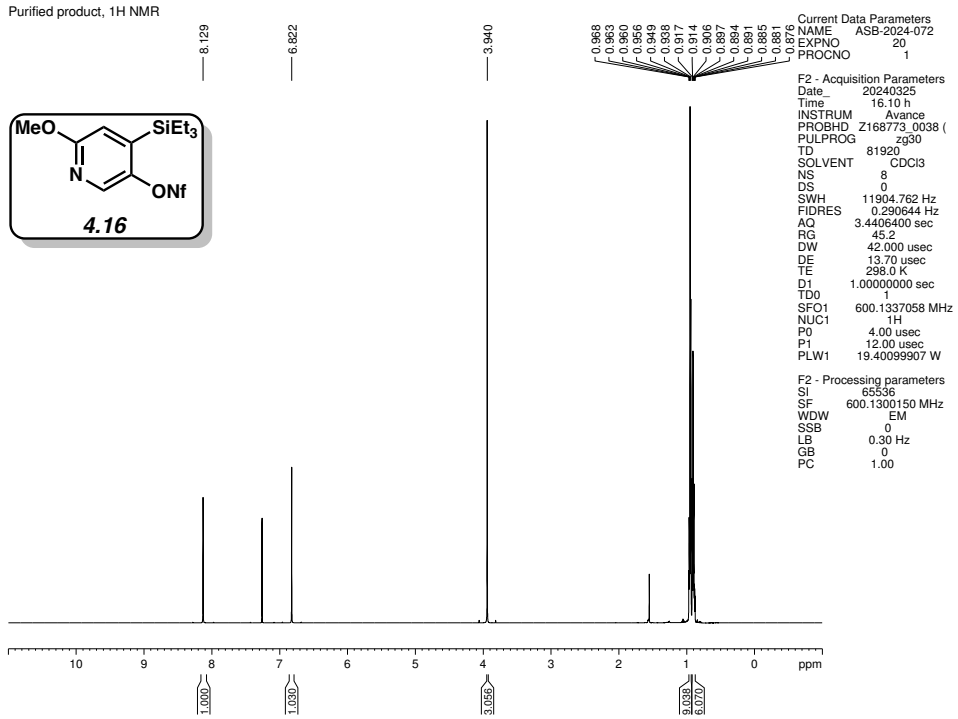

Figure 4.24. ^{1}H NMR (600 MHz, $CDCl_3$) of compound **4.16**.

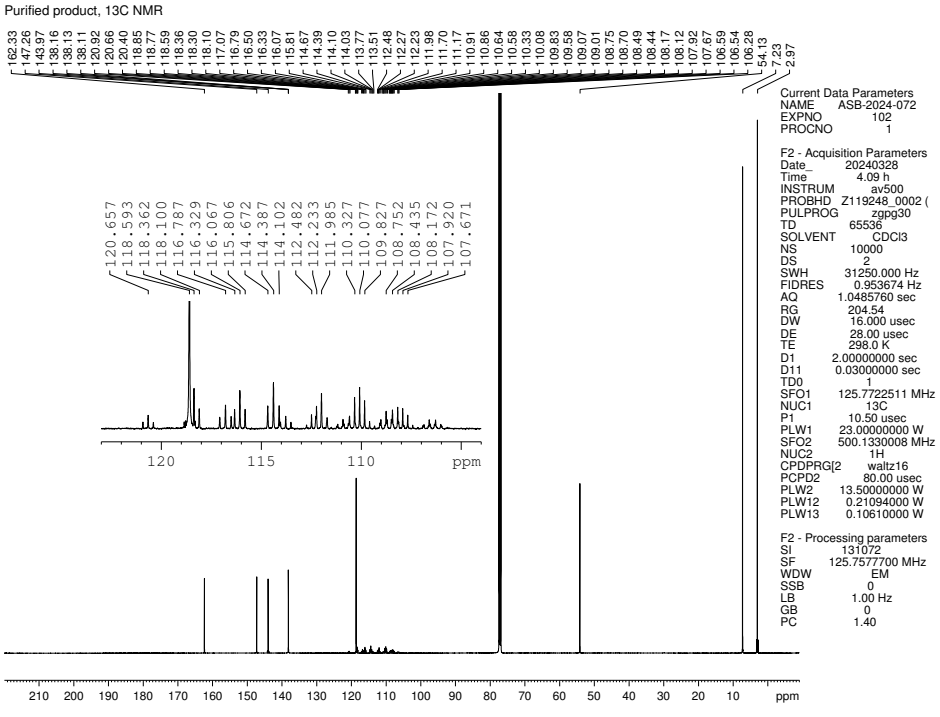

Figure 4.25. ^{13}C NMR (125 MHz, $CDCl_3$) of compound **4.16**.

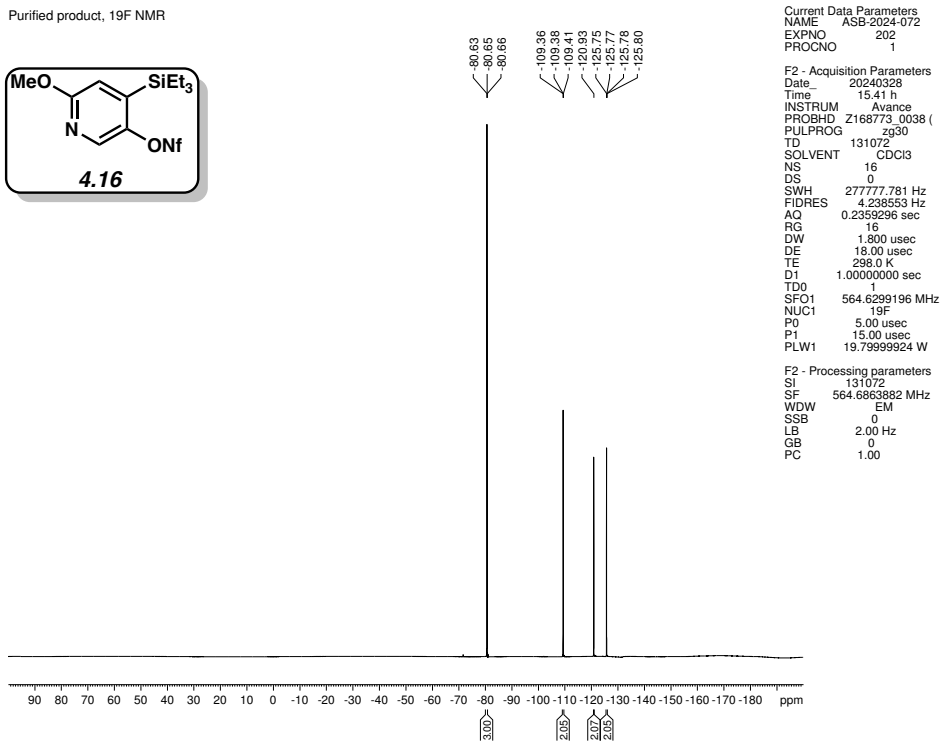

Figure 4.26. ^{19}F NMR (565 MHz, $CDCl_3$) of compound **4.16**.

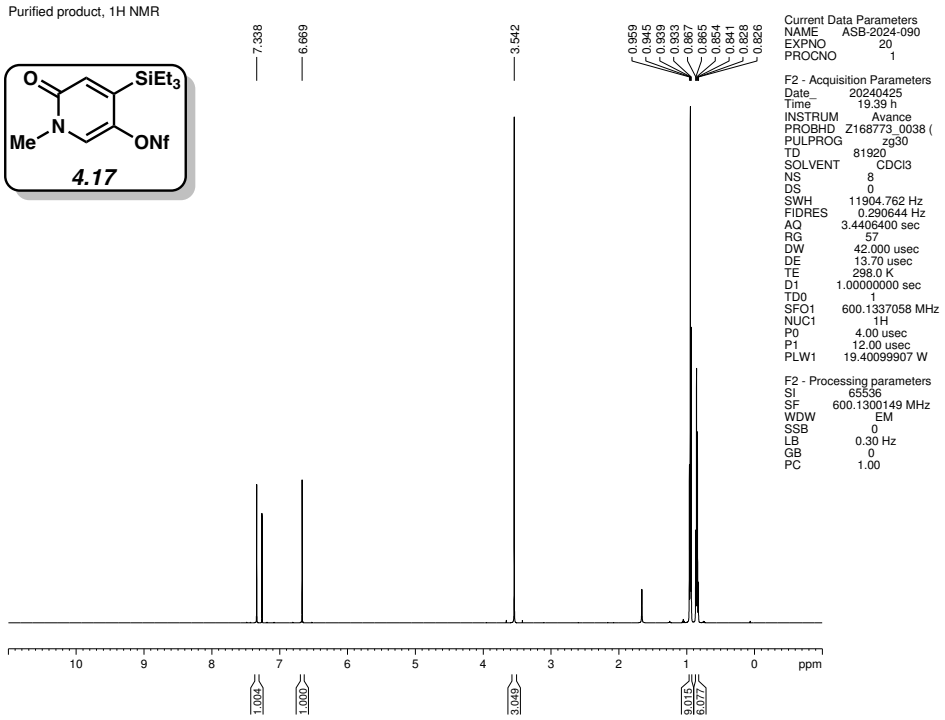

Figure 4.27. ^{1}H NMR (600 MHz, $CDCl_3$) of compound **4.17**.

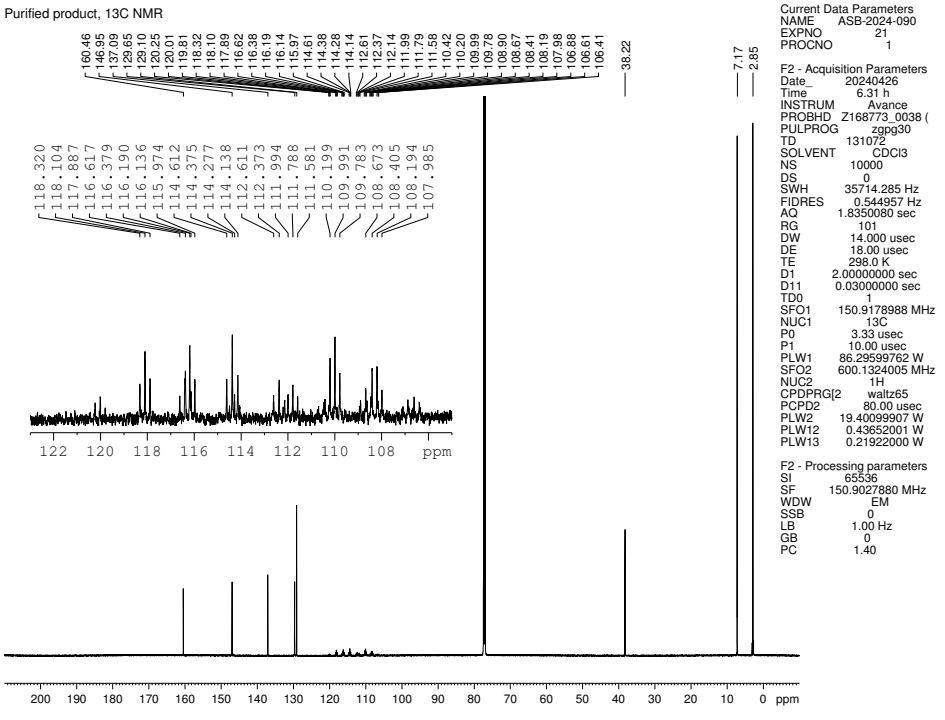

Figure 4.28. ^{13}C NMR (150 MHz, $CDCl_3$) of compound **4.17**.

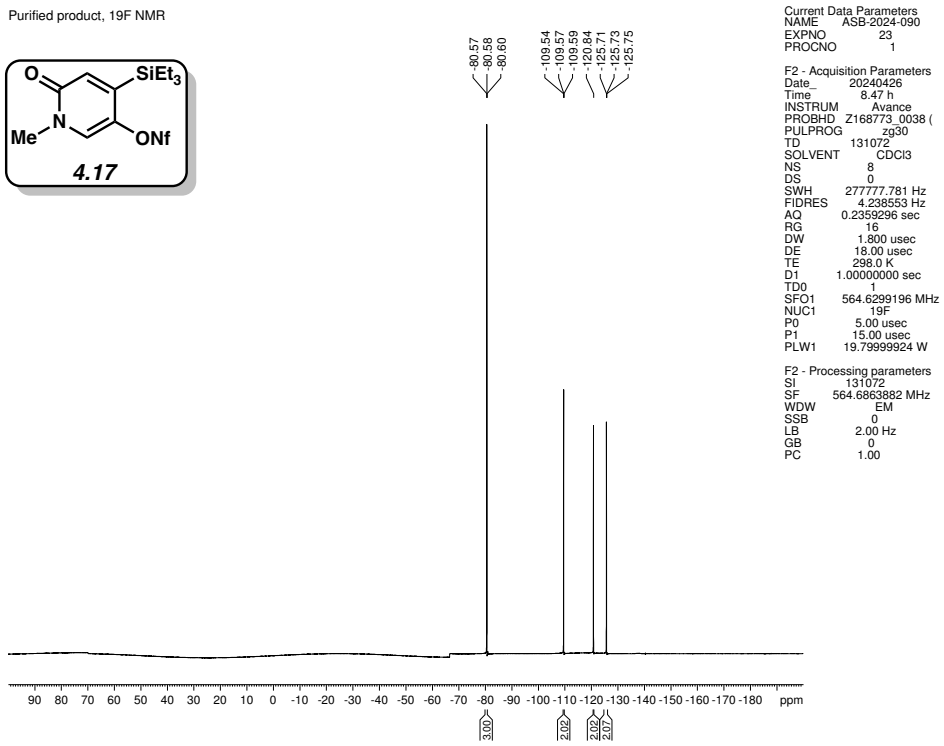

Figure 4.29. ^{19}F NMR (565 MHz, $CDCl_3$) of compound **4.17**.

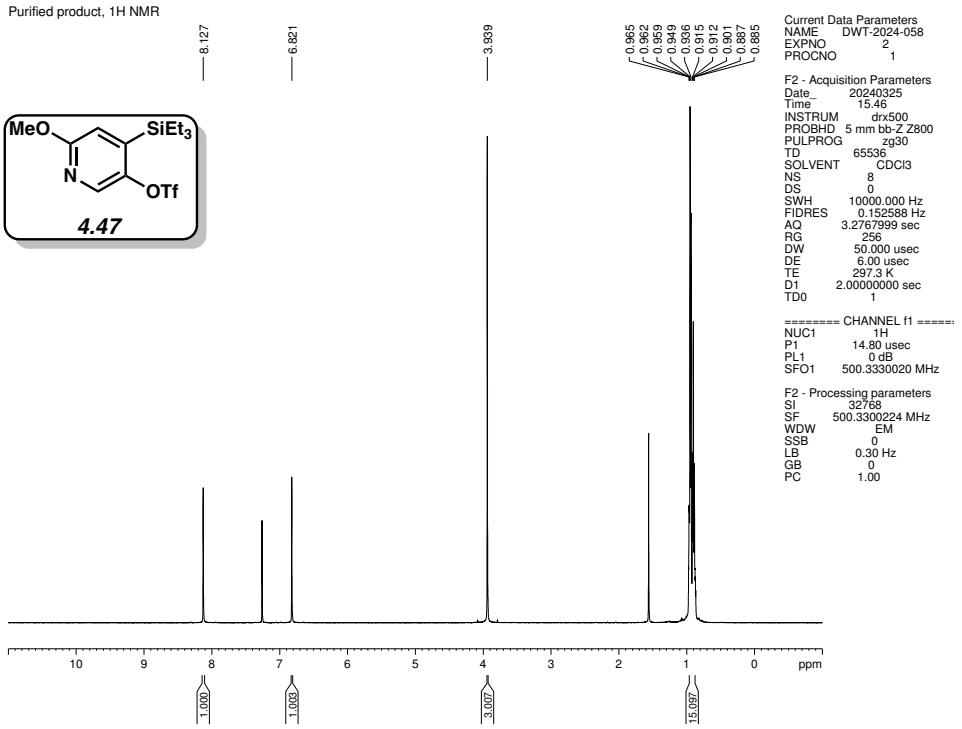

Figure 4.30. ^{1}H NMR (500 MHz, $CDCl_3$) of compound **4.47**.

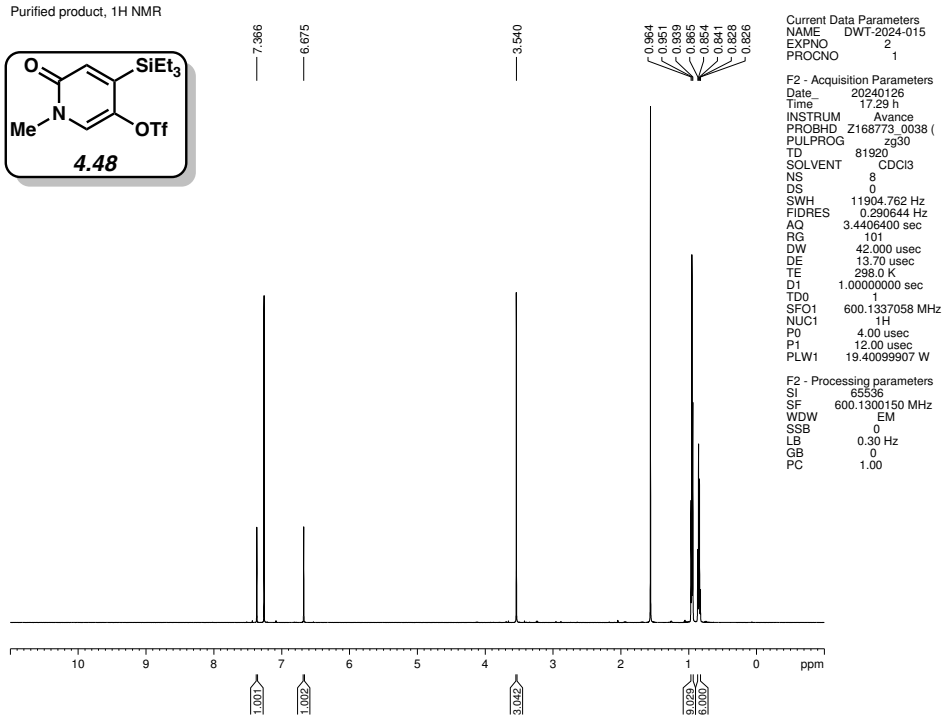

Figure 4.31. ^{1}H NMR (600 MHz, $CDCl_3$) of compound **4.48**.

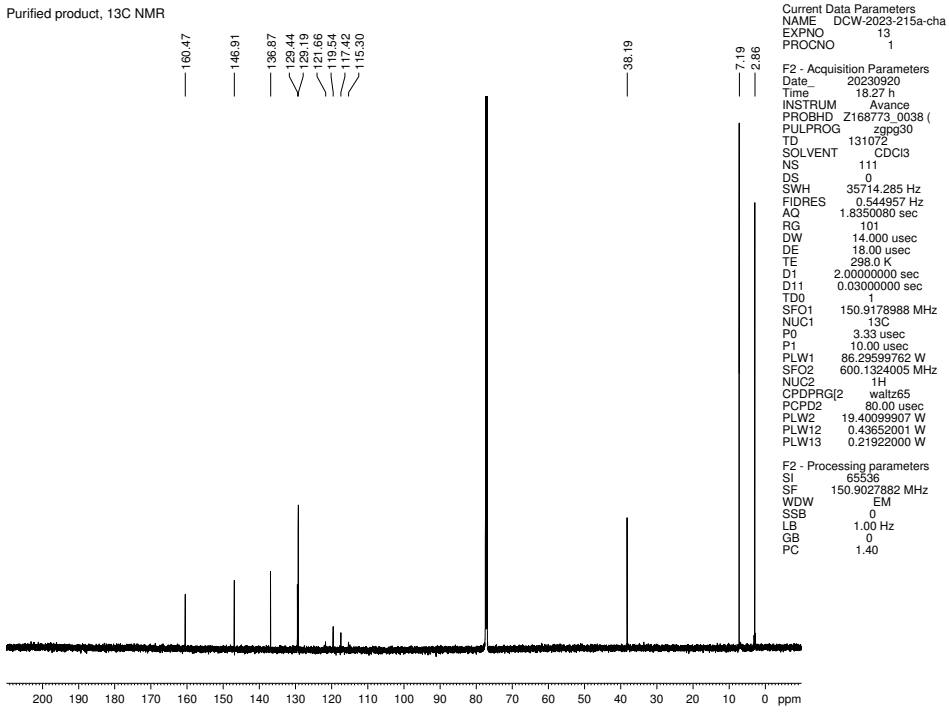

Figure 4.32. ^{13}C NMR (150 MHz, $CDCl_3$) of compound **4.48**.

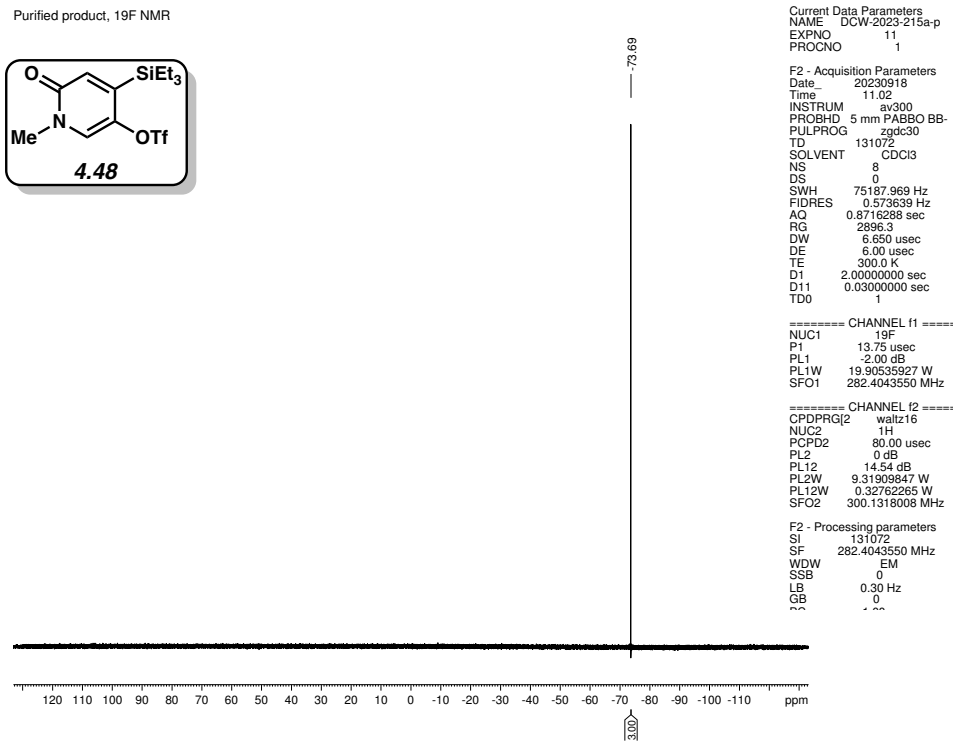

Figure 4.33. ^{19}F NMR (282 MHz, $CDCl_3$) of compound **4.48**.

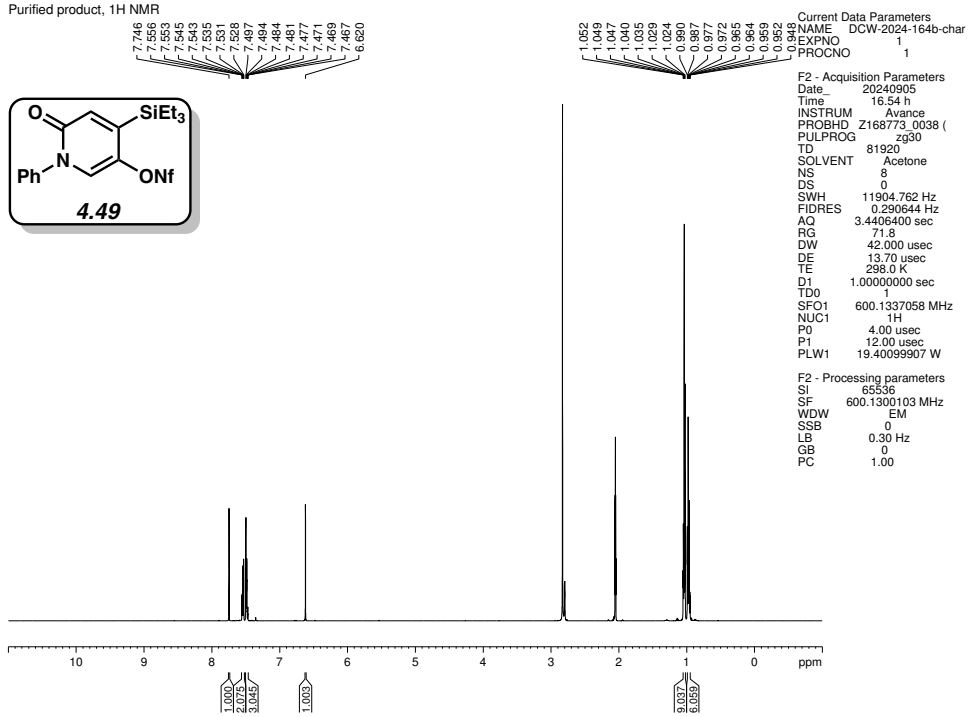

Figure 4.34. ^{1}H NMR (600 MHz, acetone-d_6) of compound **4.49**.

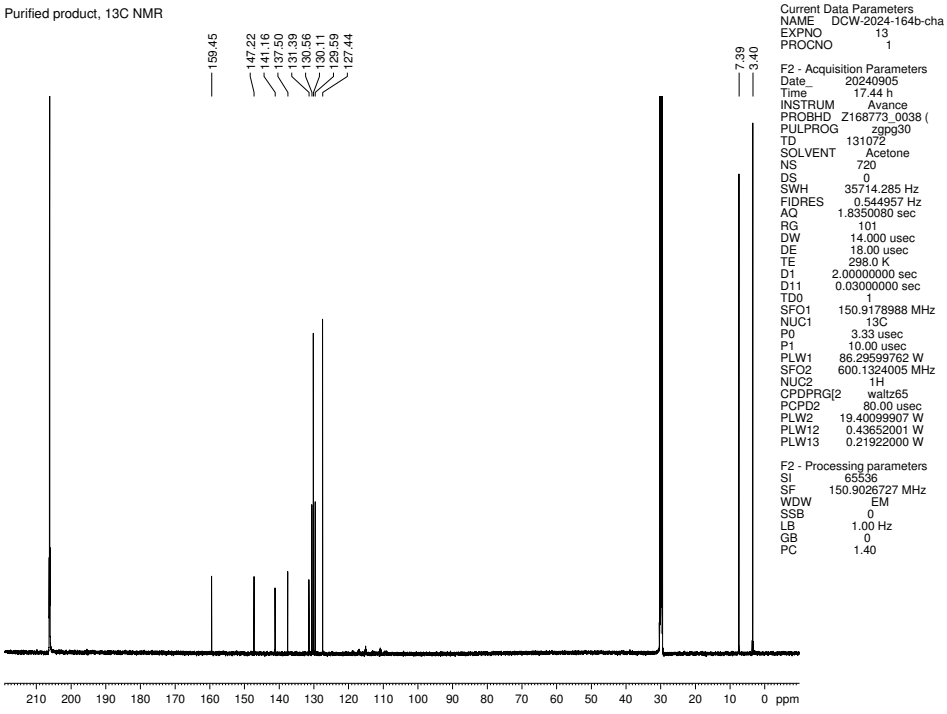

Figure 4.35. ^{13}C NMR (150 MHz, acetone-d_6) of compound **4.49**.

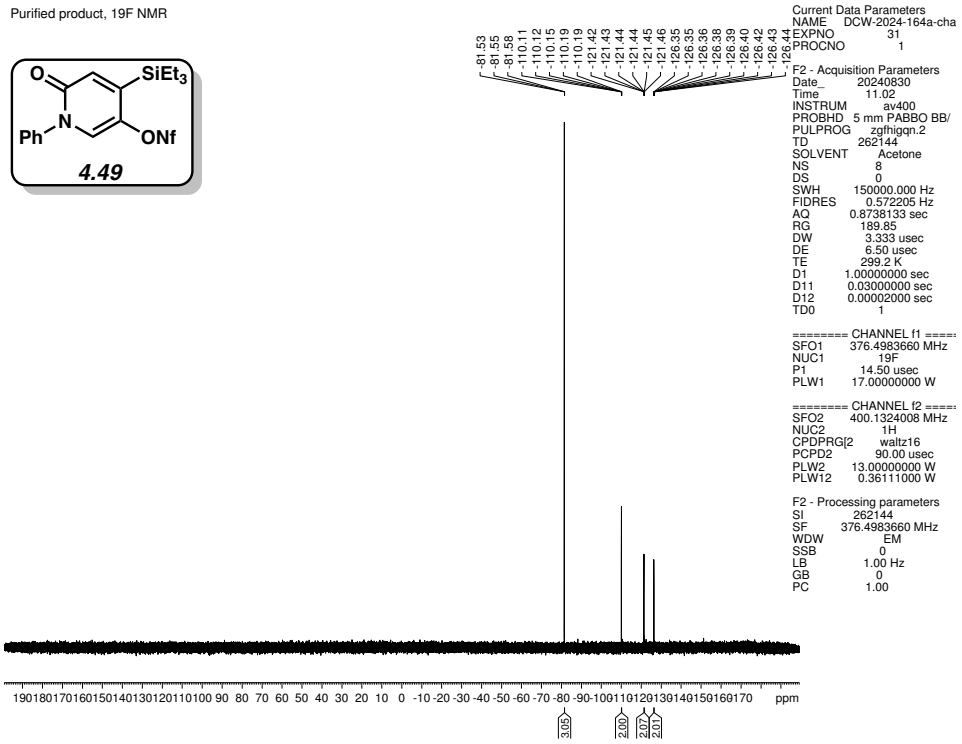

Figure 4.36. ^{19}F NMR (376 MHz, acetone-d_6) of compound **4.49**.

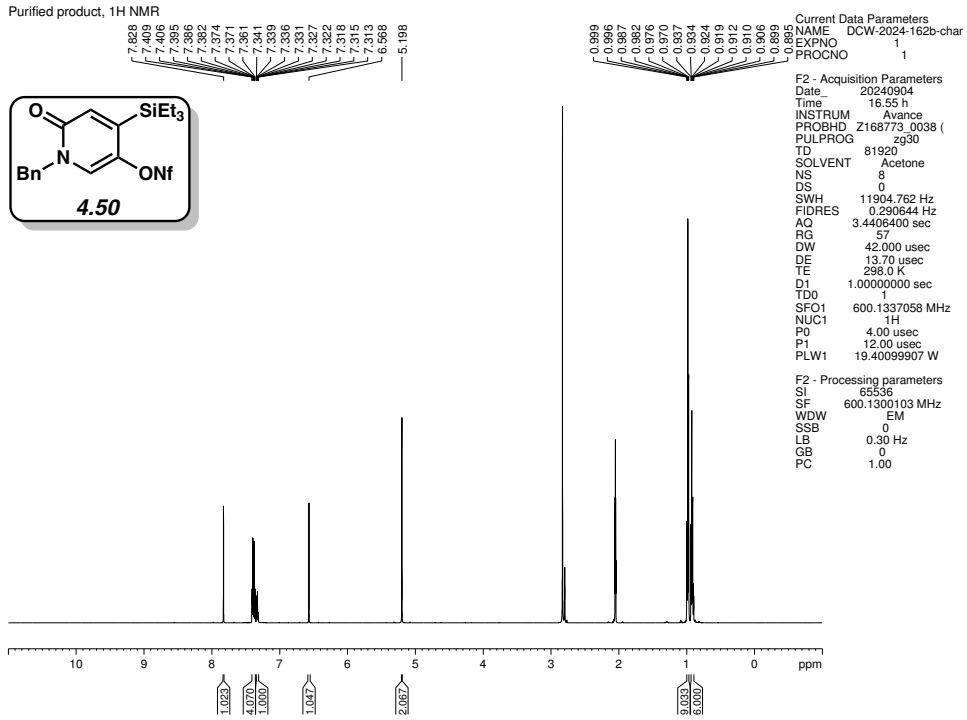

Figure 4.37. ^{1}H NMR (600 MHz, acetone-d_6) of compound **4.50**.

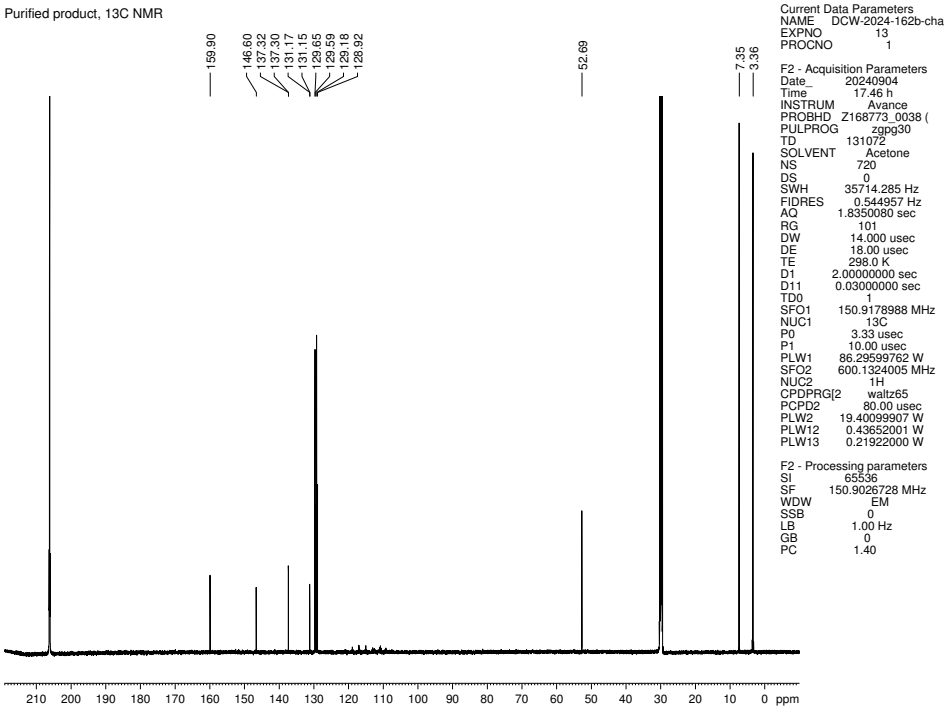

Figure 4.38. ^{13}C NMR (150 MHz, acetone-d_6) of compound **4.50**.

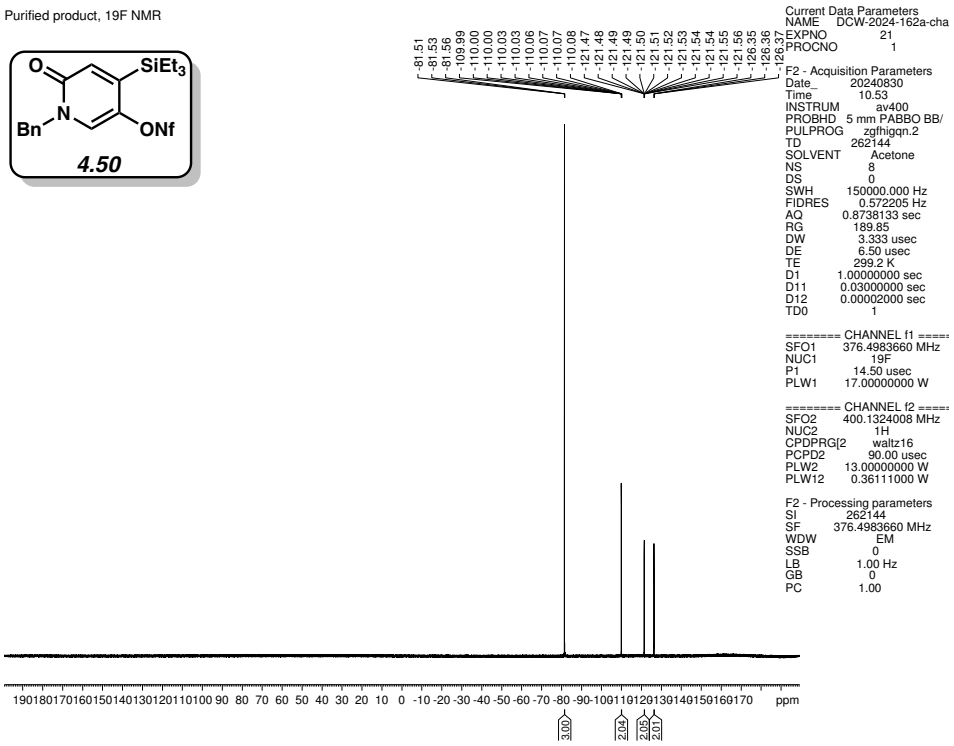

Figure 4.39. ^{19}F NMR (376 MHz, acetone-d_6) of compound **4.50**.

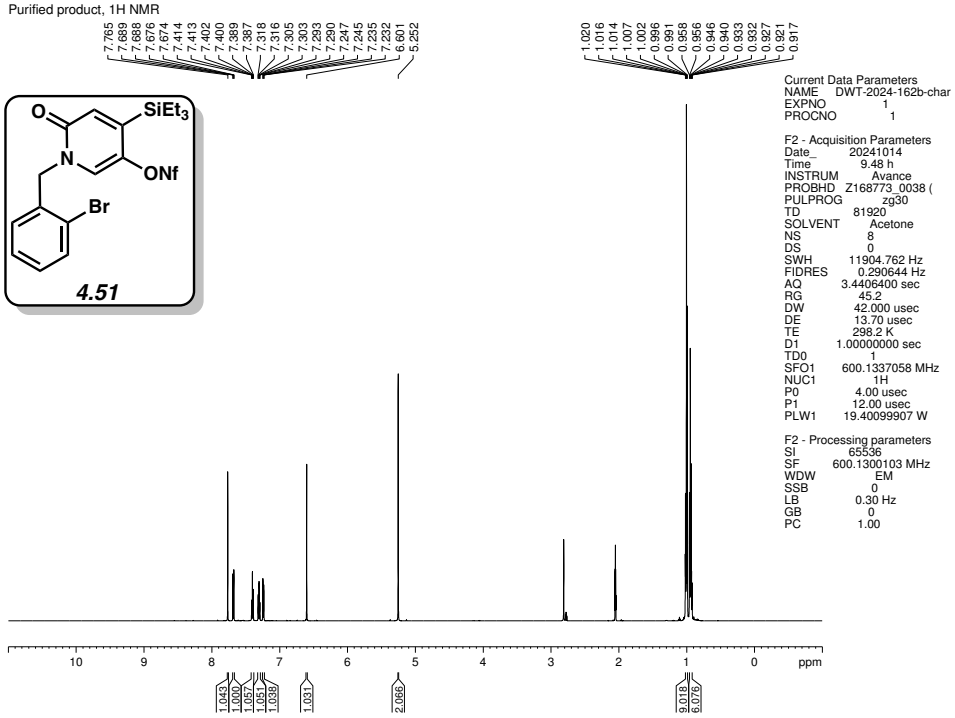

Figure 4.40. ^{1}H NMR (600 MHz, acetone-d_6) of compound **4.51**.

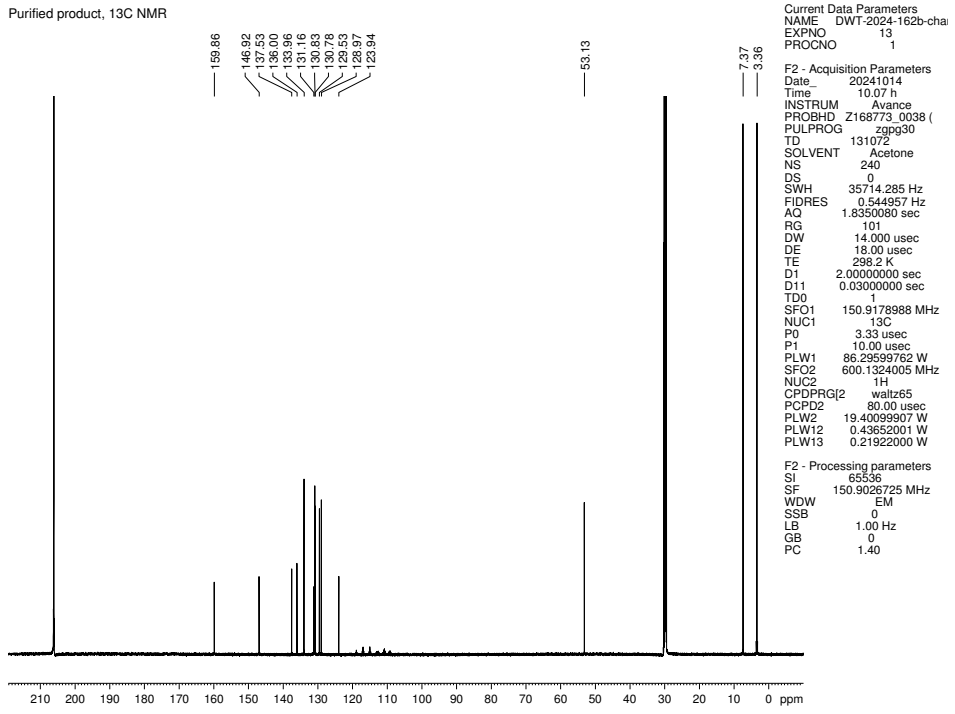

Figure 4.41. ^{13}C NMR (150 MHz, acetone-d_6) of compound **4.51**.

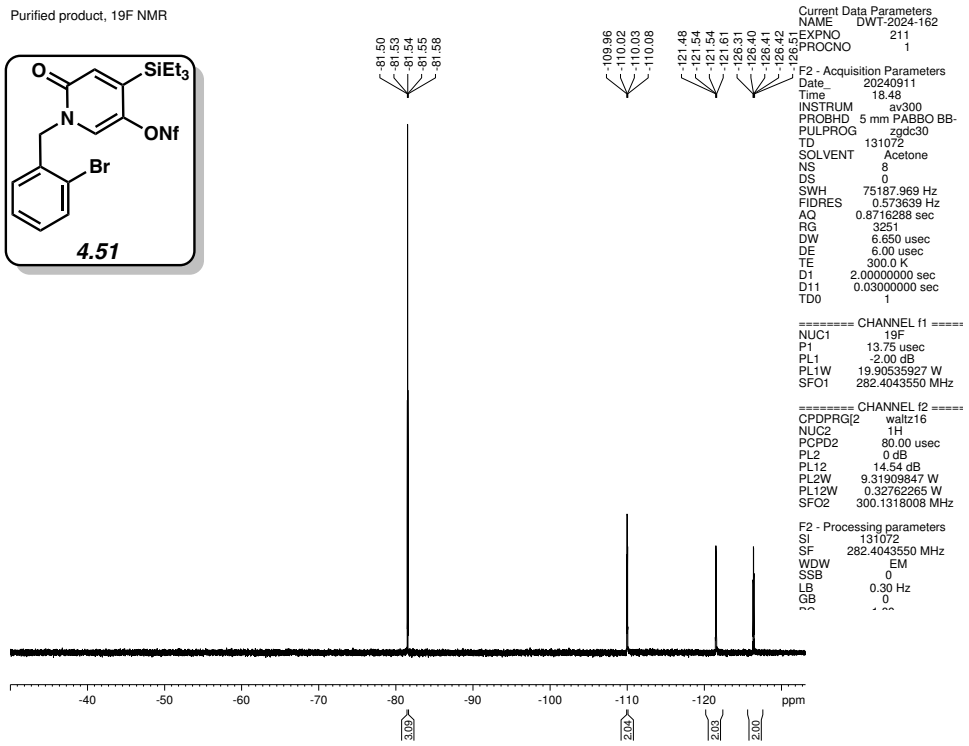

Figure 4.42. ^{19}F NMR (282 MHz, acetone-d_6) of compound **4.51**.

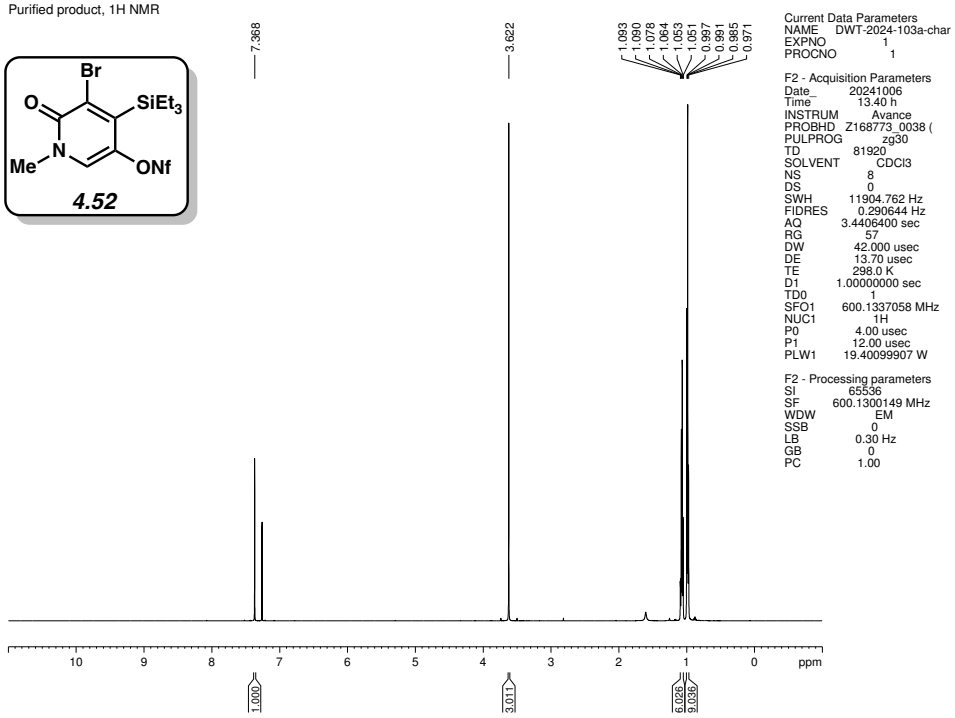

Figure 4.43. ^{1}H NMR (600 MHz, $CDCl_3$) of compound **4.52**.

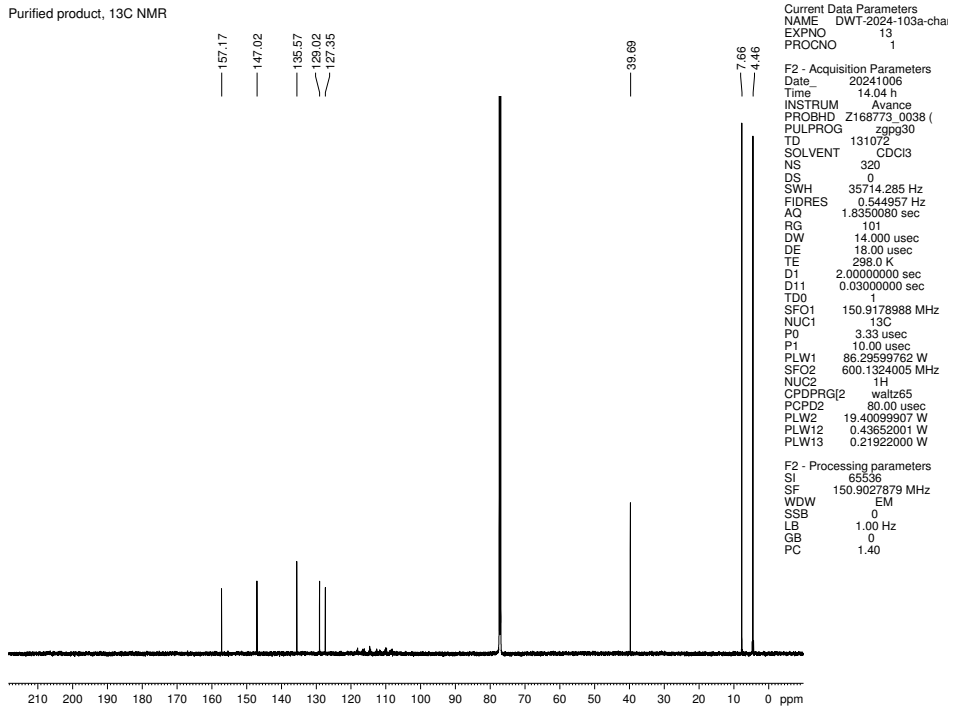

Figure 4.44. ^{13}C NMR (150 MHz, $CDCl_3$) of compound **4.52**.

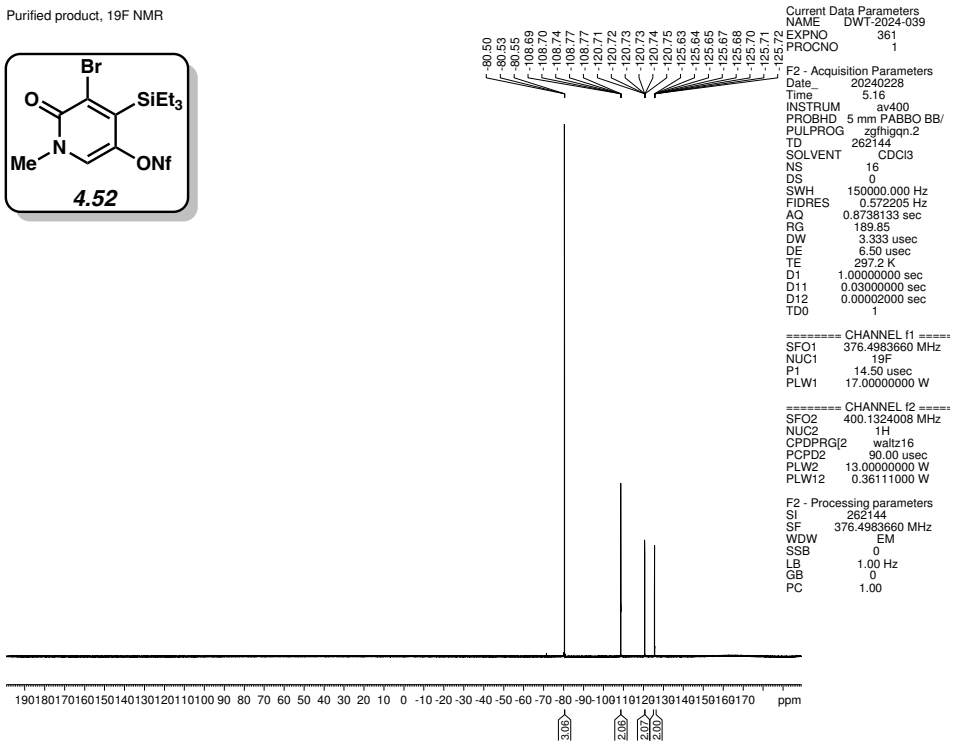

Figure 4.45. ^{19}F NMR (376 MHz, $CDCl_3$) of compound **4.52**.

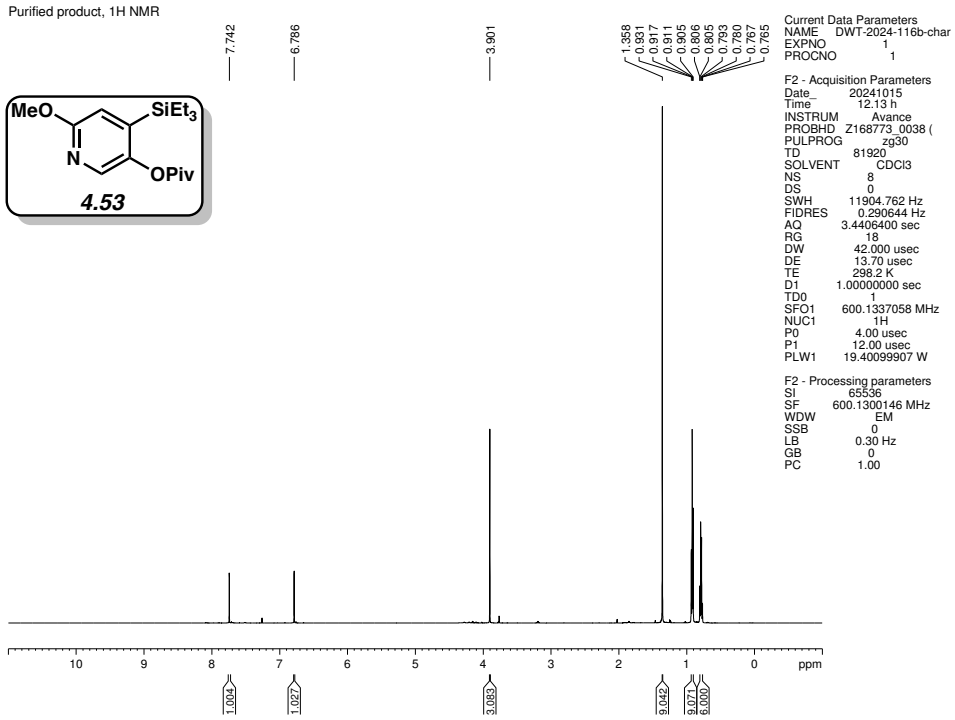

Figure 4.46. ^{1}H NMR (600 MHz, $CDCl_3$) of compound **4.53**.

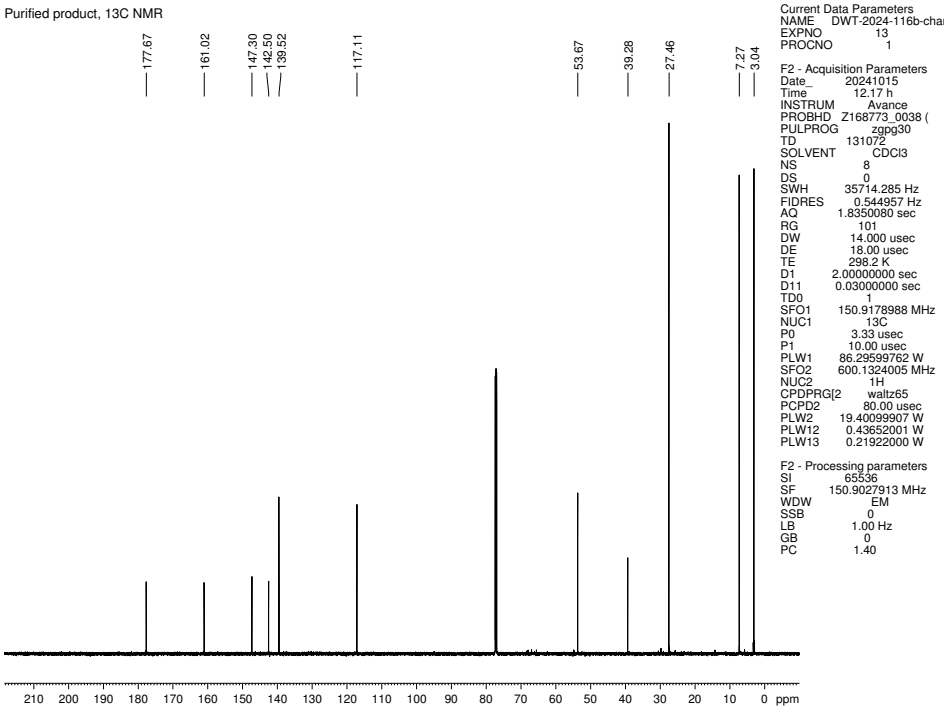

Figure 4.47. ^{13}C NMR (150 MHz, $CDCl_3$) of compound **4.53**.

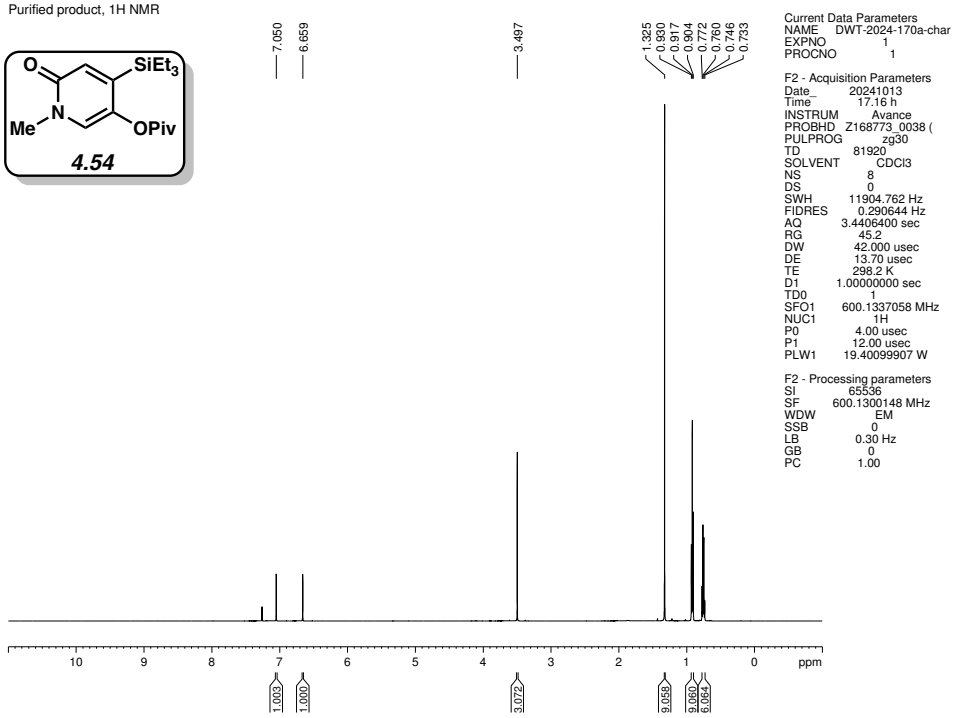

Figure 4.48. ^{1}H NMR (600 MHz, $CDCl_3$) of compound **4.54**.

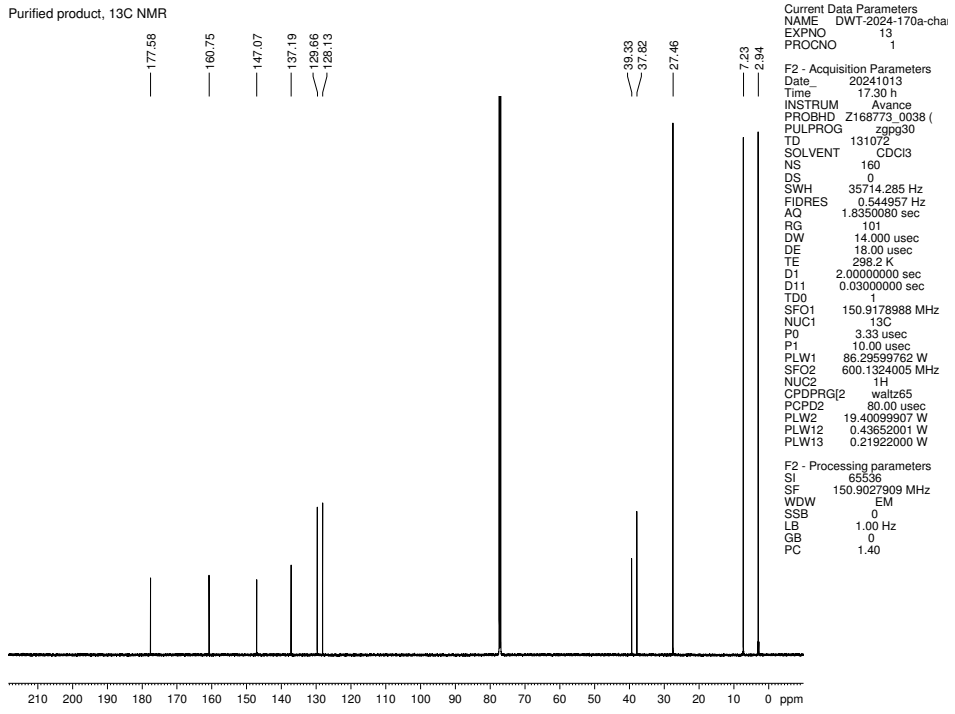

Figure 4.49. ^{13}C NMR (150 MHz, $CDCl_3$) of compound **4.54**.

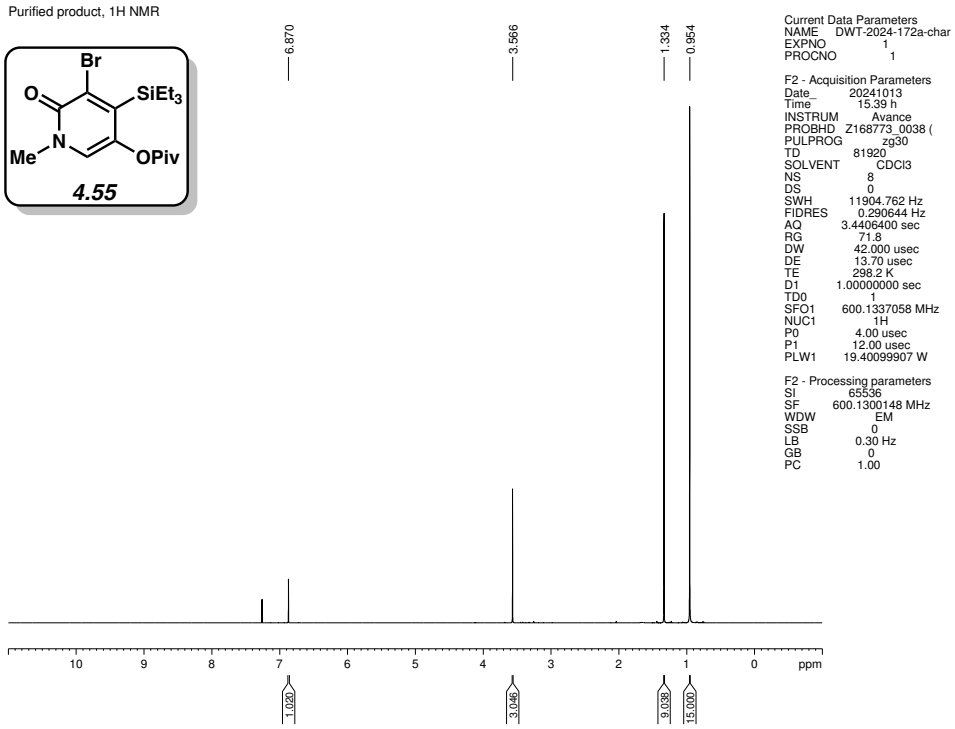

Figure 4.50. ^{1}H NMR (600 MHz, $CDCl_3$) of compound **4.55**.

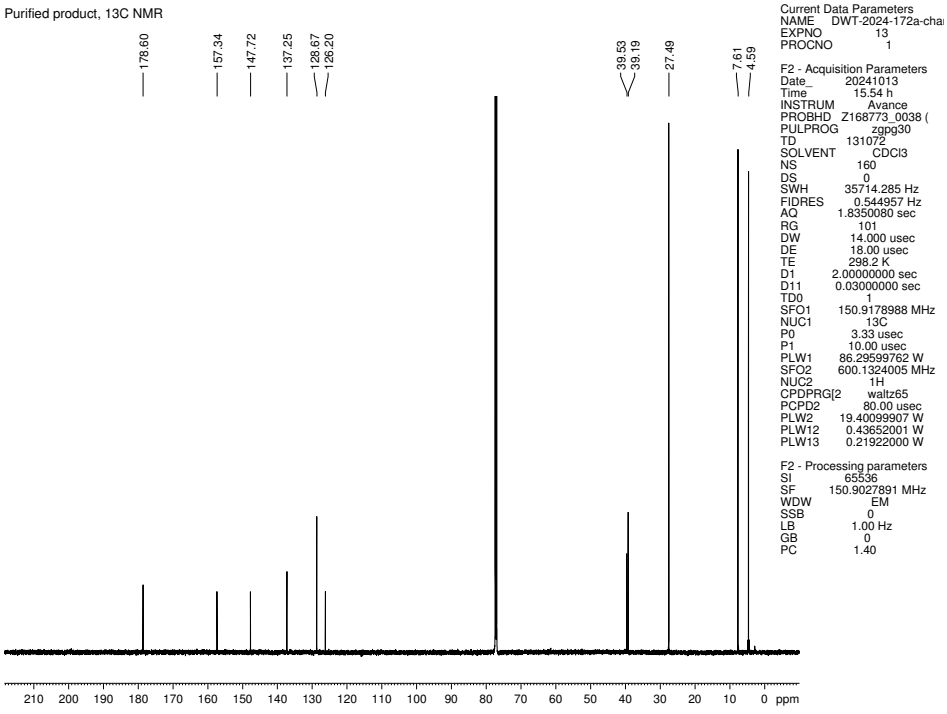

Figure 4.51. ^{13}C NMR (150 MHz, $CDCl_3$) of compound **4.55**.

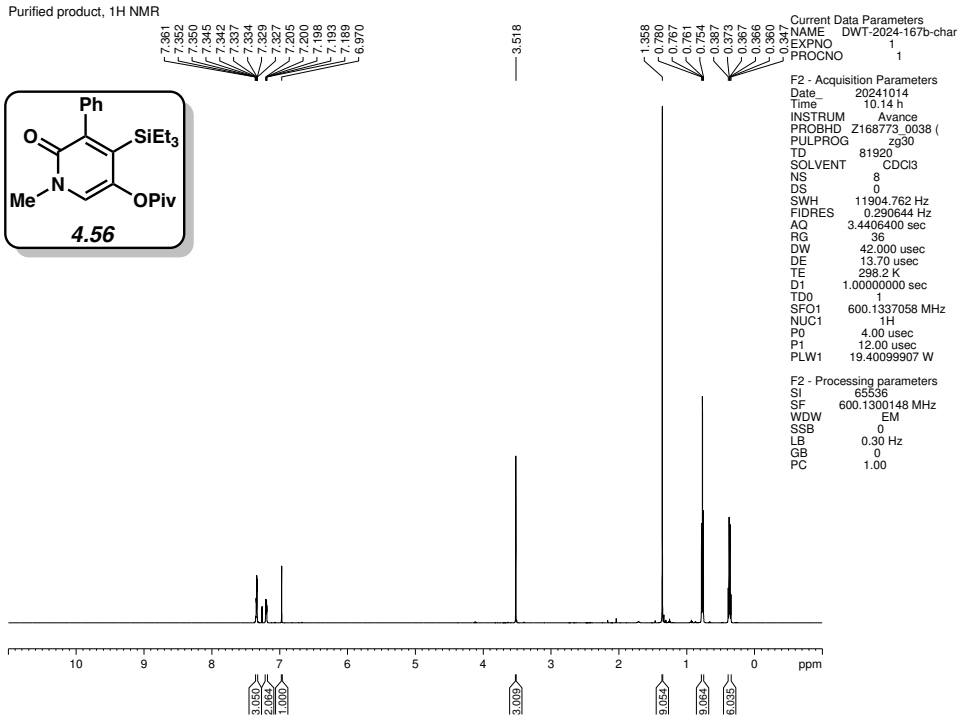

Figure 4.52. ^{1}H NMR (600 MHz, $CDCl_3$) of compound **4.56**.

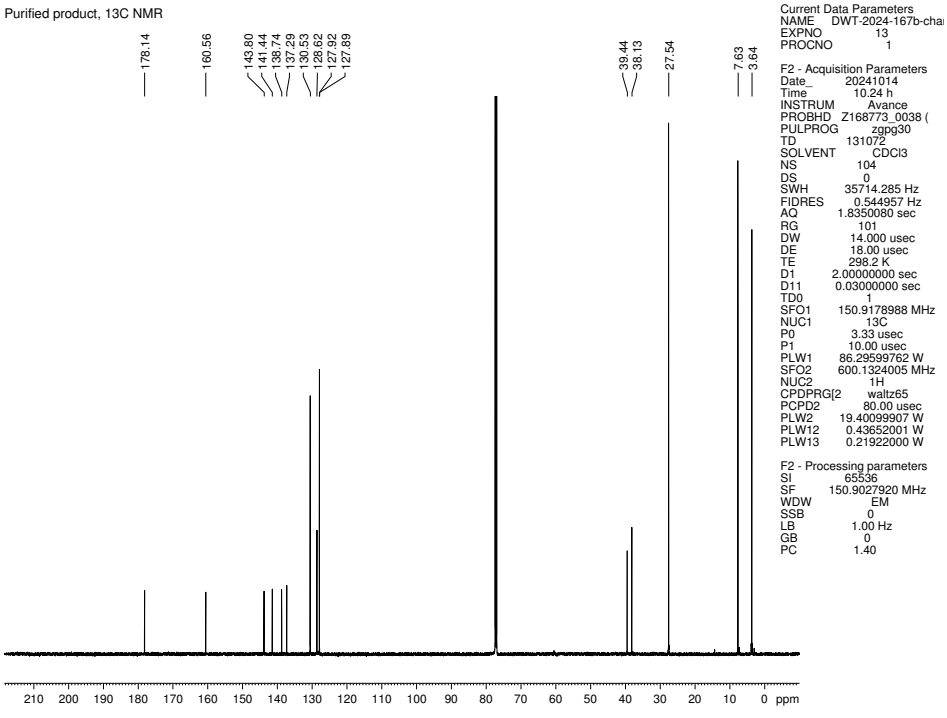

Figure 4.53. ^{13}C NMR (150 MHz, $CDCl_3$) of compound **4.56**.

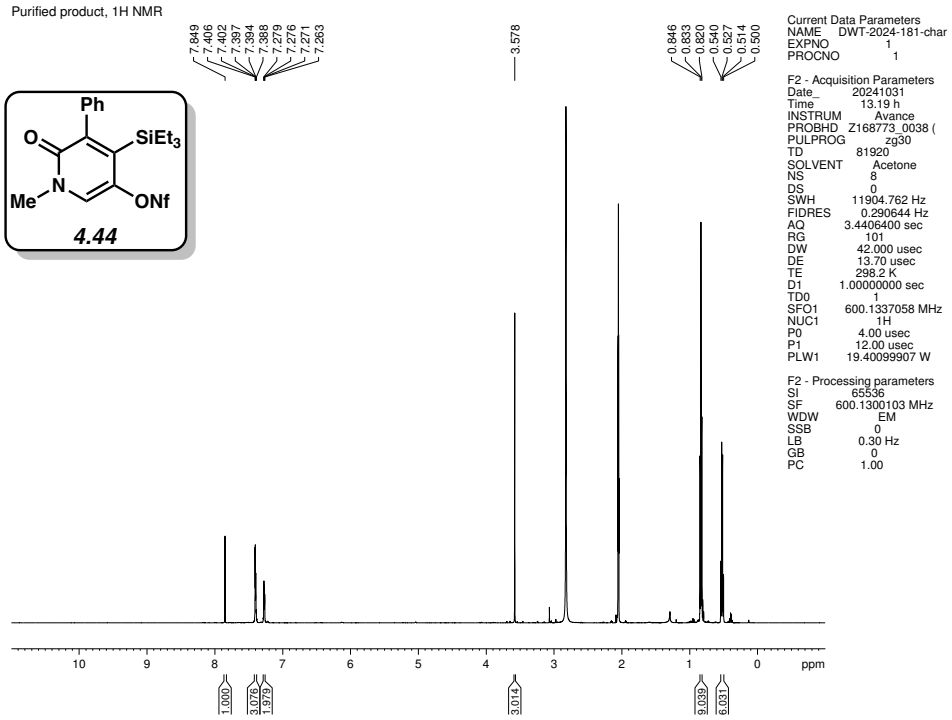

Figure 4.54. ^{1}H NMR (600 MHz, acetone-d_6) of compound **4.44**.

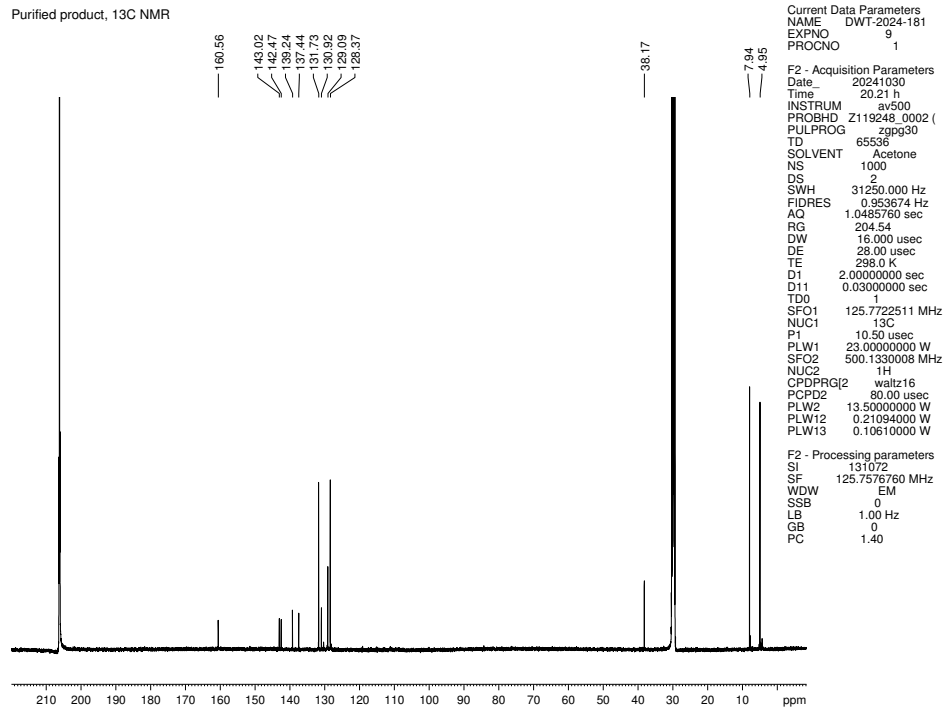

Figure 4.55. ^{13}C NMR (125 MHz, acetone-d_6) of compound **4.44**.

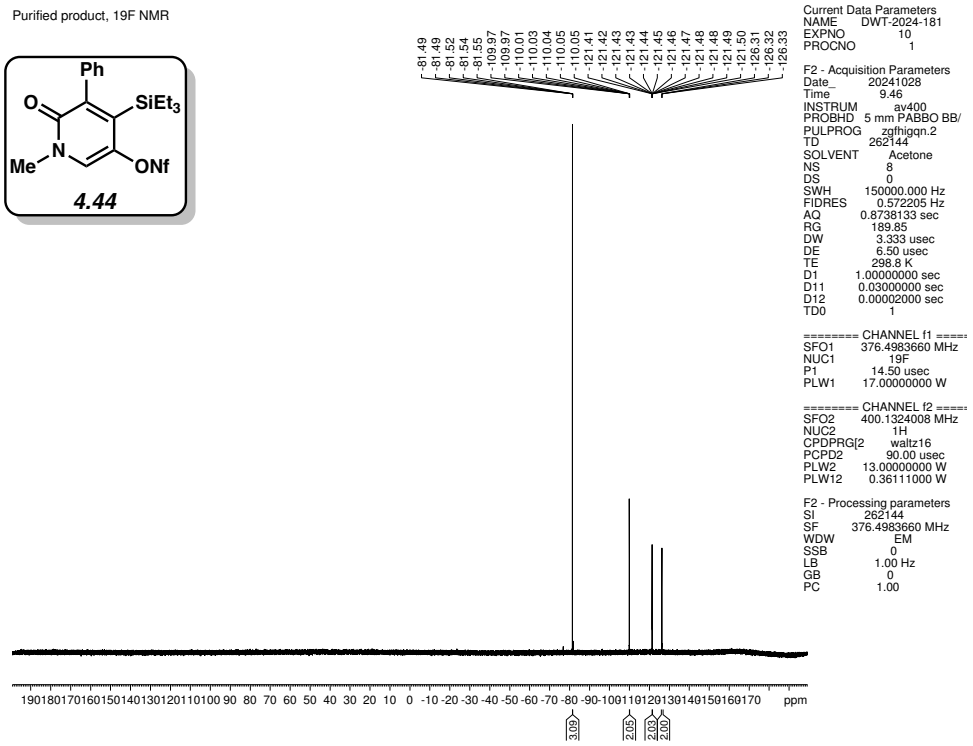

Figure 4.56. ^{19}F NMR (376 MHz, acetone-d_6) of compound **4.44**.

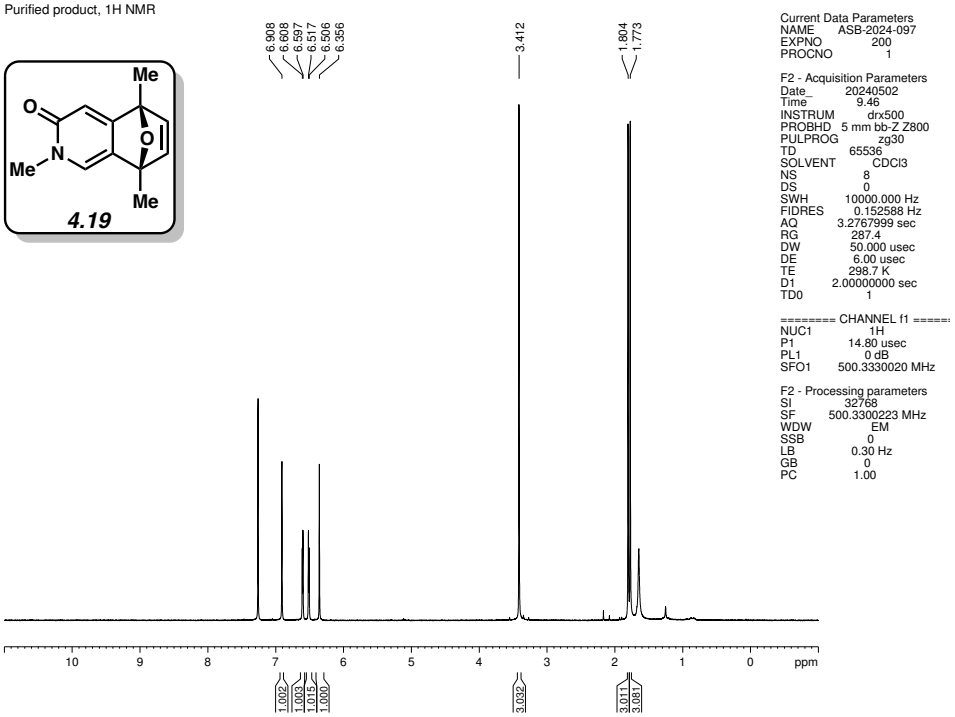

Figure 4.57. ^{1}H NMR (500 MHz, $CDCl_3$) of compound **4.19**.

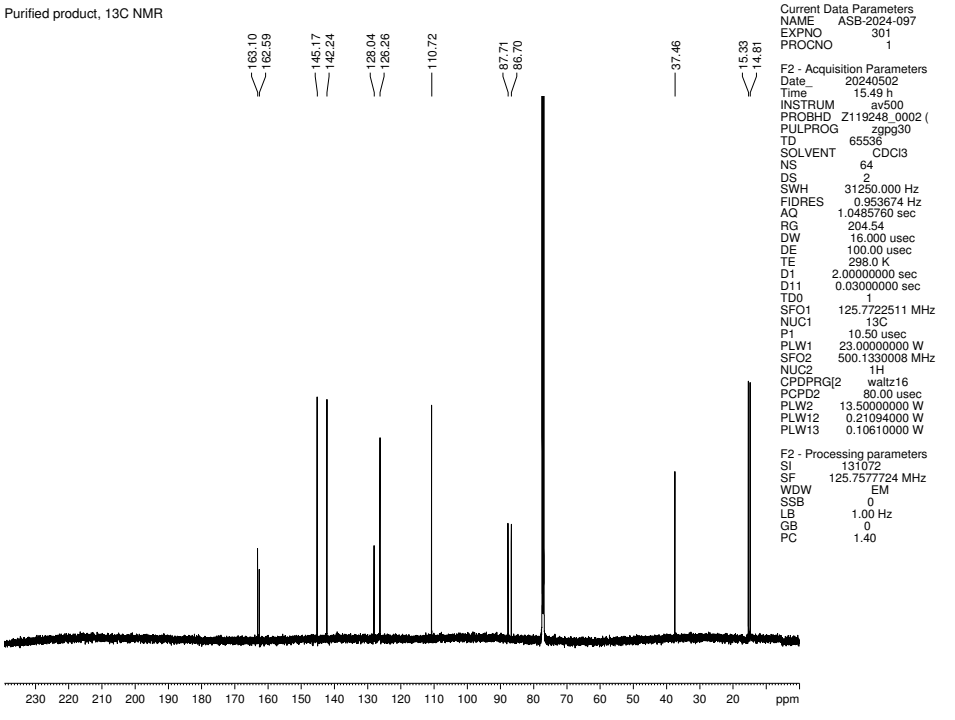

Figure 4.58. ^{13}C NMR (125 MHz, $CDCl_3$) of compound **4.19**.

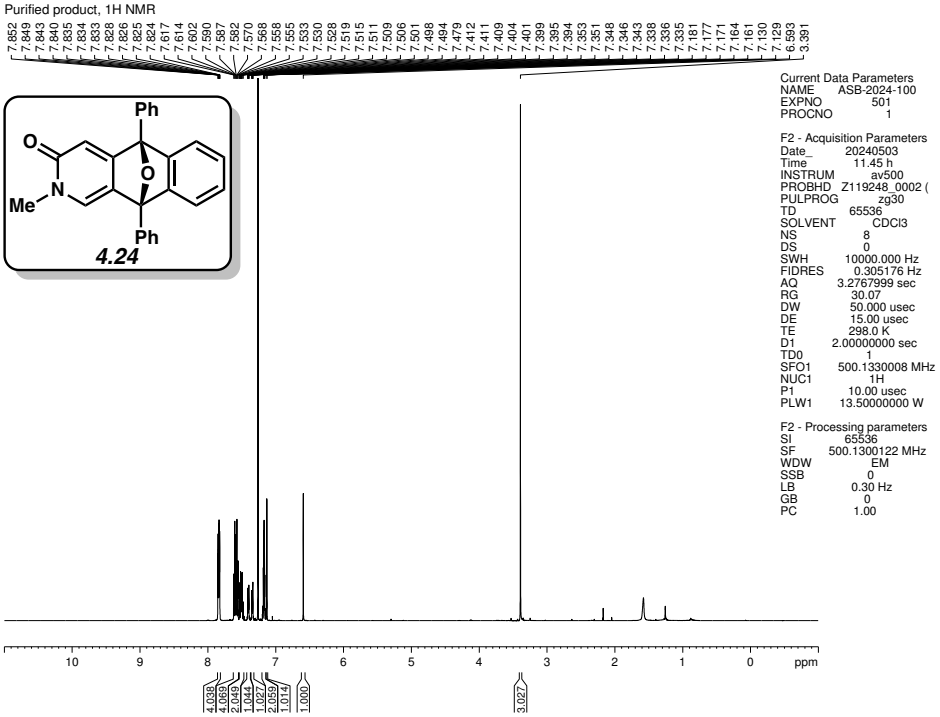

Figure 4.59. ^{1}H NMR (500 MHz, $CDCl_3$) of compound **4.24**.

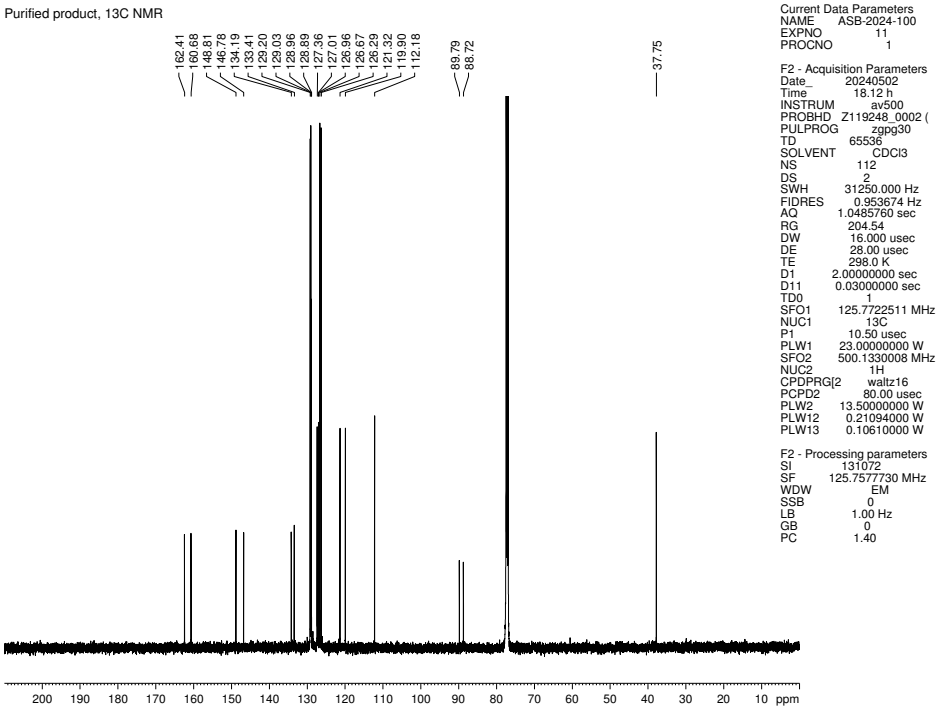

Figure 4.60. ^{13}C NMR (125 MHz, $CDCl_3$) of compound **4.24**.

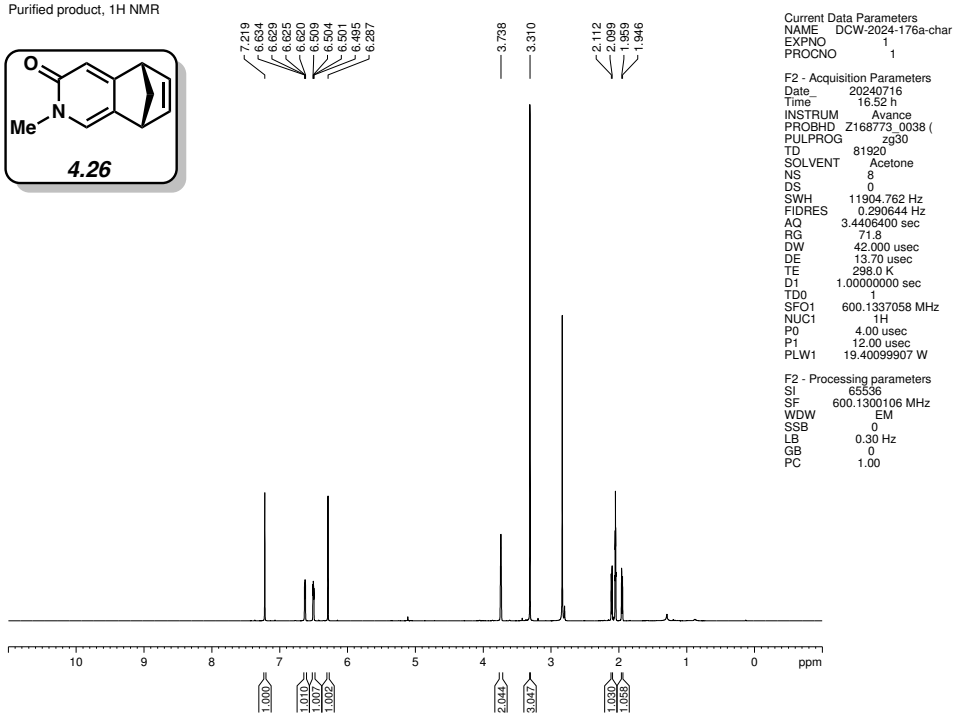

Figure 4.61. ^{1}H NMR (600 MHz, acetone-d_6) of compound **4.26**.

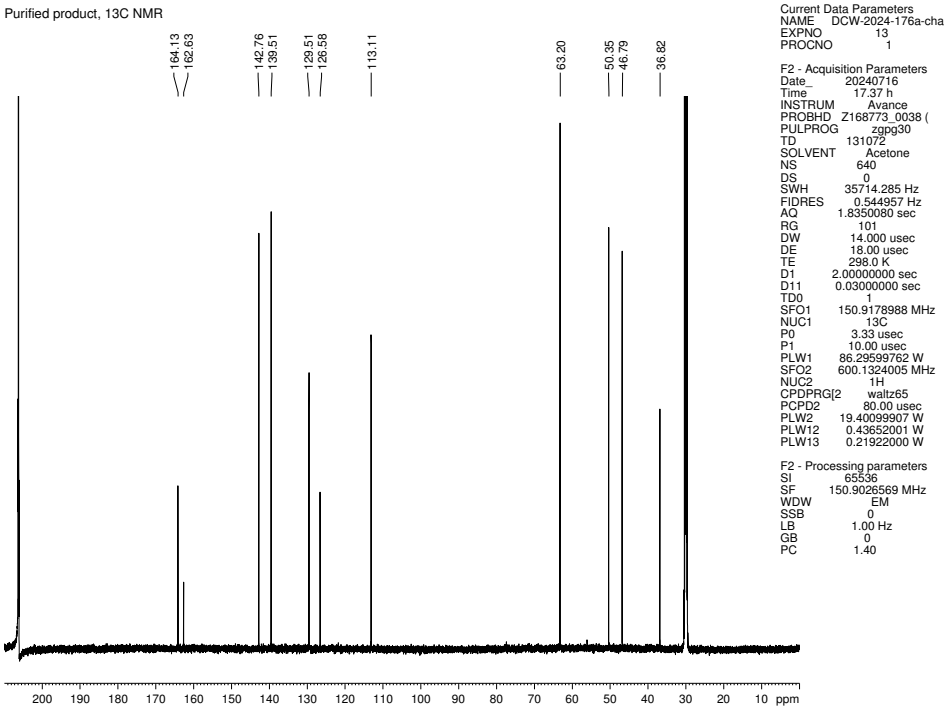

Figure 4.62. ^{13}C NMR (150 MHz, acetone-d_6) of compound **4.26**.

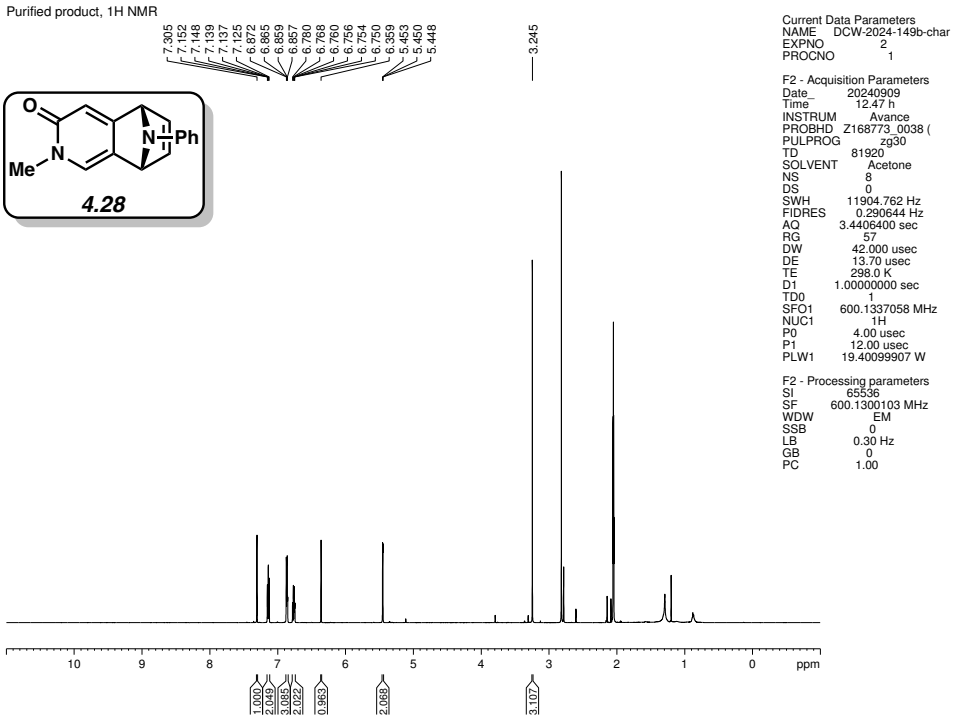

Figure 4.63. ^{1}H NMR (600 MHz, acetone-d_6) of compound **4.28**.

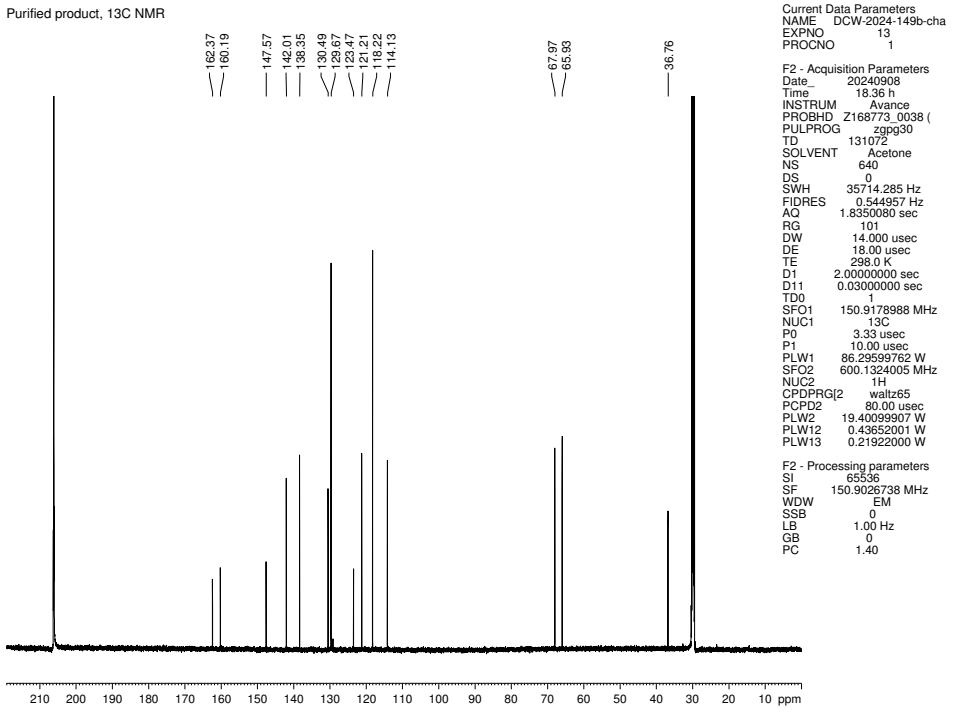

Figure 4.64. ^{13}C NMR (150 MHz, acetone-d_6) of compound **4.28**.

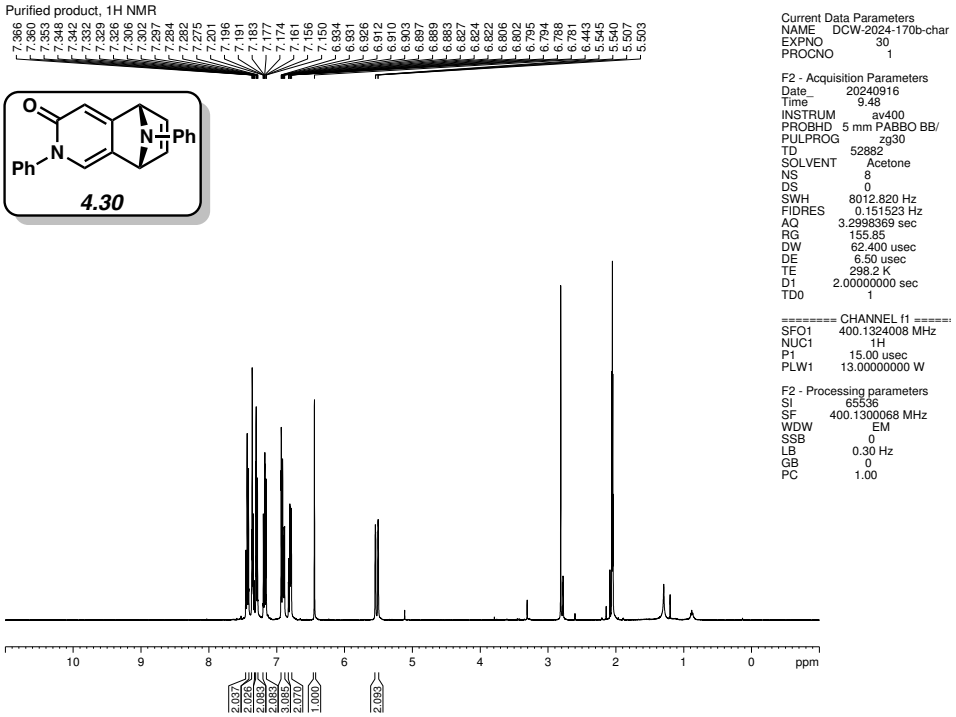

Figure 4.65. ^{1}H NMR (400 MHz, acetone-d_6) of compound **4.30**.

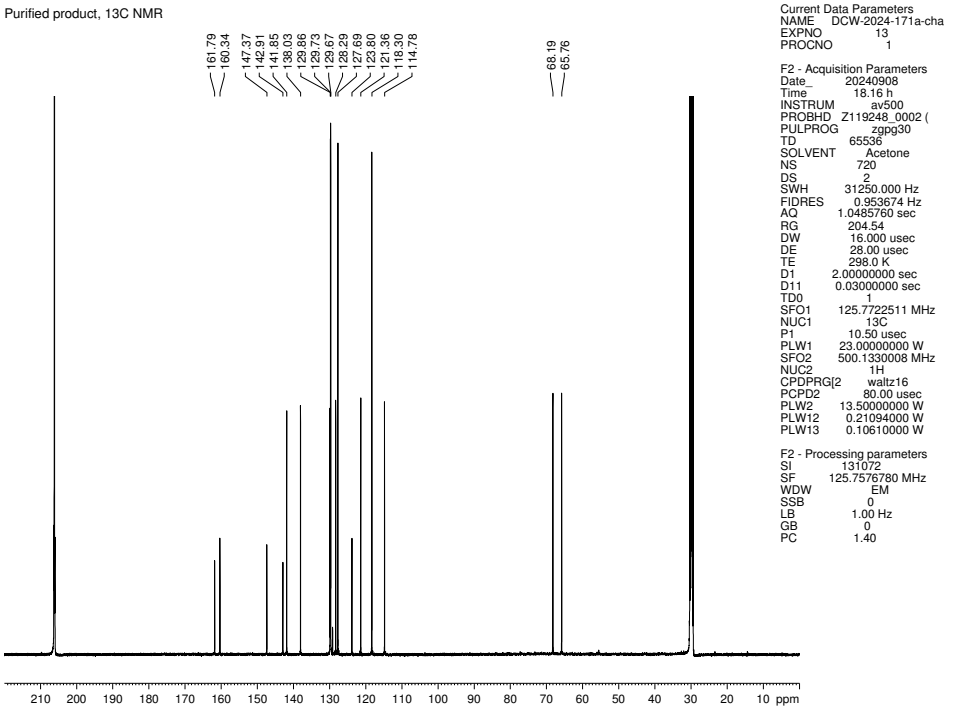

Figure 4.66. ^{13}C NMR (125 MHz, acetone-d_6) of compound **4.30**.

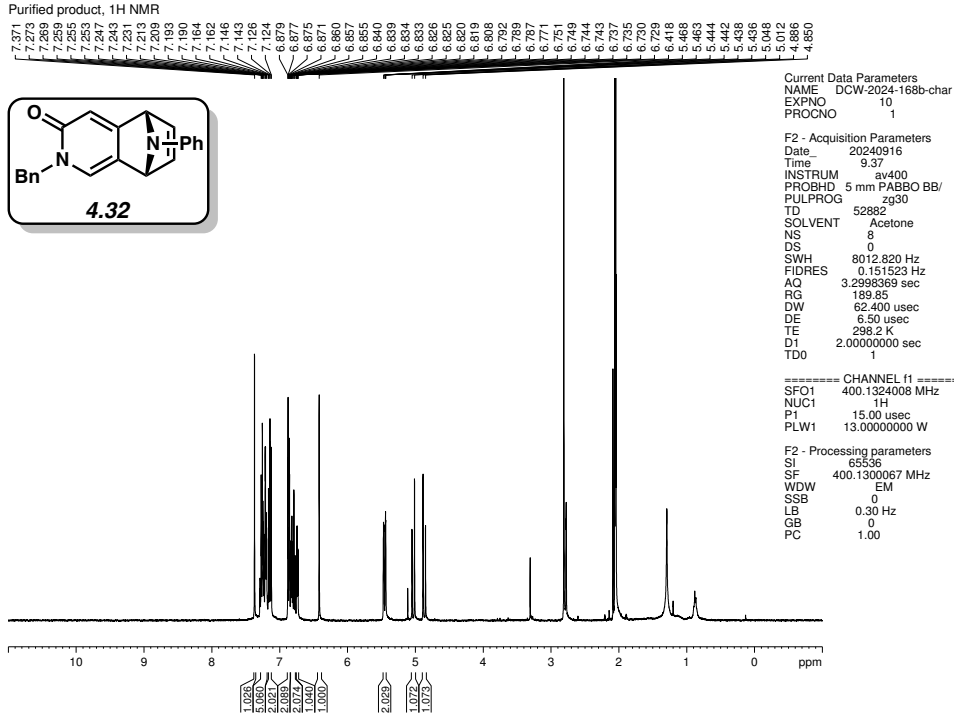

Figure 4.67. ^{1}H NMR (400 MHz, acetone-d_6) of compound **4.32**.

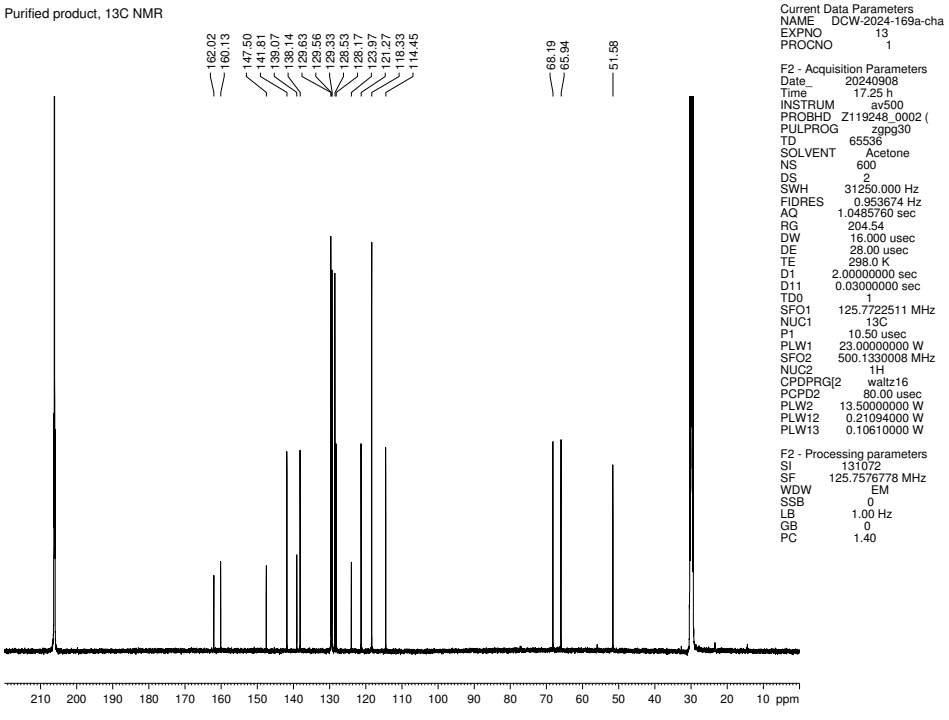

Figure 4.68. ^{13}C NMR (125 MHz, acetone-d_6) of compound **4.32**.

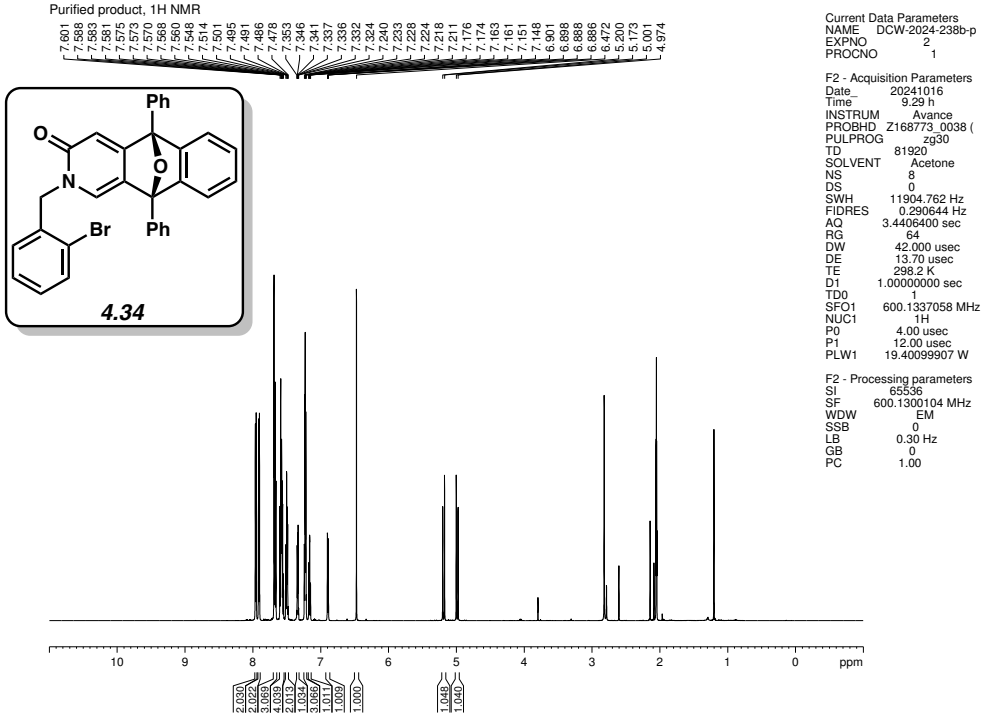

Figure 4.69. ^{1}H NMR (600 MHz, acetone-d_6) of compound **4.34**.

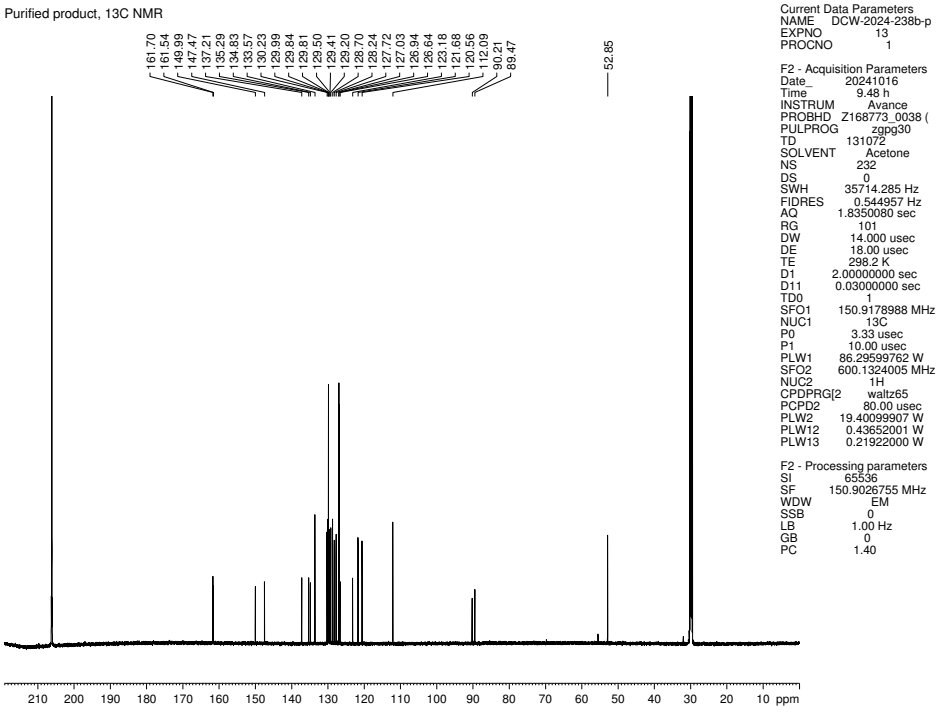

Figure 4.70. ^{13}C NMR (150 MHz, acetone-d_6) of compound **4.34**.

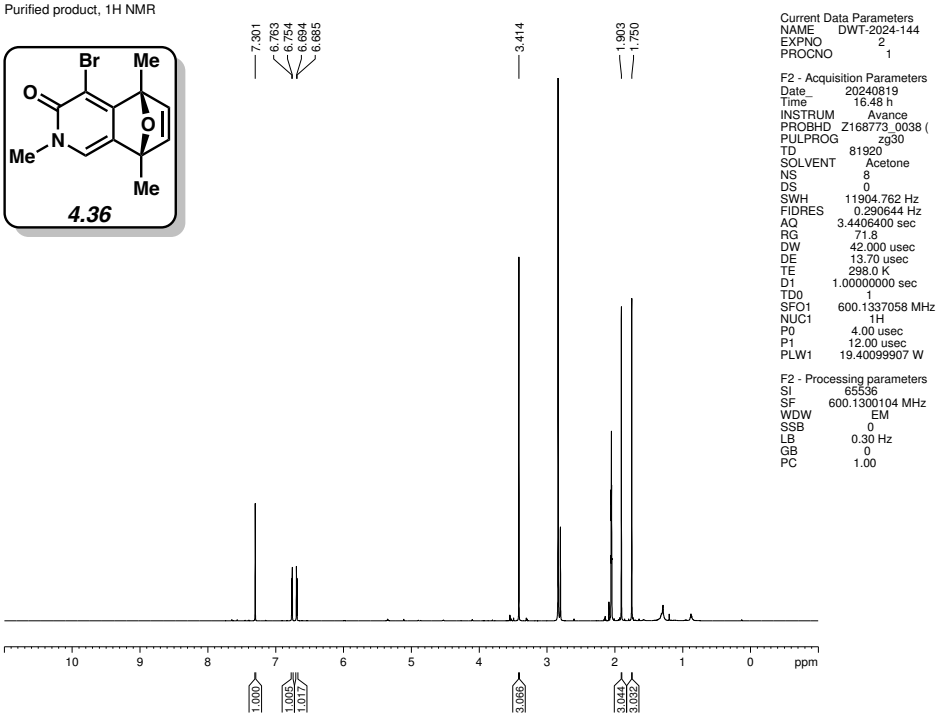

Figure 4.71. ^{1}H NMR (600 MHz, acetone-d_6) of compound **4.36**.

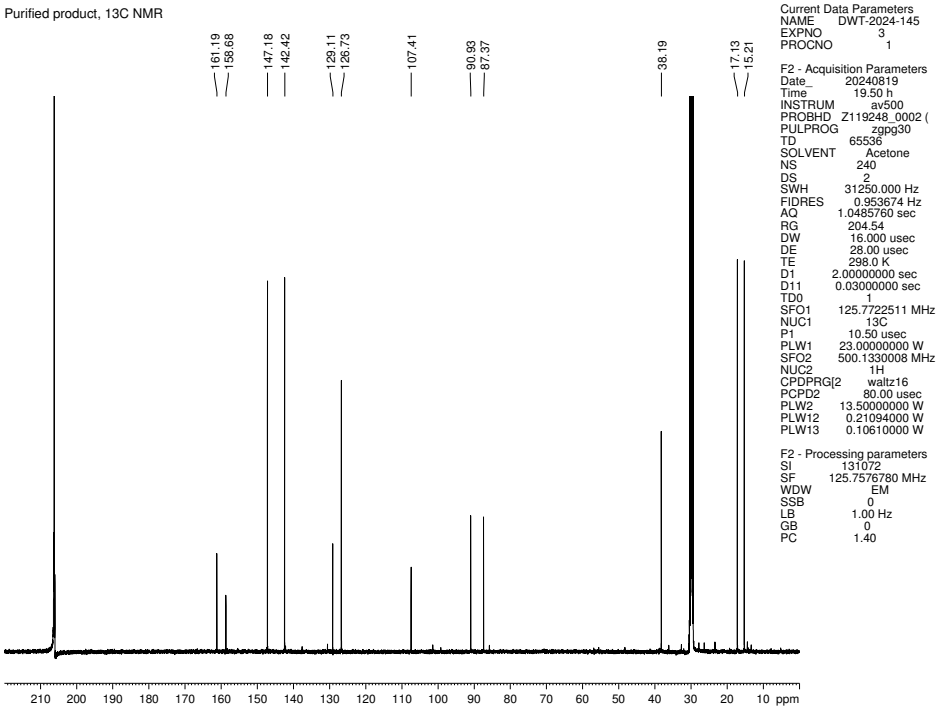

Figure 4.72. ^{13}C NMR (125 MHz, acetone-d_6) of compound **4.36**.

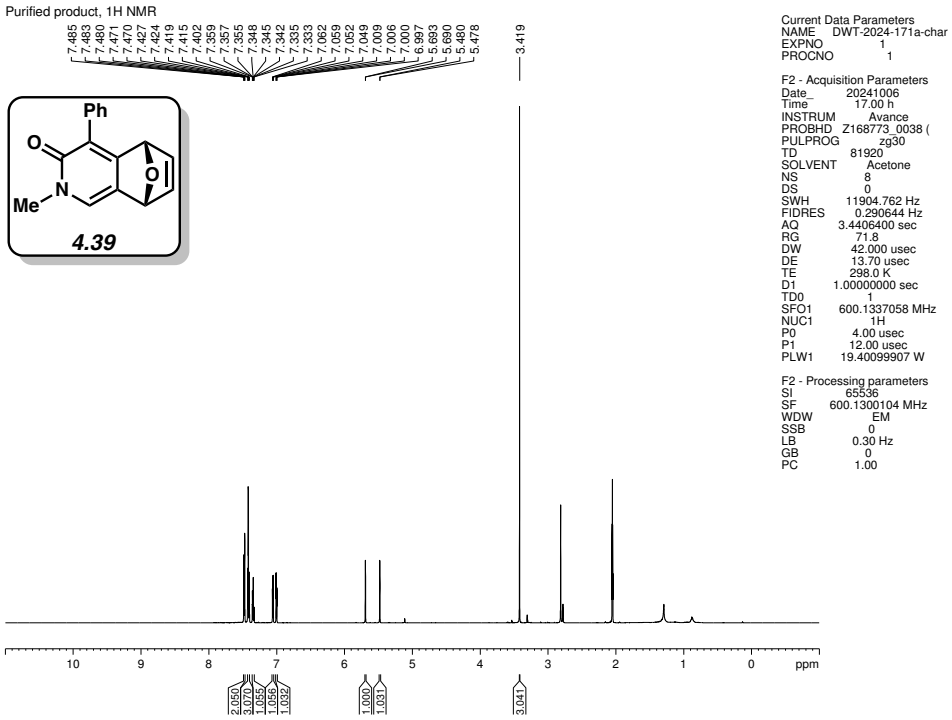

Figure 4.73. ^{1}H NMR (600 MHz, acetone-d_6) of compound **4.39**.

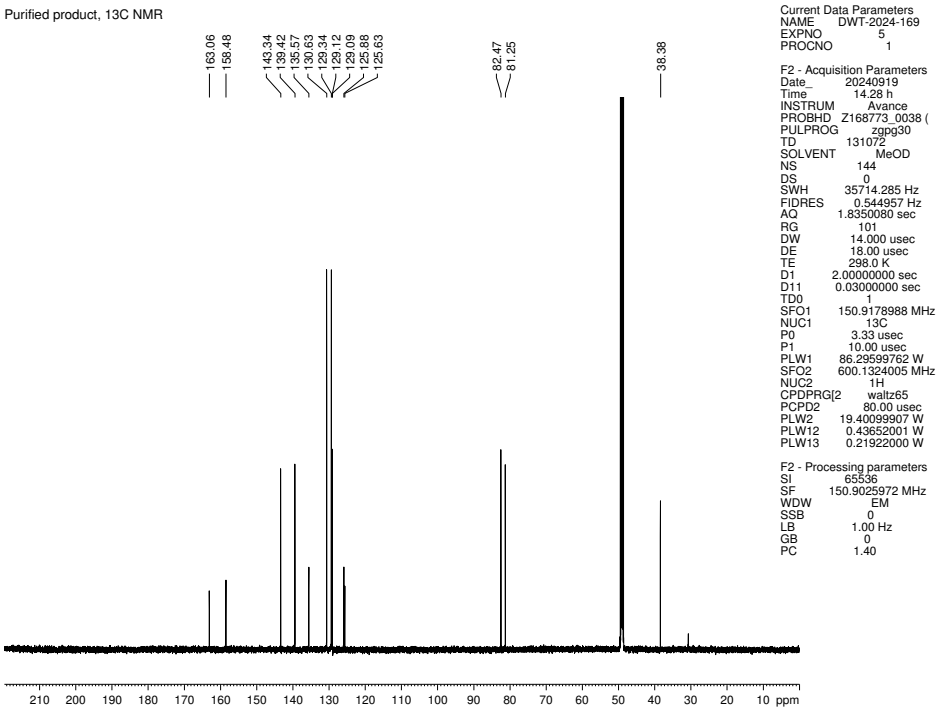

Figure 4.74. ^{13}C NMR (150 MHz, acetone-d_6) of compound **4.39**.

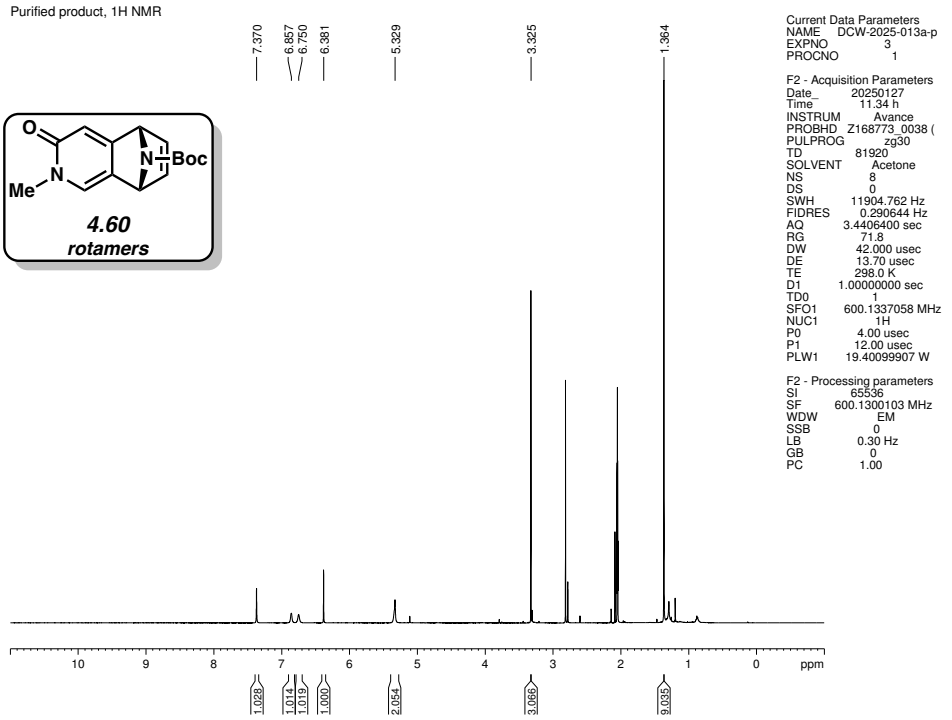

Figure 4.75. ^{1}H NMR (600 MHz, acetone-d_6) of compound **4.60**.

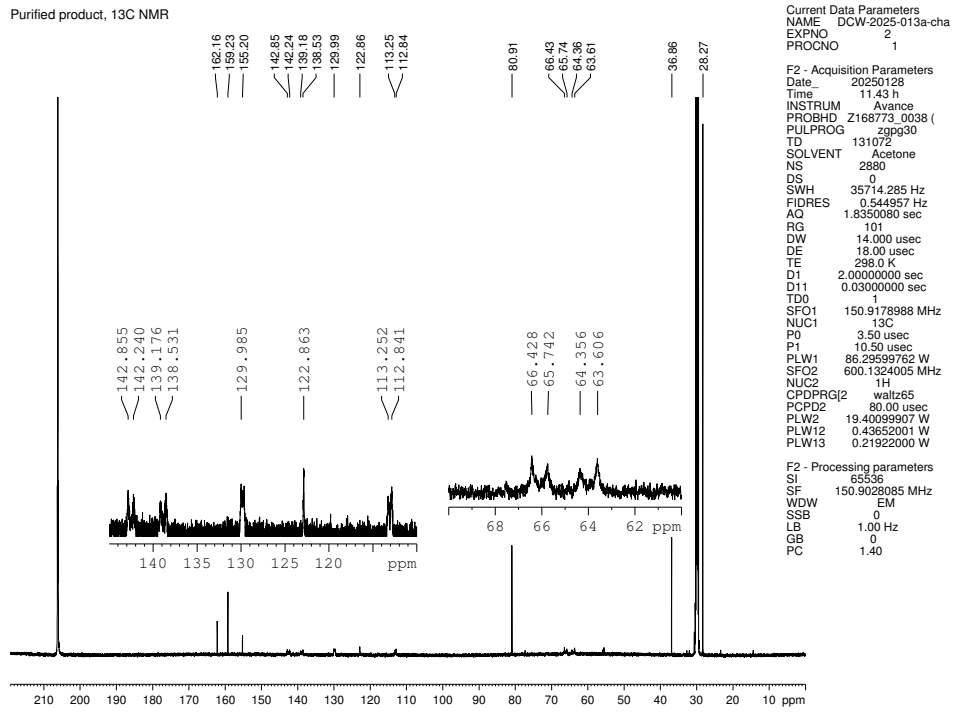

Figure 4.76. ^{13}C NMR (150 MHz, acetone-d_6) of compound **4.60**.

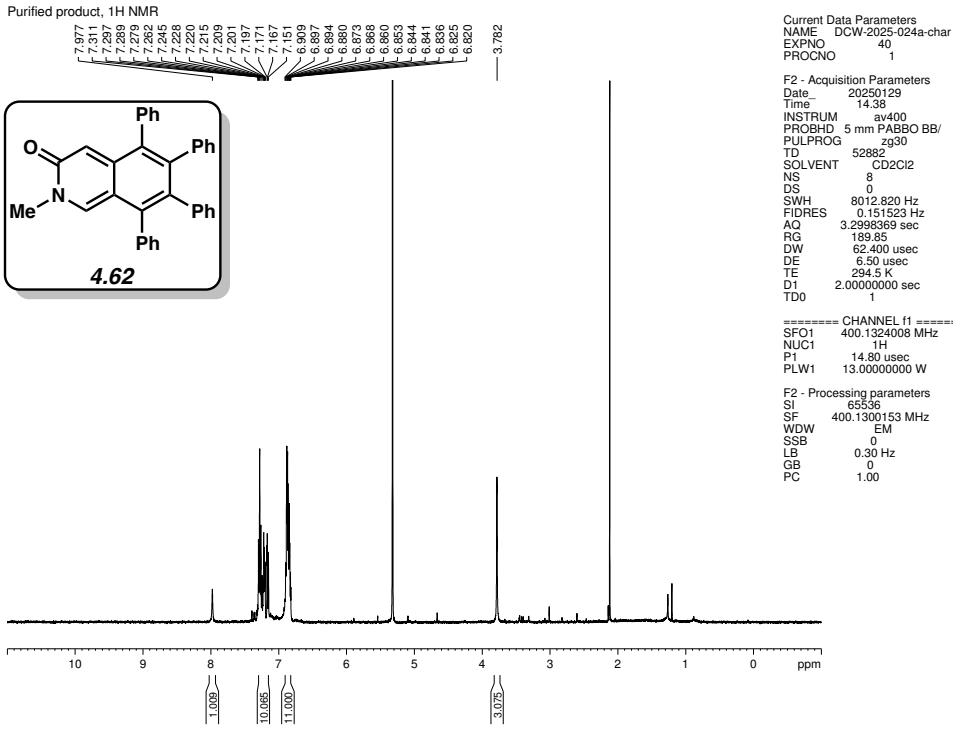

Figure 4.77. ^{1}H NMR (400 MHz, CD_2Cl_2) of compound **4.62**.

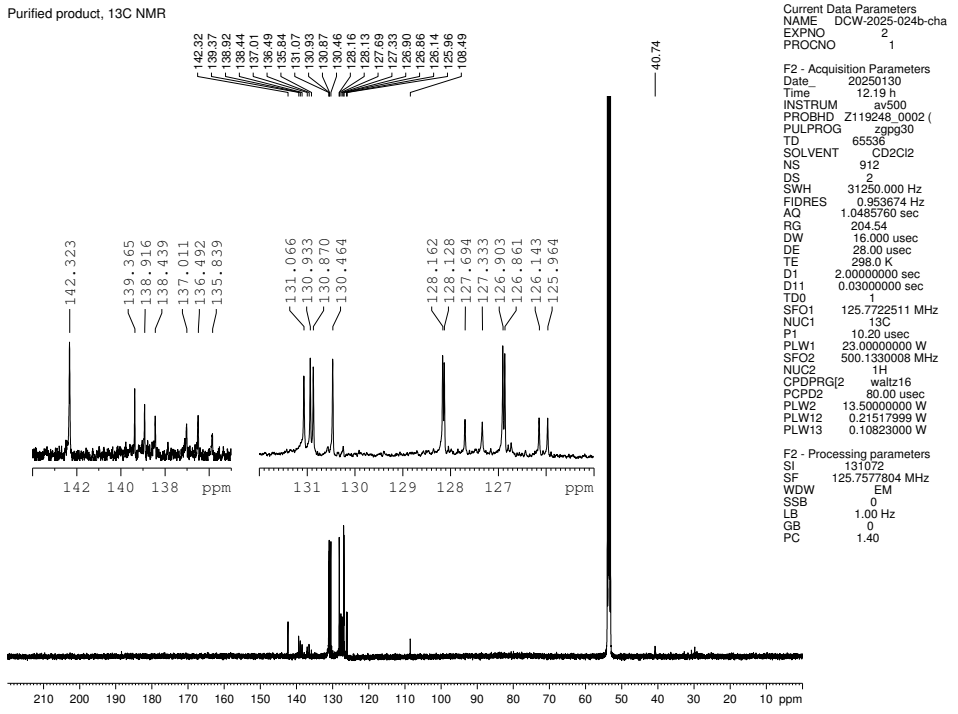

Figure 4.78. ^{13}C NMR (125 MHz, CD_2Cl_2) of compound **4.62**.

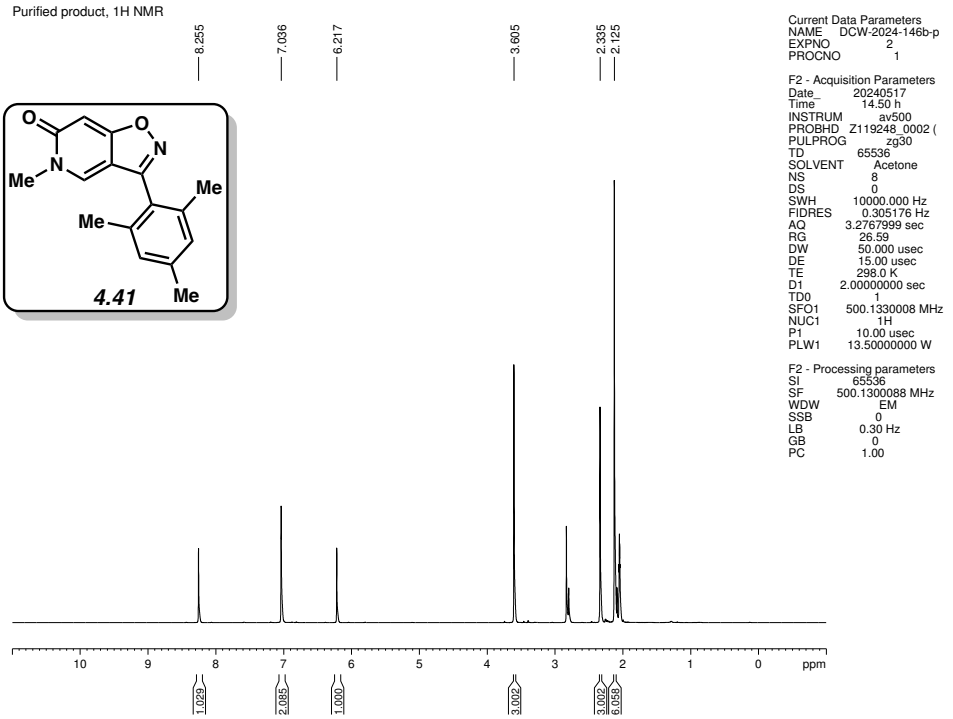

Figure 4.79. ^{1}H NMR (500 MHz, acetone-d_6) of compound **4.41**.

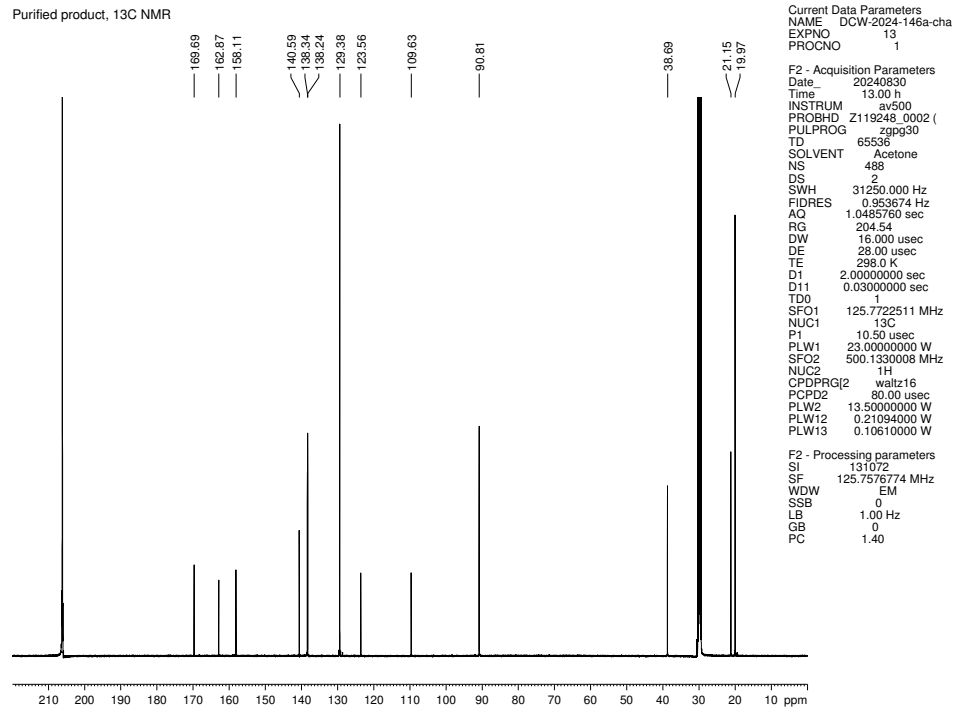

Figure 4.80. ^{13}C NMR (125 MHz, acetone-d_6) of compound **4.41**.

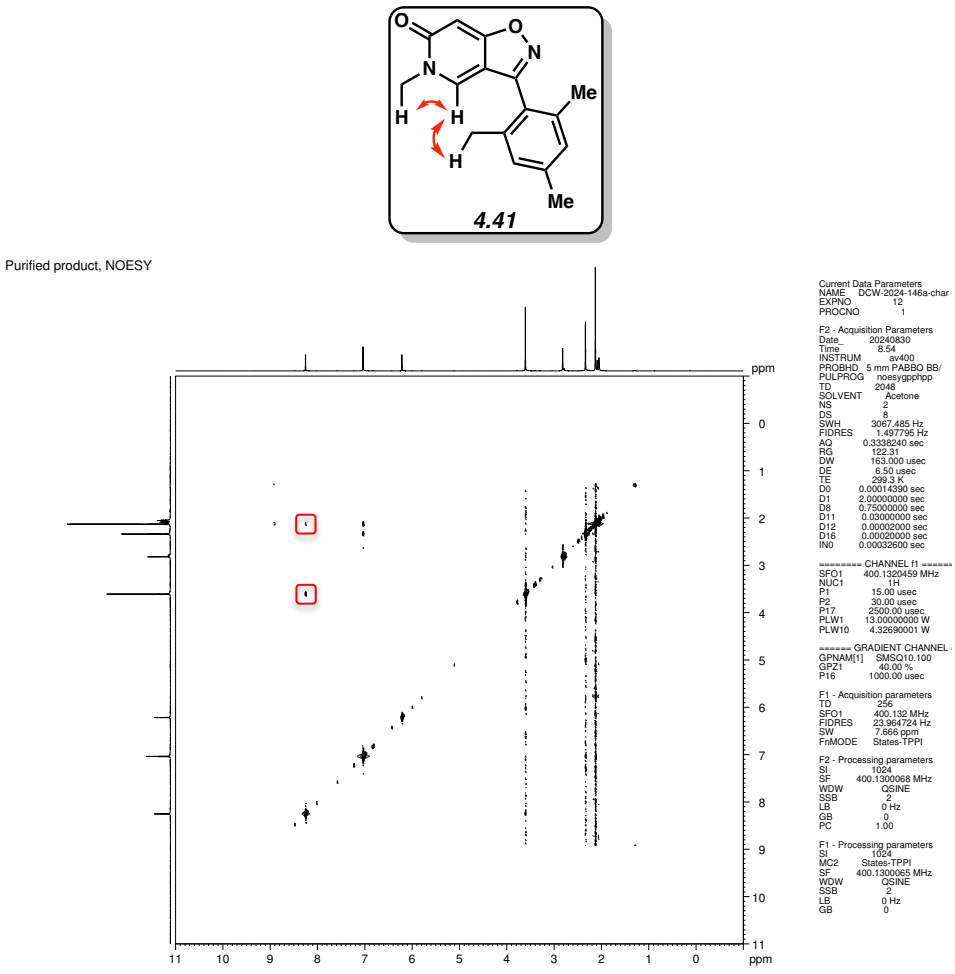

Figure 4.81. NOESY (400 MHz, acetone-d_6) of compound **4.41**.

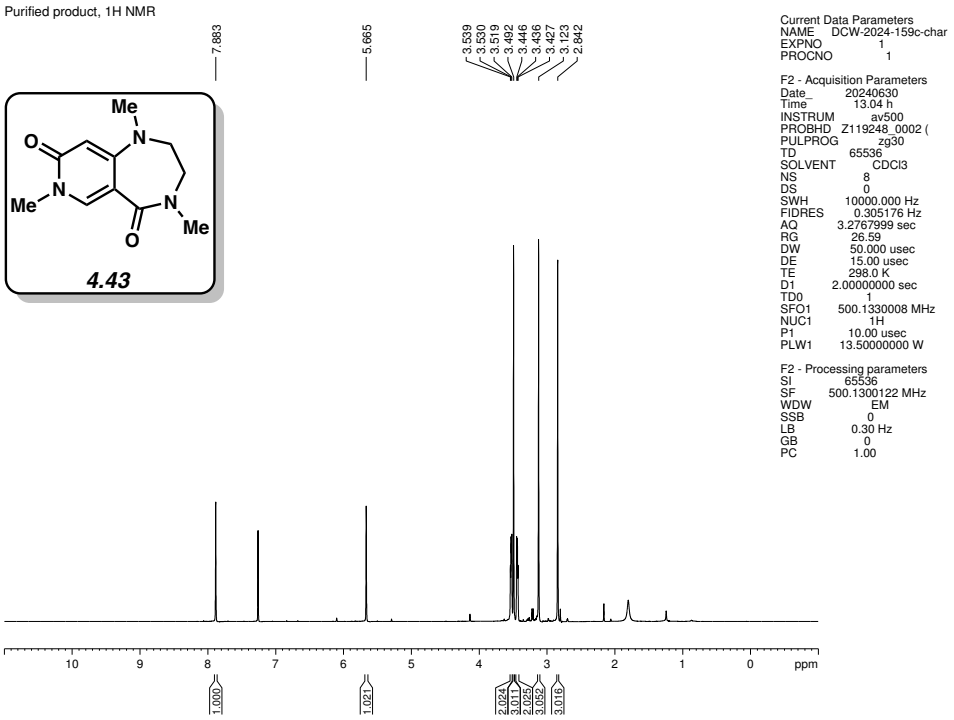

Figure 4.82. ^{1}H NMR (500 MHz, $CDCl_3$) of compound **4.43**.

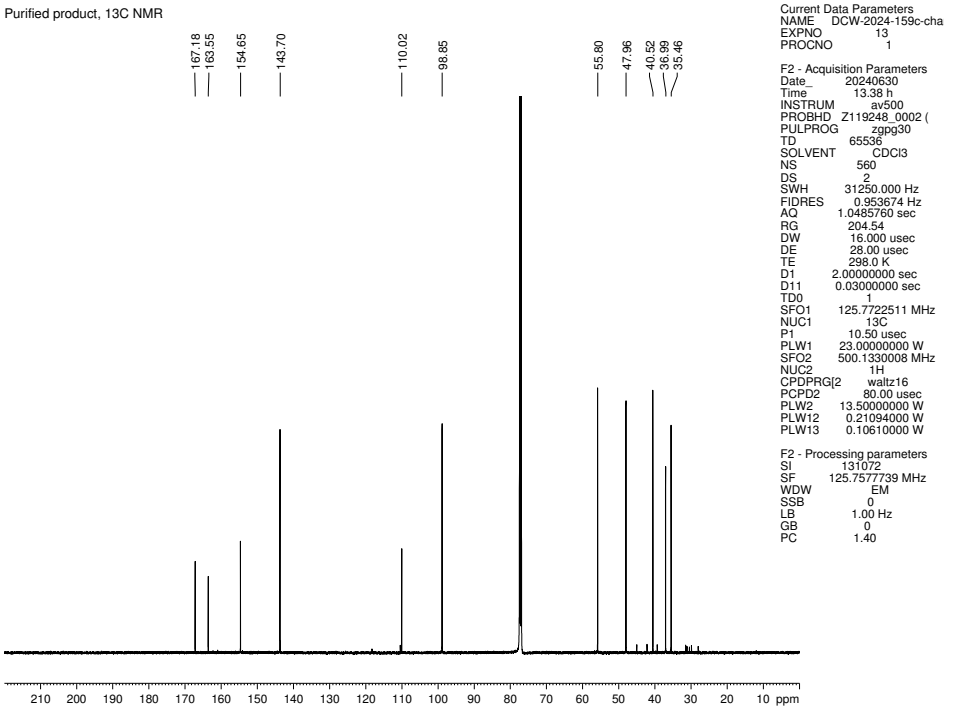

Figure 4.83. ^{13}C NMR (125 MHz, $CDCl_3$) of compound **4.43**.

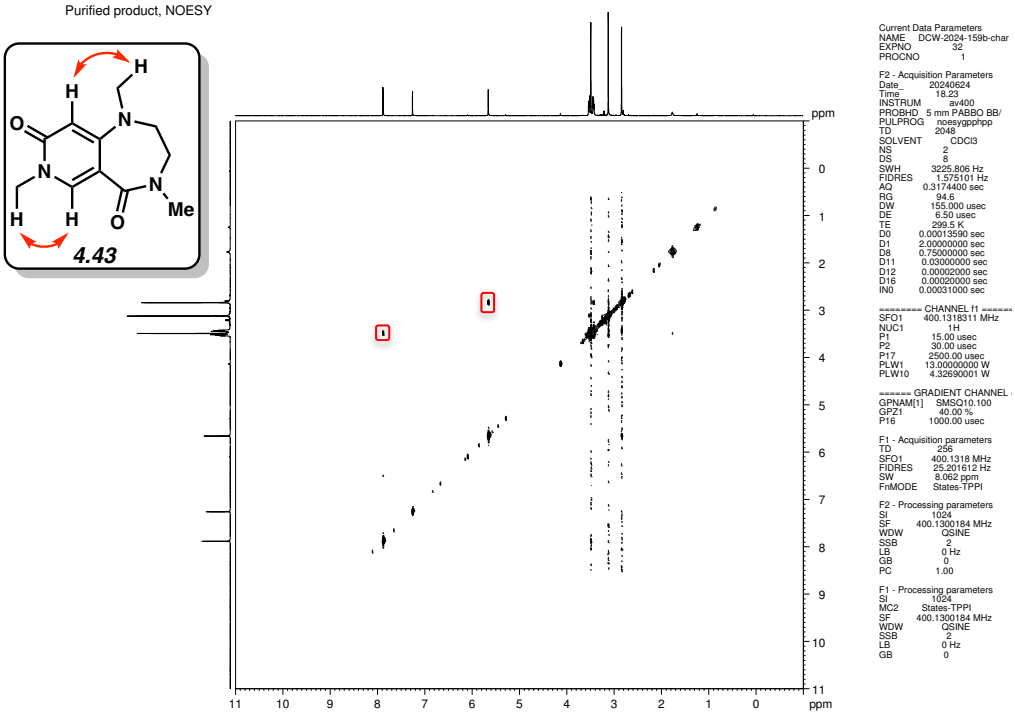

Figure 4.84. NOESY (400 MHz, $CDCl_3$) of compound **4.43**.

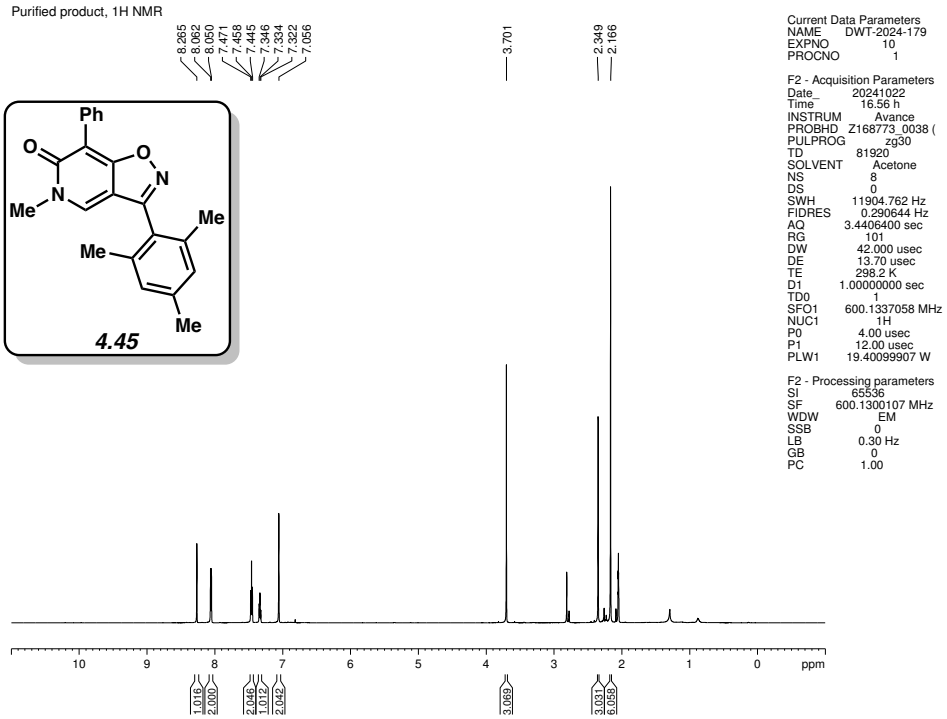

Figure 4.85. ^{1}H NMR (600 MHz, acetone-d_6) of compound **4.45**.

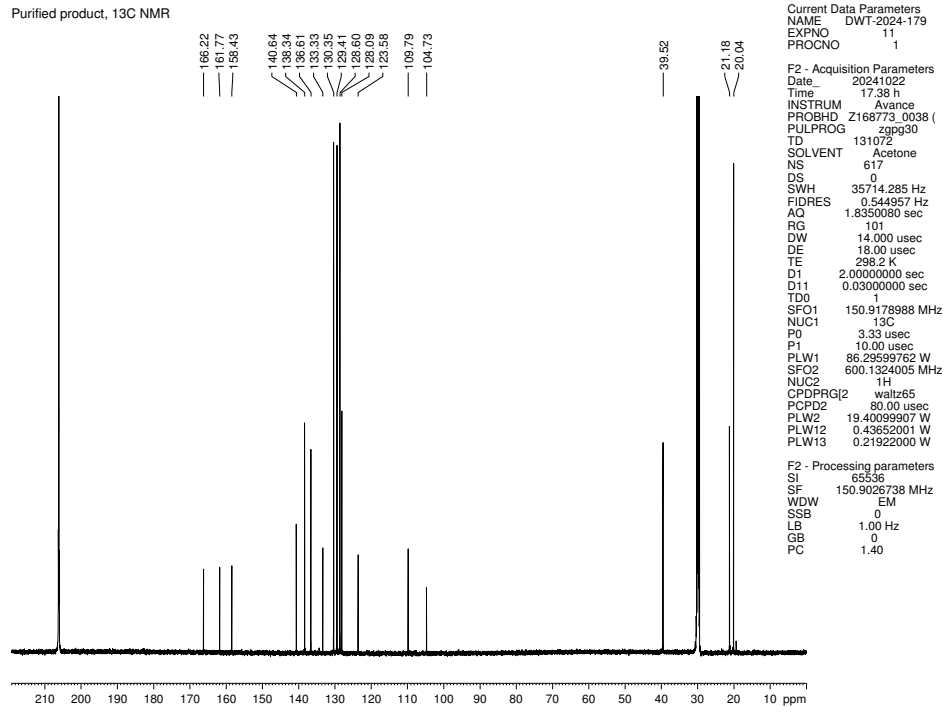

Figure 4.86. ^{13}C NMR (150 MHz, acetone-d_6) of compound **4.45**.

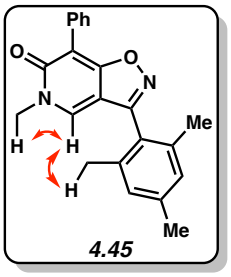

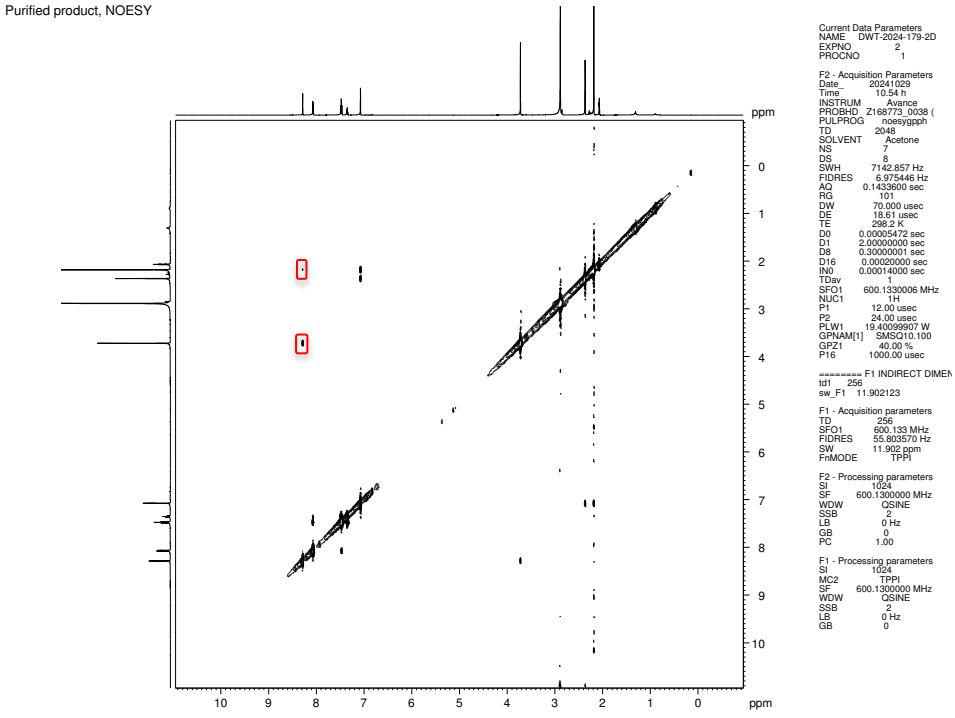

Figure 4.87. NOESY (600 MHz, acetone-d_6) of compound **4.45**.

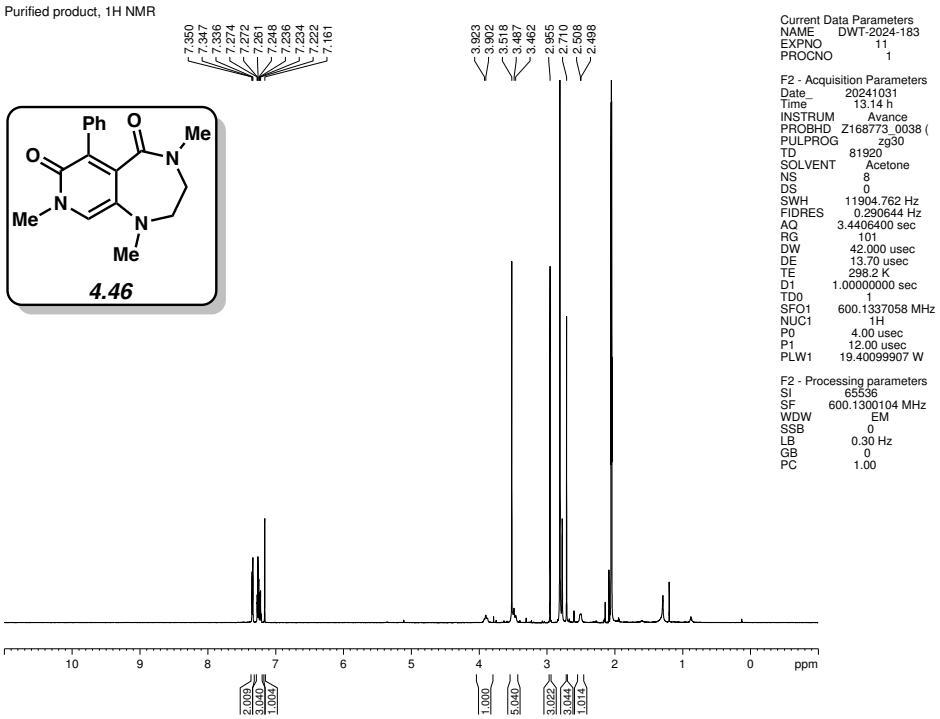

Figure 4.88. ^{1}H NMR (600 MHz, acetone-d_6) of compound **4.46**.

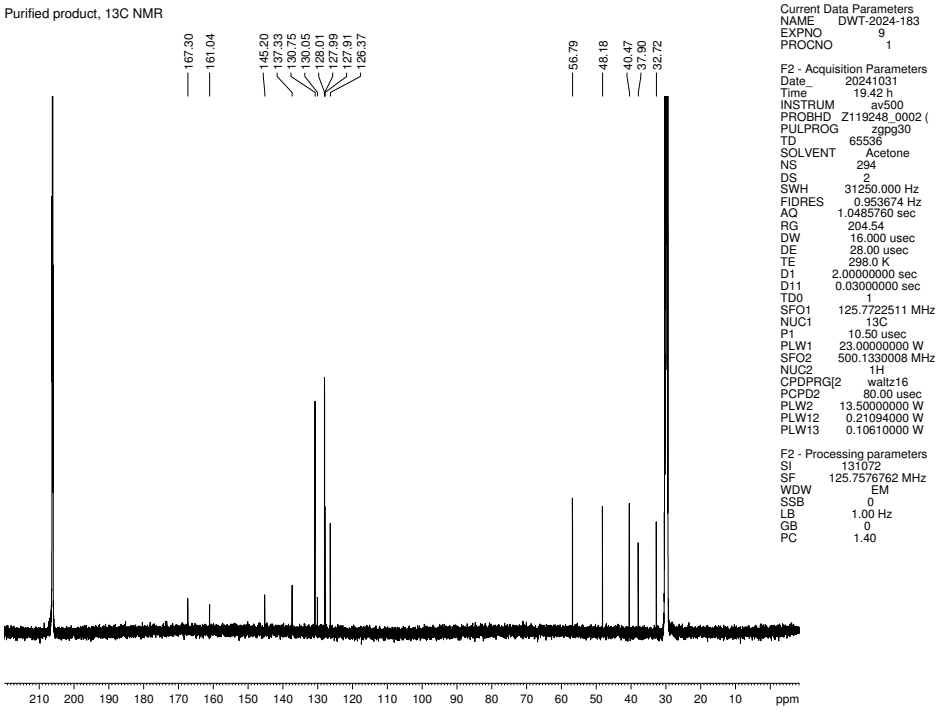

Figure 4.89. ^{13}C NMR (125 MHz, acetone-d_6) of compound **4.46**.

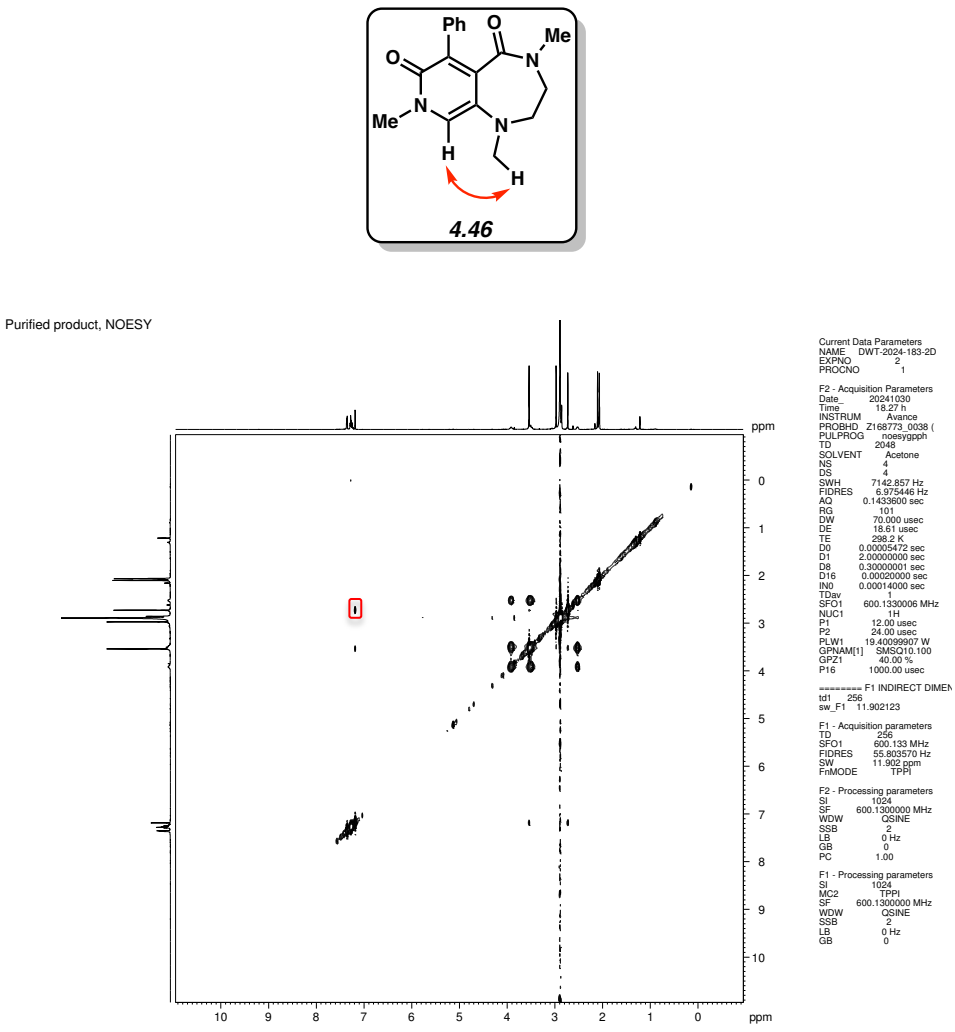

Figure 4.90. NOESY (600 MHz, acetone-d_6) of compound **4.46**.

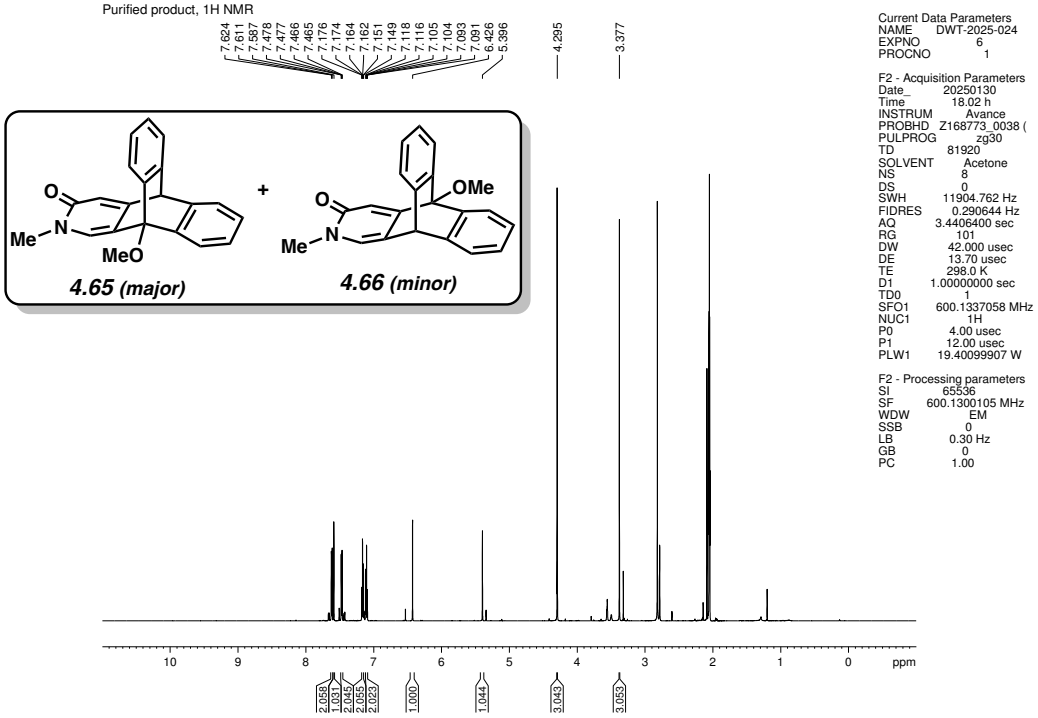

Figure 4.91. ^{1}H NMR (600 MHz, acetone-d_6) of compounds **4.65** and **4.66**.

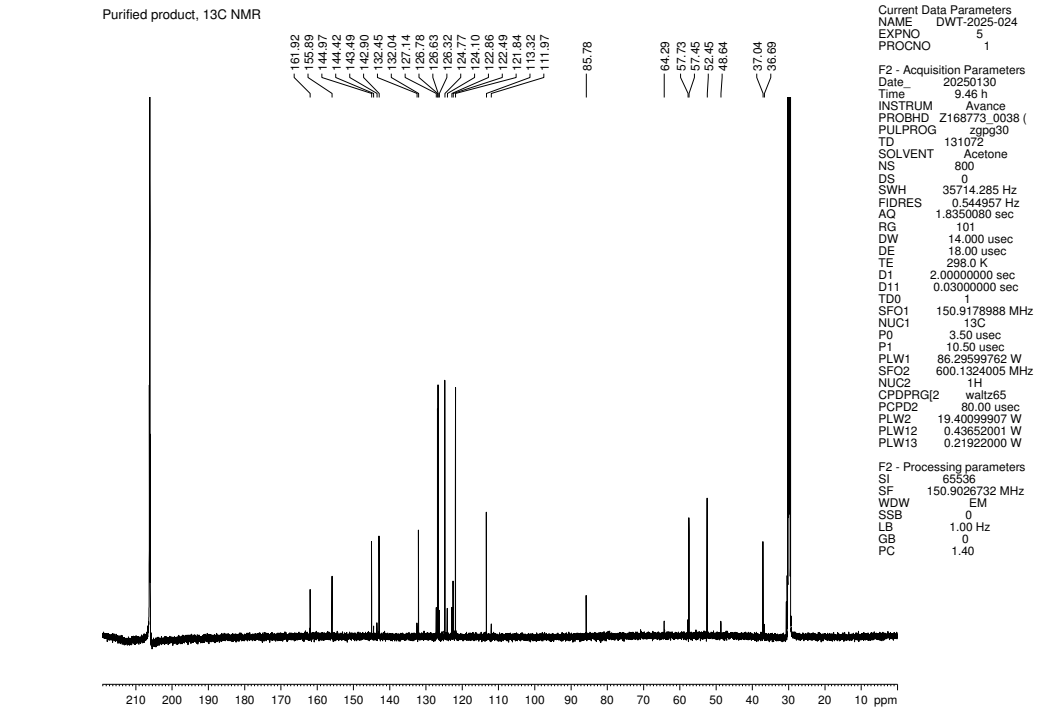

Figure 4.92. ^{13}C NMR (150 MHz, acetone-d_6) of compounds **4.65** and **4.66**.

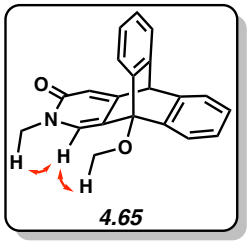

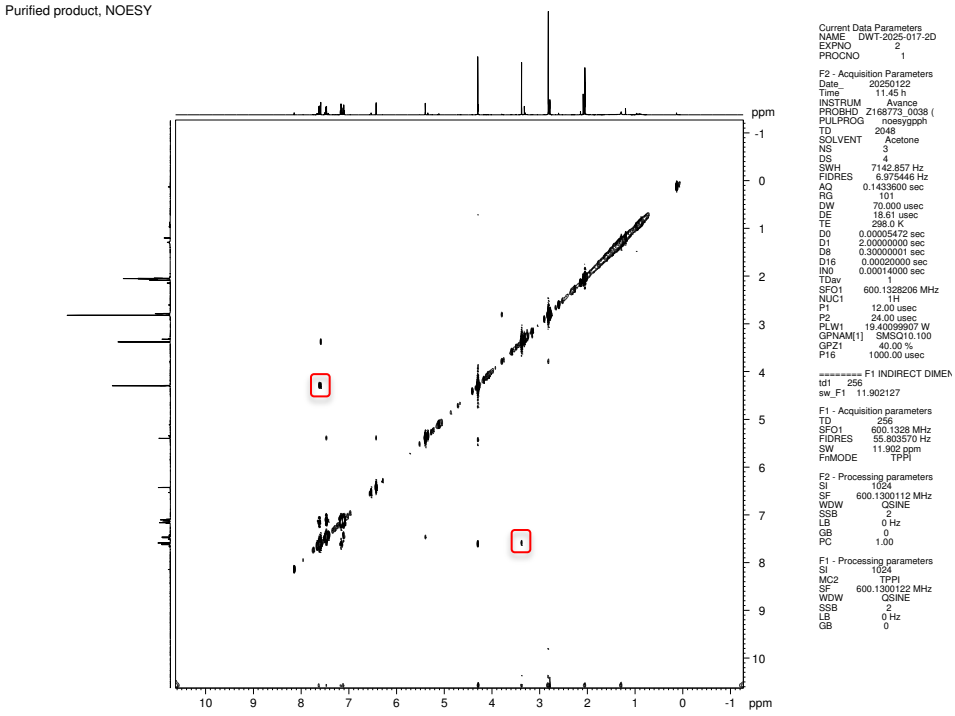

Figure 4.93. NOESY (600 MHz, acetone-d_6) of compound **4.65**.

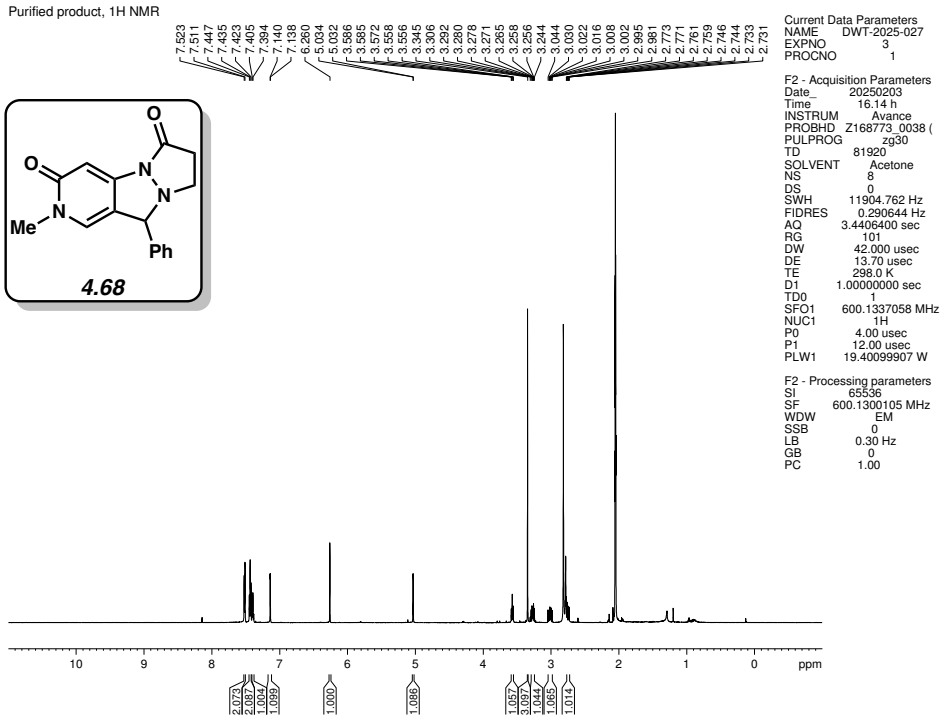

Figure 4.94. ^{1}H NMR (600 MHz, acetone-d_6) of compound **4.68**.

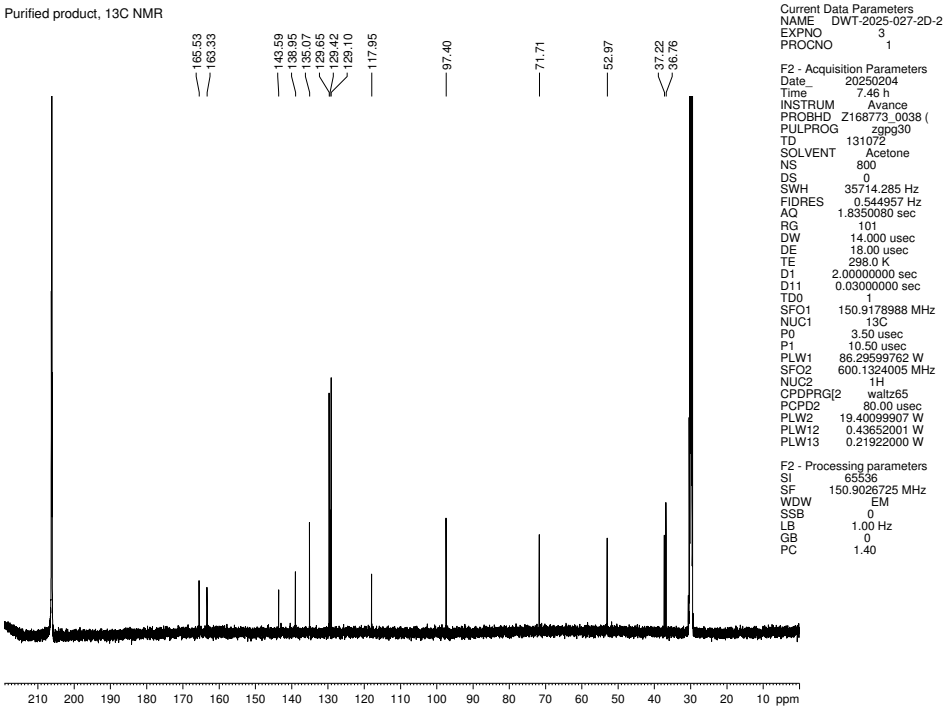

Figure 4.95. ^{13}C NMR (150 MHz, acetone-d_6) of compound **4.68**.

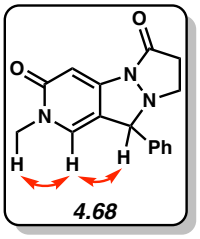

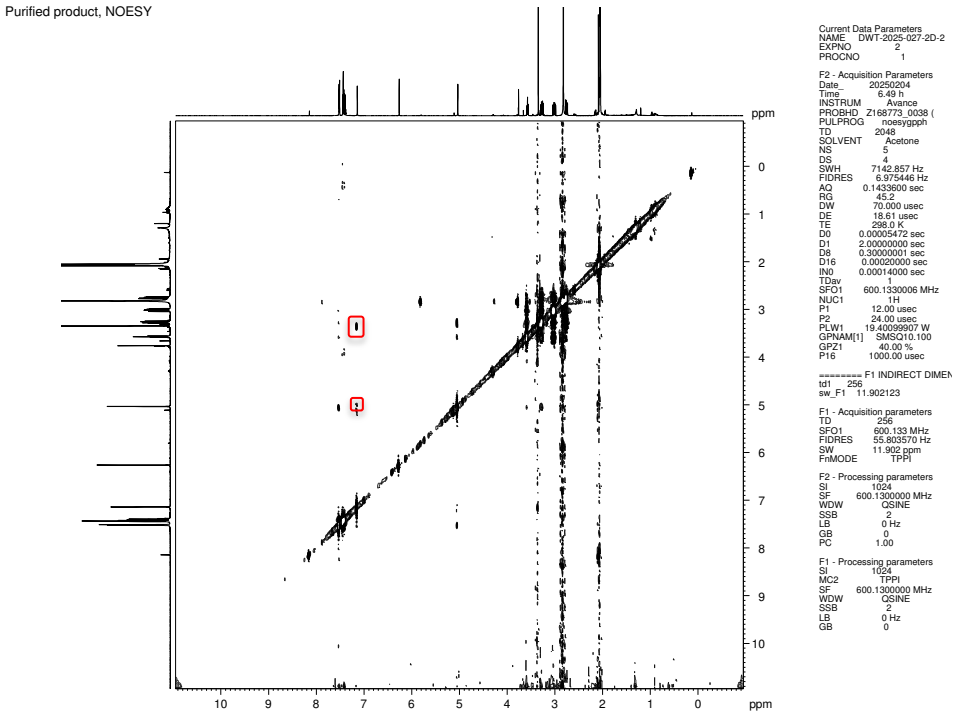

Figure 4.96. NOESY (600 MHz, acetone-d_6) of compound **4.68**.

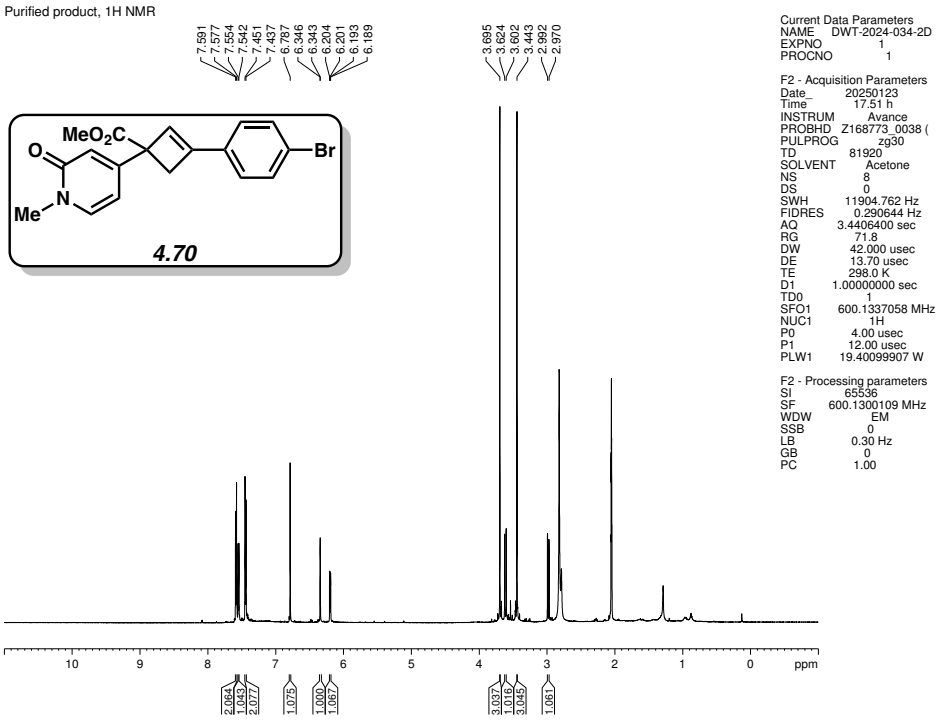

Figure 4.97. ^{1}H NMR (600 MHz, acetone-d_6) of compound **4.70**.

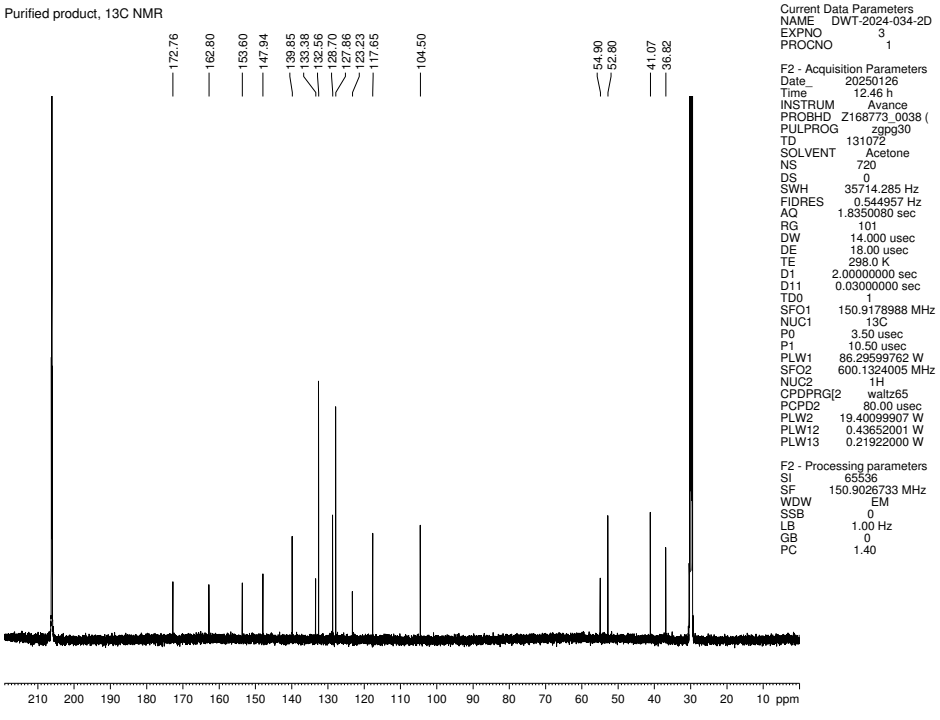

Figure 4.98. ^{13}C NMR (150 MHz, acetone-d_6) of compound **4.70**.

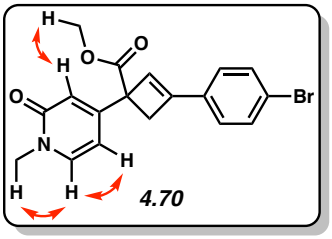

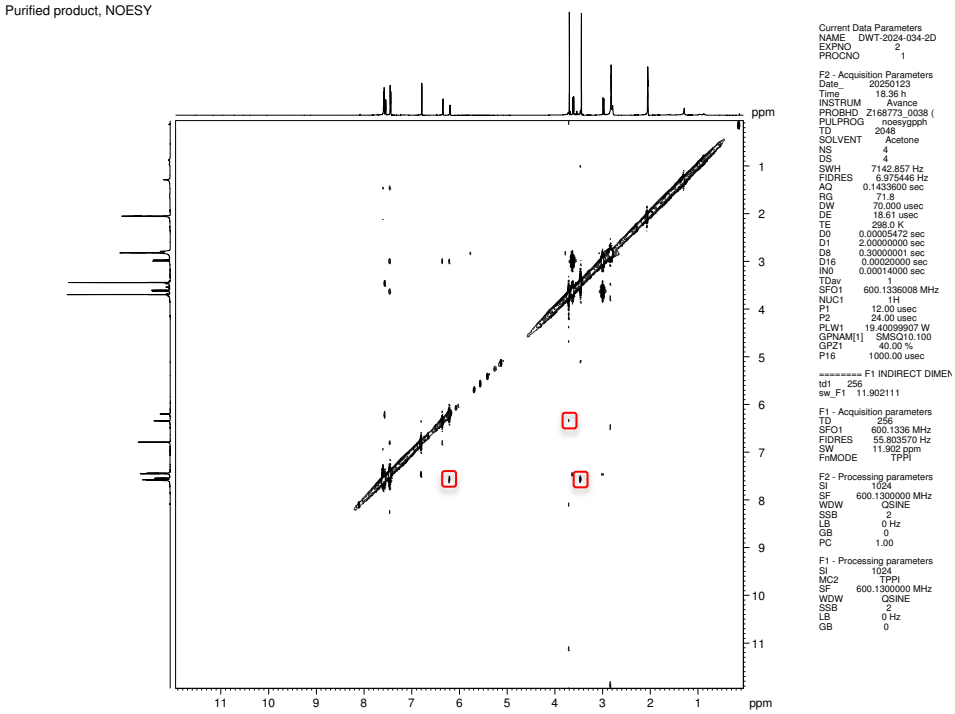

Figure 4.99. NOESY (600 MHz, acetone-d_6) of compound **4.70**.

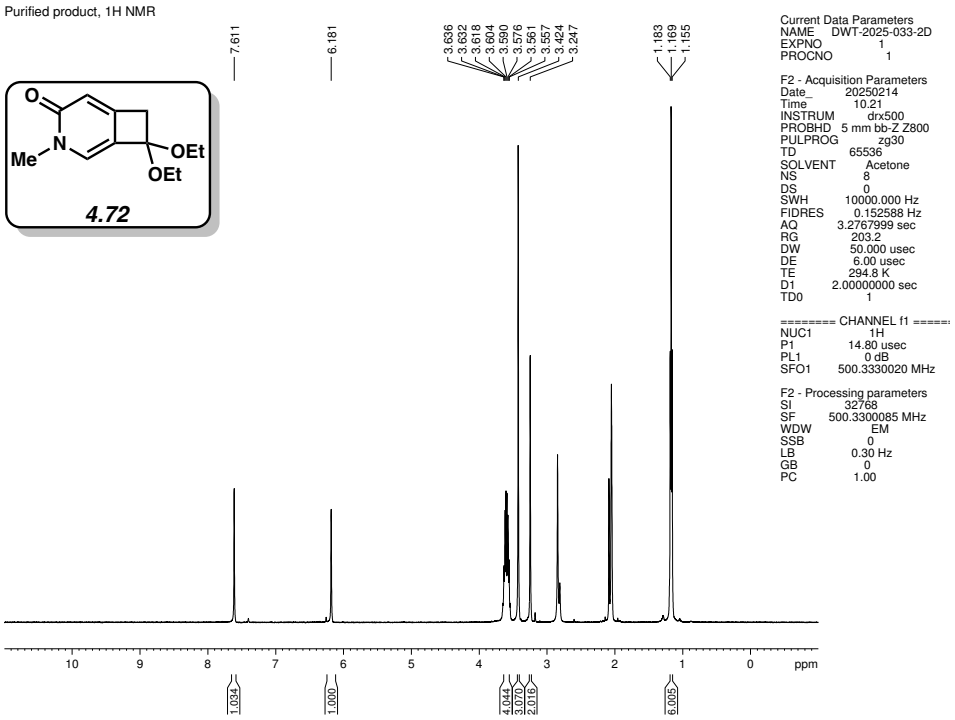

Figure 4.100. ^{1}H NMR (500 MHz, acetone-d_6) of compound **4.72**.

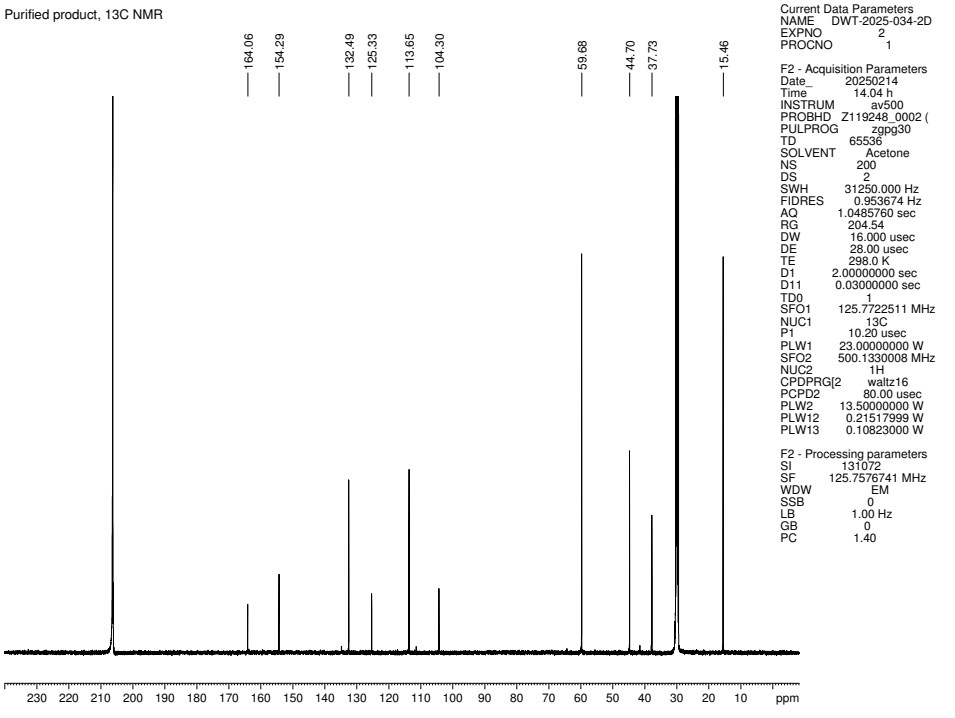

Figure 4.101. ^{13}C NMR (125 MHz, acetone-d_6) of compound **4.72**.

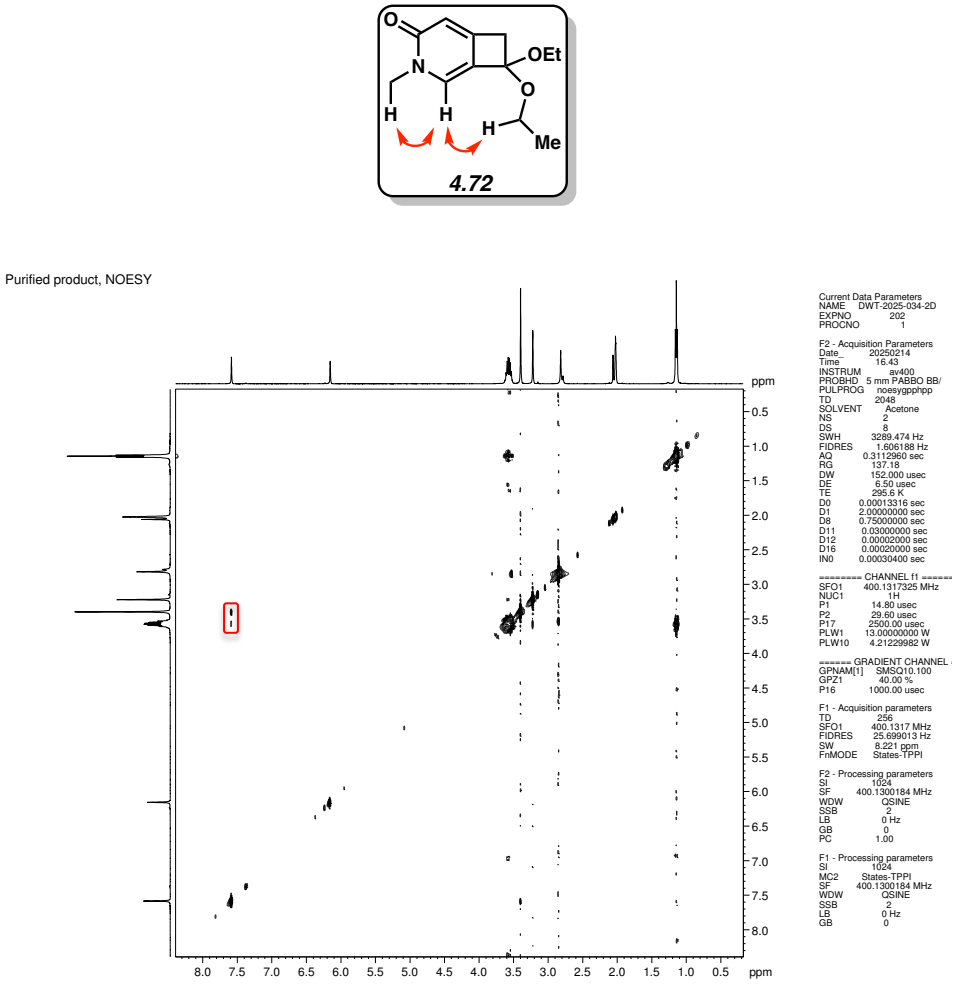

Figure 4.102. NOESY (400 MHz, acetone-d_6) of compound **4.72**.

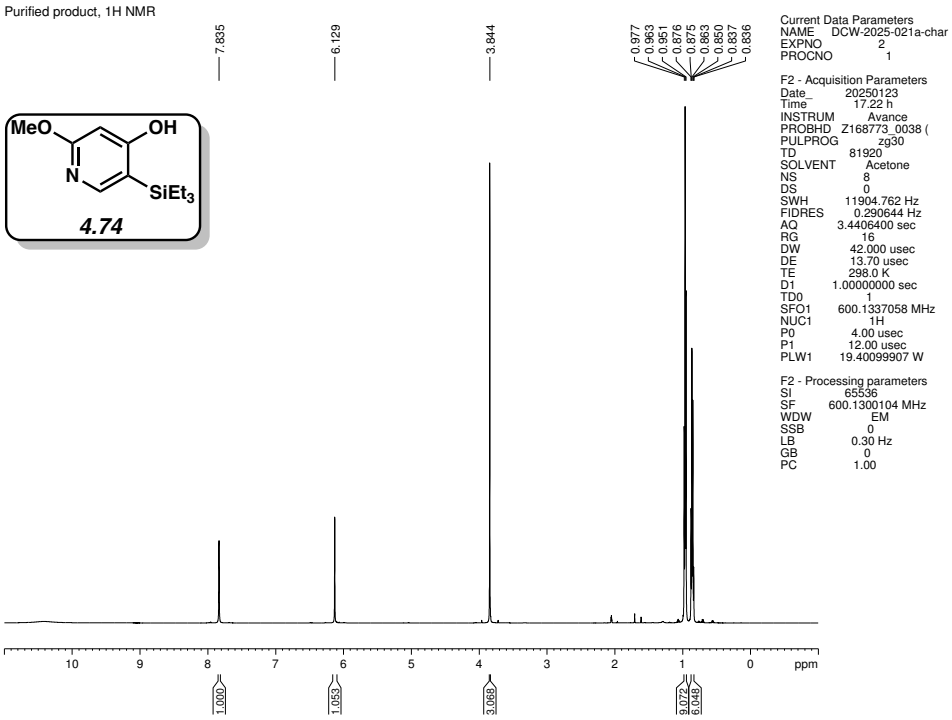

Figure 4.103. ^{1}H NMR (600 MHz, acetone-d_6) of compound **4.74**.

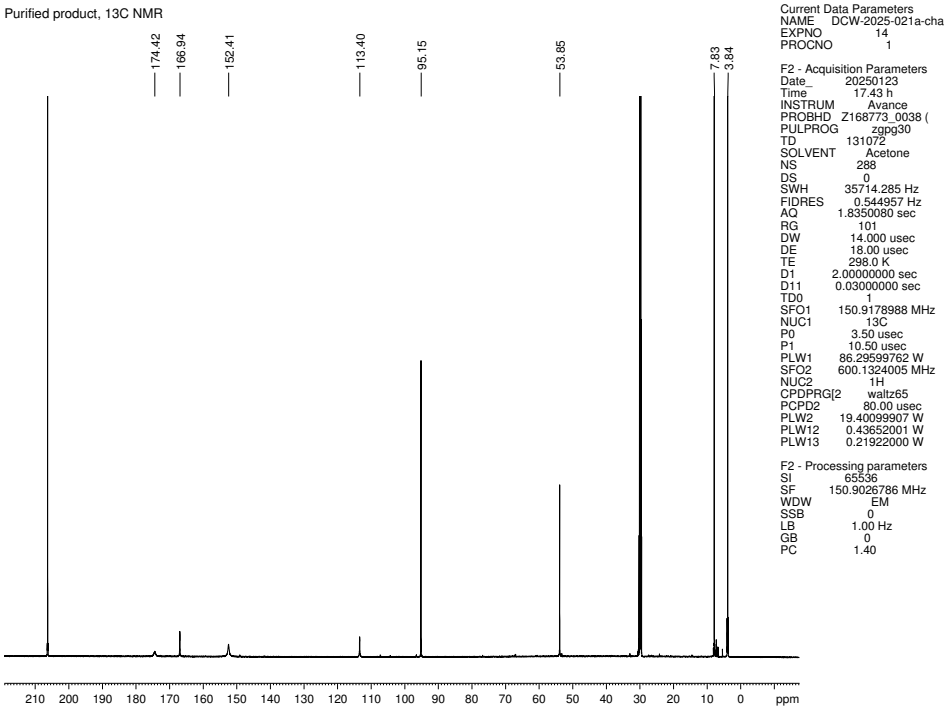

Figure 4.104. ^{13}C NMR (150 MHz, acetone-d_6) of compound **4.74**.

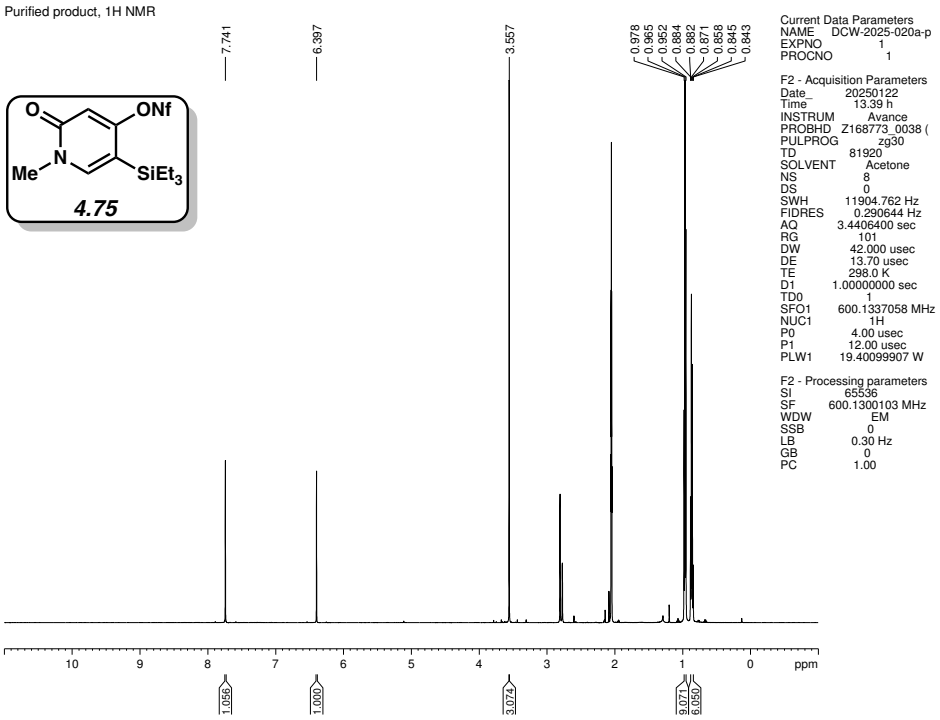

Figure 4.105. ^{1}H NMR (600 MHz, acetone-d_6) of compound **4.75**.

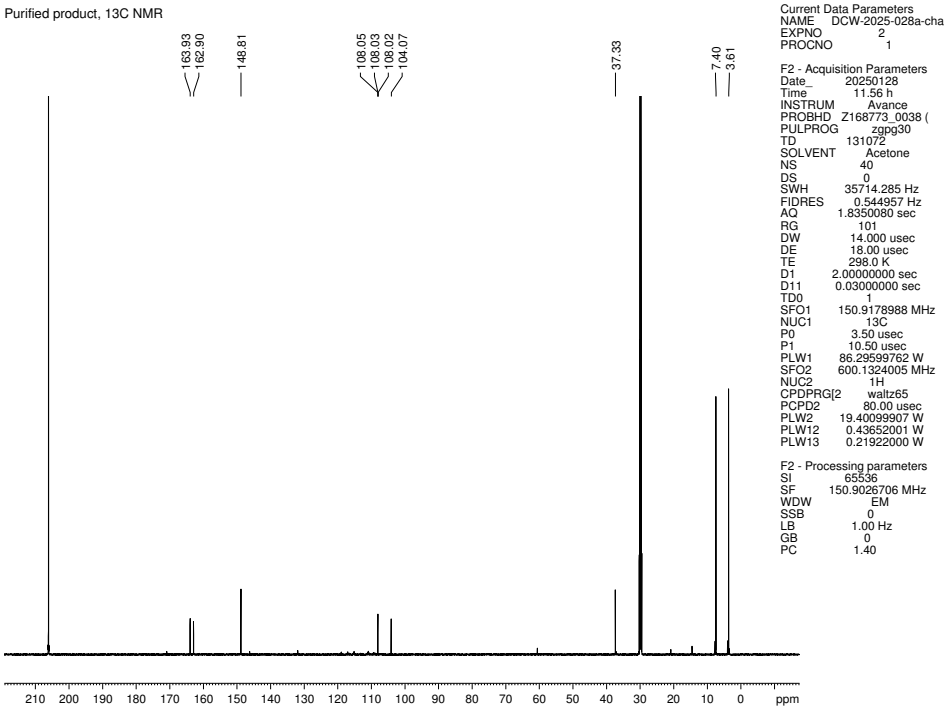

Figure 4.106. ^{13}C NMR (150 MHz, acetone-d_6) of compound **4.75**.

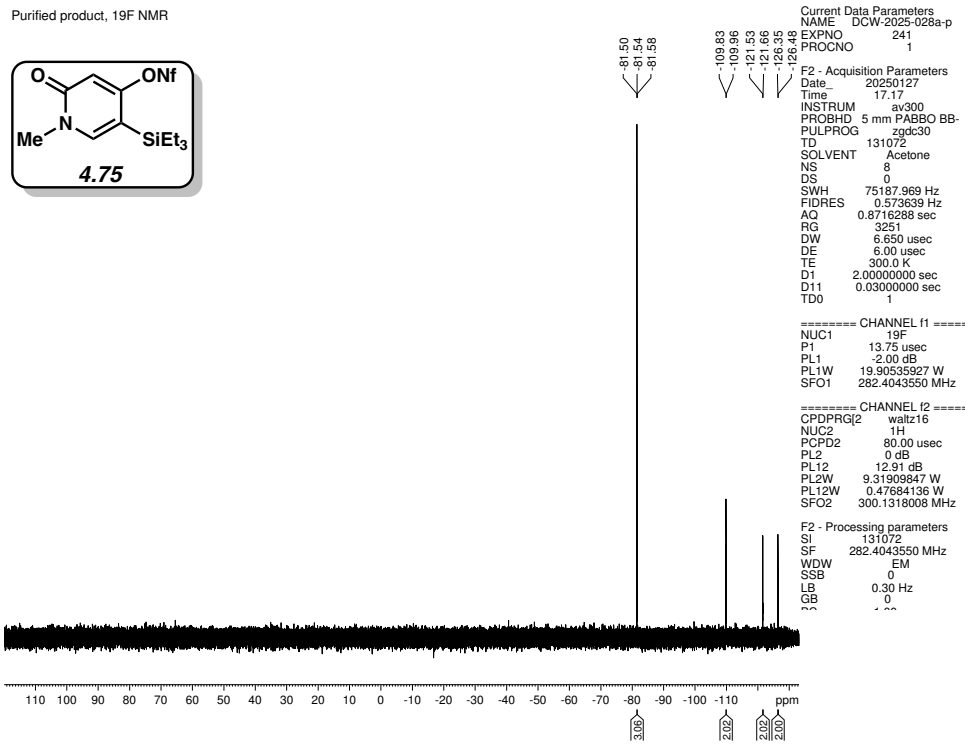

Figure 4.107. ^{19}F NMR (282 MHz, acetone-d_6) of compound **4.75**.

4.11 Notes and References

(1) Liebman, J. F.; Greenberg, A. A survey of strained organic molecules. *Chem. Rev.* **1976**, *76*, 311–365.

(2) Wenk, H. H.; Winkler, M.; Sander, W. One century of aryne chemistry. *Angew. Chem., Int. Ed.* **2003**, *42*, 502–528.

(3) Roberts, J. D.; Simmons, H. E.; Carlsmith, L. A.; Vaughan, C. W. Rearrangement in the reaction of chlorobenzene-1-C^{14} with potassium amide. *J. Am. Chem. Soc.* **1953**, *75*, 3290–3291.

(4) Wittig, G. Phenyl-lithium, der Schlüssel zu einer neuen Chemie metallorganischer Verbindungen. *Naturwissenschaften* **1942**, *30*, 696–703.

(5) Wittig, G.; Pohmer, L. Intermediäre bildung von dehydrobenzol (cyclohexa-dienin). *Angew. Chem.* **1955**, *67*, 348.

(6) Scardiglia, F.; Roberts, J. D. Evidence for *cyclo*hexyne as an intermediate in the coupling of phenyllithium with 1-chloro*cyclo*hexene. *Tetrahedron* **1957**, *1*, 343–344.

(7) Wittig, G.; Fritze, P. On the intermediate occurrence of 1,2-cyclohexadiene. *Angew. Chem., Int. Ed.* **1966**, *5*, 846.

(8) Moser, W. R. The reactions of gem-dihalocyclopropanes with organometallic reagents. Ph.D. Thesis, Massachusetts Institute of Technology: Cambridge, MA, 1964.

(9) Moore, W. R.; Moser, W. R. The reaction of 6,6-dibromobicyclo[3.1.0]hexane with methyllithium. Efficient trapping of 1,2-cyclohexadiene by styrene. *J. Org. Chem.* **1970**, *35*, 908–912.

(10) Hosoya, T.; Yoshida, S.; Nakamura, Y. Recent advances in synthetic hetaryne chemistry. *Heterocycles* **2019**, *98*, 1623–1677.

(11) Shi, J.; Li, L.; Li, Y. *o*-Silylaryl triflates: A journey of Kobayashi aryne precursors. *Chem. Rev.* **2021**, *121*, 3892–4044.

(12) Tadross. P. M.; Stoltz, B. M. A comprehensive history of arynes in natural product total synthesis. *Chem. Rev.* **2012**, *112*, 3550–3577.

(13) Gampe, C. M.; Carreira, E. M. Arynes and cyclohexyne in natural product synthesis. *Angew. Chem., Int. Ed.* **2012**, *51*, 3766–3778.

(14) Takikawa, H.; Nishii, A.; Sakai, T.; Suzuki, K. Aryne-based strategy in the total synthesis of naturally occurring polycyclic compounds. *Chem. Soc. Rev.* **2018**, *47*, 8030–8056.

(15) Ippoliti, F. M.; Adamson, N. J.; Wonilowicz, L. G.; Nasrallah, D. J.; Darzi, E. R.; Donaldson, J. S.; Garg, N. K. Total synthesis of lissodendoric acid A via stereospecific trapping of a strained cyclic allene. *Science* **2023**, *379*, 261–265.

(16) Pérez, D.; Peña, D.; Guitián, E. Aryne cycloaddition reactions in the synthesis of large polycyclic aromatic compounds. *Eur. J. Org. Chem.* **2013**, *2013*, 5981–6013.

(17) Westphal, M. V.; Hudson, L.; Mason, J. W.; Pradeilles, J. A.; Zécri, F. J.; Briner, K.; Schreiber, S. L. Water-compatible cycloadditions of oligonucleotide-conjugated strained allenes for DNA-encoded library synthesis. *J. Am. Chem. Soc.* **2020**, *142*, 7776–7782.

(18) Angus, R. O., Jr.; Johnson, R. P. Small-ring cyclic cumulenes: The structure and energetics of cyclic butatrienes and the synthesis of 1,2,3-cyclononatriene. *J. Org. Chem.* **1984**, *49*, 2880–2883.

(19) Daoust, K. J.; Hernandez, S. M.; Konrad, K. M.; Mackie, I. D.; Winstanley, J.; Johnson, R. P. Strain estimates for small-ring cyclic allenes and butatrienes. *J. Org. Chem.* **2006**, *71*, 5708–5714.

(20) Zahradník, R.; Hobza, P.; Burcl, R.; Hess, B. A., Jr.; Radziszewski, J. G. Strained unsaturated molecules. Theoretical study of acyclic and cyclic cumulenes and acetylenes. *J. Mol. Struct. THEOCHEM* **1994**, *313*, 335–349.

(21) Tokoyama, H.; Yamakado, H.; Maeda, S.; Ohno, K. Exploration of isomers of benzene by GRRM/SCC-DFTB. *Chem. Lett.* **2014**, *43*, 702–704.

(22) Tokoyama, H.; Yamakado, H.; Maeda, S.; Ohno, K. Isomers of benzene on its global network of reaction pathways. *Bull. Chem. Soc. Jpn.* **2015**, *88*, 1284–1290.

(23) Li, Z.; Rogers, D. W.; McLafferty, F. J.; Mandziuk, M.; Podosenin, A. V. Ab initio calculations of enthalpies of hydrogenation, isomerization, and formation of cyclic C_6 hydrocarbons. Benzene isomers. *J. Phys. Chem. A* **1999**, *103*, 426–430.

(24) Dinadayalane, T. C.; Priyakumar, U. D.; Sastry, G. N. Exploration of C_6H_6 potential energy surface: A computational effort to unravel the relative stabilities and synthetic feasibility of new benzene isomers. *J. Phys. Chem. A* **2004**, *108*, 11433–11448.

(25) Shakespeare, W. C.; Johnson, R. P. 1,2,3-Cyclohexatriene and cyclohexen-3-yne: Two new highly strained C_6H_6 isomers. *J. Am. Chem. Soc.* **1990**, *112*, 8578–8579.

(26) Yin, J.; Abboud, K. A.; Jones, W. M. Synthesis of zirconocene complexes of a 1,2,3-cyclohexatriene and a cyclohexen-3-yne. *J. Am. Chem. Soc.* **1993**, *115*, 8859–8860.

(27) Hickey, E. R.; Paquette, L. A. Torsional angel decompression is not the source of facial selectivity in Diels–Alder cycloadditions involving cyclic dienes fused to bicyclic

frameworks. The case study of 1,2,3,4,6,7-hexahydro-1,4-methanonaphthalene. *Tetrahedron Lett.* **1994**, *35*, 2309–2312.

(28) Hickey, E. R.; Paquette, L. A. Experimental and theoretical analysis of the effects of strain diminution on the stereoselectivity of dienophilic capture by π-facially nonequivalent homologs of isodicylopentadiene. *J. Am. Chem. Soc.* **1995**, *117*, 163–176.

(29) Burrell, R. C.; Daoust, K. J.; Bradley, A. Z.; DiRico, K. J.; Johnson, R. P. Strained cyclic cumulene intermediates in Diels–Alder cycloadditions of enyne and diynes. *J. Am. Chem. Soc.* **1996**, *118*, 4218–4219.

(30) Sakura, M.; Ando, S.; Hattori, A.; Saito, K. Reaction of cyclohexa-1,2,3-triene with *N*,α-diphenylnitrone: Formation of seven-membered cyclic amines via piradone derivatives. *Heterocycles* **1999**, *51*, 547–556.

(31) Matsuoka, S.; Jung, S.; Miyakawa, K.; Chuda, Y.; Sugimoto, R.; Hamura, T. Didehydroisobenzofuran: A new reactive intermediate for the construction of isoacenofuran. *Chem. Eur. J.* **2018**, *24*, 18886–18889.

(32) Schulz, F.; García, F.; Kaiser, K.; Pérez, D.; Guitián, E.; Gross, L.; Peña, D. Exploring a route to cyclic acenes by on-surface synthesis. *Angew. Chem., Int. Ed.* **2019**, *58*, 9038–9042.

(33) Kelleghan, A. V.; Bulger, A. S.; Witkowski, D. C.; Garg, N. K. Strain-promoted reactions of 1,2,3-cyclohexatriene and its derivatives. *Nature* **2023**, *618*, 748–754.

(34) Bulger, A. S.; Turner, D. W.; Zhou, Q.; Houk, K. N.; Garg, N. K. Evaluation of retro-aldol vs retro-carbonyl-ene mechanistic pathways in a complexity-generating C–C bond fragmentation. *Org. Lett.* **2024**, *26*, 3602–3606.

(35) Vitaku, E.; Smith, D. T.; Njardarson, J. T. Analysis of the structural diversity, substitution patterns, and frequency of nitrogen heterocycles among U. S. FDA approved pharmaceuticals. *J. Med. Chem.* **2014**, *57*, 10257–10274.

(36) Marshall, C. M.; Federice, J. G.; Bell, C. N.; Cox, P. B.; Njardarson, J. T. An update on the nitrogen heterocycle compositions and properties of U.S. FDA-approved pharmaceuticals (2013–2023). *J. Med. Chem.* **2024**, *67*, 11622–11655.

(37) Jampilek, J. Heterocycles in medicinal chemistry. *Molecules* **2019**, *24*, 3839–3842.

(38) Joule, J. A. Natural products containing nitrogen heterocycles—Some highlights 1990–2015. *Adv. Heterocycl. Chem.* **2016**, *119*, 81–106.

(39) Tlais, S. F.; Danheiser, R. L. *N*-Tosyl-3-azacyclohexyne. Synthesis and chemistry of a strained cyclic ynamide. *J. Am. Chem. Soc.* **2014**, *136*, 15489–15492.

(40) Medina, J. M.; Jackl, M. K.; Susick, R. B.; Garg, N. K. Synthetic studies pertaining to the 2,3-pyridyne and 4,5-pyrimidyne. *Tetrahedron* **2016**, *72*, 3629–3634.

(41) Kelleghan, A. V.; Tena Meza, A.; Garg, N. K. Generation and reactivity of unsymmetrical strained heterocyclic allenes. *Nat. Synth.* **2024**, *3*, 329–336.

(42) Yadav, N.; Sangwan, S.; Kumar, R.; Chauhan, S.; Duhan A.; Singh, A.; Arya, R. K. Comprehensive overview of progress in functionalization of 2-pyridone and 2,4-dihydroxy pyridine: Key constituents of vital natural products. *ChemistrySelect* **2021**, *6*, 11792–11821.

(43) Hirano, K.; Miura, M. A lesson for site-selective C–H functionalization on 2-pyridones: Radical, organometallic, directing group and steric controls. *Chem. Sci.* **2018**, *9*, 22–32.

(44) Bickelhaupt, F. M.; Houk, K. N. Analyzing reactions rates with the distortion/interaction activation strain model. *Angew. Chem., Int. Ed.* **2017**, *56*, 10070–10086.

(45) McMahon, T. C.; Medina, J. M.; Yang, Y.-F.; Simmons, B. J.; Houk, K. N.; Garg, N. K. Generation and regioselective trapping of a 3,4-piperidyne for the synthesis of functionalized heterocycles. *J. Am. Chem. Soc.* **2015**, *137*, 4082–4085.

(46) Goetz, A. E.; Garg, N. K. Regioselective reactions of 3,4-pyridynes enabled by the aryne distortion model. *Nat. Chem.* **2013**, *5*, 54–60.

(47) Shah, T. K.; Medina, J. M.; Garg, N. K. Expanding the strained alkyne toolbox: Generation and utility of oxygen-containing strained alkynes. *J. Am. Chem. Soc.* **2016**, *138*, 4948–4954.

(48) Bent, H. A. An appraisal of valence-bond structures and hybridization in compounds of the first-row elements. *Chem. Rev.* **1961**, *61*, 275–311.

(49) Medina, J. M.; McMahon, T. C.; Jiménez-Osés, G.; Houk, K. N.; Garg, N. K. Cycloadditions of cyclohexynes and cyclopentyne. *J. Am. Chem. Soc.* **2014**, *136*, 14706–14709.

(50) Medina, J. M.; Mackey, J. L.; Garg. N. K.; Houk, K. N. The role of aryne distortions, steric effects, and charges in regioselectivities of aryne reactions. *J. Am. Chem. Soc.* **2014**, *136*, 15798–15805.

(51) Ikawa, T.; Nishiyama, T.; Nosaki, T.; Takagi, A.; Akai, S. A domino process for benzyne preparation: Dual activation of *o*-(trimethylsilyl)phenol by nonafluorobutanesulfonyl fluoride. *Org. Lett.* **2011**, *13*, 1730–1733.

(52) Ikawa, T.; Masuda, S.; Nakajima, H.; Akai, S. 2-(Trimethylsilyl)phenyl trimethylsilyl ethers as stable and readily accessible benzyne precursors. *J. Org. Chem.* **2017**, *82*, 4242–4253.

(53) Luo, J.; Jensen, A. H.; Brooks, N. R.; Sniekers, J.; Knipper, M.; Aili, D.; Li, Q.; Vanroy, B.; Wübbenhorst, M.; Yan, F.; Van Meervelt, L.; Shao, Z.; Fang, J.; Luo, Z.-H.; Binnemans, K.; Fransaer, J. 1,2,4-Triazolium perfluorobutanesulfonate as an archetypal pure protic organic ionic plastic crystal electrolyte for all-solid-state fuel cells. *Energy Environ. Sci.* **2015**, *8*, 1276–1291.

(54) Högermeier, J.; Reissig, H.-U. *Nine times fluoride can be good for your syntheses.* Not just cheaper: Nonafluorobutanesulfonates as intermediates for transition metal-catalyzed reactions. *Adv. Synth. Catal.* **2009**, *351*, 2747–2763.

(55) Ikawa, T.; Urata, H.; Fukumoto, Y.; Sumii, Y.; Nishiyama, T.; Akai, S. Concise synthesis of multisubstituted isoquinolines from pyridines by regioselective Diels–Alder reactions of 2-silyl-3-4-pyridynes. *Chem. Eur. J.* **2014**, *20*, 16228–16232.

(56) Van de Poël, H.; Guillaumet, G.; Viaud-Massaurd, M. C. Synthesis of melatonin analogues derived from furo[2,3-b]- and [2,3-c]pyridines by use of a palladium-copper catalyst system. *Heterocycles* **2002**, *57*, 55–71.

(57) Joy, M. N.; Bodke, Y. D.; Khader, K. K. A.; Padusha, M. S. A.; Sajith, A. M.; Muralidharan, A. A rapid and modified approach for C-7 amination and amidation of 4-methyl-7-nonafluorobutylsulfonyloxy coumarins under microwave irradiation. *RSC Adv.* **2014**, *4*, 19766–19777.

(58) Voelkel, M. H. H.; Engelage, E.; Kondratiuk, M.; Huber, S. M. Evaluation of 6-halogenated 2-pyridone moieties as halogen bond donors. *Eur. J. Org. Chem.* **2022***, 2022*, e202200211.

(59) Maity, S.; Das, D.; Sarkar, S.; Samanta, R. Direct Pd(II)-catalyzed site-selective C5-arylation of 2-pyridones using aryl iodides. *Org. Lett.* **2018**, *20*, 5167–5171.

(60) Liu, S.; Li, Y.; Lan, Y. Mechanistic study of the fluoride-induced activation of a Kobayashi precursor: Pseudo-S_N2 pathway via a pentacoordinated silicon ate complex. *Eur. J. Org. Chem.* **2017**, *42*, 6349–6353.

(61) Smith, O.; Hindson, M. J.; Sreenithyna, A.; Tataru, V.; Paton, R. S.; Burton, J. W.; Smith, M. D. Harnessing triaryloxonium ions for aryne generation. *Nat. Synth.* **2024**, *3*, 58–66.

(62) Yoshida, H.; Shirakawa, E.; Honda, Y.; Hiyama, T. Addition of ureas to arynes: Straightforward synthesis of benzodiazepine and benzodiazocine derivatives. *Angew. Chem., Int. Ed.* **2002**, *41*, 3247–3249.

(63) Ess, D. H.; Houk, K. N. Distortion/interaction energy control of 1,3-dipolar cycloaddition reactivity. *J. Am. Chem. Soc.* **2007**, *129*, 10646–10647.

(64) Cheong, P. H.-Y.; Paton, R. S.; Bronner, S. M.; Im, G.-Y. J.; Garg, N. K.; Houk, K. N. Indolyne and aryne distortions and nucleophilic regioselectivities. *J. Am. Chem. Soc.* **2010**, *132*, 1267–1269.

(65) Saito, N.; Nakamura, K.; Shibano, S.; Ide, S.; Minami, M.; Sato, Y. Addition of cyclic ureas and 1-methyl-2-oxazolidone to pyridynes: A new approach to pyridodiazepines, pyridodiazocines, and pyridooxazepines. *Org. Lett.* **2013**, *15*, 386–389.

(66) Iwayama, T.; Sato, Y. Nickel(0)-catalyzed [2 + 2 + 2] cycloadditions of diynes and 3,4-pyridynes: Novel synthesis of isoquinoline derivatives. *Chem. Commun.* **2009**, 5245–5247.

(67) Altintas, O.; Glassner, M.; Rodriguez-Emmenegger, C.; Welle, A.; Trouillet, V.; Barner-Kowollik, C. Macromolecular surface design: Photopatterning of functional stable nitrile oxides. *Angew. Chem., Int. Ed.* **2015**, *54*, 5777–5783.

(68) Bielawski, M.; Olofsson, B. High-yielding one-pot synthesis of diaryliodonium triflates from arenes and iodine or aryl iodides. *Chem. Commun.* **2007**, 2521–2523.

(69) Hirao, Y.; Saito, T.; Kurata, H.; Kubo, T. Isolation of a hydrogen-bonded complex based on the anthranol/anthroxyl pair: Formation of a hydrogen-atom self-exchange system. *Angew. Chem., Int. Ed.* **2015**, *54*, 2402–2405.

(70) Shintrani, R.; Fu, G. C. A new copper-catalyzed [3 + 2] cycloaddition: Enantioselective coupling of terminal alkynes with azomethine imines to generate five-membered nitrogen heterocycles. *J. Am. Chem. Soc.* **2003**, *125*, 10778–10779.

(71) Liu, Y.; Li, H.; Chiba, S. Photo-induced cross-coupling of aryl iodides with alkenes. *Org. Lett.* **2021**, *23*, 427–432.

(72) Due to complex C–F splitting patterns, ^{13}C peaks of nonaflates are typically not reported.

(73) Spartan'20 Wavefunction, Inc., Irvine, CA.

(74) Grimme, S.; Bannwarth C.; Dohm, S.; Hansen, A.; Pisarek, J.; Pracht, P.; Seibert, J.; Neese, F. Fully automated quantum-chemistry-based computation of spin–spin-coupled nuclear magnetic resonance spectra. *Angew. Chem., Int. Ed.* **2017**, *56*, 14763–14769.

(75) Grimme, S. Exploration of chemical compound, conformer, and reaction space with meta-dynamics simulations based on tight-binding quantum chemical calculations. *J. Chem. Theory Comput.* **2019**, *15*, 2847–2862.

(76) Grimme, S.; Bannwarth, C.; Shushkov, P. A robust and accurate tight-binding quantum chemical method for structures, vibrational frequencies, and noncovalent interactions of large molecular systems parametrized for all spd-block elements (Z = 1–86). *J. Chem. Theory Comput.* **2017**, *13*, 1989–2009.

(77) Bannwarth, C.; Ehlert, S.; Grimme, S. GFN2-xTB–An accurate and broadly parametrized self-consistent tight-binding quantum chemical method with multipol electrostatics and density-dependent dispersion contributions. *J. Chem. Theory Comput.* **2019**, *15*, 1652–1671.

(78) Pracht, P.; Caldeweyher, E.; Ehlert, S.; Grimme, S. A robust non-self-consistent tight-binding quantum chemistry method for large molecules. *ChemRxiv* **2019**, preprint. DOI: 10.26434/chemrxiv.8326202.v1.

(79) Frisch, M. J.; Trucks, G. W.; Schlegel, H. B.; Scuseria, G. E.; Robb, M. A.; Cheeseman, J. R.; Scalmani, G.; Barone, V.; Petersson, G. A.; Nakatsuji, H.; Li, X.; Caricato, M.; Marenich, A. V.; Bloino, J.; Janesko, B. G.; Gomperts, R.; Mennucci, B.; Hratchian, H. P.; Ortiz, J. V.; Izmaylov, A. F.; Sonnenberg, J. L.; Williams-Young, D.; Ding, F.; Lipparini, F.; Egidi, F.; Goings, J.; Peng, B.; Petrone, A.; Henderson, T.; Ranasinghe, D.; Zakrzewski, V. G.; Gao, J.; Rega, N.; Zheng, G.; Liang, W.; Hada, M.; Ehara, M.; Toyota, K.; Fukuda, R.; Hasegawa, J.; Ishida, M.; Nakajima, T.; Honda, Y.; Kitao, O.; Nakai, H.; Vreven, T.; Throssell, K.; Montgomery, Jr., J. A.; Peralta, J. E.; Ogliaro, F.; Bearpark, M. J.; Heyd, J.

J.; Brothers, E. N.; Kudin, K. N.; Staroverov, V. N.; Keith, T. A.; Kobayashi, R.; Normand, J.; Raghavachari, K.; Rendell, A. P.; Burant, J. C.; Iyengar, S. S.; Tomasi, J.; Cossi, M.; Millam, J. M.; Klene, M.; Adamo, C.; Cammi, R.; Ochterski, J. W.; Martin, R. L.; Morokuma, K.; Farkas, O.; Foresman, J. B.; Fox, D. J. *Gaussian 16 Revision C.01*, Gaussian, Inc., Wallingford, CT, 2016.

(80) Becke, A. D. Density-functional thermochemistry. III. The role of exact exchange. *J. Chem. Phys.* **1993**, *98*, 5648.

(81) Lee, C.; Yang, W.; Parr, R. G. Development of the Colle–Salvetti correlation-energy formula into a functional of the electron density. *Phys. Rev. B* **1988**, *37*, 785–789.

(82) Marenich, A. V.; Cramer, C. J.; Truhlar, D. G. Universal solvation model based on solute electron density and on a continuum model of the solvent defined by the bulk dielectric constant and atomic surface tensions. *J. Phys. Chem. B* **2009**, *113*, 6378–6396.

(83) Luchini, G.; Alegre-Requena, J. V.; Funes-Ardoiz, I.; Paton, R. S. GoodVibes: Automated thermochemistry for heterogeneous computational chemistry data. *F1000Research* **2020**, *9*, 291.

(84) Grimme, S. Supramolecular binding thermodynamics by dispersion-corrected density functional theory. *Chem. Eur. J.* **2012**, *18*, 9955–9964.

(85) Li, Y.; Gomes, J.; Sharada, S. M.; Bell, A. T.; Head-Gordon, M. Improved force-field parameters for QM/MM simulations of the energies of adsorption for molecules in zeolites and a free rotor correction to the rigid rotor harmonic oscillator model for adsorption enthalpies. *J. Phys. Chem. C* **2015**, *119*, 1840–1850.

(86) Dennington, R.; Keith, T. A.; Millan, J. M. GaussView, Version 6, (Semichem Inc., 2016).

(87) Goetz, A. E.; Bronner, S. M.; Cisneros, J. D.; Melamed, J. M.; Paton, R. S.; Houk, K. N.; Garg, N. K. An efficient computational model to predict the synthetic utility of heterocyclic arynes. *Angew. Chem., Int. Ed.* **2012**, *51*, 2758–2762.

(88) Dkhissi, A.; Houben, L.; Smets, J.; Adamowicz, L.; Maes, G. Density functional theory and ab-initio computational study of the 2-hydroxypyridine/2-pyridone system: A comparison with FT-IR date from matrix isolation experiments. *J. Mol. Struct.* **1999**, *484*, 215–227.

(89) Rondan, N. G.; Domelsmith, L. N.; Houk, K. N.; Bowne, A. T.; Levin, R. H. The relative rates of electron-rich and electron-deficient alkene cycloadditions to benzyne. Enhanced electrophilicity as a consequence of alkyne bending distortions. *Tetrahedron Lett.* **1979**, *35*, 3237–3240.

(90) Kaneko, H.; Ikawa, T.; Yamamoto, Y.; Arulmozhiraja, S.; Tokiwa, H.; Akai, S. 3-(Triflyloxy)benzenes enable the regiocontrolled cycloaddition of cyclic ureas to synthesize 1,4-benzodiazepine derivatives. *Synlett* **2018**, *29*, 943–948.

(91) Witkowski, D. C.; Turner, D. W.; Bulger, A. S.; Houk, K. N.; Garg, N. K. Synthesis and reactivity of nitrogen-containing strained cyclic 1,2,3-trienes. *Nat. Synth.* **2025**, DOI: 10.1038/s44160-025-00793-9

CHAPTER FIVE

Mechanisms of Kobayashi Eliminations for the Generation of Highly-Strained Arynes, Cyclic Cumulenes, and Anti-Bredt Olefins

Zach G. Walters,[†] Dominick C. Witkowski,[†] K. N. Houk, and Neil K. Garg

Manuscript submitted.

5.1 Abstract

First disclosed in 1983, the Kobayashi method for generating transient strained intermediates from 1,2-silyltriflate precursors, has become an indispensable tool in organic synthesis. More than 1,300 Kobayashi precursors to strained intermediates have been reported to date, leading to the use of these precursors in more than 17,000 strained intermediate trapping reactions. Surprisingly, the mechanism of the Kobayashi elimination to form strained intermediates has been studied only for the formation of benzyne. We report computational studies that determine the timing of Si–C and C–O cleavage, as well as the thermodynamics of strained intermediate formation. The calculated pathway for generating anti-Bredt olefins from Kobayashi precursors differs compared to the mechanism for strained intermediate generation of other species, with a particular dependence on the Si–C–C–O dihedral angle. These studies establish the mechanisms of Kobayashi eliminations and enable the rational design of new strained intermediate precursors for future use in synthesis.

5.2 Introduction

Arynes and related strained intermediates have become common building blocks in organic synthesis.[1,2,3,4] Despite being avoided historically and having short life-times, such transient species have shown value in many areas, such as natural product synthesis,[5,6] heterocycle synthesis,[7,8] medicinal chemistry,[9] ligand synthesis,[10] organometallic and materials chemistry,[11,12] agrochemistry,[13] DNA-encoded library synthesis,[14] and more.[15] Thousands of studies of such intermediates have been reported, with the field continuing to inspire new developments in synthesis.

A key technological advance that has fueled the widespread use of arynes and related strained intermediate in modern synthesis is the discovery of 1,2-silyltriflate precursors to strained intermediates.[16] This strategy first was reported by Kobayashi and coworkers in 1983 and is highlighted in Figure 5.1A. Reaction of silyltriflate **5.1** with furan (**5.2**) in the presence of tetramethylammonium fluoride (Me_4NF) delivers cycloadduct **5.4**, presumably through the intermediacy of benzyne (**5.3**).

This methodology was first applied to the preparation of benzyne, but it has been extended to the preparation of many other strained intermediates, such as other arynes,[17,18] non-aromatic cyclic alkynes,[19,20,21] cumulated alkenes (such as cyclic allenes and cyclic 1,2,3-trienes),[22,23,24,25,26,27,28] and anti-Bredt olefins[29] (see **5.5**–**5.12**, Figure 5.1B). More than 1,300 distinct Kobayashi precursors to alkenes and alkynes are known,[30] including heterocyclic Kobayashi precursors (e.g., **5.13**–**5.16**),[31,32,33,34] which have collectively been deployed in more than 17,000 reactions reported in the literature.[30] Factors that have rendered Kobayashi methodology so practical include: a) mild conditions for strained intermediate generation; b) functional group compatibility; c) safe use;[35] d) enablement of different modes of reactivity

(including pericyclic reactions, nucleophilic additions and annulations, cascade and tandem reactions, multi-component reactions, metal-catalyzed reactions,[36,37] and σ-bond insertions[38]); and e) the aforementioned versatility in accessing distinct strained intermediate classes. Of note, transformations of strained intermediates generated from Kobayashi precursors commonly form two bonds and are increasingly used to access to structurally- and stereochemically-complex products.[2,4]

What are the mechanisms of Kobayashi eliminations for formation of strained arynes, cycloalkynes, cumulenes, and alkenes? Many theoretical studies of arynes and related intermediates exist, but these largely focus on structure and reactivity of the strained intermediates. For example, studies of ground state geometries,[39,40,41] strain,[42,43,44,45] energy of dehydrogenation,[46] reaction kinetics,[29,38,47,48] regioselective trappings,[24,27,33,34,49,50] and further computational studies of trapping reactions are known.[51,52,53] In contrast, how and why the Kobayashi elimination takes place has been reported in just two prior computational studies of the formation of benzyne.[54,55]

The aforementioned Yu et al. study was performed at the B3LYP/6-31G(d) level of theory and Biju et al. with M06-2X-D3/6-31G(d,p); both predict fluoride attack to give a pentavalent Si intermediate as the rate determining step, with subsequent Si–C cleavage having a small barrier and C–O cleavage negligible, leaving considerable uncertainty about the E2 or E1cB mechanism of the elimination. Furthermore, the mechanisms by which other classes of strained intermediates, such as cyclic alkyne **5.5**, cyclic allene **5.7**, cyclic 1,2,3-triene **5.9**, and anti-Bredt olefin **5.11** are formed from Kobayashi precursors have not been studied computationally.

We report computational studies of the mechanisms of Kobayashi eliminations to form strained intermediates (**5.17a** or **5.17b** → **5.18a** or **5.18b** using fluoride (**5.19**), Figure 5.1C). Density functional theory (DFT) calculations of the thermodynamics of formation of several

distinct classes of strained intermediates are reported, along with mechanisms of generation of **5.3**, **5.5**, **5.9**, and **5.11**.[56] While the fluoride-promoted elimination of the 1,2-silyltriflate motif ensures favorable thermodynamics in all cases, different elimination mechanisms are operative depending on the substrate. These studies not only serve to determine reaction mechanisms for Kobayashi eliminations, but provide guidance for the rational design of new strained intermediate precursors for use in synthesis.

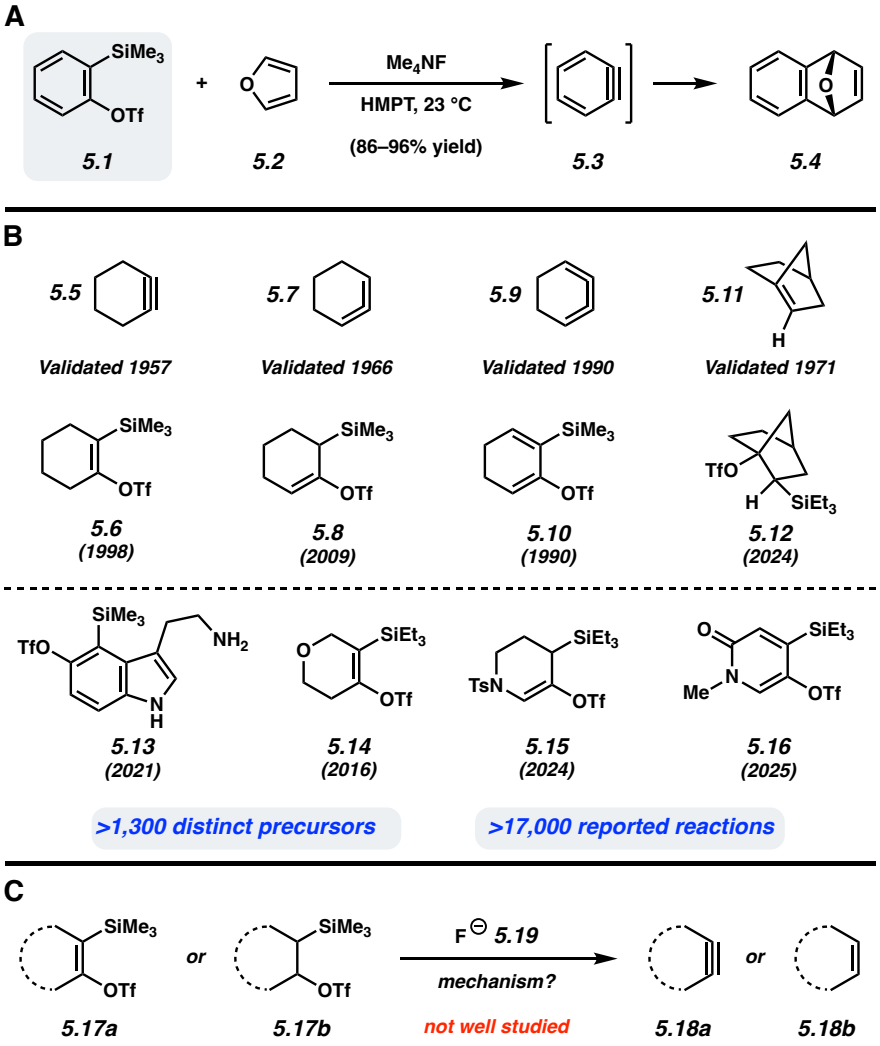

Figure 5.1. Background and overview. (A) Seminal report by Kobayashi (1983).[16] (B) Representative strained intermediates and Kobayashi-type precursors. (C) Overview of current study of the mechanism of Kobayashi eliminations.

5.3 Thermodynamics of Kobayashi Elminations to Form Strained Intermediates

The transient intermediates depicted in Figure 5.1A and 5.1B, each validated many decades ago,[23,57,58,59] are well known to possess significant strain energies, ranging from ~30 to >50 kcal mol^{-1}.[29,42,44,45] Nonetheless, Kobayashi eliminations can be used to access these high-energy species at ambient temperatures. We have computed the thermodynamics of formation of these strained intermediates via Kobayashi's fluoride-promoted elimination from different precursors.

As shown in Figure 5.2, we examined reactions where a Kobayashi precursor, generally shown as **5.17a** or **5.17b**,[60] is reacted with fluoride (**5.19**) to form alkynes **5.18a** or alkenes **5.18b**, respectively. The process is accompanied by the loss of Me_3SiF (**5.20**) and the triflate anion (**5.21**). This process was studied using DFT calculations, at the ωB97X-D/def2-QZVPP//ωB97X-D/6-31+G(d,p) level of theory, using SMD models of solvents used in experiments. This high level of theory was recently used to study aryne generation, albeit via a different base-mediated elimination mechanism.[61,62] We are only aware of computations of the thermodynamics for the generation of benzyne from a Kobayashi precursor,[54,55] whereas the corresponding computations for the generation of other strained cyclic intermediates (e.g., nonaromatic alkynes, cumulated alkenes, and anti-Bredt olefins) have not been reported.

Results from the computational evaluation of thermodynamic favorability are summarized in Figure 5.2. Beginning with the Kobayashi elimination of **5.1** to give benzyne (**5.3**), the reaction is calculated to be exergonic by 8.8 kcal mol^{-1} (entry 1).[63] The generation of cyclohexyne (**5.5**) from **5.6** is even more thermodynamically favorable (ΔG = –22.6 kcal mol^{-1}, entry 2), which is reasonable given the reduced strain present in **5.5** relative to **5.3**.[21,45] The generation of 1,2-cyclohexadiene (**5.7**) from precursor **5.8** is also computed to be energetically favorable (entry 3).[56]

The more negative ΔG of –31.7 kcal mol^{-1} again tracks with reduced strain of **5.7**, relative to **5.3** or **5.5**.[44] We also considered the generation of 1,2,3-cyclohexatriene (**5.9**) and anti-Bredt olefin **5.11** (entries 4 and 5, respectively). Whereas the thermodynamics for the generation of **5.9** are akin to that of benzyne (**5.3**) (ΔG = –3.3 kcal mol^{-1}, entry 4), the formation of anti-Bredt olefin **5.11** from silyltriflate **5.22** is energetically downhill by 21.2 kcal mol^{-1} (entry 5).

Several lessons are as follows: a) computations on the thermodynamics for Kobayashi generation of various strained intermediates generally correlate with experimental findings; b) for similar types of strained intermediates, the relative ΔG values are generally consistent with relative strain energies; c) the formation of Me_3SiF (**5.20**) and the loss of a suitable leaving group (i.e., triflate anion **5.21**; pK_a TfOH ca. –15) are essential for the success of these reactions; and d) although different leaving groups can be used in Kobayashi eliminations,[2] the use of silicon species and fluoride to trigger strained intermediate formation is essential, presumably due to the pronounced strength of the forming Si–F bond (bond dissociation energy (BDE) ≅ 135 kcal mol^{-1}).[64] Lastly, for practitioners designing new Kobayashi precursors to strained intermediates, the straightforward computations of the type show in Figure 5.2 are an excellent method to assess thermodynamic feasibility, prior to embarking on experiments.

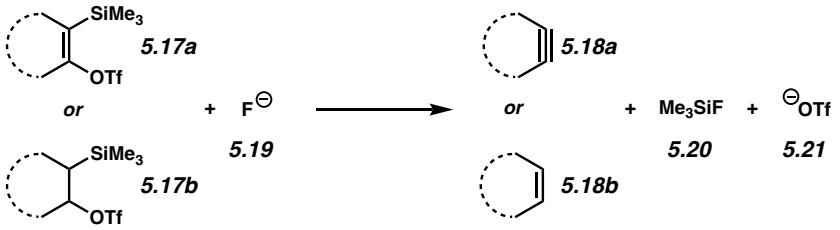

Entry	Silyl Triflate	Strained Intermediate	ΔG (kcal mol^{-1})
1	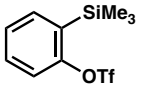 5.1	5.3	–8.8
2	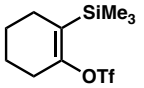 5.6	5.5	–22.6
3	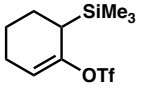 5.8	5.7	–31.7
4	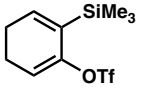 5.10	5.9	–3.3
5	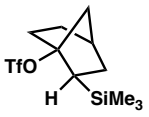 5.22	5.11	–21.2

Figure 5.2. ΔG values for the fluoride-mediated generation of strained intermediates from their trimethylsilyltriflate precursors. All energies are reported in kcal mol^{-1}. Calculations were performed at the ωB97X-D/def2-QZVPP/SMD(solvent)//ωB97X-D/6-31+G(d,p)/SMD(solvent) level. Solvent = MeCN for entries 1–3, DMSO for entry 4, and toluene for entry 5 to mimic experimental conditions.

5.4 Kobayashi Elimination to Form Benzyne (5.3)

As noted earlier, computational studies of aryne trapping processes are well-known; however, studies pertaining to how arynes (and other strained intermediates) are actually generated from Kobayashi precursors are sparse, with seminal contributions by Li & Yan in 2017[54] and by

Jindal & Biju in 2021.[55] Thus, we first computed the energy profile for the reaction of silyltriflate **5.1** with fluoride (**5.19**) to generate benzyne (**5.3**) (Figure 5.3). Although this has been computed previously using B3LYP/6-31G(d),[54] we sought to examine the transformation using a higher level of theory (ωB97X-D/def2-QZVPP/SMD(MeCN)//ωB97X-D/6-31+G(d,p)/SMD(MeCN)), consistent with the computational methods used earlier in the present study.[61] Indeed, the more advanced functional used here predicts an overall free energy change of –9 kcal mol^{-1} versus the earlier B3LYP value of –31 kcal mol^{-1}.[54]

As shown in Figure 5.3, addition of fluoride (**5.19**) to silyltriflate **5.1**, gives pre-complex **5.23**. From **5.23**, formation of silicate **5.24** proceeds via **TS-5.1**, which is the rate determining step ($\Delta G^{\ddagger}$ = 9.4 kcal mol^{-1}). Silicate **5.24** then undergoes dissociation via **TS-2** ($\Delta G^{\ddagger}$ = 7.5 kcal mol^{-1}) to furnish anion **5.25**. The loss of Me_3SiF[65] (**5.20**) provides a driving force for the reaction (10.4 kcal mol^{-1} downhill), given the notable strength of the Si–F bond[64] as discussed earlier. Benzyne (**5.3**) is then formed via elimination of triflate anion **5.21** from **5.25** via **TS-5.3**, with a barrier ($\Delta G^{\ddagger}$) of 5.7 kcal mol^{-1}. The overall reaction of silyltriflate **5.1** and fluoride anion (**5.19**) to give benzyne (**5.3**), Me_3SiF (**5.20**), and triflate anion **5.21** is thermodynamically favorable by 8.8 kcal mol^{-1} as previously discussed.

We also considered an alternative pathway from **5.25** that has occasionally been observed experimentally for silyltriflates in specialized cases, which is the thia-Fries rearrangement to give phenoxide **5.26** (Figure 5.3).[66,67,68,69] The mechanism of the thia-Fries rearrangement was expected to also proceed via aryl anion **5.25**, lending some support for the intermediacy of **5.25** since it is common to both pathways (i.e., aryne formation and thia-Fries rearrangement).[70] We examined this rearrangement mechanism and identified **TS-5.4** as a plausible transition state. However, the barrier for this process is 15.2 kcal mol^{-1} ($\Delta G^{\ddagger}$) and formation of benzyne (**5.3**) is favored by 9.5

kcal mol^{-1} ($\Delta\Delta G^{\ddagger}$). This explains why thia-Fries rearrangement is typically not observed in reactions of silyltriflate **5.1** under typical Kobayashi elimination conditions, but may be observed in other systems.[71]

Several additional considerations should be noted. First, a concerted, E2-like transition state that would allow for the direct conversion of silicate **5.24** to benzyne (**5.3**), via postulated **TS-5.5**, was not found (Figure 5.3). In addition, the elimination of **5.25** to form **5.3** has a barrier of only 5 kcal mol^{-1}. As proposed in Kobayashi's seminal report[16] the barrier to elimination is likely less than the barrier for the bimolecular reaction that would be required for the protonation of **5.25**, especially given the aprotic reaction conditions typically used in experiments. With the hope of finding experimental support for the intermediacy of **5.25**, we have performed aryne generation experiments in the presence of excess *t*-BuOH and indeed observe the formation of some aryltriflate.[72] Overall, we conclude that the Kobayashi elimination to form benzyne (**5.3**) involves aryl anion **5.25** as a key intermediate and proceeds via an E1cB mechanism, whereas the direct elimination from silicate **5.24** to give benzyne (**5.3**) is disfavored.

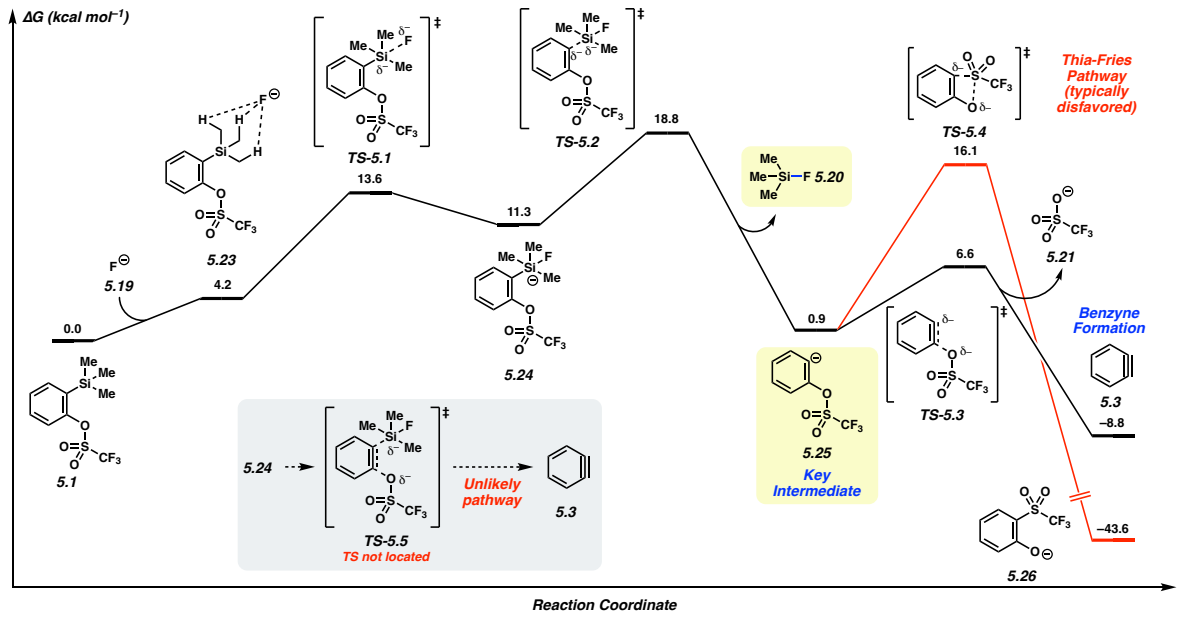

Figure 5.3. Calculated energy profile for the fluoride-mediated elimination of silyltriflate **5.1** to generate benzyne (**5.3**) (ωB97X-D/def2-QZVPP/SMD(MeCN)//ωB97X-D/6-31+G(d,p)/SMD(MeCN)). All energies are reported in kcal mol^{-1}.

5.5 Mechanisms of Kobayashi Eliminations to Form Cyclohexyne (5.5) and 1,2,3-Cyclohexatriene (5.9)

Despite possessing differing functional groups (i.e., alkyne vs. cumulene), cyclohexyne (**5.5**) and 1,2,3-cyclohexatriene (**5.9**) are conceptually similar to benzyne (**5.1**), in that each possesses: a) a functional group that ordinarily prefers a linear geometry, but is bent due to ring constraints; and b) a highly reactive π bond that is essentially orthogonal to the other alkene or alkenes present in the strained intermediate. Kobayashi precursors to these intermediates and their derivatives have been reported, along with their use in many cycloaddition reactions.[19,21,23,24]

As the mechanisms for the Kobayashi eliminations to give **5.5** or **5.9** from **5.6**[19] or **5.10**,[23] respectively, have not been reported previously, we studied both computationally (Figure 5.4). The energy profiles were determined to be very similar to what we calculate for benzyne (**5.3**; see Figure 5.3) and the full reaction coordinate diagrams are available in Sections 5.9.6 and 5.9.7,

respectively. Most notably, for both pathways, computations support a mechanism involving silicate formation (not shown), generation of a discrete carbanion (**5.27** or **5.28**) with formation of Me_3SiF (**5.20**), followed by loss of the triflate anion (**5.21**) to give the strained intermediate (via transition state **TS-5.6** or **TS-5.7**).[73] We note the following findings: a) the formation of **5.20** and **5.21** are important driving forces for these processes, leading to the overall reactions being downhill by 22.6 and 3.3 kcal mol^{-1}, respectively as noted earlier (see Figure 5.2); b) in the case of cyclohexyne (**5.5**), elimination of vinyl anion intermediate **5.27** is a barrierless pathway, whereas the corresponding elimination of vinyl anion intermediate **5.28** proceeds with an activation barrier ($\Delta G^{\ddagger}$) of 6.9 kcal mol^{-1}; c) this difference is rationalized by comparing the relative strain energies of the two intermediates (~40 kcal mol^{-1} vs ~50 kcal mol^{-1} for **5.5** vs **5.3**, respectively), and is consistent with the relative exothermicities of the eliminations, and d) we calculated similar reaction energy profiles and mechanisms for the Kobayashi eliminations to give two other 1,2,3 cyclic trienes, including an azacyclic 1,2,3-triene[34] (see Sections 5.9.8 and 5.9.9, respectively).

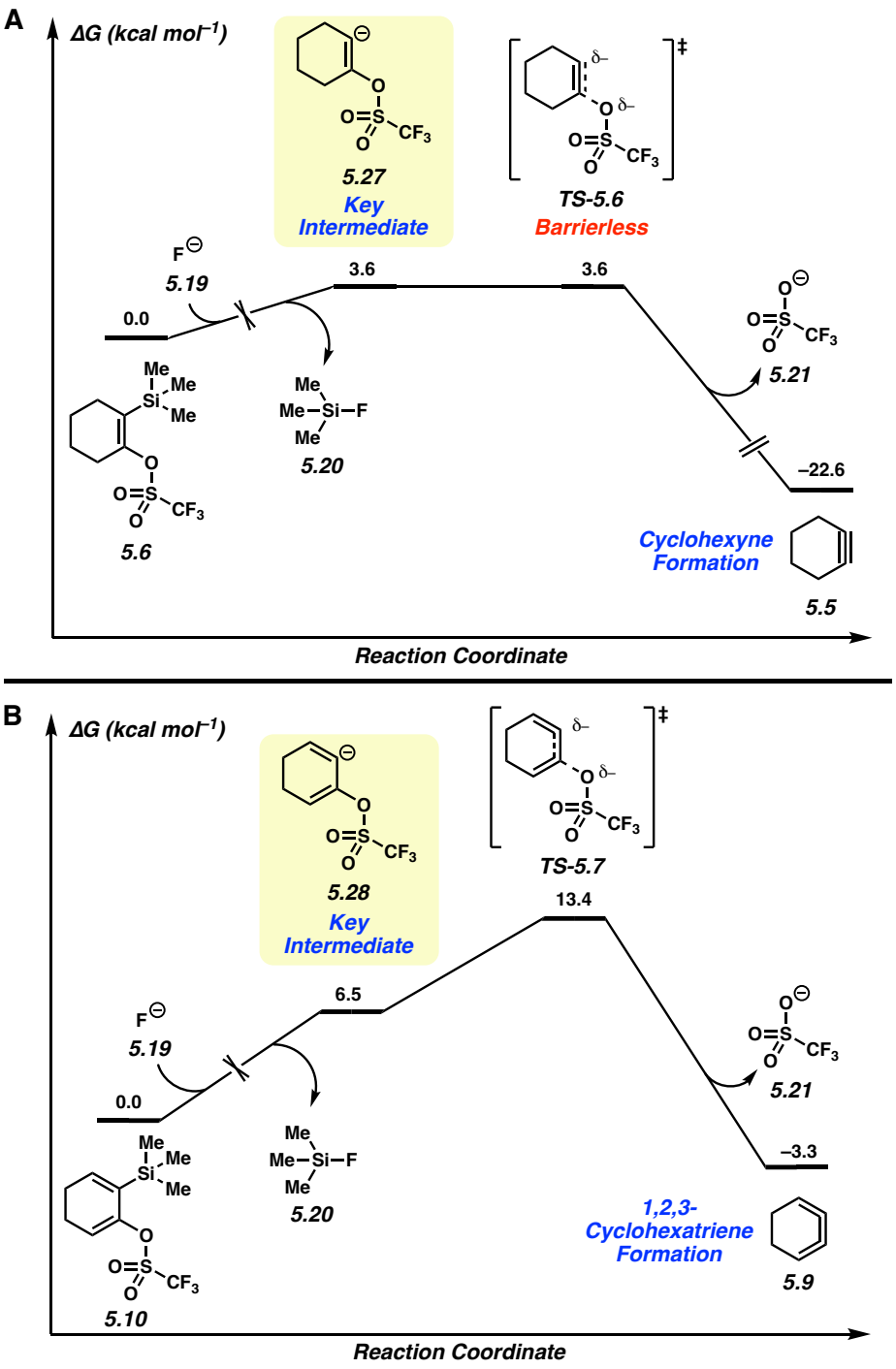

Figure 5.4. (A) Abbreviated energy profile for the generation of cyclohexyne (**5.5**) (ωB97X-D/def2-QZVPP/SMD(MeCN)//ωB97X-D/6-31+G(d,p)/SMD(MeCN)). All energies are reported in kcal mol^{-1}. (B) Abbreviated energy profile for the generation of 1,2,3-cyclohexatriene (**5.9**) (ωB97X-D/def2-QZVPP/SMD(MeCN)//ωB97X-D/6-31+G(d,p)/SMD(MeCN)). All energies are reported in kcal mol^{-1}.

5.6 Kobayashi Eliminations to Form Anti-Bredt Olefins

Another intriguing class of Kobayashi precursors are those that allow for the generation of anti-Bredt olefins. The Kobayashi approach to anti-Bredt olefins was only recently disclosed[29] as a general method to overcome Bredt's rule and access alkenes that possess severe geometric distortion. A unique aspect of Kobayashi precursors to anti-Bredt olefins is that the substrates typically bear both the silicon and leaving group substituents on saturated carbons. This leads to variations in the relationship of the Si–C and C–O bonds, as well as lower stability of the presumed carbanion that would be generated if Si–C bond cleavage occurred, prior to alkene formation, as seen in the aforementioned cases. We have examined the Kobayashi elimination to generate anti-Bredt olefin **5.11**, including stereochemical ramifications, computationally.

Figure 5.5 shows the calculated free energy profile and mechanism for the reaction of silyltriflate **5.22** to give [2.2.1] anti-Bredt olefin **5.11**. The feasibility of this overall conversion is supported by experiments.[29] Beginning with **5.22**, the Si–C–C–O dihedral angle is 33°. Addition of fluoride anion (**5.19**) via precomplex **5.29** leads to transition state **TS-5.8**, with a very small overall barrier of 4.9 kcal mol^{-1}. Formation of silicate **5.30** is exergonic by 2.7 kcal mol^{-1}.

From **5.30**, we examined two pathways for generating anti-Bredt olefin **5.11**. One pathway, the E1cB mechanism, involves formation of carbanion **5.31**, which would be akin to the pathways found for the other strained intermediates discussed earlier (see benzyne (**5.3**), cyclohexyne (**5.5**), 1,2,3-cyclohexatriene (**5.9**); Figures 5.3 and 5.4). However, a transition state to arrive at carbanion **5.31** from **5.30** could not be located, which is reasonable considering that carbanion **5.31** would be unstabilized and highly disfavorable.[74,75] Regarding the alternative pathway, silicate **5.30** is calculated to undergo facile E2-type elimination through **TS-5.9**, with an activation barrier ($\Delta G^{\ddagger}$) of 8.9 kcal mol^{-1}, to give anti-Bredt olefin **5.11**. Of note, as the reaction proceeds, there is a

progressive contraction of the Si–C–C–O dihedral angle (θ), beginning at 33° in **5.22**, decreasing to 27° in silicate **5.30**, and finally adopting an angle of 20° in **TS-5.9**. This suggests a strong stereoelectronic requirement for Kobayashi elimination on strictly aliphatic systems. As noted earlier, the overall process is 21.2 kcal mol^{-1} downhill, driven by the energetically favorable release of Me_3SiF (**5.20**) and the triflate anion (**5.21**).

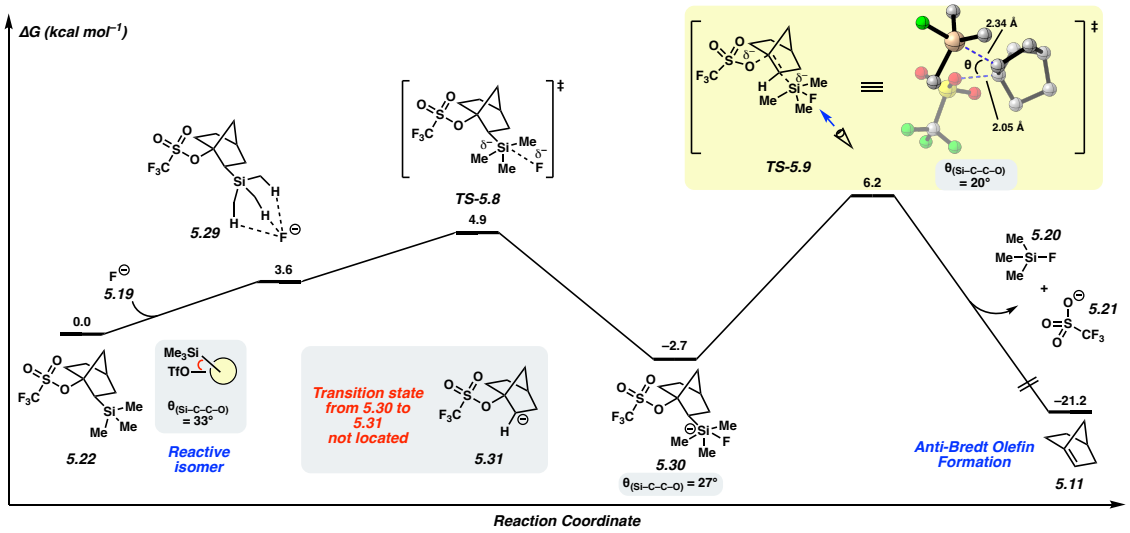

Figure 5.5. Mechanism and energy profile for the fluoride-mediated generation of anti-Bredt olefin **5.11** from silyltriflate **5.22** (ωB97X-D/def2-QZVPP/SMD(toluene)//ωB97X-D/6-31+G(d,p)/SMD(toluene)). All energies are reported in kcal mol^{-1}.

We also performed computations of the epimeric Kobayashi precursor, ***epi*-5.22**, with select results shown in Figure 5.6. In this unreactive substrate, the Si–C–C–O dihedral angle is 72°. Silicate ***epi*-5.30** can be generated analogously to **5.30** (see Section 5.9.11); however, this was found to be an unproductive intermediate. More specifically, transition states leading to concerted 1,2-elimination or formation of a discrete carbanion could not be located. Direct elimination of the silicate, which is predicted to occur for epimer **5.30** (see Figure 5.5), is presumably not feasible for ***epi*-5.30** due to poor orbital overlap between the breaking C–Si σ orbital and C–O σ* orbital of the breaking bond, as the Si–C–C–O dihedral angle in silicate ***epi*-5.30** is 70°. Overall, these

calculations are consistent with ***epi*-5.22** not undergoing fluoride-mediated Kobayashi elimination experimentally[29] and further underscore the importance of the Si–C–C–O dihedral angle in allowing for generation of the strained intermediate.

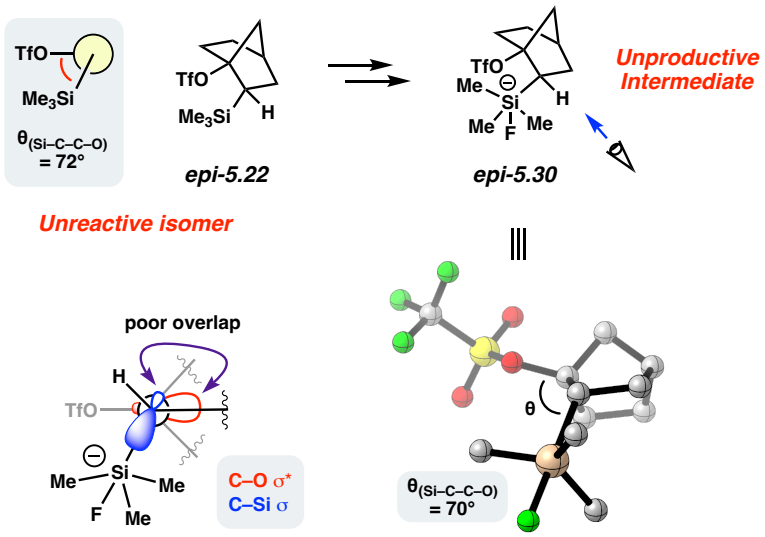

Figure 5.6. Study of unreactive substrate (***epi*-5.22**) under fluoride-mediated conditions ((U)ωB97X-D/def2-QZVPP/SMD(toluene)//(U)ωB97X-D/6-31+G(d,p)/SMD(toluene)).

5.7 Study of Impact of Dihedral Angle on Kobayashi Eliminations of Aliphatic Systems

In order to further understand the importance of the Si–C–C–O dihedral angle for successful Kobayashi elimination to generate strained cyclic alkenes, such as anti-Bredt olefins, we performed computations involving the simplest silyltriflate, **5.32**, as a model (Figure 5.7A).[76] Kobayashi elimination of this model system would give ethylene (**5.34**). By systematically constraining the Si–C–C–O dihedral angles (θ) from 180° (*anti*-periplanar) to 0° (*syn*-periplanar), we could determine the impact of dihedral angle on the transition state barrier for elimination. Thus, optimized structures of silyltriflates **5.32** and their corresponding silicate anions **5.33** were calculated for structures with θ constrained to 180°, 0°, and angles at 15° intervals within those boundaries.[77] Additionally, concerted elimination transition states **TS-5.10** were located for each constrained silicate **5.33** to give ethylene (**5.34**).

Figure 5.7A shows a plot of the ΔG of the elimination across the dihedral angles examined. Barriers are lowest for *anti*- or *syn*-eliminations, where θ is constrained to roughly 180° (**TS-5.10a**, ΔG ≅ 11 kcal mol^{-1}) or 0° (**TS-5.10c**, ΔG ≅ 13 kcal mol^{-1}), as these orientations lead to optimal overlap between the C–Si σ orbital and the C–O σ* orbital. *Anti*-elimination pathways (i.e., **TS-5.10a**) are most favorable, as is generally known for E2 eliminations.[78] The activation barrier for Kobayashi elimination increases dramatically as θ approaches 90° (**TS-5.10b**, ΔG ≅ 22 kcal mol^{-1}), reflective of poor orbital overlap in the transition state for elimination and the high strain of the eventual product with p orbitals oriented in an approximately perpendicular fashion.

TS-5.10a, **TS-5.10b**, and **TS-5.10c** are shown in Figure 5.7B. The transition state geometries show very similar bond lengths in the favorable transition states **TS-5.10a** (θ = 180°) and **TS-5.10c** (θ = 0°). The breaking C–Si bond is 2.11 Å in both cases, whereas the breaking C–O bond is 1.69 Å or 1.74 Å, respectively. In contrast, the C–Si and C–O bonds in the disfavored transition state **TS-5.10b** are elongated to 2.16 Å or 1.93 Å, respectively, indicative of a later transition state.

Finally, computations on plausible Kobayashi precursors of constrained aliphatic substrates are a valuable predecessor to substrate synthesis, since they can reveal difficulties that might arise in achieving the elimination.[79] The geometries seen in such Kobayashi precursors tend to be similar to that seen in the intermediate silicates formed after fluoride addition and, therefore, reasonably approximate the expected Si–C–C–O dihedral. Dihedral angles between 180–120° and 35–0° are appropriate for successful Kobayashi eliminations.

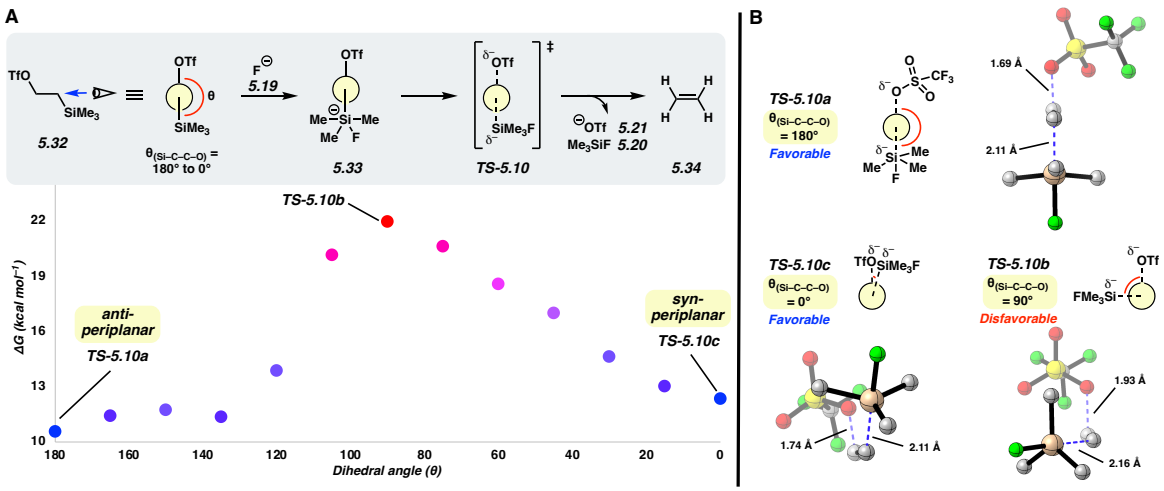

Figure 5.7. (A) Computational study of fluoride-mediated generation of ethylene (**5.34**) from silyltriflate **5.32** with varying Si–C–C–O dihedral angles θ (ωB97X-D/def2-QZVPP/SMD(MeCN)//ωB97X-D/6-31+G(d,p)/SMD(MeCN)). (B) Key transition states **TS-5.10a-c** and geometric parameters. All energies are reported in kcal mol^{-1}.

5.8 Conclusion

Kobayashi precursors to strained intermediates have become valuable building blocks in organic synthesis, resulting in >17,000 chemical reactions, with applications across numerous fields. Kobayashi precursors to arynes, cyclic alkynes, cyclic 1,2,3-trienes, cyclic allenes, and strained alkenes, such as anti-Bredt olefins, have been developed. Although the formation of benzyne had been studied previously, we studied that mechanism in detail, as well as mechanisms for other classes of strained intermediates: strained alkenes, alkynes, and 1,2,3-trienes.

We find that: a) Kobayashi eliminations, despite leading to highly strained intermediates, are thermodynamically favorable as a result of formation of the strong Si–F bond, as well as the loss of the excellent triflate leaving group; b) all mechanisms proceed via initial formation of a fluorosilicate anion; and c) the mechanism of elimination varies, either proceeding through desilylative carbanion formation, followed by elimination (for arynes, cyclic alkynes, cyclic 1,2,3-trienes), or direct elimination of the fluorosilicate anion (for anti-Bredt olefins) in cases where the

intermediate carbanion is very unstable, so that triflate loss occurs with breaking of the Si–C bond. In the latter case, stereoelectronic requirements dictate the barrier of elimination. In future substrate design of aliphatic Kobayashi precursors to strained alkenes, targeting Si–C–C–O dihedral angles between 180–120° and 35–0° in the substrate will optimize chances of successful Kobayashi elimination.

Our studies provide fundamental insight regarding the thermodynamics and mechanisms of Kobayashi eliminations, which enable the rational design of new strained intermediate precursors for future uses in synthesis.

5.9 Computational Section

5.9.1 Method for Literature Searches for Kobayashi Precursors and Reactions

The values included for the number of distinct Kobayashi Precursors were obtained using a substructure search in Scifinder^{n}, utilizing a three-membered ring, with all bonds replaced with dashed bonds (unspecified bonds). A silyl group with three "A" substituents (any atom but hydrogen) was singly bound to one carbon, and a triflate group was singly bound to an adjacent carbon. The third atom in the three membered ring was an "A" atom, and repeating group brackets were placed on this atom with a range from 1–10 atoms. Reference availability was set to available, and the reference role was set to "reactant or reagent". In order to determine the number of reported reactions with these precursors, a reaction substructure search was performed on the same structure described above. The substance role was set to "reactant and reagent," and the reagents in the reaction were restricted to include fluoride sources

.

5.9.2 Computational Methods

Initial structures were optimized in Gaussian 16 A.03[80] at the ωB97X-D[81]/6-31+G(d,p)/SMD[82] (MeCN, DMSO, or toluene) level of theory. All geometries were verified as stationary points on the potential energy surface and characterized as transition states or minima by frequency calculations. Intrinsic reaction coordinate (IRC) calculations were performed at the same level of theory to confirm the intermediates linked by each transition state. Single point energies were computed at the ωB97X-D/def2-QZVPP[83]/SMD(MeCN, DMSO, or toluene) level of theory. GoodVibes[84] (v. 3.2) with quasi-harmonic entropy[85] and enthalpy[86] treatment (frequency cut-off value: 100 cm^{-1}) was used to obtain corrected Gibbs free energies and enthalpies at either 298.15 K 1 atm. Optimized structures are presented using CYLview.[87]

5.9.3 Calculated Energies of Selected Kobayashi Precursors and Strained Intermediates

Table 5.1. Computed energies for formation of benzyne (**5.3**), cyclohexyne (**5.5**), and 1,2-cyclohexadiene (**5.7**) at 23 °C (298.15 K) at the ωB97X-D/def2-QZVPP/SMD(MeCN)//ωB97X-D/6-31+G(d,p)/SMD(MeCN) level of theory. All units are in Hartrees. E = electronic energy; SPC = single-point correction; ZPE = zero-point energy; H = enthalpy; T = temperature; S = entropy; G(T) = Gibbs free energy; qh-S = quasi-harmonic corrected entropy; qh-G(T) = quasi-harmonic corrected Gibbs free energy.

Structure	E_SPC	E	ZPE	H_SPC	T.S	T.qh-S	G(T)_SPC	qh-G(T)_SPC
5.19	-100.004288	-99.966694	0.000000	-100.001927	0.016519	0.016519	-100.018446	-100.018446
5.20	-509.251385	-509.121674	0.113649	-509.128828	0.041040	0.040990	-509.169480	-509.169818
5.21	-961.803851	-961.453330	0.027431	-961.768384	0.040379	0.039939	-961.808763	-961.808832
5.1	-1601.996156	-1601.489570	0.222400	-1601.752861	0.070171	0.066956	-1601.823032	-1601.822970
5.3	-230.925032	-230.843142	0.075665	-230.843858	0.032953	0.032957	-230.876810	-230.876830
5.6	-1604.41376	-1603.906983	0.268441	-1604.123320	0.071891	0.068879	-1604.195211	-1604.195493
5.5	-233.364615	-233.282062	0.122056	-233.235870	0.035372	0.035381	-233.271241	-233.271315
5.8	-1604.412257	-1603.904822	0.268143	-1604.122271	0.072562	0.068852	-1604.194833	-1604.194404
5.7	-233.37776	-233.296732	0.121813	-233.249526	0.035059	0.034987	-233.284584	-233.284705

Table 5.2. Computed energies for formation of 1,2,3-cyclohexatriene (**5.9**) at 23 °C (298.15 K) at the ωB97X-D/def2-QZVPP/SMD(DMSO)//ωB97X-D/6-31+G(d,p)/SMD(DMSO) level of theory. All units are in Hartrees. E = electronic energy; SPC = single-point correction; ZPE = zero-point energy; H = enthalpy; T = temperature; S = entropy; G(T) = Gibbs free energy; qh-S = quasi-harmonic corrected entropy; qh-G(T) = quasi-harmonic corrected Gibbs free energy.

Structure	E_SPC	E	ZPE	H_SPC	T.S	T.qh-S	G(T)_SPC	qh-G(T)_SPC
5.19	-100.004766	-99.967157	0	-100.002405	0.016519	0.016519	-100.018925	-100.018925
5.20	-509.249081	-509.119351	0.113640	-509.126133	0.041076	0.041024	-509.167209	-509.167550
5.21	-961.804839	-961.454311	0.027466	-961.769358	0.040265	0.039891	-961.809622	-961.809732
5.10	-1603.175077	-1602.668053	0.244253	-1602.909054	0.072379	0.068755	-1602.981433	-1602.981180
5.9	-232.096190	-232.014142	0.097089	-231.992448	0.035508	0.035494	-232.027956	-232.028105

Table 5.3. Computed energies for the reaction formation of anti-Bredt olefin (ABO) **5.11** at 23 °C (298.15 K) at the ωB97X-D/def2-QZVPP/SMD(toluene)//ωB97X-D/6-31+G(d,p)/SMD(toluene) level of theory. All units are in Hartrees. E = electronic energy; SPC = single-point correction; ZPE = zero-point energy; H = enthalpy; T = temperature; S = entropy; G(T) = Gibbs free energy; qh-S = quasi-harmonic corrected entropy; qh-G(T) = quasi-harmonic corrected Gibbs free energy.

Structure	E_SPC	E	ZPE	H_SPC	T.S	T.qh-S	G(T)_SPC	qh-G(T)_SPC
5.19	-99.946659	-99.910028	0	-99.944298	0.016519	0.016519	-99.960817	-99.960817
5.20	-509.249804	-509.119426	0.114199	-509.126325	0.039995	0.039941	-509.16632	-509.16666
5.21	-961.77215	-961.421632	0.027597	-961.736551	0.04019	0.039876	-961.776742	-961.776885
5.22	-1643.744124	-1643.225699	0.299995	-1643.422077	0.072261	0.0691	-1643.494337	-1643.494394
5.11	-272.688451	-272.59575	0.153012	-272.529153	0.03487	0.034876	-272.564023	-272.564054

5.9.4 Transition State Analysis for Reaction of Precursor 5.1 to Form Benzyne (5.3)

The reaction mechanism for the generation of benzyne (**5.3**) from precursor **5.1** was studied computationally (see Figure 5.3).[16] The optimized geometries of **TS-5.1**, **TS-5.2**, **TS-5.3**, and **TS-5.4** are shown in Figure 5.8. To explore the reaction pathways leading from **5.24** to **5.3**, we also evaluated a concerted, E2-like elimination (see Figure 5.3). No transition state (**TS-5.5**) was located on the potential energy surface connecting **5.24** to **5.3**, suggesting that this step is not feasible. Furthermore, a geometry scan from **5.24** to **5.3** was performed to further support this conclusion.

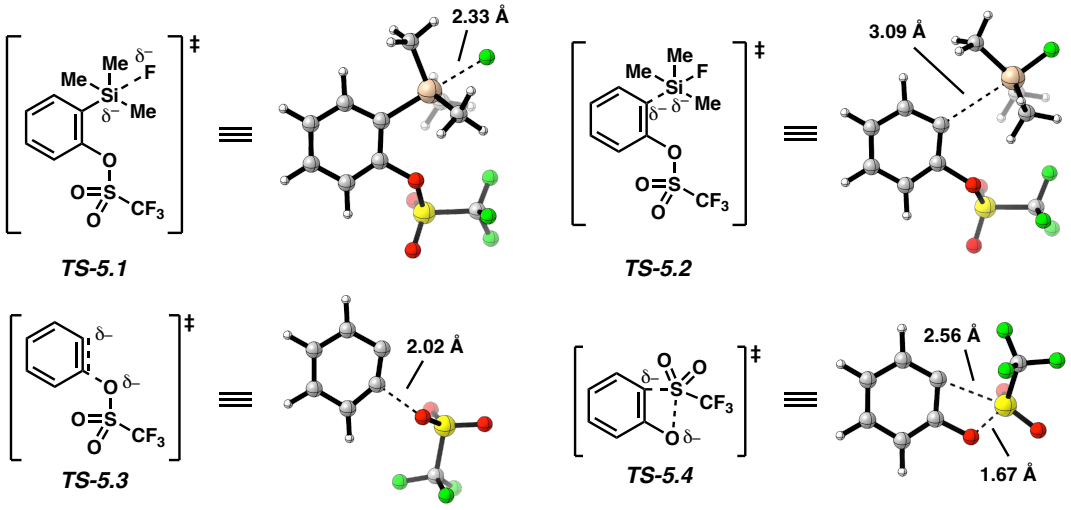

Figure 5.8. Geometries of **TS-5.1**–**TS-5.4** calculated at the ωB97X-D/def2-QZVPP/SMD(MeCN)//ωB97X-D/6-31+G(d,p)/SMD(MeCN) level of theory.

Table 5.4. Computed energies for the reaction of **5.1** to form benzyne (**5.3**) at 23 °C (298.15 K) at the ωB97X-D/def2-QZVPP/SMD(MeCN)//ωB97X-D/6-31+G(d,p)/SMD(MeCN) level of theory. All units are in Hartrees. E = electronic energy; SPC = single-point correction; ZPE = zero-point energy; H = enthalpy; T = temperature; S = entropy; G(T) = Gibbs free energy; qh-S = quasi-harmonic corrected entropy; qh-G(T) = quasi-harmonic corrected Gibbs free energy.

Structure	E_SPC	E	ZPE	H_SPC	T.S	T.qh-S	G(T)_SPC	qh-G(T)_SPC
5.19	-100.004288	-99.966694	0.000000	-100.001927	0.016519	0.016519	-100.018446	-100.018446
5.20	-509.251385	-509.121674	0.113649	-509.128828	0.041040	0.040990	-509.169480	-509.169818
5.21	-961.803851	-961.453330	0.027431	-961.768384	0.040379	0.039939	-961.808763	-961.808832
5.1	-1601.996156	-1601.489570	0.222400	-1601.752861	0.070171	0.066956	-1601.823032	-1601.822970
5.23	-1702.002155	-1701.456813	0.222584	-1701.755951	0.080779	0.074107	-1701.836730	-1701.834687
TS-5.1	-1701.992158	-1701.444297	0.223050	-1701.747130	0.072406	0.069069	-1701.819537	-1701.819668
5.24	-1701.996310	-1701.445961	0.223329	-1701.750705	0.069370	0.069370	-1701.823116	-1701.823363
TS-5.2	-1701.980915	-1701.426099	0.221363	-1701.737237	0.074649	0.070235	-1701.811886	-1701.811405
5.25	-1192.735764	-1192.307518	0.106324	-1192.616273	0.054993	0.052084	-1192.671266	-1192.670223
TS-5.3	-1192.724473	-1192.294150	0.104293	-1192.606900	0.054876	0.052187	-1192.661776	-1192.661065
5.3	-230.925032	-230.843142	0.075665	-230.843858	0.032953	0.032957	-230.876810	-230.876830
TS-5.4	-1192.713655	-1192.291141	0.106209	-1192.595248	0.050532	0.493190	-1192.645780	-1192.645907
5.26	-1192.808550	-1192.391754	0.107109	-1192.688354	0.053205	0.051229	-1192.741559	-1192.741154

5.9.5 Control Experiments to Support Proposed Mechanism

Materials and Methods. Reactions were conducted in flame-dried glassware under an atmosphere of nitrogen, and commercially obtained reagents were used as received. Anhydrous solvents were passed through activated alumina columns prior to use. Precursor **5.35** was obtained from TCI.

CsF was obtained from Strem. *t*-BuOH was obtained from Fischer. CD_3CN was obtained from Cambridge Isotope Laboratories. 2,5-dimethylfuran was obtained from Sigma-Aldrich. Reaction temperatures were controlled using an IKAmag temperature modulator. Silicycle Siliaflash P60 (particle size 40 – 63 μm) was used for flash column chromatography. Thin layer chromatography (TLC) was conducted with EMD gel 60 F254 pre-coated plates (0.25 mm for analytical chromatography and 0.50 mm for preparative chromatography) and visualized using UV light. ^{1}H NMR spectra were recorded on Bruker spectrometers (at 300 and 400 MHz) and are reported relative to the residual solvent signal. ^{19}F NMR spectra were recorded on Bruker spectrometers (at 282 and 376 MHz).

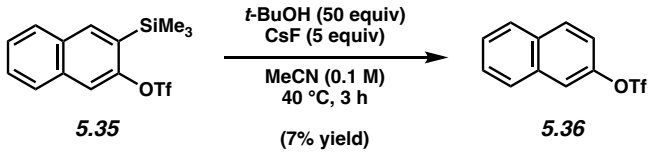

Evidence of protodesilylation under protic conditions. A 1-dram vial equipped with a stir bar was charged with silyltriflate **5.35** (34.6 mg, 99.3 μmol, 1.0 equiv) and *t*-BuOH (368 mg, 472 μL, 4.97 mmol, 50 equiv) and diluted in MeCN (1.0 mL, 0.1 M). To the solution was added CsF (75.4 mg, 497 μmol, 5.0 equiv) and the suspension was stirred at 900 rpm for 40 °C for 3 h. After this time, the reaction was allowed to cool to 23 °C and was filtered through a 0.5 x 2 cm silica gel plug, eluting with EtOAc (5 mL). The eluate was concentrated under reduced pressure then purified by preparative TLC (9:1 hexane:EtOAc) to provide aryl triflate **5.36** (1.8 mg, 6.5 μmol, 7% yield). Spectral data matched those reported in the literature.[88]

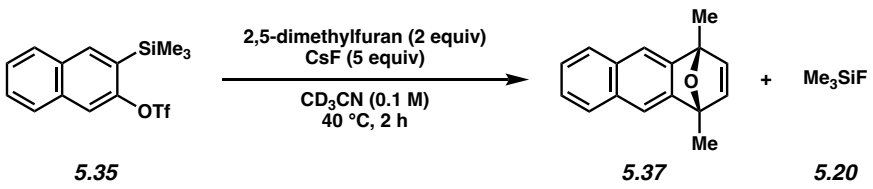

5.35 *5.37* *5.20*

Evidence of Me_3SiF formation. A 1-dram vial equipped with a stir bar was charged sequentially with silyltriflate **5.35** (24.0 mg, 69.0 μmol, 1.0 equiv), 2,5-dimethylfuran (13.0 mg, 140 μmol, 2.0 equiv), CD_3CN (0.7 mL, 0.1 M), and CsF (52.0 mg, 340 μmol, 5.0 equiv). The suspension was stirred at 900 rpm for 40 °C for 2 h. The mixture was then allowed to cool to 23°C and was filtered through a 0.5 x 1 cm celite plug. Analysis by ^1H and ^{19}F NMR showed the formation of cycloadduct **5.37** and Me_3SiF (**5.20**). Spectral data matched those reported in the literature.[89,90]

5.9.6 Reaction Energy Profile and Mechanism for Formation of Cyclohexyne (5.5)

The reaction mechanism for the generation of cyclohexyne (**5.5**) from precursor **5.6** was studied computationally (see Figure 5.4A and Figure 5.9).[19] The optimized geometries of **TS-5.11, TS-5.12**, and **TS-5.6** are shown in Figure 5.10. To explore the reaction pathways leading from **5.39** to **5.5**, we also evaluated a concerted, E2-like elimination. No transition state (e.g., **TS-5.13**) was located on the potential energy surface connecting **5.39** to **5.5**, suggesting that this step is not feasible. Furthermore, a geometry scan from **5.39** to **5.5** was performed to further support this conclusion.

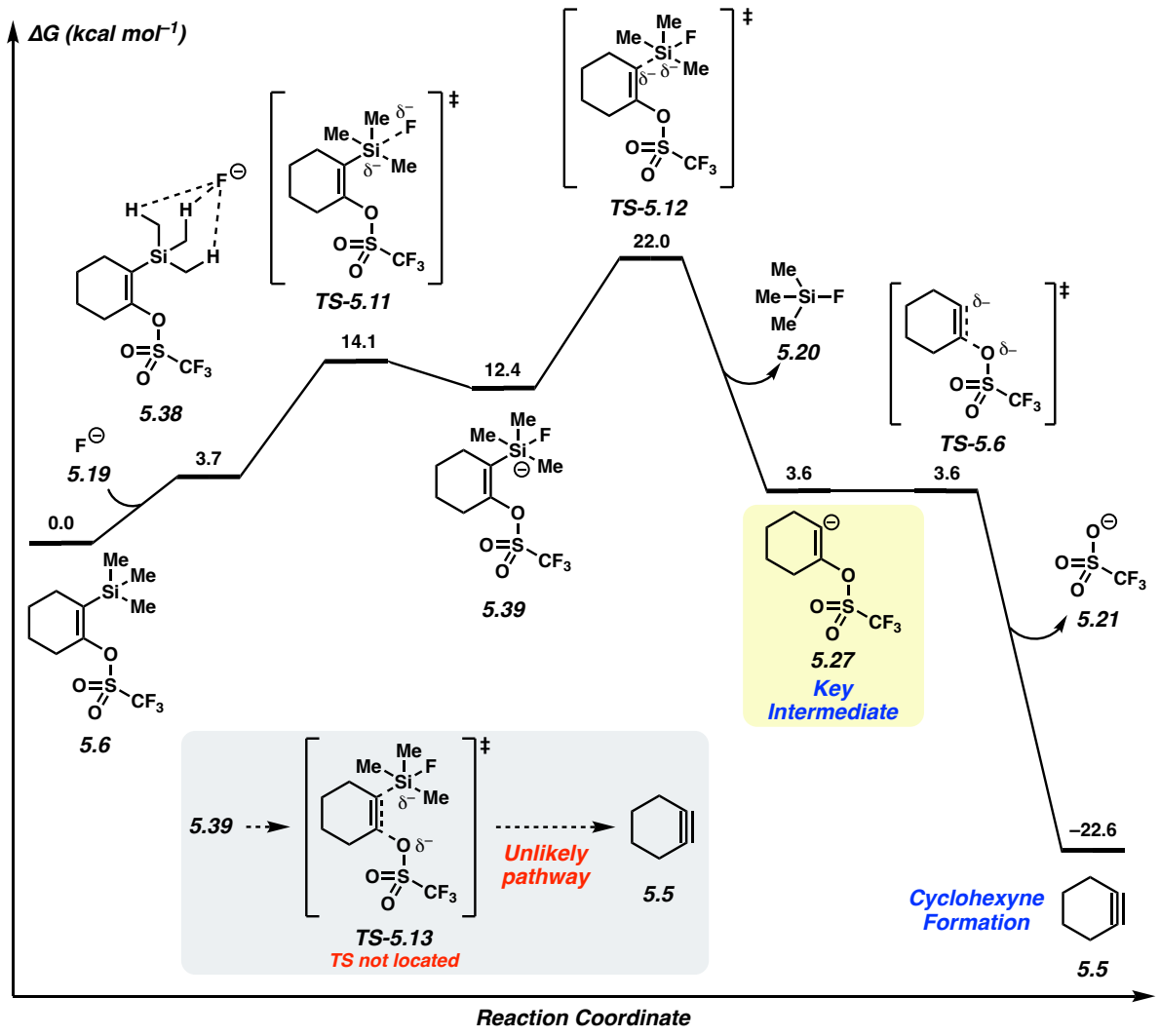

Figure 5.9. Calculated free energy profile for formation of cyclohexyne (**5.5**) from precursor **5.6** at the ωB97X-D/def2-QZVPP/SMD(MeCN)//ωB97X-D/6-31+G(d,p)/SMD(MeCN) level of theory.

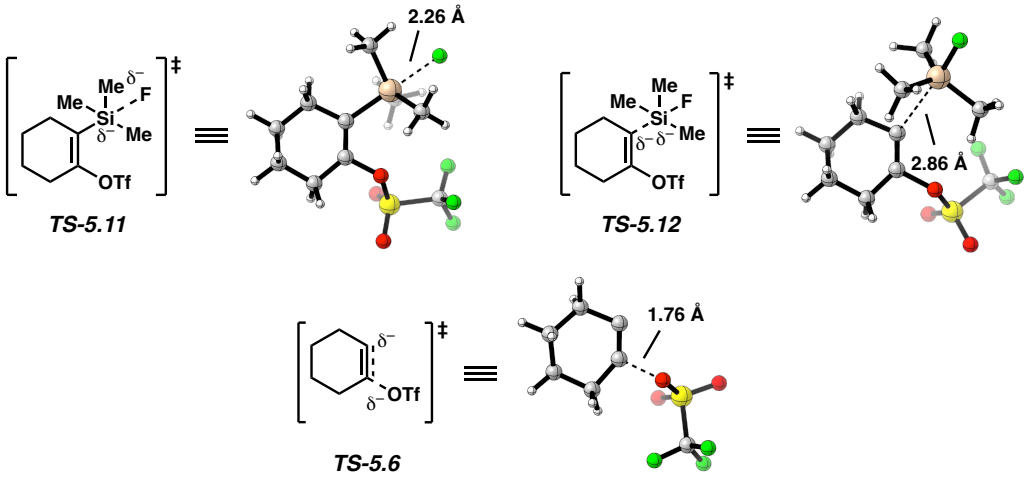

Figure 5.10. Geometries of **TS-5.11**, **TS-5.12**, and **TS-5.6** calculated at the ωB97X-D/def2-QZVPP/SMD(MeCN)//ωB97X-D/6-31+G(d,p)/SMD(MeCN) level of theory.

Table 5.5. Computed energies for the reaction of **5.6** to form cyclohexyne (**5.5**) at 23 °C (298.15 K) at the ωB97X-D/def2-QZVPP/SMD(MeCN)//ωB97X-D/6-31+G(d,p)/SMD(MeCN) level of theory. All units are in Hartrees. E = electronic energy; SPC = single-point correction; ZPE = zero-point energy; H = enthalpy; T = temperature; S = entropy; G(T) = Gibbs free energy; qh-S = quasi-harmonic corrected entropy; qh-G(T) = quasi-harmonic corrected Gibbs free energy.

Structure	E_SPC	E	ZPE	H_SPC	T.S	T.qh-S	G(T)_SPC	qh-G(T)_SPC
5.19	-100.004288	-99.966694	0	-100.001927	0.016519	0.016519	-100.018446	-100.018446
5.20	-509.251385	-509.121674	0.113649	-509.128828	0.041040	0.040990	-509.169480	-509.169818
5.21	-961.803851	-961.453330	0.027431	-961.768384	0.040379	0.039939	-961.808763	-961.808832
5.6	-1604.41376	-1603.906983	0.268441	-1604.123320	0.071891	0.068879	-1604.195211	-1604.195493
5.38	-1704.420389	-1703.874895	0.268575	-1704.127062	0.082720	0.076168	-1704.209782	-1704.208032
TS-5.11	-1704.408550	-1703.860322	0.269044	-1704.116367	0.075060	0.071311	-1704.191427	-1704.191515
5.39	-1704.411340	-1703.861109	0.269304	-1704.122306	0.075897	0.071862	-1704.194408	-1704.194168
TS-5.12	-1704.394886	-1703.839505	0.267735	-1704.104029	0.074858	0.071338	-1704.178887	-1704.178956
5.27	-1195.148215	-1194.719245	0.151749	-1194.982007	0.057312	0.054339	-1195.039319	-1195.038368
TS-5.6	-1195.147856	-1194.717822	0.150747	-1194.982939	0.055971	0.053505	-1195.038910	-1195.038389
5.5	-233.364615	-233.282062	0.122056	-233.235870	0.035372	0.035381	-233.271241	-233.271315

5.9.7 Reaction Energy Profile and Mechanism for Formation of 1,2,3-Cyclohexatriene (5.9)

The reaction mechanism for the generation of 1,2,3-cyclohexatriene (**5.9**) from precursor **5.10** was studied computationally (see Figure 5.4B and Figure 5.11).[23] The optimized geometries of **TS-5.14**, **TS-5.15**, and **TS-5.7** are shown in Figure 5.12. To explore the reaction pathways leading from **5.41** to **5.9**, we also evaluated a concerted, E2-like elimination. No transition state (e.g., **TS-**

5.16) was located on the potential energy surface connecting **5.41** to **5.9**, suggesting that this step is not feasible. Furthermore, a geometry scan from **5.41** to **5.9** was performed to further support this conclusion.

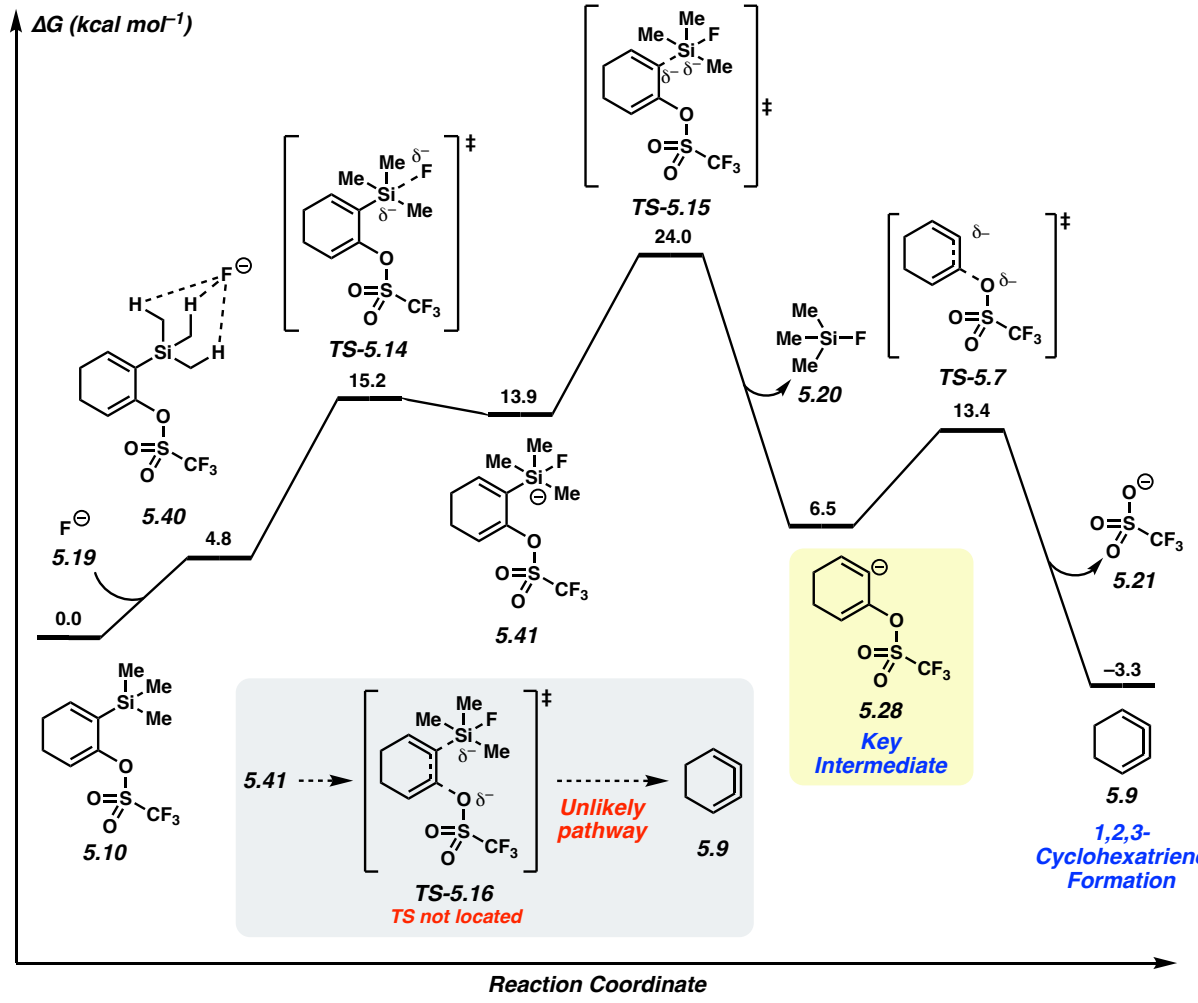

Figure 5.11. Calculated free energy profile for formation of 1,2,3-cyclohexatriene (**5.9**) from precursor **5.10** at the ωB97X-D/def2-QZVPP/SMD(DMSO)//ωB97X-D/6-31+G(d,p)/SMD(DMSO) level of theory.

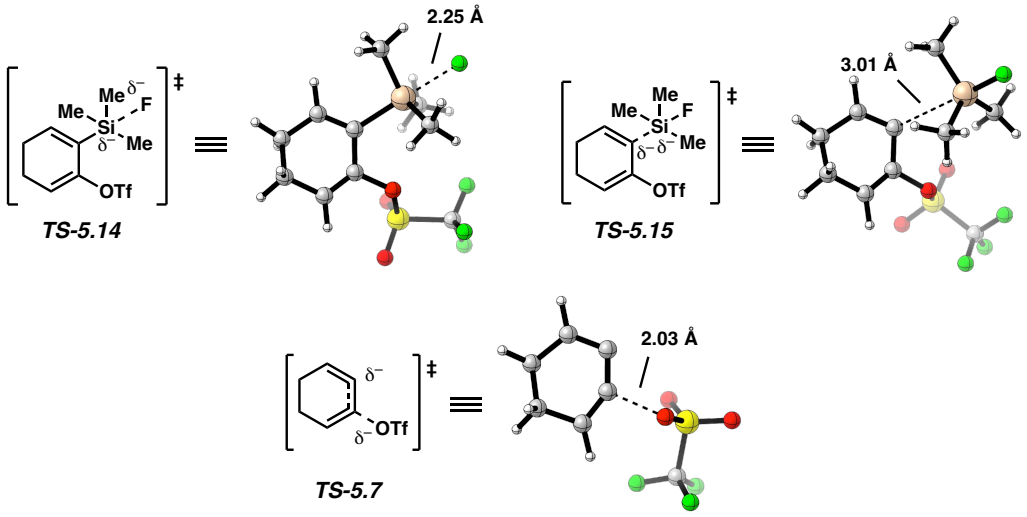

Figure 5.12. Geometries of **TS-5.14**, **TS-5.15**, and **TS-5.7** calculated at the ωB97X-D/def2-QZVPP/SMD(DMSO)//ωB97X-D/6-31+G(d,p)/SMD(DMSO) level of theory.

Table 5.6. Computed energies for the reaction of **5.10** to form 1,2,3-cyclohexatriene (**5.9**) at 23 °C (298.15 K) at the ωB97X-D/def2-QZVPP/SMD(DMSO)//ωB97X-D/6-31+G(d,p)/SMD(DMSO) level of theory. All units are in Hartrees. E = electronic energy; SPC = single-point correction; ZPE = zero-point energy; H = enthalpy; T = temperature; S = entropy; G(T) = Gibbs free energy; qh-S = quasi-harmonic corrected entropy; qh-G(T) = quasi-harmonic corrected Gibbs free energy.

Structure	E_SPC	E	ZPE	H_SPC	T.S	T.qh-S	G(T)_SPC	qh-G(T)_SPC
5.19	-100.004766	-99.967157	0	-100.002405	0.016519	0.016519	-100.018925	-100.018925
5.20	-509.249081	-509.119351	0.113640	-509.126133	0.041076	0.041024	-509.167209	-509.167550
5.21	-961.804839	-961.454311	0.027466	-961.769358	0.040265	0.039891	-961.809622	-961.809732
5.10	-1603.175077	-1602.668053	0.244253	-1602.909054	0.072379	0.068755	-1602.981433	-1602.981180
5.40	-1703.181693	-1702.635781	0.244742	-1702.912651	0.081504	0.075107	-1702.944155	-1702.992419
TS-5.14	-1703.169988	-1702.621471	0.245290	-1702.902081	0.073760	0.070270	-1702.975841	-1702.975814
5.41	-1703.172238	-1702.621997	0.245531	-1702.903704	0.074193	0.070793	-1702.977896	-1702.977892
TS-5.15	-1703.152539	-1702.597162	0.243406	-1702.886103	0.076355	0.071749	-1702.962458	-1702.961909
5.28	-1193.910226	-1193.481164	0.128627	-1193.767856	0.054655	0.052525	-1193.822511	-1193.822232
TS-5.7	-1193.895297	-1193.464801	0.125965	-1193.755204	0.056811	0.053864	-1193.812016	-1193.811145
5.9	-232.096190	-232.014142	0.097089	-231.992448	0.035508	0.035494	-232.027956	-232.028105

5.9.8 Reaction Energy Profile and Mechanism for Formation of 1,2,3-Triene 5.45

Figure 5.13 shows the corresponding reaction mechanism for the generation of dimethyl-substituted 1,2,3-triene **5.45** from precursor **5.42**.[24] Beginning with precursor **5.42**, fluoride (**5.19**) was found to form pre-complex **5.43**, which is slightly higher in energy (ΔG = 4.3 kcal mol^{-1}). From **5.43**, two pathways were identified. Formation of 1,2,3-triene **5.45** could proceed via **TS-5.17** ($\Delta G^{\ddagger}$ = 29.5 kcal mol^{-1}). This concerted, E2-like transition state that directly links precomplex

5.43 to 1,2,3-triene **5.45** is distinct from the transition states located for the other arynes, cyclohexynes, and 1,2,3-cyclohexatrienes that we have studied. However, a stepwise pathway with a lower activation energy was also identified. Formation of anion **5.44** proceeds via **TS-5.18** ($\Delta G^{\ddagger}$ = 23.3 kcal mol^{-1}). This S_N2-like transition state is different than what was found for 1,2,3-cyclohexatriene's (**5.9**) mechanism (see Section 5.9.7) as there is no discrete silicate intermediate (e.g., **5.41**). Finally, elimination of the triflate anion (**5.21**) can occur via **TS-5.19** to form **5.45**, with a small activation barrier ($\Delta G^{\ddagger}$) of 5.3 kcal mol^{-1}. The optimized geometries of **TS-5.17**, **TS-5.18**, and **TS-5.19** are shown in Figure 5.14. Notably, the generation of 1,2,3-triene **5.45** is thermodynamically favorable (ΔG = –11.7 kcal mol^{-1}).

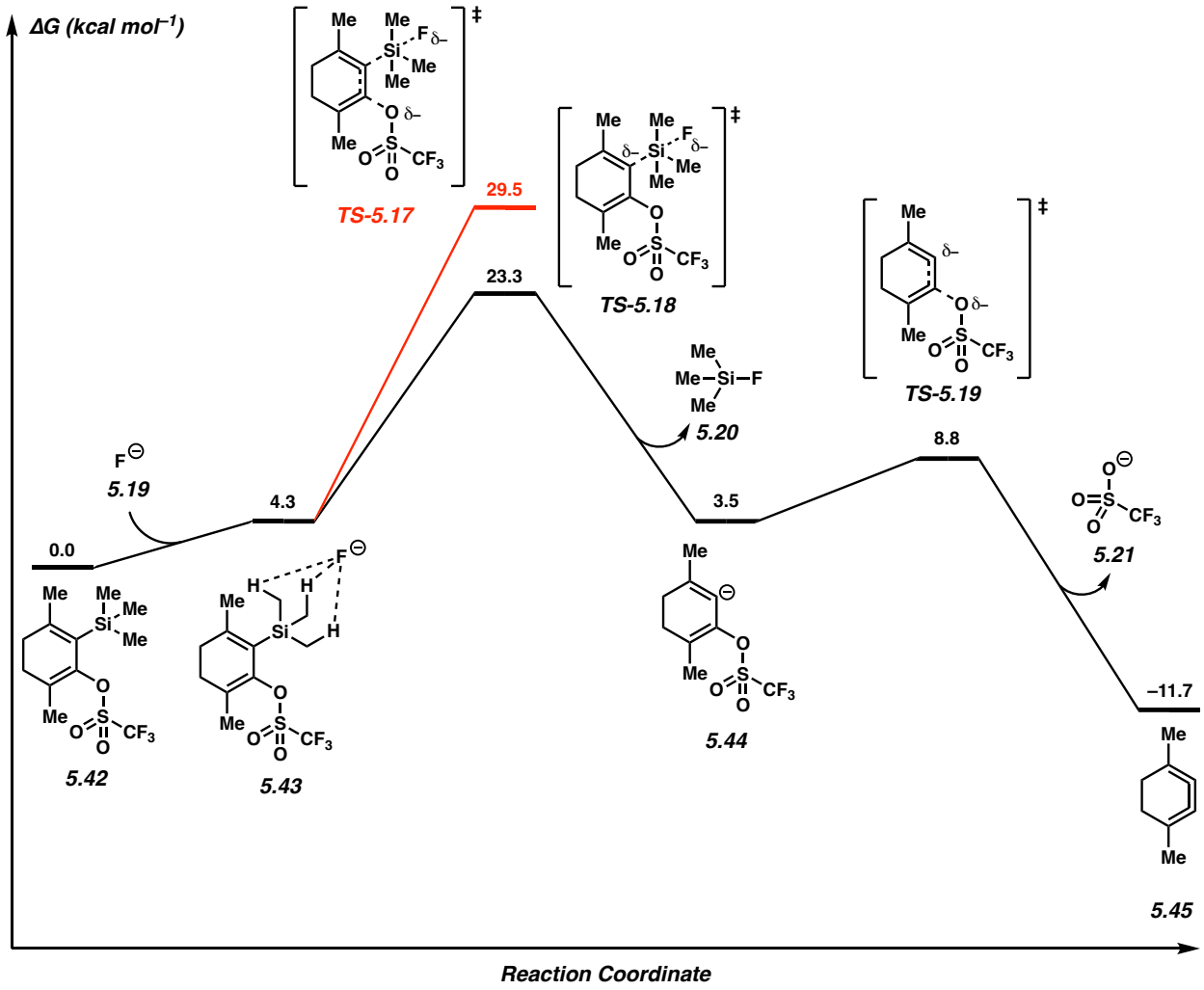

Figure 5.13. Calculated free energy profile for formation of 1,2,3-triene **5.45** from precursor **5.42** at the ωB97X-D/def2-QZVPP/SMD(MeCN)//ωB97X-D/6-31+G(d,p)/SMD(MeCN) level of theory.

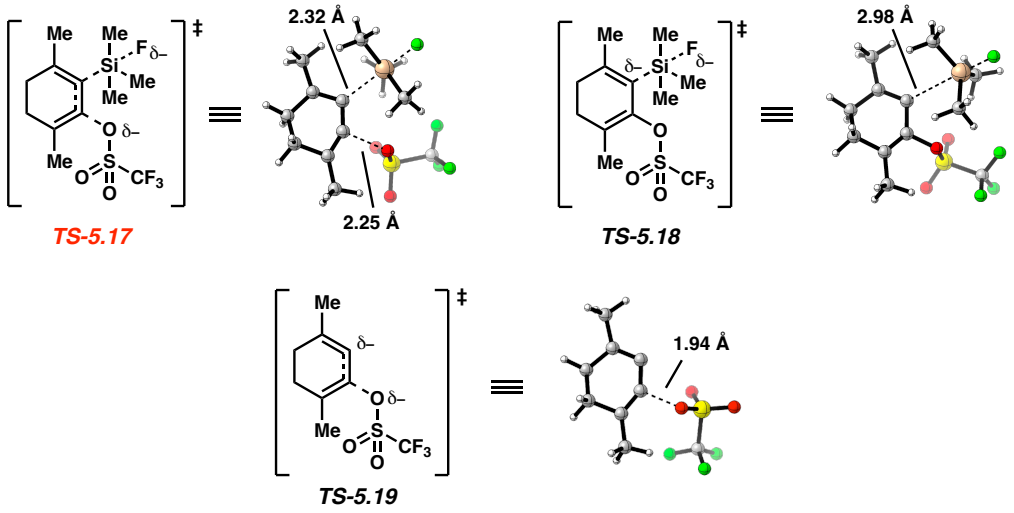

Figure 5.14. Geometries of **TS-5.17**–**TS-5.19** calculated at the ωB97X-D/def2-QZVPP/SMD(MeCN)//ωB97X-D/6-31+G(d,p)/SMD(MeCN) level of theory.

Table 5.7. Computed energies for the reaction of **5.42** to form 1,2,3-triene **5.45** at 23 °C (298.15 K) at the ωB97X-D/def2-QZVPP/SMD(MeCN)//ωB97X-D/6-31+G(d,p)/SMD(MeCN) level of theory. All units are in Hartrees. E = electronic energy; SPC = single-point correction; ZPE = zero-point energy; H = enthalpy; T = temperature; S = entropy; G(T) = Gibbs free energy; qh-S = quasi-harmonic corrected entropy; qh-G(T) = quasi-harmonic corrected Gibbs free energy.

Structure	E_SPC	E	ZPE	H_SPC	T.S	T.qh-S	G(T)_SPC	qh-G(T)_SPC
5.19	-100.004288	-99.966694	0	-100.001927	0.016519	0.016519	-100.018446	-100.018446
5.20	-509.251385	-509.121674	0.113649	-509.128828	0.041040	0.040990	-509.169480	-509.169818
5.21	-961.803851	-961.453330	0.027431	-961.768384	0.040379	0.039939	-961.808763	-961.808832
5.42	-1681.823397	-1681.290811	0.300422	-1681.498331	0.077314	0.073921	-1681.575645	-1681.575871
5.43	-1781.829274	-1781.257896	0.300538	-1781.501343	0.087597	0.081012	-1781.588940	-1781.587408
TS-5.17	-1781.789537	-1781.208963	0.298296	-1781.464608	0.082971	0.078215	-1781.547579	-1781.547302
TS-5.18	-1781.801429	-1781.220351	0.299619	-1781.475894	0.081717	0.077037	-1781.557611	-1781.557144
5.44	-1272.558204	-1272.103577	0.184014	-1272.357124	0.062240	0.059381	-1272.419364	-1272.418878
TS-5.19	-1272.547631	-1272.091138	0.182011	-1272.348495	0.062497	0.059608	-1272.410992	-1272.410537
5.45	-310.753654	-310.645175	0.152945	-310.590900	0.043116	0.042626	-310.634016	-310.634245

5.9.9 Reaction Energy Profile and Mechanism for Formation of 1,2,3-Triene 5.50

Figure 5.15 shows the corresponding reaction mechanism for the generation of azacyclic 1,2,3-triene **5.50** from precursor **5.46**.[34] Beginning with precursor **5.46**, fluoride (**5.19**) was found to form pre-complex **5.47**, which is slightly higher in energy ($\Delta G = 4.4$ kcal mol^{-1}). From **5.47**, attack of fluoride (**5.19**) via **TS-5.20** ($\Delta G^{\ddagger} = 8.4$ kcal mol^{-1}) leads to silicate **5.48**. Formation of anion **5.49** proceeds via **TS-5.21** ($\Delta G^{\ddagger} = 6.3$ kcal mol^{-1}). Finally, elimination of the triflate anion (**5.21**)

can occur via **TS-5.22** to form **5.50**, with an activation barrier ($\Delta G^{\ddagger}$) of 12.0 kcal mol^{-1}. The elimination of the triflate anion is the rate-determining step which is in contrast to the mechanisms for formations of 1,2,3-trienes **5.9** and **5.45**. The optimized geometries of **TS-5.20**, **TS-5.21**, and **TS-5.22** are shown in Figure 5.16. Notably, the generation of 1,2,3-triene **5.50** is thermodynamically favorable (ΔG = –8.8 kcal mol^{-1}). To explore the reaction pathways leading from **5.48** to **5.50**, we also evaluated a concerted, E2-like elimination. No transition state (e.g., **TS-5.23**) was located on the potential energy surface connecting **5.48** to **5.50**, suggesting that this step is not feasible. Furthermore, a geometry scan from **5.48** to **5.50** was performed to further support this conclusion.

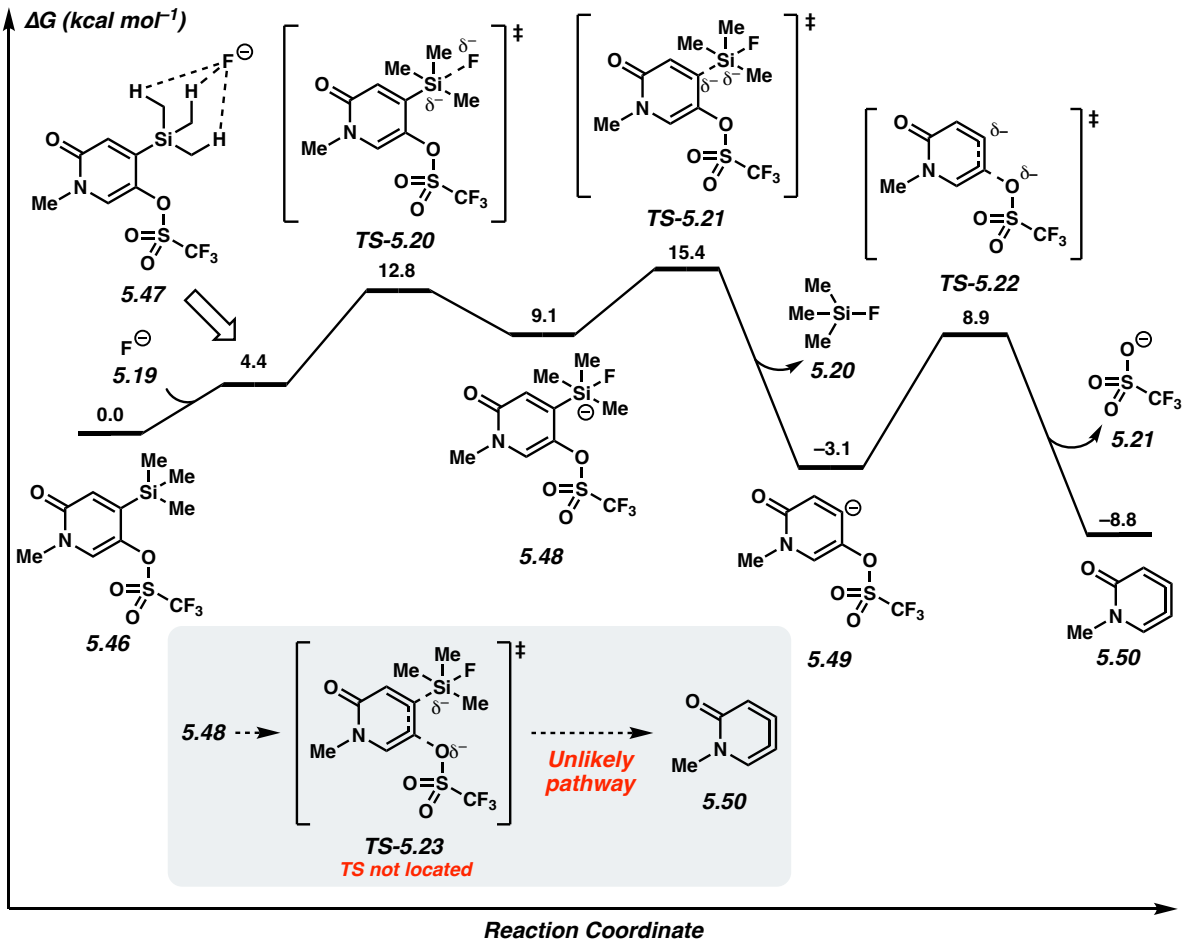

Figure 5.15. Calculated free energy profile for formation of azacyclic 1,2,3-triene **5.50** from precursor **5.46** at the ωB97X-D/def2-QZVPP/SMD(MeCN)//ωB97X-D/6-31+G(d,p)/SMD(MeCN) level of theory.

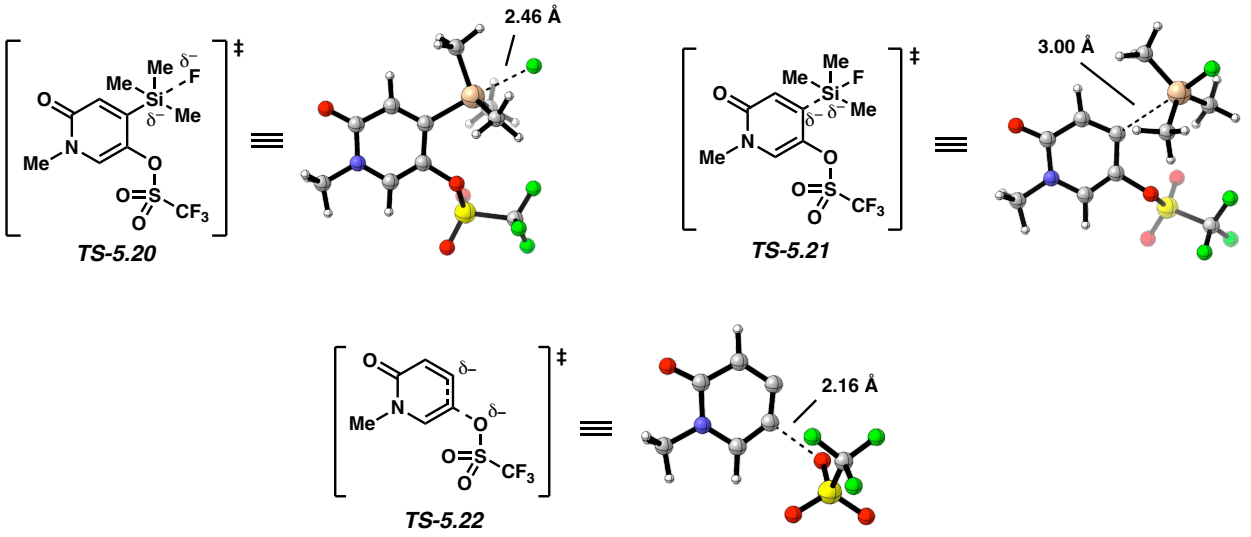

Figure 5.16. Geometries of **TS-5.20**–**TS-5.22** calculated at the ωB97X-D/def2-QZVPP/SMD(MeCN)//ωB97X-D/6-31+G(d,p)/SMD(MeCN) level of theory.

Table 5.8. Computed energies for the reaction of **5.46** to form 1,2,3-triene **5.50** at 23 °C (298.15 K) at the ωB97X-D/def2-QZVPP/SMD(MeCN)//ωB97X-D/6-31+G(d,p)/SMD(MeCN) level of theory. All units are in Hartrees. E = electronic energy; SPC = single-point correction; ZPE = zero-point energy; H = enthalpy; T = temperature; S = entropy; G(T) = Gibbs free energy; qh-S = quasi-harmonic corrected entropy; qh-G(T) = quasi-harmonic corrected Gibbs free energy.

Structure	E_SPC	E	ZPE	H_SPC	T.S	T.qh-S	G(T)_SPC	qh-G(T)_SPC
5.19	-100.004288	-99.966694	0	-100.001927	0.016519	0.016519	-100.018446	-100.018446
5.20	-509.251385	-509.121674	0.113649	-509.128828	0.041040	0.040990	-509.169480	-509.169818
5.21	-961.803851	-961.453330	0.027431	-961.768384	0.040379	0.039939	-961.808763	-961.808832
5.46	-1732.603634	-1732.042812	0.243413	-1732.336635	0.076341	0.072547	-1732.412976	-1732.413013
5.47	-1832.609745	-1832.010116	0.243525	-1832.340007	0.086257	0.079316	-1832.426264	-1832.424451
TS-5.20	-1832.601556	-1832.000017	0.244342	-1832.332612	0.078541	0.074586	-1832.411153	-1832.411131
5.48	-1832.608095	-1832.003443	0.244833	-1832.338510	0.078629	0.074615	-1832.417140	-1832.416947
TS-5.21	-1832.595224	-1831.986638	0.243057	-1832.327399	0.080784	0.075668	-1832.408183	-1832.407344
5.49	-1323.350342	-1322.867883	0.128088	-1323.206808	0.058820	0.056381	-1323.265627	-1323.26527
TS-5.22	-1323.327435	-1322.842532	0.125445	-1323.186067	0.061280	0.057925	-1323.247347	-1323.246464
5.50	-361.530260	-361.393761	0.097141	-361.425379	0.038495	0.038456	-361.463873	-361.464054

Figure 5.17 shows the corresponding reaction mechanism for the generation of azacyclic 1,2,3-triene **5.50** from precursor **5.51** (a constitutional isomer of precursor **5.46**).[34] Overall, the mechanism proceeds the same as what is described in Figure 5.15, albeit with the step with the largest $\Delta G^{\ddagger}$ being fluoride addition (i.e., **TS-5.24**) and not elimination of the triflate (i.e., **TS-5.26**). The optimized geometries of **TS-5.24**, **TS-5.25**, and **TS-5.26** are shown in Figure 5.18. Notably, the generation of 1,2,3-triene **5.50** is thermodynamically favorable (ΔG = –4.0 kcal mol^{-1}).

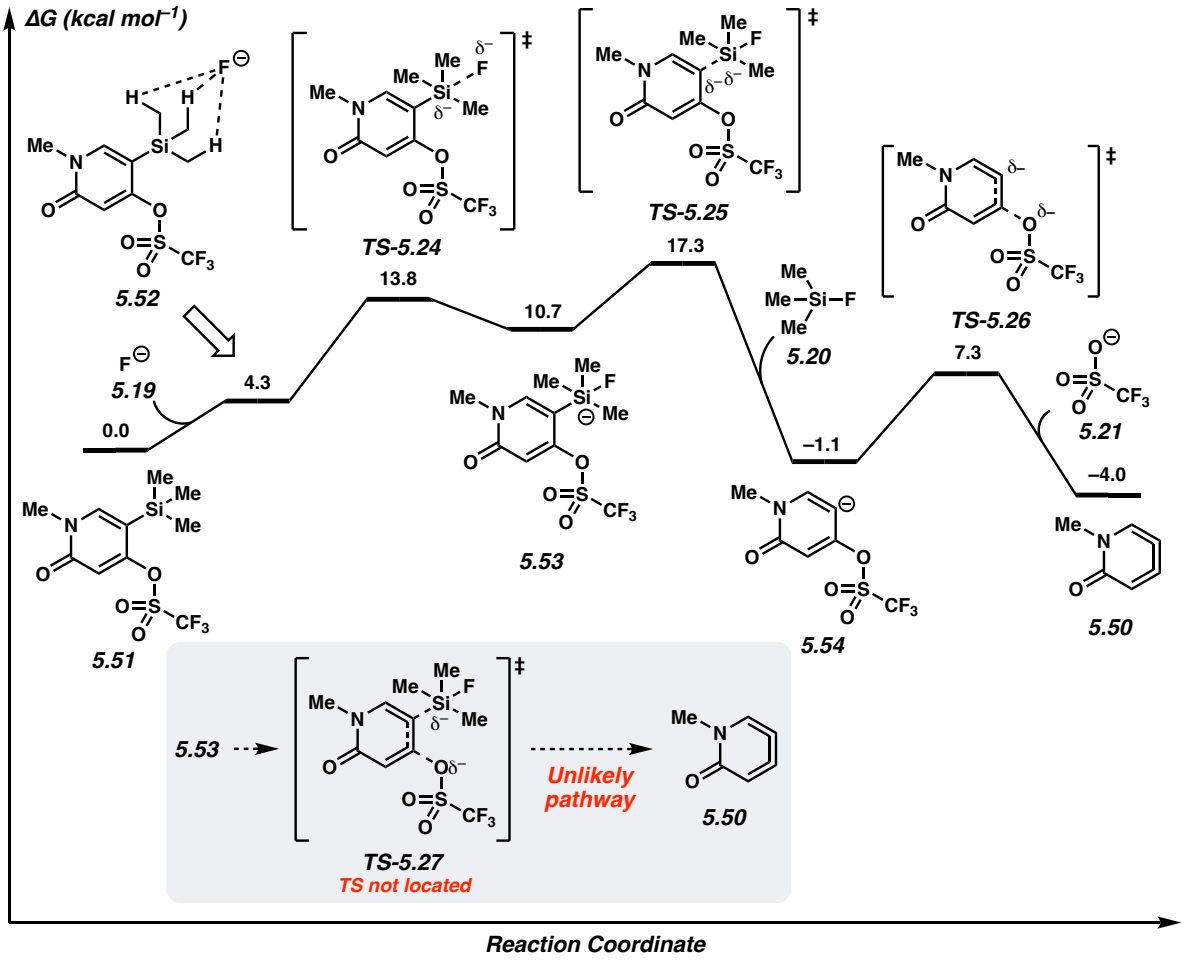

Figure 5.17. Calculated free energy profile for formation of azacyclic 1,2,3-triene **5.50** from precursor **5.51** at the ωB97X-D/def2-QZVPP/SMD(MeCN)//ωB97X-D/6-31+G(d,p)/SMD(MeCN) level of theory.

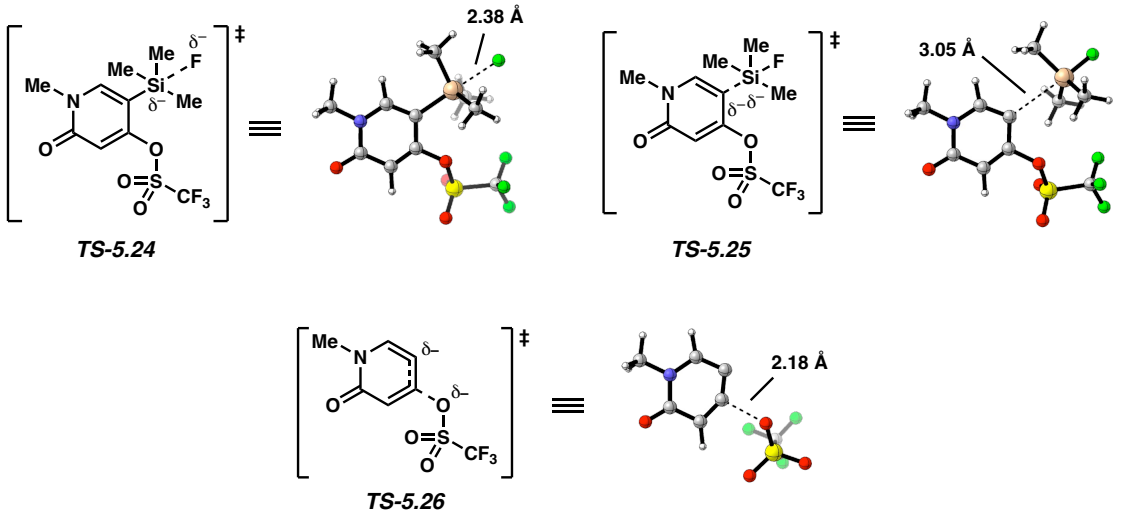

Figure 5.18. Geometries of **TS-5.24**–**TS-5.26** calculated at the ωB97X-D/def2-QZVPP/SMD(MeCN)//ωB97X-D/6-31+G(d,p)/SMD(MeCN) level of theory.

Table 5.9. Computed energies for the reaction of **5.51** to form 1,2,3-triene **5.50** at 23 °C (298.15 K) at the ωB97X-D/def2-QZVPP/SMD(MeCN)//ωB97X-D/6-31+G(d,p)/SMD(MeCN) level of theory. All units are in Hartrees. E = electronic energy; SPC = single-point correction; ZPE = zero-point energy; H = enthalpy; T = temperature; S = entropy; G(T) = Gibbs free energy; qh-S = quasi-harmonic corrected entropy; qh-G(T) = quasi-harmonic corrected Gibbs free energy.

Structure	E_SPC	E	ZPE	H_SPC	T.S	T.qh-S	G(T)_SPC	qh-G(T)_SPC
5.19	-100.004288	-99.966694	0	-100.001927	0.016519	0.016519	-100.018446	-100.018446
5.20	-509.251385	-509.121674	0.113649	-509.128828	0.04104	0.04099	-509.169480	-509.169818
5.21	-961.803851	-961.453330	0.027431	-961.768384	0.040379	0.039939	-961.808763	-961.808832
5.51	-1732.611203	-1732.049478	0.243419	-1732.344218	0.076400	0.072486	-1732.420618	-1732.420523
5.52	-1832.617415	-1832.01691	0.243671	-1832.34748	0.086624	0.079488	-1832.434104	-1832.432183
TS-5.24	-1832.60808	-1832.005500	0.244532	-1832.339144	0.077916	0.074055	-1832.417060	-1832.416943
5.53	-1832.612915	-1832.007855	0.244167	-1832.34454	0.077109	0.073490	-1832.421649	-1832.42175
TS-5.25	-1832.599710	-1831.990483	0.242775	-1832.332094	0.080163	0.075419	-1832.412257	-1832.411942
5.54	-1323.354309	-1322.871238	0.127994	-1323.210827	0.059292	0.056621	-1323.270119	-1323.26959
TS-5.26	-1323.337804	-1322.852755	0.125561	-1323.196467	0.060776	0.057548	-1323.257243	-1323.256428
5.50	-361.530260	-361.393761	0.097141	-361.425379	0.038495	0.038456	-361.463873	-361.464054

5.9.10 Reaction Energy Profile and Mechanism for Formation of Anti-Bredt Olefin 5.11

The reaction mechanism for the generation of ABO **5.11** from precursor **5.22** was studied computationally (see Figure 5.5).[29] The optimized geometries of **TS-5.8** and **TS-5.9** are shown in Figure 5.19. To explore the reaction pathways leading from **5.30** to **5.11**, we also evaluated a stepwise elimination. No transition state was located on the potential energy surface connecting **5.30** to alkyl anion **5.31**, suggesting that this step is not feasible. Finally, attempted optimization

of the ground state of anion **5.31** resulted in spontaneous elimination of the triflate anion.[74]

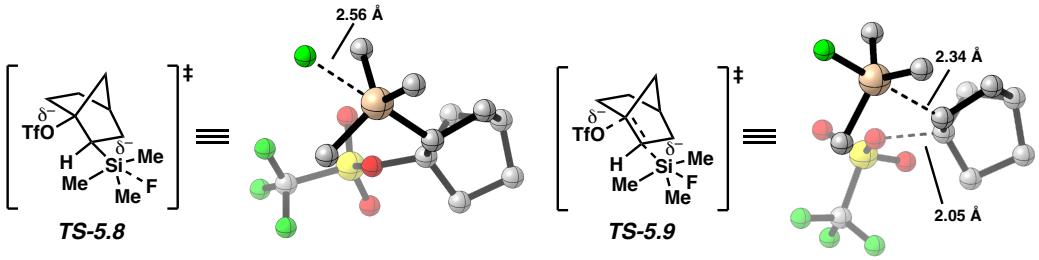

Figure 5.19. Geometries of **TS-5.8** and **TS-5.9** calculated at the ωB97X-D/def2-QZVPP/SMD(toluene)//ωB97X-D/6-31+G(d,p)/SMD(toluene) level of theory.

Table 5.10. Computed energies for the reaction of **5.22** to form ABO **5.11** at 23 °C (298.15 K) at the ωB97X-D/def2-QZVPP/SMD(toluene)//ωB97X-D/6-31+G(d,p)/SMD(toluene) level of theory. All units are in Hartrees. E = electronic energy; SPC = single-point correction; ZPE = zero-point energy; H = enthalpy; T = temperature; S = entropy; G(T) = Gibbs free energy; qh-S = quasi-harmonic corrected entropy; qh-G(T) = quasi-harmonic corrected Gibbs free energy.

Structure	E_SPC	E	ZPE	H_SPC	T.S	T.qh-S	G(T)_SPC	qh-G(T)_SPC
5.19	-99.946659	-99.910028	0	-99.944298	0.016519	0.016519	-99.960817	-99.960817
5.20	-509.249804	-509.119426	0.114199	-509.126325	0.039995	0.039941	-509.16632	-509.16666
5.21	-961.77215	-961.421632	0.027597	-961.736551	0.04019	0.039876	-961.776742	-961.776885
5.22	-1643.744124	-1643.225699	0.299995	-1643.422077	0.072261	0.0691	-1643.494337	-1643.494394
5.29	-1743.700063	-1743.141469	0.302203	-1743.374534	0.075059	0.071636	-1743.449593	-1743.449581
TS-5.8	-1743.697796	-1743.137605	0.301243	-1743.373758	0.073504	0.070431	-1743.447262	-1743.44746
5.30	-1743.709118	-1743.145307	0.300747	-1743.385167	0.074137	0.070984	-1743.459303	-1743.459522
TS-5.9	-1743.692732	-1743.125962	0.299019	-1743.370409	0.075154	0.07163	-1743.445563	-1743.445379
5.11	-272.688451	-272.59575	0.153012	-272.529153	0.03487	0.034876	-272.564023	-272.564054

5.9.11 Reaction Energy Profile and Mechanism for Formation of Anti-Bredt Olefin *epi*-5.11

Figure 5.20 shows the corresponding reaction mechanism for the formation of silicate ***epi*-5.30** from precursor ***epi*-5.22** (see Figure 5.6 for further discussion).[29] The optimized geometry of ***epi*-TS-5.8** is shown in Figure 5.21. To explore the possible reaction pathways leading from ***epi*-5.22** to ***epi*-11**, we evaluated both concerted and stepwise eliminations (Figure 5.22). No transition states were located on the potential energy surface connecting ***epi*-5.30** to alkyl anion ***epi*-5.31**, or directly to ***epi*-5.11** suggesting that this step is not feasible. Furthermore, geometry scans from ***epi*-**

5.30 to ***epi*-5.11** or **5.11** were performed to further support this conclusion. When ***epi*-5.11** was optimized with an unrestricted method, spontaneous isomerization to **5.11** occurred.

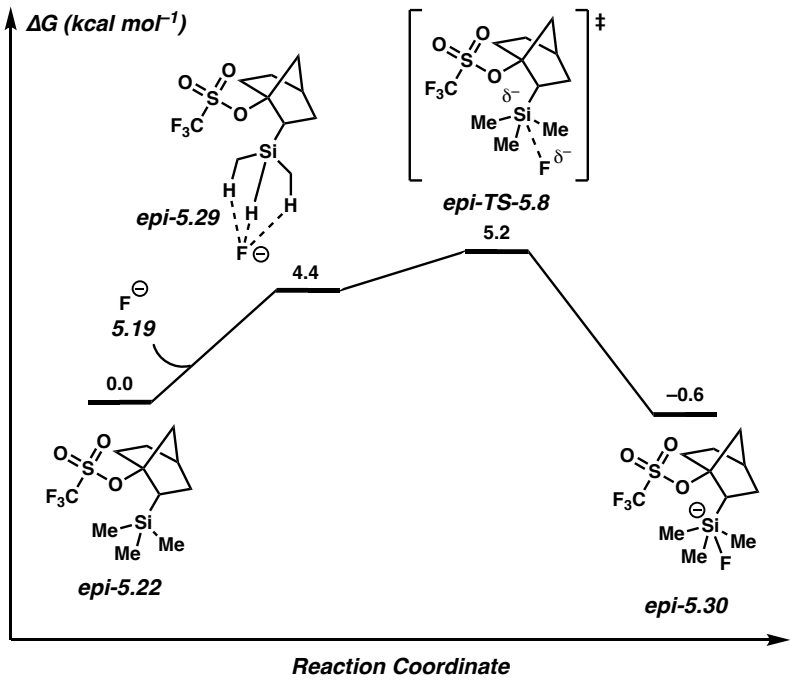

Figure 5.20. Calculated free energy profile for formation of silicate ***epi*-5.30** from precursor ***epi*-5.22** at the ωB97X-D/def2-QZVPP/SMD(toluene)//ωB97X-D/6-31+G(d,p)/SMD(toluene) level of theory.

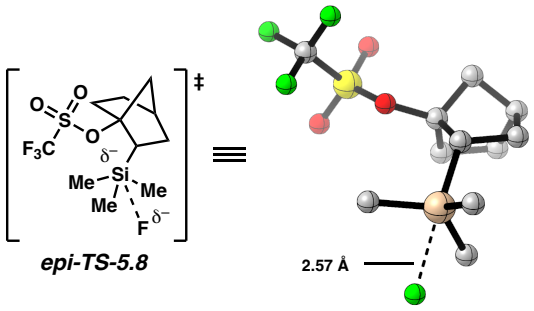

Figure 5.21. Geometry of ***epi*-TS-5.8** calculated at the ωB97X-D/def2-QZVPP/SMD(toluene)//ωB97X-D/6-31+G(d,p)/SMD(toluene) level of theory.

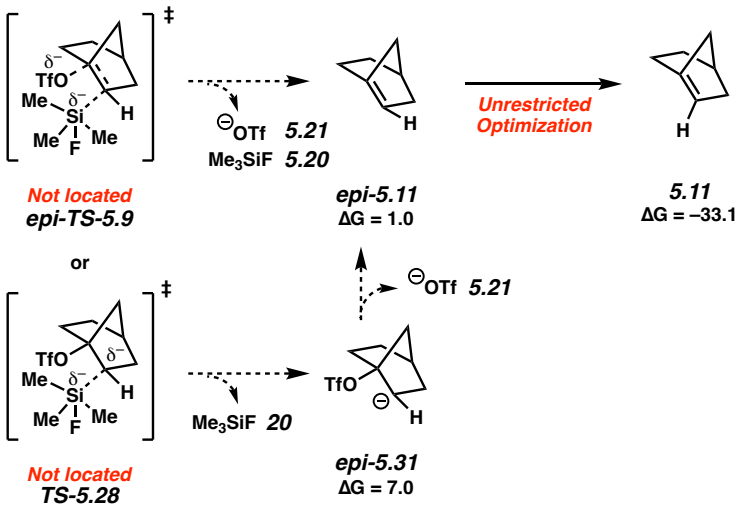

Figure 5.22. Unlocated transition states ***epi*-TS-5.9** and **TS-5.28**, anion ***epi*-5.31**, and ABO ***epi*-5.11** at the ωB97X-D/def2-QZVPP/SMD(toluene)//ωB97X-D/6-31+G(d,p)/SMD(toluene) level of theory.

Table 5.11. Computed energies for the investigation of the unobserved reaction of ***epi*-5.22** to form ABO ***epi*-5.11** at 23 °C (298.15 K) at the ωB97X-D/def2-QZVPP/SMD(toluene)//ωB97X-D/6-31+G(d,p)/SMD(toluene) level of theory. All units are in Hartrees. E = electronic energy; SPC = single-point correction; ZPE = zero-point energy; H = enthalpy; T = temperature; S = entropy; G(T) = Gibbs free energy; qh-S = quasi-harmonic corrected entropy; qh-G(T) = quasi-harmonic corrected Gibbs free energy.

Structure	E_SPC	E	ZPE	H_SPC	T.S	T.qh-S	G(T)_SPC	qh-G(T)_SPC
5.19	-99.946659	-99.910028	0	-99.944298	0.016519	0.016519	-99.960817	-99.960817
5.20	-509.249804	-509.119426	0.114199	-509.126325	0.039995	0.039941	-509.16632	-509.16666
5.21	-961.77215	-961.421632	0.027597	-961.736551	0.04019	0.039876	-961.776742	-961.776885
***epi*-5.22**	-1643.743538	-1643.224522	0.299848	-1643.421611	0.072953	0.069191	-1643.494564	-1643.494083
***epi*-5.29**	-1743.699881	-1743.14097	0.30296	-1743.373941	0.073738	0.070701	-1743.447679	-1743.447814
***epi*-TS-5.8**	-1743.697113	-1743.136566	0.301232	-1743.373167	0.073607	0.070251	-1743.446774	-1743.446578
***epi*-5.30**	-1743.707017	-1743.143156	0.301358	-1743.382818	0.072829	0.070073	-1743.455646	-1743.455934
***epi*-5.31**	-1234.418413	-1233.976449	0.182267	-1234.22183	0.055364	0.053507	-1234.277193	-1234.277064
***epi*-5.11**	-272.632474	-272.540246	0.15167	-272.474163	0.035523	0.03553	-272.509685	-272.509736

5.9.12 Effect of Dihedral Angle on Kobayashi Eliminations

Figure 5.23 shows the generalized reaction mechanism for the generation of ethylene (**5.34**) from precursor **5.32** (see Figure 5.7 for further discussion). Calculations were performed in MeCN as this is a common solvent for strained intermediate generation. Gas phases calculations were also attempted, and provided qualitatively similar results, although several transition states could not be located, possibly due to barrierless reaction in the gas phase.

In order to perform the calculations, optimization of the starting silyltriflate **5.32** and silicate **5.33** were performed using the optimization keyword opt=modredundant and dihedral constraints on the Si–C–C–O bond set to the given angle. In several cases, these structures featured imaginary frequencies corresponding to bond rotation along this angle due to adopting unfavorable conformations. Transition states **TS-5.10a-m** were then located by first scanning along the C–Si bond length of the constrained silicate to identify an energetic maximum, before elimination occurred, which was spontaneous after the bond was lengthened past the maximum. The maximum structure was then optimized with the optimization keywords opt=(ts,modredundant,calcfc,noeigen), with constraints placed upon the Si–C–C–O dihedral angle. The obtained transition states **TS-5.10a-m** featured a single imaginary frequency corresponding to elimination, and IRC calculations connected silicate **5.33** to ethylene **5.34** through the repsective transition state **TS-5.10**, although the dihedral constraints did not remain in the IRC. The optimized geometries of **TS-5.10a-m** are shown in Figure 5.24.

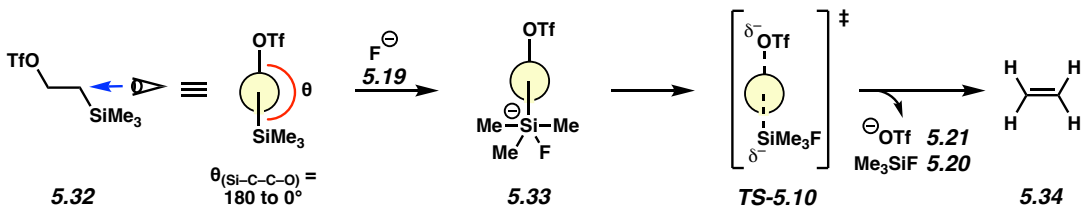

Figure 5.23. Calculated generalized pathway for formation of ethylene **5.34** from precursor **5.32** at the ωB97X-D/def2-QZVPP/SMD(MeCN)//ωB97X-D/6-31+G(d,p)/SMD(MeCN) level of theory.

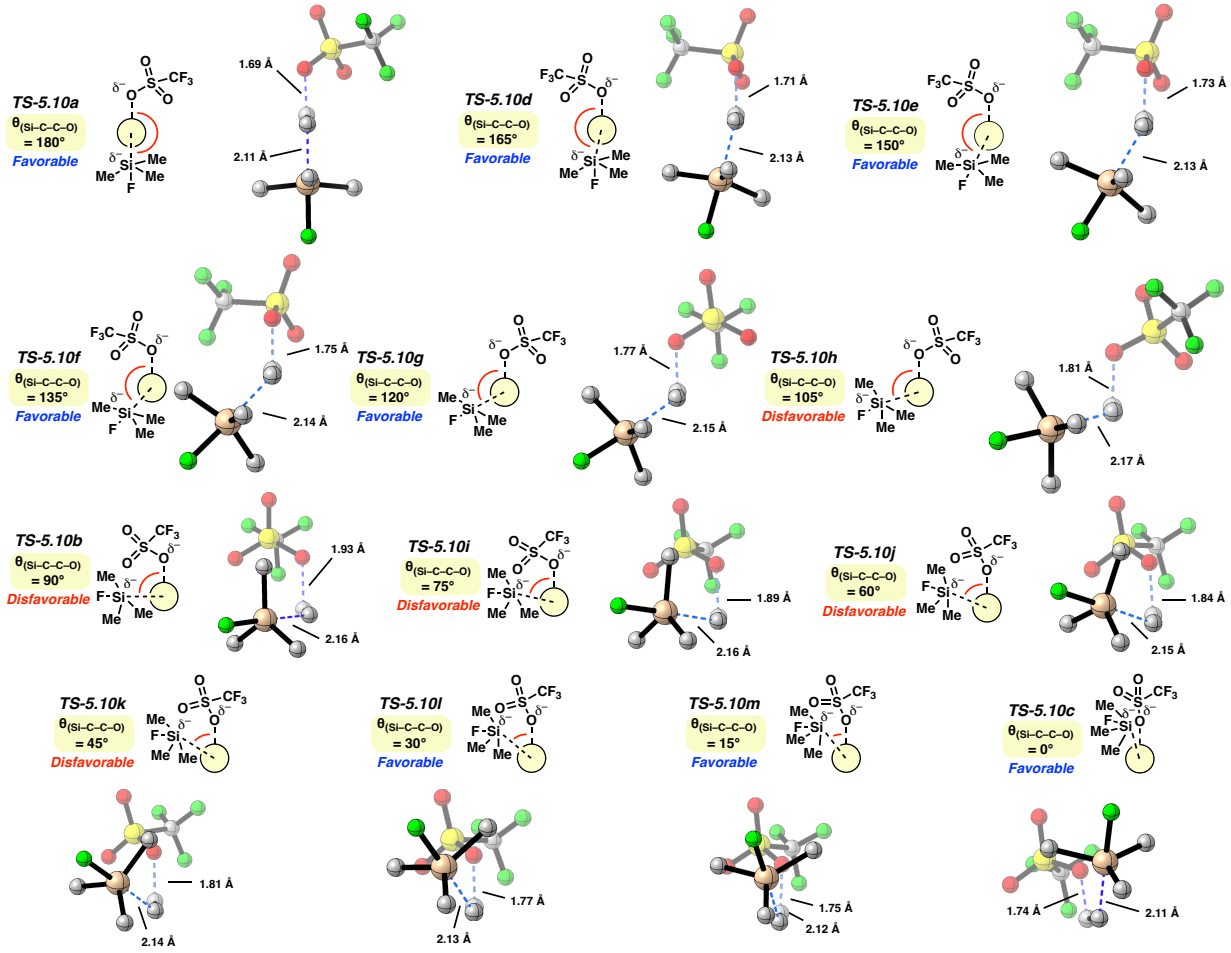

Figure 5.24. Geometry of **TS-5.10** at various dihedral angles calculated at the ωB97X-D/def2-QZVPP/SMD(MeCN)//ωB97X-D/6-31+G(d,p)/SMD(MeCN) level of theory.

Table 5.12. Computed energies for the elimination from **5.32** to form **5.34** (298.15 K) at the ωB97X-D/def2-QZVPP/SMD(MeCN)//ωB97X-D/6-31+G(d,p)/SMD(MeCN) level of theory. All units are in Hartrees. E = electronic energy; SPC = single-point correction; ZPE = zero-point energy; H = enthalpy; T = temperature; S = entropy; G(T) = Gibbs free energy; qh-S = quasi-harmonic corrected entropy; qh-G(T) = quasi-harmonic corrected Gibbs free energy.

Structure	E_SPC	E	ZPE	H_SPC	T.S	T.qh-S	G(T)_SPC	qh-G(T)_SPC
5.19	-100.004288	-99.966694	0	-100.001927	0.016519	0.016519	-100.018446	-100.018446
5.32a (180°)	-1449.575749	-1449.118477	0.197621	-1449.358936	0.068097	0.0642	-1449.427033	-1449.426069
5.33a (180°)	-1549.574495	-1549.073732	0.197659	-1549.355929	0.07191	0.067531	-1549.427839	-1549.426982
TS-5.10a	-1549.574673	-1549.072843	0.196749	-1549.357456	0.071119	0.066664	-1549.428575	-1549.427624
5.32d (165°)	-1449.575053	-1449.11781	0.197369	-1449.358345	0.068938	0.064659	-1449.427283	-1449.426093
5.33d (165°)	-1549.573962	-1549.073438	0.197819	-1549.355293	0.07228	0.067666	-1549.427573	-1549.426452
TS-5.10d	-1549.573648	-1549.071964	0.196728	-1549.356507	0.070513	0.066465	-1549.42702	-1549.426314
5.32e (150°)	-1449.573181	-1449.11594	0.197443	-1449.356457	0.068298	0.0644	-1449.424755	-1449.423843
5.33e (150°)	-1549.572094	-1549.071483	0.197833	-1549.35343	0.072319	0.067679	-1549.425749	-1549.424565
TS-5.10e	-1549.571117	-1549.069401	0.196777	-1549.353971	0.070262	0.066293	-1549.424233	-1549.423582
5.32f (135°)	-1449.57088	-1449.113607	0.197359	-1449.355125	0.065066	0.062109	-1449.420191	-1449.41977
5.33f (135°)	-1549.569522	-1549.068814	0.197861	-1549.350823	0.072161	0.067397	-1549.422984	-1549.421785
TS-5.10f	-1549.566978	-1549.065078	0.196414	-1549.35009	0.070895	0.066637	-1549.420985	-1549.420104
5.32g (120°)	-1449.569462	-1449.112165	0.197179	-1449.353793	0.065738	0.062543	-1449.419531	-1449.418939
5.33g (120°)	-1549.567071	-1549.066777	0.198057	-1549.349202	0.067404	0.064651	-1549.416607	-1549.416669
TS-5.10g	-1549.562353	-1549.060233	0.196456	-1549.345444	0.070411	0.066429	-1549.415855	-1549.41529
5.32h (105°)	-1449.573771	-1449.116617	0.197147	-1449.358902	0.064009	0.061076	-1449.422912	-1449.42238
5.33h (105°)	-1549.565597	-1549.065224	0.198141	-1549.347623	0.068307	0.065076	-1549.41593	-1549.415566
TS-5.10h	-1549.555209	-1549.053242	0.196141	-1549.338528	0.071156	0.066713	-1549.409683	-1549.408698
5.32b (90°)	-1449.572025	-1449.114603	0.197623	-1449.356263	0.064007	0.061362	-1449.42027	-1449.42004
5.33b (90°)	-1549.566615	-1549.066395	0.198085	-1549.348657	0.068206	0.064962	-1549.416862	-1549.416633
TS-5.10b	-1549.548905	-1549.04625	0.194971	-1549.333232	0.070859	0.066718	-1549.404091	-1549.403458
5.32i (75°)	-1449.573557	-1449.116163	0.197938	-1449.356703	0.066641	0.063136	-1449.423344	-1449.422619
5.33i (75°)	-1549.567907	-1549.067723	0.198767	-1549.348784	0.06902	0.065683	-1549.417805	-1549.417581
TS-5.10i	-1549.554932	-1549.052689	0.195781	-1549.338668	0.069934	0.066115	-1549.408603	-1549.40819
5.32j (60°)	-1449.573905	-1449.116854	0.197776	-1449.357118	0.067582	0.063687	-1449.4247	-1449.423605
5.33j (60°)	-1549.567915	-1549.067736	0.198565	-1549.348743	0.070482	0.066507	-1549.419225	-1549.418754
TS-5.10j	-1549.55932	-1549.05701	0.196124	-1549.342732	0.07039	0.066274	-1549.413122	-1549.412458
5.32k (45°)	-1449.573136	-1449.1163	0.197303	-1449.356526	0.068793	0.064568	-1449.425319	-1449.424138
5.33k (45°)	-1549.568088	-1549.067962	0.198628	-1549.348913	0.070487	0.066438	-1549.419401	-1549.418657
TS-5.10k	-1549.060465	-1549.060465	0.19634	-1548.843713	0.070785	0.066473	-1548.914497	-1549.415466
5.32l (30°)	-1449.571387	-1449.114534	0.197363	-1449.355558	0.06735	0.063242	-1449.422907	-1449.421485
5.33l (30°)	-1549.567885	-1549.067757	0.198591	-1549.34884	0.069038	0.065797	-1549.417878	-1549.417789
TS-5.10l	-1549.564534	-1549.06286	0.19672	-1549.347481	0.069753	0.065855	-1549.417234	-1549.416621
5.32m (15°)	-1449.569724	-1449.112826	0.197433	-1449.353806	0.066059	0.062552	-1449.419865	-1449.419131
5.33m (15°)	-1549.567284	-1549.067037	0.198576	-1549.349135	0.066847	0.064022	-1549.415982	-1549.415806
TS-5.10m	-1549.565242	-1549.063803	0.196969	-1549.348014	0.069243	0.065534	-1549.417257	-1549.416826
5.32c (0°)	-1449.569215	-1449.112286	0.197571	-1449.353247	0.065288	0.062087	-1449.418535	-1449.418083
5.33c (0°)	-1549.566982	-1549.066697	0.19866	-1549.348776	0.066563	0.063916	-1549.415338	-1549.415297
TS-5.10c	-1549.565406	-1549.06394	0.197153	-1549.348057	0.069515	0.065626	-1549.417571	-1549.416816

5.9.13 Cartesian Coordinates of Optimized Geometries

Cartesian coordinates for the optimized structures will be reported in the literature.[91]

5.10 Notes and References

(1) Wenk, H. H.; Winkler, M.; Sander, W. One century of aryne chemistry. *Angew. Chem., Int. Ed.* **2003**, *42*, 502–528.

(2) Shi, J.; Li, L.; Li, Y. *o*-Silylaryl triflates: A journey of Kobayashi aryne precursors. *Chem. Rev.* **2021**, *121*, 3892–4044.

(3) Anthony, S. M.; Wonilowicz, L. G.; McVeigh, M. S.; Garg, N. K. Leveraging fleeting strained intermediates to access complex scaffolds. *JACS Au* **2021**, *1*, 897–912.

(4) McDermott, L.; Walters, Z. G.; Clark, A. M.; Garg, N. K. Geometric distortion as an enabling tool for organic synthesis. *Nat. Synth.* **2025**, *4*, 421–431.

(5) Tadross, P. M.; Stoltz, B. M. A comprehensive history of arynes in natural product total synthesis. *Chem. Rev.* **2012**, *112*, 3550−3577.

(6) Gampe, C. M.; Carreira, E. M. Arynes and cyclohexyne in natural product synthesis. *Angew. Chem., Int. Ed.* **2012**, *51*, 3766–3778.

(7) Dubrovskiy, A. V.; Markina, N. A.; Larock, R. C. Use of benzynes for the synthesis of heterocycles. *Org. Biomol. Chem.* **2013**, *11*, 191–218.

(8) Goetz, A. E.; Shah, T. K.; Garg, N. K. Pyridynes and indolynes as building blocks for functionalized heterocycles and natural products. *Chem. Commun.* **2015**, *51*, 34–45.

(9) Coe, J. W.; Brooks, P. R.; Wirtz, M. C.; Bashore, C. G.; Bianco, K. E.; Vetelino, M. G.; Arnold, E. P.; Lebel, L. A.; Fox, C. B.; Tingley, F. D.; Schulz, D. W.; Davis, T. I.; Sands, S. B.; Mansbach, R. S.; Rollema, H.; O'Neill, B. T. 3,5-Bicyclic aryl piperidines: A novel class of α4β2 neuronal nicotinic receptor partial agonists for smoking cessation. *Bioorg. Med. Chem. Lett.* **2005**, *15*, 4889–4897.

(10) Mauger, C. C.; Mignani, G. A. An efficient and safe procedure for the large-scale Pd-catalyzed hydrazonation of aromatic chlorides using Buchwald technology. *Org. Process Res. Dev.* **2004**, *8*, 1065–1071.

(11) Chari, J. V.; Spence, K. A.; Susick, R. B.; Garg, N. K. A platform for on-the-complex annulation reactions with transient aryne intermediates. *Nat. Commun.* **2021**, *12*, 3706–3715.

(12) Wang, Z.-Y.; Xu, Y.-Z.; Cui, Z.; Zhang, L.; Lu, J.-Y.; Zheng, Y.-Q.; Zhu, R. Chain-growth synthesis of extensively cross-conjugated polyenes. *Nat. Synth.* **2025**, DOI: 10.1038/s44160-025-00760-4.

(13) Schleth, F.; Vettiger, T.; Rommel, M.; Tobler, H. Process for the preparation of pyrazole carboxylic acid amides. International patent WO 2011131544 A1, Oct 27, 2011.

(14) Westphal, M. V.; Hudson, L.; Mason, J. W.; Pradeilles, J. A.; Zécri, F. J.; Briner, K.; Schreiber, S. L. Water-compatible cycloadditions of oligonucleotide-conjugated strained allenes for DNA-encoded library synthesis. *J. Am. Chem. Soc.* **2020**, *142*, 7776–7782.

(15) Svatunek, D.; Wilkovitsch, M.; Hartmann, L.; Houk, K. N.; Mikula, H. Uncovering the key role of distortion in bioorthogonal tetrazine tools that defy the reactivity/stability trade-off. *J. Am. Chem. Soc.* **2022**, *144*, 8171–8177.

(16) Himeshima, Y.; Sonoda, T.; Kobayashi, H. Fluoride-induced 1,2-elimination of o-trimethylsilylphenyl triflate to benzyne under mild conditions. *Chem. Lett.* **1983**, *12*, 1211–1214.

(17) Goetz, A. E.; Garg, N. K.; Enabling the use of heterocyclic arynes in chemical synthesis. *J. Org. Chem.* **2014**, *79*, 846–851.

(18) Nakamura, Y.; Yoshida, S.; Hosya, T. Recent advances in synthetic hetaryne chemistry. *Heterocycles* **2019**, *98*, 1623–1677.

(19) Atanes, N.; Escudero, S.; Pérez, D.; Guitián, E.; Castedo, L. Generation of cyclohexyne and its Diels-Alder reaction with α-pyrones. *Tetrahedron Lett.* **1998**, *39*, 3039–3040.

(20) Tlais, S. F.; Danheiser, R. L. *N*-Tosyl-3-azacyclohexyne. Synthesis and chemistry of a strained cyclic ynamide. *J. Am. Chem. Soc.* **2014**, *136*, 15489−15492.

(21) Medina, J. M.; McMahon, T. C.; Jimeńez-Oseś, G.; Houk, K. N.; Garg, N. K. Cycloadditions of cyclohexynes and cyclopentyne. *J. Am. Chem. Soc.* **2014**, *136*, 14706−14709.

(22) Quintana, I.; Peña, D.; Pérez, D.; Guitián, E. Generation and reactivity of 1,2-cyclohexadiene under mild reaction conditions. *Eur. J. Org. Chem.* **2009**, *2009*, 5519–5524.

(23) Shakespeare, W. C.; Johnson, R. P. 1,2,3-Cyclohexatriene and cyclohexen-3-yne: Two new highly strained C_6H_6 isomers. *J. Am. Chem. Soc.* **1990**, *112*, 8578–8579.

(24) Kelleghan, A. V.; Bulger, A. S.; Witkowski, D. C.; Garg, N. K. Strain-promoted reactions of 1,2,3-cyclohexatriene and its derivatives. *Nature* **2023**, *618*, 748–754.

(25) Lofstrand, V. A.; West, F. G. Efficient trapping of 1,2-cyclohexadienes with 1,3-dipoles. *Chem. Eur. J.* **2016**, *22*, 10763–10767.

(26) Almehmadi, Y. A.; West, F. G. A mild method for the generation and interception of 1,2-cycloheptadienes with 1,3-dipoles. *Org. Lett.* **2020**, *22*, 6091–6095.

(27) Barber, J. S.; Yamano, M. M.; Ramirez, M.; Darzi, E. R.; Knapp, R. R.; Liu, F.; Houk, K. N.; Garg, N. K. Diels–Alder cycloadditions of strained azacyclic allenes. *Nat. Chem.* **2018**, *10*, 953–960.

(28) Jankovic, C. L.; McIntosh, K. C.; Lofstrand, V. A.; West, G. F. Stereoselective intramolecular [2+2] trapping of 1,2-cyclohexadienes: a Route to rigid, angularly fused tricyclic scaffolds. *Chem. Eur. J.* **2023**, *29*, e202301668.

(29) McDermott, L.; Walters, Z. G.; French, S. A.; Clark, A. M.; Ding, J.; Kelleghan, A. V.; Houk, K. N.; Garg, N. K. A solution to the anti-Bredt olefin synthesis problem. *Science* **2024**, *386*, eadq3519.

(30) On the basis of a SciFinder structure search; see Section 5.9.1 for details; Scifinder-n; Chemical Abstracts Service: Columbus, OH; https://scifinder-n.cas.org (accessed May 7, 2025).

(31) Anthony, S. M.; Tona, V.; Zou, Y.; Morrill, L. A.; Billingsley, J. M.; Lim, M.; Tang, Y.; Houk, K. N.; Garg, N. K. Total synthesis of (−)-strictosidine and interception of aryne natural product derivatives "strictosidyne" and "strictosamidyne." *J. Am. Chem. Soc.* **2021**, *143*, 7471–7479.

(32) Shah, T. K.; Medina, J. M.; Garg, N. K. Expanding the strained alkyne toolbox: Generation and utility of oxygen-containing strained alkynes. *J. Am. Chem. Soc.* **2016**, *138*, 4948–4954.

(33) Kelleghan, A. V.; Tena Meza, A.; Garg, N. K. Generation and reactivity of unsymmetrical strained heterocyclic allenes. *Nat. Synth.* **2024**, *3*, 329–336.

(34) Witkowski, D. C.; Turner, D. W.; Bulger, A. S.; Houk, K. N.; Garg, N. K. Synthesis and reactivity of nitrogen-containing strained cyclic 1,2,3-trienes. *Nat. Synth.* **2025**, DOI: 10.1038/s44160-025-00793-9.

(35) Kelleghan, A. V.; Busacca, C. A.; Sarvestani, M.; Volchkov, I.; Medina, J. M.; Garg, N. K. Safety assessment of benzyne generation from a silyl triflate precursor. *Org. Lett.* **2020**, *22*, 1665–1669.

(36) Dhokale, R. A.; Mhaske, S. B. Transition-metal-catalyzed reactions involving arynes. *Synthesis* **2018**, *50*, 1–16.

(37) Spence, K. A.; Meza, A. T.; Garg, N. K. Merging Metals and Strained Intermediates. *Chem Catalysis* **2022**, *2*, 1870–1879.

(38) Tena Meza, A.; Rivera, C. A.; Shao, H.; Kelleghan, A. V.; Houk, K. N.; Garg, N. K. σ-Bond insertion reactions of two strained diradicaloids. *Nature* **2025**, *640*, 683–690.

(39) Medina, J. M.; Mackey, J. L.; Garg, N. K.; Houk, K. N. The role of aryne distortions, steric effects, and charges in regioselectivities of aryne reactions. *J. Am. Chem. Soc.* **2014**, *136*, 15798–15805.

(40) Cheong, P. H.-Y.; Paton, R. S.; Bronner, S. M.; Im, G.-Y. J.; Garg, N. K.; Houk, K. N. Indolyne and aryne distortions and nucleophilic regioselectivities. *J. Am. Chem. Soc.* **2010**, *132*, 1267–1269.

(41) Im, G.-Y. J.; Bronner, S. M.; Goetz, A. E.; Paton, R. S.; Cheong, P. H.-Y.; Houk, K. N.; Garg, N. K. Indolyne experimental and computational studies: Synthetic applications and origins of selectivities of nucleophilic additions. *J. Am. Chem. Soc.* **2010**, *132*, 17933–17944.

(42) Liebman, J. F.; Greenberg, A. A survey of strained organic molecules. *Chem. Rev.* **1976**, *76*, 311–365.

(43) Novak, I. Molecular modeling of anti-Bredt compounds. *J. Chem. Inf. Model.* **2005**, *45*, 334–338.

(44) Daoust, K. J.; Hernandez, S. M.; Konrad, K. M.; Mackie, I. D.; Winstanley, J.; Johnson, R. P. Strain estimates for small-ring cyclic allenes and butatrienes. *J. Org. Chem.* **2006**, *71*, 5708–5714.

(45) Johnson, R. P.; Daoust, K. J. Interconversions of cyclobutyne, cyclopentyne, cyclohexyne, and their corresponding cycloalkylidenecarbenes. *J. Am. Chem. Soc.* **1995**, *117*, 362–367.

(46) Goetz, A. E.; Bronner, S. M.; Cisneros, J. D.; Melamed, J. M.; Paton, R. S.; Houk, K. N.; Garg, N. K. An efficient computational model to predict the synthetic utility of heterocyclic arynes. *Angew. Chem., Int. Ed.* **2012**, *51*, 2758–2762.

(47) Yamano, M. M.; Kelleghan, A. V.; Shao, Q.; Giroud, M.; Simmons, B. J.; Li, B.; Chen, S.; Houk, K. N.; Garg, N. K. Intercepting fleeting cyclic allenes with asymmetric nickel catalysis. *Nature* **2020**, *586*, 242–247.

(48) Xu, Q.; Hoye, T. R. A distinct mode of strain-driven cyclic allene reactivity: Group migration to the central allene carbon atom. *J. Am. Chem. Soc.* **2023**, *145*, 9867–9875.

(49) Goetz, A. E.; Garg, N. K. Regioselective reactions of 3,4-pyridynes enabled by the aryne distortion model. *Nat. Chem.* **2013**, *5*, 54–60.

(50) McMahon, T. C.; Medina, J. M.; Yang, Y.-F.; Simmons, B. J.; Houk, K. N.; Garg, N. K. Generation and regioselective trapping of a 3,4-piperidyne for the synthesis of functionalized heterocycles. *J. Am. Chem. Soc.* **2015**, *137*, 4082–4085.

(51) Ramirez, M.; Svatunek, D.; Liu, F.; Garg, N. K.; Houk, K. N. Origins of *endo* selectivity in Diels–Alder reactions of cyclic allene dienophiles. *Angew. Chem., Int. Ed.* **2021**, *60*, 14989–14997.

(52) Viesser, R. V.; Donald, C. P.; May, J. A.; Wu, J. I. Can twisted double bonds facilitate stepwise [2 + 2] cycloadditions? *Org. Lett.* **2024**, *26*, 3778-3783.

(53) Picazo, E.; Anthony, S. M.; Giroud, M.; Simon, A.; Miller, M. A.; Houk, K. N.; Garg, N. K. Arynes and cyclic alkynes as synthetic building blocks for stereodefined quaternary centers. *J. Am. Chem. Soc.* **2018**, *140*, 7605–7610.

(54) Liu, S.; Li, Y.; Lan, Y. Mechanistic study of the fluoride-induced activation of a Kobayashi precursor: Pseudo-S_N2 pathway via a pentacoordinated silicon ate complex. *Eur. J. Org. Chem.* **2017**, *2017*, 6349–6353.

(55) Bhattacharjee, S.; Deswal, S.; Manoj, N.; Jindal, G.; Biju, A. T. Aryne three-component coupling involving CS_2 for the synthesis of *S*-aryl dithiocarbamates. *Org. Lett.* **2021**, *23*, 9083–9088.

(56) A study of the mechanism for Kobayashi eliminations to form cyclic allenes will be reported elsewhere, as the systems are sufficiently complex to warrant independent investigation using experimental and computational techniques.

(57) Scardiglia, F.; Roberts, J. D. Evidence for cyclohexyne as an intermediate in the coupling of phenyllithium with 1-chlorocyclohexene. *Tetrahedron* **1957**, *1*, 343–344.

(58) Wittig, G.; Fritze, P. On the intermediate occurrence of 1,2-cyclohexadiene. *Angew. Chem., Int. Ed.* **1966**, *5*, 846.

(59) Keese, R.; Krebs, E.-P. Concerning the existence of 1-norbornene. *Angew. Chem., Int. Ed. Engl.* **1971**, *10*, 262–263.

(60) For computational ease and to allow for comparisons, calculations were performed using trimethylsilyltriflate substrates. In practice, different silicon substituents and different sulfonates are commonly used in Kobayashi eliminations.

(61) Smith, O.; Hindson, M. J.; Sreenithya, A.; Tataru, V.; Paton, R. S.; Burton, J. W.; Smith, M. D. Harnessing triaryloxonium ions for aryne generation. *Nat. Synth.* **2024**, *3*, 58–66.

(62) As strained intermediate generation from Kobayashi precursors has been achieved using a variety of fluoride counterions (e.g., Cs^+, K^+, and NBu_4^+), the role of the counterion was omitted from our studies. Additionally, the role of cations is further complicated by the possibility of cation exchange in many reactions, as well as possible solvent-cation interactions.

(63) Prior computational studies done at the B3LYP/6-31G(d)/SMD(MeCN) level of theory by Li and Lan report that the elimination to give **5.3** is favorable by –31.4 kcal mol^{-1} (see ref 54). A more recent study by Jindal and Biju performed using M06-2X-D3/def2-TZVPP/SMD(THF)//M06-2X-D3/6-31G(d,p) gave the corresponding ΔG of –16.2 kcal mol^{-1} (see ref 55).

(64) Balaraman, K.; Wolf, C. Chemodivergent Csp^3–F bond functionalization and cross-electrophile alkyl-alkyl coupling with alkyl fluorides. *Science Advances* **2022**, *8*, eabn7819.

(65) We have verified the formation of $SiMe_3F$ by ^1H and ^{19}F NMR spectroscopy; see Section 5.9.5 for details.

(66) Yoshioka, E.; Kakigi, K.; Miyoshi, S.; Kawasaki, Y.; Miyabe, H. Aryne precursors for selective generation of 3-haloarynes: Preparation and application to synthetic reactions. *J. Org. Chem.* **2020**, *85*, 13544–13556.

(67) Hall, C.; Henderson, J. L.; Ernouf, G.; Greaney, M. F. Tandem thia-Fries rearrangement – cyclisation of 2-(trimethylsilyl)phenyl trifluoromethanesulfonate benzyne precursors. *Chem. Commun.* **2013**, *49*, 7602–7604.

(68) Rasheed, O. K.; Hardcastle, I. R.; Raftery, J.; Quayle, P. Aryne generation *vs*. Truce–Smiles and Fries rearrangements during the Kobayashi fragmentation reaction: A new bi-aryl synthesis. *Org. Biomol. Chem.* **2015**, *13*, 8048–8052.

(69) Medina, J. M.; Jackl, M. K.; Susick, R. B. Garg, N. K. Synthetic studies pertaining to the 2,3-pyridyne and 4,5-pyrimidyne. *Tetrahedron* **2016**, *72*, 3629–3634.

(70) Charmant, J. P. H.; Dyke, A. M.; Lloyd-Jones, G. C. The anionic thia-Fries rearrangement of aryl triflates. *Chem. Commun.* **2003**, 380–381.

(71) In cases where the thia-Fries rearrangement is observed, we suspect there are subtle structural factors that stabilize the aryl anion and/or destabilize the elimination pathway.

(72) When reacted under highly protic conditions (*t*-BuOH (50 equiv), CsF (5.0 equiv), MeCN, 40°C), 2,3-naphthalyne precursor (2-(trimethylsilyl)-3-naphthyl trifluoromethanesulfonate) undergoes protodesilylation, along with presumed aryne generation and other undesired pathways, resulting in the formation of 2-naphthyl trifluoromethanesulfonate (see Section 5.9.5).

(73) We also considered direct E2-like elimination of the silicate intermediate in both cases but were unable to locate transition states for those possible pathways. However, in our

computational studies of a substituted cyclic 1,2,3-triene and its Kobayashi precursor (see Section 5.9.8), the barrier for this type of direct elimination was located. The barrier for the silicate intermediate undergoing direct elimination was found to higher than the barrier for vinyl anion formation, supporting the notion that vinyl anion formation is the preferred pathway.

(74) Prior studies have shown this carbanion is not a stationary point on the potential energy surface and undergoes spontaneous elimination upon attempted geometry optimization; see: Breton, G. W.; Ridlehoover, J. V. Spontaneous formation of strained anti-Bredt bridgehead alkenes upon computational geometry optimization of bicyclic β-halo carbanions. *Organics* **2024**, *5*, 205–218.

(75) The aliphatic anion is expected to be 10^5–10^{10} times less stable than those seen in the previously discussed systems, as aryl and vinyl anions have pK_a values roughly 5–10 units lower than aliphatic anions.

(76) Calculations were performed in MeCN as this is a common solvent for strained intermediate generation.

(77) Optimization of the starting silyltriflate **5.32** and silicate **5.33** were performed using dihedral constraints on the Si–C–C–O bond set to the given angle. See Section 5.9.12 for further details.

(78) DePuy, C. H.; Thurn, R. D.; Morris, G. F. Concerted bimolecular eliminations and some comments on the Effect of dihedral angle on E2 reactions. *J. Am. Chem. Soc.* **1962**, *84*, 1314–1315.

(79) In unconstrained aliphatic systems, free rotation or conformational changes may be readily achieved, which may render such calculations unnecessary. Thus, what we propose is likely most valuable on rigid or otherwise constrained systems, such as anti-Bredt olefins.

(80) Frisch, M. J.; Trucks, G. W.; Schlegel, H. B.; Scuseria, G. E.; Robb, M. A.; Cheeseman, J. R.; Scalmani, G.; Barone, V.; Petersson, G. A.; Nakatsuji, H.; Li, X.; Caricato, M.; Marenich, A. V.; Bloino, J.; Janesko, B. G.; Gomperts, R.; Mennucci, B.; Hratchian, H. P.; Ortiz, J. V.; Izmaylov, A. F.; Sonnenberg, J. L.; Williams-Young, D.; Ding, F.; Lipparini, F.; Egidi, F.; Goings, J.; Peng, B.; Petrone, A.; Henderson, T.; Ranasinghe, D.; Zakrzewski, V. G.; Gao, J.; Rega, N.; Zheng, G.; Liang, W.; Hada, M.; Ehara, M.; Toyota, K.; Fukuda, R.; Hasegawa, J.; Ishida, M.; Nakajima, T.; Honda, Y.; Kitao, O.; Nakai, H.; Vreven, T.; Throssell, K.; Montgomery, Jr., J. A.; Peralta, J. E.; Ogliaro, F.; Bearpark, M. J.; Heyd, J. J.; Brothers, E. N.; Kudin, K. N.; Staroverov, V. N.; Keith, T. A.; Kobayashi, R.; Normand, J.; Raghavachari, K.; Rendell, A. P.; Burant, J. C.; Iyengar, S. S.; Tomasi, J.; Cossi, M.; Millam, J. M.; Klene, M.; Adamo, C.; Cammi, R.; Ochterski, J. W.; Martin, R. L.; Morokuma, K.; Farkas, O.; Foresman, J. B.; Fox, D. J. *Gaussian 16 Revision C.01*, Gaussian, Inc., Wallingford, CT, 2016.

(81) Chai, J.-D.: Head-Gordon, M. Long-range corrected hybrid density functionals with damped atom-atom dispersion corrections. *Phys. Chem. Chem. Phys.* **2008**, *10*, 6615–6620.

(82) Marenich, A. V.; Cramer, C. J.; Truhlar, D. G. Universal solvation model based on solute electron density and on a continuum model of the solvent defined by the bulk dielectric constant and atomic surface tensions. *J. Phys. Chem. B* **2009**, *113*, 6378–6396.

(83) Weigend, F.; Ahlrichs, R. Balances bases sets of split valence, triple zeta valence and quadruple zeta valence quality for H to Rn: Design and assessment of accuracy. *Phys. Chem. Chem. Phys.* **2005**, *7*, 3297–3305.

(84) Luchini, G.; Alegre-Requena, J. V.; Funes-Ardoiz, I.; Paton, R. S. GoodVibes: Automated thermochemistry for heterogeneous computational chemistry data. *F1000Research* **2020**, *9*, 291.

(85) Grimme, S. Supramolecular binding thermodynamics by dispersion-corrected density functional theory. *Chem. Eur. J.* **2012**, *18*, 9955–9964.

(86) Li, Y.; Gomes, J.; Sharada, S. M.; Bell, A. T.; Head-Gordon, M. Improved force-field parameters for QM/MM simulations of the energies of adsorption for molecules in zeolites and a free rotor correction to the rigid rotor harmonic oscillator model for adsorption enthalpies. *J. Phys. Chem. C* **2015**, *119*, 1840–1850.

(87) Legault, C. Y. *CYLview, 1.0b*; Université de Sherbrooke: Quebec, Montreal, Canada, 2009. http://www.cylview.org.

(88) Boehm, P.; Roediger, S.; Bismuto, A.; Morandi, B. Palladium-catalyzed chlorocarbonylation of aryl (pseudo)halides through in situ generation of carbon monoxide. *Angew. Chem., Int. Ed.* **2020**, *59*, 17887–17896.

(89) Qi, X.; Tao, L.; Hahn, H.; Schultz, C.; Gallus, D. R.; Cao, X.; Nowak, S.; Röser, S.; Li, J.; Cekic-Laskovic, I.; Rad, B. R.; Winter, M. Lifetime limit of tris(trimethylsilyl) phosphite as electrolyte additive for high voltage lithium ion batteries. *RSC Adv.* **2016**, *6*, 38342–38349.

(90) Sumida, Y.; Kato, T.; Hosoya, T. Generation of arynes via ate complexes of arylboronic esters with an *ortho*-leaving group. *Org. Lett.* **2013**, *15*, 2806–2809.

(91) Walters, Z. G.; Witkowski, D. C.; Houk, K. N.; Garg, N. K. Mechanisms of Kobayashi Eliminations for the Generation of Highly-Strained Arynes, Cyclic Cumulenes, and Anti-Bredt Olefins. *Manuscript submitted*.